

Millie Pant

Kusum Deep

Atulya Nagar

Jagdish Chand Bansal *Editors*

Proceedings of the Third International Conference on Soft Computing for Problem Solving

SocProS 2013, Volume 1



Springer

Advances in Intelligent Systems and Computing

Volume 258

Series editor

Janusz Kacprzyk, Warsaw, Poland

For further volumes:
<http://www.springer.com/series/11156>

About this Series

The series “Advances in Intelligent Systems and Computing” contains publications on theory, applications, and design methods of Intelligent Systems and Intelligent Computing. Virtually all disciplines such as engineering, natural sciences, computer and information science, ICT, economics, business, e-commerce, environment, healthcare, life science are covered. The list of topics spans all the areas of modern intelligent systems and computing.

The publications within “Advances in Intelligent Systems and Computing” are primarily textbooks and proceedings of important conferences, symposia and congresses. They cover significant recent developments in the field, both of a foundational and applicable character. An important characteristic feature of the series is the short publication time and world-wide distribution. This permits a rapid and broad dissemination of research results.

Advisory Board

Chairman

Nikhil R. Pal, Indian Statistical Institute, Kolkata, India
e-mail: nikhil@isical.ac.in

Members

Emilio S. Corchado, University of Salamanca, Salamanca, Spain
e-mail: escorchado@usal.es

Hani Hagrass, University of Essex, Colchester, UK
e-mail: hani@essex.ac.uk

László T. Kóczy, Széchenyi István University, Győr, Hungary
e-mail: koczy@sze.hu

Vladik Kreinovich, University of Texas at El Paso, El Paso, USA
e-mail: vladik@utep.edu

Chin-Teng Lin, National Chiao Tung University, Hsinchu, Taiwan
e-mail: ctlin@mail.nctu.edu.tw

Jie Lu, University of Technology, Sydney, Australia
e-mail: Jie.Lu@uts.edu.au

Patricia Melin, Tijuana Institute of Technology, Tijuana, Mexico
e-mail: epmelin@hafsamx.org

Nadia Nedjah, State University of Rio de Janeiro, Rio de Janeiro, Brazil
e-mail: nadia@eng.uerj.br

Ngoc Thanh Nguyen, Wroclaw University of Technology, Wroclaw, Poland
e-mail: Ngoc-Thanh.Nguyen@pwr.edu.pl

Jun Wang, The Chinese University of Hong Kong, Shatin, Hong Kong
e-mail: jwang@mae.cuhk.edu.hk

Millie Pant · Kusum Deep
Atulya Nagar · Jagdish Chand Bansal
Editors

Proceedings of the Third International Conference on Soft Computing for Problem Solving

SocProS 2013, Volume 1

 Springer

Editors

Millie Pant
Department of Paper Technology
Indian Institute of Technology Roorkee
Roorkee, Uttarakhand
India

Kusum Deep
Department of Mathematics
Indian Institute of Technology Roorkee
Roorkee, Uttarakhand
India

Atulya Nagar
Department of Mathematics
and Computer Science
Liverpool Hope University
Liverpool
UK

Jagdish Chand Bansal
Department of Applied Mathematics
South Asian University
New Delhi
India

ISSN 2194-5357

ISSN 2194-5365 (electronic)

ISBN 978-81-322-1770-1

ISBN 978-81-322-1771-8 (eBook)

DOI 10.1007/978-81-322-1771-8

Springer New Delhi Heidelberg New York Dordrecht London

Library of Congress Control Number: 2014931408

© Springer India 2014

This work is subject to copyright. All rights are reserved by the Publisher, whether the whole or part of the material is concerned, specifically the rights of translation, reprinting, reuse of illustrations, recitation, broadcasting, reproduction on microfilms or in any other physical way, and transmission or information storage and retrieval, electronic adaptation, computer software, or by similar or dissimilar methodology now known or hereafter developed. Exempted from this legal reservation are brief excerpts in connection with reviews or scholarly analysis or material supplied specifically for the purpose of being entered and executed on a computer system, for exclusive use by the purchaser of the work. Duplication of this publication or parts thereof is permitted only under the provisions of the Copyright Law of the Publisher's location, in its current version, and permission for use must always be obtained from Springer. Permissions for use may be obtained through RightsLink at the Copyright Clearance Center. Violations are liable to prosecution under the respective Copyright Law. The use of general descriptive names, registered names, trademarks, service marks, etc. in this publication does not imply, even in the absence of a specific statement, that such names are exempt from the relevant protective laws and regulations and therefore free for general use.

While the advice and information in this book are believed to be true and accurate at the date of publication, neither the authors nor the editors nor the publisher can accept any legal responsibility for any errors or omissions that may be made. The publisher makes no warranty, express or implied, with respect to the material contained herein.

Printed on acid-free paper

Springer is part of Springer Science+Business Media (www.springer.com)

Preface

SocProS is a 3-year old series of International Conferences held annually under the joint collaboration between a group of faculty members from IIT Roorkee, South Asian University Delhi and Liverpool Hope University, UK.

The first SocProS was held at IE(I), RLC, Roorkee, December 20–22, 2011, with General Chairs as Prof. Kusum Deep, Indian Institute of Technology Roorkee and Prof. Atulya Nagar, Liverpool Hope University, UK. It was a huge success and attracted participation from all over the world, including places like UK, US, France, South Africa, etc.

The second SocProS was held at JKLU, Jaipur, December 28–30, 2012 and was as successful as SocProS 11. Encouraged by the success of first two SocProS Conferences, this year this flagship conference—SocProS 13, which is the Third International Conference on Soft Computing for Problem Solving is being held at the Greater Noida Extension Centre of IIT Roorkee during December 26–28, 2013.

This year SocProS 13 was held as a part of the Golden Jubilee Celebrations of Saharanpur Campus of IIT Roorkee.

Like other SocProS conferences, the focus of SocProS 13 lies in Soft Computing and its applications to solve real life problems occurring in different domains ranging from medical and health care to supply chain management to image processing and cryptanalysis, etc.

SocProS 2013 attracted a wide spectrum of thought-provoking research papers on various aspects of Soft Computing with umpteen applications, theories, and techniques. A total of 158 research papers are selected for publication in the form of proceedings, which is in Volumes 1 and 2.

The editors would like to express their sincere gratitude to the Plenary Speakers, Invited Speakers, Reviewers, Programme Committee Members, International Advisory Committee, Local Organizing Committee, without whose support the quality and standards of the Conference as well as these Proceedings would not have seen the light of the day.

On the Institutional side, we would like to express our gratitude to Saharanpur Campus of Indian Institute of Technology Roorkee Campus, Roorkee, India to provide us a platform to host this Conference. Thanks are also due to the various sponsors of SocProS 2013.

We hope that the papers contained in this proceeding will prove helpful toward improving the understanding of Soft Computing at teaching as well as research level and will inspire more and more researchers to work in the field of Soft Computing.

Roorkee, India
New Delhi, India
Liverpool, UK

Millie Pant
Kusum Deep
Jagdish Chand Bansal
Atulya Nagar

About the Book

The proceedings of SocProS 2013 serve as an academic bonanza for scientists and researchers working in the field of Soft Computing. This book contains theoretical as well as practical aspects of Soft Computing, an umbrella term for techniques like fuzzy logic, neural networks and evolutionary algorithms, swarm intelligence algorithms etc.

This book will be beneficial for the young as well as experienced researchers dealing with complex and intricate real world problems for which finding a solution by traditional methods is very difficult.

The different areas covered in the proceedings are: Image Processing, Cryptanalysis, Supply Chain Management, Newly Proposed Nature Inspired Algorithms, Optimization, Problems related to Medical and Health Care, Networking etc.

Contents

Computational Study of Blood Flow Through Elastic Arteries with Porous Effects	1
Anil Kumar and S. P. Agrawal	
A Modified Shuffled Frog Leaping Algorithm for Long-Term Generation Maintenance Scheduling	11
G. Giftson Samuel and C. Christober Asir Rajan	
Key-Based Steganographic Textual Secret Sharing for Confidential Messaging	25
Neil Buckley, Atulya K. Nagar and S. Arumugam	
AnimVSS: Frame-Based Visual Secret Sharing.	35
Neil Buckley, Atulya K. Nagar and S. Arumugam	
Searching Partially Bounded Regions with P Systems.	45
Hepzibah A. Christinal, Ainhoa Berciano, Daniel Díaz-Pernil and Miguel A. Gutiérrez-Naranjo	
Power System Stability Enhancement Using Fuzzy Logic Based Power System Stabilizer	55
V. K. Tayal, J. S. Lather, Piyush Sharma and S. K. Sinha	
An Improved Quantum Inspired Firefly Algorithm with Interpolation Operator.	69
A. Manju and M. J. Nigam	
Discrete Wavelet Transform Based Fault Detection and Classification in a Static Synchronous Series Compensated Transmission System	85
M. Geethanjali, M. Anju Alias and T. Karpaga Senthil Pandy	

SVM and Random Forest Classification of Satellite Image with NDVI as an Additional Attribute to the Dataset	95
K. Joshil Raj and S. SivaSathya	
Bi-directional Pixel-Value Differencing Approach for Steganography	109
Himakshi, Harsh Kumar Verma, Ravindra Kumar Singh and Charan Kamaljit Singh	
Unsupervised Classification of Mixed Data Type of Attributes Using Genetic Algorithm (Numeric, Categorical, Ordinal, Binary, Ratio-Scaled)	121
Rohit Rastogi, Saumya Agarwal, Palak Sharma, Uarvarshi Kaul and Shilpi Jain	
RoHeMaSys: Medical Revolution with Design and Development of Humanoid for Supporting Healthcare	133
Deepshikha Bhargava and Sameer Saxena	
Synergy of Differential Evolution and Particle Swarm Optimization	143
Kedar Nath Das and Raghav Prasad Parouha	
Energy Management Routing in Wireless Sensor Networks	161
Vrince Vimal and Sanjeev Maheshwari	
Axially Symmetric Vibrations of Circular Sandwich Plates of Linearly Varying Thickness	169
Rashmi Rani and Roshan Lal	
Solve Shortest Paths Problem by Using Artificial Bee Colony Algorithm	183
P. Mansouri, B. Asady and N. Gupta	
Speed Control of Three Phase Induction Motor Drive Using Soft Computing Technique	193
Arunesh Kumar Singh, D. K. Chaturvedi and Jitendra Singh	
Edge Detection in Images Using Modified Bit-Planes Sobel Operator	203
Rashi Agarwal	

Application of Rule Based Fuzzy Inference System in Predicting the Quality and Quantity of Potato Crop Yield in Agra 211
 Darpan Anand, Manu Pratap Singh and Manish Gupta

A Novel Variant of Self-Organizing Migrating Algorithm for Global Optimization 225
 Dipti Singh, Seema Agrawal and Nidhi Singh

User Ranking by Monitoring Eye Gaze Using Eye Tracker. 235
 Chandan Singh and Dhananjay Yadav

Invalidating Security Compromised Nodes by Releasing its Energy in MANETs 247
 N. Chandrakant

Administrating MANETs Via Brain Computer Interface 259
 N. Chandrakant

Parameter Estimation and Soft Computing Techniques 267
 D. K. Chaturvedi and Mayank Pratap Singh

Development of a Genetic Algorithm Toolkit in LabVIEW. 281
 Vineet Kumar, K. P. S. Rana, Amit Kumar, Richa Sharma, Puneet Mishra and Sreejith S. Nair

A Soft Calibration Technique for Thermistor Using Support Vector Machine. 297
 K. V. Santhosh and B. K. Roy

Discrete Cuckoo Search Optimization Algorithm for Combinatorial Optimization of Vehicle Route in Graph Based Road Network 307
 Chiranjib Sur and Anupam Shukla

Introducing a Novel Parameter in Generation of Course Timetable with Genetic Algorithm 321
 Ravitashaw Bathla, Shubham Jain and Rajeev Singh

Application of AI Techniques in Implementing Shunt APF in Aircraft Supply System 333
 Saifullah Khalid and Bharti Dwivedi

Differential Evolution for Supplier Selection Problem: A DEA Based Approach	343
Sunil Jauhar, Millie Pant and Aakash Deep	
Social Engineering Prevention by Detecting Malicious URLs Using Artificial Bee Colony Algorithm	355
Tushar Bhardwaj, Tarun Kumar Sharma and Manu Ram Pandit	
New Lightweight Conditional Encryption Schemes for Multimedia . . .	365
Sakshi Dhall, Saibal K. Pal and Kapil Sharma	
Comparative Study of Controller Optimization Techniques for a Robotic Manipulator	379
Richa Sharma, K. P. S. Rana and Vineet Kumar	
Hybridization of P Systems and Particle Swarm Optimization for Function Optimization	395
Garima Singh and Kusum Deep	
Image Security Using Cellular Automata Rules	403
Manoj Diwakar, Pratibha Sharma, Sandip Swarnakar and Pardeep Kumar	
Cuckoo Search Algorithm for the Selection of Optimal Scaling Factors in Image Watermarking	413
Musrrat Ali, Chang Wook Ahn and Millie Pant	
Identifying and Prioritizing Human Capital Measurement Indicators for Personnel Selection Using Fuzzy MADM	427
Remica Aggarwal	
Application of ANN to Predict Liquefaction Potential of Soil Deposits for Chandigarh Region, India.	441
Abha Mittal, Gayatri Devi and P. K. S. Chauhan	
Survey of Curve and Surface Reconstruction Algorithms from a Set of Unorganized Points	451
Kavita Khanna and Navin Rajpal	
Reconstruction of Noisy Bezier Curves Using Artificial Neural Networks	459
Kavita Khanna and Navin Rajpal	

SBM-DEA Model Based Efficiency Assessment of Public Sector Hospitals in Uttarakhand, India 467
 Sandeep Kumar Mogha, Shiv Prasad Yadav and S. P. Singh

Recognizability of Triangular Picture Languages by Triangular Wang Automata 481
 V. Devi Rajaselvi, T. Kalyani, V. R. Dare and D. G. Thomas

Role of Information Technology in Financial Inclusion 495
 Satya Narayan Singh, Om Prakash Dubey, Kusum Deep and Ajay Prasad

Harmony Search Based Algorithm for Complete Information Equilibrium in Infinite Game 503
 Riccardo Alberti and Atulya K. Nagar

A Proposed Architecture for Efficient Data Delivery and Route Maintenance in a Sparsely Deployed Mobile Ad Hoc Network 513
 Monit Kapoor and Manish Prateek

Multi-carrier Based Radar Signal Optimization Using Genetic Algorithm 525
 Gabriel Lellouch and Amit Kumar Mishra

Additive and Multiplicative Inverse of Generalized Fuzzy Numbers with Different Left Heights and Right Heights 535
 Gourav Gupta, Amit Kumar and M. K. Sharma

Cryptanalysis of “A New Method of Cryptography Using Laplace Transform” 539
 Praneesh Gupta and Prasanna Raghaw Mishra

A Design of Longitudinal Control of an Aircraft Using a Fuzzy Logic Based PID Controller 547
 S. N. Deepa and G. Sudha

Evaluation of Content Based Spam Filtering Using Data Mining Approach Applied on Text and Image Corpus 561
 Amit Kumar Sharma, Prabhjeet Kaur and Sanjay Kumar Anand

Comparison of Lattice Form Based and Direct Form Based Complex Adaptive Notch Filter 579
 Bhawya Kumar, Rahul Vijay and Pankaj Shukla

An Ensemble Pruning Approach Based on Reinforcement Learning in Presence of Multi-class Imbalanced Data.	589
Lida Abdi and Sattar Hashemi	
Fusion of Fingerprint and Iris Biometrics Using Binary Ant Colony Optimization.	601
Minakshi Gogoi and Dhruba Kr. Bhattacharyya	
Efficient Resource Allocation Strategies for Video on Demand Services	615
Alok Kumar Prusty and Bibhudatta Sahoo	
A Novel Co-swarm Gravitational Search Algorithm for Constrained Optimization	629
Anupam Yadav and Kusum Deep	
An Analytical Investigation on Thermally Induced Vibrations of Non-homogeneous Tapered Rectangular Plate	641
Anupam Khanna and Narinder Kaur	
Building of a Competent Mobility Model for Ad Hoc Wireless Networks.	653
Arvind Kumar Shukla, C. K. Jha and Vimal Kumar Mishra	
Single Axis Position Control of a Precision Gimbal.	667
Kamna Ashu, Sanoj Kumar and Kanika Chawla	
An Investigation of Fuzzy PSO and Fuzzy SVD Based RBF Neural Network for Multi-label Classification.	677
Jitendra Agrawal, Shikha Agrawal, Shilpy Kaur and Sanjeev Sharma	
A Peer-to-Peer Single Objective Particle Swarm Optimizer	689
Hrishikesh Dewan, Raksha B. Nayak and V. Susheela Devi	
F-FDRPSO: A Novel Approach Based on Hybridization of Fuzzy C-means and FDRPSO for Gene Clustering.	709
Arpit Jain, Shikha Agrawal, Jitendra Agrawal and Sanjeev Sharma	
Metaheuristic Approaches for Multiprocessor Scheduling.	721
Lakshmi Kanth Munganda and Alok Singh	
Fuzzy Slack Based Measure of Data Envelopment Analysis: A Possibility Approach	733
Shivi Agarwal	

Application of Ant Algorithm Variants to Single Track Railway Scheduling Problem 741
 G. S. Raghavendra and N. Prasanna Kumar

An ICA Mixture Model Based Approach for Sub-pixel Classification of Hyperspectral Data. 755
 N. Prabhu, Manoj K. Arora, R. Balasubramanian and Kapil Gupta

Network Connectivity in VANETs 767
 Ranjeet Singh Tomar, Brijesh Kumar Chaurasia, Shekhar Verma and Rajendra Singh Kushwah

Proposal and Survey of Various Data Mining Aspects in Mobile Computing Environment 777
 Harcharan Singh Pabla, Sukhdeep Singh, Niyati Gupta, Palak Makhija, Prabhjot Kaur and Gurpal Singh

Ant Colony Optimization Model for Discrete Tomography Problems 785
 Divyesh Patel and Tanuja Srivastava

Object Recognition Using Gabor Wavelet Features with Various Classification Techniques. 793
 Divya Sahgal and Manoranjan Parida

Cryptanalytic Attacks and Countermeasures on RSA 805
 Manish Kant Dubey, Ram Ratan, Neelam Verma and Pramod Kumar Saxena

Applications of Genetic Algorithms in Cryptology 821
 Ram Ratan

An Ontology and Pattern Clustering Approach for Activity Recognition in Smart Environments. 833
 K. S. Gayathri, Susan Elias and S. Shivashankar

A Note on Constructing Fuzzy Homomorphism Map for a Given Fuzzy Formal Context. 845
 Prem Kumar Singh and Aswani Kumar Ch.

Application of Ratio Property in Searching of M-Ambiguous Words and Its Generalization 857
 Amrita Bhattacharjee and Bipul Syam Purkayastha

Two Storage Inventory Model for Deteriorating Items Under Fuzzy Environment. 867
S. R. Singh and Anuradha

Fuzzy Optimal Solution of Interval-Valued Fuzzy Transportation Problems. 881
Deepika Rani and T. R. Gulati

Comparative Study for Brain Tumor Classification on MR/CT Images. 889
Ankit Vidyarthi and Namita Mittal

Anonymous Remote User Authentication and Key Agreement for Cloud Computing 899
Raghavendra Mishra

Automatic Identification of an Epileptic Spike Pattern in an EEG Signals Using ANN. 915
Mohd. Zuhair, Sonia Thomas, Anup Kumar Keshri, Rakesh Kumar Sinha, Kirat Pal and Dhruves Biswas

About the Editors 925

Author Index 927

Computational Study of Blood Flow Through Elastic Arteries with Porous Effects

Anil Kumar and S. P. Agrawal

Abstract In this paper, two different non-Newtonian models for blood flow, first a simple power law model displaying shear thinning viscosity, and second a generalized Maxwell model displaying both shear thinning viscosity and oscillating flow viscous-elasticity have been considered. The investigation depicts that the model considered here is capable of taking into account the rheological properties affecting the blood flow and hemodynamical features, which may be important for medical doctors to predict diseases for individuals on the basis of the pattern of flow for an elastic artery in porous effects. The governing equations have been solved by Crank-Nicholson technique. The results are interpreted in the context of blood in the elastic arteries keeping the porous effects view.

Keywords Elastic artery model · Crank-Nicholson technique · Porosity · Wall shear stress

1 Introduction

The control of the blood pressure has been possible by using porous effect in cases of cholesterol and related diseases. Physiological fluid dynamics is relatively new area that deals with fluid dynamics of porous medium of biological fluids. The study of flow of Non-Newtonian fluid has gained considerable importance in various disciplines in recent years, several researchers like Liepsch and Moravec [8] studied the flow of a shear thinning blood, analog fluid in pulsatile flow through arterial branch model and observed large differences in velocity profile relative to these measured

A. Kumar (✉)

Applied Mathematics, World Institute of Technology, Sohna, Gurgaon, India
e-mail: dranilkumar07@gmail.com

S. P. Agrawal

Civil Engineering, World Institute of Technology, Sohna, Gurgaon, India

with Newtonian fluids having the high shear rate viscosity of the analog fluid. Nazemi et al. [9] made important contributions to the identification of atherogenic sites. Rodkiewicz et al. [14] used several different non-Newtonian models for blood for simulation of blood flow in large arteries and they observed that there is no effect of the yield stress of blood on either the velocity profiles or the wall shear stress. Perktold et al. [12] modeled the flow in stenotic vessels as that of an incompressible Newtonian fluid in the rigid vessels. Sharma and Kapoor [5] investigated a mathematical analysis of blood flow through arteries using finite element method. Srivastava [17] analysed the problem of blood flow through an axially non-symmetric mild stenosis blood is represented by a Casson fluid and Newtonian fluid.

Application of the porous medium has been realised as an elegant device for flow control in fluid flow. Datta and Tarbell [2] studied the two different rheological models of blood displaying shearing thinning viscosity and oscillatory flow viscoelasticity. Katiyar and Mbah [4] investigated the effects of a grown mild stenosis in the flow of blood through the elastic artery. Lee and Libby [7] made a study of vulnerable atherosclerotic plaque containing a large necrotic core, and covered by this fibrous cap. Korenga et al. [6] considered biochemical factor such as gene expression and albumin transport in atherogenesis and in plaque rupture these have been shown to be activated by hemodynamic factors in wall shear stress. Rees and Thompson [13] studied a simple model derived from laminar boundary layer theory to investigate the flow of blood in arterial stenoses up to Reynold's number of 1,000. Tang et al. [20] analysed triggering events are believed to be primarily hemodynamic including cap tension, bending of torsion of the artery. Kumar [26] studied a mathematical model of Blood flow in Arteries with Porous Effects.

Berger and Jou [1] investigated a wall shear stress down stream of axisymmetric stenoses in the presence of hemodynamic forces acting on the plaque, which may be responsible for plaque rupture. Karner and Perktold [5] investigated the influence of endothelial damage and of blood process on albumin accumulation in the arterial wall. Stroud et al. [18] founded the difference in flow fields and in quantities such as wall shear stress among stenotic vessels with same degree of stenosis. Sharma et al. [16] developed a mathematical analysis of blood flow through arteries using finite element Galerkin's approach.

In the present study we are interested in the analysis of blood flow in elastic arteries in the presence porous effects. In the present paper we extend the local flow calculations to include the non-Newtonian rheology of blood in order to examine the effects of the shear thinning visco-elasticity of blood on flow phenomena in large elastic arteries in the porous effects using a Crank-Nicholson technique.

2 Mathematical Model

In the present investigation of the local flow formulation for Newtonian fluid in elastic artery in the porous effects has been considered. Here we consider a model blood flow using a homogeneous, incompressible fluid in an isotropic thin walled

tube with longitudinal constant when the fluid is subjected to an oscillatory pressure gradient. The equations of motion are simplified by making the long wave-length approximation $|\frac{\omega R}{C}| \leq 1$ where w is angular naturally R the vessel radius, C represents wave-speed [3, 10, 11, 15]. The governing momentum equation and continuity equation are in cylindrical coordinates as given below:

$$\frac{\partial w}{\partial t} + u \frac{\partial w}{\partial r} + w \frac{\partial w}{\partial z} = -\frac{1}{\rho} \frac{\partial p}{\partial z} - \frac{1}{\rho r} \frac{\partial}{\partial r} (r\tau) - \frac{w}{K}, \quad (1)$$

and

$$\frac{\partial u}{\partial r} + \frac{\partial w}{\partial z} + \frac{u}{r} = 0, \quad (2)$$

where u , w are velocity components in the r and z axis respectively; t time, p pressure; ρ the density; K the permeability parameter. For a purely elastic model, a relation which is quite accurate for arteries [9] as given below:

$$R = R(p) \quad (3)$$

The boundary conditions in the radial direction are:

$$\frac{\partial w}{\partial r} = 0, \quad u = 0 \quad \text{at } r = 0, \quad (4)$$

and $w = 0$,

$$u = \frac{\partial R}{\partial t} \quad \text{at } r = R(t,z), \quad (5)$$

Transforming coordinates by using the relation $\xi = \frac{r}{R(t,z)}$, transformed governing equation are [4].

$$\begin{aligned} \frac{\partial w}{\partial t} + \left(\frac{u}{r} - \frac{\xi}{R} \right) \frac{\partial w}{\partial \xi} - \frac{w}{R} \left(\frac{\partial u}{\partial \xi} + \frac{u}{\xi} \right) &= -\frac{1}{\rho} \frac{\partial p}{\partial z} - \frac{1}{\rho R} \frac{\partial \tau}{\partial \xi} - \frac{\tau}{\rho R \xi} - \frac{w}{K}, \\ \text{or } \frac{\partial w}{\partial t} &= -\frac{1}{\rho} \frac{\partial p}{\partial z} - \frac{1}{\rho R} \frac{\partial \tau}{\partial \xi} - \frac{\tau}{\rho R \xi} + \left(\frac{\xi}{R} \frac{\partial R}{\partial t} - \frac{u}{r} \right) \frac{\partial w}{\partial \xi} + \frac{w}{R} \left(\frac{\partial u}{\partial \xi} + \frac{u}{\xi} \right) - \frac{w}{K}, \end{aligned} \quad (6)$$

$$u = \frac{\partial R}{\partial P} \frac{\partial P}{\partial t} \left[\xi w - \frac{2}{\xi} \left(\int_0^{\xi} \xi w d\xi - \frac{\int_0^1 \xi w d\xi}{\int_0^1 \xi w d\xi} \int_0^{\xi} \xi w d\xi \right) \right] + \frac{1}{\xi} \frac{\partial R}{\partial t} \frac{\int_0^{\xi} \xi w d\xi}{\int_0^1 \xi w d\xi}, \quad (7)$$

where the derivative $\frac{\partial R}{\partial P}$ explain to the elastic response of the artery and experimental values for this are available [21, 22, 24, 25].

The transformed boundary conditions are:

$$\frac{\partial w}{\partial r} = 0, \quad u = 0 \quad \text{at } \xi = 0, \quad (8)$$

and $w = 0$,

$$u = \frac{\partial R}{\partial t} \quad \text{at } \xi = 1, \quad (9)$$

we present have the formulation for the power law model of Walburn and Schneck [23] and the visco elastic model of Thruston [19]. To solve the flow problem for a power law fluid equation is written as [26]:

$$\tau = -k \left| \frac{\partial w}{\partial r} \right|^{n-1} \frac{\partial w}{\partial r}, \quad (10)$$

where shear rate (γ) has been replaced by $(-\frac{\partial w}{\partial r})$ for one dimensional tube flow and the absolute value has been introduced to insure that the viscosity is always positive. Equation (4) and (10) is transformed into the new coordinate system.

$$\tau = -\frac{k}{R} \left| \frac{w_\xi}{R} \right|^{n-1} \frac{\partial w}{\partial \xi}, \quad (11)$$

The momentum and continuity Eqs. (11) and (7) can be solved subject to boundary conditions (8) and (9) to complete the flow field of non-Newtonian fluid in an elastic artery with the porous effects.

In the initial simulation we will concentrate on simple oscillatory function containing a single harmonic [27–30].

$$\frac{\partial P(t)}{\partial z} = \bar{K} + k \cos(\omega t), \quad (12)$$

$$R(t) = \bar{R}(1 + k_R \cos(\omega t - \phi)), \quad (13)$$

where \bar{R} and \bar{K} are the mean parameters, k and k_r are amplitude parameter, ϕ the phase angle and ω the frequency.

$$Q(t) = \bar{Q}(1 + k_\theta \cos(\omega t - \theta)), \quad (14)$$

And

$$\tau_w(t) = \bar{\tau}(1 + k_r \cos(\omega t - \phi)), \quad (15)$$

where $Q(t)$ and $\tau_w(t)$ are the flow rate and wall shear stress respectively. For our simulation the amplitude of second harmonics has always less then 8 % of the first harmonics indicating very small distortion.

3 Computational Method

The spatially discrete form of the governing equations is obtained using Crank-Nicholson scheme. The index for time usually appears as superscript in C.F.D., where n denotes conditions at time (t) and $(n + 1)$ denotes the conditions at time ($t + \Delta t$) [31]. The semi-discretized governing equations are written in the following form:

$$\begin{aligned} & \frac{w_i^{n+1} - w_i^n}{\Delta t} \frac{1}{p_i^n} \frac{P_i^{n+1} - P_i^n}{\Delta z} - \frac{1}{p_i^n R_i^n} \frac{\tau_i^{n+1} - \tau_i^n}{\Delta \zeta} - \frac{\tau_i^n}{p_i \zeta_i^n R_i^n} + \left[\frac{\zeta_i^n}{R_i^n} \left(\frac{R_i^{n+1} - R_i^n}{2\Delta t} \right) - \frac{u_i^n}{R_i^n} \right] \frac{w_i^{n+1} - w_i^n}{\Delta \zeta} \\ & + \frac{w_i^n}{R_i^n} \left\{ \left(\frac{u_i^{n+1} - u_i^n}{\Delta \zeta} \right) - \frac{u_i^n}{\zeta_i^n} \right\} - \frac{w_i^n}{K} \end{aligned} \quad (16)$$

where $\frac{\partial v}{\partial t} = \frac{v_i^{n+1} - v_i^n}{\Delta t}$, $\frac{\partial v}{\partial x} = \frac{v_i^{n+1} - v_i^n}{\Delta x} + O(\Delta x)^2$ and the unknown w_i^{n+1} is not only expressed in terms of the known quantities at time index n . The grid point i can not by itself result in the solution of w_i^{n+1} . The system of algebraic equations form which the unknown w_i^{n+1} is to be found, for all i can be solved simultaneously. The discretized boundary conditions are:

$$\left(\frac{\partial w}{\partial \zeta} \right)_i = \frac{w_i^{n+1} - w_i^n}{\Delta \zeta} + O(\Delta \zeta)^2 = 0, \text{ at } \zeta = 0, \quad (17)$$

$$w = 0, u = \left(\frac{\partial R}{\partial t} \right)_i = \frac{R_i^{n+1} - R_i^n}{\Delta t}, \text{ at } \zeta = 0, \quad (18)$$

The discretization technique avoids the viscous stability constraints which can be quite restriction for these type of the computation. The algebraic equations are solved by using Gauss-Siedal method.

The axial velocity are computed by solving the axial momentum Eq. (16) supplemented by the appropriate constitutive equations and the radial velocity calculated from Eq. (7). The pressure gradient parameters (\bar{K}, k) were initially chosen so that the flow wave forms produced for Newtonian fluid in the rigid tube would have an amplitude approximately equal to the mean ($k_Q = 1$ and mean flow rates characteristic of the thoracic aorta under normal $Q = 7.7$ L/min, $\alpha = 12$, $k = 18$ dynes/cm³, $K = 1$). Physiological flow simulation required iterative computation in order to match the radius (R) and flow (Q) wave-forms with system.

4 Results and Discussion

The results have been numerically worked out for various combinations of the parameters involved in the solution. Figure 1 depicts that the mean wall shear stress is the same for all models considered. This simply reflects the fact that in a

Fig. 1 Comparison of WSS for different rheological models in a rigid artery with a fixed pressure gradient wave form with the porous effects

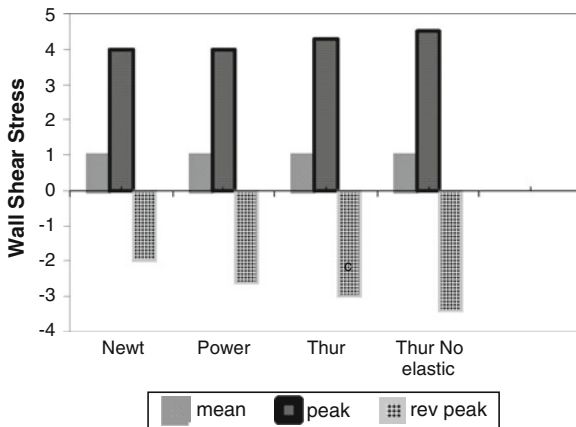
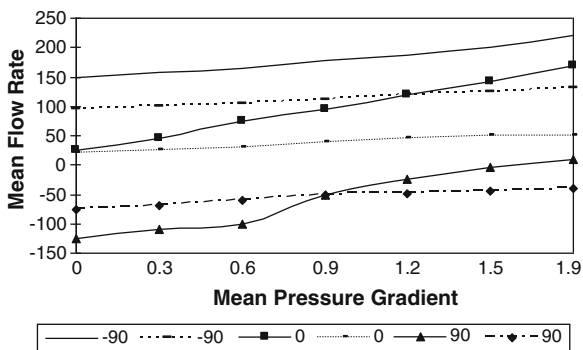


Fig. 2 Mean flow rate versus mean pressure gradient in an elastic artery for different parameters, $k = 18 \text{ dynes/cm}^3$, $a = 12$, $R = 1.9 \text{ cm}$, $K = 1$



rigid tube in the porous effects the mean wall shear stress should be independent of fluid rheology depending only on the mean pressure gradients, as can be described by time and space averaging the axial momentum equations. Figure 2 display the mean flow rate as a functions of the mean pressure gradient at $a = 12$, $\bar{R} = 1.9 \text{ cm}$, for different values of the P-Q phase angle.

Figure 3 depicts that the non-Newtonian effects on mean flow are significant, there is vary small effects shear thinning behaviour on mean wall shear stress with porous effects. Figure 4 exhibits the mean wall shear stress and mean flow rate. We use the mean flow rate rather then the mean pressure gradient to estimate mean wall shear stress in an elastic artery in the porous effects. The solid line denotes the results for rigid tube with porous effects. Figure 5 depicts the amplitude of the first harmonic of the flow rate drawn against the mean pressure gradient. Figure 6 displays the dependence of wall shear stress amplitudes on mean pressure gradient for fixed pressure gradient amplitude. Figure 7 represents the effect rheology on the wall shear stress waveforms, when the flow wave from a fixed. The mean wall shear stress increase for a power law fluid compared to a Newtonian fluid whereas for a rigid tube in the porous effects with a Newtonian fluid. The increase in mean

Fig. 3 Mean Wall Shear Stress versus mean pressure gradient in an elastic artery for different parameter, $k = 18 \text{ dynes/cm}^3$, $a = 18$, $R = 1.4$, $K = 1$

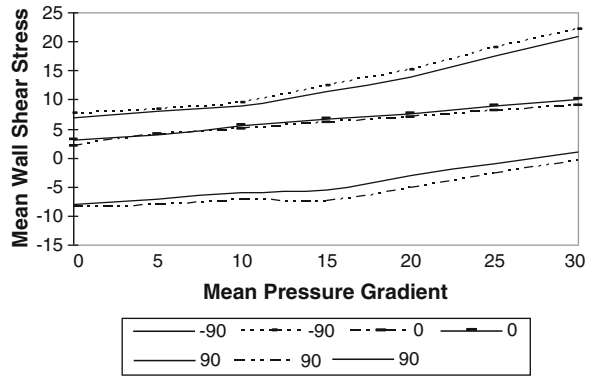


Fig. 4 Mean WSS versus mean flow rate for the Power law model for different parameters, *Solid lines* — rigid artery, *Broken lines*— elastic artery, (-90, 0, 90) impedance angle, $k = 18 \text{ dynes/cm}^3$, $a = 12$, $R = 1.9 \text{ cm}$, $K = 1$

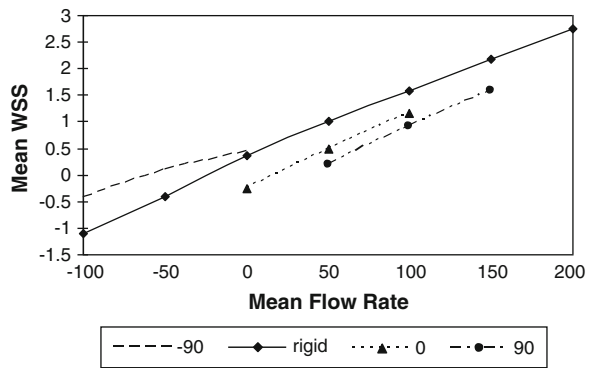
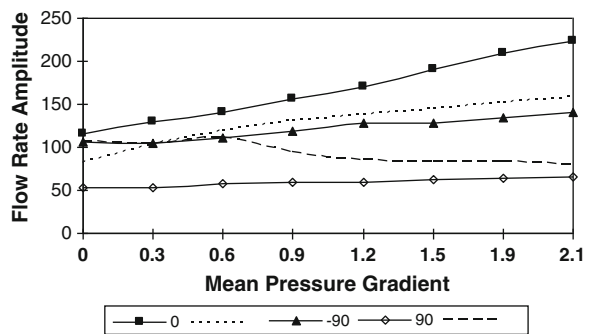


Fig. 5 Flow rate amplitude versus mean pressure gradient in an elastic artery with the porous effects, Power (*broken*), Newt. (*solid*), $k = 18 \text{ dynes/cm}^3$, $a = 12$, $R = 1.9 \text{ cm}$, $K = 1$



wall shear stress for the non-Newtonian fluid is due to the higher mean pressure gradient. This is consistent with our sinusoidal flow simulations where it is observed that the wall shear stress amplitudes were smaller for the power law fluid than the Newtonian fluid at the same pressure gradient (Fig. 6).

Fig. 6 WSS amplitudes versus mean pressure gradient in an elastic artery with the porous effects, $k = 40.5 \text{ dynes/cm}^3$, $a = 18$, $R = 1.4 \text{ cm}$, $K = 1$

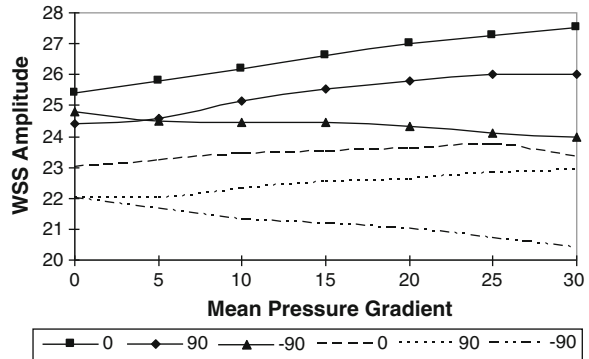
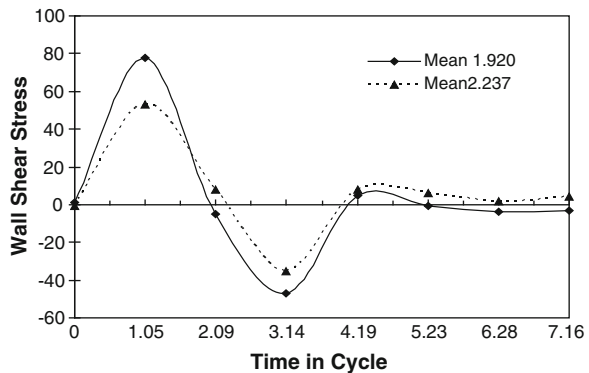


Fig. 7 WSS wave forms for an elastic artery model of ascending aorta for Newtonian (*solid line*) and Power law model (*broken line*) with porous effects



5 Conclusions

The present algorithm is economical and efficient having a sharp convergence. It is noticed that the porous effects has significant effect on the flow phenomena. The investigation shows that the model considered here is capable of taking into account the rheological properties affecting the blood flow and hemodynamic dynamic features, which may be important for medical doctors to predict diseases for individuals on the basis of pattern of flow for the in elastic artery in the porous effects.

Acknowledgment Authors are grateful to **World Institute Technology Sohna Gurgaon** affiliated to MD University, Rohtak India, for providing facilities and encouragement to complete this work. Also the corresponding authors are thankful to the learned referees for their fruitful suggestions for improving the presentation of this work.

References

1. Berger, S.A., Jou, L.D.: Flows in Stenotic vessels. *Annu. Rev. Fluid Mech.* **32**, 347–384 (2000)
2. Datta, A., Tarball, J.M.: Influence of non-Newtonian behavior of blood on flow in an elastic artery model. *ASME, J. Biomech. Eng* **118**, 111–119 (1996)
3. Greenfield, J.C., Patel, D.J.: Relation between pressure and diameter in the ascending Aorta of man. *Circ. Res.* **10**, 778 (1962)
4. Katiyar, V.K., Mbah, G.C.: Effect of time dependant stenosis on the pulsetile flow through an elastic tube. In: *International Conference on Mathematical and its Application in Engineering and Industries*, pp. 439–447. Narosa Publishing House (1997)
5. Karner, G., Perktold, K.: Effect of endothelial and increased blood process on albumin accumulation in the arterial wall: a numerical study. *J. Biomech.* **33**, 709–715 (2000)
6. Korenga, R., Ando, J., Kamiya, A.: The effect of laminar flow on the gene expression of the adhesion molecule in endothelial cells. *Jpn. J. Med. Electron. Bio. Eng.* **36**, 266–272 (1998)
7. Lee, R., Libby, P.: The unstable atheroma, atherosclerosis thrombosis vascular Biology. **17**, 1859–1867 (1997)
8. Liepsch, D., Moravec, S.: Pulsatile flow of non-Newtonian fluid in distensible models of human arteries. *Biorheology* **21**, 571–583 (1984)
9. Milnor, W.R.: *Hemodynamics*, 2nd edn. Williams and Wilkins, Baltimore (1989)
10. Nazemi, M., Kleinstreuer, C., Archie, J.P.: Pulsatile two-dimensional flow and plaque formation in a carotid artery bifurcation. *J. Biomech.* **23**(10), 1031–1037 (1990)
11. Patel, D.J., Janicki, J.S., Vaishnav, R.N., Young, J.T.: Dynamic anisotropic visco-elastic properties of the aorta in living dogs. *Circ. Res.* **32**, 93 (1973)
12. Perktold, K., Thurner, E., Kenner, T.: Flow and stress characteristics in rigid walled compliant carotid artery bifurcation models. *Med. Biol. Eng. Compu.* **32**, 19–26 (1994)
13. Rees, J.M., Thompson, D.S.: Shear stress in arterial stenoses: a momentum integral model. *J. Biomech.* **31**, 1051–1057 (1999)
14. Rodkiewicz, C.M., Sinha, P., Kennedy, J.S.: On the application of constitutive equation for whole human blood. *J. Biomech. Eng.* **112**, 198–206 (1990)
15. Sharma, G.C., Kapoor, J.: Finite element computation of two-dimensional arterial flow in the presence of a transverse magnetic field. *Int. J. numerical methods in fluid dynamics* **20**, 1153–1161 (1995)
16. Sharma, G.C., Jain, M., Kumar, A.: Finite element Galerkin’s approach for a computational study of arterial flow. *Appl. Math. Mech, China* **22**(9), 1012–1018 (2001)
17. Anil Kumar, C.L., Varshney, G. C., Sharma.:Computational technique for flow in blood vessels with porous effects. *Int. J. Appl. Math. Mech. (Engl. Ed)* **26**(1) 63–72 (2005)
18. Anil Kumar, C.L., Varshney, G.C., Sharma.: Performance modeling and analysis of blood flow in elastic arteries, *Int. J. Appl. Math. Mech (Engl. Ed)* **26**(3) 345–354 (2005)
19. Srivastava, V.P.: Arterial blood flow through a non-symmetrical stenosis with applications. *Jpn. J. Appl. Phy* **34**, 6539–6545 (1995)
20. Stroud, J.S., Berger, S.A., Saloner, D.”: Influence of stenosis morphology on flow through severely stenotic vessels; implications for plaque rupture, *J. Biomech*, **33**, pp. 443–455 (2000)
21. Thurston, G.B.: Rheological parameter for the viscosity, visco-elasticity and Thrixotropy of blood. *Biorheology* **16**, 149–155 (1979)
22. Tang, D., Yang, C., Huang, Y., Ku, D.N.: Wall stress and strain analysis using a three-dimensional thick wall model with fluid-structure interactions for blood flow in carotid arteries with stenoses. *Comput. Struct* **72**, 341–377 (1999)
23. Walburn, F.J., Schneck, D.J.: A constitutive equation for whole human blood. *Biorheology* **18**, 201 (1976)
24. White, K.C.: Hemo-dynamics and wall shear rate measurements in the abdominal aorta of dogs. Ph.D. thesis, The Pennsylvania State University (1979)

25. Anil Kumar: Mathematical model of Blood flow in Arteries with Porous Effects, International Federation for Medical and Biological Engineering (IFMBE). Conference 6th World Congress on Biomechanics (WCB 2010). In: Edited by C.T. Lim and J.C.H. Goh (Eds.): WCB 2010, International Federation for Medical and Biological Engineering (IFMBE) Proceedings 31 Springer Publishing, DOI: [10.1007/978-3-642-14515-5_5](https://doi.org/10.1007/978-3-642-14515-5_5) pp. 18–21, 2010
26. Shigeru, T., Tarbell, J.M.: Interstitial flow through the internal elastic lamina affects shear stress on arterial smooth muscle cells. *Am J. Physiol—Heart and Circulatory Physiol*, Vol. **278** pp. H1589-H1597 (2000)
27. Mishra, J.C., Sinha, A.: Effects of hall current and heat radiation on flow of a fluid through a porous medium subject to an external magnetic field. *Spl. Topics Rev. Porous Media—An Int. J.*, DOI: [10.1615/SpecialTopicsRevPorousMedia.v4.i2.40](https://doi.org/10.1615/SpecialTopicsRevPorousMedia.v4.i2.40) pp. 147–158 (2013)
28. Tiwari, A., Satya Deo.: pulsatile flow in a cylindrical tube with porous walls: applications to blood flow, DOI: [10.1615/JPorMedia.v16.i4.50](https://doi.org/10.1615/JPorMedia.v16.i4.50) *J. Porous Media*, pp. 335–340 (2013)
29. Tang1, A.Y-S., Chan1, H-N., Tsang2, A.C-O., GK-K Leung2, Leung3, K-M., Yu4, A.C-H., Chow1.K-W.: The effects of stent porosity on the endovascular treatment of intracranial aneurysms located near a bifurcation, *J. Biomed Sci Eng.* **6**, pp. 812–822 (2013)
30. Li, W.G., Hill, N.A., Going, J., Luo, X.Y.: Breaking analysis of artificial elastic tubes and human artery. *J. Appl. Mech.* ISSN **0021–8936**, 55–67 (2013)
31. Mekheimer, KhS, Haroun, M.H., Elkot, M.A.: Induced magnetic field influences on blood flow through an anisotropically tapered elastic arteries with overlapping stenosis in an annulus. *Can. J. Phys.* **89**, 201–212 (2011)

A Modified Shuffled Frog Leaping Algorithm for Long-Term Generation Maintenance Scheduling

G. Giftson Samuel and C. Christofer Asir Rajan

Abstract This paper discuss a modified Shuffled frog leaping algorithm to Long-term Generation Maintenance Scheduling to Enhance the Reliability of the units. Maintenance scheduling establishes the outage time scheduling of units in a particular time horizon. In a monopolistic power system, maintenance scheduling is being done upon the technical requirements of power plants and preserving the grid reliability. While in power system, technical viewpoints and system reliability are taken into consideration in maintenance scheduling with respect to the economical viewpoint. In this paper present a modified Shuffled frog leaping algorithm methodology for finding the optimum preventive maintenance scheduling of generating units in power system. The objective function is to maintain the units as earlier as possible. Varies constrains such as spinning reserve, duration of maintenance and maintenance crew are being taken into account. In case study, test system consist of 24 buses with 32 thermal generating units is used.

Keywords Generation maintenance schedule • Optimization • Shuffled frog leaping algorithm

1 Introduction

The efficient operation of an electric power system requires the solution of several inter related problems. One problem that has proven to be particularly unyielding is that of determining when the thermal generating units should be taken off line

G. G. Samuel (✉)

Department of EEE, Anna University, Chennai 600025, India
e-mail: giftsam2k@yahoo.com

C. C. A. Rajan

Department of EEE, Pondicherry Engineering College, Pondicherry 605014, India
e-mail: asir_70@pec.edu

for preventive maintenance. This is typically a long planning problem for power companies and it is recognized to be a significant part of the overall operations management of an electric power utility. As a result, utilities are interested in including a unit maintenance scheduling component as a part of an Energy management system.

The unit maintenance scheduling has been tackled by many authors using a variety of objective functions. They are maximizing the minimum reserve, leveling the risk of generation shortage, minimizing production cost and system unreliability. Most of the earlier work in maintenance scheduling uses optimization techniques have been employed to approach the problem. More specifically, these are the Dynamic Programming method (DP), the Mixed Integer Programming method (MIP), the Lagrangian relaxation method (LR), the Branch and Bound method (BB), the Fuzzy Theorem (FT), the Artificial Neural Network (ANN), the Simulated Annealing method (SA) and so on. The major limitation of these approaches is to consider each generating unit separately in selecting its outage interval, large computational time and complexity in programming.

Power system scheduling is to minimize the total generation cost subject to system demand and reserve requirement and individual unit constraints. It has been an active research over the years because of its significant economic impact. To solve this difficult MIP problem, many optimization based methods have been developed [1]. Among them, LR and its extensions are among the most successful ones [2–6]. Many new requirements such as transmission network and environment constraints have also been incorporated in the problem formation. Fuzzy optimization techniques have been developed to solve optimal power flow with fuzzy constrains [7–9], and to schedule manufacturing system with possible breakdowns [10] The Generic Algorithm method mimics the principles of natural genetics and natural selection to constitute search and optimization procedures. Simulated annealing mimics the cooling phenomenon of molten metal's to constitute a search procedure. The Generic Algorithm and Simulated Annealing approaches have been reported to solve a range of optimization problems in electrical power systems with encouraging results [11]. Fuzzy optimization techniques have been developed to solve optimal power flow with fuzzy constrains [12–14], and to schedule manufacturing system with possible breakdowns [15] The major limitation of these approaches is to consider each generating unit separately in selecting its outage interval, large computational time and complexity in programming.

2 Problem Formulation

The objective is to find the generation maintenance scheduling, such that minimize total operating cost over the operational planning period, subject to unit maintenance and variety of system constraints.

$$\begin{aligned} \text{Min } F_T = & \sum_{t=1}^T \sum_{i=1}^N \{F_{it}(P_{it}) \cdot n_t\} U_{it} + \sum_{t=1}^T \sum_{i=1}^N \{(P_{it} + R_{it}) \cdot \text{OMVC} \cdot n_t\} U_{it} \\ & + \sum_{t=1}^T \sum_{i=1}^N \{P_{\text{maxi}} \text{OMFC } n_t\} / 8760 \end{aligned} \quad (1)$$

$$\text{Profit} = \sum MCP * P_{it} - F_T \quad (2)$$

where

$$F_{it}(P_{it}) = A_i P_{it}^2 + B_i P_{it} + C_i \text{ Rs/hr} \quad (3)$$

The objective function represents the profit, which is calculated as the difference between its total revenues and its corresponding costs which include production cost, fixed cost and variable maintenance cost.

There are typical constraints for maintenance scheduling problems. Any maintenance timetable must satisfy a given set of constraints. In order to make the maintenance schedule feasible, certain constraints should be fulfilled. Some of basic constrains which should be set up are continuousness maintenance of some unit, maintenance manpower, maintenance window, maintenance duration and so on.

2.1 Generator Output Limit

Each unit is designed to work between minimum and maximum power capacity. The following constraint ensures that unit is within its respective rated minimum and maximum capacities.

$$U_{it} P_{i\text{min}} \leq P_{it} \leq U_{it} P_{i\text{max}} \quad (4)$$

2.2 Spinning Reserve

Spinning reserve is a safety margin that usually is given as a demand proportion. This indicates that the total capacity of the units running at each interval should not be less than the specified spinning reserve for that interval.

$$\sum_{i=1}^N U_{it} P_{i\text{max}} \geq D_t (1 + r_t \%) \quad (5)$$

2.3 Maintenance Resources

$$\sum_{i=1}^N R_i(k) (1 - U_{it}) \leq \alpha_t(k) \quad (6)$$

2.4 Maintenance Window

The maintenance timetable stated in terms of maintenance variables (S_i). The unit maintenance may not be scheduled before their earliest period or after latest period allowed for maintenance.

$$U_{it} = \begin{cases} 1 & t \leq e_i \text{ or } t \geq l_i + d_i \\ 0 & s_i \leq t \leq s_i + d_i \\ 0, 1 & e_i \leq t \leq l_i \end{cases} \quad (7)$$

2.5 One-Time Maintenance

Each unit has an outage for maintenance just once along the time horizon considered.

$$\sum_{t=1}^T sv_{it} = 1 \quad (8)$$

2.6 Reliability Indices

For simplicity most of the time, no uncertainty is considered which means that appropriate unit are provided. Nevertheless, unit forced outage rates can be approximately taken into account derating their corresponding capacities.

$$P_{\max i}^+ = (1 - for_i) * U_{it} * P_{maxi} \quad (9)$$

$$\sum_{i=1}^N P_{\max i} * (1 - for_i) - \sum_{i=1}^N P_i(t) \geq \%r_t * d_t \quad (10)$$

$$I(t) = \frac{\sum_{i=1}^N \sum_{t=1}^T P_{it}(1 - U_{it})(1 - for_i) - D_t}{\sum_{i=1}^N \sum_{t=1}^T P_{it}(1 - for_i) - D_t} \quad (11)$$

In this paper, we can see that researchers have focused much attention on maintenance scheduling problems for power systems in order to improve the economic posture of the generation companies. Reducing the total generation cost, including the fuel cost, operation and maintenance cost is one of the main objectives in power system maintenance scheduling.

3 Shuffled Frog Leaping Algorithm

The Shuffled frog leaping algorithm is a meta-heuristic optimization method which is based on observing, imitating, and modeling the behavior of a group of frogs when searching for the location that has the maximum amount of available food [16]. Shuffled frog leaping algorithm, originally developed by Eusuff and Lansey in 2003, can be used to solve many complex optimization problems, which are nonlinear, non differentiable, and multi-modal [17]. SFLA has been successfully applied to several engineering optimization problems such as water resource distribution [18], bridge deck repairs [19], job-shop scheduling arrangement [20], and traveling salesman problem (TSP) [21]. The most distinguished benefit of Shuffled frog leaping algorithm is its fast convergence speed [22]. The Shuffled frog leaping algorithm combines the benefits of the both the genetic-based memetic algorithm (MA) and the social behavior-based PSO algorithm [23, 24].

The flowchart of Shuffled frog leaping algorithm is illustrated in Fig. 1. Shuffled frog leaping algorithm is a population based random search algorithm inspired by nature memetics. In the Shuffled frog leaping algorithm, a population of possible solution defined by a group of frogs that is partitioned into several communities referred to as memeplexes. Each frog in the memeplexes is performing a local search. Within each memeplex, the individual frog's behavior can be influenced by behaviors of other frogs, and it will evolve through a process of memetic evolution. After a certain number of memetics evolution steps, the memeplexes are forced to mix together and new memeplexes are formed through a shuffling process. The local search and the shuffling processes continue until convergence criteria are satisfied (12).

The varies steps are as follows:

- (1) The Shuffled frog leaping algorithm involves a population 'P' of possible solution, defined by a group of virtual frogs(n).
- (2) Frogs are sorted in descending order according to their fitness and then partitioned into subsets called as memeplexes (m).
- (3) Froges i is expressed as $X_i = (X_{i1}, X_{i2}, \dots, X_{is})$ where S represents number of variables.
- (4) Within each memeplex, the frog with worst and best fitness are identified as X_w and X_b .
- (5) Frog with globe best fitness is identified as X_g .
- (6) The frog with worst fitness is improved according to the following equation.

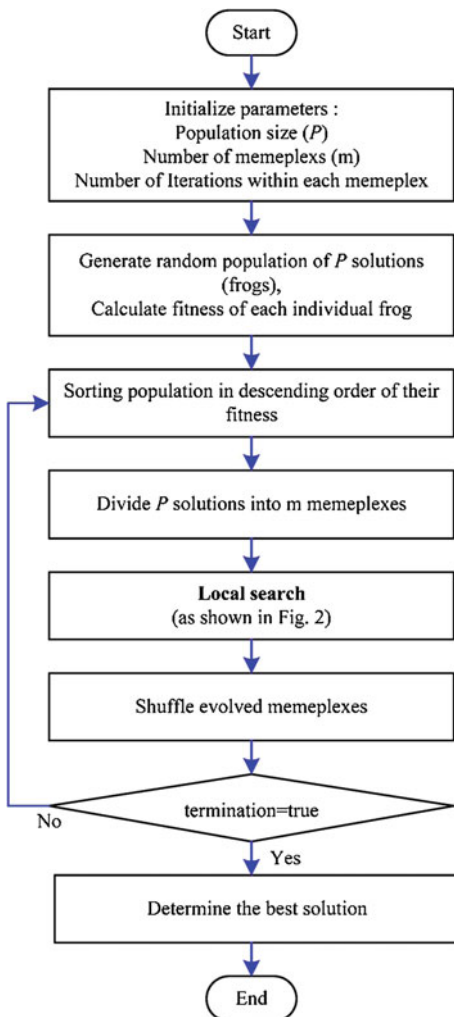
$$D_i = \text{rand}() \cdot (X_b - X_w) \quad (12)$$

$$X_{\text{neww}} = X_{\text{oldw}} + D_i \quad (-D_{\text{max}} \leq D_i \leq D_{\text{max}}) \quad (13)$$

where rand is a random number in the range of [0,1];

D_i is the frog leaping step size of the i-th frog and D_{max} is the maximum step allowed change in a frog's position. If the fitness value of new X_w is better than the

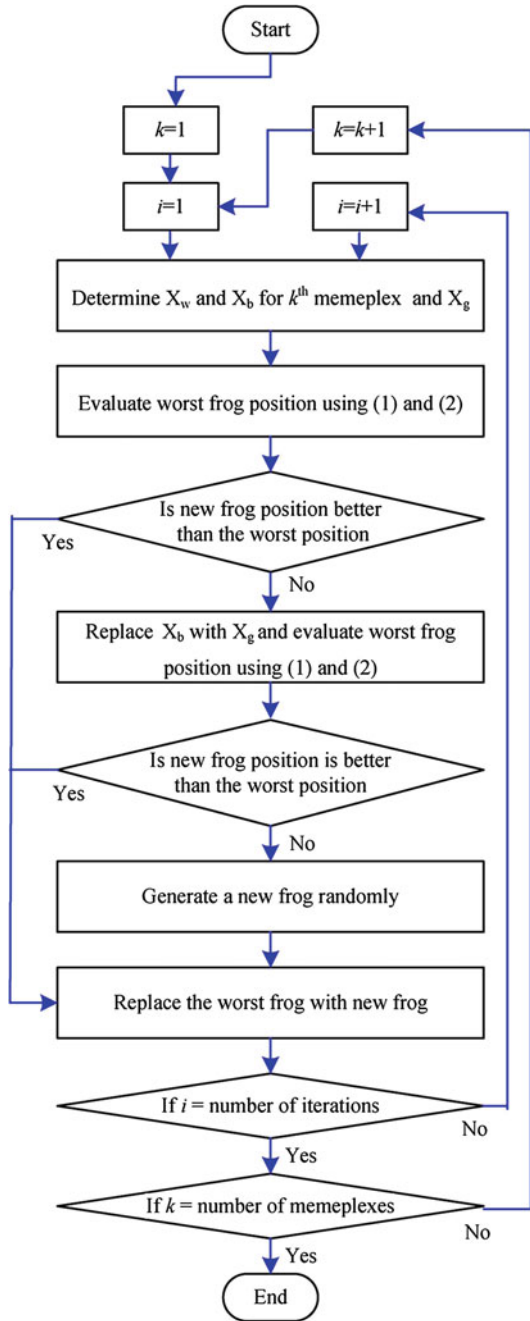
Fig. 1 Flowchart of SFLA



current one, X_w will be accepted. If it isn't improved, then the calculated (12) and (13) are repeated with X_b replaced by X_g . If no improvement becomes possible in the case, a new X_w will be generated randomly. Repeat the update operation for a specific number of iterations. The flowchart of local search of Shuffled frog leaping algorithm is illustrated in Fig. 2.

After a predefined number of memetic evolutionary steps within each memplex, the solutions of evolved memplexes are replaced into new population. This is called the shuffling process. The shuffling process promotes a global information exchange among the frogs. Then, the population is sorted in order of decreasing performance value and updates the population best frog's position, repartition the frog group into memplexes, and progress the evolution within each memplex until the conversion criteria are satisfied.

Fig. 2 Flowchart of local search



4 Simulation Result

The total operating cost of the GMS problem is expressed as the sum of fuel costs, operation and maintenance variable costs (OMVC), operation and maintenance fixed costs (OMFC) of the generating units. The fuel cost is the major component of the operating cost, which is normally modeled by a quadratic input/output curve.

The developed Shuffled frog leaping algorithm program has been carried out on a Pentium IV 2-GHz PC with a 512 Mb RAM in MATLAB 7.3. Software package and the test problem were simulated for ten independent trials using Shuffled frog leaping algorithm.

A 24 bus system with thirty two generating units has been considered as a case study. A time period of 52 weeks is considered and maintenance schedule problem is solved for the thirty two unit systems.

The proposed methodology was tested for the test system [25]. IEEE RTS (reliability test system) is a IEEE twenty four bus system with thirty two thermal units. Tables 1 and 2 show the generator data for thirty two units. When we take annual maintenance for generator, the forced outage is also considered. So the grid collapse is avoided.

The annual peak load for the thirty two generator test system is 2,850 MW. Table 3 gives data on weekly peak load in percentage of annual peak load.

The main parameters of Shuffled frog leaping algorithm have been selected as suggested in [26]. The Shuffled frog leaping algorithm has an initial population of 200 solutions, a set of 20 memplexes, and twelve generations within each memplex (before shuffling).

The Shuffled frog leaping algorithm has been tested on the thirty two unit systems over a scheduling period of 52 weeks. The thirty two generator units system Profit/cost factor are compared with result of DP, LR and GA are listed in Table 4.

The result of the generation Maintenance scheduling of the best solution of Shuffled frog leaping algorithm for thirty two unit systems is given in Table 5. It is obvious that the total cost obtained by Shuffled frog leaping algorithm is less than that of other methods.

EAs have a stochastic nature and in different cases do not converge to the some solution. Therefore, the average of different cases is calculated for each problem. It is obvious that the Shuffled frog leaping algorithm has satisfactory results in comparison with other methods.

Figure 3 shows the performance of objective function of the Shuffled frog leaping algorithm, when maintenance scheduling of the generating units solved for thirty two unit systems. In this figure, the average function fitness of the memplexes is illustrated. Figure 4 show maintenance scheduling of generating units based on its desired objective. Its reliability profit is shown in Fig. 5.

Table 1 Generator data for 32 units

Units	P_{\max} (MW)	Forced outage rate (for)	Schedule maintenance weeks/year	Manpower required per week
1–5	12	0.02	1	10
6–9	20	0.1	1	10
10–13	76	0.02	3	15
14–19	100	0.04	4	15
20–23	155	0.04	5	15
24–29	197	0.05	6	20
30	350	0.08	8	20
31 and 32	400	0.12	8	20

Table 2 The fixed and variable cost of 32 units

Units	P_{\max} (MW)	Fixed O and M cost (Rs/MW-year)	Variable O and M cost (Rs/MWh)
1–5	12	4,50,000	18,000
6–9	20	4,05,000	15,000
10–13	76	4,00,000	13,500
14–19	100	3,50,000	11,250
20–23	155	3,15,000	9,500
24–29	200	3,10,000	9,000
30	350	2,70,000	7,300
31 and 32	400	2,25,000	5,750

Table 3 Weekly peak load in percent of annual peak

Week	Peak load	Week	Peak load	Week	Peak load	Week	Peak load
1	86.2	14	75.0	27	75.5	40	72.4
2	90.0	15	72.1	28	81.6	41	74.3
3	87.8	16	80.0	29	80.1	42	74.4
4	83.4	17	75.4	30	88.0	43	80.0
5	88.0	18	83.7	31	72.2	44	88.1
6	84.1	19	87.0	32	77.6	45	88.5
7	83.2	20	88.0	33	80.0	46	90.9
8	80.6	21	85.6	34	72.9	47	94.0
9	74.0	22	81.1	35	72.6	48	89.0
10	73.7	23	90.0	36	70.5	49	94.2
11	71.5	24	88.7	37	78.0	50	97.0
12	72.7	25	89.6	38	69.5	51	100
13	70.4	26	86.1	39	72.4	52	95.2

The reserve capacity profiles corresponding to thirty two unit systems are as shown in Fig. 5 and maintenance scheduling based on desire objective function for thirty two unit systems is shown in Table 5.

Table 4 Profit/cost factor for 32 units scheduling

System	Method	Total cost (pu)	CPU time (s)
32 units	DP	1.0535	918
	LR	1.0687	850
	EP	1.0392	422
	PSO	1.0387	417
	SFLA	1.0385	414

Table 5 Generation maintenance scheduling for 32 units

Start of outage (week)	Unit	Start of outage (week)	Unit	Start of outage (week)	Unit
1	–	19	17, 25, 31	37	32
2	24	20	17, 25, 31	38	4, 8, 22, 32
3	24	21	17, 25, 31	39	18, 22, 32
4	14, 16, 24	22	17, 31	40	12, 18, 22, 32
5	14, 16, 24	23	9, 23, 31	41	12, 18, 22, 32
6	14, 16, 24	24	6, 23, 31	42	12, 18, 22, 32
7	14, 16, 24	25	20, 23, 31	43	–
8	26	26	13, 20, 23	44	1
9	26, 27	27	2, 13, 20, 23	45	28
10	7, 26, 27, 30	28	13, 20	46	21, 28
11	26, 27, 30	29	15, 20	47	21, 28
12	26, 27, 30	30	3, 15, 19	48	21, 28
13	26, 27, 30	31	15, 19, 29	49	21, 28
14	10, 11, 27, 30	32	15, 19, 29	50	5, 21, 28
15	10, 11, 30	33	19, 29	51	–
16	10, 11, 25, 30	34	29	52	–
17	25, 30	35	29, 32		
18	25, 31	36	29, 32		

Fig. 3 Performance of object function for 32 units

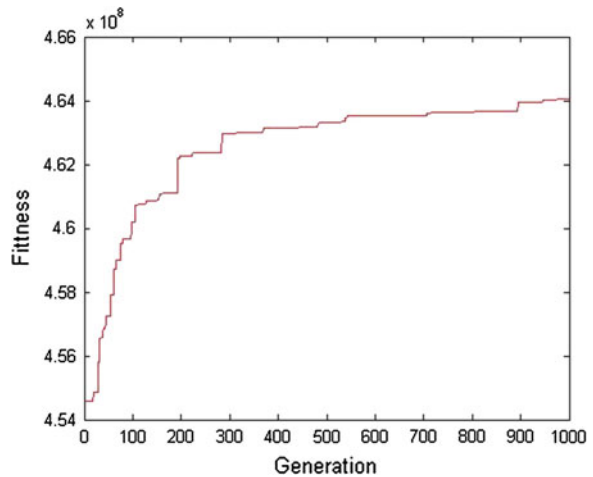


Fig. 4 Scheduling of objective function for 32 units

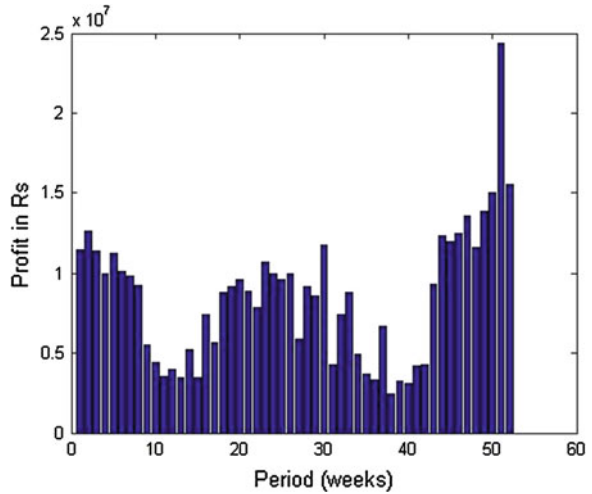
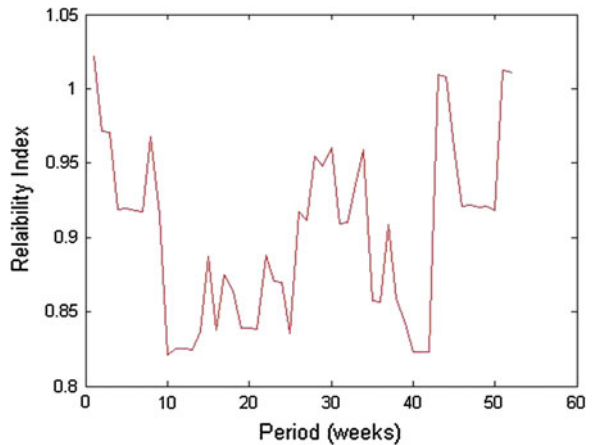


Fig. 5 Reliability index for objective function for 32 units



5 Conclusion

In this paper, a new approach for solving the generation maintenance scheduling problem based on modified Shuffled frog leaping algorithm and the optimum maintenance scheduling over the planning period have been presented. The algorithm has been tested on thirty two generating unit system.

The proposed method has been compared with other methods. The result obtained is compared with the results of other method such as DP, LR and PSO. From the result it is shown that the proposed algorithm provides true optimal solution for minimum fuel cost and computation timing in all cases.

Appendix

A_i, B_i, C_i	the cost function parameters of unit I (Rs/MW ² hr, Rs/MW hr, Rs/hr)
$F_{it} (P_{it})$	production cost of unit I at a time t (Rs/hr)
P_{it}	output power from unit i at time t (MW)
PD_t	system peak demand at hour t (MW)
N	Number of available generating units
R_{it}	reserve contribution of unit i at time t
n_t	number of units
U_{it}	commitment state of unit i at time t (on = 1, off = 0)
OMVC	operation and maintenance variable cost
OMFC	operation and maintenance fixed cost
T_s and T_e	Starting and ending stage of the time interval for jth unit
$I(t)$	Reliability index of grid in period t
$\alpha_t(k)$	kth maintenances resource at the tth period
β	Maximum number of maintenance generator in the same area
d_i	Maintenance duration of the ith generator
s_i	Maintenance starting period of the ith generator

Biographies



G. Giftson Samuel received his B.E. degree (Electrical and Electronics) from the Madurai Kamaraj University, Madurai, India in 1999 and M.E. degree (Power Electronics and Drives) from the Anna University, Chennai, India in 2004. He is currently pursuing Ph.D in Power System at Anna University, Chennai, India. He published technical papers in International and National Journals and Conferences. He is currently working as Assistant Professor in National Institute of Technology—Puducherry, Karaikal, India. His area of interest is power system optimization. He acquired Member in IEEE and Life member of ISTE.



C. Christofer Asir Rajan born on 1970 and received his B.E. (Distn.) degree (Electrical and Electronics) and M.E. (Distn.) degree (Power System) from the Madurai Kamaraj University (1991 and 1996), Madurai, India. And he received his postgraduate degree in D.I.S. (Distn.) from the Annamalai University, Chidambaram. He received his Ph.D in Power System at Anna University, Chennai, India. He published technical papers in International & National Journals and Conferences. He is currently working as Professor in Electrical Engineering Department at Pondicherry Engineering College, Puducherry, India. His area of

interest is power system optimization, operational planning and control. He acquired Member in ISTE and MIE in India and Student Member in Institution of Electrical Engineers, London.

References

1. Cohen, A., Sherkat, V.: Optimization based methods for operations scheduling. Proc. IEEE **75**(12), 1574–1591 (1987)
2. Renaud, A.: Daily generation management at electricity de france: from planning towards real time. IEEE Trans. Autom. Control **38**(7), 1080–1093 (1993)
3. Ferreira, L.A., Anderson, T., Imparato, C.F., Vojdani, A.F.: Short term resource scheduling in multi-area hydrothermal power systems. Electr. Power Energy Syst. **11**(3), 200–212 (1989)
4. Shaw J.J., Bertsekas, D.P.: Optimal scheduling of large hydrothermal power system. IEEE Trans. Power Apparatus Syst. (PAS) **104**, 286–293 (1985)
5. Shaw, J.: A direct method for security constrain unit commitment, pp. 25–31. IEEE/PES Summer Meeting, San Francisco (1994)
6. El-Kaib, A., Ma, H., Hart, J.: Environmentally constrained economic dispatch using Lagrangian relaxation method. IEEE Trans. Power Syst. **9**(4), 1723–1729 (1994)
7. Guan, X., Luh, P.B.: Power system scheduling with fuzzy reserve requirements. IEEE Trans. Power Syst. **11**(2), 864–869 (1996)
8. Tomsovic, Y.: A fuzzy linear programming approach to the reactive power/voltage control problem. IEEE Trans. Power Syst. **7**(1), 287–293 (1992)
9. Miranda, V., Saraiva, J.T.: Fuzzy modeling of power system optimal load flow. IEEE Trans. Power Syst. **7**(2), 843–849 (1992)
10. Li, Y., Luh, P.B., Guan, X.: Fuzzy optimization-based scheduling of identical machines with possible breakdown. In: Proceedings of IEEE 1994 International Conference on Robotics, San Diego, pp. 3347–3452 (1994)
11. Shahidehpour, M., Marwali, M.: Maintenance scheduling in restructured power system. Kluwer, Norwell (2000)
12. Leou, R.C.: A Flexible unit maintenance scheduling considering uncertainties. IEEE Trans. Power Syst. **16**(3), 552–559 (2001)
13. Endrenyi, J.: The present status of maintenance strategies and the impact of maintenance on reliability. IEEE Trans. Power Syst. **16**(4), 638–646 (2001)

14. Yamin, H.Y., Shahidehpour, S.M.: Long-term transmission and generation maintenance scheduling with network, fuel and emission constraints. *IEEE Trans. Power Syst.* **14**(3), 1160–1165 (1999)
15. Rajan, C.C.A., Mohan, M.R., An evolutionary programming based tabu search for solving the unit commitment problem. *IEEE Trans. Power Syst.* **19**(1), 577–589 (2004)
16. Eusuff, M.M., Lansey, K.E., Pasha, F.: Shuffled frog-leaping algorithm: a memetic meta-heuristic for discrete optimization. *Eng. Optim.* **38**(2), 129–154 (2006)
17. Zhang, X., Hu, X., Cui, G., Wang, Y., Niu, Y.: An improved shuffled frog leaping algorithm with cognitive behavior. In: *Proceedings of the 7th World Congress Intelligent Control and Automation* (2008)
18. Eslamian, M., Hosseinian, S.H., Vahidi, B.: Bacterial foraging-based solution to the unit-commitment problem. *IEEE Trans. Power Syst.* **24**(3), 1478–1488 (2009)
19. Elbehairy, H., Elbeltagi, E., Hegazy, T.: Comparison of two evolutionary algorithms for optimization of bridge deck repairs. *Comput. Aided Civ. Infrastruct. Eng.* **21**, 561–572 (2006)
20. Rahimi-Vahed, A., Mirzaei, A.H.: Solving a bi-criteria permutation flow-shop problem using shuffled frog-leaping algorithm. In: *Soft Computing*. Springer-Verlag, New York (2007)
21. Luo, X.-H., Yang, Y., Li, X.: Solving TSP with shuffled frog-leaping algorithm. *Proc. ISDA* **3**, 228–232 (2008)
22. Elbeltagi, E., Hegazy, T., Grierson, D.: Comparison among five evolutionary-based optimization algorithms. *Adv. Eng. Inf.* **19**(1), 43–53 (2005)
23. Kennedy, J., Eberhart, R.C.: Particle swarm optimization. *Proc. IEEE Conf. Neural Netw.* **4**, 1942–1948 (1995)
24. Huynh, T.H.: A modified shuffled frog leaping algorithm for optimal tuning of multivariable PID controllers. In: *Proceedings of the ICIT 2008*, pp. 1–6
25. The IEEE reliability test system—1996. *IEEE Trans. Power Syst.* **14**(3), 1010–1020 (1999)
26. Elbeltagi, E., Hegazy, T., Grierson, D.: A modified shuffled frog leaping optimization algorithm: application to project management. *Struct. Infrastruct. Eng.* **3**(1), 53–60 (2007)

Key-Based Steganographic Textual Secret Sharing for Confidential Messaging

Neil Buckley, Atulya K. Nagar and S. Arumugam

Abstract Many email communications remain unencrypted between end points, raising the need for additional encryption. This paper addresses the need by proposing a new cryptographic scheme, which first encrypts a message using key-based Shamir's secret sharing (using multiple polynomial terms as opposed to only the constant) and discretely hides the shares throughout a cover image using a steganographic technique with number padding. It thus employs multi-layer security requiring the key, the original cover image and the decryption algorithm implementation to unlock the message. Its security is analysed, confirmed and an example given.

Keywords Shamir's secret sharing · Steganography · Email security · Internet privacy

1 Introduction

Email and other electronic textual communication has become a mainstay of life, but people rarely consider how secure their messages are from interception by unintended parties. Although end-to-end email encryption is handled by the respective networks, there is no de facto security ensuring privacy during

N. Buckley (✉) · A. K. Nagar
Department of Mathematics and Computer Science, Liverpool Hope University,
Liverpool, UK
e-mail: 08008783@hope.ac.uk

A. K. Nagar
e-mail: nagara@hope.ac.uk

S. Arumugam
National Centre for Advanced Research in Discrete Mathematics, Kalasalingam University,
Anand Nagar, Krishnankoil, Tamil Nadu 626126, India
e-mail: s.arumugam.klu@gmail.com

transmission. Indeed, few users consider this security gap and less than half of companies address it, even though third-party software exists [2].

It is relatively simple to intercept email, particularly for other users on the same network, and its plain text format makes it easy prey. It is also worth noting that cloud-based email is often temporarily stored in the local cache, raising a further security risk on shared computers [1].

It is therefore wise not to send private information via email, such as bank details, date of birth or other information risking identify theft. After all, as pointed out by [2], we would not consider writing such information on a postcard, but use a sealed letter.

Nevertheless, the sending of private information, such as commercial activity, is often inevitable and there is the additional risk of the email accidentally arriving at the wrong email address.

In this paper, we propose applying our key-based version of Shamir's secret sharing (SSS) algorithm [9] to bring about "textual secret sharing" for confidential messaging. This technique relies on the fact that a number can be encoded into several "shares" using polynomial curve properties. When a subset of the shares are reunited, the secret number is revealed.

We contrast this with the related field of visual cryptography (VC), wherein the content of an email can be converted into an image, which is divided into shares using the algorithm originally proposed by [7]. Its power lies in the fact that, when the shares are stacked, only human vision is required for decryption.

However, we propose that textual secret sharing is beneficial here, as VC results in a noisy reconstruction, and we inevitably require computational decryption to precisely reconstruct the original text.

2 Aims and Objectives

We propose a key-based extension to Shamir's secret sharing and hybridise this with steganography. The email message is encrypted into a (3, 3)-SSS, i.e. three shares, all of which are required for decryption. However, although SSS conventionally encodes the secret number into the polynomial's constant term, we propose an additional key of length κ digits. Reducing the digits to modulo 3 provides the sequence of coefficient indices into which each κ -block of characters is encoded.

In short, our objectives are summarized as follows:

- Use our version of SSS to sparsely encode an email message across the three colour channels of a cover image (Sect. 4.1).
- Demonstrate successful encryption and decryption (Sects. 4.1 and 4.2, respectively).
- Discuss examples and applications in the real world (Sects. 5.1 and 5.2, respectively).
- Analyse the security of our method (Sect. 5.3).

3 Related Work

As discussed in Sect. 1, VC is often used to encrypt text. For example, [5] created the VCRYPT software, which takes financial documents as input. They overcome the contrast loss of VC using binary thresholding of gray levels in the decrypted image to precisely reconstruct the original.

Similarly, [6] apply VC to CAPTCHA codes, storing their corresponding text as share images in separate databases, then computationally reconstructing the image on a webpage, algorithmically reducing the contrast loss.

Since schemes, such as those above, rely on computational decryption, we propose Shamir's secret sharing [9] as a better alternative for share generation, as no extra algorithms are required for reversal of contrast reduction. It is simple to implement, and requires Lagrangian polynomial interpolation for decryption.

Indeed, it is used to great effect by [10] to encrypt and share medical data. Obviously, in such a context, VC would be unsuitable, due to contrast loss.

Rishiwal et al. [8] propose an alternative to Shamir's scheme, but conceal the shares within cover images, stating that "data can be transmitted more securely by converting it into an image". Their method, however, still relies on polynomial properties.

On the other hand, [3] propose secret number sharing based on the properties of circles in multi-dimensional space. Their scheme requires the construction of a circle in $k-1$ dimensions, where k is the threshold for cardinality of the qualified superset. Furthermore, they claim considerably faster execution times than for Lagrangian methods.

Wu et al. [11] apply SSS to image encryption and concealment in cover images, but use a "bit location map", involving the steganographic shifting of the two least significant bits of colour values. They refer to their scheme as "reversible", meaning the secret image is losslessly recovered. Interestingly, they use the mean squared error (MSE) with peak-to-noise ratio (PNSR) to measure and minimize the disruption caused to cover images. Similarly, [4] use LSB concealment, but interestingly correct for pixel value disruptions using genetic algorithms.

4 Proposed Method

4.1 Encryption

A confidential message comprises a sequence of ASCII characters up to a certain length. Algorithm 1 describes its encryption into a cover image. The original image can be in any format, but it is important that the stego-image remains undistorted, for example, by jpeg encoding, so a raw bitmap is desirable. It is also crucial that only the sender and recipient have access to the original image. The key should also be kept confidential, but is useless without the original image.

Guide to Notation.

ρ = number of pixels required per character

c_{ascii} = character ASCII value

w = image width

h = image height

l = message length (no. of characters)

i = key length

$K = \{k_1, \dots, k_i\}$ = digits 1 to i of the key

B = vector of binomial coefficients

$\chi^{\{1,2,3\}} \in X^{\{1,2,3\}}$ = set of three collections of vectors, each comprising ρ -sized vectors of padded Shamir y -coordinates.

(Note that χ_q^p denotes the q -th character encoded on the p -th channel, and $\chi_q^p[r]$ refers to the r -th digit within that code.)

Algorithm 1: y -Coordinate Calculation.

$\rho \leftarrow wh / l$, $charCount \leftarrow 1$

For each message character, c , **do**,

$c_{ascii} \leftarrow$ numeric ASCII value of c

$\kappa \leftarrow k_{charCount \pmod i} \pmod 3$

$r_1, r_2 \leftarrow rand[1 \dots 100]$ //I.E. RANDOM VALUES FROM 1 TO 100

If $\kappa = 0$, **then** $B \leftarrow \{c_{ascii}, r_1, r_2\}$

Else If $\kappa = 1$, **then** $B \leftarrow \{r_1, c_{ascii}, r_2\}$

Else If $\kappa = 2$, **then** $B \leftarrow \{r_1, r_2, c_{ascii}\}$

For each channel, 1 to 3, **do**,

//(TAKE THE CURRENT CHANNEL AS SHAMIR'S X -COORDINATE)//

$y_{channel} \leftarrow B_1 + B_2 * channel + B_3 * channel^2$

$i \leftarrow \lceil \log_{10} |y_{channel}| \rceil + 1$

Pad $y_{channel}$ with $\rho - i$ leading zeros

$\chi_{charCount}^{channel} \leftarrow y_{channel}$

End For

$charCount \leftarrow charCount + 1$

End For

As we can see, $y_{\{1,2,3\}}$ evaluate from binomials whose coefficients are the ASCII value of the current character and two random numbers. The key is implemented in the index of the non-random (ASCII value) coefficient.

For example, with the key “13579246”, character indices 1, 9, 17, etc. are encrypted by taking the constant of the polynomial as the ASCII code, characters 2, 10, 18, etc. take it as the coefficient of “ x^2 ”, characters 3, 11, 19, etc. take it as the coefficient of “ x ”, and so on.

After zero-padding the y -coordinates, they are steganographically embedded into the cover image, as formulated in Algorithm 2, which assumes the cover image has been loaded.

Algorithm 2: Steganographic Encryption.**For each** channel 1 to 3, **do**,*Begin at the top-left pixel of the cover image.* $val \leftarrow$ pixel value (0 to 255) of current channel $charCount \leftarrow 1$ **For each** message character, c , **do**,**For** digit = 1 to ρ , **do**,**If** $val \geq 255 - \chi_{charCount}^{channel}[digit]$, **then** $sign \leftarrow -1$ **Else If** $val \leq \chi_{charCount}^{channel}[digit]$, **then** $sign \leftarrow +1$ **Else** $sign$ randomly set to ± 1 , **End If** $val \leftarrow val + sign * \chi_{charCount}^{channel}[digit]$ *Current pixel value $\leftarrow val$, and move to next pixel of cover image***End For** $charCount \leftarrow charCount + 1$ **End For****End For** $\rho' \leftarrow$ left-padded with zeros to create four digits, and $\chi_1[1..4] \leftarrow \rho'$

Here, each pixel of the modified cover image encodes a single digit of an encoded message character, such that $val_{modified} - val_{original} = digit$. (Also note that ρ is encoded into the start of the red channel, which is needed for decryption.) The sender can then attach this image to an email and transmit it.

4.2 Decryption

On receipt of the email, the recipient downloads the attachment and proceeds to compare it with his/her copy of the original image. A pre-requisite for decryption is the extraction of Shamir's y-coordinates, but we must first decipher the underlying code digits, detailed in Algorithm 3.

Algorithm 3: Code Digit Extraction. $w, h \leftarrow$ resp. width and height of image $numImgPixels \leftarrow wh$, and $codeDigits^{\{1..3\}} \leftarrow$ collection of three empty vectors**For each** image pixel $1 \leq y \leq h, 1 \leq x \leq w$, **do**, $\{r, g, b\} \leftarrow$ colour values of current pixel in original image $\{r', g', b'\} \leftarrow$ values of current pixel in downloaded (amended) cover image $codeDigits^1 \leftarrow codeDigits^1 + |r - r'|$ $codeDigits^2 \leftarrow codeDigits^2 + |g - g'|$ $codeDigits^3 \leftarrow codeDigits^3 + |b - b'|$ **End For**

The resulting $codeDigits^{\{1..3\}}$ are a concatenation of all encoded characters, therefore comprise mostly zeros, sparsely interspersed with the actual Shamir's y-coordinates. The next step, detailed in Algorithm 4, is the recovery of these

numbers, i.e. the conversion of `codeDigits` back to a list of y-coordinates, denoted henceforth by χ .

Algorithm 4: y-Coordinate Extraction.

$numDigitsInCode \leftarrow \text{length}(\text{codeDigits}^1)$

$spaceReqForChar \leftarrow \text{codeDigits}^1[1\dots4]$

$\text{codeDigits}^1[1\dots4] \leftarrow "0000"$

$numChars := numDigitsInCode / spaceReqForChar$

$yCoords \leftarrow \text{empty vector}$

For each char code, c , in $\{1\dots numChars\}$ in colour channel $\{1\dots 3\}$, **do**,

$yCoord \leftarrow \text{codeDigits}^{channel}[c * spaceReqForChar, \dots, (c+1) * spaceReqForChar + 1]$

Convert $yCoord$ to numerical value by stripping its leading zeros

$yCoords_c \leftarrow yCoord$, and $\chi_c^{channel} \leftarrow yCoord$

End For

The result of Algorithm 4 is the list of y-coordinates $\chi^{\{1\dots 3\}}$ for respective channels, and we know from Algorithm 1 that the equivalent x-coordinates equate to the respective colour channel index, i.e. $x = 1$ (red), $x = 2$ (green) and $x = 3$ (blue). Therefore, we can use Lagrangian basis polynomials to extract the desired coefficient.

Shamir [9] pointed out that, using such an interpolative method, an n-degree polynomial requires $n + 1$ coordinate pairs to fully resolve its coefficients. Given our three channels (and Algorithm 1), we know that, for a given secret character, c , we must interpolate a binomial using the respective coordinates

$$x \in \{1..3\}, y \in \chi_c^{\{1..3\}} \quad (1)$$

From this, we construct a linear combination, L , such that,

$$L_1 = \frac{x - x_2}{x_1 - x_2} \cdot \frac{x - x_3}{x_1 - x_3}, L_2 = \frac{x - x_1}{x_2 - x_1} \cdot \frac{x - x_3}{x_2 - x_3}, L_3 = \frac{x - x_1}{x_3 - x_1} \cdot \frac{x - x_2}{x_3 - x_2} \quad (2)$$

Since $x_i = i$, we arrive at,

$$L_1 = 1/2x^2 - 5/2x + 3, L_2 = -x^2 + 4x - 3, L_3 = 1/2x^2 - 3/2x + 1 \quad (3)$$

Also, given that our required binomial is given by,

$$f(x) = \sum_{channel=1}^3 y_{channel} L_{channel} \quad (4)$$

we derive the following from the resulting coefficients:

$$\begin{aligned} \forall k_n = 0, c_{ascii} &= 3y_1 - 3y_2 + y_3 \\ \forall k_n = 1, c_{ascii} &= -5/2y_1 + 4y_2 - 3/2y_3 \\ \forall k_n = 2, c_{ascii} &= 1/2y_1 - y_2 + 1/2y_3 \end{aligned} \quad (5)$$

Here, depending on the current character index modulus i and the value of that key digit modulus 3, we use Lagrange's theorem to extract one of the three binomial coefficients, evaluating to the ASCII value of the respective character.

All that then remains is to convert each value back to the original character to decrypt the secret email message.

5 Discussion

5.1 An Example

We exemplify encryption and decryption using a notional 2000-character message beginning with "A". For brevity, we focus only on this first character. We use the key "8219" and a (notional) 250×250 cover image.

Here, $c_{ascii} = 65$, and since the character index is 1, we use the first key digit, "8". Now, $8 \bmod 3 = 2$, so we take one of the binomial terms as $65x^2$. The other coefficients are randomly set to give the following binomial and coordinates:

$$f(x) = 65x^2 + 45x + 19$$

$$x = \{1 \dots 3\}, y_{\{1 \dots 3\}} = \{129, 369, 739\}$$

Given that, $l = 2000$, $wh = 250.250 = 62500$, $\rho = \{3, 3, 3\}$, the zero-padding gives us,

$$x_1^{channel} = \overbrace{000 \dots}^{\lfloor wh/l - p_1 \rfloor = 28} y_{channel}$$

Here, $wh/l = 31$, so first four pixels of the cover image's red channel are shifted by, respectively, 0, 0, 3 and 1 values, in random directions, and character indices 29 to 31 are likewise shifted by 1, 2 and 9 in the red channel, 3, 6 and 9 in the green channel and 7, 3 and 9 in the blue channel.

Every message character is henceforth encoded in this way. It is worth noting the low computational cost of encryption, taking less than three seconds per 100 characters using a laptop PC. Decryption proved likewise computationally inexpensive.

5.2 Application to Banking

Let us imagine a company, such as a bank, with a customer base with whom it must communicate confidential information on a regular basis. If an action is required from the customer, the bank must either communicate by post, incurring paper and mailing costs, and/or via the customer's online account. In the latter case, the bank has no control over when the customer will next log in.

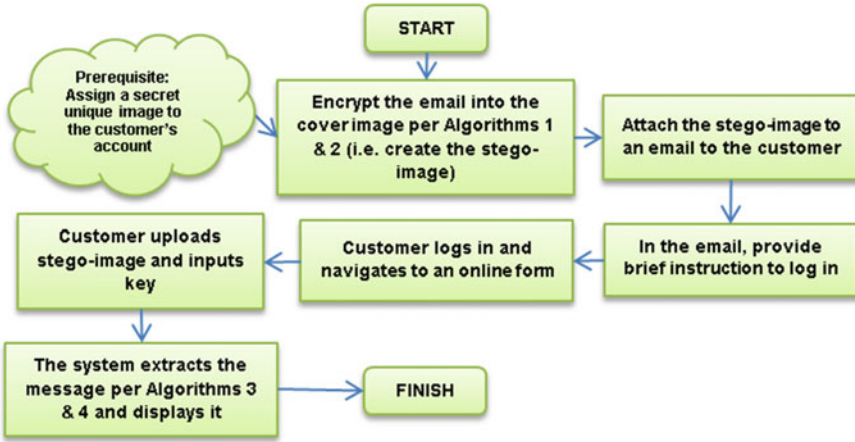


Fig. 1 Banking application of textual secret sharing with steganography

The bank will likely, however, hesitate to communicate via email, due to the security flaws highlighted in Sect. 1. We therefore propose our method as an ideal solution. Figure 1 illustrates how it could be implemented.

To this, we add the following points:

- The original (cover) image is not released by the bank, even to the customer, as it could be misused.
- The decryption key could be an existing password or one chosen specifically for this.
- Algorithms 1 and 2 would be implemented in a proprietary system only accessible by authorized personnel.

Furthermore, Algorithms 3 and 4 could be implemented using a server-side scripting language, available for use by the customer.

5.3 Security Analysis

If the email containing the stego-image is intercepted by a malicious third party, that person has no access to the secret message, even with complete access to the user's online account, as the decryption key is known only to the user.

It is possible for an incorrect key, K' to unlock the message if $K' \equiv K \pmod{3}$, but the probability of guessing K' in a single brute-force attempt is $\frac{1}{3^i}$. For $i = 8$ digits, this evaluates to $\frac{1}{6561}$. It is wise, nevertheless, to limit the number of incorrect key input attempts to guard against multiple brute-force attacks. An alternative is to increase the key length by employing a secret phrase, which reduces to the key by ASCII conversion.



Fig. 2 a Original cover image. b Stego-image

The strength of our method nevertheless lies in the need to infiltrate multiple points, i.e. the user’s email address to access the stego-image, the decryption key, the original image, the decoding application, as well as any further login credentials, which would necessitate an extremely concerted attempt.

Even with such a concerted attempt, we must remember that each new communication entails a new stego-image, rendering the previously hacked stego-image useless.

A hacking attempt will, of course, only take place if an email interceptor guesses the true purpose of the attached image, so the use of an innocent-looking cover image is beneficial.

In addition to image appearance, it is worth ensuring the image does not have a “noisy” appearance, arousing suspicion. To this end, we measure the peak-to-signal noise ratio.

We embedded a 2763-character message into the cover image in Fig. 2a. The result is the stego-image in Fig. 2b.

First, we measure the mean square error of shifted pixel values as,

$$MSE_{channel} = \frac{1}{wh} \sum_{x=1}^w \sum_{y=1}^h (c_{x,y} - s_{x,y})^2 \approx \{1.395, 1.963, 5.257\} \quad (6)$$

where w and h are the image dimensions, $c_{x,y}$ is the respective colour value (on the current channel) for the cover image, and likewise $s_{x,y}$ for the stego-image. Then, we take the mean of the individual errors to arrive at $MSE \approx 2.872$. We can now plug this value into the calculation,

$$PSNR = 20 \log_{10} 255 - 10 \log_{10} MSE \approx 43.5494dB \quad (7)$$

By comparison, a jpeg compression on this image results in a PSNR of 43.0751 dB.

6 Conclusion and Further Work

In this paper, we developed a steganographic encryption algorithm with stego-image pixel values calculated by our proposed key-based version of Shamir's secret sharing.

The secret message is spread throughout the three dimensions of a stego-image (taking colour depth as the third dimension) by splitting it into three shares and storing each share in its own channel such that each y -coordinate is zero-padded to fill the available space.

Furthermore, unlike the conventional Shamir algorithm, we encode respective ASCII values in one of three polynomial coefficients, as opposed to always using the constant. The coefficient index is taken as the current key digit modulus 3.

We confirmed the security of our method, highlighting the need for multiple points of attack, and a PSNR analysis confirmed that the stego-image is quantitatively indistinguishable from a jpeg compression.

Future work will focus on improving security, for example by encrypting the message text itself before embedding it, giving an extra security layer.

It is also worth noting the static nature of (5), i.e. the coefficients of $y_{\{1...3\}}$ remain constant. This is because we are using a (3, 3)-SSS. By using a (3, n)-SSS with $n > 3$, where respective n values are encoded using the key, the coefficients would alter, owing to differing share combinations. This would render it considerably more difficult for an interceptor in possession of the original and stego-images to guess the decryption algorithm.

References

1. Carnegie Mellon University: Interception. <http://www.mysecurecyberspace.com/secure/email/threats/interception.html> (2007)
2. Farrell, S.: Why don't we encrypt our email?. *IEEE Internet Comput.* **13**(1), 82–85 (2009)
3. Ge, L., Tang, S.: Sharing multi-secret based on circle properties. In: CIS 2008, pp. 340–344 (2008)
4. Gupta, R., Jain, A.: Integrating steganography using genetic algorithm and visual cryptography for robust encryption in computer forensics. *Int. J. Electron. Comput. Sci. Eng.* **7436**, 794–801 (2012)
5. Hawkes, L.W., Yasinsac, A., Cline, C.: An Application of Visual Cryptography to Financial Documents, pp. 1–7. Florida State University, Florida (2000)
6. James, D., Philip, M.: A novel anti phishing framework based on visual cryptography. *Int. J. Distrib. Parellel Syst.* **3**(1), 207–218 (2012)
7. Naor, M., Shamir, A.: Visual cryptography. In: EUROCRYPT'94, pp. 1–12 (1994)
8. Rishiwal, V., Yadav, M., Arya, K.V.: A robust secret image sharing scheme. In: 5th ICETET, pp. 11–14 (2008)
9. Shamir, A.: How to share a secret. *Comm. ACM* **22**(11), 612–613 (1979)
10. Ulutas, M., Ulutas, G., Nabiyeve, V.V.: Medical image security and EPR hiding using Shamir's secret sharing scheme. *Syst. Softw.* **84**(3), 341–353 (2011)
11. Wu, C., Kao, S., Hwang, M.: Reversible secret image sharing based on Shamir's scheme. In: 5th International Conference on Intelligent Information Hiding and Multimedia. *Signal Process.* pp. 1014–1017 (2009)

AnimVSS: Frame-Based Visual Secret Sharing

Neil Buckley, Atulya K. Nagar and S. Arumugam

Abstract Visual secret sharing is a cryptographic paradigm encrypting images into a number of individually random “shadow images”. When stacked, they reveal a contrast-reduced version of a secret image. In this paper, we consider random grid shadow images, which have gained increasing attention in recent years due to lack of pixel expansion inherent in Naor-Shamir visual cryptography. We propose a methodology to use such grids to encode series of frames comprising short animations, useful in situations when a mere static image is insufficient to convey a secret instruction. Although this method results in significant contrast degradation with longer animations, a method is devised to isolate the signal from the noise in a computational *XOR*-based decryption.

Keywords Visual secret sharing · Random grids · Cryptography · Animation

1 Introduction

Information security is a mounting concern in today’s digital world, bringing about the need for secure encryption of private and sensitive data. Although conventional cryptographic algorithms often meet this need, they can entail complex key management/distribution and decryption requirements.

N. Buckley (✉) · A. K. Nagar
Department of Mathematics and Computer Science, Liverpool Hope University,
Liverpool, UK
e-mail: 08008783@hope.ac.uk

A. K. Nagar
e-mail: nagara@hope.ac.uk

S. Arumugam
National Centre for Advanced Research in Discrete Mathematics, Kalasalingam University,
Anand Nagar, Krishnankoil 626126 Tamil Nadu, India
e-mail: s.arumugam.klu@gmail.com

Naor and Shamir [8] proposed an alternative cryptographic paradigm called visual cryptography (VC), whereby the secret, in the form of a binary image, is split into shares, such that subsets of them can be printed onto transparencies and stacked to reveal the secret. As such, human vision is sufficient for decryption.

The decoded image unfortunately loses at least half its contrast. This and pixel expansion comprise the major disadvantage of VC, hence there is much prior literature [7, 14] aiming to optimize these metrics.

Since each share must be random, maintaining security, the stacking (binary *OR*) operation renders contrast loss inevitable, however pixel expansion is avoidable using other visual secret sharing (VSS) methods, such as random grids.

Devised by [5], random grids (RG) comprise a randomly generated initial share and subsequent shares built in such a way that, when stacked with the first share, the required binary image is revealed. However, due to their limitation to $(2, n)$ and (n, n) secret sharing schemes, VC became the prominent methodology, because of its more robust (k, n) sharing capability, where $k \leq n$. (That is, at least k of the n shares are required.)

Although various methods have been developed to encode multiple secrets, as discussed in Sect. 3, the ability to encode a short animation within two shares has not been explored. As such, animation VSS is the subject of this research. We take advantage of the optimality of random grid-based VSS to generate “AnimVSS” (animation visual secret sharing) schemes.

2 Aims and Objectives

In this paper, we propose the creation of animation VSS shares using random grids, encoding each frame individually and arranging share pixel columns to reveal each frame upon computational “shift-stacking”. The objectives and layout of this paper are summarized as follows:

In Sect. 4.1, random grid theory is explained and we use $(2, 2)$ -RG to split each frame into shares. We also introduce the two core metrics of frame count and distance.

In Sect. 4.2, we discuss frame preprocessing and the composition of the AnimVSS shares.

The results are given in Sect. 5, with a comparison of *OR*- and *XOR*-based stacking, and the calibration of the two metrics.

In Sect. 6, we analyse our method with a comparative analysis against other shift-stacking and multiple image methods in the literature, and discuss the security and computational cost of our proposal.

Finally in Sect. 7, we conclude this work and propose future research.

3 Related Work

The work of [4] bears similarity to ours in its shift-stacking shares to hide multiple secrets. They focus on the use of two shares to hide two secrets, revealed by sliding one across the other. They build the shares on a column-wise basis, enforcing the respective secret image to be revealed upon the stacking of the respective share when shifted a given number of pixels.

Trujillo et al. [10] similarly use shift-stacking, but for cheat-prevention in VC. They use only two shares, but conceal two additional verification images, i.e. watermarks, such that watermark 1 is revealed by shifting share 2 halfway down share 1, and watermark 2 is revealed by shifting share 1 halfway down share 2.

This concept of concealing multiple secrets is indeed widely researched. There are many ways of revealing respective secret images, but [6], for instance, go to the extreme of taking an access structure of a scheme as a multi-image graph, each node and edge associated with a distinct grayscale image, such that each share is itself a grayscale cover image, and when two shares at either end of a respective edge are stacked, a unique image is revealed.

Such methods rely on pixel expansion-based VC, but many researchers, such as [14], avoid pixel expansion using probabilistic VC schemes (PVCS), as opposed to conventional VC, which is deterministic. In a PVCS, each secret pixel is represented by only one “subpixel” per shadow image, as opposed to a matrix of them. Normally, contrast is further lost using this method, but the aforementioned work avoids this by adapting a deterministic scheme to a probabilistic one.

RG, however, is emerging as the preferred VSS method, not just for avoiding pixel expansion, but the codebooks and basis matrices of VC. Indeed, [2] recently overcame the aforementioned limitations of RG, developing an algorithm for general threshold (k, n) schemes.

They achieve this by *XOR*ing the respective secret pixel with a random bit, then iteratively applying the same operation to the result. They then assign elements of the resulting bit sequence to random k shares and randomize the bit at the same position in the remaining $n-k$ shares.

4 Proposed Method

4.1 Frame-Wise Grid Creation

We denote the VCS of the i th animation frame, F^i , as G^i , comprising random grids $G_j^i, i \in \{1 \dots \phi\}, j \in \{1, 2\}$, where ϕ is the number of frames. G_j^i is randomly generated, such that $T = 1/2$, where T is the light transmission rate, i.e. the amount of light that passes through the grid if bit 0 is assumed transparent.

Crucially, a random grid must exhibit $T^b = 1/2$ and $T^w = 1/2$, i.e. the mean transmission rates of grid pixels corresponding spatially to resp. black and white frame pixels are one half.

$G_2^i, i \in \{1 \dots \phi\}$ is then generated according to Algorithm 1. The value at a required coordinate is denoted $X_j^i[x, y], x \in \{1 \dots w\}, y \in \{1 \dots h\}$, where $X \in \{F, G\}$ and w and h are the image (equal to grid) dimensions. Furthermore, the overbar indicates the binary operation $\bar{b} = NOT(b)$.

Algorithm 1: Complementary Grid Calculation.

For each coordinate $1 \leq y \leq h, 1 \leq x \leq w$, do,

If $F^i[x, y] = 1$, then $G_2^i[x, y] \leftarrow G_1^i[x, y]$

Else, $G_2^i[x, y] \leftarrow \overline{G_1^i[x, y]}$

End For

Here, G_2^i is itself a random grid, as proved by Shyu (2012) and others. Hence the result is a valid RG pair for each frame.

4.2 Merging the Grids

The aim is to merge all G^j into a (ϕ, δ) -AVSSS (Animated Visual Secret Sharing Scheme), where ϕ is the frame count and δ is the frame distance, i.e. the number of columns the shares must be shifted relative to each other to reveal successive frames. We refer to these as a scheme's core parameters.

The (ϕ, δ) -AVSSS comprises AnimVSS grids $AG_j, j \in \{1, 2\}$, constructed from the columns of our existing grids. Therefore, we denote the x th column as $(A)G_j[x]$. Algorithm 2 constructs AG_1 .

Algorithm 2: AnimVSS RG Construction.

For frame number $i = 1$ to ϕ , do,

Rescale F^i to width $\omega w / \phi$

End For

offset1, offset2 $\leftarrow 0$

For $x = 1$ to w , do,

For frame number $i = 1$ to ϕ , do,

offset1 \leftarrow offset1 + 1

offset2 \leftarrow offset2 + 1 + $\delta(i - 1)$

A $G_1[\text{offset1}] \leftarrow G_1^i[x]$

A $G_2[\text{offset2}] \leftarrow G_2^i[x]$

End For

End For

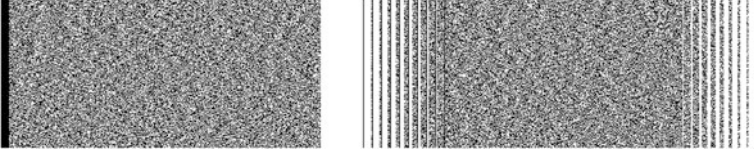


Fig. 1 Complimentary shares of a (10, 2)-AVSSS with $\omega = 2$

Note the first routine in this algorithm, rescaling frame widths according to the frame count and parameter ω . Without this step, the animation grid width grows to ϕw during construction. For this rescaling, we use nearest-neighbour interpolation. As the frame count increases, the amount by which we must down-scale the frame image also increases, reducing its quality. The purpose of ω is therefore to permit a customized rescaling amount, allowing for higher quality. The result is the AnimVSS grid pair in Fig. 1.

5 Results

5.1 OR Versus XOR Shift Stacking

If the position of grid AG_1 is constant, then the frames are reconstructed by shifting AG_2 leftward across it. Hence we denote this shifted second grid as $AG_2^{(\sigma)}$, where σ is the total pixel shift. The intended result of Algorithm 2 is therefore

$$AG_1 \oplus AG_2^{(i\delta)} \overset{1/\phi}{\approx} F^i, \text{ where } \oplus \text{ is the XOR operation and } 1/\phi \text{ is the contrast loss.}$$

Although [11] proved that reconstruction using this operation is perfect for (n, n)-VSS, such as this, there is contrast loss here, given the redundant random columns hiding the other respective frames. In physical stacking, however, half the contrast is lost in a (2, 2)-RG, so the use of the *OR* (\otimes) operation results in a total contrast degradation of $1/2\phi$.

Figures 2 and 3 show the computationally reconstructed frames of a (5, 1)-AVSSS using *OR* and *XOR*, respectively. As we can see, *XOR* gives a clearer reconstruction.

Unfortunately, contrast further degrades as ϕ increases. As we see in Fig. 4b, which is one reconstructed frame of the (10, 2)-AVSSS in Fig. 1.

To ameliorate this situation, Algorithm 3 isolates the signal from the noise for each respective frame.

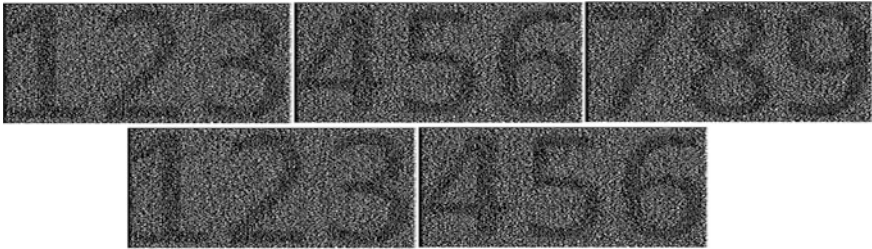


Fig. 2 Computational *OR*-based stacking of a (5, 1)-AVSSS

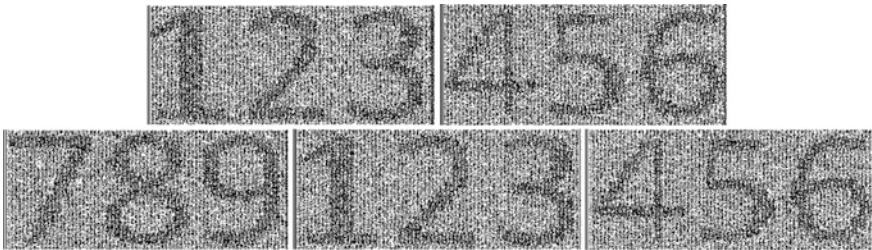


Fig. 3 Computational *XOR*-based stacking of a (5, 1)-AVSSS

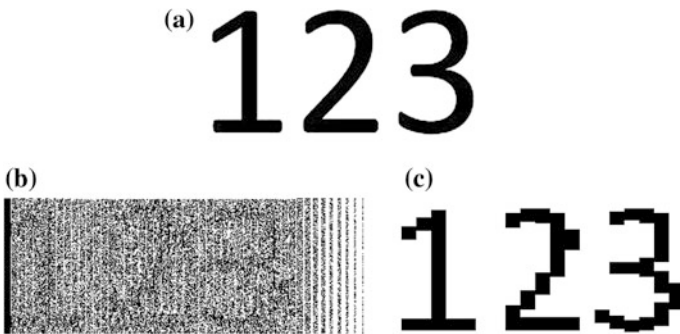


Fig. 4 **a** Original frame, **b** *XOR*-stack of a (10, 2)-AVSSS, **c** The result of Algorithm 3

Algorithm 3: Signal-from-noise Isolation.

currentFrame \leftarrow empty collection of column *h*-vectors

fx \leftarrow current column index of *currentFrame* \leftarrow 0

For $x = 1$ to $w\omega\phi$, **do**,

If $x \bmod \phi = 0$, **then**,

For $i = 1$ to ϕ , **do**,

$fx \leftarrow fx + 1$

$currentFrame[fx] \leftarrow (A G_1 \oplus A G_2^{(\sigma)})[x]$

End For

End If

End For

Here, every ϕ th frame is extracted from the stack and placed into a new matrix for the final reconstruction of the current frame, and a simple column replication technique is used to go some way toward reversing the effect of the rescaling in Algorithm 2. (Note that nearest-neighbour interpolation gives a similar result, but although efficient, carries more computational cost.)

5.2 Parameter Calibration

Using Algorithm 2, a valid AnimVSS scheme does not result from all parameter ϕ and δ values. Interestingly, for example, not all frames in the (4, 1)-AVSSS are reconstructable. This is because G_2^i columns ($i \in \{1 \dots \phi\}$) copied into AG_2 are subsequently overwritten as index i loops back to the next $\{1 \dots \phi\}$ iteration.

In the parameter intervals $1 \leq \phi, \delta \leq 10$, there are indeed 63 % valid schemes, as illustrated in Fig. 5a, in which a black block signifies the presence of a valid scheme.

Also interestingly, if we expand Fig. 5a to $1 \leq \phi, \delta \leq 200$, we obtain the validity plot in Fig. 5b. We can see that if $\phi = 1$ is omitted, the validity plot is perfectly symmetrical about the descending diagonal. Furthermore, if $\delta = 1$, only odd-numbered frame counts are valid. Finally, we can see in Fig. 5b that the probability of a valid scheme with arbitrary parameters tends to unity as $\phi, \delta \rightarrow \infty$.

6 Discussion

6.1 Comparisons with Other Shift-Stacking Research

To the best of our knowledge, this is the first study on the encryption of an arbitrary number of secret images in the guise of animation frames using only two shares, but we carry out a brief comparative study here against similar research involving shift-stacking (Table 1).

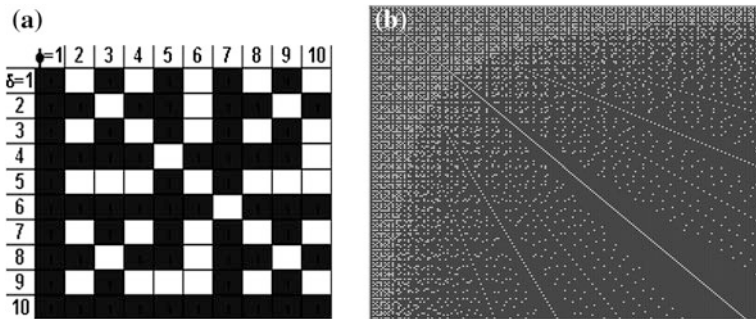


Fig. 5 Validity plots of AnimVSS schemes with varying parameter values up to 10 in A and 200 in B

Table 1 Comparative study with other multi-image shift-stacking research

	Proposed method	Method in [1]	Method in [10]	Method in [4]
Image (frame) count	Any	2	2	Any, but limited by number of shares
VSS methodology	RG	RG	VC	VC
Purpose	Animation	Multi-image encryption	Watermarking	Multi-image encryption and animation
Pixel expansion	1 or user-defined	1	2 or more	$(c-1)/r$ for (n, n) and $(c-jg)/r$ for (k, n) (c = column count, r = row count, j = stacked shares count, g = arbitrary parameter)
Observed reconstruction quality	Not discussed	Degrades with increasing frame-count, requiring Alg. 3 for signal-from-noise isolation	Presence of noise with low shift values and perfect with high shift values	Faint in contrast but recognizable

As we can see, our proposed method is advantageous over comparable research for the purpose of animation in its ability to encode any number of frames into two shares. However, it suffers from severe contrast loss, entailing the need for Algorithm 3. (On that note, it is worth observing that the value of ω should be set to higher values with increasing frame counts, to counter the additional degradation resulting from rescaling. Experiments indicate $\omega = \begin{cases} \phi/10, & \text{if } \phi > 10 \\ 1, & \text{otherwise} \end{cases}$.)

6.2 Security and Complexity Analysis

AnimVSS relies solely on $(2, 2)$ -VSS, therefore is not vulnerable to cheating through fake share creation in (k, n) -VC, as discovered by [3]. Furthermore, using Algorithm 1 ensures each frame is encoded by two purely random grids, i.e. $T^b = T^w = 1/2$, as shown by [9]. Therefore, none of the frames can be extracted by a malicious outsider in possession of either individual AG_j .

Computational cost can be considered as both the construction of the animation shares using Algorithms 1 and 2, and the signal-from-noise isolation using Algorithm 3. We implemented the algorithms on a laptop Windows 7 PC with dual-core 2.09 GHz processor and 3 GB RAM using various parameter choices in the range $2 \leq \phi, \delta \leq 30$. In all cases, share construction took less than 15 s and Algorithm 3 took less than one second to extract and display each frame.

7 Conclusion and On-Going Research

This paper proposed a method to use random grid-based VSS to encrypt an arbitrary number of secret images, in the guise of animation frames, in only two grids. Successive frames are revealed by shifting one grid in relation to the other. However, severe contrast loss is encountered with increasing frame counts, due to the fact that increasing amounts of data are being stored into the same space.

More work is therefore required in the creation of AnimVSS schemes to improve the quality. To this end we are investigating the void-and-cluster algorithm, as devised by [12] and used to great effect by [13] to harmonise the previously poor (k, n) -RG secret image reconstructions.

In addition, it is worth noting that individual frame encryptions are independent of each other. We are therefore seeking a method to “co-encrypt” grids for different neighbouring frames such that they maximally aid each other’s visual quality after reconstruction.

On this note, we are also investigating the use of a fixed AG_1 , taking advantage of the fact that it is possible to build any number of G_2 grids from this fixed share using Algorithm 1 taking the respective frame images as the different inputs. By doing this, it will be possible for a participant to be in possession of a permanent AnimVSS master share to decrypt the frames of any of an infinite number of correctly constructed AG_2 shares without having to be sent a new AG_1 . This will further improve the security of our method, as only one indecipherable grid has to be transmitted over potentially unsecured media.

References

1. Chang, J.J., Juan, J.S.: Two-Secret image sharing scheme by shifting random grids. In: 29th Workshop on Comb. Math, pp. 109–114 (2012)
2. Chen, T., Tsao, K.: Threshold visual secret sharing by random grids. *J. Syst. Softw.* **84**(7), 1197–1208 (2011)
3. Horng, G., Chen, T., Tsai, D.: Cheating in visual cryptography. *Des. Codes Cryptogr.* **38**(2), 219–236 (2006)
4. Ibrahim, M.H.: New Capabilities of Visual Cryptography. *Int J. Comput. Sci. Issues* **9**(5), 225–231 (2012)
5. Kafri, O., Keren, E.: Image encryption by multiple random grids. *Opt. Lett.* **12**(6), 377–379 (1987)
6. Lu, S., Manchala, D., Ostrovsky, R.: Visual cryptography on graphs. *J. Comb. Optim.* **21**(1), 47–65 (2011)
7. Mandal, J.K., Ghatak, S.: A Novel Technique for Secret Communication through Optimal Shares using Visual Cryptography (SCOSVC). In: 2011 Symp. on Electron. Syst. Des. 329–334 (2011)
8. Naor, M., Shamir, A.: Visual Cryptography. In: EUROCRYPT'94. pp. 1–2 (1994)
9. Shyu, S.J.: Visual cryptography and random grids. In: Cimato, S., Yang, C. (eds.) *Visual Cryptography and Secret Image Sharing*, pp. 185–220. Taylor & Francis Group (2012)
10. Trujillo, A.E., Miyatake, M.N., Iwamoto, M., Meana, H.P.: A cheating prevention EVC scheme using watermarking techniques. *Rev. Fac. Ing., Universidad de Antioquia.* 30–42 (2012)
11. Tuyls, P., Hollmann, H.D.L., Van Lint, J.H., Tolhuizen, L.: XOR-based visual cryptography schemes. *Des. Codes Cryptogr.* **37**(1), 169–186 (2005)
12. Ulichney, R.: The void-and-cluster method for dither array generation. In: *IS&T/SPIE Symposium on Electron. Imaging and Science*, vol. 1913, pp. 332–343 (1993)
13. Wu, X., Sun, W.: Improving the visual quality of random grid-based visual secret sharing. *Signal Process.* **93**(5), 977–995 (2013)
14. Yang, C., Wu, C., Liu, F.: Construction of general (k, n) probabilistic visual cryptography scheme. *J. Electron. Sci. Technol.* **9**(4), 317–324 (2011)

Searching Partially Bounded Regions with P Systems

Hepzibah A. Christinal, Ainhoa Berciano, Daniel Díaz-Pernil and Miguel A. Gutiérrez-Naranjo

Abstract The problem of automatically marking the interior and exterior regions of a simple curve in a digital image becomes a hard task due to the noise and the intrinsic difficulties of the media where the image is taken. In this paper, we propose a definition of the *interior* of a partially bounded region and present a bio-inspired algorithm for finding it in the framework of Membrane Computing.

Keywords Partially bounded region · Membrane Computing · Tissue P system

1 Introduction

In Mathematics, the apparently naive concepts of interior and exterior regions of a *simple closed curve* have a long list of approaches and further refinements. From the initial definition of a simple closed curve (or *Jordan curve*) in the plane \mathbb{R}^2 as

H. A. Christinal (✉) · A. Berciano · D. Díaz-Pernil
CATAM Research Group—Department of Applied Mathematics I, University of Seville,
Seville, Spain
e-mail: hepzi@yahoo.com

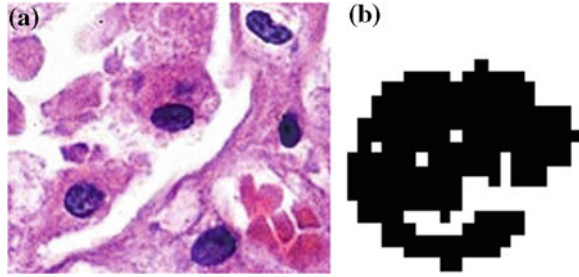
D. Díaz-Pernil
e-mail: sbdani@us.es

A. Berciano
Departamento de Didáctica de la Matemática y de las Ciencias Experimentales,
University of the Basque Country, Donostia, Spain
e-mail: ainhoa.berciano@ehu.es

H. A. Christinal
Karunya University, Coimbatore, Tamilnadu, India

M. A. Gutiérrez-Naranjo
Research Group on Natural Computing, Department of Computer Science and
Artificial Intelligence, University of Sevilla, 41012 Sevilla, Spain
e-mail: magutier@us.es

Fig. 1 Images taken from a IgA nephropathy



the image of an injective continuous map of a circumference into the plane, $\phi : S_1 \rightarrow \mathbb{R}^2$ and the well-known *Jordan theorem* which claims that the complement of a Jordan curve in the plane has two connected components, many extensions, refinements and new proofs have been necessary [11]. Some of them were generalizations of higher dimensions, and some other due to *mathematical monsters* [5] as nowhere differentiable curves or Jordan curve of positive area.

In Digital Image Analysis, the problem of fixing the interior and exterior of a curve has new features. First of all, in Digital Image Analysis, the image is not infinitely divisible (as mathematical curves). The basic unit is the pixel and the concepts of connection of components, frontiers and bounds must be based on it. Such concepts have been widely studied in the literature. Nonetheless, the use of real-world images provides a new type of problem. The noise, the resolution of the picture or the intrinsic difficulties of the media where the image is taken are sources of misleading interpretations in the concepts of interior or exterior of a plain curve.

In this paper, we propose a definition and an algorithm for considering whether a black connected component (BCC) *surrounds*, in some sense, a portion of white region in a binary image. The practical application is immediate, since the BCC can be considered as an *imperfect closed curve*, and the surrounded region as an *imperfect topological hole* of the BCC. The definition of such *partially bounded regions* is a hard task even for human experts. A typical case study is a medical image where the expert must decide whether a set of pixels *enclose* a region or not. As an example, Fig. 1a shows the detail of an image associated with the IgA nephropathy, the most common glomerulonephritis throughout the world [1]. Figure 1b shows an amplified region of the image after a binarization process and the algorithm presented in [4] for detecting connected components. Even for the human eye, it is difficult to decide whether the black pixels surrounds a white region. A computer assistant for such decision must consider that the hole can be *imperfectly surrounded* by 4-adjacent black pixels.

Next, a novel definition of *Partially Bounded Region* of an image and an algorithm for automatically finding them based on Membrane Computing¹

¹ We refer to [9] for basic information in this area, to [10] for a comprehensive presentation and the web site <http://ppage.psyste.ms.eu> for the up-to-date information.

techniques are presented. As it will be shown below, such techniques are inspired in the flow of metabolites between cells of a living tissue or between the organelles in a eucaryotic cell. This flow of metabolites takes place in parallel in Nature and can be interpreted as a flow of information.

The paper is organized as follows: Firstly, we recall the computational bio-inspired used model used (Sect. 2). Next, our definition of *Partially Bounded Region* is presented, together with our Membrane Computing algorithm (Sect. 4). Finally, some conclusions are shown.

2 Membrane Computing

Membrane Computing [10] is a model of computation inspired by the structure and functioning of cells as living organisms able to process and generate information. The computational devices in Membrane Computing are called *P systems*. Roughly speaking, a P system consists of a membrane structure, in whose compartments one places multisets of objects which evolve according to given rules. These multisets encode the information and the rules deal with them performing the computation. Following a biological inspiration, the multisets of objects represent the chemicals placed in a vesicle of a living being. Such chemicals are sent to other vesicles or transformed according to biochemical reactions, represented here by computational rules. These rules are usually applied in a synchronous non-deterministic maximally parallel manner. In this paper, the so-called (because of their membrane structure) *tissue P Systems* [6] are considered.

2.1 Tissue P Systems

The chosen P system model in this paper is the *tissue P systems model* which has been widely used to solve computational problems in other areas (see, e.g., [2, 3]), but recently, they have been also used in the study of digital images (see, e.g., [4, 7, 8] and references therein).

Informally, a *tissue P system* of degree $q \geq 1$ can be seen as a set of q cells labeled by $1, 2, \dots, q$. The cells are the nodes of a virtual graph, where the edges connecting the cells are determined by the communication rules, i.e., as usual in tissue P systems, the edges linking cells are not provided explicitly: If a rule $(i, u/v, j)$ is given, then cells i and j are considered linked. The application of a rule $(i, u/v, j)$ consists of trading the multiset u (initially in the cell i) against the multiset v (initially in j). After the application of the rule, the multiset u disappears from the cell i and it appears in the cell j . Analogously, the multiset v disappears from the cell j and it appears in the cell i . In what follows we assume the reader is familiar with the basic notions and the terminology underlying P systems.

Formally, a *tissue P system* of degree $q \geq 1$ is a tuple of the form $\Pi = (\Gamma, \Sigma, \mathcal{E}, w_1, \dots, w_q, \mathcal{R}, i_{in}, i_{out})$ where q is the number of cells and

1. Γ is a finite alphabet, whose symbols will be called objects. These objects can be placed in the cells or in the surrounding space (called the *environment*),
2. $\Sigma \subseteq \Gamma$ is the input alphabet. The *input* of the computation performed by the P system is encoded by using this alphabet,
3. $\mathcal{E} \subseteq \Gamma$ is a finite alphabet representing the set of the objects in the environment. Following a biological inspiration, the objects in the environment are available in an arbitrary large amount of copies;
4. w_1, \dots, w_q are strings over Γ representing the multisets of objects placed inside the cells at the starting of the computation;
5. \mathcal{R} is a finite set of rules of type $(i, u/v, j)$ for $0 \leq i \neq j \leq q$, $u, v \in \Gamma^*$
6. $i_{in}, i_{out} \in \{1, 2, \dots, q\}$ denotes the input cell and output cell, respectively.

The biological inspirations of this model are intercellular communication and cooperation between neurons. Rules are used as usual in the framework of membrane computing, that is, in a maximally parallel way (a universal clock is considered).

A *configuration* is an instantaneous description of the tissue P system and it is represented as a tuple (w_1, \dots, w_q) . Given a configuration, we can perform a computation step and obtain a new configuration by applying the rules in a parallel manner as it is shown above. A configuration is *halting* when no rules can be applied to it. A *computation* is a sequence of computation steps such that either it is infinite or it is finite and the last step yields a halting configuration (i.e., no rules can be applied to it). Then, a computation halts when the P system reaches a halting configuration. The output of a computation is the multiset placed in the output cell in a halting configuration collected from its halting configuration by reading the objects contained in the output cell.

2.2 Example

Let us consider the following tissue P system with cell division of degree 3, $\Pi = (\Gamma, \Sigma, \mathcal{E}, w_1, w_2, w_3, \mathcal{R}, i_{\Pi}, i_0)$, where $\Gamma = \{a_1, a_2, b, c, p, q, r, x\}$, $\Sigma = \{a_1, a_2\}$ and $\mathcal{E} = \{x\}$. The multisets in the initial configuration are $w_1 = b$, $w_2 = c$ and $w_3 = r$. The set of rules are $R_1 \equiv (1, a_1b/x^3, 0)$, $R_2 \equiv (1, x/p, 2)$, $R_3 \equiv (1, x/q, 2)$, $R_4 \equiv (1, q/r, 3)$ and $R_5 \equiv [c]_2 \rightarrow [p]_2 [q]_2$. Finally, the input cell is $i_{\Pi} = 1$ and the output cell is $i_0 = 3$. Notice that rules $R_1 \dots, R_4$ determine a virtual graph with the cells as nodes. From R_2 and R_3 we can consider an edge between cell 1 and cell 2. Analogously, R_4 determines an edge between cell 1 and cell 3. We also know by rule R_1 that cell 1 can trade some objects with the environment.

Let us consider as input of our computation the multiset a_1a_2 (one copy of a_1 and two copies of a_2) placed in the input cell 1. By considering the input, the initial

configuration C_0 has three cells, labelled with 1, 2, 3 and with the multisets $w_1 = a_1a_2^2b$, $w_2 = c$ and $w_3 = r$. In the first step of computation, rules R_1 and R_5 are applied. Rule 1 interchanges the objects a_1b from cell 1 with three copies of x taken from the environment. Rule 5 divides the cell 2. Hence, the configuration C_1 has four cells: two of them labelled with 1 and 3 (respectively) and the other two cells have the label 2. The multiset in the cell labelled by 1 is $w_1 = x^3a_2$, the cell labelled by 3 contains the multiset $w_3 = r$ and the cells labelled by 2 have, respectively, the multisets $w_2 = p$ and $w_2 = q$. In the following step of computation rules R_2 and R_3 are applied. These rules send one copy of the object x to the corresponding cell labelled by 2 against one copy of p and q (respectively). Therefore, the configuration C_2 has the same four cells as in the configuration C_1 , but with the multisets $w_1 = xa_2pq$, $w_3 = r$ and the cells labelled by 2 have the same multiset $w_2 = x$. Finally, in the third computation step the rule R_4 is applied and the object q in the cell 1 is interchanged with the object r in the cell 3. We get the final configuration C_3 with $w_1 = xa_2^2pr$, $w_3 = q$ and $w_2 = x$ in both cells labelled by 2. As the output cell is cell 3, the multiset r placed in this cell in the last configuration is the output of the configuration.

3 Digital Imagery

A *point set* is simply a topological space consisting of a collection of objects called points and a topology which provides for such notions as *nearness* of two points, the *connectivity* of a subset of the point set, the *neighborhood* of a point, *boundary points*, and *curves* and *arcs*. For a point set X in Z , a *neighborhood function* from X in Z , is a function $N : X \rightarrow 2^Z$. For each point $x \in X$, $N(x) \subseteq Z$. The set $N(x)$ is called a *neighborhood* for x .

There are two neighborhood function on subsets of \mathbf{Z}^2 which are of particular importance in image processing, the *von Neumann neighborhood* and the *Moore neighborhood*. The first one $N : X \rightarrow 2^{\mathbf{Z}^2}$ is defined by $N(x) = \{y : y = (x_1 \pm j, x_2) \text{ or } y = (x_1, x_2 \pm k), j, k \in \{0, 1\}\}$, where $x = (x_1, x_2) \in X \subset \mathbf{Z}^2$. While the Moore neighborhood $M : X \rightarrow 2^{\mathbf{Z}^2}$ is defined by $M(x) = \{y : y = (x_1 \pm j, x_2 \pm k), j, k \in \{0, 1\}\}$, where $x = (x_1, x_2) \in X \subset \mathbf{Z}^2$. The von Neumann and Moore neighborhood are also called the *four neighborhood* (4-adjacency) and *eight neighborhood* (8-adjacency), respectively.

An Z -valued image on X is any element of Z^X . Given an Z -valued image $I \in Z^X$, i.e. $I : X \rightarrow Z$, then Z is called the set of possible range values of I and X the spatial domain of I . The graph of an image is also referred to as the *data structure representation* of the image. Given the data structure representation $I = \{(x, I(x)) : x \in X\}$, then an element $(x, I(x))$ is called a *picture element* or *pixel*. The first coordinate x of a pixel is called the *pixel location* or *image point*, and the second coordinate $I(x)$ is called the *pixel value* of I at location x .

For example, X could be a subset of \mathbf{Z}^2 where $x = (i, j)$ denotes spatial location, and Z could be a subset of \mathbf{N} or \mathbf{N}^3 , etc. So, given an image $I \in \mathbf{Z}^{\mathbf{Z}^2}$, a pixel of I is the form $((i, j), I(x))$, which be denoted by $I(x)_{ij}$. We call the *set of colors* or *alphabet of colors of I* , $\mathcal{C}_I \subseteq Z$, to the image set of the function I with domain X and the image point of each pixel is called *associated color*. We can consider an order in this set. Usually, we consider in digital image a predefined alphabet of colors $\mathcal{C} \subseteq Z$. We define $h = |\mathcal{C}|$ as the size (number of colors) of \mathcal{C} . In this paper, we work with images in grey scale, then $\mathcal{C} = \{0, \dots, 255\}$, where 0 codify the black color and 255 the white color.

A *region* could be defined by a subset of the domain of I whose points are all mapped to the same (or similar) pixel value by I . So, we can consider the region R_i as the set $\{x \in X : I(x) = i\}$ but we prefer to consider a region r as a maximal connected subset of a set like R_i . We say two regions r_1, r_2 are adjacent when at less a pair of pixel $x_1 \in r_1$ and $x_2 \in r_2$ are adjacent. We say x_1 and x_2 are *border pixels*. If $I(x_1) < I(x_2)$ we say x_1 is an *edge pixel*. The set of connected edge pixels with the same pixel value is called a *boundary* between two regions.

4 Partially Bounded Regions

Given a binary 2D digital image, the HGB2I problem consists on calculating the number of connected components and the representative curves of the holes of these components. We can divide this problem in two sub-problems: the H_0 *problem* consists on calculating the number of connected components and the H_1 *problem*, which consists on calculating the number of holes. In [4], the HGB2I problem was solved by using tissue P systems. In this paper, we extend the design of such P systems in order to find *Partially Bounded Regions* (PBR).

Definition 1 *Let I be a black and white image and C_1 a connected component of black pixels of I . Let P be a white pixel of the image I .*

- *We will say that C_1 bounds the pixel P on the north (resp. south, east and west) if there is at least one black pixel of the image I on the north (resp. south, east and west) of P and the first of such black pixels belongs to C_1 .*
- *We will say that the region of white pixels C_2 is partially bound by C_1 if it is connected, all its pixels are bounded by C_1 at least on three sides (from north, south, east or west) and it is maximal, i.e., it is not a proper subset of a region with these properties.*

4.1 Looking for Partially Bounded Regions

Given an input image, the stages of our algorithm for automatically finding such regions are: *Stage 1*: Distinguishing BCCs; *Stage 2*: Minimal region containing

a BCCs; *Stage 3*: Marking candidates as possible PBRs; and *Stage 4*: Choosing PBRs.

Stage 1: Distinguishing BCCs. The first step for marking the PBR is to identify the different BCCs of the image. The algorithm from [4] to solve H_0 problem assigns a different label to each of them. So, up to now, we consider we have applied the previous algorithm, i.e., we have all the BCC labeled, and each component with a different label.

Stages 2 and 3: Minimal region containing a BCCs. The minimal rectangle containing the connected component \mathbb{C} is found. All the white pixels in such rectangle receive the same label as the black pixels of the BCC. (Rules R_1 to R_2 in the tissue P System described below.)

Marking candidates as possible PBRs. Each white pixel inside of a minimal rectangle is associated to a label. We associate the label N to this pixel if there is a black or a white pixel with this label above it, the label S if there is a black or a white pixel with this label below it; and we follow exactly the same way for the labels E (right) and O (left). (Rules R_3 to R_{10} in the tissue P system). We keep the pixels with at least the three labels from $\{N, S, E, O\}$ (Rule R_{11}).

We define a family of tissue P system to develop the steps considered in the stages 2 and 3. For each image \mathcal{I} with size n^2 , we define a tissue P system, $\Pi(n) = (\Gamma, \Sigma, \mathcal{E}, w_1, \mathcal{R}, i_{in}, i_{out})$ where:

- $\Gamma = \{w_{ij} : 1 \leq i, j \leq n\} \cup \{(a_{ij}, (k, l)) : a \in \{b, r, w\} \wedge 1 \leq i, j, k, l \leq n\}$
 $\cup \{N, S, O, E\}, \Sigma = \{(a_{ij}, (k, l)) : a \in \{b, w\} \wedge 1 \leq i, j, k, l \leq n\},$
 $\mathcal{E} = \{(a_{ij}, (k, l)) : a \in \{b, r, w\} \wedge 1 \leq i, j, k, l \leq n\},$
- $w_1 = \emptyset,$
- $i_{in} = i_{out} = 1$ is the output cell.

\mathcal{R} is the following set of rules:

- First, we will paint the white pixels adjacent to black pixels, maintained the label:
- $R_1 \equiv (1, (w_{i'j'})(b_{ij}, (k, l)) / (r_{i'j'}, (k, l))(b_{ij}, (k, l)), 0)$ for $(i, j), (i', j')$ adjacent positions in the image.
- Now, we will find the corners of our new red line and we will expand this connected component using these corners. In this way, the red component will be expanded if and only if it is concave, so it will grow in the interior part of the black connected components. Anyway, it will be able to grow on the exterior part too, but it will stop (see Fig. 2b), because of it will not be bigger than the minimal rectangle that contains this connected component.
- $R_2 \equiv \begin{array}{cc} (1, (x, (k, l)) & (y, (k, l)) \\ (z, (k, l)) & w \end{array} / \begin{array}{cc} (x, (k, l)) & (y, (k, l)) \\ (z, (k, l)) & (r, (k, l)), 0) \end{array}$
 where $x, y, z \in \{b, r\}$
- Once any rule of type R_2 cannot be activated, we will start working with the colored pixels with the same label as our connected component. The important key is to transfer to each red pixel in which direction it has black pixels with the

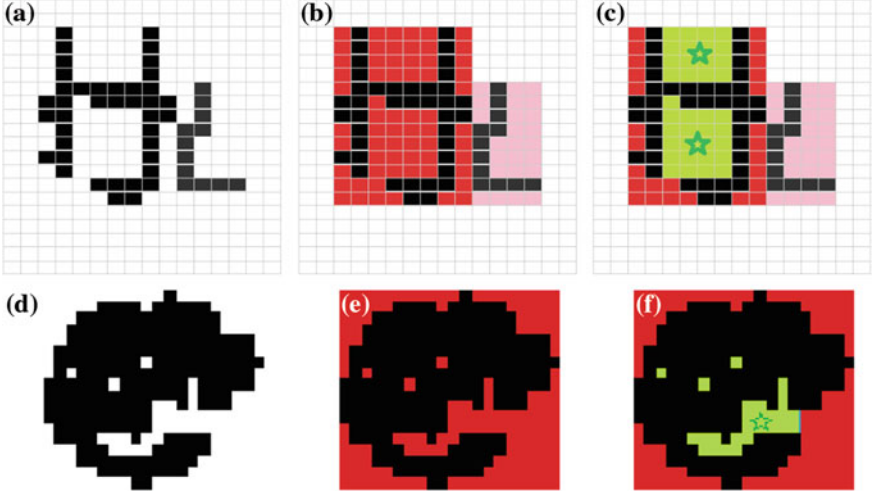
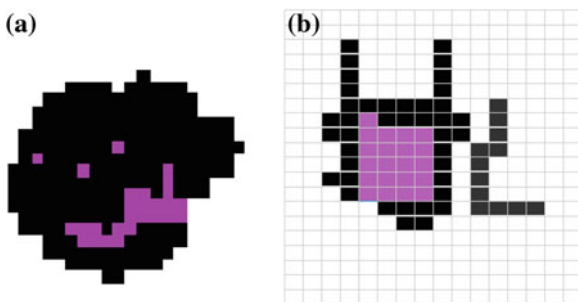


Fig. 2 **a** and **d** Input images; **b** and **e** Minimum regions containing a BCC. We can see two labels (colors), one of each connected component **c** and **f** Candidate regions to PBRs (marked with an star)

same label. We will preserve the red pixels which has black pixels (with the same label) in the four directions. To do this, we will work with the following rules:

- $R_3 \equiv (1, (b_{ij}, (k, l))(r_{ij+1}, (k, l)) / (b_{ij}, (k, l))(r_{ij+1}, (k, l), E), 0)$
- $R_4 \equiv (1, (r_{ij}, (k, l), u)(r_{ij+1}, (k, l), v) / (r_{ij}, (k, l), u)(r_{ij+1}, (k, l), vE), 0)$ for $u, v \in \{N, S, E, O\}^*$, $E \in u$ and $E \notin v$. In this case it is only possible to transfer from left to right. That is, if a pixel adjacent to the given one, that is not on the left of the first one, has the label E , this rule will not be executed.
- $R_5 \equiv (1, (b_{ij}, (k, l))(r_{ij-1}, (k, l)) / (b_{ij}, (k, l))(r_{ij-1}, (k, l), O), 0)$
- $R_6 \equiv (1, (r_{ij}, (k, l), u)(r_{ij-1}, (k, l), v) / (r_{ij}, (k, l), u)(r_{ij-1}, (k, l), vO), 0)$ for $u \in \{N, S, E, O\}^*$ and $O \in u$ and $O \notin v$. In this case it is only possible to transfer from right to left. That is, if a pixel adjacent to the given one, that is not on the right of the first one, has the label O , this rule will not be executed.
- $R_7 \equiv (1, (b_{ij}, (k, l))(r_{i+1j}, (k, l)) / (b_{ij}, (k, l))(r_{i+1j}, (k, l), S), 0)$
- $R_8 \equiv (1, (r_{ij}, (k, l), u)(r_{i+1j}, (k, l), v) / (r_{ij}, (k, l), u)(r_{i+1j}, (k, l), vS), 0)$ for $u \in \{N, S, E, O\}^*$ and $S \in u$ and $S \notin v$. In this case, the unique possibility is to transfer from down to up. That is, if a pixel adjacent to the given one, that is not at the bottom of the first one, has the label S , this rule will not be executed.
- $R_9 \equiv (1, (b_{ij}, (k, l))(r_{i-1j}, (k, l)) / (b_{ij}, (k, l))(r_{i-1j}, (k, l), N), 0)$
- $R_{10} \equiv (1, (r_{ij}, (k, l), u)(r_{i-1j}, (k, l), v) / (r_{ij}, (k, l), u)(r_{i-1j}, (k, l), vN), 0)$ for $u \in \{N, S, E, O\}^*$ and $N \in u$ and $N \notin v$. In this case, it is only possible to transfer from up to down. That is, if a pixel adjacent to the given one, that is not at the top of the first one, has the label N , this rule will not be executed.

Fig. 3 **a** and **b** PBRs of the images in Fig. 2a and d, respectively



- Just the previous rules conclude, the colored pixels that have black pixels (with the same label) in their four directions, will be assigned a new label by rule R_{11} .
- $R_{11} \equiv (1, (r_{ij}, (k, l), XYZ)/(g_{ij}, (k, l)), 0)$ for $X \neq Y \neq Z$ and $X, Y, Z \in \{N, S, E, O\}$.

Stage 4: Choosing PBRs. We take the pixels belonging to a candidate region and adjacent to a white pixel in the input image. If their number is lower than a threshold then this region is a PBR, but if number is greater than this threshold then it is rejected. This threshold is taken in function of the maximal distance between two pixels of the minimal region containing the BCCs. The definition of a family of tissue P systems to develop this stage is extremely easy. We can see a similar family in [7]. We can see in Fig. 3 the results of our algorithm when it is applied in the images of Fig. 2a, b.

5 Conclusions

Biological and medical images are intrinsically full of imperfect data. Even with the current technology, the noise cannot be fully avoided. The resolution of the camera, the absence of the proper light or an aqueous media can affect the accuracy of the image. In some technical areas, it is crucial to determine the interior of a connected set of pixels, even in case of it is not limited by a clear frontier. Solving such problem is a hard task even for expert human eyes.

In this paper, we propose a definition of partially bounded region which can help in this task. Finding a definition which cover each possible case is not possible, since the number of different cases from real-life images goes beyond any definition, but the proposed one can help in a vast amount of cases.

In this paper, we also use techniques from the bio-inspired paradigm of Membrane Computing. This new computational paradigm have features which makes it suitable for dealing with digital images and it has been successfully applied recently to Digital Image Analysis. For example, the subset of the integer plane or space taken to be the *support* of the image and the set of possible features associated to each 2D point can be considered finite and hence, the transformation

of an image into another can be performed in a *discrete* way. Other of such features is that the treatment of the image can be parallelized and locally modified. Regardless how large is the picture, the process can be performed in parallel in different local areas of it. Another interesting feature is that the information of the image can also be easily encoded in the data structures used in Membrane Computing.

Acknowledgments MAGN acknowledges the support of the project TIN2012-37434 of the Ministerio de Economía y Competitividad of Spain.

References

1. D'amico, G.: The commonest glomerulonephritis in the world: Iga nephropathy. *QJM: Int. J. Med.* **64**(3), 709–727 (1987)
2. Díaz-Pernil, D., Gutiérrez-Naranjo, M.A., Pérez-Jiménez, M.J., Riscos-Núñez, A.: Solving the independent set problem by using tissue-like P systems with cell division. In: Mira, J. et al. (ed.) *IWINAC* (1). *Lecture Notes in Computer Science*, vol. 5601, pp. 213–222. Springer, Heidelberg (2009)
3. Díaz-Pernil, D., Gutiérrez-Naranjo, M.A., Pérez-Jiménez, M.J., Riscos-Núñez, A.: A linear time solution to the partition problem in a cellular tissue-like model. *J. Comput. Theoret. Nanosci.* **7**(5, SI), 884–889 (2010)
4. Díaz-Pernil, D., Gutiérrez-Naranjo, M.A., Real, P., Sánchez-Canales, V.: Computing homology groups in binary 2D imagery by tissue-like P systems. *Rom. J. Inform. Sci. Tech.* **13**(2), 141–152 (2010)
5. Feferman, S.: Mathematical intuition versus mathematical monsters. *Synthese* **125**(3), 317–332 (2000)
6. Martín-Vide, C., Pădun, G., Pazos, J., Rodríguez-Patón, A.: Tissue P systems. *Theoret. Comput. Sci.* **296**(2), 295–326 (2003)
7. Peña-Cantillana, F., Daz-Pernil, D., Berciano, A., Gutiérrez-Naranjo, M.A.: A parallel implementation of the thresholding problem by using tissue-like P systems. In: Real, P., et al. (ed.) *CAIP* (2). *Lecture Notes in Computer Science*, vol. 6855, pp. 277–284. Springer, Heidelberg (2011)
8. Peña-Cantillana, F., Daz-Pernil, D., Christinal, H.A., Gutiérrez-Naranjo, M.A.: Implementation on CUDA of the smoothing problem with tissue-like P systems. *Int. J. Nat. Comput. Res.* **2**(3), 25–34 (2011)
9. Păun, G.: *Membrane Computing. An Introduction*. Springer, Heidelberg (2002)
10. Păun, G., Rozenberg, G., Salomaa, A. (eds.): *The Oxford Handbook of Membrane Computing*. Oxford University Press, Oxford (2010)
11. Ross, F., Ross, W.T.: The Jordan curve theorem is non-trivial. *J. Math. Arts* **5**, 213–219 (2011)

Power System Stability Enhancement Using Fuzzy Logic Based Power System Stabilizer

V. K. Tayal, J. S. Lather, Piyush Sharma and S. K. Sinha

Abstract In this paper a linearized Heffron-Philips model of a Single Machine Infinite Bus (SMIB) power system with a Fuzzy Logic Power System Stabilizer (FPSS) is developed for different membership functions. For FPSS, speed deviation and acceleration deviation are taken as inputs. Comparison of the effectiveness (steady state error, ess, overshoot (Mp) and settling time (ts) of FPSS for different membership functions with conventional PSS and without PSS is done. The performance of the SMIB system has improved significantly compared to SMIB system without PSS/with PSS. The results of the simulation show that for low frequency oscillations, FPSS is more effective in damping compared to conventional controllers. Further this paper investigates the design and implementation of a Reduced Rule Fuzzy Logic Power System Stabilizer (RLFPSS). A Reduced Rule Fuzzy Logic Power System Stabilizer for different membership functions is proposed. The effectiveness of the RLFPSS for different membership functions is illustrated with simulation carried out in MATLAB.

Keywords Heffron–Philips model • Power system stabilizer • Fuzzy logic power system stabilizer • Reduced rule fuzzy logic power system stabilizer • Controller • Membership functions

V. K. Tayal (✉) · J. S. Lather
Department of Electrical Engineering, National Institute of Technology,
Kurukshetra, Haryana, India
e-mail: vikysm09@gmail.com

J. S. Lather
e-mail: jslather@gmail.com

P. Sharma
School of Electrical, Electronics and Communication Engineering, Galgotias University,
Greater Noida, India
e-mail: piyushsharma034@gmail.com

S. K. Sinha
Electrical and Electronics Engineering Department, Amity University, Noida, India
e-mail: sinha.sanjay66@gmail.com

1 Introduction

In the present scenario of modern era the stability of electric power system is one of the most important concerns in any electric power system network. This can be traced from the fact that in steady state the average electrical speed of the generators must be in synchronism. The stability of power system can be defined as that property.

Power system stability [1] can be classified into: Transient stability and Small signal stability. Transient stability of a system was conventionally suppressed using AVR (Automatic voltage regulator), has the electric system has been seen with oscillations of frequencies ranging from 0.1 to 2 Hz. These regulators have high gain leading to destabilizing effect on power system and also these are designed for specific operating condition hence limiting to specific level of performance [2]. The solution to this problem is provided by fuzzy logic control. Fuzzy Logic [3–5] has the features of simple concept, easy implementation, and computational efficiency. This provides an easy method to draw the definite conclusion from hazy, uncertain or inexact information. So in this paper the fuzzy logic based power system stabilizer model is evaluated on a single machine infinite bus (SIMB) power system, and then the performance of Conventional power system stabilizer (CPSS), Fuzzy logic based power system stabilizer (FPSS) and Reduce Rule based on Fuzzy logic based Power system stabilizer for different membership functions have been compared. The paper is organized as follows; Sect. 2 describes the modelling of power system. The designs of the conventional power system stabilizer and Fuzzy logic based power system stabilizer have been described in Sect. 3. The MATLAB/SIMULINK simulation results are presented and discussed in Sect. 4. The conclusion is mentioned in Sect. 5. Appendix includes various parameters of the system and controllers.

2 Modeling of Power System

SMIB (Single Machine Infinite Bus) system consists of a synchronous machine connected to an infinite bus through a transmission line as shown in Fig. 1.

The fourth-order nonlinear system is described by the following set of equations.

$$\begin{aligned}\dot{\delta} &= \omega \\ \dot{\omega} &= \frac{1}{M}(T_m + T_e + D.\omega) \\ \dot{e}'_q &= \frac{1}{T'_{do}}(E_{fd} - e'_q - (X_d - X'_d)i_d)\end{aligned}$$

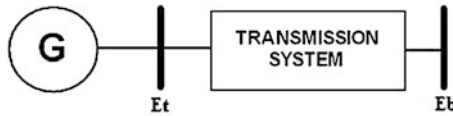


Fig. 1 Single machine infinite bus system (SMIB)

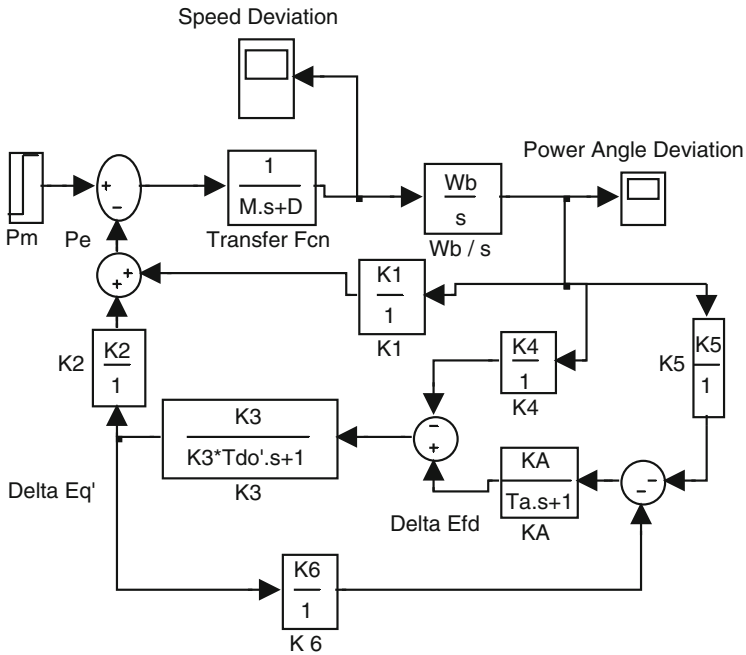


Fig. 2 MATLAB/SIMULINK model of Heffron and Phillips without controller

$$\dot{E}_{fd} = \frac{1}{T_a} [K_A (V_{ref} - V_t)] - \frac{1}{T_a} E_{fd}$$

Figure 2 shows the block diagram of Single Machine infinite bus (SMIB) power system model. This diagram was developed by Heffron and Phillips so to represent a single synchronous generator connected to the grid through a transmission line. Heffron and Phillips model [6] is a linear model. It is quite accurate for studying LFOs and stability of power systems. It has also been successfully used for designing classical power system controllers, which are still active in most power utilities.

3 Controllers

Controller is a device fabricated in a chip form, analogue electronics, or computer that supervise and actually alters the working conditions of a considered dynamical system. This paper deals with two types of power system controllers discuss below.

3.1 Conventional Power System Stabilizer (CPSS)

The Power System Stabilizer is used to provide a sufficient damping to electro-mechanical oscillations in SMIB energy system. So CPSS [7–11] is used to achieve desired transient behavior and low steady state error. The input to controller is speed deviation $\Delta\omega$. The PSS as represented in Fig. 3 has three components. These are phase compensation block, signal washout block and gain block.

The controller gain K_s is an important factor as the damping provided by the PSS increase in proportion to an increase in the gain up to a certain critical gain value, after which the damping begins to decrease. The phase compensator block is used to make the system “settle down” quickly. The outcome value of the controller has to be gradually drawn towards zero in steady state condition. Therefore a washout transfer function $[T_w.S/(T_w.S + 1)]$, which has a steady state gain zero is used. The value of washout time constant T_w , may be in the range of 1–20 s.

3.2 Fuzzy Logic Controlled Power System Stabilizer (FPSS)

The fuzzy power system stabilizer is a two-input component which have single output. These inputs are angular speed deviation and angular acceleration while output of fuzzy logic controller is a voltage signal.

3.2.1 Fuzzy Logic Control System

Aristotle, 384–322 BC defines Logic as the mark of an instructed mind to rest satisfied with that degree of precision which the nature of the subject admits, and not to seek exactness where only an approximation of the truth is possible.

Concept of fuzzy logic has been given by Lotfi Zadeh in 1965. This logic is used in many applications in the industry because of some advantages: simple and faster methodology, reduce a design development cycle, simple to implement, reduce hardware cost, improve the control performance, simplify design complexity. So it is used as a controller in a power system as a fuzzy power system stabilizer [12–20]. The designing process is carried out with the help of MATLAB 2009a (MATLAB, The MathWorks Inc., 1995). A fuzzy controller comprises of three stages: fuzzification, fuzzy rule and defuzzification.

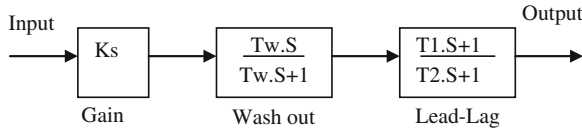


Fig. 3 Structure of conventional lead-lag controller

Table 1 Rule base of fuzzy logic controller

Speed Deviation	Acceleration						
	NH	NM	NS	ZR	PS	PM	PH
NH	NH	NH	NH	NH	NM	NM	NS
NM	NH	NM	NM	NM	NS	NS	ZR
NS	NM	NM	NS	NS	ZR	ZR	PS
ZE	NM	NS	NS	ZR	PS	PS	PM
PS	NS	ZR	ZR	PS	PS	PM	PM
PM	ZR	PS	PS	PM	PM	PM	PH
PH	PS	PM	PM	PH	PH	PH	PH

3.3 Fuzzification

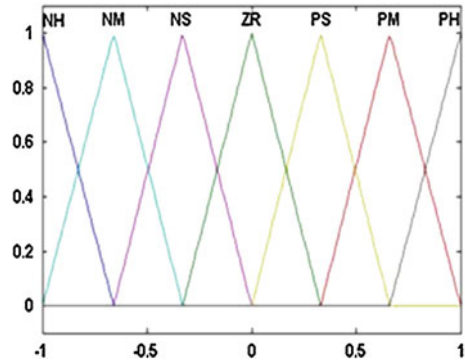
Fuzzification is the process of making a crisp quantity to fuzzy. This paper simply recognizes that many of the quantities which are considered to be crisp and deterministic are actually not deterministic at all. They carry considerable uncertainty. If the uncertainty forms arise because of elusiveness, vagueness or ambiguity then fuzzy may be variable and can be represented by a membership function. In this system there are two input speed and acceleration which is converting into fuzzy value. Each of the input and output fuzzy variables [21, 22] is assigned seven linguistic labels. Seven membership functions are generating better result proved by some testing are defined as NH (Negative High), NM (Negative Medium), NS (Negative-Small), ZR (Zero), PS (Positive-Small), PM (Positive-Medium), PH (Positive High) membership functions are used to convert the fuzzy values between 0 and 1 for inputs and output value both which are shown in Table 1.

Membership functions are used to convert the fuzzy values between 0 and 1 for inputs and output value both as shown in Fig. 4.

3.4 Fuzzy Rule Base System

Fuzzy rules are defined to reduce the error in the system after analyzing the function of controller. For each fuzzy value there are seven membership functions, so 49 combinations are possible which are shown in Table 1 of speed and acceleration. There is an output for each of the membership functions and the linguistic variables can be determined by using IF-Then fuzzy rules [23].

Fig. 4 Membership functions for fuzzy controller for input and output variables



In a defuzzification part fuzzy values which are obtained from inference system converts into the specific values. For the inference Mamdani's minimum fuzzy implication and Max–Min compositional rule are used. For the defuzzification centroid method is used. At first, a parameters satisfying FLC is designed, according to design rules and with assumption given in Sect. 3. Figure 5 shows the Heffron Phillips MATLAB/SIMULINK Model of Single Machine Infinite bus (SMIB) equipped with FLC.

3.5 Reduced Rule Fuzzy Based Power System Stabilizer

In Sect. 4 for a two input fuzzy controller 7 membership functions for each input were used. Due to large rule-base system, the design of a Fuzzy PSS is very tedious task. In the proposed Fuzzy PSS, only two fuzzy membership functions [23] are used for the two inputs angular speed and acceleration and three membership functions for the output parameter as shown in Fig. 6. Depending upon the nature of output (increasing or decreasing) four rules are derived for the fuzzy logic controller (Table 2). These four rules are sufficient to cover all possible situations.

4 Simulation Results

Figures 7, 8, 9, 10, 11, 12, 13 and 14 shown the Speed Deviation ($\Delta\omega$), Power angle Deviation ($\Delta\delta$) of the SMIB system without controller, controlled by conventional controller, FLC and Reduced Rule fuzzy PSS respectively for the different types of membership functions. The System parameters (a) Speed Deviation ($\Delta\omega$) (b) Power angle Deviation ($\Delta\delta$) of generator obtained with the proposed controllers are given in Table 3. The outputs of SMIB system without PSS (a) Speed Deviation ($\Delta\omega$) (b) Power angle Deviation ($\Delta\delta$) of generator are shown in Fig. 7.

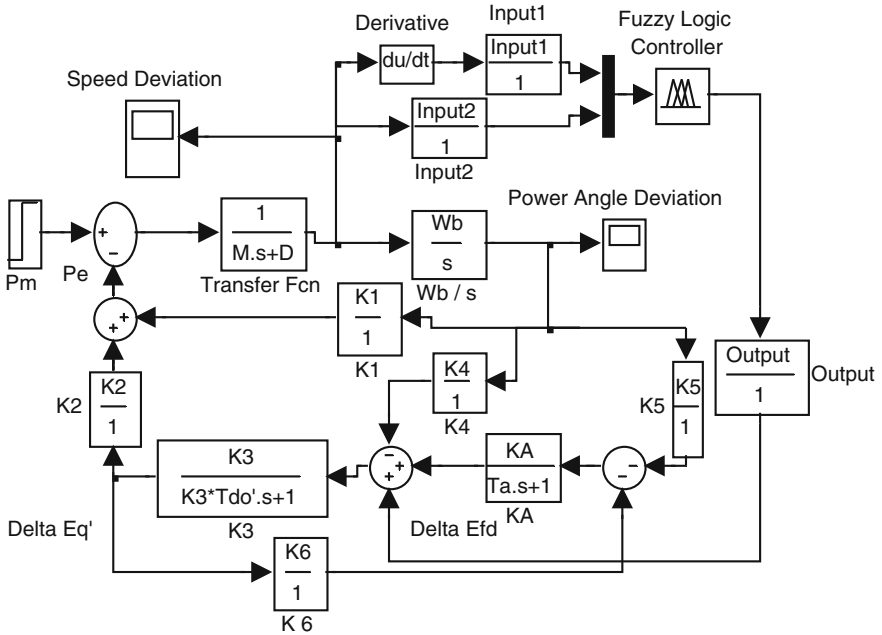


Fig. 5 MATLAB/SIMULINK model of plant controlled by fuzzy power system stabilizer

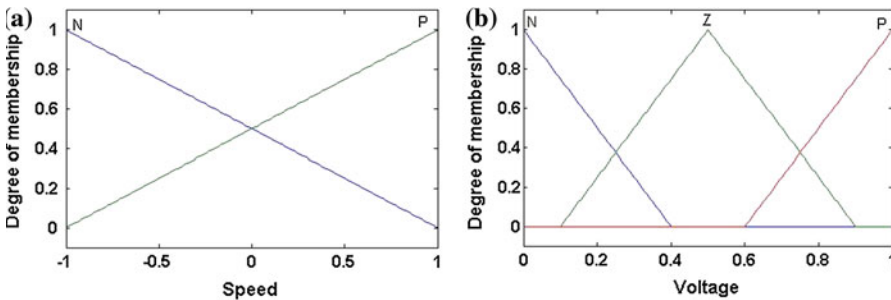


Fig. 6 Reduced membership function for a input speed and acceleration, b output voltage

Table 2 Reduced rule base of a Fuzzy PSS

	Output	Acceleration	
		N	P
Speed	N	N	Z
	P	Z	P

The responses clearly show that system has large overshoot (M_p), large settling time (t_s) and error steady state is 0 and 2 for Speed Deviation and Power angle respectively.

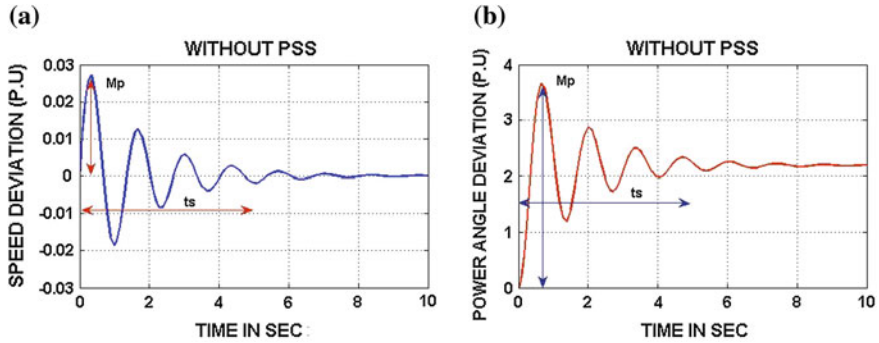


Fig. 7 Output of SMIB system without PSS **a** Speed Deviation ($\Delta\omega$), **b** Power angle Deviation ($\Delta\delta$) of generator

The outputs of SMIB systems with conventional PSS (a) Speed Deviation ($\Delta\omega$) (b) Power angle Deviation ($\Delta\delta$) of generator are shown in Fig. 8. The responses show that system has still larger overshoot (M_p), larger settling time (t_s) and error steady state is 0 and 2 for Speed Deviation and Power angle respectively. This can be further improved by fine tuning of controller parameters.

The outputs of SMIB system with Fuzzy PSS for a triangular membership function (a) Speed Deviation ($\Delta\omega$) (b) Power angle Deviation ($\Delta\delta$) of generator are shown in Fig. 9. The responses show that system has smaller overshoot (M_p), smaller settling time (t_s) and error steady state is 0 and 2 for Speed Deviation and Power angle respectively. So performance improved by using Fuzzy PSS. This can be further improved by fine tuning of controller parameters.

The outputs of SMIB system with Fuzzy PSS for a Trapezoidal membership function (a) Speed Deviation ($\Delta\omega$) (b) Power angle Deviation ($\Delta\delta$) of Generator are shown in Fig. 10. The responses show that system has smaller overshoot (M_p), smaller settling time (t_s) and error steady state is 0 and 2 for Speed Deviation and Power angle respectively. So performance improved by using Fuzzy PSS. This can be further improved by fine tuning of controller parameters.

The outputs of SMIB system Fuzzy PSS for a Gaussian membership function (a) Speed Deviation ($\Delta\omega$) (b) Power angle Deviation ($\Delta\delta$) of Generator are shown in Fig. 11. The responses show that system has smaller overshoot (M_p), smaller settling time (t_s) and error steady state is 0 and 2 for Speed Deviation and Power angle respectively. So performance improved by using Fuzzy PSS. This can be further improved by fine tuning of controller parameters.

The outputs of SMIB system with Reduced Rule Based Fuzzy PSS for a Triangular membership function (a) Speed Deviation ($\Delta\omega$) (b) Power angle Deviation ($\Delta\delta$) of Generator are shown in Fig. 12. The responses clearly show that system has much smaller overshoot (M_p), much smaller settling time (t_s) and error steady state is zero for both Speed Deviation and Power angle.

Table 3 System parameters with different controller

S. no.	System parameter	Fuzzy PSS				Reduced rule fuzzy PSS			
		With conventional PSS controller	Triangular membership function	Trapezoidal membership function	Gaussian membership function	Triangular membership function	Trapezoidal membership function	Gaussian membership function	
1	Speed Deviation ($\Delta\omega$)	Large overshoot (Mp), peak value = 0.025 pu, large settling time (ts), ess = 0	Smaller overshoot (Mp), peak value = 0.0125 pu, smaller settling time (ts), ess = 0	Smaller overshoot (Mp), peak value = 0.013 pu, smaller settling time (ts), ess = 0	Smaller overshoot (Mp), peak value = 0.013 pu, smaller settling time (ts), ess = 0	Smaller overshoot (Mp), peak value = 0.0125 pu, smaller settling time (ts), ess = 0	Smaller overshoot (Mp), peak value = 0.005 pu, smaller settling time (ts), ess = 0	Smaller overshoot (Mp), peak value = 0.0165 pu, smaller settling time (ts), ess = 0	
2	Power Angle Deviation ($\Delta\delta$)	Large overshoot (Mp), peak value = 3.5 pu, large settling time (ts), ess = 2	Smaller overshoot (Mp), peak value = 2.1 pu, smaller settling time (ts), ess = 2	Smaller overshoot (Mp), peak value = 2.24 pu, smaller settling time (ts), ess = 2	Smaller overshoot (Mp), peak value = 2.01 pu, smaller settling time (ts), ess = 2	Smaller overshoot (Mp), peak value = 0.4 pu, smaller settling time (ts), ess = 0	Smaller overshoot (Mp), peak value = 0.3 pu, smaller settling time (ts), ess = 0	Smaller overshoot (Mp), peak value = 0.4 pu, smaller settling time (ts), ess = 0	

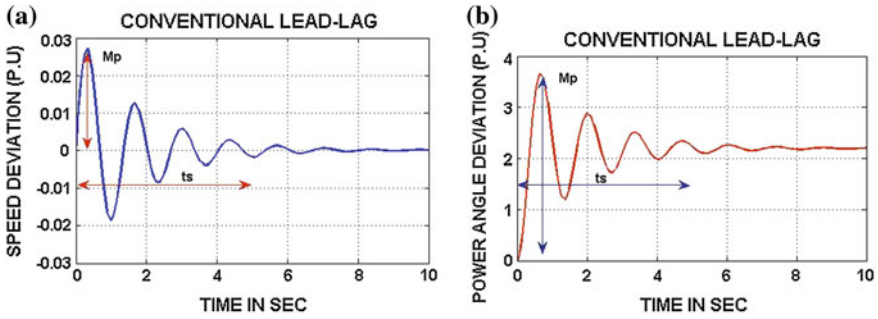


Fig. 8 Output of SMIB system conventional lead-lag PSS **a** Speed Deviation ($\Delta\omega$), **b** Power angle Deviation ($\Delta\delta$) of generator

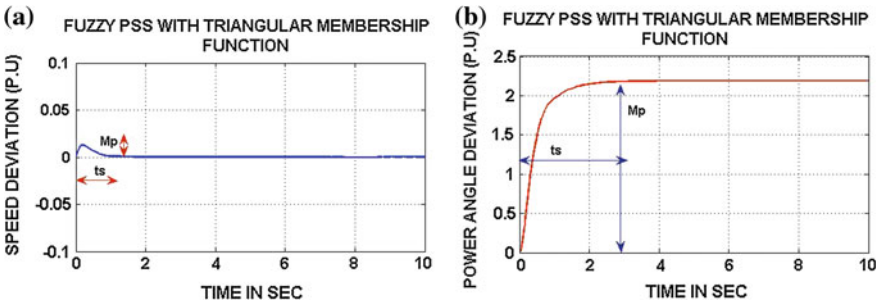


Fig. 9 Output of SMIB system fuzzy PSS for triangular membership function **a** Speed Deviation ($\Delta\omega$), **b** Power angle Deviation ($\Delta\delta$) of generator

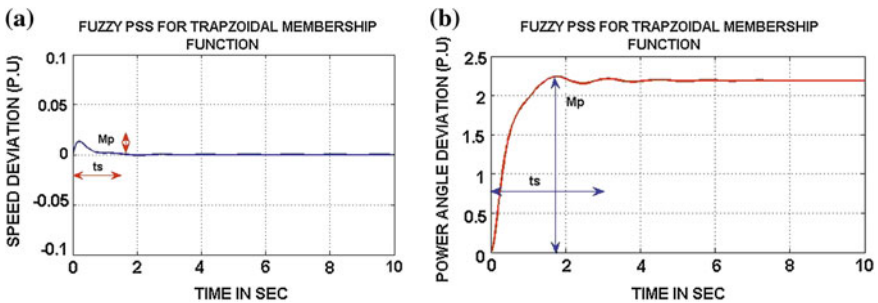


Fig. 10 Output of SMIB system Fuzzy PSS for Trapezoidal membership function **a** Speed Deviation ($\Delta\omega$), **b** Power angle Deviation ($\Delta\delta$) of generator

The outputs of SMIB system with Reduced Rule Based Fuzzy PSS for a Trapezoidal membership function (a) Speed Deviation ($\Delta\omega$) (b) Power angle Deviation ($\Delta\delta$) of Generator are shown in Fig. 13. The responses clearly show that

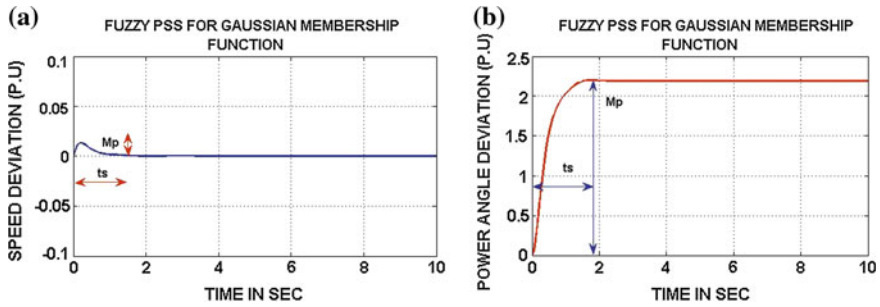


Fig. 11 Output of SMIB system Fuzzy PSS for Gaussian membership function **a** Speed Deviation ($\Delta\omega$), **b** Power angle Deviation ($\Delta\delta$) of generator

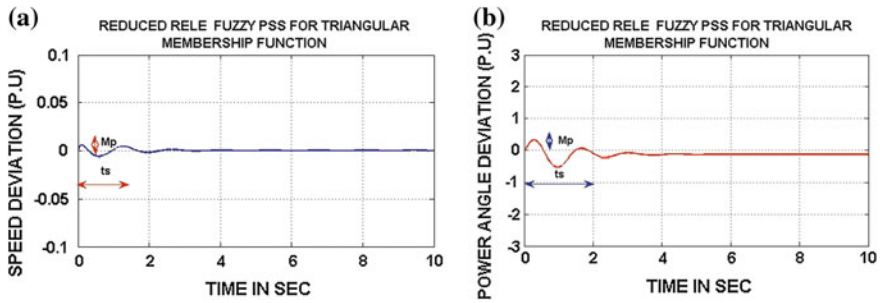


Fig. 12 Output of SMIB system reduced rule Fuzzy PSS for triangular membership function **a** Speed Deviation ($\Delta\omega$) **b** Power angle Deviation ($\Delta\delta$) of generator

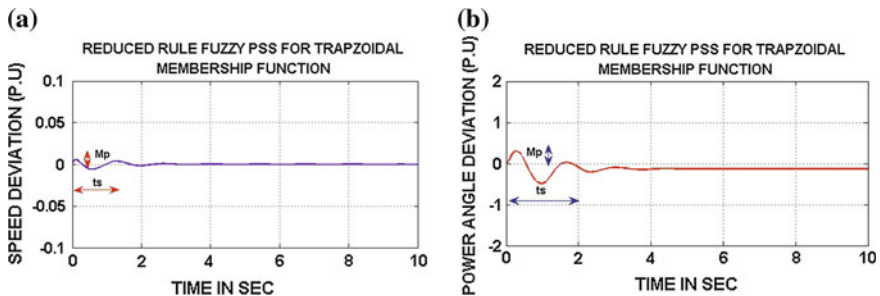


Fig. 13 Output of SMIB system reduced rule Fuzzy PSS for trapezoidal membership function **a** Speed Deviation ($\Delta\omega$), **b** Power angle Deviation ($\Delta\delta$) of generator

system has much smaller overshoot (M_p), much smaller settling time (t_s) & error steady state is for both Speed Deviation and Power angle.

The outputs of SMIB system with Reduced Rule Based Fuzzy PSS for a Gaussian membership function (a) Speed Deviation ($\Delta\omega$) (b) Power angle

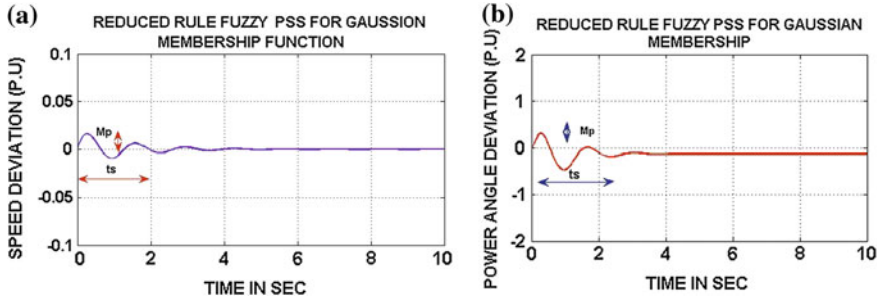


Fig. 14 Output of SMIB system reduced rule Fuzzy PSS for Gaussian membership function **a** Speed Deviation ($\Delta\omega$), **b** Power angle Deviation ($\Delta\delta$) of generator

Deviation ($\Delta\delta$) of generator are shown in Fig. 14. The responses clearly show that system has much larger overshoot (M_p), smaller settling time (t_s) and error steady state 0 and 1.5 for Speed Deviation and Power angle respectively.

5 Conclusion

In this paper initially the effectiveness of power system stabilizer is reviewed. The proposed method has been simulated on a SMIB Energy system with FLC and conventional controller using complete state space model. The Matlab/Simulink simulation results showed that in the presence of small disturbances in the system, fuzzy controller is more effective as compared to the conventional controller. The Fuzzy Logic Power System Stabilizer gives zero steady state error, smaller overshoot and settling time as compared to conventional power system stabilizer. The Fuzzy PSS with SMIB system is simulated for Triangular, Trapezoidal and Gaussian membership functions for input and output. The Fuzzy PSS for Triangular membership function gives best performance (Table 3).

The simulation results further confirmed that the proposed Reduced Rule Fuzzy logic Power System Stabilizer with simple design approach and smaller rule base can provide better performance for different membership functions as compared to the conventional power system stabilizer (CPSS) and Fuzzy Logic Power system stabilizer (Table 3). The Reduce Rule Fuzzy Logic Power System Stabilizer gives zero steady state error, much smaller overshoot and settling time compared to conventional and Fuzzy PSS.

Further, the Reduced Rule Fuzzy PSS is tested for Triangular, Trapezoidal and Gaussian membership functions for input and output. The Reduced Rule Fuzzy PSS with Trapezoidal membership function provide best performance (Table 3).

Appendix

Parameter Values

Generator: $M = 7.0$ s., $D = 0$, $X_d = 1.8$, $X_q = 1.76$, $X'_d = 0.3$, $T'_{do} = 7.2940$,
 $\omega_b = 314$

Exciter: (IEEE Type ST1): $K_A = 200$, $T_A = 0.02$ s.

$T_1 = 0.154$, $T_2 = 0.033$, $K_S = 9.5$, $T_W = 1.4$

$K_1 = 0.7636$, $K_2 = 0.8644$, $K_3 = 0.3231$, $K_4 = 1.4189$, $K_5 = 0.1463$, $K_6 = 0.4167$

Input1 = 1.8, Input2 = 29.56, Output = 1.06.

References

1. Kundur, P.: Power System Stability and Control. McGraw-Hill, New York (1994)
2. Gupta, N., Jain, S.K.: Comparative analysis of fuzzy power system stabilizer using different membership functions. *Int. J. Comput. Electr. Eng.* **2**(2) (2010)
3. Zadeh, L.A.: Outline of a new approach to the analysis of complex systems and decision processes. *IEEE Trans. Syst. Man Cybern.* **3**, 28–44 (1973)
4. Zadeh, L.A.: A theory of approximate reasoning. In: Hayes, J.E., Mikulich, L.I. (eds.) *Machine Intelligence*, pp. 149–196. Ellis Horwood/Wiley, New York (1979)
5. Zadeh, L.A.: A rationale for fuzzy control. *J. Dyn. Syst. Meas. Contr. Trans. ASME, Series G (USA)* **94**, 3–4 (1974)
6. Gurralla, G., Sen, I.: A modified heffron-phillip's model for the design of power system stabilizers. In: *Joint International Conference on Power System Technology and IEEE Power India Conference, POWERCON 2008*, pp. 1–6 (2008)
7. Larsen, E., Swann, D.: Applying power system stabilizers part i, ii, iii: practical considerations. In: *IEEE Transactions on Power Apparatus and Systems*, vol. PAS-100, no. 6, pp. 3034–3046, June 1981
8. Laskowski, T.L., DeMello, F.P., Nolan, P.J., Undrill, J.: Coordinated application of stabilizers in multi machine power system. In: *Proceedings of the Twenty-First Annual North-American Power Symposium*, vol. 9, no. 10, pp. 175–184, July 1989
9. Vournas, C., Mantzaris, J.: Application of pss modeling to stabilizer design for interarea oscillations. *IEEE Trans. Power Syst.* **25**(4), 1910–1917 (2010)
10. Watson, W., Manchur, G.: Experience with supplementary damping signals for generator static excitation systems. In: *IEEE Transactions on Power Apparatus and Systems*, vol. PAS-92, no. 1, pp. 199–203, Jan 1973
11. Radman, G., Smali, Y.: Performance evaluation of pid power system stabilizer for synchronous generator. In: *Southeastcon '88, IEEE Conference Proceedings*, pp. 597–601, April 1988
12. Lin, Y.: Systematic approach for the design of a fuzzy power system stabilizer. In: *International Conference on Power System Technology, PowerCon 2004*, vol. 1, pp. 747–752, Nov 2004
13. Roosta, A., Khorsand, H., Nayeripour, M.: Design and analysis of fuzzy power system stabilizer. In: *Innovative Smart Grid Technologies Conference Europe (ISGT Europe), 2010 IEEE PES*, pp. 1–7, Oct 2010
14. Taher, A., Shemshadi, S.A.: Design of robust fuzzy logic power system stabilizer. *World Acad. Sci. Eng. Technol.* **2**(2), 153–159 (2007)

15. Kothari, M., Kumar, T.: A new approach for designing fuzzy logic power system stabilizer. In: International Power Engineering Conference, IPEC 2007, pp. 419–424, Dec 2007
16. Hussein, T., Saad, M., Elshafei, A., Bahgat, A.: Damping inter-area modes of oscillation using an adaptive fuzzy power system stabilizer. In: 16th Mediterranean Conference on Control and Automation, pp. 368–373, June 2008
17. Gupta, R., Bandyopadhyay, B., Kulkarni, A.: Design of power system stabiliser for single-machine system using robust periodic output feedback controller. In: IEE Proceedings of Generation, Transmission and Distribution, vol. 150, no. 2, pp. 211–216, March 2003
18. Dobrescu, M., Kamwa, I.: A new fuzzy logic power system stabilizer performances. In: Power Systems Conference and Exposition, IEEE PES, vol. 2, pp. 1056–1061, Oct 2004
19. Dysko, A., Leithead, W., O'Reilly, J.: Enhanced power system stability by coordinated pss design. In: IEEE Transactions on Power Systems, vol. 25, no. 1, pp. 413–422, Feb 2010
20. Gupta, R., Sambariya, D., Gunjan, R.: Fuzzy logic based robust power system stabilizer for multimachine power system. In: IEEE International Conference on Industrial Technology, ICIT 2006, pp. 1037–1042, Dec 2006
21. Hong, T.P., Lee, C.: Induction of fuzzy rules and membership functions from training examples. *Fuzzy Sets Syst.* **84**, 33–47 (1996)
22. Rose, T.J.: *Fuzzy Logic With Engineering Applications*. McGrawHill Inc, Newyork (1997)
23. Tayal, V.K., Lather, J.S.: Digital simulation of reduced rule fuzzy logic power system stabilizer for analysis of power system stability enhancement. *Int. J. Comput. Appl.* **47**(7), 888–975 (2012)

An Improved Quantum Inspired Firefly Algorithm with Interpolation Operator

A. Manju and M. J. Nigam

Abstract Firefly Algorithm (FA), a population based algorithm has been found superior over other algorithms in solving optimization problems. Later the authors formulated a quantum Delta potential well model for FA (QFA) by placing the fireflies in an exponent atmosphere with global updating operator and weighting function. In this paper, to improve the speed of convergence and provide a proper balance between local and global search ability of QFA, an interpolation based recombination operator for generating a new solution vector in the search space has been introduced. Above algorithm is compared with various other algorithms using several benchmark functions. Statistical performance using t-test on the results exhibits the superiority of proposed QFA.

Keywords Quantum inspired FA · QPSO · Exponential atmosphere · Interpolation

1 Introduction

Nature inspired optimization algorithms have been gaining its importance over past several decades wherein the steps in the process of evolution, communication between the animals in search of food, mates, territory etc. have been mathematically formulated. Quantum inspired version of such algorithms is found to meet the increase in complexity of technology and various real world problems [1]. Recent

A. Manju (✉) · M. J. Nigam
Department of Electronics and Computer Engineering,
Indian Institute of Technology Roorkee,
Roorkee, Uttarakhand 247667, India
e-mail: manju.senthil@gmail.com

A. Manju
SKP Engineering College, Tiruvannamalai, Tamilnadu 606611, India

member of such population based algorithm is firefly algorithm (FA) introduced by Yang [2] which can obtain global as well as local optima simultaneously and effectively. FA is superior over other algorithms in the sense that it could handle multimodal problems of combinational and numerical optimization more naturally and efficiently [3, 4].

In fact, FA befits exploiting search space not only by improving individuals' experience, but also obtaining a population of local optimal solutions simultaneously [5]. Another advantage is the independent working of fireflies making it suitable for parallel implementation. Fireflies accumulates strongly around each optimum and does not jump like Genetic algorithms (GA) [6]. Fireflies are assumed to be present in atmosphere of uniform density [2]. Motivated by the fact that the density of the atmosphere decays exponentially with height, named as exponential atmosphere model [7], recently the authors have improved the FA by placing the fireflies in exponential atmosphere where the extinction coefficient varies with distance between the fireflies [8]. Above algorithm when carried out using Global and weighing operator, provides an insight of analogy with the Quantum inspired particle swarm optimization (QPSO). Movement of fireflies in the exponential atmosphere has been found to be equivalent to a particle moving in a multi dimensional space, represented by a dirac delta function. Based on such analogy quantum Delta potential well model for FA (QFA) has been proposed by the authors [9]. Employing QFA on well known Benchmark problems exhibits stronger local and global searching capability of the algorithm.

Like any other evolutionary algorithm (EA), the performance of QFA deteriorates with the increase in dimensionality of the objective function. In an attempt to improve QFA, a quadratic interpolation based recombination operator has been used along with the algorithm. Quadratic interpolation enhances PSO and QPSO [10] which motivates the authors to employ it with QFA. The proposed algorithm is employed on various benchmark functions and comparison of the algorithm based on Statistical analysis (t-test) with other algorithms has been performed. Rest of the paper is organized as follows: In Sect. 2, the basic QFA is outlined, and Sect. 3 describes the proposed improved QFA. Experimental settings and results are presented in Sect. 4. Finally, the conclusion and further research are discussed in Sect. 5.

2 Quantum Inspired Firefly Algorithm

FA proposed by Yang [2] employs three idealized rules: (1) all fireflies are unisex so that one firefly will be attracted to other fireflies regardless of their sex; (2) Attractiveness is proportional to their brightness, thus for any two flashing fireflies, the less brighter one will move towards the brighter one. The attractiveness is proportional to the brightness and they both decrease as their distance increases. If there is no brighter one than a particular firefly, it will move

randomly; (3) The brightness of a firefly is affected or determined by the landscape of the objective function.

In FA, there is a swarm of m agents (fireflies) and x_i represents a solution for firefly i . Initially all fireflies are dislocated in S (randomly or employing some deterministic strategy). Each firefly has its distinctive attractiveness β which implies how strong it attracts other members of the swarm. Firefly attractiveness can be represented by monotonically decreasing function of the distance $r_j = d(x_i, x_j)$ to the chosen firefly j , e.g. the exponential function: $\beta = \beta_0 e^{-\gamma r_j}$, where $\beta_0 \in (0, 1)$ and $\gamma \in (0, 1)$ are predetermined algorithm parameters: maximum attractiveness value and absorption coefficient, respectively.

Furthermore every member of the swarm is characterized by its light intensity which can be directly expressed as an inverse of a cost function $f(x_i)$. To effectively explore the considered search space it is assumed that each firefly i is changing its position iteratively based on two factors: attractiveness of other swarm members with higher light intensity i.e. $I_j > I_i; \forall j = 1, \dots, m, j \neq i$ which is varying across distance and a fixed random step vector u_i : where $u_i = \alpha(r \text{ and } -\frac{1}{2})$, with $\alpha \in (0, 1)$, being algorithm's parameter. It should be noted as well that only if no brighter firefly can be found such randomized step is being used [2, 11].

It is worth pointing out that the exponent γr can be replaced by other functions such as γr^m when $m > 0$. Distance between any two fireflies i and j at x_i and x_j is measured as Cartesian distance.

The firefly i movement is attracted to another more attractive (brighter) firefly j is determined by:

$$x_i = x_i + \beta_0 e^{-\gamma r_{ij}^2} (x_j - x_i) + u_i \quad (1)$$

where the second term is due to the attraction, while the third term is randomization with the vector of random variable being drawn from a Gaussian distribution. Yang in [12] used Levy distribution instead of Gaussian one. The absorption coefficient γ is customized based on the characteristic length as given in [12].

Above firefly algorithms employed either constant or varying attenuation coefficient based on characteristic length of the search space. Fireflies are assumed to be present in atmosphere of uniform density. But typically, the density of the atmosphere decays exponentially with height named as exponential atmosphere model [7].

Using the above concept the attenuation coefficient in Eq. (1) is assumed to be exponentially varying with distance [8] as $\gamma = e^{-\delta r_{ij}}$, where the coefficient δ , proportional constant of density can be adjusted such as $\gamma \in (0, 1)$.

Inspired by Quantum mechanics and trajectory analysis of PSO [13] Delta potential well model of PSO was introduced by Sun et al. [14]. Unlike PSO, QPSO needs no velocity vectors for particles, and has fewer parameters to adjust, making it easier to implement. The iterative equation of QPSO is very different from that of PSO as given below

$$X_i(t + 1) = p_i(t) \pm \beta \cdot |mbest(t) - X_i(t)| \cdot \ln(1/u) \quad (2)$$

where *mbest* is the mean value of the pbest positions of all particles [14] and β is the only parameter of adjustment of speed of convergence, named as contraction-expansion coefficient.

Adding a global updation term and inertia weight factor to the FA updation formula of fireflies in exponential atmosphere [8] a quantum Delta potential well model for FA (QFA) has been arrived [9]. In the process of formulation of QPSO in [14] the potential energy of the particle, $V(x)$ is equated to a dirac delta function. In Basic FA with fireflies in atmosphere with constant attenuation coefficient, the velocity function does not constitute a dirac delta function. But when the fireflies are placed in exponentially varying attenuation coefficient, the potential energy of the particle can be equated to the function $V(x)$ in [14]. Searching procedure of proposed QFA is similar to that of QPSO except for the updation part which happens only when it finds the brighter ones.

3 Improved QFA with Interpolation Operator

Like any other EA, the performance of QFA deteriorates with the increase in dimensionality of the objective function. As suggested in [15], integration and hybridization of swarm algorithm with evolutionary parameters is performed to overcome each others weakness leading to a new approach. In an attempt to improve QFA, a quadratic interpolation based recombination operator has been used along with the algorithm. Quadratic operators are nonlinear multiparent (polygamy) crossover operator which makes use of three particles (parents) of the swarm to produce a particle (offspring) which lies at the point of minima of the quadratic curve passing through the three selected particles. This was found enhancing PSO and QPSO [10] which motivates the authors to employ it with QFA.

A new firefly in the search space is generated by invoking quadratic interpolation recombination operator [16]. At the end of each generation the new firefly is accepted in the algorithm if it is better than the worst particle. The process is repeated until a better solution is obtained. In this way diversity is increased as a new solution is created and included in the algorithm, apart from the usual way of retaining particle having the best fitness function value to take part in recombination process.

$$\text{The new solution } \tilde{x}^i = \frac{1}{2} \frac{(b^2 - c^2)f(a) + (c^2 - a^2)f(b) + (a^2 - b^2)f(c)}{(b^i - c^i)f(a) + (c^i - a^i)f(b) + (a^i - b^i)f(c)} \quad (3)$$

where $a = x_{\min}$ (the firefly having minimum (or best) fitness function value), $\{b, c\}$ = randomly chosen fireflies from the remaining members. (a, b and c should be three different fireflies). The computational steps of the improved algorithm is given below

- Step 1: Initialize the current positions and personal best positions of all the fireflies
 Step 2: For $t = 1$ to the maximum number of iterations, execute the following steps
 Step 3: Compute mean best position m_{best}
 Step 4: For each firefly in the population, execute from step 5 to 7.
 Step 5: Compute fitness value $f(x_i)$; if $f(x_i) < f(P_i)$ then $P_i = X_i$;
 Step 6: Select the gbest position $g = \arg \min (f(P_i))$; among fireflies.
 Step 7: Update each fireflies position using Eq. (2).
 Step 8: Find a new particle using Eq. (3)
 Step 9: If the new firefly is brighter than the worst firefly in the population
 Then replace the worst firefly by the new firefly.
 Step 10: Go to step 2 until maximum iterations reached.

4 Experiment Results

Proposed algorithm is tested on Five Benchmark functions, all minimization problems with minimum value zeros. Asymmetrical initialization as in [17] is employed. Mean best fitness and standard deviation are recorded for 100 trial runs. Scalability of the algorithm is investigated by considering different population sizes M and different dimensions. The population sizes are 20, 40 and 80 and the maximum generation is set as 1,000, 1,500 and 2,000 corresponding to the dimensions 10, 20 and 30 for five functions, respectively. The algorithms used for comparison are (i) Standard FA algorithm (FA), (ii) FA based on characteristic length (FA1), (iii) algorithm with exponential atmosphere concept (FA2), (iv) Global weighed FA (FA3), (v) QFA and (vi) QFA with interpolation operator. In all the cases value of β_0 is set to 1 and $\alpha = 0.2$, as in [12] and w decreases linearly from 0.9 to 0.4. $\gamma_0 = 0.8$ in characteristic length based FA and Proportional constant of density (δ) is set as 0.3 in case of exponential atmosphere.

Further to exhibit the superiority of the proposed algorithm, Standard PSO and QPSO algorithms described in [17] is also considered with the same experimental settings. Mean best fitness and standard deviation values for the functions are given in Tables 1, 2, 3, 4 and 5 revealing the striking potential of the proposed algorithm in obtaining the optimal solution with high precision. As in Tables 6, 7, 8, 9 and 10, all t-test values are high, exhibiting the improvement of QFA by the Interpolation operator for higher dimensions also. From Table 2 and 3 we can see that the standard deviation of FA3 is higher than the proposed QFA, exhibiting the spread of the fitness value from the mean. This is due to the introduced global operator in FA, predominant in multimodal function and unimodal with long curves. Above effect is vivid from their t- test values also.

Figures 1, 2, 3, 4 and 5 give the comparison of convergence processes of proposed QFA with other algorithms, when the population size is 20, dimension 30 and number of generations is 2,000. Sphere and Dejong's functions being unimodal are used to test local search ability of the algorithm. Faster convergence exhibited by the QFA with interpolation operator proves the corresponding

Table 1 Mean best fitness and standard deviation values for Sphere function

M	D	Gen	PSO		QPSO		FA		FA1		FA2		FA3		QFA		Proposed QFA	
			Mean	SD	Mean	SD	Mean	SD	Mean	SD	Mean	SD	Mean	SD	Mean	SD	Mean	SD
20	10	1000	1.18E-20	6.11E-20	1.69E-42	1.30E-41	2.19E-03	3.90E-03	4.77E-04	3.23E-04	9.63E-04	1.20E-03	9.56E-03	7.23E-03	2.59E-74	2.59E-73	1.82E-92	1.82E-91
20	1500	9.63E-12	1.98E-11	4.69E-24	1.58E-23	6.00E-03	3.06E-03	2.26E-03	9.11E-04	4.50E-03	2.18E-03	2.83E-02	2.39E-02	7.52E-73	7.50E-72	3.01E-124	2.99E-124	
30	2000	4.90E-08	9.49E-08	4.05E-16	1.44E-15	1.15E-02	3.70E-03	5.22E-03	1.59E-03	8.95E-03	2.65E-03	4.68E-02	3.80E-02	9.01E-91	8.63E-90	6.17E-170	0	
40	10	1000	7.79E-25	2.10E-24	1.71E-65	1.36E-64	2.26E-04	1.05E-04	2.39E-04	1.06E-04	2.47E-04	1.38E-04	4.92E-03	4.75E-03	1.28E-113	1.21E-112	5.94E-115	5.93E-114
20	1500	4.63E-15	1.90E-14	1.28E-36	1.10E-35	1.74E-03	6.39E-04	1.64E-03	5.11E-04	1.47E-04	4.92E-04	1.06E-04	1.09E-04	4.16E-141	3.12E-140	1.03E-159	1.02E-158	
30	2000	9.15E-11	1.95E-10	5.17E-25	3.09E-24	4.46E-03	1.30E-03	4.71E-03	1.34E-03	4.30E-03	1.17E-03	1.68E-02	2.05E-02	3.63E-176	3.63E-176	6.28E-209	0	
80	10	1000	3.12E-28	8.90E-28	3.80E-85	2.89E-84	1.84E-04	8.30E-05	1.96E-04	1.06E-04	1.87E-04	1.82E-03	2.22E-03	8.82E-136	8.81E-135	1.15E-141	1.01E-140	
20	1500	8.28E-18	4.68E-17	5.35E-52	2.94E-51	1.29E-03	4.62E-04	1.54E-03	5.71E-04	1.25E-04	4.95E-04	4.89E-03	6.50E-03	1.18E-181	1.18E-181	3.46E-194	0	
30	2000	1.82E-13	2.66E-13	8.02E-36	3.13E-35	3.62E-03	1.08E-03	4.63E-03	1.33E-03	3.68E-03	9.89E-04	9.09E-03	9.84E-03	2.25E-227	2.25E-227	2.44E-248	0	

Table 2 Mean best fitness and standard deviation values for Rosenbrock function

M	D	Gen	PSO		QPSO		FA		FAI		FA2	
			Mean	SD	Mean	SD	Mean	SD	Mean	SD	Mean	SD
20	10	1000	65.582	168.61	39.57	119.25	53.408	87.125	38.629	67.961	36.678	66.472
	20	1500	109.67	188.8	99.38	154.21	48.112	59.622	53.69	67.868	66.741	86.349
	30	2000	200.65	298.67	154.81	224.14	67.882	72.027	60.781	54.062	52.203	46.36
40	10	1000	46.564	112.07	11.19	16.789	22.497	43.206	23.918	45.671	23.01	50.077
	20	1500	92.531	213.95	44.224	43.275	52.332	72.799	31.892	42.829	47.191	71.556
	30	2000	141.34	211.33	62.852	55.626	56.239	70.8	49.391	64.428	58.354	73.408
80	10	1000	35.475	76.205	11.345	16.697	14.886	31.825	9.9847	26.548	17.915	44.333
	20	1500	71.857	111.17	45.069	40.055	42.707	68.296	50.189	65.255	35.226	44.333
	30	2000	101.19	187.22	48.856	37.756	41.52	62.834	44.523	61.53	47.539	64.878
M	D	Gen	FA3		QFA		Proposed QFA					
			Mean	SD	Mean	SD	Mean	SD				
20	10	1000	3.8119	1.3023	87.356	348.02	1.4479	2.8307				
	20	1500	23.197	2.8709	8.8819	8.85	4.9321	7.9534				
	30	2000	37.262	5.521	13.913	13.986	6.9208	12.05				
40	10	1000	8.9847	0.12347	45.911	216.19	0.90061	2.1651				
	20	1500	19.133	0.32548	18.033	88.533	2.8416	6.3147				
	30	2000	29.291	0.51942	23.851	79.232	5.8933	11.156				
80	10	1000	8.7266	1.2351	140.19	1034.8	0.14932	0.85376				
	20	1500	18.829	0.037857	6.4221	7.9161	1.0958	4.0181				
	30	2000	28.749	0.084254	10.196	12.819	2.5669	7.7411				

Table 3 Mean best fitness and standard deviation values for Rastrigin function

M	D	Gen	PSO		QPSO		FA		FAI		FA2	
			Mean	SD	Mean	SD	Mean	SD	Mean	SD	Mean	SD
20	10	1000	5.1563	2.4418	4.7148	3.4909	88.413	38.115	84.094	34.743	87.214	38.533
		1500	22.121	7.6619	15.208	6.016	138.18	84.484	146.93	72.955	162.99	78.447
		2000	45.724	11.315	28.43	7.2859	182.81	108.95	190.29	117.45	189.88	120.05
40	10	1000	3.3357	1.7706	3.1818	1.5456	5.4518	2.0305	4.98	2.3563	5.5358	2.0628
		1500	17.775	5.0668	11.469	3.9025	13.071	3.0708	14.679	4.7938	13.289	3.9222
		2000	36.73	9.2756	20.796	6.1488	20.26	3.67	23.258	10.398	20.405	4.0231
80	10	1000	2.2632	1.2555	2.1785	1.3371	4.1824	1.6572	3.1697	1.5	4.4783	1.9858
		1500	13.008	4.1074	8.2033	2.7839	13.338	4.014	12.415	3.9411	12.834	3.8901
		2000	28.607	8.6669	16.014	4.1973	20.923	4.9036	21.926	5.3552	20.102	4.5524
M	D	Gen	FA3		QFA		Proposed QFA					
			Mean	SD	Mean	SD	Mean	SD				
20	10	1000	3.9196	1.4599	8.6952	10.022	1.194	3.2495				
		1500	13.54	7.6727	21.155	31.211	3.6171	7.675				
		2000	19.544	13.739	44.691	57.094	6.8983	12.61				
40	10	1000	2.1617	1.1806	5.8208	9.2427	1.1964	3.212				
		1500	4.8702	6.349	15.026	21.844	1.9899	5.9998				
		2000	4.9653	5.7706	36.711	47.19	2.9849	8.9997				
80	10	1000	1.1368	1.2995	5.7036	7.7815	0.50421	2.2097				
		1500	3.4943	4.3938	13.926	20.678	0.98501	4.3161				
		2000	3.8439	3.4826	17.907	27.151	3.5819	9.7486				

Table 4 Mean best fitness and standard deviation values for Griewank function

D	Gen	PSO		QPSO		FA		FA1		FA2	
		Mean	SD	Mean	SD	Mean	SD	Mean	SD	Mean	SD
10	1000	0.09379	0.04139	0.056091	0.02684	20.784	6.2839	16.773	5.9496	9.5548	5.4478
20	1500	0.03038	0.02551	0.023126	0.027403	24.805	6.4427	17.979	6.1461	13.089	5.9867
30	2000	0.0167	0.01977	0.009603	0.016281	30.327	7.8781	12.146	5.6935	16.042	5.9259
10	1000	0.08145	0.04116	0.051093	0.044666	11.247	3.9142	9.2343	4.489	5.0876	3.2736
20	1500	0.02746	0.0251	0.021885	0.026903	1.3131	0.77201	0.23411	0.25348	0.1904	0.36629
30	2000	0.01369	0.02099	0.010742	0.01381	0.20118	0.34643	0.07252	0.07285	0.02512	0.03523
10	1000	0.07301	0.03723	0.037018	0.025545	10.397	4.6273	5.7382	2.9013	2.2372	1.5758
20	1500	0.03104	0.02305	0.014062	0.01345	0.11979	0.33642	0.3264	0.37002	2.2372	0.39164
30	2000	0.01283	0.01533	0.009763	0.014969	0.02347	0.022503	0.11947	0.0981	0.02873	0.03191
D	Gen	FA3		QFA		Proposed QFA					
		Mean	SD	Mean	SD	Mean	SD	Mean	SD	Mean	SD
10	1000	46.912	47.133	9.57E-02	1.65E-01	1.33E-02	7.48E-02				
20	1500	105.13	106.03	7.58E-03	5.63E-02	4.44E-18	2.19E-17				
30	2000	142.75	155.62	1.27E-16	4.31E-16	3.33E-18	2.47E-17				
10	1000	61.079	57.095	4.63E-02	9.66E-02	2.79E-02	7.92E-02				
20	1500	119.98	108.61	3.46E-03	3.46E-02	1.11E-18	1.11E-17				
30	2000	148.56	174.76	1.80E-03	1.80E-02	0	0				
10	1000	77.006	61.454	2.48E-02	6.18E-02	2.39E-02	6.19E-02				
20	1500	131.76	116.55	3.33E-18	2.47E-17	0	0				
30	2000	134.88	148.83	4.44E-18	3.50E-17	0	0				

Table 5 Mean best fitness and standard deviation values for De Jong's function

M	D	Gen	PSO		QPSO		FA		FA1		FA2	
			Mean	SD	Mean	SD	Mean	SD	Mean	SD	Mean	SD
20	10	1000	7.13E-32	2.54E-31	5.41E-31	5.38E-65	2.58E-01	2.42E+00	1.37E-06	2.91E-06	3.86E-06	7.05E-06
20	1500	4.02E-13	2.57E-12	4.14E-30	3.78E-29	5.29E-03	4.27E-02	2.45E-05	1.91E-05	1.91E-05	1.24E-04	1.68E-04
30	2000	8.90E-07	2.98E-06	1.33E-19	7.85E-19	1.91E-03	1.87E-03	1.49E-04	1.02E-04	1.02E-04	7.16E-04	5.60E-04
40	10	1000	4.36E-37	4.20E-36	6.35E-97	6.35E-96	1.40E-07	1.44E-07	6.92E-08	6.36E-08	1.31E-07	1.78E-07
20	1500	3.82E-18	1.79E-17	3.98E-51	3.67E-50	6.96E-06	6.08E-06	3.65E-06	2.82E-06	2.82E-06	6.05E-06	4.11E-06
30	2000	3.65E-10	1.10E-09	2.10E-33	1.01E-32	5.25E-05	3.11E-05	3.17E-05	1.67E-05	1.67E-05	4.58E-05	2.40E-05
80	10	1000	1.27E-45	5.11E-45	7.43E-132	7.43E-131	4.96E-08	6.19E-08	5.02E-08	5.98E-08	6.41E-08	9.91E-08
20	1500	1.22E-22	6.08E-22	2.15E-71	1.60E-70	3.25E-06	2.99E-06	2.68E-06	1.85E-06	1.85E-06	2.87E-06	2.14E-06
30	2000	7.72E-14	3.11E-13	1.72E-46	9.92E-46	3.20E-05	2.19E-05	2.24E-05	1.34E-05	1.34E-05	2.58E-05	1.59E-05
M	D	Gen	FA3		QFA		Proposed QFA					
			Mean	SD	Mean	SD	Mean	SD				
20	10	1000	1.30E-04	1.98E-04	3.57E-148	2.59E-147	3.16E-172	0				
20	1500	1.25E-03	1.74E-03	1.09E-181	0	3.72E-262	0					
30	2000	2.66E+07	1.90E+08	2.67E-204	0	0	0					
40	10	1000	2.54E-05	4.35E-05	7.13E-193	0	4.41E-227	0				
20	1500	3.28E-04	5.28E-04	3.53E-274	0	0	0					

(continued)

Table 5 (continued)

M	D	Gen	FA3		QFA		Proposed QFA	
			Mean	SD	Mean	SD	Mean	SD
80	30	2000	7.49E-04	1.78E-03	0	0	0	0
	10	1000	4.70E-06	9.71E-06	6.81E-274	0	1.55E-266	0
	20	1500	1.32E-04	4.37E-04	0	0	0	0
	30	2000	3.02E-04	1.22E-03	0	0	0	0

Table 6 t-test value for Sphere function: comparison of proposed QFA with other algorithms

M	D	Gen	PSO	QPSO	FA	FA1	FA2	FA3	QFA
20	10	1000	1.93E + 00	1.3009	5.619082	14.78231	8.045625	13.2164	1.0011196
	20	1500	4.87E + 00	2.976255	19.61559	24.85507	20.62131	11.85208	1.0034552
	30	2000	5.16E + 00	2.813225	31.17322	32.87982	33.71603	12.32457	1.0442879
40	10	1000	3.71E + 00	1.258081	21.56479	22.52706	17.9471	10.35812	1.0013954
	20	1500	2.43E + 00	1.157876	27.28169	32.15622	29.8959	0.097958	1.3351077
	30	2000	4.68E + 00	1.672562	34.33377	35.03385	36.94447	8.185147	+ inf
80	10	1000	3.50E + 00	1.313831	22.17579	18.47386	17.4736	8.212404	0
	20	1500	1.77E + 00	1.822145	27.88343	26.95178	25.18045	7.513184	+ inf
	30	2000	6.84E + 00	2.565003	33.58867	34.88048	37.23554	9.232777	+ inf

Table 7 t-test value for Rosenbrock function: comparison of proposed QFA with other algorithms

M	D	Gen	PSO	QPSO	FA	FA1	FA2	FA3	QFA
20	10	1000	3.80E + 00	3.195922	5.960711	5.466207	5.295192	7.586887	2.4684
	20	1500	5.54E + 00	6.116499	7.178686	7.135396	7.127861	21.60073	3.3195222
	30	2000	6.48E + 00	6.588558	8.347646	9.72405	9.4534	22.8911	3.7875401
40	10	1000	4.07E + 00	6.078315	4.992206	5.034172	4.410958	37.27762	2.0818786
	20	1500	4.19E + 00	9.462447	6.772793	6.710337	6.173865	25.76496	1.7115544
	30	2000	6.40E + 00	10.03967	7.024308	6.652375	7.065332	20.9505	2.2443327
80	10	1000	4.64E + 00	6.696456	4.62887	3.702839	4.006583	57.12631	1.3533111
	20	1500	6.36E + 00	10.92338	6.082255	7.509064	7.667172	44.13134	5.9997838
	30	2000	5.26E + 00	12.01023	6.152848	6.765471	6.882973	33.82019	5.0945489

Table 8 t-test value for Rastrigin function: comparison of proposed QFA with other algorithms

M	D	Gen	PSO	QPSO	FA	FA1	FA2	FA3	QFA
20	10	1000	9.75E + 00	7.382311	22.80041	23.75724	22.24476	7.651063	7.1198325
	20	1500	1.71E + 01	11.88589	15.8623	19.5362	20.21946	9.143454	5.4565818
	30	2000	2.29E + 01	14.78467	16.03902	15.52522	15.15873	6.781026	6.463609
40	10	1000	5.83E + 00	5.56989	11.19847	9.497934	11.3676	2.820784	4.7260531
	20	1500	2.01E + 01	13.24394	16.44084	16.52287	15.7631	3.297269	5.754693
	30	2000	2.61E + 01	16.34099	17.77414	14.7421	17.67105	1.852424	7.0203458
80	10	1000	6.92E + 00	6.48258	13.31674	9.980397	13.37677	2.467692	6.4276015
	20	1500	2.02E + 01	14.05422	20.95808	19.55603	20.39247	4.074135	6.1263052
	30	2000	1.92E + 01	11.71316	15.89119	16.49256	15.35445	0.253091	4.9657022

improvement in local search process (Figs. 1 and 5). Multimodal functions like Rastrigin and Griewank demands slower searching as the sign of improvement in global search. But significant improvement in exploration is not found as the required minima are obtained very soon (around 250 generations in case of Griewank and 1,000 for Rastrigin function) and the process of Global searching is not improved (Figs. 2 and 3). Monomodal function like Rosenbrock, with long curves and slightly decreasing valley where the particles are ought to escape from the

Table 9 t-test value for Griewank function: comparison of proposed QFA with other algorithms

M	D	Gen	PSO	QPSO	FA	FA1	FA2	FA3	QFA
20	10	1000	9.41E + 00	5.377823	33.05142	28.16716	17.51268	9.950268	4.5569569
	20	1500	1.19E + 01	8.439222	38.50094	29.2527	21.86346	9.915118	1.3466719
	30	2000	8.45E + 00	5.898348	38.49532	21.3331	27.07099	9.172985	2.8565368
40	10	1000	6.00E + 00	2.551025	28.65671	20.50562	15.45156	10.69289	1.4746499
	20	1500	1.09E + 01	8.134781	17.00885	9.235837	5.198067	11.04686	1
	30	2000	6.52E + 00	7.778421	5.807234	9.953469	7.130529	8.500801	1
80	10	1000	6.80E + 00	1.958846	22.41517	19.69117	14.03474	12.52678	0.1013027
	20	1500	1.35E + 01	10.45502	3.560728	8.821145	57.12389	11.30502	1.3470981
	30	2000	8.37E + 00	6.522279	10.42839	12.17851	9.00188	9.062689	1.2687561

Table 10 t-test value for Dejong function: comparison of proposed QFA with other algorithms

M	D	Gen	PSO	QPSO	FA	FA1	FA2	FA3	QFA
20	10	1000	2.80E + 00	1.005255	1.064479	4.694397	5.472177	6.58523	1.3792252
	20	1500	1.56E + 00	1.094861	1.238772	12.82747	7.382698	7.172007	+ inf
	30	2000	2.99E + 00	1.697209	10.20559	14.67721	12.79232	1.400179	+ inf
40	10	1000	1.04E + 00	1.000299	9.738858	10.87919	7.332287	5.838485	+ inf
	20	1500	2.14E + 00	1.083669	11.44347	12.95319	14.73208	6.201063	+ inf
	30	2000	3.31E + 00	2.084407	16.85759	19.06727	19.11422	4.20384	+ inf
80	10	1000	2.48E + 00	1	8.015767	8.396435	6.475084	4.844067	+ inf
	20	1500	2.01E + 00	1.340916	10.9005	14.4946	13.40723	3.024149	+ inf
	30	2000	2.49E + 00	1.734166	14.62463	16.67362	16.21199	2.469169	+ inf

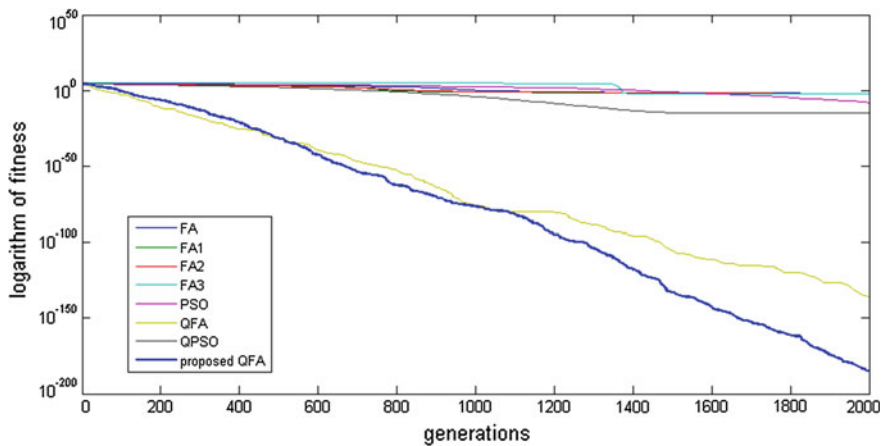


Fig. 1 Comparison of convergence process in Sphere function

narrow area of the optimal solution, tests both the local and global search ability of the algorithm. QFA offers better results when compared to QFA with interpolation operator in such cases (Fig. 4).

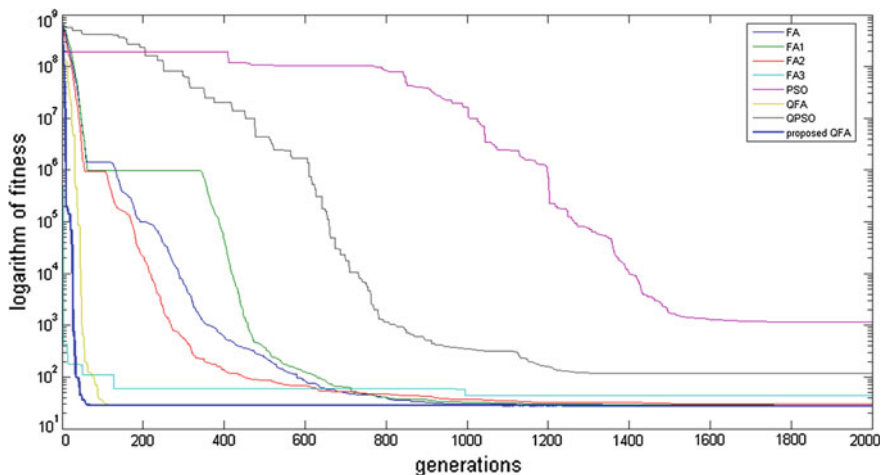


Fig. 2 Comparison of convergence process in Rosenbrock function

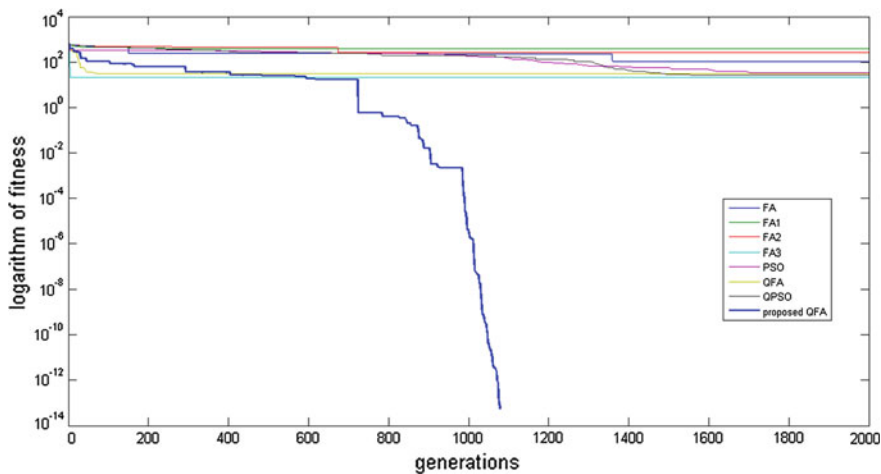


Fig. 3 Comparison of convergence process in Rastrigrin function

Since the parameter setting in QFA is same as in QFA with interpolation operator, faster convergence of QFA with interpolation operator owes to the effect of variation operator. Presence of such recombination operator leads the fireflies to converge quickly to the global best, thereby improving local searching at the stake of global searchability.

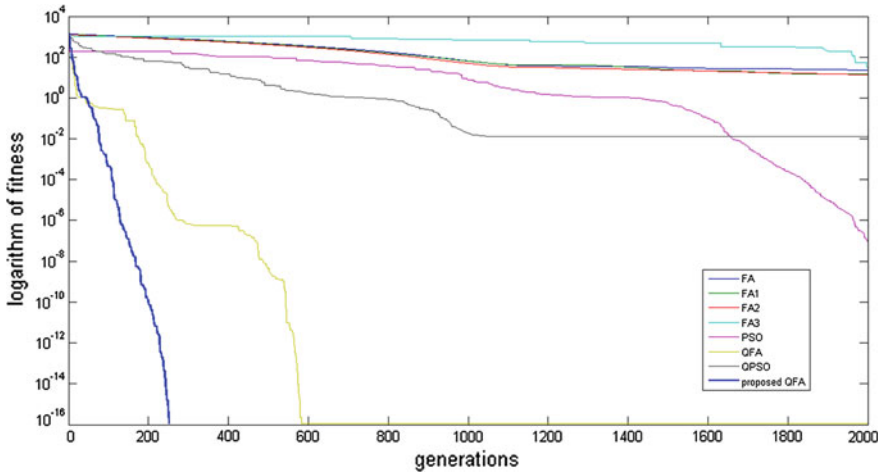


Fig. 4 Comparison of convergence process in Griewank function

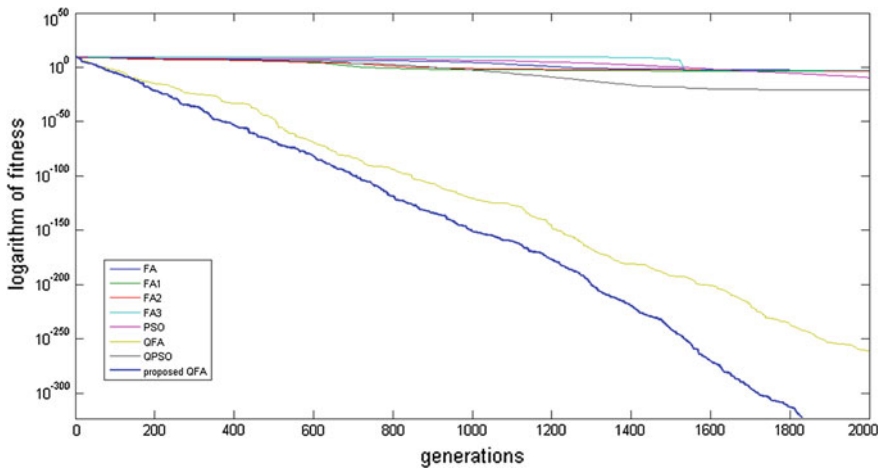


Fig. 5 Comparison of convergence process in De Jong's function

5 Conclusions and Further Research

Following the foot steps of formulation of QPSO from PSO algorithm, we have described the quantum-behaved Firefly algorithm from FA. Searching process of QFA is improved using Interpolation based recombination operator. Disadvantage of premature and slow convergence of QFA has been dealt by the proposed algorithm as demonstrated by the simulation results. Introduction of various other operators and hybridization of the algorithm to improve the tradeoff between exploration and exploitation would be an interesting direction in future.

References

1. Manju, A., Nigam, M.J.: Applications of quantum inspired computational intelligence: a survey. *Art. Intel. Rev.* (2012). doi:[10.1007/s10462-012-9330-6](https://doi.org/10.1007/s10462-012-9330-6)
2. Yang, X.S.: *Nature-Inspired Metaheuristic Algorithms*. Luniver Press, UK (2008)
3. Yang, X.S.: Firefly algorithm, stochastic test functions and design optimization. *Int. J. Bio-Insp. Comput.* **2**, 78–84 (2010)
4. Yang, X.S., Hosseini, S.S., Gandomi, A.H.: Firefly algorithm for solving non-convex economic dispatch problems with valve loading effect. *App. Soft Comp.* **12**, 1180–1186 (2012)
5. Chai-ead, N., Aungkulanon, P., Luangpaiboon, P.: Bees and firefly algorithms for noisy non-linear optimisation problems. In: *Proceedings of International Multi Conference of Engineers and Computer Scientists*, vol. 2, pp. 1449–1454 (2011)
6. Gandomi, A.H., Yang, X.-S., Talatahari, S., Alavi, A.H.: Firefly algorithm with chaos. *Comm. Nonlinear Sci. Num. Sim.* **18**, 89–98 (2013)
7. Tewari, A.: *Atmospheric and space flight dynamics modeling and simulation with MATLAB and Simulink*. Birkhäuser, Basel, Berlin, Boston (2007)
8. Manju, A., Nigam, M.J.: Application of exponential atmosphere concept in improving firefly algorithm. 3rd International Conference on Computing and Communication Networking Technology (ICCCNT), pp. 1–6 (2012). doi:[10.1109/ICCCNT.2012.6395946](https://doi.org/10.1109/ICCCNT.2012.6395946)
9. Manju, A., Nigam, M.J.: Firefly algorithm with fireflies having quantum behavior. In: *Proceedings of 2012 International Conference on Radar, Communication and Computing (ICRCC)*, pp. 117–119 (2012). doi: [10.1109/ICRCC.2012.6450559](https://doi.org/10.1109/ICRCC.2012.6450559)
10. Pant, M., Radha, T., Abraham, A.: A new quantum behaved particle swarm optimization. In: *Proceedings of 10th Annual Conference on Genetic and Evolutionary Computation (GECCO-08)*, pp. 87–94 (2008)
11. Lukasik, S., Zak, S.: Firefly Algorithm for Continuous Constrained Optimization Tasks. In: Nguyen, N., Kowalczyk, R., Chen, S.-M. (eds.) *Computational collective intelligence. Semantic Web, Social Networks and Multiagent Systems*, LNCS, vol. 5796, pp. 97–106. Springer, Heidelberg (2009)
12. Yang, X.S.: Firefly algorithm, levy flights and global optimization. In: Bramer, M., Ellis, R. (eds.) *Research and Development in Intelligent Systems*, vol. 26, pp. 209–218 (2010)
13. Clerc, M., Kennedy, J.: The particle swarm: explosion, stability, and convergence in a multidimensional complex space. *IEEE Trans. Evol. Comput.* **6**, 58–73 (2002)
14. Sun, J., Feng, B., Xu, W.B.: Particle swarm optimization with particles having quantum behavior. In: *IEEE Proceedings of Congress on Evolutionary Computation*, 325–331. (2004)
15. Angeline, P.J.: Evolutionary optimization versus particle swarm optimization: philosophy and performance difference. In: *7th Annual Conference on evolutionary programming*, San Diego, USA (1998)
16. Ali, M.M., Torn, A.: Population set based global optimization algorithms: Some modifications and numerical studies. www.ima.umn.edu/preprints/ (2003)
17. Xi, M., Sun, J., Xu, W.: An improved quantum-behaved particle swarm optimization algorithm with weighted mean best position. *App. Math. Compu.* **205**, 751–759 (2008)

Discrete Wavelet Transform Based Fault Detection and Classification in a Static Synchronous Series Compensated Transmission System

M. Geethanjali, M. Anju Alias and T. Karpaga Senthil Pandey

Abstract Protection of a transmission line which includes Flexible AC Transmission system (FACTS) devices using distance protection is a challenging task. In this paper, a power system with Static Synchronous Series Compensator (SSSC) is placed at the center of the transmission line is taken into analysis. In this paper a statistical algorithm is proposed which detects and classifies the type of fault and locates it in the SSSC compensated transmission line. The proposed algorithm is based on wavelet transform of the three phase current measured on the sending end of the line and Classification And Regression Tree (CART), a commonly available statistical method is used to classify the fault. Wavelet transform of current signal provides the hidden information of the fault location which is the input to the CART. The algorithm developed is simple and effective in detecting, classifying, and estimating the location of fault. The effective and efficient way of handling faults are exhibited using various fault cases and their corresponding simulation also shows it.

Keywords Series compensation · Fault classification · SSSC · Discrete wavelet transform and wavelet entropy

M. Geethanjali (✉) · M. Anju Alias · T. Karpaga Senthil Pandey
Department of Electrical and Electronics Engineering, Thiagarajar College of Engineering,
Madurai, India
e-mail: mgeee@tce.edu

M. Anju Alias
e-mail: anjualiasm@gmail.com

T. Karpaga Senthil Pandey
e-mail: tkspandy@gmail.com

1 Introduction

In the present energy scenario, it is not easy to develop new generation facilities and transmission infrastructure to meet the energy crisis and environmental consensus. Therefore it is vital to utilize the energy generated properly and to enhance the power transfer capability of the present power transmission system. The power flow is a function of the transmission line impedance, magnitude of the sending and receiving end voltages and the phase angle between two voltages. By controlling anyone of these power flow parameter, it is possible to control active and reactive power flow in the transmission line. The above technique is accomplished with the help of FACTS devices. During fault, the presence of FACTS devices in the network affects the steady state and transient character of the current and voltage signal which has the impact in the operation of the relay and its function.

Few researchers determined the fault location and fault resistance with the use of current and voltage signals without classifying the fault type and phases involved [1]. Protection of compensated and uncompensated transmission line is discussed in literatures [2, 3]. A number of algorithms insisting series compensation as well as TCSC compensation were proposed for fault location and classifying them through numerical methods, fuzzy logic and wavelet transform [1–5].

In this paper, a static synchronous series compensators (SSSC) is used as FACTS device in the power transmission system. SSSC is placed at the midpoint of the transmission system and provides required compensation for the system. The SSSC generates nearly three phase sinusoidal voltage that is in quadrature with line current with help of power electronics based voltage source converter. As the name of FACTS indicates it is connected in series to the transmission line using series coupled transformer. The SSSC is designed to provide inductive or capacitive compensation as per power system loading condition [6]. The SSSC is preferred over the TCSC compensated transmission line. The problems encountered with TCSC are as follows: (i).Significant increase of steady state current with series compensation which may be greater than line to ground fault current (ii). The protection arrangement using metal oxide varistor (MOV) protects the capacitor from overvoltage during fault. (iii). Inversion of voltage and current and The harmonics in voltage and current signal produced due to the decaying DC component due to resonance between the system inductance and capacitance and other non fundamental frequency related issues in the system [7–11].

In this paper, a test system is built using MATLAB/SIMULINKVersion7.10.0.499 (R2010a). The proposed power system model is a simple 11 kV network equipped with the SSSC at the midpoint of transmission line via series coupling transformer.

The test system is shown in Fig. 1.

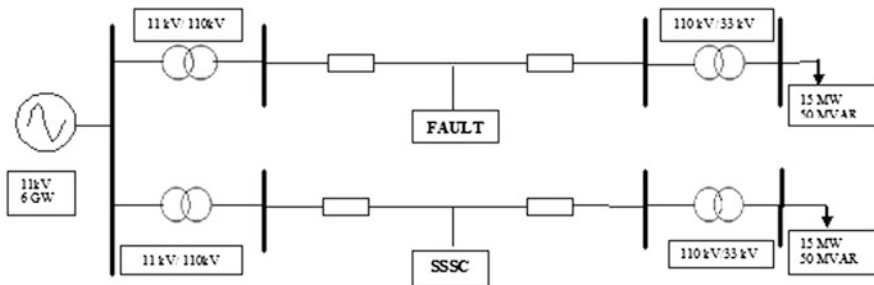


Fig. 1 One line diagram of test system

2 Wavelet Analysis

Wavelet transform is a mathematical high precise tool for signal processing and specially suited for non stationary and non periodic wide band signals. The Wavelet transform produces a time scale which is used for localizing both time and frequency. The continuous wavelet transform (CWT) of a continuous signal $x(t)$ is given by Eq. (1).

$$CWT(a, b) = \int_{-\infty}^{\infty} x(t) \Psi_{a,b}^* dt \tag{1}$$

where $\Psi(t)$ is called as the mother wavelet because it belongs a family of special wavelets which is given by $\psi_{a,b}(t) = \frac{1}{\sqrt{a}} \Psi_{a,b}^* \left(\frac{t-b}{a}\right)$ are its scaled and shifted versions, the constants ‘a’ corresponds to scaling parameter and constant ‘b’ corresponds to the shifting parameter. In this paper, DWT is used for the fault classification purpose. The DWT of a digital signal $x(t)$ is given by Eq. (2).

$$DWT(x, m, n) = \frac{1}{\sqrt{a_0^m}} \sum_m \sum_n x(k) \psi * \left(\frac{k - nb_0 a_0^m}{a_0^m}\right) \tag{2}$$

where $a = a_0^m$ $b = nb_0$ a_0^m ; a_0 , b_0 are fixed constants and generally assigned as $a_0 = 2$ and $b_0 = 1$. k , m and n are integers.

The DWT is implemented by multi resolution analysis (MRA). In this DWT process, the input signal is analyzed at various frequency bands and resolution. The signal is decomposed into approximate and detailed versions with the help of successive high pass and low pass filters. Every stage of decomposition are called as level. The details obtained at various levels comprises of the features for the fault detection and classification.

3 SSSC Mathematical Model

The SSSC is operated in voltage control mode, and therefore, a voltage-controlled voltage source inverter (VC-VSI) is used as SSSC hardware. The SSSC injects three-phase voltages in series with the line connecting the load with the supply system. For the SSSC, an energy storage device is used on the DC bus of the inverter to produce the desired (phase and magnitude) output voltages. The SSSC circuit can be represented by following mathematical equations.

$$e_{a,b,c} = (R_c + R_t)i_{ca,cb,cc} + (L_c + L_t) \frac{di_{ca,cb,cc}}{dt} \quad (3)$$

where $R_t = R_{ts} + R_{tp}$ is the injection transformer windings resistance and $L_t = L_{ts} + L_{tp}$ is the injection transformer windings leakage inductance. The quantities (e_a, b, c) are the inverter (SSSC power converter) pole voltages. The three-phase output currents of the SSSC are obtained by solving the differential equations in Eq. (3). As shown in Eq. (4), for series compensation, the injected voltage vectors produced by the SSSC are added with the supply voltage vectors, resulting in compensation of the desired reactive power.

$$v_{sa, sb, sc} = v_{an, bn, cn} - R_s i_{sa, sb, sc} - L_s \frac{di_{sa, sb, sc}}{dt} + v_{abc_inj} \quad (4)$$

The injected voltage ($V_{a-inj}, b-inj, c-inj$) imposed on the injection transformer primary are realised by the voltage control of the SSSC power circuit. The mathematical relationship between the injected voltages and inverter currents are given in Eq. (5).

$$v_{abc_inj} = (R_{ts} + R_{tp})i_{ca,cb,cc} + (L_{ts} + L_{tp}) \frac{di_{ca,cb,cc}}{dt} \quad (5)$$

3.1 SSSC Control Scheme

Unlike Shunt compensation, the SSSC system requires a constant DC bus voltage, which is ensured by using a 700 V DC supply to feed power to SSSC DC bus. The load currents (i_{La}, L_b, L_c) are sensed, and the voltages appearing at both sides ((V_{aS}, bS, cS) and (V_{Sa}, Sb, Sc)) of the injection transformer are computed to determine the real (p) and reactive (q) powers consumed by the load and fed by the supply system. The difference between the reactive power consumed by the load and supplied by the source is produced by the SSSC. The instantaneous value of real (p) and reactive (q) powers consumed by the load and supplied by the source are expressed in Eq. (6).

$$\begin{aligned}
p_{supply} &= v_{\alpha s} i_{s\alpha} + v_{\beta s} i_{s\beta} \\
q_{supply} &= -v_{\beta s} i_{L\alpha} + v_{\alpha s} i_{L\beta} \\
p_{load} &= v_{\alpha s} i_{s\alpha} + v_{\beta s} i_{s\beta} \\
q_{load} &= -v_{\beta s} i_{L\alpha} + v_{\alpha s} i_{L\beta}
\end{aligned} \tag{6}$$

To eliminate voltage sag at the PCC, it is preferred that the majority of the reactive power consumed by the load be produced by the SSSC via PI controller based scheme, The required reactive power (q) is obtained from the difference between the load side reactive power demand and the supply side reactive power output. Shown in Eq. (7) the SSSC reference voltages in α - β frame ($v^*\alpha_{inj}$, $v^*\beta_{inj}$) are computed using the desired value of reactive power that is to be supplied from the SSSC.

$$\begin{bmatrix} v_{\alpha}^*_{inj} \\ v_{\beta}^*_{inj} \end{bmatrix} = \begin{bmatrix} i_{L\alpha} & i_{L\beta} \\ -i_{L\beta} & i_{L\alpha} \end{bmatrix}^{-1} \begin{bmatrix} p = 0 \\ \bar{q}^* \end{bmatrix} \tag{7}$$

In Eq. (7), setting the real power (p) equal to zero ensures that the SSSC feeds only reactive power and requires the minimal amount of energy storage on its DC bus. For voltage control, the α - β frame ($v^*\alpha_{inj}$, $v^*\beta_{inj}$) reference voltages are transformed into the abc reference frame. After being transformed into the abc reference frame, these reference voltages are compared with the actual injected voltages (voltages across injection transformer). The obtained difference voltage signals are compared with a triangular waveform control signal. Comparison of the difference voltage signals with the triangular wave form results in switching signals for the SSSC devices. The switching signals ensure that actual injected voltages follow the reference injected voltages.

4 Wavelet Transform and Entropy Calculation

In this paper, the wavelet entropy theory is applied to detect, classify and to identify the fault position. Wavelet entropy (WE) is formed by combining Wavelet transform and Shannon entropy together. The collective operation of the wavelet entropy will ensure the usage of advantage of both methods to explain the characteristics of the signal. Wavelet transform of transient signal is expressed by multi-resolution decomposition fast algorithm. The approximation coefficients are the high-scale, low-frequency components of the signal produced by filtering the signal by a low-pass filter. The detailed coefficients are the low-scale, high-frequency components of the signal produced by filtering the signal by a high-pass filter.

Let $x(n)$ be the discrete input signal. The input signal $x(n)$ is transformed at instant 'k' and with scale 'i'. It has a high frequency component coefficient $D_i(k)$

and a low frequency component coefficient $A_i(k)$. The reconstruction is made through $D_i(k)$ and $A_i(k)$.

$$\begin{aligned}
 D_i(k) &: [2^{-(i+1)}f_s, 2^{-i}f_s] \\
 A_i(k) &: [0, 2^{-(i+1)}f_s] \quad i = 1, 2, \dots, m
 \end{aligned}
 \tag{8}$$

where f_s is the sampling frequency.

The original input signal $x(n)$ [7] can be described by the sum of all components

$$\begin{aligned}
 x(n) &= D_1(n) + A_1(n) + D_2(n) + A_2(n) \\
 &= \sum_{i=1}^n D_i(n) + A_i(n)
 \end{aligned}
 \tag{9}$$

Non Normalized Shannon entropy is used in this paper. The non normalized Shannon entropy is given by [7] Eq. (10)

$$E_i = - \sum_k E_{ik} \log E_{ik}
 \tag{10}$$

where E_{ik} is the wavelet energy spectrum at scale i and instant k and it is defined as in Eq. (11)

$$E_{ik} = |D_i(k)|^2
 \tag{11}$$

5 Proposed Wavelet Entropy Algorithm

1. Get the values of three phase current and ground current. Ground current is obtained as a sum of three phase current.
2. Apply the discrete wavelet transform and compute the entropy of current coefficient.
3. Compute the summation of absolute entropies of the coefficients of each current (sumia, sumib, sumic, sumig).
4. Denote PP1 with the phase having maximum entropy sum (A, B, C).
5. Denote PP2 with the phase having second maximum entropy sum (A, B, C).
6. Denote PP3 with the phase having minimum entropy sum (A, B, C).
7. Check if sumig < threshold:- No Fault condition is observed.
8. Check else if sumig < 1:- LL Fault (Line to Line Fault), Phases included:- PP1 and PP2, Distance measurement is performed on basis of PP1.
9. Check else if sumig < PP3:- LLLG Fault (Three Phase Fault), Phases included:- PP1, PP2, PP3 and Ground, Distance measurement is performed on basis of PP1.
10. Check else if sumig < PP2:- LLG Fault (Double Line to Ground Fault), Phases included:- PP1, PP2 and Ground, Distance measurement is performed on basis of PP1.
11. Check else if sumig < PP1:- LG Fault (Single Line to Ground Fault), Phases included:- PP1 and Ground, Distance measurement is performed on PP1.

Table 1 Sum of absolute entropies of current coefficients

Fault type	Sumia	Sumib	Sumic	Sumig
AG	2.5483×10^7	5.8703×10^5	4.1480×10^5	1.6964×10^7
BG	4.5765×10^5	2.8271×10^7	4.0080×10^5	1.9092×10^7
CG	3.7388×10^5	6.6103×10^5	2.9192×10^7	1.9740×10^7
ABG	4.6055×10^7	4.0620×10^7	4.2309×10^5	1.0481×10^7
BCG	4.2071×10^5	5.5829×10^7	4.8236×10^7	1.2320×10^7
CAG	3.9857×10^7	6.5025×10^5	4.9017×10^7	1.2789×10^7
ABCG	4.9467×10^7	5.9098×10^7	6.0642×10^7	2.6895×10^6
AB	4.7952×10^7	3.9743×10^7	3.3125×10^5	0.0062
BC	3.2136×10^5	4.4413×10^7	4.2364×10^7	0.0054
CA	4.0987×10^7	5.3583×10^5	3.8513×10^7	0.0049
No fault	3.2134×10^5	5.3581×10^5	3.3126×10^5	0

6 Results and Discussion

As shown in Table 1, in case of no fault in the system, 'sumig' is less than threshold which is equal to 4×10^{-4} i.e. almost zero. In LL fault, 'sumig' is less than 1. For example, for a BC fault, 'sumib' and 'sumic' are greater than sumia. In the case of other faults like LLLG, LLG and LG faults 'sumig' is greater than 1000, because ground is included in each case. In LG fault, for example an AG fault, 'sumia' is greater than 'sumib' and 'sumic'. Similarly in case of LLG fault, for example an ABG fault, 'sumia' and 'sumib' are greater than sumic and so on (Fig. 2).

As shown in Table 2, the maximum absolute entropy sum (PP1) decreases according to the fault location varies from source end to load end. Fault location of LLLG fault is determined from the fault current. For example, if the fault current is between 3.4333×10^8 and 2.6072×10^8 , then fault location is between 5 and 9.9 % of transmission line. In the same way other fault locations are determined.

Appendix: System Parameters of Fig. 1. (Base MVA = 100)

Generator	Rated Voltage: 11 kV Short Circuit Level: 6GW X/R Ratio: 7
Transformer1(Y/Y)	Rated Voltage: 11 kV/110 kV
Transformer2(Y/Y)	Rated Power: 250 MVA Leakage Resistance: 0.002pu Leakage Resistance: 0.08 pu

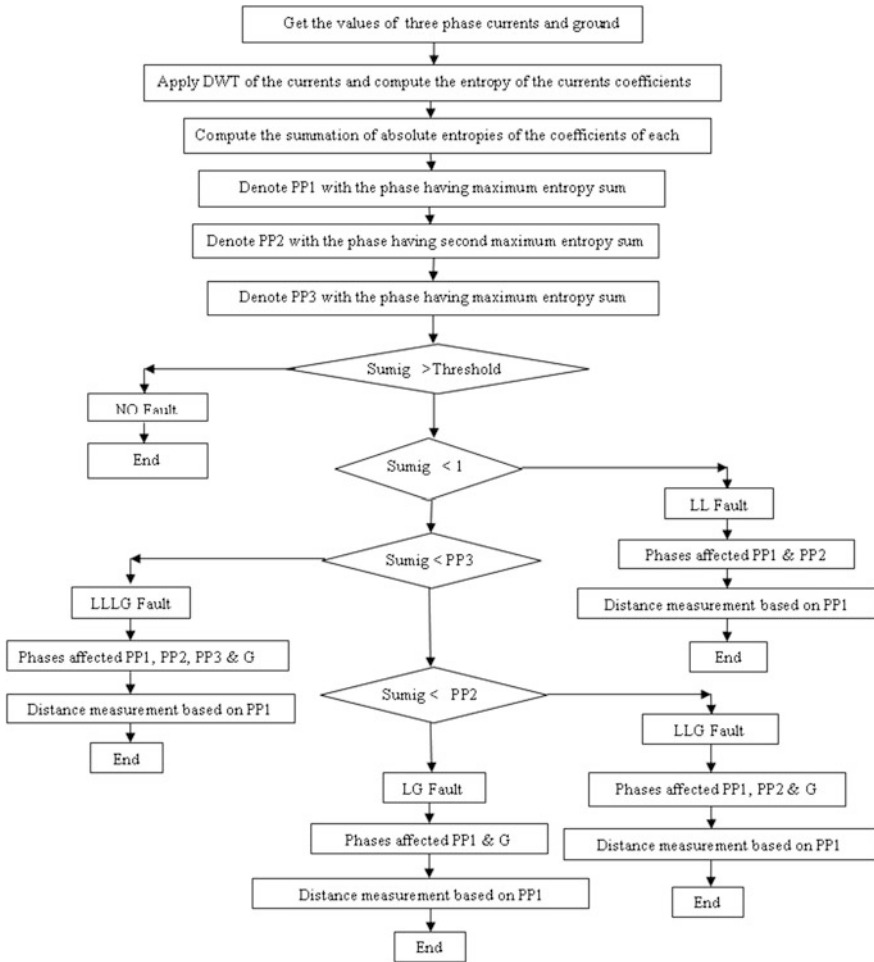


Fig. 2 Flow chart of the proposed wavelet entropy algorithm used to detect and classify fault in a static synchronous series compensated transmission system

Transformer3(Y/Y)
Transformer4(Y/Y)

Rated Voltage: 110 kV/33 kV
Rated Power: 300 MVA
Leakage Resistance: 0.002 pu
Leakage Resistance: 0.08 pu
Resistance: 0.01809 pu
Reactance: 0.0195 pu
Active Power: 15 MW
Reactive Power: 50 MVAR

Transmission Line

Load1
Load2

Table 2 Fault location of LLLG fault

Maximum absolute entropy sum	Location (%)
Greater than 3.4334×10^8	Below 4.9
Between 3.4333×10^8 and 2.6072×10^8	Between 5 and 9.9
Between 2.6071×10^8 and 2.0385×10^8	Between 10 and 14.9
Between 2.0384×10^8 and 1.6181×10^8	Between 15 and 19.9
Between 1.6180×10^8 and 1.3326×10^8	Between 20 and 24.9
Between 1.3325×10^8 and 1.1079×10^8	Between 25 and 29.9
Between 1.1078×10^8 and 9.3978×10^7	Between 30 and 34.9
Between 9.3977×10^7 and 8.0792×10^7	Between 35 and 39.9
Between 8.0791×10^7 and 7.1749×10^7	Between 40 and 44.9
Between 7.1748×10^7 and 6.0643×10^7	Between 45 and 49.9
Between 6.0642×10^7 and 5.3637×10^7	Between 50 and 54.9
Between 5.3636×10^7 and 4.9868×10^7	Between 55 and 59.9
Between 4.9867×10^7 and 4.2068×10^7	Between 60 and 64.9
Between 4.2067×10^7 and 3.7841×10^7	Between 65 and 69.9
Between 3.7842×10^7 and 3.3695×10^7	Between 70 and 74.9
Between 3.3694×10^7 and 3.0676×10^7	Between 75 and 79.9
Between 3.0675×10^7 and 2.8870×10^7	Between 80 and 84.9
Between 2.8871×10^7 and 2.8533×10^7	Between 85 and 89.9
Between 2.8532×10^7 and 2.6611×10^7	Between 90 and 94.9
Less than 2.6610×10^7	Above 95

SSSC

Rated power: 70 MVA

Nominal DC Voltage: 700 V

Nominal AC Voltage: 6.6 kV

Number of Pulses: 12

Series Coupling Transformer

Rated Voltage: 6.6 kV/48 kV

Rated power: 70 MVA

Leakage Resistance: 0.001 pu

Leakage Reactance: 0.05 pu

Acknowledgments The authors are thankful to the authorities of Thiagarajar College of Engineering, Madurai-625015, India, for providing all the facilities to do the research work.

References

1. Sadeh J., Adinehzadeh A.: "Accurate fault location algorithm for transmission line in the presence of series connected FACTS devices. *Electr. Power Energy Syst.* **32**, 323–328 (2010)
2. Samantray, S.R., Dash P.K., "Pattern recognition based digital relaying for advanced series compensated line." *Electr. Power Energy Syst.* **30**, 102–112 (2007)

3. Samantaray S.R., Dash P.K., Upadhyay, S.K.: “Adaptive kalman filter and neural network based high impedance fault detection in power distribution networks.” *Electr. Power Energy Syst.* **31**, 167–172 (2009)
4. Dash, P.K., Samantray, S.R.: “Phase selection and fault section identification in thyristor controlled series compensated line using discrete wavelet transform.” *Electr. Power Energy Syst.* **26**, 725–732 (2004)
5. Pardhan, A.K., Routray, A., Pati, S., Pardhan, D.K.: “Wavelet fuzzy combined approach for fault classification of a series-compensated transmission line.” *IEEE Trans. Power Delivery* **19**, 1612–1618 (2004)
6. Singh, BN., Singh, B., Chandra, A., Rastgoufard, P., Al-Haddad, K.: “An improved control algorithm for active filters.” *IEEE Trans. Power Delivery* **22**(2), 1009–1020 (2007)
7. El-Zonkoly, A.M., Desouki, H.: “Wavelet entropy based algorithm of fault detection and classification in FACTS compensator transmission line.” *Electr. Power Energy Syst.* **33**, 1368–1374 (2011)
8. Santoso, S., Powers, E.J., Grady, W.M., Hofmann, P.: “Power quality assessment via wavelet transform analysis”. *IEEE Trans. Power Delivery* **11**(2), 924–930 (1996)
9. Mallet, S.G.: A theory for multi-resolution signal decomposition: the wavelet representation. *IEEE Trans. Pattern Anal. Mach. Intell.* **11**(7), 674–693 (1989)
10. Torres, G.V., Ruiz P.H.F.: “High impedance fault detection using discrete wavelet transform.” In: *IEEE Electronics, Robotics and Automotive Mechanics Conference (CERMA)*, pp. 325, 329, 15–18 Nov 2011
11. Silva, KM., Neves, L.A., Souza, B.A.: “Distance protection using a wavelet-based filtering algorithm”. *Electr. Power Syst.Res.* **80**(1), 84–90, (2010) ISSN 0378-7796

SVM and Random Forest Classification of Satellite Image with NDVI as an Additional Attribute to the Dataset

K. Joshil Raj and S. SivaSathya

Abstract Image Classification is a widely researched subject both in the academic circles as well as industry having varied use in wide ranging applications in a multidisciplinary area. These techniques are being used in the fields of robotics, military applications, telecom, Oil and gas exploration, agriculture, creation of mapping products for military/civil applications and also by various departments of the Government for assessment of environmental damage, land use monitoring, radiation monitoring, urban planning, growth regulation, soil evaluation, and crop yield assessment. This paper addresses the issue of use of SVM and Random Forest algorithms for the classification of the Alwar satellite image data set. The normalized difference vegetation index (NDVI) is an estimate of the photosynthetically absorbed radiation over the land surfaces. We use NDVI as an additional attribute in the satellite image dataset to study the impact on the classification accuracy by these two algorithms. The experiments were performed using Alwar satellite image dataset, which has been previously classified using various other classification algorithms. The prediction accuracy and the kappa coefficient achieved for training data and the classified image generated from the test dataset after use of both the classifier systems is finally compared.

Keywords Satellite image classification · SVM · RF · WEKA · NDVI

K. Joshil Raj (✉) · S. SivaSathya
Department of Computer Science, Pondicherry University, Pondicherry, India
e-mail: joshlion89@gmail.com

S. SivaSathya
e-mail: ssivasathya@gmail.com

1 Introduction

Image Classification is a widely researched subject both in the academic circles as well as industry having varied use in wide ranging applications in a multidisciplinary area [1]. It is widely used to generate land use pattern maps, for land cover classification, soil pattern classification and for prediction of underground mineral/water deposits [2]. These techniques help in reducing or eliminating the requirement of an actual ground survey and also provide information of inaccessible terrains. Recent advances in remote sensing technologies and the increasing availability of satellite data with high resolution provide an enormous amount of spatial information for the exploitation in real life problems.

Image classification was initially done manually (by visual identification by experts or by ground survey) which was later replaced by Statistical techniques [3] like Parallelepiped Classification, Minimum Distance to Mean Classification, Maximum Likelihood Classification and Computational techniques. As the computational power increased and with the latest research in the field of Computational Intelligence, several new techniques have been proposed for Image Classification with great efforts for improving the classification accuracy. Image classification is the task of extracting information classes from a multiband raster image. The intent of the classification process is to categorize all pixels in a digital image into one of several land cover classes.

The organization of the paper is as follows: [Sect. 2](#) presents a brief note on the data set used for performing the experiments and also the related work that has been used in the previously published research works using different approaches for classifying this satellite image data set. [Section 3](#) gives out a review of the algorithms used in the proposed work (SVM and Random Forest). [Section 4](#) describes the procedure used in the preparation of the dataset and the conduct of the experiments using the different algorithms. [Section 5](#) has detailed experimental results obtained after using various combinations of the algorithms and datasets, each with different error matrices and accuracies. It also presents a comparison of the proposed classifiers with the various other classifiers used in the previously published work on this satellite image data set. [Section 6](#) presents Conclusion and future scope of the proposed work.

2 Satellite Image Dataset

Remote sensing data are available as multispectral and hyperspectral data. Each pixel has values corresponding to different bands of the electromagnetic spectrum. Classification techniques are used to identify pixels having similar values for different bands so as to classify them into different classes. Multispectral satellite data of size 472×576 (257712 pixels) of the Alwar region Rajasthan has been sourced from the Digital Terrain Research Lab (DTRL), a DRDO lab. This data

have been cited and used by many researchers for the purpose of image classification. This is an Indian Remote Sensing satellite's (IRS-P6) optical band image dataset with data for Green (G), Red (R), Near-Infrared (N) and Middle-Infrared (M) bands. The ground resolution of these images is 23.5 m and is taken from LISS (Linear Imaging Self Scanning Sensor)-III, sensor. The dataset also contains values for attributes of Radarsat microwave images Radarsat-1 (RS1) and Radarsat-2 (RS2) and Digital Elevation Model (DEM). Major land-use types of the area are vegetation, urban, water, rocky and barren.

2.1 Vegetation Index

There are a variety of vegetation indices that help in monitoring the vegetation in a satellite image. Reflectance is low in the red region (0.6–0.7 μ) because of the absorption of leaf pigments (chlorophyll). The infrared region (0.8–0.9 μ) shows high reflectance because of the scattering by the cell structure of the leaves. Vegetation index can be achieved by comparing the measure of infrared reflectance to that of the red reflectance. Normalized Difference Vegetation Index (NDVI) [1] can be calculated by taking the difference of (NIR-red) and normalizing it to balance out the effects of uneven illumination such as the shadows of clouds or hills.

$$NDVI = (NIR - red)/(NIR + red)$$

We also create a new training data with Normalized Difference Vegetation Index (NDVI) as an additional attribute. Thus the new dataset has 8 attributes (Red, Green, NIR, MIR, RS1, RS2, DEM and NDVI).

There has been several reported work using various algorithms like Minimum Distance Mean classifier, Maximum likelihood classifier, ACO, CAnt Miner Algorithm, Hybrid ACO—BBO, ACO/SOM, Hybrid ACO2/PSO, Hybrid ACO2/PSO/BBO [4], Semantic web based classifier, Cuckoo search Algorithm [5], Fuzzy classification, Rough Set/BBO + Ant Miner, Rough – Fuzzy Tie up approach, Fuzzy/BBO, Rough Set/BBO, BBO [6] and FPAB/BBO [7] on Alwar satellite image data set for image classification.

3 Classification Using SVM and RF Algorithms

3.1 SVM

SVMs are a set of related supervised learning methods used for classification and regression. An SVM [8] constructs a hyperplane or a set of hyperplanes in a high-dimensional space, which can be used for classification, regression and density

estimation problems. Intuitively, a good separation is achieved by the hyperplane that has the largest distance to the nearest training data points of any class since in general the larger the margin the lower the generalization error of the classifier. SVM proposed by Vapnik [9], maps input (real-valued) feature vectors into a high dimensional feature space through some nonlinear mapping. Computing the hyper plane to separate the data points i.e. training an SVM leads to a quadratic optimization problem. SVM uses a feature called kernel to solve this problem. For nonlinearly separable problems SVM transforms the data into a higher dimensional feature space and subsequently employs a linear hyperplane. There are many kernel functions; like a polynomial, radial basis functions etc. SVMs classify data by using support vectors, which are members of the set of training inputs that outline a hyper plane in feature space [10]. The primary advantage of SVMs is the lowest expected probability of generalization errors. The other advantages of using SVMs for classification are speed and scalability [11]. SVMs are relatively insensitive to the number of data points and the classification complexity does not depend on the dimensionality of the feature space, so they can potentially learn a larger set of patterns and thus be able to scale better.

3.2 Random Forest

Random forest [12] is an ensemble classifier that consists of many decision trees and outputs the class that is the mode of the class's output by individual trees. It runs efficiently on large databases, generates an internal unbiased estimate of the generalization error as the forest building progresses and can handle thousands of input variables without variable deletion. Random forests (RF) are a combination of predictors such that each predictor depends on the values of a random vector sampled independently and with the same distribution for all predictors in the forest. The generalization error of a forest of classifiers depends on the strength of the individual classifier in the forest and the correlation between them. To grow these ensembles, often random vectors are generated that govern the growth of each classifier in the ensemble. After a large number of classifiers are generated, they vote for the most popular class. We call these procedures random forests.

4 Procedure for Satellite Image Classification Using SVM and RF

SVM and RF of the Weka [13] data mining tool is used to generate 10 fold cross validation accuracy and the kappa coefficient on the training data set. Fine tuning of the parameters of the algorithms is done to generate the maximum accuracy and the kappa coefficient. The classification model is also generated using the training

Table 1 Parameters of SVM

SVM type	C-SVC
Cost	1
Gamma	0.0001
Kernel	RBF
Cross validation	10 folds

Table 2 Parameters of RF

Random features	4
Number of trees	10
Out of bag error	0.014
Cross validation	10 folds

dataset for classification of the test dataset. Test dataset is prepared in MATLAB [14] using the seven tiff images of the same area in different bands. The test image dataset is also classified using the same algorithms. Display of the classified image depicting the land cover information as a tiff image is done in MATLAB. The parameters used for SVM and Random Forest classifications are shown in Tables 1 and 2 respectively.

4.1 NDVI as an Additional Attribute

The NDVI index is used as an additional attribute for each pixel for the purpose of classification of the training and the test data set. Display of the vegetation information of the test dataset using the NDVI index with different thresholds is compared with vegetation information of the test dataset derived after image classification.

5 Experimental Results

The results (land cover information) obtained by applying the algorithms (SVM and Random Forest) on the Alwar dataset are shown in Figs. 1, 2 and 3.

The confusion matrices generated by the SVM and Random Forest classifications are given in the Tables 3, 4 and 5.

Fig. 1 Classified image using SVM

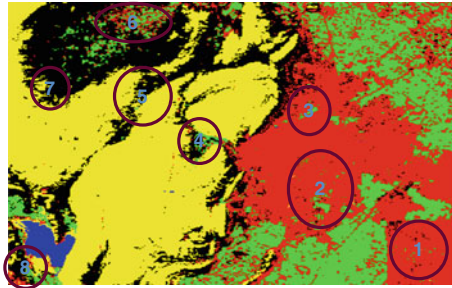


Fig. 2 Classified image using RF

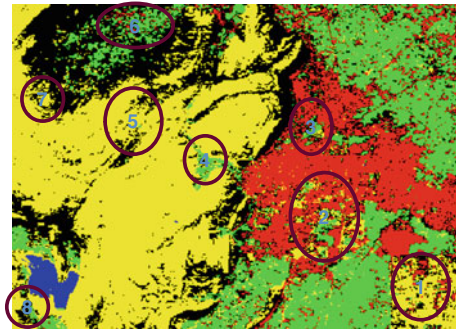
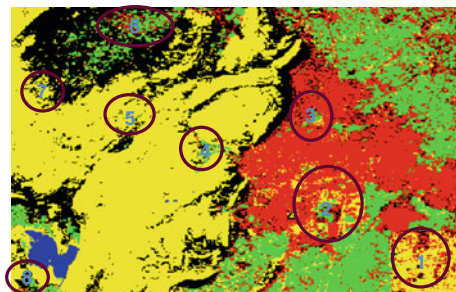


Fig. 3 Classified image using random forest with NDVI as an attribute



5.1 Accuracy Assessment

The producer's accuracy and user's accuracy are given in the Tables 6 and 7 respectively. Also the overall accuracy and Kappa coefficient of each algorithm is illustrated in Table 8.

Table 3 Confusion matrix of SVM classification

	Barren	Rocky	Urban	Veg	Water	Total
Barren	190	0	1	0	0	191
Rocky	2	286	0	0	0	288
Urban	1	0	415	1	0	417
Veg	0	0	0	329	0	329
Water	0	0	0	0	206	206
Total	193	286	416	330	206	1431

Table 4 Confusion matrix of RF classification

	Barren	Rocky	Urban	Veg	Water	Total
Barren	189	1	1	0	0	191
Rocky	2	286	0	0	0	288
Urban	0	0	416	1	0	417
Veg	0	0	0	329	0	329
Water	0	0	0	0	206	206
Total	191	287	417	330	206	1431

Table 5 Confusion matrix of RF classification (with NDVI attribute)

	Barren	Rocky	Urban	Veg	Water	Total
Barren	190	1	0	0	0	191
Rocky	2	286	0	0	0	288
Urban	0	0	416	1	0	417
Veg	0	0	0	329	0	329
Water	0	0	0	0	206	206
Total	192	287	416	330	206	1431

Table 6 Producer's accuracy

	SVM	Random forest	Random forest (With NDVI)
Barren	98.44	98.95	99.47
Rocky	100	99.65	99.65
Urban	99.75	99.76	100
Vegetation	99.69	99.69	99.69
Waterbody	100	100	100

Table 7 User's accuracy

	SVM	RF	RF (NDVI)
Barren	99.47	98.95	99.47
Rocky	99.30	99.30	99.30
Urban	99.52	99.76	99.76
Veg	100	100	100
Water	100	100	100

Table 8 Overall accuracy and kappa coefficient

	Overall accuracy	Kappa coefficient
SVM	99.65 %	0.9955
RF	99.65 %	0.9955
RF (NDVI)	99.725 %	0.9964

5.2 Comparisons with Existing Classification Techniques

Comparisons with previous published classification results on the Alwar satellite image dataset in various papers has been collated and shown in Table 9.

It can be seen after comparison of the results with previously published work, that both SVM and Random Forest are able to achieve a higher kappa coefficient and overall accuracy.

5.3 Comparison of the Image Classification Results of SVM and RF Algorithms

The satellite image classified using SVM and Random Forest algorithms were compared and also related to the actual terrain data of the area as obtained from the recent high resolution Google satellite data of Alwar region. Even though, both SVM and Random Forest generate similar 10 fold cross validation accuracy and the Kappa coefficient on the training data set, however their classification results vary greatly on the test dataset. As can be seen from the Table 11, the number of pixels classified as rocky and urban varies greatly among the different classified images. This can also be seen in the figures depicting classified images using the different algorithms. We could identify eight areas with major differences in the image classification results and they have been highlighted in the images with a circle. The comparison is also given in the Table 10.

The reason for such a variance in the classified image using the different algorithms is due to the heterogeneity of the pixel data in different bands and the requirement of a large training data for some of the algorithms. SVM performs better on the test data since it requires very less training data to generate the support vectors at boundary locations between the different classes. Thus the results depict that SVM gives more accurate results on the test satellite image data

Table 9 Comparison of kappa coefficient and overall accuracy achieved using various algorithms on the Alwar image dataset

S. No	Algorithms	Kappa Coefficient	Overall Accuracy
1.	Cuckoo search algorithm	0.9465	0.957
2.	BBO	0.6715	0.742
3.	Fuzzy classification	0.9134	–
4.	Rough-fuzzy tie up approach	0.9700	–
5.	CAnt miner algorithm	0.964	–
6.	Hybrid ACO–BBO	0.96699	0.986
7.	Hybrid ACO2/PSO	0.975	–
8.	Hybrid ACO2/PSO/BBO	0.98182	0.974
9.	Semantic web based classifier	0.9881	–
10.	Minimum distance mean classifier	0.7364	–
11.	Maximum likelihood classifier	0.7525	–
12.	Fuzzy/BBO	0.6921	0.757
13.	ACO/SOM	0.70755	0.77
14.	Rough set/BBO	0.67150	0.742
15.	ACO/BBO	0.76369	0.814
16.	FPAB/BBO	0.67927	0.748
17.	Rough set/BBO + ant miner	0.97	–
18.	SVM	0.99	0.996
19.	Random forest	0.99	0.997

as compared to the Random Forest algorithm. In case of circle 1 and 2, the results are extremely different when compared with recent high resolution Google maps Satellite data of Alwar region. This can attributed to the low resolution of our dataset which increases the problem of mixed pixels due to the heterogeneity of the pixel data and also the temporal variation of the data. Our dataset is old as compared to the Google data which is of very recent origin. Circle 1 is depicts the cantonment area in Alwar and shows more vegetation in the Google data which has increased over a period of time. Circle 2 depicts the residential area in Alwar which shows more urban characteristics in the recent Google data (Table 10).

5.4 Use of NDVI as an Additional Attribute

It can be seen that using NDVI as an additional attribute in the data set increases the classification accuracy of the Random Forest algorithm. However there is no change in the classification accuracy by using NDVI as an additional attribute in classification by SVM. The classification accuracy remains the same as the original dataset. It can also be seen from Figs. 4 and 5 that the vegetation indices like NDVI can provide an indication to the presence of vegetation in an image. The vegetation land cover information derived using SVM and RF are shown in Figs. 6, 7 and 8 respectively. It is seen that even though simply displaying NDVI

Table 10 Comparison of classified images using SVM and RF algorithms on the Alwar image dataset

S no	Locations marked in a circle in the classified image (refer Figs. 1, 2 and 3)	Image classification results by various algorithms			Actual data as seen in recent high resolution Google maps satellite data of Alwar region
		SVM	RF	RF (with NDVI)	
1.	Circle 1	Urban (94 %) Veg (3 %) Barren (3 %)	Urban (15 %) Veg (3 %) Barren (7 %) Rocky (75 %)	Urban (25 %) Barren (5 %) Rocky (70 %)	Urban (40 %) Veg (40 %) Barren (10 %)
2.	Circle 2	Urban (94 %) Veg (6 %)	Urban (65 %) Veg (15 %) Rocky (10 %) Barren (5 %)	Urban (60 %) Veg (5 %) Rocky (30 %) Barren (5 %)	Urban (100 %) No rocky
3.	Circle 3	Urban (94 %) Veg (3 %) Barren (3 %)	Urban (65 %) Veg (20 %) Barren (10 %)	Urban (75 %) Veg (5 %) Barren (5 %)	Urban (90 %) Veg (5 %) Barren (5 %)
4.	Circle 4	Rocky (45 %) Barren (45 %) Veg (10 %)	Rocky (5 %) Rocky (65 %) Barren (5 %) Veg (30 %)	Rocky (15 %) Rocky (70 %) Barren (10 %) Veg (17 %) Urban (3 %).	Rocky (50 %) Barren (50 %)
5.	Circle 5	Rocky (50 %) Barren (50 %) Veg (50 %)	Rocky (80 %) Barren (20 %) Veg (75 %)	Rocky (90 %) Barren (10 %) Veg (60 %)	Rocky (50 %) Barren (50 %) Veg (65 %)
6.	Circle 6	Urban (25 %) Barren (80 %) Rocky (20 %)	Urban (5 %) Barren (20 %) Barren (30 %) Rocky (70 %)	Urban (10 %) Barren (30 %) Barren (30 %) Rocky (70 %)	Urban (25 %) Barren (10 %) Barren (80 %) Rocky (20 %)
7.	Circle 7	Rocky (30 %) Barren (45 %) Urban (15 %)	Rocky (60 %) Barren (30 %) Veg (10 %)	Rocky (60 %) Barren (25 %) Urban (5 %) Veg (10 %)	Rocky (50 %) Barren (30 %) Urban (20 %)
8.	Circle 8	Urban (15 %) Veg (5 %)	Urban (30 %) Veg (10 %)	Urban (5 %) Veg (10 %)	Urban (20 %)

Table 11 Number of pixels classified as different land cover type using SVM and RF algorithms

Algorithms Land cover type	No of pixels		
	SVM	Random forest	Random forest (with additional NDVI feature)
Barren	50296	48155	60704
Rocky	85430	105544	99847
Urban	74250	55645	42298
Vegetation	44885	45674	52123
Waterbody	2851	2694	2740
Total	257712	257712	257712

Fig. 4 Vegetation highlighted (*green*) using the NDVI (threshold > 0.4)

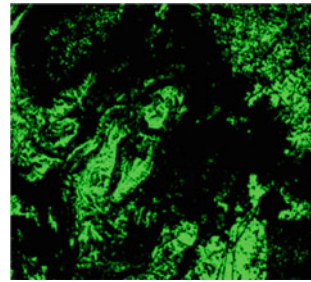


Fig. 5 Vegetation highlighted (*green*) using the NDVI (threshold > 0.5)

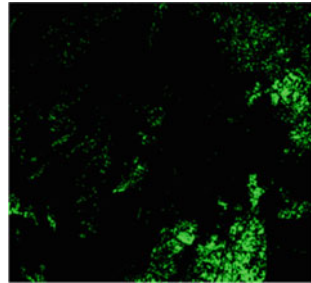


Fig. 6 Vegetation highlighted (*green*) in the SVM classified image

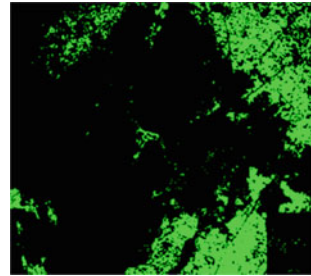


Fig. 7 Vegetation highlighted (*green*) in the RF classified image

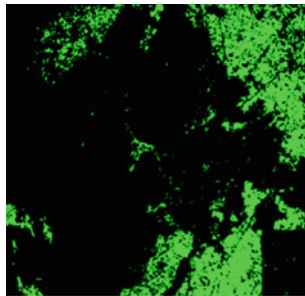
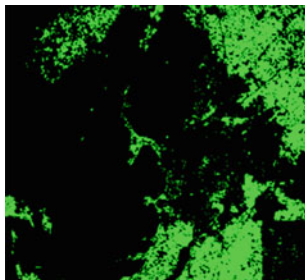


Fig. 8 Vegetation highlighted (*green*) in the RF classified image with NDVI



also gives the indication of the presence of vegetation, however use of image classification algorithms for identifying the vegetation land cover information are much more accurate.

6 Conclusion

In this paper we have presented two classification techniques to classify high resolution satellite images. We have compared our results achieved using SVM and Random Forest algorithms with the previously published results using various other algorithms on this dataset. We have also classified a test satellite image data set and compared the results. In addition, use of NDVI as an additional attribute to the dataset and its effect on the image classification task has been studied. The inclusion of an NDVI as an additional attribute has contributed to the increase in the classification accuracy as well as the kappa coefficient. Further research will include attribute reduction/feature selection wherein the aim will be to reduce the number of attributes (bands) to achieve the same accuracy or greater accuracy and the Kappa coefficient for the satellite image data set. The endeavor will also be to try out another novel algorithms and study their performance on this dataset.

Acknowledgments I would also like to present my special thanks to Dr. V. K. Panchal, Scientist 'G', DTRL, DRDO who provided me the Satellite Data for the experimental study.

References

1. Lu, D., Weng, Q.: A survey of image classification methods and techniques for improving classification performance. *Int. J. Remote Sens.* **28**(5), 823–870 (2007)
2. Shine, J.A., Carr, D.B.: A comparison of classification methods for large imagery data sets. In: *Statistics in an ERA of Technological Change-Statistical Computing Section, JSM 2002*, pp. 3205–3207, New York, 11–15 Aug 2002
3. Lilles, T.M., Kiefer, R.W.: *Remote Sensing and Image Interpretation*, 6th edn. Wiley, New York (2008)
4. Goel, L., Panchal, V.K., Gupta, D.: Embedding expert knowledge to hybrid bio-inspired techniques—an adaptive strategy towards focusing land cover feature extraction. *Int. J. Comput. Sci. Inf. Secur.* **8**(2), 244–253 (2010)
5. Bharadwaj, A., Gupta, D., Panchal, V.K.: Applying nature inspired metaheuristic technique to capture the terrain features. In: *Proceedings of the 2012 International Conference on Artificial Intelligence (ICAI-2012)*, vol. 1 (2012)
6. Panchal, V.K., Goel, S., Bhatnagar, M.: Biogeography based land cover feature extraction. In: *IEEE Proceedings of NaBiC'09*
7. Arora, P., Kundra, H., Panchal, V.K.: Fusion of biogeography based optimization and artificial bee colony for identification of natural terrain features. *Int. J. Adv. Comput. Sci. Appl.* **3**(10), 107–111 (2012)
8. Prasad, S., Krishna, I.: Classification of multispectral satellite images using clustering with SVM classifier. *Int. J. Comput. Appl.* **35**(5), 32–44 (2011)
9. Vapnik, V.N.: *The Nature of Statistical Learning Theory*. Springer, Berlin (1995)
10. Perumal, K., Bhaskaran, R.: SVM-based effective land use classification system for multispectral remote sensing images. *Int. J. Comput. Sci. Inf. Secur.* **6**(2), 95–107 (2009)
11. Cristianini N., Shawe-Taylor, J.: (2003) *Support Vector and Kernel Methods, Intelligent Data Analysis: An Introduction*. Springer, New York
12. Breiman, L.: Random forests. *Mach. Learn.* **45**(1), 5–32 (2001)
13. WEKA software: Machine Learning. <http://www.cs.waikato.ac.nz/ml/weka/>. The University of Waikato, Hamilton
14. MATLAB (7.0): Mathworks. <http://www.mathworks.com>

Bi-directional Pixel-Value Differencing Approach for Steganography

Himakshi, Harsh Kumar Verma, Ravindra Kumar Singh
and Charan Kamaljit Singh

Abstract A hybrid image steganographic approach has been proposed in this paper to enlarge the data hiding capability of cover image as well as to improve the quality of stego image. This research is a hybrid combination of cryptography, steganography and data compression. The basic building block of this approach is Wu and Tsai's method (PVD), LZW compression scheme, Vernam cipher and gray code. In this approach, chunks of the secret data are embedded by altering the pixel values of the consecutive pixels in the cover image according to their hiding capacity. The hiding capacity of the two consecutive pixels depends on their difference value, which is calculated by pixel-value differencing technique (PVD). Two layer data hiding is the key feature of this approach that's why it is called a Bi-Directional approach. Two layer data hiding approach improves the data hiding capacity and quality of stego image as well. In second layer data hiding we consider left pixel of the pixel pair as the right pixel and vice-versa. It improves the quality of stego image. In this technique stego image is totally indistinguishable from the original image by the human eye. It is also secure against the RS detection attack.

Keywords Steganography · Compression · Cryptography · PVD · Stego image · Cover image · RS detection attack · LZW · Verman cipher · Gray code

Himakshi (✉) · H. K. Verma · R. K. Singh
Department of CS, NIT Jalandhar, Jalandhar, Punjab, India
e-mail: himakshi.nitj@gmail.com

H. K. Verma
e-mail: vermah@nitj.ac.in

R. K. Singh
e-mail: ravindra1987singh@gmail.com

C. K. Singh
Department of CSE, SSCET Badhani, Badhani, Punjab, India
e-mail: aug10_ck@yahoo.co.in

1 Introduction

In recent years, enormous research efforts have been invested in the development of digital image steganographic techniques. The major goal of steganography is to enhance communication security by inserting secret message into the digital image, modifying the nonessential pixels of the image [1]. The image after the embedding of the secret message, so-called stego image, is then sent to the receiver through a public channel. In the transmission process, the public channel may be intentionally monitored by some opponent who tries to prevent the message from being successfully sent and received [2]. The opponent may randomly attack the stego image if he/she doubts the stego image carries any secret message because the appearance of the stego image shows obvious artifacts of hiding effect [3]. For this reason, an ideal steganography scheme, to keep the stego image from drawing attention from the opponent, should maintain an imperceptible stego image quality. That is to say, if there are more similarities between the cover image and the stego image, it will be harder for an attacker to find out that the stego image has important secret data hidden inside it. This way, the secret data is more likely to travel from the sender to the receiver safe and sound [4]. An alternative was proposed by [5], it make use of a stego key to provide additional security on the secret data.

For the past decade, many steganographic techniques for still images have been presented. A simple and well-known approach is directly hiding secret data into the least-significant bit (LSB) of each pixel in an image. One method proposed by Jarmo Mielikainen [6] is a modified version of the least-significant-bit (LSB) method, resulting in improved imperceptibility. It allows an embedding of the same amount of information as LSB matching but with fewer changes to the cover image. This makes the detection of the proposed method harder than the conventional LSB matching method [7]. Proposed a statistical method for detection in LSB technique. Although LSB technique is susceptible to noise over the network but it is useful when one have to store valuable information like Pan Card details, Form16 etc., on a system which is accessible to many of them. The LSB-based methods mentioned above, directly embed the secret data into the spatial domain in an unreasonable way without taking into consideration the difference in hiding capacity between edge and smooth areas. In general, the alteration tolerance of an edge area is higher than that of a smooth area [8].

That is to say, an edge area can conceal more secret data than a smooth area. With this concept in mind, Wu and Tsai presented steganographic scheme that offers high imperceptibility to the stego image by selecting two consecutive pixels as the object of embedding [9]. The payload of Wu and Tsai's scheme is determined by the difference value between the pixels. In Wu and Tsai's method, they determine whether the two consecutive pixels belong to an edge or smooth area by checking out the difference value between the two consecutive pixels. If the difference value is large, that means the two pixels are located in an edge areas, and more secret data can be hidden here. On the contrary, if the difference value is

small, that means the two pixels are located in a smooth area, and less secret data can be embedded. Therefore, their scheme produces stego images that are more similar to the original images than those produced by LSB substitution schemes, which directly embed secret data into the cover image without considering the differences between adjacent pixels. Furthermore, Chung-Ming Wang has proposed a new method based on modulus function to resolve the issue of falling-off-boundary problem [10]. Tri-way pixel-value differencing (TPVD) is also used to improve the capacity of the hidden secret information and to provide an imperceptible stego image for human vision [11]. PVD method was also modified for more robust histogram quantization [12].

2 Wu and Tsai's Method

The *embedding process* of Wu and Tsai's method uses a cover image F sized $M \times N$. F_i is a sub-block of F that has two consecutive pixels broken down by partitioning F in raster scan order such that $F = \{F_i | i = 1, 2, \dots, \frac{M \times N}{2}\}$. By definition each F_i has two elements $P_{(i,L)}$ and $P_{(i,R)}$. The pixel values of $P_{(i,L)}$ and $P_{(i,R)}$ are $P_{(i,x)}$ and $P_{(i,y)}$ respectively. The difference value d_i of $P_{(i,x)}$ and $P_{(i,y)}$ can be derived by Eq. (1).

$$d_i = |P_{(i,x)} - P_{(i,y)}| \quad (1)$$

On the other hand, they design a range table R which consists of n contiguous sub-ranges R_j ; in other words $R = \{R_j | j = 1, 2, \dots, n\}$. The major job of the range table is to provide information about the hiding capacity of each F_i . Each sub-range R_j has its lower and upper bound values, say l_j and u_j , so that we have $R_j \in [l_j, u_j]$. The width w_j of each R_j is selected to be a power of 2, and can be computed by $w_j = u_j - l_j + 1$. Each sub-block F_i relates to its sub-range R_j from the range table R such that $R_j = \min(d_i, w_j)$ and $d_i \in [l_j, u_j]$. This way, hiding capacity of two consecutive pixels can be obtained by

$$t_i = \lfloor \log w_j \rfloor \quad (2)$$

Here, t_i is the number of bits that can be hidden in F_i . Read t_i bits from the binary secret data stream and transform into its decimal value t'_i . A new difference value d'_i can be generated by putting l_j and t'_i together: $d'_i = t'_i + l_j$. Now the secret data can be embedded into F_i by modifying its $P_{(i,x)}$ and $P_{(i,y)}$ such that $d_i = d'_i$. The details of the embedding criteria are as follows:

$$\left(P'_{(i,x)}, P'_{(i,y)} \right) = \begin{cases} (P_{(i,x)} + \lceil m/2 \rceil, P_{(i,y)} - \lfloor m/2 \rfloor), \\ \quad \text{if } P_{(i,x)} \geq P_{(i,y)} \text{ and } d'_i > d_i; \\ \\ (P_{(i,x)} - \lceil m/2 \rceil, P_{(i,y)} + \lfloor m/2 \rfloor), \\ \quad \text{if } P_{(i,x)} < P_{(i,y)} \text{ and } d'_i > d_i; \\ \\ (P_{(i,x)} - \lfloor m/2 \rfloor, P_{(i,y)} + \lceil m/2 \rceil), \\ \quad \text{if } P_{(i,x)} \geq P_{(i,y)} \text{ and } d'_i \leq d_i; \\ \\ (P_{(i,x)} + \lfloor m/2 \rfloor, P_{(i,y)} - \lceil m/2 \rceil), \\ \quad \text{if } P_{(i,x)} < P_{(i,y)} \text{ and } d'_i \leq d_i; \end{cases} \quad (3)$$

where $m = |d'_i - d_i|$.

We can gain new pixel values $P'_{(i,x)}$ and $P'_{(i,y)}$ after the calculation in Eq. (3) and replace $P_{(i,x)}$ and $P_{(i,y)}$ in the cover image with the new values so that the embedding process is accomplished. An illustration of how $P_{(i,x)}$ and $P_{(i,y)}$ can be adjusted by Wu and Tsai's scheme for the purpose of hiding secret data is shown in Table 1.

In Table 1, assume the pixel values of sub-block F_i are $P_{(i,x)} = 32$, $P_{(i,y)} = 32$, and the width w_j of their sub-range is 8 with $l_j = 0$ and $u_j = 7$. Then, 3 bits of the secret data is taken out and put into F_i . All the possible ways of adjusting $P_{(i,x)}$ and $P_{(i,y)}$ are shown in Table 1. Obviously, the falling-off-boundary problem will occur and would not conform Eq. (3) if $0 \leq P_{(i,x)} \leq 3$ and $0 \leq P_{(i,y)} \leq 3$.

The recovery process of Wu and Tsai's method is quite simple and easy. Given two consecutive pixels $P'_{(i,x)}$ and $P'_{(i,y)}$ of the stego image, compute their difference value d'_i and obtain $d'_i = |P'_{(i,x)} - P'_{(i,y)}|$. Use the original range table R in the embedding phase to obtain the same R_j and w_j . The length t_i of the hiding capacity also can be gained by using Eq. (2). Calculate the real difference value $d''_i = d'_i - l_j$ and convert the decimal value d''_i into a binary string whose length is t_i bits. For example, assume $d''_i = 5_{10}$ and $t_i = 3$, and then secret data 101_2 is extracted.

3 Proposed Method

Proposed method is a two layer data hiding scheme. The motivation behind this approach is to improve the quality of stego image as well as to maximize the data hiding capacity of cover image. A basic building block of this approach includes Wu and Tsai's method [9, 10], LZW compression scheme [13, 14], Vernam cipher [15, 16] and gray code [17]. Wu and Tsai's method is used to hide data in gray

Table 1 An illustration of Wu and Tsai's embedding process

Secret data (decimal value)	$P_{(i,x)} = 32$	$P_{(i,y)} = 32$	New difference value of $P_{(i,x)}$ and $P_{(i,y)}$
0	No modify	No modify	0
1	+1	No modify	1
2	+1	-1	2
3	+2	-1	3
4	+2	-2	4
5	+3	-2	5
6	+3	-3	6
7	+4	-3	7

level image and LZW compression scheme is used to compress data. Vernam cipher provides an essential security on the secret data using a user key. Seemingly insignificant use of gray code can play a vital role in data compression. Gray code provides a high level movement of bits, which in effect improves the compression ratio.

Step wise explanation of this approach is give below.

3.1 The Embedding Process

- Step 1: Take a “key”, “secret message” and a gray level image “cover image” form user.
- Step 2: Apply “Vernam cipher” on the “secret message” using the “key”. It produces “cipher text”.
- Step 3: Concatenate a “start string” (\$) or any other) at the start of the “cipher text” and a “finish string” (*\$ or any other) at the end of the “cipher text”.
- Step 4: Apply “LZW compression” scheme on the “cipher text” to make it compact. This compact message is known as “compressed message”.
- Step 5: Apply “Wu and Tsai's embedding process” to hide “compressed message” in the “cover image”. It is the first layer data hiding and produced image is called as “intermediate Image”.
- Step 6: If complete “compressed message” has been hidden in the “cover image” then goto Step15.
- Step 7: Find the “pixel difference value” d_i , “lower bound” l_j , “upper bound” u_j and its “hiding capacity” t_i using Wu and Tsai's method and calculate “1st layer difference” $d1_i$, by $d1_i = d_i - l_j$ for each pair of “intermediate image”.
- Step 8: Create a “difference string” by concatenating binary values of “1st layer difference” in t_i bits.
- Step 9: Convert “difference string” into “gray code” (for getting better compression ratio on “difference string”).

- Step 10: Apply “LZW compression” on “gray code” of “difference string”.
- Step 11: Concatenate “difference string” with “remaining compressed message” using a “joint string” (‘_’ or any other). “Joint string” will be used to separate the “difference string” from “remaining compressed message”.
- Step 12: Apply “Wu and Tsai’s embedding process” once again to hide “difference string” in the “intermediate image”. Here we consider left pixel as right pixel of the pair and vice versa (it will improve the quality of stego image, because in first layer data hiding we add $[m/2]$ in left pixel and subtract $[m/2]$ from right pixel. Now it will add in right pixel and subtract from left pixel. So the pixel difference of the stego image and cover image will be very close).
- Step 13: If complete “difference string” has been hidden in the “intermediate image” then goto Step16.
- Step 14: goto Step1 and choose a bigger image.
- Step 15: Apply “Wu and Tsai’s method” once again to hide “compressed message” in the “intermediate image”. It will improve the quality of the image. Here we consider left pixel as right pixel of the pair and vice versa.
- Step 16: “Intermediate image” will be your “stego image”.

3.2 The Recovery Process

- Step 1: Take a gray level image “stego image” and a “key” (which is used at the sender end) from user.
- Step 2: Apply “Wu and Tsai’s recovery process” to extract the message from the “stego image”. Here we consider left pixel as right pixel of the pair and vice versa.
- Step 3: Apply “LZW de-compression” scheme on the “extracted message” to get full length message.
- Step 4: If “start string” (\$) or any other) and “finish string” (\$) or any other) are found in the “extracted message” then chop the message between it. And goto step13.
- Step 5: (Ignore Step3 & 4) Find “difference string” and “remaining compressed message” from the “extracted message”. Message after the “joint string” (‘_’ or any other) will be the “remaining compressed message”. And string before the “joint string” (‘_’ or any other) will be the “difference string”.
- Step 6: Apply “LZW de-compression” scheme on the “difference string”.
- Step 7: “Difference string” is in “gray code” so convert it into binary.
- Step 8: Find the “lower bound” l_j and its “hiding capacity” t_i using “Wu and Tsai’s method”. Read t_i bit from the “difference string” and convert it into decimal value, this is called the “1st layer difference” d_{1i} . Now add

“lower bound” l_j in “1st layer difference” to find the “difference” $d_i = d1_i + l_j$ for each pair of stego image.

Step 9: Now extract the data of 1st layer hiding by considering d_i as “difference” of the pixel pairs, l_j as “lower bound” and t_i as “hiding capacity” using “Wu and Tsai’s recovery process”.

Step 10: Now concatenate “extected message” with “remaining compressed message”.

Step 11: Apply “LZW de-compression” scheme once again.

Step 12: Chop “cipher text” between “start string” (\$) or any other) and “finish string” (\$ or any other)

Step 13: Apply “Vernam cipher” to decrypt the “cipher text” to get the original “secret message”.

4 Results and Analysis

4.1 Basic Terms

4.1.1 Range Table (R)

A range table R consisting of 6 sub-ranges R_j , for $j = 1, 2, \dots, 6$ are being considered for this approach (Table 2).

4.1.2 Peak Signal-to-Noise Ratio (PSNR)

The peak signal-to-noise ratio (PSNR) is considered to evaluate the stego image quality. A larger PSNR value indicates the fact that the discrepancy between the cover image and the stego image is more invisible to the human eye. The PSNR is defined as follows:

$$PNSR = 10 \log_{10} \frac{255^2}{MSE} dB$$

And

$$MSE = \left(\frac{1}{M \times N} \right) \sum_{i=0}^{M-1} \sum_{j=0}^{N-1} (\alpha_{ij} - \beta_{ij})^2$$

Here, α_{ij} is the pixel of the cover image where the coordinate is (i, j) , and β_{ij} is the pixel of the stego image where the coordinate is (i, j) . M and N represent the size of the image.

Table 2 Range table

Sub ranges [R _j]	Range	Lower bound [l _j]	Upper bound [u _j]	Width [w _j]
R1	0–7	0	7	8
R2	8–15	8	15	8
R3	16–31	16	31	16
R4	32–63	32	63	32
R5	64–127	64	127	64
R6	128–255	128	255	128

4.1.3 RS Detection Attack

In this section, we analyze the performance of the proposed method in terms of the stego image quality and the robustness against the RS detection attack. If pixel value alteration is less, then it will be considered as optimal quality. And if pixel value alteration is more then it will be considered as worst quality [10].

The RS detection method by [18] can directly judge whether the stego image is secure without visual inspection. Fridrich et al. [18] utilize the dual statistics method to classify all the pixels of a stego image into three pixel groups: the regular group R_m or R_{-m} , the singular group S_m or S_{-m} , and the unusable group. The stego image will pass the RS steganalysis when $R_m \cong R_{-m}$ and $S_m \cong S_{-m}$. Otherwise, the stego image will be judged as a suspicious object.

4.2 Experimental Results

For implementation of the proposed method, four gray level cover images (jpeg format) shown in Fig. 1a, c, e, g of size 256×256 pixels namely aircraft, baboon, baby and lena were considered. We implemented Wu and Tsai's method (PVD) along with our proposed method in matlab to hide text message in these cover images. We used 5 different input set for the evaluation purpose. Hiding capacity of cover image and PSNR value of the image were calculated for each input data set, and their cumulative average is taken for the final result. Table 3 shows the hiding capacity and quality of stego image for both algorithms.

Figure 1b, d, f, h are the stego images of our proposed method.

4.2.1 Peak Signal to Noise Ratio

According to experimental results proposed method is 1.08 times better than PVD method in context of stego image's quality (Fig. 2). Stego image of proposed method is totally indistinguishable from the original image by the human eye. And it is secure against the RS detection attack.

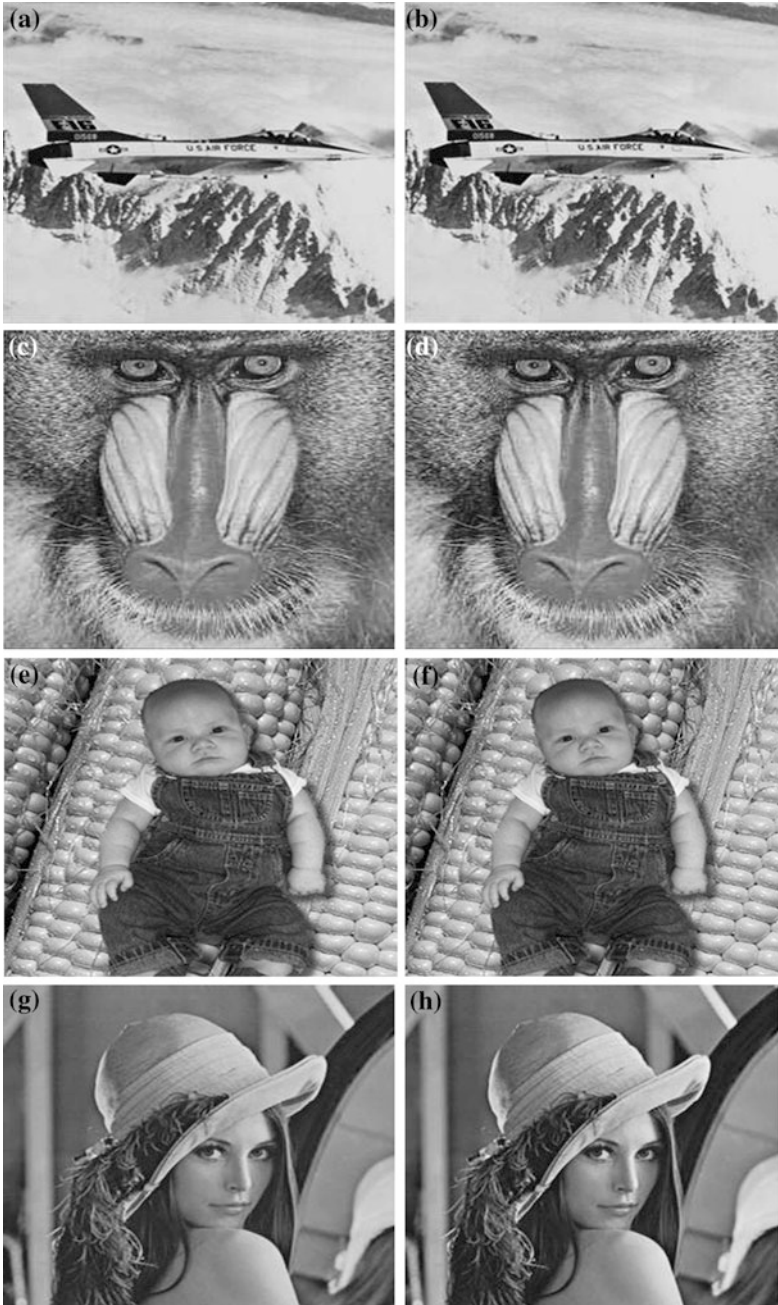


Fig. 1 Cover images and Stego images. **a** Aircraft (*Cover image*), **b** aircraft (*Stego image*), **c** baboon (*Cover image*), **d** baboon (*Stego image*), **e** baby (*Cover image*), **f** baby (*Stego image*), **g** lena (*Cover image*), **h** lena (*Stego image*)

Table 3 Test data set

Cover image	File size (bytes)	Wu and Tsai’s method (PVD)		Proposed method	
		Hiding capacity (bits)	PSNR (dB)	Hiding capacity (bits)	PSNR (dB)
aircraft	19288	268523	46.9216	971343	49.6182
baboon	22620	345783	45.1823	1272746	47.9731
baby	34232	262125	48.0274	969435	53.8732
lena	17061	252761	47.9402	945276	51.3205

Fig. 2 PSNR values of proposed method and Wu and Tsai’s method

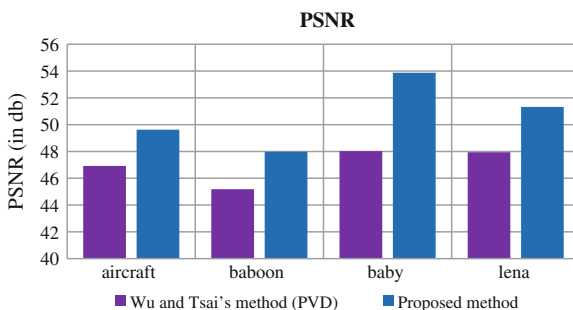
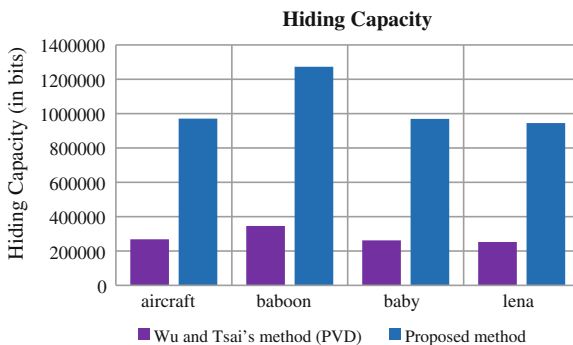


Fig. 3 Data hiding capacity of proposed method and Wu and Tsai’s method



4.2.2 Data Hiding Capacity

Data hiding capacity is the key feature of the proposed method. It makes use of LZW compression scheme and two layer data hiding for the same. Experimental results explore that proposed method is 3.68 times better than PVD method in context of data hiding capacity (Fig. 3).

5 Conclusion

Proposed method is a two layer data hiding approach. It uses LZW compression scheme, Vernam cipher and Wu and Tsai's method (PVD) to improve its performance. Verman cipher provides an essential level of security, LZW compression provide a lossless compression and PVD hide the secret message in the cover image. Proposed method has been implemented on matlab and experimental results concluded that proposed method performances better than Wu and Tsai's scheme in terms of data hiding capacity and quality of stego image. Data hiding capacity of proposed method is 3.68 times of PVD method and quality of stego image is 1.08 times better than PVD method. Besides, the proposed method is secure against the RS detection attack.

References

1. Feng, J.B., Lin, I.C., Tsai, C.S., Chu, Y.P.: Reversible watermarking: current status and key issues. *Int. J. of Network Secur.* **2**, 161–170 (2006)
2. Salomon, D.: *Data Compression: The Complete Reference*, 4th edn. Springer, London (2007)
3. Liao, Z., Huang, Y., Li, C.: Research on data hiding capacity. *Int. J. Network Secur.* **5**, 140–144 (2007)
4. Harmsen, J., Pearlman, W.: Steganalysis of additivenoise modelable information hiding. In: *Proceedings of SPIE Security Watermarking Multimedia Contents*, vol. 5020, pp. 131–142, (2003)
5. Sharp, T.: An implementation of key-based digital signal steganography. In: *Proceedings of Information Hiding Workshop*, vol. 2137, pp. 13–26. Springer LNCS (2001)
6. Ahirwal, R.R., Ahirwal, D., Jain, Y. K.: A high capacitive and confidentiality based image steganography using private stego-key. In: *Proceedings of the International Conference on Information Science and Applications*, Chennai (2010)
7. Hivrare, S.P., Sawarkar, S.D., Bhosale, V., Koregaonkar, S.: Statistical Method for Hiding Detection in LSB of Digital Images: An Overview. In: *Proceedings of World Academy of Science, Engineering and Technology*, vol. 32, pp. 2070–3740. August 2008
8. Zhang, H., Geng, G., Xiong, C.: Image steganography using pixel-value differencing. *Second International Symposium on Electronic Commerce and Security*, 2009
9. Wu, D.C., Tsai, W.H.: A steganographic method for images by pixel-value differencing. *Pattern Recogn. Lett.* **24**, 1613–1626 (2003)
10. Wang, C.-M., Wu, N.-I., Tsai, C.-S., Hwang, M.-S.: A high quality steganographic method with pixel-value differencing and modulus function. *J. Syst. Softw.* **81**(1), 150–158. ELSEVIER. January (2008)
11. Sherly, A.P., Amritha, P.P.: A compressed video steganography using TPVD. *Int. J. Database Manage. Syst. (IJDMS)* **2**(3), 67–80 (2010)
12. Zaker, N., Hamzeh, A., Katebi, S.D., Samavi, S.: Improving security of pixel value differencing steganographic method. In: *IEEE 978-1-4244-6273-5/09/\$26.00 ©2009* (2009)
13. Lempel–Ziv–Markov chain algorithm “wikipedia.org”. http://en.wikipedia.org/wiki/Lempel-Ziv-Markov_chain_algorithm
14. Lempel Ziv Markov algorithm and 7-Zip, “blogs.oracle.com”. https://blogs.oracle.com/clayb/entry/lempel_ziv_markov_algorithm_and
15. The vernam cipher, “cryptomuseum.com”. <http://www.cryptomuseum.com/crypto/vernam.htm>

16. Das, D., Nath, J., Mukherjee, M., Chaudhury, N., Nath, A.: An integrated symmetric key cryptography algorithm using generalized vernal cipher method and DJSA method: DJMNA symmetric key algorithm. In: Proceedings of IEEE International conference: World Congress WICT-2011 held at Mumbai University, 2011
17. Doran, R.W.: The gray code1. *J. Univers. Comput. Sci.* **13**(11), 1573–1597 (2007)
18. Miroslav G, Jessica J. F., Rui D.: Distortion-free data embedding for images. In: Proceedings of 4th International Workshop, 27–41, (2001) Print ISBN 978-3-540-42733-9

Unsupervised Classification of Mixed Data Type of Attributes Using Genetic Algorithm (Numeric, Categorical, Ordinal, Binary, Ratio-Scaled)

Rohit Rastogi, Saumya Agarwal, Palak Sharma,
Uarvarshi Kaul and Shilpi Jain

Abstract Data mining discloses hidden, previously unknown, and potentially useful information from large amounts of data. As comparison to the traditional statistical and machine learning data analysis techniques, data mining emphasizes to provide a convenient and complete environment for the data analysis. Data mining has become a popular technology in analyzing complex data. Clustering is one of the data mining core techniques. In the field of data mining and data clustering, it is a highly desirable task to perform cluster analysis on large data sets with mixed numeric, categorical, ordinal, and ratio-scaled with binary and nominal values. However, most already available data merging and grouping through clustering algorithms are effective for the numeric data rather than the mixed data set. For this purpose, this paper makes efforts to present a new amalgamation algorithm for these mixed data sets by modifying the common cost function, trace of the within cluster dispersion matrix. The genetic algorithm (GA) is used to optimize the new cost function to obtain valid clustering result. We can compare and analyze that the GA-based clustering algorithm is feasible for the high-dimensional data sets with mixed data values that are obtained in real life results. **Core Idea of Our Paper:** By this paper, we try to describe a technique for estimating the cost function metrics from mixed numeric, categorical and other

R. Rastogi (✉) · S. Agarwal · P. Sharma · U. Kaul · S. Jain
Computer Science and Engineering Department, ABES Engineering College,
Ghaziabad, Uttar Pradesh, India
e-mail: rohit.rastogi@abes.ac.in

S. Agarwal
e-mail: mail4somya.ag@gmail.com

P. Sharma
e-mail: sharma.palak595@ymail.com

U. Kaul
e-mail: saniakaul27@gmail.com

S. Jain
e-mail: shilpijain474@gmail.com

type databases by using an uncertain grade-of-membership clustering model with the efficiency of Genetic Algorithm. This technique can be applied to the problem of opportunity analysis for business decision-making. This general approach could be adapted to many other applications where a decision agent needs to assess the value of items from a set of opportunities with respect to a reference set representing its business. For processing numeric attributes, instead of generalizing them, a prototype may be developed for experiments with synthetic and real data sets, and comparison with those of the traditional approaches. The results confirmed the feasibility of the framework and the superiority of the extended techniques.

Keywords Clustering algorithms · Categorical dataset · Numerical dataset · Clustering · Data mining · Pattern discovery · Genetic algorithm

1 Introduction

The basic operation in Data Mining is partitioning a set of objects in database into homogeneous groups or clusters. It is useful in a number of tasks, such as unsupervised classification, image processing, sequence analysis, market research, pattern recognition, spatial analysis, economics etc.

An important characteristic is that data in data mining often contains all types of mixed attributes in real life practical applications. The traditional way to treat categorical, nominal, ratio-scaled or ordinal attributes as numeric with the help of dissimilarity matrices (after calculating Euclidean/Manhattan/Minkowski distances is by applying normalization (standard deviation/Z-score or min-max normalization on the results) and the related algorithms for numeric values, but the drawback of this process is that it does not always produce meaningful results, because many categorical domains are not ordered [1].

Most of the already available unsupervised classification algorithms either can handle both data types but are not efficient when clustering large data sets or can handle only the numeric attributes efficiently. To process such large data sets with mixed numeric and categorical and other values, we define a new cost function for clustering by modifying the common used trace of the within cluster dispersion matrix. For minimizing the cost function (to get optimal solution) we introduce genetic algorithm (GA) in clustering process. Since GA uses search strategy globally and fits for implementing in parallel, the benefit of high search efficiency is achieved in GA based clustering process, which is suitable for clustering large data sets [2].

The rest of the paper is organized as follows. The next section gives some mathematical preliminaries of the algorithm. Then we discuss the Genetic-Algorithm briefly with modified and efficient cost function for all the data sets. In last section there are summaries to the discussions.

2 Betterment by Using of Genetic Algorithm and Cost Function

With the basic features of GA like encoding, crossover, mutation, appropriate fitness function and reproduction with survivor selection, the GA can be able to design better clustering and unsupervised classification operations [3].

The proposed approach can be described with experiments and their results. The algorithm can be run on real-life datasets to test its clustering performance against other algorithms. At the same time, its properties are also empirically studied. One observation from the above analysis is that our algorithm’s computation complexity is determined by the component clustering algorithms. So far, many efficient clustering algorithms for large databases are available, it implicate that our algorithms will effective for large-scale data mining applications, too [4].

Cost function is a function that determines the amount of residual error in a comparison and needs to be minimized in optimization experiment. Let $X = \{x_1, x_2, \dots, x_n\}$ denote a set of n objects and $X_i = \{x_{i1}, x_{i2}, \dots, x_{im}\}^T$ be an object represented by m attribute values. Let k be a positive integer. The objective of clustering X is to finds a partition that divides objects in X into k disjoint clusters.

For a given number of objects n, the number of possible partitions of the object-set is definite but highly large. It is not practical to investigate every partition in order to find abetter one for a classification problem. A common solution is to choose a clustering criterion to guide the search for a partition. A clustering criterion is called cost function.

3 Cost Function for Numeric Data and Mixed Data Clustering

The widely used cost function is the trace of the within cluster dispersion matrix. Oneway to define the cost function is

$$C(W) = \sum_{i=1}^k \sum_{j=1}^n w_{ij}^2 (d(x_j, x_i))^2, w_{ij} \in \{0, 1\} \tag{1}$$

Here, w_{ij} is the membership degree of x_j belonging to cluster i. W is an $k \times n$ order partition matrix. The function $d(\cdot)$ is a dissimilarity measure often defined as the Euclidean distance. For the data set with real attributes, i.e., $X \subset R^m$, we have

$$d(x_j, x_i) = \left(\sum_{l=1}^m |x_{jl} - x_{il}|^2 \right)^{1/2} \tag{2}$$

Since, w_{ij} indicates x_j belonging to cluster i, and $w_{ij} \in [0, 1]$ we call W to be a hard k-partition. For Mixed Data Clustering cost function can be calculated by following rules.

For clustering the numeric data, we use max–min normalization for numeric data. First we will normalize numeric data so as to prevent the dominance of particular attribute. For which the normalization formula is as follows:-

$$n_i = \frac{x_i - \min(x_i)}{\max(x_i) - \min(x_i)} \times (Rh - Rl) + Rl \quad (3)$$

where, x_i is the i th object, Rh and Rl are the higher and lower ranges respectively. N is the new normalized matrix containing all types of data.

For normalizing the ratio scaled values, first, we will take log of the ratio-scaled values, given as

$$f(n) = \log(n) \quad (4)$$

For normalizing the ordinal values, First we assign ranks to the values as, better the value higher the rank and vice versa. Now, based on their ranks we will normalize them. Give 1 to the highest rank and 0 to the lowest one and other ranks get the value as:

$$\sphericalangle(r) = \frac{1}{\text{no. of different ordinal values} - 1} \times (r - 1) \quad (5)$$

For normalizing the categorical scaled values, If the two values match put value 1 and otherwise 0.

$$\delta(a, b) = \begin{cases} 0 & a = b \\ 1 & a \neq b \end{cases} \quad (6)$$

4 Re-defining Cost Function

When N has attributes with numeric and mixed values, assuming that each object is denoted by $n_i = [n_{i1}^r, \dots, n_{it}^r, n_{i,t+1}^r, \dots, n_{im}^c, n_{i,m+1}^r, \dots, n_{iy}^b, n_{i,y+1}^o, \dots, n_{iu}^o, n_{i,q+1}^r, \dots, n_{is}^{rs}]$, the dissimilarity between two mixed-type objects n_i and n_j can be measured by the following Eq. (7).

$$\begin{aligned} d(n_i, n_j) = & \left[\left(\sum_{l=1}^t |n_{il}^r - n_{jl}^r| \right)^2 + \sphericalangle_1 \cdot \left(\sum_{l=t+1}^m |n_{il}^c - n_{jl}^c| \right)^2 \right. \\ & + \sphericalangle_2 \cdot \left(\sum_{l=m+1}^y |n_{il}^b - n_{jl}^b| \right)^2 + \sphericalangle_3 \cdot \left(\sum_{l=y+1}^u |n_{il}^o - n_{jl}^o| \right)^2 \\ & \left. + \sphericalangle_4 \cdot \left(\sum_{l=y+1}^u |n_{il}^{rs} - n_{jl}^{rs}| \right)^2 \right]^{1/2} \quad (7) \end{aligned}$$

where all the terms are squared Euclidean distance measure on the mixed attributes [5].

Using Eq. (7) for mixed-type objects, we can modify the cost function of Eq. (1) for mixed data clustering. In addition, to extend the hard k-partition to fuzzy situation, we further modify the cost function for fuzzy clustering as:

$$\begin{aligned}
 C(w) = & \sum_{l=1}^k \left(\sum_{j=1}^n w_{ij}^2 \sum_{l=1}^t |x_{jl}^r - p_{il}^r|^2 + \alpha_1 \cdot \sum_{j=1}^n w_{ij}^2 \sum_{l=t+1}^m |x_{jl}^c - p_{il}^c|^2 \right. \\
 & + \alpha_2 \cdot \sum_{j=1}^n w_{ij}^2 \sum_{l=m+1}^y |n_{il}^b - n_{il}^b|^2 \\
 & \left. + \alpha_3 \cdot \sum_{j=1}^n w_{ij}^2 \sum_{l=y+1}^u |n_{il}^o - n_{il}^o|^2 + \alpha_4 \cdot \sum_{l=y+1}^u |n_{il}^{rs} - n_{il}^{rs}|^2 \right), \\
 & w_{ij} \in [0, 1]
 \end{aligned} \tag{8}$$

Let

$$\begin{aligned}
 C_i^r &= \sum_{j=1}^n w_{ij}^2 \sum_{l=1}^t |x_{jl}^r - p_{il}^r|^2 \\
 C_i^c &= \alpha_1 \cdot \sum_{j=1}^n w_{ij}^2 \sum_{l=t+1}^m |x_{jl}^c - p_{il}^c|^2 \\
 C_i^b &= \alpha_2 \cdot \sum_{j=1}^n w_{ij}^2 \sum_{l=m+1}^y |n_{jl}^b - n_{il}^b|^2 \\
 C_i^o &= \alpha_3 \cdot \sum_{j=1}^n w_{ij}^2 \sum_{l=y+1}^u |n_{jl}^o - n_{il}^o|^2
 \end{aligned} \tag{9}$$

We rewrite Eq. (8) as:

$$C(W) = \sum_{i=1}^k (C_i^r + C_i^c + C_i^b + C_i^o) \tag{10}$$

5 GA-Based Clustering Algorithm for Mixed Data

To obtain the optimal fuzzy clustering of the large data set with mixed values, genetic algorithms are employed to minimize the cost function. Since GA is a global search strategy in random fashion, it has high probability to achieve the global optima. Moreover, GA is fit for implementation in parallel, so GA-based clustering algorithm will be suitable for large data set. GA is a search strategy based on the mechanism of natural selection and group inheritance in the process of biology evolution. It simulates the cases of reproduction, mating and mutation in reproduction. GA looks each potential solution as an individual in a group (all possible solutions), and encodes each individual into a character string. By a pre-specified objective function, GA can evaluate each individual with a fitness value [6]. In the beginning, GA generates a set of individuals randomly, then some genetic operations, such crossover, mutation and etc., are used to perform on these

individuals to produce a group of offspring. Since these new individuals inherit the merit of their parents, they must be better solution over their predecessors. In this way, the group of solution will evolve toward more optimal direction [7].

6 GA-Based Clustering Algorithm

6.1 Algorithm

- Step 1. Begin
- Step 2. Define pop-size as desired population size
- Step 3. Randomly initializes pop-size population
- Step 4. While (Ideal best found or certain number of generations met)
 - Evaluate fitness
 - While (number of children = population size)
 - Select parents
 - Apply evolutionary operators to create children
 - End while
- Step 5. End While
- Step 6. Return Best solution
- Step 7. End

To employ GA to solve the clustering, the following three problems should be settled first.

- (1) How to encode the clustering solution into the gene string?
- (2) How to design a reasonable fitness function for our clustering problem?
- (3) How to select or design genetic operators including their parameters to guarantee fast convergence.

6.2 Encoding, Fitness Function and Genetic Operators

From the cost function in Eqs. (1) and (8), it is clear that the objective of clustering is to obtain a (fuzzy) partition matrix \mathbf{W} . Then using the fitness function (stated below) we can improve the chances of a particular data point to be chosen. Then after selecting that particular cluster we can further subdivide the data points in the cluster, based on their fitness values [8].

Note that since we process data with mixed attributes, besides the numeric parameters, there are other mixed parameters in gene string. Due to this, it is not ordered for the binary attributes; they can be directly encoded rather than should be normalized first [9].

We are taking the fitness function such that fitness value is inversely proportional to the cost function value, i.e., the smaller the cost function is, the

better the fuzzy clustering partition. For this case, the GA asks for a bigger fitness value. Hence, we define the fitness function by using the clustering cost function. Exponentially increased cost function will sharply reduce the fitness function.

$$f(g) = \frac{1}{1 + e^{C(W)}} \quad (11)$$

Our GA-based clustering algorithm involves all the basic genetic operators, such as selection, reproduction, crossover and mutation. What we need to do is to specify the probability parameters for each operator. For the N individuals in a generation of population, we sort their fitness value in ascending order and label each individual with its order. The selection probability is specified as:

$$P_s(g_{(i)}) = \frac{f(g_i)}{\sum_{i=1}^n f(g_i)} \quad (12)$$

The operation probabilities for crossover and mutation are adaptively assigned as

$$P_c(g_i, g_j) = \begin{cases} \frac{\alpha_1(f_{max} - f')}{f_{max} - \bar{f}} & f' \geq \bar{f} \\ \alpha_2 & otherwise \end{cases} \quad (13)$$

$$P_m(g_i) = \begin{cases} \frac{\alpha_3(f_{max} - f(g_i))}{f_{max} - \bar{f}} & f(g_i) \geq \bar{f} \\ \alpha_4 & otherwise \end{cases} \quad (14)$$

where, $f_{max} = \max_{l=1}^N \{f(g_l)\}$

$\bar{f} = \sum_{l=1}^N f(g_l)$, $f' = f(g_j)$, and $\alpha_i \in [0, 1]$

Apart from above operators, we define a new operator for the clustering algorithm, Gradient operator. The changes in the existing weights are done as per the formula: Here, The gradient operator includes two steps iteration as:

$$w_{ij} = \sum_{l=1}^k \frac{(d(x_j, x_i))^2}{(d(x_j, x_l))^2}, \forall i, j \quad (15)$$

7 A Real-Life Practical Sample Data Table of Mixed Data Types

We are representing the real life concept of our approach by taking the data of 5 employees working in a company. Here we will use every kind of data (related to all data types) to show that our method works for every kind of data. In this example, we are taking the weighted matrix (w_{ij}) as (Table 1) [10].

Table 1 Weighted matrix

	1	2	3	4	5
1	0				
2	0.4	0			
3	0.2	0.2	0		
4	0.1	0.3	0.2	0	
5	0.5	0.2	0.1	0.4	0

Test-1 contains salary of an employee (numeric data)

Test-2 shows whether the employee is male or female(binary data- Male = 1/Female = 0)

Test-3 shows the department to which employee belong (categorical data)

Test-4 depicts the ability of an employee (ordinal values)

Exc.-Excellent, Fair or Good

Test-5 shows avg. credit points allotted according totheir performance (ratio-scaled values)

Last Column shows the log value of ratio-scaled data type

Table 2 Table representing data of five employees

Object-id	Test-1 (K)	Test-2	Test-3	Test-4	Test-5	Log
1	25	M	Code-A	Exc.	445	2.65
2	40	F	Code-B	Fair	22	1.34
3	55	M	Code-C	Good	164	2.21
4	27	M	Code-A	Exc.	1210	3.08
5	53	F	Code-B	Fair	38	1.58

Table 3 Normalised matrix

	1	2	3	4	5
1	0	0	0	0	0
2	0.5	1	1	1	1.31
3	1	0	1	0.5	0.44
4	0.0666	0	0	0	0.43
5	0.9333	1	1	1	1.07

Table 4 Table evaluated using expression 16

	1	2	3	4	5
1	0				
2	4.9961	0			
3	2.4436	2.2569	0		
4	0.1893	3.962	2.1213	0	
5	5.0159	0.2453	1.6153	4.1607	0

Table 5 Further evaluated table

	1	2	3	4	5
1	0				
2	0.0799	0			
3	0.0977	0.0903	0		
4	0.0018	0.3566	0.0848	0	
5	1.2539	0.0098	0.0165	0.6571	0

Table 6 Table representing fitness value using expression 11

1	1.3455
2	0.5366
3	0.2013
4	1.1063
5	1.9373

Table 7 Further evaluated table

1	0.2066
2	0.3689
3	0.4498
4	0.2497
5	0.1259

Table 8 Table representing selection probability

1	0.1474
2	0.2633
3	0.3204
4	0.1782
5	0.0898

The Table 2 is converted into the normalized matrix using the above Eqs. (3), (4), (5), and (6) (Table 3).

We calculate the expression (stated below) to be further used in Eq. (8) (Tables 4, 5).

$$\sum_{j=1}^n d(x_j, x_i) \tag{16}$$

Now for Eq. (8) we are calculating the value of the expression:

$$\sum_{j=1}^n w_{ij}^2 (d(x_j, x_i))^2 \tag{17}$$

Now we will calculate the expression:

$$\sum_{i=1}^k \sum_{j=1}^n w_{ij}^2 (d(x_j, x_i))^2 \quad (18)$$

Now using the Eq. (11) we find the fitness value of the above calculated values (above 5 tuples) (Tables 6, 7).

First we arrange the above values in ascending order and label each one of them and then using Eq. (12), Calculate the selection probability $P_s(g_{(i)})$ (Table 8).

8 Analyses on our Experimental Results

By the above calculated tables, we can easily verify the dissimilarity matrices of our real life experimental data shown in tabular structure.

We can comfortably decide the set of clusters based on the fitness values. We are taking the threshold value for our method to be 0.22. Data item 1 and 5 whose fitness value lie below the threshold value can be grouped together in the cluster and the other three tuples can be grouped in another.

Now these clusters can be improved using GA and using the selection probability.

Result. So there can be two clusters:

C1 data items 1 and 5.

C2 data items 2, 3 and 4.

9 Conclusions

Here we have presented the genetic algorithm to cluster large data sets. The clustering performance of the algorithm can be evaluated using a large data set. The proposed results can be used to demonstrate the effectiveness of the algorithms in discovering structures in data.

The emphasis of this paper is put on the issue that employs the genetic algorithm to solve the clustering problem. Though the application is specific for the business, our approach is general purpose and could be used with a variety of mixed-type databases or spreadsheets with categorical, numeric and other data values, and temporal information. With improved metrics, artificial intelligence algorithms and decision analysis tools can yield more meaningful results and agents can make better decisions.

This approach, then, can ultimately lead to vastly improved decision-making and coordinating among business units and agents alike. If a class attribute is involved in the data, relevance analysis between the class attribute and the others

(or feature selection) should be performed before training to ensure the quality of cluster analysis. Moreover, most variants of the GA use Euclidean-based distance metrics. It is interesting to investigate other possible metrics like the Manhattan distance or Cosine-correlation in the future. To faithfully preserve the topological structure of the mixed data on the trained map, we integrate distance hierarchy with GA for expressing the distance of categorical values reasonably.

Acknowledgments The authors would like to thank the reviewers for their valuable suggestions. They would also like to thank rev. HOD-CSE, Prof. Dr. R. Radhakrishnan for his involvement and valuable suggestions on soft-computing in the early stage of this paper. We would like to thank our friends, family and seniors for their motivation and encouragement. Last but definitely not the least we would thank the almighty god without whose grace this paper would not have achieved success.

References

1. Li, J., Gao, X., Jiao, L.-C.: A GA-based clustering algorithm for large data sets with mixed numeric and categorical values. In: National Key Laboratory of Radar Signal Processing, Xidian University, Xi'an
2. Huang, Z.: A fast clustering algorithm to cluster very large categorical data sets in data mining. In: Proceedings of the SIGMOD Workshop on Research Issues on Data Mining and Knowledge Discovery, pp.1-8, Department of Computer Science, The University of British Columbia, Canada
3. Krovi, R.: Genetic Algorithm for Clustering: A Preliminary Investigation pp. 504-544. IEEE press, Piscataway (1991)
4. Huang, Z., Ng, M.K.: A fuzzy k -modes algorithm for clustering categorical data. *IEEE Trans. Fuzzy Syst.* 7(4), 446-452 (1999)
5. Christian, H., Liao, T.F.: How to find an appropriate clustering for mixed-type variables with application to socio-economic stratification. In: University College London, UK and University of Illinois, Urbana-Champaign
6. Pinisetty, V.N.P., Valaboju, R., Rao, N.R.: Hybrid Algorithm for Clustering Mixed Data Sets. <http://www.iosrjournals.org>
7. Yang, S.-B., Wu Y.-G.: Genetic algorithm for clustering mixed-type data. *Electron Imaging* 20(1), 013003 (10 April 2010, 12 August 2010, 03 December 2010, 08 February 2011). doi:10.1117/1.3537836
8. Chatzis, S.P.: A fuzzy c-means-type algorithm for clustering of data with mixed numeric and categorical attributes employing a probabilistic dissimilarity functional. In: *Expert Systems with Applications* 38, 8684-8689 (2011). doi:10.1016/j.eswa.2011.01.074 , Source: DBLP
9. Holland, J.H.: *Adoption in Natural and Artificial System.* University of Michigan Press, Ann Arbor (1975)
10. Hortaa, D.: *Evolutionary Fuzzy Clustering of Relational Data.* ICMC—USP, São Carlos (2012)

RoHeMaSys: Medical Revolution with Design and Development of Humanoid for Supporting Healthcare

Deepshikha Bhargava and Sameer Saxena

Abstract Healthcare robot technology is one of the emerging issues in the field of robotics, and not only researchers are working in the field of Humanoid but also many companies and institutes have develop Humanoids. The humanoid on healthcare has abilities to support physical and mental health which pertain to functions and interaction with a person. This paper presents an overview towards building an agent based humanoid that will work for the purpose of improving healthcare processes using a system called Robot Healthcare Management System. This paper highlights upon, a healthcare system with a humanoid by using speech, gesture, and emotions. This paper begins with the Introduction and the need of the system in Sect. 1. The Sect. 2 explores the literature relevant to research area. Further this paper discusses the motivation of research and its objectives in Sects. 3 and 4 respectively. The next section highlights upon the role, multi-agent architecture and the functionality of agent engine. At the last paper explores the research methodology and finally concludes.

Keywords RoHeMaSys · Agents · Visual agent (VA) · Audio agent (A2) · Visual-audio agent (VA2)

1 Introduction

The Robot Healthcare Management System is an agent based system will provides functionality as a Humanoid to support physical and mental health of a human. This system is abbreviated as “RoHeMaSys” in this paper. According to the

D. Bhargava (✉) · S. Saxena

Amity Institute of Information Technology, Amity University Rajasthan, Jaipur,
Rajasthan, India

e-mail: dbhargava1@jpr.amity.edu

S. Saxena

e-mail: ssaxena1@jpr.amity.edu

Health Insurance Portability and Accountability Act (HIPAA), “Healthcare is broadly defined as the treatment, management and prevention of illness and the preservation of the physical and mental well being of a person with the help of medical and allied health professionals”. The goal of a healthcare system, according to the World Health Organization is to ensure the good health and respond to the expectations of the population as well as fair financial contribution from the people and the government [28].

1.1 Humanoids

A humanoid is a robot with its overall appearance based on that of the human body [34]. In general humanoid robots have a torso with a head, two arms and two legs, although some forms of humanoid robots may model only part of the body, for example, from the waist up. Some humanoid robots may also have a ‘face’, with ‘eyes’ and ‘mouth’. Androids are humanoid robots built to resemble a male human, and Gynoids are humanoid robots built to resemble a human female [21]. A humanoid may be defined as something that looks like a human and having characteristics like opposable thumb, ability to move to the different directions and even able to give some facial expression [35–37]. A Humanoid robot is fully automated and it can [29,30] adapt to its surroundings and can continue with its goals as given by Human. Humanoid may be friend, teach our children and also can make some decisions [31,33]. The humanoids may change the interaction with machine. Apart from their traditional roles, humanoid robots can be used to explore theories of human intelligence [22]. The concept of Humanoids is being widely implemented in Robotics and these robots are called Humanoid Robots or may be simply “Humanoids”[38–40].

1.2 Need of Humanoid Based Healthcare System

To live with a healthy and happy life in any age is most important issues for a human. So the Researchers, companies are more concentrated on healthcare technology. Healthcare robot technology is one of the challenging issues in the robotics field, and lots of companies and institutions are trying to develop a healthcare robot technology. The healthcare robot must have certain abilities that should allow it to help a person mentally and/or physically. Management of complex medication for older people poses a significant challenge wherein use of information technology could play an important role in improving clinical efficacy and safety of treatment. The use of computing devices, however, presents a special challenge to older/Sick people/children suffering from some mental and health problem given their physical and cognitive limitations. Robotic platforms show the functionality of the user interface to make personalized interaction engaging and empowering, and for proactively reaching out to older/Sick people/children suffering from some mental and health problem to support their healthcare.

The recent trends in robotics are to develop a new generation of robots that are capable of moving and acting in human centric environment, interacting with people, and participating in our daily lives. This has introduced the need for building robotic systems able to learn how to use their bodies to communicate and to react to their users in a social and engaging way. Social robots that interact with humans have thus become an important focus of robotics research [7]. KASPAR which is particularly suitable for human-robot interaction studies specially those who are suffering from autism [14]. Future service robots applications in health-care may require systems to be adaptable in terms of verbal and non-verbal behaviours to ensure patient perceptions for quality healthcare [8].

2 Literature Survey

The concept of human-like automatons is nothing new. Already in the second century BC, Hero of Alexandria constructed statues that could be animated by water, air and steam pressure. In 1495 Leonardo da Vinci designed and possibly built a mechanical device that looked like an armoured knight. It was designed to sit up, wave its arms, and move its head, exile neck while opening and closing its jaw. By the eighteenth century, mechanical dolls were able to write short phrases, play musical instruments, and these dolls can perform other simple, life-like acts [23–26].

Wabot-1 was the first full-scale anthropomorphic robot built in the world. An anthropomorphic manipulator was also developed at NRad in the middle 1980s and was nick-named Greenman. The robot musician Wabot-2 is able to communicate with a person, read a normal musical score with his eyes and play tunes of average difficulty on an electronic organ. The WHL-11 biped walking robot was developed by Hitachi Ltd based on the WL-10R with a computer and hydraulic pump installed. The WASUBOT was another musician robot. Manny was a full scale anthropomorphic manikin. It took 12 researchers 3 years and \$2 million to develop this robot. An anthropomorphic robot called “Hadaly” was also developed in 1995, to study human-robot communication. Honda also introduced 6 feet tall and weighs about 460 pounds “Human” robot a light-weight, human-size and low-cost humanoid robot was developed named Saika. This robot combining a touch screen and voice based interface could offer an effective platform to improve quality of life in elder care [5, 32]. KASPAR [14], a humanoid robot, equipped with tactile sensors able to distinguish a gentle from a harsh touch, and to respond accordingly [27].

3 Motivation of Research

The paper reviewed in Sect. 2 motivated the researcher to pursue the research as mentioned below (Fig. 1):

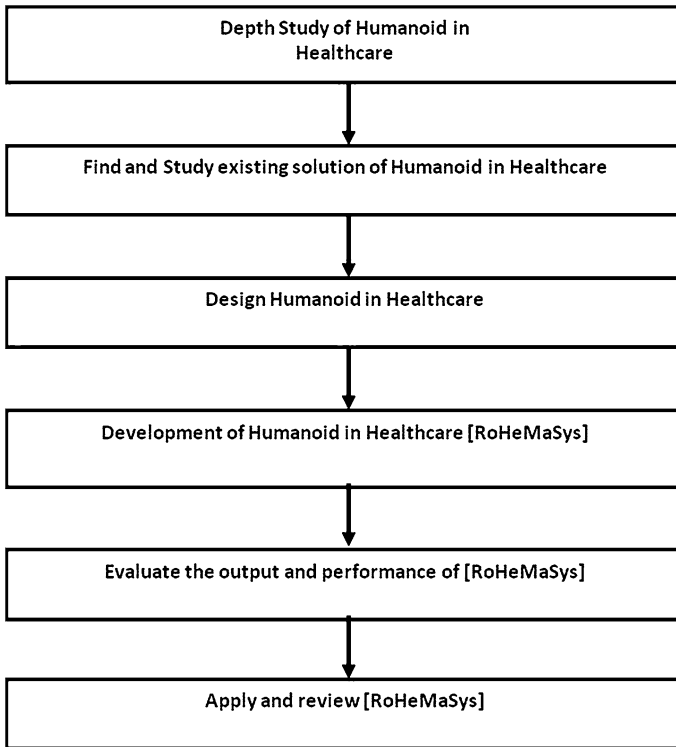


Fig. 1 Research methodology

- (i) To understand that how a robot will be helpful in healthcare [7].
- (ii) To explore the new area to design a new interface of humanoid for the purpose of reaching out to users [5].
- (iii) To discover the high level communication with humans in the form of humanlike skills such as gestures, dialog communication with mutual sympathy [3].
- (iv) To explore the humans-in sensing, kinematics configuration and performance with the help of software agents [4].
- (v) To design & development of humanoid for healthcare [14, 27].

4 Objectives

The objective of this research is to design and develop a Robot Healthcare Management System (RoHeMaSys) with the help of Humanoid. To achieve the research goal the research objective are:

- (i) Identify the problem area wherein the humanoid can be improvised and explored.
- (ii) Formulate the design of Robot healthcare management system using humanoid.
- (iii) Develop a humanoid for the purpose of providing solution in healthcare.
- (iv) Demonstrate the utility of the proposed system.
- (v) Test and Implement the System.
- (vi) Performance Analysis of the System.
- (vii) Identify and review application areas.

5 Agent Based RoHeMaSys

In this paper the agent based architecture is used to provide the solution to the problem. Here the agent used in the system is a multi-agent wherein different agents are used like intelligent agent, information agent and interface agent [50]. The RoHeMaSys is an agent which is interacting with the users like old age persons, patients suffering from Autism and kids; and then responds to the user according to the object at specific distance d . The role of RoHeMaSys can be seen in Fig. 2.

As mentioned above, RoHeMaSys is following a multiagent architecture wherein the user is getting the response from the agent with the help of following agents:

- (i) *Interface Agent*: For interact with the user with response or actions.
- (ii) *Information Agent*: To search, send and receive the information or decision from Knowledgebase.
- (iii) *Intelligent Agent*: To learn the old or new actions/decision from or to knowledgebase.
- (iv) *Visual Agent (VA)*: To identify the visual object and forward the data.
- (v) *Audio Agent (A^2)*: To identify the audio object and forward the data.
- (vi) *Visual-Audio Agent (VA^2)*: To identify the Visual and Audio objects and forward the data.

The above mentioned agents work under the umbrella activities of Agent Engine RoHeMaSys as mentioned in Fig. 3:

The agent based system of RoHeMaSys functions for the purpose providing correct information about the object to the user. The following steps are followed to perform these functions:

- Step # 1 Users (Old age persons, Patient suffering from Autism, kids etc.) are linked with the agent RoHeMaSys called Agent Engine.
- Step # 2 The interface agent of Agent Engine collects and forwards the information of the object which is in front of the user at distance d . This agent is also responsible for identifying the object whether it is Visual, Audio or a combination of both.

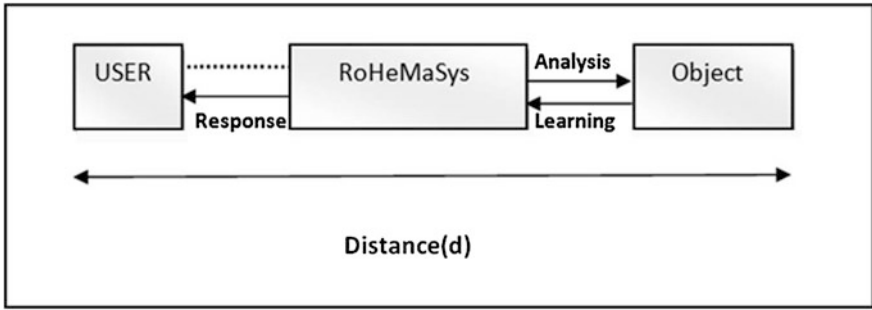


Fig. 2 Role of RoHeMaSys

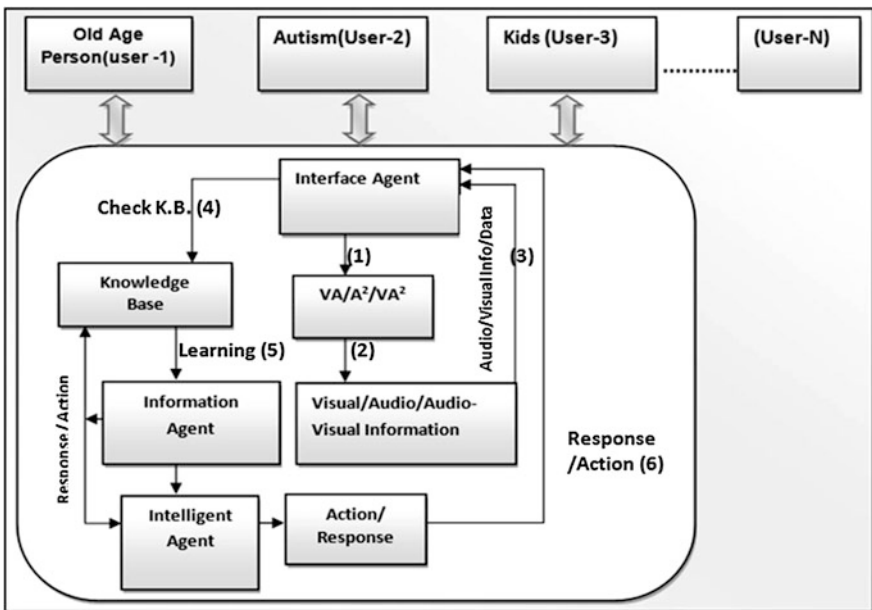


Fig. 3 Multi-agent architecture of RoHeMaSys

- Step # 3 Based upon this result the information of the object will be transferred to the relevant agent like VA or A2 or VA2.
- Step # 4 As per the information collected, the concerned agent will send the relevant information (visual, audio or Mix) to Information agent.
- Step # 5 The information agent will search in any one of the knowledgebase for availability of object data.

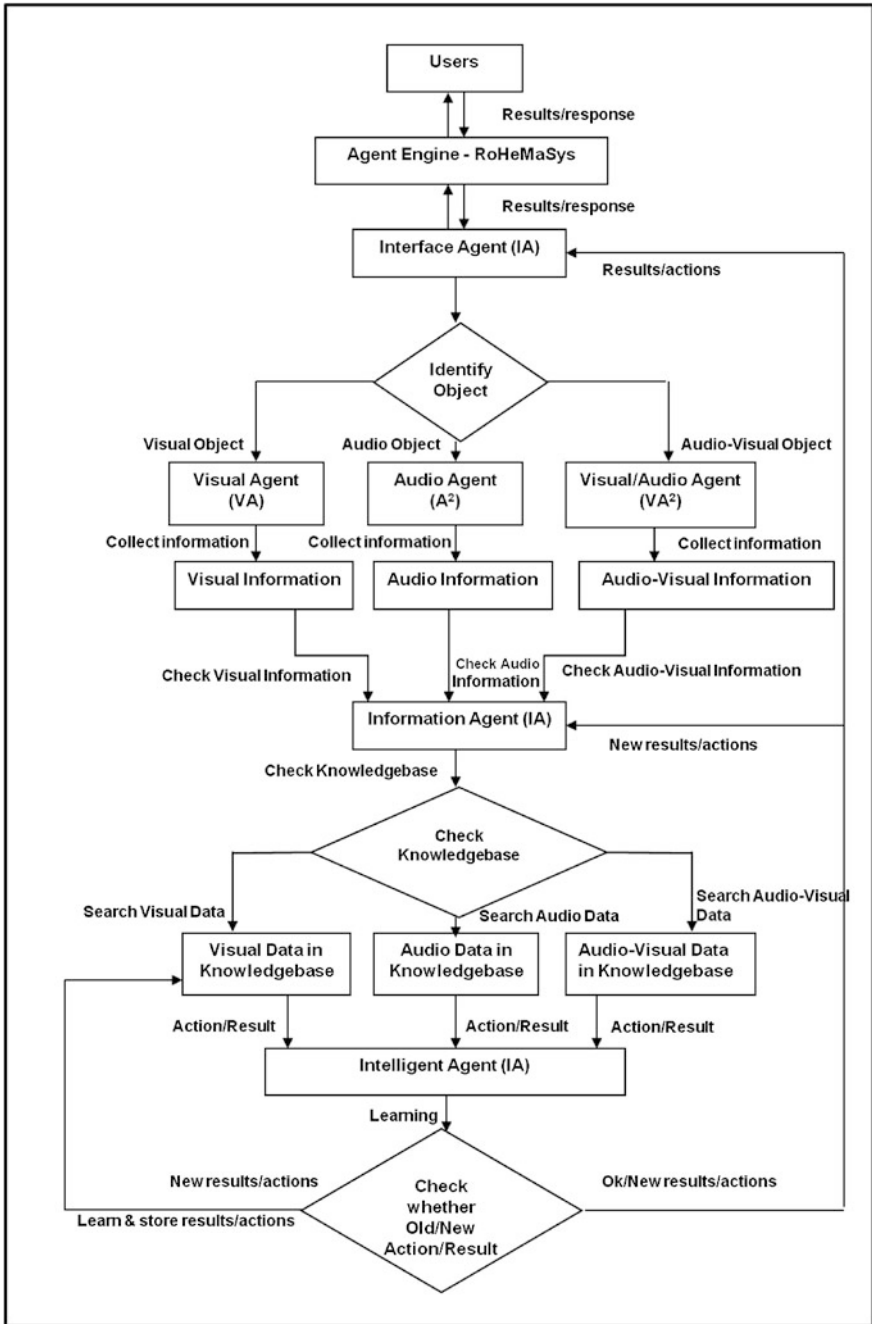


Fig. 4 Functionality of agent engine-RoHeMaSys

- Step # 6 The intelligent agent will identify whether the object is new or the old one. If the object is new then the response and the actions will be stored in relevant knowledgebase and also sends the same response to the interface and information agent for the purpose of storage and response to the user.
- Step # 7 If the object is old then the results or actions will be directed to the interface agent which in-turn will respond to the user.
- Step # 8 The functionality of agent engine RoHeMaSys can be explored through Fig. 4:

6 Conclusion

If we have a specific physical disability the humanoid robots will be programmed to mitigate that disability. If we have a specific mental disability, humanoid robots may help us to adjust and, if necessary, the humanoid may be programmed to detect, identify, and respond to any abnormal behaviour to influence positive outcomes.

To provide care to the society with old age who are suffering with Alzheimer, dementia, arthritis, osteoporosis, and countless other diseases. Some may be lucky and live as healthy as a horse in old age, but most will experience disease that may require assistance with medicine, bathing and feeding until a cure is found for any specific disease, the elderly must turn to their friends, their family, their aides, their service animals—or to their humanoid robots.

The security of the kids is another major issue, the humanoid can inform if the child is in danger area or humanoid can be used to even play with child. The agent based Humanoid can provide therapy to children suffering with autism. Humanoid can also work as a security guard in the offices, shopping mall and other public areas.

The future work concentrates upon design and development of a system to provide solutions in above stated area.

References

1. Park, M., et al. Automatic configuration recognition methods in modular robots. *Int. J. Robot. Res.* **27**(3–4), 403–421 (2008)
2. Yi, Sungil, et al.: Healthcare robot technology development. *World Congress*, vol. 17, no. 1 (2008)
3. Jung, H.-W., Seo, Y.-H., Ryoo, M.S., Yang H.S.: Affective communication system with multimodality for humanoid robot. In: *AMI,IEEE/RAS International Conference on Humanoid Robots*, vol. 2, pp. 690–706 (2004)
4. Cheng, G., Hyon, S.-H., Morimoto, J., Ude, A., Hale, J.G., Colvin, G., Scroggin, W., Jacobsen, S.C.: CB: A humanoid research platform for exploring neuroscience. *Adv. Rob.* **21**(10), 1097–1114 (2007)
5. Priyesh, T., Warren, J., Day, K., MacDonald, B., Jayawardena, C., Kuo, I., Igic, A., Datta, C.: Feasibility study of a robotic medication assistant for the elderly. In: *Australasian User Interface Conference* (2011)

6. Cynthia, B., Brooks, A., Chilongo, D., Gray, J., Hoffman, G., Kidd, C., Lee, H., Lieberman, J., Lockerd, A.: Working collaboratively with humanoid robots. In: Humanoid Robots, 4th IEEE/RAS International Conference on IEEE, vol. 1, pp. 253–272 (2004)
7. Tapus, A.: Assistive robotics for healthcare and rehabilitation. In: Proceedings of the 17th International Conference on Control Systems and Computer Science (CSCS) (2009)
8. Swangnetr, M., Zhu, B., Kaber, D., Taylor, K.: Meta-analysis of user age and service robot configuration effects on human-robot interaction in a healthcare application. In: 2010 AAAI Fall Symposium Series (2010)
9. Bischoff, R., Jain, T.: Natural communication and interaction with humanoid robots. In: Second International Symposium on Humanoid Robots (1999)
10. Peters, R.A., Wilkes, D.M., Gaines, D.M., Kawamura, K.: A software agent based control system for human-robot interaction. In: Proceedings of the Second International Symposium on Humanoid Robot (1999, October)
11. Inamura, T., Inaba, M., Inoue, H.: Acquisition of probabilistic behavior decision model based on the interactive teaching method. In Ninth International Conference on Advanced Robotics (ICAR), pp. 523–528 (1999)
12. Swinson, M.L., Bruemmer, D.D.J.: In: IEEE Intelligent Systems Special Issue on Humanoid Robotics, July/August 2000 GUEST. Expanding Frontiers of Humanoid Robotics. Strategic Analysis
13. Sobh, T.M., Wang, B., Coble, K.W.: Experimental robot musicians. *J. Intell. Rob. Syst.* **38**(2), 197–212 (2003)
14. Dautenhahn, K., Nehaniv, C.L., Walters, M.L., Robins, B., Kose-Bagci, H., Assif Mirza, N., Blow, M.: KASPAR—a minimally expressive humanoid robot for human-robot interaction research. *Appl. Bionics Biomech.* **6**(3–4), 369–397 (2009)
15. Laschi, C., Dario, P., Carrozza, M.C., Guglielmelli, E., Teti, G., Taddeucci, D., Leoni, F., Massa, B., Zecca, M., Lazzarini, R.: Grasping and manipulation in humanoid robotics. In: First IEEE-RAS International Conference on Humanoid Robots, Cambridge, MA (2000)
16. Baltes, J., McCann, S., Anderson, J.: Humanoid robots: abarenbou and daodan. In: RoboCup-Humanoid League Team Description (2006)
17. Jiang, S., Nagashima, F.: Biologically Inspired Spinal locomotion Controller for Humanoid Robot, 19th Annual Conference of the Robotics Society of Japan, 517–518 (2001)
18. Wong, C.-C., Cheng, C.-T., Huang, K.-H., Yang, Y.-T.: Design and implementation of humanoid robot for obstacle avoidance. In: FIRA Robot World Congress, San Francisco, CA (2007)
19. Haring, K.S., Mougnot, C., Ono, F., Watanabe, K.: Cultural differences in perception and attitude towards robots. In: International Conference on Kansei Engineering and Emotion Research, Penghu, Taiwan (2012)
20. Lutfi, S.: Will domestic robotics enter our houses? : a study of implicit and explicit associations and attitudes towards domestic robotics (2012) <http://purl.utwente.nl/essays/62205>
21. As given http://www.sciencedaily.com/articles/h/humanoid_robot.htm
22. Adams, B., Breazeal, C., Brooks, R.A., Scassellati, B.: Humanoid robots: a new kind of tool. *Intell. Syst. Appl. IEEE* **15**(4), 25–31 (2000)
23. Behnke, S.: Humanoid robots—from fiction to reality? *Künstliche Intelligenz Heft* **4**, 5–9 (2008)
24. As Given <http://www.androidworld.com/prod06.htm>
25. Dickstein-Fischer, L., et al.: An affordable compact humanoid robot for autism spectrum disorder interventions in children. In: Engineering in Medicine and Biology Society, EMBC, 2011 Annual International Conference of the IEEE (2011)
26. Levin, E.: Software architecture for a humanoid robot for autism spectrum disorder interventions in children Diss. Worcester Polytechnic Institute, Worcester (2012)
27. Costa, S., et al.: “Where is Your Nose?”-Developing body awareness skills among children with autism using a humanoid robot. In: ACHI 2013, The Sixth International Conference on Advances in Computer-Human Interactions (2013)

28. <http://www.whatishealthcare.org>
29. Becker-Asano, C., Wachsmuth, I.: Affective computing with primary and secondary emotions in a virtual human. *Auton. Agent. Multi-Agent Syst.* **20**(1), 32–49 (2010)
30. Do Hoang, Q.A., et al.: Human-robot interactions: model-based risk analysis and safety case construction. In: 6th European Congress on Embedded Real-Time Software and Systems (2012)
31. Fong, T., Nourbakhsh, I., Dautenhahn, K.: A survey of socially interactive robots. *Robot. Auton. Syst.* **42**(3), 143–166 (2003)
32. Pineau, J., Montemerlo, M., Pollack, M., Roy, N., Thrun, S.: Towards robotic assistants in nursing homes: challenges and results. *Robot. Auton. Syst.* **42**(3), 271–281 (2003)
33. Broadbent, E., Jayawardena, C., Stafford, R.Q., MacDonald, B.A.: Human-robot interaction research to improve quality of life in elder care—An approach and issues. In: *Human-Robot Interaction in Elder Care: Papers from the 2011 AAAI Workshop*. WS-11–12, pp. 13–19 (2011)
34. Carlson Tom, Jose del R. Millan: Brain-controlled wheelchairs: a robotic architecture, *IEEE Robot. Autom. Mag.* **20**(1), 65–73 (2013) doi:[10.1109/MRA.2012.2229936](https://doi.org/10.1109/MRA.2012.2229936)
35. Habibizad navin, A., Mirnia, M.K., Branch, T.: A new algorithm to classify face emotions through eye and lip features by using particle swarm optimization. In: 2012 4th International Conference on Computer Modeling and Simulation (ICCMS 2012) IPCSIT, vol. 22 (2012) © Islamic Azad University, Tabriz, Iran (2012, in IACSIT, Singapore press)
36. Shan, C., Gong, S., McOwan, P.W.: Facial expression recognition based on statistical local features. *Universal short title catalogue book* (2009)
37. Mpipiperis, I., Sotiris, M., Strintzis, M. G.: Bilinear models for 3-D face and facial expression recognition. *Information Forensics and Security, IEEE Transactions on* **3**, 498–511 (2008)
38. Hornung, A., Wurm, K.M., Bennewitz, M.: Humanoid robot localization in complex indoor environments. *International Conference on Intelligent Robots and Systems (IROS), 2010 IEEE/RSJ*, (2010)
39. Behnke, S., et al.: NimbRo RS: a low-cost autonomous humanoid robot for multi-agent research. In: *Proceedings of Workshop on Methods and Technology for Empirical Evaluation of Multi-Agent Systems and Multi-robot Teams (MTEE) at the 27th German Conference on Artificial Intelligence (KI2004)*, Ulm, Germany, (2004)
40. Dautenhahn, K., Werry, I.: Issues of robot-human interaction dynamics in the rehabilitation of children with autism. *Proc. From animals to animats* **6**, 519–528 (2000)
41. Khatib, O., Sentis, L., Park, J.-H.: A unified framework for whole-body humanoid robot control with multiple constraints and contacts. In: *European Robotics Symposium*. Springer, Berlin, Heidelberg (2008)
42. Brock, O., et al.: A framework for learning and control in intelligent humanoid robots. *Int. J. Humanoid Rob.* **2**(03), 301–336 (2005)
43. Pai, S., Ayare, S., Kapadia R.: Eye controlled wheelchair. *Int. J. Sci. Eng. Res.* **3**(10), ISSN 2229–5518 (2012)
44. Arai, K., Mardiyanto, R.: Eyes based electric wheel chair control system. *Int. J. Adv. Comput. Sci. Appl.* **2**(12), 98–105 (2011)
45. Platt, R., Brock, O., Fagg, A. H., Karupiah, D., Rosenstein, M., Coelho, J., Huber, M., Piater, J., Wheeler, D., Grupen, R.: A framework for humanoid control and intelligence, in *Proceedings of the IEEE International Conference on Humanoid Robots (HUMANOIDS-03)*, Karlsruhe & Munich, Germany, 2003
46. <http://www.ai.mit.edu/projects/humanoid-robotics-group/>
47. <http://www.mitpressjournals.org/doi/abs/10.1162/jocn.1991.3.1.71>
48. Arsenio, A.: M. Towards pervasive robotics. Massachusetts Institute of Technology Cambridge Artificial Intelligence Lab, Cambridge (2003)
49. Asada, M., et al.: Cognitive developmental robotics as a new paradigm for the design of humanoid robots. *Robot. Auton. Syst.* **37**(2), 185–193 (2001)
50. Bhargava, D., Sinha, M.: Design and implementation of agent based inter process synchronization manager. *Int. J. Comput. Appl.* **46**(21), 17–22 (2012)

Synergy of Differential Evolution and Particle Swarm Optimization

Kedar Nath Das and Raghav Prasad Parouha

Abstract A novel hybrid swarm intelligent algorithm of DE and PSO is proposed in this paper based on a tri-breakup concept in the population. The algorithm thus design is named as DE-PSO-DE, shortly DPD algorithm. By this proposed mechanism, all individuals in the population are portioned into three group's namely inferior, mid and superior group, based on their fitness values. DE is employed to the inferior and superior group whereas; PSO is used in the mid group. Initially the suitable mutation operators for both DEs (used in DPD) are investigated. Later, top 4 DPDs (Viz. DPDs those use best 4 combinations of mutation strategies in DE) are chosen for further study. DPD combines the global search ability of DE and the local search ability of PSO. The process of hybridization offsets the weaknesses of each other. In addition, two strategies namely *Elitism* and *Non-redundant search* have been incorporated in DPD cycle. The supremacy of DPD is realized over a set of typical unconstrained benchmark suite problems. Lastly, all top 4 DPDs are used in solving *three* real life problems. The numerical and graphical results confirm that the proposed DPD yields more accurate values with faster convergence rate. Finally, a particular DPD is recommended as the best amongst all DPDs to solve unconstrained global optimization problems.

Keywords Differential evolution • Particle swarm optimization • Non-redundant search • Elitism

K. N. Das (✉) • R. P. Parouha
NIT Silchar, Assam, India
e-mail: kedar.iitr@gmail.com

R. P. Parouha
e-mail: rparouha@gmail.com

1 Introduction

Optimization plays a very significant role in different applications. There are quite a good number of modern algorithms proposed in the last two decades to solve optimization problems. Due to the variant characteristics in the problem structure, no single algorithm performs consistently for all range of problems. There are many algorithms recommended by different authors in the literature for this task. Differential evolution (DE) is a population-based parameter optimization technique originally proposed by Storn and Price [1]. In DE new individuals are generated by mutation and crossover. Although DE is very powerful, there is very limited theoretical understanding of how it works and why it performs well. The particle swarm optimization (PSO) is motivated from the simulation of simplified social behavior first developed by Kennedy and Eberhart [2]. Due to its simplicity in coding and consistency in performance, it has already been widely used in many areas.

In recent years, some attempts have been made to combine the merits of DE and PSO. Hendtlass [3] proposed a hybrid model that each individual obeys the conventional swarm algorithm, but from time to time the DE is run which may move one individuals from a poorer area to a better area to continue the search. Pant and Thangaraj [4] proposed a new hybrid version of DE and PSO for solving both test and real life global optimization problems. Ming-Feng Han et al. [5] proposed a dynamic group-based differential evolution using a self-adaptive strategy using 1/5th rule (namely GDE). It is based on partitioned the population in two parts in order to applied two different mutation strategies of DE for an effective search of optimal solution. It has both exploitation and exploration abilities.

In this paper, a novel hybrid global optimization method, termed as DPD (DE-PSO-DE), is introduced as an efficiency solver for global optimization problems. DPD is based on a tri-breakup population scheme, in which the individuals of first and last population is enhanced by DE and the individuals of the middle population is evolved by PSO. The mechanism of hybridization inspires the system to keep a good balance between exploration and exploitation in the search space. Moreover it also helps to maintain the diversity in the population during simulation.

The rest of the paper is organized as follows. [Section 2](#) describes the Components of Hybridization Arrangement. [Section 3](#) motivates and in describes the proposed DPD algorithm. [Section 4](#) uses benchmark problems for experimental analysis of result. [Section 5](#) contains the results and discussions. Three different real life problems are solved in [Sect. 6](#). The conclusion is drawn at the last in [Sect. 7](#).

2 Components of Hybridization

The components participated in framing the hybrid system (DPD) is briefly described in this section as follows.

2.1 Differential Evolution (DE)

The three main operators of DE are mutation, crossover and selection.

(a) **Mutation:** There are many mutation strategies in DE, some well-known mutation strategies are listed as follows:

- i. “DE/rand/1/bin”: $v_i = x_{r_1} + F \times (x_{r_2} - x_{r_3})$
- ii. “DE/rand/2/bin”: $v_i = x_{r_1} + F \times (x_{r_2} - x_{r_3}) + F \times (x_{r_4} - x_{r_5})$
- iii. “DE/best/1/bin”: $v_i = x_{best} + F \times (x_{r_2} - x_{r_3})$
- iv. “DE/best/2/bin”: $v_i = x_{best} + F \times (x_{r_2} - x_{r_3}) + F \times (x_{r_4} - x_{r_5})$
- v. “DE/rand-to-best/1/bin”: $v_i = x_{r_1} + F \times (x_{best} - x_{r_2}) + F \times (x_{r_3} - x_{r_4})$
- vi. “DE/current-to-best/1/bin”: $v_i = x_i + F \times (x_{best} - x_i) + F \times (x_{r_2} - x_{r_3})$
- vii. “DE/rand-to-best/2/bin”: $v_i = x_{r_1} + F \times (x_{best} - x_{r_2}) + F \times (x_{r_3} - x_{r_4}) + F \times (x_{r_5} - x_{r_6})$
- viii. “DE/current-to-best/2/bin”: $v_i = x_i + F \times (x_{best} - x_i) + F \times (x_{r_2} - x_{r_3}) + F \times (x_{r_4} - x_{r_5})$

where $F \in [0, 1]$ is the mutation coefficient, x_{best} represents the best individual in the current generation, $i \neq r_1 \neq r_2 \neq r_3 \neq r_4 \neq r_5 \neq r_6$, $i, r_1, r_2, r_3, r_4, r_5, r_6 \in \{1, \dots, N_p\}$, x_i is referred to the *target* vector; v_i is the *mutant* vector.

(b) **Crossover:**

$$U_{j,i,G+1} = \begin{cases} V_{j,i,G+1}; & \text{if } (rand_j \leq CR) \text{ or } (j=j_{rand}) \\ X_{j,i,G}; & \text{if } (rand_j > CR) \text{ or } (j \neq j_{rand}) \end{cases} \quad (1)$$

where $j = 1, 2, \dots, D$; $rand_j \in [0, 1]$; CR is the crossover constant takes values in the range $[0, 1]$ and $j_{rand} \in \{1, 2, \dots, D\}$ is the randomly chosen index.

(c) **Selection:**

$$x_{i,G+1} = \begin{cases} U_{i,G+1}; & \text{if } f(U_{i,G+1}) \leq f(X_{i,G}) \\ X_{i,G}; & \text{otherwise} \end{cases} \quad (2)$$

2.2 Particle Swarm Optimization (PSO)

Particle swarm optimization is a stochastic global optimization method inspired by the choreography of a bird flock. PSO relies on the exchange of information between individuals (called particles) of the population (called swarm). In PSO, each particle adjusts its trajectory stochastically towards the positions of its own

previous best performance (*pbest*) and the whole swarm global best performance (*gbest*). In PSO particle's velocity and position are updated as follows:

$$v = \omega \cdot v + c_1 r_1 (pbest - x) + c_2 r_2 (gbest - x) \quad (3)$$

$$x_{iN} = x_{iN} + v_{iN} \quad (4)$$

where ω is called the “*inertia weight*”; c_1 and c_2 are “*acceleration coefficients*”, r_1 and r_2 are random numbers uniformly distributed in the interval [0, 1].

2.3 *Elitism*

If crossover or mutation performed in an EA algorithm then good candidates may be lost in offspring that are weaker than the parents. Often the EA will re-discover these lost improvements in a subsequent generation but there is no guarantee. To combat this we can use a feature known as *elitism*. Elitism is therefore is a mechanism to retain the overall best individuals. At the end of iteration both the populations obtained (before and after the iterations) are combined and the best half is considered for next generation.

2.4 *NRS Algorithm*

In proposed algorithm, Non-redundant search (NRS) [6] is used as a local search. The NRS algorithm improves the search ability to find the optimal solution for mainly two reasons: (i) Deletion of individuals with the same chromosome in the current population. (ii) Addition of new individuals selected randomly instead of these redundant ones. Consequently NRS helps in improving the search ability.

3 Proposed Method: DE-PSO-DE (DPD)

Each of DE and PSO has some advantages and disadvantages. With hybridization they co-operate to each other for throwing out their inherent drawbacks. Hence, researchers started applying hybridization techniques between them. In fact, the hybrid techniques, being powerful, yields promising results in solving specific problems. In the past decade, numerous hybrids of DE and PSO have been suggested with diverse design ideas from many researchers. GDE (a group-based DE) developed by authors in [5], for global optimization problem. In each cycle of GDE algorithm, the population is being partitioned into two groups according to their fitness, in order to apply two different strategies of mutation in DE. The local mutation model is applied to the superior group in order to explore the search

space near the current best and the global mutation model is applied to the inferior group in order to search the overall potential solution. Inspired by [5] the following observations are noted. Due to the robust behavior of mutation operators, DE has the ability to balance exploration and exploitation, over search space. As reported in [5], DE works better at two different situations where the local search or the global search is essential. However, due to the inherent shortcomings of DE, sometimes, stacking in some local minimal or choosing the path to premature convergence is unavoidable. Hence many a time the diversity in the population need to be maintained.

Therefore introduction of another mechanism becomes essential in the group based hybridization methods, proposed in [5]. It is also observed that the behavior of PSO is to wildly seek the potential solution. It diversifies the candidate solutions in a better way and probably also helps in avoiding some shortcomings of DE, in the hybrid system. Hybridization process hopefully helps to get rid of falling in premature convergence and getting trapped in local optima.

The purpose of incorporating these two giant techniques in a single one is to provide a better and more robust algorithm for solving global optimization problems. Keeping in view the above observations and inspired by the concept of GDE, a tri-breakup-population based mechanism is proposed in this paper. It initiates with a random population. The strings are then sorted according to the increasing order of their fitness. Now the population is being allowed to break into three groups A, B and C namely inferior group, mid group and superior group respectively. Of course the population size is kept fixed to a multiple of 3 to favor the tri-breakup mechanism. According to the local and global searching behavior of DE (as observed above), it is allowed to being employed in both the inferior and superior groups. At the same time Particle Swarm Optimization (PSO) is used in the mid-group to overcome the shortcomings of DE. Therefore the synergy of DE-PSO-DE (DPD) is the hybrid method proposed in this paper. The detailed mechanism (flow diagram) of the proposed DPD is also outlined in Fig. 1.

4 Experiment Setting and Benchmark Problems

4.1 Selection of Mutation Operators for DE in DPD

In DE Algorithm, the role of mutation operator is as a kernel operator. On the basis of review of the past literature [4, 8], researcher used many mutation strategies in DE. For DE, selecting a mutation operator is indeed a difficult task.

Therefore, in the present study, 8 different strategies of most efficient mutation operators have been reconsidered for analysis. The list of those strategies is

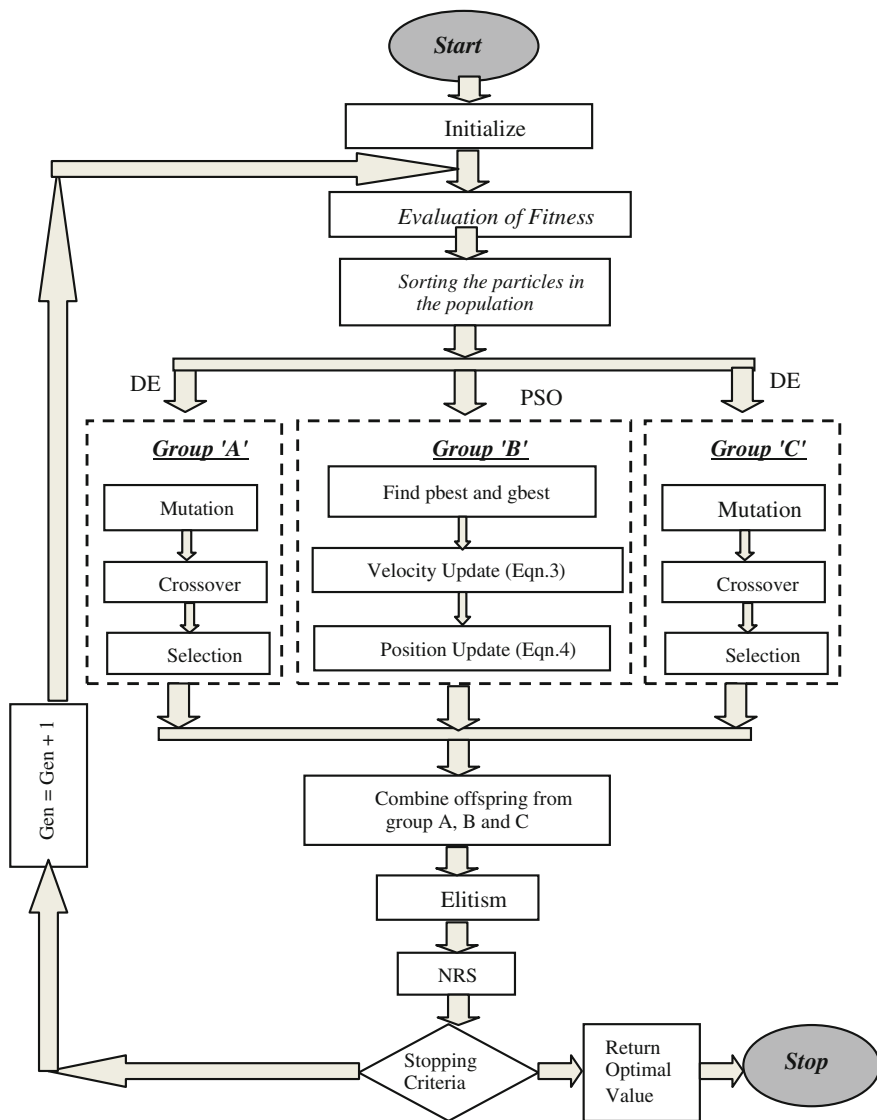


Fig. 1 Flowchart of DPD algorithm

reported in Sect. 2.1. While dealing with DPD, DE is being used two times in a generation. Hence, all combinations of mutation strategies are considered a **(DE with 8 different strategies of mutation) + PSO + (DE with 8 different strategies of mutation) = DPD**

Therefore, a total of $8 \times 8 = 64$ combinations with all possible permutation of mutation operators, are generated by considering one case at a time. For comparison, all combinations (i.e. all forms of DPD) are tested in a set of 23 benchmark problems (quoted in [7]) which is a mixture of both scalable and non-scalable functions. 20 independent runs with 200 iterations are fixed to start the simulation. The average function value of 20 runs for each function is recorded by each of 64 combinations. For a fixed function, the top 20 combinations are collected according to the better function values obtained. The numbers of functions solved by each of the combinations out of 23 problems are reported in Table 2. It is observed from the Table 1 that, since **(3, 3)**, **(3, 7)**, **(3, 5)**, **(3, 1)** mutation combinations solved maximum no of benchmark problems, which is shown in bold face. Hence, they are being renamed as **DPD-1**, **DPD-2**, **DPD-3**, and **DPD-4**, respectively. These four top DPDs are considered for further study.

4.2 Experimental Setting

In order to evaluate the performance of the proposed DPD algorithms, a test suite quoted in [5, 8] (reported in Table 2) with different characteristics have been picked up. Simulations were conducted on a CORE i3, 2.8 GHz computer, 2 GB of RAM, in the C-Free Standard 4.0 Environment.

In the first phase, DPD compared with DE-PSO [4] and HSO [7]. For PSO, the acceleration constants C_1 and C_2 are both set to 2.0, the inertial weights are set to $W_{\max} = 0.9$, $W_{\min} = 0.4$. However for DE in DPD, the mutation factor in group 1 i.e. $F_A = 0.5$ and for group 3 i.e. $F_C = 0.8$; and the crossover weight $CR_A = CR_C = 0.9$. The population size for DPD is set to a value, multiple of 3 to favor the population-tri-breakup system. After an extensive analysis, for dimensions 30, 50, 100 it is fixed to 30, 51, and 99 respectively, for all problems in [4] and [7]. Termination criteria for DPD algorithm are same as DE-PSO [4] and HSO [7].

5 Experiment Results and Discussion

Considering the 30, 50, 100-dimensional 12 benchmark problem set [4] (taken from Table 2) as test bed, the mean function values obtained by top 4 DPDs are reported in Table 3 with DE-PSO [4] results. Better values are highlighted by bold face against each function. It is observed from Table 3 that all DPDs outperform of 12 benchmark test functions, in general. DPD-1 performs better than rest three DPDs.

Table 1 Selection of mutation operator for DPD in 64 different combinations

Combination	No. of functions solved	Combination	No. of functions solved	Combination	No. of functions solved	Combination	No. of functions solved
(1, 1)	04	(3, 1)	20	(5, 1)	01	(7, 1)	13
(1, 2)	09	(3, 2)	19	(5, 2)	01	(7, 2)	11
(1, 3)	06	(3, 3)	23	(5, 3)	01	(7, 3)	15
(1, 4)	08	(3, 4)	18	(5, 4)	03	(7, 4)	12
(1, 5)	08	(3, 5)	20	(5, 5)	02	(7, 5)	11
(1, 6)	05	(3, 6)	19	(5, 6)	01	(7, 6)	11
(1, 7)	08	(3, 7)	21	(5, 7)	02	(7, 7)	13
(1, 8)	05	(3, 8)	18	(5, 8)	02	(7, 8)	10
(2, 1)	02	(4, 1)	16	(6, 1)	10	(8, 1)	09
(2, 2)	01	(4, 2)	19	(6, 2)	09	(8, 2)	06
(2, 3)	00	(4, 3)	13	(6, 3)	08	(8, 3)	08
(2, 4)	01	(4, 4)	18	(6, 4)	10	(8, 4)	06
(2, 5)	02	(4, 5)	16	(6, 5)	09	(8, 5)	07
(2, 6)	01	(4, 6)	17	(6, 6)	10	(8, 6)	10
(2, 7)	03	(4, 7)	17	(6, 7)	10	(8, 7)	09
(2, 8)	03	(4, 8)	17	(6, 8)	10	(8, 8)	07

Only for function f_{11} (30-dim) DE-PSO performed marginally better solution in terms of mean values. From Table 3 it is noted that in general, DPDs are more stable than DE-PSO, as they can be executed with less standard deviations.

Again DPD algorithm applied to standard benchmark problems from [7] (Table 2) and the results were averaged over 50 runs. The results were compared with HSO [7]. Table 4 lists the comparison results including the best values, mean values and standard deviations. Better values are highlighted by bold face. It is observed from Table 4 that all top 4 DPDs produced better or highly similar results as HSO algorithm for all function. Comparing between DPDs, DPD-1 performs better than rest three DPDs. Only for Quartic Function, DPD-2 produced better result as compared to rest three DPDs as well as HSO. From Table 4 the standard deviation of DPD is significantly low compared with HSO. This illustrated that the results generated by DPD is robust.

Overall, among non-DPDs (i.e. DE-PSO and HSO), HSO performs better, but it is worse than DPDs. Therefore, HSO is considered for convergence-comparison graph with all DPDs. In order to visualize the rate of convergence of DPDs, a set of 6 typical test functions with varying difficulty levels, are considered. These functions are Sphere, Schwefel, Rosenbrock, Rastrigrin, Ackley and Griewank. Staring from the same seed, all algorithms allowed running over generations for a fair comparison, it implies all the methods start from same initial population. For the above 6 functions, the convergence graphs are shown in Fig. 2a–f. Undoubtedly from Fig. 2a–f, it is clear that for each of the functions DPDs converges faster than HSO, within few initial generations only. In the other hand, while comparing the convergence amongst DPDs, DPD-1 is the best one.

Table 2 Benchmark functions used in the experimental study, S is the domain of the variables, f_{min} is the function value at global minima, and C is function characteristics with values U: unimodal, M: multimodal, S: separable, N: non-separable

F		Function name	S	C	f_{min}
f_1		Rastrigin	[-5.12, 5.12]	MS	0
f_2		Sphere	[-5.12, 5.12]	US	0
f_3		Griewank	[-600, 600]	MN	0
f_4		Rosenbrock	[-30, 30]	UN	0
f_5		Schwefel	[-500, 500]	MS	-418.9829 * n
f_6		Schwefel 2.22	[-10,10]	UN	0
f_7		Schwefel 1.2	[-100, 100]	UN	0
f_8		Schwefel 2.21	[-100, 100]	US	0
f_9		Penalized	[-50, 50]	MN	0
f_{10}	$f_{10(a)}$	Penalized 1	[-50, 50]	MN	0
	$f_{10(b)}$	Penalized 2	[-50, 50]	MN	-1.1428
f_{11}		Ackley	[-32, 32]	MN	0
f_{12}	$f_{12(a)}$	Quartic	[-1.28, 1.28]	US	0
	$f_{12(b)}$	Dejong's noisy			
f_{13}		Step function	[-100, 100]	US	0
f_{14}		Foxholes	[-65.536, 65.536]	MS	0.998004
f_{15}		Kowalik	[-5, 5]	MN	0.0003075
f_{16}		Six hump camel	[-5, 5]	MN	-1.0316285
f_{17}		Branin	[-5, 10] and [0,15]	MS	0.398
f_{18}		Goldstein-price	[-2, 2]	MN	3
f_{19}		Hertman3	[0, 1]	MN	-3.86
f_{20}		Hertman6	[0, 1]	MN	-3.32
f_{21}		Shekel5	[0, 10]	MN	-10.1532
f_{22}		Shekel7	[0, 10]	MN	-10.4029
f_{23}		Shekel10	[0, 10]	MN	-10.5364

6 Real World Application

In this section three popular real life non-linear optimization problems taken from [4], which are listed below (RP 1–RP 3). These problems are:

RP-1: Gas transmission design

RP-2: Optimal thermohydraulic performance of an artificially roughened air heater

RP-3: Optimal capacity of gas production facilities

Table 3 Experimental result of DPDs with DE-PSO [4] in terms average (standard)

f	Dim	DPD				
		DE-PSO	DPD-1	DPD-2	DPD-3	DPD-4
f ₁	30	1.6141 (3.885)	0.00(0.00)	0.0(0.00)	0.00(0.0)	0.00(0.00)
	50	24.578 (14.62)	0.00(0.00)	0.0(0.00)	0.00(0.0)	0.00(0.00)
	100	251.49 (8.267)	0.000(0.0)	0.00(0.0)	0.00(0.0)	0.000(0.0)
f ₂	30	4.077e-48	1.52e-187	4.13e-181	8.52e-180	2.53e-175
	50	1.593e-47	(4.5e-193)	(6.3e-187)	(1.2e-188)	(9.3e-181)
	100	2.753e-49	4.27e-191	6.32e-181	2.13e-176	5.52e-174
f ₃	30	(1.401e-49)	(6.13e-194)	(4.3e-194)	(1.3e-194)	(8.3e-186)
	50	1.093e-40	8.72e-177	5.36e-169	5.83e-169	7.54e-166
	100	(1.769e-40)	(2.4e-183)	(3.9e-174)	(2.2e-176)	(5.9e-171)
f ₄	30	0.000 (0.00)	0.00(0.00)	0.00(0.00)	0.00(0.00)	0.00(0.00)
	50	5.4e-20 (0)	0.00 (0.00)	0.00(0.00)	0.00(0.00)	0.00(0.00)
	100	1.084e-19	0.00(0.00)	0.00(0.00)	0.00(0.00)	0.00(0.00)
f ₅	30	24.202	8.51e-12	6.66e-11	5.71e-10	4.84e-11
	50	(12.3086)	(1.73e-12)	(3.85e-12)	(2.43e-11)	(3.52e-11)
	100	44.741	8.51e-12	6.66e-11	5.71e-10	4.84e-11
f ₆	30	(1.402)	(1.73e-12)	(3.85e-12)	(2.43e-11)	(3.52e-11)
	50	91.024	2.32e-06	3.19e-04	3.19e-04	7.46e-02
	100	(3.400)	(4.14e-08)	(1.41e-04)	(1.41e-04)	(5.19e-02)
f ₇	30	-12545.8	-12569.5	-12569.5	-12569.5	-12569.5
	50	(47.3753)	(0)	(0)	(0)	(0)
	100	-20913.6	-20929.6	-20929.6	-20929.6	-20929.6
f ₈	30	(54.2753)	(26.142)	(26.142)	(26.142)	(26.142)
	50	-41898.3(0.0)	-41898.3(0)	-41898.3(0)	-41898.3(0)	-41898.3(0)
	100	-41898.3(0.0)	-41898.3(0)	-41898.3(0)	-41898.3(0)	-41898.3(0)

(continued)

Table 3 (continued)

f	Dim	DE-PSO	DPD			
			DPD-1	DPD-2	DPD-3	DPD-4
f ₆	30	2.474e-6	9.6e-133	2.9e-123	6.4e-122	9.2e-123
		(1.440e-06)	(4.4e-139)	(3.7e-129)	(3.4e-126)	(4.5e-128)
f ₈	50	3.697e-5	1.2e-126	1.96e-119	1.96e-119	2.37e-112
		(7.255e-06)	(2.68e-138)	(9.6e-122)	(9.6e-122)	(3.6e-119)
f ₉	30	4.792e-27	1.5e-187	4.3e-181	8.2e-180	2.5e-175
		(4.52e-27)	(4.5e-193)	(6.3e-187)	(1.2e-188)	(9.3e-181)
f ₉	50	2.320e-27	1.62e-183	3.65e-179	5.39e-172	8.92e-169
		(1.21e-27)	(5.3e-190)	(2.3e-183)	(2.3e-176)	(7.2e-176)
f _{10(b)}	100	1.016e-22	9.33e-168	2.56e-153	2.56e-153	8.38e-124
		(1.19e-23)	(2.2e-176)	(5.2e-162)	(5.2e-162)	(2.4e-156)
f ₁₁	30	5.504e-13	1.32e-32	1.32e-32	1.32e-32	1.32e-32
		(0.000)	(2.88e-48)	(2.88e-48)	(2.88e-48)	(2.88e-48)
f ₁₁	50	3.303e-13	1.32e-32	1.32e-32	1.32e-32	1.32e-32
		(0.00000)	(2.88e-48)	(2.88e-48)	(2.88e-48)	(2.88e-48)
f _{10(b)}	30	-1.150(0.0)	-1.15(0.00)	-1.150(0.0)	-1.150(0)	-1.150(0.00)
		(-1.15044(0))	(-1.15044(0))	(-1.15044(0))	(-1.15044(0))	(-1.15044(0))
f ₁₁	50	-1.150(0.0)	-1.15(0.00)	-1.150(0.0)	-1.150(0)	-1.150(0.00)
		(3.697e-15(0))	(4.16e-15(0))	(4.16e-15(0))	(4.16e-15(0))	(4.16e-15(0))
f ₁₁	100	7.250e-15	4.52e-15	4.91e-15	4.91e-15	4.67e-15
		(1.56e-15)	(0.00)	(0.00)	(0.00)	(0.00)
f ₁₁	100	1.025e-15	1.002e-15	1.136e-15	1.136e-15	1.28e-15
		(2.50e-14)	(1.5e-15)	(1.0e-15)	(1.0e-15)	(1.7e-14)

(continued)

Table 3 (continued)

f	Dim	DE-PSO	DPD			
			DPD-1	DPD-2	DPD-3	DPD-4
f _{12(b)}	30	0.0076(0.002)	2.4e-2(1.2e-2)	5.3e-2(3.2e-2)	5.3e-2(1.2e-2)	6.2e-2(3.2e-2)
	50	0.011(0.001)	5.1e-2(3.9e-2)	5.9e-2(3.1e-2)	7.3e-2(6.8e-2)	1.08e-1 (9.2e-2)
f ₁₃	100	0.0358(0.015)	1.3e-1(4.8e-2)	3.7e-1(1.1e-1)	4.7e-1(1.1e-1)	5.8e-1 (3.0e-1)
	30	0.00(0.000)	0.000(0.00)	0.00(0.00)	0.00(0.00)	0.000(0.00)
	50	0.00(0.000)	0.000(0.00)	0.00(0.00)	0.00(0.00)	0.000(0.00)
	100	0.00(0.000)	0.000(0.00)	0.00(0.0)	0.00(0.00)	0.000(0.00)

Table 4 Experimental result of top 4 combinations of DPD with HSO [7]

f	HSO	DPD			
		DPD-1	DPD-2	DPD-3	DPD-4
f ₁ (G = 9000)	0	0	0	0	0
	0	0	0	0	0
	0	0	0	0	0
	7.64e-26	2.2e-186	5.9e-179	3.7e-174	2.5e-173
f ₂ (G = 1500)	1.42e-24	1.3e-184	3.9e-177	6.7e-172	1.8e-171
	3.33e-24	2.4e-186	5.6e-181	1.1e-174	1.7e-173
	0	0	0	0	0
	6.66e-18	0	0	0	0
f ₃ (G = 2000)	3.45e-17	0	0	0	0
	1.90e-06	2.34e-12	4.92e-12	2.92e-12	1.61e-11
	5.70e-04	8.51e-12	6.66e-11	5.71e-10	4.84e-11
	1.77e-03	1.73e-12	3.85e-12	2.43e-11	3.52e-11
f ₅ (G = 9000)	-12569	-12569.5	-12569.5	-12569.5	-12569.5
	-12569	-12569.5	-12569.5	-12569.5	-12569.5
	3.33e-24	0	0	0	0
	4.84e-18	5.3e-133	8.3e-126	3.6e-124	3.1e-123
f ₆ (G = 2000)	1.39e-17	9.6e-133	2.9e-123	6.4e-122	9.2e-123
	8.52e-18	4.4e-139	3.7e-129	3.4e-126	4.5e-128
	5.12e-86	4.2e-098	3.4e-083	5.1e-083	3.4e-075
	1.21e-83	6.8e-088	4.4e-081	8.6e-083	4.6e-072
f ₇ (G = 5000)	5.19e-83	5.3e-111	3.1e-086	4.6e-089	8.8e-077
	1.04e-04	3.3e-189	1.9e-183	3.9e-182	6.9e-177
	1.77e-02	1.5e-187	4.3e-181	8.2e-180	2.5e-175
	3.65e-02	4.5e-193	6.3e-187	1.2e-188	9.3e-181

(continued)

Table 4 (continued)

f	HSO	DPD			
		DPD-1	DPD-2	DPD-3	DPD-4
f ₉ (G = 1500)	6.67e-25	1.69e-32	1.69e-32	1.69e-32	1.69e-32
	2.11e-23	4.71e-32	4.71e-32	4.71e-32	4.71e-32
	2.77e-23	1.15e-47	1.15e-47	1.15e-47	1.15e-47
f _{10(a)} (G = 1500)	1.47e-22	1.32e-32	1.32e-32	1.32e-32	1.32e-32
	2.05e-20	1.32e-32	1.32e-32	1.32e-32	1.32e-32
	2.74e-20	2.88e-48	2.88e-48	2.88e-48	2.88e-48
f ₁₁ (G = 9000)	8.36e-11	4.16e-15	4.44e-15	4.44e-15	4.16e-15
	2.13e-11	4.16e-15	4.44e-15	4.44e-15	4.16e-15
	4.45e-11	0	0	0	0
f _{12(a)} (G = 1500)	3.29e-04	1.64e-04	1.73e-05	1.92e-04	3.27e-04
	8.87e-04	5.92e-04	5.32e-05	5.52e-04	5.29e-03
	4.46e-04	4.52e-04	1.39e-05	2.15e-04	7.28e-05
f ₁₃ (G = 1500)	0	0	0	0	0
	0	0	0	0	0
	0	0	0	0	0
f ₁₄ (G = 100)	0.998	0.998004	0.998004	0.998004	0.998004
	0.998	0.998004	0.998004	0.998004	0.998004
	2.68e-14	2.90e-18	1.49e-16	4.44e-15	3.43e-15
f ₁₅ (G = 4000)	3.07e-04	3.07e-04	3.07e-04	3.07e-04	3.07e-04
	3.07e-04	3.07e-04	3.07e-04	3.07e-04	3.07e-04
	5.94e-19	1.57e-21	2.48e-19	2.14e-12	2.66e-17
f ₁₆ (G = 100)	-1.0316	-1.03162	-1.03162	-1.03162	-1.03162
	-1.0316	-1.03162	-1.03162	-1.03162	-1.03162
	1.01e-07	2.58e-37	1.28e-28	3.61e-18	5.67e-19

(continued)

Table 4 (continued)

f	HSO	DPD			
		DPD-1	DPD-2	DPD-3	DPD-4
f ₁₇ (G = 100)	0.39789 0.39789 4.30e-06	0.397887 0.397887 2.18e-18	0.397887 0.397887 4.16e-12	0.397887 0.397887 1.27e-16	0.397887 0.397887 4.52e-09
f ₁₈ (G = 100)	3 3 3.38e-11	3 3 4.28e-18	3 3 4.21e-12	3 3 4.56e-14	3 3 9.56e-06
f ₁₉ (G = 100)	-3.8628 -3.8628 5.31e-11	-3.8628 -3.8628 1.21e-21	-3.8628 -3.8628 2.14e-11	-3.8628 -3.8628 5.28e-08	-3.8628 -3.8628 1.61e-07
f ₂₀ (G = 100)	-3.322 -3.322 1.45e-11	-3.322 -3.322 9.63e-16	-3.322 -3.322 5.69e-21	-3.322 -3.322 1.23e-12	-3.322 -3.322 6.83e-11
f ₂₁ (G = 100)	-10.15 -10.15 1.02e-04	-10.1532 -10.1532 0	-10.1532 -10.1532 0	-10.1532 -10.1532 0	-10.1532 -10.1532 0
f ₂₂ (G = 100)	-10.40 -10.40 2.07e-05	-10.4029 -10.4029 0	-10.4029 -10.4029 0	-10.4029 -10.4029 0	-10.4029 -10.4029 0
f ₂₃ (G = 100)	-10.54 -10.54 7.26e-04	-10.5364 -10.5364 0	-10.5364 -10.5364 0	-10.5364 -10.5364 0	-10.5364 -10.5364 0

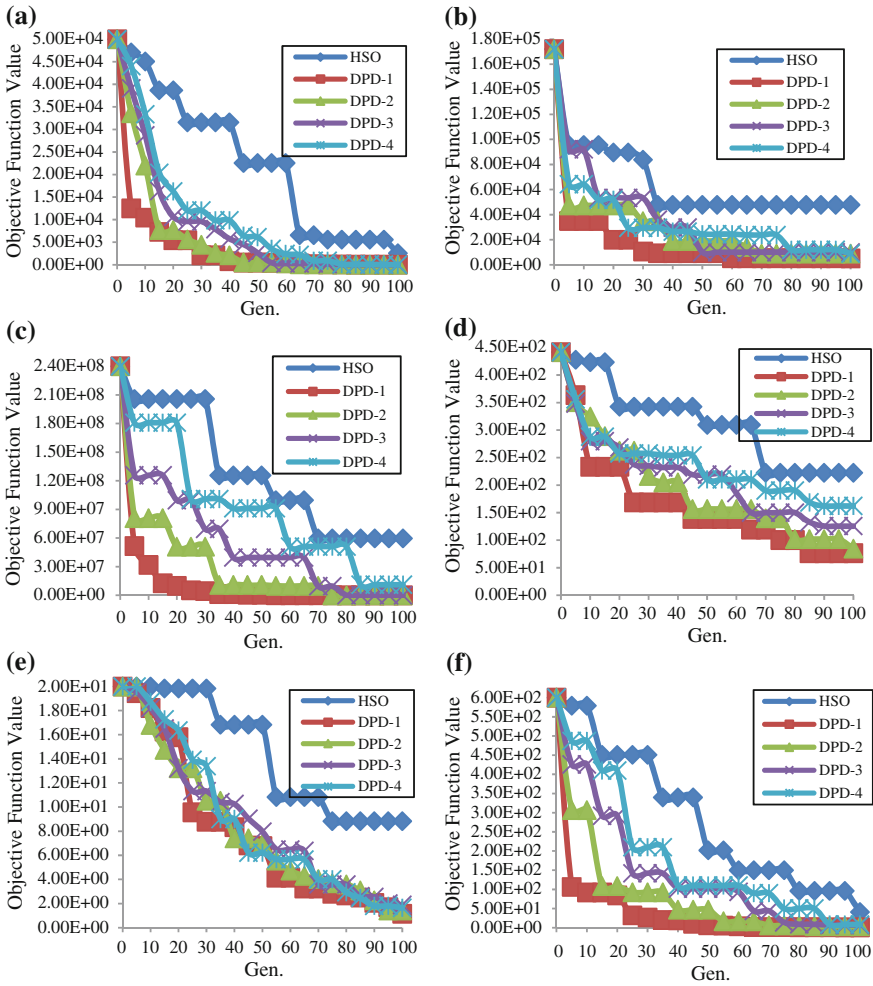


Fig. 2 Convergence graphs of DPDs with HSO. **a** Convergence for sphere (30-dim), **b** convergence for Schwefel (30-dim), **c** convergence for Rosenbrock (30-dim), **d** convergence for Rastrigin (30-dim), **e** convergence for Ackley (30-dim), **f** convergence for Griewank (30-dim)

6.1 Results and Discussion

For the real world problems, results from DE-PSO [4] are considered for comparison. To run all 3 problems, the parameter setting for DPDs are same reported in Sect. 4.2. Termination criteria for DPD are same as DE-PSO [4]. The comparative result is reported in Table 5 best results are shown in bold face. From Table 5, it is seen that out of 3 real life problems, all 4 DPDs achieved marginally better solution. Moreover, DPDs are more stable than DE-PSO. However, while comparing among top 4 DPDs, DPD-1 is the better option.

Table 5 Result comparison for real life problems

Item	DE-PSO	DPD			
		DPD-1	DPD-2	DPD-3	DPD-4
RP1: Gas transmission compressor design					
x_1	53.4474	54.99997	54.99997	54.99997	54.99979
x_2	1.1901	1.1	1.1	1.1	1.100001
x_3	24.7186	10	10	10	10
$f(x)$	296.436e + 4	173.1614e + 04	173.1614e + 4	173.1614e + 4	173.1619e + 4
G_{Avg}	129.6	110.5	110.5	110.5	126.3
RP2: Optimal thermohydraulic performance of an artificially roughened air heater					
x_1	0.15301	0.1155168	0.003760192	0.005937828	0.1047784
x_2	10	10	10	10	10.00001
x_3	3000	4168.170	15198.12	8988.574	4666.775
$f(x)$	4.21422	4.214220	4.214220	4.214220	4.214220
G_{Avg}	83.9	83.5	86.8	86.8	87.39
RP3: Optimal capacity of gas production facilities					
x_1	17.5	17.5	17.5	17.5	17.5
x_2	600	599.9921	600	600	597.4764
$f(x)$	169.844	169.8437	169.8437	169.8437	169.8538
G_{Avg}	9.9	9.1	9.1	9.1	9.4

7 Conclusion

Based on DE and PSO algorithm, an integrated swarm intelligent approach (DPD) is presented. By using global information obtained from DE and PSO, the exploration and exploitation abilities of DPD algorithm are balanced. The DE population uses the global best to generate offspring in every generation. The PSO acquires the best individual after few generations. DPD uses an information exchange mechanism that helps to avoid the premature convergence. Population uses the global best to generate offspring every generation. Form the numerical results it can be concluded that DPD performs better than other compared algorithms for most of the benchmark functions under consideration. Therefore, tri-beak-up technology for the population really makes the DE-PSO-DE faster and robust. Secondly, based on the searching process of an efficient mutation operator, it is worth to conclude that DPD-1 (that uses the scheme “DE/best/1/bin”: $V_i = x_{best} + F \times (x_{r_2} - x_{r_3})$) in both DEs used in DPD is recommended, because the same conclusion is drawn from both numerical result comparison and convergence graph.

References

1. Storn, R., Price, K.: Differential evolution—a simple and efficient heuristic for global optimization over continuous spaces. *J. Global Optim.* **11**(4), 341–359 (1997)
2. Kennedy, J., Eberhart, R.C.: Particle swarm optimization. In: *Proceeding of IEEE International Conference on Neural Networks*. pp. 1942–1948 (1995)
3. Hendtlass, T.: A combined swarm differential evolution algorithm for optimization problems. *Lect. Notes Comput. Sci.* **2070**, 11–18 (2001)
4. Pant, M., Thangaraj, R.: DE-PSO: a new hybrid meta-heuristic for solving global optimization problems. *New Math. Nat. Comput.* **7**(3), 363–381 (2011)
5. Han, M.F., Liao, S.H., Lin, C.T.: *Dynamic group-based differential evolution using a self-adaptive strategy for global optimization problems*. Springer, New York (2012)
6. Zhang, H., Ishikawa, M.: An extended hybrid genetic algorithm for exploring a large search space. In: *2nd International conference on autonomous robots and agents*. pp. 13–15 (2004)
7. Tuba, M., Brajevic, I., Jovanovic, R.: Hybrid seeker optimization algorithm for global optimization. *Appl. Math. Inf. Sci.* **7**(3), 867–875 (2013)
8. Ali, M., Pant, M., Abraham, A.: Simplex differential evolution. *Acta Polytech. Hung.* **6**(5), 95–115 (2009)

Energy Management Routing in Wireless Sensor Networks

Vrince Vimal and Sanjeev Maheshwari

Abstract Wireless Sensor Networks sensor nodes collect, process, and communicate data acquired from the physical environment to an external Base-Station (BS). Its flexibility in terms of the shape of the network and mobility of the sensor nodes makes it special. Sensor nodes in WSNs are normally battery-powered, so energy has to be carefully utilized in order to avoid early termination of sensors' lifetimes. Also sensors position in network is also initially not determined so sensor should be capable of generating optimal routing path and transmitting data to the base station. Second constraint with the sensors is bandwidth. Considering these two limitations it is necessary routing and sensing algorithm that use innovative methods to preserve energy of sensors. In this paper we use neural network to conserve energy of WSN and increase the life of network.

Keywords WSN · Neural network · Energy optimization

1 Introduction

Wireless Sensor Networks (WSNs) comes under wireless ad hoc networks in which sensor nodes collect, process, and communicate data acquired from the physical environment to an external Base-Station (BS). Some of them are capable of sensing a special phenomenon in the environment and send the data back to one or several base stations. A quality of WSN that makes it unique is its flexibility in terms of the shape of the network and mobility of the sensor nodes. WSN can be

V. Vimal (✉) · S. Maheshwari
MIT, MIET Group, Meerut, India
e-mail: vrince.vimal@gmail.com

S. Maheshwari
e-mail: smm_miet@rediffmail.com

deployed in areas where regular sensor networks (even wired networks) cannot operate. Today the application of Sensor Networks can be seen in different aspects of our lives; it is successfully applied in medical applications, military purposes, disaster area monitoring, etc. [1, 2].

But these networks are facing various challenges such as, sensor nodes in WSNs are normally battery-powered, and hence energy has to be carefully utilized in order to avoid early termination of sensors' lifetimes [3]. Since wireless sensors are not physically connected to any central resource of energy, they are completely dependent on their battery source to operate.

Each wireless sensor node is physically not connected to any source of energy, and thus its own battery is the only dependable power supply for it. Sensor nodes are also constrained on bandwidth. Considering these two limitations, it is necessary to design routing and sensing algorithms that use innovative methods to preserve the energy of the sensors [4]. Since the lifetime of the network is highly dependent on the lifetime of the sensor's batteries [5]. The lifetime of the network can only increase by preserving the energy in the sensor nodes. Number of techniques has been evolved to increase the lifetime of the wireless sensor network. Since most of the energy consumption of each node is due to sensing and routing operations, many of the proposed techniques try to optimize these two tasks. Some approaches update the routing path when a sensor node in a path is low in energy [6].

For efficient energy management it is also important monitor a network resources continuously. This same concept has been already investigated in many other environments, e.g., power plants [7], and in many distributed systems [8]. Many recent experimental studies have shown that, especially in the field of sensor networks where low power radio transmission is employed, wireless communication is far from being perfect [9–12].

In this paper we are using neural networks to conserve the energy of WSNs and increase the lifetime of the network. Next sections describe how neural network can be used for efficient distribution of energy in WSNs.

2 Feed Forward Neural Network

The feed forward neural network can learn the input–output pattern pairs by defining the error between desired output and actual output [13].

$$E_x = \frac{1}{2} \sum [T_j - A_j]^2 \quad (1)$$

This represents the total error performance of the network during the training. Here, T_j be the target output and A_j be the actual output. To minimize the error signal, each coupling-strength is to be updated by an amount proportional to the partial derivative of E_x with respect to w_{jh} (weights between hidden and output layer units).

$$\begin{aligned}
\frac{\partial E_x}{\partial w_{hj}} &= \frac{1}{2} \frac{\partial}{\partial w_{hj}} \left[T_j - f \left(\sum_j w_{hj} S_j^h \right) \right]^2 = \{A_j - T_j\} \cdot f' \left(\sum_j w_{hj} S_j^h \right) \cdot S_j^h \\
&= [\{A_j - T_j\} \cdot A_j (1 - A_j)] \cdot S_j^h \\
\frac{\partial E_x}{\partial w_{hj}} &= \delta_j^o \cdot S_j^h
\end{aligned} \tag{2}$$

Where S_j^h is the output from hidden layer?

Similarly the partial derivative of E_x with respect to w_{ih} (weights between input and hidden layer units)

$$\begin{aligned}
\frac{\partial E_x}{\partial w_{ih}} &= \frac{1}{2} \frac{\partial}{\partial w_{ih}} \left[T_j - f \left(\sum_j w_{hj} S_j^h \right) \right]^2 \\
&= \sum_j \{A_j - T_j\} \frac{\partial}{\partial w_{ih}} f \left(w_{hj} S_j^h \right) \\
&= \sum_j \{T_j - A_j\} f' \left(\sum_j w_{hj} S_j^h \right) \left(w_{hj} \frac{\partial S_j^h}{\partial w_{ih}} \right) \\
&= \sum_j \{A_j - T_j\} \{A_j (1 - A_j)\} \left[w_{hj} \left\{ \frac{\partial f \left(\sum_j w_{hj} S_j^h \right)}{\partial w_{ih}} \right\} \right] \\
&= \left[\sum_j \{A_j - T_j\} \{A_j (1 - A_j)\} \{w_{hj} S_j^h (1 - S_j^h)\} \right] S_j^i \\
\frac{\partial E_x}{\partial w_{ih}} &= \delta_j^h \cdot S_j^i
\end{aligned} \tag{3}$$

Here S_j^i is the input, which are critical temperatures

$$\begin{aligned}
\delta_j^h &= \sum_j \{A_j - T_j\} A_j (1 - A_j) S_j^h (1 - S_j^h) w_{hj} \\
\delta_j^h &= \delta_j^o S_j^h (1 - S_j^h) w_{hj}
\end{aligned}$$

so that we can write Eq. (3) as:

$$\frac{\partial E_x}{\partial w_{ih}} = \delta_j^o S_j^h (1 - S_j^h) w_{hj} S_j^i \tag{4}$$

In both Eqs. (2) and (4), is common, which is back-propagated from the units of output layer to the units of hidden layer and coupling strengths will be changed in order to reduce the error signal of the network.

The coupling strengths of output and hidden layers can be updated by following equations.

$$\Delta w_{jh}(s+1) = -\eta \sum_{n=1}^{N_n} \frac{\partial E_x}{\partial w_{hj}} + \alpha [\Delta w_{hj}(s)] \quad (5)$$

and,

$$\Delta w_{ih}(s+1) = -\eta \sum_{n=1}^{N_n} \frac{\partial E_x}{\partial w_{ih}} + \alpha [\Delta w_{ih}(s)] \quad (6)$$

where, s represents the sweep number (i.e. the number of times the network has been through the whole set of cases at which time the coupling strengths are updated), n runs over all cases, N_n is the total number of cases, η represents the learning rate parameter and α represents the momentum term which is the relative contribution of previous change in coupling strengths.

2.1 Most Significant Node Prediction Using Neural Networks

In order to predict Most Significant Node (MSN) in a WSN we are depicting a set of input patterns for a five layered feed forward neural network. These input patterns belong to one wireless sensor node and by using them as the inputs of the neural network we can predict the energy level of the sensor at the last of WSN's lifetime. These patterns may be in the form of features coded from sensor node's distance from the neighboring border, node's distance from sink, Sensor's number of neighbors, the number of neighbors which initially route their data through this sensor. After deploying sensor nodes, base-station receives sensor nodes positions and neighbors' information, thus it can easily calculate these patterns for each sensor and the neural network can be able to predict their final energy level. The neural network can be trained with different network parameters. A well-trained neural network would be able to receive each sensor's features as the inputs and predict its final energy level. Thus, if the neural network be executed for each one of WSN at the start of the WSN's lifetime it would be possible to predict the Most Significant Sensor nodes of the WSN. The result of this prediction is dependent of initial energy management scheme followed by the WSN.

3 Experiment-1

To train our neural network architecture we did an experiment. Our experiment generates random WSNs and calculates all the mentioned characteristic features for each sensor, then it continues to operate until the lifetime of the network ends; at this point our experiment calculated all the sensor's final energy levels and thus

it can use them as the training output of our neural network. Having all the characteristic features and final energy levels of each sensor, the experiment trains the neural network with these input–output feature patterns. Considering equal energy level for all the sensor nodes, the wireless sensor network starts to operate and use the battery of all the sensor nodes. We have also considered a working cycle for all the nodes, meaning that each node is equipped with an internal clock and operates at specific time periods which give the node enough time to route the gathered data. Thus the WSN works in discrete amount of time. The experiment implemented in Visual C++ and Mat lab. In our experiment we used 150 randomly generated WSNs with 90 sensor nodes. At the end of each WSN’s lifetime our experiment runs a training operation on the neural network and trains the neural network using the information from all 90 sensors. The experiment repeats this operation for each one of the 150 random WSNs. After training, we tested the neural network with some newly generated WSNs and the results thus obtained are according to our predictions.

Each WSN is simulated to have 50 randomly scattered sensor nodes. The simulation results showed that in average the lifetime of the network is 24.09. This value is very much dependent on the neural network precision in predicting the energy levels of the sensor nodes; thus it is possible to increase this average lifetime of the WSN by increasing the training iterations which results in creating a more precise neural network. We applied different iterations to our neural network and for each one of these iterations, we observed the average lifetime of 50 random networks. Figure 1 showing the result thus obtained. It can be seen that on increasing the number of iterations and having a more precise neural network, the average lifetime of the random 50 WSNs increased.

3.1 Most Significant Node Prediction Using Neural Networks

The set of Group Head nodes can be selected on the basis of the routing cost metric explored by the equation

$$R_{CM} = \frac{E_k}{A_r \{E^T(N_k^S, N_m^D) + E^R(N_k^S, N_m^D)\}} \quad (7)$$

where, E_k be the energy associated with the delivery ratio of the packet, delivered correctly from source node N^S to the destination node N^D , $E^T(N_k^S, N_m^D)$ is the energy transmitted from N^S and $E^R(N_k^S, N_m^D)$ is the energy received at N^D , A_r be the range area of the network.

The densely populated areas of the network will be overcrowded with Group Head nodes, while the barely populated areas will be left without any Group Head node. In such a situation, it is likely that the high cost sensors from poorly covered

Fig. 1 Average life time of WSN versus training epochs of NN

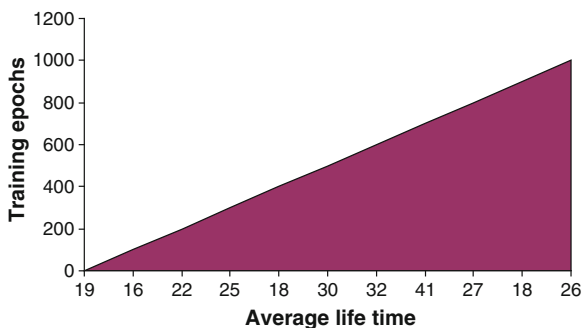
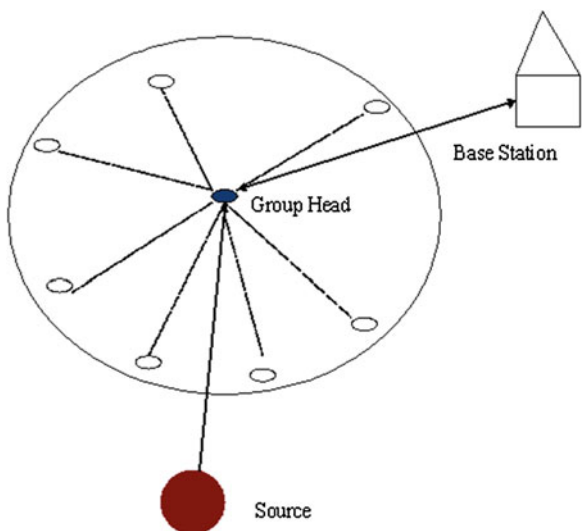


Fig. 2 Layout of a simple WSN

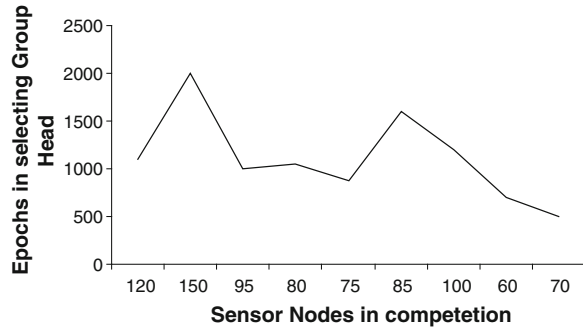


areas will have to perform expensive data transmissions to distant Group Head nodes which will further reduce their lifetime (Fig. 2).

We are using here, five layered feed forward neural network architecture system just like in Fig. 1. We have provided input patterns in form of the sensor nodes competing for Group Head. The node with smallest value of is selected as Group Head.

4 Experiment-2

Now, we have designed the similar experiment to Experiment 1 with a different task. In this experiment we used 600 randomly generated WSNs with 400 sensor nodes. The node’s sensing range was considered 50 m. We provide arbitrary

Fig. 3 Selecting group head

number of competing sensor to our neural network system and seek the convergence for selecting Group Head. The experiment convergence was found to be extremely slow for large data range but is quite good for low range data. Figure 3 reports the convergence of the network while successful selection of the Group Head.

5 Conclusion

In this paper we proposed a neural network approach for energy conservation routing in a wireless sensor network. Our designed neural network system has been successfully applied to our scheme of energy conservation. We have applied neural network to predict Most Significant Node and selecting the Group Head amongst the association of sensor nodes in the network. After having a precise prediction about Most Significant Node, we would like to expand our approach in future to different WSN power management techniques and observe the results. Here, we used arbitrary data for our experiment purpose; it is also expected to generate a real time data for the experiment in future. The selection of Group Head is proposed using neural network with feed forward learning method. And the neural network found able to select a node amongst competing nodes as Group Head.

References

1. Akyildiz, I.F., Su, W., Sankarasubramania, Y., Cayirci, E.: A survey on sensor networks. *IEEE Commun. Mag.* **40**(8), 102–114, (2002)
2. Chong, C-Y., Kumar, S.P.: Sensor networks: evolution, opportunities, and challenges. *Proc. IEEE* **91**(8), 1247–1256 (2003)
3. Al-Karaki, N., Kamal, A.E.: Routing techniques in wireless sensor networks: a survey. *IEEE Wirel. Commun.* **11**(6), 6–28 (2004)
4. Al-Karaki, J.N., Kamal, A.E.: Routing techniques in wireless sensor networks: a survey. *IEEE Wirel. Commun.* **11**(6), 6–28 (2004)

5. Heinzelman, W., Chandrakasan, A., Balakrishnan, H.: Energy-efficient communication protocol for wireless microsensor networks. In: Proceedings of the 33rd Hawaii International Conference on System Sciences (HICSS '00) (2000)
6. Hu, L., Li, Y., Chen, Q., Liu, J-Y., Long, K-P.: A new energy-aware routing protocol for wireless sensor networks. International conference on wireless communications, networking and mobile computing (WiCom 2007), pp. 2444–2447, 21–25 Sept 2007
7. Bates, P.: Debugging heterogeneous distributed systems using event based models of behavior. *ACM Trans. Comput. Syst.* **13**, 1 (1995)
8. Frei, C.: Abstraction techniques for resource allocation in communication networks. Ph.D. Dissertation, Swiss Federal Institute of Technology (EPFL), Lausanne, Switzerland, 2000
9. Cerpa, A., Busek, N., Estrin, D.: Scale: a tool for simple connectivity assessment in lossy environments. Tech. Rep. 21, Center for Embedded Networked Sensing, University of California, Los Angeles (2003)
10. Yarvis, M., Conner, W., Krishnamurthy, L., Chhabra, J., Elliott, B., Mainwaring, A.: Real-world experiences with an interactive ad hoc sensor network. In: Proceedings of the 31st IEEE International Conference on Parallel Processing Workshops (ICPPW), IEEE Computer Society, Vancouver (2002)
11. Zhao, J., Govindan, R.: Understanding packet delivery performance in dense wireless sensor networks. In: Proceedings of the 1st ACM International Conference on Embedded Networked Sensor Systems, SENSYS, ACM Press, Los Angeles (2003)
12. Okdem, S., et al.: Routing in WSN using ant colony optimization router chip. *Sensors* **9**, 909–921. ISSN: 1424-8220 (2009)
13. Sharma, N.K., Kumar, S., Singh, M.P.: Conjugate descent formulation of backpropagation error in feed forward neural network. *ORION* **25**(1), 69–86, ISSN: 0529-191-X (2009)

Axially Symmetric Vibrations of Circular Sandwich Plates of Linearly Varying Thickness

Rashmi Rani and Roshan Lal

Abstract In this paper axisymmetric vibration of circular sandwich plates with honeycomb core of linearly varying thickness has been studied. The facings are of the same thickness and of the same material, are treated as membranes. The facings take the shape of conical shell due to linear thickness variation in the core and hence membranes forces of the facings contribute to the transverse shear of the core. The equations of motion for such a plate have been derived by Hamilton's energy principle. The frequency equations have been obtained by employing differential quadrature method for three different boundary conditions at the edge, namely, clamped, simply supported and free. The lowest three roots of these frequency equations have been obtained for various values of different plate parameters and reported as the frequencies for the first three modes of vibration. Three dimensional mode shapes for specified plates have been presented. Comparison of results with published work has been made.

Keywords Sandwich plate · Honeycomb core · Differential quadrature method

1 Introduction

Sandwich structures are widely used to build large portions of aerospace, automotive and ship structures since past few decades because of their high specific bending stiffness ratio, damping characteristics, excellent fatigue tendency, variety of design and strength properties. Examples are aerodynamic fairings (belly fairing, leading and trailing edge fairings) or control surfaces (rudders, ailerons) [1].

R. Rani (✉) · R. Lal

Department of Mathematics, Indian Institute of Technology Roorkee, Roorkee 24766, India
e-mail: rani.msashmi9@gmail.com

R. Lal

e-mail: rlatmfma@iitr.ernet.in

Sandwich plates of variable thickness are commonly used as structural elements in many industrial applications, and thus help the designer in reducing the weight and size of a structure without compromising its strength and stiffness. Hence, it becomes necessary to analyze the dynamic behavior of sandwich plates with fair amount of accuracy.

In the literature, dynamic behavior of sandwich plates of uniform/non-uniform thickness of various geometries have been investigated by many researchers and reported in references [2–12], to mention a few. Out of these, Ref. [2, 3] are the excellent survey of the work up to 2008 on numerical assessment of classical and refined theories for the analysis of sandwich plates. In these studies, various numerical methods such as Bessel functions [4], Galrkin's method [5], spline finite point method [6], B-spline FSM [7], Discrete layer annular finite element method [8], isoparametric finite element method [9], Finite element method [10], 3D FEM [11], Cubic spline method [12] have been used to obtain the natural frequencies of various models under different constraints.

Recently, differential quadrature method has been emerged as a successful numerical technique with remarkable accuracy to analyze the vibrational characteristics of homogeneous/composite plates in numerous studies and few of them are listed in references [13–16]. Keeping this in view, the present work is an attempt to apply this method to study the axisymmetric vibration of circular sandwich plates of linearly varying thickness. This analysis takes into account the contribution of the face sheets membrane forces to the stresses of the core due to linear thickness variation in the core. The governing differential equations of motion are obtained by Hamilton's principle. Differential quadrature method has been employed to obtain the frequency equations for three different boundary conditions. These frequency equations have been solved numerically using MATLAB. The lowest three roots of these equations have been reported as first three natural frequencies corresponding to the first three modes of vibration. Effect of various plate parameters such as taper parameter, core thickness and face thickness has been studied graphically on the natural frequencies for all the three boundary conditions. Three-dimensional mode shapes have been plotted for specified plate. The frequency parameter has been compared.

2 Equation of Motion

2.1 Displacement–Strain Relations

Consider a circular sandwich plate of radius a and thickness $2(h_c + h_f)$ referred to cylindrical polar coordinate (r, θ, z) , $z = 0$ being the middle surface of the plate and also the plane of symmetry. The line $r = 0$ is the axis of the plate. A cross-sectional view of the plate with linearly varying core thickness $h_c(r)$, the facing thickness $h_f (<< h_c)$ and facing slope ϕ is shown in Fig. 1. Any location in the

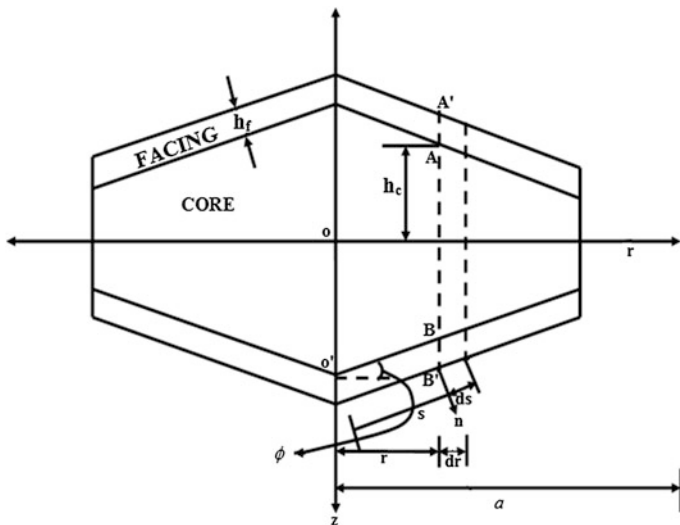


Fig. 1 Cross-section of circular sandwich plate with core of linearly varying thickness

lower or upper facing is identified by its r -coordinate or by its s -coordinate, where $s = s(r)$. The thickness variation of core with radial distance is given by:

$$\frac{dh_c}{dr} = -\tan \phi, \quad h_c = h_o(1 - \alpha \frac{r}{a}), \tag{1}$$

where α is taper parameter and h_o is the thickness of the core at the centre of the plate. The variables s and r are connected by $ds = \sec \phi dr$. During axisymmetric vibration, the movement of the line element $A'B'$ will consist of a rotation $\psi(r, t)$ about the midpoint in the vertical plane parallel to the r -axis and a vertical displacement $w(r, t)$, both assumed to be small. These movements will impart to any point in the core and on the line element $A'B'$ a radial displacement $u_r(r, z, t) = z\psi(r, t)$ and a vertical displacement $u_z(r, z, t) = w(r, t)$. These displacement components give rise to the strain

$$\epsilon_{c_{rz}} = \frac{\partial w}{\partial r} + \psi \tag{2}$$

in the core. All the other strain components $\epsilon_{c_r}, \epsilon_{c_\theta}, \epsilon_{c_{\theta z}}$ and $\epsilon_{c_{r\theta}}$ can be neglected due to the assumption of honeycomb core.

The displacement at the interface of the core and lower facing i.e. at the point B of line element $A'B'$ in the radial and vertical direction are given by

$$\{u_r(r, z, t)\}_{z=h_c} = h_c\psi, \quad \{u_z(r, z, t)\}_{z=h_c} = w(r, t). \tag{3}$$

Using Eq. (3), the tangential (*s*—wise) and normal (*n*—wise) components of displacement of point *B* at the interface of the core and the lower facing are given by

$$u_s = h_c \psi \cos \phi - w \sin \phi, \quad u_n = w \cos \phi + h_c \psi \sin \phi. \quad (4)$$

The displacements given in Eq. (4) give rise to the following meridional and circumferential strains

$$\left. \begin{aligned} \varepsilon_{f_s} &= \frac{\partial u_s}{\partial s} = \left(\frac{dh_c}{dr} \psi + h_c \frac{\partial \psi}{\partial r} \right) \cos^2 \phi - \frac{\partial w}{\partial r} \sin \phi \cos \phi, \\ \varepsilon_{f_\theta} &= \frac{1}{r} (u_s \cos \phi + u_n \sin \phi) = \frac{h_c}{r} \psi, \end{aligned} \right\} \quad (5)$$

in the lower facing. The corresponding strains in the upper facing are $-\varepsilon_{f_s}$ and $-\varepsilon_{f_\theta}$. The suffixes *c* and *f* are used for core and face sheet.

2.2 Stress–Strain Relations

The face sheets and the core are assumed to be homogeneous and isotropic, with the following stress–strain relations:

$$\begin{aligned} \sigma_{c_{rz}} &= G_c \varepsilon_{c_{rz}}, \quad \sigma_{f_s} = \lambda_f (\varepsilon_{f_s} + \nu_f \varepsilon_{f_\theta}), \\ \sigma_{f_\theta} &= \lambda_f (\varepsilon_{f_\theta} + \nu_f \varepsilon_{f_s}) \end{aligned} \quad (6)$$

where E_c , E_f and ν_c , ν_f are Young's moduli and Poisson's ratio of the core and the facings, respectively.

3 Equations of Motion

By Hamilton's energy principle, the equations of motion are obtained as

$$\frac{\partial M_r}{\partial r} + \frac{1}{r} (M_r - M_\theta) - \bar{Q}_r = 2 \left(\rho_c \frac{h_c^3}{3} + \rho_f h_f h_c^2 \sec \phi \right) \frac{\partial^2 \psi}{\partial t^2}, \quad (7)$$

$$\frac{\partial Q_r}{\partial r} + \frac{1}{r} Q_r = 2 (\rho_c h_c + \rho_f h_f \sec \phi) \frac{\partial^2 w}{\partial t^2}, \quad (8)$$

where

$$M_r = M_{c_r} + 2h_c N_{f_s} \cos \phi, \quad M_\theta = M_{c_\theta} + 2h_c N_{f_\theta} \sec \phi,$$

$$Q_r = Q_{c_r} - 2N_{f_s} \sin \phi, \quad \bar{Q}_r = Q_{c_r} + 2 \frac{dh_c}{dr} N_{f_s} \cos \phi,$$

The stress resultant given by

$$\begin{aligned}
 (Q_{c_r}, M_{c_r}, M_{c_\theta}) &= \int_{-h_c}^{h_c} (k_s \sigma_{c_{rz}}, z \sigma_{c_r}, z \sigma_{c_\theta}) dz, \\
 (N_{f_s}, N_{f_\theta}) &= \int_0^{h_f} (\sigma_{f_s}, \sigma_{f_\theta}) dn
 \end{aligned}$$

where k_s is the shear constant. Using non dimensional variable the Eqs. (7) and (8) can be written as

$$x = r/a, \bar{W} = w/a, H_f = h_f/a, H_c = h_c/a, H_o = h_o/a, R_c = \lambda_c/\mu_c, R_f = \lambda_f/\mu_c,$$

$$U_0 \frac{d^2 \Psi}{dx^2} + U_1 \frac{d\Psi}{dx} + (U_2 - \Omega^2 P_2) \Psi + U_3 \frac{d^2 W}{dx^2} + U_4 \frac{dW}{dx} = 0, \quad (9)$$

$$U_5 \frac{d^2 \Psi}{dx^2} + U_6 \frac{d\Psi}{dx} + U_7 \Psi + U_8 \frac{d^2 W}{dx^2} + U_9 \frac{dW}{dx} - \Omega^2 P_{10} W = 0, \quad (10)$$

where

$$U_0 = 3R_f H_f H_c \cos^3 \phi x^2, \quad U_1 = 3R_f H_f x \cos^3 \phi (H_c + 2 \frac{dH_c}{dx}),$$

$$U_2 = 3R_f H_f (x \frac{dH_c}{dx} \cos^3 \phi - H_c \sec \phi) - 3k_s x^2, \quad P_2 = -x^2 H_c (H_c + 3H_f R_\rho \sec \phi),$$

$$U_3 = -3R_f H_f x^2 \sin \phi \cos^2 \phi, \quad U_4 = 3R_f H_f x \sin \phi (v_f - \cos^2 \phi) - 3x^2,$$

$$U_5 = -R_f H_f H_c x \sin \phi \cos^2 \phi,$$

$$U_6 = H_c x - R_f H_f \sin \phi (2x \frac{dH_c}{dx} \cos^2 \phi + v_f H_c + H_c \cos^2 \phi),$$

$$U_7 = R_f H_f \sin \phi (\sin \phi \cos \phi - v_f \frac{dH_c}{dx}) + H_c + x \frac{dH_c}{dx},$$

$$U_8 = x (k_s H_c + R_f H_f \cos \phi \sin^2 \phi),$$

$$U_9 = R_f H_f \cos \phi \sin^2 \phi + H_c + x \frac{dH_c}{dx}, \quad P_{10} = -x (H_c + H_f R_\rho \sec \phi),$$

$$\Omega^2 = \rho_c a^2 \omega^2 / G_c \text{ and}$$

$$R_\rho = \rho_f / \rho_c$$

The solution of Eqs. (9) and (10) in conjunction with the boundary conditions at the edge $x = 1$ together with regularity condition at the center constitute a boundary value problem in the range (0, 1). Due to the presence of variable

coefficients in above equations, their exact solution is not possible. Keeping this in view, an approximate solution is obtained by employing differential quadrature method.

4 Method of Solution

Let x_1, x_2, \dots, x_m be the m grid points in the applicability range $[0, 1]$ of the plate. According to differential quadrature method [17], the n th order derivatives of $W(x)$ and $\Psi(x)$ w.r.t. x can be expressed discretely at the point x_i as follows:

$$W_x^n(x_i) = \sum_{j=1}^m C_{ij}^n W(x_j), \tag{11}$$

$$\Psi_x^n(x_i) = \sum_{j=1}^m C_{ij}^n \Psi(x_j), \quad n = 1, 2 \quad i = 1, 2, \dots, m. \tag{12}$$

where C_{ij}^n are weighting coefficients given by

$$C_{ij}^{(1)} = \frac{M^1(x_i)}{(x_i - x_j)M^1(x_j)}, \quad i, j = 1, 2, \dots, m, \text{ but } j \neq i, \tag{13}$$

$$\text{in which } M^1(x_i) = \prod_{\substack{j=1 \\ j \neq i}}^m (x_i - x_j) \tag{14}$$

and

$$C_{ij}^{(n)} = n(C_{ii}^{(n-1)} C_{ij}^{(1)} - \frac{C_{ij}^{(n-1)}}{x_i - x_j}), \quad i, j = 1, 2, \dots, m, \text{ but } j \neq i, \text{ and } n = 2, \tag{15}$$

$$C_{ii}^{(n)} = - \sum_{\substack{j=1 \\ j \neq i}}^m C_{ij}^{(n)}, \quad i = 1, 2, \dots, m, \text{ and } n = 2, \tag{16}$$

Now, discretizing Eqs. (9) and (10) at the grid points $x = x_i, i = 2, 3, \dots, (m - 1)$, and substituting the values of first two derivatives of W and Ψ from Eqs. (11) and (12), we get

$$\sum_{j=1}^m (U_{0,i} C_{ij}^{(2)} + U_{1,i} C_{ij}^{(1)}) \Psi_j + \sum_{j=1}^m (U_{3,i} C_{ij}^{(2)} + U_{4,i} C_{ij}^{(1)}) W_j + (U_{2,i} - \Omega^2 P_{2,i}) \Psi_i = 0, \tag{17}$$

$$\sum_{j=1}^m (U_{5,i}C_{ij}^{(2)} + U_{6,i}C_{ij}^{(1)})\Psi_j + \sum_{j=1}^m (U_{8,i}C_{ij}^{(2)} + U_{9,i}C_{ij}^{(1)})W_j + U_{7,i}\Psi_i - \Omega^2 P_{10,i}W_i = 0, \tag{18}$$

The satisfaction of Eqs. (17) and (18) at $(m - 2)$ internal grid points $x_i, i = 2, \dots, (m - 1)$ provide a set of $(2m - 4)$ equations in terms of unknowns $W_j = W(x_j)$ and $\Psi_j = \Psi(x_j), j = 1, 2, \dots, m$. The resulting system of equations can be written in matrix form as

$$[U][C] = [0], \tag{19}$$

where U and C are the matrices of orders $(2m - 4) \times 2m$ and $2m \times 1$, respectively. The above $(m - 2)$ internal grid points chosen for collocation are the zeros of shifted Chebyshev polynomial of order $(m - 2)$ with orthogonality range $(0, 1)$, given by

$$x_{k+1} = \frac{1}{2} \left[1 + \cos\left(\frac{2k - 1}{m - 2} \pi\right) \right], k = 1, 2, \dots, (m - 2).$$

5 Boundary Conditions and Frequency Equations

The following three sets of boundary conditions have been considered here:

- (i) Clamped (C) (ii) Simply supported (S) (iii) Free (F).
- (i) $\Psi = W = 0$: for clamped edge, (ii) $W = M_r = 0$: for simply supported edge,
- (iii) $M_r = Q_r = 0$: for free edge,

By satisfying the relations (i), (ii) and (iii) together with the regularity condition (iv) $W = Q_r = 0$ at $x = 0$ a set of four homogeneous equations has been obtained. These equations together with the field Eq. (19) give a complete set of $2m$ equations in terms of $2m$ unknowns. For a clamped plate, the set of these $2m$ homogeneous equations can be written as

$$\begin{bmatrix} U \\ U^C \end{bmatrix} [C] = [0], \tag{20}$$

where U^C is a matrix of order $4 \times 2m$.

For a non-trivial solution of Eq. (20), the frequency determinant must vanish and hence

$$\begin{vmatrix} U \\ U^C \end{vmatrix} = 0. \tag{21}$$

Similarly, for supported and free plates, the frequency determinants can be written as

$$\begin{vmatrix} U \\ U^S \end{vmatrix} = 0, \quad (22)$$

$$\begin{vmatrix} U \\ U^F \end{vmatrix} = 0, \quad (23)$$

respectively.

6 Results and Discussions

The numerical values of the frequency parameter Ω have been obtained by calculating the roots of the characteristic polynomial obtained from Eqs. (21–23) employing DQ method. The lowest three roots have been reported as the first three natural frequencies corresponding to different boundary conditions. The values of various plate parameters for these three modes of vibration are taken as $\alpha = -0.5(0.5)0.5$, $H_o = 0.1(0.1)0.30$, $H_f = 0.005, 0.010, 0.02$.

The material for the core and facings are to be aluminum honeycomb and aluminum respectively, for which the various constant are $R_f = 4800.00$, $\nu_f = 0.30$ and $R_\rho = 26.70$ [18]. In order to choose the appropriate number of grid point a computer programme has been developed to evaluate the frequencies, was run for $m = 5(1)18$ for different sets of plate parameters for all the three boundary conditions. The numerical values show a consistent improvement with the increase in the number of grid points m . In all the computations, the number of grid points has been taken as $m = 14$, since further increase in m does not improve the result even in the fourth place of decimal. In this regard, the normalized frequency parameter Ω/Ω^* for first three modes of vibration for a specified plate i.e $\alpha = -0.5$, $H_o = 0.10$, $H_f = 0.005$ are presented in Fig. 2a, b and c for clamped, simply supported and free plates, respectively as maximum deflection were observed for this data.

Figure 3a, b and c shows the effect of taper parameter α on the natural frequencies for clamped, simply supported and free plate respectively. From this graph it is observed that the values of frequency Ω for clamped plate are grater then simply supported plate but less then free plate. The values of frequency parameter decrease with increase in negative values of α up to $\alpha = 0$ for all the three boundary conditions and after then it increased for clamped and free plate except the second and third mode of vibration for $H_o = 0.1$ while, for simply supported plate the frequency parameter increase for the positive values of α for $H_o = 0.2$. This may be attributed to the fact that with the increases in positive values of α , the facings membrane forces are increased, which reduce the core shear stress and therefore deflection due to shear.

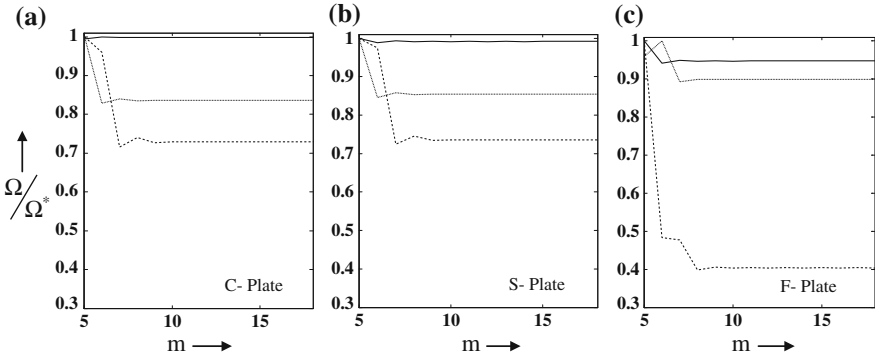


Fig. 2 Convergence of frequency parameter Ω/Ω^* for the first three modes of vibration with grid refinement for $\alpha = -0.50, H_o = 0.10, H_f = 0.005$
 First Mode — Second Mode Third Mode - - -

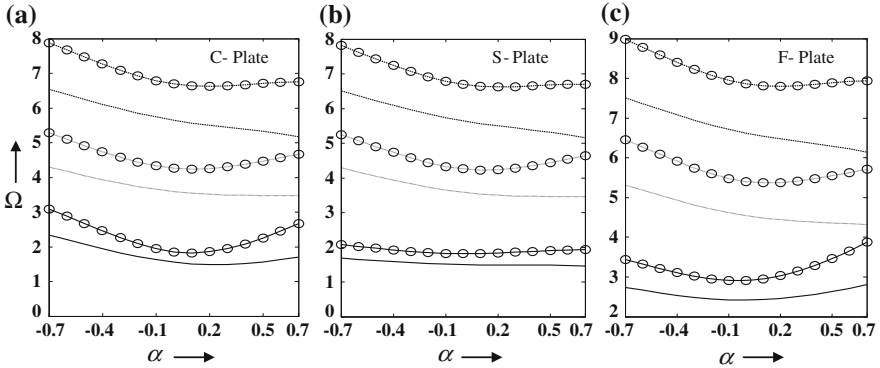


Fig. 3 Taper parameter α versus frequency parameter Ω for $H_f = 0.005$

Key: $\left. \begin{matrix} \text{First Mode} & \text{—} \\ \text{Second Mode} & \text{.....} \\ \text{Third Mode} & \text{- - -} \end{matrix} \right\} H_o = 0.1$ $\left. \begin{matrix} \text{O O O} \\ \text{O..O..O} \\ \text{O _O O} \end{matrix} \right\} H_o = 0.2$

Figure 4a, b and c depict the effect of core thickness at the centre H_o on the frequency parameter Ω for $\alpha = -0.5$ for clamped, simply supported and free plate, respectively. From the figure it is clear that the frequency parameter increases for increasing values of H_o first rapidly and then slowly for all the three boundary conditions. This rate of increase with increasing value of H_f and in the order of boundary condition $F > C > S$. The difference between the frequency parameter Ω for $H_f = 0.005$ and $H_f = 0.010$ decrease with the increase in the core

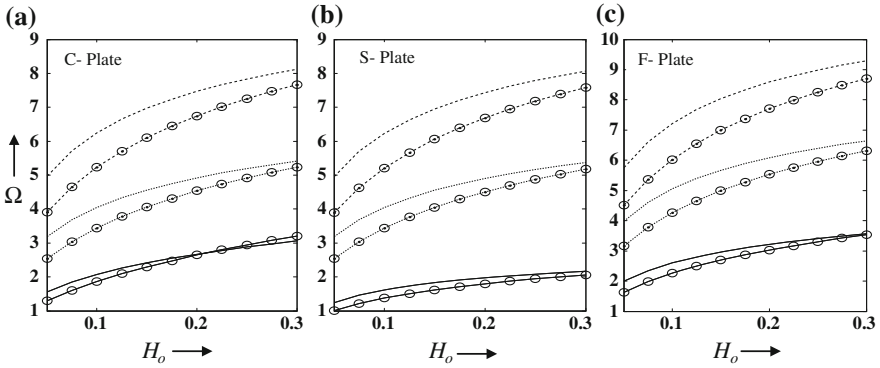


Fig. 4 Core thickness at the centre H_o versus frequency parameter Ω for $\alpha = -0.5$

Key: $\left\{ \begin{array}{l} \text{First Mode} \text{---} \\ \text{Second Mode} \text{.....} \\ \text{Third Mode} \text{- - -} \end{array} \right\} H_f = 0.005$ $\left\{ \begin{array}{l} \text{---} \\ \text{.....} \\ \text{- - -} \end{array} \right\} H_f = 0.010$

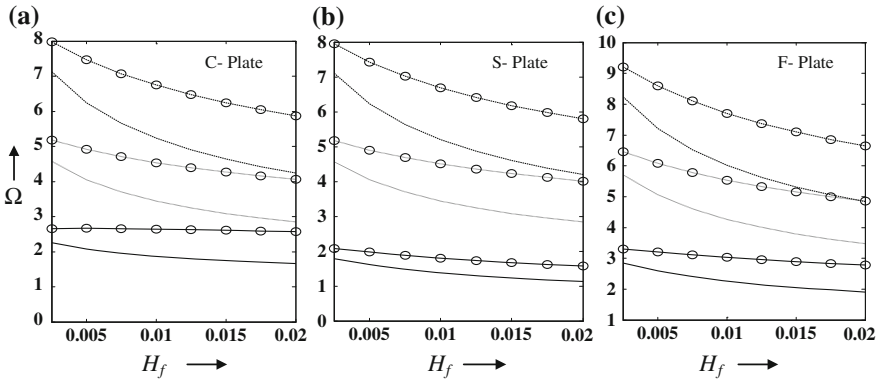


Fig. 5 Face thickness H_f versus frequency parameter Ω for $\alpha = -0.5$

Key: $\left\{ \begin{array}{l} \text{First Mode} \text{---} \\ \text{Second Mode} \text{.....} \\ \text{Third Mode} \text{- - -} \end{array} \right\} H_o = 0.1$ $\left\{ \begin{array}{l} \text{---} \\ \text{.....} \\ \text{- - -} \end{array} \right\} H_o = 0.2$

thickness at the centre. This may be due to the fact that the transverse shear of the core plays a significant role for higher values of H_o as compared to the bending stiffness of the plate.

Figure 5a, b and c shows the effect of face thickness H_f on the frequency parameter Ω for all the boundary conditions namely clamped, simply supported and free plate, respectively and for all the three modes of vibration. It is clear from the figure that the frequency parameter decreases with the increasing values of H_f

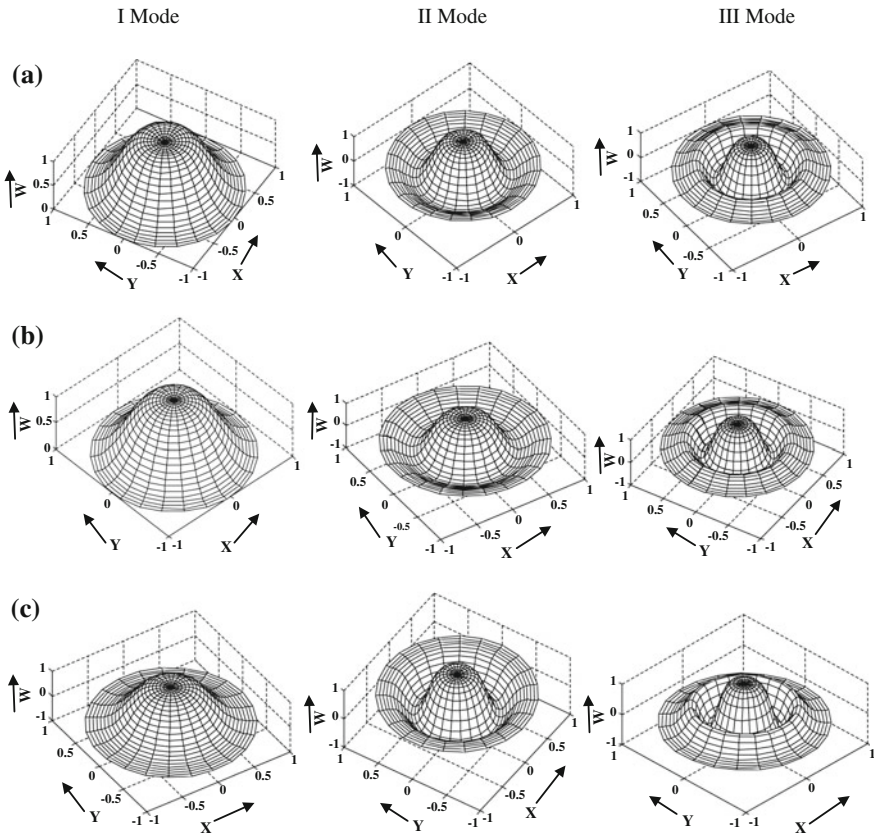


Fig. 6 Normalized transverse displacements for clamped, simply supported and free plate: $H_o = 0.10$, $H_f = 0.005$, $\alpha = -0.5$. **a** Clamped plate, **b** simply supported plate, **c** free plate

for all the three boundary conditions. This rate of decrease increase from $H_o = 0.1$ to $H_o = 0.2$ for all the three modes of vibration and for all the three plates. This rate of decrease for simply supported plate is greater than clamped plate but smaller then free plate. This can be attributed the fact that bending stiffness of the plate increases with the increasing values of H_f . Three dimensional mode shapes for specified sandwich plates taking, and have been plotted and shown in Fig. 6a, b and c for clamped simply supported and free plate respectively. A comparison of numerical results for circular sandwich plates with those of obtained by Chebyshev method has been presented in Table 1. A close agreement for all the three boundary conditions has been found.

Table 1 Comparison of frequency parameter for $H_f = 0.005$

α	Clamped plate					
	$H_o = 0.1$					
	I	II		III		
-0.5	2.0752	2.0753 ^a	4.0518	4.0520 ^a	6.2469	6.2473 ^a
0.0	1.5565	1.5565 ^a	3.5913	3.5913 ^a	5.6483	5.6483 ^a
0.5	1.5673	1.5674 ^a	3.4802	3.4804 ^a	5.3291	5.3295 ^a
Simply supports plate						
-0.5	1.6158	1.6159 ^a	4.0506	4.0508 ^a	6.2240	6.2246 ^a
0.0	1.5010	1.5010 ^a	3.5863	3.5863 ^a	5.6470	5.6470 ^a
0.5	1.4848	1.4849 ^a	3.4631	3.4633 ^a	5.3196	5.3199 ^a
Free plate						
-0.5	2.5985	2.5988 ^a	5.0543	5.0543 ^a	7.2167	7.2178 ^a
0.0	2.4207	2.4207 ^a	4.5431	4.5431 ^a	6.6240	6.6240 ^a
0.5	2.6317	2.6320 ^a	4.3622	4.3624 ^a	6.2957	6.2962 ^a

^a Ref. [18]

7 Conclusions

Axisymmetric vibrations of circular sandwich plate of variable thickness have been investigated. In this analysis, face sheets are treated as membranes while the core is taken to be of linearly varying thickness. Energy formulations have been obtained for the governing differential equation for such plates which have been solved employing the differential quadrature method. It is found that frequency parameter for C plate is higher than that for S plate and lower than that for F plate for the same set of the values of plate parameters.

Acknowledgments One of the authors, Rashmi Rani is thankful to Ministry of Human Resources and Development (MHRD), India for the financial support to carry out this research work.

References

1. Heimbs, S., Middendorf, P., Hampf, C., Hähnel, F., Wolf, K.: Aircraft sandwich structures with folded core under impact load. In: Ferreira, A.J.M. (ed.) 8th International Conference on Sandwich Structures, ICSS, vol. 8, (2008)
2. Altenbach, H.: Theories for laminated and sandwich plates. *Mech. Compos. Mater.* **34**, 333–348 (1982)
3. Carrera, E., Brischetto, S.: A survey with numerical assessment of classical and refined theories for the analysis of sandwich plates. *Appl. Mech. Rev.* **62**, 010803–010819 (2009)
4. Mirza, S., Singh, A.V.: Axisymmetric vibration of circular sandwich plates. *AIAA J.* **12**, 1418–1420 (1974)

5. Sherif, H.A.: Free flexural vibrations of clamped sandwich circular plates. *J. Sound Vib.* **157**, 531–537 (1992)
6. Zhou, H.B., Li, G.Y.: Free vibration analysis of sandwich plates with laminated faces using spline finite point method. *Comput. Struct.* **59**, 257–263 (1996)
7. Yuan, W.X., Dawe, D.J.: Free vibration of sandwich plates with laminated faces. *J. Numer. Methods Engrg.* **54**, 195–217 (2002)
8. Chen, Y.R., Chen, L.W.: Axisymmetric parametric resonance of polar orthotropic sandwich annular plates. *Compos. Struct.* **65**, 269–277 (2004)
9. Chang, J.S., Chen, H.C., Lin, H.T.: Numerical and experimental studies on aluminium sandwich plates of variable thickness. *J. Chinese Inst. Eng.* **29**, 851–862 (2006)
10. Gupta, A.P., Jain, M.: Axisymmetric vibrations of annular sandwich plates of linearly varying thickness. *J. Sound Vib.* **80**(3), 329–337 (1982)
11. Burlayenko, V.N., Sadowski, T.: Analysis of structural performance of sandwich plates with foam-filled aluminum hexagonal honeycomb core. *Comput. Mater. Sci.* **45**, 658–662 (2009)
12. Sadowski, T., Bec, J.: Effective properties for sandwich plates with aluminium foil honeycomb core and polymer foam filling—static and dynamic response. *Comput. Mater. Sci.* **50**, 1269–1275 (2011)
13. Malekzadeh, P., Karami, G., Farid, M.: A semi-analytical DQEM for free vibration analysis of thick plates with two opposite edges simply supported. *Comput. Methods Appl. Mech. Engrg.* **193**, 4781–4796 (2004)
14. Gupta, U.S., Lal, R., Sharma, S.: Vibration analysis of non-homogeneous circular plate of nonlinear thickness variation by differential quadrature method. *J. Sound Vib.* **298**, 892–906 (2006)
15. Tornabene, F., Liverani, A., Caligiana, G.: Laminated composite rectangular and annular plates: a GDQ (generalized differential quadrature method) solution for static analysis with a posteriori shear and normal stress recovery. *Compos. B* **43**, 1847–1872 (2012)
16. Kumar, Y., Lal, R.: Prediction of frequencies of free axisymmetric vibration of two-directional functionally graded annular plates on Winkler foundation. *J. Mech. A-Solids.* **42**, 219–228 (2013)
17. Bert, C.W., Jang, S.K., Striz, A.G.: Two new approximate methods for analyzing free vibration of structural components. *AIAA J.* **26**, 612–618 (1988)
18. Jain, S.K.: *Vibration of Non-Uniform Composite Plates*, University of Roorkee, Roorkee (1994)

Solve Shortest Paths Problem by Using Artificial Bee Colony Algorithm

P. Mansouri, B. Asady and N. Gupta

Abstract Nature-inspired algorithms are among the most powerful algorithms to solve optimization problems. This paper intends to provide a detailed description of a new iterative method to solve the shortest path problem for given directed graph(dgraph) $G = (V, E)$ from source node s to target node t . Each edge $(i, j) \in E$ has an associated weight w_{ij} . This problem is known as NP-hard problems, so an efficient solution is not likely to exist. Weights are assigned by the network operator. A path cost is the sum of the weights of the edges in the path. The efficiency of this approach is shown with some numerical simulations. For large data network, this method reaches to shortest path from s to t in polynomial time.

Keywords Shortest path problem · Optimization · Artificial bee colony algorithm

1 Introduction

One of the most fundamental algorithmic graph problems is shortest paths problem(SPP), also it is an NP-hard combinatorial optimization problem that has long challenged researchers. The objective of the SPP is to find the shortest paths between two nodes with minimum weights(cost). For solving this problem some

P. Mansouri (✉) · B. Asady
Department of Mathematics, Arak Branch, Islamic Azad University, Arak, Iran
e-mail: p-mansouri@iau-arak.ac.ir; pmansouri393@yahoo.com

B. Asady
e-mail: basadi@iau-arak.ac.ir

P. Mansouri · N. Gupta
Department of Computer Science, Delhi University, Delhi, India
e-mail: ngupta.cs.du@gmail.com

traditional methods as the network simplex method are, $O(n^3)$ Bellman-Ford algorithm, $O(n^2)$ Dijkstra algorithm, Floyd-Warshall algorithm, and so on [1]. However, for more complex and large scale problems, decreasing of computing time is important, when applying the conventional methods. Bio-inspired algorithms are among the most powerful algorithms for optimization [2–8], especially for the NP-hard problems same as the traveling salesman problem and etc. Particle swarm optimization (PSO) was developed by Kennedy and Eberhart in 1995 [9], based on the swarm behavior such as fish and bird schooling in nature, the so-called swarm intelligence. Though particle swarm optimization has many similarities with Genetic algorithms, but it is much simpler because it does not use mutation/crossover operators. Instead, it uses the real-number randomness and the global communication among the swarming particles. In this sense, it is also easier to implement as it uses mainly real numbers. Yuster presented an approximation algorithm for the all pairs shortest path problem in weight graphs in 2012 [12]. His algorithm solved the APSA problem for weighted directed graphs, with positive real weights. Artificial bee colony algorithm (ABC) defined by Dervis Karaboga in 2005, motivated by the intelligent behavior of honey bees [10, 11]. It is as simple as Particle Swarm Optimization (PSO) and Differential evolution (DE) algorithms, Genetic algorithm (GA) [5], biogeography based optimization (BBO), and uses only common control parameters such as colony size and maximum cycle number. ABC as an optimization tool, provides a population-based search procedure in which individuals called foods positions are modified by the artificial bees with time and the bee's aim is to discover the places of food sources with high nectar amount and finally the one with the highest nectar. In ABC system, artificial bees fly around in a multidimensional search space and some (employed and onlooker bees) choose food. Development of an ABC algorithm for solving generalized assignment problem which is known as NP-hard problem is presented in detail along with some comparisons [11]. Sources depending on the experience of themselves and their nest mates, and adjust their positions. In this paper, we focus on the single source shortest paths problem: given a dgraph $G = (V, E)$ with m vertices, we want to find a shortest path from a given source vertex $s \in V$ to each target vertex $t \in V$. In Sect. 2, the ABC algorithm and Shortest path problem are described. In Sect. 3, presenting the accuracy and complexity of proposed method with some examples. Finally, in Sect. 4, we discuss about ability of the proposed method.

2 Artificial Bee Colony Algorithm

Artificial bee colony algorithm (ABC) is an algorithm based on the intelligent foraging behavior of honey bee swarm, purposed by Karaboga in 2005 [10]. In ABC model, the colony consists of three groups of bees: employed bees, onlookers and scouts. It is assumed that there is only one artificial employed bee for each

1. Initial food sources are produced for all employed.
2. Repeat UNTIL (requirements are met)
 - (a) Each employed bee goes to a food source in her memory and determines a neighbor source, then evaluates its nectar amount and dances in the hive.
 - (b) Each onlooker watches the dance of employed bees and chooses one of their sources depending on the dances, and then goes to that source. After choosing a neighbor around that, she evaluates its nectar amount.
 - (c) Abandoned food sources are determined and are replaced with the new food sources discovered by scouts. item The best food source found so far is registered.

Fig. 1 Artificial bee colony algorithm

food source. In other words, the number of employed bees in the colony is equal to the number of food sources around the hive. Employed bees go to their food source and come back to hive and dance on this area. The employed bee whose food source has been abandoned becomes a scout and starts to search for a new food source. Onlookers watch the dances of employed bees and choose food sources depending on dances. The pseudo-code of the ABC algorithm is given in Fig. 1.

In ABC which is a population based algorithm, the position of a food source represents a possible solution to the optimization problem and the nectar amount of a food source corresponds to the quality (fitness) of the of solutions in the population. At the first step, a randomly distributed initial population (food source positions) is generated. After initialization, the population is subjected to repeat the cycles of the search processes of the employed, onlooker, and scout bees, respectively. An employed bee produces a modification on the source position in her memory and discovers a new food source position. Provided that the nectar amount of the new one is higher than that of the previous source, the bee memorizes the new source position and forgets the old one. Otherwise she keeps the position of the one in her memory. After all employed bees complete the search process, they share the position information of the sources with the onlookers on the dance area. Each onlooker evaluates the nectar information taken from all employed bees and then chooses a food source depending on the nectar amounts of sources. As in the case of the employed bee, she produces a modification on the source position in her memory and checks its nectar amount. Providing that its nectar is higher than that of the previous one, the bee memorizes the new position and forgets the old one. The sources abandoned are determined and new sources are randomly produced to be replaced with the abandoned ones by artificial scouts.

3 The Artificial Bee Colony Algorithm for Solving Shortest Paths Problem

We want to present a procedure for solving a Shortest Paths Problem (SPP) by using the ABC algorithm (ABC-SPP). In Order to, we define the mathematical model of the SPP as following.

3.1 Mathematical Model

Let $G = (V, E)$ be a directed graph of given network with n nodes. Assume that each edge $(i, j) \in E$ has an associated length (or weight) $w_{ij} \geq 0$ and it contains a directed path from source node s to every other node in the network. Our propose is to find the shortest path from source node s to target node t that has minimum cost, or a path that takes least time to traverse. This viewpoint gives rise to the following linear programming formulation of the SPP. The objective cost function is as following (Fig. 2):

$$\begin{aligned} \min z &= \sum_i \sum_j x_{ij} w_{ij}, (i, j), \\ \text{s.t} & \\ \sum_{j, (i,j) \in E} x_{ij} - \sum_{k, (k,i) \in E} x_{ki} &= \begin{cases} 1, & i = s, \\ 0, & i \neq s, t, \\ -1, & i = t. \end{cases} \\ x_{ij} \in [0, 1], w_{ij} &\geq 0, \end{aligned}$$

Corresponding to linear programming formulation of the SPP, with penalty function term it is converted into one of the following unconstrained minimization problems

$$\begin{aligned} \min E(x, K) &= z + [K_1 (\sum_{j, (1,j) \in E} x_{1j} - 1) + K_2 (1 + \sum_{i, (i,m)} x_{im})] + \\ &K_3 \sum_i (\sum_j (\sum_k (x_{ij} - x_{ki}))), ((i, j), (k, i) \in E), i \neq s, t, \end{aligned} \tag{1}$$

where $z = \sum_i \sum_j x_{ij} w_{ij}, (i, j) \in E, i, j, k = 1, 2, \dots, m, i \neq j \neq k$, and penalty coefficients are $K_i \gg 1, i = 1, 2, 3$. Based on the above explanation of mathematical model of SPP, the main steps of the proposed method is as following:

In the first step, initial population P of $n \geq 2$ solution p_k is generated randomly by using ABC algorithm, that included of some edges $(i, j) \in E, i, j = 1, 2, \dots, m, i \neq j, k = 1, 2, \dots, n$ between nodes s and t (it is clear that in the initial population, there exist a solution p that included some edges relates to a path between s and t and is not optimal solution). In the second step, if in each solution(path), first node and last nodes are s and t respectively, go to next step and compute penalty

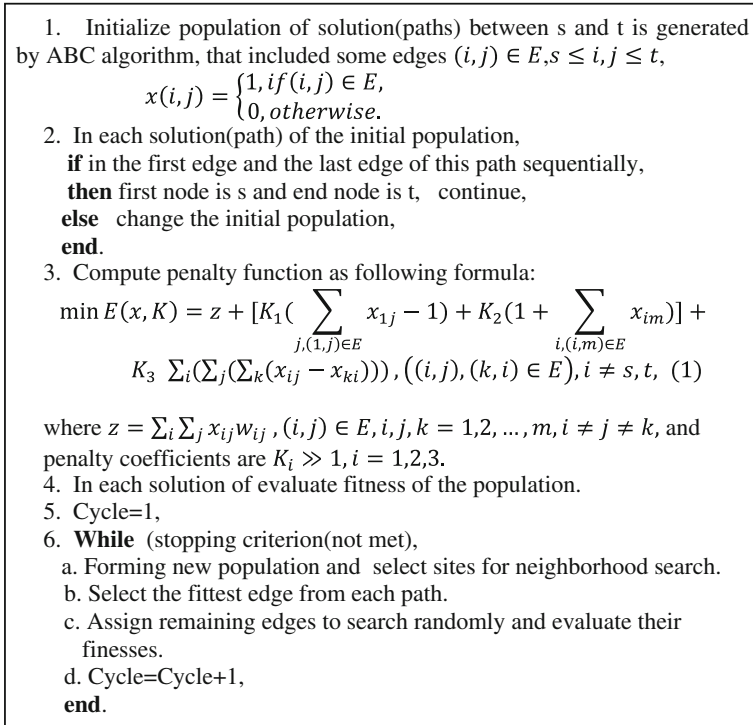


Fig. 2 Main steps of the ABC-SPP

function, else change population of solution. AS ABC algorithm is a optimization algorithm, then after some iteration, propose method reach to optimal solution of function (1). So, shortest path from node s to node t will be achieved without need to visit all paths between s and t. We illustrate propose method with some examples.

4 Numerical Example

4.1 Example 1

In this example, we want to find shortest path between node 1 and node 14 by using ABC-SPP algorithm. Consider a network with 14 nodes and 29 edges in the Fig. 3.

When there are no negative weights(costs). This problem is formulated i th proposed method as following:

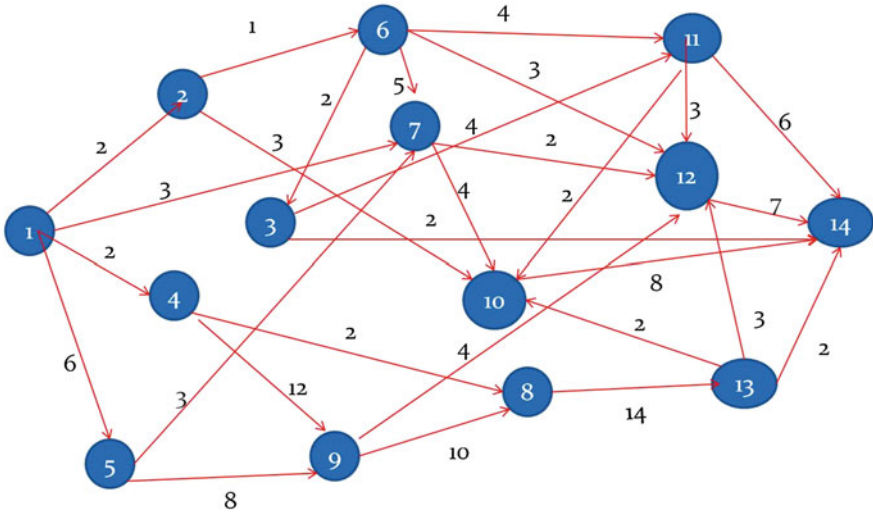


Fig. 3 A directed network in Example 1

$$\begin{aligned} \min E(x, K) = & x_{12} + 3x_{17} + 2x_{14} + 6x_{15} + x_{26} + 3x_{210} + 4x_{311} \\ & + 2x_{314} + 2x_{48} + 12x_{49} + 8x_{59} + 3x_{57} + 4x_{611} + 3x_{612} + 5x_{67} + 2x_{63} \\ & + 2x_{712} + 4x_{710} + 14x_{813} + 10x_{98} + 4x_{912} + 8x_{1014} + 2x_{1110} + 3x_{1112} \\ & + 6x_{1114} + 7x_{1214} + 2x_{1310} + 3x_{1312} + 2x_{1314} + K[(x_{12} + x_{17} + x_{14} - 1) \\ & + (x_{26} + x_{210} - x_{12}) + (x_{311} + x_{314} - x_{63}) + (x_{48} + x_{49} - x_{14}) \\ & + (x_{59} + x_{57} - x_{15}) + (x_{611} + x_{612} + x_{67} + x_{63} - x_{26}) \\ & + (x_{712} + x_{710} - x_{67} - x_{57} - x_{17}) + (x_{813} - x_{48} - x_{98}) \\ & + (x_{98} + x_{912} - x_{49} - x_{59}) + (x_{1014} - x_{210} - x_{710} - x_{1110} - x_{1310}) \\ & + (x_{1110} + x_{1112} + x_{1114} - x_{311} - x_{611}) \\ & + (x_{1214} - x_{612} - x_{712} - x_{912} - x_{1112} - x_{1312}) \\ & + (x_{1310} + x_{1312} - x_{813}) + (x_{314} + x_{1014} + x_{1214} + x_{1314} - 1)] \end{aligned}$$

Assumption that $K = 1000$. By using Table 1 and proposed method the optimal solution is same as $z^* = 7$ and optimal solution is :

$$X^* = [1, 0, 0, 0, 1, 0, 1, 0, 0, 0, 0, 0, 1, 0, 0, 0, 0, 0, 0, 0, 0, 0, 0, 0].$$

Therefore, shortest path between node 1 and node 14, which is corresponding to the optimal solution is

$$1 \rightarrow 2 \rightarrow 6 \rightarrow 3 \rightarrow 14.$$

Table 1 The weight of edges

Edge	Weight	Edge	Weight	Edge	Weight
(1,2)	1	(5,9)	8	(9,12)	4
(1,7)	3	(5,7)	3	(10,14)	8
(1,4)	2	(6,11)	4	(11,10)	2
(1,5)	6	(6,12)	3	(11,12)	3
(2,6)	1	(6,7)	5	(11,14)	6
(2,10)	3	(6,3)	2	(12,14)	7
(3,11)	4	(7,12)	2	(13,10)	2
(3,14)	2	(7,10)	4	(13,12)	3
(4,8)	2	(8,13)	14	(13,14)	2
(4,9)	12	(9,8)	10		

4.2 Example 2

Consider a network with 18 nodes and 44 edges in the Fig. 4.

When there are no negative weights (costs). This problem is formulated with proposed method as following:

$$\begin{aligned}
 \min E(x, K) = & x_{12} + x_{13} + 3x_{17} + 2x_{14} + 6x_{15} + \\
 & 4x_{18} + x_{26} + 3x_{210} + 2x_{213} + 4x_{311} + 2x_{318} + 3x_{39} + \\
 & 12x_{414} + 2x_{49} + 8x_{59} + 9x_{510} + 4x_{513} + 4x_{611} + \\
 & 3x_{612} + 5x_{67} + 2x_{63} + 2x_{712} + 4x_{713} + 4x_{811} + \\
 & 14x_{814} + 10x_{914} + 8x_{912} + 4x_{1013} + 8x_{1015} + 8x_{1112} + \\
 & 2x_{1118} + 3x_{1113} + 6x_{1218} + 7x_{1215} + 6x_{1318} + \\
 & 3x_{1317} + 2x_{1416} + 3x_{1417} + 2x_{1415} + 4x_{1517} + \\
 & 3x_{1618} + 3x_{1612} + 2x_{1617} + 6x_{1718} + K[(x_{12} + x_{17} + \\
 & x_{13} + x_{14} + x_{15} + x_{18} - 1) + (x_{26} + x_{210} + x_{213} - \\
 & x_{12}) + (x_{311} + x_{318} + x_{39} - x_{13} - x_{63}) + (x_{414} + x_{49} - \\
 & x_{14}) + (x_{59} + x_{510} + x_{513} - x_{15}) + (x_{611} + x_{612} + \\
 & x_{67} + x_{63} - x_{26}) + (x_{712} + x_{713} - x_{17} - x_{67}) + \\
 & (x_{811} + x_{814} - x_{18}) + (x_{912} + x_{914} - x_{39} - x_{49} - \\
 & x_{59}) + (x_{1013} + x_{1015} - x_{210} - x_{510}) + (x_{1112} + \\
 & x_{1113} + x_{1118} - x_{311} - x_{611} - x_{811}) + (x_{1215} + x_{1218} - \\
 & x_{612} - x_{712} - x_{912} - x_{1112}) + (x_{1318} + x_{1317} - x_{213} - \\
 & x_{513} - x_{713} - x_{1013} - x_{1113}) + (x_{1416} + x_{1417} + \\
 & x_{1415} - x_{414} - x_{814} - x_{914}) + x_{1517} - x_{1015} - x_{1215} - \\
 & x_{1415}) + (x_{1618} + x_{1612} + x_{1617} - x_{1416}) + (x_{1718} - \\
 & x_{1317} - x_{1417} - x_{1517})]
 \end{aligned}$$

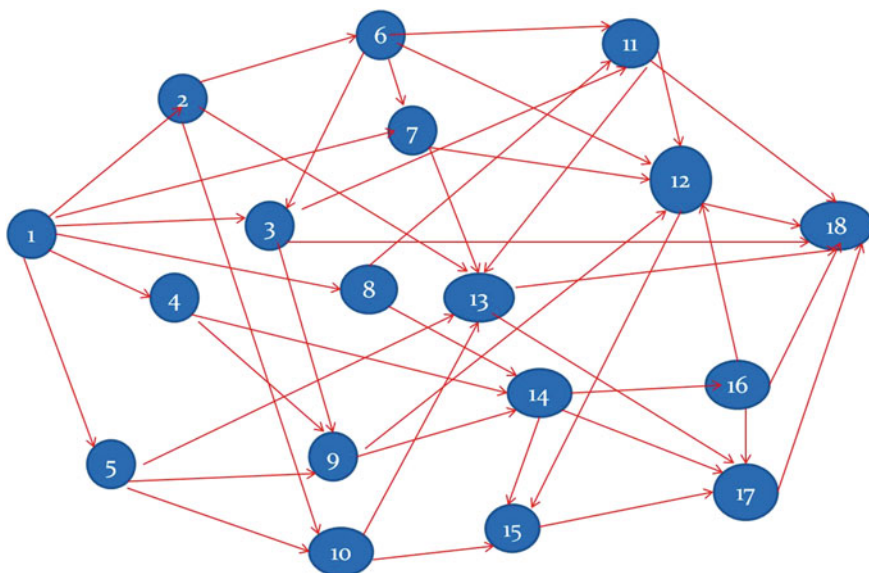


Fig. 4 A directed network in Example 2

Table 2 The weight of edges

Edge	Weight	Edge	Weight	Edge	Weight	Edge	Weight
(1, 2)	1	(9,14)	10	(10,13)	4	(16,12)	3
(1, 3)	1	(5, 9)	8	(10,15)	8	(16,17)	2
(1, 7)	3	(5,10)	9	(11,12)	8	(16,18)	3
(1, 4)	2	(5,13)	4	(11,18)	2	(17,18)	6
(1, 5)	6	(6,11)	4	(11,13)	3	(4,14)	12
(1, 8)	4	(6,12)	3	(12,18)	6	(2, 6)	1
(6, 7)	5	(12,15)	7	(2,10)	3	(6, 3)	2
(13,18)	6	(2,13)	2	(7,12)	2	(13,17)	3
(3, 9)	3	(7,13)	4	(14,16)	2	(3,11)	4
(8, 11)	4	(14,17)	3	(3,18)	2	(8,14)	14
(14,15)	2	(4, 9)	2	(9,12)	8	(15,17)	4

Assumption that $K = 1000$. By using Table 2 and proposed method the optimal solution is same as $z^* = 3$ and optimal solution is

$$X^* = [0, 0, 1, 0, 0, 0, 0, 0, 0, 0, 1, 0, 0, 0, 0, 0, 0, \dots, 0, 0, 0]$$

Therefore, shortest path between node 1 and node 18, which is corresponding to the optimal solution is

$$1 \rightarrow 3 \rightarrow 18.$$

5 Conclusion

In this work, we present a new iterative method to solve the shortest paths problem for given directed graph by using ABC algorithm. For this purpose, we used the penalty function to construct the optimization problem. By solving optimization problem, we find the optimal solution of penalty function that occur at shortest path between given nodes s and t .

References

1. Abeyesundara, S., Giritharan, B., Kodithuwakku, S: A genetic algorithm approach to solve the shortest paths problem for road maps. In: Proceedings of the International Conference on Information and Automation, Colombo, Sri Lanka, pp. 272–275 (2005)
2. Ahuja, R.K., Magnanti, T.L., Orlin, J.B: Network Flows: Theory, Algorithms, and Applications. Prentice-Hall, New Jersey (1993)
3. Deb, K: Optimisation for Engineering Design. Prentice-Hall, New Delhi (1995)
4. Goldberg, D.E.: Genetic Algorithms in Search, Optimisation and Machine Learning. Addison Wesley, Reading (1989)
5. Karaboga, D: An idea based on honey bee swarm for numerical optimization. Technical Report-TR06, Erciyes University, Engineering Faculty, Computer Engineering Department (2005)
6. Karaboga, D., Basturk, B.: On the performance of artificial bee colony (ABC) algorithm. *Appl. Soft Comput.* **8**, 687–697 (2008)
7. Kennedy, J., Eberhart, R.C: Particle swarm optimization. In: Proceedings of IEEE International Conference on Neural Networks, Piscataway, NJ, pp. 1942–1948 (1995)
8. Kennedy, J., Eberhart, R., Shi, Y: Swarm Intelligence. Academic Press, San Francisco (2001)
9. Yang, X.S: Biology-derived algorithms in engineering optimization (Chapter 32). In: Olariu, S., Zomaya, A. (eds.) *Handbook of Bioinspired Algorithms and Applications*. Chapman and Hall/CRC, Boca Raton (2005)
10. Yang, X.S: Nature-Inspired Metaheuristic Algorithms. Luniver Press, Frome (2008)
11. Yuster, R.: Approximate shortest in weighted graphs. *J. Comput. Syst. Sci.* **78**, 632–637 (2012)
12. Zakzouk, A.A.A., Zaher, H.M., El-Deen, R.A.Z: An ant colony optimization approach for solving shortest paths problem with fuzzy constraints. In: Proceedings of the 7th International Conference on Informatics and Systems (INFOS) (2010)

Speed Control of Three Phase Induction Motor Drive Using Soft Computing Technique

Arunesh Kumar Singh, D. K. Chaturvedi and Jitendra Singh

Abstract Variable speed AC Induction motors powered by switching power converters are becoming more and more popular, because of advances in solid state power devices, microprocessors and evaluation of soft computing technique. The most common principle of this kind, is the constant V/Hz principle. By making V/f constant, the magnitude of the magnetic field in the stator is kept at an approximately constant level throughout the operating range. So three-phase induction motor drive systems driven by V/f (V/Hz) controlled PWM voltage source inverter have been widely used in the industrial applications. Soft Computing (SC) techniques are recently having significant impact on power electronics and motor drives, which is already a complex and multidisciplinary technology that is going through dynamic evolution in the recent years. Fuzzy Logic, Neural Networks, Neuro-Fuzzy and Evolutionary Computations are the core methodologies of soft computing (SC). In this paper, ANN controller and Fuzzy logic controller has been implemented for speed control of 3-phase induction motor by using soft computing techniques. Out of these two techniques ANN based control takes less settling time and has almost no overshoot. The result of the ANN controller is smoother than the fuzzy logic controller but its output can be improved by tuning it.

Keywords Induction motor speed control · Soft computing · Fuzzy controller · ANN controller

A. K. Singh (✉)
Jamia Millia Islamia, New Delhi, India
e-mail: aru_dei@yahoo.com

D. K. Chaturvedi
Dayalbagh Educational Institute, Agra, India
e-mail: dkc.foe@gmail.com

J. Singh
IEC-CET, Gt. Noida, Noida, India
e-mail: jitendramtech0109@gmail.com

1 Introduction

The three-phase induction motors are the most widely used electric motors in industry. They run at essentially constant speed from no-load to full-load when they are directly connected to service mains/supply. However, the speed is frequency dependent and consequently these motors are not easily adapted to speed control. We usually prefer d.c. motors when large speed variations are required. Nevertheless, the 3-phase induction motors are simple, rugged, low-priced, easy to maintain as compare to d.c. motor and can be manufactured with characteristics to suit most industrial requirements. By controlling the speed of induction motor, we can use it for various industrial applications.

Switching power converters offer an easy way to regulate both the frequency and magnitude of the voltage and current applied to a motor. As a result much higher efficiency and performance can be achieved by these motor drives with less generated noises. The most common principle of this kind is the constant V/Hz principle [1] which requires that the magnitude and frequency of the voltage applied to the stator of a motor maintain a constant ratio.

The energy that a switching power converter delivers to a motor is controlled by soft computing based Space vector Pulse Width Modulated (SVPWM) signals applied to the gates of the power transistors. PWM signals are pulse trains with fixed frequency and magnitude and variable pulse width. However, the width of the pulses changes from period to period according to a modulating signal. When a SVPWM signal is applied to the gate of a power transistor, it causes the turn on and turn-off intervals of the transistor to change from one PWM period to another PWM period according to the same modulating signal. The frequency of a SVPWM signal must be much higher than that of the modulating signal, the fundamental frequency, such that the energy delivered to the motor and its load depends mostly on the modulating signal.

The aim of this paper is that it shows the dynamics response of speed with design the fuzzy logic controller and ANN controller [2–7] to control a speed of motor when the load torque is constant. This paper presents design and implements a voltage source inverter type space vector pulse width modulation (SVPWM) for control a speed of induction motor. This paper also introduces a comparative analysis of fuzzy logic controller and ANN controller when reference speed varies and load torque is fixed [8–16].

2 Inverter Control Scheme

There are various control schemes to control the inverter output voltage and frequency which are given below:

Multilevel Inverter Control Scheme: Fundamental switching frequency (SVM, SHE-PWM) and High Switching frequency (SVM, SHE-PWM, SPWM).

Fig. 1 Voltage source inverter fed 3-phase induction motor

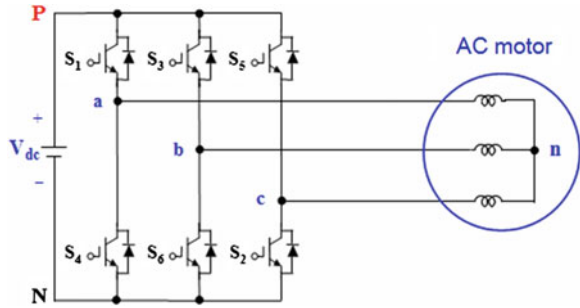
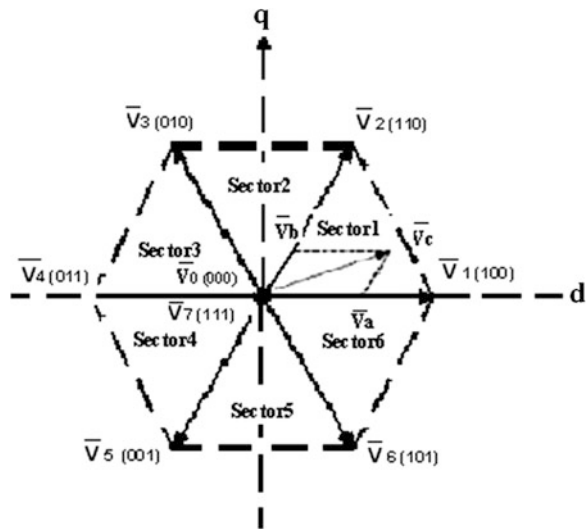


Fig. 2 Space vector of voltage



Space vector modulation (SVM) has recently grown as a very popular pulse width modulation for voltage fed converter ac drives because of its superior harmonic quantity and extended linear range of operation. In this paper, the space vector pulse width modulation technique is defined for the speed control of induction motor.

2.1 Space Vector Pulse Width Modulation

The typical power stage of the three phase inverter and the equivalent circuit of a machine are presented in Fig. 1 as given below:-

A three phase bridge inverter has 8 permissible switching states. In the SVPWM scheme, the 3-phase output voltage is represented by a reference vector, as shown in Fig. 2, which rotates at an angular speed of $\omega = 2\pi f$. The task of SVM is to use the combinations of switching states.

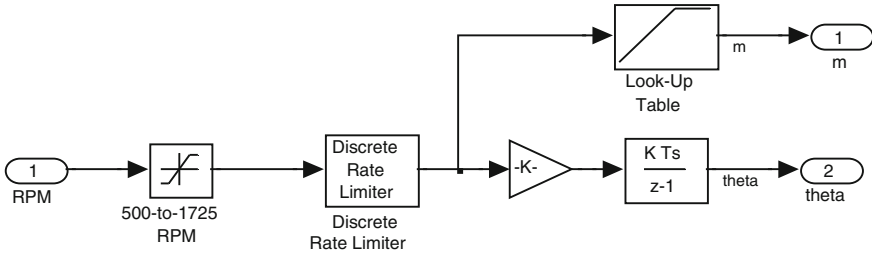


Fig. 3 Simulink block for V/f control

The three phase sinusoidal and balance voltages are given by following equations:

$$V_{An} = V_m \cos(\omega t) \quad (1)$$

$$V_{Bn} = V_m \cos\left(\omega t - \frac{2\pi}{3}\right) \quad (2)$$

$$V_{Cn} = V_m \cos\left(\omega t + \frac{2\pi}{3}\right) \quad (3)$$

$$\dot{V} = \frac{2}{3} [V_{An} + aV_{Bn} + a^2V_{Cn}] \quad (4)$$

The double edge modulation of reference voltages V_{Ao} , V_{Bo} and V_{Co} are given as:

$$V_{Ao} = V_{An} + V_{n0} \quad (5)$$

$$V_{Bo} = V_{Bn} + V_{n0} \quad (6)$$

$$V_{Co} = V_{Cn} + V_{n0} \quad (7)$$

where

$$V_{n0} = \frac{1}{2} \text{median}(V_{An}, V_{Bn}, V_{Cn}). \quad (8)$$

The voltages are applied to the three phase induction motor by using Eq. (4).

2.2 Simulink Model of V/f and SVPWM Generator Block

For making the constant V/f [1], the simulation model is shown in Fig. 3. This is simulated to avoid the danger of saturation in induction motor. In this Simulink model the required speed is taken at the input side and the modulation index (m) and theta are taken at the output side.

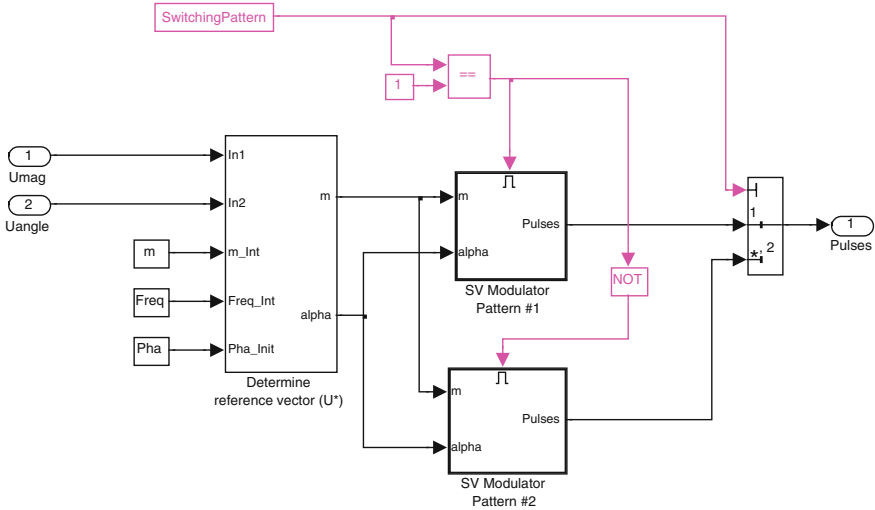


Fig. 4 SV PWM generator simulink block

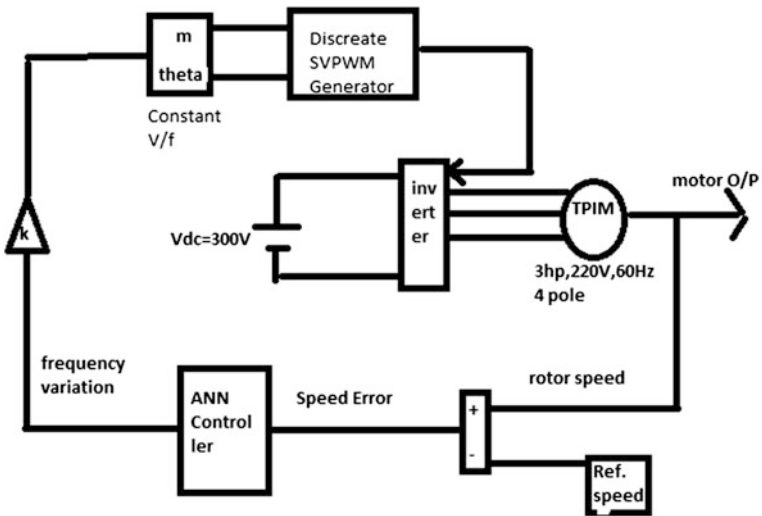


Fig. 5 ANN based speed control of three phase IM

For switching the inverter, space vector pulse width modulation technique is used. SVM pulses are generated the Simulink model as given in Fig. 4.

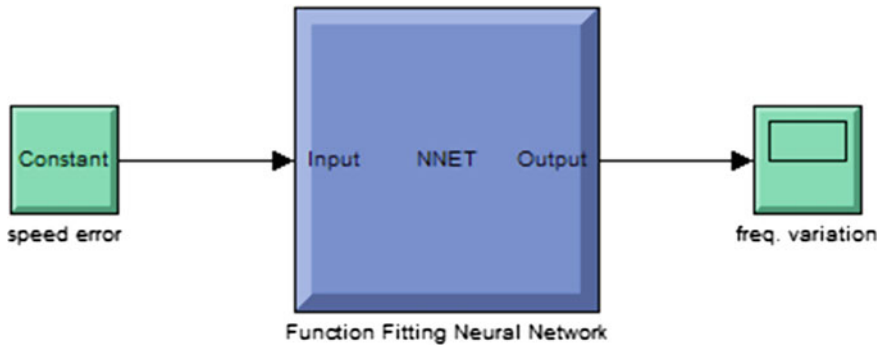


Fig. 6 ANN controller

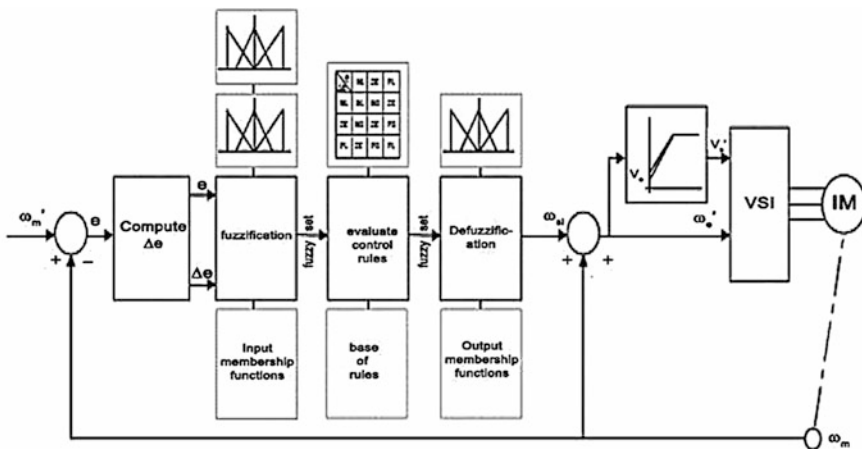


Fig. 7 Fuzzy based model of speed control of three phase IM

3 Modeling of ANN Based Control System

Block diagram for speed control of three phase induction motor is shown in Fig. 5. Simulink model has been designed according to this block diagram.

ANN controller has been design as shown in Fig. 6. Its input is speed error and output is frequency variation. First rotor output speed is compared to the reference speed and then neural network [17–20] is trained for the required frequency variation for that speed error.

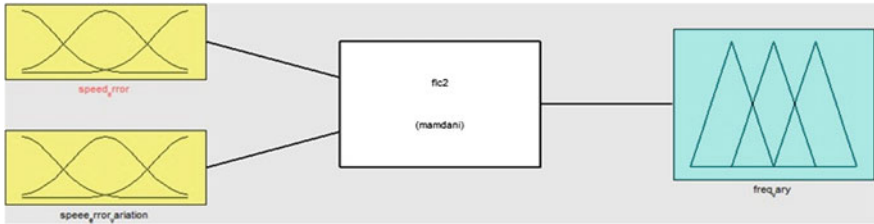


Fig. 8 Fuzzy logic controller

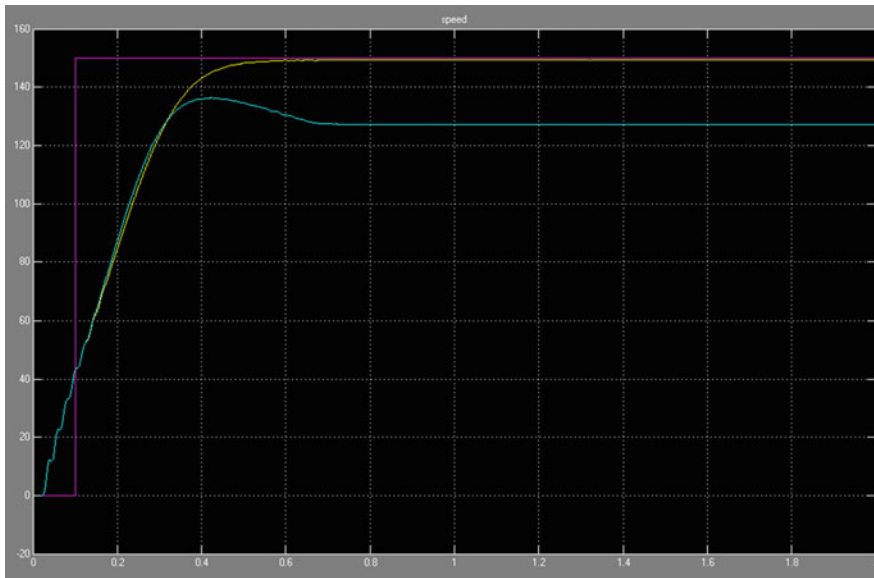


Fig. 9 Rotor speed response of ANN and fuzzy controller technique

4 Modeling of Fuzzy Logic Based Control System

Fuzzy logic based speed controller model is shown in Fig. 7. The design of a Fuzzy Logic Controller requires the choice of Membership Functions. The membership functions should be chosen such that they cover the whole universe of discourse. It should be taken care that the membership functions overlap each other. This is done in order to avoid any kind of discontinuity with respect to the minor changes in the inputs. To achieve finer control, the membership functions near the zero region should be made narrow. Wider membership functions away from the zero region provides faster response to the system [21–27].

The fuzzy logic controller is shown in Fig. 8. The inputs to the Fuzzy Logic Controller are two: 1. Speed Error (e) and 2. Change in Error (Δe) or derivative of speed error.

Table 1 Analysis result in tabular form

Analyzing quantity	Fuzzy based control	ANN based control
Settling time of speed and electromagnetic torque waveform	0.5 s	0.38 s
FFT of speed waveform	79.44 %	61.42 %
FFT of electromagnetic torque waveform	163.90 %	26.26 %

5 Comparative Analysis

The rotor speed response has been analyzed for ANN controller and fuzzy controller, which is shown in Fig. 9. This analysis shows that neural based model has less settling time and almost no overshoot. The rotor speed in fuzzy based control is 79.44 % while in neural based control rotor speed it is 61.42 %, which show speed fluctuation is more in fuzzy based control and speed is not controlled much more smoothly as in the case of neural based control. These analysis outcomes are given in Table 1.

6 Conclusion

The speed control of IM can be done by various methods. We have used soft computing based V/f technique to control the speed of a three phase IM. The soft computing techniques based controllers like the ANN controller and Fuzzy logic controller have been implemented. The constant V/f close loop technique is used because it modifies the output accordingly and reduces the settling time to reach steady state. As from the above discussion it is clear that Neural based control taking less settling time and has almost no overshoot. By comparing the soft computing techniques, results of the ANN controller are smoother than the fuzzy logic controller but its output can be improved by tuning it.

References

1. Proca, A.B., Keyhani, A.: Identification of variable frequency induction motor models from operating data. *IEEE Trans. Electrical Energy* **17**(1), 24–31 (2002)
2. Pinto, J.O.P., Bose, B.K., da Silva, L.E.B., Kazmierkowski, M.P.: A neural network based space vector PWM controller for voltage-fed inverter induction motor drive. *IEEE Trans. Ind. Appl.* **36**, 1628–1636 (2000)
3. Mondal, S.K., Pinto, J.O.P., Bose, B.K.: A neural network based space vector pwm controller for a three level voltage fed inverter induction motor drive. *IEEE Trans. Ind. Appl.* **38**(3), 660–669 (2002)
4. Lee, Y.H., Suh, B.S., Hyun, D.S.: A novel PWM scheme for a three-level voltage source inverter with GTO thyristors. *IEEE Trans. Ind. Appl.* **32**, 260–268 (1996)

5. Koyama, M., Fujii, T., Uchida, R., Kawabata, T.: Space voltage vector based new PWM method for large capacity three-level GTO inverter. In: Proceedings IEEE IECON'92, pp. 271–276 (1992)
6. Luo, Y.-C., Chen, W.-X.: Sensorless stator field orientation controlled induction motor drive with a fuzzy speed controller. *Comput. Math. Appl.* **64**(5), 1206–1216 (2012)
7. Yager, R.G.: Fuzzy logics and artificial intelligence. *J. Fuzzy Sets Syst.* **90**, 193–198 (1997)
8. Buhl, M., Lorenz, R.D.: Design and implementation of neural networks for digital current regulation of inverter drives. In: Conference Record IEEE-IAS Annual Meeting, pp. 415–421 (1991)
9. Singh, B., Bhuvanawari, G., Garg, B.: Harmonic mitigation in AC–DC converters for vector controlled induction motor drives. *IEEE Trans. Energy Convers.* **22**(3), 637–646 (2007)
10. Xiang-Dong, S., Kang-Hoon, K., Byung-Gyu, Y., Matsui, M.: Fuzzy-logic-based V/f control of an induction motor for a DC grid power leveling system using flywheel energy storage equipment. *IEEE Trans. Ind. Electron.* **56**(8), 3161–3168 (2009)
11. Marcelo Suetake, I.N., da Silva, A.G.: Embedded DSP-based compact fuzzy system and its application for induction-motor V/f speed control. *IEEE Trans. Ind. Electron.* **58**(3), 750–760 (2011)
12. Wang, Y., Song, J., Zhang, B.: Fuzzy sliding-mode variable structure control for fan filter units motor speed regulation system. *Procedia Eng.* **15**, 969–973 (2011)
13. Ustun, S.V., Demirtas, M.: Modeling & control of V/f controlled induction motor using genetic-ANFIS algorithm. *Energy Convers. Manage.* **50**, 786–791 (2009)
14. Tsai-Jiun Ren, T.-C.C.: Robust speed controlled induction motor drive based on recurrent neural network. *Electr. Power Syst. Res.* **76**(12), 1064–1074 (2006)
15. Tsai, C.-H., Yeh, M.-F.: Application of CMAC neural network to the control of induction motor drives. *Appl. Soft Comput.* **9**(4), 1187–1196 (2009)
16. Bose, B.K.: *Power Electronic and Drives*, pp. 264–276. Prentice-Hall, Englewood Cliffs (1986)
17. Gao, X.Z., Gao, X.M., Ovaska, S.J.: A modified Elman neural network model with application to dynamical system identification. In: Proceeding of the IEEE International Conference on Systems, Man and Cybernetics, pp. 1376–1381. Beijing, China (1996)
18. Lima, F., Kaiser, W., Nunes da Silva I., de Oliveira, A.A.: Speed neuro-fuzzy estimator applied to sensorless induction motor control. *Latin Am. Trans. IEEE (Revista IEEE America Latina)*, **10**, 2065–2073 (2012)
19. Oguz, Y., Dede, M.: Speed estimation of vector controlled squirrel cage asynchronous motor with artificial neural networks. *Energy Convers. Manage.* **52**(1), 675–686 (2011)
20. Haykin, S.: *Neural Networks. A Comprehensive Foundation*. Macmillan Collage Publishing company, Inc., New York (1994)
21. Kim, S.-M., Han, W.-Y.: Induction motor servo drive using robust PID-like neuro-fuzzy controller. *Control Eng. Pract.* **14**(5), 481–487 (2006)
22. Ye, Z., Sadeghian, A., Wu, B.: Mechanical fault diagnostics for induction motor with variable speed drives using adaptive neuro-fuzzy inference system. *Electr. Power Syst. Res.* **76**(9–10), 742–752 (2006)
23. Lee, C.C.: Fuzzy logic in control systems: fuzzy logic controller—Part I, II. *IEEE Trans. Syst. Man Cybern.* **20**(2), 404–435 (1990)
24. Limongi, L.R., Bojoi, R., Griva, G., Tenconi, A.: Performance comparison of DSP-based current controllers for three-phase active power filters. In: Proceedings of IEEE International Symposium on Industrial Electronic, pp. 136–141 (2008)
25. Al-Odienat, A.I., Al-Lawama, A.A.: The advantages of PID fuzzy controllers over the conventional types. *Am. J. Appl. Sci.* **5**(6), 653–658 (2008)
26. Karanayil, B., Rahman, M.F., Grantham, C.: Online stator and rotor resistance estimation scheme using artificial neural networks for vector controlled speed sensorless induction motor drive. *IEEE Trans. Ind. Electron.* **54**(1), 167–176 (2007)
27. Bose, B.K.: *Modern Power Electronics and AC Drives*. Prentice-Hall, Upper Saddle River (2002)

Edge Detection in Images Using Modified Bit-Planes Sobel Operator

Rashi Agarwal

Abstract The detection of edges in images is a vital operation with applications in various fields. There are a number of methods developed already for the same. We have developed a ‘global method’ for extraction of edges which is a modification of the existing Sobel operator. We have first extracted the bit planes of each image and have applied the Sobel operator on each bit plane for enhanced results. After this we have recreated the image by adding up the Sobel edge detected planes in their order of importance. This is a fairly simple global method which yields very good results. The computations are simpler and faster as well.

Keywords Edge detection · Bit-planes · Sobel operator

1 Introduction

Edge detection is a vital operation in image processing with numerous applications in scene analysis and object recognition. Various algorithms with different complexities and tradeoffs exist for detection of edges. Numerous studies have been done in the past to assess these algorithms [1]. Detection of edges refers to the process of identifying and locating sharp discontinuities in an image. The discontinuities are abrupt changes in pixel intensity which characterize boundaries of objects in a scene. Classical methods of edge detection involve convolving the image with an operator (a 2-D filter), which is constructed to be sensitive to large gradients in the image while returning values of zero in uniform regions.

There are two main approaches for edge detection:

R. Agarwal (✉)
IT Department, UIET, CSJM University, Kanpur, India
e-mail: dr.rashiagrawal@gmail.com

- Gradient:** The gradient method detects the edges by looking for the maximum and minimum in the first derivative of the image.
- Laplacian:** The Laplacian method searches for zero crossings in the second derivative of the image to find edges. An edge has the one-dimensional shape of a ramp and calculating the derivative of the image can highlight its location.

In the former method, the discontinuities are enhanced by neighborhood operators. The Robert's, Prewitt and Sobel operators are examples of this method. A quantitative assessment of these is done in [2]. All the gradient-based algorithms have kernel operators that calculate the strength of the slope in directions which are orthogonal to each other, commonly vertical and horizontal. Later, the contributions of the different components of the slopes are combined to give the total value of the edge strength.

Most edge detection methods work on the assumption that the edge occurs where there is a discontinuity in the intensity function or a very steep intensity gradient in the image. Using this assumption, if one take the derivative of the intensity value across the image and find points where the derivative is be located. The gradient is a vector, whose components measure how rapid pixel value are changing with the distance in the x and y direction.

Edge detection in noisy environment can be treated as an optimal linear filter design problem. Canny formulated edge detection as an optimization problem and defined an optimal filter, which can be efficiently approximated by the first derivative of Gaussian function in the one-dimensional case. Canny's filter was further extended to recursive filters, which provide a more efficient way for image noise filtering and edge detection [3].

Other edge detection methods include differentiation based edge detection using logarithmic image processing (LIP) models [4], contrast-based methods [5], relaxation labeling techniques [6] and anisotropic diffusion [7]. In fact, these methods can be combined to achieve better performance.

In our study we have used a modified version of the simple Sobel mask to find out edges. We have applied the mask to various bit planes of an image as described in the next section and combined the obtained masks in order of their significance to get the final edge image effectively.

2 Methodology

A. Bit Plane Slicing

Given an X-bit per pixel image, slicing the image at different planes (bit-planes) plays an important role in image processing. In general, 8-bit per pixel images are

processed. We can slice an image into the following bit-planes. Zero is the least significant bit (LSB) and 7 is the most significant bit (MSB) [8]:

- 0 which results in a binary image, i.e., odd and even pixels are displayed
- 1 which displays all pixels with bit 1 set: 0000.0010
- 2 which displays all pixels with bit 2 set: 0000.0100
- 3 which displays all pixels with bit 3 set: 0000.1000
- 4 which displays all pixels with bit 4 set: 0001.0000
- 5 which displays all pixels with bit 5 set: 0010.0000
- 6 which displays all pixels with bit 6 set: 0100.0000
- 7 which displays all pixels with bit 7 set: 1000.0000.

Shown below is an 8-bit per pixel image and how each plane represents information on that plane.

These bit planes can be combined in their order, back again to get the original image.

2.1 Sobel Operator

The Sobel operator performs a 2-D spatial gradient measurement on an image. Typically it is used to find the approximate absolute gradient magnitude at each point of an input grayscale image. The Sobel edge detector uses a pair of 3×3 convolution masks, one estimating gradient in the x-direction and the other estimating gradient in y-direction. In the Sobel mask operator consists of a pair of 3×3 convolution kernels as shown in Fig. 1. One kernel is simply the other rotated by 90° [9, 10].

+1	+2	+1
0	0	0
-1	-2	-1

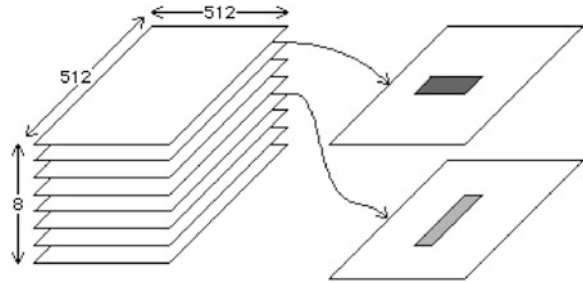
Gy

-1	0	+1
-2	0	+2
-1	0	+1

Gx

These kernels are designed to respond maximally to edges running vertically and horizontally relative to the pixel grid, one kernel for each of the two perpendicular orientations. The kernels can be applied separately to the input image, to produce separate measurements of the gradient component in each orientation

Fig. 1 Bit planes of an 8 bit image (512 × 512 size)



(call these G_x and G_y). These can then be combined together to find the absolute magnitude of the gradient at each point and the orientation of that gradient. The gradient magnitude is given by:

$$|G| = \sqrt{G_x^2 + G_y^2}$$

Typically, an approximate magnitude is computed using:

$$|G| = |G_x| + |G_y|$$

which is much faster to compute.

The angle of orientation of the edge (relative to the pixel grid) giving rise to the spatial gradient is given by:

$$\theta = \arctan(G_y/G_x)$$

3 Results and Discussion

The process of extraction of edges was carried out on each bitplane of the image and these edges were then recombined to give the final result. Below are shown images of “lena” which are most popular in the image processing fraternity. We have named our method the Modified Biplane Sobel Operator (MBSO).



The various bitplanes extracted and their corresponding edges are shown as follows.



Bitplane 7 of original image



Bitplane 7 edge



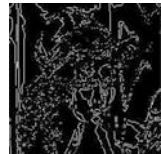
Bitplane 6 of original image



Bitplane 6 edge



Bitplane 5 of original image



Bitplane 5 edge



Bitplane 4 of original image

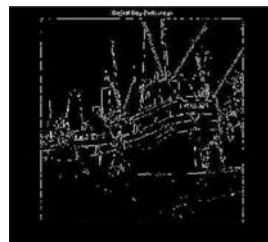


Bitplane 4 edge

Another image, “Ships” showed following results



Original ‘Ships’ image



Edge extraction by Sobel operator

(continued)

(continued)



Edge extraction by MBSO

The “cameraman” image gave the following results:



Original 'Cameraman' image



Edge extraction by Sobel operator



Edge extraction by MBSO

The ‘barn’ image gives following results:



Original ‘Cameraman’ image



Edge extraction by Sobel operator



Edge extraction by MBSO

Table 1 Signal to noise ratio with noise = 1 using Sobel operator

Image	SNR = 1	SNR = 0.6
Lena	0.91	0.56
Ships	0.84	0.51
Cameraman	0.88	0.52
Barn	0.92	0.60

Table 2 Signal to noise ratio with noise = 1 using modified bitplanes sobel operator

Image	SNR = 1	SNR = 0.6
Lena	0.95	0.62
Ships	0.88	0.53
Cameraman	0.89	0.55
Barn	0.94	0.64

Signal to Noise Ratio (SNR) and Average Risk (AVR) [11, 12] are our chosen criteria to compare different algorithms. Both the original Sobel edge detector and the bitplane Sobel edge detector in the context of the above mentioned classification, are selected and then tested. The above sets of images resulting from the applying of those algorithms are presented next. Tables 1, 2 describe the corresponding values of the SNR for each edge detector.

4 Conclusion

The Sobel mask is easy to implement as compared to other operators. Although the Sobel operator is slower to compute, it's larger convolution kernel smoothes the input image to a greater extent and so makes the operator less sensitive to noise. The larger the width of the mask, the lower its sensitivity to noise and the operator also produces considerably higher output values for similar edges. Sobel operator effectively highlights noise found in real world pictures as edges though the detected edges could be thick. The Bitplane Sobel operator is computationally a little expensive but the results when compared take it worth it. The visual comparison of the above sets of images can lead us to the subjective valuation of the performances of selected edge detectors. The SNR values also show improvement with the new developed technique. Additional tests and statistical investigations are necessary for a more detailed evaluation of the techniques.

References

1. Sharifi, M., Fathy, M., Mahmoudi, M.T.: Classified and comparative study of edge detection algorithms. In: Proceedings of the International Conference on Information Technology: Coding and Computing, pp. 117–120 (2002)
2. Abdou, I.E., Pratt, W.K.: Quantitative design and evaluation of enhancement edge detectors. In: Proceedings of IEEE, vol. 67, pp. 753–763 (1979)
3. Canny, J.: A computational approach to edge detection. *IEEE Trans. Pattern Anal. Mach. Intell.* **PAMI-8**, 679–698 (1986)
4. Deng, G., Pinoli, J.-C.: Differentiation-based edge detection using the logarithmic image processing model. *J. Math. Imaging Vis.* **8**, 161–180 (1998)
5. Johnson, R.P.: Contrast based edge detection. *Pattern Recogn.* **23**, 311–318 (1990)
6. Iyengar, S.S., Deng, W.: An efficient edge detection algorithm using relaxation labeling technique. *Pattern Recogn.* **28**, 519–536 (1995)
7. Perona, P., Malik, J.: Scale-space and edge detection using anisotropic diffusion. *IEEE Trans. Pattern Anal. Mach. Intell.* **12**, 629–639 (1990)
8. Agarwal, R.: Bit planes histogram equalization for tone mapping of high contrast images. In: *IEEE Proceedings of Computer Graphics, Imaging and Visualisation Conference*, Singapore, pp. 33–38 (2011)
9. Gonzalez, R.C., Woods, R.E.: *Digital Image Processing*, 3rd edn. Prentice Hall, Upper Saddle River, NJ (2008)
10. Vincent, O.R., Folorunso, O.: A descriptive algorithm for sobel image edge detection. In: *Proceedings of Informing Science & IT Education Conference InSITE* (2009)
11. Speeuwers, L.J., van der Heijden, F.: An edge detector evaluation method based on average risk. In: Forstner, Ruwiedel (eds.) *Robust Computer Vision*, Wichmann, Karlsruhe 40–49 (1992)
12. Heath, M., Sarker, S., Sanocki, T., Bowyer, K.: Comparison of edge detectors: a methodology and initial study. In: *Proceedings of CVPR'96 IEEE Computer Society Conference on Computer Vision and Pattern Recognition*, pp. 143–148 (1996)

Application of Rule Based Fuzzy Inference System in Predicting the Quality and Quantity of Potato Crop Yield in Agra

Darpan Anand, Manu Pratap Singh and Manish Gupta

Abstract Conservatory growers want steadfast amount of yields so as to precisely meet the demand. Objective of this paper is to apply rule based fuzzy inference system (RBFIS) to forecasting crop yield by using ecological parameters. Inputs to RBFIS are derived from a crop development model (temperature, humidity, water/irrigation, available soil, fertilizers and seed quality). RBFIS has two output nodes, for the quality and the quantity of yield, with potato as a case.

Keywords Crop yield · Fuzzy system · Inference · Rule based fuzzy system

1 Introduction

The real-world problems are complex, having lot of inter-dependent parameters deriving the results. The deficiency on explored hypothesis and the lack of knowledge on analyzed phenomena along with high operating cost on experts need classy methods of preparing precise intelligent systems competent to reflecting

Agra (27° 11'0" North, 78° 1'0" East), Uttar Pradesh, India, Asia.

D. Anand (✉)
Mahamaya Technical University, Noida, India
e-mail: darpan.anand.agra@gmail.com

D. Anand · M. Gupta
HITM, Agra, India
e-mail: manish_dabra@yahoo.com

M. P. Singh
Dr. Bhim Rao Ambedkar University, Agra, India
e-mail: Manu_p_singh@hotmail.com

certainty to specify their knowledge even for unexpected cases. The fuzzy system is a tool capable of building a machine with intelligence.

The concept of fuzzy sets initiated by Attanasov [1] is an expansion of the concept of fuzzy sets, found to be more rational and realistic as the non-membership function is self-determining of the membership function but both are linked to each other through a condition.

Fuzzy system is used in this paper because of its nearness to real life implementations in execution of a work, happening in agriculture system too. Ultimately, it will be illustrated that the use of fuzzy systems lifts up an effective workable accumulation to the field of Artificial Intelligence and conceivably more generally to formal mathematics as a whole [1].

The inference system as shown in Fig. 1, is a tool to solve the problem like crop prediction, therefore an inference engine is a software program that endeavors to obtain solutions from a knowledge base (KB). It is the 'mind' that expert systems bring into play to cause the information in its KB, participate in decision making to formulate new results and conclusions.

An inference system contains three major sub systems. 1. Knowledge Base, 2. Inference Engine, 3. User Interface. To develop the inference system based on fuzzy for crop prediction for potato. Process includes collection of vague data and converts this in fuzzy membership functions and also develop a knowledge based on fuzzy inputs and fuzzy outputs of the problem i.e. agriculture management on potato.

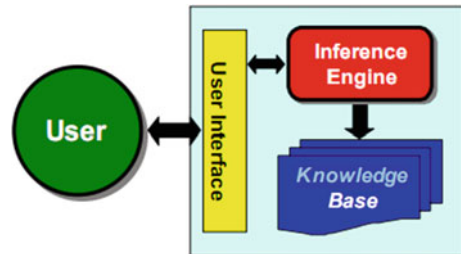
A RBFIS commenced by Zadeh (1971) is now considered fundamental in further research, helping implementation to derive the Mamdani-Assilian (1975) linguistic Fuzzy Inference System (FIS).

This paper proposes a technique, based on RBFIS to predict the quality and quantity of the crop yield of potato. In this method six input parameters influencing the yield (soil, water, humidity, fertilizer, seed and temperature), and two output parameters (quality and quantity) are taken.

2 Literature Survey

The RBFIS has been acknowledged as a constructive approach to model many multifaceted phenomena in the field of forecasting prediction. These mathematical models bring into play different equations and formulae to resolve such problems. However, when resolving real-life problems, linguistic information is often came upon that is regularly hard to enumerate using conventional mathematical methods. Basic results linked to the growth of fuzzy logic data from Zadeh (1973) and Mamdani and Assilian (1975). Approximate Reasoning, a concept, successfully introduced by Zadeh, showed that fuzzy logical statements permit the formation of algorithms that can use vague data to derive fuzzy inferences. Zadeh understood his approach would be advantageous above all in the study of complex humanistic systems. Recognized that Zadeh's approach could be effectively applied to various

Fig. 1 An inference system [2]



filed of controlling and forecasting, Mamdani and Assilian (1975) applied it to control a pilot-scale steam engine. They used fuzzy logic in order to convey linguistic rules. As regards the application of fuzzy logic in engineering, the tutorials given by Mendel (1995) are of importance.

Rule based Fuzzy Logic is a straightforward (yet very influential) problem solving method with wide-range applicability. It is at present used in the fields of business, systems control, electronics and traffic engineering. The system can be used to produce solutions to problems based on “vague, ambiguous, qualitative, incomplete or imprecise information”.

Others models are based on statistical inference as multiple regression equations. The Large Area Crop Inventory Experiment LACIE (McDonald 1984) and AgRISTARS (Ferguson 1982) demonstrated studies on considering Crop yield models. The applicability of crop forecasting systems has been deemed by the leading crop as a simulation model (Gommes 1998). In an attempt to correct the atmospheric and soil spectral effects on remotely-sensed data, Spectral vegetation indices have been developed (Broge and Mortensen 2002). Similar systems within government agencies for the management of agricultural prices and distribution in China have already proven precious to decision-makers and analysts (Bingfng and Chenglin 1998).

A subtractive based fuzzy inference system is introduced to estimate the potato crop parameters like biomass, leaf area index, and plant height and soil moisture. The plant height, biomass, and leaf area index of potato crop and soil moisture measured at its various growth stages were used as the target variables during the training and validation of the network [3].

This work investigates the yield modeling and prediction process in Apples using the dynamic influence graph of Fuzzy Cognitive Maps (FCMs). In this work, a data driven non-linear FCM learning approach was chosen to categorize.

Yield in Apples, where very few decision making techniques were investigated. Through the proposed methodology, FCMs were designed and developed to represent experts’ knowledge for yield prediction and crop management. The developed FCM model consists of nodes linked by directed edges, where the nodes represent the main soil factors affecting yield, [such as soil texture (clay and sand content), soil electrical conductivity (EC), potassium (K), phosphorus (P), organic matter (OM), calcium (Ca) and zinc (Zn) contents], and the directed edges show the cause-effect (weighted) relationships between the soil properties and yield [4].

Table 1 Standard function to define Fuzzy parameters

Function	Description
Dsigmf	Built-in membership function composed of difference between two sigmoidal membership functions
gauss2mf	Gaussian combination membership function
Gaussmf	Gaussian curve built-in membership function
Gbellmf	Generalized bell-shaped built-in membership function
Pimf	Π-shaped built-in membership function
Psigmf	Built-in membership function composed of product of two sigmoidally shaped membership functions
Sigmf	Sigmoidally shaped built-in membership function
Smf	S-shaped built-in membership function
Trapmf	Trapezoidal-shaped built-in membership function
Trimf	Triangular-shaped built-in membership function
Zmf	Z-shaped built-in membership function

3 System Model

To get the effective outputs by formulation and mapping of given inputs based on fuzzy logic, is called as fuzzy inference. The process of fuzzy inference entails all of the pieces like: If-Then Rules, Logical Operations, and Membership Functions.

For this proposed system, as per advised by the domain experts and survey, meet the point that in initial phase [5], some important input parameters for the potato crop production in context of the AGRA district i.e. six input parameters and two output parameters. The fuzzy parameters input or output is defined by some standard functions. Some standard functions are illustrated in the Table 1.

For this modeling the **trapmf function**. The trapezoidal curve is a function of a vector, x , and depends on four scalar parameters a , b , c , and d , as given.

$$f(x; a, b, c, d) = \max\left(\min\left(\frac{x - a}{a - b}, 1, \frac{d - x}{d - c}\right), 0\right) \tag{1}$$

or in general the Eq. (1) can be written as:

$$f(x; a, b, c, d) = \begin{cases} 0, & x \leq a \\ \frac{x-a}{b-a}, & a \leq x \leq b \\ 1, & b \leq x \leq c \\ \frac{d-x}{d-c}, & c \leq x \leq d \\ 0, & d \leq x \end{cases} \tag{2}$$

The operation of the Mamdani rule base can be broken down into four parts:

- 1) Mapping each of the crisp inputs into a fuzzy variable (**fuzzification**);
 - 2) Determining the output of each rule given its fuzzy antecedents;
 - 3) Determining the aggregate output(s) of all of the fuzzy rules;
 - 4) Mapping the fuzzy output(s) to crisp output(s) (**defuzzification**).
- 1) Fuzzification

The rules, however, are given in terms of fuzzy variables. The membership of each fuzzy input variable is evaluated for the given crisp input, and the resulting value is used in evaluating the rules.

2) Evaluating the Rules

Second step is determined the values of parameters using the membership function and according to the compositional rule of inference, the rules are evaluated. The result is an output fuzzy set that is some concise version on the user-specified output fuzzy set. The height of this clipped set depends on the minimum height of the antecedents.

3) Aggregating the Rules

After the previous step, fuzzy output defined for each of the rules in the rule base, and then need to combine these fuzzy outputs into a single fuzzy output. Mamdani defines that the output of the rule base should be the maximum of the outputs of each rule.

4) Defuzzification

After the previous step, fuzzy output defined for the rule base. It needs to convert this output into a crisp output. To do this, the centroid (first moment) of the fuzzy output is used.

3.1 The System Model

For the modeling of proposed system, first we need to identify the components of the system. The Rule based fuzzy inference system has the following components:

1. ***Parameters:*** These are the variables for the system to determine the output. The non-fuzzy data converted into the fuzzy input variables. For fuzzification process, it required some function. Triangular-shaped built-in membership function is used in this modeling [6]. These parameters can be further divide into two types as:
 - a. ***Input Parameters:*** These are the independent of the system. The output of the system is derived by these input parameters. Each input parameter is dividing into three membership functions. These membership functions are defined by the Triangular-shaped built-in membership function. The crisp data has taken from the government records.
 - b. ***Output Parameters:*** These parameters wrap the inference value of the system. It means system executes the process and according to the input parameters the system gives the output. For determining the output parameters, it derives into five membership function and each membership function is defined by triangular-shaped built-in membership function.

2. **Rule base:** Among the parameter, there are various relations. These relations are defined by the rules. The collection of these rules is called as the Rule base. The relation between the parameters can be defined by the following operators:

<i>a.</i> AND	<i>b.</i> OR	<i>c.</i> NOT
---------------	--------------	---------------

The AND, OR and NOT are the logical operator applied between the various combination of the input and output parameter. For example say IP1 and IP2 are two input parameters defined by three membership functions, High, Medium and Low. There is one output parameter as OP1. The rule may be defines as:

If IP1 is high AND IP2 is low
Then OP1 is Medium

The above rule explained as if the input parameter IP1’s value is high and input parameter IP2’s value is low then the system out is OP1 and the value is Medium.

Similarly a number of rules developed for any system and the relationship is defined by the above explained operators. The knowledge of these relationships is gathered from the domain expert of the field.

There are five steps to develop the rule based fuzzy inference system. The steps are:

- Step1: Fuzzify Input
- Step2: Apply Fuzzy Operator
- Step3: Apply Implication Method
- Step4: Aggregate All Outputs
- Step5: Defuzzification

For defining the parameters, analyses the previous records of the Agra city. The statistical department of Uttar Pradesh Government helped us to collect the data. On the bases of it we develop the membership functions of input and output parameters.

Triangular and trapezoid methods are used for defining these inputs and output membership function. For de-fuzzification, system uses centroid method [7].

So system is look like as in Fig. 2.

3.1.1 Input Parameters

1. **SOIL:** Soil is the base for the agriculture. Soil is the layer of minerals and organic matter, in thickness from centimeters to a meter or more, on the land surface [8]. As far as Agra is concerned, the total area for agriculture land is the key to derive land parameter. Land can be further divide into its various type depend on its texture but for this paper, the area of agriculture utilized land as one of the input parameter. This input can be defined as below and shown in Fig. 3.

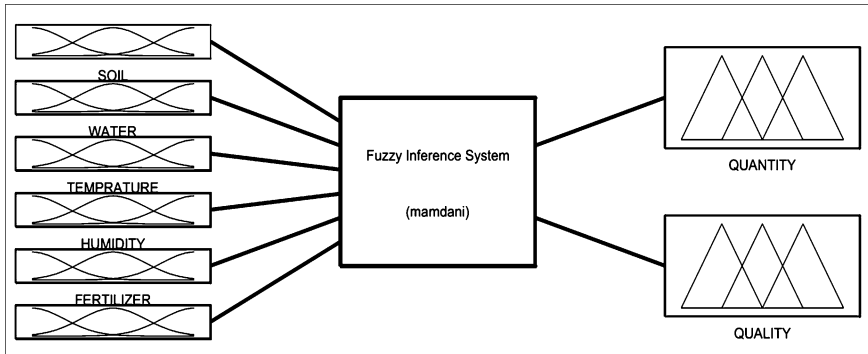


Fig. 2 Membership fuzzy inference system for potato crop

The total area of agriculture utilized land = AUA in hectares.

LOW	MEDIUM	HIGH
$0 < AUA < 263230$	$262000 \leq AUA \leq 265000$	$268400 \leq AUA < \infty$

2. **WATER:** The second input parameter is water is require for the irrigation of crop i.e. Diet for the crop. Because this crop is the type of 'RABI' that means the crop is going to develop in winter season therefore water irrigations are slightly minimum as compare to other season's crop. In Agra perspective, the total number of water resources available in Agra includes walls, tube wells and other resources. The input can be defined as:

$$\text{Total Number of Water Resources} = \text{WR}$$

LOW	MEDIUM	HIGH
$0 < \text{WR} \leq 139450$	$139400 \leq \text{WR} \leq 139700$	$139600 \leq \text{WR} \leq \infty$

In case of potato crop, it needs 2–3 times of irrigation. Therefore in this way the MEDIUM type of irrigation gives the maxim productivity, so the membership function of water can be illustrated as in Fig. 3.

3. **TEMPERATURE:** Temperature is the next input parameter for this inference. As discussed earlier that the potato crop comes under the RABI season. It means that, minimum temperature at this level required for production.

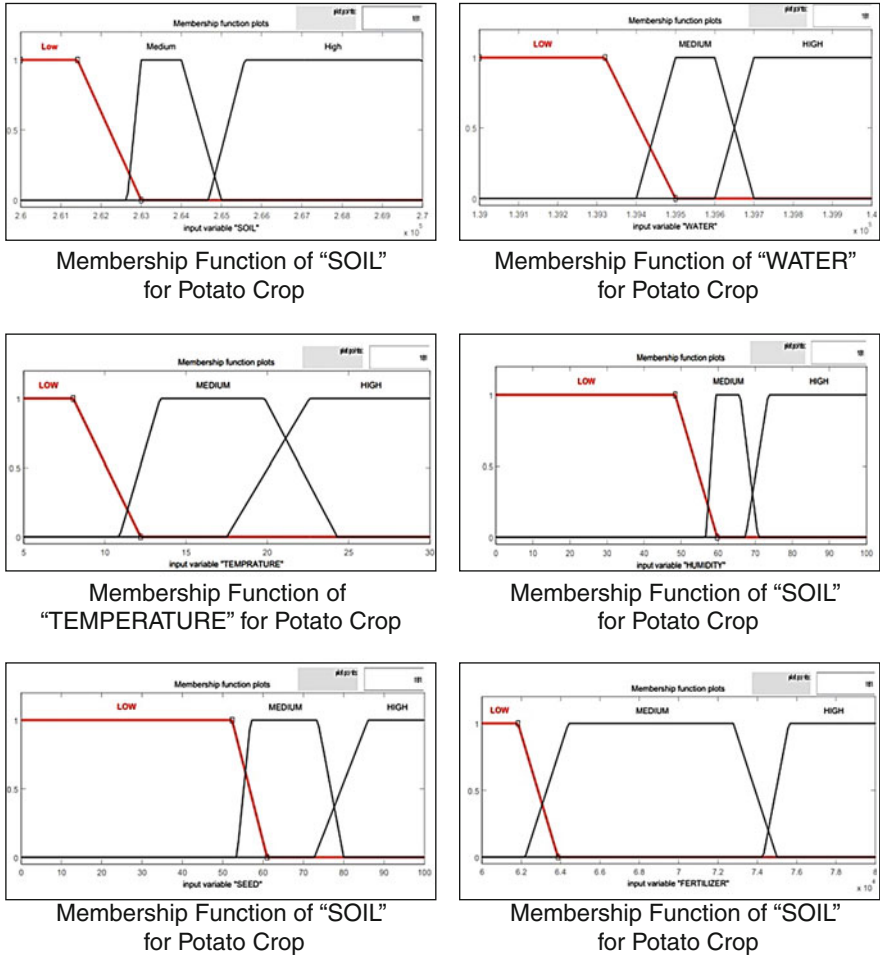


Fig. 3 Membership function of input parameters

Therefore for the agriculture life cycle the temperature range can divide in three levels as:

LOW	MEDIUM	HIGH
under 12 degree	11–24 degree	above 17.5 degree

This parameter is totally depending on the nature, no one can control this parameter so the membership function of the temperature can be drawn as Fig. 3.

4. **HUMIDITY:** Humidity can make the temperature of the surrounding air feel like it is warmer than the actual temperature, because the cooling effect of evaporation. So high humidity favored the growth of the crop, therefore with understanding these factors are divided this factor in three categories as:

LOW	MEDIUM	HIGH
below 60	in between 57 to 71	above 68

This parameter is also depending upon the nature so the membership function for this can be drawn as Fig. 3.

5. **FERTILIZERS:** A substance that provides nutrients to plants. Some, such as manure, are natural; others are human-made or synthetic. In Agra region farmers uses both type of fertilizers i.e. organic and synthetic, first they prepare the farms using organic compost then mean while of the crop production they apply the chemical fertilizer. These fertilizers basically provided by the state government. So the membership function for the fertilizers can be defined with respect to the amount distributed by the government. So the fertilizers (FLZ) in metric tons can be shown as:

LOW	MEDIUM	HIGH
$FLZ < 62000$	$6 \times 10^4 < FLZ < 75 \times 10^4$	$FLZ > 73 \times 10^4$

Therefore the membership functions for the fertilizers shown in Fig. 3.

6. **SEEDS:** Seed is the part of a plant that can make another plant. Usually a plant makes flowers, and then once the flowers have been pollinated, they turn into fruit. The seeds are inside the fruit. Seeds can be spread by wind, water, or animals. Then, when they are in a new place with water and nutrients, they can grow into a new plant. Sometimes an animal eats some fruit, and then poops the seeds out someplace, and a new plant grows there. Potato itself used as a seed for potato crop itself.

The seed quality is the factor which emphasis the quality and quantity of the total crop. So this can be dividing the range of this parameter in three categories as:

LOW	MEDIUM	HIGH
$SEED < 60 \%$	$55 \% < SEED < 80 \%$	$SEED > 75 \%$

So the membership functions for the seeds shown in Fig. 3.

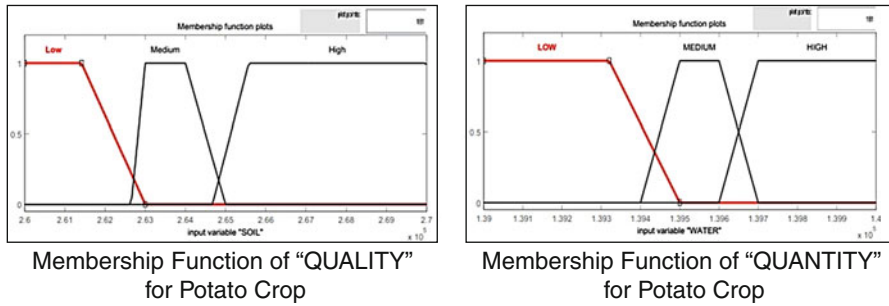


Fig. 4 Membership function of quality and quantity for potato crop

3.1.2 Output Parameters

The output of any crop is the quantity and quality of the production. Therefore for this proposed system two parameters for output as:

1. **QUANTITY:** This parameter can be scale in scale 0 to 1, define the quality in five categories as:

VERY LOW	LOW	MEDIUM	HIGH	VERY HIGH
QT < 193	221 < QT < 231	229 < QT < 239	238 < QT < 249	QT > 245

100 is the scale of previous year production. The membership function for this output parameter can be shown as in Fig. 4.

2. **QUALITY:** This parameter can be scale in scale 0 to 1, define the quantity in five categories as:

VERY LOW	LOW	MEDIUM	HIGH	VERY HIGH
QL < 50 %	41 % < QL < 63 %	58 % < QL < 83 %	78 % < QL < 97 %	QL > 92 %

100 is the scale of previous year production. The membership function for this output parameter can be shown as in Fig. 4.

Rule base:

There are 6 inputs and 2 outputs. Each input is divided into three membership functions and according to the combination of these inputs, will produce the output. MATLAB support AND, OR and NOT operations to combine the inputs, rule base have 729 combinations of these inputs so the rule base size is 729 which can illustrate all possible combinations.

Table 2 Values of three years data of city of Agra

Input parameter	Y-2009	Y-2010	Y-2011
Temperature (°c)	16.2	15.6	14.6
Humidity (%)	70.2	72.4	72.7
Water Resources (#)	139514	139542	140548
Useful Soil (ha)	263230	264454	266459
Uses of Fertilizers (m tones)	68117	68117	112237

Table 3 Output Parameters in terms of production

Output Parameter	Y-2009	Y-2010	Y-2011
Actual Yield Output	230.63	241.84	251.49
	Medium	High	Very High
Measured Output	226	235	245
	Medium	High	Very High
Error in (percentage) %	2	2.8	2.58

4 Simulation and Results

For test this system, the government statistical book data is used which illustrate the data of past years. The quality of seeds is not in the statistics of Agra. Other five parameters for past three years are available and illustrated by the following Table 2.

Test the system on the above data and the result of the system is mentioned in Table 3. We apply the inputs as given in Table 1 and the output of the system is given in the Table 2. Under limitation of the accuracy of the data and information the results are fruitful.

The results are also shown using the graph as Fig. 5.

Test results Analyses:

The graph ‘-.-’ shown in Fig. 5, the actual yield production (data given by the government agency), graph ‘—’ shows the output from system and below the ‘-o-’ shows the error of the system’s output with respect to the actual output for past three years i.e. 2009, 2010 and 2011. Because system’s output came in terms of fuzzy system. After defuzzification, the System produces the output in terms of the actual number. So the Table 2 and Fig. 5 shows that there is an error in analytical data but the fuzzy term data does not have error. So the graph in Fig. 5 illustrated that, our hypotheses is correct under the circumstances and limitations of the development of the system. The last rows of the Table 2 show the errors. For the year 2009 error is 2 %, for year 2012 error is 2.8 % and for the year 2011 the error is 2.5 %. But in terms of the fuzzy data error is NIL. So it means our hypotheses are proved and system is valid for these hypotheses.

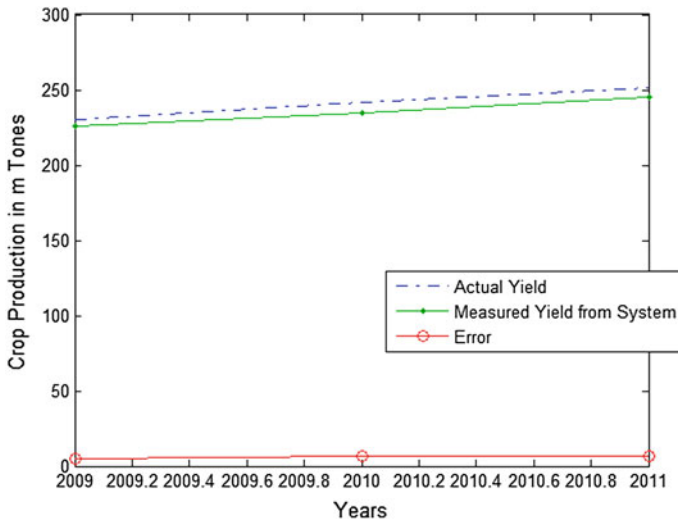


Fig. 5 Graphs of actual, measured and error graph with respect to the year

5 Conclusion

The evaluations between considered and simulated values meet the expense of it a role in forecasting of potato crop. The proposed system design and simulation work could also lead to the new possibilities in the field of crop forecasting with available measurements of parameters. However our anticipated fuzzy inference system estimates the quantity and quality of potato crop.

Under the limitations of the parameters values and accuracy of the exact rules, we can say the system's outputs are near to the actual outputs. But we can improve the system by adding the more accurate data, more parameters and improved rules. But in terms of fuzzy, the output is accurate and acceptable. This system fulfilled our proposed hypothesis and also it can be used for betterment and development of agriculture and planned the future business related to the particular crop.

References

1. Chai, Y., Jia, L., Zhang, Z.: Mamdani model based adaptive neural fuzzy inference system and its application. *Int. J. Inf. Math. Sci.* **5**, 1 (2009)
2. Athar, Atifa, et al.: A fuzzy inference system for synergy estimation of simultaneous emotion dynamics in agents. *Int. J. Sci. Eng. Res.* **2**(6), 35–41 (2011)
3. Pandey, Abhishek, et al.: Crop parameters estimation by fuzzy inference system using X-band scatterometer data. *Advances in space research* (2012)
4. Papageorgiou, E.I., et al.: Yield prediction in apples using fuzzy cognitive map learning approach. *Comput. Electron. Agric.* **91**, 19–29 (2013)

5. <http://research.cip.cgiar.org/confluence/display/wpa/India> (2013)
6. <http://www.mathworks.co.uk/help/fuzzy/fuzzy-inference-process.html> (2012)
7. Fitz-Rodríguez, E., Giacomelli, G.A.: Yield prediction and growth mode characterization of greenhouse tomatoes with neural networks and fuzzy logic. *Trans. ASABE* **52**(6), 2115–2128 (2009)
8. Mitchell, J., Gaskell, M., Smith, R., Fouche, C., Koike, S.T.: Soil management and soil quality for organic crops. Vegetable research and information centre, California

A Novel Variant of Self-Organizing Migrating Algorithm for Global Optimization

Dipti Singh, Seema Agrawal and Nidhi Singh

Abstract This paper presents a novel variant SOMAQI of population based optimization technique self organizing migrating algorithm (SOMA). This variant uses the quadratic approximation or interpolation for creating a new solution vector in search space. To validate the efficiency of this algorithm it is tested on 10 benchmark test problems and the obtained results are compared with already published results using the same quadratic approximation. On the basis of comparison it is concluded that the presented algorithm shows better performance in terms of number of population size and function mean best.

Keywords Self organizing migrating algorithm • Particle swarm optimization • Quadratic interpolation • Global optimization

1 Introduction

Hybrid technique is regarded as an effective method of improving the performance of a population based technique for solving complex optimization problems. The good exploration capabilities are often used to locate some promising zones within the wide solution space, while the local optimization methods exploit the located promising zones to achieve the best solution quickly and accurately. Many

D. Singh (✉)

Department of Applied Sciences, Gautam Buddha University, Greater Noida, India
e-mail: diptima@rediffmail.com

S. Agrawal

Department of Mathematics, S.S.V.P.G. College, Hapur, India
e-mail: Seemagrwl7@gmail.com

N. Singh

School of Engineering, Gautam Buddha University, Greater Noida, India
e-mail: nidhi@gbu.ac.in

attempts have been made in literature to hybridize population based techniques with other exiting approaches such as Quadratic Approximation. A random search technique for global optimization based on the quadratic approximation was developed by Mohan and Shankar (now Deep) [1]. Deep and Das proposed four variants of quadratic approximation based hybrid genetic algorithm for function optimization and tested its performance on the set of benchmark test problems [2]. Deep and Bansal [3] presented the hybridization of PSO with quadratic approximation operator (QA) and the presented results showed the efficiency of hybrid technique [4]. A variant of Quantum behaved Particle Swarm optimization for solving global optimization problems was presented by Millie et al. To improve the performance of real coded genetic algorithm Deep and Das [5] hybridized it with quadratic approximation. Millie et al. presented a new variant of Particle Swarm optimization named QPSO for solving global optimization problems and tested it on various benchmark problems. Analysis of results showed that the use of multiparent quadratic interpolation operator outperformed basic PSO [6]. Deep and Bansal [3] developed a variant of PSO with hybridization of quadratic approximation operator for economic dispatch problems with valve-point effects.

This paper presents a variant (SOMAQI) of Self Organizing Migrating Algorithm (SOMA) which uses the quadratic approximation or interpolation for creating a new solution vector in the search space. Quadratic Approximation is an operator which produces the minima of the quadratic curve passing through the three chosen individuals and substantially improves the performance of SOMA. SOMA is an emergent search technique based on the self-organizing behavior of groups of individuals in a social environment. Like other evolutionary algorithm it also works with a population of solutions. The main feature of this algorithm which makes it distinguished as compared to other algorithms is that no new solutions are created during the search. Instead, only the positions of the solutions are changed during a generation, called a migration loop. The proposed algorithm SOMAQI creates new point in the search space using Quadratic Interpolation in such a way that diversity of the search domain can be maintained by newly generated points and can be thoroughly exploited. The direction of the search can be a little bit guided. The Competitive- Cooperative behavior can achieve the global optimal solution with a small population size in less number of function evaluations. A set of 10 well known test problem has been used to evaluate the performance of SOMAQI.

The paper is organized as follows. In [Sect. 2](#), preliminaries are presented. In [Sect. 3](#), the proposed Algorithm SOMAQI is presented. In [Sect. 4](#), the numerical results are discussed. Finally, the paper concludes with [Sect. 5](#) drawing the conclusions of the present study.

2 Preliminaries

In this section two algorithms SOMA and PSO has been described. SOMA has been used for hybridization and PSO has been used for comparison.

2.1 Self Organizing Migrating Algorithm

Self-Organizing migrating Algorithm is a population based stochastic search technique which is based on the social behavior of a group of individuals [7, 8]. At each generation the individual with highest fitness value is known as leader and the worst is known as active. Rather than competing with each other, the active individual proceeds in the direction of the leader. This algorithm moves in migration loops and in each migration loop active individual travels a certain distance towards the leader in n steps of defined length. This path is perturbed randomly by PRT parameter. PRT vector is created before an individual proceeds towards leader. This parameter has the same effect as mutation in Genetic Algorithm (GA). It is defined in the range (0, 1). The movement of an individual is given as follows:

$$x_{i,j}^{MLnew} = x_{i,j,start}^{ML} + (x_{L,j}^{ML} - x_{i,j,start}^{ML})t PRTVector_j \quad (1)$$

where $t \in (0, \text{by step to, PathLength})$ and ML is actual migration loop

$x_{i,j}^{MLnew}$ is the new positions of an individual, $x_{i,j,start}^{ML}$ is the positions of active individual.

$x_{L,j}^{ML}$ is the positions of leader.

The computational steps of SOMA are given as follows:

- Step 1: generate initial population;
- Step 2: evaluate all individuals in the population;
- Step 3: generate PRT vector for all individuals;
- Step 4: sort all of them;
- Step 5: select the best fitness individual as leader and worst as active;
- Step 6: for active individual new positions are created using Eq. (1). Then the best position is selected and replaces the active individual by the new one;
- Step 7: if termination criterion is satisfied stop else go to step 2;
- Step 8: report the best individual as the optimal solution.

```

Initialize particles, do
Calculate fitness value of each particle
If fitness value of the particle is better than pbest set current value as the new pbest
Set gbest to the best fitness value of all particles
For each particle
Calculate particle velocity according equation (2)
Update particle position according equation (3)
End for
While termination criterion is satisfied

```

Fig. 1 PSO pseudo code

2.2 Particle Swarm Optimization

Particle swarm optimization is a population based stochastic search algorithm developed by Eberhart et al. [9]. It is inspired by the social behavior of bird flocking and fish schooling. PSO consists of a swarm of particles. Particles move towards the best position in the search space with a velocity remembering each particle's best known position (pbest) and global best known position (gbest). The velocity and position of a particle is updated according to the following equations:

$$v_i^{k+1} = wv_i^k + c_1r_1(p_i - x_i^k) + c_2r_2(p_g - x_i^k) \quad (2)$$

$$x_i^{k+1} = x_i^k + v_i^k \quad (3)$$

In which: $i = 1, \dots, N$; N -the population of the group particles; k -the maximum number of iteration; r_1, r_2 -the random values between $[0,1]$, which are used to keep the diversity of the group particles; c_1, c_2 -the learning coefficients, also are called acceleration coefficients; v_i^k —the velocity of particle i in k -th iteration; x_i^k —the position of particle i in k -th iteration; p_i —the best known position of particle i ; p_g —global best known position of the group particles. The pseudo-code of PSO is given in Fig. 1.

3 Proposed SOMAQI Algorithm

In this section SOMAQI has been presented which uses the quadratic interpolation for creating the new solution member in the search space. As discussed in the introductory section in the working of SOMA, no new solutions are created during the search instead only the positions of the solutions are changed. For maintaining the diversity of the population, new points using Quadratic Interpolation are created in the search space. The methodology of this algorithm is given as follows:

First the individuals are generated randomly. At each generation the individual with highest fitness value is selected as leader and the worst one as active individual. Now the active individual moves towards leader in n steps of defined length. The movement of this individual is given in Eq. (1). Then we again select the best and worst individual from the population. A new point is created using quadratic interpolation at the end of each generation using Eq. (4). For this we choose three particles R_1 , R_2 and R_3 , where R_1 is the leader and R_2 and R_3 are randomly chosen particles from the remaining population. This new point is accepted only if it is better than active individual and is replaced with active individual.

Mathematically, the new point $x' = (x'_1, x'_2, \dots, x'_n)$ is given as

$$x' = \frac{1}{2} \frac{[(R_2^2 - R_3^2) * f(R_1) + (R_3^2 - R_1^2) * f(R_2) + (R_1^2 - R_2^2) * f(R_3)]}{[(R_2 - R_3) * f(R_1) + (R_3 - R_1) * f(R_2) + (R_1 - R_2) * f(R_3)]} \quad (4)$$

The computational steps of SOMAQI are given as follows:

- Step 1: generate initial population;
- Step 2: evaluate all individuals in the population;
- Step 3: generate PRT vector for all individuals;
- Step 4: sort all of them;
- Step 5: select the best fitness individual as leader and worst as active;
- Step 6: for active individual new positions are created using Eq. (1). Then the best position is selected and replaces the active individual by the new one;
- Step 7: create new point by QI from R_1 , R_2 and R_3 using Eq. (4);
- Step 8: if new point is better than active replace active with the new one;
- Step 9: if termination criterion is satisfied stop else go to step2;
- Step 10: report the best individual as the optimal solution.

4 Main Results

The proposed algorithm is coded in C++ and run on a Pentium IV 2.39 GHz computer. We have tested the proposed SOMAQI algorithm on the 10 unconstrained benchmark problems given below. All the problems are highly multimodal. Since SOMAQI is probabilistic technique and rely heavily on the generation of random numbers, therefore 50 trials of each are carried out, each time using a different seed for the generation of random numbers. A run is considered to be a success if the optimum solution obtained falls within 1 % accuracy of the known global optimal solution. The stopping criteria is fixed number of iterations are performed.

$$f_1(x) = \sum_{i=1}^n (x_i^2 - 10 \cos(2\pi x_i) + 10)$$

$$f_2(x) = \frac{1}{4000} \sum_{i=0}^{n-1} x_i^2 - \prod_{i=0}^{n-1} \cos\left(\frac{x_i}{\sqrt{i+1}}\right) + 1$$

$$f_3(x) = \sum_{i=0}^{n-1} 100(x_{i+1} - x_i^2)^2 + (x_i - 1)^2$$

$$f_4(x) = - \sum_{i=1}^n x_i \sin\left(\sqrt{|x_i|}\right)$$

$$f_5(x) = \left(\sum_{i=0}^{n-1} (i+1)x_i^4 \right) + \text{rand}[0, 1]$$

$$f_6(x) = 20 + e - 20 \exp\left(-0.2 \sqrt{\frac{1}{n} \sum_{i=1}^n (x_i^2)}\right) - \exp\left(\frac{1}{n} \sum_{i=1}^n \cos(2\pi x_i)\right)$$

$$f_7(x) = \max|x_i|, 0 \leq i < n$$

$$f_8(x) = \sum_{i=0}^{n-1} \left[x_i + \frac{1}{2} \right]^2$$

$$f_9(x) = \sum_{i=0}^{n-1} |x_i| + \prod_{i=0}^{n-1} |x_i|$$

$$f_{10}(x) = \sum_{i=0}^{n-1} \left(\sum_{j=0}^i x_j \right)^2$$

Initialization range and the optimum values for the functions are given in Table 1. The obtained results for functions f_1 – f_3 are given in Table 2. Results for f_4 – f_{10} are given in Table 3 along with already published results.

We have tested functions f_1 , f_2 and f_3 for three dimension sizes 10, 20 and 30. The population size taken for all dimensions is 10. The maximum number of iterations corresponding to 10, 20 and 30 dimensions is set as 1000, 1500 and 2000. We have tested functions from f_4 to f_{10} for three dimension sizes 10, 30 and 50 and the maximum number of iterations is set as 3000 for dimension 50. For the valid comparison all the parameters are taken same as in Ref. [10].

Different values of parameter PRT is taken as 0.005, 0.05, 0.1, 0.3, 0.5 and 0.9 for different functions. A total of 50 runs for each experimental setting are conducted. It is clear from the Table 2 that for function f_1 , the proposed algorithm is showing better results than BPSO and QPSO and giving comparative results than

Table 1 Initialization range and optimum values of the functions

Function	Initialization range	Optimum
f_1	[2.56, 5.12]	0
f_2	[300, 600]	0
f_3	[15,30]	0
f_4	[-500, 500]	-418.9829*n
f_7	[-1.28, 1.28]	0
f_6	[-32, 32]	0
f_7	[-100,100]	0
f_8	[-100, 100]	0
f_9	[-10,10]	0
f_{10}	[-100, 100]	0

Table 2 Comparison results of functions f_1 - f_3 (mean best)

Function	Dim	% of success	BPSO	QPSO	Q-QPSO	SOMAQI (mean best)	Standard deviation
f_1	10	100	5.5382	5.2543	$4.915e^{-19}$	0	0
	20	96	23.1544	16.2673	$7.806e^{-19}$	$2.7e^{-011}$	0
	30	96	47.4168	31.4576	$6.071e^{-19}$	$3.2264e^{-009}$	0
f_2	10	46	0.09217	0.08331	0.062657	$9.09092e^{-05}$	0.00019719
	20	54	0.03002	0.02033	0.005091	$2.25846e^{-06}$	0.00000856
	30	58	0.01811	0.01119	0.015442	$2.72336 e^{-05}$	0.00009506
f_3	10	66	94.1276	59.4764	5.544203	5.71912	0.359886
	20	72	204.336	110.664	15.53810	16.16542	0.42757
	30	72	313.734	147.609	25.68707	26.28846	0.77181

Q-QPSO for all the dimensions taken. For function f_2 the proposed algorithm is giving better results than BPSO, QPSO and Q-QPSO for all dimensions taken. For function f_3 , though the percentage of success obtained by proposed algorithm is zero but mean best value is better than BPSO and QPSO and comparative to Q-QPSO. From Table 3, we can easily say that for functions f_4 - f_{10} the proposed algorithm outperforms BPSO, QPSO and Q-QPSO for all dimensions taken. Other existing algorithms use different population sizes for different dimensions. Whereas the main advantage of using proposed algorithm is that it works with very small population size (10) for all dimensions.

5 Conclusions

This paper presents a variant SOMAQI incorporating the concept of Quadratic Interpolation. The proposed algorithm is tested on ten standard unconstrained benchmark problems and results are compared with BPSO, QPSO and Q-QPSO.

Table 3 Comparison results of functions f_4 – f_{10} (mean best)

Function	Dim	% of Success	BPSO	QPSO	Q-QPSO	SOMAQI (mean best)	Standard Deviation
f_4	10	94	-2389.36	-3871.03	-3898.67	-4080.191	88.47912
	30	78	-6466.18	-8967.29	-9998.00	-12274.205	156.0609
	50	92	-10473.0	-13105.9	-14783.6	-20418.080	184.8745
f_5	10	78	0.50267	0.452975	0.376021	0.00033651	0.00024
	30	64	0.61722	0.501799	0.497801	0.00028473	0.00023
	50	72	0.78832	0.598823	0.537782	0.00026446	0.00022
f_6	10	100	$6.965e^{-12}$	$4.407 e^{-15}$	$1.210 e^{-15}$	$-5.8872e^{-15}$	0
	30	100	$3.618 e^{-05}$	$7.568 e^{-12}$	$5.828 e^{-15}$	$-5.8872 e^{-15}$	0
	50	100	3.43866	$1.018 e^{-06}$	$6.267 e^{-14}$	$-5.8872 e^{-15}$	0
f_7	10	96	$3.793e^{-06}$	$1.0981 e^{-09}$	$7.937 e^{-13}$	$2.7643 e^{-15}$	0
	30	94	7.836	4.11969	0.005714	$3.8742 e^{-05}$	0.000023
	50	90	27.8394	21.1619	0.2213	0.00279532	0.005437
f_8	10	100	0.00000	0.00000	0.00000	0	0
	30	100	0.05	0.00000	0.00000	0	0
	50	100	1.7	0.1	0.00000	0	0
f_9	10	100	$2.414 e^{-14}$	$2.0205 e^{-32}$	$3.327e^{-34}$	0	0
	30	100	$2.047e^{-07}$	$3.2466 e^{-13}$	$7.943 e^{-16}$	0	0
	50	100	7.73949	$1.6757 e^{-08}$	$8.667 e^{-11}$	0	0
f_{10}	10	100	$2.515 e^{-22}$	$5.5161 e^{-54}$	$1.009 e^{-62}$	0	0
	30	100	$1.343e^{-07}$	$1.4434 e^{-21}$	$2.999 e^{-27}$	$3.0790 e^{-33}$	0
	50	88	0.000176	$1.0679 e^{-10}$	$3.786 e^{-17}$	$2.9746 e^{-18}$	0

The results are obtained by using population size 10 only for all dimensions. On the basis of the results and discussion it is concluded that the proposed algorithm outperforms BPSO, QPSO and Q-QPSO in terms of mean best and population size.

References

1. Mohan, C., Shankar, K.: Random search technique for global optimization. *Asia. Pac. JOR* **11**, 93–101 (1994)
2. Deep, K., Das, K.: Quadratic approximation based hybrid genetic algorithm for function optimization: original research article. *Appl. math. Comput.* **203**, 86–98 (2008)
3. Deep, K., Bansal, J.C.: Quadratic approximation PSO for economic dispatch problems with valve-point effects. In: *International Conference on Swarm, Evolutionary and Memetic Computing*, SRM University, Chennai, 460–467 Springer (2010)
4. Deep, K., Bansal, J.C.: Hybridization of particle swarm optimization with quadratic approximation. *Opsearch.* **46**, 3–24 (2009)
5. Deep, K., Das, K.: Quadratic approximation based hybrid genetic algorithm function optimization. *Appl. Math. Comput.* **203**, 86–98 (2008)
6. Pant, M., Thangaraj, R., Abraham, A.: A new PSO algorithm with crossover operator for global optimization problems: 2nd international symposium on hybrid artificial intelligent systems (HAIS’07), softcomputing series. In: Corchado, E. et al. (ed.) *Innovations in Hybrid Intelligent Systems*, vol. 44, pp. 215–222. Springer Verlag, Germany (2007)
7. Zelinka, I., Lampinen, J.: SOMA—self organizing migrating algorithm. In: *Proceedings of the 6th International Mendel Conference on Soft Computing*, pp. 177–187 Brno (2000)
8. Zelinka, I.: SOMA—self organizing migrating algorithm. In: Onwubolu, G.C., Babu, B.V (eds.) *New Optimization Techniques in Engineering*. Springer, Berlin (2004)

9. Eberhart, R.C., Kennedy, J.: Particle swarm optimization. In: Proceedings IEEE International Conference on Neural Networks, IEEE Service Center, Piscataway, vol. 4, pp. 1942–1948, Perth (1995)
10. Pant, M., Thangaraj, R., Abraham, A.: A new quantum behaved particle swarm optimization. In: Proceedings of the 10th Annual Conference on Genetic and Evolutionary Computation, GECCO, 87–94 (2008)

User Ranking by Monitoring Eye Gaze Using Eye Tracker

Chandan Singh and Dhananjay Yadav

Abstract Image and video processing has been an intensive field of research for last two decades. Human Computer Interaction is one of the important domains that come under image and vision processing. This paper contains conversion of text into text-image format (words with its pixel position), this conversion is used to calculate efficiency of a user by calculating user ranking based on correct answer lines recorded by eye gaze tracker (mounted on user's eye). After reading of text, questions are asked to user, time is measured to find the answer lines for given questions (page time T_1). Score is inversely proportional to time taken by the user to reach on answer line. Finally, the user gets score and rank among the existing users on the basis of time.

Keywords Eye gaze · Eye tracker · Monitoring eye gaze

1 Introduction

In the field of human computer interaction, the growth of eye tracking system has increased exponentially, it is used in area like image and visual processing, human psychology, human reading behavior and graphics display system, where fixation and saccade are vital for eye tracking. Eye tracking methodologies are used in five broad disciplines namely: Industrial Engineering, Psychology, Marketing/Advertising, Neuroscience and Computer Science. When a user concentrates on some

C. Singh

Indian Institute of Information Technology Allahabad, Allahabad, India
e-mail: chandan.hbti@gmail.com

D. Yadav (✉)

Department of Mathematics, Indian Institute of Technology Roorkee, Roorkee, India
e-mail: dhananjayadav@gmail.com

text on a computer or web, in this process eye-gaze provides much information about his reading pattern such as on which words, image user spent more time; X and Y coordinate of words, image on the screen, fixation duration given to the words, image by the user, speed and acceleration of eye-gaze [1]. Mosconi et al. [2] developed an eye-gaze based system. It monitors user's behavior when they read on-line newspaper i.e. where user pays more attention. Some user are interested in business news, some other are interested in sports news, where as some user interested in political news etc. Xu et al. [3] proposed a method in which it uses algorithm during reading a document to predict the time spent on every word in that document by using semantic analysis. Recently Smith [4] studied the Eye tracking as a measure of noticing: a study of explicit recasts in SCMC.

One of the challenging problems to those people, who are working on Human Computer Interface, is to develop improved and user friendly interface between computer and a human. This problem motivates me to develop an efficient and enjoyable human-computer-interaction based on Eye-gaze method. Many modules which are partially related to the "user ranking by monitoring eye gaze using eye tracker" have been developed but these are very limited. So, there may be some enhancement and integration over these modules. The recent developments in the field of artificial intelligence enable us to get information regarding the significance of words occurrence in a corpus. In this research work the reading behavior of the user will be identified by tracking his eye movements and according to his efficiency rank will be evaluated and provided to him.

2 Features of User Ranking by Monitoring Eye Gaze Using Eye Tracker

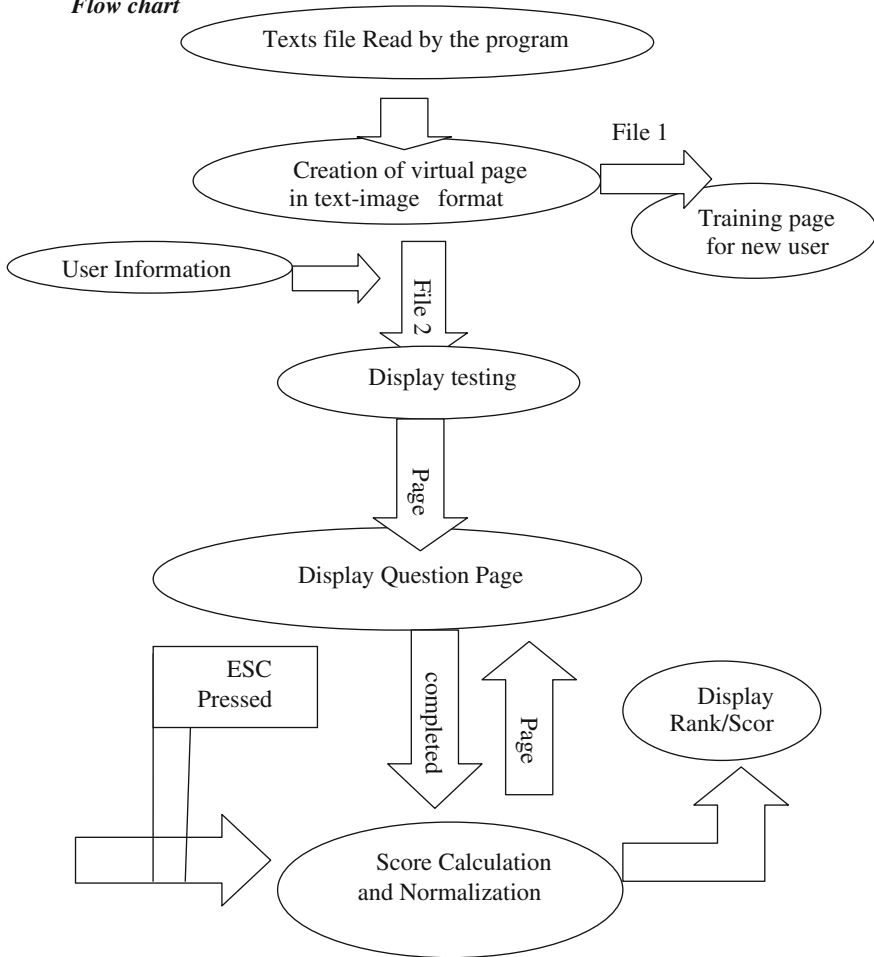
User is important for any application software. User decides how software is running and decides the efficiency of software. Finally user gives the preference according to his demand. So ranking system is always there for software depends on user requirement. This software application provides rank to the user on basis of their learning rate in respect of time taken by the user in reading comprehension. Ranking system is applied in respect of domain. This application software clusters the user not only in respect of domain but take care of level of the user i.e. beginner, intermediate or professional.

This application program reads a text file for selected domain and level of the user. Uploaded file in memory is converted in text image format i.e. creation of virtual page and create an index for each word. After successful creation and transfer of x, y coordinates by Host PC. Application software utilizes the received data from Host pc in mapping between user eye gaze and x and y coordinates of virtual page. Successful mapping returns an index of word which helps to calculate the time on page and time on answer line. The time on page and time on answer line are stored to calculate the score and rank of the user in respective domain.

This application program use four functional key CURS_UP, CURS_DOWN, PAGE_UP, PAGE_DOWN to make program easily accessible. Functional keys are used for following functionality:

CURS_UP for Next Page, CURS_DOWN for Previous Page. PAGE_UP for Question page, PAGE_DOWN for Testing Page.

Flow chart



2.1 Training Page for New User

The main purpose of training page is to be familiar to new user with eye tracker system. It will help new user how the system is working i.e. when user see computer screen there is exact mapping between User and computer screen is

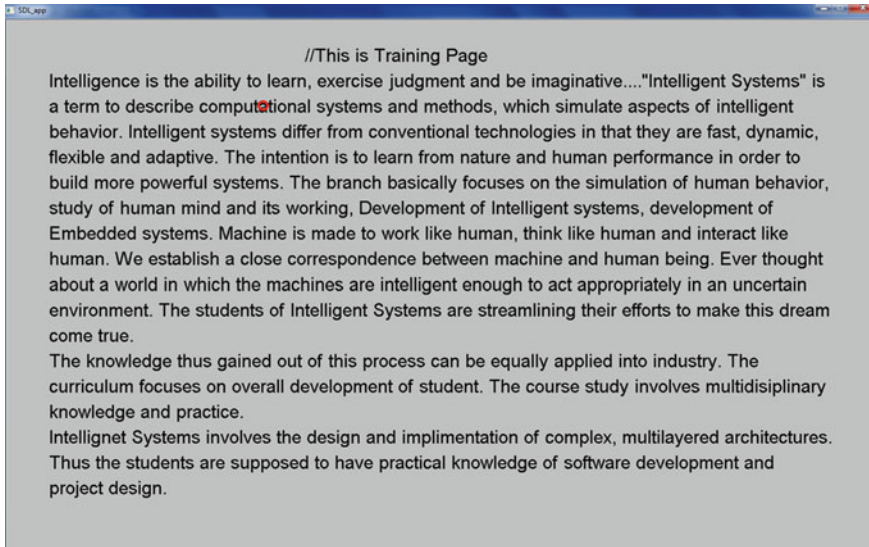


Fig. 1 Training page

occurring or not. The main advantage of training page is user will familiar with gaze cursor, which moves along with eye gaze of the user. User can judge the position of gaze cursor is matching with word selected by user's eye gaze (see Fig. 1), if not user exits from the program.

2.2 User Information Page

User information page contain essential information for this application program. Name, enrolment number, age and class/level are the required field. Name and enrolment number are required for to save and access the score. User rank displays along with the name score. Age and class are used to cluster the user rank (see Fig. 2). Age help to access data between minimum and maximum (say 18–35) age from score cluster i.e. it helps to display rank between age group. Class/level of user is another parameter for clustering for user i.e. beginner, intermediate, professional. Passage length and number of questions varies for beginner, intermediate, professional respectively.

2.3 Testing Page

Passage comprehension is required to check learning ability of user. In passage there are some important lines which decide the user attention toward the passage. These lines are used to check learning rate and reading effectiveness. Testing page

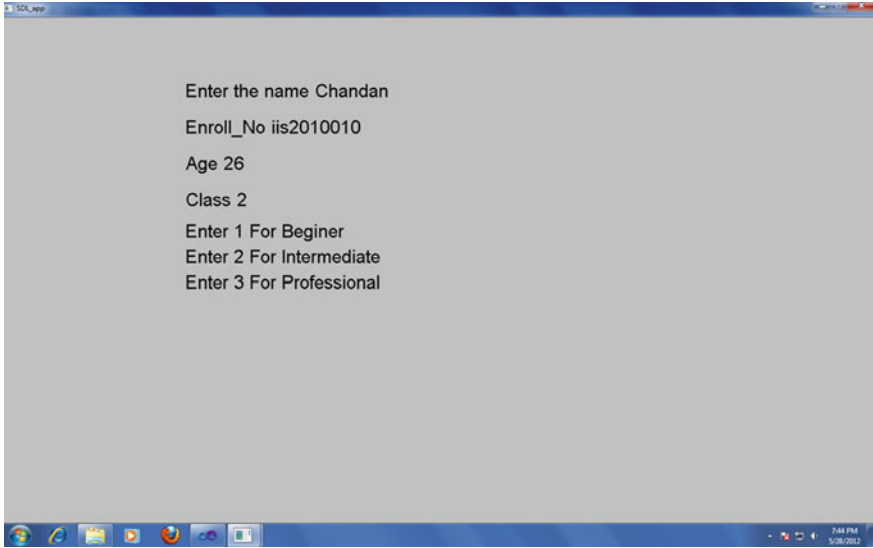


Fig. 2 User information page



[1.0]INTRODUCTION

An operating system is a program that manages the computer hardware. It also provides a basis for application programs and acts as an intermediary between the computer user and the computer hardware. An amazing aspect of operating system is how varied they are in accomplishing these tasks. Mainframe operating systems are designed primarily to optimize utilization of hardware. Personal computer (PC) operating systems support complex games, business applications, and everything in between. Operating systems for handheld computers are designed to provide an environment in which a user can easily interface with the computer to execute programs. Thus, some operating systems are designed to be convenient, others to be efficient, and others some combination of the two. Before we can explore the details of computer system operation, we need to know something about system structure. We begin by discussing the basic functions of system startup, I/O, and storage.

We also describe the basic computer architecture that makes it possible to write a functional operating system. Because an operating system is large and complex, it must be created piece by piece. Each of these pieces should be a well-delineated portion of the system, with carefully defined inputs, outputs, and functions.

[1.1]WHAT OPERATING SYSTEMS DO

Fig. 3 Testing page

is extremely important module of this project. Testing page basically combination of words and its position i.e. words are stored with its X, Y coordinates (see Fig. 3). Testing page contains the information regarding the user domain subject. In testing page there are some useful lines where user is more emphasized.

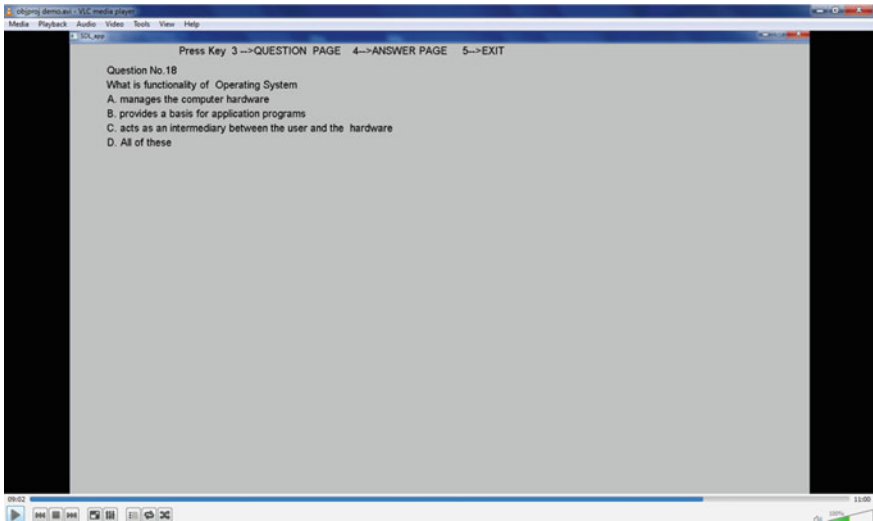


Fig. 4 Question page

2.4 Question Page

User read testing page effectively and attentively, turns on the question page and tries to make confidence of comprehension. Comprehension is measured by number of correct answer and correct lines read by the user. Question page is designed to check the comprehension ability of user. Question page is display before giving the answer to monitor line read by the user (see Fig. 4). It is combination of word and its position. Questions are objective types, after reading question user turns on current test page.

2.5 Score Calculation

Time is a vital parameter of score calculation. If user taking more time to reach the answer line than user is less efficient. Let say T_1^i is time spent by the user to reach on answer line. For score calculation, T_1^i should be greater than the threshold value. To obtain the maximum score and good rank, the value of $1/T_1^i$ should high.

$Score = \sum_{i=1}^N \frac{1}{T_1^i}$ and normalized score = Score*100, where T_1^i is the time spent by user to reach on answer lines and N is the total number of questions.

2.6 Algorithms

1. Program reads text file for training page.
 - 1.1 Conversion of text file in to image data text file .Text image data are stored a vector called word vector.
word_vector= Virtual_page(text_file);
 - 1.2 Calling of function Realtime_data() to get real time data and draw gaze cursor for user eye movement and fixation.


```
Realtime_data();
if(x and y are not missing)
Draw_gazecursor();
else
pause();
```
2. Enter user information by keyboard_typing() function, keyboard typing function detect the keyboard, implemented through SDL programming.
 - 2.1 user_name=keyboard_typing();
 - 2.2 user_enrollno= keyboard_typing();
 - 2.3 user_age= keyboard_typing();
 - 2.4 user_level= keyboard_typing();
3. Text file for testing page
 - 3.1 Conversion of text file in to image data text file Text image data are stored in a vector called word vector.
word_vector= Virtual_page(text_file);
 - 3.2 call of function real time data to get real time data, draw gaze cursor and mapping function. Mapping function returns the index of word which is read by the user.


```
If(x&y! missing)
{ Mapping(x,y);
Draw_gazecursor(); }
```
4. If CURS_UP key is pressed then load next page loaded in memory by checking the value of start and new_start variables not crossing the upper limit.


```
If (CURS_UP)
{new_start=start+1;
start = new_start;
page[p]=new start;
p = p+1;}
```

 Next page loaded by implementation of above line.
5. If CURS_DOWN key is pressed then load next page loaded in memory by checking the value of start and new_start variables not crossing the lower limit.


```
if (CURS_DOWN)
{ start=page [p-1];
new_start=start;
p=p-1;}
```

 Previous page loaded by implementation of above line.
6. if PAGE_UP key is detected than by checking of upper limit of no. of question. if question no not reach to upper limit than question page display on screen.

```

6.1 if(PAGE_UP)
    {if(question_no<=No_question)
      print_question(question_no); }

```

6.2 If user skipped the question than score of this question is calculated as zero by calling the function print dwell. print_dwell() function is used for both time calculation.

```

    If(question is skipped by user)
    {print_dwell();
    reset_dwell();
      question_no = question_no +1;}

```

By implementation of above function (6.1) Question Page display on screen.

7. if PAGE_DOWN key is detected than by checking of upper limit of no. of question. if question no not reach to upper limit than testing page display on screen.

```

7.1 if( PAGE_DOWN)
    If(question_no<=No_question)
    {print_dwell();
    reset_dwell(); }

```

7.2 By implementation of above function testing page displays with user option.

8. If Escape is pressed or successful execution of application program score of reder question wise rank and score displays.

```

8.1 If(ESC or All_Question)
    {score_question();
    display_rank(list);}

```

3 Result and Analysis

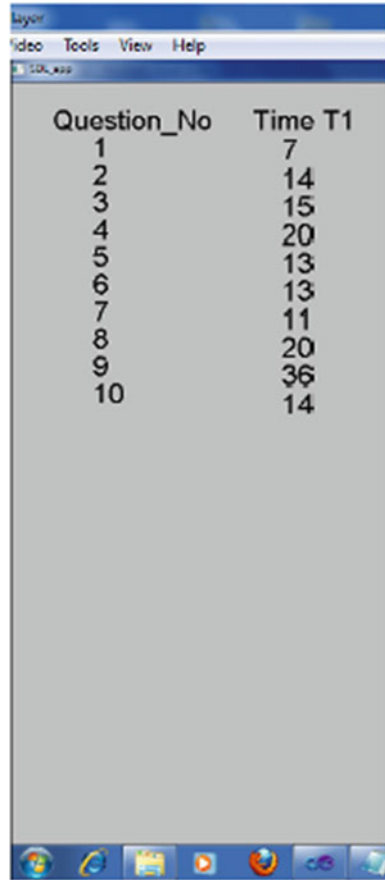
This application is developed in C ++ with SDL, EyeLink libraries in Microsoft Windows environment. EyeLink monitors eye movement and accordingly generates data like location where eye is looking, time duration for which it is looking, speed, acceleration and saccades. All of the data is stored in EDF (EyeLink Data File). SDL stands for Simple DirectMedia Layer. This has been used for keyboard event handling and text display. All experimentation is realized on Windows 7 Operating System on computer with processor Intel Core 2 Duo and 2 GB RAM.

Current research work provides user rankings after user is done with reading the passage and time spend to find the answer of related questions. Figure 5 represents a demonstration of time spent on to find the answer line. Score is calculated on the basis of time spent by the user on testing page to find the answer line T_1 .

Figure 6 represents a demonstration of how different users are ranked accordingly. It shows user name, score and their respective rank.

The user scores obtained in Fig. 6 are plotted on a graph in terms of histogram showcasing a comparison of scores of all users as shown in Fig. 7. X-axis

Fig. 5 Question wise score of user

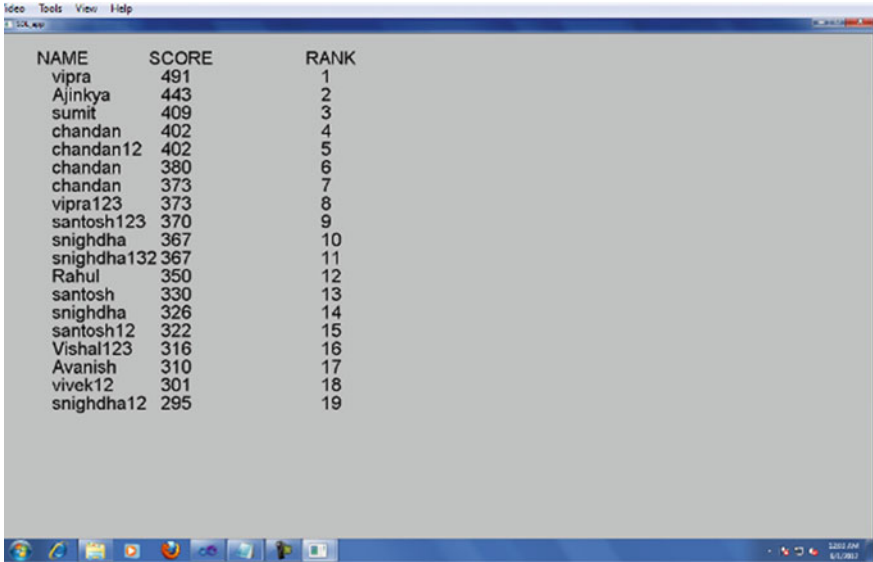


Question_No	Time T1
1	7
2	14
3	15
4	20
5	13
6	13
7	11
8	20
9	36
10	14

represents the user number and Y-axis represents their score. Figure 7 clearly shows the variation of scores of different users.

Figure 8 analyses scores of a particular user for same passage on repetition. X-axis represents number of questions and Y-axis represents score for each question. Red bars stand for scores on first attempt, green bars show scores for same questions in second attempt for same passage.

Figure 9 showcases score variation on second attempt but for different users on the same passage. X-axis shows number of users. Y-axis shows their score. Red bar represents each users score on first attempt and Green bar shows their score on second attempt.



A screenshot of a Notepad window titled 'Notepad - vipra.kwp'. The window contains a table with three columns: NAME, SCORE, and RANK. The data is as follows:

NAME	SCORE	RANK
vipra	491	1
Ajinkya	443	2
sumit	409	3
chandan	402	4
chandan12	402	5
chandan	380	6
chandan	373	7
vipra123	373	8
santosh123	370	9
snighdha	367	10
snighdha132	367	11
Rahul	350	12
santosh	330	13
snighdha	326	14
santosh12	322	15
Vishal123	316	16
Avanish	310	17
vivek12	301	18
snighdha12	295	19

Fig. 6 User rank and score

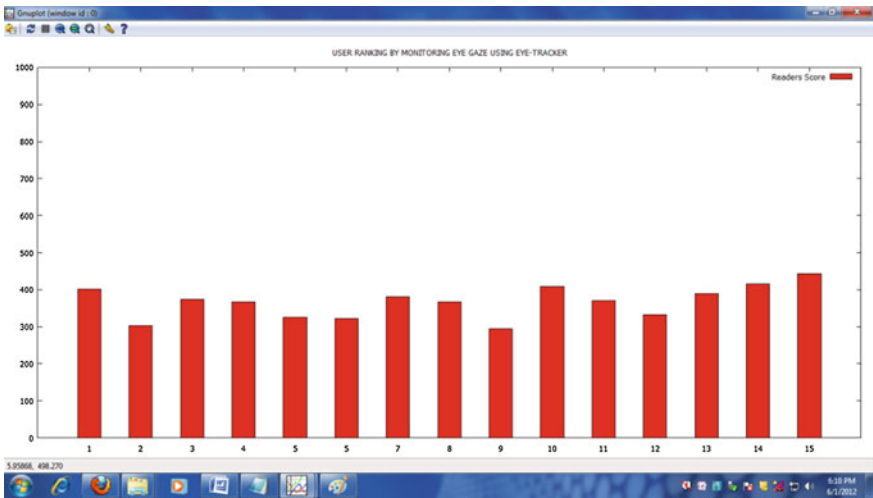


Fig. 7 Users score histogram

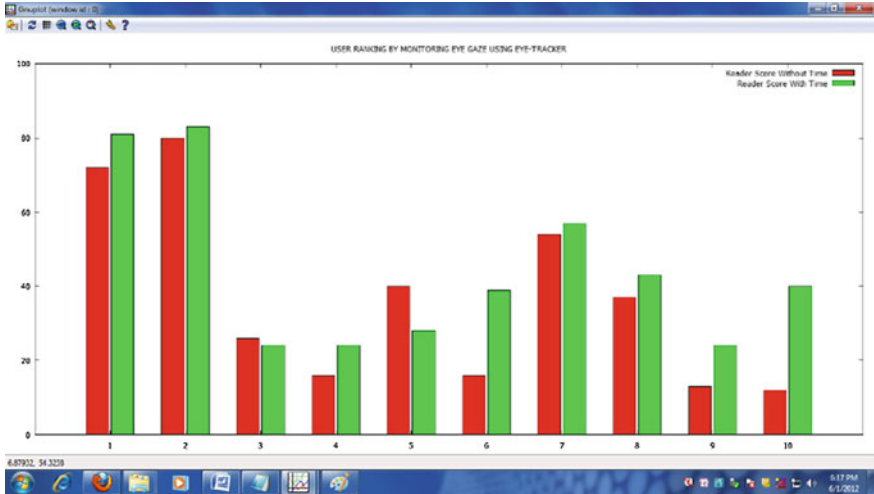


Fig. 8 Score variation of single user first attempt versus second attempt

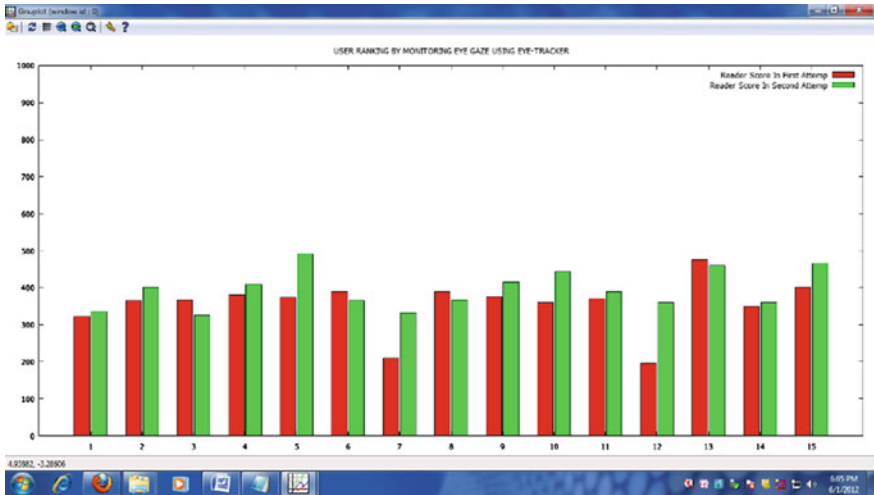


Fig. 9 Score variation of users first attempt versus second attempt

4 Conclusions

This paper presents a novel idea of ranking on the basis of efficiency of a user on the basis of time spent in identifying the location of the correct answer for question presented to him from the comprehension corpus. However, the system as of now is static in terms of learning the answers and questions and their answers for each

passage has to be pre-defined thus making a cumbersome task of manually identifying potential questions for each passage. For comprehension database to be large, this requires a lot of work and time. This concept can be implemented in class room teaching to monitor the behavior of students. By monitoring eye gaze of a student, system can generate a summary student had what study in classroom.

References

1. Rayner, K.: Eye movements in reading and information processing. 20 years of research. *Psychol. Bull.* **124**(3), 372–422 (1998)
2. Mauro, M., Marco, P., Alice, R.: On-line newspapers and multimedia content: an eye tracking study. In: *Proceedings of the 26th Annual ACM International Conference on Design of Communication*, pp. 55–64. Lisbon, Portugal (2008)
3. Xu, S., Jiang, H., Lau, F.C.M: User-Oriented Document Summarization Through Vision-Based Eye-Tracking. *IUI 2009. Proceedings of the 14th international conference on Intelligent user interfaces*, February 8–11, pp. 7–16. Sanibel Island, (2009)
4. Smith, B.: Eye tracking as a measure of noticing: a study of explicit recasts in SCMC. *Lang. Learn. Technol.* **16**(3), 53–81 (2012)

Invalidating Security Compromised Nodes by Releasing its Energy in MANETs

N. Chandrakant

Abstract MANETs are having very limited resources like memory, CPU speed, Bandwidth, battery life etc. In spite of having higher secured nodes and security algorithms in Ad Hoc network, some time, the genuine nodes can be attacked or accessed by fraud/malicious nodes, and also a node itself can turn into a malicious behaviour. In such scenarios, human may not be able to acquire and catch them to avoid adversary affect or misusing node's data for different purpose which is dangerous in some cases like Border Monitoring. As a different approach to avoid such dangerous circumstances, this paper is proposing a novel approach to exhaust the valuable resources of MANETs is called retiring or invalidating a node e.g., turning node's battery level to zero and other approaches can be used to make invalidate a node.

Keywords MANET · Invalidate · Self-retirement

1 Introduction

Security in a MANET is very important in scenarios such as a battlefield, deep forest, deep sea etc. The common network goals of security like confidentiality, data availability, integrity, authenticity and non-repudiation are little difficult to achieve in wireless network like MANET, WSN etc., this can be due to its open environment where all nodes co-operate in forwarding the packets in the network like hop-by-hop, comparing to wired networks, wireless networks has problems in detecting fraud nodes or malicious nodes. Hence, considering overall research and

N. Chandrakant (✉)
Bangalore, India
e-mail: nadhachandra@gmail.com

its upcoming security challenges, it is relatively difficult to design a hundred percent secured protocol for WSN/MANET.

This paper try to address the problem which occurs after a node compromising with malicious node/network in order to not to loose its crucial data or not to misuse the data.

Figure 1 shows a typical architecture of a wireless sensor network (WSN) [1]. MANETs are responsible for self-organizing after first deployment with hop-to-hop connections between nodes. Usually the committed sensors will start collecting auditory, infrared or magnetic information and seismic about the environment using either continuous or event driven working modes.

The rest of this paper is arranged as follows: In Sect. 2, it details about past research in security of MANETs communication. Detailed techniques of design and its implementation with results has been explained in Sect. 3. Finally, Sect. 4 concludes the paper and gives an direction of future research.

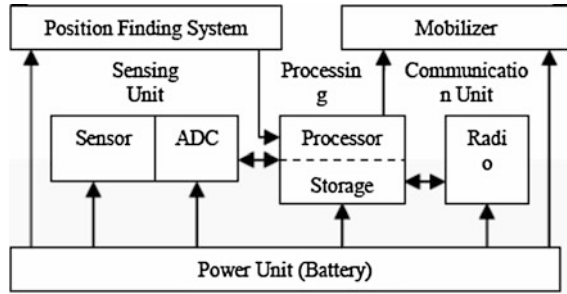
2 Literature Survey

Though there are no exact supporting papers to this topic as it is a negative approach to avoid data misusing. However, we can start referring security related papers in MANETs and highlighted same in below paragraphs.

MANETs supports hop-by-hop routing in the dearth of base station, hence topology modifies over a time due to the node movement associated with the connection failure and creation, limited in radio resources and bandwidth, limited energy power and calculating capability pose challenges in packet routing in MANET. Utkarsh et al. [2] proposed a Energy Saving Ad hoc Routing (ESAR) algorithm goals to accomplish better energy proficient with a longer network life time. The algorithm chooses a path for routing by bearing in mind the definite distance between the source and destination along with the minimum offered energy of a node in the path. The chosen path is considered as the best path for packet transmission till any node in the path drains battery power after a threshold value. At this point of time, a support path is selected as an alternate path for packet transmission. The progression is repeated till all the paths from the same source to destination are pooped with their battery power. Their simulation result shows that ESAR has enhanced the existing routing algorithms. This can be helpful nowadays since energy-constrained mobile devices rely on some kind of payments, secured by means of public key cryptography; these transactions may lead to energy overhead in the network.

Furthmuller and Waldhorst [3] has proposed a approach where they evaluate the energy overhead of an incentive system based on hash coins. Therefore they created a prototype of a hash coin based incentive system in a MANET and conducted energy measurements. The results are evaluated to solutions based on non-private key cryptography. Using the familiarity regarding the energy

Fig. 1 Architecture of a sensor node in MANET



utilization of these approaches helped them to choose the finest suited incentive system and reasonable system parameters for an encouragement system in a MANET.

Accurate state information about energy level should be available to support energy-efficient routing in MANETs. However due to bandwidth limitations, transmission costs, high loss rate and the dynamic topology of MANETs, gathering and maintaining up-to-date situation information is a non-trivial task. Hence Kunz [4] team came up with a solution where they use Optimized Link State Routing (OLSR) as the primary routing protocol and focus on residual power level as QoS metric, which has been used for routing judgment in many energy-efficient routing protocol schemes. The experiments shows that, nodes have at best rough state information, particularly under high traffic rates. They evaluated two additional techniques to reduce inaccuracies and compare them against the basic OLSR protocol. These techniques shown significant improvements in accuracy levels. In picky, a method Smart Prediction attains highly precise apparent residual energy levels under all traffic loads, mobility scenarios, and radio models.

In MANETs, to perform any network tasks, it needs energy and other resources, hence it is requested cooperate networking nodes with others. Tamilarasi and Sundararajan [5] has proposed a 2ACK scheme, which can be simply add-on to any source routing protocol. They carried out an analysis of the power needs for various cryptographic primitives with the purpose of using this data as a foundation for devising energy-efficient security protocols along with delay measurement, packet delivery ratio and routing overhead to evaluate finest security algorithm.

Nodes in MANET communicates directly with each other when they are both within the same signal range. Otherwise, they depends on their neighbours to relay messages. Shakshuki et al. [6] has analysed the study of self-configuring nodes in MANET. The open communication medium and broad distribution of nodes make MANET susceptible to malevolent attackers. In this case, it is vital to develop proficient intrusion-detection mechanisms to guard MANET from attacks. With the developments of the technology and cut in hardware costs. To regulate to such trend, they muscularly believed that it is essential to address its possible security issues. Finally, they anticipated and implemented a new intrusion-detection system named Enhanced Adaptive ACKnowledgment (EAACK) particularly designed for

MANETs. Compared to modern approaches, EAACK demonstrates higher malicious-behaviour-detection rates in definite situation while does not greatly influence the network performances.

3 Proposed Techniques and Implementation

Node retirement is essential when there were a crucial information is broadcasted by genuine node which is compromised with malicious node/network. This kind of node(s) can be sacked/invalidated/bounced/neglected by using following methods,

A Release Battery

Here, if a node is compromised with malicious network or if a node itself turns into malicious (behaviour changes), then such node's battery or energy can be turned to zero so that it can not broadcast or leak crucial data.

B Encode Data

The data should be encoded such that no one can decode it except the known node.

C Physical Damage

If a node is physically reachable, then it can be damaged physically, so that we cannot use it again.

D Self Loop Access (Query Processing)

Make it busy itself with junk data, so that it cannot send any data to anybody.

E Mute the Node (Sleeping)

Based on a flag data, it should be mutable or unmutable using a key technique.

F Memory Overflow

Since nodes are having small size memory and it can be overflowed by any computation or flooding packets.

G Key Change

Here, after evaluating/declaring a node as malicious by its own network, then all valid or genuine nodes would generate/receive a global/public key and private keys except malicious node, hence communication of genuine nodes cannot be affected.

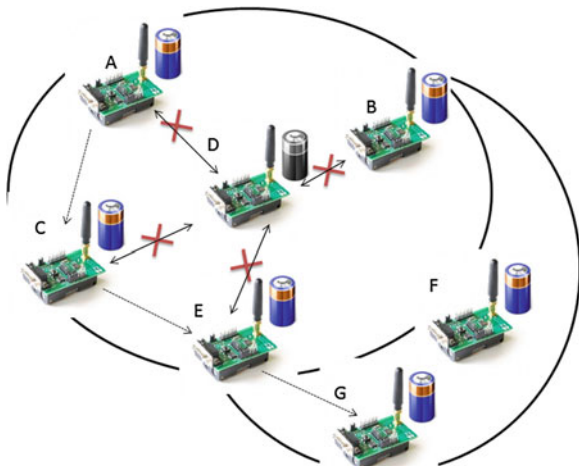
In this paper, we are considering Battery Release when a node misbehaves in the network. An example of MANET is shown in Fig. 2 where D is turned into malicious node and its battery is released until zero.

The power depleted in transmission of a single bit [7–9] is specified by

$$e_{tx}(d) = e_{t1} + e_{d1} * d^n \quad (1)$$

where e_{t1} is the power dissolute per bit in the transmitter circuitry and $e_{d1} * d^n$ is the power dissipated for transmission of a single bit over a space d , n being the path loss exponent (usually $2.0 = n = 4.0$). The latency of a (one-hop) message movement consists of the time needed to send the wakeup signal (T_{tone}), and the

Fig. 2 Example of node retirement in MANET



real transfer time over the primary radio (T_{msg}) [10]. This transfer time includes waking up the radio, receiving the message (including headers), and sending back an acknowledge frame. For simplicity, transmission errors and collisions are not considered; hence, retransmissions are not modelled.

$$T_{tone} = 10/F_{wu} \tag{2}$$

$$L_{wu} = T_{tone} + T_{msg} \tag{3}$$

$$P_{wu} = P_{wu} + F_{msg} \times ((T_{tone} + T_{msg}) \times P_{TX} + T_{msg} \times P_{RX} + (N - 1) \times T_{hdr} \times P_{RX}) \tag{4}$$

The average power consumed by a node depends on the frequency at which messages are sent through the network, denoted by T_{msg} . Each message transfer adds energy to the basic costs of the wakeup circuitry (P_{wu}). Receiving the message also takes T_{msg} time.

If the distance between the transmitter and receiver is less than threshold value d_0 [9], the proposed method will adopt the free space model (d^2 power loss), else it will adopts the multi-path (hop-by-hop) fading channel model (d^4 power loss). So if the transmitter sends an 1-bit message to the receiver up to a distance of d , the power consumption of the transmitter and t receiver can be computed by the following equations:

$$E_{Tx}(n, d) = \begin{cases} E_{elec} * n + \epsilon_{fs} * n * d^2, & d < d_0. \\ E_{elec} * n + \epsilon_{mp} * n * d^4, & d \geq d_0. \end{cases} \tag{5}$$

$$E_{Rx}(n) = E_{elec} * n \tag{6}$$

Where, $E_{Tx}(n, d)$ is the energy consumption of the transmitter who sends an n-bit message to the receiver up to a distance of d .

$E_{Rx}(n)$ is the energy consumption of the receiver who receives an n-bit message.

E_{elec} is the energy consumption of the wireless send-receive circuit.

ϵ_{fs} and ϵ_{mp} represent the energy consumption factor of amplification in the two radio models. A node's lifetime can be computed as follows,

$$Lifetime\ of\ a\ Node = (E_{TOTAL_CAP} / (E_t + E_r + E_{g/AP} - 2 * E_o) / (t - FRAME)) \quad (7)$$

A Network lifetime can be computed as follows,

$$Lifetime\ of\ a\ Node = (E_{TOTAL_CAP} / (E_t + E_r + E_{g/AP} + (N - 3) - 2 * E_o) / (t - FRAME)) \quad (8)$$

Where, N is the number of nodes in the network and E_{TOTAL_CAP} is the total energy capacity of a single node. t_{FRAME} is time to complete frame cycle. E is Energy and t, r, g, o, AP are Transmitter, Receiver, Gateway, Other and Access Point respectively.

There many ways to make battery power zero or make node's lifetime zero which includes following methods,

A Packet Sending/Receiving/Resending

Basically energy is converted into Joules by multiplying the Power with Time. Joules required to transmit/receive the packets of n size in the following equation,

$$\begin{aligned} E_{tx}(n) &= (TP * n) / 2 * 10^6 \\ E_{rx}(n) &= (RP * n) / 2 * 10^6 \end{aligned} \quad (9)$$

Where, TP is Transmitted Power and RP is Receiving Power.

B Complex Computations [11]

A complex equations or computations can spend more time and energy of a node.

$$E_{TC} = E_C + E_W \quad (10)$$

Where, E_{TC} is total energy spent for entire computation, E_C is energy spent for computation after having all input values, and E_W is energy spent for delay in getting a substitutional values for variables.

C Increase Distance between Nodes

Distances between neighbouring nodes and/or central node does affect energy consumption as given below,

$$Ed = \{(u, v) \in V^2 | d(u, v) \leq R\} \quad (11)$$

Where, Ed is Edges. Ad hoc network is represented by a graph $G = (\text{Vertices}, \text{Edges})$ or $G = (V, E)$ where V is the set of nodes and $E \subseteq V^2$ is the edge set. Nodes u, v belongs to E means that u can send messages to v . The $d(u, v)$ is the distance between nodes u and v , R is transmission Radius.

The general energy consumption equation is as follows,

$$E_u = \begin{cases} r(u)^\alpha + c, & \text{if } r(u) \neq 0 \\ 0, & \text{Otherwise} \end{cases} \quad (12)$$

Where, E_u is transmitting a unit message depends on the range of the emitter u . α is a real constant greater than 2 and $r(u)$ is the range of the transmitting node and c is constant.

Energy level and the distance of the node i are given by e_i and d_i respectively. The energy-distance factor ρ is computed as follows,

$$\rho = (e_i * d_i) / (\sum_{i=1}^n e_i * d_i) \quad (13)$$

Where, n is number of nodes.

D Packet Collision [12]

The amount of energy consumption at a node N due to collisions on the link (T, R), denoted by $E_{(T,R)}^N$ where T is Transmitter and R is Receiver, using the collision model [13] by assuming that a packet collides at most once with a given hidden node is specified by following equation,

$$E_{(T,R)}^N = \left(\sum_{i=1}^{n_{\text{hidden}}} i (E_T^N + E_R^N) \delta_i / 1 + \sum_{i=1}^{n_{\text{hidden}}} \delta_i \right) \quad (14)$$

where,

δ_i is the probability of encountering i successive collisions on a packet as given in below equation,

$$\delta_i = \left(t_{\text{trans}}^i / \prod_{j=0}^{i-1} t_j \right) \quad (15)$$

$$E_T^N = \begin{cases} E_{T_{\text{pk}}}, & \text{if } N \equiv T \\ E_{R_{\text{pk}}}, & \text{if } N \text{ can receive packets from } T \\ 0, & \text{Otherwise} \end{cases} \quad (16)$$

$$E_R^N = \begin{cases} E_{T_{ack}}, & \text{if } N \equiv R \\ E_{R_{ack}}, & \text{if N can receive packets from R} \\ 0, & \text{Otherwise} \end{cases} \quad (17)$$

E Idle/Sleep Mode

Turning a node's status to sleep where it consumes low-power.

$$T_{sleep} = T_{frame} - T_{listen} \quad (18)$$

Where, T_{frame} is protocol Frame Time (500 ms), T_{listen} is listening period. In idle status, the node is neither transmitting nor receiving any data packets. However it consumes energy because the nodes have to listen to the wireless medium continuously in order to detect a packet that it should receive or needs sense environment, so that the node can then switch back into receive mode from idle. Then power consumed in Idle Mode is:

$$E = P_R$$

Where E is power consumed in Idle Mode and P_R is power consumed in Reception Mode.

F Traffic/Congestion

MANET can have shared resources including neighbouring nodes, where multiple senders compete for link bandwidth, so our responsibility is to adjust the data rate used by each sender in order to avoid network overloading. Usually packets that arrive at a router and cannot be forwarded for some amount of time are dropped, many packet can be dropped if consequently an excessive amount of packets arriving at a network bottleneck [14].

When there is too much data traffic at a node, that slows down or starts losing data known as network congestion. The energy spent for congestion is dependent on many parameters,

$$E_C = E_D + E_L + E_O \quad (19)$$

Where, E_C is total energy spent for congestion process, E_D is energy spent for delaying packet delivery, E_L is energy spent for packet lost and retransmitting it again, E_O is energy spent for other side effects like collision, etc.

G Path/Link/Signal Lost

A link is a route between two nodes takes place through wireless environments, link loss rates when evaluating the path's performance. If link loss occurs in a MANET, then it is necessary to resend the packet.

$$E_{LL} = E_W + E_{RT} \quad (20)$$

Where, E_{LL} is total energy spent for link loss and packet retransmission, E_W is energy spent for waiting for a acknowledgement or waiting till Threshold time expires, E_{RT} is energy spent for retransferring the packet.

H Interference

Interference is anything which modifies or alters or disrupts or unwanted signals adding to a packet as it travels along a channel between a sender and a receiver. During the transmission of data from a node s to its destination, its signal to interference plus noise ratio (SINR) can be evaluated in the following equation, the data is transmitted with a constant power ρ to its intended destination and both are positioned with a fixed D distance away [15].

$$SINR = \left(\rho D^{-\beta} \right) / \left(\sigma + \sum_s \rho d_s^{-\beta} \right) \quad (21)$$

Where, d is the distance between the nodes, σ is the channel noise and β is the link/path loss attenuation factor $\beta > 2$.

I High Packet Size

If packet size is more, it is probably a energy consuming and time consuming too. The below equation shows how packet size matters in energy consumption,

$$\begin{aligned} E_{tx} &= (P_{tx} * 8 * PS / BW) \\ E_{rx} &= (P_{rx} * 8 * PS / BW) \end{aligned} \quad (22)$$

Where E_{tx} and E_{rx} are used for energy consumption for transmitting and receiving a packet. P_{tx} and P_{rx} indicates transfer power and receive power respectively. PS and BW are Packet Size and Bandwidth respectively.

J Full Overhearing

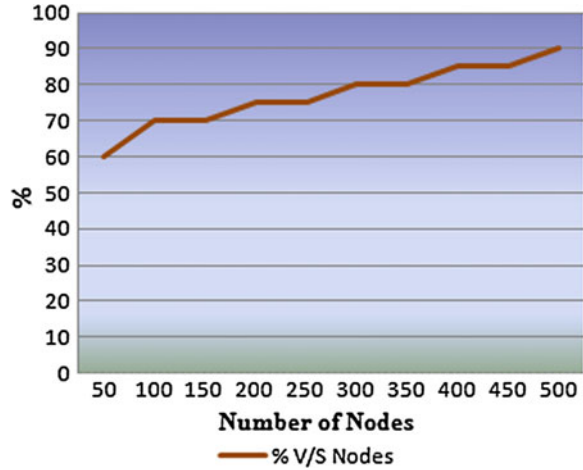
When a node receives data packets that are not intended for it called as overhearing mode and it may consume the same amount of energy used in receiving the packet. The power consumed in overhearing mode is,

$$P_O = P_R \quad (23)$$

Where, P_O is power consumed in Overhearing Mode and P_R is power consumed in Reception Mode.

In this paper we have implemented few of the above approaches to make malicious node unconscious in the communication via simulation using Java Language. In this network, we have considered maximum 500 nodes with 1 % as malicious node(s) chosen randomly in the network, and trying to make energy free

Fig. 3 Number of nodes versus percentage of success in making to zero energy



of malicious node(s) so that it cannot participate in the communication. Figure 3 shows the simulation results of the proposed strategies and it encourages when number of nodes are more in the network due to many reasons like, many nodes can participate in the operation with less cost of individual to beat the malicious node. Hence, this paper makes a very good novel approach to defence our deployed network and preserve the data misuse.

4 Conclusions

This paper has presented a negative approach for data misusing which is essential due to lack of security in the MANETs. Some time, the genuine nodes can be attacked or accessed by fraud or malicious nodes, and also a node itself can turn into a malicious behaviour. To address such problems, a novel approach has been proposed to exhaust the valuable resource of the MANETs called invalidating/retiring a node where we need to turn the node's battery level to zero so that it cannot participate in the communication, hence data misuse can be avoided.

References

1. Singh, S.K., Singh, M.P., Singh, D.K.: A survey of energy-efficient hierarchical cluster-based routing in wireless sensor networks. *Int. J. Adv. Networking Appl.* **2**, 570–580 (2010)
2. Utkarsh, Mishra, M., Chinara, S.: ESAR: an energy saving ad hoc routing algorithm for MANET. In: *Fourth International Conference on Advanced Computing (ICoAC)*, 2012, p. 15 (2012)
3. Furthmuller, J., Waldhorst, O.P.: Evaluating the energy consumption of an incentive system for resource sharing in manets. In: *IEEE International Conference on Communications (ICC)*, 2012, pp. 6293–6297 (2012)

4. Kunz, T.: Accurately predicting residual energy levels in manets. In: Proceedings of the 2008 IEEE International Conference on Wireless and Mobile Computing, Networking and Communication, WIMOB 08, Washington, DC, USA, 2008. IEEE Computer Society, pp. 44–50 (2008)
5. Tamilarasi, M., Sundararajan, T.VP.: Secure enhancement scheme for detecting selfish nodes in MANET. In: International Conference on Computing, Communication and Applications (ICCCA), 2012, p. 15, (2012)
6. Shakshuki, E.M., Kang, N.,Sheltami, T.R.: EAACK: a secure intrusion-detection system for MANETs. IEEE Trans. Ind. Electron. **60**, 1089–1098 (2013)
7. Seetharam, A., Acharya, A., Bhattacharyya, A., Naskar, M.K.: An energy efficient data gathering protocol for wireless sensor networks. J. Appl. Comput. Sci. **1**, 30–34 (2008)
8. Chandrakant, N., Deshpande, H., Tejas, J., Shenoy, P.D., Venugopal, K.R., Patnaik L.M.: Emid: maximizing lifetime of wireless sensor network by using energy efficient middleware service. Int. J. Innovative Technol. Creative Eng. **1**, 20–24 (2011)
9. Rana, G., Zhangb, H., Gong, S.: Improving on leach protocol of wireless sensor networks using fuzzy logic. J. Inf. Comput. Sci. **7**, 767–775 (2010)
10. Doorn, B.V.D., Kavelaars, W., Langendoen, K.: A prototype low-cost wakeup radio for the 868mhz band. Int. J. Sens. Netw. **5**(1), 22–32, (2009)
11. Seddik-Ghaleb, A., Ghamri-Doudane, Y., Senouci, S.-M.: Tcp computational energy cost within wireless mobile ad hoc network. In: Proceeding of LCN (2008)
12. Allard, G., Minet, P., Nguyen, D.-Q., Shrestha, N.: Evaluation of the energy consumption in MANET. Ad Hoc Mobile Wireless Netw. **4104**, 170–183 (2006)
13. Nguyen, D., Minet, P.: Evaluation of the bandwidth needed at the mac 802.11b level. Research Report, INRIA-RR-5553, INRIA, France (2005)
14. Lochert, C., Scheuermann, B., Mauve, M.: A survey on congestion control for mobile ad-hoc networks. Wiley Wireless Commun. Mobile Comput. **7**, 655–676 (2007)
15. Suseendran, G., Chandrasekaran, E.: Interference reduction technique in mobile adhoc networks using mathematical prediction filters. Int. J. Comput. Appl. **60**, 916 (2012)

Administrating MANETs Via Brain Computer Interface

N. Chandrakant

Abstract The electroencephalogram (EEG) based Brain-Computer Interfaces (BCIs) has been considerably extended to the multidisciplinary and challenging nature of BCI study. The algorithms of Digital signal processing and pattern recognition certainly constitute necessary components of a BCI system which are applied to the EEG signals to decode mental states those are relevant for BCI operation. The basic BCI concepts such as: brain activity monitoring, BCI operation, and the relevant mental states for BCI are applied to WSN. The major types of relevant mental states for BCI, namely motor imagery (ERD/ERS), steady state visual evoked potentials (SSVEP) are also mapped to MANET's behaviour. The multivariate nature of the EEG combined with the neuroscience familiarity on hemispheric brain specialization is favourably taken into account to derive optimal combinations of the individual signals composing the EEG. BCI provides a non-muscular channel for sending commands to the external world using the electroencephalographic activity or other electrophysiological process of the brain function. A necessary factor in the successful operation of BCI systems is the methods used to process the brain signals. The processed data has been applied on to nodes of MANET where each set of sensor nodes are used for particular application. Based on the output of BCI commands, the MANET is operated and controlled with using only activities of neurons of brain, hence this approach could be more helpful to physically differently abled people or medically injured people.

Keywords WSN · BSP · ANN · BCI (Brain Computer Interface)

N. Chandrakant (✉)
Bangalore, India
e-mail: nadhachandra@gmail.com

1 Introduction

A Brain Computer Interface (BCI)/Mind Machine Interface (MMI)/Direct Neural Interface/Brain Machine Interface (BMI)/Direct Communication Pathway between the brain and an external digital device which are often directed at assisting, augmenting, or repairing human cognitive or networking functions, sensory-motor functions [1].

Human brains are made up of neurons with entity nerve cells connected to one another by dendrites and axons. Whenever we think, move, feel or remember something, our neurons are at work which is carried out by small electric signals that zip from neuron to neuron as fast as 250 mph. The signals are produced by differences in electric potential carried by ions on the covering of each neuron. We can analyse the signals and process as understandable words.

The applications of BCI can include,

- (a) You can sense the thoughts of Aliens if scientists proves its existence.
- (b) Benefits for stroke.
- (c) Benefits for disabilities like paralyzed including oral problems.
- (d) Study of Animal's behaviour.
- (e) Identify thoughts of thieves.
- (f) BCI system will facilitate an augmentative communication method for patients with severe motor disabilities.
- (g) Monitor unmanned areas.

The rest of this paper is arranged as follows: In [Sect. 2](#), gives some helpful input information for this paper. Detailed design and its implementation with results has been explained in [Sect. 3](#). Finally, [Sect. 4](#) concludes the paper and gives future trends.

2 Literature Survey

Starlab Neuroscience [1, 2] Research offers advanced data analysis services for their clients in research and in industry. They have a sister company Neuroelectronics, where they offer custom solutions for data capture and analysis based on clients needs.

Intendix [3] provides 3 major solution areas, they are, Personal EEG Based Spelling System, Screen Overlay Control Interface and Paint by Thoughts. This system can work with passive, active, or new dry EEG electrodes. Using these systems, apart from writing text, the patient can also use the system to trigger an alarm, let the computer speak the written text, print out or copy the text into an e-mail or to send commands to external devices.

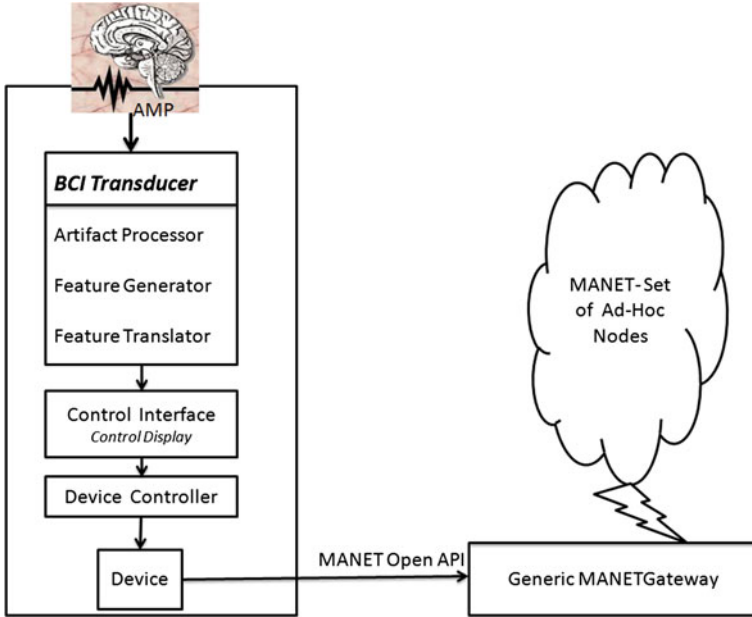


Fig. 1 Overall architecture of BCI-MANET computing

Algorithm 1 *main(args[], addlInfo[])*

Require: Initialize $i \leftarrow 0, j \leftarrow 0, rule[] \leftarrow null, n \leftarrow numberOfNodes$

```

1: while  $i++ \leq numberOfRules$  do
2:   if  $args[i] == 'BCI\_Value'$  then
3:     rule = getInstructions(addlInfo[i])
4:     while  $j++ \leq n$  do
5:       if  $rule[i].nodeId == j$  then
6:         if  $rule[i] == isAlreadyApplied()$  then
7:           Then ignore this instructions and donot execute on MANET.
8:         else
9:           executeOperationOnNode(rule[i], j)
10:        end if
11:      end if
12:    end while
13:  else
14:    Take the default behaviour of the network/algorithm
15:  end if
16: end while
    
```

Paper [4] proposed a new multi-stage procedure for a real time BCI which allows a BCI [5] user to movement including four directions and to stop a small car (any object) on the computer display screen in real time. The results shows high performance of the proposed on-line BCI system which has conducted extensive experiments with 5 young healthy subjects.

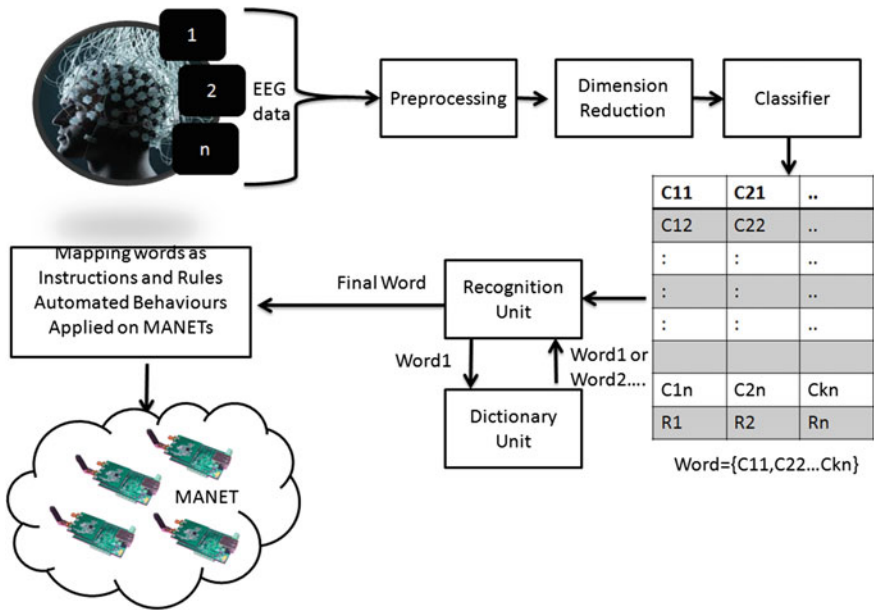


Fig. 2 Architecture of proposed system

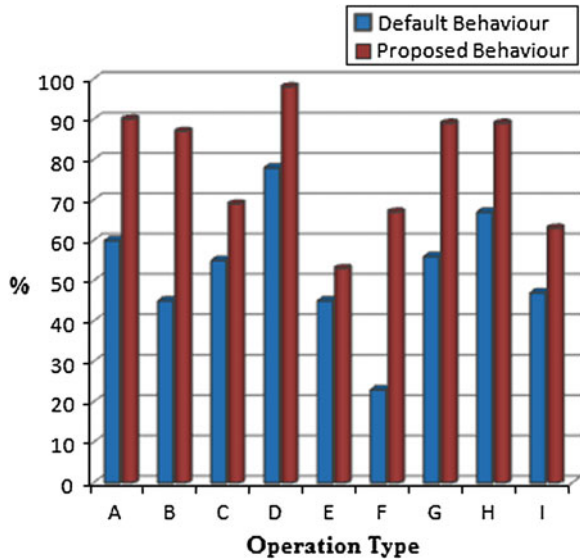
Paper [6] presents a new classification technique of uninterrupted EEG recordings based on a network of spiking neurons. The EEG signals were pre-processed using Wavelet Transform to take out the noise and to extract the low frequency substance and analysis of the signals was carried out on the ensemble EEG and the task of the neural network was to recognize the P300 component in the signal. The network engaged leaky-integrate-and-fire (LIF) neurons as nodes in a multi-layered arrangement which does formation of multiple weak classifiers to perform voting and combined results are used for final classification.

3 Proposed System and Design

The overall Architecture is shown in Fig. 1. A transducer device will converts variations in a physical quantity, such as pressure or brightness into an electrical signal or vice versa.

Electrodes of Electro Encephalo Graph (EEG) will read the brain signals after placing electrodes in the specific area of the brain where the suitable signals are generated. The electrodes compute minute differences in the voltage between neurons and this signal is further amplified, filtered and interpreted by a computer program.

Fig. 3 Performance of default and proposed behaviour of a MANET



The proposed system is shown in Fig. 2. Electroencephalography (EEG) is the sensing of electrical action along the scalp which measures the voltage fluctuations resulting from ionic current flows between the neurons of the brain. In the medical context, EEG records the brain’s spontaneous electrical activity over a short period of time, typically 20–40 min, as recorded from numerous electrodes placed on the scalp (Fig. 3).

Then preprocessing includes, Epoching which is cutting the data into chunks referenced to stimulus presentation and Averaging which is calculating the mean value for each time-point across all epochs.

Dimension reduction is generally used to decrease the necessary training time of the classifiers with a few degree of precision lost. The dimension reduction is typically performed on either feature or electrode space.

The processing and matching of words with help of dictionary out of the EEG data can be evoked by potential components, like the P300 or the N400. This will indicate collective macroscopic activities of neurons that are reflected in the EEG as speech.

The final matching word(s) is (are) mapped to certain set of instructions and rules and intern these instructions are applied as operations on MANETs which can help network to increase its throughput/performance. Sometime human intervention gives more advantages than auto-operations. MANET operations can be invoked by above strategy/algorithm and operations are as follows,

- A. **Routing Path Adjustment:** Detecting efficient path for packet routing. It includes even deciding central node for other node’s communication. Dynamic/Hybrid path can be calculated on-demand, hence it is more efficient.

- B.** Topology Adjustment: The structure of the network is reconstructed based on the requirements.
- C.** Resource Management: Limited bandwidth available between two intermediate nodes, hence managing it efficiently. Node may have limited memory and power and thus computations need to be energy-efficient.
- D.** Energy Management: Energy is a very important resource of MANET, a node/network is alive till energy/power is lost. Hence, it should be preserved as much as we can by analysing its usages.
- E.** Traffic management: The traffic can exhaust energy of the network and lost of packets too, hence transferring of packets needs to do intelligently. It includes even link management like failures and redirecting traffic.
- F.** Memory Management: Memory is one of the essential resource of MANET and also its memory is very small. Hence, memory must be used intelligently.
- G.** Sleep/Wakeup Strategy: If a node is useful or participating in the communication or transferring repeated data, in such cases, we can toggle the nodes's status to sleep or wakeup.
- H.** Enabling/Disabling Security: A hierarchy of security is enabled or disabled based on cost in terms of network performance and energy consumption.
- I.** Miscellaneous: Unspecified or customized operations can be done on MANETs, e.g., node retirement etc.

The basic algorithm is specified in Algorithm 1. The algorithm has many variables and methods, *numberOfRules* is number of rules or instructions applied on set of nodes. *BCI_Value* is the value of braincomputer interface which is generated out of EEG data. The *getInstructions(addyInfo[i])* is the process of extracting instructions out of array data. The *isAlreadyApplied()* is used to check weather instructions are already executed on the network or not. The *execute-OperationOnNode(rule[i], j)* is the process of applying the operation specified in *rule[i]* on a particular node(*j*).

The performance graph of default and proposed behaviour is shown in Fig. 3 with comparison of percentage. The simulation experiment is implemented in JAVA with 500 nodes as network size. Where operation type is termed as actions/rules/instructions to be performed on node(s). Operation Types are, Routing, Topology, Resource, Energy, Traffic, Memory, Sleep/Wakeup, Security and Miscellaneous. In this experiment, we have considered Routing operation type and we simulated 9 times for the same type which is named from *A* to *I*.

It is obvious that human intelligence is more dynamic than default behaviour. Hence, our experiment proves the same and have achieved more performance than the default behaviour. Similarly, same kind of experiment can be conducted for other operation types and we believe that human intervention always fetches more performance than automated, but everything has its own merits and demerits.

4 Conclusions

A novel approach is proposed where integration of MANETs and BCI devices are linked and commands are processed using neuron's (brain) signals. The brain's data is processed and provided as input to the nodes of MANET where each set of mobile nodes are used for different applications. Based on the output of BCI system, the MANET is operated and controlled using only activities of neurons of a brain, hence this approach could be more helpful/useful to physically differently abled people, medically injured people or even lazy people too!

References

1. BCI. Braincomputer interface: <http://en.wikipedia.org/wiki/Brain>
2. StarLab: <http://starlab.es/neuroscience>
3. Intendix: <http://www.intendix.com/>
4. Martinez, P., Bakardjian, H., Cichocki, A.: Fully-online, multi- command brain computer interface with visual neurofeedback using SSVEP paradigm. <http://www.bsp.brain.riken.jp/publications/2007/BCICIN.pdf> (2007)
5. Santhanam, G., Ryu, S.I., Yu, B.M., Afshar, A., Shenoy, K.V.: A high-performance brain-computer interface. *Nature* **44**(2), 195–198 (2006)
6. <http://www.port.ac.uk/research/iir/research/currentresearch/dataanalysis/braincomputerinterface/>. Spiking Neural Network Based Approach to EEG Signal Analysis

Parameter Estimation and Soft Computing Techniques

D. K. Chaturvedi and Mayank Pratap Singh

Abstract The paper presents an overview of parameter estimation of three phase induction motor using different techniques. The techniques mainly described in the paper are conventional techniques and soft computing techniques. The soft computing techniques considered in the paper are fuzzy system, artificial neural network (ANN), Neuro-Fuzzy, genetic algorithms (GA) and particle swarm optimization (PSO).

Keywords Induction motor · Parameter estimation · Soft computing techniques · ANN · GA · PSO

1 Introduction

The induction motor parameter estimation is the art and science of building mathematical models of dynamic systems from observed input–output data. It can be seen as the interface between the real world of applications and the mathematical world of control theory and model abstractions. The knowledge of all the machine parameters is very important to tune the controllers of a high performance motor drive system. The accurate knowledge of the induction motor parameters is critical for the sensorless drive strategies based on the stator flux estimation [1]. This fact has stimulated the development of specific techniques to determine the

D. K. Chaturvedi (✉) · M. P. Singh
Department of Electrical Engineering, D.E.I., Dayalbagh, Agra, India
e-mail: dkc.foe@gmail.com

M. P. Singh
e-mail: mayankpratapsinghonline@yahoo.com

induction motor parameter [2]. There are various techniques to estimate the induction motor parameters, such as:

1. Conventional techniques
2. Soft computing techniques
 - a. Fuzzy system
 - b. Artificial neural network
 - c. Genetic Algorithms
 - d. PSO
 - e. Integration of above techniques.

1.1 Conventional Methods

There are various conventional methods available with their merits and demerits [3, 4]. There are many ways to detect mechanical and electrical problems in induction motors, either directly or indirectly, such as motor current signature analysis, line neutral voltage signature, instantaneous reactive power signature, stator current and motor efficiency, electromagnetic field monitoring, chemical analysis, temperature measurement, infrared measurement, acoustic noise analysis, partial discharge measurement and vibration monitoring and fault detection based on parameter adaption [5].

The Knowledge of all the machine parameters is very important to tune the controllers of a high performance motor drive system [6–8]. For several decades, the Kalman filter has proved to be a powerful tool for state and parameter estimation of linear and nonlinear systems and has been applied in induction motor for estimation of flux [9, 10] and its parameters [11].

Induction motor parameters change with temperature, frequency and saturation. The consequence of any mismatch between the parameter values used in the controller and those in the motor is that the actual rotor flux position does not coincide with the position assumed by the controller.

The parameters that may need to be identified offline or tracked online depend on the vector control scheme under consideration [12]. The most important offline identification and online parameter estimation techniques are reviewed.

1.1.1 Offline Parameter Estimation Techniques

It is often the case in practice that one manufacturer supplies the inverter with a vector controller, while the machine comes from another manufacturer. It is then not possible to set the parameters of the controller in advance and these have to be

set onsite, once when the inverter is connected to the machine. Such a situation has led to the development of the so-called self-commissioning procedures for vector controlled induction machines. The main idea behind this concept is that the controller automatically determines all of the parameters of an induction machine, required for vector control. The automated procedure of testing and calculation is done following the first enabling of the controller. As the induction motor may already be coupled to a load, the tests aimed at self-commissioning have to identify the required parameters at standstill. The identification is therefore performed with single-phase supply to the machine. In principle, two types of excitation may be applied—dc or ac. The one ideal for true self-commissioning is dc. From applied dc voltage and resulting dc steady state current, one finds the value of the stator resistance. Determination of the remaining parameters is then based most frequently on transient current response that follows application of the dc voltage. Self-commissioning schemes that rely on this approach are those described in [13]. The methods regarded as suitable for commissioning but inappropriate for self-commissioning are those that either require some special conditions to be satisfied during the commissioning (for example, the machine is allowed to rotate) or they require substantially more complicated mathematical processing of the measurement results, when compared to the self-commissioning methods. For example, procedures described in [14] are all based on some tests with single-phase supply to the machine. The maximum likelihood estimation method described in [15], which requires application of the recursive least squares algorithm, this being the same as for the procedure of [16]. The second possible excitation for parameter identification at standstill is single-phase ac. Standstill frequency response for the parameter identification [17]. A method based on trial- error and essentially does not require any computations. Some of the offline identification procedures surveyed so far enables identification of the machine's magnetizing curve in addition to other rated parameter values [18].

It should be noted that accuracy of parameter determination in all offline identification techniques depends on the sample rate selection, quantization errors, resolution and accuracy of sensors [19]. Identified parameter values will therefore always be characterized with certain error margin. The major problem encountered in offline parameter identification at standstill is undoubtedly the inverter lock-out time and nonlinearity, which make the accurate parameter determination on the basis of reconstructed voltages very difficult without prior knowledge of the inverter voltage drop characteristics. A technique for overcoming this problem has recently been proposed based on recursive least squares [20].

1.1.2 Online Rotor Time Constant Estimation Techniques

The major effort has been put into development of rotor time constant (rotor resistance) online estimation methods. Due to a huge number of proposed solutions of very different nature, these are further classified into four subgroups.

A. Spectral Analysis Techniques

This group of methods encompasses all of the cases where online identification is based on the measured response to a deliberately injected test signal or an existing characteristic harmonic in the voltage/current spectrum [21]. Stator currents and/or voltages of the motor are sampled and the parameters are derived from the spectral analysis of these samples. In spectral analysis, a perturbation signal is used because under no-load conditions of the induction motor, the rotor induced currents and voltages become zero, so slip frequency becomes zero, and hence, the rotor parameters cannot be estimated. In Matsuo and Lipo [21] the disturbance to the system is provided by injecting negative sequence components. An online technique for determining value of the rotor resistance was used by detecting the negative sequence voltage. The main drawback of this method is that the strong second harmonic torque pulsation is induced due to the interaction of positive and negative rotating components of MMF.

B. Observer-Based Techniques

Loron and Laliberté [22] describe the motor model and the development and tuning of an extended Kalman filter (EKF) for parameter estimation during normal operating conditions without introducing any test signals. The proposed method requires terminal and rotor speed measurements and is useful for auto-tuning an indirect field-oriented controller or an adaptive direct field-oriented controller. Zai et al. [23] proposed a method for detection of the inverse rotor time constant using the EKF by treating the rotor time constant as the state variable along with the stator and rotor currents. This is similar to a previously mentioned method that injected perturbation in the system, except that in this case, the perturbation is not provided externally. Instead, the wide-band harmonics contained in a PWM inverter output voltage serve as an excitation. This method works on the assumption that when the motor speed changes, the machine model becomes a two-input/two output time-varying system with superimposed noise input. The drawbacks are that this method assumes that all other parameters are known and the variation in the magnetizing inductance can introduce large errors into the rotor time constant estimation. The application of the EKF for slip calculation for tuning an indirect field oriented drive is proposed in [24, 25]. Using the property that in the steady state the Kalman gains are asymptotically constant for constant speeds, the Riccati difference equation is replaced by a look-up table that makes the system much simpler. The disadvantage is that, although the complexity of the Riccati equation is reduced, the full-order EKF is computationally very intensive as compared to the reduced order-based systems.

C. Model Reference Adaptive System-Based Techniques

The third major group of online rotor resistance adaptation methods is based on principles of model reference adaptive control. This is the approach that has

attracted most of the attention due to its relatively simple implementation requirements. The basic idea is that one quantity can be calculated in two different ways. The first value is calculated from references inside the control system. The second value is calculated from measured signals. One of the two values is independent of the rotor resistance (rotor time constant). The difference between the two is an error signal, whose existence is assigned entirely to the error in rotor resistance used in the control system. The error signal is used to drive an adaptive mechanism (PI controller) which provides correction of the rotor resistance. Any method that belongs to this group is based on utilization of the machine's model and its accuracy is therefore heavily dependent on the accuracy of the applied model [26].

D. Other Methods

There exist a number of other possibilities for online rotor resistance (rotor time constant) adaptation, such as those described in [27]. It is based on a special switching technique of the current regulated PWM inverter, which allows measurement of the induced voltage across the disconnected stator phase. The rotor time constant is then identified directly from this measured voltage and measured stator currents. The technique provides up to six windows within one electric cycle to update the rotor time constant, which is sufficient for all practical purposes.

1.1.3 Online Estimation of Stator Resistance

An accurate value of the stator resistance is of utmost importance in this case for correct operation of the speed estimator in the low speed region. If stator resistance is detuned, large speed estimation errors and even instability at very low speeds result. It is for this reason that online estimation of stator resistance has received considerable attention during the last decade [28, 29]. The other driving force behind the increased interest in online stator estimation was the introduction of direct torque control (DTC), which in its basic form relies on estimation of stator flux from measured stator voltages and currents.

1.2 Soft Computing Techniques

The soft Computing Techniques have been employed to assist the fault-detection task to correctly interpret the fault data, such as expert systems, fuzzy logic, fuzzy NN, artificial neural network (ANN), wavelet transform technique and genetic algorithm.

a. Fuzzy System for Parameter Identification

A higher order fuzzy system (FS) identification method was drawn attention of many researchers for nonlinear dynamic system parameter identification [30].

To perform fault analysis on an induction motor using both experiments and simulation, and to study failure identification techniques applied for condition monitoring of the motor and finally to design an On-line condition monitoring system, fuzzy logic system using Lab View was suggested [31].

b. Artificial Neural Network Technique

Artificial Neural Network (ANN) is a system based on the operation of biological neural networks; it is an abstract simulation of a real nervous system. ANN's have been applied with astonishing success in fields ranging from computer science to engineering to medicine.

The Induction motor is a nonlinear multivariable dynamic system with parameters that vary with temperature, frequency, saturation, and operating point. The rotor parameters are the most important parameters for the control of the induction motor drives. The rotor resistance can change up to 150 % over the entire operation [32, 33]. The rotor parameter estimation is proposed by estimating the rotor temperature in [33]. This is based on the fact that the temperature influences the fundamental frequency component of the terminal voltage for a given input current.

In many papers, the use of ANN has been tried for estimating the rotor angular speed. Among the methods used, it is possible to note two types of ANN designs. One is based on the machine model and the other one uses stator currents and voltages for direct speed estimation.

c. Integration of ANN and FS

ANNs and fuzzy logic are widely used in the areas of modelling, identification, diagnostics and control of nonlinear systems. There are numbers of methods that can provide true on-line adaptation process of a fuzzy model. One of example is a Takagi–Sugeno–Kang fuzzy model, where the input space is automatically partitioned using a modified fuzzy adaptive resonance theory (ART) mechanism [34].

A simple fuzzy controller implemented in the motor drive speed control has a narrow speed operation and needs much manual adjusting by trial and error if high performance is required [35]. On the other hand, it is extremely tough to create a training data for ANN that can handle all the operating modes [36]. A neuro-fuzzy controller (NFC) for the induction motor drive has the advantages of both FLC and ANN. Over the last decade, researchers reported works on the application of NFC

for variable speed drives [37]. However, the conventional NFCs utilized in earlier works have a large number of membership functions and rules.

d. Genetic Algorithm (GA)

The basic procedure to develop a genetic algorithm was described and the examples of its application for parameter identification were introduced. In order to simplify the offline identification of induction motor parameters, a method based on optimization using a multi objective genetic algorithm was proposed [38].

Estimation of parameters of three-phase induction motor in order to conduct on-site energy audits of existing motors was used to project a cost savings. This technique used only a few sets of data (voltage, current, speed, power factor or torque if possible) from the field test of motor (on-site), instead of the no load and blocked rotor tests, coupled with the genetic algorithm for evaluating the equivalent circuit parameters [39].

e. Particle Swarm Optimization (PSO)

Over the past few decades, with the indirect field-oriented control and non sinusoidal measurements, most of the methods can be roughly divided into three categories: signal injection-based method [40], model reference adaptive system-based technique [41], and optimization techniques [42]. The signal injection-based method is to improve the estimation of low speed performance of sensor less schemes or to excite the machine to create various response signals. They often require extra hardware for signal injection. Applications of signal injection have been presented in dealing with the stator and rotor winding temperatures. The model reference adaptive system uses the error between the estimated and the reference signals to calculate the parameters. In optimization techniques, parameter estimation has been investigated by using the artificial intelligence including the particle swarm optimization (PSO) and the least squares strategy. These techniques have been reported to minimize the consequences of parameter sensitivity in vector controlled drives.

2 Results and Discussion

See Figs. 1 and 2.

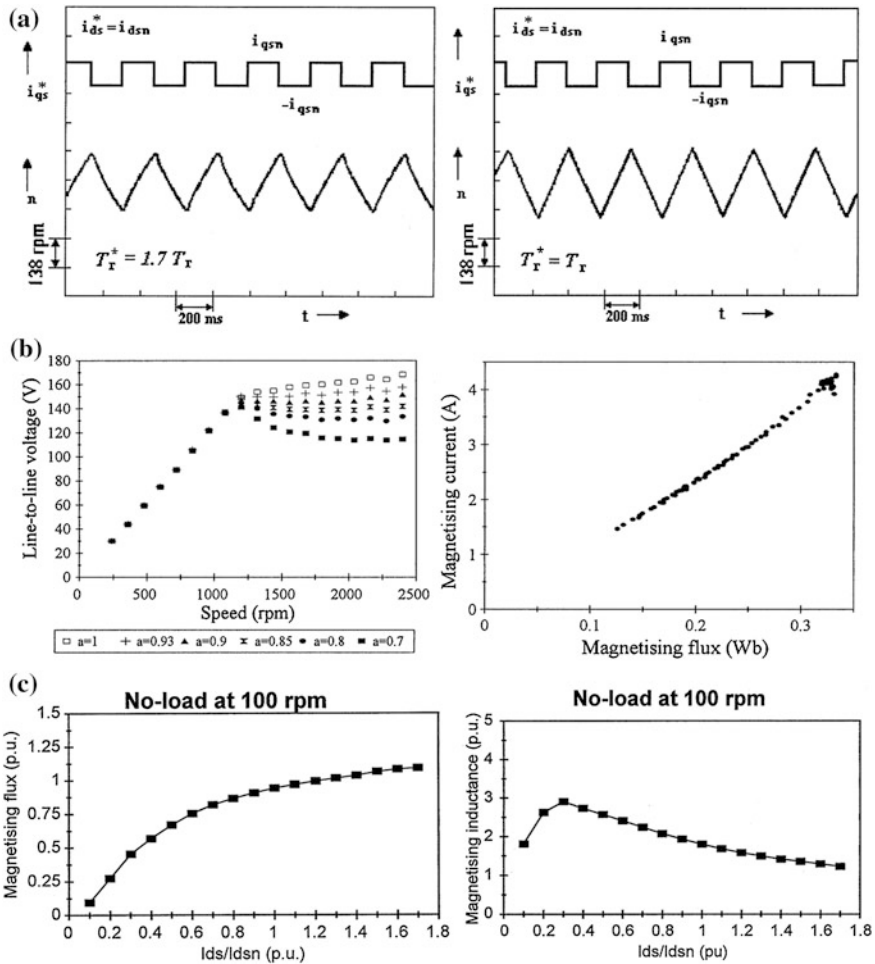


Fig. 1 Results of induction motor parameter estimation. **a** An experimental trial-and-error method of rotor time constant tuning in indirect vector controller: speed response to alternating square-wave torque command with correct rotor time constant and with 1.7 times correct rotor time constant (0.75-kW machine). Speed response is a triangular function of time when the rotor time constant is correctly set [12] **b** Measured fundamental stator voltage for different settings of the parameter a of the inverse magnetizing curve per-unit analytical approximation $i = a \Phi + (1-a) \Phi^7$ and reconstructed magnetizing curve (2.3-kW machine, field-weakening starts at 1150 r/min]). The correct value is $a = 0.9$ since it gives the flattest voltage behaviour in the field-weakening region [43] **c** Experimentally identified magnetizing curve and magnetizing inductance (100 r/min, no-load conditions, 7-kW machine) [44] **d** Fundamental component of the iron loss identified using the procedure and the corresponding equivalent iron loss resistance (4-kW machine) [45] **e** Rotor inductance and rotor resistance identification using conventional method [46] **f** Experimental recording of the operation of the rotor resistance adaptation in indirect rotor flux oriented induction machine, using the method [47] **g** Estimated and actual rotor time constant [48]

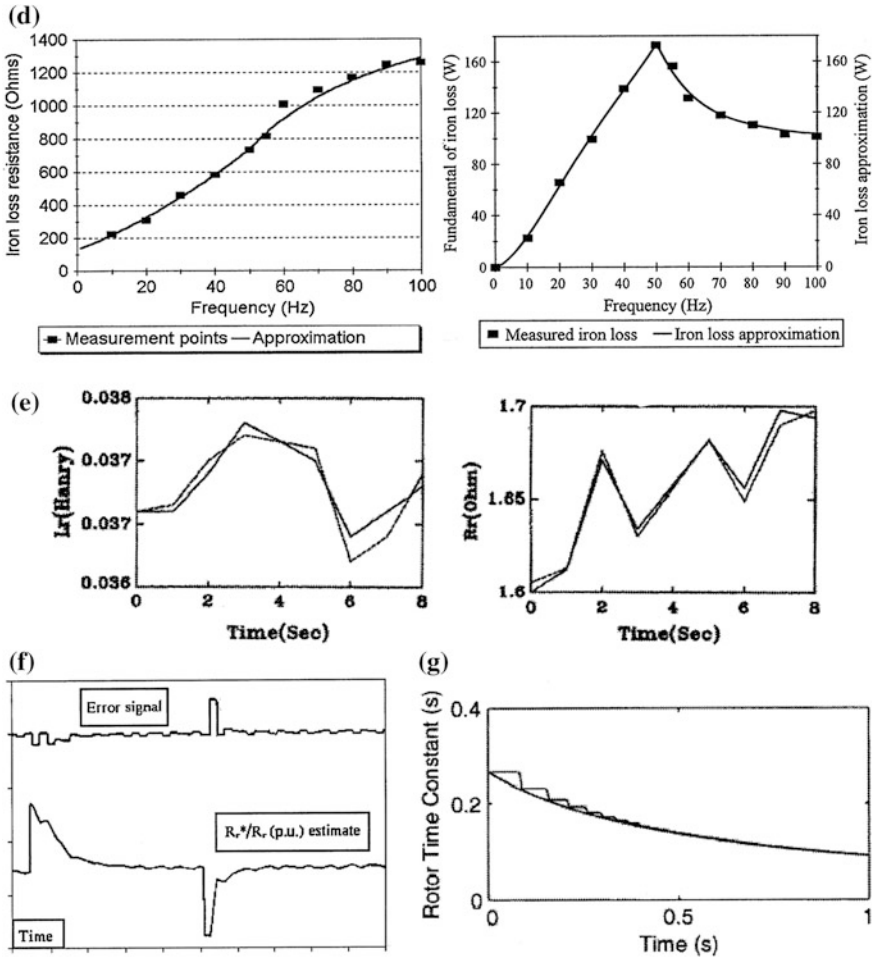


Fig. 1 continued

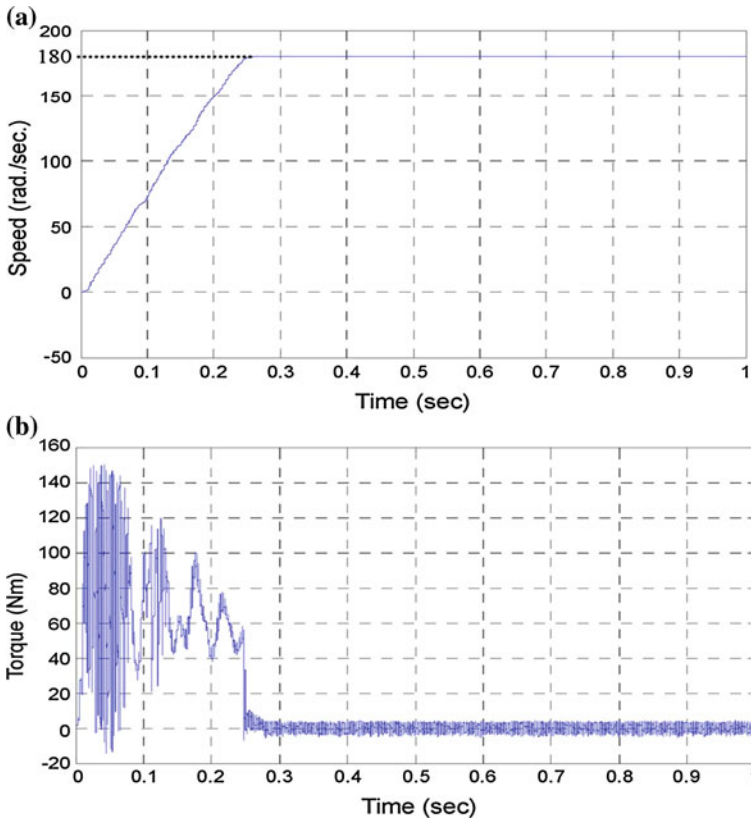


Fig. 2 Simulated starting responses of the 3-hp IM Drive with neuro-fuzzy controller. **a** Speed. **b** Torque [49]

3 Conclusion

The parameters of induction motor may vary due to several factors such as: machine internal temperature, machine ageing, magnetic saturation, the coupling effect between the internal system and external system. In this paper, an overview of estimation of induction motor parameters has been presented using conventional and soft computing techniques. The soft computing techniques are better than conventional techniques in terms of adaptability and flexibility.

References

1. Holtz J., Quan J.: Sensorless vector control of induction motors at very low speed using a nonlinear inverter model and parameter identification. In: Proceedings of the IEEE-IAS Annual Meeting, pp. 2614–2621 (2001)
2. Ribeiro, L.A. de S., Jacobina, C.B., Lima, A.M.N., Oliveira A.C.: Parameter sensitivity of MRAC models employed in ifo controlled ac motor drive. *IEEE Trans. Ind. Electron.* 44, 536–545 (1997)
3. Ponci F., Cristaldi L., Faifer M., Lazzaroni M.: Innovative approach to early fault detection for induction motors. In: Proceedings of the IEEE SDEMPED, pp. 283–288 (2007)
4. Benbouzid M.: A review of induction motors signature analysis as a medium for faults detection. *IEEE Trans. Ind. Electron.* 47(5), 984–993 (2000)
5. Barrera, P.M. de la, Bossio, G.R., Garcia, G.O., Solsona, J.A.: Stator core fault diagnosis for induction motors based on parameters adaptation. In: Proceedings of the IEEE SDEMPED, pp. 1–6 (2009)
6. Vélez-Reyes, M., Minami, K., Verghese, G.C.: Recursive speed and parameter estimation for induction machines. In: Proceedings of the IEEE-IAS Annual Meeting, pp. 607–611 (1989)
7. Stephan, J., Bodson, M., Chiasson, J.: Real-time estimation of the parameters and fluxes of induction motors. *IEEE Trans. Ind. Appl.* 30, 746–759 (1994)
8. Bose B.K., Simoes M.G., Creclius D., Rajashekara K., Martin R.: Speed sensorless hybrid vector controlled induction motor drive. In: Proceedings of the IEEE-IAS Annual Meeting, pp. 137–143 (1995)
9. Cava, M.L., Picardi, C., Ranieri, F.: Application of the extended Kalman filter to parameter and state estimation of induction motors. *Int. J. Model. Simul.* 9(3), 85–89 (1989)
10. Atkinson, D.J., Acarney, P., Finch, J.: Observers for induction motor state and parameter estimation. *IEEE Trans. Ind. Appl.* 27(6), 1119–1127 (1991)
11. Wade, S., Dunnigan, M., Williams, B.: A new method of rotor resistance estimation for vector-controlled induction machines. *IEEE Trans. Ind. Electron.* 44(2), 247–257 (1997)
12. Levi E.: Impact of iron loss on behaviour of vector controlled induction machines. *IEEE Trans. Ind. Applicat.* 31, 1287–1296 (1995)
13. Globevnik, M.: Induction motor parameters measurement at standstill. In: Proceedings of the IEEE Industry Electronics Society Annual Meeting, pp. 280–285 (1998)
14. Ruff, M., Grotstollen H.: Identification of the saturated mutual inductance of an asynchronous motor at standstill by recursive least squares algorithm. In: Proceedings of the European Conference Power Electronics Applications vol. 5, pp. 103–108 (1993)
15. Moon, S.I., Keyhani, A.: Estimation of induction machine parameters from standstill time-domain data. *IEEE Trans. Ind. Appl.* 30, 1606–1615 (1994)
16. Consoli, A., Fortuna L., Gallo A.: Induction motor identification by a microcomputer-based structure. *IEEE Trans. Ind. Electron.* 34, 422–428 (1987)
17. Bünte A., Grotstollen H.: Offline parameter identification of an inverter-fed induction motor at standstill. In: Proceedings of the European Conference Power Electronics Applications, pp. 3.492–3.496 (1995)
18. Kwon, W.H., Lee, C.H., Youn, K.S., Cho, G.H.: Measurement of rotor time constant taking into account magnetizing flux in the induction motor. In: Proceedings of IEEE Industry Applications Society Annual Meeting, pp. 88–92 (1994)
19. Borgard, D.E., Olsson, G., Lorenz, R.D.: Accuracy issues for parameter estimation of field oriented induction machine drives. *IEEE Trans. Ind. Applicat.* 31, 795–801 (1995)
20. Bertoluzzo, M., Buja, G.S., Menis, R.: Inverter voltage drop-free recursive least-squares parameter identification of a PWM inverter-fed induction motor at standstill. In: Proceedings of the IEEE International Symposium on Industry Electronics, pp. 649–654 (1997)
21. Matsuo, T., Lipo, T.A.: A rotor parameter identification scheme for vector controlled induction motor drives”, *IEEE Trans. Ind. Applicat.* 1A-21, 624–632 (1985)

22. Loron, L., Laliberté, G.: Application of the extended Kalman filter to parameters estimation of induction motors. In: Proceedings of the European Conference Power Electronics Applications, vol. 5, pp. 85–90 (1993)
23. Zai, C., Marco, C., Lipo, T.: An extended Kalman filter approach to rotor time constant measurement in PWM induction motor drives. *IEEE Trans. Ind. Appl.* **28**(6), 96–104 (1992)
24. Finch, J.W., Atkinson, D.J., Acamley, P.P.: Full-order estimator for induction motor states and parameters. *Proc. IEEE Power Appl.* **145**(3), 169–179 (1998)
25. Kataoka, T., Toda, S., Sato, Y.: On-line estimation of induction motor parameters by extended Kalman filter. In: Proceedings of the European Conference Power Electronics Applications vol. 4, pp. 325–329 (1993)
26. Krishnan, R., Pillay, P.: Sensitivity analysis and comparison of parameter compensation schemes in vector controlled induction motor drives. In: Proceedings of IEEE Industrial Applications Society Annual Meeting, pp. 155–161 (1986)
27. Toliyat, H., Arefeen M.S., Rahman, K.M., Ehsani, M.: Rotor time constant updating scheme for a rotor flux oriented induction motor drive. *IEEE Trans. Power Electron.* **14**, 850–857 (1999)
28. Akin E., Ertan H. B., and Uctug M. Y., (1994), “A method for stator resistance measurement suitable for vector control”, *Proc. IEEE Ind. Electron. Soc. Annu. Meeting*, pp. 2122–2126
29. Umanand, L., Bhat, S.: Online estimation of stator resistance of an induction motor for speed control applications. *IEE Proc. Electr. Power Appl.* **142**, 97–103 (1995)
30. Yassine, Koubaa: Recursive identification of induction motor parameters. *Simul. Model. Pract. Theory* **12**(2004), 363–381 (2004)
31. Saravana Kumar, R., Vinoth Kumar, K., Ray, K.K.: Fuzzy Logic based fault detection in induction machines using Lab view. *IJCSNS Int. J. Comput. Sci. Netw. Secur.* **9**(9), 226–243 (2009)
32. Toliyat, H.A., Levi, E., Raina, M.: A review of RFO induction motor parameter estimation techniques. *IEEE Trans. Energy Convers.* **18**(2), 271–283 (2003)
33. Loser, F., Sattler, P.: Identification and compensation of the rotor temperature of AC drives by an observer. In: Conference Record IEEE IAS Annual Meeting, pp. 532–537 (1984)
34. Tzafestas, S.G., Zikidis, K.C.: Neuro FAST: On-line neuro-fuzzy ART-based structure and parameter learning TSK model. *IEEE Trans. Syst. Man Cybern. B* **31**, 797–802 (2001)
35. Uddin, M.N., Radwan, T.S., Rahman, M.A.: Performances of fuzzy-logic-based indirect vector control for induction motor drive. *IEEE Trans. Ind. Appl.* **38**(5), 1219–1225 (2002)
36. Uddin, M.N., Abido, M.A., Rahman, M.A.: Development and implementation of a hybrid intelligent controller for interior permanent magnet synchronous motor drive. *IEEE Trans. Ind. Appl.* **40**(1), 68–76 (2004)
37. Consoli, A., Cerruto, E., Raciti, A., Testa, A.: Adaptive vector control of induction motor drives based on a neuro-fuzzy approach. In: Proceedings of IEEE PESC, pp. 225–232 (1994)
38. Treerong, J.: Induction Motor Fault Detection Based on Parameter Identification Using Genetic Algorithm. *J. KMUTNB.* **20**(3) (2010)
39. Phumiphak, T., Chat-uthai, C.: Estimation of Induction Motor Parameters Based on Field Test Coupled with Genetic Algorithm. Mahanakorn University of Technology, Thailand (1999)
40. Holtz J.: Sensorless control of induction machines—With or without signal injection? *IEEE Trans. Ind. Electron.* **53**(1), 7–30 (2006)
41. Telford, D., Dunnigam, M.W., Williams, B.W.: Online identification of induction machine electrical parameters for vector control loop tuning. *IEEE Trans. Ind. Electron.* **50**(2), 253–261 (2003)
42. Abdelhadi, B., Benoudjit, A., Nait-Said, N.: Application of genetic algorithm with a novel adaptive scheme for the identification of induction machine parameters. *IEEE Trans. Energy Convers.* **20**(2), 284–291 (2005)
43. Levi, E., Sokola, M., Vukosavi, S.N.: A method for magnetizing curve identification in rotor flux oriented induction machines. *IEEE Trans. Energy Convers.* **15**, 157–162 (2000)

44. Levi, E., Vukosavic, S.N.: Identification of the magnetizing curve during commissioning of a rotor flux oriented induction machine. *Proc. IEEE Power Appl.* **146**(6), 685–693 (1999)
45. Levi, E., Sokola, M., Boglietti, A., Pastorelli, M.: Iron loss in rotor flux oriented induction machine: identification, assessment of detuning and compensation. *IEEE Trans. Power Electron.* **11**, 698–709 (1996)
46. Toliyat H. A. and Hosseiny A. A. GH.,(1993), “Parameter estimation algorithm using spectral analysis for vector controlled induction motor drives,” in *Proc. IEEE Int. Symp. Ind. Electron*, pp. 90–95
47. Vukosavic, S.N., Stojic, M.R.: On-line tuning of the rotor time constant for vector-controlled induction motor in position control applications. *IEEE Trans. Ind. Electron.* **40**, 130–138 (1993)
48. Toliyat, H., Arefeen, M.S., Rahman, K.M., Ehsani, M.: Rotor time constant updating scheme for a rotor flux oriented induction motor drive. *IEEE Trans. Power Electron.* **14**, 850–857 (1999)
49. Nasir Uddin, M., Wen Hao.: Development of a self-tuned neuro-fuzzy controller for induction motor drives. *IEEE Trans. Ind. Appl.* **43**(4), 1106–1115 (2007)
50. Nemeč, M., Makuc, D., Ambrožič, V., Fišer, R.: Simplified Model of Induction Machine with Electrical Rotor Asymmetry. ICEM, Rome, Italy (2010)

Development of a Genetic Algorithm Toolkit in LabVIEW

Vineet Kumar, K. P. S. Rana, Amit Kumar, Richa Sharma,
Puneet Mishra and Sreejith S. Nair

Abstract It is a well known fact that LabVIEW is one of the finest tools for measurement and control applications. Requirement of intelligent controller tuning methods like Genetic Algorithm (GA) has been felt at times in the LabVIEW environment as there is no standard LabVIEW GA toolkit supplied with the package. In this paper, a GA Toolkit developed in LabVIEW environment, has been presented. The developed toolkit is used for optimizing the gains of the PID (Proportional plus Integral plus Derivative) controller for the given performance indices of a closed loop system. For the purpose of tuning, the algorithm mimics the biological evolution and is used to find the suitable values of PID gains in order to improve the response of the given system. An integrated performance index comprising of rise time, settling time, overshoot, integral absolute error (IAE), integral square error (ISE), integral time weighted absolute error (ITAE) or a combination of these forms the objective function for the optimization. In this toolkit four selection methods, three crossover methods and three mutation methods have been incorporated. To test the developed toolkit a simulation example is also performed and results have been presented.

Keywords Genetic Algorithm · Virtual instrument (VI) · Selection · Crossover · Mutation · PID · Controller optimisation

V. Kumar (✉) · K. P. S. Rana · R. Sharma · P. Mishra · S. S. Nair
Division of Instrumentation and Control Engineering, Netaji Subhas Institute of Technology,
Sector-3, Dwarka, New Delhi 110078, India
e-mail: vineetkumar27@gmail.com

K. P. S. Rana
e-mail: kpsrana1@gmail.com

A. Kumar
Bhabha Atomic Research Centre, Trombay, Mumbai 400085, India

1 Introduction

PID controllers are most widely used controllers in industries. This is mainly because they have simple control structures, easy to maintain and provide good static and dynamic responses [1, 2]. However, to reach such an objective its parameters must be properly tuned. Improper controller tuning can lead to poor performance, or even to system instability. In control literature, there exist mainly two classes of tuning methods: traditional methods and intelligent methods. Among traditional methods, Ziegler-Nichols (ZN) method is most popular [3]. ZN method is used for linear system which is based on quarter decay ratio. For a wide range of practical processes, this fine-tuning approach works quite well to produce adequate settings of classical PID controllers. ZN technique has some predefined performance indices and in general is not customizable. With the advent of high speed computational power now it has been possible to tune a PID controller to a specific need. Nature-inspired algorithms like GA [4] and particle swarm optimization (PSO) [5] come under the banner of intelligent optimizing techniques offering the above mentioned capability for controller optimization.

GA is known as one of the most effective methods to solve the complex, multi-objective non-linear optimization problems. It is a stochastic global optimization method inspired by biological mechanisms of natural selection and natural genetics which was first developed by Holland [6] and has been widely used in optimizing parameters of PID controller since then [7–10]. This paper endeavors to provide a GA Toolkit designed and developed in LabVIEW 8.6 Development System to tune PID controller. It implements GA using several selection, mutation and crossover methods. A special kind of mutation operator based on PSO is also included [11–14].

The paper is organized as follows. In Sect. 2, a brief about the PID controller have been presented. A general overview of GA has been presented in Sect. 3. A modular approach was adopted for the toolkit development. Details of each module developed have been presented. All the Virtual Instruments (VIs) required in building of complete Toolkit have been dealt with in Sect. 4. To validate the Toolkit, controller gains for a chosen process have been optimized and presented in Sect. 5. Finally, conclusion has been drawn in Sect. 6.

2 PID Controller

Eq. (1) defines the PID controller transfer function.

$$G_{\text{PID}}(s) = K_p + \frac{K_i}{s} + K_d s \quad (1)$$

where $G_{\text{PID}}(s)$ is PID controller transfer function; K_p is proportional gain; K_i is Integral gain; K_d is Derivative Gain and $G(s)$ is plant transfer function.

3 GA Based Tuning

In the developed toolkit, K_p , K_i and K_d of PID controller are optimized with the help of GA in order to get a desired system response. In the context of tuning of PID controller, according to GA terminology, $\{K_p, K_i, K_d\}$ are treated as ‘individuals’, since it is based on the biological evolution. Thus, throughout this paper, individuals and $\{K_p, K_i, K_d\}$ are used interchangeably.

GA operates on a set of individuals called population. In the proposed toolkit, size of the population is user selectable. GA proceeds iteratively, operating on a given population to produce next set of generations. First of all, a group of individuals or one generation set is created randomly. In a given population certain individuals who are found to be ‘fitter’ than others are allowed to mate, thus implementing Charles Darwin’s theory of ‘Survival of the fittest’. Fitness of an individual is measured by a function called fitness function, which involves computation of the output response parameters of the plant using particular values of K_p , K_i , and K_d . The response parameters with which fitness function is evaluated are rise time, settling time, overshoot, IAE, ISE and ITAE. The individuals, who are selected for mating, are called ‘parents’ and are subjected to genetic operators, to produce next set of generation. The genetic operators commonly used in GA are Crossover and Mutation. Crossover is a technique in which pair of individuals is combined together in a variety of fashions to produce a different pair of individuals, whereas Mutation is a technique in which some random changes are introduced in an individual in order to preserve genetic diversity of population. After applying such operators to selected parents, set of individuals produced are called children. Finally, those ‘parents’ which are found to be weaker than their ‘children’ are eliminated and the best set of individuals among parents and children form the next set of generation.

In next section, various VIs (Virtual Instruments) implementing selection, crossover and mutation techniques required for the Toolkit have been explained.

4 Development of Toolkit

In order to develop the proposed GA Toolkit, several modular VIs are developed and then integrated together in a main VI called as Genetic Algorithm.vi. This is done in order to utilize the modular object oriented programming approach of development of GA Toolkit to tune PID controller. Initially, a random array generator VI is used to create the initial population, and then several VIs are developed for selection, crossover and mutation respectively. As there are four techniques for selection, three for crossover, and three for mutation therefore a large number of VIs were required to be developed and integrated into a main program.



Fig. 1 SubVI: random array generator.vi

4.1 Random Array Generator.vi

This VI is used to generate three arrays of random numbers i.e. an array each for K_p , K_i and K_d . Since the random number generator in LabVIEW produces numbers between 0 and 1, so the generated numbers are multiplied by a suitable constant (50) to generate values $\{K_p, K_i, K_d\}$ in a suitable range (0.001–50). It is invoked three times to generate initial population. In subsequent iterations, more optimum values of $\{K_p, K_i, K_d\}$ are evolved. In this case size of the array, population size is given as 50 to this VI which can be altered by user. Figure 1 shows the corresponding subVI.

4.2 Fitness Evaluation.vi

GA determines the fitness of an individual by some sort of fitness function. Fitter the individuals are, more are their chances of being carried forward to the next generation or producing children for the next generation. The Fitness evaluation.vi computes the fitness scores of each individual in a given generation. Values of set of 50 individuals $\{K_p, K_i, K_d\}$ are used by this VI. PID controller is then cascaded with the plant transfer function with the help of standard Control Design (CD) Create PID Academic Model.vi and standard CD Series.vi. Unity gain negative feedback is constructed through standard CD Feedback.vi. Step response parameters of open loop plant function are also computed by standard CD Parametric Time Response.vi. Integral performance indices of closed loop system with PID controller are computed for all sets of $\{K_p, K_i, K_d\}$ as given below.

$$ISE = \sum_{n=0}^N e^2[n]; IAE = \sum_{n=0}^N |e[n]|; ITAE = \sum_{n=0}^N n|e[n]|$$

where, $e[n]$ is calculated using standard CD Get IO time data.vi and standard CD Step Response.vi. Rise time (RT), settling time (ST), overshoot (OS) associated with each individual are calculated using standard CD Parametric Time Response.vi. The used fitness function is defined as

$$\frac{1}{0.001 + w_1 * RT + w_2 * ST + w_3 * OS + w_4 * IAE + w_5 * ISE + w_6 * ITAE} \quad (2)$$

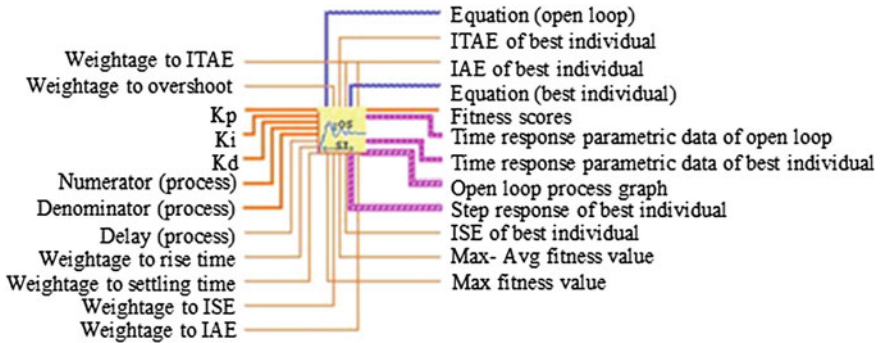


Fig. 2 SubVI: fitness evaluation.vi

where, w_1, w_2, w_3, w_4, w_5 and w_6 are the corresponding weights assigned to RT, ST, OS, IAE, ISE and ITAE. The weights are fed as an input to Fitness Evaluation.vi. The user can choose the weights as required for a specific case under study. All the weights must sum up to one. All the above mentioned parameters as well as step response associated with best individual are obtained as an output of Fitness Evaluation.vi. The block diagram of the developed VI is as shown in Fig. 2.

4.3 VIs for Selection

According to GA implementation requirements, on the basis of fitness scores, parents are to be selected which will undergo further operations like mutation and crossover to generate next set of population. For selection process, four methods are implemented in the developed toolkit and thus, four separate VIs are developed as described below.

4.3.1 Roulette Wheel Selection.vi

This VI implements roulette wheel selection technique. Every individual score i.e. fitness score associated with the set $\{K_p, K_i, K_d\}$ in a given population is mapped to a number between 0 and 1.

$$\text{Modified fitness score} = \frac{\text{Individual fitness Score}}{\sum \text{individuals' scores in population}} \quad (3)$$

To implement Roulette Wheel Algorithm a random number between 0 and 1 is initially generated. Now, the modified fitness scores are summed one by one until the sum is greater than or equal to generated random number. The individual whose value makes the sum over the generated random number is the one which

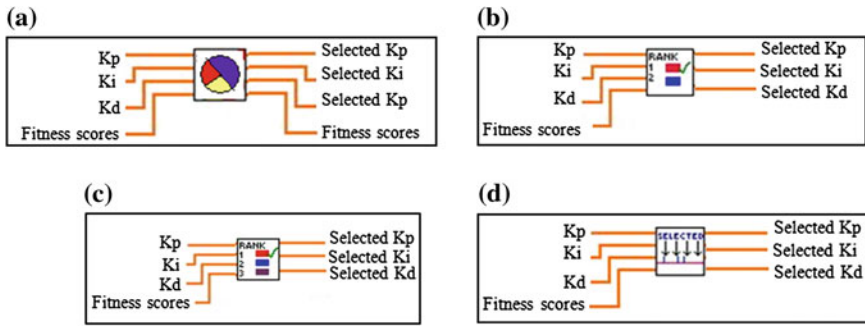


Fig. 3 Selection SubVIs **a** Roulette wheel selection.vi, **b** Rank based selection.vi, **c** Tournament selection.vi, **d** Stochastic universal sampling.vi

gets selected. Roulette Wheel Selection.VI is shown in Fig. 3a. It selects one individual at a time and hence this VI can be invoked as many times as the number of desired parents.

4.3.2 Rank Based Selection.vi

Rank based Selection.VI is shown in Fig. 3b. It selects at random any two individuals in the population and the fitter out of the two is selected. This also may be repeated as many times as the number of desired parents. In the developed toolkit, the number of parents taken was 10 thus requiring the VI to be invoked 10 times.

4.3.3 Tournament Selection.vi

Tournament based Selection.VI as shown in Fig. 3c randomly selects N individuals out of the population and the fittest individual is selected out of them. In the toolkit, N is taken as five thus, a tournament is held between randomly selected five individuals and individual associated with best fitness is finally selected.

4.3.4 Stochastic Universal Sampling.vi

This VI as shown in Fig. 3d implements the algorithm very similar to Roulette Wheel. Unlike the Roulette Wheel, it is able to select the required number of parents in a single go and hence, this VI is not required to be invoked multiple times.

Algorithm followed for Stochastic Universal Sampling is:

- i. For all individuals $\{K_p, K_i, K_d\}$ in a given population, the individual fitness score is normalized to between 0 to 1 to produce modified fitness scores by the formula as mentioned in Eq. (3).


```

ii. The no. of parents selected: 10.
iii. Say variable  $x = 1/10 = 0.1$ 
iv. A random number  $n$  is generated having value between 0 and  $x$ .
v.  $m = 0$ 
vi. for  $i : 1$  to  $N$ 
        while
             $m = m +$  modified fitness score of  $i^{\text{th}}$  individual;
        if ( $m > n$ )
            Select  $i^{\text{th}}$  individual;
            Exit while loop;
        End if
        End while
     $n = n + x$ ;
    End for
End

```

4.4 VIs for Crossover

After individuals are selected, they are required to undergo crossover and mutation process to generate next set of population. In the developed toolkit, three methods of crossover namely Arithmetic Crossover, Single Point Crossover and Two Point Crossover are implemented maintaining a probability of 0.75.

4.4.1 Arithmetic Crossover.vi

Parents' pool is prepared by a selection process which is divided into pairs and the children are produced by following formulae.

$$(k_p, k_i, k_d)_{child1} = x * (k_p, k_i, k_d)_{parent1} + (1 - x) * (k_p, k_i, k_d)_{parent2} \quad (4)$$

$$(k_p, k_i, k_d)_{child2} = x * (k_p, k_i, k_d)_{parent2} + (1 - x) * (k_p, k_i, k_d)_{parent1} \quad (5)$$

where, x is a random number between 0 and 1. Thus, weighted mean of pair of parents is used to generate pair of children as shown in Fig. 4a.

4.4.2 Single Point Crossover.vi

This VI as shown in Fig. 4b is implemented in three stages.

Step1: In this stage, individuals are binary encoded and then concatenated. For example, if gains (K_s) are 8 bit encoded as,

K_p : 10011010

K_i : 10101010

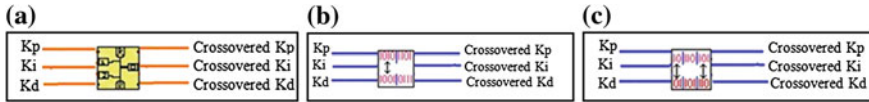


Fig. 4 Crossover SubVIs **a** Arithmetic Crossover.vi, **b** Single point crossover.vi, **c** Two point crossover.vi

K_d : 10110011

Then, the concatenated individual will be a 24 bit number after concatenating K_p , K_i and K_d respectively, i.e. 100110101010101010110011. Concatenation in LabVIEW is done by using $k_p * 2^{16} + k_i * 2^8 + k_d$. Where, K_p , K_i , and K_d are each in the form of 8-bit binary number. As the upper bound on K_p , K_i , and K_d was 50 all these gains could be well represented as 8-bit binary numbers format.

Step 2: This array is further split into two arrays and pairs of parents are formed between corresponding position from 1st and 2nd array. Now, a random crossover site is chosen among a given pair of parents and bits next to crossover site are exchanged to produce encoded children. For example in below mentioned parents crossover site is 4th, the pair of children produced will be as:

Parent1: 10011010 1010 1010 1011| 0011

Parent2: 10011001 1001 1001 1001| 0111

Child1: 1001 1010 1010 1010 1011| 0111

Child2: 1001 1001 1001 1001 1001| 0011

Stage 3: The pairs of children thus produced are combined into a single array using a standard Interleaved 1D Arrays.vi. Then, the concatenated $\{K_p|K_i|K_d\}$ has to be split into individuals K_p , K_i and K_d . Let $\{K_p|K_i|K_d\}$ represents the concatenated individual obtained after crossover, then separate gains are produced as:

$$k_p = \{k_p|k_i|k_d\} \ggg 16 \tag{6}$$

$$k_i = \{k_p|k_i|k_d\} \ggg 8 - [\{k_p|k_i|k_d\} \ggg 16] * 2^8 \tag{7}$$

$$k_d = \{k_p|k_i|k_d\} - [\{k_p|k_i|k_d\} \ggg 8] * 2^8 \tag{8}$$

4.4.3 Two Point Crossover.vi

The difference between the single point crossover and the two point crossover methods is that the two random crossover sites, instead of one, are selected among pair of parents encoded in the binary number. Thus, the only difference between the Two Point Crossover.vi and Single Point Crossover.vi is that the second step is performed twice in it as shown in Fig. 4c.

4.5 VIs for Mutation

After the crossover process next operation is mutation process. Three techniques for mutation namely Uniform Mutation, Mutation based on PSO and Flipping Based Mutation are implemented. These are described as follows.

4.5.1 Uniform Mutation.vi

This VI as shown in Fig. 5a simply replaces any five individuals $\{K_p, K_i, K_d\}$ by some randomly generated individuals. The random number generator is used for both random selection of an individual from the current population and to replace it with a new random value. This mutation is done with the probability of 10 % ($5/50 = 0.1$).

4.5.2 Mutation Based on PSO.vi

In this kind of mutation [11], an individual to be mutated, is updated with the help of PSO algorithms. For example, if X is the new individual after the PSO based mutation operation and X_i is the individual before it. The mutation operation based on the idea of PSO as shown in Fig. 5b is implemented by the following formula.

$$X = w * x + c_1 * r_1 * (50 - X_i) + c_2 * r_2 * (x - X_i) \quad (9)$$

where, 50 is used as the upper bound of K_p, K_i and K_d as adopted in algorithm, x is the optimal individual of former generation, w is inertia weight coefficient, c_1, c_2 are positive constants and r_1 and r_2 are random numbers between 0 and 1. According to the literature [15], $w = 0.7298$ and $c_1 = c_2 = 1.49445$ has been used.

4.5.3 Flipping Based Mutation.vi

This is again implemented in three steps. In the first step, encoded K_p, K_i, K_d values are concatenated as in Single Point Crossover.vi. In the second step, any five bits in array of 50 encoded individuals are flipped and finally, in the third step the concatenated $\{K_p, K_i, K_d\}$ are split into separate K_p, K_i and K_d . So, first step and the third step of this VI is similar to Single Point Crossover.vi. The second step is described as follows.

Let $[K_p, K_i, K_d]_a$ represents a-th element in array of concatenated individuals and $[K_p, K_i, K_d]_{m_a}$ represents the mutated element at ath place of new array produced.

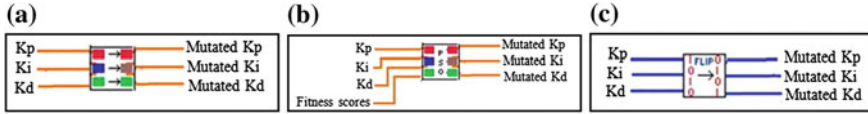


Fig. 5 Mutation SubVIs **a** Uniform mutation.vi, **b** Mutation based on PSO.vi, **c** Flipping based mutation.vi

Step 2:

```

For i : 1 to 5
    j= random number (0,1) * (size of array-1)
    k(binary number) = 2^|(23*random number(0,1))|
    [Kp, Ki, Kd]mj = k xor concatenated [Kp, Ki, Kd]j.
End For
    
```

Thus, in this way any randomly selected kth bit of randomly selected jth element is flipped with the help of standard Exclusive Or.vi. This mutation has been done with probability $(5/(24*10)) = 0.02$. This Vi is shown in Fig. 5c.

4.6 Replacement.vi

After 10 children are produced in given iterations of GA, best 50 individuals out of 50 parents and 10 children are selected based on the fitness score and passed on to the next generation. The algorithm implemented in Replacement.vi is as described below and the code is as shown in Fig. 6.

4.7 Delete Error-Prone Individuals.vi

There might be such values of $\{K_p, K_i, K_d\}$ evolved that result in highly unstable closed loop system and computation of time response parameters like rise time, settling time, overshoot etc. is not possible for them. Such values correspond to a high fitness score of 1000 or above because other parameters are kept zero as they are not computed. To stop such individuals from participating in process of evolution, they are deleted by this VI even before the process of selection takes place. This VI is invoked in Fitness Evaluation.vi so as to consider scoring only after deleting such individuals and then invoked in Replacement.vi to delete unsuitable children. It has Coerce out of bound individuals.vi present in it so that both VIs can be together invoked in main VI. It is shown in Fig. 7.

4.8 Coerce out of Bound Individuals.vi

In the developed Toolkit as mentioned before upper bound on values of $K_p, K_i,$ and K_d is taken as 50 and lower bound is kept at 0. So any $\{K_p, K_i, K_d\}$ crossing such

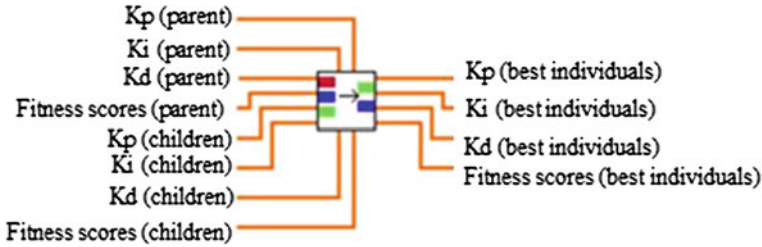
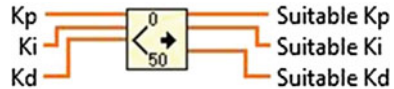


Fig. 6 SubVI : replacement.vi

Fig. 7 SubVI: delete error-prone individuals.vi



Fig. 8 SubVI: coerce out of bound individuals.vi



limit is coerced to 0 or 50 whichever bound is more suitable. This VI as shown in Fig. 8 is invoked in Fitness Evaluation.vi to compute fitness scores of coerced individuals. To pass such coerced individuals in main program Genetic Algorithm.vi, this VI is also invoked in Delete error-prone individuals.vi.

4.9 Genetic Algorithm.vi

The main virtual instrument called Genetic Algorithm.vi integrates all the above mentioned VIs in a coherent way thus acting as a Toolkit for PID controller tuning. The outline of interconnection of VI is shown in Fig. 9. First of all; three random arrays are produced by Random Array Generator.vi for K_p , K_i and K_d respectively. Then Fitness Evaluation.vi computes the fitness of each individual thus obtained. Now the out of bound individuals.vi deletes unsuitable individuals. The VIs for selections are enclosed in a case structure thus asking from user to choose a particular selection method making the program user friendly and interactive. This way several optimizing options are available to the user for exploring various combinations of selections, crossovers and mutation. Then there is Replacement.vi to prepare individuals for next iteration. Appropriate action is invoked for out of bounds individuals. This process is repeated iteratively till the desired results are achieved or user terminated. This yields optimum values of PID parameters as desired.

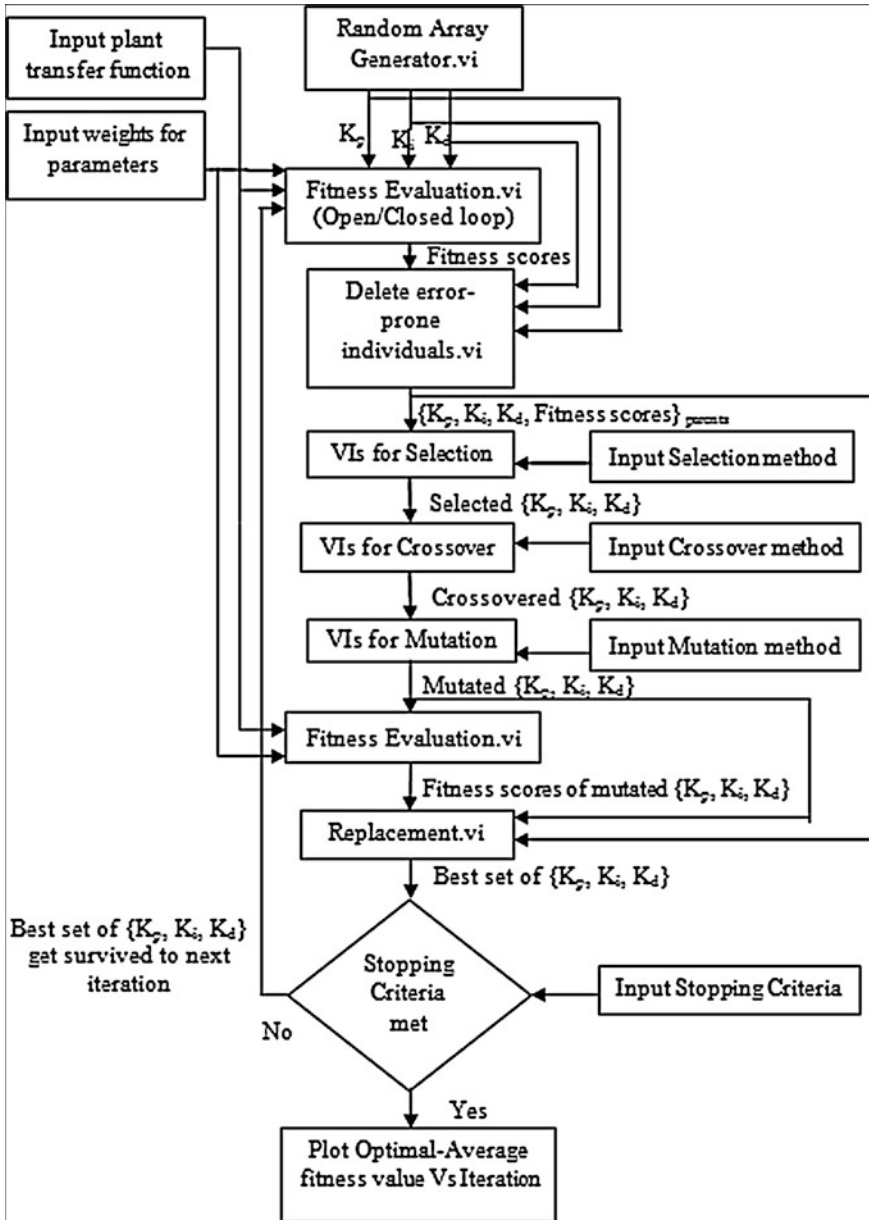


Fig. 9 Interconnection of VIs in genetic algorithm.VI

Fig. 10 Open loop response

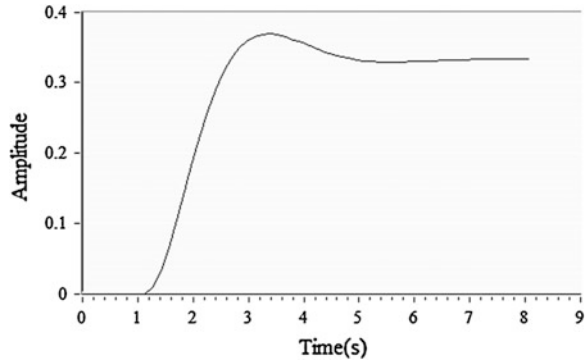


Fig. 11 Time response parameters (open loop)

Time Response Parametric Data of open loop	
Rise Time (s)	Overshoot (%)
0.989949	10.8183
Peak Time (s)	Steady-State Gain
3.39411	0.333333
Settling Time (s)	Peak Value
5.9397	0.369394

5 Simulations and Results

To demonstrate the working step and to test the developed toolkit flowing second order plant with delay of 1s was chosen.

$$G(s) = \frac{e^{-s}}{s^2 + 2s + 3}$$

This plant is optimized for a population of 50 members using tournaments selection, arithmetic crossover and PSO based mutation method. The number of generation is kept 100. The fitness function was design using a weightage of 0.25 for rise time, 0.24 for settling time, 0.5 for over shoot, 0.05 for ISE, 0.05 for ITAE and 0.0 for IAE.

Fig. 12 Best individual

Best individual		
Kp	Ki	Kd
23.8393	29.9618	10.6893

Fig. 13 Closed loop transfer function (optimum solution)

Equation of optimal solution in current iteration

$$e^{-s} \frac{10.6893s^2 + 23.8393s + 29.9618}{s^3 + 12.6893s^2 + 26.8393s + 29.9618}$$

Fig. 14 Time response parameters (optimum solution)

Time Response Parametric Data of best individual		
IAE of best individual	Rise Time (s)	Overshoot (%)
57.7779	0.192639	0.0457099
ISE of best individual	Peak Time (s)	Steady-State Gain
54.9284	4.83525	1
ITAE of best individual	Settling Time (s)	Peak Value
32.771	1.36774	1.00046

5.1 Open Loop Response

Open loop response is the step response of Plant in open loop. Time Response Parameters are also shown among equation of open loop plant and its step response. Open loop response of transfer function of plant to be optimized is shown in Fig. 10 and the corresponding computed time response parameters are shown in Fig. 11.

5.2 Optimal Solution

In every iteration, population consisting of several $\{K_p, K_i, K_d\}$ are evolved because GA doesn't deal with one solution. It deals with certain population of solutions. Since plotting step responses corresponding to all values of $\{K_p, K_i, K_d\}$ would be cumbersome and also difficult to analyze visually together in given iteration, so the step response of closed loop system implemented with PID having most optimum $\{K_p, K_i, K_d\}$ present in given population at each iteration was only plotted. Time response parameters as well as equation of closed loop were also shown. Additionally, a graph is plotted, showing convergence of algorithm indicated by decreasing difference between best fitness score and average fitness score

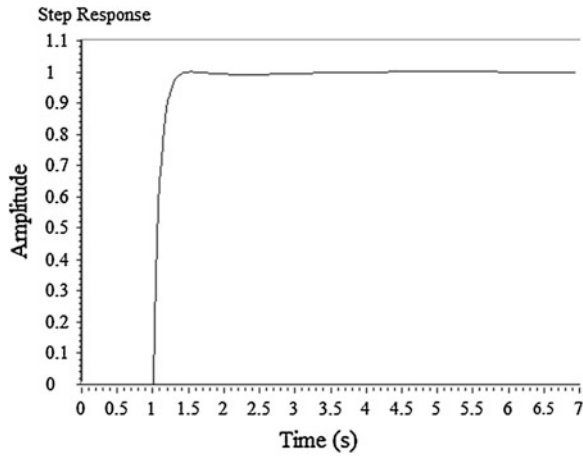


Fig. 15 Step response

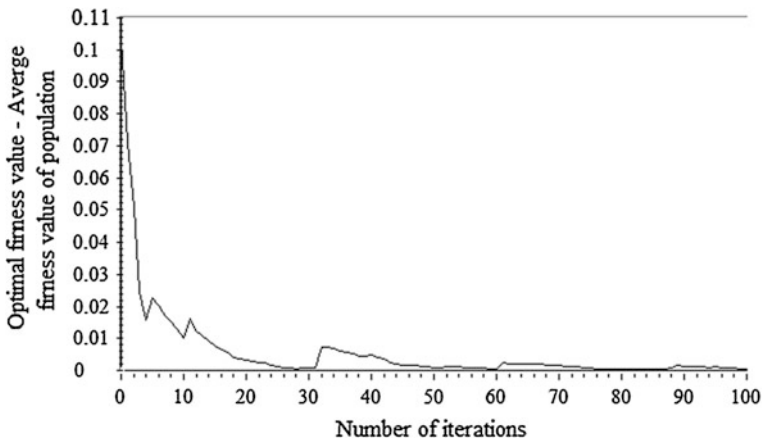


Fig. 16 Convergence graph (optimum solution)

of population. The details of the optimal response after 100 iterations (set as a generation limit) for the chosen second order system to be optimized are shown in Figs. 12, 13, 14, 15 and 16.

5.3 Current Population Archive

This plot shows the convergence plot of the developed toolkit for the test case. The value of the fitness function is plotted against the number of iterations. As seen, very small value of fitness function is obtained, around 70 iterations meaning thereby that the desired solution has been obtained.

6 Conclusion

A step by step procedure has been described for the development of GA Toolkit in LabVIEW environment. LabVIEW, being a software package of very high importance in the measurement and control domain worldwide and the standard package till date is not available with intelligent optimization methods such as GA. This experimentation has demonstrated the capability of LabVIEW for such state of the art optimization method. The experience gain can be extended further for Ant Colony, PSO, Bee, Simulated Annealing, Cuckoo Search, Fish Schooling, Mimetic Optimization etc. The developed toolkit is being used to train the undergraduate/postgraduate students in the Advanced Process Control Laboratory of our Institute. It has been a well appreciated and successful tool among the students offering 144 combinations of various methods. This process will go a long way extending its applications in other areas of engineering optimization.

References

1. Kuo, B.C.: Automatic Control Systems, 5th edn. Prentics-Hall, Englewood Cliffs (1987)
2. Astrom, K., Hagglund, T.: The future of PID control. *Control Eng. Pract.* **9**(11), 1163–1175 (2011)
3. Ziegler, J.G., Nichols, N.B.: Optimum setting for automatic controllers. *Trans. ASME* **64**, 759–768 (1942)
4. Holland, J.H.: Outline for a logical theory of adaptive systems. *J. ACM* **3**, 297–314 (1962)
5. Kennedy, J., Eberhart, R.: Particle Swarm Optimization. IEEE Press, USA (1995)
6. Holland, J.H.: Adaptation in Natural and Artificial Systems. University Michigan Press, Ann Arbor, MI (1975)
7. Wang, P., Kwok, D.P.: Auto-tuning of Classical PID Controllers Using an Advanced Genetic Algorithm. IEEE Press, USA (1992)
8. Zhang, H., Cai, Y., Chen, Y.: Parameter optimization of PID controllers based on genetic algorithm. In: Proceedings of the 2010 IEEE International Conference on E-Health Networking, Digital Ecosystems and Technologies, pp. 47–49 (2010)
9. Fan, L., Joo, E.M.: Design for auto-tuning PID controller based on genetic algorithms. *IEEE ICEA*, pp. 1924–1928 (2009)
10. Sivanandam, S.N., Deepa, S.N.: Introduction to Genetic Algorithm. Springer-Verlag, New York (2008)
11. Zhang, G., Dou, M., Wang, S.: Hybrid genetic algorithm with particle swarm optimization technique. In: Proceedings of the 2009 IEEE, International Conference on Computational Intelligence and security, pp. 103–106 (2009)
12. Galeel, A., Nazir, A., Gautham, Swajan, R., Binu, L.S.: A simplified genetic algorithm for online tuning of PID controller in LabVIEW. In: Proceedings of the 2009 IEEE World Congress on Nature and Biologically Inspired Computing (NaBIC), pp. 1516–1519 (2009)
13. Travis, J., Kring, J.: LabVIEW for Everyone: Graphical Programming Made Easy and Fun, 3rd edn. Prentice-Hall PTR, Upper Saddle River (2006)
14. Manual “LabVIEW Control Design and Simulation Module”. <http://digital.ni.com> (2010). Accessed Jun 2010
15. Bai, M.M., Gan, N.: Improvement and analysis of particle swarm optimization. *J. Sci. Mosaic* **7**(4), 23–26 (2008)

A Soft Calibration Technique for Thermistor Using Support Vector Machine

K. V. Santhosh and B. K. Roy

Abstract This paper aims at designing an calibration technique for temperature measurement using support vector machine. The objectives of the present work are: (i) to extend the linearity range of measurement to 100 % of input range, and (ii) to make measurement technique adaptive to variations in physical parameters of thermistor like reference resistance and temperature coefficient. Support vector machine (SVM) is trained to achieve the proposed objectives. The proposed measurement technique is tested considering variations in physical parameters of thermistor like reference resistance (R_o) and temperature coefficient. Results show that the proposed intelligent technique has fulfilled the set objectives.

Keywords Calibration • Thermistor • SVM • Adaption • Self-retirement

1 Introduction

Temperature is one of the most frequently used process measurements. Almost all chemical processes and reactions are temperature dependent. In chemical plants, temperature is frequently the indication of the progress of a process. Where the temperature is critical to the reaction, a considerable loss of product may result from incorrect measurement of temperatures. In some cases, loss of control of temperature can result in catastrophic plant failure with consequent damages and

K. V. Santhosh (✉)

Department of Instrumentation and Control Engineering, Manipal Institute of Technology,
Manipal, India
e-mail: kv.santhu@gmail.com

B. K. Roy

Department of Electrical Engineering, National Institute of Technology Silchar,
Silchar, India
e-mail: bkr_nits@yahoo.co.in

possible loss of life. There are many other areas of industry in which temperature measurement is essential. Such applications include steam raising and electricity generation, plastics manufacture and moulding, milk and dairy products, and many other areas of food industries. Thus, an accurate and precise measurement of temperature is very important.

Many methods have been developed for measuring temperature. Most of these rely on measuring some physical property of a working material that varies with temperature. Thermistor is one such sensor which finds a wide application in a process industry because of its characteristics like high sensitivity and precision. However in the thermistor the problem of non linearity has restricted its applications. To solve the problem of linearizing a sensor, there are in general two methods, the first one requires nonlinear analog circuit and the second uses numerical methods that are computed by microprocessor or personal computer [1]. The first method has a few practical drawbacks. Further, the whole circuitry may be altered or replaced when there is need to change thermistor to achieve different sensitivity, cost etc. This increases the time and effective cost of the instrument. The last method is preferred because computer is used today for data acquisition and also it has the advantage of linearization on taking into account the effect of disturbing variables. Artificial neural networks are broadly useful in a wide range of applications such as signal and image processing, pattern recognition [2], control systems [3] and recently instrumentation [4].

Literature survey suggests that in [5, 7], linearization of thermistor using neural network algorithms in PSPICE platform. Linearization of thermistor with the help of analog circuits is discussed in [6], for thermistors having Chebyshev-Optimal linearity error. In [8, 11], Linearization over a certain range of thermistor is done using analog circuits. A Generalized method of using neural network for linearization of sensor output is discussed in [9]. Thermistor is linearized over a certain range using LabVIEW software is reported in [10]. Temperature measurement using thermistor is discussed in [12], linearization of sensor is achieved using the frequency modulation techniques. Linearization of thermistor using a dual slope digital converter is reported in [13]. In [14], software is programmed to calculate temperature output from the RTD output over a linear range. Softwares like LabVIEW and Multisim is used to design a calibration circuit for thermistor to linearize its output in [15]. A temperature measurement technique for heat flux measurement in fluid mixing plant using thermistor is discussed in [16], linearization of thermistor sensor is done with the help of analog circuits. Neural network algorithms are used to linearize a certain range of thermistor output is discussed in [17], implementation on FPGA is also reported. In [18], Temperature measurement using thin film gauges for fire fighters gloves is discussed. Linearization of sensor is achieved with the help of analog circuits.

Literature survey suggests a lot of work have been reported on linearization of thermistor output. But most of the reported work concentrates on linearizing a certain range of full scale. Though a few reported works talk on extending the linearity range of sensors, it doesnt talk about making the output of sensor adaptive to variations of physical parameters of sensors. To overcome the above drawbacks

a technique is proposed in this paper, to extend linearity range of thermistor sensor to full scale of input range. Make output adaptive for variation in physical parameters. All these are achieved with use of soft calibration technique trained by SVM.

The paper is organised as follows: after introduction in Sect. 1, a brief description on thermistor model is given in Sect. 2. A brief note on data conversion is given in Sect. 3. Section 4 deals with the problem statement followed by proposed solution in Sect. 5. Result and analysis is given in Sect. 6. Finally, conclusion is discussed in Sect. 7.

2 Thermistor

Thermistors are thermally sensitive resistors and have a negative (NTC) or positive (PTC) resistance/temperature coefficient [19–21]. The negative exponential function that best describes the resistance–temperature (R–T) characteristic of an NTC thermistor can be interpolated using different equations. The Steinhart-Hart equation:

$$R_T = R_o \left(e^{\frac{B(T_o - T)}{T_o}} \right) \quad (1)$$

where

R_T Resistance at T °C

R_o Resistance at T_o °C

B temperature coefficient

3 Data Conversion Unit

The block diagram representation of the proposed instrument is given in Fig. 1.

A voltage divider (also known as a potential divider) is a simple linear circuit that produces an output voltage (V_1) that is a fraction of its reference voltage (V). Voltage division refers to partitioning of a voltage among the components of the divider. The formula governing a voltage divider is given as:

$$V_1 = V \left(\frac{R_T}{R_t + R_T} \right) \quad (2)$$

The output of voltage divider circuit is fed to a buffer amplifier as shown in Fig. 2. The buffer amplifier is a unity gain amplifier. A buffer amplifier is used to transfer a voltage from a first circuit, having a high output impedance level, to a second circuit with a low input impedance level [22, 23].

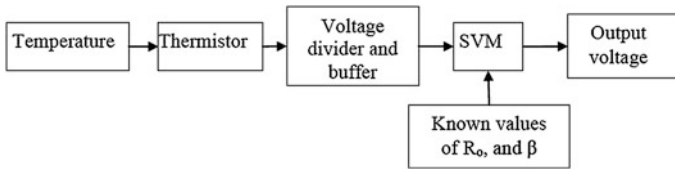
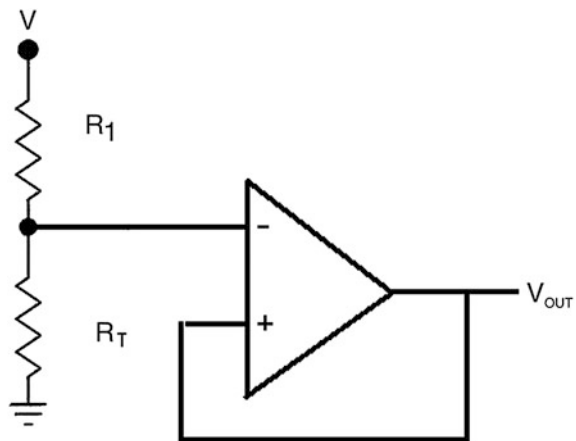


Fig. 1 Block diagram of the proposed measuring technique

Fig. 2 Data conversion circuit for thermistor



4 Problem Statement

In this section characteristic of thermistor is simulated to understand the difficulties associated with available measuring scheme. For this purpose, simulation is carried out with three different reference resistance (R_o) and temperature coefficient (B). These are $R_o = 2000, 4000, \text{ and } 6000$. Further three different B . These are $B = 4000, 8000, \text{ and } 12000$ are used to find the output resistance of thermistor with respect to various values of input temperature considering a particular R_o and B . These output resistances are used as input of data conversion unit and output voltages are generated. Finally voltage signals corresponding to change in temperature is plotted as below.

The MATLAB environment is used of and the following characteristics are simulated.

Figures 3 and 4 show variation of voltages with change in temperature considering different values of reference resistance and temperature coefficient. It has been observed from above graphs that the output from data converter circuit has a non linear relation. Datasheet of thermistor suggests that of 10 to 60 % of full scale input range is used in practice. The output voltage varies with change in reference resistance and temperature coefficient. These are reasons which have made user to go for calibration techniques using some circuits. These conventional techniques have drawbacks that these are time consuming and need to be calibrated every

Fig. 3 Affect of R_o on temperature measurement with thermistor

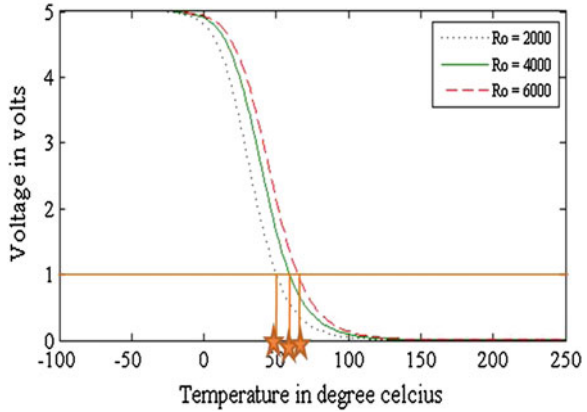
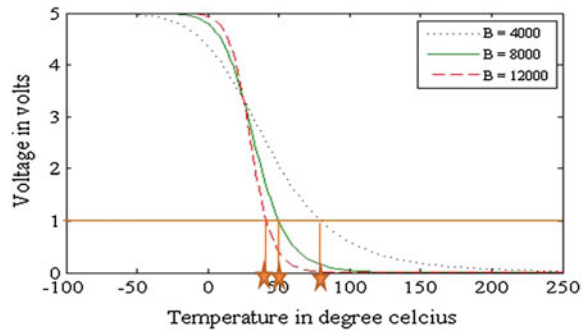


Fig. 4 Affect of B on temperature measurement with thermistor



time when thermistor is changed in the system. Further the use is restricted to a portion of full scale of input range.

In view of all these drawbacks discussed, an attempt has been made for an intelligent temperature measurement by designing an Adaptive Calibration Technique (ACT). The problem statement is as given below: Design an ACT for temperature measurement using thermistor, so as to achieve the following objectives.

1. Linearity range needs to be extended to 100 % of input scale.
2. Same setup of measurement should be capable of giving accurate measurement with changes in R_o and B , all within certain range.

5 Problem Solution

The drawbacks discussed in the earlier section are overcome by adding a Lagrangian Support Vector Machine (LSVM), replacing the conventional calibration circuit, in cascade with data converter unit.

Table 1 Summary of SVM model proposed

Parameters of the SVM model				
Database	20 % training for CV		18	
	20 % training for CV		18	
Projection algorithm	K-mean clustering			
O/P dimension	50 %			
Input optimization	Back elimination			
Input		Temp	R_o	B
	Min	-80 °C	2 k	4000
	Max	240 °C	6 k	12000

When we establish a calibration model of thermistor sensor based on LSVM, we should solve a regression problem indeed. Support Vector Machines provide a framework for regression problem and it can be applied to regression analysis. There is only one kind of sample in LSVM regression analysis and the optimal hyper plane is not to separate the two kinds of samples, but to minimize the margin between all samples and optimal hyper planes [24, 25].

The calibration principle based on LSVM makes use of the input parameters mapped to high-dimensional space by nonlinear transformation function, thus regression analysis can be performed in the high-dimensional space, and finally the Input/Output function can be obtained [26–29].

Considering a set of training data about the thermistor sensor input and output: x_{ik}, y_{ik} , $i = 1, \dots, n$, where x_{ik} R_m is input parameter of thermistor sensor data conversion output for variations in temperature, at different reference resistance and temperature coefficients. y_{ik} R is output parameter of measurement technique for variation of temperature and independent of reference resistance and temperature coefficient.

First, the calibration model should be trained to get the corresponding parameters of the calibration model, such as kernel function, chastisement parameter and error bias and so on. Second, calibration model should make use of the training sampling data to obtain the values of coefficients so as make the relation between input temperature and output voltage linear, and adaptive to variations in temperature coefficients (B), and reference resistance (R_0). If the output error is satisfied, the training ends. Otherwise the calibration model parameters should be adjusted according to the error. Finally, the verifying sampling data should be used to verify the calibration model to determine the parameters of the calibration model (Table 1).

6 Results and Analysis

The proposed LSVM is trained and is subjected to various test inputs corresponding to different temperature with a particular reference resistance and temperature coefficient, all within the specified range. The testing data used are different from data used for training. For testing purposes, various parameters are

Table 2 Simulation results of proposed intelligent temperature measurement with thermistor

AT in °C	R_o in ohms	B	MT in °C	% error
-80	3000	4500	-80.0078	-0.0098
-80	3500	4800	-79.9993	0.0009
-80	3800	5100	-80.0099	-0.0124
-40	4000	5000	-40.0022	-0.0055
-40	4500	5200	-39.9973	0.0067
-40	5200	6900	-40.0064	-0.0160
0	5000	5700	0.00033	0.000
0	5500	6200	-0.00095	0.000
0	5280	7100	0.00026	0.000
40	3250	6750	40.0055	-0.0137
40	3750	7250	39.9993	0.0018
40	4120	7630	40.0066	-0.0165
80	4250	7750	80.0058	-0.0072
80	4750	8250	79.9922	0.0098
80	4400	9100	80.0091	-0.0114
120	5250	8610	120.0103	-0.0086
120	5750	9250	119.9899	0.0102
160	3100	10200	159.9833	0.0104
160	3400	10850	160.0136	-0.0085
160	5800	7050	159.9864	0.0085
200	3600	11350	199.9962	0.0019
200	3800	8600	199.9892	0.0054
200	4200	6500	199.984	0.0080
240	4100	1580	239.983	0.0071
240	5800	1895	240.036	-0.0150
240	5200	6000	239.984	0.0067

chosen within the specified ranges, the range of temperature is considered from -80 to 240 °C. The outputs of the proposed technique with LSVM are noted corresponding to various input pressures with different values of R_o and B . The results are listed in Table 2.

where

- AT Actual temperature in °C
- MT Measured temperature in °C

It is evident from Table 2, that the proposed measurement technique has incorporated intelligence. Mean square of % error for 27 different simulated test conditions is 0.00911 %. It has increased the linearity range of the thermistor to 100 % of input range. Also, the output is made adaptive to variations in the reference resistance and temperature coefficient (Figs. 5 and 6).

Fig. 5 Actual vs measured temperature in simulation for temperature measurement with thermistor

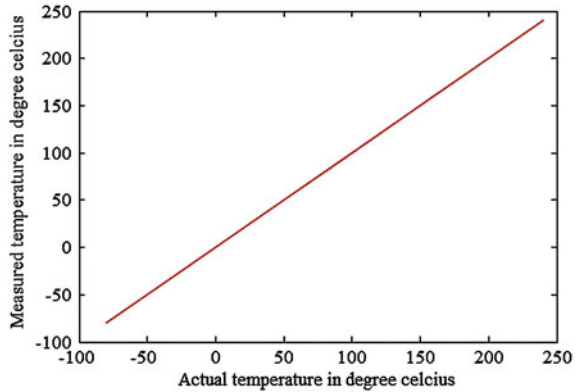
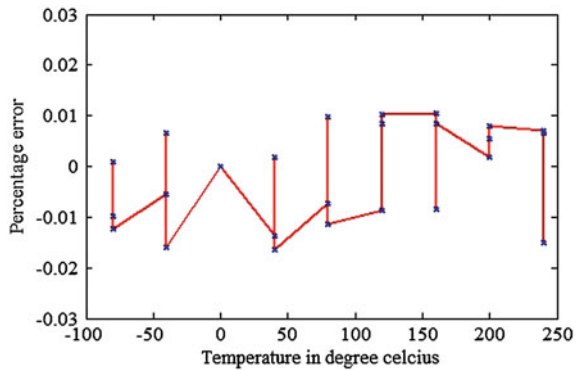


Fig. 6 Percentage error in simulation for temperature measurement with thermistor



7 Conclusion and Future Scope

Available reported works have discussed different techniques for calibration of temperature measurement, but these are not adaptive of variations in physical parameters, like reference resistance and temperature coefficient. Hence, repeated calibration is required for any change of physical parameters of thermistor like reference resistance and temperature coefficient. Sometime the calibration circuit may itself be replaced which is a time consuming and tedious procedure. Further, most of the reported works have not utilized the full scale of measurement. In comparison to these, the proposed measurement technique achieves linear input output characteristic for full scale input range and makes the output adaptive to variations in physical parameters of thermistor, reference resistance, and temperature coefficient.

In the present proposed technique is tested with simulation work, real life implementation and testing is planned as for future.

References

1. Attari, M.: Methods For Linearization of Non-Linear Sensors. In: Proceedings of CMMNI-4, Fourth Maghrebin Conference on Numerical Methods of Engineering, Algiers (Algeria), vol. 1, pp. 344–350 (1993)
2. Freeman, J.A.: Neural Networks—Algorithms, Applications, and Programming Techniques. Addison-Wesley, Massachusetts (1992)
3. Aggoune, M.E., Boudjema, F., Bensenouci, A., Hellal, A., Vadari, S.V., El Mesai, M.R.: Design of an adaptive-structure voltage regulator using artificial neural networks. In: Proceedings of the 2nd IEEE Conference on Control Applications, Vancouver, Canada, Sept 1993, pp. 337–343 (1993)
4. Pau, L.F., Johansen, F.S.: Neural Network Signal Understanding for Instrumentation. IEEE Trans. Instrum. Meas. **39**(4), 558–564 (1990)
5. Wang, L.M., Ma, L.Y., Huang, Y.: A general neural network-based approach to modeling sensors in PSPICE simulation. In: Proceedings of International Conference on Natural Computation, Hainan, China (2007)
6. Renneberg, C., Lehman, T.: Analog circuits for thermistor linearization with Chebyshev-optimal linearity error. In: Proceedings of European Conference on Circuit Theory and Design, Seville (2007)
7. Wang, L.M., Deng, Y.F., Zhao, X.L., Liu, B.L.: A neural network-based approach for creating a ntc thermistor model library for PSPICE. In: Computational Intelligence and Security Workshop, Hong Kong, Oct 2008 (2008)
8. Nenova, Z.P., Nenov, T.G.: Linearization circuit of the thermistor connection. IEEE Trans. Instrum. Meas. **58**(2), 441–449 (2009)
9. Khan, S.A., Shahani, D.T., Agarwala, A.K.: Sensor Calibration and Compensation using Artificial Neural Network. ISA Trans. **48**, 143–144 (2009)
10. Tsai, C.-F., Li, L.-T., Li, C.-H., Young, M.-S.: Implementation of thermistor linearization using LabVIEW. In: Proceedings of International Conference on Intelligent Information Hiding and Multimedia Signal Processing, Kyoto, Japan (2009)
11. Balraj, A., Patvardhan, A., Renuka Devi, V., Aiswarya, R., Prasen, V.: Embedded temperature monitoring and control unit. In: Proceedings of International Conference on Recent Trends in Information, Telecommunication and Computing, Kochi, India (2010)
12. Dey, D., Munshi, S.: Simulation studies on a new intelligent scheme for temperature measurement using thermistor in 555 timer circuit. Int. J. Smart Sens. Intell. Syst. **3**(2), 217–229 (2010)
13. Madhu Mohan, N., Jagadeesh Kumar, V., Sankaran, P.: Linearizing dual-slope digital converter suitable for a thermistor. IEEE Trans. Instrum. Meas. **60**(5), 1515–1521 (2011)
14. Hambali, N., Saat, S., Ramli, M.S., Hazmi, M.: Automatic detection computer-based (ADCob) system for temperature measurement calibration of RTD. In: Proceedings of International Conference on Electrical, Control and Computer Engineering, Pahang, Malaysia (2011)
15. Weng, Z., Zhou, R.: Design and simulation of temperature measurement circuit based on LabVIEW and multisim. In: Proceedings of Second International Conference on Mechanic Automation and Control Engineering, Mongolia, China (2011)
16. DAleo, F.P., Prasser, H.-M.: Design, calibration and testing of a thin film temperature gauge array for temperature and heat flux measurements in fluid mixing experiments. J. Flow Meas. Instrum. **24**, 29–35 (2012)
17. Sonowal, D., Bhuyan, M.: FPGA implementation of neural network for linearization of thermistor characteristics. In: Proceedings of International Conference on Devices, Circuits and System, Coimbatore, India (2012)
18. Mrugala, D., Ziegler, F., Kostelnik, J., Lang, W.: Temperature sensor measurement system for firefighter gloves. In: Proceedings of Eurosensors, Poland (2012)
19. Steinhart, J.S., Hart S.R.: Calibration curves for thermistors. Deep Sea Res. **15**, 497 (1968)

20. Neubert, H.K.P.: Instrument Transducers—an Introduction to their Performance and Design. Clarendon Press, Oxford (1975)
21. Bosson, G., Guttman, F., Simmons, L.M.: Relationship between temperature and resistance of a thermistor. *J. Appl. Phys.* **21**(12), 1267–1268 (1950)
22. Deoblin, E.O.: Measurement Systems Application and Design, 3rd edn. Mc Graw Hill, New York (2005)
23. Pallas-Areny, R., Webster, J.G.: Sensors and signal conditioning, 2nd edn. A Wiley-Interscience Publication, New York (2001)
24. Chang, C.-C., Lin, C.-J.: LIBSVM. A library for support vector machines (2001). Available via <http://www.csie.ntu.edu.tw/~cjlin/libsvm>
25. Xuegong, Z.: Statical learning theory and support vector machines. *Acta Automatica Sinica.* **26**(1), 32–42 (2000)
26. Suykens, J.A.K., Vandewalle, J.: Least Squares Support Vector Machine Classifiers. Kluwer Academic Publisher, Netherlands (1999)
27. Schokopf, B., Smola, A.: Learning with Kernels: Support Vector Machines, Regularization, Optimization and Beyond. MIT Press, Cambridge (2002)
28. Suykens, J.A.K., Gestel, T.V., Brabanter, J.D., Moor, B.D., Vandewalle, J.: Least Squares Support Vector Machines. World Scientific Publishers Co, Singapore (2002)
29. Gestel, T.V., Suykens, J.A.K., Baesens, B., Viaene, S., Vanthienen, J., Dedene, G., De Moor, B., Vandewalle, J.: Benchmarking least squares support vector machine classifiers. *J. Mach. Learn.* **54**(1), 5–32 (2004)

Discrete Cuckoo Search Optimization Algorithm for Combinatorial Optimization of Vehicle Route in Graph Based Road Network

Chiranjib Sur and Anupam Shukla

Abstract Cuckoo Search (CS) Algorithm is a well-known and successful nature inspired meta-heuristics which mimics the salient life-style feature of cuckoo bird and has been widely applied in various continuous domain problems, search analysis and optimization. The algorithm mostly depends on the random placement of the constrained value(s) of variable at the solution set and is being evaluated by the fitness function. There is also provision for slow increment of the solution variable for local search. But here in this paper we have concentrated on the development and application of a modified version of the algorithm called Discrete Cuckoo Search Optimization Algorithm (DCSO) for discrete problem domain like that of the graph based problem and other combinatorial optimization problems like traveling salesman problem etc. The algorithm is first tested on the Travelling Salesman Problem benchmark datasets and then it is applied on a road based graph network for optimization with respect to a non-weighted fitness function of travel time and waiting time and is compared with Ant Colony Optimization (ACO) and Intelligent Water Drop (IWD).

Keywords Discrete cuckoo search · Combinatorial optimization · Path planning heuristics · Travelling salesman problem · Road network optimization

C. Sur (✉) · A. Shukla

Soft Computing and Expert System Laboratory, ABV-Indian Institute of Information Technology and Management, Gwalior, India
e-mail: chiranjibsur@gmail.com

A. Shukla

e-mail: dranupamshukla@gmail.com

1 Introduction

Path planning in a graph based environment has always been challenging combinatorial optimization problem when the problem environment is large, unexplored and multi-objective optimization is required through a fitness value consisting of a weighted summation of two factors. It requires quick searching and at the same time near optimal solution because for a huge graph the normal shortest path finding algorithms will take a huge amount of time. Due to the dynamic parameters of the network if the results obtained are not quick enough then it will be of no use. Hence the researcher has indulged on random dependent heuristics which has proven to have sought out solution much quicker and efficiently. One such group of heuristic algorithm mimics the various principles of the nature and its habitats. Cuckoo Search is such a nature inspired meta-heuristics which has been widely used for optimization, but in continuous ones. In this paper a discrete version of the CS is introduced which suits constrained graph based and combinatorial optimization problems. The requirement of the discrete version was badly felt due to the large number of discrete optimization problems which are present in the real world and need to be addressed. One such problem is the route optimization of the road network confining within the present infrastructure. After primary test of the algorithm for the TSP, the road network is simulated with it and considerable improvement is achieved (against minimum distance preference) for optimized path with respect to total, travelling and waiting time. The rest of the paper is arranged as [Sect. 2](#) describing the road network and assumptions considered for simplification, [Sect. 3](#) provides brief of cuckoo's lifestyle, [Sects. 4](#) and [5](#) describe cuckoo search and its discrete version, [Sect. 6](#) illustrates its scope with [Sect. 7](#) providing the results of its application for TSP benchmarks, [Sect. 8](#) presents the algorithm for route search with computational results in [Sect. 9](#) and conclusions in [Sect. 10](#).

2 Model for Road Network

The Discrete Cuckoo Search Optimization Algorithm is being applied on a road network for route optimization for proper guidance and management of vehicles and the results have shown its ability for optimization as a heuristics. The road network graph (consisting of 25 nodes and 45 edges) is shown in [Fig. 1](#).

The network possess several paths and each of the edges has distance and average waiting time as its parameters and the overall fitness is calculated by the summation of all the parameters of the edges of the derived path. The fitness function is kept simple and non-linear non-weighted sum of traveling time and waiting time. The main purpose of the CSOA algorithm is finding the best path for the vehicles and analyzes the variation in total time and thus compare with the Ant Colony Optimization and Intelligent Water Drop algorithms for optimized path.

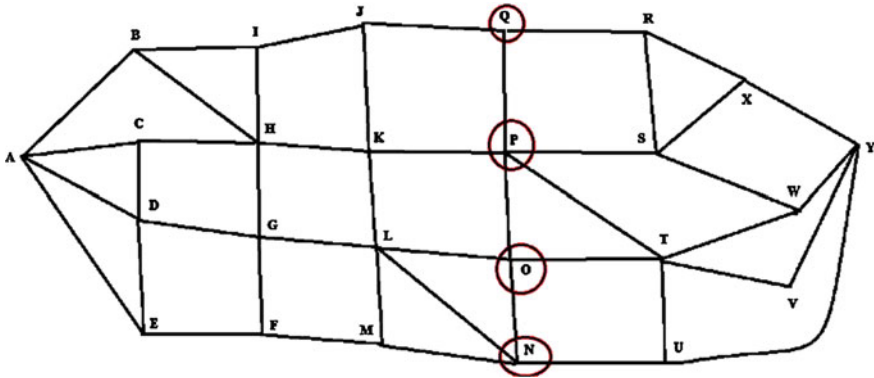


Fig. 1 Road network graph used for simulation

$$f_1 = \sum_{k=1}^{K=n} D_k \ \& \ f_2 = \sum_{k=1}^{K=n} AWT_k \tag{1}$$

where f_1 and f_2 are the two equations and D_k is the distance and AWT_k is the average waiting time for the path $k \in \{i, j\}$ where i and j are the two nodes and there exist a link between them. Fitness function is defined as $f = (f_1/V + f_2)$ where V is the velocity normalization factor to make both f_1 and f_2 of the same time unit and f_1/V becomes travelling time.

There are various assumptions considered for the simplicity of the road network and its vehicles and all agents and calculations are regarded as ideal. The road is considered to be of same width but the lengths between two nodes are considered as the distance which varies according to the model. So at times change in velocity when a broad road meet a narrow one and vice versa are ignored because the aim of the paper and its results totally focus on the performance of the nature inspired meta-heuristics. The vehicles are considered as of uniform dimension and capable of moving with non-accelerating velocity and thus the unnecessary minute details of the vehicle movement and also the minute variations are abstracted from the calculation. Another important assumption is the average waiting time, which is in constant variation with respect to overall road network. It is assumed that the presence of other vehicles in the road network produces an overall change in the waiting time and is considered as approximate average waiting time.

3 Life-Style and Breeding Habit of Cuckoo Bird

Before describing the Discrete Cuckoo Search Optimization Algorithm it is justified if the lifestyle of the bird is studied, so that the steps and its implications are clear and acceptable. The cuckoo bird has the typical “obligate brood parasitism” characteristic also called belligerent reproduction tactic and requires the home

(nests), parental attention and feedings of other birds for fledging their hatched young so that the young bird is raised under the surrogate parents. So they breed by laying eggs on other bird's nest and are intelligent enough to make sure that the size and other visible characteristics of the host bird matches with its own. Also to make space and to keep the count of the eggs near constant, the cuckoo is brutal enough to push down the eggs of the host bird, which also does the same of throwing away the suspected eggs out of the nest or dump the whole nest if anyhow it can detect the eggs present are not its own. Later when the young cuckoo hatches, they also show significant intelligence by pushing down the host bird's eggs to ensure gathering of larger share of the food from the host bird. Not only that they even mimicry the screaming of the host bird's chick to create more feeding opportunity. These features of cuckoo bird are being molded to suit the optimization problem scenario considering the bird as the operator and the eggs (also young hatched cuckoo) as the individual variable value of the solution set. In the subsequent sections the details of the algorithm is discussed along with the modifications and enhancements done to suit the algorithm for the graph based problem.

4 Cuckoo Search Optimization Algorithm

Cuckoo Search was introduced by Xin-she Yang and Deb [1] and then on several works has been done using the meta-heuristics and has reached a successful status with its usage ranging from nurse scheduling [2], optimization of web service composition [3], neural network training [4] and spiking neural network [5] training, data fusion in wireless sensor network domain [6], test data generation and structural soft-ware testing and nonetheless the traditional knapsack problem solution [7]. The basics of the classical Cuckoo Search [1] Algorithm, on which the operations are dependent, are:

1. Each cuckoo one egg at a time, and dumps it in a randomly chosen nest;
2. The best nests with high quality of eggs (solutions) will carry over to the next generations;
3. The number of available host nests is fixed, and a host can discover an alien egg with a probability $p_a \in [0, 1]$. In this case, the host bird can either throw the egg away or abandon the nest so as to build a completely new nest in a new location.
4. A Levy flight is performed by $x(t+1) = x(t) + \alpha * Levy(\lambda)$ for $\alpha > 0$.

The algorithm works well for the continuous domain problems and the Levy flight has helped the algorithm in creating a local search of the algorithm. But if it is utilized for the discrete combinatorial problems then Levy flight will be of no utilization. Hence a modified version of the algorithm called Discrete Cuckoo Search Optimization Algorithm is developed with some extra operations which will favor the graph based search problems.

5 Discrete Cuckoo Search Optimization

The Discrete Cuckoo Search Optimization Algorithm is described in the following steps with details of the steps:

Step 1: Nests Creation by host birds [Random Initialization of solution sets]

Step 2: Cuckoo lays eggs at an arbitrary nest [Generate node number, nest number and position for the operation]

Step 3: Cuckoo may throw away (replace existing solution) the host bird eggs or may not (add the solution), before laying. [Strategy depends on the problem, like in TSP the former suits while the latter suits graph search problems like in route planning problem]

Step 4: The host bird (upon detection with probability P_d) may throw away eggs as alien eggs. [Reject some nodes randomly from any position of existing solution set]

Step 5: Newly hatched cuckoo bird may push the host eggs down [Considering that the eggs, both host's and cuckoo's, and the newly hatched birds are solutions that constitute the solution set. Now difference between Step 4 and Step 6 is that in Step 4, certain numbers of random eggs are thrown away randomly irrespective of fitness, but in Step 6 the worst eggs are thrown away by the newly hatched birds born out of better eggs.]

Step 6: The newly hatched mimics the cries of the host and tries to attract more share of attention and food. [This step is vital for problems where the sequence of the nodes is necessary and very important and is a prevention for constrained discrete problems where may happen that the right node may not matched up with the right position due to probability and hence this step will actually provoke right nodes attracting right nodes through the process of checking each an arbitrary node with irregularity of the node sequence, but is actually employed at the later iteration stage when may be many of the solution sets of constrained scenario need one node for completion. This step is equivalent to the process that only the hungry bird is fed.]

Step 7: The host bird may throw away the eggs or abandon the nest for a new one. [This is equivalent to rejecting the worst set of solutions and gets the best lot for the next iteration/generation of the next generation or iteration. However if the system is dynamic and the system parameters are changing like that of the road network or processes in a factory chain, then the previous generation is not required for the next generation as no more it remains the best solution lot. It is better to start a new search or let the whole population survive considering that one from the worst lot may be-come the global best of the next solution.]

Step 8: The best nests pass on to the next generation.

6 Scope of Discrete Cuckoo Search

The Discrete Cuckoo Search Optimization Algorithm has wide number of application in the discrete domain of problems starting from combinatorial optimization problems like quadratic assignment problem, knapsack problem, n-queen problem, vehicle routing problem, etc. (of which travelling salesman problem is already taken up in the paper and is simulated with several datasets) and graph based problems like optimized route planning, graph coloring problem, etc. Not only this it has application in various optimization problems fields of other fields and can be utilized in VLSI design optimization, software development cycle optimization, process scheduling problems, cost minimization problems and all other problems where it is required to use random searches in an unknown environment and the solution needs to be taken out of huge number of combination possibilities. The most important feature of the CSOA is the adaptiveness it can incorporate in the solution set through variable numbers of solution members and is most suitable for problems like vehicle routing problem, multi-processor task scheduling where all the processors/vehicles may not be taking part in the event.

7 Results of Application of DCSO in TSP

The travelling salesman problem (TSP) is a famous discrete combinatorial problem which has various real life applications starting from graph based problems, to VLSI, and many mechanical engineering problems and is being widely considered as a benchmark test bed for consideration of analysis of performance of heuristic algorithms. In this work we have tested the DCSO for eight different dimensional TSP and each of them are run for 15000, 35000 and 50000 iterations and the variations of result are investigated. Tables 1, 2 and 3 has shown the result of simulation of the DCSO on the various dimensions of the TSP of the dataset repository [8]. The table has provided the dataset Id, dimensions, mean, standard deviations (SD), best case, worst case, and error. The patterns of the Global Best with change in iterations number for the various dimensions of the TSP are also plotted in Fig. 2.

Form the plot of Fig. 2 it is clear that with the increase in the dimension, we can get better minimal optimization with increase in the number of iterations.

8 Methods and Algorithms

The details of the algorithm and the data structures applied on the road network are described in this section.

Table 1 Results of application of DCSO for different TSP datasets (15000 iteration)

Data set id	Cities	Mean	SD	Global best	Global worst
bayg29.tsp	29	1.77E + 04	566.3376	1.7104e + 004	3.3938e + 004
berlin52.tsp	52	2.24E + 04	666.6126	2.1651e + 004	3.6037e + 004
kroA100.tsp	100	1.39E + 05	1434.8984	1.3783e + 005	2.0331e + 005
ch130.tsp	130	3.86E + 04	303.9852	3.8193e + 004	6.1777e + 004
ch150.tsp	150	4.65E + 04	334.3546	4.6016e + 004	5.4882e + 004
rat195.tsp	195	1.92E + 04	469.11433	1.8571e + 004	2.5892e + 004
a280.tsp	280	3.03E + 04	293.92799	3.0033e + 004	3.8126e + 004
pa561.tsp	561	2.01E + 05	645.2067	1.9979e + 005	2.2633e + 005

Table 2 Results of application of DCSO for different TSP datasets (35000 iteration)

Data set id	Cities	Mean	SD	Global best	Global worst
bayg29.tsp	29	1.75E + 04	330.7355	1.7280e + 004	3.4699e + 004
berlin52.tsp	52	2.19E + 04	505.8623	2.1338e + 004	3.5732e + 004
kroA100.tsp	100	1.37E + 05	1784.8667	1.3454e + 005	2.1247e + 005
ch130.tsp	130	3.90E + 04	198.6043	3.8784e + 004	5.3383e + 004
ch150.tsp	150	4.55E + 04	728.57321	4.4689e + 004	6.2446e + 004
rat195.tsp	195	1.95E + 04	195.35011	1.9335e + 004	2.6335e + 004
a280.tsp	280	3.03E + 04	139.4322	3.0206E + 004	3.7782E + 004
pa561.tsp	561	1.98E + 05	1222.4123	1.9743E + 005	2.2869E + 005

Table 3 Results of application of DCSO for different TSP datasets (50000 iteration)

Data set id	Cities	Mean	SD	Global best	Global worst
bayg29.tsp	29	1.74E + 04	341.7806	1.7122e + 004	3.4679e + 004
berlin52.tsp	52	2.21E + 04	364.03606	2.1627e + 004	3.5749e + 004
kroA100.tsp	100	1.33E + 05	1956.7724	1.3039e + 005	2.0847e + 005
ch130.tsp	130	3.92E + 04	153.08059	3.9071e + 004	5.3585e + 004
ch150.tsp	150	4.54E + 04	419.3745	4.4973e + 004	6.1946e + 004
rat195.tsp	195	1.92E + 04	127.1757	1.9108e + 004	2.6140e + 004
a280.tsp	280	3.00E + 04	364.5216	2.9741E + 004	3.8255E + 004
pa561.tsp	561	1.97E + 05	2814.6211	1.9365E + 005	2.2737E + 005

DCSO FOR OPTIMIZED ROUTE SEARCH

Step 1: Initialize Road Network Graph matrix and Road parameter matrix for edges $\{p_1, p_2, \dots, p_k\}$ for k parameters. Here $k = 2$.

Step 2: Initialize N nests (solution sets) and each of the nests with a short random length solution for each nest. A unit bit string marker is initialized with 0 (for incomplete path) and can be 1 (for complete path)

Step 3: Initialize the fitness matrix

Step 4: Prevent Duplicity of nodes and Evaluate the fitness of the initial strings

Step 5: Perform Cuckoo lays eggs at an arbitrary nest

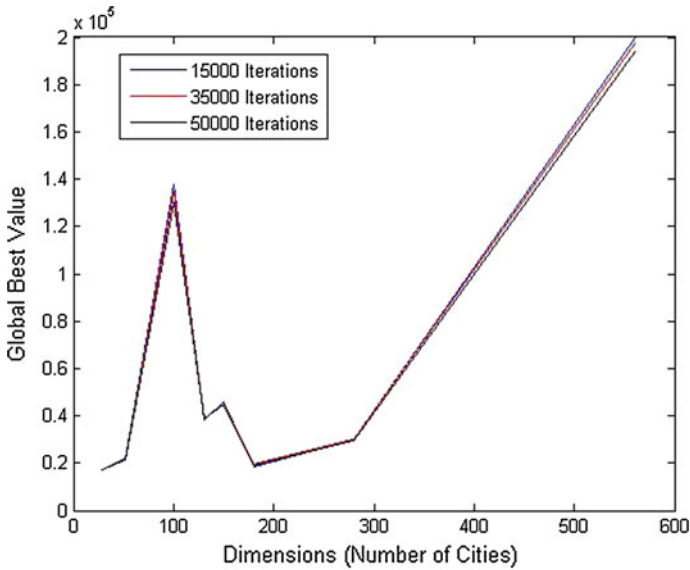


Fig. 2 Variation of the global best with change in dimensions and iterations

Step 6: Perform Cuckoo may throw away the host bird eggs or may not, before laying.

Step 7: Perform The host bird (upon detection with probability P_d) may throw away eggs as alien eggs.

Step 8: Perform Newly hatched cuckoo bird may push the host eggs down

Step 9: Perform The newly hatched mimicry the cries of the host and tries to attract more share of attention and food.

Step 10: Perform The host bird may throw away the eggs or abandon the nest for a new one.

Step 11: Perform The best nests passes on to the next iteration.

Step 12: If the path is found complete then mark the string marker as 1 and no operations are performed on it.

Step 13: Evaluate Fitness of each complete string set of solution or with string marker as 1.

Step 14: When the numbers of solutions are greater than a certain percentage of the total number of strings then Update the Global Best result with the best complete path depending upon the Primary Fitness.

Step 15: Check Condition for stopping or Start from Step 1. [As the system is dynamic the next iteration must start from the initialization]

Step 16: If iteration is complete provide the Best path for guiding the vehicles.

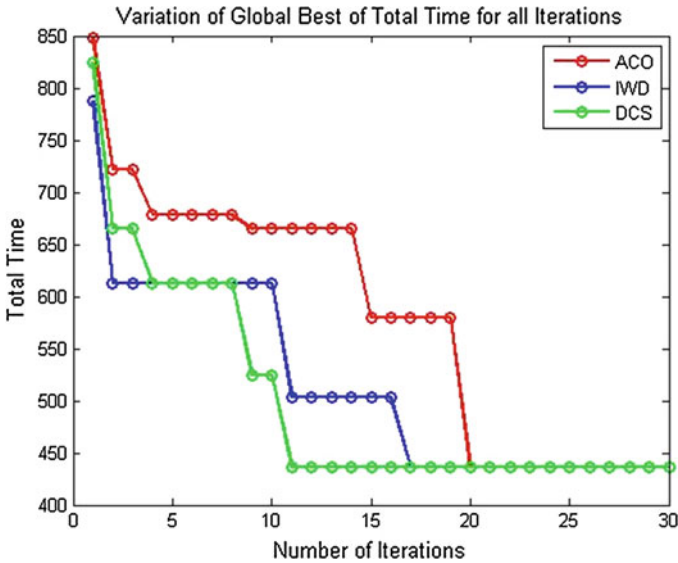


Fig. 3 Variation of the global best of total time for all iterations

9 Results of DCSO Applied in Road Network

The following are resultant graphs of the simulation carried out on the road network shown in Figs. 3, 4, 5, 6, 7, 8, 9, 10 and 11. From Figs. 3, 4 and 5 the change in global best or the convergence rate is revealed where it has shown that the Discrete Cuckoo Search has better performance mainly in total time analysis.

Our focus was on total time and the simulation was executed on Total time analysis. However the two parameters separately are also plotted to see how the algorithm perform. It must be noted that the Travelling time and Waiting time analysis is not done separately but on the run when Total time (Travelling time + Waiting time) analysis is performed. Figures 6, 7 and 8 has shown how the cumulated optimized Total time, Travelling time and Waiting time look for the same event. The average of the same cumulated optimized Total time, Travelling time and Waiting time is shown in Figs. 9, 10 and 11.

In most cases DCSO has out-performed the other two algorithms. In the cases of Travelling time and Waiting time, the performance of DCSO is not up to the mark because of Step 10 of Sect. 8. Where the elimination of the nest or solution set is based on Total time and hence only the best paths with respect to Total time survived which may not have been enough for optimization with respect to Travelling time and Waiting time.

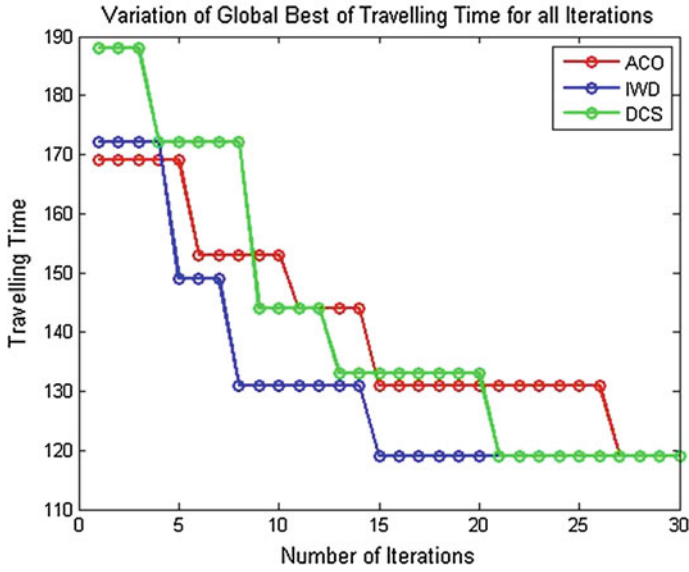


Fig. 4 Variation of the global best of travelling time for all iterations

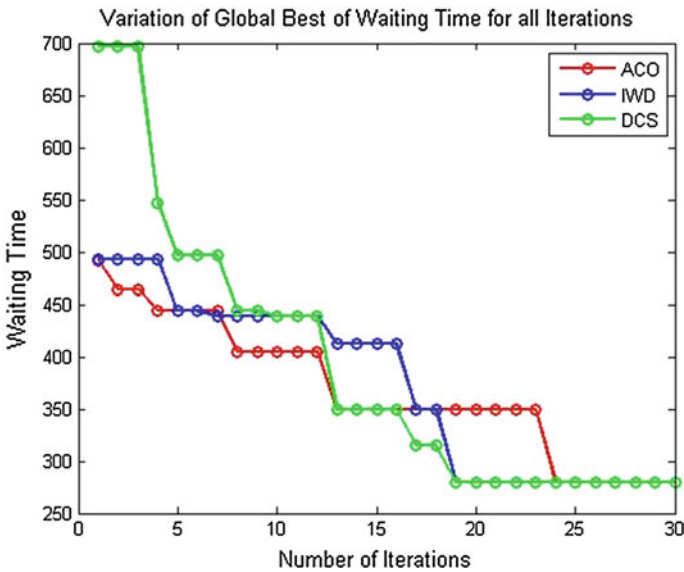


Fig. 5 Variation of the global best of waiting time for all iterations

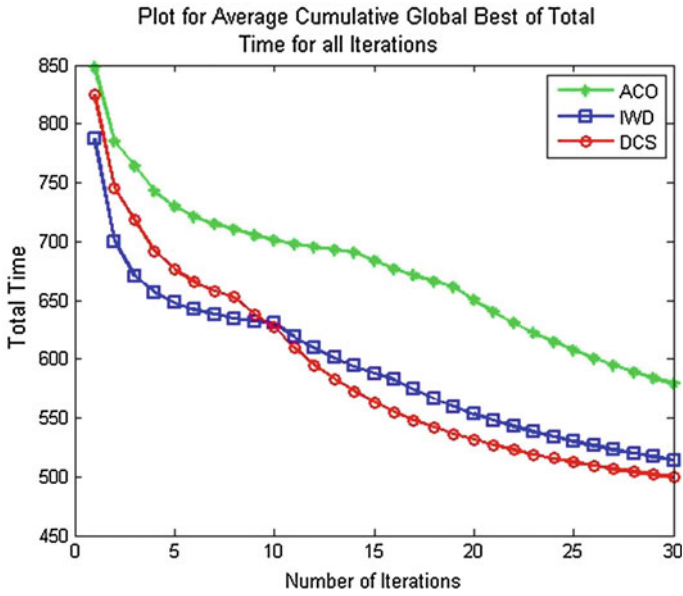


Fig. 6 Plot for average cumulative global best of total time for all iterations

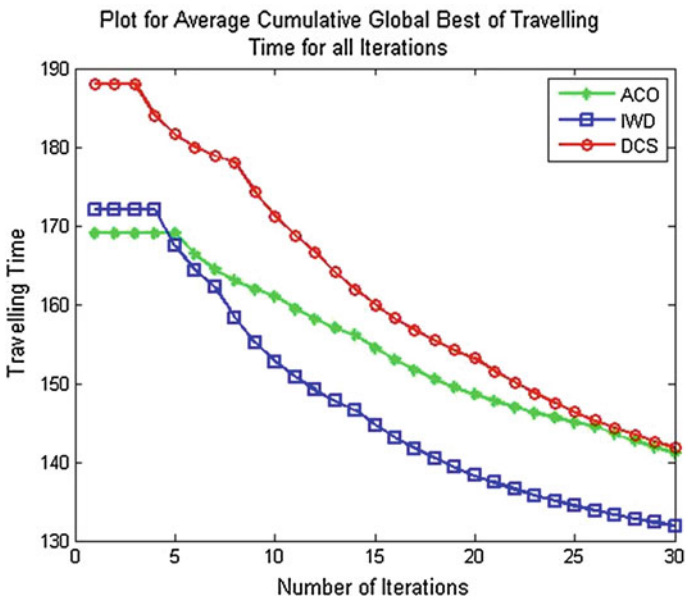


Fig. 7 Plot for average cumulative global best of travelling time for all iterations

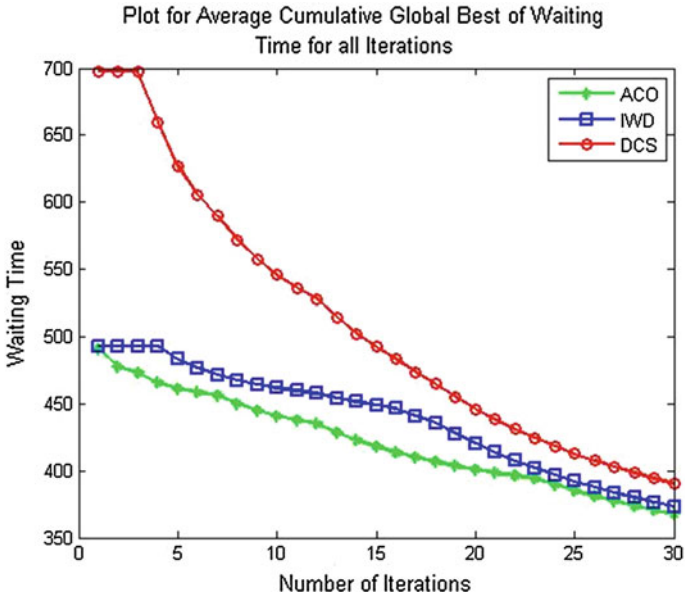


Fig. 8 Plot for average cumulative global best of waiting time for all iterations

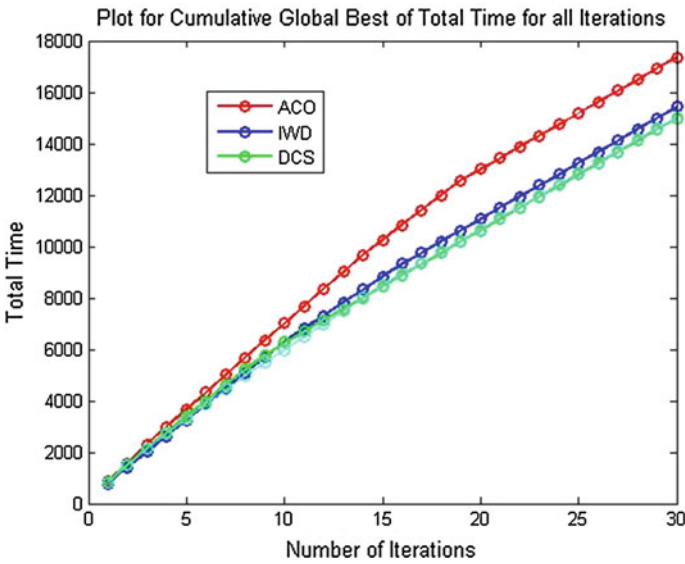


Fig. 9 Plot for cumulative global best of total time for all iterations

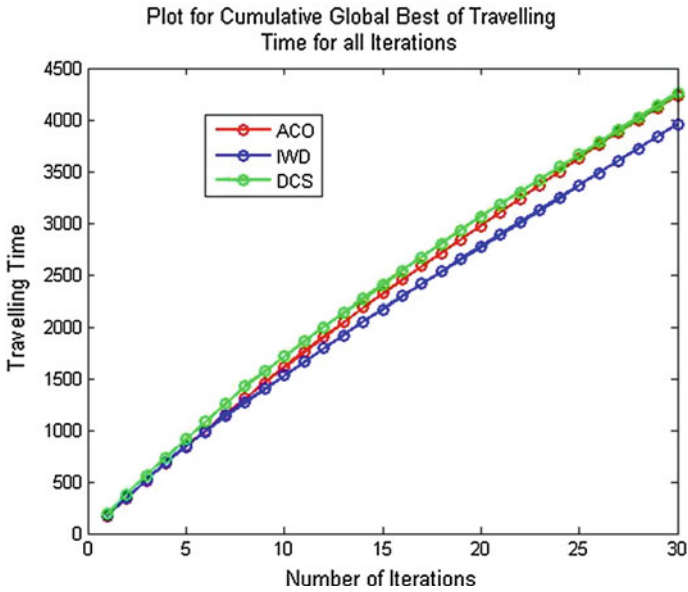


Fig. 10 Plot for cumulative global best of total time for all iterations

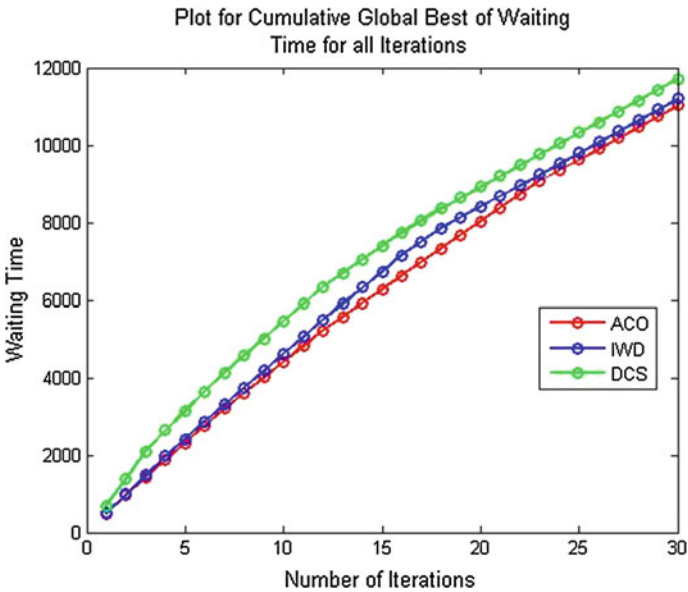


Fig. 11 Plot for cumulative global best of total time for all iterations

10 Conclusion

So a modified version of Cuckoo Search called Discrete Cuckoo Search, which can be applied for graph based and discrete event based problems, is presented. The results shown in the above section clearly indicate the capability of the Discrete Cuckoo Search Optimization Algorithm in handling graph based combinatorial optimization problems and generated good result for the routing problem for the road network system and has actually helped in finding the least time based route. Instead of choosing the least travel time route the problem has opt for the optimized route with respect to the total time. Overall it can be seen that in the road graph, DCSO has been able to perform well cumulatively for waiting time, total time and travel time. Also the results of the TSP dataset have given its ability and scalability for a wide range and gradual increase in performance with the increase in iterations.

References

1. Yang, X.-S., Deb, S.: Cuckoo search via levy flights. In: Proceedings of World Congress on Nature Biologically Inspired Computing (NaBIC 2009), pp. 210–214, 2009
2. Tein, L.H., Ramli, R.: Recent advancements of nurse scheduling models and a potential path. In: Proceedings 6th IMT-GT Conference on Mathematics, Statistics and its Applications (ICMSA 2010), pp. 395–409, 2010
3. Chifu, V.R., Pop, C.B., Salomie, I., Suia, D.S., Niculici, A.N.: Optimizing the semantic web service composition process using cuckoo search. In: Intelligent Distributed Computing V, Studies in Computational Intelligence, vol. 382, pp. 93–102, 2012
4. Valian, E., Mohanna, S., Tavakoli, S.: Improved cuckoo search algorithm for feedforward neural network training. *Int. J. Artif. Intell. Appl.* **2**(3), 36–43 (2011)
5. Vazquez, R.A.: Training spiking neural models using cuckoo search algorithm. In: 2011 IEEE Congress on Evolutionary Computation (CEC'11), pp. 679–686, 2011
6. Dhivya, M., Sundarambal, M.: Cuckoo search for data gathering in wireless sensor networks. *Int. J. Mobile Commun.* **9**, 642–656 (2011)
7. Layeb, A.: A novel quantum inspired cuckoo search for knapsack problems. *Int. J. Bio-Inspired Comput.* **3**(5), 297–305 (2011)
8. TSP Datasets—<http://www.iwr.uni-heidelberg.de/groups/comopt/software/TSPLIB95/tsp/>
9. Yang, X.-S., Deb, S.: Engineering optimization by cuckoo search. *Int. J. Math. Model. Numer. Optim.* **1**, 21–32 (2010)
10. Sur, C., Sharma, S., Shukla, A.: ‘Analysis and modeling multi-breed mean-minded ant colony optimization of agent based road vehicle routing management’. In: 2012 International Conference for Internet Technology and Secured Transactions, pp. 634–641, Dec 2012
11. Sur, C., Sharma, S., Shukla, A.: “Egyptian vulture optimization algorithm—a new nature inspired meta-heuristics for knapsack problem”. In: The 9th International Conference on Computing and Information Technology (IC2IT2013), vol. 209, pp. 227–237, 2013
12. Sur, C., Sharma, S., Shukla, A.: “Solving travelling salesman problem using Egyptian vulture optimization algorithm—a new approach”. In: 20th International Conference on Intelligent Information Systems, (IIS 2013), vol. 7912, pp. 254–267, 2013
13. Sur, C., Sharma, S., Shukla, A.: “Multi-objective adaptive intelligent water drops algorithm for optimization and vehicle guidance in road graph network”. In: 2013 International Conference on Informatics, Electronics and Vision (ICIEV), pp. 1–6, 17–18 May 2013

Introducing a Novel Parameter in Generation of Course Timetable with Genetic Algorithm

Ravitashaw Bathla, Shubham Jain and Rajeev Singh

Abstract In this paper, we introduce a new Happiness parameter along with Genetic Algorithm for generating course timetable. This happiness parameter will generate appropriately feasible solution and account for the comfort and happiness of the instructor and students both (indicating the appropriateness of the resulting solution). The final result obtained from this approach shows that the solution space is reduced considerably and hence a feasible solution is obtained. Using this parameter, it can also be analysed that the solution obtained from Genetic Algorithm without Happiness Parameter are unfavourable most of the times. We perform experiments on data of Department of Computer Engineering, G.B. Pant University of Agriculture and Technology, Pantnagar and are able to produce promising results.

Keywords Genetic algorithm · Timetable · Scheduling · Happiness parameter

1 Introduction

The university timetabling problem can be considered as the task of assigning a number of events, such as lectures, exams; to a limited set of timeslots (and rooms), in accordance with a set of constraints. The constraints vary greatly from

R. Bathla (✉) · S. Jain · R. Singh
Department of Computer Engineering, G.B. Pant University of Agriculture and Technology,
Pantnagar, Uttarakhand, India
e-mail: ravitashawbl_270@hotmail.com

S. Jain
e-mail: sj38711@gmail.com

R. Singh
e-mail: rajeevpec@gmail.com

university to university, since all have their own specific requirements. The timetabling problem is an NP-Hard problem [1]. This is very difficult to solve using conventional methods or manually and costs a lot of resources, time and money [2].

Among several timetable related problems in academic domain, the Course Timetabling and Exam Scheduling problem are prominent one. The two problems exhibit very similar characteristics and have different requirements depending upon institutional needs. The course timetable problem deals with assigning one event per room per timeslot and involve allocation of events to a fixed set of timeslots. The exam scheduling problem involves multiple event scheduling in a single classroom at the same time (provided seating capacity constraints are not violated) and allow flexibility in number of timeslots. In this paper, we have chosen the Course Timetable Problem as it provides more versatile problem domain and the set of constraints are robust.

The various constraints that might be imposed on a particular timetabling problem also varies according to the level of impact and importance of each of the constraint. The constraints are usually divided into two categories: Hard constraints, and the soft constraints [3]. The priority is given to hard constraints over soft constraints. A timetable is considered feasible if all the hard constraints are satisfied [4] and are usually same for most of the universities. Meanwhile, soft constraints are those that should be obeyed if possible, and vary with universities. Most universities will have their own idiosyncratic set of constraints according to their requirement that make their timetabling problem different from others. These eccentric behavior of soft constraints for each university make it very difficult for the generalization of the problem [5].

We propose to generate an appropriate feasible timetable solution using our new Happiness parameter along with Genetic Algorithm. The Happiness parameter is implemented after the application of Genetic Algorithm, on those solutions that have fitness value of 1.0. Using this parameter, feasible solution(s) is (are) obtained and the solution space is reduced considerably.

The rest of paper consists of 7 sections. [Section 2](#) showcases related work done in the field. [Section 3](#) describes the problem description in detail. [Section 4](#) presents the standard Genetic Algorithm. [Section 5](#) presents the proposed methodology including the new happiness parameter. [Section 6](#) contains results and discussions of the experiments performed and finally [Sect. 7](#) concludes the work done.

2 Related Work

The work done by Bambrick [6], presents Genetic Algorithm for solution of timetable problem with repair strategy. The final solution is selected stochastically from all the random solutions that have fitness count of 1.0. Sometimes least feasible (non-appropriate) solutions are obtained as final solution because the

solution space is wide enough. These non-appropriate solutions also exists with feasible solution, all having fitness 1.0.

According to the work presented by Abdullah and Turabieh [7], local search is used for optimization of the solution after implementation of Genetic Algorithm. Local search technique optimizes the solution by reducing the number of soft constraints. An additional computational cost is incurred in doing this optimization. The optimization is implemented on the fittest solution in the population which limits the final solution, as final solution is the result of further optimization of that fittest solution.

Yang and Jat [8] have implemented local search and guided search technique along with Genetic Algorithm for solution of the course timetable problem. An additional data structure in guided search technique was used that stores information about the events that have zero penalty value [2]. This data structure is used every time a new generation is produced for passing of traits to new generations.

3 Problem Description

In course timetable problem, a set of events (Lectures, Practical and Tutorials) have to be allotted to fixed number of rooms and timeslots within a week for instructors and group of students [7].

In this paper, we generate the timetable of Department of Computer Engineering, G.B. Pant University of Agriculture and Technology. The course structure is defined such that each course bears a number of credit hours. The credit hours designates the total number of lectures and practical. The tutorials are not mandatory for all courses. They are not included in the total credit hours. A course titled Operating System with course number TCT324 having 3 credits with 2 lectures, 2 tutorials and 1 practical is represented as TCT324(2-2-1).

The basic data for our problem is:

1. 12 courses of different credits (including 7 practical for 7 different courses)
2. 7 instructors to which the above courses have been assigned
3. 2 rooms where the lectures would be held.

The detailed list of courses of Department of Computer Engineering, G.B. Pant University for a selected semester are described in the Table 1.

The hard constraints that are incorporated in the problem, as described in [6] are as:

1. A classroom must not be booked twice at one time.
2. Each event must be allotted exactly once.
3. Students must not have multiple classes simultaneously.

Table 1 Data of Department of Computer Engineering, G.B. Pant University of Agriculture and Technology of a selected semester for generation of course timetable

S. No.	Abbreviation	Course name	Credits	Year
1	DS	Data structure	3(3-1-0)	II
2	DSS	Discrete structure	3(3-0-0)	II
3	FLAT	Finite language and automata theory	3(3-1-0)	II
4	FCCS	Fundamentals of computer communications systems	4(3-1-1)	II
5	PL	Programming language	3(3-1-0)	II
6	SYP	System programming	4(3-0-1)	III
7	DBMS	Database management system	4(3-0-1)	III
8	ORS	Operational research	2(2-1-0)	III
9	MIS	Management information system	3(2-0-1)	III
10	CA	Computer architecture	3(2-1-1)	IV
11	DMW	Data mining and warehousing	3(2-1-1)	IV
12	CGA	Computer graphics and animations	4(3-0-1)	IV

4. The classroom must have enough capacity to hold the allotted group of students.
5. Instructors must not be booked twice for one particular timeslot.
6. An instructor must not be allotted a lecture, laboratory or tutorial when he/she is unavailable. E.g. an instructor might have prior commitments.

The soft constraints, as described in [6] have been exempted from consideration since they vary greatly with respect to departments and universities.

4 Genetic Algorithm

Genetic Algorithms (GA) are adaptive systems inspired by natural evolution used for solving complex problems and for searching of large problem spaces. The power of GA lies in the fact that they are capable of finding the global optimum in multi-modal spaces [9]. This characteristic makes GA a well suited tool for timetabling problem.

4.1 Evolutionary Process

The Genetic Algorithm is derived from the process of evolution in nature, as stated by Charles Darwin [10]. This is done by generating a population of individuals represented as Chromosomes, in essence a set (an array) of character, binary or decimal strings [11]. The individuals in the population go through the process of evolution. Thus, producing new individuals in the population.

Initially, a fixed amount of random chromosomes (individuals) are generated equal to the population size. The fitness of these randomly generated individuals are evaluated using the defined constraint data. The individuals that are most fit i.e. having the highest maximum fitness value, are used for breeding to generate new chromosomes. This process is called Selective Breeding [6]. The chromosome produced after breeding is named as Generation. The new individual generated is again evaluated for its fitness value and if it has a better fitness value than the remaining in the population, the chromosome is added to the population and the one with least fitness value is discarded from consideration. The total number of individuals in a population (population size) remains constant throughout [10]. This process is repeated either depending upon the requirements or until a valid solution is obtained.

4.2 Genetic Algorithm Operators

4.2.1 Crossover

Once fitness of a chromosome is calculated, parents are chosen for breeding with maximum fitness value. A new creature is produced by selecting a part (a gene) of the chromosome from the first parent and another gene from the second parent. This process of combining genes is called Crossover. A crossover point is selected where the genes are formed from the chromosome. If one point is selected, it is called single-point crossover. Once the new chromosome has been produced it is added into the population [2, 12].

4.2.2 Mutation

After performing Crossover and before releasing child into the population there are chances that mutation may need to be performed. The probability of occurrence of mutation is called mutation rate [11]. Mutation is a process of injecting small genes or noise into the existing or newly generated chromosome. The need of mutation arises when the chromosome produced is very unfit or has the solution that is far from required. Thus, a noise is injected into the chromosome, for increasing its chances to be included in the chromosome [2, 5, 13].

5 Proposed Methodology

Initially, a colony is established using random variables with colony size equal to population size. The fitness value of these randomly generated individuals (chromosomes) are calculated and sorted accordingly. Since, the colony size is equal to the population size no offspring is discarded (killed) at this time.

If the randomly generated individuals have fitness value of 1.0, the happiness value is calculated (one at a time) for such chromosomes directly. This happiness value is initially stored in the memory. If there is more than one individual with fitness value of 1.0, the happiness value is calculated for all such individuals. The initially stored happiness value in the memory is overridden, if at later stages the individuals are found to have happiness value greater than the value stored previously.

If the randomly generated individuals do not have fitness value of 1.0, they are bred to generate offspring. The breeding is performed on those individuals (parents) which have maximum fitness value. The two parents bred together to generate an offspring. Again, the fitness value of the newly generated offspring is calculated. If the newly generated offspring has fitness value greater than the minimum value of fitness in the colony, the newly generated offspring is added into the colony and the offspring with the minimum fitness is discarded from the colony. This process of breeding continues until offspring with fitness value of 1.0 is not obtained.

The Happiness value is calculated for the new individuals in the colony with fitness value of 1.0. And again, if the happiness value is found to be greater than the value stored in the memory; the old value is overridden with new happiness value. This entire process is repeated until total generations are produced. The flow chart for genetic algorithm along with happiness parameter is shown as a schematic diagram in Fig. 1.

Before calculating fitness value, the timetables are checked for any error that might occur as a result of random timetable generation or due to breeding. A concept of repair strategy is used to produce repaired timetables. This is a part of hybrid Genetic Algorithm, as suggested by Gen and Cheng [14].

Some genes of the chromosomes are outside the search space. This might include for example, two timetable bred to form a new timetable and in the resulting timetable one class has more than one instance [2, 6].

In this paper, there are two stages of repair strategy used for repairing errors caused by breeding of timetables as proposed by Bambrick [6]. Firstly, a class may be booked more than once in a timetable. The total number of one type of classes booked are calculated and if more than one instance of the class is found, a randomly chosen class is altered as null booking. Secondly, a class may not be booked at all in the resulting timetable. Thus, all rooms are searched for that class and if no room is found with that class, a null booking is taken randomly and class is allotted to that null booking.

5.1 Repair Strategy

Before calculating fitness value, the timetables are checked for any error that might occur as a result of random timetable generation or due to breeding. A concept of repair strategy is used to produce repaired timetables. This is a part of hybrid Genetic Algorithm, as suggested by Gen and Cheng [14].

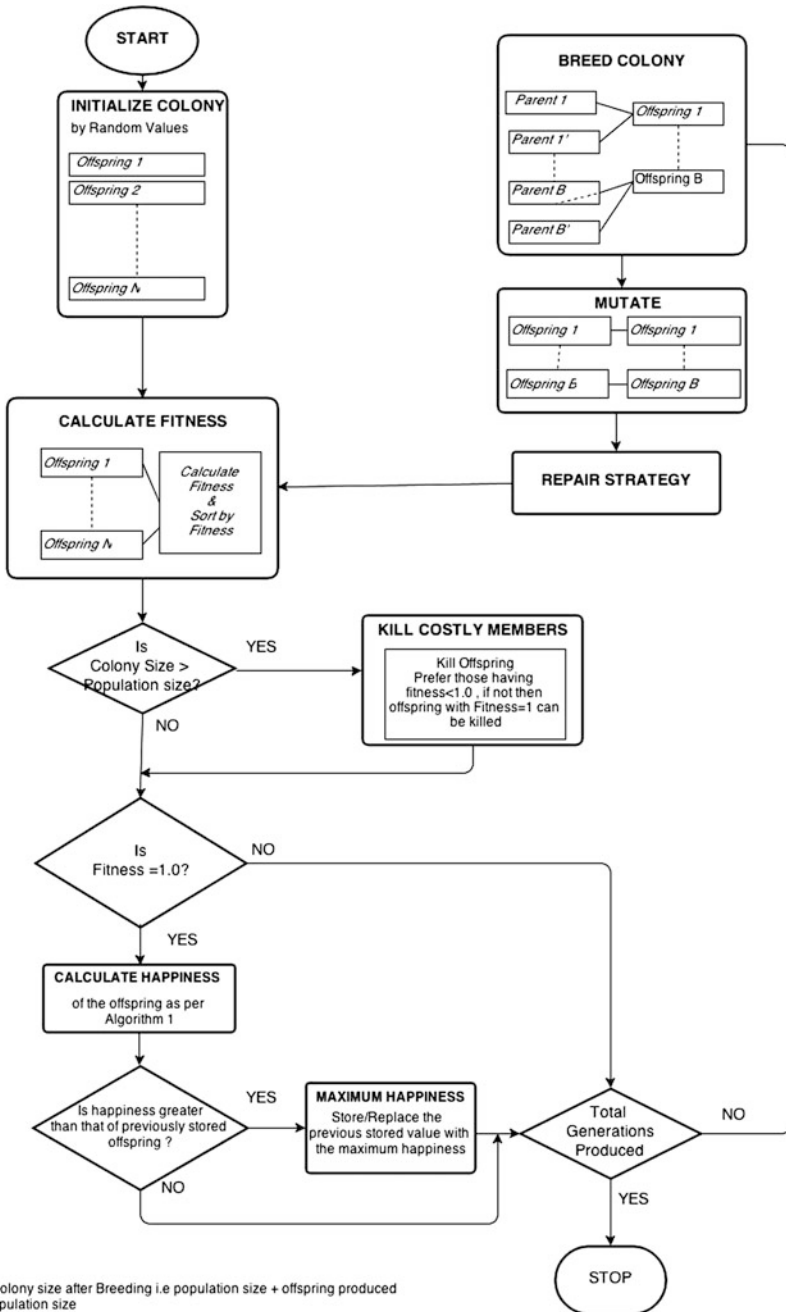


Fig. 1 Flowchart for generating course timetable using GA and happiness parameter

5.2 Happiness Parameter

The happiness parameter calculates happiness of the entire timetable. The happiness parameter is calculated after implementation of GA on those individuals that have fitness value of 1.0.

The Happiness parameter is the sum of number of free time slots an instructor has after which no lectures are scheduled for that particular day, for all days of the week. A penalty (-1) is added for every lecture scheduled early morning 08:00–09:00 and/or immediately after lunch (13:00–14:00) from 14:00–15:00. The algorithm to calculate happiness parameter is shown in Algorithm 1.

The formula to calculate the Happiness value is:

$$\text{Happiness} = \sum_{i=0}^n \{(\text{Total Timeslots (i.e. 8)} - \text{Position of last lecture for } i \text{ day}) - p\}$$

Where, i = Number of Working days {Mon, Tue, Wed, Thu, Fri, Sat}, and

$$\text{Penalty, } p = \begin{cases} -1, & \text{If a lecture is scheduled at 08:00 – 09:00 OR 14:00 – 15:00} \\ -2, & \text{If a lecture is scheduled at 08:00 – 09:00 AND 14:00 – 15:00} \end{cases}$$

Algorithm 1: Algorithm for calculating Happiness Parameter

Input: Timetable

Output: Happiness parameter value

```

var day = {Mon, Tue, Wed, Thu, Fri, Sat}
var timeslot = {08:00-09:00, 09:00-10:00, 10:00-11:00,
11:00-12:00, 12:00-13:00, 13:00-14:00, 14:00-15:00,
15:00-16:00, 16:00-17:00}
var Happiness = 0;
var free_timeslots = 0;
var last_allocated_timeslot = 0;
var total_timeslot = size of 'timeslot' array;
for days = 0 to 5 do
  Calculate last_allocated_timeslot;
  free_timeslots = total_timeslot - last_allocated_timeslot;
  Happiness = Happiness + free_timeslots;
  for timeslot = 0 to 8 do
    if Lecture allocated at timeslot = 08:00-09:00
      OR 14:00-15:00
    then
      Happiness = Happiness - 1;
    end
    else If Lecture allocated at timeslot =
      08:00-09:00 AND 14:00-15:00
    then
      Happiness = Happiness - 2;
    end
  end
return Happiness;
end

```

Table 2 Specification for genetic algorithm

S. No.	Parameters	Quantity
1	Number of generations	20,000
2	Population size	50
3	Number of working days	6
4	Number of timeslots each day	8

6 Results and Discussion

The proposed algorithm was programmed using C++ and Java (for GUI) and simulation was performed on Intel core i3 processor 2.4 GHz running Windows Operating system and tested on the data of Department of Computer Engineering, G.B. Pant University of Agriculture and Technology. The specification considered for the GA are mentioned in Table 2. The Table 3 shows the result of simulations obtained by executing the algorithm on the same data set. The number of generations with maximum and minimum Happiness are also specified in the Table.

The generations with fitness value of 1.0 are relatively very large in number and the solution with maximum happiness are very small in number. There are many generations in which the Happiness is negative and the minimum Happiness value has been specified in the table.

The graphs with varying fitness and happiness values depicting the simulation result are shown in Figs. 2, 3. Figure 2 shows the fitness value on the Y axis and number of generations on the X-axis. Similarly, Fig. 3 show the Happiness parameter value on the Y axis and number of generations on the X-axis. The graph clearly states that the number of generations with positive happiness are very less and the generations with negative happiness are greater in number. The average Happiness was calculated for the simulations and was found to be negative. In Fig. 3 we have shown the best possible curve of Happiness factor.

The probability that the selected solution is having negative happiness is calculated using following formula.

$$\begin{aligned}
 & \text{Probability of selecting solution with negative Happiness} \\
 & = \frac{\text{Total number of Generations with negative Happiness}}{\text{Total Number of Generations having Fitness}}
 \end{aligned}$$

The Table 4 represents the probability of selection of a timetable with negative happiness for all the iterations done in Table 3. The values in Table 4 clearly depicts that there are more than 90 % (approx.) chances of selection of non-appropriate timetable without using Happiness parameter. Hence, using Happiness parameter the probability of selection of an appropriate feasible solution is greatly increased and that of non-appropriate solution reduces gradually.

Table 3 Simulation results on application of algorithm 1

S. No.	G_0	$G(H_{neg})$	H_{max}	$G(H_{max})$	H_{min}	$G(H_{min})$	H_{avg}
1	14288	13566	5	2	-12	19	-4.608133
2	14317	13488	6	4	-13	6	-4.650268
3	14228	13300	6	1	-14	1	-4.556508
4	14190	13476	6	8	-12	5	-4.834179
5	14254	13514	6	11	-13	4	-4.687877
6	14427	13537	6	10	-13	17	-4.635198
7	14300	13192	7	2	-13	2	-4.419161
8	14422	13461	8	1	-12	6	-4.498613
9	14290	13298	5	9	-12	14	-4.348775
10	14158	12842	6	15	-13	3	-4.323138

Where, G_0 = Generations with Fitness = 1.0,
 $G(H_{max})$ = Generations with Maximum Happiness,
 $G(H_{min})$ = Generations with Minimum Happiness,
 $G(H_{neg})$ = Generations with negative Happiness,
 H_{max} = Maximum Happiness,
 H_{min} = Minimum Happiness,
 H_{avg} = Average Happiness.

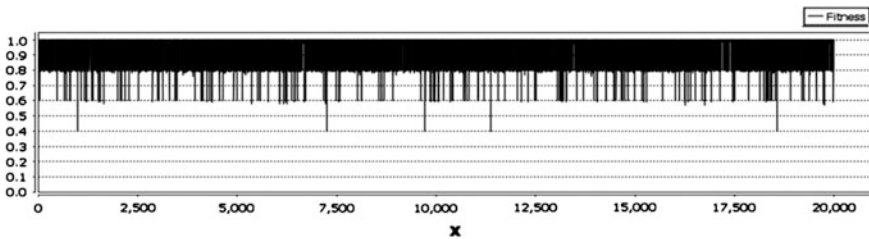


Fig. 2 Simulation graph with Fitness = 1.0

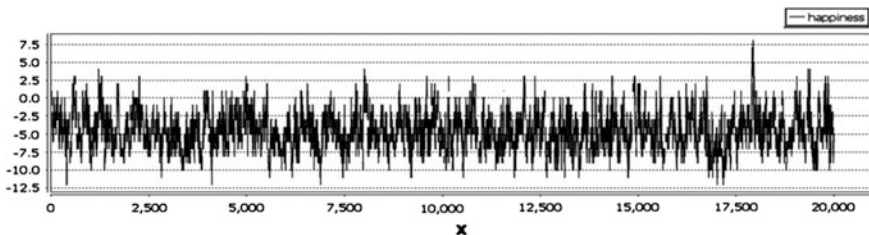


Fig. 3 Simulation graph with maximum Happiness = 8.0

We believe that adding this happiness parameter in the genetic algorithm will narrow the solution space and would generate timetables that will meet the comfort of the instructors and the students. The solutions with less happiness would be discarded from consideration of final solution.

Table 4 Probability of selecting solutions with negative Happiness

S. No.	G_0	$G(H_{neg})$	Probability of selecting offspring with H_{neg}
1	14288	13566	0.94946
2	14317	13488	0.93855
3	14228	13300	0.93477
4	14190	13476	0.94968
5	14254	13514	0.94808
6	14427	13537	0.93831
7	14300	13192	0.92251
8	14422	13461	0.93336
9	14290	13298	0.93058
10	14158	12842	0.90704

7 Conclusion

This paper introduces a Happiness parameter with Genetic Algorithm. We have shown that using Happiness parameter, an appropriate and feasible timetable solution is obtained. Depending upon the conditions the non-appropriate solutions are discarded. Future work will be aimed to enhance the algorithm by providing Happiness for individual Instructors. We will also aim for making this parameter versatile so that it can be used for other problems like motorcycle assembling in the field of production.

References

1. Cooper, T.B., Kingston, J.H.: The complexity of timetable construction problems. In: Burke, Edmund, Ross, Peter (eds.) *Practice and Theory of Automated Timetabling*. Lecture Notes in Computer Science, vol. 1153, pp. 281–295. Springer, Berlin (1996)
2. Hosny, M., Fatima, S.: A survey of genetic algorithms for the university timetabling problem. In: *International Proceedings of Computer Science and Information Technology*, vol. 13, (2011)
3. Come, D., Ross, P.: Peckish initialisation strategies for evolutionary timetabling. In: *Selected papers from the First International Conference on Practice and Theory of Automated Timetabling*, pp. 227–240. Springer, London (1996)
4. Zibran, M.F.: *A Multi-phase Approach to University Course Timetabling*. University of Lethbridge, Canada (2007). Canadian theses
5. Lewis, R., Paechter, B.: Finding feasible timetables using group-based operators. *IEEE Trans. Evol. Comput.* **11**(3), 397–413 (2007)
6. Bambrick, L.: *Lecture Timetabling Using Genetic Algorithms*. The University of Queensland, Brisbane (1997)
7. Abdullah, S., Turabieh, H.: Generating university course timetable using genetic algorithms and local search. In: *3rd International Conference on Convergence and Hybrid Information Technology*, 2008. ICCIT '08, vol. 1, pp. 254–260. (2008)
8. Yang, S., Jat, S.N.: Genetic algorithms with guided and local search strategies for university course timetabling. *IEEE Trans. Syst. Man Cybern. Part C Appl. Rev.* **41**(1), 93–106 (2011)

9. Hacker, K.A., Eddy, J., Lewis, K.E.: Efficient global optimization using hybrid genetic algorithms. In: 9th AIAA/ISSMO Symposium on Multidisciplinary Analysis and Optimization, pp. 4–6. (2002)
10. Holland, J.H.: Adaptation in natural and artificial systems: an introductory analysis with applications to biology, control, and artificial intelligence. University of Michigan Press, Michigan (1975)
11. Davis, L.: Handbook of genetic algorithms. VNR computer library. Van Nostrand Reinhold, New York (1991)
12. Abdullah, S., Turabieh, H., McCollum, B., Burke, E.K.: An investigation of a genetic algorithm and sequential local search approach for curriculum-based course timetabling problems. In: Proceedings of Multidisciplinary International Conference on Scheduling: Theory and Applications (MISTA 2009), Ireland, pp. 727–731. (2009)
13. Sapru, V., Reddy, K., Sivaselvan, B.: Time table scheduling using genetic algorithms employing guided mutation. In: IEEE International Conference on Computational Intelligence and Computing Research (ICCIC), 2010, pp. 1–4. (2010)
14. Gen, M., Cheng, R.: Genetic algorithms and engineering design (engineering design and automation). Wiley, New York (1997)

Application of AI Techniques in Implementing Shunt APF in Aircraft Supply System

Saifullah Khalid and Bharti Dwivedi

Abstract A new improved ANN control based aircraft shunt filter has been proposed in this paper. The shunt active power filter model has been improved using Genetic Algorithm and fuzzy logic. Genetic Algorithm has been used to find the optimum value of filter inductor; whereas fuzzy logic controller has been used in voltage control loop of the filter. The improvement in the control scheme using ANN control makes APF versatile for compensation of reactive power, harmonic currents, and unbalance in source currents. Proposed aircraft shunt filter also provide proper solution to the neutral current in the system. The simulated results using MATLAB model are presented and they clearly prove the effectiveness of the proposed control method of aircraft shunt APF.

Keywords Artificial intelligence (AI) · Artificial neural network (ANN) · Active power filter (APF) · Genetic algorithm · Total harmonics distortion (THD) · Fuzzy logic

1 Introduction

In contrast to normal supply system which is having source frequency of 50 Hz, aircraft ac power system is using source frequency of 400 Hz [1–3]. Aircraft power utility is having source voltage of 115/200 V. The loads associated with the aircraft ac system are quite different from the normal loads used in 50 Hz supply system [1]. When we consider the generation portion; aircraft system will remain

S. Khalid (✉) · B. Dwivedi
Department of Electrical Engineering, I.E.T., Lucknow, India
e-mail: saifullahkhalid@outlook.com

B. Dwivedi
e-mail: bharti_dwivedi@yahoo.com

AC driven from the engine for aircraft primary power. Fuel cell technology can be used to produce a DC output for ground power where its silence operation would match up to satisfactorily with the Auxiliary Power Unit (APU). However when considering the distribution of primary power, whether AC or DC; each approach has its merits.

While discussing Aircraft Power Systems we also need to consider increased power electronics application in aircraft which creates harmonics, large neutral currents, waveform distortion of both supply voltage and current, poor power factor and excessive current demand. Furthermore if a number of non linear loads are impressed upon a supply their effects are additive. Therefore good power quality of the generation system is of particular interest to the Aircraft manufacturer.

Now days, advance soft computing techniques are used widely in automatic control system or for optimization of the system applied. Some of them are such as fuzzy logic [4–8], optimization of active power filter using GA [9–12], power loss minimization using particle swarm optimization [13], neural network control [14–18] applied in both machinery and filter devices.

In this paper, three different AI techniques i.e. GA, Fuzzy and ANN have been used to make a complete optimized active filter for reduction of harmonics and others problem created into the aircraft electrical system due to the non linear loads [1]. The simulation results clearly show their effectiveness. The simulation results obtained with new model are much better than those of traditional methods.

The paper has been organized in the following manner. The complete system used in this paper has been discussed in Sect. 2. The control algorithm for APF is discussed in Sect. 3, which also discusses about the brief detail of the different intelligent algorithms used in the system. MATLAB/Simulink based simulation results are discussed in Sect. 4 and finally Sect. 5 concludes the paper.

2 Aircraft System Description

The aircraft electrical system is a three-phase power system with source frequency of 400 Hz. Shunt Active Power filter improves the power quality and compensates the harmonic currents in the system [7, 9, 10, 13, 15, 20]. The shunt APF is realized by using one voltage source inverters (VSIs) connected at point of common coupling (PCC) with a common DC link voltage [5, 7, 8, 19].

The loads used in this paper are a combination of unbalanced and balanced non-linear loads. They have been tested together to check the affectivity of the system. First load used is three-phase rectifier parallel with inductive load and an unbalanced load connected a phase with midpoint. Second load used is the three-phase rectifier connects a pure resistance directly and third one is three-phase inductive load linked with the ground point. The values of the circuit parameters and load under consideration are given in Appendix.

3 Control Theory

The proposed control of APF depends on Constant instantaneous power control strategy improvised with artificial intelligent techniques such as Genetic algorithm, fuzzy logic and ANN [4–18]. The following section deals with basic application of Genetic algorithm, fuzzy logic and overall control scheme using ANN based on constant source current control strategy [4, 5, 14].

In this paper, GA is applied to the system simulated using MATLAB Simulink and has been used to search the optimum value inductor filter (L_f). The boundary and limits of parameters in the filter has been defined and a program using genetic algorithm has been written to give the best value of the filter inductor.

The fuzzy logic control has been used in the dc voltage control loop of the active power filter. In fuzzy, the design uses centrifugal defuzzification method. There are two inputs; error and its derivative and one output, which is the command signal. The two inputs uses Gaussian membership functions while the output uses triangle membership function. Table 1 presents the fuzzy control rule. Figure 1 shows the membership functions used.

In this paper, the Constant instantaneous power control strategy based current controller has been modeled, by an artificial neural network (ANN) using two hidden layers with 12 neurons each, and one output layer with 3 neurons. As seen in the Constant instantaneous power control strategy theory, the current controller has seven inputs and three outputs. The network type used is feed forward back prop. TRAINLM has been used as a training function and LEARNM has been used as adaptive linear function. In this model each neurons of the hidden layers has n inputs and it varies based on the function of chosen hidden layer. The adaptation of the weights (W) and bias (b) in the ANN, is based, initially, on the calculation of the mean square error (MSE) between the outputs of the Constant instantaneous power control technique and those of the ANN, and secondly, on TRAINLM algorithm.

3.1 Control Scheme

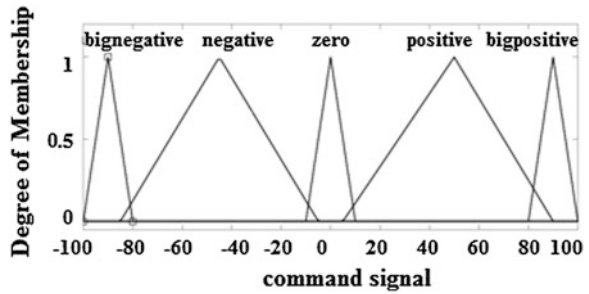
In this paper Constant instantaneous power control strategy [4, 5, 8] has been used for active power filter with the application of artificial intelligent techniques as shown in the Fig. 2. The intelligent techniques like Fuzzy logic; genetic algorithm and ANN technique have been used to optimize the system so that the system will give the best performance under different load conditions connected together or alone.

We know that, the hysteresis controllers produce high switching frequency, which is very harmful for aircraft power utility of 400 Hz. So, we have applied the space vector modulation technique to this HB controller so that the disadvantages of the hysteresis controller can be reduced. SVM technique treats the inverter as a

Table 1 Fuzzy control rule

de/dt	Error		
	Negative	Zero	Positive
Negative	Big negative	Positive	Big positive
Zero	Big negative	Zero	Big positive
Positive	Big negative	Negative	Big positive

Fig. 1 Membership functions



whole unit, which is different when compared to normal PWM technique. This configuration can produce a better current shape by using a significant bandwidth of the hysteresis control [8, 21].

The whole system based on Constant instantaneous power control strategy [9, 14] utilizing SVM based HB [21] has been implemented using MATLAB/Simulink to give the filter currents which will compensate the harmonics and make the system clean and well within standard limit [11].

4 Simulation Results and Discussions

The proposed scheme of APF is simulated in MATLAB environment to estimate its performance. The proposed control scheme has been simulated to compute the performance of APF and analysis through total harmonic distortion (THD) of source and load current as well as the compensation time, which in turn shows the speed of the system to improve the power quality. The simulation results clearly demonstrate that the scheme is able to successfully reduce the significant amount of THD in source current and voltage within limits. Simulation results have been analyzed on the basis of THD and compensation time obtained.

Simulation has been done for 15 cycles. Three loads have been used. Load 1 (three-phase rectifier parallel with inductive load and an unbalanced load connected a phase with midpoint) is always connected (firing angle = 30°), Load 2 (three-phase rectifier connected a pure resistance directly) is initially connected and disconnect after every 2.5 cycles, Load 3 (three-phase inductive load linked with the ground point) is connected after every half cycle.

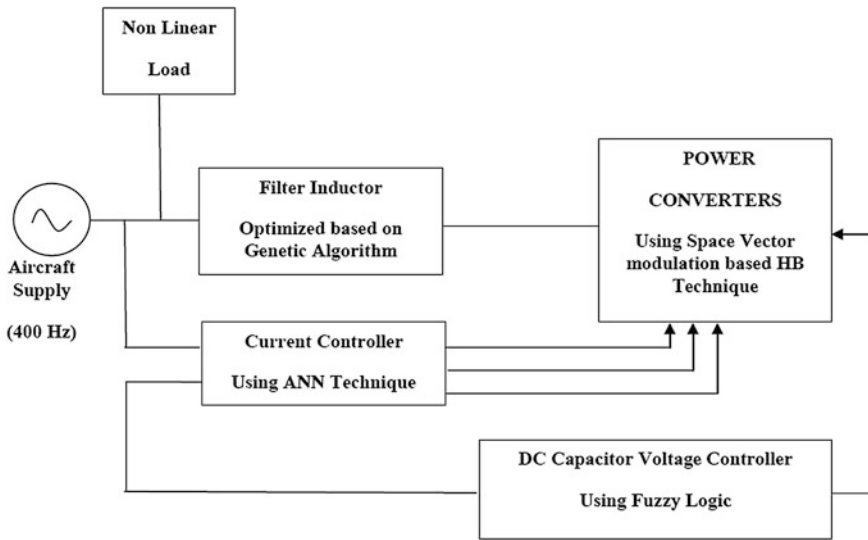


Fig. 2 Block diagram of the optimized active filter using GA, fuzzy logic and ANN techniques

4.1 Uncompensated System with Combined All Three Loads Connected at Different Time Interval

After doing simulation in MATLAB/Simulink without using any filter (Fig. 3) i.e. for *Uncompensated System*, it has been observed that the THD of source current found while using all three loads simultaneously connected with the system at different time is 9.5 % and THD of source Voltage were 1.55 %. By observing these data and waveforms shown in Fig. 4, we can easily understand that system has been polluted and unbalanced when loads has been connected.

4.2 Performance of APF Under Combined All Three Loads Connected at Different Time Interval

During the analysis of simulation results based on THD, this has been observed (Fig. 4) that while doing simulation of Shunt Active power based on Conventional constant source instantaneous power Strategy that the THD of source current found was 2.73 % and THD of source Voltage were 1.70 %; whereas when model has been optimized using Genetic Algorithm, Fuzzy Logic and current controller developed using ANN control techniques has been used, it has been observed that the THD of source current reduces to an amazing 1.67 %, and THD of source voltage reduces to 1.65 % which is absolutely the improvement from conventional one.

Fig. 3 Source voltage and source current waveforms of uncompensated system for all three loads connected together at different time interval

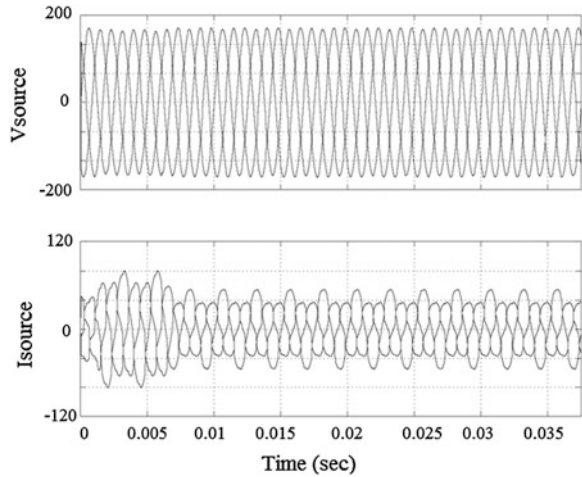
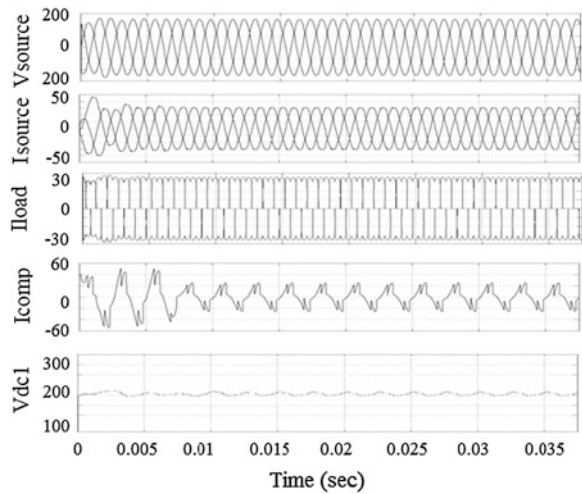


Fig. 4 Source voltage, source current, compensation current (phase b), load current and DC link voltage waveforms of active power filter using GA-FL with neural network controller with all three loads connected for aircraft power utility



During the analysis of simulation results based on compensation time, this has been observed that after the comparison of both model i.e. Conventional constant instantaneous power control Strategy model and improved model using Genetic Algorithm, Fuzzy Logic and current controller developed using ANN control techniques, the response time of new improved model was only 0.0062 s; as comparison from old simple conventional model 0.0082 s, we found that new model is better than old conventional model. THD-I and THD-V present the total harmonic distortion for source current and total harmonic distortion for source voltage respectively.

The simulation waveforms shown and the results have been tabulated in Table 2. We can see from the second column of Table 2 that the THD for source

Table 2 THDs and response time of compensated system

Techniques and loads details	THD-I (%)	THD-V (%)	Compensation time (sec)
Uncompensated system	9.5	1.55	NA
All three loads connected (using conventional technique)	2.73	1.7	0.0082
All three loads connected (using GA-FL-ANN technique)	1.67	1.65	0.0062

Fig. 5 Graphical representation of THD-I and THD-V for uncompensated system, conventional and GA-FL-ANN control strategy for Load 1, 2 and 3 connected together

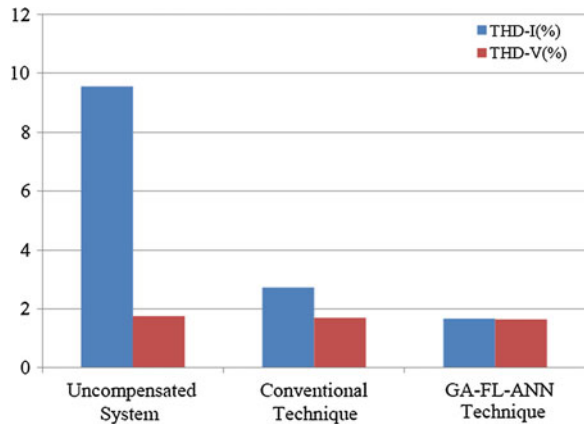
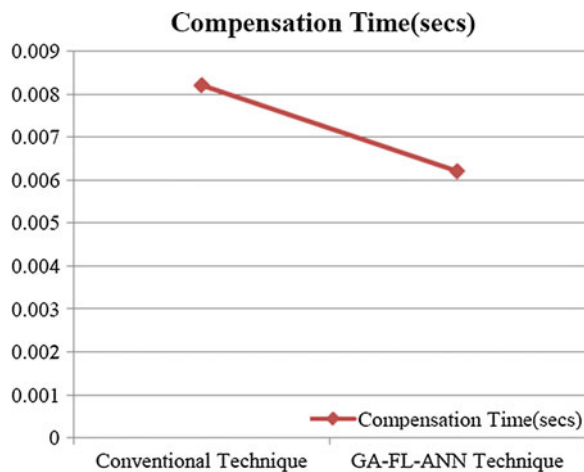


Fig. 6 Graphical representation of compensation time for uncompensated system, conventional and GA-FL-ANN control strategy for Load 1, 2 and 3 connected together



current has been in decreasing order which means that conventional system reduces it to within the international standard limits and when it has been modified using the improved GA-FL-ANN control based Shunt APF, it has been reduced further, which shows that it can compensate the system efficiently.

We can clearly see from the bar chart shown in Fig. 5 that the THD for current has been continuously decreasing and least for AI (GA-FL-ANN) technique. Whereas, Fig. 6 shows that AI technique applied is fast as compared to conventional technique.

5 Conclusion

A novel GA-FL-ANN control aircraft shunt active filter has been reported which clearly demonstrate its fast compensation ability. This also has been observed that Genetic Algorithm, Fuzzy Logic and ANN have well optimized the model and increased the ability of conventional model. From the simulation results, this can be easily seen that the proposed novel active filter can be effectively applied in higher frequency system.

Appendix

The system parameters used are as follows [1]:

Three-phase source voltage: 115 V/400 Hz, Filter inductor = 0.25 m H, Filter capacitor: 5 μ F, Dc voltage reference: 400 V, Dc capacitor: 4700 μ F.

References

1. Chen, D., Guo, T., Xie, S., Zhou, B.: Shunt active power filters applied in the aircraft power utility. 36th Power Electronics Specialists Conference. PESC '05, pp. 59–63. IEEE, (2005)
2. Li, Z., Li, Y., Wang, P., Zhu, H., Liu, C., Gao, F.: Single-loop digital control of high-power 400-Hz ground power unit for airplanes. *IEEE Trans. Industr. Electron.* **57**(2), 532–543 (2010)
3. Lavopa, E., Zanchetta, P.: Real-time estimation of fundamental frequency and harmonics for active shunt power filters in aircraft electrical systems. *IEEE Trans. Industr. Electron.* **56**(8), 2875–2884 (2009)
4. Aredes, M., Monteiro, L.F.C., Miguel, J.M.: Control strategies for series and shunt active filters. *IEEE Bologna Power Tech Conference*, pp. 101–106. Bologna, 23–26 June (2003)
5. Aredes, M., Hafner, J., Heumann, K.: Three-phase four-wire shunt active filter control strategies. *IEEE Trans. Power Electron.* **12**(2), 311–318 (1997)
6. Khalid, S., Dwivedi, B., Kumar, N., Agrawal, N.: A review of state of art techniques in active power filters and reactive power compensation. *Natl. J. Technol.* **3**(1), 10–18 (2007)
7. Peng, F.Z., Akagi, H., Nabae, A.: A new approach to harmonic compensation in power systems – a combined system of shunt passive and series active filters. *IEEE Trans. Ind. Appl.* **6**(26), 983–990 (1990)
8. Bose, B.K.: Recent advances in power electronics. *IEEE Trans. Power Electron.* **7**(1), 2–15 (1992)

9. Dugan, R.C., McGranaghan, M.F., Beaty, H.W.: *Electrical Power Systems Quality*. McGraw-Hill, New York (1996)
10. Sankaran, C.: *Power Quality*. CRC Press, Boca Raton (2002)
11. IEEE Recommended Practices and Requirements for Harmonic Control in Electrical Power Systems. IEEE Standard 519, (1992)
12. Khalid, S., Vyas, N.: *Application of Power Electronics to Power System*. University Science Press, New Delhi (2009)
13. Mohan, N., Undeland, T., Robbins, W.: *Power electronics, converters, applications and design*, 2nd edn. Wiley, Canada (1995)
14. Akagi, H., Watanabe, E.H., Aredes, M.: *Instantaneous Power Theory and Applications to Power Conditioning*. Wiley, New Jersey (2007)
15. Emadi, A., Nasiri, A., Bekiarov, S.B.: *Uninterruptible Power Supplies and Active Power Filters*. CRC Press, New York (2005)
16. Khalid, S., Dwivedi, B., Singh, B.: New optimum three-phase shunt active power filter based on adaptive tabu search and genetic algorithm using ANN control in unbalanced and distorted supply conditions. *Elektrika: J. Electr. Eng.* **14**(2), 09–14 (2012)
17. Kumar, N., Thapa, K.B., Khalid, S.: A novel series active power filter scheme using adaptive tabu search algorithm for harmonic compensation. *Int. J. Appl. Innov. Eng. Manage. (IJAIEM)*. **2**(2), 155–159 (2013)
18. Dehini, R., Bassou, A., Ferdi, B.: Artificial neural networks application to improve shunt active power filter. *Int. J. Comput. Info. Eng.* **3**(4), 247–254 (2009)
19. Singh, B., Al-Haddad, K., Chandra, A.: A review of active filters for power quality improvement. *IEEE Trans. Industr. Electron.* **46**(5), 960–971 (1999)
20. Ghosh, A., Ledwich, G.: *Power Quality Enhancement Using Custom Power Devices*. Kluwer, Boston (2002)
21. Ling, L.P.: SVM based hysteresis current controller for a three phase active power filter. M.E. thesis, Department of Electrical Engineering, Universiti Teknologi Malaysia, Skudai (2004)

Differential Evolution for Supplier Selection Problem: A DEA Based Approach

Sunil Jauhar, Millie Pant and Aakash Deep

Abstract Deciding an appropriate approach for supplier selection is however a demanding research task as there are often thousands of potential suppliers and identifying a subset of these suppliers can be a difficult practice. During last few years, Differential Evolution has come out as a dominant tool used for solving a wide range of problems arising in numerous fields. In the current study, we present an approach to solve the supplier selection problem mathematical modeled with Data envelopment analysis using differential evolution. A case study demonstrates the application of the present approach.

Keywords Supplier selection • Supply chain management • DE • DEA

1 Introduction

Developing an efficient and robust supply chain (also known as supply chain management) is a crucial task for the success of a business firm. One of the most important factors that help in building a strong supply chain is the supplier selection process. It is natural that for a particular product, large numbers of suppliers/vendors are available in the market. Now, it is the duty of the purchasing managers to identify the most suitable set of suppliers for their product.

S. Jauhar (✉) · M. Pant
Indian Institute of Technology, Roorkee, India
e-mail: suniljauhar.iitr@gamil.com

M. Pant
e-mail: millidma@gamil.com

A. Deep
Jaypee University of Engineering and Technology, Guna, India
e-mail: aakash791@gamil.com

Differential evolution (DE) algorithm was proposed by Storn and Price in 1995 [1]. It is a population set based evolutionary algorithm to solve global optimization problem. During some past years DE has been applied in the many real life application of engineering and science field [2], chemical engineering [3], engineering design problem [4], neural network [5], multi-objective [6], and so on. Global optimization is necessary in fields such as engineering, statistics and finance.

In the present study DE is used for solve the supplier selection problem modeled with the help of data envelopment analysis (DEA). The purpose of the paper is to use DE in DEA to measure and analyze the relative efficiency of 12 suppliers on the basis of experimental data given by [7]. The mathematical model of the problem is constrained in nature for which Pareto ranking method is embedded in DE.

The rest of the paper is organized as follows. The supplier selection, Motivation for using DE, Mathematical model formulation, Differential evolution, Experimental data, Parameter settings for DE and results are discussed in Sects. 2–8 respectively. Discussions and conclusions drawn from the present study are given in Sect. 9.

2 Supplier Selection

Supplier selection and evaluation forms an integral part of a supply chain. A wrong choice or decision may lead to unpleasant circumstances and in worst case may even lead to the deterioration of the entire supply chain's financial and operational position.

Research on supplier selection can be traced back to the early 1960s when it was called vendor selection. The early research activities are summarized in a literature review by [8]. Later, [9] provided a short but insightful overview of supplier selection research. Some researchers emphasize strategic decision making [10–12]. A majority of researchers treated it as an optimization problem and proposed solution methodologies like linear programming, non-linear programming etc. for its solution [13–18].

3 Motivation for Using DE

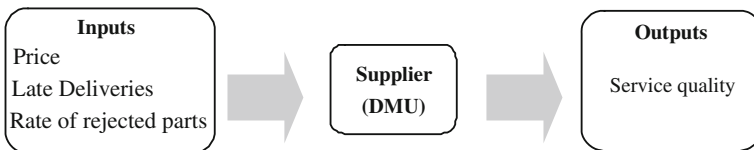
DE is a development version of the “Genetic algorithm”. Principally it is based on the evolution of biological analogy, the individual seeking the best solution. It is a population-based stochastic method to solve global optimization problem, used to optimize the functions. The motivations for using DE are listed below.

- Simple in structure.
- Fast convergence speed.
- Few control parameter required.

- Easy applicable to various problems.
- Generally good accuracy for real world problems.
- Easy to implement as same parameter settings work fine for a wide range of problem.
- The benefits of DE are its ease of practice, speed and robustness.
- To our best knowledge, this is the first time that the DE algorithm is applied to the supplier selection.

4 Mathematical Model Formulation

DEA is a linear programming based method for determining the efficiency of Decision-Making Unit (DMU) on the basis of multiple inputs and outputs [19]. DMU can comprise manufacturing units, departments of big organizations such as universities, schools, hospitals, power plants, police stations, tax offices, prisons, a set of firms etc. [20]. Most of the DMU are non-profit organizations, where the measurement of Performance efficiency is tough. The DMU well-defined in this study with input and output criteria are as follows:



The performance of DMU is estimated in DEA by the concept of efficiency or productivity, which the ratio of weights sum of outputs to the weights sum of inputs [21] i.e.

$$Efficiency = \frac{Weighted\ sum\ of\ outputs}{Weighted\ sum\ of\ inputs} \tag{1}$$

The two basic DEA models are the CCR (Charnes, Cooper and Rhodes) model [22] and the BCC (Banker, Charnes and Cooper) model [23]. These two models distinguish on the returns to scale assumed. The former assumes constant returns-to-scale whereas the latter assumes variable returns-to-scale [20]. A comprehensive text with the DEA model variations and applications can be found in [24]. In the current study we use CCR model which is well-defined further down:

Assume that there are N DMUs and each unit have I input and O outputs then the efficiency of m th unit is obtained by solving the following model which is proposed by Charnes et al. [22].

$$\begin{aligned} \text{Max } E_m &= \frac{\sum_{k=1}^O w_k \text{Output}_{k,m}}{\sum_{l=1}^I z_l \text{Input}_{l,m}} \\ 0 \leq \frac{\sum_{k=1}^O w_k \text{Output}_{k,n}}{\sum_{l=1}^I z_l \text{Input}_{l,n}} &\leq 1; n = 1, 2, \dots, m, \dots, N \end{aligned} \quad (2)$$

Where

E_m is the efficiency of the m th DMU, $k = 1$ to O , $l = 1$ to I and $n = 1$ to N .

$\text{Output}_{k,m}$ is the k th output of the m th DMU and w_k is weight of output $\text{Output}_{k,m}$

$\text{Input}_{l,m}$ is the l th input of m th DMU and z_l is the weight of $\text{Input}_{l,m}$

$\text{Output}_{k,n}$ and $\text{Input}_{l,n}$ are the k th output and l th input respectively of the n th DMU,

Where $n = 1, 2, \dots, m, \dots, N$

The fractional program shown in Eq. 2 can be converted in a linear program which is shown in Eq. 3

$$\begin{aligned} \text{Max } E_m &\sum_{k=1}^O w_k \text{Output}_{k,m} \\ \text{s.t.} & \\ \sum_{l=1}^I z_l \text{Input}_{l,m} &= 1 \\ \sum_{k=1}^O w_k \text{Output}_{k,n} - \sum_{l=1}^I z_l \text{Input}_{l,n} &\leq 0, \forall n \\ w_k, z_l &\geq 0; \forall k, l \end{aligned} \quad (3)$$

To determine the efficiency score of each DMU we run the above program run N times. A DMU is considered efficient if the efficiency score is 1 otherwise it is considered as inefficient.

5 Differential Evolution

Introduced by Storn and Price in 1995, It is Population-based search technique for global optimization. DE algorithm is a kind of evolutionary algorithm, used to optimize the functions. In current study DE refers to the DE/rand/1/bin scheme [25].

DE starts with a randomly generated set of solutions when we have not any preliminary knowledge about the solution space. This set of solutions is term as population. Suppose we want to optimize a function with Dimension of the solution

space (D). Let $P = \{X_{1,G}, X_{2,G}, \dots, X_{NP,G}\}$ be the population at any generation G , where NP is population size and the Target vectors have the form: $X_{i,G} = \{X_{1,i,G}, X_{2,i,G}, \dots, X_{D,i,G}\}$, $i = 1, 2, \dots, N$, where G is the generation number.

Population is initialized between $[X_{lower}, X_{upper}]$ as;

$$\begin{aligned} &\text{For } i = 1 : NP \\ &\{ \\ &\quad \text{For } j = 1 : D \\ &\quad \quad X_{j,i,G} = X_{lower} + (X_{upper} - X_{lower}) * rand(0, 1) \\ &\quad \} \end{aligned}$$

Where, $rand$ = Uniform random number between 0 & 1.

For simple DE (*DE/rand/1/bin*), the mutation, crossover, and selection operators are defined as follows:

5.1 Mutation

Mutation enlarges the search space, For a given Target vector $X_{i,G}$ randomly Select three random vector $X_{r1,G}, X_{r2,G}, X_{r3,G}$ where $i \neq r_1 \neq r_2 \neq r_3$ and add the weighted difference of two of the vectors to the third then the mutant vector $V_{i,G} = \{v_{1,i,G}, v_{2,i,G}, \dots, v_{D,i,G}\}$ is defined as;

$$V_{i,G} = X_{r1,G} + F(X_{r2,G} - X_{r3,G}) \tag{4}$$

This is called *DE/rand/1* Mutation Strategy, F is scaling factor having value between (0, 2) and control the amplification of differential variation ($X_{r2} - X_{r3}$).

5.2 Crossover

Crossover is to increase diversity of mutant vectors. Crossover integrates fruitful solutions from the preceding generation, The trial vector $U_{i,G+1}$ is developed from the elements of the target vector, $X_{i,G,1}$ and the elements of the mutant vector, $V_{i,G+1}$.

Let $V_{i,G} = \{v_{1,i,G}, v_{2,i,G}, \dots, v_{D,i,G}\}$ be the mutant vector and $X_{i,G}$ be the target vector, then trial vector $U_{i,G}$ is generated as;

$$u_{j,i,G} = \begin{cases} v_{j,i,G} & \text{if } rand_j \leq Cr \vee j = j_{rand} \\ x_{j,i,G} & \text{otherwise} \end{cases} \tag{5}$$

Where, Cr = Crossover Probability, j_{rand} is any number from $1, 2, \dots, D$.

5.3 Selection

“Survival of the fittest” principle in selection: The trial vector $U_{i,G}$ is compared with the target vector $X_{i,G+1}$ and that on with a better fitness is admitted to the next generation.

Select fittest vector from target vector and trial vector to the population of next generation.

$$X_{i,G+1} = \begin{cases} U_{i,G} & \text{if } f(U_{i,G}) \leq f(X_{i,G}) \\ X_{i,G} & \text{Otherwise} \end{cases} \quad (6)$$

Mutation, crossover and selection continue until some stopping criterion is reached.

Pseudo Code of DE Algorithm

```

1   Begin
2   Generate uniformly distribution random population  $P = \{X_{1,G}, X_{2,G}, \dots, X_{NP,G}\}$ .
    $X_{i,G} = X_{lower} + (X_{upper} - X_{lower}) * rand(0,1)$ , where  $i = 1, 2, \dots, NP$ 
3   Evaluate  $f(X_{i,G})$ 
4   While (Termination criteria is met )
5   {
6     For  $i=1:NP$ 
7     {
8       Select three random vector  $X_{r1,G}, X_{r2,G}, X_{r3,G}$  where  $i \neq r1 \neq r2 \neq r3$ 
9         Perform mutation operation
10        Perform crossover operation
11        Evaluate  $f(U_{i,G})$ 
12        Select fittest vector from  $X_{i,G}$  and  $U_{i,G}$  to the population of next generation
13      }
14      Generate new population  $Q = \{X_{1,G+1}, X_{2,G+1}, \dots, X_{NP,G+1}\}$ 
15    } /* end while loop*/
16  END

```

5.4 Constraint Handling

For the constraint problems various methods have been suggested in literature. A survey of different methods for constraint handling can be found in [26] and [27]. In this paper Pareto-Ranking method is used for handling the constraints [28, 29].

6 Experimental Data

To efficient suppliers selection, companies need to keep comprehensive supplier information files which should include a list of items available from each supplier, such as the as price, late deliveries, rate of rejected parts and service quality.

In the present study we have considered a case (data is taken from [7]) of selecting a supplier out of 12 potential suppliers. In our supplier selection case two set of criteria were formulated: Input (traditional purchasing criteria) and Output criteria. The criteria considered for selection as given below:

1. Input criteria: which include price, late deliveries, rate of rejected parts.
2. Output criteria: including service quality of the product and services.

This case presented here to illustrate the present approach; the underlying data is shown in Table 1 with the supplier’s database covering Input (traditional purchasing criteria) such as price, late deliveries, rate of rejected parts and Output criteria is service quality of an item provided in the shipment of a company.

On the basis of the above data the DEA model of *K*th DMU will be as follows:

$$\begin{aligned}
 &Max SQ_m \\
 &s.t. \\
 &z_1 PR_m + z_2 LD_m + z_3 RR_m = 1 \\
 &w SQ_n - (z_1 PR_n + z_2 LD_n + z_3 RR_n) \leq 0 \\
 &\forall n = 1, \dots, m, \dots 12
 \end{aligned}
 \tag{7}$$

7 Parameter Setting for DE Algorithm

In this paper we have applied DE to solve the DEA model. The parameter settings for DE are given in Table 2.

The program is implemented is DEV C++ and all the uniform random number is generated using the inbuilt function *rand ()* in DEV C++. The fitness value is taken as the average fitness value in 30 runs and the program is terminate when reach to Max-Iteration.

Table 1 Data of 12 different suppliers [7]

Criteria	Inputs			Output
	Price (PR)	Late deliveries (LD) %	Rate of rejected (RR) %	Service quality (SQ)
Suppliers				
1	290	7	3	95
2	240	3	5	98
3	300	4	6	12
4	255	5	3	100
5	295	10	8	65
6	250	3	3	110
7	245	7	4	92
8	285	6	4	73
9	270	6	6	75
10	270	12	4	81
11	285	3	5	112
12	275	5	8	85

Table 2 Parameter setting for DE

Pop size (NP)	100
Scale factor (F)	0.5
Crossover rate (Cr)	0.9
Max iteration	3000

7.1 Weight Selection

Because of its easy practice the weighted point model is of practical significance in purchasing management. It makes it appropriate to examine its applicability. The selection of weights in most of the circumstances takes place in advance as part of a group assessment. With the help of a program is implemented in DEV C++, we are examining a weight system by which the multi-criteria can influence the decision making.

For this purpose with the help of program which is implemented is DEV C++, we intended to generate all the uniform random number using the inbuilt function *rand ()* in DEV C++, to assist the selection of the weights for input as well as output factors in a manner to permit the control the end result of the selection process.

Table 3 Average efficiency and weighted of 12 suppliers in 30 runs

Suppliers	Value of input and output weight				Efficiency
	Z[1]	Z[2]	Z[3]	W	
1	0	0	0.33337	0.00909282	0.863818
2	0.00352436	0.0225639	0.0172946	0.0102042	1
3	0.00333337	0	0	0.00757585	0.0909102
4	0	0	0.333337	0.00909102	0.909102
5	0.00338987	0	1.42974e017	0.00830173	0.539612
6	0.000230935	0.158028	0.156064	0.00909102	1
7	0	0	0.250003	0.00681827	0.62728
8	0.00350881	0	9.0241e-017	0.00797458	0.582144
9	0.00370374	1.62202e017	0	0.00841761	0.631321
10	0.00370374	0	7.15911e-018	0.00841761	0.681826
11	0.000131411	0.317989	0.0038805	0.00892868	1
12	0	0.191415	0.00536679	0.00536679	0.456178

Fig. 1 Histogram of all suppliers with their efficiency score



Table 4 Suppliers efficiency score

Suppliers	Efficiency	Suppliers	Efficiency
1	0.863818	7	0.62728
2	1	8	0.582144
3	0.0909102	9	0.631321
4	0.909102	10	0.681826
5	0.539612	11	1
6	1	12	0.456178

8 Results

In the Table 3 results of all DMUs are given. From this Table we can see that for suppliers 2, 6 and 11, the efficiency score is 1 so these supplier are assumed to be 100 % efficient while efficiency score for all other supplier are less than 1. So these suppliers are not as efficient and among these, supplier no. 3 is probably the most inefficient in comparison to all other suppliers.

In the Table 4 results of all DMUs are given and (Fig. 1) shows the histogram of all suppliers with their efficiency score.

9 Discussions and Conclusion

The research of efficient supplier selection problem can obtain a recommended combination of efficient suppliers 2, 6 and 11 using differential evolution algorithm gives the better solution.

For the current research conducted in 18 suppliers, the results are:

1. Suppliers 2, 6 and 11, the efficiency score is 1 so these suppliers are assumed to be 100 % efficient.
2. Supplier 3 is probably the most inefficient in comparison to all other suppliers.
3. Suppliers 2, 6 and 11 would be the most suitable set of suppliers (or key suppliers).
4. By using this DE, the company can obtain a recommended combination of efficient suppliers.
5. Combination of suppliers 2, 6 and 11 would be the recommended supplier set while the company needing single-item suppliers.
6. The results of the case indicate that the DE algorithm can solve the problem effectively.

DE has proven its versatility in solving a wide range of real life application problems. In this study, we present a comprehensive supplier selection framework. The first step is to construct a criterion set that containing both Input and Output factors, which is suitable for real world applications. We then presents an approach to solve the multiple-criteria supplier selection problem with the application of DE, for DEA based mathematical model. By using this approach, the company can obtain a recommended combination of efficient suppliers. Numerical results validate the efficiency of DE for dealing with such problems.

References

1. Storn, R., Price, K.: Differential Evolution—A Simple and Efficient Adaptive Scheme for Global Optimization over Continuous Spaces. Tech. Rep TR-95-012, Berkeley (1995)
2. Plagianakos, V., Tasoulis, D., Vrahatis, M.: A review of major application areas of differential evolution. In: *Advances in Differential Evolution*, vol. 143, pp. 197–238. Springer, Berlin (2008)
3. Wang, F., Jang, H.: Parameter estimation of a bio reaction model by hybrid differential evolution. In: *Proceedings of IEEE Congress on Evolutionary Computation (CEC-2000)*, pp. 410–417. San diego (2000)
4. Joshi, R., Sanderson, A.: Minimal representation multi sensor fusion using differential evolution. *IEEE Trans. Syst. Man Cybern. Part A Syst. Hum.* **29**(1), 63–76 (1999)
5. Ilonen, J., Kamarainen, J., Lampine, J.: Differential evolution training algorithm for feed-forward neural networks. *Neural Process. Lett.* **17**(1), 93–105 (2003)
6. Ali, M., Siarry, P., Pant, M.: An efficient differential evolution based algorithm for solving multi-objective optimization. *Eur. J. Oper. Res.* **217**, 404–416 (2011)

7. Shirouyehzad, H., Lotfi, F.H., Dabestani, R.: A data envelopment analysis approach based on the service quality concept for vendor selection. Paper presented at the international conference on computers and industrial engineering (CIE 2009), pp. 426–430, 6–9 July 2009. doi:[10.1109/ICCIE.2009.5223823](https://doi.org/10.1109/ICCIE.2009.5223823)
8. Weber, C.A., Current, J.R., Benton, W.C.: Vendor selection criteria and methods. *Eur. J. Oper. Res.* **50**(1), 2–18 (1991)
9. Ghodspour, S.H., O'Brien, C.: A decision support system for supplier selection using an integrated analytic hierarchy process and linear programming. *Int. J. Prod. Econ.* **56–57**, 199–212 (1998)
10. Davidrajuh, R.: Modeling and implementation of supplier selection procedures for e-commerce initiatives. *Ind. Manage. Data Syst.* **103**(1), 28–38 (2003)
11. Huang, S.H., Uppal, M., Shi, J.: A product driven approach to manufacturing supply chain selection. *Supply Chain Manage. Int. J.* **7**(3/4), 189–199 (2002)
12. Fisher, M.L.: What is the right supply chain for your product? *Harvard Bus. Rev.* **75**, 105–116 (1997)
13. Talluri, S., Narasimhan, R.: Vendor evaluation with performance variability: a max–min approach. *Eur. J. Oper. Res.* **146**(3), 543–552 (2003)
14. Talluri, S., Narasimhan, R.: A note on “a methodology for supply base optimization”. *IEEE Trans. Eng. Manage.* **52**(1), 130–139 (2005)
15. Ng, W.L.: An efficient and simple model for multiple criteria supplier selection problem. *Eur. J. Oper. Res.* **186**(3), 1059–1067 (2008)
16. Talluri, S.: A buyer–seller game model for selection and negotiation of purchasing bids. *Eur. J. Oper. Res.* **143**(1), 171–180 (2002)
17. Hong, G.H., Park, S.C., Jang, D.S., Rho, H.M.: An effective supplier selection method for constructing a competitive supply-relationship. *Expert Syst. Appl.* **28**(4), 629–639 (2005)
18. Ghodspour, S.H., O'Brien, C.: The total cost of logistics in supplier selection, under conditions of multiple sourcing, multiple criteria and capacity constraints. *Int. J. Prod. Econ.* **73**, 15–27 (2001)
19. Dimitris, K.S., Lamprini, V.S., Yiannis, G.S.: Data envelopment analysis with nonlinear virtual inputs and outputs. *Eur. J. Oper. Res.* **202**, 604–613 (2009)
20. Ramanathan, R.: *An Introduction to Data Envelopment Analysis: A Tool for Performance Measurement*. Sage Publication Ltd., New Delhi (2003)
21. Srinivas, T.: *Data envelopment analysis: models and extensions*. In: *Production/Operation Management Decision Line*, pp. 8–11 (2000)
22. Charnes, A., Cooper, W.W., Rhodes, E.: Measuring the efficiency of decision making units. *Eur. J. Oper. Res.* **2**(6), 429–444 (1978)
23. Banker, R.D., Charnes, A., Cooper, W.W.: Some models for estimating technical and scale inefficiencies in data envelopment analysis. *Manage. Sci.* **30**, 1078–1092 (1984)
24. Cooper, W.W., Seiford, L.M., Tone, K.: *Data envelopment analysis*. Springer, US (2007)
25. Das, S., Abraham, A., Chakraborty, U., Konar, A.: Differential evolution using a neighborhood-based mutation operator. *IEEE Trans. Evol. Comput.* **13**(3), 526–553 (2009)
26. Jouni, L.: A constraint handling approach for differential evolution algorithm. In: *Proceeding of IEEE Congress on Evolutionary Computation (CEC 2002)*, pp. 1468–1473 (2002)
27. Coello, C.A.C.: Theoretical and numerical constraint handling techniques used with evolutionary algorithms: a survey of the state of the art. *Comput. Methods Appl. Mech. Eng.* **191**(11–12), 1245–1287 (2002) [Differential Evolution for Data Envelopment Analysis 319]
28. Ray, T., Kang, T., Chye, S.K.: An evolutionary algorithm for constraint optimization. In: Whitley D., Goldberg D., Cantu-Paz E., Spector L., Parmee I., Beyer H.G. (eds.) *Proceeding of the Genetic and Evolutionary Computation Conference (GECCO 2000)*, pp. 771–777 (2000)
29. Kumar, P., Mogha, S.K., Pant, M.: Differential evolution for data envelopment analysis. In: *Proceedings of the International Conference on Soft Computing for Problem Solving (SocProS 2011)*, 20–22 December 2011. doi:[10.1007/978-81-322-0487-9_30](https://doi.org/10.1007/978-81-322-0487-9_30)

Social Engineering Prevention by Detecting Malicious URLs Using Artificial Bee Colony Algorithm

Tushar Bhardwaj, Tarun Kumar Sharma and Manu Ram Pandit

Abstract Social Engineering is an emerging concept that was initially coined in the year (1980s). Initially it was encountered, when people use to fool others by masquerading names and contact details to steal the assets of others. As the needle moves on the whole world is affected by this disease. It came across many cyber attacks like phishing, spamming, hacking etc. In all the methods the basic thing which prevails most is the presence of malicious URLs. These URLs plays an important role in making social engineering a success. In this paper we have proposed a solution that prevents this type attack by helping in detecting the malicious URLs. The model uses the Artificial Bee Colony approach to optimize and detect that the target website is genuine or not. Once we come to know that the link we are going to click is safe enough than maximum percent of the problem is solved.

Keywords Social engineering · Malicious URLs · Swarm intelligence · ABC

1 Introduction

For a lay man, “Social engineering can be defined as the technique or practice of deceiving a person on phone or computer in order to gain the information”. If we look at the future, this kind of attack lies in social engineering and malware. The main aim is to convince people to click and install applications that may have

T. Bhardwaj (✉)
M. T. U Noida, Noida, India
e-mail: tusharbhardwaj19@gmail.com

T. K. Sharma
IIT Roorkee, Roorkee, India
e-mail: taruniitr1@gmail.com

M. R. Pandit
B. I. T. S Pilani, Pilani, India
e-mail: manupandit123@gmail.com

background agents. The present scenario of social engineering lies in the hands of attacks like phishing, spamming. The main goal is detect and block the malicious URLs which are the root cause of social engineering. Just think of net banking system. We often neglect the security issues and land onto giving our important credentials to a fake webpage that is controlled by a third party or hacker. The degree of social engineering threat is increasing exponentially. We have tried to detect the malicious URLs using and optimize it using one of the evolutionary algorithm i.e. ABC. It reduces the training time of detection of the malicious URLs.

2 Literature Review

In Sect. 1 we have seen that malicious URLs are the key weapon for a social engineer. There are various methods used in detecting the malicious URLs. Xin (Robert) Luo et al. describes the human factors that help the social engineers. This article examines human factors that can lead to social engineering intrusions. Christophe Chong et al. have described in their work on web vulnerabilities on the smart phones or mobile devices. They have focused on a machine learning solution that identifies malicious URLs using a combination of URL lexical features, JavaScript source features. Monther Aldwairi and Rami Alsalman uses the Naive approach for the detection process for the authenticity of the URL under scanner. Justin Ma et al. also highlighted in their paper a model that helps in extracting and automatically analyzing tens of thousands of features potentially indicative of suspicious URLs.

In all the above mentioned research work it has been found that there are certain features which can be used as the training sets for the optimization.

3 Our Framework

In this part of the paper we will showcase the methodology and the proposed techniques by which the malicious URLs can be detected. But before hitting the deck let us study the key points which encompass the whole paper.

3.1 *Social Engineering Threats*

Social engineering is the most upcoming threats in the field of cyber security. In the earlier stages the social engineers were in the form teller-callers those gave fake calls to the people and deceive them to gain control over important information.

The current face of social engineering is in the form of phishing, malware, spamming, etc. In which the user thinks that the URL in front of them is authentic enough to give the credentials.

3.2 Malicious URL

Malicious URLs Examples (*Kindly enlarge the images for better view*) (Figs. 1, 2, 3).

3.3 Methodology

In [Sect. 3.3](#) we will study the process by which we will detect the malicious and useful URLs. The primary goal is to identify the fake web pages so as to prevent the social engineering attacks [1]. First of all we will discuss the framework or flow of activities which shows the working of the model.

In [Fig. 4](#) we can see the flow of activities that will be followed so as to complete the detection of malicious URLs. The first step is to get a collection of 50 malicious and benign web URLs [2]. Secondly, the features from those URLs will be extracted. All about the features will be discussed in [Sect. 4](#). Third step contains the model generation. In fourth step ABC is used for the population evolution and the fitness function is maximized. The last step contains the detection of the malicious web URLs and their testing.

So, let us have a look over the five steps of the flow chart in detail.

4 Features Extraction

Features are basically of three kinds:

1. Lexical Tokens.
2. Web-based features.
3. Network features.

4.1 Lexical Tokens

In [Sect. 4.1](#) we will study the different parameters by which a webpage or URL is being identified when we talk about URL, i.e. Uniform Resource Locator and URI i.e. [3] Uniform Resource Identifier, these tools are used to identify any webpage on the internet. URL can be bifurcated into three parts:

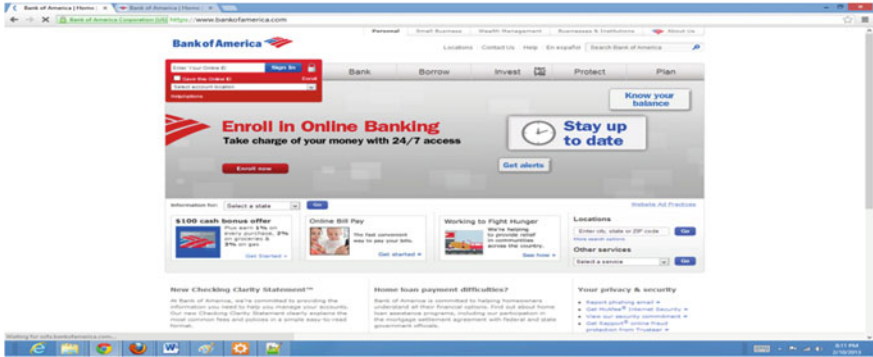


Fig. 1 Original Bank of America Site

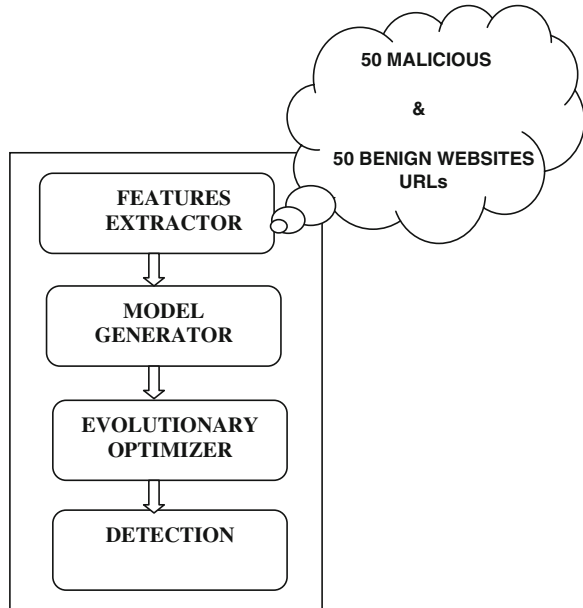


Fig. 2 The Forged Site



Fig. 3 Observe the difference between URL and link Highlighted Page

Fig. 4 Flowchart: The framework or flow of activities



1. The protocol.
2. Hostname.
3. Path.

Take the example of a URL “<http://www.nutrisicag.com/home/about.pdf>” [4]. So, the mentioned URL have three parts, protocol is “http://”, hostname is “www.nutrisicag.com”, and last but not the least path is “home/about.pdf”. In addition to the given information we have certain features known as “bag-of-words” like ‘?’, ‘+’, ‘-’, ‘&’, ‘_’.

4.2 Web-Based Features

In addition to the lexical tokens there are host based features such as IP address, domain name services, time to live (TTL), DNS A, DNS PTR and DNS MX. These features are used for the classification and detection process [5].

4.3 Network Features

Beside and fore mentioned lexical and host based features there are network features which helps in the smooth running of the system. Such features includes

Features		
Java Script	DNS	Path Tokens
Document frequency DF	Connection speed	Last token value
Title tag	DNS record	TLD
IP address	URLs	DNS TTL
Lexical tokens	Meta data	Meta Tags

Fig. 5 Features

JS Enable/Disable, 3-4-5 grams (n grams), HTML tags, Term Frequency and Inverse Document Frequency (TF-IDF) [6, 7]. All the features mentioned above have their specific tasks, so it is not possible and needed to discuss them here [8].

5 Model Generation

The starting phase consists of the data acquisition. In which 50 benign and malicious website being mined. For benign URLs we have used a crawler on the Alexa ranking website. On the other hands for malicious website we have mined malware database (<http://support.clean-mx.de/cleanmx/%20viruses>). It is quite obvious that duplicate URLs may be present after collecting them from the source. So we have eliminated the duplicate one's by matching the lexical tokens of the URL. After this a training dataset is being created as shown in Fig. 5.

5.1 Training Dataset

In this section, the author have created a training data set that comprises of Java Script, Domain Name Service (DNS), and Path Tokens. All the three mentioned characteristics are quite responsible and helpfull in detecting the malicious URLs. See Fig. 5.

6 Artificial Bee Colony Algorithm

6.1 Introduction

ABC, proposed by Karaboga in 200 is a relatively recent bio-inspired meta heuristic optimization algorithm that mimics the natural intelligent foraging behavior of honey bees. Initially ABC was proposed and developed for solving continuous

optimization problems. Since the introduction of ABC, it has also been applied to solve a wide variety of optimization problems arising in various disciplines. The detailed survey can be studied in ABC comprises of three kinds of bees namely (a) Scout (b) Employed and (c) Onlooker bees [9]. The bees intelligently organize themselves and divide the labor to perform the tasks like searching for nectar, sharing information about the food source etc.

The position of a food source represents a possible solution to the optimization problem and the nectar amount of a food source corresponds to the quality (fitness) of the associated solution. A brief overview and mathematical model of ABC is presented in Sect. 3.2.

6.2 Outline of Artificial Bee Colony

6.2.1 Unconstrained ABC

ABC tries to model natural behavior of real honey bees in food foraging. The colony of artificial bees comprises of three groups of bees: employed bees which takes the responsibility for exploiting the food sources and communicate the information to the onlooker bees, which are waiting in the hive. Onlooker bees chooses the food sources by watching the waggle dance performed by employed bees while scouts explores the food sources randomly based on some external clue [10]. The basic steps of unconstrained ABC are discussed below:

Initialization of Food Sources (Population of Solutions): The first step of ABC is generation of initial population. Suppose, the initial population consists of SN number of n -dimensional real-valued vectors, representing the food sources, which are generated randomly. Suppose $X_i = \{x_{i,1}, x_{i,2}, \dots, x_{i,n}\}$ denotes the i th food source in the population, where each food source is initialized as:

$$x_{i,j} = x_{\min,j} + rand(0, 1)(x_{\max,j} - x_{\min,j}) \quad (1)$$

where $i \in 1, 2, \dots, SN$; $j \in 1, 2, \dots, n$. $x_{\max,j}$ and $x_{\min,j}$ denotes the upper and lower bound constraints respectively of decision variable. These food sources are assigned randomly to SN number of employed bees and their fitness is determined [11].

Determination of new food locations (Employed Bees Stage): The duty of employed bees is to determine new food source say, v_i with the help of the food source x_i assigned to it during the initialization phase. The employed bees exploit the food source. The equation used is:

$$v_{ij} = x_{ij} + \phi_{ij}(x_{ij} - x_{kj}) \quad (2)$$

where $k \in \{1, 2, \dots, SN\}$ and $j \in \{1, 2, \dots, n\}$; Control parameter $\phi_{ij} \in [-1, 1]$ gives the step length which decides the movement of bees. k is generated randomly such that, $k \neq i$. After a new food source has been generated by the employed bee, a

tournament selection is held between v_i and x_i and the one with a better fitness value becomes the member of the population.

Evaluation of Nectar Information or quality of solution (Onlookers Phase): The work of onlookers is to enhance the exploration capability of ABC. An onlooker evaluates the nectar information (i.e. the fitness of solutions) collected from all the employed bees and selects a food source x_i using probability P_i as:

$$P_i = f_i / \sum_{k=1}^{SN} f_k \quad (3)$$

where f_i denotes the fitness value of the i th food source. The onlooker after selecting the food source x_i , modifies it by using Eq. (2). Once again a tournament is held between the food source selected and the food source modified by the onlooker and once again as in previous step, the one with better fitness value becomes a member of the population. Therefore, good food sources attract more onlooker bees compared to bad ones.

Diversity mechanism in ABC (Significance of Scouts): The main work of scouts is to induce diversity in ABC. An employed bee which is not able to improve the fitness value of a food source becomes a scout. A scout is activated when it is observed that the fitness of a food source x_i shows no betterment even after a specified number of trials limit. Stagnation in the fitness value of a food source indicates that the particular food source may be replaced with a new food source. Scout produces a new food source with the help of Eq. (1).

7 Detection and Results

We have implemented the proposed model using JSP language and Microsoft Access as a database. For the collection of the malicious URLs we have used Chrome plug-in. We have a precision ratio mentioned below in Eq. (4) which is used to evaluate the accuracy of the model using different features.

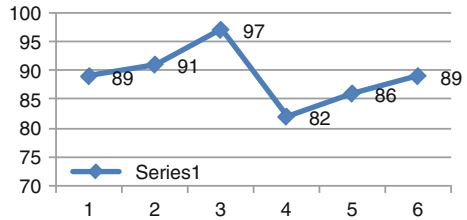
$$Q = \frac{\text{number of URLs classified correctly}}{\text{total number of URLs}} \quad (4)$$

As we have used ABC the precision percentage is 89 %. We have taken a small amount just half of the dataset. So to conclude we may say that if we take a large amount of dataset than the precision ratio can improve to a great deal.

Let us observe the precision percentage with the help of graph.

We have divided the result into 6 subsets and calculated the precision using ABC. The result is shown with the help of a graph as given in the Fig. 6. It is clearly shown that the average of the precision using ABC is 89 %. We can't neglect the fact that we have applied DE to the fitness function which is working on a smallest dataset of 100 malicious and benign website URLs.

Fig. 6 The precision percentage



8 Conclusion

In the work above we have proposed a method by which the social engineering can be prevented. The root cause of social engineering is some basic cyber attacks like phishing, spamming etc. So we have tried to detect the malicious websites. Once we can know that the link or URL we are going to click is malicious the work is half done. We have used DE to expand the population of the training dataset. As a larger set of the malicious dataset will be proved helpful in detecting the malicious link. The training time is reduced by using DE to a great deal. The experimental results shows that the average system precision is 89 %. In our future work we are looking to embed more evolutionary algorithms to get a better results.

References

1. CISCO IRONPORT.: IronPortWeb Reputation: Protect and defend against URL-based threat. <http://www.ironport.com>
2. ALEXA.: The web information company. <http://www.alexa.com> (1996)
3. Aldwairi, M., Alsalman, R.: MALURLs: Malicious URLs Classification System. In: Proceedings of the Annual International Conference on Information Theory and Applications (ITA), Singapore (2011)
4. Ma, J., Saul, L., Savage, S., Voelker, G.: Beyond blacklists: learning to detect malicious websites from suspicious URLs. In: Proceedings of the ACM SIGKDD Conference, Paris, France (2009)
5. Choi, Y.H., Kim, T., Choi, S.J.: Automatic Detection for JavaScript obfuscation attacks in web pages through string pattern analysis. <http://www.sersc.org/journals/IJSIA/vol4%20no2%202010/2.pdf>
6. DNS-BH.: Malware prevention through domain blocking. <http://www.malwaredomains.com>
7. Google.: Google Toolbar. <http://tools.google.com/firefox/toolbar/>
8. Antonakakis, M.: Kopis: detecting Malware domains at the upper DNS hierarchy. <http://static.usenix.org/%20events/sec11/tech/slides/antonakakis.pdf>
9. Karaboga, D.: An idea based on honey bee swarm for numerical optimization. Technical Report TR06, Erciyes University, Engineering Faculty, Computer Engineering Department (2005)
10. Karaboga, D., Basturk, B.: On the performance of artificial bee colony (ABC) algorithm. *Appl. Soft Comput.* **8**(1568–4946), 687–697 (2007)
11. Karaboga, D., Basturk, B.: A powerful and efficient algorithm for numerical function optimization: artificial bee colony (ABC) algorithm. *J. Global Optim.* **39**(0925–5001), 459–471 (2007)

New Lightweight Conditional Encryption Schemes for Multimedia

Sakshi Dhall, Saibal K. Pal and Kapil Sharma

Abstract The unprecedented advancement in multimedia technology and the upsurge of social networking as an indispensable part of day to day life, has brought forth an unimaginable necessitate for voluminous data transfer over inherently insecure networks. Besides security, another major aspect today is to design lightweight encryption schemes which can perform effectively on hand-held devices like mobiles and provide security as per the requirements of the applications. The standard encryption schemes address the security aspect of only plain textual data and are not suitable for securing voluminous real-time data transfers, having significant level of redundancies, over resource-constrained environments. Focusing on this requirement introduced as the need of the hour, the paper proposes novel lightweight encryption schemes, based on conditional approach, using simple S-Box look-ups, shifting, negation and XORing (standard Exclusive OR) as the basic building blocks. To address the issue of significant redundancy present in the plain text, pixel position has been introduced as one of the parameters in the encryption process. The results of empirical analysis demonstrate the strength of the proposed schemes and they perform equally well for worst case scenarios (white image). The comparative results demonstrate complete removal of redundancies in the proposed cipher with much higher computational efficiency as compared to the standard schemes like AES.

Keywords Image encryption · S-Box · Computational efficiency · Avalanche effect

S. Dhall (✉)

Jamia Millia Islamia University, New Delhi 110025, India
e-mail: sakshidhall@gmail.com

S. Dhall · K. Sharma

Delhi Technological University, New Delhi 110042, India
e-mail: kapil@ieee.org

S. K. Pal

Scientific Analysis Group, DRDO, New Delhi 110054, India
e-mail: skptech@yahoo.com

1 Introduction

In today's world, bulk data exchange has become a necessary and indispensable part of many applications thereby leading to an apparent and intense upsurge among researchers for devising security solutions for the voluminous transmissions over insecure and inherently vulnerable networks. Cryptography [1, 2] is the science dealing with designing algorithms to convert plaintext to non-perceivable forms thereby facilitating secure transmission of sensitive information from the source to the destination.

Earlier, transmissions largely constituted textual data but there has been a drastic shift in the nature of data required to be transmitted over susceptible and penetrable network channels. Advancement in mobile and multimedia technologies [3, 4] and the boon in social networking have given an altogether different dimension to data transfer requirements. They have opened up space for multimedia content [5], like images, audio and video, to become part of major data exchanges happening today.

Unlike textual data, multimedia content has two major characteristics—it normally has significant redundancies and is much bulkier in terms of data-rate and bandwidth & storage requirements. These characteristics attributed to multimedia content evoke an apparent need for separate encryption schemes to address the special issues which remain unhandled with the traditional block cipher schemes like AES, IDEA or DES [6], which are otherwise suitable for textual data.

Block cipher schemes encrypt a block of data at a time and generate equal-sized cipher using key which is symmetric. The basic design of block ciphers normally involves several rounds of a fixed set of operations wherein the secret part is the round key. Substitution and transposition are two of the fundamental building blocks for any block cipher algorithm. Round key generation, S-Box and number of rounds are some of the key critical aspects of block cipher design where the trade-off remains between the strength of the cipher and the number of operations involved, and depending on the nature of application a balance is required to be achieved.

Multimedia encryption schemes [7–9] also follow fundamentally similar primitives and design approach as any block cipher. Besides the bulkier nature of multimedia, due to the wide range of real time applications in the varied fields of entertainment, social networking, medical science, military etc., multimedia encryption schemes need to be computationally light [10] and at the same time they also need to ensure that the redundancies in the plaintext do not get propagated and reflected in the cipher [11]. There are two feasible approaches for designing cryptosystems for multimedia security—one is to design new primitive schemes based on new design constructs to suit multimedia requirements, and the other is to introduce suitable modifications in the operations to accommodate the special characteristics attributed to multimedia while maintaining the high level structure similar to that of standard schemes like AES. The former approach will require rigorous analysis before its strength could be established while the latter approach is better as it will be based on an already proven standard for security. With this as the

underlined rationale, the paper proposes three variants of lightweight block cipher [12] based on conditional encryption. The paper is an extension of our previously authored work [13] with the intent of customizing it to suit the multimedia requirements, increasing the security without significantly increasing the computational cost and keeping it in line with the basic conditional approach.

The rest of the paper is organized as follows. Section 2 briefs about the original algorithm followed by our implementation describing the three proposed variants customized to suit multimedia data in Sect. 3. Section 4 reports the observations and subsequent analysis of our schemes. This is followed by the conclusion section.

2 Block Cipher Based on Conditional Encryption

The algorithm [13] uses 128 bit key to generate eight 128 bit round keys, one per round, and encrypts a block of 128 bits. Each round comprise of two phases—Readjustment Phase followed by Substitution & Shifting Phase. The 128 bit key is denoted by 16 bytes $k[0], k[1] \dots k[15]$. Also $rk[i], P[i], C[i]$ denote the i th byte of the round key, plain text and cipher respectively and n represents the total number of bytes in the round key. The operators \wedge, \lll, \ggg denote XOR, left circular shift and right circular shift respectively. Also ‘ q ’ represents the number of non-zero bytes (of round key) with even parity and ‘ r ’ represents the parity of 128 bit round key. Following are the details of the operations performed as part of the base algorithm:

- (a) **Re-adjustment Phase:** This is the first phase per round in the overall encryption process. It re-arranges and/or negates part or all bits of the plain text and/or the round key. The intent of this phase is to perform minor operations on the plain text and round key based on the conditional approach where the decision of the operations performed is based on the parity of the round key and the number of non-zero even parity bytes in the round key.

```

If r is even {
    If q is even {
        Swap the two 64-bit halves of the round key
        Negate 1st half (first 64-bits) of the plain text
    }
} else {
    If q is even {
        Negate all 128-bits of the plain text
        Swap the two 64-bit halves of the plain text
    } else {
        Negate 1st 64 bits of the round key
        Negate last 64 bits of the plain text
        Swap the two 64-bit halves of the plain text
    }
}
    
```

- (b) **Encryption:** The encryption process involves 8 rounds and each round begins with the readjustment phase as described above, followed by substitution using AES S-Box. This is further followed by conditional bitwise shifting and XOR operations on the readjusted plain text to generate the cipher, where bytes_XOR refers to $rk[0] \wedge rk[1] \dots \wedge rk[15]$.

Generate_round_key(k)

Per round operation

Perform Re-Adjustment Phase

$C = \text{AES_SBox_based_Substitution}$

if bytes_XOR = even {

 for i = 0 to 15

$C[i] = P[i] \lll (rk[i] \% 8)$

 } else {

 for i = 0 to 15

$C[i] = P[i] \lll (rk[n-1-i] \% 8)$

 }

$C[0] = C[0] \wedge rk[0]$

for i = 1 to 15

$C[i] = C[i-1] \wedge C[i] \wedge rk[i]$

3 Implementation

The scheme described in the earlier section is built on computationally less expensive fundamental operations like shifting, XORing, substitution and negation. With block size of 128 bits it showed impressive results for textual data but is not found suitable when applied directly to multimedia due its fixed block size. In this paper, we propose three variants of the described scheme having customizable block size, maintaining low operational cost, addressing the issue of redundancy in the plain text, and therefore making them suitable for multimedia applications. In all the three proposed variants, position of the pixels has been brought out as a parameter so as to overcome the redundancies present in the plain multimedia. The variants maintain the key size of 128 bits and as the block size is customizable so the entire image can be encrypted in one go or in parts as per the application's security requirements. As mentioned, to bring pixel position as one of the parameters determining the cipher, the intermediate cipher is XORed with the pixel position in all the variants. We now present the three proposed variants in details where we let 'n' be the customizable block size (in bytes).

3.1 First Scheme

This variant introduces conditional left or right rotation of the AES S-Box [14] before performing the substitution as per the base algorithm. The round key dependent **sBoxRoundConstant** determines the number of rotations of the S-Box. Also, the intermediate cipher is parameterized as per the pixel positions by introduction of XORing operation with the pixel positions.

(a) **Re-adjustment Phase**

```

If r is even {
    If q is even {
        Swap the two 64-bit halves of the round key
        Negate 1st half (first 64-bits) of the plain text
        sBoxRotationDirection = left
    } else {
        sBoxRotationDirection = right
    }
} else {
    if q is even {
        Negate all 128-bits of the plain text
        Swap the two 64-bit halves of the plain text
        sBoxRotationDirection = left
    } else {
        Negate 1st 64 bits of the round key,
        Negate last 64 bits of the plain text
        Swap the two 64-bit halves of the plain text
        sBoxRotationDirection = right
    }
}

```


(b) Image Encryption

Generate_round_key(k)

Per round operation

sBoxRotationConst = 0

sBoxRotationDirection = ''

for i = 0 to 15 {

sBoxRotationConst= sBoxRotationConst^rk[i]

}

Perform Re-Adjustment Phase

C = AES_SBox_based_Substitution_with_rotation
 (sBoxRotationConst, sBoxRotationDirection)

for i = 0 to n-1 {

C[i] = C[i]^ (i&0xFF)

}

If bytes_XOR = even {

 for i = 0 to n-1

 C[i] = P[i] <<< (rk[i%16] %8)

} else {

 for i = 0 to n-1

 C[i] = P[i] <<< (rk[15-(i%16)] %8)

}

C[0] = C[0] ^ rk[0]

for i = 1 to n-1

 C[i] = C[i-1]^C[i]^rk[i%16]

Each round of the encryption process starts with the readjustment phase which besides readjusting the plain text and/or round key as per the base algorithm, in this variant, also determines the sBoxRotationConst value and the sBoxRotationDirection for subsequent S-Box rotation for the substitution operation. After the readjustment phase, follows the substitution based on the key based rotated S-Box. The intermediate cipher bytes are then XORed with their respective positions in the image, and finally the shift and XOR operations are applied to yield the cipher.

3.2 Second Scheme

The second variant involves generation of key-based S-Box [15] for substitution instead of performing conditional left or right rotation of the AES S-Box as done in Variant 1. Also, unlike variant 1, there is no change in the Re-adjustment Phase as compared to the base algorithm.

The strength of this variant lies in the key-based S-Box generation. And to ensure the pixel position determines the cipher output, as in variant 1 here again, the intermediate cipher bytes are XORed with the respective pixel positions.

The second variant is an improvement over the first variant in terms of efficiency. The first variant involved key based conditional left or right rotation of the AES S-Box in each round thereby involving higher computation, while this variant generates key based S-Box once for all the rounds thereby making it even lighter.

3.3 Third Scheme

This variant is an extension of the second variant to increase the strength of the algorithm. FAN transform [16, 17] based scrambling of the image is included as the preprocessing step adding another layer of security to this variant thereby enhancing its strength.

FAN transform provides a one to one mapping for carrying out transposition of the image pixels from one pixel location to the other. Application of several iteration of the FAN transform reduces correlation among the pixels and converts the image to incomprehensible form. After the application of FAN transform, the scrambled image is made to undergo key-based generated S-Box substitution followed by the XOR and shifting operations as done in variant 2.

The next section discusses the observations of all the three discussed schemes in details.

4 Observations and Analysis

The strength of the three variants is judged based on a number of observations taken on 512×512 sized 8-bit grayscale images; however the schemes can be extended to other color planes without any modification. Figure 1 shows the original and encrypted Peppers image (Variant 1). The encrypted image does not contain any textured regions indicating that the redundancies in the original image are not propagated in the encrypted counter-part. The histogram and entropy values are studied. The histogram of the cipher image is found to be smoothly distributed and the variation in entropy across the cipher image is also nearly uniform. Figure 2 displays the histogram of the original and encrypted image (Variant 1) and Fig. 3 represents the block-wise entropy of the encrypted image (Variant 1) observed by dividing the image into 64 equal blocks of size 64×64 . Observations taken with Variant 2 and Variant 3 also show similar results with complete removal of redundancies after encryption, smooth histograms and uniform block-wise entropy across the cipher image.

Further, the avalanche properties for the three variants are also studied by observing:

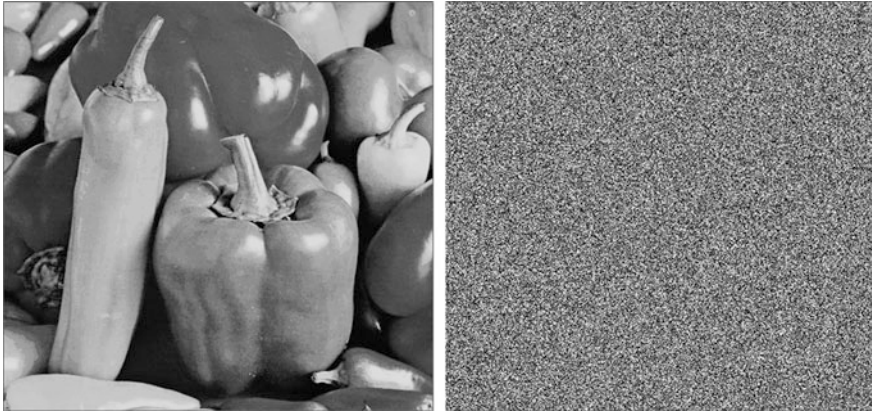


Fig. 1 Original and encrypted Peppers image

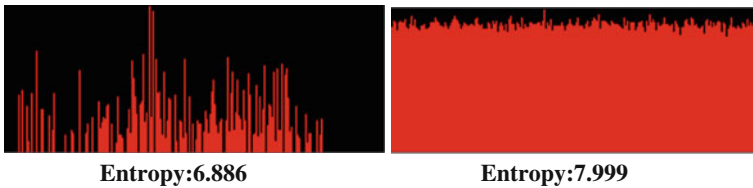


Fig. 2 Histograms & entropy of original and encrypted Peppers image

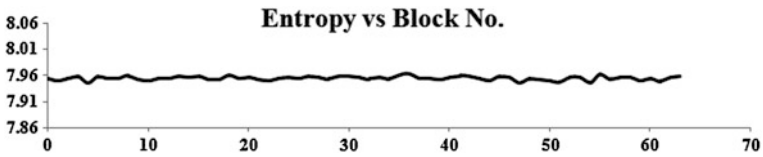


Fig. 3 Blockwise entropy plot of encrypted Peppers image

- (i) Number of bits changed in the cipher with one bit changed per pixel.
- (ii) Number of bits changed in the cipher with one bit change in the key.
- (iii) Number of bits changed in the decrypted image when decrypted using a key having one bit changed as compared to the original key used while encryption.

The graphs for all the above set of observations show variation within the acceptable range, and average to around 50 % change of bits in all the above scenarios, thereby indicating strong avalanche properties. Figures 4, 5 and 6 shows some of the avalanche observations for the three variants.

Fig. 4 Number of bits changed in the cipher with one bit changed per pixel (Peppers image, Variant 1)

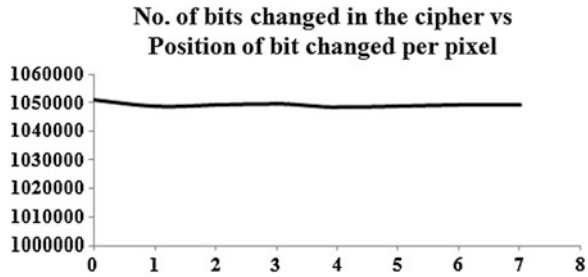


Fig. 5 Number of bits changed in the cipher with one bit change in the key (Peppers image, Variant 2)

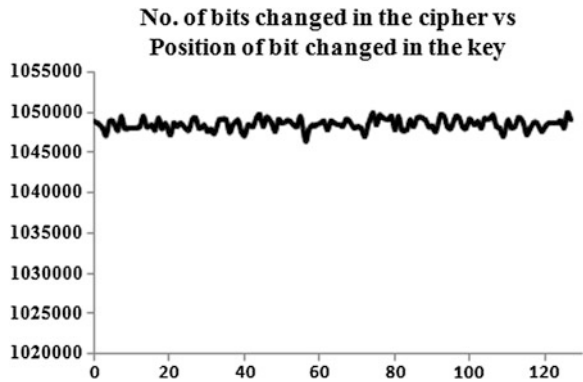
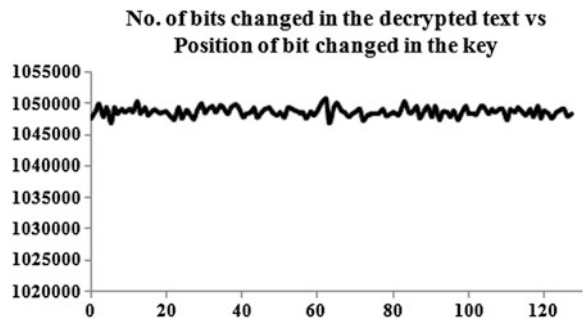


Fig. 6 Number of bits changed in the decrypted cipher with one bit changed while decryption (Peppers image, Variant 3)



Also, similar set of observations were taken on plain white image and the results were identical. Figures 7 and 8 shows the histogram and one of the avalanche property observations respectively, obtained with Variant 2 for plain white image.

In addition to the above, the NPCR, UACI [18] and Correlation-coefficient values were taken for the three variants on Peppers and Plain White Image. NPCR (Number of Pixel Change Rate) is a metric to identify the rate at which number of pixels is changed in the cipher with one pixel changed in the original image. Likewise, UACI (Unified Average Change Intensity) measures the average change in intensity of the pixels in the cipher with one pixel change in the original image.

Fig. 7 Histogram & entropy of encrypted *White image*

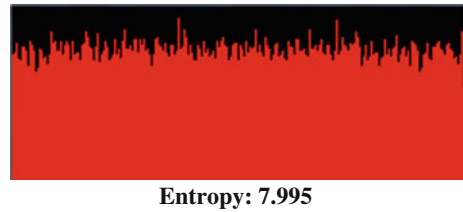
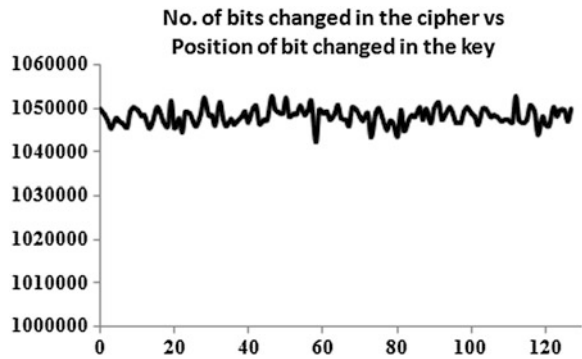


Fig. 8 Number of bits changed in the cipher with one bit change in the key (*White image, Variant 2*)



Both these values lie between 0 and 1 and higher the values, better is the observation in terms of security.

While NPCR and UACI are calculated between two cipher images with one bit changes in the original images, correlation coefficient is evaluated between the original image and the cipher image. It is an indicator of the relationship between the original image and the encrypted one. Its value lies between -1 and 1 , where values closer to 1 indicate strong correlation, values closer to -1 indicate strong anti-correlation and values closer to 0 indicate minimal relation between the original and the cipher image.

The NPCR, UACI and correlation coefficient observations are specified in Table 1 as under:

As the high level structure of the proposed schemes is similar to that of AES, involving multiple rounds with each round constituting transposition and non-linear substitution operations with an additional conditional approach, thus a comparative study with the standard AES algorithm is also done. It shows that the cipher generated using AES in ECB mode contains significant redundancies while the same are completely removed in the ciphers generated with the proposed schemes. Figure 9 shows a magnified section of the ciphers generated using AES (containing textured areas) and proposed scheme (Variant 2) for Peppers image (redundancies completely removed).

Further AES in CBC mode is not a feasible option as it involves a significant increase in the computation for bulky multimedia content and also recovering and decrypting back the plain text becomes difficult in case of packet loss on the network.

Table 1 Security analysis & image quality measures

Variant	Image	NPCR	UACI	Correlat ⁿ Coefficient
1	Peppers	0.99599	0.33522	-0.001894
	White	0.99545	0.33601	-
2	Peppers	0.99610	0.33500	-0.000991
	White	0.99597	0.33565	-
3	Peppers	0.99620	0.33451	-0.000683

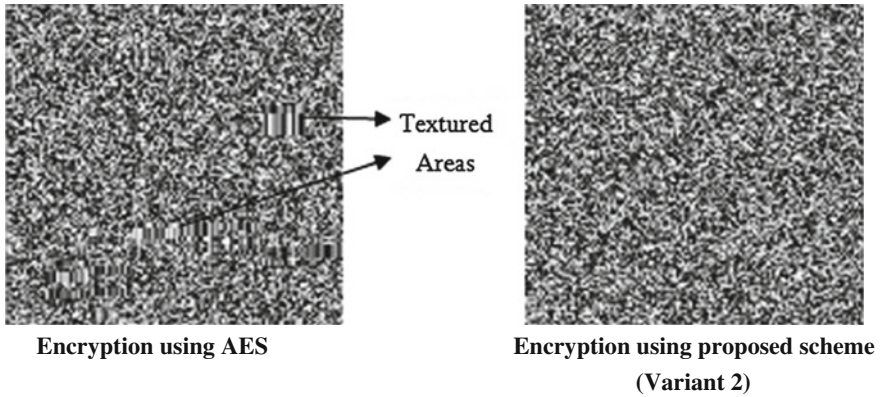


Fig. 9 Comparison of encryption using AES and proposed scheme

In addition to the above, time observations show that Variant 1 takes around 40 % less time and Variant 2 takes around 50 % less time as compared to AES thereby highlighting the computational efficiency of these schemes,.

5 Conclusions

New lightweight schemes with customizable block size for multimedia encryption were proposed in this paper. The proposed schemes utilize simple operations like XORing, negation and shifting which are computationally less expensive hence suitable for securing bulky multimedia content. Also, the conditional approach ensures dynamic behavior in the algorithm itself hence making it more difficult for attackers and the introduction of pixel position as one of the parameters in the encryption process addresses the issue of high levels of redundancy in the plain text.

Comparison with the standard AES algorithm shows that standard schemes otherwise suitable for plain textual data neither prove to be efficient to sustain the bulkiness attributed to multimedia, nor are they able to prevent the redundancies

prevalent in the plain text to get propagated to the generated cipher. On the other hand, observations taken on Peppers and Plain White Image show strong avalanche properties by all the three variants. Uniform and consistent results especially for the first two variants, for plain white images display their strength irrespective of the level of redundancy in the plain text. This testifies high resistance against various cryptanalytic attacks. The smooth histograms, uniform block-wise entropy, correlation coefficient value approaching zero and NPCR and UACI values as high as 0.99 and 0.33 respectively, showcase the strength of the proposed schemes.

Also the observations demonstrate that out of the three variants, the Variant 2 is the lightest hence making it suitable for security requirements on resource constraint hand-held devices. Variant 1 is computationally little higher expensive as compared to Variant 2 yet it is far lighter than standard algorithms like AES and hence is suitable for multimedia applications where resource availability is adaptive. Variant 3 involves an extra layer of security in the form of FAN transform hence making it suitable for multimedia applications with high security requirements where resource constraint is not a major determining factor.

The future work would relate to identification and design of more constructs for providing computational efficiency with adequate amount of security depending on the nature of the evolving applications. Rigorous security analysis and cryptanalysis of the proposed schemes as block ciphers shall also be addressed as part of the future work to establish the usability and applicability as standard block ciphers. Also, theoretical and cryptanalysis will be attempted for other multimedia encryption schemes with an approach of improving their security.

References

1. Stinson, D.R.: *Cryptography: Theory and Practice*, 3rd edn. Chapman & Hall, Boca Raton (2005)
2. Menezes, A. (ed.): *Handbook of Applied Cryptography*. CRC-Press, Boca Raton (1996)
3. Furht, B. (ed.): *Encyclopedia of Multimedia*. Springer, New York (2005)
4. Gonzalez, R.C., Woods R.E.: *Digital Image Processing*, 3rd edn. Prentice Hall, Upper Saddle River (2007)
5. Leitold, H., Markatos, E.: *Communication & multimedia security: In: Proceedings of the 10th IFIP International Conference, LNCS*, Springer (2006)
6. Stallings, W.: *Cryptography & Network Security Principles and Practices*, 3rd edn. Pearson Education (2004)
7. Lian, S., Zhang, Y.: *Handbook of research on secure multimedia distribution*, Information Science Reference, IGI Global (2009)
8. Lian, S.: *Multimedia Content Encryption—Techniques and Applications*, pp. 21–42. CRC Press, Taylor & Francis Group, New York (2009)
9. Kang, X., Peng, A., Xu, X., Cao, X.: Performing scalable lossy compression on pixel encrypted images. *EURASIP J. Image Video Process.* **2013**, 32. <http://jivp.urasipjournals.com/content/2013/1/32>
10. Agrawal, P., Rajpoot, M.: Partial encryption algorithm for secure transmission of multimedia messages. *Int. J. Comp. Sci.* **3**(1), 467–470 (2012)

11. Lini, A., Neenu, D.: Secure image encryption algorithms: a review. *Int. J.Sci. Technol. Res.* **2**(4) (2013) ISSN 2277-8616
12. Ahmed, F., Resch, C.L.: Characterizing cryptographic primitives for lightweight digital image encryption. In: *Proceeding of Mobile Multimedia/Image Processing, Security, and Applications*. SPIE 7351, 73510G, pp. 10G 1–11, (2009)
13. Dhall, S., Pal S.K.: Design of a new block cipher based on conditional encryption, ITNG 2010. IEEE Computer Society/CPS, IEEE Conference Publishing Services, Las Vegas, pp. 714–718 (2010)
14. Krishnamurthy, G.N., Ramaswamy, V.: Making AES stronger: AES with key dependent S-box. *Int. J. Comput. Sci. Netw. Secur.* **8**(9), 388–398 (2009)
15. Abd-ElGhafar, I., Rohiem, A., Diao, A., Mohammed, F.: Generation of AES key dependent S-boxes using RC4 algorithm. In: *13th International Conference on Aerospace Sciences & Aviation Technology (ASAT-13)*, 26–28 May 2009
16. Jing, F., Fei, H.: FAN transform in image scrambling encryption application. (2009) doi:978-1-4244-5668-0/09
17. Li, B., Xu, J.: Period of Arnold transformation & its application in image scrambling. *J. Central South Univ. Technol.* **12**(1), 278–282 (2005)
18. Wu, Y., Noonan, J.P., Agaian, S.: NPCR and UACI randomness tests for image encryption, cyber journals: multidisciplinary journals in science and technology. *J. Sel. Areas Telecommun.* (2011)

Comparative Study of Controller Optimization Techniques for a Robotic Manipulator

Richa Sharma, K. P. S. Rana and Vineet Kumar

Abstract A robotic manipulator is a highly nonlinear, highly coupled, Multi-Input Multi-Output (MIMO) and dynamic system. Being complex in nature conventional Proportional-Integral-Derivative (PID) controller tuning methods, in general, are not applicable to these systems. For the past two decades, with the advent of efficient and high speed computing power, optimization techniques are being applied for complex non-linear processes for tuning of controllers. These techniques yield optimized performance for customised performance indexes. This paper presents a detailed comparative study of performances of three optimization techniques for the tuning of PID controllers for a two-link planar rigid robotic manipulator. In this work tuning of PID controllers has been carried out using three techniques namely Particle Swarm Optimization (PSO), Simulated Annealing (SA) and Genetic Algorithm (GA). Two performance indices namely Integral of Absolute Error (IAE) and Integral of Absolute Change in Control Output (IACCO) with equal weightage for both the links are considered for optimization. The robustness testing of optimized controllers is done for the trajectory tracking, model uncertainties and disturbance rejection. The simulation results clearly indicate that the PSO outperforms both SA and GA.

Keywords Two-link planar robotic manipulator · PID controller · Particle swarm optimization · Simulated annealing · Genetic algorithm · Trajectory tracking · Robustness testing

R. Sharma (✉) · K. P. S. Rana · V. Kumar
Instrumentation and Control Engineering Division, Netaji Subhas Institute of Technology,
Dwarka, New Delhi 110078, India
e-mail: richasharma_7@yahoo.co.in

K. P. S. Rana
e-mail: kpsrana1@gmail.com

V. Kumar
e-mail: vineetkumar27@gmail.com

1 Introduction

For the past few years, the applications of robotic manipulators in the field of industry, space, nuclear plants and medical has increased due to their effectiveness in accurate positioning and the trajectory tracking tasks [1]. Essentially it requires the effective control of end-effector of the robotic manipulators. PID controllers with different implementations have been cited for control of robotic manipulators by several authors [2–6]. The critical issue has been the tuning of the PID controller so that it would provide accurate control signal for the end-effector. With the advancement in the computational intelligence, the intelligent optimization techniques such as real coded GA [7], PSO [8, 9], Multi-Objective GA (MOGA) [4, 10], Tabu Search [11, 12], Differential Evolution (DE) [13], Ant Colony Optimization (ACO) [14, 15] and Non-Linear Programming (NLP) [16] have also been used for the tuning of PID controllers. The literature survey indicates the need of the comparative study of various optimization techniques for PID controller tuning for a two-link planar robotic manipulator. This will enable the user to tune the controller effectively.

This paper is organized as follows. The model of a two-link planar rigid robotic manipulator is presented in Sect. 2. In Sect. 3 the trajectory to be tracked has been described. In Sect. 4 an overview of the PID controller is presented. Section 5 presents the brief of the used optimization techniques. The simulation results are presented in Sect. 6. Finally, the conclusion is drawn in Sect. 7.

2 Model of Two-Link Planar Rigid Robotic Manipulator

The mathematical model of two-link planar rigid robotic manipulator as shown in Fig. 1 has been described in [4].

Following Eqs. (1) and (2) show the relationship between control output or torque (τ) and link position (θ) for both the links. Table 1 lists the relevant parameters.

$$\begin{aligned} \tau_1 = & l_2^2 m_2 \left(\frac{d^2 \theta_1}{dt^2} \right) + l_1^2 (m_1 + m_2) \left(\frac{d^2 \theta_1}{dt^2} \right) + m_2 g l_2 \cos \theta_1 \cos \theta_2 + (m_1 + m_2) l_1 g \cos \theta_1 \\ & - m_2 l_1 l_2 \sin \theta_2 \left(\frac{d\theta_2}{dt} \right)^2 - 2m_2 l_1 l_2 \sin \theta_2 \left(\frac{d\theta_1}{dt} \right) \left(\frac{d\theta_2}{dt} \right) + m_2 l_1 l_2 \cos \theta_2 \left(2 \frac{d\theta_1^2}{dt^2} + \frac{d\theta_2^2}{dt^2} \right) \end{aligned} \quad (1)$$

$$\begin{aligned} \tau_2 = & m_2 l_1 l_2 \sin \theta_2 \left(\frac{d\theta_1}{dt} \right)^2 + m_2 l_1 l_2 \cos \theta_2 \left(\frac{d\theta_1^2}{dt^2} \right) + m_2 l_2^2 \left(\frac{d\theta_1^2}{dt^2} + \frac{d\theta_2^2}{dt^2} \right) \\ & + m_2 l_1 g \cos \theta_1 \cos \theta_2 \end{aligned} \quad (2)$$

Fig. 1 Two-link planar robotic manipulator

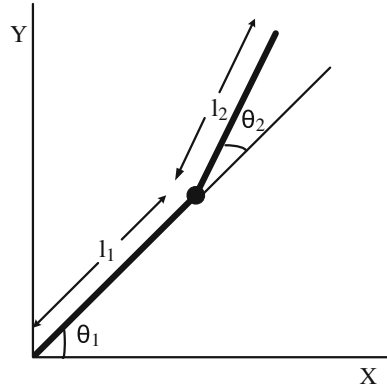


Table 1 Parameters for a two-link planar rigid robotic manipulator

Parameters	Link1	Link2
Mass (kg)	0.1	0.1
Length (m)	0.8	0.4
Acceleration gravity (g) in (m/s ²)	9.81	9.81

where m_1 and m_2 are mass of Link1 and Link2 respectively; l_1 and l_2 are lengths of Link1 and Link2 respectively; θ_1 and θ_2 are the positions of Link1 and Link2 respectively; τ_1 and τ_2 are the control output signals (torque) for Link1 and Link2 respectively.

3 Trajectory

The trajectory which is to be tracked is of a polynomial nature as given in Eq. (3).

$$\theta_{desired} = \theta_{initial} + \left(6 \frac{t^5}{t_s^5} - 15 \frac{t^4}{t_s^4} + 10 \frac{t^3}{t_s^3} \right) (\theta_{final} - \theta_{initial}) \tag{3}$$

where $\theta_{desired}$ is the desired position for Link1 and Link2 separately; $\theta_{initial} = 0$ is the initial positions for both Link1 and Link2 respectively; the final position for Link1 is $\theta_{final} = \pi/2$ and for Link2 is $\theta_{final} = \pi/6$. Also, $t_s = 2$ s is the time taken to reach the final position by both links [17].

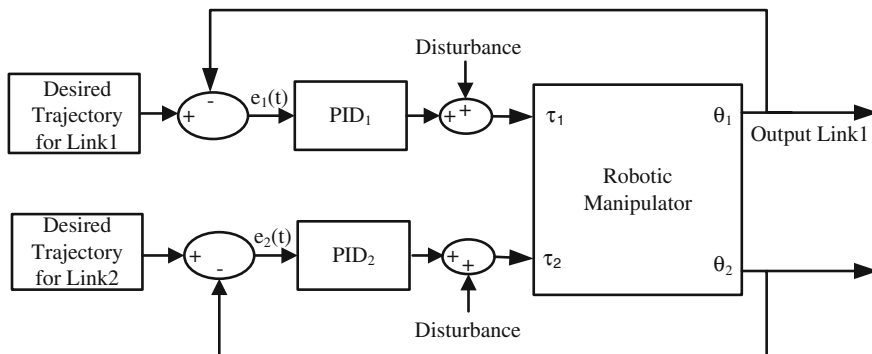


Fig. 2 Block Diagram of PID controllers applied to two-link planar rigid robotic manipulator

4 PID Controller

The block diagram of PID controllers applied to a two-link planar rigid robotic manipulator is shown in Fig. 2.

The control law for PID controller for both links in s-domain is as follow:

$$\tau_j(s) = (K_{pj} + \frac{K_{ij}}{s} + K_{dj}s)E_j(s) \tag{4}$$

where K_{pj} , K_{ij} and K_{dj} ($j = 1, 2$ stands for Link1 and Link2) are proportional, integral and derivative gains for the PID controllers for respectively. The gains are required to be tuned for the efficient functioning of the controller. Also, error $e_j(t) = \theta_{desired}(t) - \theta_{actual}(t)$ is the difference between the desired position and the actual position tracked by the robotic manipulator.

5 Optimization Techniques

For tuning of the controller parameters, one requires a fitness function which is subjected to optimization process. The fitness function is tried out for minimization, varying the controller parameters within the predefined bounds. This Section presents the fitness function definition and the brief description about the used optimization techniques.

5.1 Fitness Function

The fitness function chosen includes IAE of both the links (f_1) and IACCO of both the links (f_2). For all of the three optimization techniques, a single fitness function

F comprising of equally weighted f_1 and f_2 . The main purpose of employing these fitness functions is to minimize the effects of error between actual and desired trajectories and also, to minimize the effects of change in the control signal for better trajectory tracking. The fitness functions used are given as follows:

$$f_1 = \int |e_1(t)|dt + \int |e_2(t)|dt \quad (5)$$

$$f_2 = \int |\Delta\tau_1|dt + \int |\Delta\tau_2|dt \quad (6)$$

$$F = w_1f_1 + w_2f_2 \quad (7)$$

where $e_1(t)$ and $e_2(t)$ are the errors for Link1 and Link2 respectively; $\Delta\tau_1$ and $\Delta\tau_2$ are changes in the control output signal for Link1 and Link2 respectively. Also, w_1 and w_2 are the weights of f_1 and f_2 respectively.

5.2 Particle Swarm Optimization

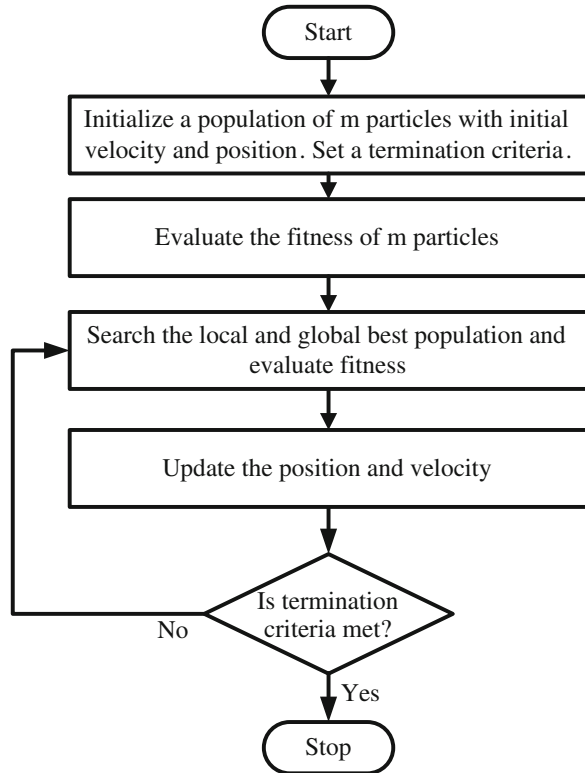
PSO was introduced by Kennedy and Eberhart [8]. PSO is an iterative algorithm used to optimize the best solution in a search space. It is found to be suitable for optimization of continuous nonlinear problems [8]. It works on the movement of m particles, each particle having its position and velocity for moving in the search space. The best feature of PSO is that each particle remembers its past best position. The best solution is achieved both with the best past position of the particle and the global best past position of the entire population [18]. The velocity and position of the particles is calculated according to the following two equations [19]:

$$V_p(t+1) = w_p V_p(t) + q_1 r_1 (P_p(t) - X_p(t)) + q_2 r_2 (g_p(t) - X_p(t)) \quad (8)$$

$$X_p(t+1) = X_p(t) + V_p(t+1) \quad (9)$$

where w_p is the inertial weight, q_1 and q_2 are acceleration constants, r_1 and r_2 are random numbers or constants in the range $[0, 1]$ [19]. Also, $V_p(t)$ is the particle's previous velocity, $X_p(t)$ is the particle's previous position, $g_p(t)$ is the best position achieved by the particle, $P_p(t)$ is the best position achieved by the rest of the particles. The implementation of PSO algorithm used is described in Fig. 3 [20]. In the present work, PSO algorithm was programmed in the MATLAB.

Fig. 3 Flowchart of PSO algorithm



5.3 Simulated Annealing

SA is a simple and efficient optimization technique. It works on the principle of annealing which means metals or some substances are melted with high temperature and then gradually cooled down until they regain into solid metal [22]. The purpose is to attain the lowest energy state as a result of minimization of energy. It means here the energy factor acts as the fitness function which needs to be minimized. This is different from other optimization techniques because of its ability to use uphill moves or some bad moves which helps in achieving the global or best minima [21, 22]. The mechanism of the simulated annealing is expressed by Boltzmann probability as

$$\text{Probability } P_{sa} = e^{-(\Delta E/KT_a)} \quad (10)$$

Where ΔE is the change in energy from one point to the next point, T_a is the temperature and K is the Boltzmann's constant. The mechanism of SA is based on the rule given by Metropolis et al. in 1953. They proposed an algorithm for annealing based on the sequential moves. This includes that the probability with

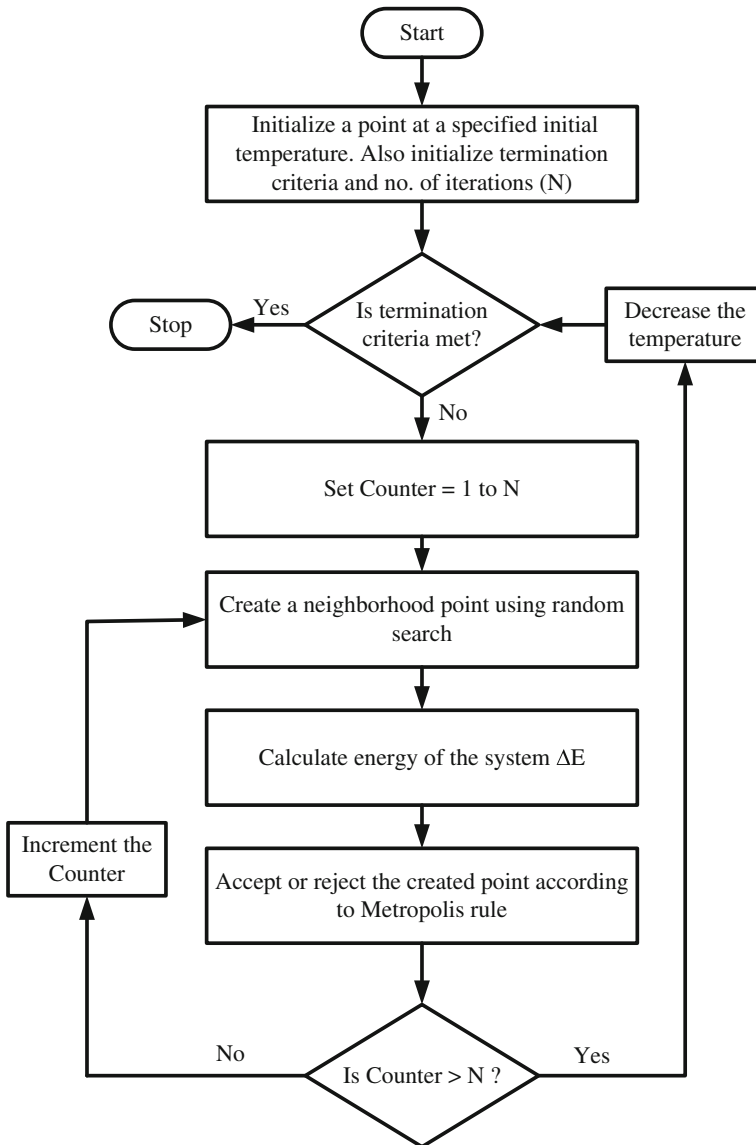
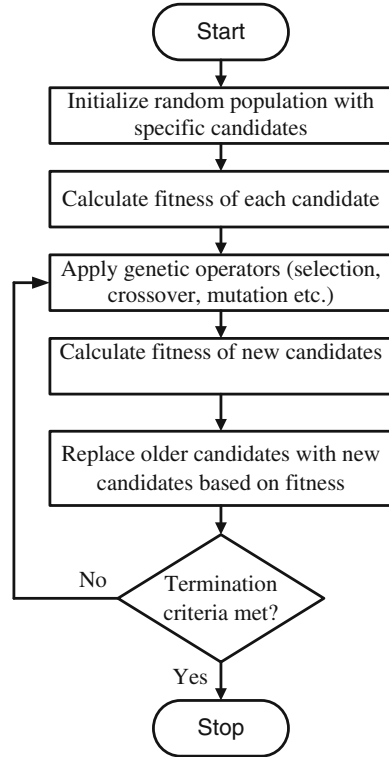


Fig. 4 Flowchart of SA algorithm

which system changes its state from one energy state to another is given by Eq. (10). Also, it indicates that if the new energy state is smaller than current energy state then the system will accept the new energy state otherwise the energy change is probabilistic [21]. The stepwise SA algorithm is given in flowchart as shown in Fig. 4 [23, 24]. In the present work, MATLAB Toolbox was used for implementing the SA algorithm.

Fig. 5 Flowchart of GA algorithm



5.4 Genetic Algorithm

GA has been proposed by Prof. John Holland, his students and his colleagues. It is an efficient search algorithm based on the natural selection and the theory of survival of the fittest [25]. The three main genetic operators involved in the search algorithm are Reproduction, Crossover and Mutation. Reproduction generally involves the selection of chromosomes for mating based on the best fitness value as in the natural selection does. The selection methods generally used are rank selection, roulette wheel selection, tournament selection etc. After the selection process, the crossover is done between two selected parents or chromosomes by exchanging some bits and a new offspring or child is produced. Mutation is the method of altering some bits in the parent chromosome and an offspring having different characteristics from the parent chromosome may be developed. It generally improves the diversity in the population and also solves premature convergence [4, 26]. The flowchart shown in Fig. 5 presents the implementation of GA [4]. In this work, real-coded GA using MATLAB Toolbox was implemented for the simulation.

Table 2 Parameters used for PSO, SA and GA

Parameters	Parameter values (PSO)	Parameter values (SA)	Parameter values (GA)
Lower bounds [$K_{p1}, K_{i1}, K_{d1}, K_{p2}, K_{i2}, K_{d2}$]	[0 0 0 0 0 0]	[0 0 0 0 0 0]	[0 0 0 0 0 0]
Upper bounds [$K_{p1}, K_{i1}, K_{d1}, K_{p2}, K_{i2}, K_{d2}$]	[400 400 400 400 400 400]	[400 400 400 400 400 400]	[400 400 400 400 400 400]
Population size	40	–	40
Mutation fraction	–	–	0.2
Crossover fraction	–	–	0.8
Iterations	100	100	100
Acceleration coefficients	2, 2	–	–
Inertial weight	0.25	–	–
Random number	[0 1]	–	–
Velocity factor	0.3	–	–
Initial values	–	[0 0 0 0 0 0]	–
Initial temperature	–	100	–

Table 3 List of tuned PID gains, IAE and fitness values for PSO, SA and GA

Parameters	PSO		SA		GA	
	Link1	Link2	Link1	Link2	Link1	Link2
Proportional gains	363.745700	358.45310	79.93040	135.16410	27.29610	35.47150
Integral gains	35.411800	307.98020	29.92440	14.69960	9.35420	25.78390
Derivative gains	6.798000	17.73530	4.09360	41.10830	4.84020	2.82650
IAE	0.002806	0.00425	0.01243	0.01981	0.03439	0.04643
Fitness values	0.00016		0.00038		0.00088	

6 Simulation Results

The simulation is done with MATLAB/SIMULINK software version R2009b. A Simulink model was developed for Eqs. (1) and (2) which was solved using the 4th order Runge–Kutta method. The simulation time was kept 2 s. The sampling time used during the simulation was 1 ms. The torque constraints for both links were bounded to $[-10\ 10]$ N-m during the simulation. The various parameters used for PSO, SA and GA during the optimization process are listed in the Table 2.

6.1 Controller Optimization for Trajectory Tracking

This Section presents the performance of trajectory tracking problem. The value of IAE and the Fitness Values are provided in the Table 3. It is observed that the value of IAE for both links, in case of PSO, is superior to both SA and GA. The

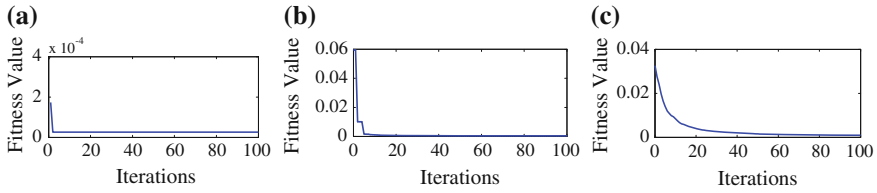


Fig. 6 Fitness Values versus Iterations. **a** PSO. **b** SA. **c** GA

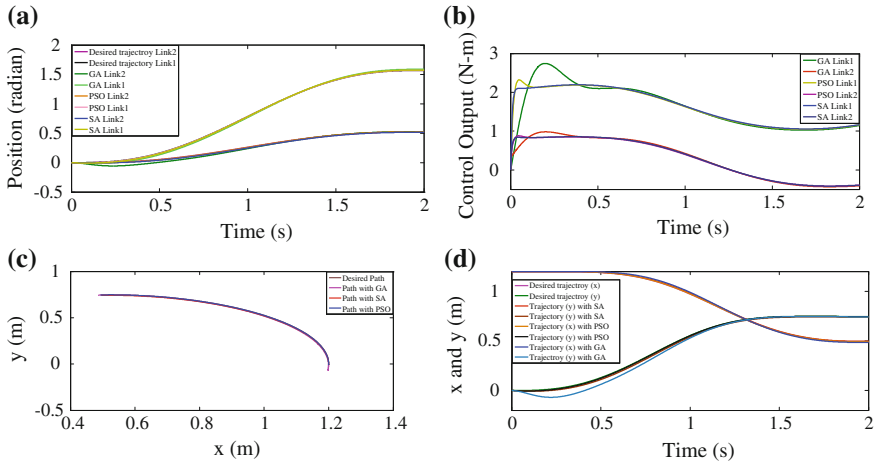


Fig. 7 **a** Trajectory tracking performance. **b** Controller output. **c** Path tracked by end-effector. **d** x and y versus time variations for the end-effector all for PSO, SA and GA

Fitness Values versus Iterations graphs for PSO, SA and GA are shown in Fig. 6a, b and c respectively. The trajectory tracking and change in control output graphs for the tuned parameters for PSO, SA and GA are shown in Fig. 7a and b respectively. The path tracked, x and y versus time variations by the end-effector of the robotic manipulator are shown in Fig. 7c and d respectively.

6.2 Effects of Model Uncertainties on Controller Performance

Robustness of the optimized PID controllers was studied for model uncertainties. The model uncertainties include the mass changes from the actual 0.1 kg value.

For robustness testing, the mass of the robotic manipulator was increased by 5, 10 and 15 % of the actual value in m_1 , m_2 and both masses simultaneously.

Table 4 IAE for Link1 and Link2 under mass changes

Increase in link mass (%)	PSO		SA		GA		
	Link1	Link2	Link1	Link2	Link1	Link2	
m ₁	5	0.002806	0.004329	0.01243	0.02026	0.03439	0.04733
	10	0.002806	0.004408	0.01243	0.02070	0.03440	0.04823
	15	0.002806	0.004487	0.01243	0.02115	0.03440	0.04914
m ₂	5	0.002947	0.004385	0.01305	0.02036	0.03615	0.04790
	10	0.003088	0.004520	0.01368	0.02091	0.03792	0.04938
	15	0.003229	0.004655	0.01431	0.02146	0.03969	0.05087
m ₁ , m ₂	5	0.002947	0.004463	0.01305	0.02081	0.03616	0.04879
	10	0.003088	0.004677	0.01368	0.02180	0.03793	0.05116
	15	0.003229	0.004890	0.01431	0.02280	0.03971	0.05353

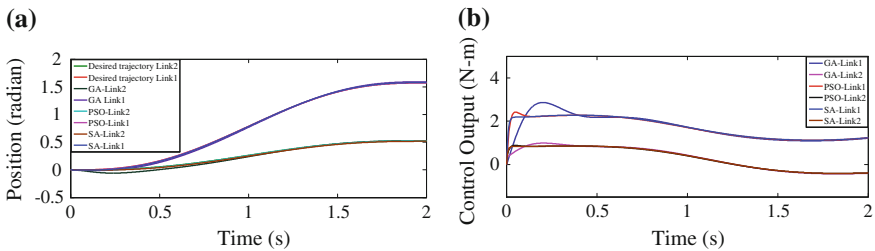


Fig. 8 a Trajectory tracking. b Controller output for PSO, SA and GA for 10 % change in m₁

The IAE for the PSO, SA and GA for increase in the value of masses of Link1, Link2 and both links are presented in the Table 4.

To demonstrate the results graphically for the trajectory tracking and control output, a special case of 10 % increase in m₁ is shown in Fig. 8a and b respectively. The graphical representations of variation in IAE for individual links with respect to mass changes are shown in Fig. 9. From the Table 4 and Fig. 9, it is observed that PSO is superior to both SA and GA for handling the model uncertainties also.

6.3 Disturbance Rejection

The IAE variations under disturbances for PSO, SA and GA are presented in this Section. Here, two cases for incorporating the disturbances were studied. First, the disturbances 0.1sin50t, 0.15sin50t and 0.2sin50t were given to the controller output of Link1, Link2 and both links for 2s individually. The IAE under disturbances for PSO, SA and GA are summarized in Table 5. The graphical representations of IAE variations with disturbances for individual link are shown in Fig. 10.

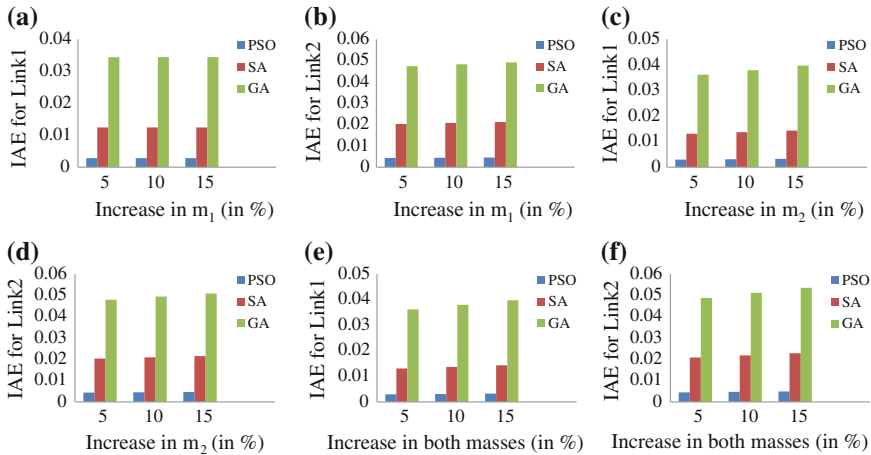


Fig. 9 Variation in IAE for **a** change in m_1 for Link1, **b** change in m_1 for Link2, **c** change in m_2 for Link1, **d** change in m_2 for Link2, **e** change in both masses for Link1, **f** change in both masses for Link2

Table 5 IAE for disturbance $0.1\sin50t$, $0.15\sin50t$ and $0.2\sin50t$

Disturbance	PSO		SA		GA		
	Link1	Link2	Link1	Link2	Link1	Link2	
Link1	0.1sin50t	0.002803	0.004250	0.01243	0.01981	0.03438	0.04642
	0.15sin50t	0.002806	0.004252	0.01243	0.01979	0.03438	0.04641
	0.2 sin50t	0.002816	0.004250	0.01243	0.01981	0.03438	0.04640
Link2	0.1 sin50t	0.002806	0.004248	0.01243	0.01980	0.03434	0.04643
	0.15sin50t	0.002808	0.004250	0.01243	0.01981	0.03432	0.04643
	0.2 sin50t	0.002806	0.004257	0.01243	0.01979	0.03430	0.04643
Both links	0.1sin50t	0.002803	0.004249	0.01243	0.01980	0.03434	0.04642
	0.15sin50t	0.002808	0.004253	0.01243	0.01979	0.03432	0.04641
	0.2sin50t	0.002816	0.004259	0.01243	0.01979	0.03429	0.04641

Second, the disturbance $0.01 + 0.1 \sin 25t$ was given for the time $t_s = 1s$ to $t_s = 2s$ to Link1, Link2 and both links individually and the graphs for the trajectory tracking and control output with disturbances are shown in Fig. 11a and b respectively. The IAE for disturbances for PSO, SA and GA are summarized in Table 6. The graphical representations of IAE variations with disturbances for individual link are shown in Fig. 12. It is inferred from the results that the PSO performs better than both SA and GA with disturbances also.

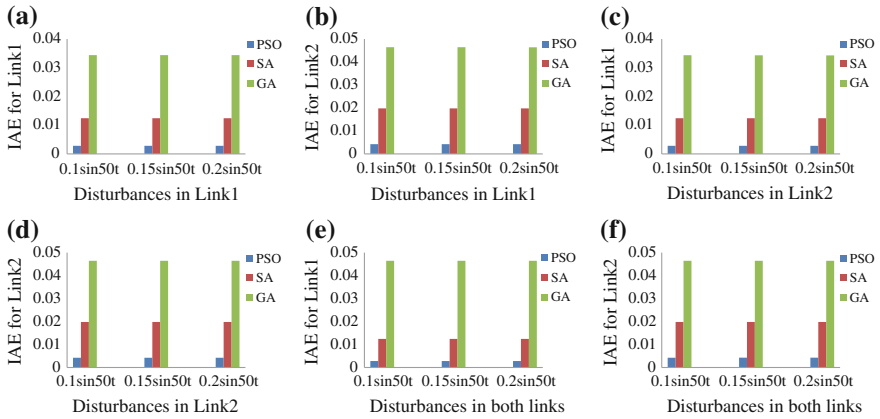


Fig. 10 Variation in IAE for **a** Link1 with disturbances in Link1. **b** Link2 with disturbances in Link1. **c** Link1with disturbances in Link2. **d** Link2 with disturbances in Link2. **e** Link1 with disturbances in both links. **(f)** Link2 with disturbances in both links

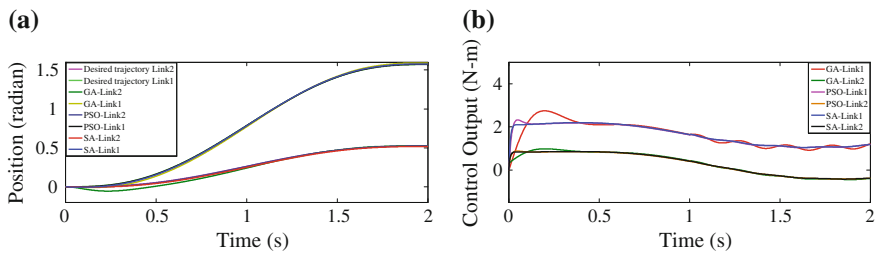


Fig. 11 a Trajectory tracking under disturbance $0.01 + 0.1 \sin 25t$. **b** Control output under disturbance $0.01 + 0.1 \sin 25t$ in both links for PSO, SA, GA

Table 6 IAE for disturbance $0.01 + 0.1 \sin 25t$

Disturbance	PSO		SA		GA	
	Link1	Link2	Link1	Link2	Link1	Link2
Link1	0.002815	0.004251	0.01239	0.01981	0.03438	0.04631
Link2	0.002806	0.004252	0.01243	0.01973	0.03450	0.04643
Both links	0.002815	0.004253	0.01239	0.01973	0.03449	0.05542

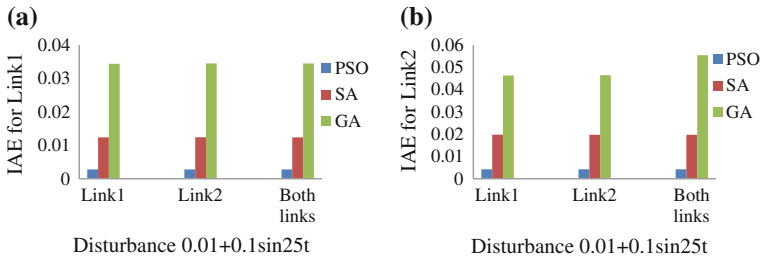


Fig. 12 Variation in IAE for **a** Link1 with disturbance ($0.01 + 0.1\sin 25t$) in Link1, Link2 and both links. **b** Link2 with disturbance ($0.01 + 0.1\sin 25t$) in Link1, Link2 and both links

7 Conclusion

This paper investigated a comparative study among three potential optimization techniques namely PSO, SA and GA for tuning of PID controllers applied to a two-link planar rigid robotic manipulator. The fitness function IAE and IACCO are chosen for the purpose of minimization of the tracking error and change in control output. The study conducted clearly indicates that PSO outperforms both SA and GA for the trajectory tracking, model uncertainties and disturbance rejection. For further study, advancement in PSO algorithm can be implemented for the similar purpose.

References

1. Panwar, V., Kumar, N., Sukavanam, N., Borm, J.-H.: Adaptive neural controller for cooperative multiple robot manipulator system manipulating a single object. *Appl. Soft Comput.* **12**, 216–227 (2012)
2. Ang, K.H., Chong, G., Li, Y.: PID control system analysis, design and technology. *IEEE Trans. Control Syst. Technol.* **13**(4), 559–576 (2005)
3. Kuc, T.-Y., Han, W.-G.: An adaptive PID learning control of robot manipulators. *Automatica* **36**, 717–725 (2000)
4. Ayala, H.V.H., Coelho, L.d.S.: Tuning of PID controller based on a multiobjective genetic algorithm applied to a robotic manipulator. *Expert Syst. Appl.* **39**, 8968–8974 (2012)
5. Li, X., Yu, W.: A systematic tuning method of PID controller for robot manipulators. In: 9th IEEE International Conference on Control and Automation, pp. 274–279 (2011)
6. Bingul, Z., Karahan, O.: Tuning of fractional PID controllers using PSO algorithm for robot trajectory control. In: Proceedings of IEEE International Conference on Mechatronics, Turkey, pp. 955–960 (2011)
7. Juang, J.-G., Huang, M.-T., Liu, W.-K.: PID control using presearched genetic algorithms for a MIMO system. *IEEE Trans. Syst. Man and Cybern. Part C Appl. Rev.* **38**, 716–727 (2008)
8. Gaing, Z.-L.: A particle swarm optimization approach for optimum design of PID controller in AVR system. *IEEE Trans. Energy Convers.* **19**(2), 384–391 (2004)
9. Zhao, J., Li, T., Qian, J.: Application of particle swarm optimization algorithm on robust PID controller tuning. *Lect. notes in Comp. Sci.* **3612**, 948–957 (2005)

10. Lin, C.-L., Jan, H.Y., Shieh, N.C.: GA-based multiobjective PID control for a linear brushless DC motor. *IEEE/ASME Trans. Mechatron.* **8**(1), 56–65 (2003)
11. Bagis, A.: Tabu search algorithm based PID controller tuning for desired system specifications. *J. Franklin Inst.* **348**, 2795–2812 (2011)
12. Puangdownreong, D., Sujitjorn, S.: Obtaining an optimum PID controller via adaptive tabu search. In: *Proceedings of the International Conference on Adaptive and Natural Computing Algorithm (ICANNGA) part II*, vol. 4432, pp. 747–755 (2007)
13. Lianghong, W., Yaonan, W., Shaowu, Z., Wen, T.: Design of PID controller with incomplete derivation based on differential evolution algorithm. *J. Syst. Eng. Elec.* **19**(3), 578–583 (2008)
14. Chen, Y., Guo, Z., Liu, J.: An improved ant colony algorithm for PID parameters optimization. In: *International Conference on Intelligence and Computing Technol. and Automation*, pp. 157–160 (2009)
15. Hai-bin, D., Dao-bo, W., Xiu-fen, Y.: Novel approach to nonlinear PID parameter optimization using ant colony optimization algorithm. *J. Bionic Eng.* **3**, 73–78 (2006)
16. Liang, X.-m., Li, S.-c., Hassan, A.B.: A novel PID controller tuning method based on optimization techniques. *J. Cent. South. Univ. Technol.* **17**, 1036–1042 (2010)
17. Subudhi, B., Morris, A.S.: Dynamic modeling, simulation and control of a manipulator with flexible links and joints. *Robot. Auton. Syst.* **41**, 257–270 (2002)
18. Selleri, S., Mussetta, M., Pirinoli, P., Zich, R.E., Matekovits, L.: Some insights over new variations of the particle swarm optimization method. *IEEE Antennas Wirel. Propag. Lett.* **5**, 235–238 (2006)
19. Zamani, M., Karimi-Ghartemani, M., Sadati, N., Parniani, M.: Design of a fractional order PID controller for an AVR using particle swarm optimization. *Control. Eng. Prac.* **17**, 1380–1387 (2009)
20. Huang, H.-C., Chen, C.-P., Wang, P.-R.: Particle Swarm Optimization for solving the inverse kinematics of 7-DOF robotic manipulators. In: *IEEE International Conference on Systems Man and Cybernetics*, pp. 3105–3110 (2012)
21. Kirkpatrick, S., Gelatt Jr, C.D., Vecchi, M.P.: Optimization by simulated annealing. *Science* **220**, 671–680 (1983)
22. Davidson, R., Harel, D.: Drawing graphs nicely using simulated annealing. *ACM Trans. Graph.* **15**, 301–331 (1996)
23. Vasan, A., Raju, K.S.: Comparative analysis of simulated annealing, simulated quenching and genetic algorithms for optimal reservoir operation. *Appl. Soft Comput.* **9**, 274–281 (2009)
24. Chen, S.-M., Chien, C.-Y.: Solving the traveling salesman problem based on the genetic simulated annealing ant colony system with particle swarm optimization techniques. *Expert Syst. Appl.* **38**, 14439–14450 (2011)
25. Goldberg, D.E.: *Genetic Algorithms in Search, Optimization & Machine Learning*. Pearson Education, India (2009)
26. Garg, D.P., Kumar, M.: Optimization techniques applied to multiple manipulators for path planning and torque minimization. *Eng. Appl. Artif. Intell.* **15**, 241–252 (2002)

Hybridization of P Systems and Particle Swarm Optimization for Function Optimization

Garima Singh and Kusum Deep

Abstract This paper describes the broad framework for the hybridization of P-systems or Membrane Computing and Particle Swarm Optimization with a view to minimize nonlinear optimization problems. The paper highlights that very few papers are available on the hybridization and concludes that a lot of scope of research is possible in this domain.

Keywords P systems · Particle swarm optimization · Intelligent hybrid algorithm

1 Introduction

To solve the complicated nonlinear optimization problems, researchers now-a-days prefer intelligent heuristic algorithms over traditional mathematic methods. Membrane computing, a nature-inspired optimization technique modeled as P systems was introduced by Paun in 1998 and was published in [1]. It is a parallel distributed computing model which derives its functionality and structure from tissues or organs of living cells. Particle Swarm Optimization, an evolutionary algorithm inspired by swarm behavior of birds was proposed in 1995 by Kennedy and Eberhart [2].

To improve the exploration ability, diversity and convergence speed of swarm and obtain more accurate results certain modifications are made in Basic PSO algorithm. They are either used with different inertia weights and acceleration constants or they are hybridized with other evolutionary algorithms. Also, to use

G. Singh (✉) · K. Deep

Department of Mathematics, Indian Institute of Technology Roorkee, Roorkee, India
e-mail: garimachauhan.iitr@gmail.com

K. Deep

e-mail: kusumdeep@gmail.com

P system and define its rules for practical purpose is still a difficulty. However, new algorithms can be designed by implementing the rules of evolutionary algorithm within the parallel and distributed computation framework provided by P system.

In recent years, a number of papers have appeared in which P-systems are hybridized with other evolutionary algorithms like Genetic Algorithms [3], Ant Colony Optimization [4], Quantum Inspired EAs [5], etc.

This paper focuses on the ways in which P-system is combined with PSO and its variants in the research field and how they are used for various applications. This paper is organized as follows. Section 2 describes the concept of P-systems and Sect. 3 provides the basic definition of PSO. Section 4 provides a framework for the hybridization of P-systems and PSO. Section 5 describes a critical review of the existing papers on the hybridization of P-systems and PSO. Finally, conclusions are drawn in Sect. 6.

2 P-systems

P-system or Membrane system is a distributed and parallelized model with the features abstracted from the way of processing compounds by biological cells. It is the hierarchical arrangement of membranes surrounding the region in which objects and rules to evolve these objects are placed. These are of three types namely cell-like, tissue-like and neural-like P system each having many of their variants. A general expression for any P system is given by

$$\Pi = (V, T, C, \mu, w_1, \dots, w_m(R_1, \rho_1), \dots, (R_m, \rho_m))$$

where V is alphabet of objects, $T \subseteq V$ is the output alphabet, $C \subseteq V - T$ is catalyst (just used to initiate certain rules without themselves taking part in it), μ is the membrane structure having m membranes each labeled by elements of set $H = \{1, 2, \dots, m\}$, m is known as degree of Π , $w_i (1 \leq i \leq m)$ is the multiset defined over V associated with the region i . While each region i , is associated a finite set of evolution rules given by R_i having a priority relation defined by ρ_i .

3 Particle Swarm Optimization

Particle Swarm Optimization is swarm intelligence method used as optimization technique in which each particle of the swarm contribute towards obtaining optimal result by deciding its motion on the basis of its previous best position (pbest) and global best position (gbest) of the swarm. For this each particles i update their positions $x_{ij}(t)$ and velocity $v_{ij}(t)$ in all the j dimensions in each iteration t using the equations

Fig. 1 Hybridizing of membrane computing with PSO

```

Begin
  t ← 1
  i)      Initialize membrane structure with specified
          number of membrane and X(t), V(t).
  ii)     Generate n individuals for each membrane.

          while (not termination condition) do
            for i = 1: m
  iii)    Perform PSO in the membrane
            end
  iv)    Execute communication rules

          t = t + 1
        end
end
    
```

$$v_{ij}(t + 1) = v_{ij}(t) + c_1 \times r_1 \times (pbest_{ij}(t) - x_{ij}(t)) + c_2 \times r_2 \times (gbest_j(t) - x_{ij}(t))$$

$$x_{ij}(t + 1) = x_{ij}(t) + v_{ij}(t + 1)$$

where, c_1 and c_2 are acceleration constants, r_1 and r_2 are the uniform random variable in the range [0, 1].

4 General Hybridization of P-system and PSO Algorithms

Figure 1 shows the basic idea of hybridizing PSO with P systems. The new variants of the hybrid algorithms are developed by applying one or more of the following concepts:

- i. Use different existing variants of Particle Swarm Optimization.
- ii. Using frameworks of different P systems.
- iii. By applying various ways of communications among regions.
- iv. Various techniques to enhance searching efficiency, improve the precision, escape the local minima and avoid premature convergence can be incorporated as a part of transformation/communication rules.

5 Available Hybridized Models in Literature

In literature the first attempt to hybridize P system with PSO was done by Zhou et al. in 2010 [6]. They used it for continuous function optimization. The membrane algorithm proposed was named Particle Swarm Optimization Based on P

system (PSOPS). In this algorithm, one layered membrane structure (OLMS) form of cell-like P system with transformation and communication rules is used in which the transformation rules are nothing but the evolutionary rules of PSO applied individually in each membrane. The effectiveness and validity of the proposed algorithm is established by performing experiments on 7 randomly selected benchmark continuous optimization problems. For 6 functions the problem size is 30 whereas the problem size of one problem is trivially kept to 2. They claim that PSOPS obtains significantly better solutions than PSO for the seven functions and consume less time relatively in general. They conclude that due to the fact that PSOPS employs the formal framework and communication rules, it can avoid premature convergence to a considerable degree, and hence has faster convergence rate. But the results show that out of the 7 problems considered, only 5 problems attain optimal or close-to-optimal solutions. This is probably due to the fact that the swarm size is fixed to 30, whereas only 1000 iterations are carried out. Also only 30 runs are performed. Further, a real life problem related to time-frequency analysis of a LFM radar emitter signal is solved. The problem is a 4-variable problem. The swarm size is kept to 20, maximal number of iterations is set to 200; the number of elementary membranes is set to 12, and the maximal number of generations for the skin membrane is set to 10 and the maximal number of generations for each elementary membrane randomly is 40. All experiments are executed for 20 independent runs. Based on the analysis of the results they claim that PSOPS greatly decreases the computational load of TFAD, as compared with its counterpart PSO algorithm.

In same year itself, Yang et al. [7] came up with another hybridization named as Membrane Computing Based Particle Swarm Optimization (MCBPSO). The algorithm was implementation of Basic PSO in the multi-layered membrane structure with real numbers as the objects. Although, the evolution rules are the update equations of basic PSO applied to the objects of each membrane individually, but this step is followed by cooperation, a way of communicating among membranes, and the mutation operation in each membrane. The cooperating operation was performed to improve searching efficiency while the mutation operation or reinitializing of the bad objects was done to escape local minima and hence to obtain more precise result. To test the performance MCBPSO is evaluated on five test functions but the results are not shown in the paper, although, they claim that algorithm has most satisfying precision and searching efficiency. This algorithm is then applied to build a soft-sensing model for computing component of Texaco gasifier syngas with LS-SVM. It is parameter selection problem which are estimated using 14 variables. The sample data of 277 groups is used out of which 200 groups are used to train the model and this model is then tested using 77 groups. The results are compared with four other algorithms.

Zhang et al. in 2012 [8] proposed a new variant of membrane algorithm, called HPSOPS. This algorithm was a one layered membrane structure of cell-like P system evolved using the update rules of Hybrid Particle Swarm Optimization with Wavelet Mutation (HPSOWM). Here, the claim behind using HPSOWM was its excellence in the quality and convergence of solution as compared to other PSO

approaches. Then, the algorithm is used to solve the broadcasting problem. Although, broadcasting algorithm was modelled using P system framework way back in 2010 by Lefticaru et al. [9] but first membrane algorithms to solve this problem was claimed to be HPSOPS. The swarm size for the problem is fixed to 20. The number of elementary membranes is 6. The maximal generation for elementary membrane is 40 while the maximal generation for algorithm is fixed at 1000. The experiment was conducted for trees with number of nodes increasing from 10 to 150 and nodes having sons only in range 2–10 (including). All these cases are executed for 30 runs independently. The results are compared with HPSOWM and GA. Based on their experiments they concluded that the decrease in successful rates is much slower in case of HPSOPS as compared to its counterpart.

The Bio-Inspired Algorithm Based on Membrane Computing (BIAMC) is designed by Xiao et al. in 2013 [10]. Their focus was to avoid premature convergence by using concept of neighbourhood search. BIAMC implemented update rules of PSO based on Gaussian distribution with the framework of cell-like P system with local and global neighbourhood search applied in the skin membrane as an intermediate step of send-in and send-out communication rules. To test effectiveness and efficiency it is used to numerically simulate three constrained engineering design problems and the results are compared with other algorithms. For this purpose they designed a membrane structure with 20 elementary membranes each having fixed swarm size of 8. The process is iterated at maximum 500 times. The neighbourhood radius for search is fixed to 5. For each test function 30 independent runs are conducted. Out of three problems two are four variables problem while one is three variables problem. The result shows that for pressure vessel design problem did not attain the minimum standard deviation as compared to other algorithms. Also, for the tension/compression string problem the best solution by other algorithm is better as compared to best solution found by this algorithm.

Later, in 2013, Zhong et al. [11] presented a new hybrid particle swarm optimization based on P systems. In this hybridization, the new variation is done on the basis of the topology or the way used by the population to communicate between the membranes. They used the wheel-type structure and they claimed that this technique improves the algorithm's performance in avoiding its premature convergence. To validate their claim they tested it on five optimization function having 10 dimensional search spaces and compared the results with three other algorithm. The three of the test functions are unimodal while two are multimodal. To compare the results 50 independent runs are conducted for each function. With 1,000 as the maximum number of iteration to be performed the result shows that although it performed better than other in case of multimodal functions but for unimodal functions other algorithms are to be preferred. Also the test were conducted to analysis the parameter settings and on the basis of results it is concluded that for better convergence swarm size should be 40, number of membranes should be 40, exchange-timing should be after 30 iterations, and the number of particle to be exchanged should be 15.

Latest hybridization to be found in literature is by Wang et al. [12] named as Membrane Optimization algorithm based on Mutated Particle Swarm Optimization (MO-MPSO). This algorithm is designed with a view to avoid evolution of same particles in searching process of PSOPS algorithm tending to reduce the swarm size of its elementary membrane and hence converging prematurely. The performance of the algorithm is measured on the basis of 10 benchmark problems and the results are compared with PSO and PSOPS. The test is conducted by taking three dimensions 10, 50 and 100 for each problem. For the test purpose the swarm size is kept 30 and running the algorithm for each problem 30 times independently. With the help of experiments the authors proved that due to the involvement of mutation mechanism as the dimension increases the effect of homoplasmy in elementary membrane causing prematurity is reduced. To further test it, it is used instead of BP algorithm in the MIMO PID Neural Network controller and the results are compared with other algorithms. In the algorithm, the swarm size is set as 30 with eight elementary membranes each of which restricted to maximum generation of 5 while maximum generation for skin membrane is 20. The results are compared for small swarm size with few algorithms which perform better for larger swarm size.

6 Conclusion and Future Scope

This paper has provided a survey of the various ways in which Particle Swarm Optimization technique is embedded within the framework of P systems to fully utilize the parallelism and distribution ability of membrane structure with help of easy implementation of PSO for the purpose of function optimization. Not much work is reported this direction to fully exploit the advantage of this hybridization. There are still many aspects that can be experimented as a part of future research.

References

1. Paun, G.: Computing with membranes. *J. Comput. Syst. Sci.* **61**, 108–143 (2000)
2. Kennedy, J., Eberhart, R.: Particle swarm optimization. In: *Proceedings of International Conference on Neural Networks*, pp. 1942–1948 (1995)
3. Huang, L., Wang, N.: An optimization algorithm inspired by membrane computing. In: *International Conference on Natural Computation, 2006. Lecture Notes in Computer Science*, vol. 4222, pp. 49–52 (2006)
4. Zhang, G.X., Cheng, J.X., Gheorghe, M.: A membrane-inspired approximate algorithm for travelling salesman problems. *Rom. J. Inf. Sci. Tech.* **14**, 3–19 (2011)
5. Zhang, G.X., Gheorghe, M., Wu, C.Z.: A quantum-inspired evolutionary algorithm based on P systems for a class of combinatorial optimization. *Fundam. Inform.* **87**, 93–116 (2008)
6. Zhou, F., Zhang, G., Rong, H., Gheorghe, M., Cheng, J., Ipate, F., Lefticaru, R.: A particle swarm optimization based on P systems. In: *6th IEEE International Conference on Natural Computation*, pp. 3003–3007 (2010)

7. Yang, S., Zhang, L., Gu, X.S.: Membrane computing based particle swarm optimization algorithm and its application. In: 5th IEEE International Conference on Bio-Inspired Computing: Theories and Applications (BIC-TA), pp. 631–636 (2010)
8. Zhang, G., Zhou, F., Huang, X., Cheng, J., Gheorge, M., Ipate, F., Lefticaru, R.: A novel membrane algorithm based on particle swarm optimization for solving broadcasting problems. *J. Univers. Comput. Sci.* **18**, 1821–1841 (2012)
9. Lefticaru, R., Ipate, F., Gheorghe, M., Zhang, G.X.: Tuning P-systems for solving the broadcasting problem. In: Proceedings of the 10th Workshop on Membrane Computing, pp. 337–354 (2010)
10. Xiao, J., Huang, Y., Cheng, Z.: A bio-Inspired algorithm based on membrane computing for engineering design problem. *Int J. Comput. Sci.* **10**, 580–588 (2013)
11. Zhong, Y., Nie, S.: An improved particle swarm optimization algorithm based on membrane structure. *Int. J. Comput. Sci.* **10**, 532–537 (2013)
12. Wang, J., Wang, T., Shi, P., Tu, M., Yang, F.: Membrane optimization algorithm based on mutated PSO and its application in nonlinear control systems. *Int. J. Innovative Comput. Inf. Control.* **9**, 2963–2977 (2013)

Image Security Using Cellular Automata Rules

Manoj Diwakar, Pratibha Sharma, Sandip Swarnakar
and Pardeep Kumar

Abstract In this age of universal electronic connectivity, there is no time at which security does not matter. With the increase in usage of transmission of digital images over the network, there is need of more secure systems. The main aim of this paper is to achieve two main principles of security i.e. authenticity and confidentiality, particularly for transmission of images over a network. Authenticity ensures that only the intended receiver is able to receive the message and confidentiality ensures that the message is confidential. For achieving these two principles, there are lots of mechanisms available, e.g. the most common practices for achieving authenticity are passwords, access control etc. and for achieving confidentiality, there are lots of symmetric and asymmetric encryption methods available. In this paper, a two-level security mechanism has been presented. This two level security ensures authenticity at one level and confidentiality at another level. For achieving first level of security, the image to be send is hidden behind another image using Stenographic methods and for achieving second level of security, the image would be encrypted using 2D Cellular Automata (CA) rules. If one level of security is broken, then the other level would provide security.

Keywords Cellular automata · Steganography · Cryptography

M. Diwakar (✉) · S. Swarnakar
DIT University, Dehradun, Uttarakhand, India
e-mail: manoj.diwakar@gmail.com

S. Swarnakar
e-mail: sandipswarnakar.2008@gmail.com

P. Sharma
Dronacharya College of Engineering, Farrukhnagar, Gurgaon, India
e-mail: pratibha49@gmail.com

P. Kumar
Jaypee University of Information Technology, Solan, India
e-mail: pardeepkumarkhokhar@gmail.com

1 Introduction

The requirements of information security within an organization have undergone two major changes in last several decades. Before the widespread use of data processing equipment, the security of information felt to be valuable to an organization was provided primarily by physical and administrative means. An example of former is the use of rugged filing cabinets with a combination lock for storing sensitive documents.

The second major change that affected security is the introduction of distributed systems and the use of network and communication facilities for carrying data between user and computer and between computer and computer. Network security measures are needed to protect data during their transmission.

Now, as the technology is increased for sharing of information over the internet is an explosive growth, which showing behavior of new threats and vulnerabilities in the existing systems. Stronger and reliable methodologies are required in order to handle these threats. The data shared over the internet includes text, images, audio, video, etc. Since unauthorized data access has become easier, accessibility in wireless communication networks and efficient security measures need to be applied. Data security has become a critical issue to protect valuable data from undesirable readers.

2 Cellular Automata

The cellular automata (CA) have been used since the forties of last century. It was used in many physical applications. These applications extended to fields as biological models, image processing, language recognition, simulation, computer architecture, cryptography and many other fields. The CA is one of the modern methods used to generate binary pseudo-random a sequences using registers.

The reason for choosing CA for encryption is that they evolve in complex chaotic structure in future generation from a simple input and secondly, the systems developed should be such that it can be implemented in VLSI technology and also optimize performance/cost ratio. CA is one of the fields that enable easy implementation using basic XOR gates. Also, the computation time of algorithms developed using CA is less.

The state of the given cell at time step $(t + 1)$ will be find from different states of cells at time step t . For a k -state CA, each cell can take any of the integer values between 0 and $(k - 1)$ then for 2-state CA the value of each cell is 0 or 1 [1, 2]. In general, this relationship is expressed in Eq. 1.

$$(S_i(t + 1) = f(S_i(t) + S_{neigh}(i)(t)) \quad (1)$$

where S_i denotes the state of the i th cell, t denotes the number of generations that have evolved, $S_{neigh}(i)$ denotes the set of neighbors of the i th cell.

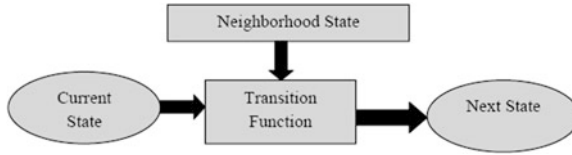


Fig. 1 Model of cellular automata

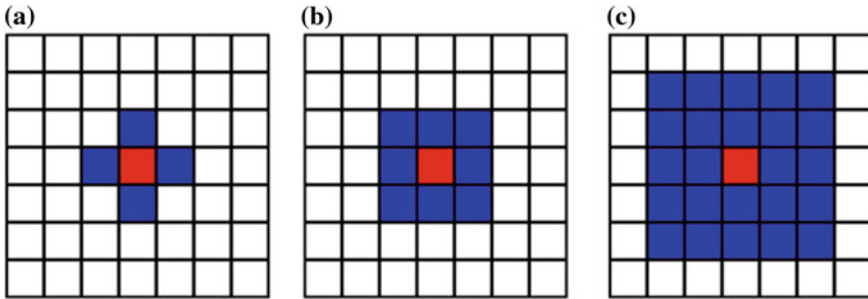


Fig. 2 Models of 2D cellular automata. **a** Von Neumann, **b** Moore Neighborhood, **c** Extended Moore

As shown in the Fig. 1, CA changes according to update rule that shows new state of every cell based on the old states and its neighbors gives the overall change of CA. After every iteration, next state is calculated according to some rules [3, 4, 5]. These rules are different in 1D and 2D CA.

Two dimensional CA were historically studied more extensively than 1D ones – though rarely with simple initial conditions. Two dimensional CA also consists of neighbors similar to 1D CA. Different definitions of neighborhoods are possible in 2D space. Considering a two dimensional lattice the following definitions are common as shown in Fig. 2.

- Von Neumann Neighborhood, four cells: The cell above and below, right and left from each cell are called the Von Neumann neighborhood of this cell. The radius of this definition is 1, as only the next layer is considered. The total number of neighbor cells including itself are 5 cells.
- Moore Neighborhood, eight cells: The Moore neighborhood is an enlargement of the von Neumann neighborhood containing the diagonal cells too. In this case, the radius $r = 1$ too. The total number of neighbor cells including itself are 9 cells.
- Extended Moore Neighborhood: It equivalent to the description of Moore neighborhood above, however the neighborhood reaches over the distance of the next adjacent cells. Hence the $r = 2$ (or larger). The total number of neighbor cells including itself are 25 cells.

In this paper Moore Neighborhood Model has been used. The dark gray cell is the center cell; the gray cells are the neighborhood cells. The states of these cells

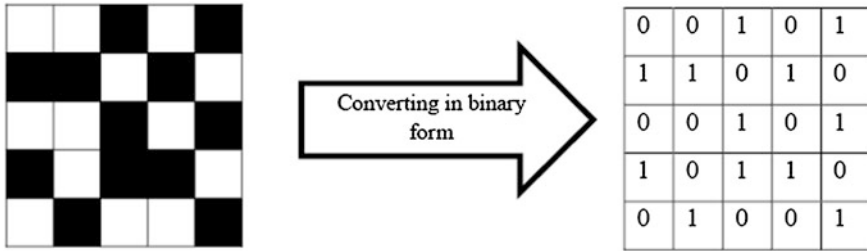


Fig. 3 Conversion in binary matrix

Fig. 4 Calculation of neighbors except boundaries

	3	4	4	
	5	4	5	
	4	3	4	

Fig. 5 Final output after applying rules of life i.e. the cells alive in next generation

	■			
		■		

are used to calculate the next state of the (dark gray) center cell according to the defined rule [6, 7]. One of the famous examples of 2D CA example is Game of Life. It was the first practical CA invented by John Conway in the late 1960s.

Now consider the following 2D CA. Here the cells are shown in black and white color. By convention white color represents dead cells and is represented by 0 after converting in binary matrix. Similarly black color represents alive cells and is represented by 1 after converting in binary matrix. The conversion is shown in Fig. 3.

After this transformation in binary matrix, calculate the number of neighbor’s matrix as shown in Fig. 4. Here, boundary cells have been left.

Then based on the 4 rules defined above, calculate next state of each cell i.e. alive or dead. Considering the cell at position (2, 2), it can be seen that it is alive cell and consists of 3 alive neighbor cells. So its next state will be alive. Cell at position (2, 3) is dead and consists of 4 neighbors, so the next state will be dead. Continuing in this fashion for every cell, the final outcome i.e. the cells that are alive in next generation is shown in Fig. 5.

This is just a simple example. Applying different rules produces different outputs and patterns.

3 Cryptography and Cellular Automata

Cryptography is the branch of applied mathematics that aims to add security by encoding messages to make them non-readable. Due to these inherent properties, CA has become an important tool to develop cryptographic methods. In addition to encryption CA finds its application in various fields like edge detection, pattern classification, error correction coding etc. The proposed classifier was built around a special class of sparse network referred to as CA. Hence CA is widely used for various applications.

4 Design and Implementation

The techniques used for implementing the two levels of security are:

- Hiding image to be send behind another image by password.
- Encryption of image using CA rules.

First of all Steganography will be used for hiding image to be send behind the cover image. The image obtained from this step will be then encrypted for making the content invisible. Encryption will be done by applying CA rules. The block diagram showing the methodology of the paper is shown in Fig. 6.

4.1 Image Hiding Behind Another Image

First image has used to be sending and another image is to be used as cover image. If size of cover image and image to be sent is different, the cover image needs to be resized according to the image to be sent. This can be accomplished using the “resize” function of Matlab.

First the sender is asked for a password. This password has to be kept secret among sender and receiver. After entering the password, the cover image needs to be resized.

After resizing, the image to be sent is hidden behind the cover image using Least Significant Bit (LSB) technique. The last two least significant bits of the cover image are cleared and the two most significant bits of the image to be sent are moved to the cleared least significant bits. At the receiver side, first the receiver

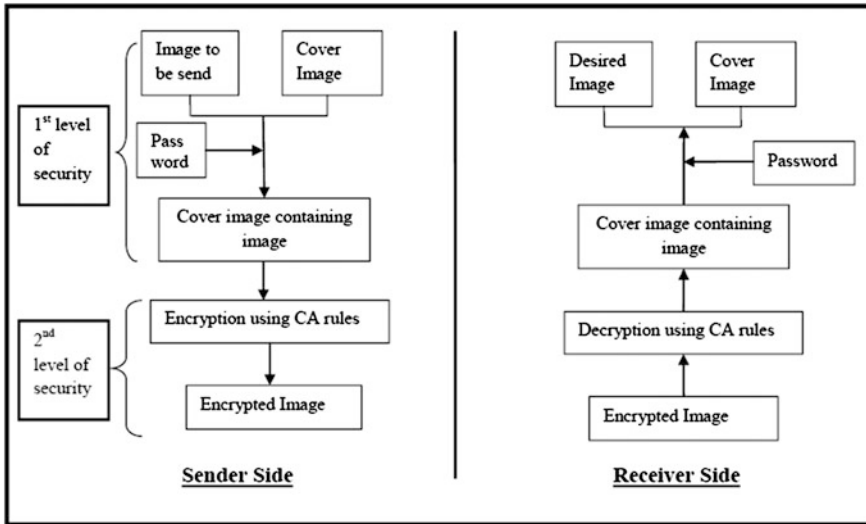


Fig. 6 Block diagram showing the two levels of security

is asked for password. If the password entered is correct only then the image can be retrieved.

4.2 Encryption Using Cellular Automata Rules

Encryption is absolutely vital to the security of all digital communications on the internet. Without encryption, you could not securely log into your social apps, shop online, or use the Internet to transmit any kind of highly personal information [8, 9, 10]. Encryption encodes the data so that it is not directly visible. The image obtained after step 1 will be encrypted, so that transmission over the network is secured. The types of CA are defined by their dimension. They can be 1D, 2D, 3D etc. There are different rules for 1D and 2D. In this paper 2D CA rules are used for encryption.

In case the cell has dependency on two or more neighboring cells, the rule number will be the arithmetic sum of the numbers of the relevant cells, which gives the linear rules of CA. So XOR operation is also linear rule of CA.

A null boundary CA is the one in which the extreme cells are connected to logic-0 states.

- Periodic boundary cellular automata (PB CA): A periodic boundary (PB) CA is the one in which the extreme cells are connected to each other.
- Uniform Cellular Automata (UCA): A uniform cellular automata (UCA) is the one in which same rules are applied to each cell.

- Hybrid Cellular Automata (HCA): If different rules are applied to different cells, then it is called as hybrid cellular automata.

In this paper PB CA has been used. Fig. 7 shows the steps involved in encryption process.

Step 1: Nonlinear CA rule (Complement) and PB CA rule-8

The length of the plain text is taken as 128 bits and the length of key as 128 bits. First the plain text is converted as 4×4 matrix with each cell containing 1 bytes (= 8 bits). Now nonlinear CA rule (complement) is applied to each bit of the plain text. Similarly 128-bits key is written in a 4×4 matrix and nonlinear CA rule (complement) is applied to each cell of the key matrix. After the complementation PB CA rule-8 is applied separately. Fig. 8 shows the use of PB CA rule-8 to the matrix.

Step 2: XOR Operation

XOR operation is applied between the resulted cipher key and cipher text providing the linear rule of cellular automata and hence providing the diffusion property of the cryptography.

Step 3: PB CA Rule 128 and PB CA Rule 32

Now the output of XOR operation is fed to PB CA rule128 and PB CA rule32 consecutively so that permutation (transposition) operations are performed providing the linear rules of CA and hence providing the diffusion property of cryptography [11]. For example, in the following matrix, applying the PB CA rule 128 to each cell of the matrix, the values in the first row have been shifted to second row, values in the second row have been shifted to third row and so on and values in the last row have been shifted to first row after applying periodic boundary (PB) CA rule-128 to each value in the cell of the matrix.

0	1	1	0			0	0	0	1
0	1	0	0	PB	CA	0	1	1	0
1	1	1	0	Rule 128		0	1	0	0
0	0	0	1			1	1	1	0

For example, in the following matrix, applying PB CA rule-32 to each cell, the values in the first column have been shifted to second column, second column values have been shifted to third column and third column values have been shifted to first column, and so on.

0	1	1	0			0	0	1	1
0	1	0	0	PB	CA	0	0	1	0
1	1	1	0	Rule 32		0	1	1	1
0	0	0	1			1	0	0	0

Since nonlinear CA rule (compliment), PB CA rule-8 (linear), XOR (linear), PB CA rule-128 (linear) and PB CA rule-32 (linear) are reversible; we can decrypt the

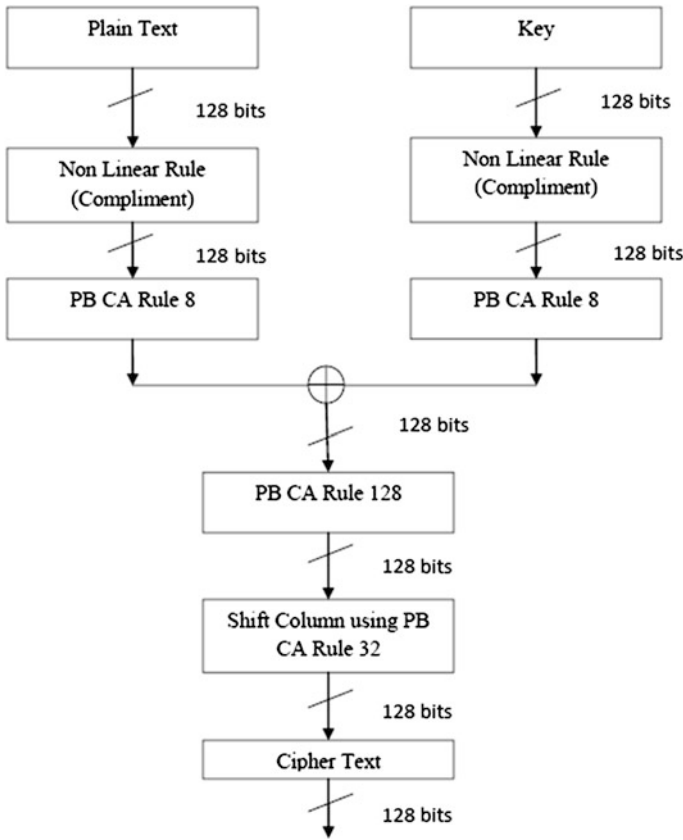


Fig. 7 Encryption steps for 1 round

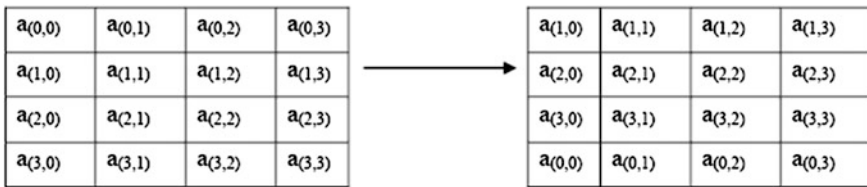


Fig. 8 PB CA rule-8

cipher text to plain text in reverse way. Hence the inverses of PB CA rule-8, PB CA rule-128 and PB CA rule-32 are PB CA rule-128; PB CA rule-8 and PB CA rule-2 respectively. Figure 9 shows the results for image encryption using 2D CA rules.

To retrieve the image at the receiver side, the receiver selects decryption task to be performed where reverse process should be processed.

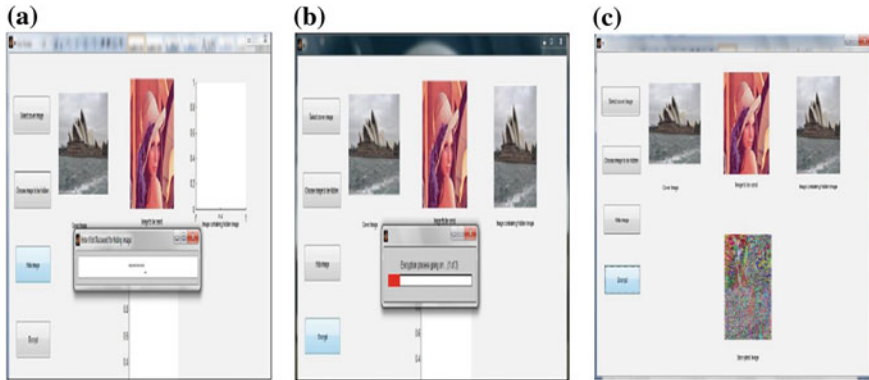


Fig. 9 Results **a** Prompt window asking 8 bit password for hiding image, **b** Prompt window showing progress of encryption, **c** Image obtained after encryption

5 Conclusion and Future Work

The proposed technique can be used to hide any format of image. The strength of the security can be greatly enhanced by combining Steganography and Cryptography concepts. For implementing Image Steganography concept, LSB technique has been used. The strength of the LSB technique used lies in the fact that it gives no idea that weather is something hidden inside it or not because the size of the cover image is doubled. The image obtained after hiding is encrypted and hence both authenticity and confidentiality are achieved. A two level security system for secure transfer of images has been developed and tested successfully.

In future, the proposed method can be improved as follows:

- As the time taken for encryption is slightly more, it can be reduced by changing rules applied
- For encryption using CA, S box can be developed.
- Hybrid CA rules can also be applied.

References

1. Younes, M.A.B., Jantan, A.: An image encryption approach using a combination of permutation technique followed by encryption. *Int. J. Comput. Sci. Netw. Secur.* **8**, 191–197 (2008)
2. Tong, X., Cui, M.: Image encryption with compound chaotic sequence cipher shifting dynamically. *Image Vis. Comput.* **26**, 843–850 (2008)
3. Pratibha, S., Diwakar, M., Lal, N.: Edge detection using Moore neighborhood. *Int. J. Comput. Appl.* **61**(3), 26–30 (2013)
4. Pratibha, S., Diwakar, M., Choudhary, S.: Application of edge detection in brain tumor detection. *Int. J. Comput. Appl.* **58**(16), 21–25 (2012)

5. Maji, Pradipta, Shaw, Chandrama, Ganguly, Niloy, Biplab, K.S., Chaudhuri, P.P.: Theory and application of cellular automata for pattern classification. *Fundamenta Informaticae* **58**, 321–354 (2003)
6. Behnia, S., Akhshani, A., Mahmodi, H., Akhavan, A.: A novel algorithm for image encryption based on mixture of chaotic maps. *Solitons Fractals* **35**, 408–419 (2008)
7. Nandi, S., Kar, B.K., and Chaudhuri, P.P.: Theory and applications of cellular automata in cryptography. *IEEE Trans. Comput.* **43**(12), 1346–1357 (1994)
8. Munshi, S., Maity, S.: A cellular automata based network security model. In: *IEEE Second International Conference on Emerging Applications of Information Technology*, 2011. pp. 75–279
9. Fateri, S., Enayatifar, R.: A new method for image encryption via standard rules of CA and logistic map function. *Int. J. Phys. Sci.* **6**(12), 2921–2926 (2011)
10. Al-Shatnawi, A.M.: A new method in image steganography with improved image quality. *Appl. Math. Sci* **6**(79), 3907–3915 (2012)
11. Ahsan, K., Kundur, D.: Practical data hiding in TCP/IP. *Proceedings of the Workshop on Multimedia Security at ACM Multimedia*, 2002

Cuckoo Search Algorithm for the Selection of Optimal Scaling Factors in Image Watermarking

Musrrat Ali, Chang Wook Ahn and Millie Pant

Abstract This paper introduces the application of an evolutionary algorithm, called the cuckoo search (CS), in finding the optimal scaling factors in digital image watermarking to improve robustness and imperceptibility. It is the first application of the cuckoo search technique to the image watermarking problem. The basic idea is to treat digital image watermarking as an optimization problem and then solve it using CS. Apply one-level redundant discrete wavelet transform (RDWT) to the cover image then the singular values of all sub bands are modified by embedding the watermark multiplied by scaling factors. The scaling factors are optimized using the cuckoo search algorithm to obtain the highest possible robustness without compromising with quality. To investigate the robustness of the scheme several attacks are applied to seriously distort the watermarked image. Empirical analysis of the results has demonstrated the efficiency of the proposed technique.

Keywords Redundant discrete wavelet transform · Singular value decomposition · Cuckoo search algorithm · Optimized scaling factors

M. Ali (✉) · C. W. Ahn
Department of Computer Science and Engineering, Sungkyunkwan University,
Suwon 440746, Republic of Korea
e-mail: musrrat.iitr@gmail.com

C. W. Ahn
e-mail: cwan@skku.edu

M. Pant
Department of Applied Sciences and Engineering, IIT Roorkee,
Roorkee 247667, India
e-mail: millifpt@iitr.ernet.in

1 Introduction

In designing of image watermarking scheme, two conflicting objectives which are the imperceptibility and robustness are often considered. The main goal of image watermarking scheme is to produce the watermarked image with low quality degradation and high robustness. In order to improve these objectives researchers have been proposed several schemes implementing in spatial as well as transformed domain. The spatial domain watermarking techniques directly embed the watermark into the cover image by altering the pixel values [1, 2]. These methods generally are less robust to image and signal processing attacks and required low computational efforts. While frequency domain methods transform the representation of spatial domain into the frequency domain and then modify its frequency coefficients to embed the watermark. There are many transform domain watermarking techniques such as discrete cosine transforms (DCT) [3–5], singular value decomposition (SVD) [6, 7], discrete Fourier transforms (DFT) [8, 9], and discrete wavelet transforms (DWT) [10–12]. These methods typically provide higher image imperceptibility and are much more robust to image manipulations but the computational cost is higher than spatial-domain watermarking methods. The performance of watermarking methods was further improved by combining two or more transformations [10–16]. The idea was based on the fact that combined transforms could compensate for the drawbacks of each other, resulting in effective watermarking. In all transformed domain watermarking schemes, there is a conflict between robustness and transparency (Imperceptibility). If the watermark is embedded in the perceptually most significant region, the scheme would be robust to attacks but it is difficult to hide the watermark. However, if the watermark is embedded in the perceptually insignificant region, it would be easier to hide the watermark but the scheme may be less resilient to attacks. Imperceptibility and robustness can also be improved by finding the suitable scaling factors and suitable embedding region. Some of the watermarking algorithms have taken the advantage of intelligent optimization techniques to improve imperceptibility and robustness, like genetic algorithm (GA) [17, 18], particle swarm optimization (PSO) [10, 19–22], and differential evolution (DE) [23]. For many decades, the selection of optimal scaling factors is a critical issue faced in watermarking

The main contribution of this work is the application the cuckoo search optimization algorithm [24, 25] for obtaining the suitable scaling factors in image watermarking. This stochastic optimization technique has been successfully applied in solving some real life application problems with promising results [26–31]. However, this emerging optimization method has not been applied to watermarking problems including image watermarking. The performance of this nature-inspired optimization method has been analyzed using several test images and ten distortion attacks. Results show that cuckoo search offers a reliable performance for solving these watermarking problems. This is an alternative of other evolutionary techniques. The major advantage of the cuckoo search algorithm is its

simplicity of implementation because it has only a single parameter, the identification probability of cuckoo eggs (pa), other than the population size NP .

The rest of the paper is structured as follows. The mathematical formulation of the proposed watermarking scheme is given in Sect. 2. Section 3 describes cuckoo search algorithm and its implementation. The experimental results are discussed in Sect. 4. Finally, Sect. 5 draws the conclusions based on this research.

2 Mathematical Formulation of the Proposed Watermarking Algorithm

This section is devoted to the mathematical formulation of the proposed watermarking algorithm. Imperceptibility, robustness and capacity or payload are the most important requirements that must be confronted in designing a watermarking scheme. Makbol and Khoo [15] recently proposed a watermarking technique based on redundant discrete wavelet transform (RDWT) and singular value decomposition (SVD). They have replaced DWT by RDWT and followed the same steps used by Ganic et al. [12]. This scheme performed well against some attacks, but have a weakness in the selection of the scaling factors which highly affect the characteristics of the watermarking technique. This method has taken the fixed values of scaling factors as 0.05 and 0.005 for low frequency and high frequency sub bands respectively. It is a hard step for choosing the suitable scaling factor actually, it is image-dependent. Different watermarks need the different scaling factors, although they are embedded in the same host image. In this paper, the metaheuristic algorithm named cuckoo search is incorporated for selecting the suitable scaling factor to satisfy the robustness and invisibility.

2.1 Embedding Process

1. Apply one-level RDWT on cover image (J) that decompose it into four blocks denoted by LL , HL , LH , and HH .
2. Perform SVD operation on all blocks obtained in step 1 (i.e. LL , HL , LH and HH).

$$A^k = U_k S_k V_k^T, \quad k \in \{LL, HL, LH, HH\} \quad (1)$$

3. Modify the singular values of diagonal matrices of LL , HL , LH and HH blocks of the cover image by adding the corresponding the watermark W and then apply SVD to them respectively.

$$S_k + \lambda_k W = U_{wk} S_{wk} V_{wk}^T, \quad k \in \{LL, HL, LH, HH\} \quad (2)$$

where: λ_k is an optimized scaling factor obtained from the cuckoo search algorithm. In our case the total number of scaling factors is equal to the number of blocks. That is anew scaling factor is used for each block.

4. Obtain the modified LL , HL , LH and HH blocks of the one level of cover image such that

$$A'^k = U_k S_{wk} V_k^T \quad (3)$$

5. Replace the original blocks at the first level of the transformed cover image by modified blocks respectively and apply the inverse redundant discrete wavelet transform (IRDWT) to get the watermarked image I_w .

2.2 Extraction Process

The watermarked image I_w is subjected to various distortions. If I_w^* is distorted watermarked image then a possibly corrupted watermark W^* can be extracted performing the following steps:

1. Apply the *steps* 1 and 2 of the embedding process on the corrupted watermarked image I_w^* to get S_{wk}^*

$$A_{wk}^* = U_{wk}^* S_{wk}^* V_{wk}^{*T} \quad (4)$$

2. Compute possibly corrupted D_k^*

$$D_k^* = U_{wk} S_{wk}^* V_{wk}^T \quad (5)$$

3. Extract the possibly corrupted watermark (W^{*k}) from each sub-band $k \in \{LL, HL, LH, HH\}$

$$W^{*k} = (D_k^* - S_k) / \lambda_k \quad (6)$$

3 Cuckoo Search Algorithm and its Implementation

3.1 Cuckoo Search Algorithm

The cuckoo search optimization algorithm, introduced by Yang and Deb in 2009 [24, 25], is inspired by the brood parasitism of the cuckoo species in association with the Lévy Flight behavior of some birds and fruit flies. The characteristic of cuckoo birds is that they never build their own nests and instead lay their eggs in

the nest of other host birds. There are two possibilities that the host bird either discovers the alien eggs or not. If then it is discovered it will either throw these alien eggs away from the nest or simply abandon its nest and build a completely new nest somewhere else. So, to reduce the chances of identification cuckoo birds carefully mimic the color and pattern of the eggs of host birds to increase the hatching probability of their own eggs. The egg-laying timing of some cuckoo species is also amazing. Parasitic cuckoos often choose a nest where the host bird just laid its own eggs. Generally, the hatching time of cuckoo eggs slightly earlier than their host eggs. As soon as the first cuckoo chick is hatched, the first instinctive action it will take is to throw out the host bird chicks and eggs that have not yet hatched to increase the food share provided by its host bird. It is also observed that a cuckoo chick can also mimic the call of host chicks to gain access to more feeding opportunity. In cuckoo search optimization algorithm, each egg in a nest represents a potential solution. The reproduction process of the cuckoo search algorithm works under three assumptions that are given as:

1. Each cuckoo lays one egg at a time and dumps it in a randomly chosen nest.
2. The best nest with high quality of eggs (solutions) will carry over to the next generation.
3. The number of available host nests is fixed, and a host can discover an alien egg with a probability of identification $p_a \in [0, 1]$. If it happens, the host can either throw away the alien egg from the nest or abandon the nest.

The initial population of NP solutions (nests) is generated by uniformly distributed random numbers over the search space. The randomly chosen initial solutions of design variables are defined in the search space by the lower (LB) and upper (UB) boundaries. The initial value of the j th variable of the i th solution is given by the following relation:

$$X_{i,j,G=0} = LB_j + rand_j \times (UB_j - LB_j) \quad (7)$$

where LB_i and UB_i are the j th variables of LB and UB , respectively; G is the number of the current generation (cycle); $rand_j \in (0, 1)$ is a uniform random number and anew for each variable.

The new nest is generated using the concept of Lévy flight. Lévy flight represents a variation of random walk, one of the ways of motion of some birds or animals in searching for food, in which the step length is determined by Lévy distribution. The important property of Levy flight is, it makes sure that the whole search space is covered, which is due to the heavy-tailed property of Levy distribution. The general equation of the reproduction scheme of the CS algorithm to generate a new solution $X_{i,G+1}$ corresponding to the solutions $X_{i,G}$ is given as:

$$X_{i,G+1} = X_{i,G} + \alpha \otimes Levy(\beta) \quad (8)$$

where α is the step-size that controls the scale of random search and depends on the scales of the optimization problems under analysis. It is recommended that the step size should be 0.01 times of the size of the search space. For larger values of

the step size the Lévy flight may become too “aggressive” that results in the new solutions may go out of the boundary of the search space. Index $i = 1, 2, \dots, NP$ denotes i th solution; \otimes is the element-wise multiplication; Levy (β) is a Levy distributed random number. There are many algorithms proposed in the literature for generating the step length s of Levy flight. The numerical algorithm proposed by Mantegna [32] is one of the most efficient and yet straightforward way to generate Levy distributed random numbers. In Mantegna’s algorithm, the step length s can be calculated by using the following expression:

$$s = \frac{u}{|v|^{1/\beta}} \quad (9)$$

where u and v are drawn from normal distributions. That is $u \sim N(0, \sigma^2)$ and $v \sim N(0, 1)$ With

$$\sigma = \left(\frac{\Gamma(1 + \beta) \sin(\pi\beta/2)}{\Gamma\left(\frac{1+\beta}{2}\right) \beta 2^{\frac{\beta-1}{2}}} \right)^{1/\beta}$$

where Γ denotes *gamma function* and $\beta \in [0, 2]$ is a *scale factor*.

The host bird can identify the cuckoo eggs with probability p_a , that is a fraction p_a of the total number of solutions is replaced by new random solutions. The new solution should be generated by a random walk manner at the location far from the current best solution to avoid being trapped in local minima. This operator is called abandon operator and it is performed as follows:

$$X_{i,G+1} = \begin{cases} X_{i,G} + rand \times (X_{r1,G} - X_{r2,G}) & \text{if } rand_i > p_a \\ X_{i,G} & \text{else} \end{cases} \quad (10)$$

where *rand* is a uniformly distributed random number in $[0, 1]$ interval; $X_{r1,G}$ and $X_{r2,G}$ are the solutions randomly selected from the population. The best nests with the fittest egg (solution) carry over to the next generation. This process is continued till the termination criteria reached and the best nest (solution) with fittest egg (objective value) is taken as the optimal value. The CS algorithm in more detail is explained in [24, 25] and recommended the parameter values, *scale factor* (β) = 1.5 and *probability of identification* (p_a) = 0.25.

3.2 Application of the Cuckoo Search Algorithm in Finding SFs

Numerous researchers have dealt with solving the problem of image watermarking as an optimization problem. The objective function, in image watermarking, may include various requirements (like, imperceptibility, robustness, capacity etc.) that should be fulfilled by the given watermarking scheme. Scaling factors (SFs) in a

watermarking technique determine the watermark strength that control the imperceptibility and robustness. Use of small scaling factor favors the invisibility of the watermark, but the watermarked image is less robust to several common attacks. On the other hand, high scaling factor favors the robustness, but the quality of watermarked image is unacceptable. Most existing watermarking schemes have been used scaling factors as a constant value; actually, it is image dependent. A constant scaling factors may be suitable for one set of images but may not be appropriate for another set. Moreover, this parameter is often tuned and adjusted “manually”. Proper setting of scaling factor for watermarking is more difficult than expected. Therefore, an efficient and powerful algorithm is required for this purpose. Due to the difficulty in finding the suitable value of the scaling factor, here we apply the cuckoo search algorithm to automatically determine these values to achieve a better performance. The multiple scaling factors together make a single solution in CS. In our case the dimension of each individual is four (i.e. Different scaling factor for each block). The procedure is started initializing the population generated by random number generator between zero and one. Different blocks of the watermark multiplied by these scaling factors are embedded in the corresponding blocks of third level decomposition of the cover image

Then the watermarked image is examined for several attacks, and from these corrupted watermarked images the watermarks are extracted using the extraction process. The fitness is computed for each individual and then the individual with smaller fitness values are selected for the next generation. Now start the main loop of CS. Perform reproduction process to generate new solutions and evaluate the fitness. Continue the process till the termination criterion not satisfied. At the end of iteration, we will obtain the near optimum scaling factors. The individual with the minimum fitness of the final generation is used for watermark embedding. The evaluation function (fitness function) that rates all individuals according to their fitness, mathematically is given as follows:

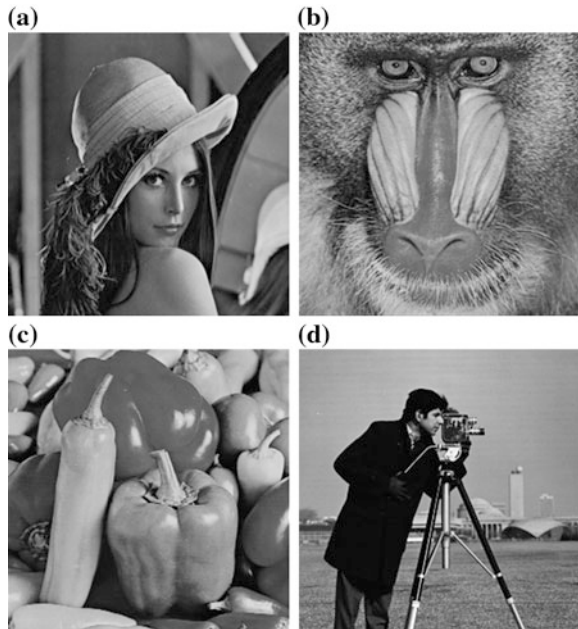
$$\text{Minimize } f = \frac{N}{\sum_{i=1}^N NC(W, W_i^*)} - NC(I, I_w) \quad (11)$$

where I and I_w denote the cover and the watermarked images, respectively; NC [17] represent the two-dimensional normalized correlation value; W and W^* indicate the watermark and the extracted watermark image, respectively; N is the number of attacking methods.

4 Results and Discussions

This section analyzes the performance of the proposed watermarking scheme under the numerous experiments. The test images “lena”, ‘baboon’ and “pepper” of size 256×256 given in Fig. 1a–c are taken as the cover images. While grayscale “cameraman” of size 256×256 given in Fig. 1d is taken as the

Fig. 1 a–c Cover images lena, baboon and pepper respectively, d watermark image cameraman



watermark image. *PSNR* (peak signal-to-noise ratio) is used to analyze the visual quality of the watermarked image. To investigate the robustness of the proposed scheme ten attacks are applied to the watermarked images: (1) Gamma correction (GC) with gamma value 0.6, (2) median filtering (MF) with window size 3×3 , (3) cropping (CR) 50 %, (4) rotation (RO) with 45° anticlockwise, (5) translation (TR) with 50 horizontal and 50 vertical pixels, (6) histogram equalization (HE), (7) Gaussian noise (GN) with zero mean and 0.01 variance, (8) JPEG compression with quality factor 50, (9) row flipping (RF), (10) column flipping. The algorithms are implemented in MATLAB environment on a PC with 4 GB RAM and Core 2 Duo processor. Normalized correlation (*NC*) coefficient is used as a similarity measure between the original and extracted watermark images. The parameter settings of CS are, population (number of nests) size $NP = 20$, and maximum generations 200. In order to justify the proposed approach, results are compared to the scheme proposed by Makhbol and Khoo [15] based on RDWT, where the scaling factors are taken fixed for all the images. For our convenience we will call it pure RDWT. To run this algorithm we have taken the recommended parameters setting.

The watermarked images obtained by proposed technique, with *PSNR* values are given in Fig. 2a–c. From a close observation of Figs. 1 and 2 one can say that there is no perceptual difference between original and watermarked images that is also supported by good *PSNR* value. It shows that the good imperceptibility is obtained by proposed technique.

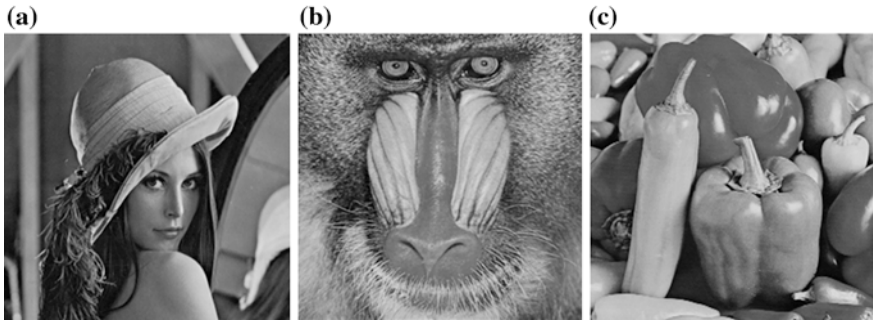


Fig. 2 a–c Watermarked images lena, baboon, and pepper respectively with their respective PSNR values. a $PSNR:36.3994$. b $PSNR:36.2858$. c $PSNR:34.6284$

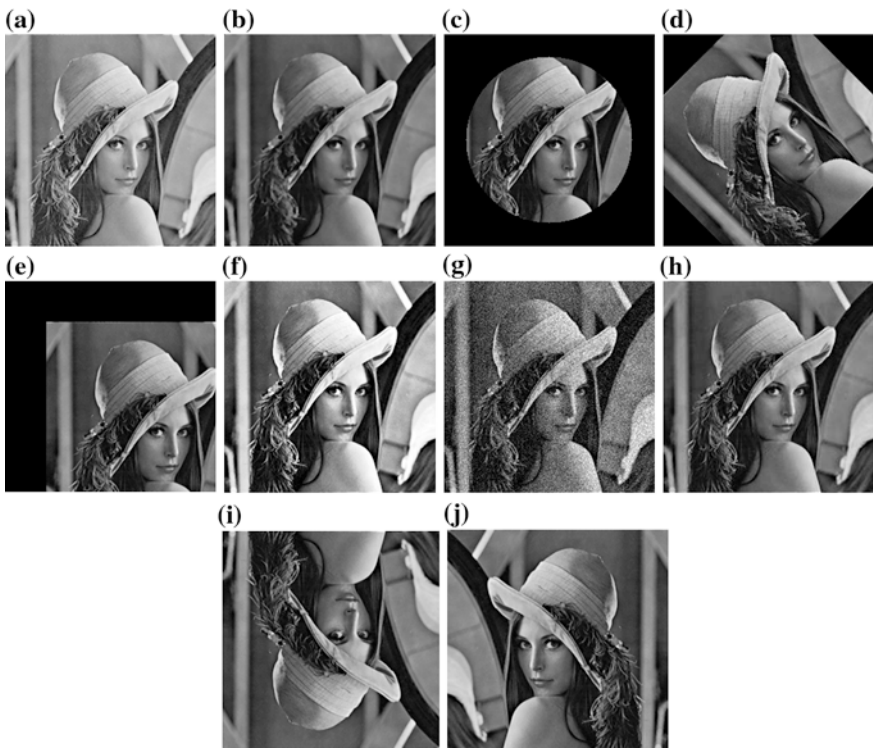


Fig. 3 a–j Watermarked images after different attacks. a Gama correction (GC). b Median filtering (MF). c Cropping (CR). d Rotation (RO). e Translation (TR). f Histogram Eq. (HE). g Gaussian noise (GN). h JPEG compression. i Row flipping (RF). j Column flipping (CF)

For the robustness experiments the distortions applied on watermarked images and a sample of distorted images is shown in Fig. 3. For the visual quality analysis of the extracted watermarks these are given in Fig. 4. From Fig. 4 it is clear that the

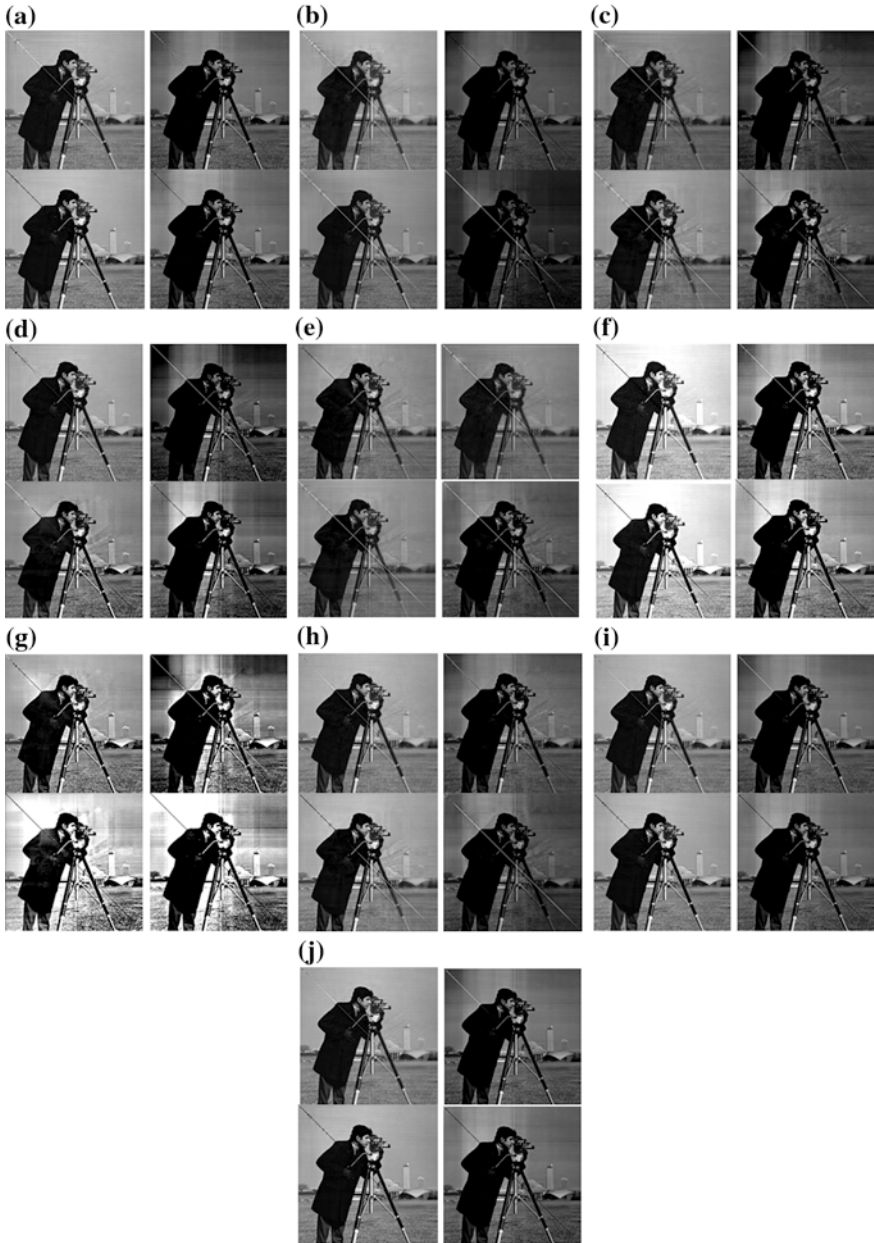


Fig. 4 A visual-perception of watermarks extracted after different attacks from the images given in Fig. 3. **a** Gama correction (GC). **b** Median filtering (MF). **c** Cropping (CR). **d** Rotation (RO). **e** Translation (TR). **f** Histogram Eq. (HE). **g** Gaussian noise (GN). **h** JPEG compression. **i** Row flipping (RF). **j** Column flipping (CF)

Table 1 PSNR comparison of the watermarked images obtained by the algorithms

Algorithm	Lena	Baboon	Pepper
Our	36.3994	36.2858	34.6284
Pure RDWT	36.8792	36.9173	35.7843

Table 2 Experimental results of the proposed scheme under different attacks

Attack	Lena		Baboon		Pepper	
	Our	Pure RDWT	Our	Pure RDWT	Our	Pure RDWT
GC	0.9988	0.9896	0.9975	0.9884	0.9992	0.9894
MF	0.9951	0.9821	0.9932	0.9622	0.9975	0.9832
CR	0.9936	0.9864	0.9906	0.9863	0.9914	0.9882
RO	0.9987	0.9828	0.9972	0.9681	0.9973	0.9825
TR	0.9959	0.9796	0.9918	0.9865	0.9919	0.9813
HE	0.9979	0.9912	0.9936	0.9762	0.9978	0.9915
GN	0.9917	0.9792	0.9945	0.9921	0.9939	0.9942
JPEG	0.9978	0.9903	0.9981	0.9933	0.9974	0.9869
RF	0.9989	0.9842	0.9990	0.9867	0.9985	0.9852
CF	0.9987	0.9848	0.9993	0.9880	0.9989	0.9843

extracted watermarks are almost similar to the original watermark. The quality of extracted watermarks is good in all the cases but the quality of the extracted watermark in the case of Gaussian noise attack is poor in comparison to the other cases. The PSNR of the watermarked images obtained by the algorithms are given in Table 1 while the normalized correlation (NC) values of extracted watermarks obtained in each case are given in Table 2. Also, the results obtained by the algorithm proposed in [15] are given in the tables for the comparison. From the Table 1 it is clear that the watermarked image quality using these two algorithms is nearly the same. There is no meaningful difference between the algorithms in the image quality aspect and the PSNR of watermarked image in all the cases is higher than 30 that is acceptable. From Table 2, it is observed that the proposed algorithm has the better correlation values than that of the pure RDWT in all the cases. The overall performance of the proposed algorithm is better than the pure RDWT algorithm.

5 Conclusions

The proposed technique in this paper has taken the advantage of an evolutionary technique called cuckoo search for finding the suitable scaling factors that are used in image watermarking. The watermark image is embedded into the cover image in the RDWT-SVD domain. The advantage of the proposed technique is that it automatically chooses the optimal scaling factors depending on the image and watermark, while for the ordinary methods it is constant and need the fine tuning for all the types of images. To investigate the robustness of the scheme several

attacks are applied to seriously distort the watermarked image. Numerical and pictorial representation of the results has shown the efficiency of the proposed technique. In most of the cases watermark is extracted with high correlation value. The experimental results comparison with the other algorithm based on RDWT has also shown the efficiency of the proposed algorithm. Thus, our proposed scheme has satisfied the capacity, robustness, imperceptibility, and security requirements that are essential for a good watermarking technique.

References

1. Nikolaidis, N., Pitas, I.: Robust image watermarking in the spatial domain. *Sig. Process.* **66**(3), 385–403 (1998)
2. Liu, J.-C., Chen, S.-Y.: Fast two-layer image watermarking without referring to the original image and watermark. *Image Vis. Comput.* **19**(14), 1083–1097 (2001)
3. Lin, S.D., Shie, S.-C., Guo, J.Y.: Improving the robustness of DCT-based image watermarking against JPEG compression. *Comput. Stand. Interfaces* **32**, 54–60 (2010)
4. Phadikar, A., Maity, S.P., Verma, B.: Region based QIM digital watermarking scheme for image database in DCT domain. *Comput. Electr. Eng.* **37**, 339–355 (2011)
5. Wu, X., Sun, W.: Robust copyright protection scheme for digital images using overlapping DCT and SVD. *Appl. Soft Comput.* **13**(2), 1170–1182 (2013)
6. Liu, R., Tan, T.: An SVD-based watermarking scheme for protecting rightful ownership. *IEEE Trans. Multimedia* **4**(1), 121–128 (2002)
7. Mohammad, A.A., Alhaj, A., Shaltaf, S.: An improved SVD-based watermarking scheme for protecting rightful ownership. *Sig. Process.* **88**(9), 2158–2180 (2008)
8. Lu, W., Lu, H., Chung, F.-L.: Feature based robust watermarking using image normalization. *Comput. Electr. Eng.* **36**, 2–18 (2010)
9. Rawat, S., Raman, B.: A blind watermarking algorithm based on fractional Fourier transform and visual cryptography. *Sig. Process.* **92**(6), 1480–1491 (2012)
10. Run, R.-S., Horng, S.-J., Lai, J.-L., Kao, T.-W., Chen, R.-J.: An improved SVD-based watermarking technique for copyright protection. *Expert Syst. Appl.* **39**, 673–689 (2012)
11. Ouhsein, M., Hamza, A.B.: Image watermarking scheme using nonnegative matrix factorization and wavelet transform. *Expert Syst. Appl.* **36**(2), 2123–2129 (2009)
12. Ganic, E., Eskicioglu, A.M.: Robust DWT-SVD domain image watermarking: embedding data in all frequencies. In: *Proceedings of the ACM Multimedia and Security Workshop*, pp. 166–174 (2004)
13. Song, C., Sudirman, S., Merabti, M.: A robust region-adaptive dual image watermarking technique. *J. Vis. Commun. Image R.* **23**, 549–568 (2012)
14. Bhatnagar, G., Wu, J.Q.M.: Biometrics inspired watermarking based on a fractional dual tree complex wavelet transform. *Future Gener. Comput. Syst.* **29**(1), 182–195 (2013)
15. Makbol, N.M., Khoo, B.E.: Robust blind image watermarking scheme based on redundant discrete wavelet transform and singular value decomposition. *Int. J. Electron. Commun. (AEÜ)* **65**, 658–663 (2012). <http://dx.doi.org/10.1016/j.aeu.2012.06.008>
16. Rastegar, S., Namazi, F., Yaghmaie, K., Aliabadian, A.: Hybrid watermarking algorithm based on singular value decomposition and radon transform. *Int. J. Electron. Commun. (AEU)* **65**, 658–663 (2011)
17. Lai, C.C.: A digital watermarking scheme based on singular value decomposition and tiny genetic algorithm. *Digit. Sig. Process.* **21**, 522–527 (2011)
18. Maity, S.P., Maity, S., Sil, J., Delpha, C.: Collusion resilient spread spectrum watermarking in M-band wavelets using, GA-fuzzy hybridization. *J. Syst. Softw.* **86**(1), 47–59 (2013)

19. Vahedi, E., Zoroofi, R.A., Shiva, M.: Toward a new wavelet-based watermarking approach for color images using bio-inspired optimization principles. *Digit. Sig. Process.* **22**, 153–162 (2012)
20. Tsai, H.-H., Jhuang, Y.-J., Lai, Y.-S.: An SVD-based image watermarking in wavelet domain using SVR and PSO. *Appl. Soft Comput.* **12**(8), 2242–2453 (2012)
21. Tsai, H.-H., Lai, Y.-S., Lo, S.-C.: A zero-watermark scheme with geometrical invariants using SVM and PSO against geometrical attacks for image protection. *J. Syst. Softw.* **86**(2), 335–348 (2013)
22. Wang, Y.-R., Lin, W.-H., Yang, L.: An intelligent watermarking method based on particle swarm optimization. *Expert Syst. Appl.* **38**(7), 8024–8029 (2011)
23. Aslantas, V.: An optimal robust digital image watermarking based on SVD using differential evolution algorithm. *Opt. Commun.* **282**, 769–777 (2009)
24. Yang, X.S., Deb, S.: Cuckoo search via levy flights. In: *Proceedings of World Congress on Nature and Biologically Inspired Computing' NABIC-2009*, pp. 210–214 (2009)
25. Yang, X.S., Deb, S.: Engineering optimisation by Cuckoo search. *Int. J. Math. Model. Numer. Optim.* **1**(4), 330–343 (2010)
26. Bhargava, V., Fateen, S.E.K., Bonilla-Petriciolet, A.: Cuckoo search: a new nature-inspired optimization method for phase equilibrium calculations. *Fluid Phase Equilib.* **337**, 191–200 (2013)
27. Gandomi, A.H., Yang, X.S., Alavi, A.H.: Cuckoo search algorithm: a metaheuristic approach to solve structural optimization problems. *Eng. Comput.* **29**, 17–35 (2013)
28. Bulatović, R.R., Đorđević, S.R., Đorđević, V.S.: Cuckoo search algorithm: a metaheuristic approach to solving the problem of optimum synthesis of a six-bar double dwell linkage. *Mech. Mach. Theory* **61**, 1–13 (2013)
29. Yildiz, A.R.: Cuckoo search algorithm for the selection of optimal machining parameters in milling operations. *Int. J. Adv. Manuf. Technol.* **64**, 55–61 (2013)
30. Valian, E., Tavakoli, S., Mohanna, S., Haghi, A.: Improved cuckoo search for reliability optimization problems. *Comput. Ind. Eng.* **64**, 459–468 (2013)
31. Moravej, Z., Akhlaghi, A.: A novel approach based on cuckoo search for DG allocation in distribution network. *Electr. Power Energy Syst.* **44**, 672–679 (2013)
32. Mantegna, R.N.: Fast, accurate algorithm for numerical simulation of Levy stable stochastic processes. *Phys. Rev.* **49**, 4677–4683 (1994)

Identifying and Prioritizing Human Capital Measurement Indicators for Personnel Selection Using Fuzzy MADM

Remica Aggarwal

Abstract Human capital constitutes an important and essential asset in any organization. Identifying and evaluating various human capital indicators or assessors is a multi-attribute decision making problem (MADM) which includes both qualitative and quantitative factors and therefore an appropriate MADM technique is required for proper evaluation and assessment of these factors or attributes. This study aims at defining a methodology based on Delphi method as well as Fuzzy Analytic Hierarchy Process (FAHP) is proposed to prioritize various human capital indicators associated with the five main attributes i.e. Talent, Integration, enabling a performance-based culture/climate, capability and leadership. The findings showed that in context with the case problem, Employees satisfaction with advancement opportunities, Internal relationship index, Employee skills, Creating results by using knowledge, Percentage of employees with access to appropriate training and development opportunities are the most important indicators for the HC in an Indian organization.

Keywords Human capital measurement indicators · Fuzzy analytic hierarchy process · Fuzzy sets · Delphi technique

1 Introduction

The Human Capital (HC) is the source of creativity in the organization. Implicit knowledge assets of the employees constitute one of the most crucial elements that affect the work performance of the company [1]. However, precise statistical data associated with the human capital measurement indicators are not readily available

R. Aggarwal (✉)
Department of Management, Birla Institute of Technology and Science,
Pilani 333031, India
e-mail: remica_or@rediffmail.com

or very hard to be extracted. In addition, decision-makers prefer natural language expressions rather than sharp numerical values in assessing these parameters which makes HC, an inherently fuzzy notion. Indeed, the uncertainty in expressions such as ‘low talent’, ‘moderate ability of knowledge creation’ or ‘high experience’, which are frequently encountered in the HC literature, is fuzziness. To handle such uncertainty based ambiguous or fuzzy information, the fuzzy set theory proposed by [2] which was later on developed by Zimmermann [3] and has been extensively used as a useful tool in multi attribute decision making. The concept of combining the fuzzy theory and MADM is referred to as fuzzy MADM (FMADM).

This paper aims at obtaining prioritization of HC measurement indicators under uncertainty or fuzziness. A Fuzzy Analytic Hierarchy Process approach is proposed to prioritize various multiple HC indicators. The findings showed that in context with the case study, Employees satisfaction with advancement opportunities, Internal relationship index, Employee skills, Creating results by using knowledge, Percentage of employees with access to appropriate training and development opportunities are the most important indicators for the HC in an Indian organization.

2 Literature Review

A. Multi-attribute decision-making techniques for prioritization

Multi-attribute decision-making (MADM) techniques have the advantage that they can assess a variety of options according to a variety of criteria that have different units. Another significant advantage is that they can analyze both quantitative and qualitative evaluation criteria together. TOPSIS, outranking and AHP are three of the most frequently used MADM techniques. TOPSIS views a MADM problem with m alternatives as a geometric system with m points in the n dimensional space. The chosen alternative is required to have shortest distance from the positive-ideal solution and the longest distance from the negative-ideal solution [4]. The outranking decision aid methods systematically compare all couples of actions on different criteria and thereby determine which actions are being preferred to the others. The most well known outranking methods are ELECTRE, ORESTE, and PROMETHEE. Analytic Hierarchy Process (AHP) developed by Saaty [5] is a method for ranking various decision alternatives available and selecting the best one in the presence of multiple criteria. This includes three main operations viz. hierarchy construction, priority analysis and consistency verification while ranking the decision alternatives. Firstly, complex multiple criteria decision problems need to break down into multiple hierarchical levels. After that, the decision makers have to compare each cluster in the same level in a pair-wise fashion based on their own experience and knowledge. Since these comparisons

involve personal or subjective judgments, some degree of inconsistency may occur. To guarantee that the judgments are consistent, consistency verification is performed to measure the degree of consistency among the pair-wise comparisons by computing the consistency ratio. If it is found that the consistency ratio is >0.1 , the decision makers should review and revise the pair wise comparisons. Once all pair-wise comparisons are carried out at every level, and are proved to be consistent, the judgments can then be synthesized to find out the priority ranking of each criterion and its attributes.

B. Fuzzy AHP methods

The earliest work in fuzzy AHP appeared in [6] which compared fuzzy ratios described by triangular membership functions. Thereafter different approaches to FAHP have been cited in the literature, amongst the recent ones are by [7–10]. This paper proposes the Fuzzy Analytic Hierarchy Process as suggested by [10] to assess and prioritize various performance measurement indicators of Human Capital (HC) in an Indian organization.

3 Objectives of the Study

The aims of this research are as follows: (1) enumerate various HC performance measurement indicators through a review of the literature and industry interviews; (2) to select appropriate indicators for the case problem taken using Fuzzy Delphi Technique (FDT); (3) use FAHP (Fuzzy Analytic Hierarchy Process) to find the fuzzy weights of the indicator (assessors) as well as their final ranking or priorities; and (4) provide suggestions based on the research results for HC assessment and serve as a reference for future research in this field.

4 Research Methodology

The paper proposes a process integrating fuzzy Delphi and fuzzy AHP approach to select and assess various HC performance indicators. The selection of attributes requires a thorough check on different aspects from each attribute and the requirement of the company. Based on extensive literature survey by the research wing of the department, five main attributes has been selected to maximize HC in an organization. These attributes are Talent (Tal), Integration (Int), enabling a performance-based culture/climate (Cul), Capability (Cap) and Lead: leadership (Lead). Associated with these attributes are the various human resource efficiency measures or indicators [11–14]. After the analysis, 35 indicators have been selected for measuring performance of Human Capital. Thereafter, based on the

subjective judgment data of a group of experts, this is further shortlisted to around 20 using Fuzzy Delphi method. After short listing, these are then assessed and prioritize using the technique of Fuzzy Analytic Hierarchy Process. This section describes the Fuzzy Set theory, Fuzzy Delphi technique as well as Fuzzy Analytic Hierarchy Process techniques used in the paper.

C. Fuzzy set

A fuzzy set is characterized by a membership function, which assigns to each element a grade of membership within the interval [0, 1], indicating to what degree that element is a member of the set. A tilde “ $\tilde{}$ ” will be placed above a symbol if the symbol represents a fuzzy set. A TFN is denoted simply as (l, m, u) where the parameters l, m and u denote the smallest possible value, the most promising value and the largest possible value that describe a fuzzy event. Each TFN has linear representations on its left and right side such that its membership function can be defined as:

$$\mu_{\tilde{M}} = \begin{cases} 0, & x < l \\ (x - l)/(m - l), & l \leq x \leq m \\ (u - x)/u - m, & m \leq x \leq u \\ 0, & x > u \end{cases}$$

D. Fuzzy Delphi Method

The FDM steps [15] are as follows:

1. Collect opinions of decision group: Find the evaluation score of each alternate factor’s significance given by each expert by using linguistic variables in questionnaires.
2. Set up triangular fuzzy numbers: Assuming the evaluation value of the significance of j th element given by i th expert of n experts is $\tilde{W}_{ij} = [a_{ij}, b_{ij}, c_{ij}]$ then the fuzzy weighting \tilde{W} of j th element is $\tilde{W} = [a_j, b_j, c_j]$ among which $a_j = \min [a_{ij}]$, $b_j = \frac{1}{n} \sum_n b_{ij}$, $c_j = \max [c_{ij}]$.
3. Defuzzification: Use simple center of gravity method to defuzzify the fuzzy weight w_{ij} of each alternate element to definite value S_j ,

$$S_j = \frac{a_j + 4b_j + c_j}{6}, j = 1, 2, \dots, m.$$

4. Screen evaluation indexes: Finally proper factors can be screened out from numerous factors by setting the threshold a . The principle of screening is as follows:
 If $S_j > a$, then j th factor is the evaluation index.
 If $S_j < a$, then delete j th factor.

E. Fuzzy Analytic Hierarchy process

This study is based on FAHP method are as follows [10]:

1. Determine the evaluation criteria.
2. Set up hierarchy architecture conforming to target problems through fuzzy decision making investigating expert’s opinions.
3. Construct pair wise comparison matrices among all the elements/attribute in the dimensions of the hierarchy system. Assign linguistic terms to the pair wise comparisons by asking which are the more important of each two dimensions as following matrix A:

$$A = \begin{bmatrix} 1 & \tilde{a}_{12} & \dots & \tilde{a}_{1n} \\ \tilde{a}_{21} & 1 & \dots & \tilde{a}_{2n} \\ \cdot & \cdot & \dots & \cdot \\ \cdot & \cdot & \dots & \cdot \\ \tilde{a}_{n1} & \tilde{a}_{n2} & \dots & 1 \end{bmatrix} \text{ where,}$$

$$\tilde{a}_{ij} \begin{cases} \tilde{9}^{-1}, \tilde{8}^{-1}, \tilde{7}^{-1}, \tilde{6}^{-1}, \tilde{5}^{-1}, \tilde{4}^{-1}, \tilde{3}^{-1}, \tilde{2}^{-1}, \tilde{1}^{-1}, \tilde{1}, \tilde{2}, \tilde{3}, \tilde{4}, \tilde{5}, \tilde{6}, \tilde{7}, \tilde{8}, \tilde{9} & i \neq j \\ \tilde{1} & i = j \end{cases}$$

4. To use geometric mean technique to define the fuzzy geometric mean and fuzzy weights of each criterion given by [16]:

$$\tilde{r}_i = (\tilde{a}_{i1} \otimes \tilde{a}_{i2} \otimes \dots \otimes \tilde{a}_{in})^{\frac{1}{n}}$$

$$\tilde{w}_i = \tilde{r}_i \otimes (\tilde{r}_1 \oplus \tilde{r}_2 \oplus \dots \oplus \tilde{r}_n)^{-1}.$$

5 Numerical Illustration

This paper aims at prioritizing HC measurement indicators in an Indian organization. Among all the available criteria judged and explored after reviewing the literature, following 20 were sorted out using Fuzzy-Delphi method measurement (Table 1).

There is a pair wise judgment matrix to be filled by the representatives of the company who also are the decision makers/managers (refer appendix). The set of linguistic variables used for obtaining the opinions of the company representatives is given in Table 2.

Table 1 Sorting of indicators

Indicator	Description	Indicator	Description
I1	Employees satisfaction with advancement opportunities	I11	Succession rate of training programs
I2	Absenteeism rate	I12	Employee turnover by performance level and by controllability
I3	Percentage of payroll spent on training	I13	Internal relationship index
I4	Consistency and clarity of messages from top management and HR	I14	Employee skills
I5	Retention rates of critical human capita	I15	Percentage of employees with access to appropriate training and development opportunities
I6	Creating results by using knowledge	I16	Freely expressing the opinions
I7	Extent of cross- functional teamwork	I17	Change in employee mindset
I8	Percentage of employees development plans completed	I18	Extent of organisational learning
I9	Perception of consistent and equitable treatment of all employees	I19	Performance of newly hired applicants
I10	Total HR investments	I20	Diversity of race and gender by job category

Table 2 Set of linguistic variables

Extremely strong	(9, 9, 9)
Intermediate	(7, 8, 9)
Very strong	(6, 7, 8)
Intermediate	(5, 6, 7)
Strong	(4, 5, 6)
Intermediate	(3, 4, 5)
Moderately strong	(2, 3, 4)
Intermediate	(1, 2, 3)
Equally strong	(1, 1, 1)

6 Major Results

F. The fuzzy geometric means of responses are obtained as (Table 3)

$$\tilde{r}_i = [\tilde{a}_{i1} \otimes \tilde{a}_{i2} \otimes \tilde{a}_{i3} \otimes \tilde{a}_{i4} \otimes \tilde{a}_{i5} \otimes \dots \otimes \tilde{a}_{i20}]^{1/20}$$

Table 3 Fuzzy geometric responses of indicators

	\tilde{r}_{i1}	\tilde{r}_{i2}	\tilde{r}_{i3}
I1	3.823	4.824	5.764
I2	0.967	1.2527	1.617
I3	0.469	0.638	0.893
I4	0.619	0.843	1.118
I5	0.683	0.980	1.386
I6	0.398	0.536	0.782
I7	0.461	0.629	0.938
I8	0.532	0.780	1.143
I9	0.737	1.092	1.564
I10	0.456	0.641	0.941
I11	0.705	1.030	1.510
I12	1.150	1.591	2.153
I13	0.286	0.368	0.526
I14	0.310	0.408	0.587
I15	0.411	0.555	0.803
I16	1.590	2.162	2.727
I17	1.272	1.871	2.370
I18	1.282	1.905	2.597
I19	1.147	1.650	2.135
I20	0.687	0.861	1.104

Table 4 Fuzzy weights of indicators

	\tilde{w}_{i1}	\tilde{w}_{i2}	\tilde{w}_{i3}
W1	0.117	0.196	0.320
W2	0.030	1.252	1.617
W3	0.469	0.638	0.893
W4	0.620	0.843	1.118
W5	0.683	0.980	1.386
W6	0.398	0.535	0.781
W7	0.461	0.628	0.938
W8	0.532	0.779	1.142
W9	0.737	1.091	1.564
W10	0.456	0.641	0.9408
W11	0.705	1.029	1.509
W12	1.150	1.591	2.153
W13	0.286	0.368	0.526
W14	0.309	0.408	0.587
W15	0.411	0.555	0.802
W16	1.588	2.162	2.727
W17	1.272	1.871	2.369
W18	1.282	1.905	2.596
W19	1.147	1.649	2.135
W20	0.687	0.861	1.103

Table 5 Final ranking of indicators

Rank	Name	Weights	Normalised weights
1	I1 Employees satisfaction with advancement opportunities	2.160	0.108
2	I13 Internal relationship index	1.916	0.0959
3	I14 Employee skills	1.854	0.0927
4	I6 Creating results by using knowledge	1.646	0.0823
5	I15 Percentage of employees with access to appropriate training and development opportunities	1.611	0.0806
6	I7 Extent of cross-functional teamwork	1.111	0.0556
7	I3 Percentage of payroll spent on training	1.109	0.0555
8	I10 Total HR investments	1.055	0.0528
9	I8 Percentage of employees development plans completed	0.998	0.050
10	I4 Consistency and clarity of messages from top management and from HR	0.872	0.0437
11	I20 Diversity of race and gender by job category	0.851	0.0426
12	I5 Retention rates of critical human capita	0.799	0.034
13	I11 Succession rate of training programs.	0.660	0.331
14	I2 Absenteeism rate	0.652	0.0327
15	I9 Perception of consistent and equitable treatment of all employees	0.652	0.0327
16	I12 Employee turnover by performance level and by controllability	0.572	0.0287
17	I19 Performance of newly hired applicants	0.553	0.0277
18	I17 Change in employee mindset	0.421	0.0211
19	I18 Extent of organizational learning	0.380	0.0190
20	I16 Freely expressing the opinions	0.203	0.0180

B. Below are the fuzzy weights for each indicator (Table 4)

$$\tilde{w}_i = \tilde{r}_i \otimes [\tilde{r}_1 \oplus \tilde{r}_2 \oplus \dots \oplus \tilde{r}_{20}]^{-1}$$

C. The final ranking of each indicator (Table 5).

7 Conclusion

This research incorporates the fuzzy theory for prioritization of performance measurement indicators of HC in context of an Indian organization by objectifying the evaluators’ subjective judgments. The findings showed that in context with the case study Employees satisfaction with advancement opportunities, Internal relationship index, Employee skills, Creating results by using knowledge, Percentage of employees with access to appropriate training and development opportunities are the most important indicators for the HC in an Indian organization.

Appendix

A.1 Pair wise comparison matrix of indicators

	I1			I2			I3		
I1	1	1	1	4	5	6	3	4	5
I2	0.16	0.2	0.25	1	1	1	2	3	4
I3	0.2	0.25	0.33	0.25	0.33	0.5	1	1	1
I4	0.14	0.17	0.2	0.2	0.25	0.33	2	3	4
I5	0.11	0.12	0.14	0.2	0.25	0.33	3	4	5
I6	0.11	0.11	0.11	0.17	0.2	0.25	3	4	5
I7	0.17	0.2	0.25	0.17	0.2	0.25	0.33	0.5	1
I8	0.14	0.17	0.2	0.25	0.33	0.5	2	3	4
I9	0.12	0.14	0.17	2	3	4	2	3	4
I10	0.12	0.14	0.17	0.2	0.25	0.34	0.33	0.5	1
I11	0.17	0.2	0.25	4	5	6	0.33	0.5	1
I12	0.2	0.25	0.3	3	4	5	2	3	4
I13	0.11	0.11	0.1	0.2	0.25	0.33	0.2	0.25	0.3
I14	0.11	0.11	0.1	0.17	0.2	0.25	0.25	0.33	0.5
I15	0.12	0.14	0.16	0.2	0.25	0.33	0.25	0.33	0.5
I16	0.25	0.33	0.5	3	4	5	3	4	5
I17	0.25	0.33	0.5	4	5	6	2	3	4
I18	0.33	0.5	1	3	4	5	2	3	4
I19	0.14	0.17	0.2	1	2	3	1	2	3
I20	0.25	0.33	0.5	0.17	0.2	0.25	0.17	0.2	0.25
	I4			I5			I6		
I1	5	6	7	7	8	9	8	9	10
I2	3	4	5	3	4	5	4	5	6
I3	0.2	0.25	0.33	0.2	0.25	0.33	0.2	0.25	0.34
I4	1	1	1	0.25	0.3	0.5	1	2	3
I5	2	3	4	1	1	1	2	3	4
I6	0.3	0.5	1	0.25	0.3	0.5	1	1	1
I7	0.25	0.33	0.5	0.33	0.5	1	2	3	4
I8	0.3	0.5	1	0.25	0.3	0.5	1	2	3
I9	2	3	4	0.33	0.5	1	2	3	4
I10	0.25	0.33	0.5	0.33	0.5	1	2	3	4
I11	3	4	5	3	4	5	1	2	3
I12	2	3	4	4	5	6	3	4	5
I13	0.2	0.25	0.3	0.25	0.33	0.5	0.25	0.33	0.5
I14	0.25	0.33	0.5	0.2	0.25	0.33	0.33	0.5	1
I15	0.25	0.3	0.5	1	2	3	2	3	4
I16	4	5	6	2	3	4	3	4	5
I17	3	4	5	1	2	3	2	3	4
I18	3	4	5	1	2	3	1	2	3
I19	3	4	5	2	3	4	2	3	4
I20	0.12	0.14	0.17	0.25	0.33	0.5	0.2	0.25	0.3

(continued)

A.1 (continued)

	I7			I8			I9		
I1	4	5	6	5	6	7	6	7	8
I2	4	5	6	2	3	4	0.25	0.33	0.5
I3	1	2	3	0.25	0.33	0.5	0.25	0.33	0.5
I4	2	3	4	1	2	3	0.25	0.33	0.5
I5	1	2	3	2	3	4	1	2	3
I6	0.25	0.3	0.5	0.33	0.5	1	0.25	0.33	0.5
I7	1	1	1	0.25	0.33	0.5	0.2	0.25	0.3
I8	2	3	4	1	1	1	1	2	3
I9	3	4	5	0.33	0.5	1	1	1	1
I10	2	3	4	1	2	3	0.33	0.5	1
I11	3	4	5	1	2	3	0.33	0.5	1
I12	4	5	6	2	3	4	3	4	5
I13	0.25	0.3	0.5	0.33	0.5	1	0.25	0.33	0.5
I14	0.2	0.2	0.3	0.25	0.33	0.5	0.33	0.5	1
I15	0.25	0.3	0.5	0.33	0.5	1	0.33	0.5	1
I16	1	2	3	2	3	4	2	3	4
I17	1	2	3	3	4	5	2	3	4
I18	1	2	3	2	3	4	3	4	5
I19	1	2	3	3	4	5	1	2	3
I20	0.25	0.33	0.5	0.25	0.33	0.5	0.25	0.33	0.5
	I10			I11			I12		
I1	6	7	8	4	5	6	3	4	5
I2	2	3	4	0.17	0.2	0.25	0.2	0.25	0.333
I3	1	2	3	0.17	0.2	0.25	0.25	0.33	0.5
I4	2	3	4	0.2	0.25	0.33	0.25	0.33	0.5
I5	1	2	3	0.2	0.25	0.33	0.17	0.2	0.25
I6	0.25	0.33	0.5	0.33	0.5	1	0.2	0.25	0.3
I7	0.25	0.33	0.5	0.2	0.25	0.33	0.17	0.2	0.25
I8	0.33	0.5	1	0.33	0.5	1	0.25	0.33	0.5
I9	1	2	3	1	2	3	0.2	0.25	0.333
I10	1	1	1	0.33	0.5	1	0.25	0.33	0.5
I11	1	2	3	1	1	1	0.25	0.33	0.5
I12	2	3	4	2	3	4	1	1	1
I13	0.25	0.33	0.5	0.33	0.5	1	0.2	0.25	0.333
I14	0.25	0.33	0.5	0.33	0.5	1	0.25	0.33	0.5
I15	0.33	0.5	1	1	1	1	0.33	0.5	1
I16	3	4	5	2	3	4	2	3	4
I17	3	4	5	1	2	3	1	2	3
I18	2	3	4	1	2	3	1	2	3
I19	2	3	4	1	2	3	2	3	4
I20	3	4	5	3	4	5	5	6	7
	I13			I14			I15		
I1	8	9	10	8	9	10	6	7	8
I2	3	4	5	4	5	6	3	4	5

(continued)

A.1 (continued)

I3	3	4	5	2	3	4	2	3	4
I4	3	4	5	2	3	4	2	3	4
I5	2	3	4	3	4	5	0.33	0.5	1
I6	2	3	4	1	2	3	0.25	0.33	0.5
I7	2	3	4	3	4	5	2	3	4
I8	1	2	3	2	3	4	1	2	3
I9	2	3	4	1	2	3	1	2	3
I10	2	3	4	2	3	4	1	2	3
I11	1	2	3	1	2	3	1	1	1
I12	3	4	5	2	3	4	1	2	3
I13	1	1	1	0.33	0.5	1	0.25	0.33	0.5
I14	1	2	3	1	1	1	0.25	0.33	0.5
I15	2	3	4	2	3	4	1	1	1
I16	4	5	6	2	3	4	3	4	5
I17	3	4	5	2	3	4	2	3	4
I18	2	3	4	3	4	5	3	4	5
I19	2	3	4	3	4	5	3	4	5
I20	0.1	0.2	0.25	0.17	0.2	0.25	2	3	4
		I16			I17			I18	
I1	2	3	4	2	3	4	1	2	3
I2	0.2	0.25	0.3	0.17	0.2	0.25	0.2	0.25	0.3
I3	0.2	0.25	0.3	0.25	0.33	0.5	0.25	0.33	0.5
I4	0.17	0.2	0.25	0.2	0.25	0.33	0.2	0.25	0.3
I5	0.25	0.33	0.5	0.33	0.5	1	0.33	0.5	1
I6	0.2	0.25	0.3	0.25	0.33	0.5	0.33	0.5	1
I7	0.33	0.5	1	0.33	0.5	1	0.33	0.5	1
I8	0.25	0.3	1	0.2	0.25	0.33	0.25	0.33	0.5
I9	0.25	0.3	0.5	0.25	0.33	0.5	0.2	0.25	0.3
I10	0.2	0.25	0.3	0.2	0.25	0.33	0.25	0.33	0.5
I11	0.25	0.3	0.3	0.33	0.5	1	0.33	0.5	1
I12	0.25	0.3	0.5	0.33	0.5	1	0.33	0.5	1
I13	0.17	0.25	0.5	0.2	0.25	0.33	0.25	0.33	0.5
I14	0.25	0.3	0.5	0.25	0.33	0.5	0.2	0.25	0.3
I15	0.2	0.25	0.3	0.25	0.33	0.5	0.2	0.25	0.3
I16	1	1	1	1	2	3	1	1	1
I17	0.33	0.5	1	1	1	1	1	2	1
I18	1	1	1	0.33	0.5	1	1	1	1
I19	1	1	1	1	1	1	0.25	0.33	0.5
I20	4	5	6	5	6	7	4	5	6
		I19			I20				
I1	5	6	7	2	3	4			
I2	0.33	0.5	1	4	5	6			
I3	0.33	0.5	1	4	5	6			
I4	0.2	0.25	0.3	6	7	8			
I5	0.25	0.33	0.5	2	3	4			

(continued)

A.1 (continued)

I6	0.25	0.33	0.5	2	3	4
I7	0.33	0.5	1	2	3	4
I8	0.2	0.25	0.3	2	3	4
I9	0.33	0.5	1	2	3	4
I10	0.25	0.33	0.5	0.2	0.25	0.33
I11	0.33	0.5	0.1	0.2	0.25	0.33
I12	0.25	0.33	0.5	0.14	0.17	0.2
I13	0.2	0.25	0.3	0.25	0.33	0.5
I14	0.25	0.33	0.5	0.2	0.25	0.33
I15	0.25	0.33	0.5	0.2	0.25	0.33
I16	1	2	3	1	1	1
I17	1	1	1	1	2	1
I18	0.33	0.5	1	1	1	1
I19	1	1	1	0.25	0.33	0.5
I20	4	5	6	1	1	1

References

1. Bontis, N.: Intellectual capital: an exploratory study that develops measures and models. *Manag. Decis.* **36**, 63–76 (1998)
2. Bontis, N., Keow, W., Richardson, S.: Intellectual capital and business performance in Malaysian industries. *J. Intellect. Cap.* **1**, 85–100 (2000)
3. Bozbura, F.T.: Measurement and application of intellectual capital in Turkey. *Learn. Organ.* **2**, 357–367 (2004)
4. Bozbura, F.T., Beskese, A., Kahraman, C.: Prioritization of human capital measurement indicators using fuzzy AHP. *Expert Syst. Appl.* **32**, 1100–1112 (2007)
5. Bellman, R., Zadeh, L.: Decision-making in a fuzzy environment. *Manage. Sci.* **17**, 141–164 (1970)
6. Zimmermann, H.J.: Fuzzy programming and linear programming with several objective functions. *Fuzzy Sets Syst.* **1**, 45–55 (1985)
7. Yoon, K.P., Hwang, C.L.: Multiple attribute decision making: an introduction. In: Sage University Paper Series on Quantitative Applications in the Social Sciences, Thousand Oaks (1995)
8. Saaty, T.L.: *The analytic hierarchy process: planning, priority setting, resource allocation*. McGraw-Hill, New York (1980)
9. Van Laarhoven, P.J.M., Pedrycz, W.: A fuzzy extension of Saaty's priority theory. *Fuzzy Sets Syst.* **11**, 229–241 (1983)
10. Chan, F.T.S., Jiang, B., Tang, N.K.H.: The development of intelligent decision support tools to aid the design of flexible manufacturing systems. *Int. J. Prod. Econ.* **65**, 73–84 (2000)
11. Kahraman, C., Cebeci, U., Ulukan, Z.: Multi-criteria supplier selection using fuzzy AHP. *Logist. Inf. Manage.* **16**, 382–394 (2003)
12. Cheng, J.Z., Chen, P.T., Yu, H.C.: Establishing a MAN access strategy for future broadband service: a fuzzy MCDM analysis of SONETH/SDH and Gigabit Ethernet. *Technovation* **25**, 557–567 (2005)
13. Ravasizadeh, E., Reza, M., Ghadim, K., Jalal, H.: Identifying and evaluate E-supply chain risks using fuzzy MADM. *Am. J. Sci. Res.* **40**, 134–159 (2011)
14. Abeysekera, I., Guthrie, J.: Human capital reporting in a developing nation. *Br. Acc. Rev.* **36**, 251–268 (2004)

15. Klir, G., Yuan, B.: Fuzzy sets and fuzzy logic—theory and application. Prentice-Hall Inc., New Jersey (1995)
16. Hsieh, T.Y., Lu, S.T., Tzeng, G.H.: Fuzzy MCDM approach for planning and design tenders selection in public office buildings. *Int. J. Project Manage.* **22**, 573–584 (2004)
17. Becker, B.E., Huselid M.A., Ulrich, D.: The HR Scorecard, pp.235–250. Harvard Business Scholl Press, Boston (2001)

Application of ANN to Predict Liquefaction Potential of Soil Deposits for Chandigarh Region, India

Abha Mittal, Gayatri Devi and P. K. S. Chauhan

Abstract The phenomenon of liquefaction generally caused by dynamic factors where there is a mass of saturated soil sand. To prevent probable destruction of structures in such areas, prediction of liquefaction potential seems to be necessary. For the purpose of data collection we need to do boreholes at various locations and carry our many experiments, each of which requires a vast expenditure of time and money. Therefore, prediction of liquefaction by existing data leads us to decreasing cost of time and money. Neural networks are intelligent systems that uses specific processing characteristics of the brain The present study attempt to the prediction of liquefaction potential of soil deposits by artificial neural network approach in the Chandigarh region of India. To meet the objective 670 datasets from different boreholes were collected for the development of ANN models. ANN models were trained with seven input parameters by optimum number of hidden layers, epochs and suitable transfer function. Out of total datasets 70 % (470 datasets) of data were used for development of models and 30 % (200 datasets) of datasets were used for testing and validation. The predicted value of liquefaction potential by ANN models were compared with method [1], which shows that ANN method could predict with 95 % accuracy in Chandigarh region of India.

Keywords Artificial neural network · Chandigarh region of India · Liquefaction potential

A. Mittal (✉) · G. Devi · P. K. S. Chauhan
Geotechnical Engineering Group, CSIR-Central Building Research Institute, Roorkee, India
e-mail: abham2003@yahoo.com

G. Devi
e-mail: gaytrikapil@gmail.com

P. K. S. Chauhan
e-mail: pradeepali@yahoo.com

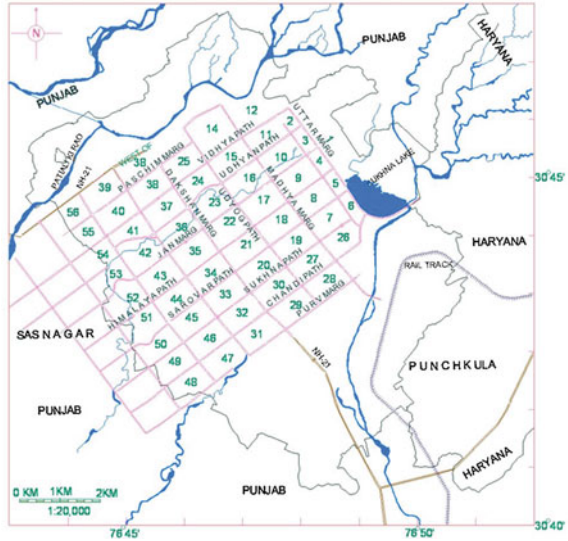
1 Introduction

Soil liquefaction during an earthquake has been one of the major thrusts for geotechnical engineers. Liquefaction is known as a phenomenon by which the soils lose all its shear strength due to increase in pore pressure caused by ground shaking during earthquake. This resulted in disastrous effects such as landslide, ground settlement, sand boiling and particularly tilting of buildings, foundation failures. It is always important that engineers should have information regarding liquefaction potential level of soil and related method for its mitigation for new construction activity in any city. Seismic microzonation of the major cities based on the liquefaction is not very much common in India unlike the other countries like USA, Japan, Australia and New Zealand etc. IS 1893 (Part-I):2002 also does not give any specific guidelines on liquefaction potential assessment and related mitigation. However, a few recent earthquakes like Chamoli (1999), Bhuj (2001) have awakened the engineers and planners for the need to properly assess the consequences of earthquakes on both existing and future construction activities.

During the last two decades, artificial intelligence (AI) has been successfully used in several applications in civil engineering because of its heuristic problem-solving capabilities. The artificial neural network (ANN) is one of the AI approaches that can be classified as “machine learning”. It has the ability to simulate the learning capabilities of the human brain by automating the process of knowledge acquisition and data mining [2, 3]. The ANN is a collection of interconnected computational elements called “neurons” that have performance characteristics similar to the biological neurons. Interconnections among neurons are established by weights, which are applied to all values passing through one neuron to another.

In literature, CPT test results were used to develop soil liquefaction assessment methods using neural network methodology [4–10]. Goh [4] developed a back propagation neural network (BPNN) to assess liquefaction potential from CPT data. He reported that neural networks were proven to be feasible tools for soil liquefaction assessments, simpler to apply, and yield more reliable results when compared to conventional methods. In this model, [4] had used a relatively small dataset, which is considered the main limitation of ANN approaches. Goh [6] developed probabilistic neural network (PNN) models to analyze the databases based on CPT and shear wave velocity data. In this model, soil particle-size information was introduced as an input data and the liquefaction potential was considered a classification problem. Barai and Agarwal [7] developed an instance based learning (IBL) model to predict soil liquefaction potential. Kumar et al. [11] has compared the predicted values of liquefaction potential using ANN model with [12] method, which exhibits that trained artificial neural networks models are capable of predicting soil liquefaction potential adequately. These versatile applications make ANN models valuable problem-solving tools in the field of geotechnical engineering, which performs the conventional techniques in terms of accuracy and efficiency.

Fig. 1 Map of Chandigarh



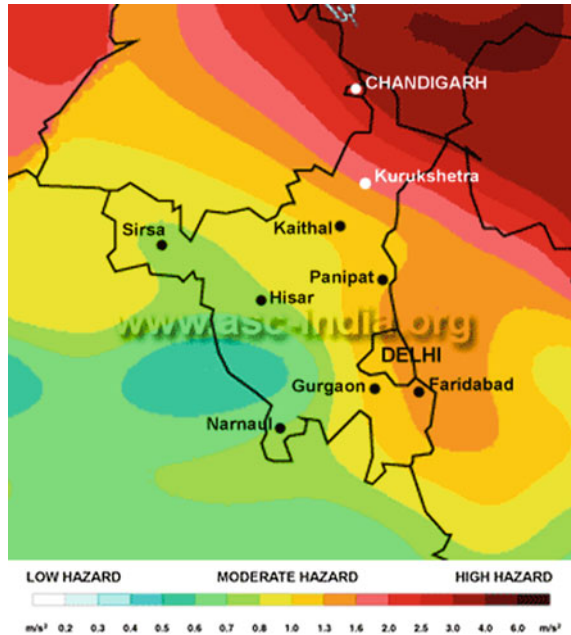
2 Geology and Seismicity of Chandigarh

Chandigarh, presently the union territory and capital city of Punjab and Haryana, located at about 250 kms North of Delhi at the foot hills of Siwaliks, is a great centre of attraction in the recent times. The union territory of Chandigarh comprises of Chandigarh city, Notified Area Committee Manimajra and 22 villages (Fig. 1) [13, 14].

Chandigarh is occupied by semi consolidated formations of Upper Siwalik of Middle Miocene age and is exposed in north eastern fringe. Indo-Gangetic Plain in the rest of the territory is occupied by the alluvium of Pleistocene age. The city lies in high earthquake prone Himalayan seismic belt (zone IV, IS 1893–2002). Also, the alluvial cover of Indo-Gangetic plain makes even distant earthquakes felt here quite strongly.

The seismicity in this region is due to movements along several faults, thrusts as well as lineaments. Himalayan earthquakes have their epicenters very close to any of the terrain bounding thrusts i.e. Main Central Thrust (MCT), Main Boundary Thrust (MBT) and Himalayan Frontal Thrust (HFT). Due to its location Chandigarh region experiences a no. of mild earthquakes every year. Large earthquakes have occurred in all parts of Himachal Pradesh, the biggest being the Kangra Earthquake of 1905. There were two more big quakes, but they were not nearly as powerful as the 1905 jolt. The first was in 1906, a 6.4 near Kullu and the second was a 6.8 in Lahual-Kinnaur Spiti in 1975 along the Indo-China Border. The Himalayan Frontal Thrust, the Main Boundary Thrust, the Krol, the Giri, Jutogh and Nahan thrusts lie in this region. Besides that there are scores of smaller faults, like the Kaurik Fault etc.

Fig. 2 Seismic hazard of Chandigarh



The area is also vulnerable to possible future large earthquakes in the Central Himalayas [15]. Number of important structures and monuments of this moderately populated city could be prone to damage due to an earthquake of considerable magnitude. According to the GSHAP (Global Seismic Hazard Assessment Program), the UT Chandigarh should expect to have maximum peak ground acceleration (PGA) of 0.08–0.32 g. The seismic effects in this zone vary from site to site depending on the geological, geomorphological and geotechnical conditions. The seismic hazard studies (www.asc-india.org) in the recent past have also indicated Chandigarh is in the high hazard zone (Fig. 2). The seismic events felt in around Chandigarh region have been presented in Table 1.

3 Sub-Surface Geology

The sub-surface geological features compiled based on the reports/borehole data available for Chandigarh city (CGWB, 2002) reveals that the topsoil comprises of clayey material and varies in thickness from less than a meter to 10 m. It is underlain by beds of clay and kankar, sand and gravel. Along Sukhna Choe, three prominent sand beds occur (interbedded with clay beds) within a depth of about 100 m. The upper sand beds are about 15 m thick and occur 8 m below land

Table 1 Historical seismic events in and around Chandigarh region

Sl. No.	Date	Location	MSK Intensity
1	15 July 1720	28.66 N–77.25 E	VII–VIII
2	04 April 1905	32.30 N–76.30 E	VII–VIII
3	14 January 1934	26.60 N–86.80 E	VII–VIII
4	15 August 1950	28.50 N–96.70 E	VII–VIII
5	27 August 1960	28.20 N–77.40 E	VI
6	20 June 1966	28.50 N–76.98 E	IV–V
7	29 July 1980	29.60 N–81.09 E	VI–VIII
8	21 October 1991	30.78 N–78.77 E	VI–VII
9	09 August 1993	36.37 N–78.87 E	VII
10	12 November 1996	29.93 N–77.21 E	IV–V
11	04 May 1997	28.98 N–76.59 E	IV
12	30 March 1998	28.21 N–76.24 E	V
13	22 March 1999	29.26 N–76.94 E	IV
14	29 March 1999	30.49 N–79.29 E	VI–VII
15	08 October 2005	34.40 N–73.56 E	VIII–IX

surface. The middle sand bed is about 18 m thick and occurs at a depth varying from 21 to 38 m below ground level. The deeper sand bed occurs at depth varying from 39 to 76 m below ground level and is about 27 m thick. Along the Patiali-ki-Rao nala a single thick sand bed has inter-layered clay lenses in northeast and southwest direction. Further, the soils in Chandigarh are loamy sand at surface and calcareous sandy loam in subsurface layers. The hard clay forms pan at depths varying between 20 and 30 m in the northern parts, the soil is sandy to sandy loam whereas it is loamy to silty loam in southern parts.

4 The Dataset

The borehole data from CGWB, CPWD and a few local agencies have been collected and compiled for various locations in different sectors. It is revealed from the data that the soil strata in general comprises of clayey silty soils in the top layers followed by sandy silt to silty sands at depths in most of the sectors. In northern parts, the soil is sandy to sandy loam whereas it is loamy to silty loam in southern parts. A few sectors (6, 12, 25, 27, 30, 36, 37, 42, 43, 52, 54 and 63) showing a significant amount of non-plastic silts and fine sands with low SPT-N values and high water table conditions [13, 14]. The sub-surface water level exists at shallow depths towards western side of the city and at deeper levels towards the eastern side. The hard/stiff strata are found to encounter at shallow depths on the NW direction and the depths increased towards the SE direction. However, boreholes available from a few sectors indicate a poorly graded and fine sands with

low SPT—N values showing signs of potential to liquefaction in case of a major earthquake. The ground water level has been observed to be nearer to surface within a range of 1.8 to 8.0 m towards Western side (Mohali) and varied to significant depths of 2.0 to 14.5 m towards Eastern side. The depth of hard strata also encountered at shallow depths on the NW side and deep towards SE side.

5 Artificial Neural Networks

ANNs are advanced tools stimulated by the physical and computational characteristics of the human brain. Like biological neurons, they consist of interconnected information processing neural elements (neurons) working in union to make decisions, classifications, and predictions. Neural networks are capable of learning linear and nonlinear functions that make them influential tools in the analysis of complex relations. Interconnections among neurons are established by weights, which are applied to all values passing through one neuron to another. Changing weights improves adaptabilities and prediction capabilities of neural networks.

Neural networks are arranged mainly in three layers namely: input layer; output layer, and the hidden layers. Through the learning process, input and output data of a specific engineering problem are given, and the aforementioned weights among neurons are updated without requiring human development of algorithms. In the validation phase, the trained network makes predictions for a new set of data that has never been introduced, during the previous phases. The neural network will provide accurate prediction, as long as large volumes of data covering all possible governing parameters and field conditions are used during the learning process.

6 Training Algorithm

The main method, which is used for training network, is called training algorithm whose function is to adjust the weight of neurons. The input parameters, which are chosen for training of artificial neural network, relate directly to the approach used for determining liquefaction potential. The parameters that can potentially produce the phenomenon of liquefaction in soil are as follows :

Depth (z), SPT-N value (N), Shear reduction factor, Fine content (F_c), Total and effective stress, maximum acceleration and earthquake magnitude etc. Other factors such as level of underground water or the density of soil is active in an indirect way. The output parameter i.e. factor of safety against liquefaction (F_s) is defined as

$$F.S. = (CRR_{7.5}/CSR).(MSF);$$

Table 2 Liquefaction hazard potential index

Factor of safety range	Severity index
<1	High
1 to 2	Moderate
2 to 3	Low
>3	Nil
Non liquefiable (NL)	Nil

Table 3 Range of input and output parameters

Sl. No.	Input/output parameters	Minimum	Maximum
1	Depth (z)	0.5	34.5
2	SPT-N Value (N _{abs})	2	86
3	Bulk density (γ)	1	19.4
4	Total stress (σ _v)	0.51	71.0
5	Effective stress (σ' _v)	1.01	71.07
6	Fine content (F _c)	0.0	100
7	Stress reduction coeff. (r _d)	0.25	1.00
8	Liquefaction potential (Factor of safety against liquefaction FS)	0.34	36.5

where CRR and CSR are cyclic resistance ratio and cyclic stress ratio which will be computed by using the input parameters define above by Youd et al. method [1]. Based on the seismic history and the data available from the seismic hazard studies, the values of M_w = 7.5 and MSF = 1.0 are assumed for assessment of liquefaction potential. Finally, the liquefaction potential level of Chandigarh city has been classified into four categories viz. high, moderate, low and very low and nil based on the value of factor of safety against liquefaction as suggested by Sitharam et al. [16] shown in Table 2. For this analysis peak acceleration has been taken as 0.08 g.

A total of 670 datasets were used. Out of 670 datasets about 30 % i.e. 200 datasets were reserved for testing and validation. The boundaries of input and output parameters of the models are listed in Table 3. The input–output data of each ANN model were scaled to lie between −1 to +1 by using the following relation

$$\alpha_{norm} = 2 \frac{\alpha_{actual} - \alpha_{min}}{\alpha_{max} - \alpha_{min}} - 1$$

where α_{norm} is the normalized value, α_{max} is the maximum value, α_{min} is the minimum value α_{actual} is the actual value.

In this study we used feed-forward back propagation technique. In this technique learning algorithm has two stages. In first stage, the inputs are forwarded from input layer to output layer. After computing the errors of each output between

Table 4 Comparison among results of hidden layers and hidden neurons

No. of hidden layers	No. of hidden neurons	Training		Testing		Validation	
		MSE	R	MSE	R	MSE	R
1	2	0.010	0.93	0.007	0.94	0.007	0.92
1	4	0.007	0.94	0.006	0.95	0.010	0.91
1	6	0.009	0.93	0.005	0.95	0.006	0.93
1	8	0.008	0.92	0.004	0.94	0.011	0.92
1	10	0.005	0.93	0.005	0.93	0.021	0.93
1	12	0.006	0.95	0.006	0.95	0.012	0.94
1	14	0.006	0.95	0.005	0.96	0.004	0.95
1	16	0.008	0.94	0.009	0.94	0.011	0.92
1	18	0.009	0.92	0.010	0.93	0.009	0.94
1	20	0.007	0.91	0.010	0.92	0.009	0.91

computed and desired output, in second stage information is send backward to the inputs which readjust the connecting weights in the hidden and output layer to minimize this [11].

Though many activation functions exist, the tan sigmoid activation functions used, which outputs a number between -1 (for low input values) and 1 (for high input values). The resultant of this function is then passed as the input to other neurons through more connections.

7 Results and Discussion

ANN tool built in MATLAB (R2010b) software was used for all operations in which networks were trained with single or double hidden layers of varying number of neurons (2–20) were used in the analysis. For choosing training algorithm the abilities of networks were compared and results are presented in Table 4. Mean square error is used to assess the rate of learning in a neural network. Comparison has been done between the hidden layers and hidden neurons. According to Table 4, network architecture at Sl. No. 7 Which has hidden neurons 14 is most suitable for learning.

At the end of training process, the 15 % of dataset that were not used in training of neural network are taken for validation. From the graphs presented in Fig. 3, it is inferred that the network at Sl. No. 8 is able to predict liquefaction potential with 95 % accuracy for Chandigarh region. In Fig. 3 regression coeff. R is given for training, testing, validation as well as for full set of data.

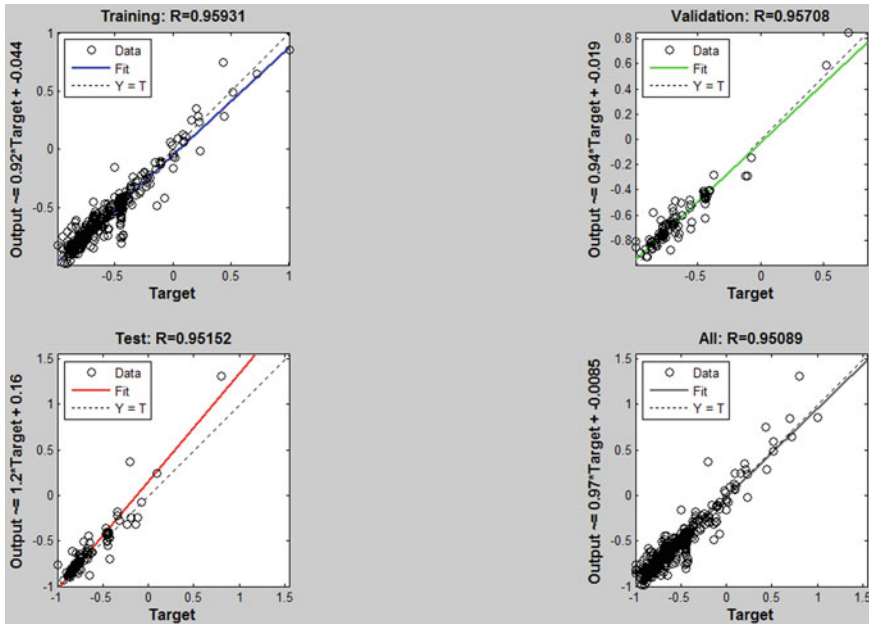


Fig. 3 Target vs output for training, testing, validation and all data

8 Conclusions

In the present paper, ANN model has been developed for the assessment of liquefaction potential based on field and laboratory test data for Chandigarh region. Regression Coefficient (R) values in all the models (in Table 4) are greater than 92 % indicate satisfactory prediction capabilities of ANN approach compared with [17] method given by Youd et al. [1]. High regression coeff. values indicates that the model is highly reliable for prediction.

Field and laboratory input parameters can be used directly as input vector for ANN models, to predict the liquefaction potential for any other site of the Chandigarh region. ANN model is more simpler than the conventional method given by Youd et al. [1] to predict liquefaction potential.

Acknowledgements The authors are grateful to the Director, CSIR-Central Building Research Institute, Roorkee for giving the permission to publish the paper.

References

1. Youd, T.L. et al.: Liquefaction resistance of soils : summary report from the 1996 NCEER and 1998 NCEER/NSF workshops on evaluation of liquefaction resistance of soils. *J. Geotech. Geoenviron. Eng. ASCE* **127**(10), 817–833 (2001)
2. Hanna, A.M., Ural, D., Saygili, G.: Neural network model for liquefaction potential in soil deposits using Turkey and Taiwan earthquake data. *Soil Dyn. Earthquake Eng.* **27**(2007), 521–540 (2007)
3. Hanna, A.M., Ural, D., Saygili, G.: Evaluation of liquefaction potential of soil deposits using artificial neural networks, 2007. *int. J. Comput. Aided. Eng. Software* **24**(1), 5–16 (2007)
4. Goh, A.T.C.: Seismic liquefaction potential assessed by neural networks, 1994. *J. Geotech. Eng.* **120**(9), 1467–1480 (1994)
5. Goh, A.T.C.: Pile driving records reanalyzed using neural networks. *J Geotech Eng. ASCE* **122**(6), 492–500 (1996)
6. Goh, A.T.C.: Probabilistic neural network for evaluating seismic liquefaction potential. *Can. Geotech. J.* **39**, 219–232 (2002)
7. Barai, S., Agarwal, G.: Studies on instance based models for liquefaction potential assessment. *Electron. J. Geotech. Eng.* (2002) available at: www.eige.com/2002/Ppr0235/Ppr0235.htm
8. Juang, C.H., Chen, C.J., Tien, Y.M.: Appraising cone penetration test based liquefaction resistance evaluation method:artificial neural network approach. *Can. Geotech. J.* **36**, 443–454 (1999)
9. Juang, C.H., Chen, C.J., Jiang, T., Andrus, R.D.: Risk based liquefaction potential evaluation using standard penetration tests. *Can. Geotech. J.* **37**, 1195–1208 (2000)
10. Baziar, M.H., Nilipour, N.: Evaluation of liquefaction potential using neural-networks and CPT results. *Soil Dyn. Earthquake Eng.* **23**(2003), 631–636 (2003)
11. Kumar, V., Venkatesh, K., Tiwari, R.P., Kumar, Y.: Applications of ANN to predict liquefaction potential. *Int. J. Comput. Eng. Res.* **2**(2), 379–389 (2012)
12. Idriss, I.M., Boulanger, R.W.: Semi-empirical procedures for evaluating liquefaction potential during earthquakes. *Soil Dyn. Earthquake Eng.* **26**(2006), 115–130 (2006)
13. Dharmaraju, R., Ramakrishna, V.V.G.S.T., Gayatri D.: Liquefaction potential assessment of Chandigarh city—a conventional approach. In: *A Workshop on Microzonation*, ©Interline Publishing, Bangalore
14. Dharmaraju, R., Ramakrishna, V.V.G.S.T., Karthigeyan, S., Gayatri D.: Liquefaction potential of Chandigarh city—a conventional approach. In: *The 12th International Conference of International Association for Computer Methods and Advances in Geomechanics (IACMAG)*, Goa, India, 1–6 Oct 2008
15. Abha, M., Dharmaraju, R., Gayatri, D.: Estimation of probable occurrence of earthquake in Chandigarh region, India. In: *The 12th International Conference of International Association for Computer Methods and Advances in Geomechanics (IACMAG)*, Goa, India, 1–6 Oct 2008
16. Sitharam, T.G., Anbazhagan, P., Mahesh, G.U., Bharathi, K., Nischala Reddy, P.: ‘Seismic Hazard studies using Geotechnical Boerhole Data and GIS’. In: *Proceedings of Symposium on Seismic Hazard Analysis and Microzonation*, Roorkee, Sep 2005
17. Youd T. L., Idriss I. M. (eds.): *NCEER Workshop on Evaluation of Liquefaction Resistance of Soils*, 1997, National Center for Research on Earthquake Engineering, State University of New York, (1997)

Survey of Curve and Surface Reconstruction Algorithms from a Set of Unorganized Points

Kavita Khanna and Navin Rajpal

Abstract Reconstruction of curves and surfaces from a set of unorganized points is a problem with a lot of practical relevance and thus has been an active area of research. In the review various curve and surface reconstruction algorithms which take an unorganized set of points have been discussed. Also it highlights the major advantages and disadvantages of these algorithms. Delaunay triangulations are most important structures used in surface reconstruction algorithms as they work without the geometric properties of the points. Most of the curve and surface reconstruction algorithms combine different approaches with Delaunay Triangulations in order to make reconstruction more systematic and robust. All such types of major issues pertaining to surface reconstruction have been reviewed and mentioned.

Keywords Surface reconstruction · Delaunay triangulations · Robust

1 Introduction

To find the mathematical description of a surface from a set of unorganized points is a task that is widely needed in reverse engineering, medical imaging and geometric modeling applications. The main issues while dealing with surface reconstruction are to deal with the samples which have non uniform sampling rate and to reconstruct surfaces with arbitrary topology. Apart from that the reconstruction process should have theoretical proofs and guarantees to support them. In this

K. Khanna (✉) · N. Rajpal
USICT, Guru Gobind Singh Indraprastha University, Delhi, India
e-mail: kvita.khanna@gmail.com

N. Rajpal
e-mail: navin_rajpal@yahoo.com

paper we study different algorithms pertaining to surface reconstruction and how these algorithms deal with the above mentioned issues of surface reconstruction.

2 Types of Surface Reconstruction

The work that has been done in Surface Reconstruction so far could be broadly divided into two categories- Approximation and Interpolation. The algorithms in the first category calculate the surface which approximates the sample points i.e. the reconstructed surface does not pass exactly through the sample points whereas the surface in second category passes through the original sample points.

3 Basic Terms

3.1 *Medial Axis*

Medial axis of a curve/surface could be defined as the closure of the set of points that have a minimum of two points at an equal distance in the given curve/surface.

3.2 *Local Feature Size*

Local feature size at a point could be defined as the distance of that point to the medial axis. So it is a function $f, f : S \rightarrow \mathbb{R}$ such that $f(x) = d(x, M)$, where S is the given surface and M is the medial axis of S .

3.3 *Sampling*

It is the process of generating points from a given curve or a surface. These are of two types- uniform sampling and non uniform sampling. For any reconstruction process to be efficient the sample should be dense. But this density should vary as the features in the curve or surface with a result fewer samples are needed in low curvature areas and more samples are needed in high curvature areas. This gave rise to the concept of a ϵ -sample.

3.4 ϵ -sample

Any sample of the given curve/surface is called an ϵ -sample if for each point x of the curve/surface there exist a sample point s such that the normed distance between x and s is less than equal to $\epsilon f(x)$, $\|x - s\| \leq \epsilon f(x)$ where $f(x)$ is the feature size and ϵ should have a value less than 1 in order to have a dense sample.

3.5 Voronoi Diagrams

Voronoi diagram of a given set of points called sites partitions it into cells called the voronoi cells such that each cell contains a set of points which are near to a site than to any other site.

3.6 Delaunay Triangulations

Delaunay triangulations are the triangulation that maximizes the minimum angle among all the triangulations. They are the duals of voronoi diagrams as both of them represent the same information but in different form.

4 Algorithms for Reconstruction

Hoppe [1, 2] has contributed significantly in the field of approximation based surface reconstruction algorithms. The algorithm given by Hoppe works by finding the zero set of the distance function which here is a signed distance function as it can have both the positive and the negative value depending upon the side to which the point lies. This zero set is the estimate for the unknown surface. In the second stage of the algorithm a continuous piecewise linear approximation to the surface is found from the zero set. For achieving this variation of the marching cubes algorithm, which was originally given by **William and Harvey [3]**, is used in which the algorithm visits only the cubes that intersect the zero set. The outcome is a mesh approximating the given surface. The complexity of the algorithm is $O(m \log n)$ where n is the number of points given in the cloud and m represents the number of cubes visited in the entire process.

Dealing with the major issues of Surface Reconstruction this algorithm works for arbitrary topologies and noisy samples whereas it assumes sampling to be uniform and surface to be a manifold i.e. non intersecting one.

The algorithms given under second approach i.e. interpolation use Voronoi diagrams and their duals Delaunay Triangulations [4, 5] for surface reconstruction.

These structures are a backbone to surface reconstruction as they do not need any geometric information in a set of unorganized points.

Crust algorithm given by **Amenta et al.** [6] was the first algorithm of curve reconstruction which had theoretical guarantees of correctness. It works in two phases. In the first phase the Voronoi diagram of the sample points is computed. The second phase computes the Delaunay Triangulation of the union of set of sample points and Voronoi vertices. Regarding the major issues the Crust algorithm works for the non uniform sample which is an ϵ -sample with $\epsilon \leq 0.25$. It is unable to reconstruct curves with sharp corners and boundaries. Also it works only for closed and smooth curves. In addition to it the Crust is not able to handle noise. The time complexity of the algorithm is $O(n \log n)$.

The crust algorithm was further advanced by **Conservative crust** given by **Dey et al.** [7]. It uses the concept of Gabriel graphs and Gabriel edges for reconstructing curves from a set of unorganized points. A user defined parameter ρ is used to fine tune the algorithm for which the range is defined to be $[1.25, 1.75]$. Dealing with the major issues the conservative crust as opposed to crust also works for open curves and is able to detect end points. But at the same time it also works only for smooth nonintersecting curves. Also the user defined parameter ρ plays a significant role in the performance of the algorithm. The performance falls when either the ρ is too small or too large. The running time of conservative crust is same as the crust algorithm i.e. $O(n \log n)$.

NN Crust is also a curve reconstruction algorithm given by **Dey and Kumar** [8] with theoretical guarantees. It introduced the concept of half neighbors and showed that only nearest neighbor edges are not sufficient to reconstruct a curve rather half neighbor edges are helpful in doing so. This concept was implemented using Delaunay triangulations. It was found that for every p belonging to sample P the shortest edge pq in Delaunay P gives the nearest neighbor of p , while the shortest edge ps so that angle $(pqs) \geq \Pi/2$ gives the half neighbor to p . Regarding the major issues, the NN-Crust works correctly for non-uniform samples which are an ϵ -sample with $\epsilon < 1/3$. It can handle only the curves which are smooth, closed and do not have boundaries. The time complexity of NN Crust is $O(n \log n)$ which is same as the crust and the conservative crust.

Gathan algorithm given by **Dey** [9] was also a step forward in the field of curve reconstruction. It works by computing the Delaunay edges and proceeds afterwards by computing the normal for each edge and pole for each point. It uses two user defined parameters ρ and α . The experimental results show that for a good reconstruction ρ should be between 1.7 and 2.0 and α between 35° and 40° . Some of the major issues of reconstruction are tackled in this algorithm as it can deal with non smooth curves and thus it can handle corners and end points. But dealing with non-intersecting curves is still not possible with this algorithm. Also there are no theoretical proofs for this algorithm. The time complexity of this algorithm is also $O(n \log n)$.

Zeng et al. [10] proposed a parameter free algorithm **DISCUR** for the reconstruction of curves. It uses a vision function to check the connectivity between a

point and a curve due to which the Delaunay edges that meet the vision function will be connected and the Delaunay edges that conflict with the vision function will be disconnected even if they are the shortest neighbors.

Regarding the major issues of Surface Reconstruction the algorithm works for curves that may be open, closed or have sharp corners. All this could be done when the sampling condition given in [10] is satisfied.

Guo [11] has given a new curve reconstruction algorithm based on Delaunay Triangulations. The algorithm first searches for medial points which lie near the medial axis of the point cloud and use Delaunay triangulations for this. Secondly all the data points are fitted by a quadratic curve segment which efficiently approaches the point cloud. The algorithm given in [11] works well on noisy data as well.

Crust algorithm in two dimensions was extended to 3-d [12, 13] for reconstruction of surfaces from a set of unorganized points. It uses a subset of voronoi vertices to remove Delaunay triangles. The algorithm uses the concept of poles which are defined to be the voronoi vertices for a sample point which are farthest and are on the opposite sides of that point. The Delaunay triangulation of the union of sample points and the poles is computed. The triangles which have all the three vertices belonging to the sample points forms the crust. Dealing with the major issues, this algorithm works only for non- uniform samples but it should be sufficiently dense. It doesn't work for surfaces with boundaries. Also it requires two Delaunay computations and so its time complexity is $O(n^2 \log n)$.

Amenta et al. [14] introduced the **CoCone** algorithm which was an improvement over the Crust algorithm. It uses only one Delaunay computation as opposed to crust which uses two of them. It constructs a piecewise linear surface from the set of sample points. A condition called cocone test is given for the Delaunay triangles to be in the set of candidate triangles which is a superset of restricted Delaunay triangles. This set is then pruned to extract a 2-manifold. Regarding the major issues this algorithm works only for smooth closed manifold. The output may have gaps and holes for sharp corners and boundaries, specifically when the sampling condition is not met. Also it gives theoretical guarantees only when ϵ -sampling condition is satisfied for $\epsilon \leq 0.05$. The complexity of this algorithm is $O(n^2)$.

Power Crust [15] is also one of the important algorithms for surface reconstruction. It uses the concept of poles and polar balls in order to approximate the medial axis transform. Dealing with the major issues it does not depend on the sampling condition and can reconstruct sharp corners. It is guaranteed to produce water tight bounded surface on any input. Also it can handle small amount of noise. And all this is attained without any additional time cost of the previous algorithms as it also runs in $O(n^2)$ time. But the major disadvantage is, it introduces some extra points as vertices in the output surface.

Tight Cocone [16] algorithm is also a famous algorithm for reconstruction. It first computes the Delaunay Tetrahedral from the input samples and then labels them as in or out as per an initial approximation of the surface. Finally all the out

tetrahedral are peeled off. The tight cocone has major advantage over the previous reconstruction algorithms, the first being that it gives water tight reconstruction and leaves no holes with under sampling. Also it introduces no extra points as vertices in the output surface. It can handle small amount of noise and works for non-uniform samples. Also it runs in $O(n^2)$ time which is same as the previous algorithms.

Kuo and Yau [17] proposed a Delaunay-based region-growing approach to surface reconstruction which interpolates the set of sample points. This approach has the advantages of both Delaunay-based and region-growing approaches. It is better than the traditional Delaunay-based approach as it requires only one Delaunay computation. Also it is better than the region growing approaches as it doesn't use user defines parameters and heuristic rules. Dealing with the major issues this approach can handle the surfaces with boundaries. It is also capable of handling sharp edges and corners when the sampling requirement given in [17] is satisfied. Also it can deal with the sample points with non-uniform distribution. It can handle noisy data but then it requires a separate hole filling method as a post processing step.

Dey and Goswami [18] proposed an algorithm for dealing with the noisy data with reasonable noise. The algorithm works with the Delaunay/Voronoi diagrams of the input points and uses the concepts of the power crust algorithm [18]. In the power crust algorithm the union of a set of Delaunay balls named polar balls approximate the solid bounded by the sampled surface. But this property does not stand true in presence of noise. This algorithm assumes a noise model and with this model some of the Delaunay balls are relatively big that play the role of the polar balls. These balls are identified and partitioned into inner and outer balls. The boundary of the union of the outer (or inner) big Delaunay balls is homeomorphic to the sampled surface. This gives a homeomorphic surface reconstruction but the reconstructed surface may not interpolate the sample points.

Dey et al. [19] recently presented an algorithm for the reconstruction of a surface with boundaries in three dimensions from a sufficiently dense sample. It uses a silver peeling approach and it guarantees that the output is isotopic to the unknown sampled surface. It was the first algorithm which guarantees isotopic or homeomorphic reconstruction of surfaces with boundaries. On the other hand it works only for uniform samples although with some heuristics proposed in [19] it can be modified to give correct outputs for non-uniform sample as well but no theoretical guarantees for reconstruction exist in this case.

Hiyoshi [20] visualised the reconstruction problem as an optimization problem and applied this approach to reconstruct both the curves and the surfaces. The algorithm first computes the Delaunay triangulation of the sample points and then it assigns a weight with each of the Delaunay edges. Now the reconstruction is based on the minimization or maximization of the edges which are included in the process of reconstruction. It gives theoretical proofs for the better reconstruction over the previous algorithms.

The recent trend in the surface reconstruction is on fast and memory efficient algorithms. **Gopi et al.** [21] gave a projection based approach to surface

reconstruction. The algorithm given in [21] starts at a data point and then finds all the triangles that are incident on to that point. Then the vertices which are adjacent to that are processed in a breadth-first manner and in this way the triangles which are incident to those points are found. The major advantage of approach given in [21] is that the worst case time complexity of the algorithm is $O(n \log n)$ whereas in practice it exhibits linear time performance. Also it is very much memory efficient as it goes through a single pass of all data points to generate the mesh. The major drawback is that it gives different triangulations for different starting points. Moreover it works only for smooth curves. Also it gives spurious boundaries for under sampled and extremely non uniform models.

Yong Joo et al. [22] gave an algorithm which reconstructs a surface with parallel implementation using graphics hardware. The algorithm starts by constructing an octree for the sample points on CPU and then downloads it to the GPU. It then finds in parallel the k -nearest neighbours of each sample point. It is based on the concept that the global triangulations could be obtained by merging all the set of local triangulations called the fans. The major disadvantage of the GPU assisted approach in [22] is that it works only for distributions which are locally uniform. Also it cannot reconstruct noisy data.

Zhou [23] gave a parallel surface reconstruction algorithm that runs entirely on GPU. The algorithm given in [22] constructs octrees on CPU whereas in this algorithm octrees are constructed using fine grained parallelism on the GPU. After that it performs the Poisson surface reconstruction on GPU.

5 Conclusion

Reconstruction of curves and surfaces forms an active area of research. A review of these reconstruction algorithms have been presented along with the major issues and challenges in each of these algorithms. Each algorithm is analyzed for its time complexity, sampling condition, topology and smoothness of surface, presence of boundaries, presence of noise and its theoretical guarantees.

References

1. Hoppe, H., DeRose, T., Duchamp, T., McDonald, J., Stuetzle, W.: Mesh optimization. In: Proceedings of SIGGRAPH, ACM, pp. 19–26 (1993)
2. Hoppe, H., DeRose, T., Duchamp, T., McDonald, J., Stuetzle, W.: Surface reconstruction from unorganized points. In: Proceedings of SIGGRAPH, ACM, pp. 71–78 (1992)
3. William, E.L., Harvey, E.C.: Marching cubes: a high resolution 3D surface reconstruction algorithm. In: Proceedings of SIGGRAPH, ACM, pp. 163–169, Jul 1987
4. de Berg, M., Cheong, O., Van Kreveld, M., Overmars, M.: Computational Geometry. Springer, Heidelberg (2008)

5. Dyer, R., Zhang, H., Moller, T.: A survey of Delaunay structures for surface representation. In: Technical Report, School of Computing Science, Simon Fraser University, Canada, Jan 16 2009
6. Amenta, N., Bern, M., Eppstein, D.: The crust and the beta skeleton: combinatorial curve reconstruction. *Graph. Models Image Process.* **60**, 125–135 (1998)
7. Dey, T.K., Mehlhorn, K., Ramos, E.A.: Curve reconstruction: connecting dots with good reason. *Comput. Geom. Theor. Appl.* **15**, 229–244 (1999)
8. Dey, T.K., Kumar, P.: A simple provable algorithm for curve reconstruction. In: Proceedings of 10th ACM/SIAM Symposium. *Discrete Algorithms*, pp 893–894, Jan 1999
9. Dey, T.K., Wenger, R.: Reconstructing curves with sharp corners. *Comput. Geom. Theor. Appl.* **19**, 89–99 (2001)
10. Zeng, Y., Nguyen, T.A., Yan, B., Li, S.: A distance-based parameter free algorithm for curve reconstruction. *Comput. Aided Des.* **40**, 210–222 (2008)
11. Guo, F.: Reconstructing curves from point clouds. In: 2nd International Conference on Materials, Mechatronics and Automation, Lecture Notes in Information Technology, pp 186–191 (2012)
12. Amenta, N., Bern, M.: Surface reconstruction by Voronoi filtering. *Discrete Comput. Geom.* **22**, 481–504 (1998)
13. Amenta, N., Bern, M., Kamvysselis, M.: A new Voronoi—based surface reconstruction algorithm. In: Proceedings of SIGGRAPH, ACM, pp. 415–421 (1998)
14. Amenta, N., Choi, S., Dey, T.K., Leekha, N.: A simple algorithm for homeomorphic surface reconstruction. In: Proceedings of the sixteenth annual symposium on Computational geometry, pp. 213–222 (2000)
15. Amenta, N., Choi, S., Kolluri, R.K.: The power crust, union of balls, and the medial axis transform. *Comput. Geom.* **19**, 127–153 (2001)
16. Dey, T.K., Goswami, S.: Tight Cocone: a water-tight surface reconstructor. *J. Comput. Inf. Sci. Eng.* **3**, 302–307 (2003)
17. Kuo, C.C., Yau, H.-T.: A Delaunay-based region-growing approach to surface reconstruction from unorganized points. *Comput. Aided Des.* **37**, 825–835 (2005)
18. Dey, T.K., Goswami, S.: Provable surface reconstruction from noisy samples. *Computational Geometry*, **35**, 124–141 (2006)
19. Dey, T.K., Edgar, K.L., Ramos, A., Wenger, R.: Isotopic reconstruction of surfaces with boundaries. In: Eurographics Symposium on Geometry Processing, pp. 1371–1382 (2009)
20. Hiyoshi, H.: Optimization-based approach for curve and surface reconstruction. *Comput. Aided Des.* **41**, 366–374 (2009)
21. Gopi, M., Krishnan, S.: A fast and efficient projection based approach for surface reconstruction. In: Proceedings of High Performance Computer Graphics, Multimedia and Visualisation, pp. 179–186 (2002)
22. Kil, Y.J., Amenta, N.: GPU—assisted surface reconstruction on locally—uniform samples. In: Proceedings of International Meshing Roundtable, pp 369–385 (2008)
23. Zhou, K., Gong, M., Huang, X., Guo, B.: Data-parallel octrees for surface reconstruction. *IEEE Trans. Vis. Comput. Graph.* **17**, 669–681 (2011)

Reconstruction of Noisy Bezier Curves Using Artificial Neural Networks

Kavita Khanna and Navin Rajpal

Abstract The current work examines the reconstruction of Bezier curves with noisy data using artificial neural networks. Feed forward network with back propagation learning is used to fit the noisy data of the Bezier curves. Different parameters like learning rate, number of hidden layer neurons and number of epochs are studied and the results are compared for different runs. The best suited parameters are established for this specific problem.

Keywords Bezier curve · Feed-forward network · Noisy data · Back-propagation learning

1 Introduction

Curves and surfaces play an important role in computer science and engineering. The technology is increasing fast and so efficient algorithms are needed for discretizing curves and surfaces in order to store them and display them efficiently. A great deal of effort is needed to the development and implementation of algorithms to manipulate curves and surfaces. Bezier curves are an important part in the family of curves and so play a significant role in computer graphics and in designing. In fact they are best suited for ab initio designs. The current work studies these Bezier curves and reconstructs them using the noisy data of these curves. Feed-forward neural networks are used for this reconstruction as these are best suited for curve fitting and interpolation problems. The next two sections discuss the basics of Bezier curves and the artificial neural networks.

K. Khanna (✉) · N. Rajpal
USICT, Guru Gobind Singh Indraprastha University, Delhi, India
e-mail: kvita.khanna@gmail.com

N. Rajpal
e-mail: navin_rajpal@yahoo.com

2 Bezier Curves

Mathematically the curves could be broadly given by two techniques:

- Curve Fitting Techniques
- Curve Fairing Techniques

Curve fitting is a term used for the curves that pass through all the given data and such types of curves are said to fit the data for example cubic splines. Curve fitting methods provide very good results to the problems related to shape description where the basic shape comes from experimental evaluation or mathematical calculation for example aircraft wings, mechanical and structural parts. But for the situations where the data points are not the true values rather an approximation to the true values then the curve that shows the correct trend of the data may not pass through any of the data points. In this case the curve is said to fair the data. The most common technique of curve fairing is least squares approximation which gives a curve with the condition that it minimizes the sum of the y-squared deviations between the actual or given data points and the derived curve. The examples of the curves that do not pass through all the data points are Bezier curves and B-Spline curves. This technique is most commonly used in shape design problems that depend on both the aesthetics and functional requirements. These problems are termed ab initio designs examples include ship hull, car bodies, aircraft fuselages, glass wares and furniture. The curve fitting techniques like cubic spline fitting method tend to become ineffective for such type of ab initio designs. The method that suitably describes such types of ab initio designs and shapes of free form curves and surfaces was developed by Pierre Bezier and is known as a Bezier curve. This curve is determined by a defining polygon and mathematically it is established that a curve which is generated with the help of the vertices of a defining polygon is dependent on some interpolation or approximation scheme to find the relationship between the curve and the polygon. This scheme is supported by the choice of a basis function. The Bernstein basis produces Bezier curves.

2.1 Properties of a Bezier curve [1]

- The basis functions are real.
- The degree of the polynomial defining the curve segment is one less than the number of defining polygon points.
- The curve follows the shape of the defining polygon.
- The first and the last points on the curve are coincident with the first and the last points of the defining polygon.
- The tangent vectors at the ends of the curve have the same direction as the first and the last polygon spans respectively.

- The curve is contained within the convex hull of the defining polygon.
- The curve is invariant under affine transformation.

2.2 Mathematically we can Define a Parametric Bezier Curve as

$$P(t) = \sum_{i=0}^n B_i J_{n,i}(t) \quad 0 \leq t \leq 1$$

where B_i are position vectors of the $n + 1$ defining polygon vertices and $J_{n,i}(t)$ is the i -th n -th- Bernstein basis function and is given by:

$$J_{n,i}(t) = \binom{n}{i} t^i (1 - t)^{(n-i)}$$

$$\binom{n}{i} = \frac{n!}{i!(n - i)!}$$

where n is the degree of the Bernstein basis function and thus of the polynomial curve segment. It is one less than the number of points in the defining polygon.

The maximum value of each blending function occurs at $t = i/n$ and is given by

$$J_{n,i}(t) = \binom{n}{i} \frac{i^i (n - i)^{n-i}}{n^n}$$

The summation of the basis function is 1 i.e.

$$\sum_{i=0}^n J_{n,i}(t) = 1$$

Cohen and Riesenfeld have generalized this representation in matrix form as:

$$P(t) = [T][N][G]$$

where $[T] = [t^n \ t^{n-1} \ t^{n-2} \ \dots \ t \ 1]$

$$(N_{i+1,j+1})_{i,j=0}^n = \binom{n}{j} \binom{n-j}{n-i-j} (-1)^{n-i-j} \quad 0 \leq i + j \leq n \text{ and } 0 \text{ otherwise.}$$

2.3 Limitations of Bernstein Basis

Number of vertices fixes the order of resulting polygon which defines the curves. It is global in nature so that a change in one vertex is felt throughout the entire curve. This eliminates the ability to produce a local change within a curve.

3 Neural Networks Basics

Artificial neural networks are commonly known as a brain in a computer. The working of a neural network is quite similar to a human brain as they are designed such that the neurons incorporate all the important features of the brain, the major ones being learning and remembering [2]. This work uses neural networks for its following advantages:

- Can store accurate functions without using excessive amounts of memory.
- Can take any set of data points and fit a curve to them with the accuracy required for the specific problem.
- Can efficiently work with noisy data.
- Can work for linear and nonlinear functions.

The type of network used here is a multilayer perceptron which is a feed-forward neural network with back propagation learning. The feed forward neural networks are the ones in which the propagation of signals is in the forward direction i.e. from input layer to the hidden layer and from the hidden layer to the output layer. Input layer represents the actual data and are connected to the hidden nodes which modifies the data which in turn is connected to the output node which represents the target. A function called a threshold or activation function is responsible for modifying the signal coming into the hidden layer nodes. In the early days of neural networks this function produced a value of 1 or 0 depending on whether the signal from the prior layer exceeded a threshold value. Now activation functions are sigmoid in shape and can take any value between 0 and 1 or between -1 and 1. The process of finding the best set of weights for the neural network is known as training or learning. Each time the network cycles through the training data it produces a predicted value for the target variable and error is computed to reduce the overall error. The goal is to minimize the sum of the squared residuals.

A 1-n-1 network is used for curve fitting and interpolation problems, where 1 denotes the input node, n the number of hidden layer nodes and 1 output node [3, 4]. The same network is used here with Log-Sigmoid function as the activation function for the hidden layer and linear function as the activation function for the output layer.

4 Simulation Results

Firstly a Bezier curve with control points is created. Then a noise of .05 is added on to the curve. This noisy curve is then given as input to the network with the target as the actual curve. Different runs of the net are made to find out the best suited parameters in terms of learning rate, number of epochs and number of hidden neurons.

Table 1 Performance of training network with varying learning rate

Learning rate	No. of epocs	No. of hidden neurons	Performance
0.01	5000	24	0.00238
0.005	5000	24	0.00228
0.009	5000	24	0.00247
0.0001	5000	24	0.00206
0.01	10000	24	0.00206
0.005	10000	24	0.00242
0.009	10000	24	0.00206
0.0001	10000	24	0.00242

Table 2 Performance of training network with varying number of epocs

Learning Rate	No. of epocs	No. of hidden neurons	Performance
0.01	1000	24	0.00245
0.01	1500	24	0.00254
0.01	2000	24	0.00232
0.01	2500	24	0.00218
0.01	3500	24	0.00228
0.01	4500	24	0.00215
0.01	5000	24	0.00231
0.01	7000	24	0.00224
0.01	9000	24	0.00223
0.01	10000	24	0.00221
0.01	20000	24	0.00210

Normally it is assumed that for simple curves the learning rate should be between .1 to .01 and for more complex curves it should be between .01 to .001. The best results are obtained here with the learning rate as .01. It is tested for 5000 and 10000 epochs. Table 1 summarizes the results:

To set up the number of epochs the network was trained initially with 1000 epochs and consequently they were increased till the performance was stabilized. The performance is best with 20000 epochs and .01 learning rate. Table 2 justifies the results:

The number of hidden neurons also plays a major role in the performance of any network. An incremental approach was used to find the number of hidden neurons that best suit this problem. It was found that the network responds best with 30 hidden neurons after which the performance does not get better. The simulation results are given in Table 3.

Figures 1, 2, 3 and 4 show the original Bezier curve constructed using 4 control points, then the noisy Bezier curve with noise added to both x and y coordinates is plotted and after that the reconstructed curve is shown and Fig. 4 a combination of all the previous curves. The result shows that the curve obtained is smooth and fits the noisy data well.

Table 3 Performance of training network with varying number of hidden neurons

Learning Rate	No. of epocs	No. of hidden neurons	Performance
0.01	20000	02	0.00223
0.01	20000	03	0.00266
0.01	20000	05	0.00243
0.01	20000	08	0.00251
0.01	20000	10	0.00256
0.01	20000	20	0.00205
0.01	20000	24	0.00210
0.01	20000	30	0.00199
0.01	20000	36	0.00244
0.01	20000	40	0.00242

Fig. 1 Curve obtained from control points

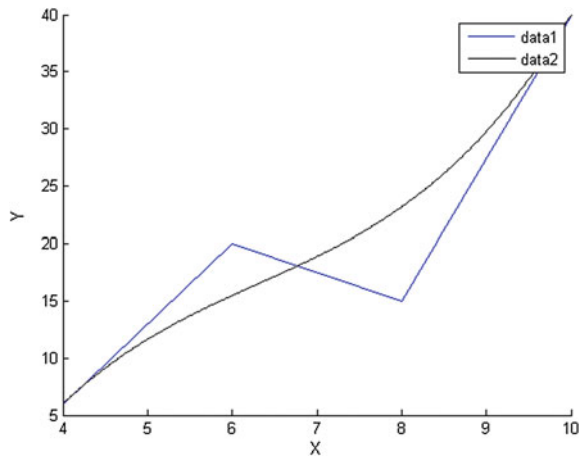


Fig. 2 Noisy curve shown with green color

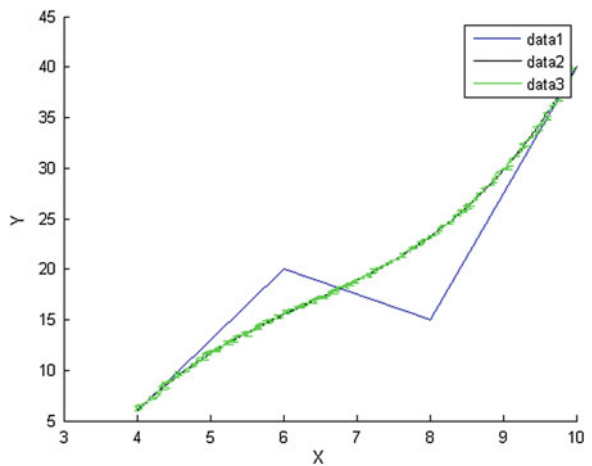


Fig. 3 Curve obtained after fitting shown with *red color*

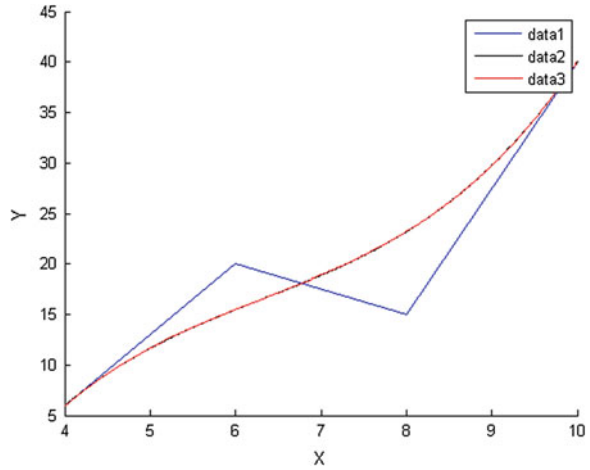
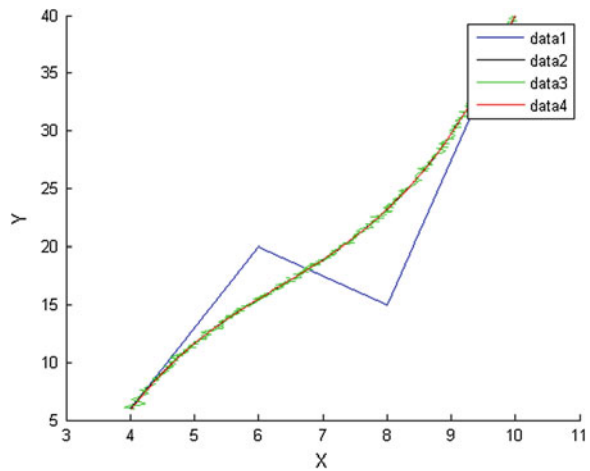


Fig. 4 Curve obtained by the dataset after fitting shown with *red color*, noise with *green color* and original curve with *blue color*



5 Conclusion and Future Work

The current work reconstructs a noisy Bezier curve using feed forward neural networks. This reconstruction could be carried out using Radial Basis Networks and the results could be compared to the one obtained from the feed forward neural networks. This work could be further extended by extracting the control points from a given curve and then reconstructing the curve using those control points.

References

1. Rogers, D.F., Adams, J.A.: *Mathematical Elements of Computer Graphics*. Tata Mc Graw Hill Publications, New Delhi (1990)
2. Uys, E.: *An investigation into using neural networks for statistical classification and regression*. University of Pretoria, Pretoria (2010)
3. Paliwal, Mukta, Kumar, Usha A.: *Neural networks and statistical techniques: a review of applications*. *Expert Syst. Appl.* **36**(1), 2–17 (2009)
4. Liu, X., Huang, H., Xu, W.: *Approximate B-Spline Surface Based on RBF Neural Networks*. *Lecture Notes in Computer Science*, vol 3514, pp. 995–1002. Springer, Heidelberg (2005)

SBM-DEA Model Based Efficiency Assessment of Public Sector Hospitals in Uttarakhand, India

Sandeep Kumar Mogha, Shiv Prasad Yadav and S. P. Singh

Abstract The present study is an attempt to provide an overview of the general status of the public sector hospitals of Uttarakhand, in terms of their productive efficiencies. The paper applies slack base model (SBM) for the measurement of efficiencies and slacks. On the basis of the status of the overall technical efficiency, it concludes that the performance of hospitals is not satisfactory and is far away from the optimal level. The average overall technical efficiency 54.10 % indicates that an average hospital has the scope of producing the outputs with the inputs 45.90 % lesser than their existing levels. The slack analysis results show that on average 12.57 % of beds, 13.16 % of doctors, 14.04 % of paramedical staff can be reduced and 17.53 % of out-door patients, 66.55 % of in-door patients, 208.23 % of major surgeries, 110.73 % of minor surgeries can be expanded if all the inefficient hospitals operate at the level of efficient hospitals.

Keywords Data envelopment analysis · SBM-model · Efficiency · Public hospitals and Uttarakhand

S. K. Mogha (✉) · S. P. Yadav
Department of Mathematics, Indian Institute of Technology Roorkee,
Roorkee 247667, India
e-mail: moghadma@gmail.com

S. P. Yadav
e-mail: yadavfma@iitr.ernet.in

S. P. Singh
Department of Humanities and Social Sciences, Indian Institute of Technology
Roorkee, Roorkee 247667, India
e-mail: singhfhs@iitr.ernet.in

1 Introduction

India is a developing country, which has made significant progress in the past several decades in improving health and well-being of its peoples. However, much progress remains to be achieved in increasing literacy, public awareness, and providing quality healthcare services to the general masses. Education and health being vital components of human development, plays significant role not only in the well-being of the people but also contribute substantially to the economic development [1].

Indian Government is still under increasing pressure to improve the efficiency of healthcare system. The increasing resources crunch, coupled with the declining efficiency and effectiveness of public investment, has put the public sector in a position of comparative disadvantage. It is observed that public health investment over the years has been comparatively low as its percentage in terms of gross domestic product (GDP) has declined from 1.30 % in 1990 to 0.90 % in 1999. However, its share has increased to 1.25 % in 2007 and further to 1.30 % in 2011. The aggregate expenditure on the health sector in India is 5.2 % of the GDP of which public sector constitutes only 17 % [2]. The scarcity of resources, coupled with structural reform programmes, has forced the policy makers to search for alternative ways of achieving maximum return from the given public healthcare services. One approach towards this end has been to examine the performance status of public hospitals on the basis of which policy decisions on the future course of action could be taken.

As Uttarakhand is a newly established state and situated mostly in hilly areas, there is a necessity to examine the status of the state in all the sectors including healthcare sector. From the establishment of the State, there are no major studies in public health sector. Only a few DEA-based studies relative to efficiency measurement have been conducted in Indian public and private healthcare sectors. Some relevant studies conducted on both the healthcare sectors are reviewed. Agarwal et al. [3] examine the year-wise performance of government sector hospitals of Uttaranchal for the period 2001–2004 using DEA-CCR and BCC output-orientated models. Dash et al. [4] assess the technical efficiencies of district hospitals in Tamil Nadu. Lakshmana [5] examine a district level analysis on existing healthcare infrastructure for children in Karnataka. Mogha et al. [6] use DEA-CCR and BCC output-oriented models for assessing the performance of 55 private sector hospitals in India for the year 2010. Mogha et al. [7] also assess the year-wise technical and scale efficiencies of Indian private sector hospitals for the 6 years period from 2004–2005 to 2009–2010.

The purpose of this study is to evaluate the performance of public sector hospitals in Uttarakhand by providing a mathematical technique to analyze the efficiency with which service is rendered. This study estimates the relative efficiencies of public sector hospitals, evaluates the reference sets and set the targets for the inefficient hospitals. The paper is organized as follows: [Sect. 2](#) contains methodology and [Sect. 3](#) contains empirical results and discussions followed by the conclusion in the last.

2 Methodology

This paper measures the overall technical efficiency (OTE), pure technical efficiency (PTE) and scale efficiency (SE) of 36 public sector hospitals of Uttarakhand State. The OTE refers to the extent to which a DMU can produce the maximum output from its chosen combination of inputs and scale efficiency refers to sub optimal activity level. DEA is a linear programming (LP) based technique for measuring the relative efficiency of homogeneous DMUs [8]. It calculates a maximal performance measure for each DMU relative to all other DMUs in the observed population with the sole requirement that each DMU lie on or below the frontier [9]. However, the radial CCR model [10] and BCC model [11] suffers from one shortcoming; they neglects the slacks in the evaluation of efficiencies. To overcome this shortcoming efficiency scores can be computed using the “slack-based” non-radial and non-oriented DEA model [12].

2.1 Data and Variables

We measure OTE of 36 public sector hospitals using the data collected from the Directorate of Medical Health and Family Welfare, Government of Uttarakhand, Dehradun, India for the year 2011. We have selected Government hospitals of Uttarakhand, having bed strength 24 or above. As per the availability of data, a total of 36 District hospitals, Base hospitals, and Combined hospitals are selected. Detailed list of selected hospitals is given in Appendix A.

To evaluate the relative efficiency of the public hospitals we have taken three inputs, namely number of beds (Input 1), number of doctors (Input 2), number of paramedical staff (Input 3), and four outputs namely, number of outdoor-patients (Output 1), number of indoor-patients (Output 2), number of major surgery (Output 3) and number of minor surgeries (Output 4).

In our sample hospitals there are some differences. All district male hospitals don't have maternity department and all district female hospitals don't have dental, orthopedic and eye departments. Therefore, to maintain the homogeneity of output measure, only number of major and minor surgery received are taken as the case-mix outputs [13] because the surgical department is common to all the hospitals. The thumb rules “the number of DMUs is expected to be larger than twice the sum of inputs and outputs” is applied for the selection of number of hospitals, inputs and outputs.

Descriptive statistics of input and output variables are given in Table 1. It is clear from the maximum and minimum values of input and output variables, and the value of standard deviations that there is a perceptible variation in the selected inputs and outputs across the hospitals.

Table 1 Descriptive statistics of inputs and outputs

	Inputs			Outputs			
	Input 1	Input 2	Input 3	Output 1	Input 2	Input 3	Input 4
Max	402	55	140	715221	22111	4128	2834
Min	24	6	11	5491	485	76	231
Mean	93.667	18.972	39.833	126792.8	7221.42	562.94	692.36
SD	66.967	9.284	25.403	122708.6	5634.79	738.65	522.97

Table 2 Correlation matrix between inputs and outputs

	Input 1	Input 2	Input 3	Output 1	Output 2	Output 3	Output 4
Input 1	1						
Input 2	0.876	1					
Input 3	0.900	0.906	1				
Output 1	0.873	0.776	0.796	1			
Output 2	0.595	0.559	0.583	0.612	1		
Output 3	0.473	0.492	0.619	0.391	0.477	1	
Output 4	0.508	0.527	0.629	0.443	0.576	0.959	1

Correlation analysis also has been worked out to know the relation between input and output variables. Correlation matrix between input and output variables is given in Table 2. It is observed that the outputs have positive correlations with the input variables.

2.2 Selection of the Model

Since in the basic CCR and BCC models the efficiency is measured either by changing inputs or by changing outputs, i.e., either input-oriented model or output-oriented model are used for the measurement. When both inputs and outputs can simultaneously be changed, i.e., the firm is able to reduce inputs and augment outputs simultaneously, a non-oriented model is used. It is known as the Additive Model (AM) or a slack-based model (SBM) and this is based on input and output slacks. This model allows managers to work on both inputs and outputs to achieve efficiency. Generally, in case of public hospitals it is difficult to choose the orientation (input or output) for the evaluation of efficiencies. It is not admirable to reduce input levels or increase output levels regarding public sector hospitals. So, in this study, a non-oriented and non-radial model known as SBM-DEA model has been used [12, 14].

In order to illustrate the model, let us assume that there are n DMUs ($DMU_j, j = 1, 2, \dots, n$) with m inputs ($x_{ij}, i = 1, 2, \dots, m$) and s outputs ($y_{rj}, r = 1, 2, \dots, s$) for each DMU. Let u_i and v_j are the weights corresponding to the i th input and j th output. Then the SBM-DEA model can be described as follows:

Table 3 Description of notations used in model 1

Symbol	Description
n	Total number of DMUs (hospitals)
m	Total number of inputs
s	Total number of outputs
i	Index of input
r	Index of output
j	Index for DMU
k	Index of specific DMU whose efficiency is being assessed
x_{ik}	Observed amount of the i th input of the k th hospital
y_{jk}	Observed amount of the j th output of the k th hospital
λ_{jk}	Multipliers used for computing linear combinations of hospital inputs–outputs
ρ	The efficiency score of a hospital by SBM model
ρ^*	The optimal efficiency score of a hospital by SBM model
s_{ik}^-	Non-negative slack or potential reduction of the i th input for the k th hospital
s_{rk}^+	Non-negative slack or potential increase of the r th output for the k th hospital
s_{ik}^{*-}	Optimal slack to identify an excess utilization of the i th input for the k th hospital
s_{rk}^{*+}	Optimal slack to identify a shortage utilization of the r th output for the k th hospital
\bar{x}_{ik}	Target for the i th input of the k th hospital after evaluation
\bar{y}_{rk}	Target for the r th output of the k th hospital after evaluation
λ_{jk}^*	Optimal value of λ_{jk}

$$\left. \begin{aligned}
 \text{Min } \rho_k &= \frac{1 - (1/m) \sum_{i=1}^m s_{ik}^- / x_{ik}}{1 + (1/s) \sum_{r=1}^s s_{rk}^+ / y_{rk}} \\
 \text{Subject to} & \\
 \sum_{j=1}^n \lambda_{jk} x_{ij} + s_{ik}^- &= x_{ik}, \forall i \\
 \sum_{j=1}^n \lambda_{jk} y_{rj} - s_{rk}^+ &= y_{rk}, \forall r \\
 \lambda_{jk} \geq 0, s_{ik}^- \geq 0, s_{rk}^+ &\geq 0, \forall i, r, j, k
 \end{aligned} \right\} \dots \text{Model 1}$$

Table 3 describes the used notations in the model.

2.3 Calculation for OTE, PTE and SE

Calculate OTE for every sample hospital by using Model 1 for the sample year. The detailed information of SBM-DEA results is given in Table 4.

If the optimal value λ_{jk}^* of λ_{jk} is non-zero, then the j th hospital represents the reference set (peers) for the k th hospital and the corresponding optimal value is known as the peer weight of the j th hospital. In the objective function of Model 1, the numerator value evaluates the mean reduction rate of inputs or input inefficiency of k th hospital. Similarly, the reciprocal of denominator evaluates the mean expansion rate of outputs or output inefficiency of k th hospital. Thus, the value of

Table 4 Resulting efficiency scores of hospitals by SBM-DEA model

Code	SBM-CRS results		Peer weights	SBM PTE	SBM SE	RTS	Peer count
	OTE	Reference set					
H1	0.375	H5, H7	0.500, 0.750	0.392	0.957	DRS	0
H2	0.657	H5, H7	1.00, 2.00	1	0.657	DRS	0
H3	1	H3	1	1	1	CRS	0
H4	0.374	H7, H12, H14	0.002, 0.704, 0.308	0.724	0.517	DRS	0
H5	1	H5	1	1	1	CRS	10
H6	0.574	H7, H14	0.500, 2.667	1	0.574	DRS	0
H7	1	H7	1	1	1	CRS	22
H8	0.353	H5, H7	0.500, 0.250	0.476	0.742	IRS	0
H9	0.669	H5, H7, H14	0.820, 0.211, 0.112	0.673	0.994	DRS	0
H10	0.246	H12, H14	1.690, 0.021	0.537	0.458	DRS	0
H11	0.487	H7, H12, H14	0.333, 0.167, 0.167	0.530	0.919	IRS	0
H12	1	H12	1	1	1	CRS	14
H13	0.241	H7	0.333	0.414	0.582	IRS	0
H14	1	H14	1	1	1	CRS	15
H15	1	H15	1	1	1	CRS	0
H16	0.336	H7, H12	0.500, 0.750	0.586	0.573	DRS	0
H17	1	H17	1	1	1	CRS	0
H18	1	H18	1	1	1	CRS	0
H19	0.173	H7	0.500	1	0.173	IRS	0
H20	0.460	H5, H12, H14	0.411, 1.401, 0.144	0.505	0.911	DRS	0
H21	0.174	H5, H7	1.00, 0.667	1	0.174	DRS	0
H22	0.314	H7, H14	0.500, 0.250	0.418	0.751	IRS	0
H23	0.319	H7	0.400	0.453	0.704	IRS	0
H24	0.373	H5, H7, H12, H14	0.102, 0.075, 2.278, 0.026	0.385	0.969	DRS	0
H25	0.208	H7	0.600	0.223	0.933	IRS	0

(continued)

Table 4 (continued)

Code	SBM-CRS results		Reference set	Peer weights	SBM PTE	SBM SE	RTS	Peer count
	OTE							
H26	1		H26	1	1	1	CRS	1
H27	1		H27	1	1	1	CRS	0
H28	0.391		H7, H12, H14	0.092, 0.115, 0.249	1	0.391	IRS	0
H29	0.214		H5, H12	0.001, 1.151	1	0.214	DRS	0
H30	0.245		H7, H12, H14	0.137, 2.780, 0.133	0.289	0.848	DRS	0
H31	0.495		H7, H12	2.00, 1.00	1	0.495	DRS	0
H32	0.212		H7, H12, H14	0.108, 2.124, 0.021	0.394	0.538	DRS	0
H33	0.269		H7, H12, H14	0.245, 2.115, 0.164	0.297	0.906	DRS	0
H34	0.393		H7, H12, H14	0.018, 1.373, 0.159	0.592	0.664	DRS	0
H35	0.273		H5, H12, H14	0.155, 1.213, 0.070	0.696	0.392	DRS	0
H36	0.669		H5, H7, H14, H26	0.022, 0.137, 0.309, 0.148	1	0.669	IRS	0
Mean	0.541				0.738	0.742		

Source: Authors' calculation

ρ_k can be interpreted as the product of input and output inefficiencies. This model is known as SBM-CRS model [12].

Model 1 is a fractional programming problem. The theory of fractional linear programming [14] makes it possible to replace Model 1 with an equivalent linear programming problem. For this, let us multiply a scalar variable $t > 0$ to both the numerator and denominator of Model 1. This causes no change in ρ_k . We adjust t so that the denominator becomes 1. This gives the new constraint as

$$t + (1/s) \sum_{r=1}^s ts_{rk}^+/y_{rk} = 1.$$

So, the objective is to minimize the numerator. Thus we have the following model:

$$\left. \begin{aligned} \text{Min } \tau_k &= t - (1/m) \sum_{i=1}^m ts_{ik}^-/x_{ik} \\ \text{Subject to} \\ t + (1/s) \sum_{r=1}^s ts_{rk}^+/y_{rk} &= 1 \\ \sum_{j=1}^n \lambda_{jk}x_{ij} + s_{ik}^- &= x_{ik}, \forall i \\ \sum_{j=1}^n \lambda_{jk}y_{rj} - s_{rk}^+ &= y_{rk}, \forall r \\ \lambda_{jk} \geq 0, s_{ik}^- \geq 0, s_{rk}^+ &\geq 0, \forall i, r, j, k \text{ \& } t > 0 \end{aligned} \right\} \dots \text{Model 2}$$

Model 2 given is a non-linear programming problem since it contains the non-linear terms ts_{ik}^- and ts_{rk}^+ . Let us transform Model 2 into a linear programming problem. Let $S_{ik}^- = ts_{ik}^-$, $S_{ik}^+ = ts_{ik}^+$ and $\delta = t\lambda$ then Model 2 becomes the following linear programming problem in t, S_{ik}^-, S_{ik}^+ and δ :

$$\left. \begin{aligned} \text{Min } \tau_k &= t - (1/m) \sum_{i=1}^m S_{ik}^-/x_{ik} \\ \text{Subject to} \\ t + (1/s) \sum_{r=1}^s S_{rk}^+/y_{rk} &= 1 \\ \sum_{j=1}^n \delta_{jk}x_{ij} + S_{ik}^- &= tx_{ik}, \forall i \\ \sum_{j=1}^n \delta_{jk}y_{rj} - S_{rk}^+ &= ty_{rk}, \forall r \\ \delta_{jk} \geq 0, S_{ik}^- \geq 0, S_{rk}^+ &\geq 0, \forall i, r, j, k \text{ \& } t > 0 \end{aligned} \right\} \dots \text{Model 3}$$

Let an optimal solution of Model 3 be $(\tau^*, t^*, \delta^*, S_{ij}^{*-}, S_{ij}^{*+})$. Then the optimal solution of Model 1 is given by $\rho_k^* = \tau^*$, $\lambda^* = \delta^*/t^*$, $s_{ij}^{*-} = S_{ij}^{*-}/t^*$, $s_{ij}^{*+} = S_{ij}^{*+}/t^*$.

The interpretation of results of the Model 1 can be given as follows:

The k th hospital is said to be Pareto efficient if all slacks are zero, i.e., $s_{ik}^{*-} = s_{rk}^{*+} = 0$ for all i and r , which is equivalent to $\rho_k^* = 1$.

The non-zero slacks and (or) $\rho_k^* \leq 1$ identify the sources and amount of any inefficiency that may exist in the k th hospital. The reference set shows how input

can be decreased and output can be increased to make the k th hospital efficient. We estimate PTE for every sample hospital by using Model 3 through adjoining the convexity constraint $\sum_{j=1}^n \delta_{jk} = 1$. Calculate scale efficiency (SE) for every hospital using $SE = OTE/PTE$. However some considerations are proven for the use of SBM-DEA model.

- (i) A hospital (DMU) is said to be SBM-efficient if and only if $\rho^* = 1$, i.e., when there is no input excess and no output shortfall in an optimal solution.
- (ii) The optimal SBM efficiency score ρ^* for any hospital (DMU) is not greater than the optimal CCR efficiency score θ^* [14].

The results of SBM-CRS and SBM-VRS models are calculated using MATLAB.

3 Results and Discussions

The efficiency scores (OTE, PTE and SE) of 36 public hospitals have been estimated for the year 2011. Table 4 presents the efficiency scores obtained from SBM-CRS and SBM-VRS models along with reference sets and peer weights of the sample hospitals. The DEA analysis evaluates the set of hospitals which construct the efficiency frontier. The hospitals achieving the efficiency score equal to 1.00 constitute the efficiency frontier and those having the value less than 1.00 are inefficient.

3.1 Overall Technical Efficiency (OTE)

Table 4 evinces that out of 36 hospitals 10 hospitals are relatively overall technical efficient as they scored $OTE = 1$, and thus they form the efficiency frontier. The remaining 26 hospitals are inefficient as they have efficiency scores less than 1. The efficient hospitals H3, H5, H7, H12, H14, H15, H17, H18, H26 and H27 are on the best practice frontier (efficiency frontier) and thus form the “reference sets”, i.e., these hospitals can set an example of good operating practice for the remaining 26 inefficient hospitals to emulate. The average OTE score is work out to be 54.10 %, which reveals that on average a hospital can reduce its resources or increase outputs by 45.90 % to become efficient. The hospital H19 is the most technical inefficient hospital as its efficiency is found to be 17.30 %. Among the inefficient hospitals only 4 hospitals H2, H6, H9 and H36 have the efficiency score above the average efficiency score.

3.2 Pure Technical Efficiency (PTE)

SBM-CRS model is based on the assumption of constant returns to scale (CRS) which does not consider the scale size of hospital to be relevant in assessing overall technical efficiency. Therefore, in order to know whether inefficiency in any hospital is due to inefficient production operation or due to unfavorable conditions displayed by the size of hospital, SBM-VRS model is also applied. SBM-VRS efficiency (PTE) is always greater than or equal to SBM-CRS efficiency (OTE). Hence number of hospitals on the frontier under SBM-VRS model is always greater than or equal to the number of hospitals on the frontier under SBM-CRS model.

The resulted efficiency scores calculated from SBM-VRS model are shown in the fifth column of Table 4. It is evident from the Table that out of 36 hospitals 18 (50 %) are pure technical efficient (VRS score = 1), while remaining 18 hospitals are inefficient as they scored efficiency score less than 1. The efficiency score obtained by this model measures how efficiently inputs are converted into output(s) irrespective of the size of the hospitals. The average PTE is worked out to be 73.80 %. This means that given the scale of operation, on average, hospitals can reduce its inputs or increase outputs by 26.20 % of its observed level to become pure technical efficient. PTE is concerned with the efficiency in converting inputs to outputs, given the scale size of hospital, so, we observe that H2, H6, H19, H21, H28, H29, H31 and H36 are overall technical inefficient but pure technical efficient. This clearly evinces that these hospitals are able to convert its inputs into outputs with 100 percent efficiency, but their OTE is low due to their scale-size.

3.3 Scale Efficiency (SE)

A comparison of the results for SBM-CRS and SBM-VRS gives an assessment of whether the size of a hospital has an influence on its OTE. Scale efficiency (SE) is the ratio of OTE to PTE scores. If SE is less than one, then the hospital appears either small or big relative to its optimum scale-size. Table 4 also represents the SE score of hospitals in the sixth column. Results show that out of 36 hospitals, 10 hospitals are scale efficient while remaining 26 hospitals are scale inefficient. The average SE is found to be 74.20 %, which indicates that on average a hospital may be able to decrease its inputs or increase its outputs by 25.80 % beyond its best practice targets under variable returns to scale (VRS), if it were to operate at constant returns to scale (CRS).

Table 5 Average slacks in inputs and outputs under SBM-CRS model

Code	Input 1	Input 2	Input 3	Output 1	Output 2	Output 3	Output 4
Mean	12.67	2.74	6.21	2340.67	2183.19	673.79	524.91

Source Authors' calculation

Table 6 Percentage reduction in inputs and augmentation in outputs for inefficient hospitals under SBM-CRS model

Code	Inputs			Outputs			
	Input 1	Input 2	Input 3	Output 1	Output 2	Output 3	Output 4
H1	22.54	0.00	32.92	0.00	225.05	124.75	201.22
H2	0.00	14.29	0.00	73.46	17.23	36.69	0.00
H4	0.00	29.86	41.65	0.00	0.00	351.08	63.07
H6	24.05	0.00	12.26	0.00	16.19	98.50	121.11
H8	31.88	0.00	26.97	0.00	334.74	158.58	75.45
H9	19.58	0.00	37.90	0.00	0.00	34.70	48.11
H10	0.00	12.70	23.87	0.00	80.85	784.95	164.33
H11	0.00	24.07	41.03	0.00	212.92	0.00	41.46
H13	41.67	27.08	0.00	0.00	616.84	172.88	131.34
H16	0.00	34.09	4.69	41.70	0.00	421.89	148.05
H19	42.11	28.57	42.11	53.80	1173.20	242.51	31.14
H20	0.00	5.16	0.00	0.00	7.30	305.68	141.58
H21	55.56	66.67	51.52	135.54	417.29	294.74	27.27
H22	0.00	39.58	19.05	0.00	249.83	224.30	133.61
H23	48.12	36.67	46.06	41.11	122.22	165.64	41.88
H24	0.00	1.18	0.00	0.00	0.00	425.56	243.35
H25	63.20	55.29	51.35	10.86	189.90	78.56	127.48
H28	0.00	43.15	25.06	0.00	0.00	334.25	57.20
H29	30.62	63.25	0.00	0.00	84.09	672.34	126.08
H30	6.10	0.00	9.29	0.00	0.00	765.96	386.25
H31	14.52	11.11	0.00	52.82	0.00	101.64	19.68
H32	0.00	1.43	28.29	0.00	0.00	951.95	346.60
H33	0.00	22.04	15.14	0.00	0.00	623.01	281.57
H34	0.00	14.13	10.05	0.00	0.00	401.89	134.70
H35	0.00	12.55	0.00	0.00	60.35	762.11	182.59
H36	0.00	25.78	0.00	0.00	0.00	128.94	17.80
Mean	12.57	13.16	14.04	17.53	66.55	208.23	110.73

Source Authors' calculation

3.4 Targets for Inefficient Hospitals

When a hospital is inefficient, DEA allows setting targets of its inputs and outputs so that it can improve its performance. Thus, each of the inefficient hospitals can become overall technical efficient by adjusting its operation to the associated target point determined by the efficient hospitals that define its reference frontier. Input and output targets, according to the SBM-DEA model, can be set by using the relations given in Eqs. (1) and (2) respectively.

$$\overline{x}_{ik} = x_{ik} - s_{ik}^{-*} \tag{1}$$

$$\overline{y}_{rk} = y_{rk} + s_{rk}^{+*} \tag{2}$$

where the description of notations used in Eqs. (1) and (2) are given in Table 3. To calculate input and output targets, slacks for each hospital are required. The average optimal input and output slacks for hospitals are given in Table 5.

Table 6 presents the target values of all inputs and outputs for inefficient hospitals along with percentage reduction in inputs and percentage augmentation in outputs. It can be observed from Table 6 that on average a hospital has significant scope to reduce the inputs and expand the outputs relative to the best practice hospital.

4 Conclusions

This paper measures the relative efficiencies (OTE, PTE and SE) of 36 public sector hospitals of Uttarakhand State using SBM-DEA model. The study finds that 10 (27.78 %) hospitals have the maximum degree of OTE. Average OTE of the hospitals 54.10 %, indicates that on average 45.90 % of the technical potential of hospitals is not in use i.e., these hospitals have the scope of producing the more outputs with lesser inputs than their existing levels. The results of SBM-VRS model show that out of 36 hospitals, 18 (50 %) are pure technical efficient as they efficiently convert their inputs into outputs. However, out of them, 8 hospitals are technical inefficient due to scale-size effect. The target setting results show that all the inputs have the significant scope to reduce and outputs to increase. The SBM model suggests that on average, inefficient hospitals may be able to reduce 12.57 % of beds, 13.16 % of doctors, 14.04 % of paramedical staff, and to expand 17.53 % of outdoor-patients, 66.55 % of indoor-patients, 208.23 % of major surgeries 110.73 % of minor surgeries can be expand if all the inefficient hospitals operate at the level of efficient hospitals.

Appendix A

Full Name and Locations of the Selected Hospitals

Code	District name	Hospital name	Code	District name	Hospital name
H1	Pauri	District Male Hospital	H19	Nanital	G.B Pant Hospital Nanital
H2	Pauri	District Female Hospital	H20	Nanital	Combined Hospital Ramnagar

(continued)

(continued)

Code	District name	Hospital name	Code	District name	Hospital name
H3	Pauri	Base Hospital Srinagar	H21	Nanital	Combined Hospital Padampuri
H4	Pauri	Combines Hospital Srinagar	H22	Almora	District Hospital Male
H5	Pauri	Combines Hospital Kotdwar	H23	Almora	District Hospital Female
H6	Dehradun	Doon male hospital	H24	Almora	Combined Hospital Ranikhet
H7	Dehradun	Female hospital Dehradun	H25	Almora	Base Hospital Almora
H8	Dehradun	Coronation Hospital	H26	US Nagar	L.D Bhatt hospital Kashipur
H9	Dehradun	SPS Hospital Rishikesh	H27	US Nagar	District Hospital Rudrapur
H10	Dehradun	St. Merry. Hospital Mussoorie	H28	Tehri	District Hospital Baurari Tehri
H11	Haridwar	HMG Hospital Haridwar	H29	Tehri	Combined Hospital Narendnagar
H12	Haridwar	CR Female Hospital	H30	Pithoragarh	District Hospital male Pithoragardh
H13	Haridwar	Mela Hospital Haridwar	H31	Pithoragarh	District Hospital Female Pithoragardh
H14	Haridwar	Combined Hospital Roorkee	H32	Chamoli	District Hospital Gopeshwar
H15	Nanital	B.D Pandey Male Hospital	H33	Uttarkashi	District Hospital Uttarkashi
H16	Nanital	B.D Pandey Female Hospital	H34	Rudraprayag	District Hospital Rudraprayag
H17	Nanital	Base hospital Haldwani	H35	Champawat	Combined Hospital Tanakpur
H18	Nanital	Female Hospital Haldwani	H36	Bageshwar	District Hospital Bageshwar

References

1. Tyson L.D.A.: For developing countries, health is wealth. Business Week. <http://www.businessweek.com/stories/2002-01-13/for-developing-countries-health-is-wealth> (2002)
2. Economic Survey: Government of India. <http://indiabudget.nic.in/index.asp> (2011–2012)
3. Agarwal, S., Yadav, S.P., Singh, S.P.: DEA technique based assessment of efficiencies of the government hospitals of Uttaranchal (India). *Int. J. Econ. Res.* **4**(1), 25–42 (2007)
4. Dash, U., Vaishnavi, S.D., Muraleedharan, V.R.: Technical efficiency and scale efficiency of district hospitals: a case study. *J. Health Manage.* **12**(3), 231–248 (2010)
5. Lakshmana, C.M.: A study on healthcare infrastructure for children in Karnataka: a district-wise analysis. *J. Health Manage.* **12**(4), 423–443 (2010)
6. Mogha, S.K., Yadav, S.P., Singh, S.P.: Performance evaluation of Indian private hospitals using DEA approach with sensitivity analysis. *Int. J. Adv. Manage. Econ.* **1**(2), 1–12 (2012)
7. Mogha, S.K., Yadav, S.P., Singh, S.P.: Estimating technical and scale efficiencies of private hospitals using a non-parametric approach: case of India. *Int. J. Oper. Res.* (2013, in Press)

8. Ramanathan, R.: *An Introduction to Data Envelopment Analysis*. Sage Publication India Pvt. Ltd., New Delhi (2003)
9. Charnes, A., Cooper, W.W., Lewin, A.Y., Saiford, L.M.: *Data Envelopment Analysis: Theory, Methodology and Application*. Kluwer Academic Publishers, Boston (1994)
10. Charnes, A., Cooper, W.W., Rhodes, E.: Measuring the efficiency of decision making units. *Eur. J. Oper. Res.* **2**(6), 429–441 (1978)
11. Banker, R.D., Charnes, A., Cooper, W.W.: Some models for the estimation of technical and scale inefficiencies in data envelopment analysis. *Manage. Sci.* **30**(9), 1078–1092 (1984)
12. Tone, K.: A slack based measure of efficiencies in data envelopment analysis. *Eur. J. Oper. Res.* **130**, 498–509 (2001)
13. Grosskopf, S., Valdmainis, V.: Evaluating hospital performance with case-mix-adjusted outputs. *Med. Care* **31**(6), 525–532 (1993)
14. Cooper, W.W., Seiford, L.M., Tone, K.: *Data Envelopment Analysis a Comprehensive Text with Models, Applications, References and DEA solver Software*. Springer, USA (1997)

Recognizability of Triangular Picture Languages by Triangular Wang Automata

V. Devi Rajaselvi, T. Kalyani, V. R. Dare and D. G. Thomas

Abstract Wang automata to recognize rectangular picture languages and iso-picture languages were studied in [6, 7]. In this paper we introduce triangular Wang automata based on triangular Wang tiles to recognize triangular picture languages. We discuss scanning strategies and prove that triangular Wang automata with a specific scanning strategy recognize the class of triangular pictures recognized by triangular tiling systems.

Keywords Triangular picture languages · Triangular tiling systems · Scanning strategy · Triangular Wang systems · Wang automaton

1 Introduction

Wang automaton is based on labeled Wang tiles. It combines features of both online tessellation acceptors and 4-way automata. (i) As in online tessellation acceptors computation assigns states to each picture position (ii) as in 4-way automata the input head visits the picture moving from one pixel to an adjacent one according to some scanning strategy.

V. D. Rajaselvi (✉)
Sathyabama University, Chennai 600119, India
e-mail: devijerson@gmail.com

T. Kalyani
Department of Mathematics, St. Joseph's Institute of Technology, Chennai 600119, India
e-mail: kalphd02@yahoo.com

V. R. Dare · D. G. Thomas
Department of Mathematics, Madras Christian College, Chennai 600059, India
e-mail: rajkumardare@yahoo.com

D. G. Thomas
e-mail: dgthomasccc@yahoo.com

Wang automata recognize the class REC that is they are equivalent to tiling acceptors and hence strictly more powerful than 4-way automata.

In this paper we extended the concept of Wang automaton to recognize triangular picture languages. We proved that triangular Wang automata with a specific scanning strategy recognize the class TREC.

This paper is organized in the following manner. In Sect. 2 we recall some basic notions of triangular pictures and triangular picture languages, triangular tiling and triangular Wang systems. In Sect. 3 we introduce polite scanning strategies for triangular pictures. In Sect. 4 we present a newer version of Wang automaton named as triangular Wang automata (TWA) and prove the theorem characterizing TREC as the class of triangular picture languages recognized by TWA.

2 Preliminaries

Here we review the notions of formal language theory relating to triangular pictures and triangular tiling systems from [4] and [6].

Let Σ be a finite alphabet of symbols. A triangular picture ‘ p ’ over the alphabet Σ is a triangular array of symbols over Σ . The set of all triangular arrays over the alphabet Σ is denoted by Σ_T^{**} . A triangular picture language over Σ is a subset of Σ_T^{**} .

With respect to a triad of three dimensional axes X, Y, Z the coordinates of each element of a triangular array can be fixed.

Given a triangular picture ‘ p ’ the number of rows (counting from the bottom to top) denoted by $r(p)$ is the size of a triangular picture. (The number of horizontal lines used to draw a triangle are called as the rows of the triangle).

Definition 1 *If $p \in \Sigma_T^{**}$ then \hat{p} is the triangular picture obtained by surrounding p with a special boundary symbol $\#$.*

Definition 2 *Let $p \in \Sigma_T^{**}$ is a triangular picture. Let Σ and Γ be two finite alphabets and $\pi : \Sigma \rightarrow \Gamma$ be a mapping which we call a projection. The projection by mapping π of a triangular picture $p' \in \Gamma^{**}$ such that $\pi(p(i, j, k)) = p'(i, j, k)$.*

Definition 3 *Let $L \subseteq \Sigma_T^{**}$ be a triangular picture language. The projection of L is the language $\pi(L) = \{p'/p' = \pi(p), p \in L\} \subseteq \Gamma_T^{**}$.*

Definition 4 *An triangular picture language L is called local if there exists a finite set Δ of triangular tiles over $\Sigma \cup \{\#\}$ such that $L = \{p \in \Sigma_T^{**} / B_2(\hat{p}) \subseteq \Delta\}$. The family of local triangular picture languages will be denoted by TLOC.*

Definition 5 *Let Σ be a finite alphabet. An triangular picture language $L \subseteq \Sigma_T^{**}$ is called recognizable if there exists local triangular picture language L' over an alphabet and a projection $\pi : \Gamma \rightarrow \Sigma$ such that $\pi(L') = L$.*

The family of recognizable triangular picture languages will be denoted by *TREC*.

Definition 6 A triangular tiling system T is a 4-tuple $(\Sigma, \Gamma, \pi, \theta)$ where Σ and Γ are finite set of symbols $\pi : \Gamma \rightarrow \Sigma$ is a projection and θ is a set of triangular tiles over the alphabet $\Gamma \cup \{\#\}$.

Definition 7 The triangular picture language $L \subseteq \Sigma_T^{**}$ is tiling recognizable if there exists a triangular picture language recognizable by triangular tiling system denoted by $\mathcal{L}(TTS)$.

2.1 Triangular Wang Automata

In this section we introduce triangular Wang automaton to recognize triangular picture language. We introduce triangular Wang tiles to define triangular Wang systems (TWS) a formalism to recognize triangular picture languages.

Definition 8 A labeled triangular Wang tile is a 4-tuple consisting of three colors chosen from a finite set of colors Q and a label from a finite alphabet Σ . The colors are placed at left down (L_d), right down (R_d) and horizontal (H) positions of the label.

Two triangular Wang tiles may be adjacent if and only if the adjacent edges are of same color.

In the rest of the paper it is supposed that the triangular Wang tilings cover the plane so that all the tiles that are beyond the borders of the considered picture will be a special tile $(\#, \#, \#)$.

Definition 9 For any direction $d \in Dirs^T = \{\swarrow, \searrow, \rightarrow\}$, A_d is the color of the edge of a triangular tile A towards the direction d . ‘ $-d$ ’ refers to the opposite direction to d . $\lambda(A)$ refers to the label of the triangular tile A .

In Fig. 1 $A_{\searrow} = q, A_{\swarrow} = p, A_{\rightarrow} = r$. The set of tiles with labels in Σ and colors in Q is Σ_{3Q} .

We also consider partial tiles, where some colors may be undefined: The set of partial tiles is denoted by Σ_Q . Domain of a tile A is the set Δ_A of directions where A is defined. Given two partial triangular tiles A, C bearing the same label, C extends to A if $C_d = A_d$ for every $d \in \Delta_A$. A triangular tile which is not partial can be called as complete. Labeled triangular Wang tiles can be used to build triangular pictures over Σ .

2.2 Triangular Wang Pictures

A triangular picture is called triangular Wang picture if all borders are colored with $\#$ and two tiles may be adjacent only if the color of the touching edges is the same.

An example of triangular Wang picture of size 4 is given in Fig. 2.

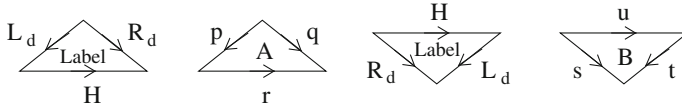


Fig. 1 Set of tiles

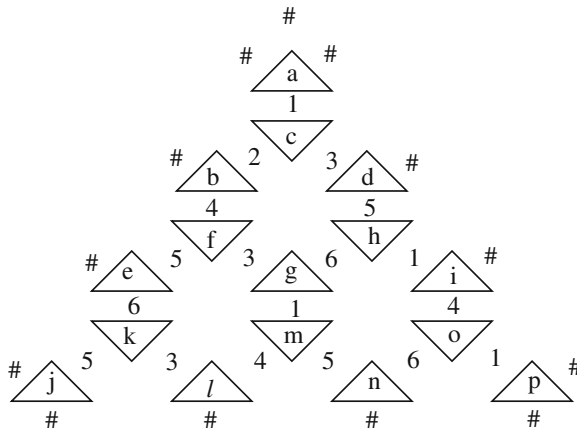


Fig. 2 Triangular Wang picture

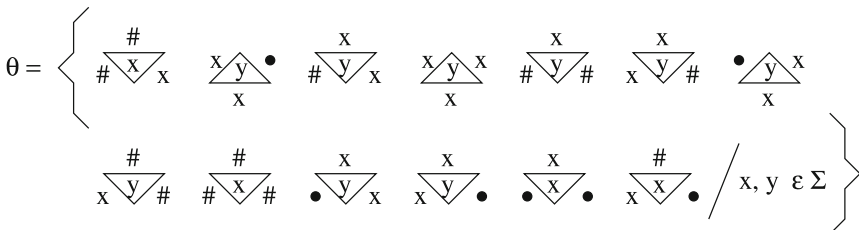
Definition 10 The label of a triangular Wang picture P over Σ_{3Q} is the picture $p = \lambda(P) \in \Sigma_T^{**}$ having the pixels of P . That is $P(i, j, k) = \lambda(P(i, j, k))$. The label of the above Wang picture is given in Fig. 3.

2.3 Triangular Wang Systems

A triangular Wang system is a triple $W = \langle \Sigma, Q, \theta \rangle$ where Σ is a finite alphabet, Q is the set of colors, θ is a subset of Σ_{3Q} . The language generated by W is the language $L(W) \subseteq \Sigma_T^{**}$ of the labels of all triangular Wang pictures is $L_W(\theta)$.

Notice that a triangular picture $p \in L(w)$ may have more than one Wang tiling in w . TREC is the class of picture languages generated by triangular Wang systems.

Example 1 Consider the language $L \subseteq \Sigma_T^{**}$ of pictures of size $n \geq 2$ with the first row like $w\bar{b}w$ where \bar{w} is the reverse of w . Then L is recognized by the triangular Wang system $\langle \Sigma, Q, \theta \rangle$ where $Q = \Sigma \cup \{\bullet, \#\}$ and



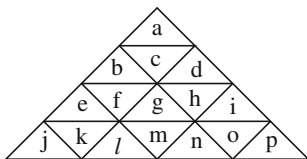


Fig. 3 Triangular picture

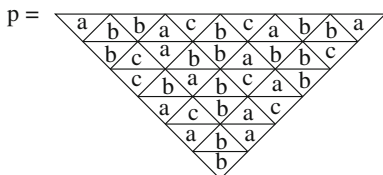


Fig. 4 Triangular tiling

The symbols on borders are used to connect each letter in w to the corresponding letter in \bar{w} along nested paths following a V-like form. In Fig. 4 we show an example of picture $p \in L$ together with its Wang tiling $P \in L_w(\theta)$ (the colors in P are used in the figure only to emphasize the V-like form of the resulting paths).

3 Triangular Scanning Strategies

Two dimensional scanning strategies for rectangular pictures are discussed [3]. The authors considered strategies that do not depend on the content of the input picture. Scanning strategies are defined in terms of partial functions; for a partial function g , if the value of g at t is not defined then $g(t) = \perp$ (Fig. 5).

Definition 11 A triangular scanning strategy is a family $\delta = \{\delta_{m \times n} : \{1, 2, \dots\} \rightarrow m \times n, p \in \Sigma^{(m,n)T}\}$ where each $\delta_{m \times n}$ is a partial function such that $\delta_{m \times n}(t) \neq \perp$ for some t implies $\delta_{m \times n}(s) \neq \perp$ for every $1 \leq s \leq t$. $\delta_{m \times n}$ is called the triangular scanning function over the triangular picture domain $(m \times n)$. A scanning strategy said to be continuous if for every t, m, n , $\delta_{m \times n}(t + 1)$ is adjacent to $\delta_{m \times n}(t)$ provided they are both defined.

Definition 12 A triangular scanning strategy is said to be one pass if each scanning function $\delta_{m \times n}$ restricted to $\{1, 2, \dots, |\text{dom}(p)|\}$ where δ is a bijection and $\delta_{m \times n}(t) = \perp$ for every $t > |\text{dom}(p)|$.

A triangular strategy provides a method to visit positions in any triangular picture domain; $\mu_{m \times n}(t)$ is the position visited in $\text{dom}(p)$ at time t . One pass strategies are those that visit each position in each domain exactly once.

Definition 13 A triangular scanning strategy is said to be blind if it proceeds locally by scanning adjacent positions. It cannot be neither triangular picture

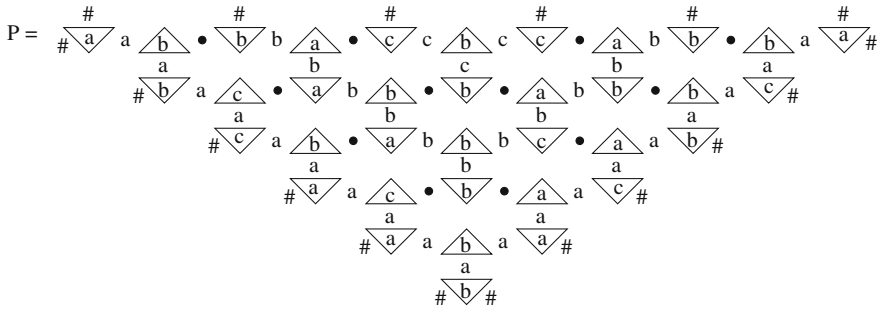


Fig. 5 Triangular Wang tiling

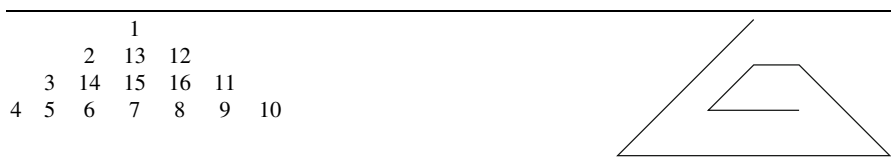
content nor its size. It can realize a border # and an already considered position when reaches it.

Examples of one pass triangular scanning strategies with the picture size 4.

Example 2 This triangular scanning strategy has a bousrophedomic behaviour (snake like)



Example 3 This triangular scanning strategy has a spiral behaviour



Example 4 This triangular scanning strategy has a digitized L-like behaviour



Example 5 This triangular scanning strategy has mixed behaviour



The following notions add some constraints to the scanning strategies to implement blindness. Given a position x , we denote by $\langle x \rangle$, the set of 3 edges adjacent to x and $d \in T \text{ dirs}$, the edge of x in the direction d is denoted by x_d and the position adjacent to x in direction d is denoted by $x * d$.

Definition 14 The next position function is a partial function $\eta : 2^{T \text{ dirs}} \times T \text{ dirs} \rightarrow T \text{ dirs}$ such that $\eta(D, d) = \perp$ if $-d \notin D$. Here η is used to choose where to go next. For a given position there may be a set of already considered edges, given by the set D of directions and d is the direction from the last considered edge.

If $|D| = 1$ then d is the unique element of D i.e., $d = -d$.

If $|D| = 2$ then d is uniquely determined.

If $1 < |D| < 2$ then d may not be unique.

After fixing any next position function η , any starting corner $cor_s \in \text{corners}\{\ell_c, r_c, u_c\}$, any starting direction $d_s \in T \text{ dirs}$ for every picture domain $m \times n$, consider the following triangular scanning function $\delta_{m \times n}$ over $m \times n$, the starting position is

$$\delta_{m \times n}(1) = \begin{cases} (1, 1) & \text{if } cor_s = u_c \\ (m, 1) & \text{if } cor_s = \ell_c \\ (m, n) & \text{if } cor_s = r_c \end{cases}$$

where $n = 2m - 1$.

We also define O_1 as the set of outer edges (that is, those adjacent to borders) of the picture domain $m \times n$ and we set $d_1 = d_s$.

The inductive definition of $\delta_{m \times n}(t + 1)$ for $t \geq 1$ is given by

$$D_t = \{d \in T \text{ dirs} : (\delta_{m \times n}(t))_d \in O_t\}.$$

$$O_{t+1} = O_t \cup \text{edges}(\delta_{m \times n}(t)).$$

$$d_{t+1} = \eta(D_t, d_t).$$

$$\delta_{m \times n}(t + 1) = \delta_{m \times n}(t) * d_{t+1}.$$

Here we should notice that $\delta_{m \times n}(1) - d_1$ must be in O_1 for $\eta(D_1, d_1)$ to be defined.

Definition 15 A scanning strategy is blind if it is induced by a triple $\langle \eta, cor_s, d_s \rangle$ where η is a next position function, cor_s a starting corner and d_s a starting direction.

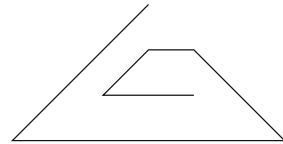
Definition 16 A triangular scanning strategy is called polite if it is blind and one pass. All the one pass scanning strategies represented from Examples 2–5 are blind and hence polite.

Example 6 \triangleleft induced by the triple $\langle \eta_{\triangleleft}, ul, \swarrow \rangle$ where its next position function is shown in the following table. The set of directions $D \in 2^{T \text{ dirs}}$ and incoming direction $d = T \text{ dirs}$ and together graphically denoted in a partially outlined triangle where marked sides corresponds to elements of D .

$D = \{ \swarrow, \rightarrow, \searrow \}$, $d = \swarrow$, is shown as #.

(D, d)	$\eta_{\triangleleft}(D, d)$
	\swarrow
	\rightarrow
	\rightarrow
	\swarrow

(D, d)	$\eta_{\triangleleft}(D, d)$
	\swarrow
	\swarrow
	\rightarrow
	\rightarrow



4 Triangular Wang Automata

We are now able to formally introduce triangular Wang automata and to show that they are equivalent to triangular tiling systems.

Definition 17 A δ -directed triangular Wang automaton $\delta(TWA)$ is a tuple $\langle \Sigma, Q, \tau, \delta, F \rangle$ where

Σ —finite input alphabet

Q —finite set of colors

$\tau : \Sigma_Q \times T \text{ dirs} \rightarrow 2^{\Sigma_Q}$ is a partial function such that the tile $\tau(A, d)$ extends A .

δ is a polite scanning strategy induced by some $\langle \eta, cor_s, d_s \rangle$ such that $\tau(A, d) \neq \phi$ implies $\gamma(\Delta_A, d) \neq \perp$.

$F \subseteq \Sigma_{3Q}$.

A triangular Wang automaton can be viewed as having a head that visits a triangular picture by moving from a position to an adjacent one and coloring at each step the edges of the position it is visiting. The elements of $\Sigma_Q \times T_{\text{dirs}}$ can be considered as states of the automaton.

For each accepting computation, the TWA produces a triangular Wang picture whose label is equal to the input picture. The movements of the head are lead by the scanning strategy δ , where as the coloring operations of automaton are determined by τ . Since triangular scanning strategy δ is polite, the automaton visits the picture positions independently of the input symbols and the choice of colors to assign to the edges is non-deterministic.

Table 1 ∇ TWA for L : δ and η stand respectively for $\delta(A, d)$ and $\eta(\Delta_A, d)$: $x, y \in Q$

A	d	δ	η	A	d	δ	η	A	d	δ	η
#		#		∇		x		∇		x	
∇	\rightarrow	∇	\searrow	x ∇	\nearrow	x ∇	\nearrow	∇	\searrow	∇	\searrow
x ∇	\searrow	x ∇	\searrow	∇	\nearrow	∇	\nearrow	x ∇	\searrow	x ∇	\searrow
x		x		x ∇	\nearrow	x ∇	\nearrow	∇	\searrow	∇	\searrow
∇	\searrow	∇	\searrow	x ∇	\nearrow	x ∇	\nearrow	∇	\searrow	∇	\searrow
x ∇	\searrow	x ∇	\searrow	∇	\nearrow	∇	\nearrow	x ∇	\searrow	x ∇	\searrow
x		x		∇	\nearrow	∇	\nearrow	∇	\searrow	∇	\searrow
∇	\searrow	∇	\searrow	∇	\nearrow	∇	\nearrow	x ∇	\searrow	x ∇	\searrow
x ∇	\searrow	x ∇	\searrow	x ∇	\nearrow	x ∇	\nearrow	∇	\searrow	∇	\searrow
x		x		∇	\nearrow	∇	\nearrow	x ∇	\searrow	x ∇	\searrow
∇	\searrow	∇	\searrow	∇	\nearrow	∇	\nearrow	∇	\searrow	∇	\searrow
x ∇	\searrow	x ∇	\searrow	∇	\nearrow	∇	\nearrow	x ∇	\searrow	x ∇	\searrow
x		x		∇	\nearrow	∇	\nearrow	∇	\searrow	∇	\searrow
∇	\searrow	∇	\searrow	∇	\nearrow	∇	\nearrow	x ∇	\searrow	x ∇	\searrow
x ∇	\searrow	x ∇	\searrow	∇	\nearrow	∇	\nearrow	∇	\searrow	∇	\searrow
x		x		∇	\nearrow	∇	\nearrow	∇	\searrow	∇	\searrow
∇	\searrow	∇	\searrow	∇	\nearrow	∇	\nearrow	∇	\searrow	∇	\searrow
x ∇	\searrow	x ∇	\searrow	∇	\nearrow	∇	\nearrow	∇	\searrow	∇	\searrow
x		x		∇	\nearrow	∇	\nearrow	∇	\searrow	∇	\searrow
∇	\searrow	∇	\searrow	∇	\nearrow	∇	\nearrow	∇	\searrow	∇	\searrow
x ∇	\searrow	x ∇	\searrow	∇	\nearrow	∇	\nearrow	∇	\searrow	∇	\searrow
x		x		∇	\nearrow	∇	\nearrow	∇	\searrow	∇	\searrow
∇	\searrow	∇	\searrow	∇	\nearrow	∇	\nearrow	∇	\searrow	∇	\searrow

More precisely the behaviour of a δ -directed TWA, $A = \langle \Sigma, Q, \tau, \delta, F \rangle$ over an input picture $p \in \Sigma^{(m,n)T}$ can be described as follows.

Configuration of TWA: $\langle conf, dr, pos \rangle$

where $conf \in \Sigma_Q^{(m,n)T}$, $dr \in T \text{ dirs}$, $pos = (i, j)$ with $1 \leq i \leq m$, $1 \leq j \leq n$.

Initial Configuration: $\langle conf_s, d_s, cor_s \rangle$

where $conf_s \in \Sigma_Q^{(m,n)T}$ is such that $\lambda(conf_s) = p$ with coloring totally undefined, except for the borders where the coloring is #.

Transition: $\langle conf, dr, pos \rangle \mapsto \langle conf', dr', pos' \rangle$ is such that

$$dr' = \eta(\Delta_{conf(pos)}, dr)$$

$$pos' = pos * dr'$$

$$conf'(pos) = \tau(conf(pos), dr)$$

$$conf'(pos * v)_{-v} = conf'(pos)_v, \forall v \in T \text{ dirs} \setminus \Delta_{conf(pos)}$$

Final Configuration: $\langle conf_F, d_F, pos_F \rangle$

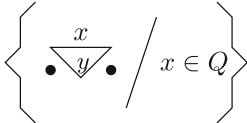
where $conf_F \in \Sigma_Q^{(m,n)T}$ and $conf_F(pos_F) \in F$.

At time $t = 0$, the head of the automaton points at the position in the starting corner cor_s and the current direction is set to d_s . At time $t > 0$, when the current direction is dr , the head is placed at position pos , the pixel and colors of borders of p at position pos are given by $conf(pos)$ and then let $dr' = \eta(\Delta_{conf(pos)}, dr)$ and $A' \in \tau(conf(pos), dr)$. Hence the automaton at time $t \geq 1$ may execute this move.

Color the borders at position pos according to A' , set the current direction to dr' , move to the position $pos * dr'$ and extend $conf$ to the triangular Wang picture $conf'$ with $conf'(pos) = A'$.

If no move is possible, TWA halts. The input triangular picture p is accepted if there is a computation such that three edges of the final position are colored according to some triangular labeled Wang tile in F .

Example 7 Consider the language L presented in Example 1 starting from the Wang system sketched in the same example, one can define an equivalent ∇ -TWA as described in Table 1. Note that $\tau(A, d)$ has atmost one element, for any A, d , so in the Table these are not represented as sets. For better readability, the table also presents the next-position function η . The set of accepting tiles is



It is interesting to note that the set of complete tiles coincides with tile-set θ of Example 1.

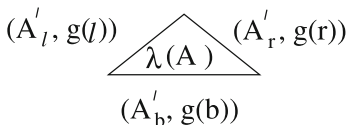
Theorem 1 For every polite triangular scanning strategy δ , we have $\mathcal{L}(\delta - TWA) = TREC$.

Proof We prove that for every polite scanning strategy δ , δ -directed Wang automata are equivalent to triangular Wang systems.

Let $T = \langle \Sigma, Q, \tau, \delta, F \rangle$ be a δ -TWA recognizing a language L . Then given $A' \in \tau(A, d)$, let $d' = \eta(\Delta_A, d)$ and for every direction y set

$$g(y) = \begin{cases} d' & \text{if } y = d' \\ d & \text{if } y = -d \\ \perp & \text{otherwise.} \end{cases}$$

If we consider the labeled triangular Wang tile $c \in \Sigma_{3(Q \times Tdirs)}$ defined by setting $\lambda(c) = \lambda(A')$ and $c_d = (A'_d, g(d))$ for any direction d . That is, c will be of the form



These labeled triangular Wang tiles C carry two information: The color C_d assigned by automaton through A'_d for the borders and the path followed by the head of the automaton, corresponding to the scanning strategy δ . For every $G \in F$,

consider all tiles $J \in \Sigma_{3(Q \times Tdirs)}$ which are like G , but exactly one edge colored with an inbound array (corresponding to current direction), while all the other edges have their second component as \perp . Let θ be the set of any such C and J . It can be easily verified that each triangular Wang picture over θ corresponds to an accepting computation of TWA. Hence L is the language generated by the triangular Wang system $W = (Q \times Tdirs, \Sigma, \theta)$.

Conversely let $W = (Q, \Sigma, \theta)$ be a triangular Wang system recognizing a language L . Then take any polite triangular scanning strategy δ and define δ -TWA. $T = \langle \Sigma, Q, \tau, \delta, F \rangle$ where F is set of all triangular Wang tiles over Q and τ is defined by setting for each direction d and partial triangular tile A :

$$\tau(A, d) = \begin{cases} \{B \in \theta/B \text{ extends } A\} & \text{if } \eta(\Delta_A, d) \neq \perp \\ \phi & \text{otherwise.} \end{cases}$$

It can be proved that the language recognized by T is L and this concludes the proof.

5 Determinism in Triangular Wang Automata

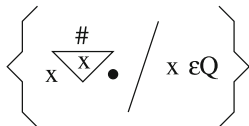
In the framework of triangular Wang automata, it is quite natural to introduce the concept of determinism.

Definition 18 A μ -TWA $\langle \Sigma, Q, \tau, \mu, F \rangle$ is deterministic if $\tau(A, d)$ has at most one element for every triangular tile $A \in \Sigma \times Q^3$ and direction d . Deterministic δ -TWA are denoted by δ -DTWA. The union of classes $\mathcal{L}(\delta$ -DTWA) over all polite scanning strategies δ is denoted by Scan-DTREC.

If τ is the transition function of δ -DTWA, we shall write $\tau(A, d) = A'$ instead of $\tau(A, d) = \{A'\}$.

Example 8 The ∇ -TWA in Example 7 is deterministic.

Example 9 Language L presented in Example 1 can be recognized also by a V-DTWA (see Table 2). The set of accepting tiles is



The first column in Table 2 is used for the outermost V, therefore going right down then left up. The second column covers internal V's following the direction right down then left up. The third column is for the other internal V's. As in Example 7 the set of complete tiles coincides with tile-set θ of Example 1.

Table 2 V-DTWA for $L : \tau$ and η stand respectively for $\tau(A, d)$ and $\eta(\Delta_A, d) : x, y \in Q$

A	d	δ	η
#		#	
# x	→	# x	x ↘
x y	↘	x y	• ↘
x		x	
# y	↘	# y	x ↘
x y	↘	x y	• ↘
x		x	
# y	↘	# y	x ↘
x y	↘	x y	x ↘
x		x	
# y	↘	# y	# ↗
x y	↗	x y	x ↗
x		x	
x y	# ↗	x y	# ↗
y	↗	• y	x ↗
x		x	
#		x	
x x	↗	x x	# ←

A	d	δ	η
#		#	
• x	→	• x	x ↘
x y	↘	x y	• ↘
x		x	
• y	↘	• y	x ↘
x y	↘	x y	• ↘
x		x	
• y	↘	• y	x ↘
x y	↘	x y	x ↘
x		x	
• y	↘	• y	• ↗
x y	↗	x y	x ↗
x		x	
x y	• ↗	x y	• ↗
y	↗	• y	x ↗
x		x	
x y	↗	x y	• ↗
x		x	
• x	↗	• x	x ↗
y	↗	y	
#		#	
x x	↗	x x	• ←

A	d	δ	η
#		#	
• x	→	• x	x ↘
x y	↘	x y	x ↘
x		x	
• y	↘	• y	• ↗
x y	↗	x y	x ↗
#		#	
x x	• ↗	x x	• ←

6 Conclusion

Triangular Wang automata can be considered as a natural model to define TREC. The scanning strategies give good alternate to the traditional diagonal strategy adopted by online tessellation automata. Since polite scanning strategies are used in TWA, the content and size of the picture is not needed which can be an eye opener for image analysis.

References

1. Anselmo, M., Giammarresi, D., Madonia, M., Restivo, A.: Unambiguous recognizable two-dimensional languages. *Theor. Inf. Appl.* **40**(2), 277–293 (2006)
2. Anselmo, M., Giammarresi, D., Madonia, M.: From determinism to non-determinism in recognizable two-dimensional languages. In: *Proceedings of the DLT 2007, Lecture Notes in Computer Science*, vol. 4588, pp. 36–47. Springer, Heidelberg (2007)
3. Anselmo, M., Giammarresi, D., Madonia, M.: Tiling automaton: a computational model for recognizable two-dimensional languages. In: *Proceedings of the CIAA 2007, Lecture Notes in Computer Science*, vol. 4783, pp. 290–302 (2007)
4. Devi Rajaselvi, V., Kalyani, T., Thomas, D.G.: Domino recognizability of triangular picture languages. *Int. J. Comput. Appl.* **57**(15), 0975–8887 (2012)
5. Inoue, K., Takanami, I.: A survey of two-dimensional automata theory. *Inf. Sci.* **55**(1–3), 99–121 (1991)
6. Kalyani, T., Dare, V.R., Thomas, D.G.: Recognizability of iso-picture languages by Wang systems. *Int. J. Imaging Syst. Technol. (Wiley Publications)* **19**, 140–145 (2009)
7. Lonati, V., Pradella, M.: Deterministic recognizability of picture languages with Wang automata. *Discrete Math. Theor. Comput. Sci.* **4**, 73–94 (2010)

Role of Information Technology in Financial Inclusion

Satya Narayan Singh, Om Prakash Dubey, Kusum Deep
and Ajay Prasad

Abstract The Indian banking sector today is stressing toward Financial Inclusion. The main reason motive is to include large population of India in the financial system of nation. This is a new avenue and a large market for banks. Where Information Technology will play an important role in reducing cost of providing banking services, particularly in the rural and the financially excluded population. The role of Information Technology can be realized from the fact that it has greater population penetration and its ability to serve at remote location at low cost which is essential requirement for Financial Inclusion.

Keywords Financial inclusion · Banks · Kiosk

S. N. Singh (✉)

Department of Information Technology, Xavier Institute of Social Service, Ranchi,
Jharkhand 834001, India
e-mail: snsinghxiss@rediffmail.com

O. P. Dubey

Department of Mathematics, Bengal College of Engineering and Technology, Durgapur,
West Bengal 713212, India
e-mail: omprakashdubeymaths@gmail.com

K. Deep

Department of Mathematics, Indian Institute of Technology, Roorkee,
Uttarakhand 247667, India
e-mail: kusumfma@iitr.ernet.in

A. Prasad

Department of Rural Management, Xavier Institute of Social Service, Ranchi,
Jharkhand 834001, India
e-mail: ajayxiss12@gmail.com

1 Introduction

The history of financial inclusion in India is actually much older than the formal adoption of the objective. The Nationalization of Banks, Lead Bank Scheme, Incorporation of Regional Rural Banks, Service Area Approach and formation of Self-Help Groups—all these were initiatives aimed at taking banking services to the masses. The brick and mortar infrastructure expanded. The number of bank branches multiplied ten-fold: from 8,000+ in 1969, when the first set of banks were nationalized, to 99,000+ today. Despite this wide network of bank branches spread across the length and breadth of the country; banking has still not reached a large section of the population [1, 2].

In mid eighties Information Technology came as enabler for the Financial Inclusion in Banking sector. Reserve Bank of India (RBI) took upon itself the task of promoting computerization in banking to improve Customer Services, Book Keeping, and Management Information System (MIS) to enhance productivity. In recent years Financial Inclusion (FI) has gained prominence in public consciousness. After observing 2005 as Year of Microfinance by United Nations (UN) and adoption of Millennium goal to reduce by half world poverty by 2015, efforts have been stepped up towards inclusive economic growth [3].

The process of ensuring access to financial services and timely and adequate credit where needed by vulnerable groups such as weaker sections and low income groups at an affordable cost.

—The Committee on Financial Inclusion [4].

To achieve the goal and process to include the excluded mass technological interventions are required to reduce cost of business, enhance business productivity.

2 Need of Information Technology for Financial Inclusion

While many public sector banks in India have launched financial inclusion initiatives, these are often due to RBI mandates rather than a desire to seize a ‘blue sky’ business opportunity. Unsurprisingly, most of these initiatives continue to remain at a pilot stage with limited impact on the ground.

While many public sector banks have undertaken major technology adoption initiatives e.g. Core Banking System implementation, other supply side stakeholders of the formal financial ecosystem including post offices, Micro Finance Institutions (MFI), Regional Rural Banks (RRB), Primary Agricultural Co-operative Society (PACS) continue to be seriously under invested in IT. Since these institutions have the primary responsibility to provide financial services to rural India, their low IT capabilities often impedes their ability to provide services efficiently and scale up their operations. Poor IT adoption also makes it difficult for

these institutions to integrate their operations with the other constituents of the financial ecosystem, both upstream and downstream.

Technology up gradation and reform could also pave the way for home banking services, especially for presently excluded mass. Apart from poverty alleviation, increasing financial inclusion may have a multiplier effect on the Indian economy. It will enable the Government to provide social development benefits and subsidies directly to the beneficiary bank accounts thereby drastically reducing leakages and pilferages in social welfare schemes and leading to a reduction in the subsidy burden. Greater financial inclusion often leads to an increase in economic prosperity which has a positive influence on inclusive growth [5].

3 Technological Developments in Banks

Development in the field of Information Technology (IT) strongly supports the growth and inclusiveness of the banking sector, thereby facilitating inclusive economic growth. The active role of RBI has enabled the integration of Information Technology in banking sector. The major Development in banking sector is:

3.1 Adoption of the Core Banking Solution (CBS)

CBS is networking of branches, which enables customers to operate their accounts and avail of banking services from any branch of the Bank on CBS network, regardless of where the customer maintains his/her account.

3.2 Growth of Automated Teller Machines (ATMs)

The banking space has seen considerable growth through the ATMs, (approximately 1,00,000 ATMs at present) but the same has been restricted principally to the urban/metro areas.

3.3 Development of National Payment Systems

The payment system could be broadly divided in two segments:

3.3.1 Paper-Based Payments

Use of paper-based instruments (like cheques, drafts etc.) account for nearly 60 % of the volume of total non-cash transactions in the country.

3.3.2 Electronic Payments

The overall thrust is to reduce the use of paper for transactions and move towards electronic mode. They are practiced under the names of Electronic Clearing Services (ECS) and National Electronic Fund Transfer (NEFT).

3.4 Pre-paid Payment Systems

Pre-paid instruments are payment instruments that facilitate purchase of goods and services against the value stored on these instruments. The pre-paid payment instruments can be issued in the form of smart cards, magnetic stripe cards, internet accounts, internet wallets, mobile accounts, mobile wallets, paper vouchers, etc.

3.5 Point of Sale (POS) Terminals/Online Transactions

There are over five lakh POS terminals in the country, which enable customers to make payments for purchases of goods and services by means of credit/debit cards [1].

Any of above technological development can't serve the purpose alone for Financial Inclusion, until adopted in any model.

4 Model Adopted by Banks for Financial Inclusion

The models adopted for FI by banks can be in the form of Branch Network, Business Correspondent/Business Facilitator model (BC/BF model) and Micro Finance Institutions. In their pursuit for achieving FI, novel initiatives like Banking on wheels an tools of technology like mobile, internet kiosk play a vital role. As these technological intervention helps to overcome barriers like distance of branch, location of customers, availability of information and literacy of the customer. With an objective of providing a viable and cost effective banking service at the door step of the financially excluded group banks in India have adopted a branchless banking model called Customer Service Points (CSPs) which

are manned by Business Correspondents (BCs). The CSPs are low cost and technology enabled alternate delivery channel that facilitate basic banking services to the rural communities, at their door step at an affordable cost [6, 7].

Two different technology enabled financial inclusion models were analyzed:

4.1 Point of Scale (POS)

A Point of Scale a smart model is a branchless banking model which facilitates opening of accounts and financial transactions. A Smart Card is a wallet sized card with an electronic chip designed to store information relating to the customer. A POS is a device with the CSPs, capable of reading a smart card. National level BCs like FINO (Financial Inclusion Network and operations) and ZMF (Zero Mass Foundation) are leading service providers of this integrated technology platform to enable sourcing and servicing of customers under FI.

Hardware requirements are Mobile phone with Public Key Infrastructure (PKI) security, POS with fingerprint scanner and printer. Smart Card with magnetic strip (contact card) or smart card with Radio Frequency Identification (RFID) also called as a contact-less card, alternatively a plain plastic card without any magnetic strip.

The mobile phone acts as a core bank branch and capable of storing up to 50,000 customer account details like complete customer ID, photograph, 4 or 6 finger print each, multiple account types and 5 years of transaction history for multiple transaction types. The system can work both online and offline and synchronization with their data server happens using GPRS. The system has up to 2 GB memory to store offline transactions. There is provision of voice prompts and local language voice over during transaction or enrollment. Transactions require the biometrics of the customer and the operator present at the CSP [8].

4.2 Kiosk Banking Model

Stationary locations at remote places enroll and services customer through internet accessing the customer accounts on core banking platform of the bank.

The service provider are social enterprise like Geosansar, Oxygen Services India Pvt. Ltd., and other Individual BCs who do not have their own technology or technology partners are the front end services providers called Kiosk Operators (KOs) at the CSPs. There is no outside technology vendor for Kiosk banking channel. The technology has been developed in house. The front end kiosk operation is integrated with 24 x 7 CBS data centers. The system requirement for functioning is a simple PC with web camera/digital camera and the speakers, Internet connectivity, Finger print scanner and Printer [9].

5 Analysis

5.1 Discontinuation of RFID Cards/Card with Memories

Though the thought of having transaction detail and the account status with oneself was good idea but this technical move was not practical in a country where the technology of developing the card was not developed.

Hence plain cards were introduced having few numbers (like ZSN) which could be used to retrieve data from the data base. Unlike RFID its maintenance and issue does not cost more than Rs. 15 where it varied from Rs. 80 to 250 and time to reissue is time consuming.

5.2 Interoperability Between the Correspondent Serving Same Branches is not Possible in POS Model

The customer enrolled by one correspondent can make transaction with other correspondent of any bank if interoperability is possible through the common gateway. Though the pilot is successfully launched by State Bank of India in Mewat district of Haryana state. It may take some time to be implemented in full spirit. Difference in structure is shown in Fig. 1.

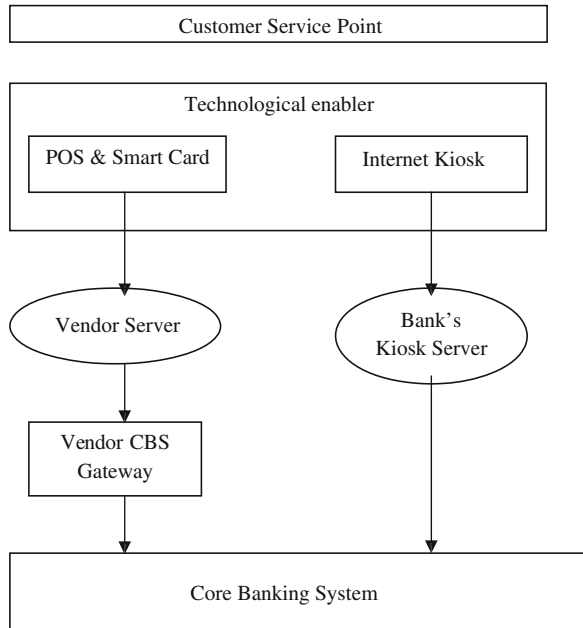
5.3 The Possibility of Fraud While Enrolment

This possibility can be sensed in spite of the secure biometric data. This fraud can be performed while enrolling the customer and while taking the finger print of the customer. By distracting the customer there is chance that the agent may get his finger scanned. This will make him the owner of the account. As a result he could withdraw or transfer money from the account. This shows a need to connect the banking operation with Aadhaar data base for secure transaction and providing a document for the identity of the excluded mass.

The above mentioned issues shows that the FI in India required to be implemented with more rigorous tests on the field making, it viable to provide an efficient structure.

Study conducted on the field showed the models strength and weakness stressing upon the point that there cannot be generalized model for implementation of FI but this possibility to initiate the Financial Inclusion is possible due to Information Technological implementation. It requires refinement for ever increasing customer base and upcoming challenges in terms of cyber threats keeping in mind the practicability of technology used for its expansion.

Fig. 1 Structure of POS and Kiosk model



6 Conclusion

Technology is the final element of financial inclusion strategy and an enabler. The choice of technology driven models is crucial decision, which could make or merge the inclusion plan. Since these services have to be provided at zero or minimal charge to the customer, banks need to lower their own cost of customer acquisition and maintenance to make this a profitable proposition. In this backdrop, financial inclusion calls for intelligent selection of a mix of business models and technology, for successful implementation of Financial Inclusion Plan.

In future the number of customer will be increasing and for the security and customer protection the database should be well protected to prevent the agents to give the biometric twice to avoid any fraud by the BC agents.

References

1. Gupta, S.K.: Financial inclusion—IT as enabler. http://www.rbi.org.in/scripts/bs_viewcontent.aspx?Id=2598
2. <http://www.rbi.org.in>
3. Khan, H.R.: Issues and challenges in financial inclusion: policies, partnerships, process and products. RBI Monthly Bulletin LXVI (8), 1447–1457 (Aug 2012)
4. Rangarajan, C.: “Report of the committee on Financial Inclusion”, (Jan 2008)

5. Rajdeep, S.: “Financial Inclusion—From Obligation to opportunity”, Tata Consultancy Services (2010)
6. Chakrabarty, K. C.: The first mile walk into financial inclusion—thinking differently. RBI Monthly Bulletin LXVI (9), 1585–1588 (Sep 2012)
7. Chakrabarty, K. C.: Financial inclusion of urban poor in INDIA. RBI Monthly Bulletin LXVII (2), 115–122 (Feb 2013)
8. Financial Inclusion: SBIRD reading material, 34–35, (Dec 2012)
9. Financial Inclusion: SBIRD reading material, 39–40, (Dec 2012)

Harmony Search Based Algorithm for Complete Information Equilibrium in Infinite Game

Riccardo Alberti and Atulya K. Nagar

Abstract In this paper we discuss and analyse a novel algorithm for the computation of approximated Nash equilibrium points in the class of infinite games with complete information. In particular we compare an established algorithm based on the principles of simulated annealing (SA) with our implementation which is a hybrid combination of SA and the basic Harmony Search algorithm. We study the method in the class of *positional games* which is a subset of the class of continuous games and it is a model for economic goods allocation in the presence of externalities. We show that our hybrid method converges to an equilibrium point faster than the plain SA algorithm though the accuracy of the solutions is slightly higher.

Keywords Computational game theory · Harmony search · Simulated annealing · Nash equilibrium · Best response · Regret function

1 Introduction

In the most general terms, game theory is a mathematical apparatus designed to analyse the strategic interactions of rational players. The basic assumption is that decision-makers pursue individual objectives taking into consideration the expectations of other participants. In this work we focus our attention on strategic non-cooperative continuous games with a finite number of players. A game is

R. Alberti (✉) · A. K. Nagar
Department of Mathematics and Computer Science, Liverpool Hope University,
Liverpool L16 9JD, UK
e-mail: 11002767@hope.ac.uk

A. K. Nagar
e-mail: nagara@hope.ac.uk

defined by the tuple $G = (\Sigma, u, I)$ where $\Sigma = \times_{i \in I} \Sigma_i$ is a compact set (every Σ_i is compact) and represents the set of joint pure strategies, u is the set of utility functions (i.e. $u_i, \forall i \in I$) which we consider to be continuous and concave and, I is the finite set of players. A solution of the game is defined as $\sigma^* = (\sigma_1^*, \dots, \sigma_I^*)$ such that $\forall i \in I u_i(\sigma_i^*, \sigma_{-i}^*) \geq u_i(\sigma_i, \sigma_{-i}^*)$. As usual we use the notation σ_{-i} to indicate the strategies of all players except for player i . This is the definition of Nash equilibrium. In words a Nash equilibrium is *a point in the joint strategy set where no player can increase her payoff by unilaterally deviate from the equilibrium strategy while the others don't*. In the original proof of existence, given by Nash in [1], the author employs the concept of best reponse (BR). BR is a correspondence that produces a subset of maximisers of i 's utility function when other players play some joint strategy σ_{-i} . Therefore a Nash equilibrium can be defined as the fixed point of the cartesian product, over the set of player I , of the BR correspondences. Eventually, another concept that we are goin to extensively use in this work, is that of regret function. The regret function is a measure that gives the maximum benefit any agent can gain by unilateral deviation. Formally it is defined as $\varepsilon(\sigma) = \max_{i \in I} \max_{a \in \Sigma_i} [u_i(a, \sigma_{-i}) - u_i(\sigma)]$. In this light a Nash equilibrium is the point that minimise the regret function. Calculating a Nash equilibrium is in the class of PPAD complexity. Though many tools that compute solutions exist, few approximation tools for any general class of infinite games are present. In this work we study a variation of the work proposed in [2] substituting a part of the proposed Simulated Annealing based algorithm with a Harmony Search algorithm. In the experimental part of this work we calculate the approximate solution to games in a class of continuous games that describe an economic model in the presence of externalities. We show that our implementation though might slightly lose in accuracy of the approximation, it gains in convergence speed.

The remainder of this paper is structured as follows.

Section 2 revises the method proposed by [2] and present a simplified version of the algorithm to be applied to continuous games of complete information. In Sects. 3 and 4 we present our implementation and discuss the results of the simulations. Eventually in Sect. 5 we draw the conclusion of our work and propose future directions of research.

2 Simulated Annealing

Simulated Annealing (SA) is a technique that has attracted significant attention as suitable for optimization problems of large scale, especially ones where a desired global extremum is hidden among many local extrema [3]. It mimics the physical process of annealing of metals whereby metals cool and anneal. At high temperatures, the molecules of a liquid move freely with respect to one another. If the liquid is cooled slowly, thermal mobility is lost. The atoms are often able to line themselves up and form a pure crystal that is completely ordered. This crystal is the state of minimum energy for this system. For slowly cooled systems, nature is

able to find this minimum energy state. The general setting of the method is summarised as follow:

- a real valued function F defined over a finite set D (let us assume that F has many global minima);
- for each $d \in D$ a set $N(d) \subset D$ containing all the neighbours of d ;
- a function $T : \mathcal{N} \rightarrow (0, \infty)$, the cooling schedule, that is coupled with the cooling rate T_r ;
- $d_0 \in D$ as a starting point;

The algorithm evolves as a discrete-time inhomogeneous Markov chain using a peculiar update rule. The acceptance/update condition is mutated by another physical observation. Even at low temperature, there is a chance, of a system being in a high energy state, thus the system moves, with some probability, to a higher energy state to get out of a local energy minimum in favor of finding a global one. The update condition has been defined by Metropolis in [4] and represents the probability of accepting a new energy state value as: $p = \exp[-(E_2 - E_1)/kT]$, where k is a natural constant (Boltzman), E_2 is the new energy value and E_1 is the current minimum.

In [2] a globally convergent SA based algorithm for finding an approximated Nash equilibrium is described. The method consists of two routines: one for the computation of the approximated best response for each player and the other for the minimisation of the joint regret function. A simplified version for continuous games with complete information is summarised here.

Approximated best response (SABR). For each player this routine is described by four steps:

1. consider an initial point $d_{k,i} \in D_i$;
2. choose a neighbour point $d_{k+1,i} \in N(d_{k,i})$ using a truncated normal distribution within i 's strategy boundaries;
3. evaluate the utility function for the current player in $d_{k+1,i}$ and $d_{k,i}$;
4. update the response using the Metropolis Acceptance (MA) rule;

The parameters used by the SABR routine are as in Table 1

Approximated equilibrium calculator (SAEC + SABR). For each tick of the cooling schedule this routine performs the following actions:

1. consider an initial point $d_k \in D$;
2. choose a neighbour point $d_{k+1} \in N(d_k)$ using a truncated normal distribution within the joint strategy boundaries;
3. calculate the maximum regret function as $\bar{\epsilon} = \max_i \{u_i(SABR(d_{k,i}), d_{k,-i}) - u_i(d_k)\}$;
4. update the regret counter using the Metropolis Acceptance (MA) rule;

The parameters used in the routine are summarised in Table 2.

Table 1 Simulated annealing parameters for SABR

Parameter	Value
F	u_i
D	Σ_i
T	1000
T_r	1.05
MA	$exp((u_i(d_{k+1,i}, d_{k,i}) - u_i(d_k))/t)$
$d_{0,i}$	random from D

Table 2 Simulated annealing parameters for SAEC

Parameter	Value
F	$SABR_i$
D	Σ
T	1000
T_r	1.05
MA	$exp((\bar{e}(d_k) - \bar{e}(d_{k+1}))/t)$
d_0	random from D

In the Sect. 3 we introduce our contribution which is based on the application of the Harmony Search algorithm.

3 Harmony Search

The HS algorithm was inspired by the improvisation process of musicians. When the musicians compose harmony, they usually try various possible combinations of the musical pitches stored in their memory [5]. The search for a perfect state of harmony is analogous to the procedure for finding the optimal solutions to engineering problems. It has been shown that HS outperforms various optimization methods in many optimization problems. One of key success factors of the algorithm is the employment of a novel stochastic derivative which can be used even for discrete variables. Instead of traditional calculus-based gradient, the algorithm utilizes musicians experience as a derivative in searching for an optimal solution. The Harmony Search (HS) algorithm combines features of others heuristic optimization methods. It preserves the history of past vectors similar to Tabu Search (TS) and ability to vary the adaptation rate as Simulated Annealing (SA). Furthermore, HS manages several vectors simultaneously in the process similarly to the Genetic Algorithm (GA). However, the major difference between GA and HS is that HS makes a new vector from all existing vectors and can independently consider each component variable in a vector, while GA utilizes only two of the existing vectors and keep the structure of gene [6]. The general parameters of the algorithm are:

Table 3 Values of the parameters HSBR

Parameter	Value
HMS	30
HMCR	0.9
PAR	0.3
MI	1000
FW	$\frac{d_u - d_l}{1000}$

- HMS harmony memory size: number of solution vectors simultaneously handled by the algorithm;
- HMCR harmony memory considering rate: is the rate ($0 \leq HMCR \leq 1$) where HS picks one value randomly from musicians memory;
- PAR pitch adjusting rate: PAR ($0 \leq PAR \leq 1$) is the rate where HS tweaks the value which was originally picked from memory;
- MI maximum improvisation: is the number of iterations;
- FW is arbitrary the amount of maximum change in pitch adjustment;

In this work we utilise such algorithm to design an alternative approximated best response (HSBR). We will incorporate our routine in the SAEC described above. In words, given a joint strategy of i 's opponents, the routine is able to determine the best response like a musician is able to determine his best contribution to the harmony produced by the rest of the orchestra.

Approximated best response (HSBR). For each player this routine is described by five steps:

- consider an initial point $d_{k,i} \in D_i$;
- initialise HM with random values taken from a uniform distribution within i 's strategy boundaries (i.e. d_u for the upper bound and d_l for the lower bound);
- if a strategy from HM is selected (HMCR) then adjust pitch (PAR) using a uniform distribution $\mathcal{U}(0, 1)$. Generate new strategy o.w;
- update HM replacing worst strategy with strategy generated;
- find best strategy in HM;

The parameters used in the routine are summarised in Table 3.

In our implementation we utilise a fixed set of values for the parameters. As anticipated the routine just described is integrated withing the SAEC routine described in the Sect. 2 substituting the original SABR routine. This constitutes an hybrid HS + SA search algorithm for the calculation of approximated Nash equilibria in continuous games with perfect information. Such modification will result in the following change in the SAEC sequence; in fact step 3. of SAEC is replaced by the following:

Calculate the maximum regret function as $\bar{e} = \max_i \{u_i(HSBR(d_{k,i}), d_{k,-i}) - u_i(d_k)\}$.

In the Sect. 4 we compare the two methods.

4 Simulation and Results

Our simulation considers a set of continuous games derived from the study of an economic model of competition in the presence of externalities. Such model generates a class called: positional non-cooperative games. In such model every player possesses a utility function defined as:

$$\delta_i(\sigma, \pi) = \frac{q_i^\pi(\sigma)}{\sum_{j \in N} q_j^\pi(\sigma)} \sum_{j \in N} q_j(\sigma) \quad (1)$$

where as usual $\sigma \in \Sigma$ is a point in the joint strategy set, the q_i s are convex functions that indicate the level of absolute consumption of a particular good and N is the number of players. Eventually π is the positionality index which indicates the *social-status* signalling capabilities of the good at stake [7]. We do not discuss the details of the economic model here. For the scope of this paper it is sufficient to know that the δ_i s are continuous and quasi-concave functions and hence every game defined as $G = (\Sigma, \delta(\sigma, \pi), I)$ has a Nash equilibrium in pure strategies.

We proceed by generating 30 games with random values for the q_i s and π s and calculating an approximate Nash equilibrium of each game. In particular we focus our attention on three performance indices:

1. the values of the maximum regret function $\bar{\epsilon}$ at equilibrium;
2. the absolute number of iteration required by the algorithm to converge to an equilibrium point (Convergence Speed);
3. the relative convergence speed (RCS) as the ratio between the number of iteration required to converge to an equilibrium point and the total number of iteration;

In Fig. 1 we report the comparison between the maximum regret function calculated with the SABR and HSBR. This measure provides an insight on the accuracy of the approximated solution. The closer to 0 the closer to the real equilibrium point. As we can see the simulated annealing based algorithm has the lowest maximum regret function. The mean (-0.0157) of the regret maximum regret function calculated by the harmony search based best response is still close to 0 but the suboptimality is evident from Fig. 1.

Though the approximations provided by our algorithm is inferior to the SA based algorithm, our implementation converges faster to the equilibrium point as one can appreciate from Fig. 2. In particular in 20 cases out of 30 (66 %) our algorithm converges faster than the implementation described in [2].

Eventually if we consider the number of steps required to converge to an equilibrium with respect to the total number of computation steps, our implementation still outperforms the simulated annealing version. In Fig. 3 the performances against this statistic is presented. In this case only 50 % of the times our implementation finds the equilibrium point faster (with respect to the previous analysis) than the SA algorithm.

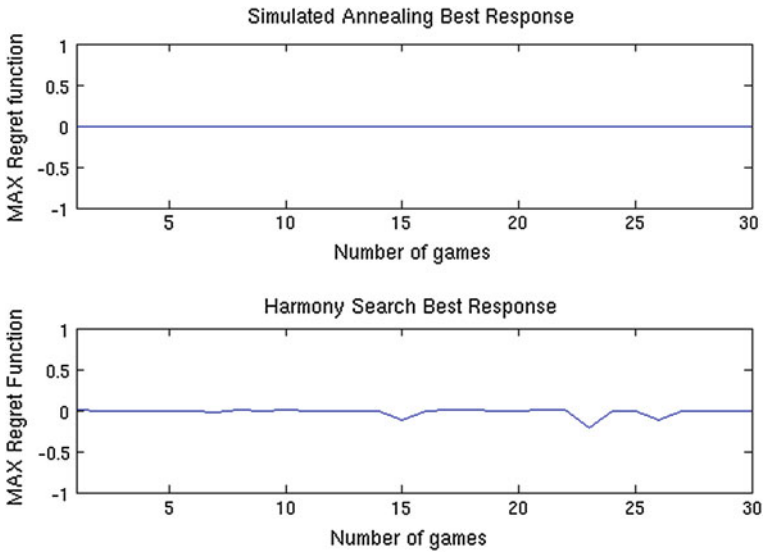


Fig. 1 Maximum regret function

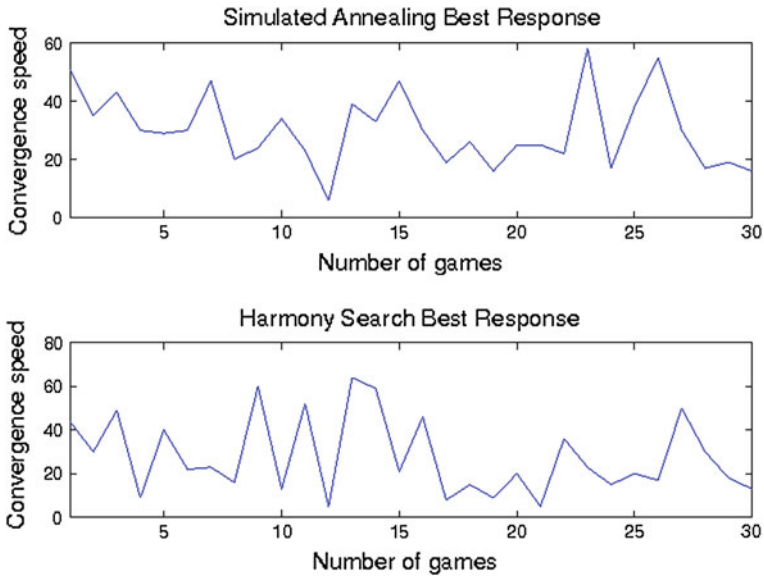


Fig. 2 Convergence speed

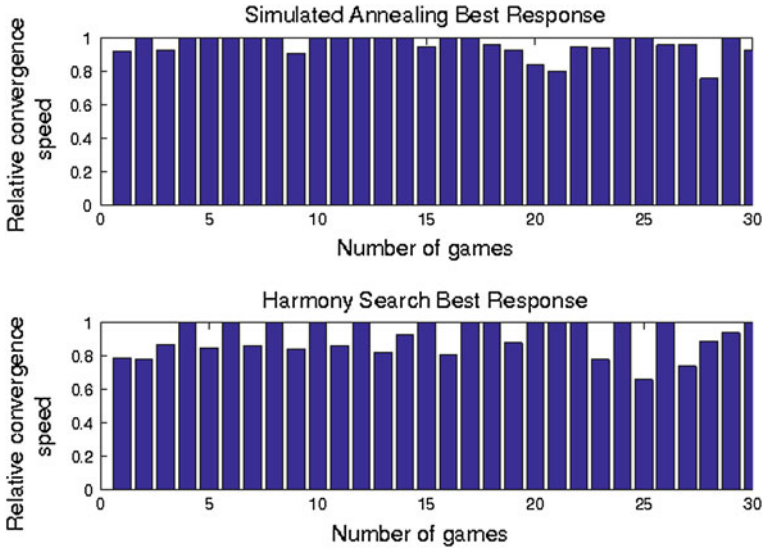


Fig. 3 Relative convergence speed

In the Sect. 5 we draw the conclusion of this work and we provide some future research directions.

5 Conclusions

In this work we have exploited the analogy between the behaviour of a rational agent that finds the best response to her opponents' strategies and that of a jazz musician that tries to find the perfect harmony to be *in tune* with the overall harmony played through a process of improvisation and improvement. We have shown that the HSBR converges faster to an equilibrium than the corresponding routine based on simulated annealing, with the cost of loosing a small fraction of accuracy in the solution. Future works will be in the direction of using a dynamic tuning for the HS parameters in order to reduce the inaccuracy but maintaining the CS. Another research direction is to consider the implementation of HS to the main routine (SAEC) in order to build a complete approximated Nash equilibrium calculator based on the harmony search approach.

References

1. Nash, J.F.: Equilibrium points in n-person games. *PNAS* **36**(1), 48–49 (1950)
2. Vorobeychik, Y., Wellman, M.P.: Stochastic search methods for Nash equilibrium approximation in simulation-based games. In: *Proceedings of 7th International Conference on Autonomous Agents and Multiagent Systems*, pp. 1055–1062 (2008)
3. Bertsimas, D., Tsitsiklis, J.: Simulated annealing. *Stat. Sci.* **8**(1), 10–15 (1993)
4. Press, W.H., Teukolsky, S.A., Vetterling, W.T., Flannery, B.P.: Simulated annealing methods (Chap. 10). In: *Numerical Recipes in C: The Art of Scientific Computing*. Cambridge University, Cambridge (1988)
5. Woo Geem, Z.: State-of-the-Art in the structure of harmony search algorithm (Chap. 1). *Recent Advances in Harmony Search Algorithm*. Springer, Heidelberg (2010)
6. Tangpattanakul, P., Meesomboon, A., Artrit, P.: Optimal trajectory of robot manipulator using harmony search algorithms (Chap. 3). *Recent Advances in Harmony Search Algorithm*. Springer, Heidelberg (2010)
7. Ball, S., Eckel, C.C., Grossman, P.J., Zame, W.: Veblen effects in a theory of conspicuous consumption. *Quart. J. Econ.* **116**(1), 161–188 (2001)

A Proposed Architecture for Efficient Data Delivery and Route Maintenance in a Sparsely Deployed Mobile Ad Hoc Network

Monit Kapoor and Manish Prateek

Abstract Mobile ad hoc networks have seen tremendous research being carried out looking into various issues in the area of routing, disruption tolerance and mobility control amongst other issues. MANET has a typical environment and in many works MANET is not treated as a case of infrastructureless network. This work aims to treat Ad Hoc networks differently than a Wireless Infrastructure Network. This work also aims at proposing a framework for route maintenance of a network of any size in case of sparsely deployed topologies and maintain the mobility of all the nodes to the advantage of the participating nodes.

Keywords Mobile ad hoc networks · Mobility management · IEEE 802.11 standards · Sparse node · Delay tolerant networks

1 Introduction

Mobile Ad Hoc Networks (MANET) are a collection of self-configuring mobile nodes which combine arbitrarily in any topology so that basic functions of a network are carried out and network is up for the duration of time for which it was established. MANETs are characterized by random mobility of nodes, frequent disruption in connectivity and limitation of resources such as buffer, battery back-up etc. and most importantly lack of infrastructure or backbone [1]. Each node in a MANET can perform network function of Packet forwarding and thus each node is

M. Kapoor (✉) · M. Prateek
Department of CSE, Centre for IT, University of Petroleum and Energy Studies,
Dehardun, India
e-mail: mkapoor@ddn.upes.ac.in

M. Prateek
e-mail: mprateek@ddn.upes.ac.in

acting like a Router, hence at each node route maintenance activity has to be carried out. Participating nodes in a MANET communicate with other nodes in the network through 802.11 MAC Layer [2]. They can be found as STA (Stations) which are part of IBSS (Independent Basic Service Set) in IEEE standards. A Collection of interacting IBSSs' is represented as Mobile ad-hoc network where the Basic Service set functionality is without any backbone as illustrated in Fig. 1 ahead in this article.

Ad-hoc networks have been named like this as they are created on the go mostly without any prior planning and they are deployed for dealing with emergency situations mostly, like battlefields, or natural disaster sites earthquake and other natural calamities etc. These networks are operative for only as long as they are needed. In emergency situations like mentioned the network partitions can last long because thick deployment of nodes shall not be done and hence the main challenges in our view shall be efficient data delivery in sparse deployment, optimal usage of resources of node. However, it has been seen over a period of time that commercially Ad Hoc network have not been in use as much as in above mentioned scenarios.

Many articles [3–5] have been dealing with a high node density scenario there by proposing protocols such as DSR, DSDV and AODV. These protocols aim to solve problems of typically “connected networks”. A connected network would be one in which node density in the network deployment area is relatively high.

Some of articles go on to indicate TCP traffic [6, 7] in a MANET which is in clear opposite to what has been proposed in 802.11 standards where as we can see in Fig. 1. Stations are part of basic service set and interacting BSS's combine to form an Ad hoc network. Since there is no portal involved here as is seen in [2] in case of wireless infrastructure network hence it can be safely concluded that Ad Hoc networks are a case of a infrastructureless network and TCP traffic can't be a characteristic of Ad Hoc networks. Hence Ad hoc network looks more suited to conditions mentioned in Delay Tolerant Networks at [8], a separate research group is working on node mobility management, data buffering amongst others.

Rest of the paper is organized as follows. Section 2 briefly discuss about various issues that concern us in design of routing protocol for Mobile Ad Hoc network. Section 3 is about related works in the area of MANET and Delay Tolerant Network environment and their co relation. Section 4 mentions about existing drawbacks in the related works. Section 5 contains description about concept of remoteness and mobility management. Section 6 provides the protocol design and framework and Sect. 7 is the conclusion section.

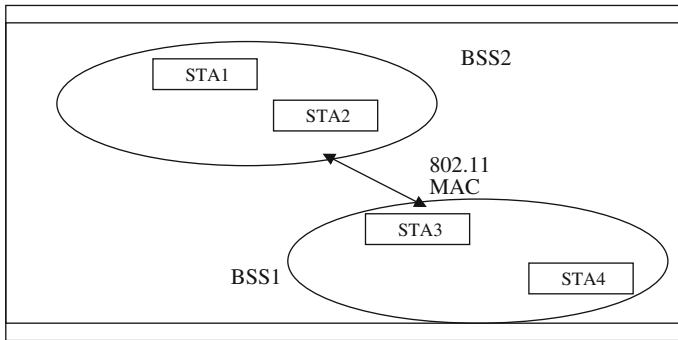


Fig. 1 IBSS as ad hoc network (Source 802.11 standards)

2 Design Issues

The identified issues in design of a routing protocol are:

- A. **Route Entries at a node:** MANET nodes are constantly moving in random direction and due to changing topology paths keep on varying and it is needed to maintain the route entries on the move. Lack of infrastructure increases the need of accurate network mapping all the time so that network function is not hampered. But doing so should be with minimum overhead.
- B. **Mobility:** Nodes are mobile and this mobility can be put to use so as the network becomes self-organizing and stable over a period of time. Mobility control again relies on network mapping at each node but is constrained by limited battery power. Inclusion of extra control information in data packets for the purpose of self-organization shall cause faster depletion of battery and has to be optimized.
- C. **Limited resources availability:** Mobile Nodes have finite battery power and limited buffer and processing capacity. Any processing overhead would result in faster consumption of battery and any increase in battery or buffer at node would lead to loss of free mobility as payload of nodes will increase.

3 Related Works

Sparse node problem has been treated by deploying ferrying techniques in [9]. Message ferrying approach deploys set of special nodes called message ferries that exploits mobility to decrease delays. OPWP technique also uses this kind of approach in [10] where ferry nodes rather than being mobile all the time show controlled mobility around, optimized waypoints. Another technique which is very similar to [9, 10], uses data mules which are moved into a sensor field to facilitate

traffic in a wireless sensor network [11], in which sensor field has a sparse deployment of nodes. Sensor nodes are pinned at one location and data mules act as carriers of information available at sensor nodes which are stationary. Ferry Access Points (FAPS) propose in [12] sticky transfers as a method to improve communication in DTN. In this node to ferry contact as and when it happens will lead to creation of a long duration contact resulting transfer of complete data. But, natural node movement is controlled during this sticky contact. Another approach is in [13] where throwboxes have been suggested in DTNs having mobile nodes so that larger contact opportunities are created and these throwboxes are present at advantage location provide routing and buffering.

In [14] DTN routing schemes are classified as deterministic, enforced and opportunistic. Deterministic routing schemes are used when a priori information about traffic demand and contact is known. Enforced Routing schemes deploy special purpose nodes to provide connectivity as already discussed in [9–13]. Enforced routing techniques also require beforehand information about design of routes or locations for placing throwboxes to facilitate traffic. Opportunistic routing schemes use flooding mechanism where multiple copies of each message is flooded in the network as provided in epidemic routing [15]. As proposed in [16] the approach aims to better [15] by limiting multiple copies being sent to next hops for better resource utilization. Another technique is proposed in spray and wait [17] in which replication of messages is present in network but the concern that how many messages stay replicated is again a concern and it is stated in [17] that source can't decide how many copies of message can stay in network. ASBIT [18] is a recent technique that identifies the significance of time intervals between two exchanges and it utilizes the same interval to predict the number of inter node contacts within the estimated delivery and delay therein. In [19] the authors provide mechanism to source packets from nodes to a node as compared to node to a base station in DSG routing where traffic is sent from a node to a base station, a sensor node and deploys distributed caching. DSG-N² routing identifies social grouping among nodes based on contact patterns between nodes.

4 Observations to Related Works

These are:

1. Special nodes are made to travel in network and in event of failure of ferry node, data mule in [9, 11] the network operation would fail. Moreover in [11] the technique suggested is for specific case for wireless sensor networks. However, the concept that some node has to act as ferry is supported.
2. In [10] ferries stop at OPWP and wait for business nodes to come at some point in network run time to offload nodes' buffer. This waiting for nodes contributes to delay.

3. In [12] mobility of nodes is governed by movement of ferries only during contact time between ferry node and network node. This is a scenario to be replicated during entire duration of network but without ferry nodes, and only for duration of node to node to data transfer.
4. In [14] throwboxes are stationary ferries that occur to contact within the travel of a node, hence the node that facilitates traffic is stationary and offloads data on nodes by assuming that node is travelling in direction of destination specific traffic acquired by throwbox. Hence, throwbox technique is again waiting for favorable node to arrive.
5. Approaches provided in [16, 17] work on concept of multiple sends and in a sparse node deployment this flooding or controlled flooding is highly taxing on resources of mobile nodes and seems improbable too.
6. In [18] it overcomes the disadvantages of [17] by utilizing the inter contact delay and it is aimed to use this significant inter-contact time for network restoration.
7. In [19] the network is managed by caching at base stations as well node to node transfers on type of request basis which suggest that it is not a case of sparsely deployed network whereas DTN environment is a typical case of sparsely deployed topology.

5 Concept of Remoteness and Mobility Management

A node can be considered a transceiver with a range around it in a circular area with node acting as radial point. The range of transmission for a node is equal to radius of the circle. This imaginary circle moves along with node's random movement. Since Ad hoc network will have node to node communication it means that receiver node has to be inside the circle of sending node for the duration of transfer. A remote node would be one that is outside the range of the broadcasting node and a node at relatively larger distance would be more remote to another node that is relatively nearer but still outside the range of the node.

Also, there can be scenario where node would be moving into the circle in the direction of center of the circle. In this scenario the node has to stop after coming inside the circle. This effort of controlling the receiver position inside the broadcasting node's transmission range would be called as mobility management.

Here BSS1 has one node in it and the node in BSS3 is remote node for BSS1. For BSS2 the node on outside boundary is to be stopped and node has to be brought in after it reaches the boundary perimeter.

The following illustration will explain this concept of node mobility management (refer (Fig. 2)).

Let R be the radius of circle of Transmission range and there be defined a threshold distance D_{th1} which is equal to R , i.e. $D_{th1} = R$.

Now $\exists Y \in Y_k$ s.t. $|Y_k - Y_0| = Y_{dis}$ and $\exists X \in X_k$ s.t. $|X_k - X_0| = X_{dis}$.

Therefore,

$$\sqrt{(Y_{\text{dis}})^2 + (X_{\text{dis}})^2} = R = D_{\text{th}1} \quad (1)$$

Let us maximum displacement threshold for any node at any location within the range is 90 % of R and minimum displacement threshold for node be 20 % of R. This can be put in inequalities 2 and 3 as below.

$$\sqrt{(Y_{\text{dis}})^2 + (X_{\text{dis}})^2} < = 0.9R \quad (2)$$

$$\sqrt{(Y_{\text{dis}})^2 + (X_{\text{dis}})^2} > = 0.2R \quad (3)$$

We shall term this as snoop location test that each node will do for its master node to get its coordinates as given by inequality 4 as under.

$$0.2R < = \sqrt{(Y_{\text{dis}})^2 + (X_{\text{dis}})^2} < = 0.9R \quad (4)$$

If the condition is violated, the node shall reset its path to align with the master node and shall keep on doing so, till the next agreed time interval when One Hop Packets are broadcast and network topology is available afresh.

6 Protocol Design and Framework

In this section, the workflow of the algorithm is described on the basis of the following assumptions derived out of favorable scenarios in previous section.

- a. Network is sparsely deployed and here we model network for 4 nodes only.
- b. We assume that all nodes are aware of maximum network size which is 4 in this case.
- c. Nodes broadcast to other nodes there one hop neighbor information after fixed interval of time and network activity is suspended during this time interval.
- d. All nodes enter the network simultaneously and if any node is entering after some time the network has started functioning it will not straight way look to connect to some neighbor, though it will be listening to its neighbors if any. It will have to wait for time interval when one hop neighbor is being broadcast by its neighbor.

Algorithm: Since the network size is 4 and node are enumerated in given set $N_i = \{n_1, n_2, n_3, n_4\}$. Each node shall maintain a 3×4 Stack of Booleans 1-D matrix for route maintenance, which is to be maintained at each node. Each row of stack matrix shall signify as nth hop entries where each column represents node ϵN_i .

Tables 1 and 2 are route maintenance matrices for nodes, n_1 and n_2 , where column are indicative of n_1, n_2, n_3, n_4 and rows are indicative of 1 hop neighbor, 2 hop neighbor and 3 hop neighbor. If any entry in table is 1 it means that

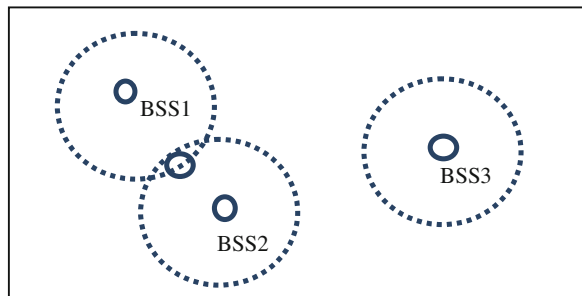
Table 1 Route Maintenance Entries in routing table for node n1

Hop no	Node1	Node 2	Node 3	Node 4
1-hop	0	1	0	0
2-hop	0	0	1	0
3-hop	0	0	0	1

Table 2 Route maintenance entries in routing table for node n2

1	0	1	0
0	0	0	1
0	0	0	0

Fig. 2 Scenario depicting remote nodes and nodes within the transmission range



corresponding node is a neighbor and row no will tell if it is 1-hop, 2-hop or 3-hop neighbor.

The entries in shaded part of Table 1 represent the presence of neighbor at a particular hop distance. From here onwards, only shaded portion of Table 1 is reproduced under different scenarios and significance of row and columns remains same.

Then, image of network for node n1 is in Fig. 2, and we assume nodes moves in direction of arrow. Let below be called Scenario A.

Zeros in last row of matrix for n2 signify that there is no three hop neighbor for node 2. Also it can be seen that same network image is available at node n1 and n2.

Let the below be called scenario B shown in Fig. 3 when nodes have moved to enter a new topology (Fig. 4).

Now the matrix for node n1 and n2 for Scenario B is in Tables 3 and 4 respectively (Fig. 5).

Here it can be seen that n2, n3 and n4 are connected in a looping topology and hence which route to be followed is not clear if say data is to be sent from 1 to 4 (Table 5).

Fig. 3 Node at center with threshold radials

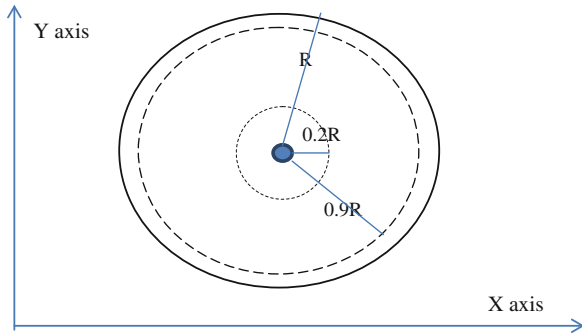


Fig. 4 Scenario A

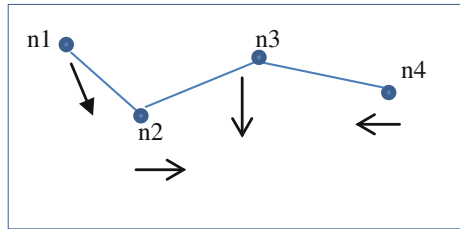


Table 3 Route maintenance entries in routing table for node n1

0	1	0	0
0	0	1	1
0	0	1	1

Table 4 Route maintenance entries in routing table for node n2

1	0	1	1
0	0	1	1
0	0	0	0

Fig. 5 Scenario B

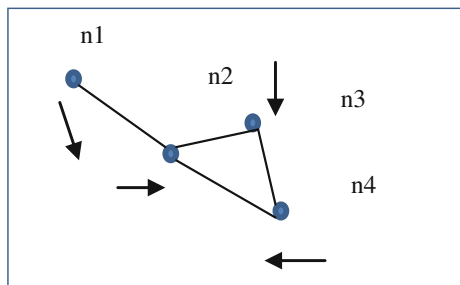


Table 5 Notations used in algorithm

Notation used	Description
RH(n)	nth hop information bits framed in size 4 bit
NS(n)	nth node's RH(n)s Stack Array of size $(n-1 \times n)$ for complete route information
AN(n)	Stack for node n for scenario A
BN(n)	Stack for node n for scenario B
RST, NR	Resetted operation, not resetted operation

So, the following algorithm is proposed.

- Step 1. Node $n \in N_i$ transmits one hop packet containing 4-bit RH(n) frame along with Control information to each one hop neighbor during the interval already known to all nodes. All nodes n broadcast one hop information received from all sources to all their one hop neighbors except the node from which it came. The source and destination information is available in one hop packet in form of control bits.
- Step 2. Each neighbor node n accepts one hop information, removes control information and pushes RH(n) on NS(n) in modulo 4 order, s.t., rows RH(n) of NS (n) are in order $(n + k) \% 4$ for $k = 0, 1, 2, 3$ where n is the node number.

Order is representative of the node number.

- 2 (a). If $(n + k) \% 4$ equals ZERO, then set order n of RH(n) being pushed onto stack NS(n) as $n = 4$.
- Step 3. In NS(n) for node (n) set the nth column bit to ZERO to avoid loopback condition.
- Step 4. Start reading 4×4 NS(n) in row major order and preserve 1's as they are encountered. For every node $n \in N_i$ don't read the bit in nth column, and entry is NR whenever 1 is encountered.
- 4 (a). Preserve 1's only if 1 is not encountered in previous row traversals, i.e., RST if already done a NR for 1 in same column.
5. Drop last row of matrix i.e. the 4th row in this case, NS(n) for network of size 4 is ready.

7 Results and Conclusions

We played this algorithm on a self-prepared computer program and found the algorithm working for a network of size 4 where duplicity of links was handled by passing only one hop information between nodes. In this way same network image is available to all nodes as we created AN(n) and BN (n) for all 4 nodes (Tables 6 and 7).

Table 6 Route maintenance entries in routing table for node n1

0	1	0	0
1	0	1	1
0	1	0	1
0	1	1	0

Table 7 Route maintenance entries in routing table for node n2

1	0	1	1
0	1	0	1
0	1	0	0
0	1	0	0

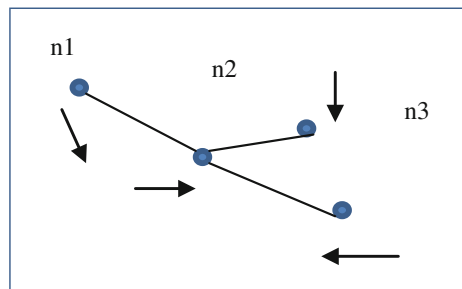
Table 8 Route maintenance entries in routing table for node n1

0	1	0	0
0	0	1	1
0	0	0	0

Table 9 Route maintenance entries in routing table for node n2

1	0	1	1
0	0	0	0
0	0	0	0

Fig. 6 Scenario emerging for both n1 and n2



After, step 2 the following Tables 6 and 7 are created on nodes n1 and n2. As it can be seen these tables have four rows whereas the actual table that has route entries has three rows. One extra row has been created due to iterations in step 2 of algorithm.

The Tables 8 and 9 are received after the Step 4 and 5 of Algorithm is played. Tables 8 and 9 are representative of same network image for both node n1 and n2. The same network image results in zero duplication of messages in the network when network will be put in operation.

The network image emerging out of Tables 8 and 9 is given in Fig. 6.

In this Paper we have tried to establish the Parameter of mobility by modeling node as a transmitter which transmits in one circular fashion and then we have tried to propose a routing protocol for the same. It is seen that duplicity of links is handled very well by the routing protocol and any node at any given point in life of network has same image of topology of the network. The controlled mobility feature allows the node to remain in close proximity to each other while data transmission is taking place. In our future work we shall propose packet format for the same and shall model it for varying network sizes.

References

1. Murthy, C.S.R., Manoj, B.S.: In: Ad-Hoc wireless networks-Architectures and Protocols, ch-5, pp. 213–245, 3rd edn. Pearson Education, Delhi (2008)
2. IEEE Standards for Information technology-Telecommunications and Information Exchange between systems: Part 11 Wireless LAN Medium access control (MAC) and Physical Layer (PHY) specifications-802.11T.M-2007, Unit 5, pp. 23–49 (2007)
3. Johnson, D., Maltz, D.: Dynamic source routing in ad hoc wireless networks. In: ACM Sigcomm. Stanford University, California (1996)
4. Perkins, C., Bhagwat, P.: Highly dynamic destination sequenced distance vector routing for mobile computers. *Comput. Commun. Rev.* **24**(4), 234–244 (1994)
5. Perkins, C., Royer, E.: Ad Hoc on demand distance vector routing in 2nd IEEE workshop on mobile computing system and applications (1999)
6. Gollakota, S., Venkata Ramana, B., Murthy, C.S.R.: Modeling TCP over ad hoc wireless networks using multi-dimensional Markov chains. In: 3rd International Conference on Broadband Communications, Networks and Systems (BROADNETS'06) (2006)
7. Oliveira, R., Braun, T.: TCP in wireless mobile ad hoc networks. <http://citeseerx.ist.psu.edu/viewdoc/summary?doi=10.1.1.1.9988>
8. <http://www.dtnrg.org>
9. Zhao, W., Ammar, M., Zegura, E.: A message ferrying approach for data delivery in sparse mobile ad hoc networks. In: Proceedings of MOBIHOC'04, Japan, 24–26 May 2004
10. Bin Tariq, M.M., Ammar, M., Zegura, E.: Message ferry route design for sparse ad hoc networks with mobile nodes. In: Proceedings of MOBIHOC'06, Florence
11. Shah, R., Roy, S., Jain S., Brunette, W.: Data mules: modeling a three tier architecture for sparse sensor networks. *Elsevier Ad Hoc Netw. J.* **1**(2), pp. 215–233 (3 Sept 2003)
12. Yasmeeny, F., Huda, N., Yamada, S., Borcea, C.: Ferry access points and sticky transfers: improving communication in ferry-assisted DTNs. <http://cs.njit.edu/~borcea/papers/aoc12.pdf>. ©IEEE (2012)
13. Zhao, W., Chen, Y., Ammar, M., Corner, M., Levine, B., Zegura, E.: Capacity enhancement using throwboxes in DTNs. http://scholarworks.umass.edu/cgi/viewcontent.cgi?article=1161&context=cs_faculty_pubs. ©IEEE (2006)
14. Zhang, Z.: Routing in intermittently connected mobile ad hoc networks and delay tolerant networks: overview and challenges. *IEEE Commun. Surv. Tutorials* **8**(1), 24–37 (2006)
15. Vahadat, A., Becker, D.: Epidemic routing for partially connected ad hoc networks. In: Duke Technical Report CS-2000–06, (2000)
16. Mundur, P., Seligman, M., Lee, G.: Epidemic routing with immunity in delay tolerant networks. <http://202.194.20.8/proc/MILCOM08/Milcom08/pdfs/1791.pdf>. ©IEEE (2008)
17. Luo, G., Zhang, J., Hunag, H., et al.: Exploiting intercontact time for routing in delay tolerant networks. In: Transactions on emerging telecommunication technologies. ©Wiley Online Library, Hoboken (2012)

18. Spyropoulos, T., Psounis, K., Raghavendra, C.S.: Spray and wait: an efficient routing scheme for intermittently connected mobile networks. In: Proceedings of the ACM SIGCOMM, Philadelphia pp. 252–259 (2005)
19. Cabanis, R., Vulli, S., Madria, S.: Social group based routing in delay tolerant networks. In: Proceedings of Wireless Networks, Springer, London (2013)

Multi-carrier Based Radar Signal Optimization Using Genetic Algorithm

Gabriel Lellouch and Amit Kumar Mishra

Abstract In this paper, we present our preliminary work on the use of single objective genetic algorithms to improve the design of multicarrier phase coded radar pulses in terms of their autocorrelation properties. The parameter over which optimization is performed is the set of complex phase codes which are applied onto the subcarriers. We show how the use of genetic algorithms is relevant in this context through several comparisons with the well-known Barker phase code structures.

Keywords Multi-carrier radar · Autocorrelation function · Genetic algorithm

1 Introduction

With the advent of powerful digital hardware, software defined radio and radar have become an active area of research and development [1]. This in turn has given rise to many new research directions in the radar community which was previously not comprehensible. One such direction is the recently investigated multi carrier radar also called OFDM radar [2, 3].

The nature of OFDM as a communication waveform is to convey information via the phase codes applied onto the various subcarriers, which can belong to any alphabet, phase shift keying (PSK) for example [4]. After several manipulations, demodulation in the receiver eventually retrieves the transmitted phase codes and in turn, recovers the binary message. In radar, the multicarrier phase coded

G. Lellouch (✉) · A. K. Mishra
University of Cape Town, Cape Town, South Africa
e-mail: gabriel.lellouch@gmail.com

A. K. Mishra
e-mail: akmishra@ieee.org

(MCPC) signal also assigns phase codes onto the subcarriers, however, if the constraint to convey information is not included the phase codes may be searched so that the resulting signal offers optimal radar features. Narrow main peak, low sidelobe level, low ambiguity level both in range and Doppler, are example of such features. An extensive review of the phase code strategies to optimize some of these features when a MCPC pulse is used is provided in [5, 6]. Emphasis is put on the mutual use of a train of MCPC pulses based on complementary sequences together with frequency weighting to reduce the autocorrelation sidelobe levels. These promising results also seem to impose several constraints on the number of subcarriers, symbols and pulses as the complementarity relies on cyclic shifts of one sequence in time and frequency. For applications such as netted radar, phase code strategies offering low cross-correlation properties between the pulses of the different nodes have been investigated [7]. More recently, Riché et al. investigated the possibilities offered by multicarrier signals to mitigate range ambiguities for SAR applications. Similarly, the problem consists in lowering the cross-correlation between consecutive pulses. Unlike Paichard, Riché et al. did not consider the phase codes but instead investigated the frequency content of the consecutive pulses.

Formulating other constraints such as minimizing the peak-to-envelope mean power ratio (PMEPR), minimizing the spectral leakage, etc. it is straightforward that the design of a code-based OFDM radar is a multi-objective engineering optimization problem. In this work, we use genetic algorithm (GA) to search for phase code sequences that would improve the design of MCPC pulses in terms of autocorrelation sidelobes.

There are two novelties in this paper. First of all, the use of coded MCPC pulse as a radar signal is in itself a new direction. Secondly, the use of GA to design MCPC radar pulses is also novel. We show that the GA based OFDM radar outperforms in some cases the classic Barker code based OFDM radar. The rest of the paper is organized as follows. [Section 2](#) describes the MCPC signal considered in this work and recalls some important properties of the multicarrier signal over which the paper builds up. [Section 3](#) discusses the phase codes generation from a GA prospect. Our objective functions are presented and the experimental setup is reviewed. In [Sect. 4](#) our preliminary results are shown and discussed before we conclude the paper in [Sect. 5](#).

2 Multi Carrier Phase Coded Based Radar

The use of phase codes in radar signals is not new. Likewise the well-known chirp pulse, phase coded pulses have been attractive from the early days of radar for their compression capabilities. The initial pulse length T is divided into K bits of identical duration $t_b = T/K$, and each bit is coded with a different phase value. Unlike communication applications that require the use of alphabets to transmit

information, radar potentially support an unlimited number of K -phase code sequences. As we mentioned earlier, many criteria exist that may be used to select a specific code. In Chap. 6 [8], Levanon et al. mention the problem of finding a code that leads to a predetermined range-Doppler resolution as very complicated. For that reason, he suggests to address the problem of phase code selection with the one dimension autocorrelation function (ACF) rather than the two dimension ambiguity function (AF). Our optimization procedure described in Sect. 3 follows the same guideline.

2.1 Single Phase Coded Correlation Properties

Interestingly, when the ACF $R(\tau)$ of the single carrier phase coded pulse is considered, only few discrete samples are necessary to reconstruct the continuous function. Levanon et al. showed that in this case $R(\tau = it_b + \eta)$, (i is a positive integer and $0 \leq \eta < t_b$) given by:

$$R(it_b + \eta) = \frac{1}{Kt_b} \left[\eta \sum_{k=1}^K a_k a_{k-i-1}^* + (t_b - \eta) \sum_{k=1}^K a_k a_{k-i}^* \right] \quad (1)$$

is obtained by connecting, in the complex plane, the values at $R(it_b)$ (noted $R[i]$) by straight lines.

$$R(\tau) = R(it_b + \eta) = \frac{1}{Kt_b} [(t_b - \eta)R[i] + \eta R[i + 1]] \quad (2)$$

In Eq. (1) we defined the phase codes a_k as zero for illegal values of k (i.e., $k > K$ or $k < 1$). Note also that the pulse has been normalized by its length Kt_b so that it exhibits unit energy. One consequence of this observation is that the following optimization problem of finding the phase codes that produce minimum side lobes or minimum area under $R(\tau)$ reduces to finding the phase codes that produce minimum value of either $|R(it_b)| \forall i$ or $\sum_{i=1}^{K-1} |R(it_b)|$. Chapter 6 in [8] elaborates further on the many codes that prove to offer these optimal autocorrelation properties.

2.2 Multi Carrier Phase Coded Correlation Properties

Unlike the single carrier case, the multicarrier pulse no longer offers a simple expression for the ACF $R(\tau)$. When the MCPC pulse is defined by:

$$u(t) = \sum_{n=1}^N \sum_{k=1}^K \omega_n a_{n,k} r_k(t) \cdot \exp(j2\pi n \Delta f t) \quad (3)$$

Levanon et al. have shown [8] in Chap. 11 that $R(\tau)$ can be expressed as:

$$|R(it_b + \eta)| = \left| \sum_{k=1}^N \exp(j2\pi k \frac{\eta}{t_b}) \times \sum_{n=1}^N \omega_n \omega_k^* \right. \\ \left. \times [I_1 \sum_{k=1}^K a_{n,k} a_{k,k-i-1}^* + I_2 \sum_{k=1}^K a_{n,k} a_{k,k-i}^*] \right| \quad (4)$$

As expressed in Eq. (3), our MCPC pulse is composed of N subcarriers equally spaced by $\Delta f = 1/t_b$. Each subcarrier is weighted by ω_n and is assigned the phase code $a_{n,k}$ where the index k denotes the symbol number ranging from 1 to K . The function $r_k(t)$ refers to the rectangular window of each of the K symbols:

$$r_k(t) = \begin{cases} 1 & kt_b \leq t \leq (k+1)t_b \\ 0 & \text{elsewhere} \end{cases}$$

In Eq. (4), I_1 and I_2 are given by $I_1 = \eta \cdot \text{sinc}(\beta) \cdot \exp(j)$ where $\beta = \pi(n-k)\frac{\eta}{t_b}$ and $I_2 = t_b \delta(n-k) - I_1$, [8]. When $N = 1$ it is easy to realize that Eq. (4) reduces to Eq. (1) except for the normalization factor, since the multicarrier pulse has not been normalized.

First null of the autocorrelation Irrespectively of the phase codes, the width of the main peak can be computed when $\eta/t_b \ll 1$ and $i = 0$. Because $I_1 \sim \eta$ and $I_2 \sim t_b \delta(n-k) - \eta$, and assuming the weights $\omega_n = 1$ (this assumption is of no harm for the global behaviour of the ACF), then:

$$|R(\eta)| \simeq Mt_b \left| \sum_{k=1}^N \exp(j2\pi k \frac{\eta}{t_b}) \right| \\ \simeq Mt_b \left| \exp(j\pi(N+1)\frac{\eta}{t_b}) \times \frac{\sin(\pi N \frac{\eta}{t_b})}{\sin(\pi \frac{\eta}{t_b})} \right| \quad (5)$$

From the second part of the expression one sees that the first null happens for $\eta = t_b/N$. Of course, the larger N the better the approximation. This result will be used in Sect. 3. Note that this expression can be rearranged into $\delta\tau = 1/B$ where $\delta\tau$ is the Rayleigh resolution and B the full signal bandwidth.

Identical sequences After all efforts spent in searching for optimal phase codes in the single carrier case, early investigations with multicarrier waveforms naturally started from those existing results. One way to design the multicarrier pulse referred to identical sequence (IS) phase coding has been to apply a certain sequence repetitively onto all N subcarriers. As a result of this design strategy, the discrete ACF of the multicarrier signal becomes a scaled version of the discrete ACF of the single carrier signal when the discrete samples are taken at integer numbers of the symbol duration. Recall Eq. (4) to realize that both continuous ACFs are no more scaled version of one another. This method has the advantage that it gives a closed form expression to these discrete values but obviously ignores the behaviour of the ACF in between. However, as we mentioned previously, the

multicarrier signal faces another severe constraint, namely the PEMPR. Because the IS strategy has proven to be a good solution in terms of PMEPR when the design of the pulse is complemented by a phasing technique, IS coding has been proposed in many cases [9] despite the little control on the resulting ACF.

3 GA Based Code Generation

In this section, we present our experiments to find optimal sequences for the multicarrier radar waveform, which we discussed in the previous section, when GA is the optimization process.

3.1 Objective Functions

As introduced earlier, our objective is to find an optimal coding sequence that will give us the least amount of sidelobes in the ACF. The two criteria that we use in our work are the peak sidelobe level ratio (PSLR) and the integrated sidelobe level ratio (ISLR). Both shall be set as low as possible. Accordingly, we define the following objective functions based on which we run our GA.

$$PSLR = \frac{\max_k |R[k]|}{|R[0]|} \quad ISLR = \frac{\sum_k |R[k]|}{|R[0]|} \quad (6)$$

where we have $R[0] = 1$ because we normalize the ACF with respect to the main peak value before considering the ratios. $R[k]$ refer to the values of the autocorrelation as defined in Eq. (4), taken outside the mainlobe. Note however that they are not as in Eq. (2) taken at integer number of the symbol duration but rather at consecutive samples of the oversampled ACF. For example, if the oversampling rate is N_{os} , the time span between $R[k]$ and $R[k + 1]$ is $t_b/(N \cdot N_{os})$. Note that the orthogonality property of the MCPC pulse imposes a critical sampling period $t_s = t_b/N$. Recall that the first null occurs around t_b/N , hence the mainlobe of the ACF is assumed to be spanning over $2 \cdot N_{os}$ samples. Lastly, we must emphasize the fact that in this work, both objectives are investigated separately and not together. As a matter of fact, our GA optimization consists in single objective optimization.

3.2 Experimental Setup

GA procedure The execution of the genetic algorithm implemented in this work is a two-stage process. Goldberg defined this class of genetic algorithms as simple

genetic algorithms (SGA) [10]. It starts with the current population, composed of L subjects. In our case, one subject is a set of $N \times K$ phase codes $[a_{n,k}]_{n,k}$ as defined in Eq. (3). In the next step, the fitness of all L subjects is assessed upon either of the two objectives given in Eq. (7). Selection is then applied. The best subject is selected twice while the weakest subject is not selected. Like this we build the intermediate population. Thereafter we randomly form pairs out of this intermediate population making sure that all pairs are composed of different elements. The next step is called recombination. Each pair produces two offsprings based on random one-point crossover. Lastly, mutation is applied in an alternate fashion. Every two generations, few elements (in our simulation we use 5) would be randomly chosen and for each element one random bit would be flipped. The condition to end the iterative optimization is based on the mean value of either fitness functions over the entire population reaching a certain threshold we would define in comparison with the results obtained with the Barker based IS MCPC pulse. Our termination condition also includes a convergence criterion on all elements of the population. Said differently, the variance of the fitness of all elements shall be small, meaning that the algorithm has reached an optimal value.

Problem encoding The first step in the implementation of any genetic algorithm is to generate an initial population. Following the canonical genetic algorithm guideline [10], this implies encoding each element of the population into a binary string. In our case, we simply encode one phase code (value between 0 and 2π) into a string of q genes and stack the $N \cdot K$ strings of q genes each into a larger string that we call chromosome, which is then made up of $Q = N \cdot K \cdot q$ genes. This chromosome constitutes one element of the population. The larger q , the finer the resolution. In our experiments, we consider the largest value authorized by *Matlab* that is $q = 18$. The resolution is $\Delta\theta = 2\pi/2^q \simeq 0.024\text{mrad}$. With the values of N and K that we consider in this paper, the size of the chromosome can be as large as 900, ($N = 10$ and $K = 5$). The search space \mathcal{S} “reduces” to the binary strings of length Q . Note that in case the range of authorized phase values is restrained by whatever design constrain, Q may decrease together with the search space dimension.

Population size To understand what the population size L shall be, we followed the guideline given in [11]. The starting point is to say that every point in the search space shall be reachable from the initial population by crossover only. This can happen only if there is at least one instance of every gene at each locus in the whole population. On the assumption that every gene is generated with random probability ($P(1) = 1/2$ and $P(0) = 1/2$) the probability that at least one gene is present at each locus is given by:

$$P = (1 - (1/2)^{L-1})^Q \quad (7)$$

In the two cases that we investigated and report in 4 ($K = 3$, $N = 3$) and ($K = 5$, $N = 10$), we have respectively $Q_1 = 162$ and $Q_2 = 900$ for the chromosome size. From Eq. (8), we calculate the population size that would insure a probability of $P = 99.9\%$. We obtain respectively $L_1 = 18.7$ and $L_2 = 21.2$. For simplicity we consider $L = 22$ in our simulations.

4 Results and Discussions

We now present the results we obtained with our genetic algorithm and compare them with the Barker based IS MCPC pulse. The latter is chosen since Barker codes are well-known for their sidelobe reduction properties. When $K = 3$, the Barker based phase sequence is $[\pi \pi 0]$ and when $K = 5$ case it is $[\pi \pi \pi 0 \pi]$.¹ The IS strategy implies that this sequence is applied onto each of the N subcarriers through the $a_{n,m}$ terms. We could also have decided to apply on each subcarrier a cyclically time shifted version of the code, but for the sake of comparison between the different cases we stick to IS.

4.1 PSLR Based GA

When the objective function is the PSLR, Fig. 1a, b tell that in both cases the GA converges quickly towards populations whose fitnesses are better than the Barker based IS MCPC pulse. In Figs. 1b and 2b we show the ACF of the MCPC pulse designed with phase codes resulting from our optimization. In both cases, the maximum sidelobe level outside the main lobe has been reduced by about 9 dB and 6 dB respectively. Although we did not stress this constraint in our objective function, the sidelobe level in the vicinity of the peak has been noticeably reduced. This is very valuable when high resolution is needed.

4.2 ISLR Based GA

Unlike PSLR, the ISLR of the Barker based IS MCPC pulse is rather good as it can be expected from the IS strategy. In the first case though ($K = 3, N = 3$), it is still possible to find optimal solutions that outperform our reference. Here, we give an example where we find an optimal solution in two steps. We start from a random initial population and converge after about 70 iterations towards an optimum (Fig. 3). We then inject four optimal elements in the initial population, complete with random elements and run again the algorithm. We observe in Fig. 4 that we converge towards optimal solutions in the vicinity of this element. This can be seen in Fig. 4b. In the other case, ($K = 5, N = 10$), one can guess, looking at Fig. 2b that the ISLR of the Barker based IS MCPC pulse is very low and might already be or not far from being an optimal solution. Starting from a fully random population, our algorithm slowly converged but still could not reach the Barker solution after many generations. Then, we decided to inject Barker sequences into

¹ Another Barker code with the very same autocorrelation properties results from interchanging 0 and π , namely $[0 0 \pi]$ and $[0 0 0 \pi 0]$.

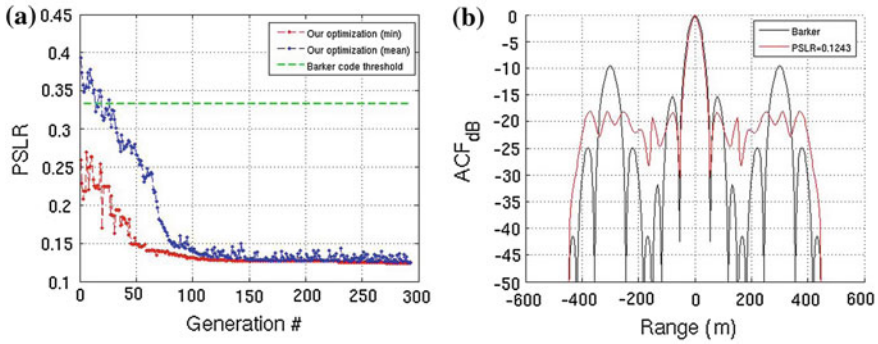


Fig. 1 The phase codes of the MCPC pulse ($N = 3, K = 3$) are optimized via our PSLR based GA. **a** Convergence of our GA, **b** ACF of the MCPC pulse. In **(b)** the ACFs of our optimized MCPC pulse and the Barker based IS MCPC pulse are compared

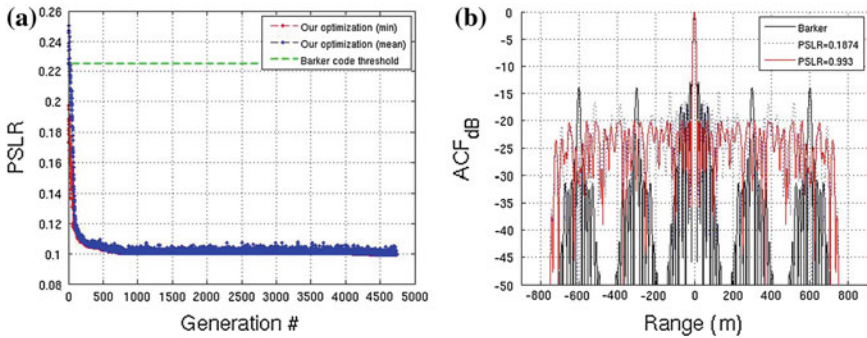


Fig. 2 The phase codes of the MCPC pulse ($N = 10, K = 5$) are optimized via our PSLR based GA. **a** Convergence of our GA, **b** ACF of the MCPC pulse. In **(b)** the ACFs of our optimized MCPC pulse and the Barker based IS MCPC pulse are compared

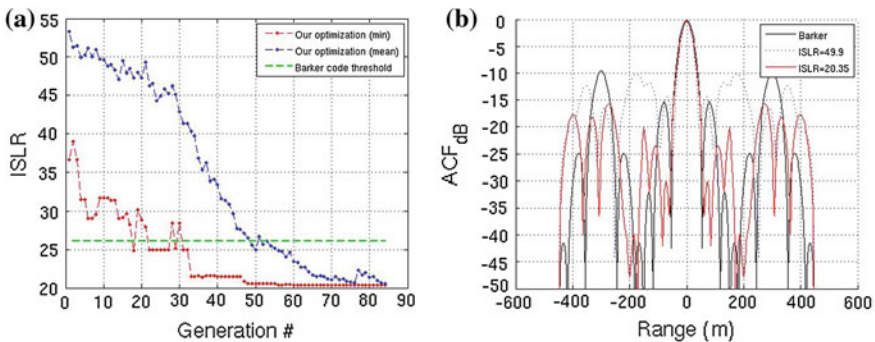


Fig. 3 The phase codes of the MCPC pulse ($N = 3, K = 3$) are optimized via our ISLR based GA. **a** Convergence of our GA, **b** ACF of the MCPC pulse. In **(b)** the ACFs of our optimized MCPC pulse and the Barker based IS MCPC pulse are compared

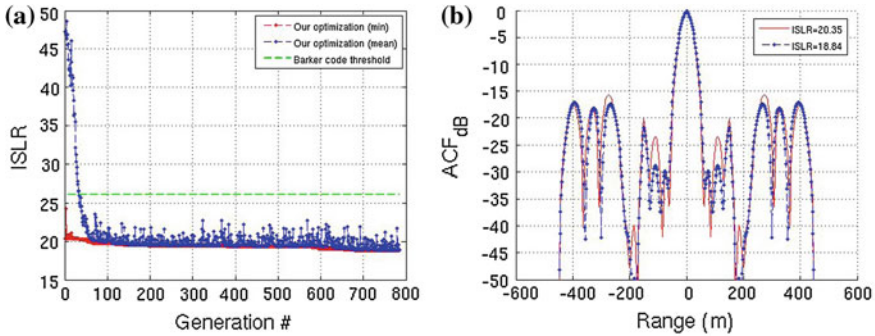


Fig. 4 The phase codes of the MCPC pulse ($N = 3, K = 3$) are optimized via our ISLR based GA. In the initial population we injected 4 good elements obtained in the previous search. **a** Convergence of our GA, **b** ACF of the MCPC pulse. In (b) the ACFs of our optimized MCPC pulse is compared to the MCPC pulse built from the initial good element

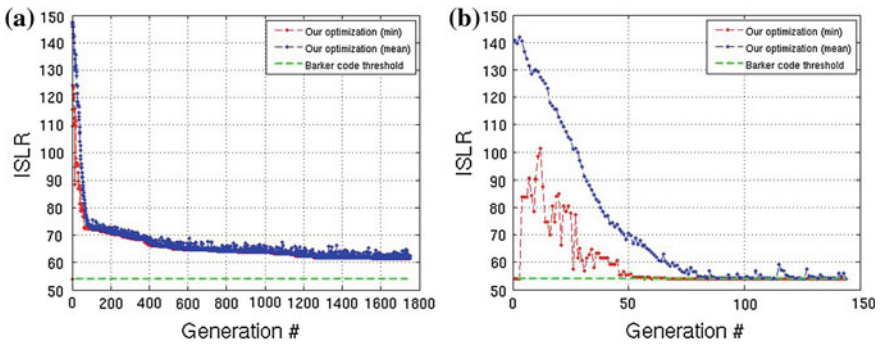


Fig. 5 **a** Convergence of our GA, **b** Convergence of our GA. In (a) one Barker based IS is injected in the initial population while in (b) four Barker based IS are injected in the initial population

Table 1 Summary of the results

	Barker	wf1	wf2	wf3	wf4
PSLR	0.33	0.12	–	–	–
ISLR	26.11	–	18.84	–	–
PSLR	0.23	–	–	0.10	–
ISLR	54.05	–	–	–	54.05

the initial population. We started with one such sequence out of the 22 which compose the initial population. Convergence is happening but after 1800 generations we are still above the reference value. We repeated the experiment with four sequences and, as seen in Fig. 5b, our genetic algorithm quickly converged towards the Barker solution. Our findings are altogether summarized in Table 1.

5 Conclusion

In this paper we showed how genetic algorithms can be used to optimize the design of MCPC radar pulses. Our optimization consisted of a single objective optimization based on either of the two objective functions, the peak sidelobe level ratio or the integrated sidelobe level ratio of the autocorrelation function. We have seen that GA permitted to find better phase code sequences than the Barker based identical sequences, at least in terms of the two objectives we defined, except in one of the cases where the latter seems to be an optimal solution. In the future, we will incorporate multiple objectives in our genetic algorithm to optimize the design of the MCPC pulse further in terms of more than one criterion, for example the peak-to-mean envelop power ratio.

References

1. Langman, A., Hazarika, O., Mishra, A.K., Inggs, M.: White RHINO: a low cost whitespace communications and radar hardware platform. In: Radioelektronika (RADIOELEKTRONIKA) Conference (2013)
2. Lellouch, G., Tran, P., Pribic, R., Van Genderen, P.: OFDM waveforms for frequency agility and opportunities for Doppler processing in radar. In: IEEE Radar Conference, May 2008, pp. 1–6
3. Lellouch, G., Pribic, R., Van Genderen, P.: Wideband OFDM pulse burst and its capabilities for the Doppler processing in radar. In: IEEE International Radar Conference, Sept 2008, pp. 531–535
4. Hara, S., Prasad, R.: Multicarrier techniques for 4G mobile communications. Artech House Publishers, Boston (2003)
5. Levanon, N.: Multifrequency complementary phase-coded radar signal. In: IEE Proceedings-Radar, Sonar and Navigation, pp. 276–284 (2000)
6. Levanon, N., Mozeson, E.: Multicarrier radar signal pulse train and CW. In: IEEE Transactions on Aerospace and Electronic Systems, pp. 707–720 (2002)
7. Paichard, Y. Orthogonal multicarrier phased coded signal for netted radar systems. In: IEEE International Waveform Diversity and Design Conference, Feb 2009, pp. 234–236
8. Levanon, N., Mozeson, E.: Radar Signals. Wiley-Interscience, New York (2004)
9. Huo, K., Deng, B., Liu, Y., Jiang, W., Mao, J.: The principle of synthesizing HRRP based on a new OFDM phase-coded stepped-frequency radar signal. In: IEEE 10th International Conference on Signal Processing (ICSP), pp. 1994–1998 (2010)
10. Whitley, D.: A Genetic Algorithm Tutorial. Colorado State University, Fort Collins
11. Reeves, C.: Handbook of Metaheuristics, pp. 55–82. Springer, Berlin (2003)
12. Riché, V., Meric, S., Baudais, J-Y., Pottier, E.: Optimization of OFDM SAR signals for Range ambiguity suppression. In Radar Conference (EuRAD), pp. 278–281 (2012)
13. Gu, C., Zhang, J., Zhu, X.: Resolution performance analysis for multicarrier phase-coded signal. In: Congress on Image and Signal Processing, pp. 193–196 (2008)

Additive and Multiplicative Inverse of Generalized Fuzzy Numbers with Different Left Heights and Right Heights

Gourav Gupta, Amit Kumar and M. K. Sharma

Abstract In this paper, with the help of Zadeh's extension principle, it is shown that there is error in the additive and multiplicative inverse of generalized fuzzy numbers with different left heights and right heights proposed by Lee and Chen [1]. To resolve the error, new additive and multiplicative inverse of generalized fuzzy numbers with different left heights and right heights are proposed. Also, it is shown that generalized fuzzy numbers with different left heights and right heights cannot be used for fuzzy risk analysis.

Keywords Generalized fuzzy numbers · Generalized fuzzy numbers with different left heights and right heights · Additive and multiplicative inverse

1 Introduction

Chang et al. [2] proposed the concept of generalized fuzzy numbers with different left heights and right heights. Lee and Chen [1] proposed the arithmetic operations of these fuzzy numbers and used the division operation for fuzzy risk analysis. Chen et al. [3] also used the same division operation for fuzzy risk analysis.

G. Gupta (✉) · A. Kumar · M. K. Sharma
School of Mathematics and Computer Applications, Thapar University,
Patiala, Punjab, India
e-mail: gouravgupta333@gmail.com

A. Kumar
e-mail: amitkdma@gmail.com

M. K. Sharma
e-mail: mksharma@thapar.edu

It is well known that the division operation is actually the multiplication of a number with the multiplicative inverse of another number and the subtraction operation is the addition of a number with the additive inverse of another number.

In this paper, it is pointed out that there is error in the additive and multiplicative inverse and hence in subtraction and division operation of generalized fuzzy numbers with different left heights and right heights proposed by Lee and Chen [1]. To resolve the error, new additive and multiplicative inverse of generalized fuzzy numbers with different left heights and right heights are proposed. Also, it is shown that the generalized fuzzy numbers with different left heights and right heights cannot be used for fuzzy risk analysis.

The rest of this paper is organized as follows. In Sect. 2, error occurring in the additive and multiplicative inverse of generalized fuzzy numbers with different left heights and right heights proposed by Lee and Chen [1] are pointed out. In Sect. 3, new additive and multiplicative inverse are defined for generalized fuzzy numbers with different left heights and right heights. In Sect. 4, it is shown that generalized fuzzy numbers with different left heights and right heights cannot be used for fuzzy risk analysis.

2 Error in Existing Additive and Multiplicative Inverse

If \tilde{A} is any fuzzy number defined on the universal set X and $\mu_{\tilde{A}}(x)$ is the membership value corresponding to $x \in X$, then by Zadeh's extension principle ([4], p. 60), the membership value of $\frac{1}{x}$ in $\frac{1}{\tilde{A}}$ will also be $\mu_{\tilde{A}}(x)$. Due to the same reason, since in the generalized fuzzy number with different left height and right height $\tilde{A} = (a, b, c, d; L, R)$ the membership values corresponding to b and c are L and R respectively. So, the membership values of $\frac{1}{b}$ and $\frac{1}{c}$ in $\frac{1}{\tilde{A}}$ should also be L and R respectively. However, according to existing arithmetic operation [1], if $\tilde{A} = (a, b, c, d; L, R)$ is generalized fuzzy number with different left height and right height then $\frac{1}{\tilde{A}} = (\frac{1}{d}, \frac{1}{c}, \frac{1}{b}, \frac{1}{a}; L, R)$, i.e., in $\frac{1}{\tilde{A}}$ the membership values corresponding to b and c are L and R respectively. While, in $\frac{1}{\tilde{A}}$ obtained by the existing arithmetic operations [1] the membership values corresponding to $\frac{1}{b}$ and $\frac{1}{c}$ are R and L respectively which is contradicting the Zadeh's extension principle ([4], p. 60), i.e., there is error in the multiplicative inverse and hence in the division operation proposed by Lee and Chen [1].

The same error is also occurring in calculating the additive inverse $-\tilde{A}$ of \tilde{A} and hence in calculating the subtraction of generalized fuzzy numbers with different left heights and right heights with the help of arithmetic operations proposed by Lee and Chen [1].

3 Proposed Additive and Multiplicative Inverse

In this section, keeping Zadeh's extension principle in mind, the additive and multiplicative inverse of a generalized fuzzy number with different left height and right height is defined.

Let $\tilde{A} = (a, b, c, d; L, R)$ be the generalized fuzzy number with different left height and right height. Then,

$$(i) -\tilde{A} = (-d, -c, -b, -a; R, L)$$

$$(ii) \frac{1}{\tilde{A}} = \left(\frac{1}{d}, \frac{1}{c}, \frac{1}{b}, \frac{1}{a}; R, L\right)$$

4 Non-applicability of Generalized Fuzzy Numbers with Different Left Heights and Right Heights in Fuzzy Risk Analysis

If $\tilde{A} = (a_1, b_1, c_1, d_1; L_1, R_1)$ and $\tilde{B} = (a_2, b_2, c_2, d_2; L_2, R_2)$ are two generalized fuzzy numbers with different left heights and right heights such that left height $(L_1) >$ right height (R_1) and left height $(L_2) >$ right height (R_2) then using the arithmetic operation proposed in Sect. 3, $\frac{1}{\tilde{B}} = \left(\frac{1}{d_2}, \frac{1}{c_2}, \frac{1}{b_2}, \frac{1}{a_2}; R_2, L_2\right)$ will be a generalized fuzzy number with different left height and right height such that left height $(R_2) >$ right height (L_2) . Since, in \tilde{A} left height $(L_1) >$ right height (R_1) while in $\frac{1}{\tilde{B}}$ left height $(R_2) >$ right height (L_2) i.e., both are different types of generalized fuzzy numbers with different left heights and right heights, so it is not possible to find the arithmetic operation $\tilde{A} \otimes \frac{1}{\tilde{B}}$. However, it is obvious from Step 1 of the existing methods [1, 3] that for the fuzzy risk analysis, there is need to find $\tilde{A} \otimes \frac{1}{\tilde{B}}$. So, generalized fuzzy numbers with different left heights and right heights cannot be used for the fuzzy risk analysis.

Acknowledgments The second author, Dr. Amit Kumar, want to acknowledge the adolescent inner blessings of Mehar (lovely daughter of his cousin sister). He believes that Mata Vaishno Devi has appeared on the earth in the form of Mehar and without her blessings it was not possible to think the ideas presented in this paper. The first and third authors would like to acknowledge for financial assistant given by University Grant Commission (F. No. 39-49/2010 (SR)).

References

1. Lee, L.W., Chen, S.M.: Fuzzy risk analysis based on fuzzy numbers with different shapes and different deviations. *Expert Syst. Appl.* **34**, 2763–2771 (2008)
2. Chang, J.R., Cheng, C.H., Kuo, C.Y.: Conceptual procedure for ranking fuzzy numbers based on adaptive two-dimensions dominance. *Soft. Comput.* **10**, 94–103 (2006)

3. Chen, S.M., Munif, A., Chen, G.S., Liu, H.C., Kuo, B.C.: Fuzzy risk analysis based on ranking generalized fuzzy numbers with different left heights and right heights. *Expert Syst. Appl.* **39**, 6320–6334 (2012)
4. Zimmermann, H.J.: *Fuzzy Set Theory and Its Applications*, 4th edn. Kluwer Academic Publisher, Dordrecht (2001)

Cryptanalysis of “A New Method of Cryptography Using Laplace Transform”

Praneesh Gupta and Prasanna Raghav Mishra

Abstract We present a cryptanalysis of an encryption scheme based on Laplace Transforms proposed by A.P. Hiwarekar. We have shown that scheme is described in a superfluous manner. We have given equivalent operations for the scheme by means of which the scheme can be described in much simpler terms. Using these operations we can break the scheme in much lesser number of trials than that is claimed by the author. We have also given an example to illustrate our cryptanalytic attack in support of our findings.

1 Introduction

“A New Method of Cryptography Using Laplace Transform” proposed by Hiwarekar [6] is an encryption scheme designed to facilitate encryption/decryption for English text. We have shown that the use of Laplace Transform is rather superfluous and the scheme can be described independent of Laplace Transform [1, 3] and this description is much simpler than the present one. The author has claimed that the scheme is secure against any type of cryptanalytic attack. However, no concrete reasoning is given in support of his claim. We have launched a ciphertext only attack [8] on the scheme. We have shown that the scheme can be broken with much lesser number of trials as compared to that is required for Brute force [7]. The organization of this paper is as follows:

P. Gupta (✉) · P. R. Mishra
Scientific Analysis Group, Defence Research and Development Organisation,
Metcalfe House Complex, Delhi 110054, India
e-mail: praneesh.jk@gmail.com

P. R. Mishra
e-mail: prasanna.r.mishra@gmail.com

In the second section we describe the scheme in brief. In the third section we put some critical observations regarding the scheme. In the fourth section we describe the simpler representation of the scheme and carry out the cryptanalysis. We have also given a technique to recover plaintext from the ciphertext without the knowledge of key. In the fifth section we present some case studies of our attack applied on ciphertexts of English plaintexts encrypted with the scheme under consideration.

2 Brief Description of the Scheme

The scheme under consideration is based on computation of Laplace Transform of a polynomial of specific form. The coefficients of the polynomial depends on the characters of the plaintext. The details of encryption/decryption process are as follows:

Encryption: Before encryption, the plaintext is coded to give a finite sequence of positive integers $0, 1, \dots, 25$. The coding scheme maps character A to 0, B to 1 and so on. Here no distinction is made between small and capital letters. Numbers and special characters are just ignored. Infact, this is a one–one onto map (say ϕ) from the set of alphabets to the set $\{0, 1, 2, \dots, 25\}$.

Let $\mathcal{P} = P_1P_2 \dots P_n$ denote the plaintext which is to be encrypted. The coded plaintext can be given as

$$\phi(\mathcal{P}) = \phi(P_1)\phi(P_2) \dots \phi(P_n).$$

The coded plaintext gives rise to an infinite sequence given as

$$G_i = \phi(P_{i+1}), \quad i = 0, 1, \dots, n-1 \text{ and } G_i = 0 \text{ for } i \geq n.$$

A polynomial $f(t)$ is formed by multiplying this sequence term by term to the expansion of te^{rt} , $r \in \mathbb{N}$.

It is clear that $f(t)$ has a finite degree as there are only finitely many non-zero terms in the sequence $\{G_i | i \in \mathbb{N}\}$. Now the Laplace transform of $f(t)$ i.e. $L\{f(t)\}$ is computed and the coefficients of Laplace transform are collected and divided by 26. Quotients are treated as key and kept secret while the remainders are positive integers in the range 0–25 which are mapped back to English alphabets and taken as ciphertext.

To illustrate the encryption process, we take $r = 2$ and the word ‘PROFESSOR’ as plaintext. The plaintext is encoded to 15 17 14 5 4 18 18 14 17. The sequence $\{G_i\}$ is given as $G_0 = 15, G_1 = 17, G_2 = 14, G_3 = 5, G_4 = 4, G_5 = 18, G_6 = 18, G_7 = 15, G_8 = 17, G_n = 0$ for $n \geq 9$. Using this sequence, we form the polynomial $f(t)$ as,

$$\begin{aligned}
f(t) &= t[G_0 1 + G_1 \frac{2t}{1!} + G_2 \frac{2^2 t^2}{2!} + G_3 \frac{2^3 t^3}{3!} + G_4 \frac{2^4 t^4}{4!} + G_5 \frac{2^5 t^5}{5!} \\
&\quad + G_6 \frac{2^6 t^6}{6!} + G_7 \frac{2^7 t^7}{7!} + G_8 \frac{2^8 t^8}{8!}] \\
&= 15t + 17 \frac{2t^2}{1!} + 14 \frac{2^2 t^3}{2!} + 5 \frac{2^3 t^4}{3!} + 4 \frac{2^4 t^5}{4!} + 18 \frac{2^5 t^6}{5!} + 18 \frac{2^6 t^7}{6!} \\
&\quad + 14 \frac{2^7 t^8}{7!} + 17 \frac{2^8 t^9}{8!}.
\end{aligned}$$

Here $f(t)$ is a polynomial in t of degree 9. We now compute Laplace transform of $f(t)$.

$$\begin{aligned}
L\{f(t)\}(s) &= L\{15t + 17 \frac{2t^2}{1!} + 14 \frac{2^2 t^3}{2!} + 5 \frac{2^3 t^4}{3!} + 4 \frac{2^4 t^5}{4!} + 18 \frac{2^5 t^6}{5!} + 18 \frac{2^6 t^7}{6!} \\
&\quad + 14 \frac{2^7 t^8}{7!} + 17 \frac{2^8 t^9}{8!}\}(s) \\
&= \frac{15}{s^2} + \frac{68}{s^3} + \frac{168}{s^4} + \frac{160}{s^5} + \frac{320}{s^6} + \frac{3456}{s^7} + \frac{8064}{s^8} + \frac{14336}{s^9} \\
&\quad + \frac{39168}{s^{10}}
\end{aligned}$$

s being a non zero real or complex number.

Now the coefficients of Laplace transform are collected and divided by 26. In our case the quotients are 0, 2, 6, 6, 12, 132, 310, 551, 1506 and remainders are 15, 16, 12, 4, 8, 24, 4, 10, 12. Now the key is given as 0, 2, 6, 6, 12, 132, 310, 551, 1506 and the remainders when mapped back to alphabets, produce ciphertext as PQMEIYEKM.

Decryption: For decryption ciphertext is mapped to integers as per encoding scheme described above. In this case ciphertext PQMEIYEKM is mapped to 15, 16, 12, 4, 8, 24, 4, 10, 12. With the use of key value, we can obtain the coefficients of Laplace transform of $f(t)$ i.e. $L\{f(t)\}$ using division algorithm [4, 5]. The values of coefficients thus obtained are 15, 68, 168, 320, 3456, 8064, 14336, 39168. Now, $L\{f(t)\}$ can be written as:

$$\begin{aligned}
L\{f(t)\}(s) &= \frac{15}{s^2} + \frac{68}{s^3} + \frac{168}{s^4} + \frac{160}{s^5} + \frac{320}{s^6} + \frac{3456}{s^7} + \frac{8064}{s^8} + \frac{14336}{s^9} \\
&\quad + \frac{39168}{s^{10}}
\end{aligned}$$

Taking inverse Laplace transform, we can get back $f(t)$. From $f(t)$, the original plaintext message can be easily recovered.

3 Observations

We have made the following observations regarding the scheme.

1. The scheme does not use pre-decided secret parameter as key, instead the key is derived from the plaintext itself. This is inconsistent with the existing design philosophy.
2. It is not stated whether the parameter r is a part of the key or a pre-shared value.
3. As per designer's claim, the encryption/decryption scheme is based on Laplace Transform. The equivalent description of the scheme (as shown in Sect. 4) shows that the scheme is actually independent of Laplace Transform.

The first two observations are related to inconsistencies present in the scheme while the last one is related to security aspects of the scheme. In the next section we describe how this security related issue can be exploited to mount a "ciphertext only" type of cryptanalytic attack on the scheme.

4 Cryptanalysis

Let the plaintext be denoted as sequence of English alphabets P_1, P_2, \dots, P_n and the corresponding ciphertext be denoted as C_1, C_2, \dots, C_n . As discussed in Sect. 2, to encrypt the given plaintext we need the Laplace transform of $\sum_{i=1}^n \frac{r^{i-1} \phi(P_i) t^i}{(i-1)!}$. We have

$$\begin{aligned}
 L\left(\sum_{i=1}^n \frac{r^{i-1} \phi(P_i) t^i}{(i-1)!}\right) &= \sum_{i=1}^n L\left(\frac{r^{i-1} \phi(P_i) t^i}{(i-1)!}\right) \\
 &= \sum_{i=1}^n \frac{r^{i-1} \phi(P_i)}{(i-1)!} L(t^i) \\
 &= \sum_{i=1}^n \frac{r^{i-1} \phi(P_i)}{(i-1)!} \int_0^{\infty} e^{-st} t^i dt \\
 &= \sum_{i=1}^n \frac{r^{i-1} \phi(P_i)}{(i-1)!} \frac{i!}{s^{i+1}} \\
 &= \sum_{i=1}^n \frac{r^{i-1} i \phi(P_i)}{s^{i+1}}.
 \end{aligned}$$

This leads us to formulate an alternate description of encryption process. The i th character of ciphertext is given as

$$C_i = \phi^{-1}((r^{i-1}i\phi(P_i)) \bmod 26)$$

and the i th key element is given as $\lfloor (r^{i-1}i\phi(P_i)/26) \rfloor$. This is clearly independent of Laplace Transform. Now we describe our analysis that leads to the breaking of the scheme. Depending upon the value of $r^{i-1}i$, we can make different guesses as described below.

1. For $r^{i-1}i \equiv 1 \pmod{26}$ we have

$$C_i = \phi^{-1}(\phi(P_i) \bmod 26) = P_i$$

2. $\gcd(r^{i-1}i, 26) = 1$. In this case we can find plaintext uniquely as

$$P_i = \phi^{-1}((y_i\phi(C_i)) \bmod 26),$$

y_i being the inverse of $r^{i-1}i$ modulo 26. In particular if $C_i = 'A'$ then from above relation we have $P_i = 'A'$ so the plaintext character is directly determined and the value of y_i need not be computed.

3. $\gcd(r^{i-1}i, 26) = 2$. Let $x = \phi(P_i)$, then to guess the possible plaintext we have to solve the congruence $r^{i-1}ix \equiv \phi(C_i) \pmod{26}$ for x . It will have 2 solutions [2]. Let one of the solution be x_1 . The other solution will be given by $x_2 \equiv x_1 + 13 \pmod{26}$. There will be two choices for P_i precisely $\phi^{-1}(x_1)$ and $\phi^{-1}(x_2)$.
4. $\gcd(r^{i-1}i, 26) = 13$. In this case the congruence equation given in (3) will have thirteen solutions. Let one of the solution be x_1 . The other solution will be given by $x_2 \equiv x_1 + 2 \pmod{26}$, $x_3 \equiv x_1 + 4 \pmod{26}$... $x_{13} \equiv x_1 + 24 \pmod{26}$. The corresponding plaintext characters will precisely be $\phi^{-1}(x_1)$, $\phi^{-1}(x_2)$... $\phi^{-1}(x_{13})$.
5. $r^{i-1}i \equiv 0 \pmod{26}$ In this case there are all 26 possibilities for plaintext character.

5 Case Studies

Some case studies are given below to illustrate our technique to recover the plaintext from ciphertext.

1. Given $C = \text{“PQMEIYEKM”}$ and $r = 2$. Now applying the ciphertext only attack as described in pervious section we have: For $i = 1$ we directly know the plaintext i.e., P.

For $i = 2$ we have, $C_2 = 'Q'$ and $\phi(C_2) = 16$. As $\gcd(r^{i-1}i, 26) = \gcd(4, 26) = 2$, there will be two choices for the possible plaintext character. To guess the plaintext character we solve the congruence $4x \equiv 16 \pmod{26}$. The solutions to the congruence are 4 and 17. The two choices the plaintext characters will be $\phi^{-1}(4)$ and $\phi^{-1}(17)$ i.e., 'E' and 'R' respectively.

Similarly, there are two choices for each of the plaintext characters at positions 3rd, 4th, 5th, 6th, 7th, 8th and 9th positions. These choices are ('B', 'O'), ('F', 'S'), ('E', 'R'), ('F', 'S'), ('F', 'S'), ('B', 'O') and ('E', 'R') respectively. Thus the plaintext word can be guessed in maximum 256 trials. The 256 guessed words are-

1.	PEBFEFFBE
2.	PRBFEFFBE
3.	PEOFFEFFBE
	:
243.	PEOFFESSOR
244.	PROFESSOR
245.	PEBSESSOR
	:
254.	PRBSRSSOR
255.	PEOSRSSOR
256.	PROSRSSOR

The correct word appears at position 244.

2. Given $C = \text{"PYOUIKWYZ"}$ and $r = 3$.

The first letter of the plaintext is determined directly i.e., P.

There are two choices for each of the plaintext characters at positions 2nd, 4th, 6th and 8th positions. Plaintext characters at positions 3, 5, 7 and 9 can be guessed uniquely. Thus the plaintext word can be guessed in maximum 16 trials. The sixteen guessed words are-

1.	PEOFFFSBR
2.	PROFFFSBR
3.	PEOFFFSBR
	:
14.	PROFESSOR
15.	PEOFFESSOR
16.	PROFFESSOR

The correct word appears at position 14.

3. Given $C = \text{"PEEWYSEWR"}$ and $r = 7$.

The directly known plaintext character is 'P'.

There are two choices for each of the plaintext characters at positions 4th, 6th, and 8th positions. Plaintext characters at positions 3, 5, 7 and 9 can be guessed uniquely. Thus the plaintext word can be guessed in maximum 16 trials. The sixteen guessed words are-

1.	PEOFEFSBR
2.	PROFEFSBR
3.	PEOSEFSBR
	⋮
14.	PROFESSOR
15.	PEOESSOR
16.	PROSESSOR

The correct word appears at position 14.

4. Given $C = \text{“POKEUUEMK”}$ and $r = 18$.

As described earlier the first plaintext character is ‘P’.

Except first, there are two choices for each of the plaintext characters at all positions. Thus the plaintext word can be guessed in maximum 256 trials. The 256 guessed words are-

1.	PEBFEFFBE
2.	PRBFEFFBE
3.	PEOFEFFBE
	⋮
243.	PEOFESSOR
244.	PROFESSOR
245.	PEBESSOR
	⋮
254.	PRBSRSSOR
255.	PEOSRSSOR
256.	PROSRSSOR

The correct word appears at position 244.

The above analysis is done with the assumption that r is a publicly known parameter. However, it is possible to break the scheme even if r is a part of key, as there are effectively 26 different values of r , the number of trials for r is bounded above by 26. The complexity of the attack will be increased at most by a factor of 26 in this case.

6 Conclusion

The cryptographic scheme proposed by Hiwarekar [6] is a weak scheme. We have proved that the encryption function of the scheme can be expressed in a simpler form which is independent of Laplace Transform. Using our alternate formulation

of encryption process we have launched a ciphertext only attack and shown that the scheme can be broken in much lesser number of trials than the exhaustive trials. With the help of examples we have illustrated how the plaintexts are recovered from the ciphertexts.

Acknowledgments The authors would like to express their gratefulness to Dr. P. K. Saxena, OS and Director, SAG for allowing them to carry out this work. Authors are thankful to Mrs. Navneet Gaba, Scientist 'F', SAG and Mr Mukesh Malhotra, Scientist 'F', SAG for giving insight for this paper. Sincere thanks are also due to Dr. Sucheta Chakrabarti, Scientist 'F', SAG for carrying out a microscopic scrutiny of this paper.

References

1. Antimirov, M.Y., Kolyshkin, A.A., Vaillancourt R.: Applied integral transforms, CRM monograph series. American Mathematical Society, Providence, Rhode Island, USA (1993)
2. Burton, D.M.: Elementary Number Theory, pp. 82–89. Allyn and Bacon, Boston (1980)
3. Davies, B.: Integral Transforms and their Applications, Texts in Applied Mathematics. Springer, New York (2002)
4. Gallian, J.A.: Contemporary Abstract Algebra, pp. 4–13. D.C. Heath and Company, Lexington (1986)
5. Herstein, I.N.: Topics in Algebra, vol. 155, pp. 18. Wiley, Hoboken (2007)
6. Hiwarekar, A.P.: A new method of cryptography using Laplace Transform. Int. J. Math. Arch. **3**(3), 1193–1197 (2012)
7. Menezes, A., Van Oorschot, P., Vanstone, S.: Handbook of Applied Cryptography. CRC Press, Florida (1997)
8. Stallings, W.: Cryptography and Network Security Principles and Practice, 5th edn, p. 36, Pearson Education Inc. New York (2011)

A Design of Longitudinal Control of an Aircraft Using a Fuzzy Logic Based PID Controller

S. N. Deepa and G. Sudha

Abstract For linear systems and nonlinear systems, classic controllers such as PID have been widely used in industrial control processes and in flight control systems because of their simple structure and robust performance in a wide range of operating conditions. Several numerical approaches such as Fuzzy Logic Controller (FLC) algorithm and evolutionary algorithms have been used for the optimum design of PID controllers. In this paper Fuzzy PID controller is developed to improve the performance for a pitch control of aircraft system. The controller is designed based on the dynamic modeling of system begins with a derivation of suitable mathematical model to describe the longitudinal motion of an aircraft. Mamdani-type-Fuzzy Logic Controller is used to tune each parameter of Proportional-integral-derivative (PID) controller by selecting appropriate fuzzy rules through simulations. The simulation results show that Fuzzy Logic Controller tuned by PID algorithm is better performance and more robust than the classical type algorithm for aircraft pitch control.

Keywords Fuzzy logic controller · Fuzzy sets · Pitch dynamics · PID controller

1 Introduction

Flight dynamics deals principally with the response of aerospace vehicles to perturbations in their flight environments and to control inputs [1–3]. In order to understand this response, it is necessary to characterize the aerodynamic and

S. N. Deepa (✉) · G. Sudha
Anna University, Regional Center, Coimbatore, Tamilnadu, India
e-mail: deepapsg@gmail.com

G. Sudha
e-mail: sudha.gunasekar@gmail.com

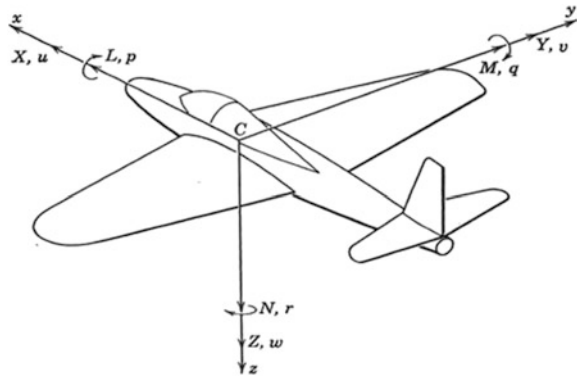
propulsive forces and moments acting on the vehicle, and the dependence of these forces and moments on the flight variables, including airspeed and vehicle orientation. The rapid advancement of aircraft design from the very limited capabilities of the Wright brothers first successfully airplane to today's high performance military, commercial and general aviation aircraft require the development of many technologies, these are aerodynamics, structures, materials, propulsion and flight control. In longitudinal control, the elevator controls pitch or the longitudinal motion of aircraft system [4, 5]. The elevator is situated at the rear of the airplane running parallel to the wing that houses the ailerons. Pitch control is a longitudinal problem and this work controls the pitch of an aircraft. Pitch is controlled by the rear part of the tail plane's horizontal stabilizer being hinged to create an elevator. By moving the elevator control backwards the pilot moves the elevator up a position of negative camber and the downwards force on the horizontal tail is increased. The angle of attack on the wings increased so the nose is pitched up and lift is generally increased. In gliders the pitch action is reversed and the pitch control system is much simpler, so when the pilot moves the elevator control backwards it produces a nose-down pitch and the angle of attack on the wing is reduced. The pitch angle of an aircraft is controlled by adjusting the angle and therefore the lift force of the rear elevator. Lot of works has been done in the past to control the pitch of an aircraft for the purpose of flight stability and yet this research still remains an open issue in the present and future works [6, 7]. Modern aircraft include a variety of automatic control system that aids the flight crew in navigation, flight management and augmenting the stability characteristics of the airplane.

2 Mathematical Model of Aircraft Dynamics

The standard notation [8] for describing the motion of, and the aerodynamic forces and moments acting upon, flight vehicle is indicated in Fig. 1. The variables x , y , z represent coordinates, with origin at the center of mass of the vehicle. The x -axis lays in the symmetry plane of the vehicle [9] and points toward the nose of the vehicle. The z -axis also is taken to lie in the plane of symmetry, perpendicular to the x -axis, and pointing approximately down. The y -axis completes a right-handed orthogonal system, pointing approximately out the right wing [10].

Angles θ , φ and δ_e represent the orientation of aircraft pitch angle in the earth-axis system and elevator deflection angle. The forces, moments and velocity components in the body fixed coordinate of aircraft system can be described as showed in Fig. 1. The aerodynamics moment components for roll, pitch and yaw axis are represent as L , M and N . The term p , q , r represent the angular rates about roll, pitch and yaw axis while term u , v , w represent the velocity components of roll, pitch and yaw axis. The angles α and β represents the angle of attack and sideslip respectively [11, 12].

Fig. 1 Force, moments, and velocity components in a body fixed coordinate



A few assumption need to be considered before continuing with the modeling process. First, the aircraft is at a steady state cruising at constant altitude and velocity, thus the thrust and drag are cancel out and the lift and weight balance out each other. Second, the change in pitch angle does not change the speed of an aircraft under any circumstance. Also, the atmosphere in which the plane flies is assumed undisturbed, thus forces and moment due to atmospheric disturbance are considered zero. Hence, considering Fig. 1, the following dynamic equations describe the longitudinal dynamics of a typical aircraft;

Force equations:

$$X - mgS_{\theta} = m(\dot{u} + qv - rv) \tag{1}$$

$$Z + mgC_{\theta}C_{\phi} = m(\dot{w} + pv - qu) \tag{2}$$

Momentum equation:

$$M = I_y\dot{q} + rq(I_x - I_z) + I_{xz}(P^2 - r^2) \tag{3}$$

Equations (1), (2) and (3) should be linearized using small disturbance theory. The equations are replaced by a reference value plus a perturbation or disturbance, as given in Eq. (4). All the variables in the equation of motion are replaced by a reference value plus a perturbation or disturbance. The perturbations in aerodynamic forces and moments are functions of both, the perturbations in state variables and control inputs.

$$\begin{aligned} u &= u_0 + \Delta u, v = v_0 + \Delta v, w = w_0 + \Delta w \\ p &= p_0 + \Delta p, q = q_0 + \Delta q, r = r_0 + \Delta r \\ X &= X_0 + \Delta X, M = M_0 + \Delta M, Z = Z_0 + \Delta Z \\ \delta &= \delta_0 + \Delta \delta \end{aligned} \tag{4}$$

For convenience, the reference flight condition is assumed to be symmetric and the propulsive forces are assumed to remain constant [13]. This implies that,

$$v_0 = p_0 = q_0 = r_0 = \phi_0 = \psi_0 = w_0 = 0 \tag{5}$$

After linearization the following equations were obtained for the longitudinal dynamics, of the aircraft.

$$\left[\frac{d}{dt} - X_u \right] u + g_o \cos \theta_0 - X_w w = X_{\delta e} \delta_e + X_{\delta T} \delta_T \tag{6}$$

$$-Z_u u + \left[(1 - Z_{\dot{w}}) \frac{d}{dt} - Z_W \right] w - [u_0 + Z_q] q + g_o \sin \theta_0 = Z_{\delta e} \delta_e + Z_{\delta T} \delta_T v \tag{7}$$

$$-M_u u - \left[(M_{\dot{w}}) \frac{d}{dt} - M_W \right] w + \left[\frac{d}{dt} - M_q \right] q = M_{\delta e} \delta_e + M_{\delta T} \delta_T \tag{8}$$

The Eq. (9) gives the transfer function for the change in the pitch rate to the change in elevator deflection angle.

$$\frac{\Delta q(s)}{\Delta \delta_e(s)} = \frac{-(M_{\delta e+} \frac{M_{\dot{z}} Z_{\delta e+}}{u_0})s - (\frac{M_{\dot{z}} Z_{\delta e+}}{u_0} - \frac{Z_{\dot{z}} M_{\delta e}}{u_0})}{s^2 - (M_q + M_{\dot{x}} + \frac{Z_{\dot{z}}}{u_0})s + (\frac{Z_{\dot{z}} M_q}{u_0} - M_x)} \tag{9}$$

The transfer function of the change in pitch angle to the change in elevator angle can be obtained from the change in pitch rates to the change in elevator angle as given in Eqs. (10), (11) and (12).

$$\Delta q = \Delta \dot{\theta} \tag{10}$$

$$\Delta q(s) = s \Delta \theta(s) \tag{11}$$

$$\frac{\Delta \theta(s)}{\Delta \delta_e(s)} = \frac{1}{s} \frac{\Delta q(s)}{\Delta \theta(s)} \tag{12}$$

Hence, the transfer function for the pitch system dynamics of an aircraft can be described by,

$$\frac{\Delta q(s)}{\Delta \delta_e(s)} = \frac{1}{s} \frac{-(M_{\delta e+} \frac{M_{\dot{z}} Z_{\delta e+}}{u_0})s - (\frac{M_{\dot{z}} Z_{\delta e+}}{u_0} - \frac{Z_{\dot{z}} M_{\delta e}}{u_0})}{s^2 - (M_q + M_{\dot{x}} + \frac{Z_{\dot{z}}}{u_0})s + (\frac{Z_{\dot{z}} M_q}{u_0} - M_x)} \tag{13}$$

For simplicity, a first order model of an actuator is employed with the transfer function as given in Eq. (14), and time constant $\tau = 0.0167$ s is employed.

$$H(s) = \frac{1}{\tau s + 1} \tag{14}$$

Modern computer-based flight dynamics simulation is usually done in dimensional form, but the basic aerodynamic inputs are best defined in terms of the

classical non-dimensional aerodynamic forms. These are defined using the dynamic pressure,

$$Q = \frac{1}{2} \rho V^2 = \frac{1}{2} \rho S L V_{eq}^2 \quad (15)$$

where ρ is the ambient density at the flight altitude and V_{eq} is the equivalent airspeed, which is defined by the above equation in which $\rho S L$, is the standard sea-level value of the density. In addition, the vehicle reference area S , usually the wing platform area, wing mean aerodynamic chord \bar{c} , and wing span b are used to non-dimensionalize forces and moments.

3 PID Structures

In the literature, several works has describing the PID structure [15–19]. According to the authors the three term form is the standard PID structure of this controller. The structure is also known as parallel form and is represented by,

$$G(s) = K_p + K_I \frac{1}{s} + K_D s = K_p \left(1 + \frac{1}{T_I s} + T_D s \right) \quad (16)$$

where K_p is proportional gain, K_I is integral gain, K_D derivative gain; T_I is integral time constant and T_D is derivative time constant. The proportional term is for providing an overall control action which is proportional to the error signal through the constant gain factor. The integral term is to reduce steady-state errors through low-frequency compensation by an integrator. The derivative term is to improve transient response through high-frequency compensation by a differentiator. Each of the controllers has its advantages and disadvantages. The disadvantages of each controller can be eliminated by combining all three controllers into a single PID controller. The selection of gains for the PID controllers can be determined by a method developed by Ziegler and Nichols, who studied the performance of PID controllers by examining the integral of the absolute error.

4 Mamdani Fuzzy Logic with PID Combination

In general, the non linear aircraft model is complex, and the complexity arises from the uncertainty in the form of ambiguity [14]. The growth of fuzzy logic approach handles ambiguity and uncertainty existing in complex problems. Fuzzy sets represents fuzzy logic provide means to model the uncertainty associated with vagueness, imprecision and lack of information regarding aircraft dynamics. Fuzzy logic operates on the concept of membership. The membership was extended to possess various “degrees of membership” on the real continues interval between the value 0

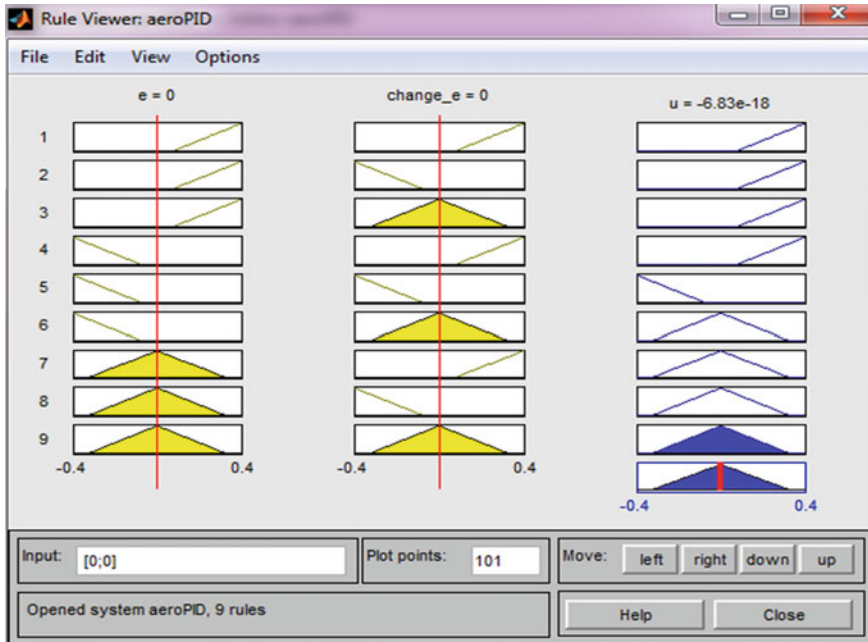


Fig. 2 Fuzzy inference in the rule viewer

and 1. Fuzzy sets are tools that convert the concept of fuzzy logic into algorithms [20]. Since fuzzy sets allow partial membership, they provide computer with such algorithms that extend binary logic and enable it to take human like decision. Fuzzy Logic Control (FLC) system is one of the main developments and successes of fuzzy sets and fuzzy logic. A FLC is characterized by four modules: fuzzifier; defuzzifier; inference engine and rule base. In terms of inference process there are two main types of Fuzzy Inference Systems (FIS) the Mamdani-type and the Takagi–Sugeno Kang (TSK) type. In terms of use, the Mamdani FIS is more widely used, mostly because it provides reasonable results with a relatively simple structure, and also due to the intuitive and interpretable nature of the rule base [22–24].

The aircraft dynamics are highly nonlinear, trial-and-error procedures and experience play an important role in defining the rules. Each fuzzy set consists of three types of membership function, which are negative (N), zero (Z) and positive (P). Here triangular membership functions are chosen for each fuzzy set. The universe of discourse is set between -0.4 to 0.4 that implies the range of pitch angle (± 0.4 radian).

The appropriate membership function to represent each fuzzy set need to be defined and each fuzzy set must have the appropriate universe of discourse. Using the FIS editor, the two inputs to the fuzzy controller are the error (e) which measures the system performance and the rate at which the error changes (Δe), whereas the output of the control signal (Δu). The FIS rule and plot of output surface viewer is shown in Figs. 2 and 3.

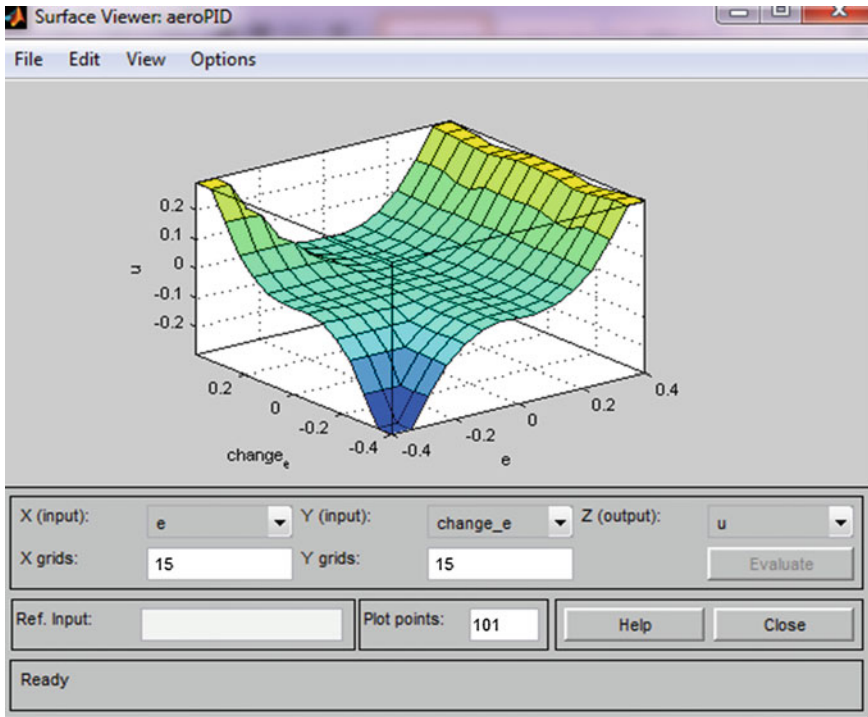


Fig. 3 Three dimensional view of output surface

5 Results and Discussion

5.1 Case 1: Classical Method

Ziegler–Nichols method is heuristic tuning method to obtain PID parameters. In this method, the K_i and K_d gains are first set to zero. The proportional gain is increased until it reaches the ultimate gain, K_u , at which the output of the loop starts to oscillate K_u and the oscillation period P_u are used to set the gains of PID parameters. The longitudinal state space matrix for aircraft dynamics is given in Eq. (17).

$$A = \begin{bmatrix} -63.17 & -203.14 & -776.4 & 0.0000 \\ 1.0000 & 0.0000 & 0.0000 & 0.0000 \\ 0.0000 & 1.0000 & 0.0000 & 0.0000 \\ 0.0000 & 0.0000 & 1.0000 & 0.0000 \end{bmatrix} \quad (17)$$

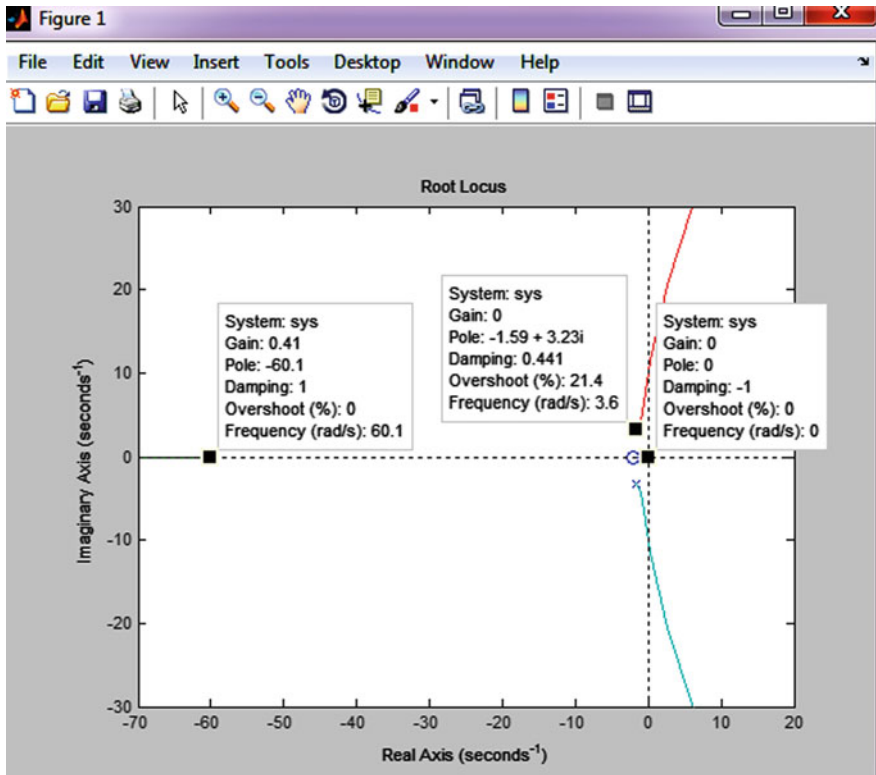


Fig. 4 Root locus of aircraft dynamics response

The eigen values of the longitudinal transport is given in Eqs. (18) and (19).

$$\lambda_{1,2} = 0, 60 \tag{18}$$

$$\lambda_{3,4} = -1.585 \pm i3.22 \tag{19}$$

When the roots are real, there is of course no period, and only parameter is the time to double or half [25]. These are the times that must elapse during which any disturbance quantity will double or halve itself, respectively. When the modes are oscillatory, it is envelope ordinate that doubles or halves. Since the envelope may be regarded as an amplitude modulation, then we may think of the doubling or halving as applied to the variable amplitude. The stability of the airplane is governed by the real parts of the eigen values, roots of the characteristics equation. The root locus of closed loop aircraft dynamics is shown in Fig. 4.

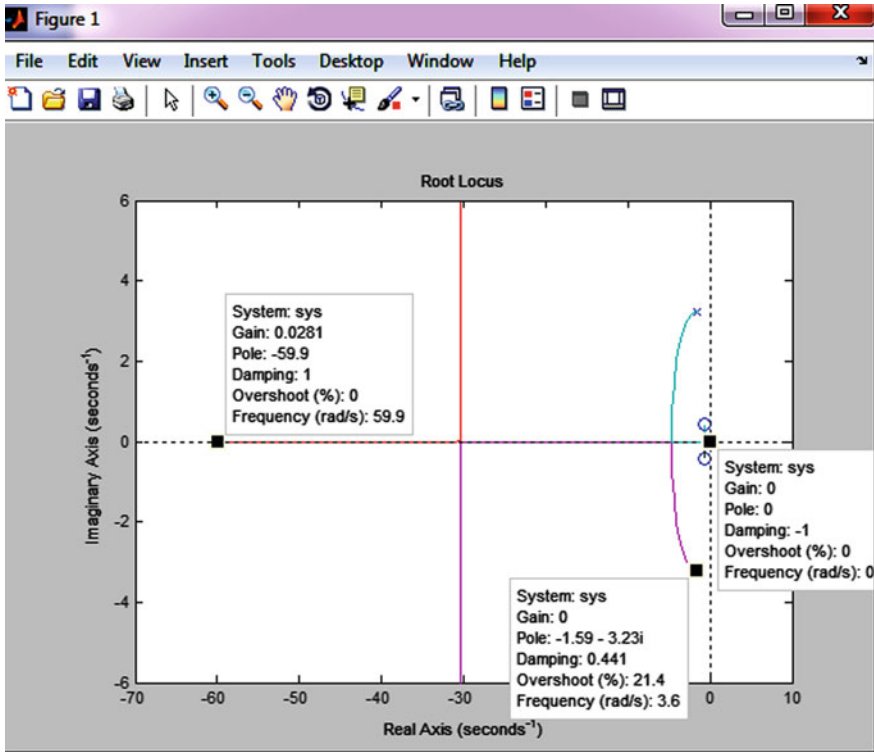


Fig. 5 Root locus of PID controller with aircraft dynamics response

The root locus of closed loop PID controller for aircraft dynamics is shown in Fig. 5. PID Controller has addition of one pole and two zeros. Addition of PID controller generally increases the order of the system. Addition of zeros will cause the root locus to bend toward the left half portion making the system more stable.

The step response of the PID controller is shown in Fig. 6. The delay time is 3 s, rise time is 8 s, settling time is 33 s, and peak overshoot is 59 %. The response is oscillatory in nature.

5.2 Case II: Hybrid Method

In the advanced modern aircrafts, the conventional PID (Proportional-Integral-Derivative) controllers are used extensively even though they are not very efficient for non-linear dynamic systems, mainly because of their intuitive nature, ease of operation and low cost. To overcome this flaw, an unconventional technique of Fuzzy Logic could be used as it has proven to be more efficient than PID controllers and depends on human experience and intuition [26]. This type of Fuzzy

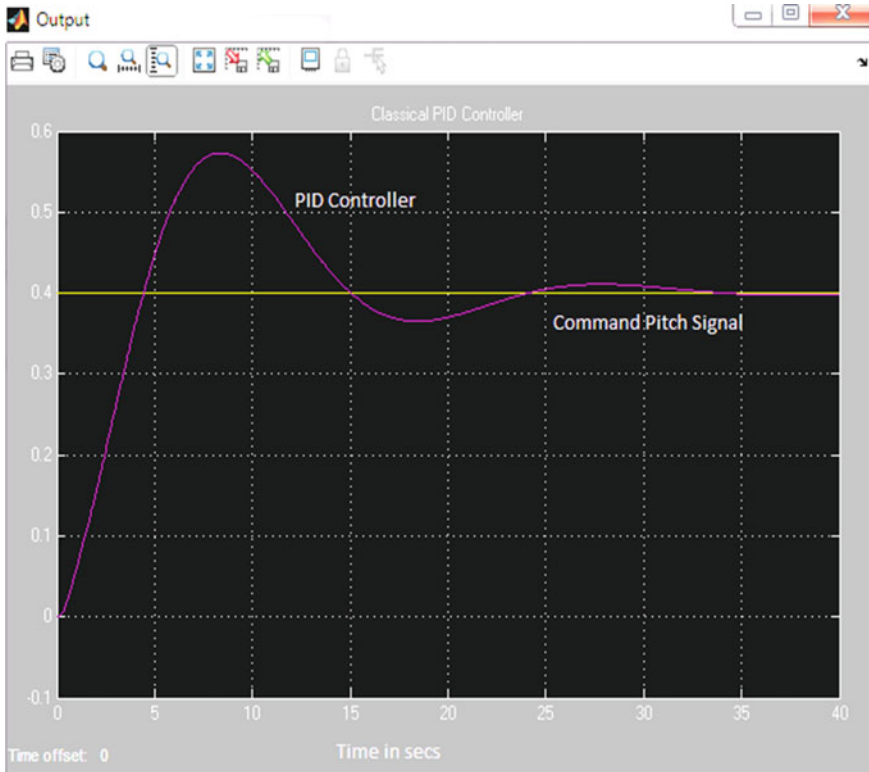


Fig. 6 PID controller response

PID control was expressed by Mamdani and is very popular compared to Takagi–Sugeno type which uses fuzzy sets to define the input variables but the output is defined by means of functions or LTI systems. The step response of the Fuzzy based PID controller is shown in Fig. 7. The delay time is 0.4 s, rise time is 0.8 s, settling time is 3.1 s, and peak overshoot is 48 %. The response is smooth in nature.

The results shown in Table 1 clearly indicates Fuzzy based PID controller is the best compared to PID Controller. The performance specifications like delay time, rise time, settling time and peak overshoot values are very less compared to PID Controller. But it has reasonable steady error as 8 %.

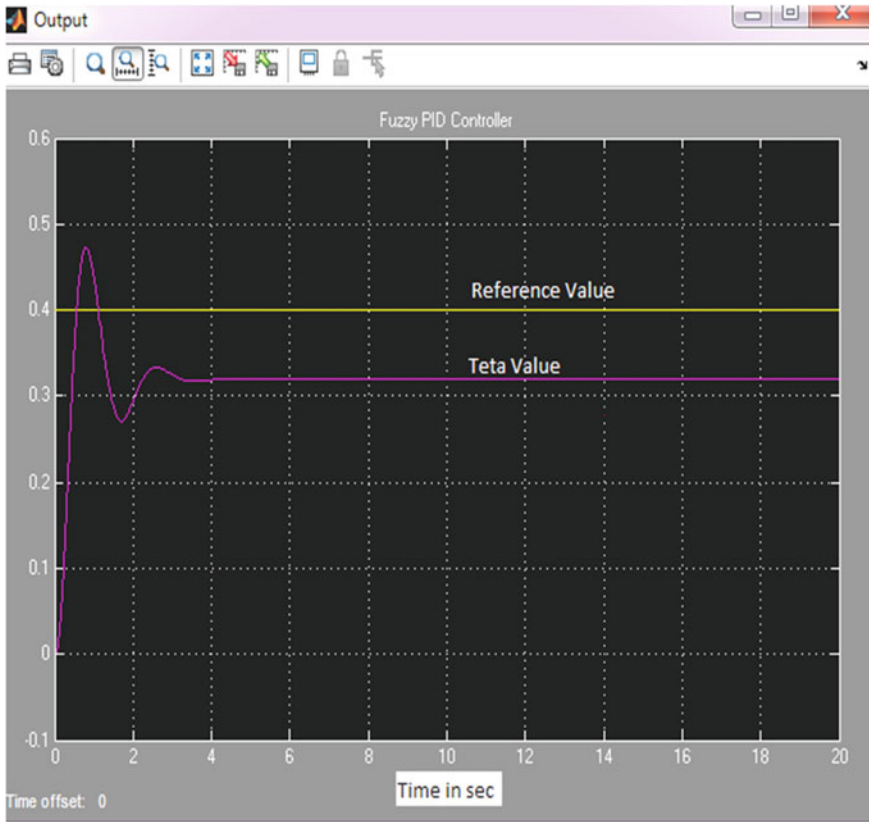


Fig. 7 Fuzzy PID controller response

Table 1 Comparison of PID and fuzzy controller

S.no	PID controller	Fuzzy PID controller
Delay time T_d in secs	3	0.4
Rise time T_r in secs	8	0.8
Settling time T_s in secs	33	3.1
Peak overshoot M_p in %	59	48
Transient behavior	Oscillatory	Smooth
% Steady state error E_{ss}	0	8 %

6 Conclusions

Hence, in this paper fuzzy logic based intelligent controller design is introduced for controlling non linear longitudinal pitch control of an aircraft. Although, there have been many developed techniques to control a dynamic system using feedback as PID control, but very few control techniques are actually implemented in the

real world flight control applications. The main reason behind not implementing the advanced optimal control techniques is that they are not intuitive and in aerospace where safety is a high priority, unintuitive techniques are not trusted enough to be implemented in real aircrafts. From the results the following parameters can be observed. The values show, the PID controller produces the response with very high settling time due to the oscillatory behavior in transient period. It has severe oscillations with a very high peak overshoot of 59 %. The proposed Fuzzy logic controller can effectively eliminate these dangerous oscillations and provides smooth operation in transient period. Also it is giving a steady state error of 8 %, which is a considerable value. The fuzzy control works very efficiently for nonlinear dynamic systems and it's simple and intuitive which is precisely what is required in the current and future aerospace industry.

References

1. Bryan, G.H., Williams, W.E.: The longitudinal stability of aerial gliders. Proc. R. Soc. Lond. A **73**, 110–116 (1904)
2. Tobak, Murray, Schiff, Lewis B.: On the formulation of the aerodynamic characteristics in aircraft dynamics. NACA TR Report-456 (1976)
3. Goman, M.G., Stolyarov, G.I., Tyrtshnikov, S.L., Usoltsev, S.P., Khrabrov, A.N.: Mathematical description of aircraft longitudinal aerodynamic characteristics at high angles of attack accounting for dynamic effects of separated flow. TsAGI Preprint No. 9 (1990)
4. Wang, Q., Stengel, R.F.: Robust nonlinear flight control of a high-performance aircraft. IEEE Trans. Control Syst. Technol. **13**(1), 15–26 (2005)
5. Snell, A., Stout, P.: Robust longitudinal control design using dynamic inversion and quantitative feedback theory. J. Guidance Navig. Control **20**(5), 933–940 (1997)
6. Bossert, D.E.: Design of robust quantitative feedback theory controllers for pitch attitude hold systems. J. Guidance Navig. Control, **17**(1), 217–219 (1994)
7. Fujimoro, A., Tsunetomo, H.: Gain-scheduled control using fuzzy logic and its application to flight control. J. Guidance Navig. Control **22**(1), 175–177 (1999)
8. Anderson, John: Introduction to Flight, 4th edn. McGraw-Hill, New York (2000)
9. Etkin, Bernard, Reid, Lloyd D.: Dynamics of Flight; Stability and Control, 3rd edn. John Wiley and Sons, New York (1998)
10. Nelson, R.C.: Flight Stability and Automatic Control, 2nd edn, McGraw-Hill, New York (1998)
11. MacDonald, R.A., Garelick, M., Grady, J.O.: Linearized mathematical models for DeHavilland Canada 'Buffalo and Twin Otter' STOL Transport, U.S. Department of Transportation, Transportation Systems Centre Reports No. DOTR-TSC-FAA-72-8, (1971)
12. Schmidt, L.V.: Introduction to Aircraft Flight Dynamics, AIAA Education Series, (1998)
13. Chen, F.C., Khalil, H.K.: Two-time-scale longitudinal control of airplanes using singular perturbation. AIAA J. Guidance Navig. Control **13**(6), 952–960 (1990)
14. Sivanandam, S.N., Deepa, S.N.: Control System Engineering using MATLAB. VIKAS Publishing company Ltd, New Delhi, India (2007)
15. Alfaro, V.M., Vilanova, R., Arrieta O.: Two-degree-of-freedom PI/PID tuning approach for smooth control on cascade control systems. In: Proceedings of the 47th IEEE Conference on Decision and Control Cancun, Mexico 9–11 Dec (2008)

16. Ang, K.H., LI, C.G, Yun.: PID control system analysis, design, and technology. In: IEEE Transactions on Control Systems Technology, vol. 13(4) (2005)
17. Yurkevich, V.D.: Advances in PID control. InTec, (2011). ISBN 978-953-307-267-8
18. Myint, M., Oo, H.K., Naing, Z.M., Myint, Y.M.: PID controller for stability of Piper Cherokee's pitch displacement using MATLAB. In: International Conference on Sustainable Development: Issues and prospects for the GMS, China (2008)
19. Zhou, X., Wang, Z., Wang, H.: Design of series leading correction PID controller. In: IEEE International Conference, (2009)
20. Chen, G., Pham, T.T.: Introduction to Fuzzy Systems, Chapman and Hall/CRC Applied Mathematics and Nonlinear Science Series, (2006)
21. Wahid, N., Rahmat, M.F., Jusoff, K.: Comparative assesment using LQR and fuzzy logic controller for a pitch control system. Eur. J. Sci. Res. **42**(2), 184–194 (2010)
22. Lee, C.C.: Fuzzy logic in control system: fuzzy logic controller I. IEEE Trans. Syst. Man Cybern. **20**, 404–418 (1990)
23. Lee, C.C.: Fuzzy logic in control system: fuzzy logic controller II. IEEE Trans. Syst. Man Cybern. **20**, 419–435 (1990)
24. Jianwen, C., Zhanjun, H., Jingcun, S., Changjian, P.: Simulation of fuzzy self-tuning PID control based on simulink. Appl. Mech. Mater. **52–54**, 1644–1649 (2011)
25. Vick, A., Cohen, K.: Longitudinal stability augmentation using a fuzzy logic based PID controller. 28th North American Fuzzy Information Processing Society Annual Conference, USA (2009)
26. Sanchez, E.N., Bacerra, H.M., Verez, C.M.: Combining fuzzy, PID and regulation for an autonomous mini helicopter. Int. J. Inf. Sci. pp. 1999–2022 (2007)

Evaluation of Content Based Spam Filtering Using Data Mining Approach Applied on Text and Image Corpus

Amit Kumar Sharma, Prabhjeet Kaur and Sanjay Kumar Anand

Abstract With the continuous growth of email users, unsolicited emails also known as Spam increases to a large extent. In current, server and client side anti spam filters are developed for detecting different features of spam emails. However, recently spammers introduced some new tricks consisting of embedding spam contents into digital image, pdf and doc files as attachments, which can make all current techniques based on the analysis of digital text in the body and subject field of emails ineffective. In this paper we proposed an anti spam filtering approach based on data mining techniques which classify the spam and ham emails. The effectiveness of proposed approach is experimentally evaluated on large corpus of simple text datasets as well as text embedded image datasets and comparisons between some classifiers such as Random Forest and Naive Bayes is done.

Keywords Spam filtering · Image spam · OCR · Stemming · Features · VSM · tf-idf · PCA · Naive Bayes · Random Forest

1 Introduction

The continuous growth of internet technology leads to various possible ways of communication, in which email system is one of the most convenient and economic method [1]. In email system, everyday we receive different types of

A. K. Sharma (✉) · P. Kaur · S. K. Anand
Central University of Rajasthan, Kishangarh, Ajmer, India
e-mail: amitchandnia@gmail.com

P. Kaur
e-mail: prabhjeetkour@gmail.com

S. K. Anand
e-mail: sanjayanand@curaj.ac.in

messages in bulk. Spam emails is a big problem having several harmful effects such as wastage of user time [2], economic loss, work productivity loss, spreading of virus and Trojans which results in degradation of users trust. Spam stands for “**Self Promotional Advertising Messages**” but now the most popular definition is “**unsolicited bulk mail**”. Spam raises the bandwidth requirement of email system and server load capacity which results in increase of annual cost. In addition, phishing spam emails are the serious threat to security of end users, that try to get personnel and confidential information like passwords and account numbers through spoof messages from on-line business transactions. Another trick has been applied by spammers that is image spam, it embed body of the message into images and send as attachments. Image spam email target different advertisement aims such as: adult, financial, product, internet, health, education, political and spiritual etc.

Spam filtering techniques are classified to segregate ham and spam emails [2]. These techniques mainly focus on three levels as email address, the subject of message and message contents [3]. Email address and subject of message is mainly based on black/white list technology [4] and pattern matching, but spammer are able to bypass both filtering and results in increased rates of false negatives. Content based spam filtering is one of the most effective solutions to detect spam. It is based on features selection and text classification methods such as Naive Bayesian classifier, Random Forest and SVM etc. [5–9]. For image based spam filtering, OCR provides the facility to extract the textual information into images that extracts clean digital text. Spammers are trying to make OCR system ineffective without compromising human readability, by placing text in form of CAPTCHA and it is the hard challenge for OCR [10, 11].

Source of Spam

Source of spam are Botnet [12], Directory Harvest Attacks [12], Internet Hoaxes and Chain Process [12], Social Networking, Backscatter [13], Unsecured Wireless Networks and Open Relays etc.

Types of Spam

There are various types of spam. Some of spam are as: Blank Spam [14], Phishing Mails [12], Email Scam [12], Trojan Horse Email, Image Spam [15, 16], Web Spam [17] and Attachment Spam [18] etc. Spammer more active at the time of festivals and important occasions such as Christmas, Diwali, New Year and World Cup etc., that time spammer attract to the users for buying products and provides several offers to lure them.

2 Image Spam

As there are various anti spam filters are available for detecting the spam with simple messages. For passing these spam filters spammer used image as spam message. Contents of image spam are URL [19], text and hyperlink of the website



Fig. 1 Image spam: health advertisement

etc. For avoid spam filtering in Image they also use some technique with image as obfuscation, split image in multiple section, add wild background, add more colors, hand written text, use of animated pictures, use of CAPTCHA, text bold trick, shorten URLs, forged header information, add Patchy font, use Cartoon etc. [15, 20]. Mostly image spam target are advertisements such as: adult contents, financial, products sell, political, internet, health (usually pharmaceuticals), educational and anti-spam messages etc. Example of image spam can be seen in (Fig. 1).

There are two big issue faced, first is imposed high computational cost to filtering process and second is spammer exploit lot of tricks to fool OCR such as CAPTCHA. In this paper our main focus is on content that are embedded in image, OCR is the useful for image spam filtering. Generally OCR extract image including hand written text, print written text and type written text into simple text. A good OCR recognizes characters in different size, fonts and style. ABBYY Fine Reader is the OCR tool that transforms scans, PDFs and digital camera images into editable and searchable formats and delivers up to 99.8 % recognition accuracy. It can recognize 189 languages and automatic language detection. ABBYY supports Image input formats in BMP, PCX, DCX, JPEG, JPEG 2000, JBIG2, PNG, TIFF, PDF, XPS, DjVu, GIF, WDP and saving formats in DOC, DOCX, XLS, XLSX, PPTX, RTF, PDF, PDF/A, HTML, CSV, TXT, ODT, EPUB, FB2, DjVu [21].

3 Spam Procedure and Remedy

3.1 Technique of Spam Email

Usually spammer use bulk mailing technique to send spam. In this technique bulk mailer send huge volume of email without going through mail server or ISP (Internet Service Provider). In this spammer use several features to hide their

tracks. Mostly bulk mailer don't use their ISP, they use open relay, open relay is SMTP server that provides to everyone to sending mails [22].

3.2 Remedy of Spam

There are two different methods to counter spam emails as:

- The first method tries to prevent bulk mailers to send spam, e.g. by incurring a cost on every email message sent, or by blocking or limiting access to mail servers for spammers. Prevention techniques are classified as Computer time based system and Money Based Systems [22].
- The second method aims to detect and remove all spam once it is sent, by applying different types of filtering techniques. These filtering techniques are as Origin based filtering [4], Challenge—Response Filter, Filtering based on traffic analysis [22], Rule based spam filter [4] and Content based spam filtering [4, 10, 23]. Our main focus in this paper is content based filtering because body of spam message is user interactive part due to attractiveness of contents every time when a user open an email.

4 Related Work

Classification techniques have been applied in textual as well as image spam filtering process. During literature survey, we can see a proposed method, where variant of Naive Bayes classifier have been applied for spam detection [23]. A Compared classification strategy including Naive Bayes, Neural Network, Decision Tree and SVM were tested on different dataset on emails [9]. In which J48 and NB classifier provides better results compare to NN and SVM. A textual classification method defined by K-NN and Genetic Algorithm for solving clustering problem [5]. After successfully done textual classification, some techniques developed for image classification, in which textual features, visual features, shape feature and template based nature have been applied on SVM classifier [11]. A binary classifier also have been proposed to detect image spam which achieves preliminary results on different datasets [15]. Image spam filtering techniques are based on pattern recognition and computer vision, in which OCR and rule based classification technique also have been applied for image spam detection [24]. At the server side a solution of image spam has been presented that suggest a combine cluster analysis based on sparse representation with clustering algorithm [19].

5 Attacks on Spam Filter

To preventing spam emails, spam filtering techniques are playing very effectively role in web security. To decrease filtering effectiveness, spammers try to various attacks on spam filters. There is various common attacks on spam filters as following:

- **Tokenization Attacks**—Spammer prevent tokenization of message by splitting or modifying features, for example putting extra spaces, or symbols like ‘-’ or ‘#’, in the middle of the words, ‘U_N_D_\$_E_R_S_T_##_A_N_D’ [12].
- **Text Obfuscation Attacks**—When message have misspelling certain keywords, such as ‘weeek’, ‘veeery’. Transposing letters or by substituting letters with numbers and symbols, for example, ‘drgs’ or ‘UN\$UBB\$CRIBE’ [12].
- **Good Word Attacks**—One of the most common technique, a spammer modifies a spam message by appending or inserting words indicative of legitimate mails [25, 26].

6 Problem Formulation

Problem with bulk of spam emails received in our mailbox are without our knowledge and these are targeted to affect our systems. For prevention from such spam many schemes has been proposed and implemented, but still problem with these is that whenever spam filters are introduced, the spammer try to find out new way to bypass these filters with new techniques to affect the targeted system. Nowadays most of spammer sends spam mails in image format using several embedding tricks. Some problems were observed literature survey are as:

- How to make more effective to spam filters?
- How to better identify spam emails and classification of ham and spam emails from large data?
- How to better identification of image spam emails from large volume of data?
- How to understand human vision used by spammer?
- Find out new tricks which applied by spammer to send image spam emails.

7 Proposed Working Model

Proposed working model is based on data mining approach for classify ham and spam emails separately to make more effective to content based spam filters at the user level. It has four major sections of data mining process as: data selection, data pre-processing, data classification and data evaluation. The effectiveness of proposed model is experimentally evaluated on simple text datasets as well text

embedded image datasets of spam emails by detecting different features of spam emails. We can see the working of proposed model in (Fig. 2).

7.1 Data Selection

We have selected simple text data from Trec07 text corpus and image data from combination of Trec07 image and Personal image corpus [23, 27]. Randomly different size of files were selected from corpuses for testing purpose.

7.2 Data Pre-processing

Today's real world databases are highly susceptible to noisy, missing, incomplete and inconsistent data due to their typically huge size and their origin from heterogeneous, multiple sources. Low quality data lead to low quality mining results. There are many data pre-processing techniques available as Data cleaning, Data integration, Data transformation and Data reduction [6]. Following steps are used for data cleaning and reducing.

Feature Selection [3, 10, 28, 29]

Feature selection approach is used to find subset of the original variables also known as variable selection or attribute selection. This is based on information gain, correlation and mutual information to filter unimportant and redundant features. We getting features from subject and body of the emails of different data sources using content based filtering.

Feature Extraction

In feature extraction relevant information is extracted from input large data that reduce set of features [28]. Here we are extracting the keywords lists (blacklist and white list) that are present into body of the emails.

Remove Stop and Irrelevant Words

Many common, irrelevant and daily uses words are frequently occurs in email files like is, are, they, has, from, to etc. that have no sense. Some common words also available in emails that are used in both spam emails and legitimate emails. In programming implementation, we are using more than 600 stop words [30] to remove from files.

Word Stemming

In word stemming process commoner morphological and inflexional ending are removed from words. Stemming algorithm based on suffix stripping was given by M. F. Porter in 1980 using English grammatical rules [31–34].

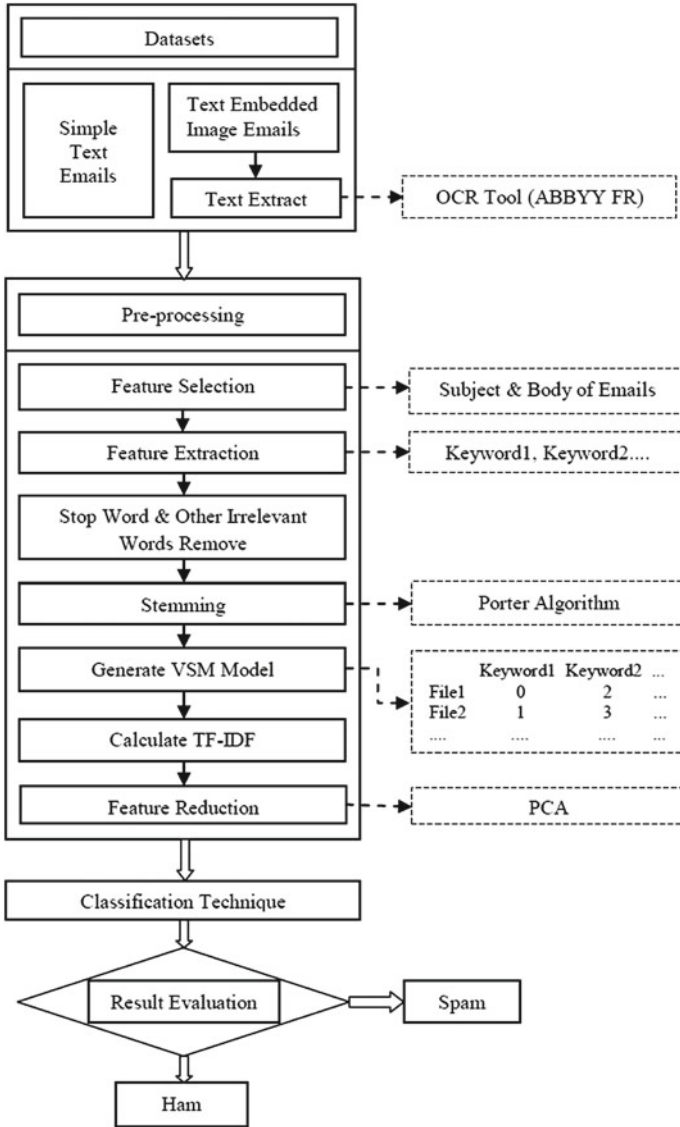


Fig. 2 Proposed working model for ham and spam classification

Tokenization

Tokenization is the process of breaking text into words, phrases, symbols, white spaces or other meaningful elements.

Table 1 Format of sparse matrix

Word frequency					
Document	Word1	Word2	Word3	–	–
File1	2	1	0	–	–
File2	3	0	4	–	–
–	–	–	–	–	–
–	–	–	–	–	–

Generate Vector Space Model (VSM)

VSM provides a sparse matrix which has word frequency for all testing files. Matrix columns represent the number of words presence in the dataset files and rows represent name of the files. The matrix form as in Table 1.

Compute tf-idf

In text mining or information retrieval, the tf-idf (term frequency inverse document frequency), is a suitable method to evaluate how a word important in a document. Calculate tf-idf and represent textual information into a VSM [35] that is algebraic model in which textual information represent as a vector and components of vector represent the importance of a term absence or presence in a document [10, 36].

Combine term frequency and inverse document frequency, to produce a composite weight for each term in each document. tf-idf weight assign to term t in document d given by

$$tf - idf_{t,d} = tf_{t,d} * idf_d$$

where $tf_{t,d}$ is term frequency, each term in a document has a associated weight for that term, that depend on the number of occurrences of the term in the document.

$$tf = P(w|d)$$

where idf_t is inverse document frequency, measured by term is common across all documents divided by cardinality of number of documents by the number of documents containing the term, and taking log of that quotient.

$$idf_t = \log(N/df_t)$$

where df_t defined to be the number of documents in the collection that contain a term t , N is total number of document (corpus of documents).

Feature Reduction

Feature reduction or dimension reduction transform the data in high dimensional to fewer dimensions. We apply principle component analysis technique for feature reduction which take less time for classification and decrease complexity of classifier.

In machine learning field, PCA (**Karl Pearson et al. 1901**) is a statistical procedure that transform correlated variable into linearly uncorrelated variable

which are ordered in reducing variability. Uncorrelated variables are combinations of the original variables. Removal of variables is applied in last with minimum loss of original data [8]. PCA is the simplest true Eigen vector based multivariate analysis. Steps to obtain Principal Component (PC):

Step 1: Dataset is given in form of covariance matrix (Σ):

$$\Sigma = \begin{pmatrix} a_{11} & a_{12} & \cdots & a_{1n} \\ & a_{22} & \cdots & a_{2n} \\ & & \cdots & \cdots \\ & & & a_{nn} \end{pmatrix}$$

Step 2: Obtain the Eigen vector correspondence to covariance matrix $|\Sigma - \lambda I| = 0$ and arrange the Eigen vector in decreasing order as $\lambda_1 \lambda_2 \dots \lambda_n$. Here I denote to the identity matrix

Step 3: Choose λ_1 and get correspond value of the λ_1 :

$$|\Sigma - \lambda I| \begin{pmatrix} \beta_1 \\ \beta_2 \\ \cdots \\ \beta_n \end{pmatrix} = 0$$

Calculate the $\beta_1, \beta_2 \dots \beta_n$ under the normality condition

Step 4: Calculate principle components (PCs). For first PC calculate $\mu_1 = \beta^{(1)'} X$

$$X = \begin{pmatrix} X_1 \\ X_2 \\ \cdots \\ X_n \end{pmatrix}$$

Same process proceeds for $\lambda_2 \dots \lambda_n$.

Properties:

1. First principle component has the maximum variability among the remaining all PCs.
2. Variance of the PC is equal to the corresponding Eigen values.
3. Percentage of variance is explained by the first r PCs, here $r < n$.

$$\%ofvariation = \frac{\sum_{i=1}^r \lambda_i}{\sum_{i=1}^n \lambda_i} \times 100$$

7.3 Data Classification

Classification technique of data mining classifies the large data into separate classes by using different classifier. We are working with Naive Bayes and random forest classifier to classify ham and spam emails. We have compared the results after applying PCA and without applying PCA.

Naive Bayes Classifier

It is a statistical classifier which help in predicting the probability of class membership. In this paper we have used Nave Bayesian classifier which is based on assumption that the effect of value of attribute belonging to a given class is independent of the values of other attribute. The spam message's calculated probability value is higher than the set threshold; then the message is classified as a spam. Before it can be used, a bayesian filter must be trained with a set of legitimate emails (ham). For each word w in the training sets the filter estimates the probability in a spam message($C = S$) or a ham message($C = H$) using

$$P(W = w/C = S) = \frac{S(w)/N_S}{S(w)/N_S + H(w)/N_H}$$

Where $S(w)$ is the number of occurrences of word w in the spam set, $H(w)$ is the number of occurrences of word w in the ham set, and N_H and N_S are the sizes of the ham and spam training sets respectively.

Random Forest Classifier

Generally, the concept of Random Forests is applied to create many classification trees. This method puts every input vector at bottom in each tree of the forest to classify a new object from an input feature vectors. Each tree in forest provides the "votes" to each tree and tree with highest "votes" are considered for classification.

7.4 Data Analysis

Data analysis is evaluation of results of different classifier applied on different datasets. K-fold cross validation is used as testing option for testing of model built by classifier. Cross validation helps to identify good parameters on the basis of which classifier predict unknown data accurately [37]. We have analysed results to find out correctly classified and incorrectly classified instances, analyse time taken to build model, detail accuracy and confusion matrix. Various parameters are as follow [3, 9, 38]

True Positive (TP): Correctly ham and spam detected rate that is actual ham and spam emails.

False Positive (FP): Incorrectly ham and spam detected rate that is not ham and spam emails.

Precision: Number of correctly classified instances of a class/number of instances classified as belonging to that class.

$$P = TP / (TP + FP)$$

Recall: Number of correctly classified instances of a class/number of instances in that class.

$$R = TP / (TP + FN)$$

Accuracy = (Correctly Classified Emails/Total Emails) * 100

Confusion Matrix: Confusion matrices are very useful for evaluating classifiers, as they provide an efficient snapshot of it’s performance, by displaying the distribution of correct and incorrect instances. Typical Weka output contains the following:

Confusion Matrix

<i>a</i>	<i>b</i>	< --	<i>classified as</i>
24	1	<i>a</i>	= <i>ham</i>
2	23	<i>b</i>	= <i>spam</i>

8 Experimental Evaluation

8.1 Experiment Setup

Experiments were carried out on different data sets, which are publicly available. We apply our strategy on image and text dataset; we made different set of files that has equal ham and spam files for both datasets. We have extracted text from image files by using ABBYY FR OCR tool. System configuration was 4 GB RAM, Core2duo 2.00GHz processor having window 7 installed.

8.2 Experiment Results

Experiment 1

Proposed scheme was applied on both image and text dataset. We get the preprocessed results after apply stemming process, remove stop words and other irrelevant words, count word frequency, compute tf-idf and generate sparse matrix. For classifying the data, applied Naive Bayes and Random Forest classifier. Results can be observed as Tables 2, 3, 4 and 5.

Table 2 Results: apply Naive Bayes classifier on simple text dataset

No. of emails	Total attributes	Correctly classified instances	Incorrectly classified instances	TP rate (%)	FP rate (%)	Acc rate (%)	Time build model
300	462	290	10	96.7	3.3	96.7	0.06
500	723	482	18	96.4	3.6	96.4	0.11
1000	1198	954	46	95.4	4.6	95.4	0.46
1500	1530	1435	65	95.7	4.3	95.7	0.72
2000	1823	1920	80	96.0	4.0	96.0	1.13

Table 3 Results: apply Random Forest classifier on simple text dataset

No. of emails	Total attributes	Correctly classified instances	Incorrectly classified instances	TP rate (%)	FP rate (%)	Acc rate (%)	Time build model
300	462	290	10	96.7	3.3	96.7	0.08
500	723	483	17	96.6	3.4	96.6	0.20
1000	1198	964	36	96.4	3.6	96.4	0.56
1500	1530	1451	49	96.7	3.3	96.7	1.11
2000	1823	1952	98	97.6	2.4	97.6	1.58

Table 4 Results: apply Naive Bayes classifier on image dataset

No. of emails	Total attributes	Correctly classified instances	Incorrectly classified instances	TP rate (%)	FP rate (%)	Acc rate (%)	Time build model
50	136	47	3	94	6	94	0
100	284	96	4	96	4	96	0.02
150	444	139	11	92.7	7.3	92.7	0.03
200	553	176	24	88	12	88	0.05

Table 5 Results: apply Random Forest classifier on image dataset

No. of emails	Total attributes	Correctly classified instances	Incorrectly classified instances	TP rate (%)	FP rate (%)	Acc rate (%)	Time build model
50	136	40	10	88	20	80	0.02
100	284	94	6	94	6	94	0.03
150	444	134	16	89.3	10.7	89.3	0.06
200	553	175	25	87.5	12.5	87.5	0.08

Experiment 2

Proposed scheme was also applied on different sets of Trec07 text dataset with PCA. Results can be observed as Table 6.

Table 6 Results: dimensionality reduction of attributes by applying PCA

No. of emails	Total attributes	Correctly classified instances	Incorrectly classified instances	TP rate (%)	FP rate (%)	Acc rate (%)	Time build model
300	157	284	16	94.7	5.3	94.7	0.08
500	261	473	27	94.6	5.4	94.6	0.16
1000	508	911	89	91.1	8.9	91.1	0.35
1500	685	1382	118	92.1	7.9	92.1	0.62
2000	850	1828	172	91.4	8.6	91.4	0.75

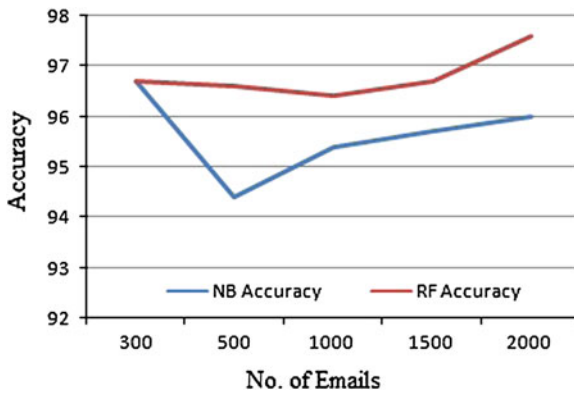


Fig. 3 Accuracy graph between NB and RF classifier

8.3 Result Evaluation

1. Experiment 1 results, tf-idf provides importance of words and removes the unusual words or attribute. Results of Naive Bayes classifier and Random Forest classifier are compared and observed that Random Forest classifier better for large volume of dataset with large features (Fig. 3). Naive Bayes classifier give better accuracy for image categorization.
2. Experiment 2 results shows that Naive Bayes classifier take less time to build model comparative Random Forest classifier (Fig. 4).
3. Experiment 2 results also shows that when we apply classifier with PCA, it reduce the dimensionality of variables and take the less time to build model. Time taken by classifier to build the model after applying PCA is less than without apply PCA (Fig. 5). When we use more instances and attribute PCA gives the almost similar results with high performance.

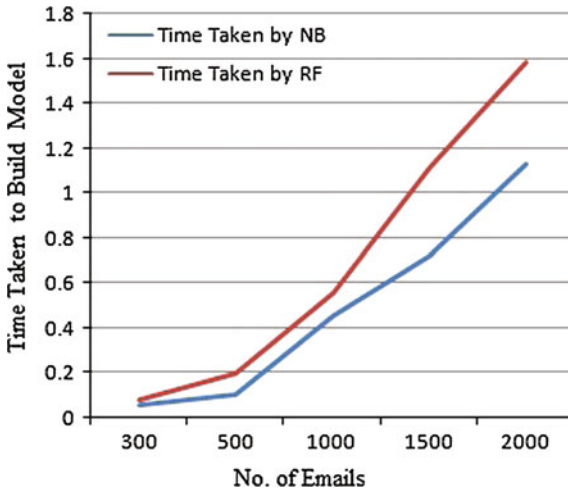


Fig. 4 Time taken to build model graph between NB and RF classifier

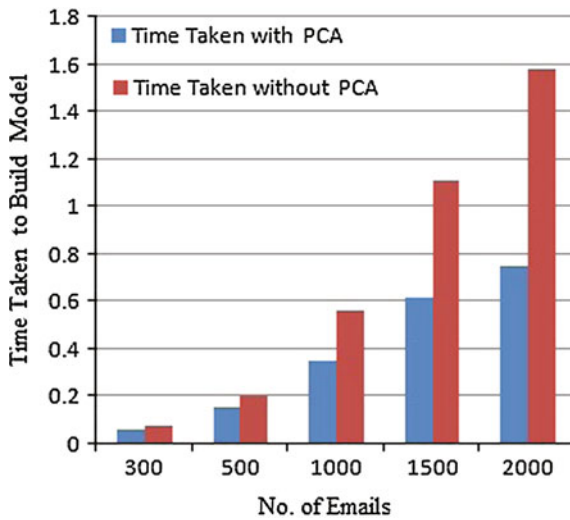


Fig. 5 Time taken to build model graph between applied PCA and without applied PCA

9 Conclusions and Future Work

Researchers are trying to implement new spam filters that can prevent to destination by blocking at client level or server level. In this work, we have presented a content based spam filtering approach using data mining techniques at the client level for classifying the spam and ham emails.

Presented approach have been successfully applied on both simple text dataset as well as image text dataset. We have compared its performance with the Naive Bayes and Random Forest classifiers. We have also compared the performance and accuracy with the using PCA and without using PCA.

We have completed experiment using large and publicly available standard databases and results indicate that the performance of proposed strategy is better. Proposed approach acquired to best average performance for all evaluated databases presenting an higher accuracy rate that is more than 96 % for all emails datasets.

We are conducting more experiments using large volume of datasets as Trec07 simple text dataset, Trec07 image dataset and Personal image dataset. OCR (ABBYY Fine Reader PE 11) tool provides the 99.8 % accuracy to extract text from scan files, pdf and digital camera image files.

Future researches need to consideration on coevolutionary problem of the spam filtering at server level, because while the spam filter tries to develop its prediction capacity, the spammer try to develop their spam messages in order to overreach the classifiers. Therefore, an efficient way to evolve for detection the changes of spam features.

Moreover, Spammer insert a large amount of noise in spam message to make the probability estimation more difficult. None of classifier can give 100 % accuracy thus, spam filters should have a flexible way to compare the term in the classifying task.

References

1. Hayat, M.Z., Basiri, J., Seyedhossein, L., Shakery, A.: Content-based concept drift detection for email spam filtering. In: 5th International Symposium on Telecommunications (IST), 2010, IEEE, pp. 531–536 (2010)
2. Caruana, G., Li, M.: A survey of emerging approaches to spam filtering. *ACM Comput. Surv. (CSUR)* **44**(2), 9 (2012)
3. Qaroush, A., Khater, I.M., Washaha, M.: Identifying spam email based-on statistical header features and sender behavior. In: Proceedings of the CUBE International Information Technology Conference, pp. 771–778. ACM, New York (2012)
4. Wu, J., Deng, T.: Research in anti-spam method based on bayesian filtering. In: Pacific-Asia Workshop on Computational Intelligence and Industrial Application, PACIIA'08, vol. 2, pp. 887–891 (2008)
5. Alguliev, R.M., Aliguliyev, R.M., Nazirova, S.A.: Classification of textual e-mail spam using data mining techniques. *Appl. Comput. Intell. Soft Comput.* **2011**, 10 (2011)

6. Han, J., Kamber, M., Pei, J.: *Data mining: concepts and techniques*. Morgan Kaufmann, San Francisco (2006)
7. Perez-Diaz, N., Ruano-Ordas, D., Fdez-Riverola, F., Mendez, J.R.: SDAI: an integral evaluation methodology for content-based spam filtering models. *Expert Syst. Appl.* **39**(16), 12487–12500 (2012)
8. Rozza, A., Lombardi, G., Casiraghi, E.: Novel IPCA based classifiers and their application to spam filtering. In: *Ninth International Conference on Intelligent Systems Design and Applications, ISDA'09*, IEEE, pp. 797–802 (2009)
9. Youn, S., McLeod, D.: A comparative study for email classification. In: Elleithy, K. (ed.) *Advances and Innovations in Systems, Computing Sciences and Software Engineering*, pp. 387–391. Springer, New York (2007)
10. Fumera, G., Pillai, I., Roli, F.: Spam filtering based on the analysis of text information embedded into images. *J. Mach. Learn. Res.* **7**, 2699–2720 (2006)
11. Mehta, B., Nangia, S., Gupta, M., Nejdil, W.: Detecting image spam using visual features and near duplicate detection. In: *Proceedings of the 17th International Conference on World Wide Web*, pp. 497–506. ACM, New York (2008)
12. Fong, M. (ed): *Spam or harm, Introduction to Artificial Intelligence Project*, 12 Dec (2008)
13. Backscatter. Source of Spam. <http://www.spamresource.com/2007/02/backscatter-what-is-it-how-do-i-stop-it.html>
14. Wikipedia. Types of email spams. http://en.wikipedia.org/wiki/Email_spam
15. Attar, A., Rad, R.M., Atani, R.E.: A survey of image spamming and filtering techniques. *Artif. Intell. Rev.* **40**(1) pp.71–105 (2013)
16. Gao, Y., Yang, M., Zhao, X., Pardo, B., Wu, Y., Pappas, T.N., Choudhary, A.: Image spam hunter. In: *IEEE International Conference on Acoustics, Speech and Signal Processing, ICASSP*, IEEE, pp. 1765–1768 (2008)
17. Hidalgo, J.M.G., Bringas, G.C., Sanz, E.P., Garcia, F.C.: Content based SMS spam filtering. In: *Proceedings of the 2006 ACM Symposium on Document Engineering*, pp. 107–114. ACM, New York (2006)
18. GFI-Microsoft Gold certified partner. Attachment spam the latest trend. <http://www.gfi.com/whitepapers/attachment-spam.pdf>
19. Sadan, Z., Schwartz, D.G.: Social network analysis of web links to eliminate false positives in collaborative anti-spam systems. *J. Netw. Comput. Appl.* **34**(5), 1717–1723 (2011)
20. Gao, Y., Choudhary, A., Hua, G.: A comprehensive approach to image spam detection: from server to client solution. *IEEE Trans. Inf. Forensics Secur.* **5**(4), 826–836 (2010)
21. ABBYY Fine Reader. Input and output supported files. http://www.abbyy.com/support/engine/10win/Product_info/Formats/
22. Garcia, F.D., Hoepman, J.H., van Nieuwenhuizen, J.: Spam filter analysis. In: *Proceedings of 19th IFIP International Information Security Conference, WCC2004-SEC*, pp. 395–410. Kluwer Academic Publishers, New York (2004)
23. Almeida, T.A., Yamakami, A.: Content-based spam filtering. In: *Proceedings of the 2010 International Joint Conference on Neural Networks (IJCNN)*, pp. 1–7 (2010)
24. Biggio, B., Fumera, G., Pillai, I., Roli, F.: A survey and experimental evaluation of image spam filtering techniques. *Pattern Recogn. Lett.* **32**(10), 1436–1446 (2011)
25. Jorgensen, Z., Zhou, Y., Inge, M.: A multiple instance learning strategy for combating good word attacks on spam filters. *J. Mach. Learn. Res.* **9**, 1115–1146 (2008)
26. Lowd, D., Meek, C.: Good word attacks on statistical spam filters. In: *Proceedings of the Second Conference on Email and Anti-spam (CEAS)*, pp. 125–132 (2005)
27. NIST (National Institute of Standard and Technology) US Govt. Trec07 Dataset. <http://trec.nist.gov/data/spam.html>
28. Gong, Y., Chen, Q.: Research of spam filtering based on Bayesian algorithm. In: *2010 International Conference on Computer Application and System Modeling (ICASM)*, vol. 4, pp. V4-678–V4-680 (2010)

29. Ribeiro, M.T., Guerra, P.H.C., Vilela, L., Veloso, A., Guedes, D., Meira, W., Jr, Chaves, M.H.P.C., Steding-Jessen, K., Hoepers, C.: Spam detection using web page content: a new battleground. In: Proceedings of the 8th Annual Collaboration, Electronic messaging, Anti-Abuse and Spam Conference, pp. 8–91. ACM, New York (2011)
30. Onix text retrieval toolkit. Stop word lists. <http://www.lextek.com/manuals/onix/stopwo-rds.html>
31. Bhat, V.H., Malkani, V.R., Shenoy, P.D., Venugopal, K.R., Patnaik, L.M.: Classification of email using beaks: behavior and keyword stemming. In TENCON 2011—2011 IEEE Region 10 Conference, IEEE, pp. 1139–1143 (2011)
32. Duke education. Stemming code. URL <http://www.cs.duke.edu/courses/compsci308/cps108/fa-1107/code/stemmer/code.pdf>
33. Issac, B., Jap, W.J.: Implementing spam detection using bayesian and porter stemmer keyword stripping approaches. In: IEEE Region 10 Conference, TENCON 2009–2009, IEEE , pp. 1–5 (2009)
34. Porter, M.F.: Porter Stemming Algorithm. <http://tartarus.org/martin/PorterStemmer/def.txt>
35. Giannakopoulos, G., Mavridi, P., Paliouras, G., Papadakis, G., Tserpes, K.: Representation models for text classification: a comparative analysis over three web document types. In: Proceedings of the 2nd International Conference on Web Intelligence, Mining and Semantics, p. 13. ACM, New York (2012)
36. Afolabi, I.T., Musa, G.A., Ayo, C.K., Sofoluwe, A.B.: Knowledge discovery in online repositories: a text mining approach. *Eur. J. Sci. Res.* **22**(2), 241–250 (2008)
37. Parimala, R., Nallaswamy, R.: A study of spam e-mail classification using feature selection package. *Glob. J. Comput. Sci. Technol.* **11**(7), 45– 54 (2011)
38. Kumar, R.K., Poonkuzhali, G., Sudhakar, P.: Comparative study on email spam classifier using data mining techniques. In: Proceedings of the International MultiConference of Engineers and Computer Scientists, vol. 1 (2012)

Comparison of Lattice Form Based and Direct Form Based Complex Adaptive Notch Filter

Bhawya Kumar, Rahul Vijay and Pankaj Shukla

Abstract In this paper we present a comparison of the tracking characteristics of Lattice based complex adaptive IIR notch filter (L-CANF) using new adaptive algorithm and Direct form based complex adaptive notch IIR notch filter (D-CANF) using simplified gradient descent adaptive algorithm for different step size parameters. Three cases are investigated, i.e., linear chirp, quadratic chirp and randomly-hopping frequency input complex signals buried complex zero mean white Gaussian noise. Computer simulations shows the better tracking performance of L-CANF based on new adaptive algorithm over D-CANF based on simplified gradient descent algorithm.

Keywords Adaptive filters • Freq-hop • Chirp • Frequency estimation • Complex notch filter

1 Introduction

Adaptive notch filters are required in many engineering applications for estimation, enhancement and suppression of unknown frequencies of periodic components, buried in additive noise. Many designs have been proposed over the years [1–10].

B. Kumar (✉)

Department of Electronics Engineering, Gurukul Institute of Engineering and Technology,
Kota, India
e-mail: bhawyabkumar@gmail.com

R. Vijay

Department of Electronics Engineering, Career Point University, Kota, India
e-mail: vijay.rahul1986@gmail.com

P. Shukla

Department of Electronics Engineering, RTU, Kota, India

An IIR based design provides better notch than FIR based design as surveyed in [1, 2].

While most of the designs focused on real coefficient filters, however complex coefficient adaptive notch filters are required for applications in communication system and signal processing particularly when input signal consist of in-phase and quadrature-phase components. Some examples include enhancement of noisy chirp signals in radar systems [3] and suppression of narrow band interference in the QPSK spread-spectrum system [4, 5].

Complex adaptive IIR notch filters can be direct form based using simplified gradient descent adaptive algorithm as presented in [5, 8] or lattice form based using new complex algorithm as proposed in [9].

In this paper we compared the tracking characteristics of lattice form based complex adaptive notch filter [9] with direct form based complex adaptive notch filter [5–8] using computer simulation. Three different cases are considered i.e. linear chirp, quadratic chirp and randomly-hoping frequency input complex signals buried complex zero mean white Gaussian noise. Our Simulation results shows that L-CANF with new adaptive algorithm provides better and faster tracking of notch frequency than D-CANF using simplified gradient descent algorithm in case of hop and chirp input signals for narrow notch bandwidth as required.

The structure of first order direct form based complex adaptive notch filter is presented in Sects. 2 and 3 presents the lattice form based complex adaptive notch filter. Input signals for different cases of experiment are defined in Sect. 4. Results of computer simulation are presented in Sect. 6 while a comparison using mean update term is shown in Sect. 6 and finally Sect. 7 contains the conclusion.

2 Direct Form Based CANF

Figure 1 shows the structure of first order direct-form complex notch filter. The input sequence is designated as $u(n)$ while output is $e(n)$.

The transfer function linking the input $u(n)$ to the output $e(n)$ of the complex notch filter can be expressed as

$$G(z) = \frac{1 + \alpha}{2} \frac{1 - e^{j\omega_1(n)} z^{-1}}{1 - \alpha e^{j\omega_1(n)} z^{-1}} \quad (1)$$

where α is the notch bandwidth coefficient and ω_1 is the notch frequency parameter. Simplified gradient descent adaptive algorithm used to estimate the input signal frequency is expressed as [5–8].

$$\omega_1(n + 1) = \omega_1(n) + \mu \text{Re}[e(n)x_1^*(n)] \quad (2)$$

Fig. 1 Flow graph of direct form complex notch filter

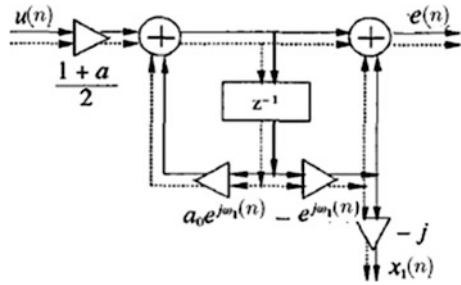
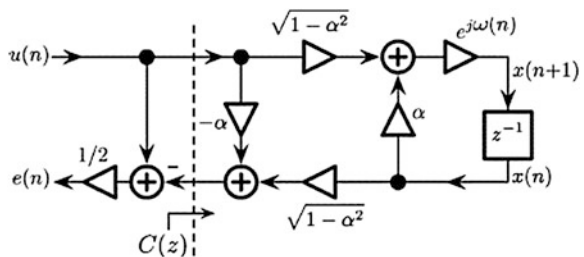


Fig. 2 Flow graph of lattice form complex notch filter



Here $\text{Re}[\cdot]$ denotes real number and $*$ denotes complex conjugate, μ is the step size parameter, $x_1(n)$ is the simplified gradient signal which is generated by the circuit whose transfer function is given by [5, 8] as

$$F(z) = \frac{1+\alpha}{2} \frac{j e^{j\omega_1(n)} z^{-1}}{1-\alpha e^{j\omega_1(n)} z^{-1}} \tag{3}$$

3 Lattice Form Based CANF

Figure 2 shows the flow graph of Lattice form complex notch filter as given by [9]. The input sequence is designated as $u(n)$ while output is $e(n)$.

The transfer function linking input $u(n)$ to the output $e(n)$ of the notch filter will be

$$H(z) = \frac{1+\alpha}{2} \frac{1 - e^{j\omega(n)} z^{-1}}{1 - \alpha e^{j\omega(n)} z^{-1}} \tag{4}$$

where α is the notch bandwidth coefficient and ω is the notch frequency parameter. Transfer function linking the input $u(n)$ to the filtered regressor $x(n)$ of notch filter can be expressed as

$$G(z) = \sqrt{1-\alpha^2} \frac{e^{j\omega(n)} z^{-1}}{1-\alpha e^{j\omega(n)} z^{-1}} \tag{5}$$

Table 1 New complex algorithm for lattice based CANF

<p>New Complex Algorithm</p> <p><i>Available at time n</i></p> <ul style="list-style-type: none"> • Notch frequency parameter (n) • Filter states x(n) • Composite input signal u(n) <p><i>Filter computations</i></p> $x(n + 1) = e^{j(n)}x(n) + e^{j(n)}\sqrt{1 - z} u(n)$ $e(n) = -\frac{\sqrt{1 - z}}{2}x(n) + \frac{1 +}{2}u(n)$ $\omega(n + 1) = \omega(n) + \mu \text{Im}[e(n)x^*(n)]$

For very slow adaptation i.e. small value of μ new complex adaptive algorithm for estimation of the input signal frequency can be written as

$$\omega(n + 1) = \omega(n) + \mu \text{Im}[e(n)x^*(n)] \tag{6}$$

where the imaginary part of the expectation i.e. $E\{e(n)x^*(n)\}$ can be found to be independent of noise induced term as shown in [9]. Here $\text{Im} [.]$ denotes the imaginary number and $*$ denotes complex conjugate, $\mu > 0$ is the step size parameter.

The upper bound for the step size parameter in the above update equation can be found by using stationarity assumption [9] as

$$0 < \mu < \frac{1}{A^2} \left(\frac{1 - \alpha}{1 + \alpha} \right)^{3/2} \tag{7}$$

The new complex algorithm for lattice based CANF is summarized in Table 1.

4 Complex Input Signal

The input to the system is taken as complex single-sided tone plus the background noise.

$$u(n) = Ae^{j(\omega_0(n)+\theta)} + v(n) \quad (8)$$

where A is scale factor (Real or complex) ω_0 is unknown frequency of input signal, θ is random phase uniformly distributed over $[0, 2\pi]$ and $v(n)$ is white complex circular Gaussian noise process whose variance is given by

$$\sigma^2 = E|v(n)|^2 = E\left\{(\text{Re}[v(n)])^2\right\} + E\left\{(\text{Im}[v(n)])^2\right\} \quad (9)$$

a. **Linear Chirp:** For Linear chirp input signal we take

$$u(n) = Ae^{j\omega(n)} + v(n) \quad (10)$$

in which linearly varying frequency is generated using $\omega(n) = \theta_1 n^2$ with $\theta_1 = 0.004$.

b. **Quadratic Chirp:** For quadratic chirp input signal

$$u(n) = Ae^{j\omega(n)} + v(n) \quad (11)$$

quadratically varying frequency is generated using

$$\omega(n) = \theta_2 n^2 + \theta_3 n^3 \quad (12)$$

with $\theta_2 = -0.004$, $\theta_3 = 1.2 \times 10^{-6}$

c. **Frequency Hop:** For generating frequency-hop input signal, its frequency ω is abruptly changes every 1000 iterations giving a piecewise stationary signal.

5 Simulation, Results and Discussion

In this section we present simulation results obtain from single run of adaptive algorithms to demonstrate the comparison of L-CANF with new complex adaptive algorithm and D-CANF with simplified gradient descent algorithm in tracking frequencies of linear chirp, quadratic chirp and frequency hop signal.

In all the cases the signal power is taken as unity ($A = 1$) and signal-to noise ratio is taken as 0 dB.

For notch bandwidth parameter $\alpha = 0.7$ and $A = 1$ the upper bound for step size parameter can be calculated using (7) as

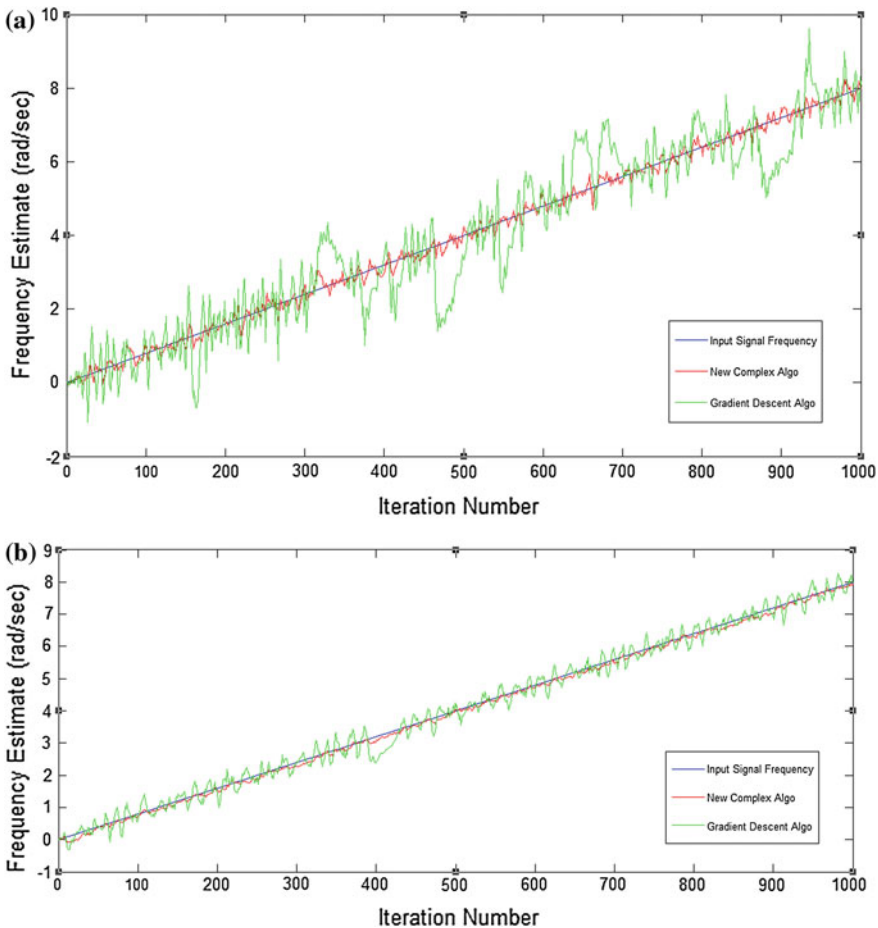


Fig. 3 **a** Linear chirp signal with $\alpha = 0.7$ and $\mu = 0.07$. **b** Linear chirp signal with $\alpha = 0.7$ and $\mu = 0.02$

$$0 < \mu < 0.07 \tag{13}$$

Figure 3a, b shows the results of tracking a frequency of a linear chirp signal. Bandwidth parameter $\alpha = 0.7$, step size parameter $\mu = 0.07$ (upper bound from (10) for Fig. 3a and $\mu = 0.02$ (roughly one-third of upper bound from (10) for Fig. 3b). It can be seen that in both cases L-CANF using new complex algorithm shows much better tracking performance than D-CANF using simplified gradient descent algorithm. Also as the step size parameter is scaled back from its upper bound the adaptive algorithms shows much better tracking capabilities as shown in Fig. 3b.

Figure 4a, b shows the results of tracking a quadratically varying frequency of a quadratic chirp signal. Bandwidth parameter $\alpha = 0.7$, step size parameter

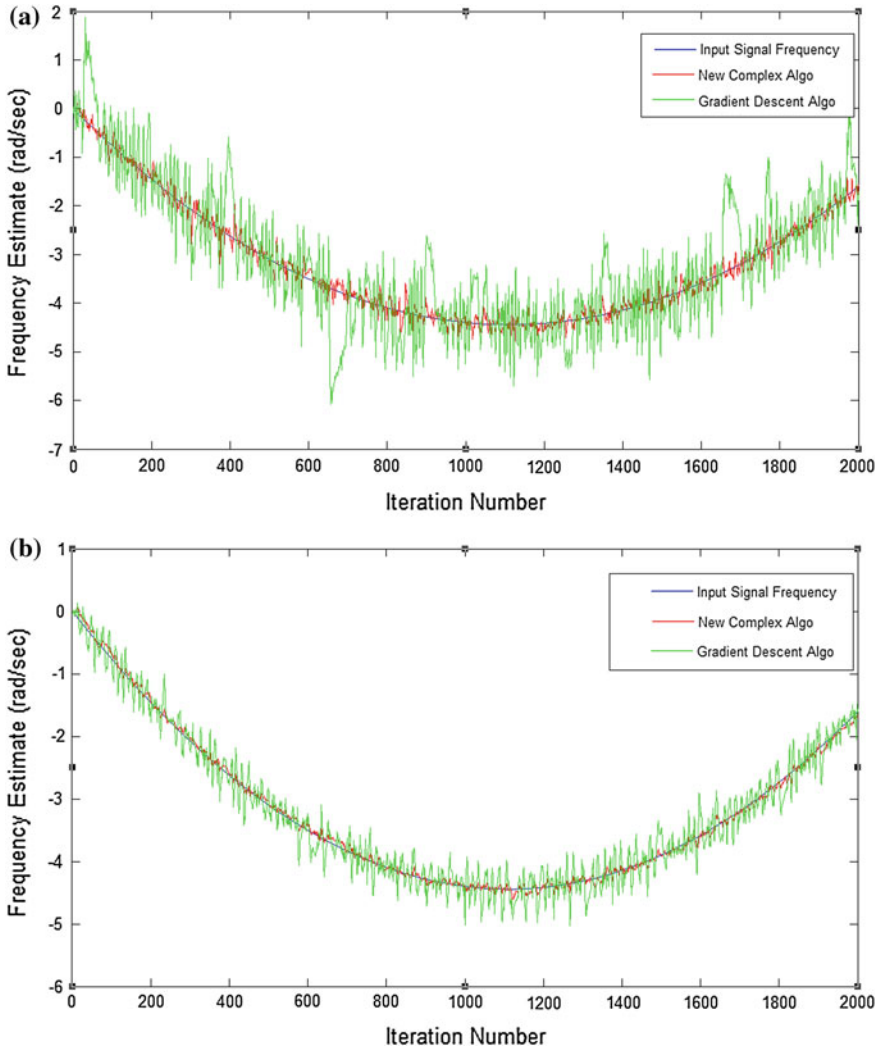


Fig. 4 **a** Quadratic chirp signal with $\alpha = 0.7$ and $\mu = 0.07$. **b** Quadratic chirp signal with $\alpha = 0.7$ and $\mu = 0.02$

$\mu = 0.07$ (upper bound from (10)) for Fig. 4a and $\mu = 0.02$ (roughly one-third of upper bound from (10)) for Fig. 4b. It can be seen that in both cases L-CANF using new complex algorithm shows much better tracking performance than D-CANF using simplified gradient descent algorithm. Also as the step size parameter is scaled back from its upper bound the adaptive algorithms shows much better tracking capabilities as shown in Fig. 4b.

Figure 5 shows the frequency estimates $\omega(n)$ (reduced modulo- 2π) obtained from single run of L-CANF using new complex algorithm and D-CANF using

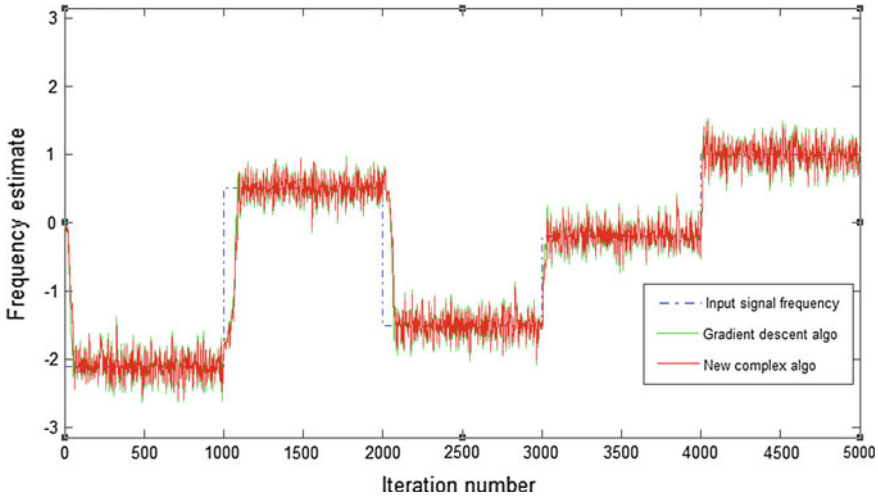


Fig. 5 Frequency hop experiment with $\alpha = 0.7$ and $\mu = 0.07$

simplified gradient descent algorithm in a frequency hop experiment, using bandwidth parameter $\alpha = 0.7$, step size parameter $\mu = 0.07$ (upper bound from (10)). It can be seen that both the adaptive filter algorithms are able to distinguish between positive and negative frequencies as required and takes almost same number of iteration for adaptation, however the variations are slightly less in case of L-CANF using new complex algorithm as compared to D-CANF using simplified gradient descent algorithm.

6 Comparison

The mean update term in case of simplified gradient descent algorithm can be found as

$$f_{\text{simgrad}} = \frac{-A^2}{4} \frac{(1 + \alpha)^2}{|1 - \alpha e^{j(\omega_0 - \omega_1)}|^2} \sin(\omega_0 - \omega_1) \tag{14}$$

and in case of new complex algorithm as given by [9].

$$f_{\text{newcomp}} = \frac{-A^2}{2} \frac{(1 + \alpha) \sqrt{1 - \alpha^2}}{|1 - \alpha e^{j(\omega_0 - \omega)}|^2} \sin(\omega_0 - \omega) \tag{15}$$

From (14) and (15) we have

$$\frac{f_{\text{simgrad}}}{f_{\text{newcomp}}} = \frac{-1}{2} \sqrt{\frac{1 + \alpha}{1 - \alpha}} \leq 1 \tag{16}$$

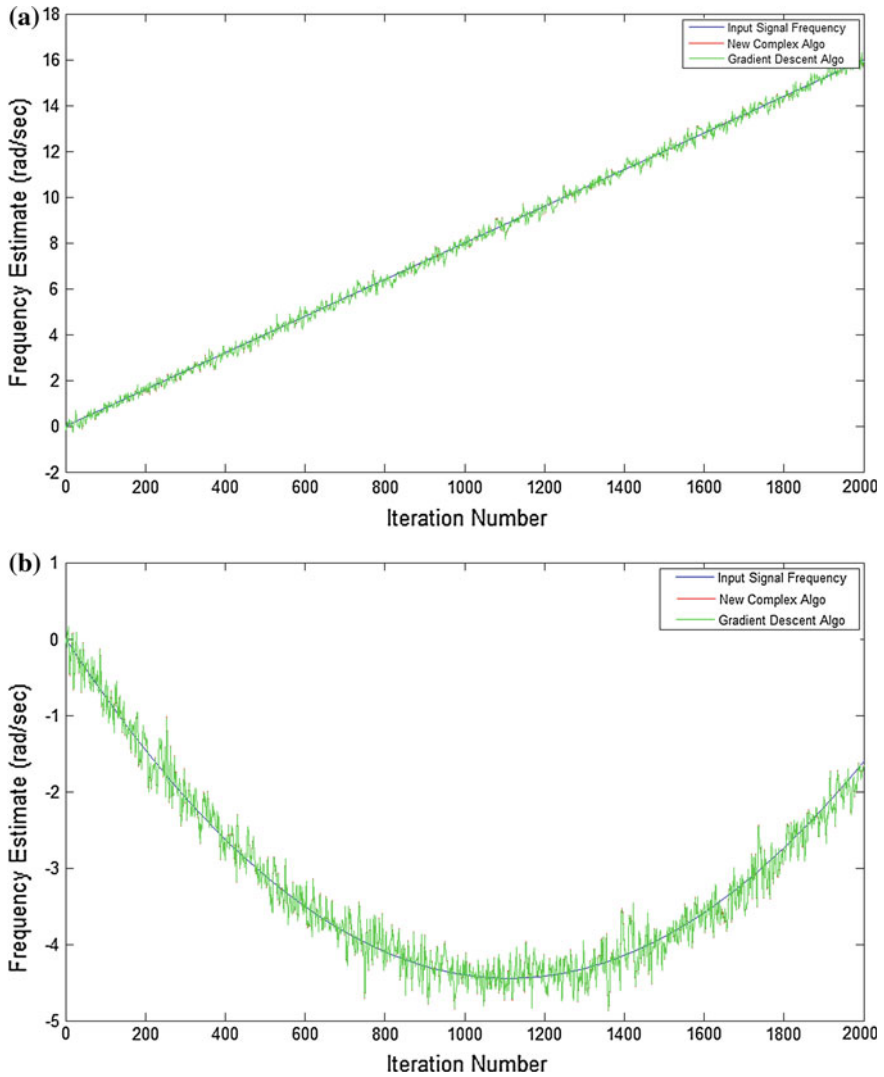


Fig. 6 **a** Linear chirp signal with $\alpha = 0.59$ and $\mu = 0.11$. **b** Quadratic chirp signal with $\alpha = 0.59$ and $\mu = 0.11$

when $\alpha \geq 0.6$.

Thus simplified gradient descent algorithm will have weaker driving force when $\alpha > 0.6$ or we can say for

$$BW_{3db} = \frac{\pi}{2} - 2\tan^{-1}\alpha < 28^\circ \tag{17}$$

At $\alpha \approx 0.6$ both the algorithms provide the similar tracking capabilities as shown in Fig. 6a for linear chirp signal experiment and in Fig. 6b for quadratic chirp signal experiment.

7 Conclusion

In this paper, tracking characteristics of lattice based CANF using new complex algorithm [9] are compared with direct form based CANF using simplified gradient descent algorithm. The comparison was made using linear chirp, quadratic chirp and frequency hop experiment. It has been observed that L-CANF using new complex algorithm shows much better tracking capabilities in estimating varying signal frequencies as compared to D-CANF using simplified gradient descent counterpart for narrow notch filter bandwidth.

References

1. Regalia, P.A.: An improved lattice-based adaptive IIR notch filter. *IEEE Trans. Sig. Process.* **39**, 2124–2128 (1991)
2. Pei, S.C., Tseng, C.C.: Complex adaptive IIR notch filter algorithm and its applications. *IEEE Trans. Circ. Syst.* **CAS-41**(2), 158–163, 1994
3. Macchi, O., Bershad, N.: Adaptive recovery of a chirped sinusoid in noise, part I: performance of the RLS algorithm. *IEEE Trans. Sig. Proc.* **39**, 583–594, 1991
4. Li, L.M., Milstein, L.B.: Rejection of pulsed CW interference in PN spread-spectrum systems using complex adaptive filters. *IEEE Trans. Commun.* **COM-31**, 10–20, 1988
5. Jiang, H.Y., Nishimura, S., Hinamoto, T.: Steady-state analysis of complex adaptive IIR notch filter and its application to QPSK communication systems. *IEICE Trans. Fundam.* **E85-A**(5), 1088–1095 (2002)
6. Nishimura, S., Jiang, H.Y.: Simplified realization of cascaded adaptive notch filters using complex coefficients. In: *Proceedings of ISCAS*, **5**, 269–272 (1998)
7. Mvuma, A., Nishimura, S., Hinamoto, T.: Tracking analyses of adaptive IIR notch filters using gradient-based algorithm. In: *Proceedings of IEEE International Symposium on Circuits and Systems (ISCAS)*, pp. 1148–1151 (2008)
8. Mvuma, A., Nishimura, S., Hinamoto T.: Complex coefficient adaptive IIR notch filter tracking characteristics. *IEEE Trans. Circuits Syst.* **MWSCAS '09**, vol.52, pp. 640–643 (2009)
9. Regalia, P.A.: A complex adaptive notch filter. *IEEE Sig. Process. Lett.* **17**(11), 937–940 (2010)
10. Regalia, P.A.: *Adaptive IIR Filtering in Signal Processing and Control*. Marcel Dekker, New York (1995)

An Ensemble Pruning Approach Based on Reinforcement Learning in Presence of Multi-class Imbalanced Data

Lida Abdi and Sattar Hashemi

Abstract In recent years, learning from imbalanced data sets has become a challenging issue in machine learning and data mining communities. This problem occurs when some classes of data have smaller number of instances than other classes. Multi-class imbalanced data sets have been pervasively observed in many real world applications. Many typical machine learning algorithms pose many difficulties dealing with these kinds of data sets. In this paper, we proposed an ensemble pruning approach which is based on Reinforcement Learning framework. In effect, we were inspired by Markov Decision Process and considered the ensemble pruning problem as a one player game, and select the best classifiers among our initial state space. These selected classifiers which can produce a good ensemble model, are employed to learn from multi-class imbalanced data sets. Our experimental results on some UCI and KEEL benchmark data sets show promising improvements in terms of minority class recall, G-mean, and MAUC.

Keywords Reinforcement learning · Markov decision process (MDP) · Ensemble pruning · Multi-class imbalanced problems

1 Introduction

In many real world applications, the presence of imbalanced data causes many problems for learning algorithms. In these data sets some class or classes of data have smaller number of instances (minor or positive classes) than other classes (major or negative classes). Multi-class imbalanced problems have been pervasively observed

L. Abdi · S. Hashemi (✉)

Department of Computer Science and Engineering, Shiraz University, Shiraz, Iran
e-mail: s-hashemi@shirazu.ac.ir

L. Abdi

e-mail: l-abdi@cse.shirazu.ac.ir

in many real world applications such as weld flaw and protein fold classifications. In imbalance learning, correctly classifying the positive class instances is of great importance. Many typical machine learning algorithms are highly biased to the majority class and ignore the minority class instances. Classification rules that can learn from positive classes are fewer and weaker than other classes. The objective is to learn a classifier which provides a high accuracy for the minority class without severely jeopardizing the accuracy of the majority class [1].

Considering imbalanced problems, there are two crucial aspects; first, which evaluation criteria should be used in order to assess the classifier's performance? Second, what are possible solutions in handling class imbalanced problems? Regarding the first aspect, it is common that accuracy and error rate are the most widely used criteria in classification. But considering the model that is induced with skewed distribution, accuracy or error rate are no longer a wise measure, since the minority class has very little impact on accuracy than other classes. As a result, other performance metrics such as G-mean, Receiver Operator Characteristics (ROC) curve analysis, F-measure, precision, and recall are the more appropriate criteria in this field.

With regard to the second aspect, solutions which have been proposed in the literature are consisting of sampling techniques, feature selection methods, and new algorithms [2]. Sampling techniques, which are commonly consisting of over-sampling and under-sampling techniques, are conducted as pre-process tasks in order to balance the distribution of the training data. These techniques suffer from over-fitting and lack of useful information, respectively. Feature selection techniques [3] attempt to choose the most informative and discriminative features among all features and can help ease the learning process. New algorithms, on the other hand, are designed to change the inductive bias of the learners. Cost sensitive methods, one class classifications, and ensemble learning approaches are among these techniques. These model-based approaches showed many improvements in dealing with skewed distributions. In particular, ensemble learning algorithms have become an effective tool in processing imbalanced data. Many researches have focused on these learning algorithms due to their effectiveness and proficiency such as SMOTEBOOST [4].

We propose an ensemble pruning method which is based on Reinforcement Learning framework. Assuming all the trained classifiers as our initial search space, we try to rank and choose the most accurate and diverse classifiers. Also, a low cost reward function is designed and used to evaluate each state of the search space. Finally, a subset of the base learners is chosen and together they will create a good ensemble model for multi-class imbalanced data sets.

The rest of the paper is organized as follows: in Sect. 2 some of the related researches in imbalanced data sets are presented. Section 3 provides the details of the proposed ensemble pruning approach. Our experimental results and analyses are presented in Sect. 4. Section 5 concludes the paper by a conclusion part.

2 Related Work

In this section some related researches in the area of imbalanced data sets are presented. Data re-sampling techniques such as random over-sampling, random under-sampling, and SMOTE over-sampling (Synthetic Minority Over-sampling Techniques) [5] are among the most widely used methods of sampling. In random oversampling, some randomly chosen instances are added to the original data set. Random under-sampling on the other hand, remove some number of randomly chosen instances from the data set. SMOTE over-sampling, which was proposed by Chawla et al., shows great success in various applications.

SMOTE generate artificial data based on the nearest neighbours of existing minority class instances. For each minority class instance that was chosen to populate, K nearest neighbours are considered. The difference between the considered sample and one of its randomly selected neighbours is computed. Then this difference is multiplied by a random number $\delta \in [0, 1]$ and added to the original sample. The new sample is generated on the connecting line segment between the considered sample and its nearest neighbour. Among model based techniques, SMOTEBOOST [4] combine both SMOTE over-sampling and AdaBoost [6] together which outperforms both of them. SMOTEBoost populates the training data in each iteration of AdaBoost. M2 algorithm with SMOTE over-sampling. Therefore, a balanced set of training data is used in each iteration of the SMOTEBoost. Particularly, in processing multi-class imbalanced data sets the most widely used technique is class decomposition.

Sun et al. [7] used Genetic Algorithm and find the optimum cost setup of each class and design a cost sensitive ensemble algorithm. Wang and Yao [8] used the idea of negative correlation learning which is a successful neural network ensemble learning model and design an algorithm which is called AdaBoost. NC to learn from multi-class imbalanced datasets. They used an ambiguity term, which represents diversity, and lead the algorithm to generate accurate and diverse ensemble members.

Liao [9] studied several over-sampling and under-sampling techniques used with OAA for weld flaw classification problem. Fernandez et al. [10] combined OAO and SMOTE in their algorithm. In order to identify different classes they used a two-step methodology. First, they applied OAO method to decompose the problem to some two-class sub-problems, and then they used SMOTE to balance the data in each sub-problem.

In this paper we designed an ensemble pruning algorithm which is inspired by [8]. In fact, Hazrati et al. [11] designed a game theoretic framework for feature selection. They introduced a Monte Carlo graph search to overcome the complexity of the problem of feature selection. Each state is referred to a subset of features and the action is choosing a feature among all other features. In order to evaluate each episode, they employ a low cost evaluation function to determine the importance of feature subsets in classification problem. The return of episode is propagated to all features that contribute in the episode.

We used the idea of feature selection from [8] and designed an ensemble pruning algorithm to learn from multi-class imbalanced data sets. Ensemble learning models are comprised of three steps: ensemble generation, ensemble pruning, and ensemble integration. In ensemble generation step, some desired number of classifiers are trained as our initial search space. Then our proposed ensemble method ranks each classifier and chooses the most effective ones. In ensemble integration part, we assigned weights to each classifier and aggregate the prediction of selected learners. The label of the coming test instance will be the weighted vote of these classifiers.

3 The Proposed Method

In this section, the proposed ensemble pruning approach which is based on Reinforcement Learning (RL) framework is introduced. We used UCT [12], a Monte Carlo tree search algorithm to generate episodes which help us to explore most promising regions in huge search space of classifiers' combinations. In each iteration, an episode is generated by a sequence of classifier selection. At the end of each iteration, the set of classifiers in the episode is evaluated. The reward of final state is divided among all classifiers in the episode. After desired number of iterations, the top ranked classifiers are selected as our final ensemble model. Weight of each classifier is considered as its weight. In the following parts the detailed explanation of each part is presented.

3.1 Problem Definition

In [12], the problem of feature subset selection has been considered as a Markov Decision Process (MDP) and the RL procedure is applied to evaluate the space. Actually, in RL techniques, it is needed to introduce states and actions. Monte Carlo is one of the RL techniques which learns from complete sample returns and is only used for episodic tasks [13]. After termination of each episode, the episode should be evaluated and the acquired reward should be traversed to each state that has been in the episode.

Inspired from [12], we can consider ensemble pruning problem as a MDP and use RL approach to select the best classifiers for the final ensemble model. Our approach can be formalized as follows: let C_T stands for all the trained classifiers that form our initial search space and C is a subset of C_T which is a state in our search space. In fact, the state space is the power set of C_T and action in this problem is referred to selecting a classifier in the considered state and going to the next state. We consider an imaginary classifier C_f which stands for the last chosen classifier. Selecting this classifier means our episode is terminated and it should be evaluated. At the beginning of each iteration, we consider an empty state and add each classifier to the previous set and go to the next state. As we know the policy π

is a process of selecting the best classifier and the best policy π^* is the one that leads to the best reward [13]:

$$\pi^*(C) = \text{Argmax}_{c \in C_T/C}(\text{Rewards}) \tag{1}$$

3.2 The Proposed Ensemble Pruning Method

In order to select the best classifiers from among all trained ones, a huge state space must be evaluated. Learning the best policy in each state means selecting the best classifier in the current state and that is the main concern of all RL problems. The proposed policy estimation relies on the Upper Confidence Tree (UCT) [14] which improves EvE (exploration versus exploitation) trade-off of the Upper Confidence Bound (UCB) algorithm [15]. Each subset of classifiers in the UCT can be represented as a node. UCT is comprised of two phases: Bandit-based phase and Random-based phase. Bandit-based phase is executed when the algorithm reaches a node which has not been seen previously. In bandit-base phase the algorithm chooses an optimal action that maximizes the UCB criterion which is

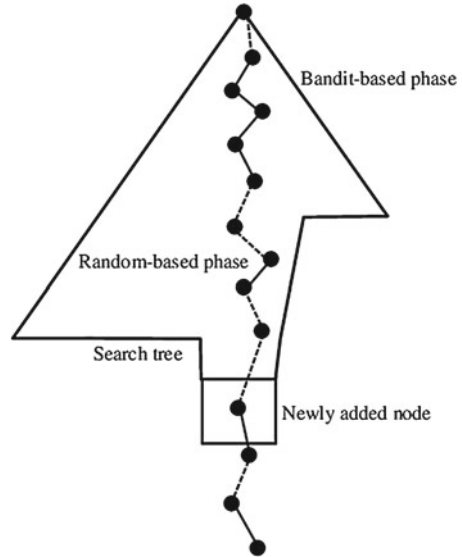
$$a^* = \text{argmax}_{a \in A} \left\{ \hat{\mu}_{C,a} + \sqrt{\frac{c_e \ln(T_C)}{t_{C,a}}} \right\} \tag{2}$$

where T_C is the number of times that node C have been visited, $t_{C,a}$ is the number of times that action a has been selected in node C , $\mu_{C,a}$ is the average reward collected when selecting action a in node C , and c_e is a parameter of the algorithm which is set to 2 in [11] and in our case. On the other hand, random-based phase is executed when the algorithm reaches a node which has not been seen previously. In this phase, the newly met node is added to our state space. In this situation the algorithm does not have any experience, so it will choose an action **randomly** (Fig. 1).

3.3 The Reward Function

In our approach, at the end of each episode we should evaluate the final state with a low cost function. Since we want to have an accurate and diverse ensemble model, we should design a suitable reward function which is able to evaluate the episode efficiently. The reward of each episode is the summation of diversity and G-mean. Each classifier which is involved in the episode gain an equal portion of this reward. Finally, classifiers are ranked with regards to the acquired reward and the ensemble model is created from top ranked classifiers. For a two-class data set we define $S = \{(x_1, y_1), \dots, (x_i, y_i), \dots, (x_t, y_t)\}$ where y_i is the true label of instance x_i and for each classifier f_j , we define $y(j, i) = 1$ if f_j recognizes x_i correctly and 0 otherwise. In order to calculate diversity, we used Q-statistic [16] which is a pairwise measure of

Fig. 1 Illustrates the UCT, a Monte Carlo tree search [12] algorithm which will grow the search tree asymmetrically in order to search the promising regions thereof. UCT proceeds by successive iterations where each iteration executes a sequence of actions which are divided to two phases: a bandit-base phase and random-based phase



diversity. It is highly recommended for its simplicity and understandability. For two classifiers f_i and f_k , the Q-statistic will be calculated as follows:

$$Q_{i,k} = \frac{N^{11}N^{00} - N^{01}N^{10}}{N^{11}N^{00} + N^{01}N^{10}} \tag{3}$$

where N^{ab} is the number of instances x_j for which $y(j, i) = a, y(j, k) = b$. When the number of existing classifiers in an episode is more than two, this measure can be calculated. So if we have m classifiers we have $(m(m - 1))/2$ pairs of classifiers. Higher Q-statistic indicates smaller diversity and lower disagreement between learners. So we can compute diversity as follows:

$$diversity = (-1) \times Q\text{-statistic} \in [-1, 1] \tag{4}$$

In order to evaluate the efficiency of the classifiers in each episode we used G-mean which is the geometric mean of the recall of all classes and can be calculated as follows:

$$G\text{-mean} = \left(\prod_{i=1}^c R_i \right)^{\frac{1}{c}} \tag{5}$$

$$R_i = \frac{TP_i}{TP_i + FN_i}, i = 1, \dots, c \tag{6}$$

where c is the number of classes. In multi-class case ($c > 2$). TP is the number of instances of positive class which are classified correctly and FN is the number of positive class instances that are misclassified. We used a reward function that is computed by adding these two metrics, diversity and G-mean. In each phase of calculating the reward function, each classifier should classify the whole training

data and then we calculate each metric. In order to decrease the computational cost of classification, at the beginning of the algorithm where we want to train initial classifiers as our state space, we classify the whole train samples and preserve the estimated labels. In order to calculate G-mean, we acquire the estimated labels of the instances by taking majority vote between existing classifiers in the episode. Then the corresponding diversity can be calculated as well. In the case that our episode contains less than two classifiers, we set diversity to -1 .

3.4 Overview of the Proposed Method

The pseudo code of the proposed ensemble pruning algorithm with its three major parts is presented in Algorithm 3.4. Main part of the algorithm initializes the search space. The desired number of classifiers is trained using sampling with replacement. We train 100 classifiers. Also, bandit-based phase and random-based phase are presented in part 2 and 3 of the algorithm.

Algorithm 1 Main algorithm “RL-based ensemble pruning approach”

Input: Number of iterations T , training data $S : \{(x_1, y_1), \dots, (x_i, y_i), \dots, (x_t, y_t)\}$, class labels $y \in \{1, 2, \dots, c\}$.

Output: Final ensemble model.

-Select n subset of training data with t samples, from S , using sampling with replacement;

-Train n classifiers on each subset of data.

for $i = 1$ to T **do**

Random-based phase();

end for

Part2: Bandit-based phase function

Add an imaginary classifier C_f to the set of classifiers and select one classifier according to equation 2.

if C is final **then**

Evaluate(C);

Update Rewards();

else if C has been seen previously **then**

Bandit-based();

else

Random-based();

end if

Part3: Random-based phase function

Add an imaginary classifier C_f to the set of classifiers and select one uniformly randomly.

if C is final **then**

Evaluate(C);

Update Rewards();

else if C has been seen previously **then**

Bandit-based();

else

Random-based();

end if

4 Experimental Design

In this section, we aim at providing some evidence which proves the efficiency of our method on 10 standard data sets from UCI [17] and KEEL [18] repository. Table 1 provides some characteristics of these data sets. We used five-fold cross validation in each algorithm to make sure that each fold of test data contains all classes of instances. Also, we used C4.5 decision tree as our base classifier in all algorithms which is implemented in Weka [19], an open source data mining tool with the default parameters. We compare our result with two other ensemble learning models Bagging and AdaBoost. The results show ensemble pruning based on Reinforcement Learning outperforms these two ensemble models in most cases.

4.1 Performance Metrics

Usually the most prevalently used performance criteria in classification tasks are accuracy and error rate. However, they can be deceiving in certain situations and are highly sensitive to changes in data [1]. In processing imbalanced data sets selecting good evaluation criteria is of great importance. We used three performance metrics here, minority class recall, G-mean, and MAUC [20]. Minority class recall which is simply the recall of the minority class is computed as follows:

$$R_{minor} = \frac{TP_{minor}}{TP_{minor} + FN_{minor}} \quad (7)$$

Precision is a measure of exactness, i.e. from among the examples labelled as positive, how many are actually labelled correctly [1]. On the other hand, recall is a measure of completeness, i.e. how many examples of the positive class were labelled correctly. F-measure incorporates both measures, precision and recall, to express the trade-off between them. Parameter β which is set to one in most cases and in our case is a coefficient to adjust the relative importance of these two metrics [1]. Precision and F-measure also provided in the following equations:

$$Precision = \frac{TP}{TP + FP} \quad (8)$$

$$F\text{-measure} = \frac{(1 + \beta^2) \text{Recall} \cdot \text{Precision}}{\beta^2 \cdot \text{Recall} + \text{Precision}} \quad (9)$$

G-mean which is the geometric mean over all classes of data is given in Eq. 5. MAUC on the other hand is the extended version of AUC for multi-class cases is the average of AUC over all pairs of classes.

Table 1 Description of ten benchmark multi-class imbalanced data sets

Data set	Size	Distribution	Class
Ecoli	327	143/77/52/35/20	5
Cleveland	303	164/55/36/35/13	5
Page	5473	4913/329/28/88/115	5
Wine	178	48/59/71	3
Contraceptive	1473	629/333/511	3
Solarflare2	1066	147/211/239/95/43/331	6
Hayes-roth	132	51/51/30	3
Pageblocks	545	492/33/8/12	4
Car	1728	1210/384/69/65	4
Glass	214	70/76/17/13/9/29	6

$$MAUC = \frac{2}{c(c-1)} \sum_{i < j} \frac{[A(i,j) + A(j,i)]}{2} \quad (10)$$

In which $A(i,j)$ is the AUC over classes i, j and can be calculated from the i th column of M . M is a $t \times c$ matrix which is provided by classifier for t instances and c classes. Each element in M , $m_{(p,q)}$, indicates the probability of belongingness of instance p to class q . In multi-class cases $A(i,j)$ and $A(j,i)$ may not be equal, so both of them should be calculated in MAUC [20].

4.2 Analyses and Observations

Our results on several multi-class imbalanced data sets are reported in Table 2. We used five-fold cross validation over each data set. The means and standard deviation of all metrics are computed. Recall is the measure of completeness; it indicates that how many positive class samples are classified correctly. Our overall results indicate improvements in terms of minority class recall, precision, F-measure, G-mean, and MAUC compared to two other ensemble learning algorithms, Bagging and AdaBoost. Minority class recall, precision, F-measure, and G-mean indicate better results over six out of ten data sets. G-Mean shows that how well a classifier can balance the recognition among different classes. In other words, it is the geometric mean of the recall over all classes of data and can indicate the ability of the algorithm in predicting the true labels over all classes. MAUC evaluates the average ability of separating any pairs of classes. It is the average of AUC over all existing class pairs. In our method this metric outperform other methods over four data sets. Although our proposed ensemble pruning approach is simple, it indicates better performance over other competing methods. By searching a huge space of classifiers and select the best performing ones, the learning process improved greatly over other popular ensemble methods. Diversity shows a positive effect on the minority class and the overall performance in terms of MAUC and G-mean [21].

Table 2 Means and standard deviations of MAUC, G-mean, minority class recall, precision, and F-measure by bagging, adaBoost and the proposed method over 10 data sets of UCI [17] and KEEL [18]. Single class metrics are computed for the smallest class of each data set. Greater values are highlighted in boldface

MAUC			
â€¢	Proposed method	Bagging	AdaBoost
Ecoli	0.953 ± 0.0141	0.948 ± 0.025	0.943 ± 0.020
Cleveland	0.616 ± 0.061	0.623 ± 0.074	0.604 ± 0.029
Page	0.971 ± 0.015	0.983 ± 0.009	0.969 ± 0.018
Wine	0.998 ± 0.002	0.996 ± 0.004	0.995 ± 0.007
Contraceptive	0.698 ± 0.028	0.704 ± 0.021	0.688 ± 0.031
Solarflare2	0.866 ± 0.016	0.891 ± 0.014	0.883 ± 0.016
Hayes-roth	0.986 ± 0.015	0.979 ± 0.011	0.972 ± 0.014
Pageblocks	0.947 ± 0.038	0.971 ± 0.031	0.948 ± 0.034
Car	0.998 ± 0.001	0.998 ± 0.001	0.998 ± 0.001
Glass	0.919 ± 0.009	0.925 ± 0.009	0.913 ± 0.031
G-mean			
	Proposed method	Bagging	AdaBoost
Ecoli	0.759 ± 0.059	0.752 ± 0.085	0.78 ± 0.077
Cleveland	0.0 ± 0.0	0.0 ± 0.0	0.0 ± 0.0
Page	0.848 ± 0.058	0.843 ± 0.04	0.837 ± 0.024
Wine	0.962 ± 0.034	0.93 ± 0.04	0.968 ± 0.013
Contraceptive	0.491 ± 0.032	0.494 ± 0.039	0.492 ± 0.020
Solarflare2	0.416 ± 0.242	0.381 ± 0.216	0.313 ± 0.289
Hayes-roth	0.879 ± 0.124	0.847 ± 0.065	0.816 ± 0.070
Pageblocks	0.615 ± 0.364	0.610 ± 0.349	0.420 ± 0.384
Car	0.961 ± 0.024	0.953 ± 0.025	0.951 ± 0.052
Glass	0.262 ± 0.36	0.507 ± 0.284	0.414 ± 0.38
Minority class recall			
	Proposed method	Bagging	AdaBoost
Ecoli	0.8 ± 0.111	0.65 ± 0.224	0.85 ± 0.137
Cleveland	0.0 ± 0.0	0.0 ± 0.0	0.0 ± 0.0
Page	0.867 ± 0.139	0.9 ± 0.091	0.9 ± 0.149
Wine	0.978 ± 0.05	0.916 ± 0.085	0.978 ± 0.05
Contraceptive	0.366 ± 0.054	0.387 ± 0.079	0.393 ± 0.046
Balance	0.02 ± 0.045	0.0 ± 0.0	0.1 ± 0.07
Solarflare2	0.158 ± 0.126	0.117 ± 0.079	0.119 ± 0.153
Hayes-roth	1.0 ± 0.0	1.0 ± 0.0	1.0 ± 0.0
Pageblocks	0.6 ± 0.418	0.8 ± 0.274	0.4 ± 0.418
Car	0.985 ± 0.034	0.954 ± 0.069	0.923 ± 0.133
Glass	0.8 ± 0.447	0.8 ± 0.447	0.6 ± 0.548
Minority class precision			
	Proposed method	Bagging	AdaBoost
Ecoli	0.883 ± 0.162	0.933 ± 0.149	0.86 ± 0.129
Cleveland	0.0 ± 0.0	0.0 ± 0.0	0.0 ± 0.0
Page	0.868 ± 0.184	0.829 ± 0.156	0.848 ± 0.155
Wine	0.964 ± 0.05	0.945 ± 0.122	0.944 ± 0.052

(continued)

Table 2 (continued)

MAUC			
$\hat{\epsilon}$	Proposed method	Bagging	AdaBoost
Contraceptive	0.425 ± 0.023	0.428 ± 0.066	0.403 ± 0.037
Solarflare2	0.293 ± 0.219	0.233 ± 0.137	0.155 ± 0.153
Hayes-roth	1.0 ± 0.0	1.0 ± 0.0	0.971 ± 0.064
Pageblocks	0.7 ± 0.447	0.9 ± 0.224	0.5 ± 0.5
Car	0.939 ± 0.102	0.91 ± 0.1	0.971 ± 0.039
Glass	0.7 ± 0.447	0.633 ± 0.415	0.533 ± 0.505
Minority class F-measure			
	Proposed method	Bagging	AdaBoost
Ecoli	0.824 ± 0.048	0.731 ± 0.091	0.849 ± 0.105
Cleveland	0.0 ± 0.0	0.0 ± 0.0	0.0 ± 0.0
Page	0.85 ± 0.102	0.856 ± 0.099	0.866 ± 0.126
Wine	0.969 ± 0.028	0.926 ± 0.084	0.959 ± 0.024
Contraceptive	0.393 ± 0.041	0.406 ± 0.072	0.398 ± 0.038
Solarflare2	0.198 ± 0.153	0.15 ± 0.089	0.123 ± 0.131
Hayes-roth	1.0 ± 0.0	1.0 ± 0.0	0.985 ± 0.034
Pageblocks	0.633 ± 0.415	0.833 ± 0.236	0.433 ± 0.435
Car	0.958 ± 0.055	0.927 ± 0.054	0.941 ± 0.07
Glass	0.733 ± 0.435	0.693 ± 0.413	0.56 ± 0.518

5 Conclusion

In this paper we proposed an ensemble pruning algorithm based on Reinforcement Learning. In other words, we consider the problem as a Markov Decision Process. By generating episode in each iteration and computing the corresponding reward we are able to rank classifiers. By employing the UCT we could search the most promising regions of the huge state space which provide a trade-off between exploration and exploitation. Our experimental results show the efficiency of our method in most cases in comparison with Bagging and AdaBoost ensemble models.

References

1. He, H., Garcia, E.A.: Learning from imbalanced data. *IEEE Trans. Knowl. Data Eng.* **21**(9), 1263–1284 (2009)
2. Wasikowski, M., Chen, X.W.: Combating the small sample class imbalance problem using feature selection. *IEEE Trans. Knowl. Data Eng.* **22**(10), 1388–1400 (2010)
3. Alibeigi, M., Hashemi, S., Hamzeh, A.: DBFS: An effective density based feature selection scheme for small sample size and high dimensional imbalanced data sets. *Data Knowl. Eng.* **8182**, 67–103 (2012)
4. Chawla, N., Lazarevic, A., Hall, L., Bowyer, K.: SMOTEBoost: improving prediction of the minority class in boosting. *Knowl. Disc Databases* **2003**, 107–119 (2003)

5. Chawla, N.V., Bowyer, K.W., Hall, L.O., Kegelmeyer, W.P.: Smote: synthetic minority over-sampling technique. *J. Artif. Intell. Res.* **16** 341–378 (2002)
6. Freund, Y., Schapire, R.E.: A decision-theoretic generalization of on-line learning and an application to boosting. *J. Comput. Syst. Sci.* **55**, 119–139 (1997)
7. Sun, Y., Kamel, M.S., Wang, Y.: Boosting for learning multiple classes with imbalanced class distribution. In: *Proceedings of the 6th International Conference on Data Mining (ICDM 06)*, pp. 592–602 (2006)
8. Wang, S., Yao, X.: Multiclass imbalance problems: analysis and potential solutions. *IEEE Trans. Syst. Man Cybern. Part B* **42**(4), 1119–1130 (2012)
9. Liao, T.W.: Classification of weld flaws with imbalanced class data. *Expert Syst. Appl.* **35**(3), 1041–1052 (2008)
10. Fernandez, A., del Jesus, M.J., Herrera, F.: Multi-class imbalanced data-sets with linguistic fuzzy rule based classification systems based on pairwise learning. *Comput. Intell. Knowl. Based Syst. Des.* **6178**, 8998 (2010)
11. Hazrati, S. M., Hamzeh, A., Hashemi, S.: A game theoretic framework for feature selection. In: *9th International Conference on. IEEE Fuzzy Systems and Knowledge Discovery (FSKD)* (2012)
12. Gaudel, R., Sebag, M.: Feature selection as a one-player game. In: *International Conference on Machine Learning*, pp. 359–366 (2010)
13. Sutton, R.S., Barto, A.G.: *Reinforcement Learning: An Introduction*, vol. 1, MIT press, Cambridge (1998)
14. Kocsis, L., Szepesvri, C.: Bandit based monte-carlo planning, *Mach. Learn.: ECML* 282–293 (2006)
15. Auer, P., Cesa-Bianchi, N., Fischer, P.: Finite-time analysis of the multiarmed bandit problem. *Mach. Learn.* **47**(2–3), 235–256 (2002)
16. Kuncheva, L.I., Whitaker, C.J.: Ten measures of diversity in classifier ensembles: limits for two classifiers, In: *Intelligent Sensor Processing, A DERA/IEE Workshop*, pp. 10–1, IET (2001)
17. Frank, A., Asuncion, A.: UCI machine learning repository. <http://archive.ics.uci.edu/ml> (2010)
18. Alcalá-Fdez, J., Fernandez, A., Luego, J., Derrac, J., Garcia, S., Sanchez, L., Herrera, F.: Keel data-mining software tool: Data set repository, integration of algorithms and experimental analysis framework. *J Multiple-Valued Logic Soft Comput.* **17**(2–3), 255–287 (2011)
19. Witten, I.H., Frank E.: *Data Mining: Practical Machine Learning Tools and Techniques*, 2nd edn. Morgan Kaufmann, San Francisco (2005)
20. Hand, D.J., Till, R.J.: A simple generalization of the area under the ROC curve for multiple class classification problems. *Mach. Learn.* **45**(2), 171–186 (2001)
21. Wang, S., Yao, X.: Relationships between diversity of classification ensembles and single-class performance measures. *IEEE Trans. Knowl. Data Eng.* **25**(1), 206–219 (2013)

Fusion of Fingerprint and Iris Biometrics Using Binary Ant Colony Optimization

Minakshi Gogoi and Dhruva Kr. Bhattacharyya

Abstract This paper presents an effective method for decision level fusion of fingerprint and iris biometrics using binary ant colony optimization (ACO) technique to identify the imposter instances. ACO is an evolutionary method. The selection of a proper set of optimization parameters for ACO is a multi-objective decision making optimization problem. Initially the matching scores for individual biometric classifiers are computed. Next, a ACO-based procedure is followed to simultaneously optimize the parameters and the fusion rules for fingerprint and iris biometrics. The proposed method has been found to perform satisfactorily on several benchmark datasets.

Keywords ACO · BACO · Iris · Fingerprint · FAR · FRR

1 Introduction

Multimodal biometrics fusion gains importance in the biometric authentication system due to its impact on higher accuracy and better performance. In score level fusion of different modalities, the performance is adversely affected by the fusion strategies. The score level fusion involves matching scores from the different sensors, and the fusion of these scores by sum, product and weighted sum rules. A major issue of fusion of multi-modal biometric is the selection of optimal rules. Some of the approaches that employ an optimal fusion are deterministic methods, probabilistic method and evolutionary computation method. Different evolutionary

M. Gogoi (✉)

Department of CSE/IT, GIMT, Guwahati, India

e-mail: m_gogoi@tezu.ernet.in

D. Kr. Bhattacharyya

Department of CSE, Tezpur University, Assam, India

e-mail: dkb@tezu.ernet.in

computation approaches are swarm intelligence (SI) [1], ant colony optimization (ACO), bacteria foraging and genetic algorithm (GA).

Our work is focused on the development of an effective method for combination of multimodal biometric data. Iris and fingerprint biometrics have been found better as compared to other available traits due to their accuracy, reliability and simplicity, which make them promising solution to the society. The features of individual iris and fingerprint traits are extracted from their preprocessed images. These features of a query image are compared with those of stored template to obtain the matching scores as in [2]. It shows the utility of adaptive multimodal biometric fusion on the real biometric samples using the Bayesian fusion rule for score level fusion. We have investigated the adaptive combination of iris and fingerprint biometric on publicly available database and the results have been found satisfactory.

The rest of the paper is organization as follows: [Sect. 2](#) describes the related multimodal biometric fusion works. In [Sect. 3](#), we discuss about the ACO optimization work. In [Sect. 4](#), we have given our method. We demonstrate the performance of the proposed method in [Sect. 5](#), followed by our concluding remarks in [Sect. 6](#).

2 Related Work

Recently, works on the fusion of multimodal biometrics are gaining significant importance due to their effectiveness in terms of cost and efficiency. In the past few years several novel methods have been introduced to address this important problem. Based on our study, it has been observed that the fusion works can be classified into six major categories as follows.

- (a) Sensor level fusion: Raghavendra et al. [3] consider biometric sensor fusion technique using PSO for face and palmprint images. The authors use decomposition technique based on wavelet transformation. They select the most discriminative wavelet coefficients from the images to produce a fused image. Singh et al. [4] use visible and infrared face images and verification. It decides based on match scores by using multiple SVMs to learn both the local and global properties of the multi-spectral face images at different granularity levels and resolution.
- (b) Representation level fusion: Nagar et al. [5] consider fusion of different features into a single multi-biometric template by converting different biometric representations into a common representation space using various embedding algorithms. Rattani et al. [6] use integrated feature sets obtained from multiple biometric traits like fingerprint and iris.
- (c) Dynamic Classifier Selection: Giacinto et al. [7] select classifier for each unknown pattern, that is more likely to classify it correctly. In another attempt, Giacinto et al. [8] design a multiclassifier selector for each pattern. It ensures that at least one classifier identifies the patterns correctly. In order to select this classifier, the training patterns with the same behaviour are considered and the classifier with the highest accuracy is chosen.

Table 1 Biometric fusion methods and their uses

Approaches	Descriptions/methods used
Sensor level (Raw data)	The authors [3] consider biometric sensor fusion technique using PSO for face and palmprint images. The authors [4] have fused visible and infrared face images and verification decision is made using match score fusion
Representation or feature level	The author [5] have considered fusion of different features into a single multi-biometric template. The author [6] have used integrated feature sets obtained from multiple biometric traits like fingerprint, iris
Dynamic classifier selection	The author [7] have aimed to select, for each unknown pattern, the classifier that is more likely to classify it correctly. The author [8] also considered to design an multiclassifier selector for each pattern
Matching score or confidence level	The author [9] introduce a rule-based approach to consider the task of combining classifiers in a probabilistic Bayesian framework based on the Bayes theorem and hypothesis. The author [10], provided a supervised approach which shows fusion strategy using a support vector machine (SVM)
Class rank-based (Class rank)	The author [11] propose fusion based on a minimum distance method for combining rankings from several biometric algorithms
Decision (abstract level)	The authors [13] introduce decision-level fusion for correlated biometric classifiers

- (d) Matching score-based fusion: Kittler et al. [9] introduce a rule-based method to combine the classifiers in a probabilistic Bayesian framework on the basis of the Bayes theorem and by using a hypothesis it obtains the ways to merge the modalities (sum, product, max, min). It is established by the authors based on experimental results that the *sumrule* outperforms the remainder due to its robustness to errors made by the individual classifiers. Fierrez-Aguilar et al. [10] provide a supervised method which shows that a fusion strategy using a support vector machine (SVM) can outperform a fusion algorithm using the *sumrule*.
- (e) Class Rank-based fusion: Rukhin et al. [11] propose a fusion technique based on a minimum distance method for combining rankings from several biometric algorithms.
- (f) Decisión Level Fusion: Veeramachaneni et al. [12] use a decisión-level fusion for correlated biometric classifiers based on likelihood ratio test (LRT) and the Chair Varshney rule (CVR).

A table of comparison of these methods in terms of two basic parameters is shown in Table 1. We enumerate the following observations based on our study:

1. In the past, several effective supervised and unsupervised methods have been introduced to address the multimodel biometric fusion problem. Most methods have been established using fingerprint and iris images.

2. Methods for multibiometric fusion can be broadly classified into six categories based on their flexibility on the measure, metric and level of representation used. A major issue with most of the these methods is the increase in false alarms. Special attempts have been made to improve the detection accuracy, and hence to minimize the false alarms.
3. Appropriate use of optimization techniques have proven to be useful in improving the performance of such multisensor-based methods. However, deciding the appropriate set of parameters/thresholds is the challenging task in such optimization techniques.

3 Background of the Work

Ant colony optimization (ACO) is a nature-inspired optimization algorithm [14, 15], motivated by the natural phenomenon that ants deposit pheromone on the ground in order to mark some favorable path that should be followed by other members of the colony. The first ACO algorithm, called the ant system, was proposed by Dorigo et al. [16]. ACO has been widely applied in various problems [17].

3.1 Ant Colony Optimization (ACO)

ACO aims to iteratively find the optimal solution of the target problem through a guided search (i.e., the movements of a number of ants) over the solution space, by constructing the pheromone information. The main characteristic of ACO algorithm is that, at each iteration the pheromone values are updated by all the k ants those have built a solution in the iteration itself. Each ant chooses its possible solutions randomly from the available possible values. Two important parameters in ACO are ‘pheromone constant’ (Q) and ‘evaporation factor’ ($\rho < 1$). The pseudo code of an ACO algorithm is given in Fig. 1.

3.2 Binary ACO for Fusion of Fingerprint and Iris

The binary ACO (BACO) algorithm used in this fusion approach of iris and fingerprint trait is (i) to make choice of sensors, (ii) to dynamically select threshold and (iii) to select fusion rule to maximize the accuracy or minimize the accuracy error. The algorithm quantifies different security level by associating error rates: global false acceptance rate (GFAR) and global false rejection rate (GFRR) given by [12] are depicted in the Table 2.

Fig. 1 Pseudo code of an ACO

```

Initialize positions of totally K ants
Initialize pheromone matrix  $\tau(0)$ 
for  $n = 1$  to  $N$  do
    for  $k = 1$  to K do
        consecutively move the  $k^{th}$  ant for  $L$  steps, according to a probabilistic rule selection
        update the pheromone matrix  $\tau(N)$ 
        make the solution decision according to the final pheromone matrix  $\tau(N)$ 
    end for
end for
    
```

Table 2 Fusion rules

Error definition	Fusion rule selected			
	Iris only	Fingerprint only	AND	OR
GFAR	FAR1	FAR2	$FAR1 \times FAR2$	$FAR1 + FAR2 - FAR1 \times FAR2$
GFRR	FRR1	FRR2	$FRR1 + FRR2 - FRR1 \times FRR2$	$FRR1 \times FRR2$

3.3 Problem Formulation with BACO for Fusion

In this problem there are $(N + 1)$ dimensions, where N is the number of biometrics. Each of the N dimensions is a threshold at which that particular biometric is set. The $(N + 1)$ th dimension is the fusion rule, which determines how all the decisions from the biometrics are fused. Hence the representation of each particle is

$$X_i = \lambda_{i1}, \lambda_{i2}, \lambda_{i3}, \lambda_{i4}, \dots, \lambda_{in}, f_{in+1} \tag{1}$$

where each $\lambda_{ij}, j = 1, 2, \dots, n$, represents a particular biometric and f_{in+1} represents the fusion rule.

The problem is to develop an effective decision level fusion method based on a score combination function ‘f’ which accepts individual scores obtained from each sensor to identify an instance X_i either as genuine or imposter w.r.t. a decision threshold.

4 Proposed Method

The biometric thresholds are continuous. In such model, a fusion rule takes an integer value which suffers slow convergence hence the need for binary ACO (BACO) algorithm, where FAR of each biometric is evolved instead of thresholds. The fusion rule is a binary number having a length of $\log_2 p$ bits, where $p = 2^{2^N}$,

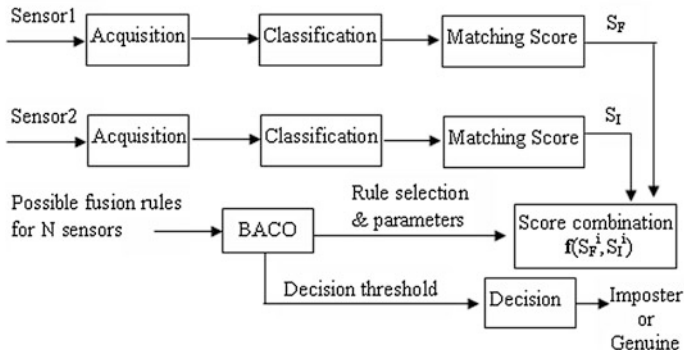


Fig. 2 Block diagram of the proposed system

with a real value varying from $0 \leq f \leq p - 1$. For binary search spaces, the binary decision model as described in [12] is being used. A binary decision model works better for moving through the decision fusion space.

The block diagram of the proposed method is shown in Fig. 2. As shown in the figure, the method accepts the match scores from the individual sensors and uses a combination function f to combine the scores, hence to decide the genuineness of an input instance.

The multimodal biometric data from fingerprint and iris biometric are used to extract the corresponding F_F and F_I feature vectors. These feature vectors are employed to generate the matching scores S_F and S_I from the corresponding templates acquired during the registration. The risk of attack on a biometric system can be varying and therefore it is critical to provide multiple levels of security. The security requirement in Bayesian sense, is quantified with two parameters; the global cost (0, 1) of falsely accepting an imposter C_{FA} and the global cost (0, 1) of falsely rejecting or accepting a genuine user C_{FR} from the installed biometric system. These two costs can be employed to adequately quantify the desired performance. The total error cost, E to be minimized by the multimodal biometrics system is the weighted sum of $GFAR$ and $GFRR$ as given by [12] is

$$E = C_{FA}GFAR(\eta) + C_{FR}GFRR(\eta) \text{ where } C_{FA} + C_{FR} = 2 \tag{2}$$

where $GFRR(\eta)$ is the global or the combined false acceptance rate and $GFRR(\eta)$ is the combined false rejection rate at decision threshold η from the multimodal biometric system. The task of multimodal biometric system as shown in Fig. 2 is to minimize the (global) cost E , i.e., the accuracy error for the system given by Eq. 2, by selecting (i) the appropriate score level combination rule, (ii) its parameters and (iii) the decision threshold. The multidimensional search among the various combination rules and their weight parameters to optimize the global cost E is achieved by the ant colony optimization (ACO) approach.

We discuss the basic steps of the proposed method as depicted in Fig. 2.

4.1 Data Acquisition

A virtual multimodal database derived from the CASIA iris database [18] and FVC fingerprint database [19] is used to evaluate the performance of the said method. The multimodal database consists of 108 users obtained by randomly pairing the first 108 users in the FVC database with the users in the CASIA database.

4.2 Feature Extractions

In case of iris, the most discriminating features of iris pattern is the phase information. Extraction of the phase information is done by using 2D Gabor wavelets according to Daugman [20]. In case of fingerprint feature extraction, two salient features, i.e., core and reference points. An algorithm developed by Hong et al. [21] is used to detect the core point but with a slight difference that maps all the block directions to the interval from -0.5 to 0.5 and then simply regards the value 0.5 corresponds to the core.

4.3 Matching

We use individual matching mechanism for each sensor output, which are discussed next. For Iris recognition, we match a pair of Iris image templates (derived based on its discriminating feature) bit-wise using the Hamming distance (HD). Two templates are considered to have been generated from the same iris image if the Hamming distance produced is lower than a user defined threshold. In case of fingerprint, we match two fingerprint feature representations at two levels. At coarse level, fingerprints are classified into whorl, arch, tented arch, left loop, right loop and twin loop. At a finer level, it is compared to the subset of the database containing that type of fingerprints only. Here, we have used our SOM-MSOM technique [2] for coarse level classification. At finer level, matching is performed based on the minutiae (i.e., ridge ending and branching points) information.

4.4 Combination Function, f

This function accepts match scores, i.e., S_I and S_F respectively, from iris and fingerprint module and computes $f(S_F^i, S_I^i)$ using the rules and parameter provided by BACO submodule.

4.5 Decision Box

This module takes the input from combination function, f and BACO to decide the class of a given input instance X_i either as genuine or imposter. It uses the decision threshold given by the BACO submodule to decide the class of X_i .

5 Performance Evaluation

In this section we report performance evaluation of our method in light of three well-known and one synthetic dataset.

5.1 Environment Used

The experiments were carried out on a workstation with Intel dual-core processor (1.86 GHz) with 1 GB of RAM. We used MATLAB 7.2 (R2006a) version in windows (64-bits) platform for the performance evaluation.

5.2 Datasets Used

We have used four datasets out of which two benchmark, and one synthetic dataset for fingerprint trait and one benchmark dataset for iris trait. The detail about the datasets are given in Table 3. The fingerprint dataset FVC2000 and FVC2004 are available in [19]. The synthetic dataset was created using tools [22], where each image size is of 300×300 pixels. The iris dataset is available in [18]. For the verification experiments, the datasets are divided into two parts training and test sets.

5.3 Result and Analysis

From the result of our experiment we have obtained different ROC curves for each biometric trait as shown in Figs. 3 and 4.

Iris biometric: For iris dataset, i.e., CASIA V.1, we obtain the matching scores for different iris images, the corresponding error rates are generated using different threshold values. The ROC curve obtained is shown in Fig. 3. The FAR and FRR values are reported in Table 4. It can be seen from the table as well as from the figure that result is satisfactory.

Table 3 Datasets used

Samples	Dataset types			
	Fingerprint			Iris
	Real		Synthetic	CASIA V.1
	FVC 2000	FVC 2004		
Training	200	200	200	324
Test	100	100	100	432

Fig. 3 ROC curve of Iris biometric (CASIA) dataset

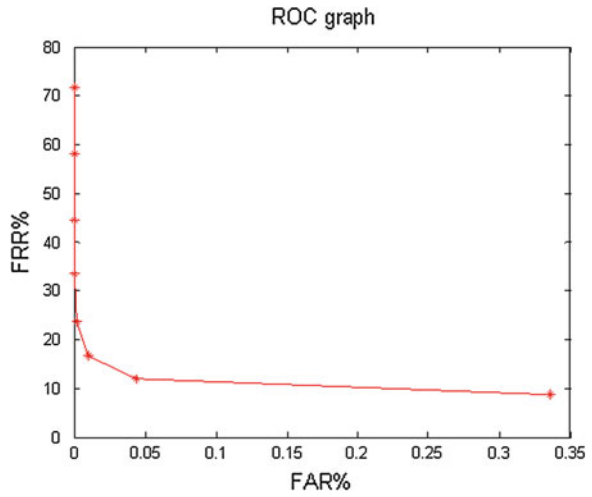


Fig. 4 ROC curve of fingerprint (FVC) dataset

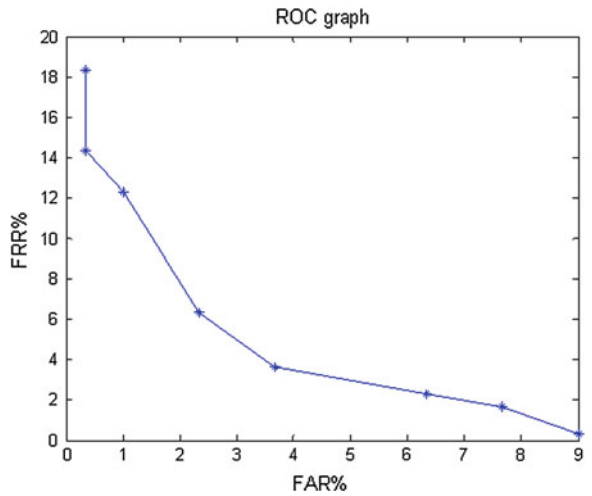


Table 4 Results of FAR/FRR values of CASIA V.1 dataset

Threshold	FAR	FRR
0.2800	0	71.6821
0.3000	0	58.0247
0.3200	0.0007	44.5988
0.3400	0.0007	33.5648
0.3600	0.0021	23.6883
0.3800	0.0100	16.8210
0.4000	0.0436	12.1142
0.4200	0.3358	8.7191

Table 5 Results of FAR/FRR values of FVC dataset

Threshold	FAR	FRR
0.6000	10	1.333
0.6250	8.6667	2.6667
0.6500	7.3333	3.3333
0.6750	4.6667	4.6667
0.7000	3.3333	7.3333
0.7250	2.0000	13.000
0.7500	1.3333	15.333
0.7750	0.6667	19.3333

The ROC curve for the CASIA V.1 Iris dataset is depicted in Fig. 3. Similarly we obtain satisfactory performance for FVC dataset as shown in Fig. 4.

Fingerprint biometric: For fingerprint biometric we obtain three sets of results for FVC2000, FVC2004 and synthetic datasets. The average results are obtained as Table 5. The corresponding ROC curve for FVC dataset is shown in Fig. 4. Like CASIA dataset, we obtain satisfactory performance for FVC dataset as shown in Fig. 4.

Multimodal biometric fusion: In this work we provide the solutions for fusion of iris and fingerprint for the range of costs 1.7 – 2.0. The algorithm ran the BACO 100 times for the same cost. The details about the parameters used is as given on the Table 6. It can be observed from Table 7 that as the value of C_{FA} approaches more towards the maximum value (i.e., 2), the sensor 1 (i.e., Iris) is dominant in the sensor suite of Fingerprint and Iris. The solutions consist of the rule and the sensor operating point defined by its false acceptance rate (FAR) and false rejection rate (FRR). From the error rates of the sensors and their distributions the sensor threshold are computed. In Table 7, we summarize the results showing a range of costs and the probable rules selected. The ‘OR’ rule is more probable when the cost of false acceptance is low i.e., less than 1.88. Due to sensor 1’s dominance, the system simply ignores the sensor 2’s (Fingerprint) decisions with higher range of costs.

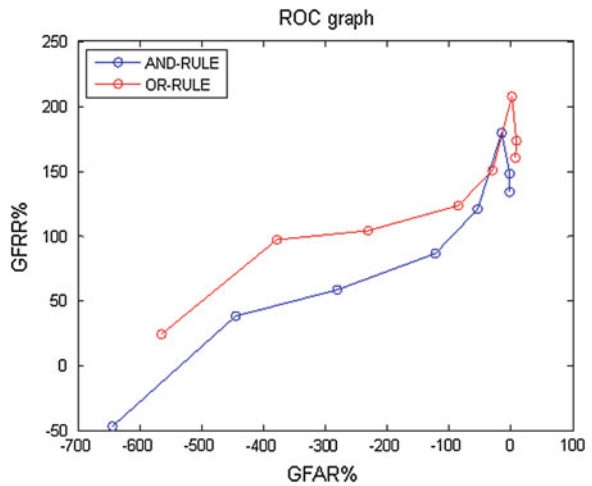
Table 6 Ant colony optimization parameters

No of ants	No of dimensions	No of rules	Pheromone constant(Q)	Evaporation factor(R)
8	2	4	0.01	0.05

Table 7 Selection of rules against different C_{FA}

C_{FA}	Probabilities of rule chosen by ACO			
	Iris only	Fingerprint only	AND rule	OR rule
1.70	0	0	0	100
1.72	0	0	0	100
1.74	0	0	0	100
1.76	0	0	0	100
1.8	0	0	0	100
1.82	0	0	0	100
1.84	0	0	0	100
1.86	0	0	0	100
1.88	94	0	0	6
1.9	95	0	0	5
1.92	100	0	0	0
1.94	100	0	0	0
1.96	100	0	0	0
1.98	100	0	0	0

Fig. 5 GFAR versus GFRR curve for AND and OR rule of Iris and Fingerprint dataset



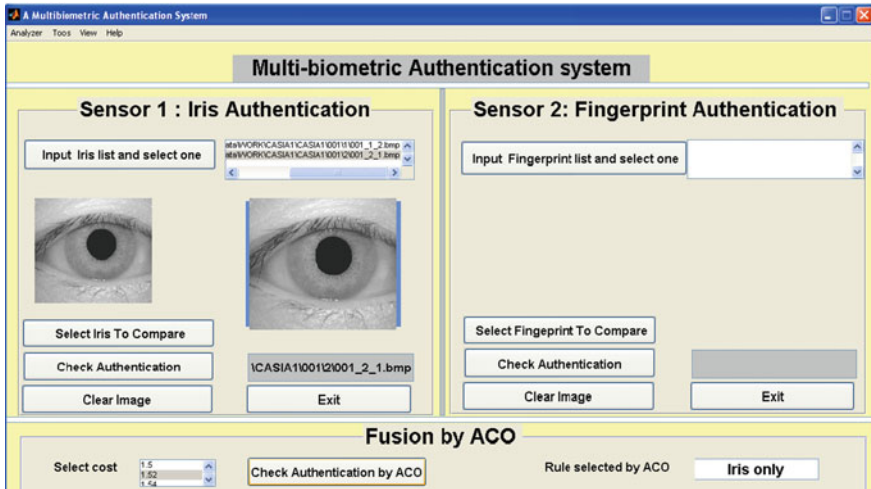


Fig. 6 Snapshot of the GUI of our system

6 Conclusions and Future Works

In this paper we have introduced a fusion method for combination of multimodal biometrics. The method has been established to perform significantly well over several benchmark datasets. In our future work, it is aimed to use other biometric traits and to explore the possibility of developing a faster approach with high detection accuracy (Figs. 5 and 6).

References

1. Kennedy, J., Eberhart, R.C., Shi, Y.H.: Swarm Intelligence. Morgan Kaufmann, CA (2001)
2. Gogoi, M., Bhattacharya, D.K.: An effective fingerprint classification method using minutiae score matching. *J. Comput. Sci. Eng.* **1**(1) (2010)
3. Raghavendra, R., Rao A., Kumar G.H.: Multimodal biometric score fusion using gaussian mixture model and Monte Carlo method. *J. Comput. Sci. Technol.* **25**(4), 771–782 (2010)
4. Singh, R., Vatsa, M., Noore, A.: Integrated multilevel image fusion and match score fusion of visible and infrared face images for robust face recognition. *Pattern Recogn.* **41**(3), 880–893 (2008). Special Issue on Multimodal Biometrics
5. Nagar, A., Jain, A.K.: On the security of non-invertible fingerprint template transforms. In: Proceedings of IEEE Workshop on Information Forensics and Security, London, UK. (2009)
6. Rattani, A., Kisku, D.R., Bicego, M., Tistarelli, M.: Feature level fusion of face and fingerprint biometrics. In: Proceedings of 1st IEEE International Conference on Biometrics, Theory, Applications and Systems, pp. 1–6. (2007)
7. Giacinto G., Roli F.: Methods for dynamic classifier selection. In: 10th International Conference on Image Analysis and Processing, pp. 659–664 Venice, Italy. (1999)

8. Giacinto G., Roli F.: Selection of classifiers based on multiple classifier behaviour. In: Proceedings of the Joint IAPR International Workshops on Advances in Pattern Recognition. (2000)
9. Kittler, J., Hatef, M., Duin, R.P.W., Matas J.: On combining classifiers. *IEEE Trans. Pattern Anal. Machine Intell.* bfseries **20**(3), 226–239 (1998)
10. Fierrez-Aguilar, J., Ortega-Garcia, J., Gonzalez-Rodriguez, J.: Fusion strategies in multimodal biometric verification. In: *IEEE International Conference on Multimedia and Expo*, pp. 5–8. IEEE Computer Society, Los Alamitos, CA, USA (2003)
11. Rukhin, L., Malioutov, I.: Fusion of biometric algorithms in the recognition problem. *Pattern Recogn. Lett.* **26**, 679–684 (2005)
12. Veeramachaneni, K., Osadciw, L. A., Varshney, P. K.: Adaptive multimodal biometric fusion algorithm using particle swarm. *SPIE* **5099**, 211–221 (2003)
13. Veeramachaneni, K., Osadciw, L., Ross, A., Srinivas, N.: Decision-level fusion strategies for correlated biometric classifiers. In: *Proceedings of IEEE Computer Society Workshop on Biometrics at the Computer Vision and Pattern Recognition (CVPR) conference*, Anchorage, USA (2008)
14. Dorigo, M., Thomas, S.: *Ant Colony Optimization*. MIT Press, Cambridge (2004)
15. Duan, H. B.: *Ant Colony Algorithms: Theory and Applications*. Science Press, Beijing (2005)
16. Dorigo, M., Maniezzo, V., Coloni, A.: Ant system: Optimization by a colony of cooperating agents: *IEEE Trans. Syst. Man Cybern. Part B* **26**, 29–41 (1996)
17. Dorigo, M., Caro, G.D., Stutzle, T.: Special issue on ant algorithms. *Future Gener. Comput. Syst.* **16**, 851–871 (2000)
18. <http://www.biometrics.idealtest.org>
19. <http://www.bias.csr.unibo.it/fvc2004>
20. Daugman J.: How iris recognition works. *IEEE Trans. Circuits Syst. Video Technol.* **14**(1), 21–30 (2004)
21. Hong, L., Jain, A.: Classification of fingerprint images. In: *Proceedings of the 11th Scandinavian Conference on Image Analysis*, Kangerlussuaq, Greenland. (1999)
22. <http://www.cubs.buffalo.edu>: SFinge

Efficient Resource Allocation Strategies for Video on Demand Services

Alok Kumar Prusty and Bibhudatta Sahoo

Abstract The Web Services have gained considerable attention over the last few years. Video-on-Demand (VoD) systems have resulted in speedy growth of the web traffic. Therefore the concept of load balancer aimed to distribute the tasks to different Web Servers to reduce response times was introduced. This paper attempts to analyze the performance of FCFS, Randomized, Genetic algorithms and Heuristics algorithms for selecting server to meet the VoD requirement. Performances of these algorithms have been simulated with parameters like makespan and average resource utilization for different server models. This paper presents an efficient heuristic called Ga-max-min for distributing the load among servers. Heuristics like min-min and max-min are also applied to heterogeneous server farms and the result is compared with the proposed heuristic for VOD Servers. Ga-max-min was found to provide lower makespan and higher resource utilization than the genetic algorithm.

Keywords Makespan · Resource utilization · FCFS · Random · Genetic · Max-min · Min-min

1 Introduction

Web server is a program that provides content like web pages over the World Wide Web. The simultaneous open connections to the web server are generally limited. Thus the waiting time becomes high when the number of requests to the

A. K. Prusty (✉) · B. Sahoo

Department of Computer Science and Engineering, National Institute of Technology Rourkela, Rourkela, Orissa 769 008, India
e-mail: aloksworld1988@gmail.com

B. Sahoo

e-mail: bdsahu@nitrkl.ac.in

web server is large resulting in DOS (Denial of Service) attack. An effective solution to this problem is the use of multiple servers known as clustered Web Servers or a server farm. Multimedia communications require continuous service, i.e. read, process and transfer the information should be done with minimum delay which is vastly improved if we use a server farm.

The performance of a server farm depends on the type of routing, server capacity and scheduling policies used. The server capacity can be homogeneous or heterogeneous. In case of homogeneous systems, each of the servers in the server farm are of equal capacity and the request is processed by the server having the least number of tasks in the queue, i.e. Join the shortest queue policy [1]. Heterogeneous systems score over homogeneous systems if tasks are of different sizes. Heterogeneous systems can also include task-specific systems, i.e. for more computation oriented tasks we can use an array processor.

Load Balancing Policy consists of load index policy, information collection policy, task location and task transfer policy. In our approach we assume that the nature of task coming to the web server is known beforehand. Load index policy keeps track of the number of tasks in the queue and information collection policy has the knowledge about the type of tasks coming to the server farm and the nature of web traffic distribution. Task transfer policy decides whether the task has to be serviced in the local servers or sent to other servers located remotely. Our main focus is on the task location policy which describes scheduling algorithm for the various tasks. We also assume an infinite capacity front end dispatcher which assigns the tasks to various servers.

In this paper we examine the different scheduling algorithms, first come first serve, random and genetic algorithm. The metric for comparing different algorithms is makespan. Makespan is defined as the maximum time taken to complete all the tasks given to the dispatcher or load balancer. An advantage for using genetic approach is that there is no need to set any threshold values on the number of tasks or utilization of the server. The server load can be represented by the following equation [2].

$$\text{Bandwidth} = \text{AverageDailyVisitors} \times \text{AveragePageViews} \times \text{AveragePageSize} \times 31 \times \text{FudgeFactor} \quad (1)$$

If people are allowed to download files from the site, the bandwidth calculation becomes:

$$\text{Bandwidth} = [(\text{AverageDailyVisitors} \times \text{AveragePageViews} \times \text{AveragePageSize}) + (\text{AverageDailyFileDownloads} \times \text{AverageFileSize})] \times 31 \times \text{Fudge Factor} \quad (2)$$

- Average Daily Visitors—The number of people expected to visit a site, on average, each day. It may vary significantly on the basis of how a site is marketed.

- Average Page Views It represents the average number of web pages visited by a person.
- Average Page Size It shows the average size of the web pages, expressed in kilobytes (KB).
- Average Daily File Downloads—The number of downloads expected to occur from a site. It depends on number of visitors and average downloads per visitor.
- Average File Size—Average size of files that are downloadable from the site.
- Fudge Factor—A number greater than 1. A fudge factor of 1.5 implies that the estimate is off by 50. Usually, bandwidth is offered in terms of Gigabytes (GB) per month. Hence the entire formula is multiplied by 31.

Video on Demand. VOD servers are different from normal web servers because they demand a consistent and higher data rate. They find applications in Video Conference (VC), IP telephony, Multimedia Mail and Digital Libraries [3]. VOD networks followed centralized architecture in the early days. But with increase in number of requests the trend has shifted to distributed architecture for VOD networks. As the number of requests increases the number of servers required to cater to those request increases which adds to additional cost. If by some heuristics or means, we can efficiently allocate the tasks to the different available servers such that it optimizes the value of a metric like makespan and throughput, then the customer requirements can be met in a better manner. The objective of this paper is twofold. Firstly to analyze the existing algorithms and heuristics in the context of VOD based systems, and secondly to analyze the performance of the proposed heuristic for two metrics namely Makespan and Average resource utilization.

2 Literature Review

Most notable of the server selection algorithms [4] are the closest server algorithm that selects server based on the proximity to the client, optimized closest server algorithm that chooses the closest server among the free channels, Register all algorithm where the clients request is added to the queue of all the servers and Maximum-MFQ-rank-first algorithm which computes the rank at the various server queues and assigns the request to the server having the best rank. Gupta et al. [1] analyzed the join the shortest queue policy on processor sharing server farms. They used a single queue approximation and investigated the sensitivity of the queuing model to variations. Niyato et al. [5] studied load balancing for Internet video and audio server. Ciardo et al. [6] devised a strategy for task allocation in web servers based on size distributions of the requested documents. Zhang et al. [7] analyzed the central load balancing model, derived average response time and the rejection rate and compared three different routing policies. The retrieval schemes for VOD can be classified into two categories, a) Disk level retrieval schemes [3] which focuses on synchronizing and efficiently using the data between different storage devices and b) server level retrieval schemes [3] which

delivers data to the client whenever the need arise. Our approach is based on the server level. Similar requests can be batched or the server can be replicated [4] to achieve low latency and thus serve a higher number of requests. Previous studies have followed the Zipfs Law to calculate the popularity of the video files [8–10]. In Zipf-like distributions, the access frequency for a file of popularity rank i is equal to C/i_a , where C is a normalization constant and $a(a > 0)$ is the distribution parameter [11]. The file usage patterns like which category of videos are accessed at which point of time during a day can also be analyzed and the cache be maintained accordingly.

3 System Architecture

The adapted Fig. 1 [12] depicts the prevalent 3-tier architecture for web servers. The main components are a set of web servers, a set of database server nodes and a switch which executes the logic for server selection. It can divide the tasks into classes on basis of quality metric like burst time, etc. The Front end servers are designed to deliver the static pages mostly and in case of any query from the client the appropriate database server is connected. The routing and firewall switch ensures authorization and authentication and forbids any unintended user from accessing the files on the servers.

The system architecture of a Video on Demand system basically consists of three major parts [13]: a client, a network, and a server. Each part can be subdivided further into components and interfaces.

VOD system from the client's point of view is a simple operation. The user makes a selection from a list of available videos and the video is delivered to the user within the accepted QoS limits. Most networks use proxy servers or replicas to minimize delay. This is done by a process called request routing which directs the request to a particular web server on the basis of certain metrics. According to [11, 14], there are 4 kinds of architecture for VOD networks a) Centralized, all the requests from the clients are handled at the original server, b) proxy based servers that are located close to the user end to reduce the load on the original server by caching, c) Content delivery networks, the servers are deployed close to the edge of the network to serve a fraction of clients request and d) hybrid, is basically a peer to peer approach.

4 Server Model and Performance Metrics

The web server infrastructure supporting VOD can be modeled as $M/M/m$ queuing system with m heterogeneous server. The heterogeneous server farm addressed here can be expressed by Kendall notation like $M/M/m$, where: (i) First M : represents exponential inter arrival times between tasks distribution (Poisson process),

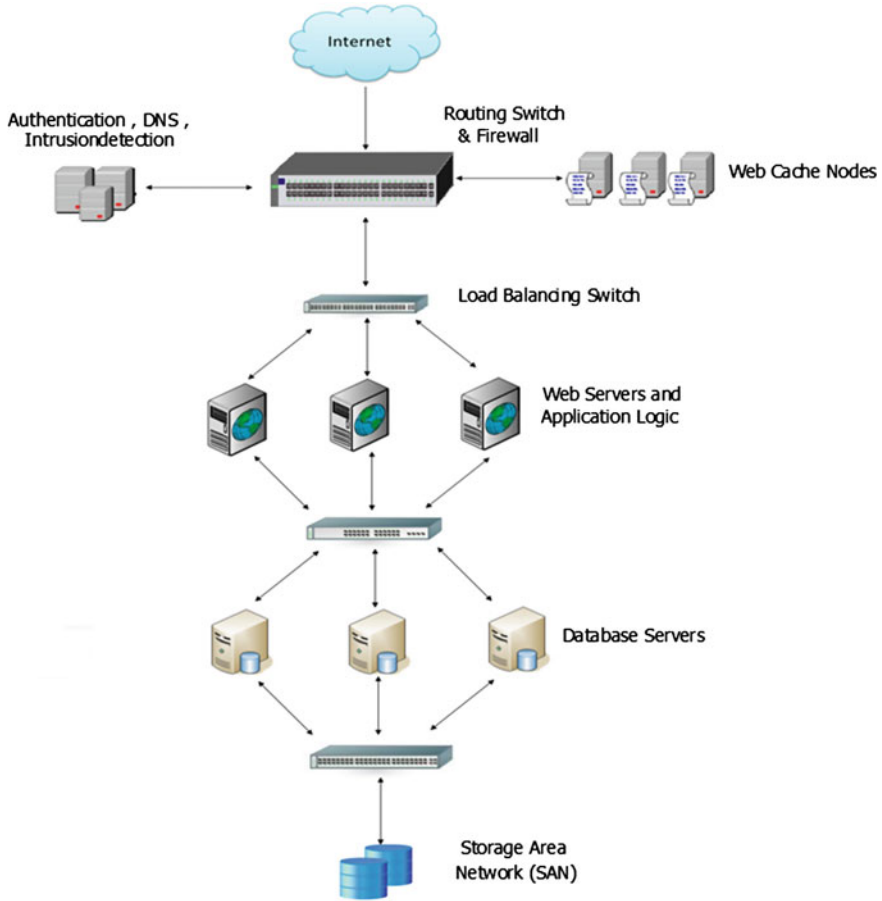


Fig. 1 Three tire architecture for web server

(ii) Second M: represents exponential execution time of jobs distribution, and (iii) m: represents number of heterogeneous computing nodes in the system. It is also assumed that the queue has infinite waiting room to accept the incoming tasks. Each computing node executes its queue of tasks in first-come first-served order. The task enters into the queue of central scheduler at mean rate λ . The distribution is assumed to be exponential with mean $1/\lambda$. A task t_i with central scheduler can be allocated to a computing node with probability a_i

$$\sum_{i=1}^m a_i = 1 \tag{3}$$

The processing time of task t_i on node M_j is modeled as an independent exponentially distributed random variable with mean $1/\mu_j$. For stability it is also assumed that tasks must not be generated faster than the HDCS can process i.e.

$$\lambda \leq \sum_{j=1}^m \mu_j \quad (4)$$

In general for HDCS with m nodes, the state of the markov chain is described by m tuples (s_1, s_2, \dots, s_m) in which s_j denotes number of task with node M_j . A task allocated to node M_j with probability a_j or executed at node M_1 with probability a_1 . Let λ_j be the arrival rate of task at the computing node M_j resulted due to allocation by central scheduler. The average utilization ρ_j can be computed as λ_j/μ_j . Let Q_j be the queue length of node M_j then the average queue length can be computed as:

$$E(Q_j) = \rho_j/(1 - \rho_j) \quad (5)$$

The average response time denoted as $E(T_j)$ and defined as

$$E(T_j) = 1/\lambda(\rho_j/(1 - \rho_j)) \quad (6)$$

As the central scheduler runs on M_1 , let a_1 is the probability that schedules the task to node M_1 locally. The probability a task will migrate to another node is $1 - a_1$ and migration probabilities to each node is identical. The average execution queue length or L_j determines how smoothly the load is balanced.

Many different metrics are used to evaluate the performance of VOD server. They can be classified as Technology based and user based [3]. We have used *Makespan* and *Resource utilization* as two metrics for comparing algorithms as defined below.

Makespan: Makespan is defined as the largest completion time of all the tasks in the system. In the VOD scenario, it is an indicator of the response time. For example; if the makespan of a group of tasks exceeds a certain threshold then the tasks are not allowed as the response time Qos is not met.

Resource Utilization: Average Resource utilization for a system is defined as the average of the resource utilization of various servers. For a single server, utilization is given by

$$\text{Resource utilization } (R_u) = (\text{Amount of time a server is idle})/\text{Total time} \quad (7)$$

Makespan indirectly refers to the Response time of the system as a certain response time of say 0.5 s implies that the requests should complete execution within 0.5 s which suggests the makespan should not exceed 0.5 s. Resource utilization suggests what fraction of the total time a server is working.

4.1 Linear Programming Problem Formulation for VOD Task

Let $A(j)$ be the set of tasks assigned to server(node) M_j ; and T_j be the total time machine M_j have to work to finish all the task in $A(j)$. Hence $T_j = \sum_{t_i \in A(j)} t_{ij}$; for all task in $A(j)$. This is otherwise denoted as L_j and defined as load on node M_j . The

basic objective of load balancing is to minimize make span, which is defined as maximum loads on any node ($T = \max_{j:1:m} (T_j)$). Let x_{ij} correspond to each pair (i, j) of node $M_j \in M$ and task $t_i \in T$.

- $x_{ij} = 0$; implies that task i not assign to node j .
- $x_{ij} = t_{ij}$; will indicate load of task i on node j .

For each task t_i we need $\sum_{j=1}^m x_{ij} = t_{ij}$; for all task $t_i \in T$. The load on node M_j can be represented as $L_j = \sum_{i=1}^n x_{ij}$, where $x_{ij} = 0$ whenever task $t_i \notin A(j)$. The load balancing problem aims to find an assignment that minimizes the maximum load. Let L be the load of a HDCS with m nodes. Hence the generalized load balancing problem on HDCS can be formulated as

Minimize L

$$\sum_{j=1}^m x_{ij} = t_{ij}, \text{ for all } t_i \in T \tag{8}$$

$$\sum_{i=1}^n x_{ij} \leq L, \text{ for all } M_j \in M \tag{9}$$

Where $x_{ij} \in \{0, t_{ij}\}$, for all $t_i \in T, M_j \in M$ and $x_{ij} = 0$ for all $t_i \notin A(j)$

. The objective function defined here is to minimize the makespan, hence used as the performance metric for evaluating various load balancing scheme through resource allocation. More over the resource utilization also used as a metric to predict effective utilization of server farm.

5 Typical Server Selection Algorithms

Let there be a task set T consisting of $n(T_1, T_2, \dots, T_n)$ tasks and let there be M servers. The basic problem is where to map a task T_i among the M possible servers. This is done by the server selection strategy. The tasks should be allocated in such a way that after allocation of all the n tasks among the M servers, the performance metrics should be optimized.

The need for server selection arises in case of distributed system architecture. Choosing a good strategy is important because of the following reasons

1. It can reduce the overall cost of maintenance of the system.
2. It can reduce the response time of the system, thereby increasing customer satisfaction.
3. It can efficiently distribute the load among various servers and thus reduces the chance of breakdown of a particular system due to server overloading.
4. It can provide robustness and easy scalability to the system.

So selecting a good strategy is of paramount importance. But each of the existing algorithms does not apply well to all the scenarios. The existing algorithms can be

further divided into Traditional and Heuristic based algorithms. Traditional ones include FCFS, Random and Genetic algorithms. There is another class of algorithms called the Heuristic algorithms which comprises of Min-min, Max-min and Weighted mean time scheduling [15]. These heuristics are applicable for heterogeneous task systems where we have servers of different capacity.

5.1 First Come First Serve

This is a simple scheduling policy used in various load balancing servers. Whichever request comes first is served first irrespective of any other criteria. This algorithm though simple to implement has serious limitations. For e.g. if a process with a high burst time is followed by a sequence of processes with low burst time then the latter has to wait for a long period of time to complete its execution. The response time for these processes is far greater than their burst times. So these processes undergo starvation.

5.2 Random

This is another scheduling policy where the tasks are distributed randomly to the available processors. If the distribution is truly random, then the random outweighs other algorithms in the long run.

5.3 Genetic

The genetic algorithm is an optimization technique that has its base on the basis of natural selection. A GA consists of candidates or populations which evolve based on some predefined rules such that each evolution produces a better population (i.e. population which minimizes the cost function). Some of the advantages of GA are

- It optimizes both continuous and discrete variables.
- It simultaneously searches from a wide sampling space.
- It is well suited for parallel computing.
- It optimizes complex cost functions quite well (there are several local minima) and produces the global minima.
- It provides a list of optimal solutions not the single best optimum solution.
- Encoding the variables is easy when they are represented in terms of genes. GA essentially operates in five steps initialization, evaluation of fitness function, selection, crossover, mutation [16].

5.4 *Min–Min*

This consists of two phases [12, 15]. First we choose a fixed arbitrary order and then for each task we choose the server with the minimum burst time. In the second phase, the task with the minimum burst time among the group chosen in phase 1 is selected and assigned the corresponding server and the ETC matrix is updated with new completion times for the remaining tasks while the chosen task is deleted from the matrix. Completion time is given by the equation.

$$CT(i,j) = ET(i,j) + r(j) \quad (10)$$

Where $r(j)$ is the ready time of machine j , i.e. the time taken by the machine to complete all its pending tasks from the moment the task i is assigned to machine j . The maximum time to complete all the tasks is represented by the makespan.

5.5 *Max–Min*

This algorithm is similar to min–min except in the second phase the task with the maximum completion time is mapped first. This algorithm is known to provide better resource utilization than the Min-min algorithm.

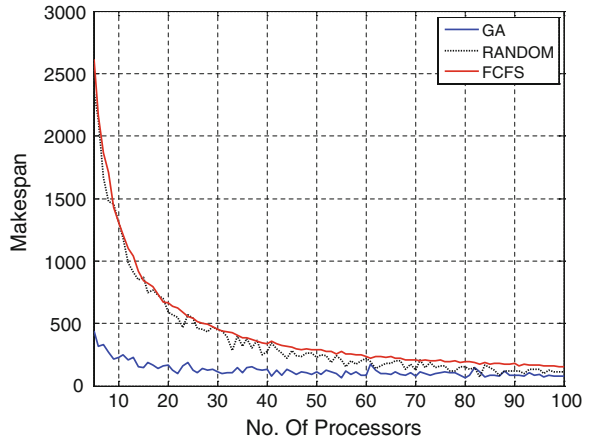
5.6 *WMTS*

The algorithm is adopted as described in [12] where the weighted sum of expected time is used. The weights are proportional to the server capacity.

5.7 *Composite GA-Max-Min Server Selection Algorithm*

This algorithm merges the genetic algorithm and the Max-min algorithm. This results in the enhancement of the performance of the genetic algorithm. So this kind of algorithm can be used where the number of tasks is very large.

Fig. 2 Comparison between GA random and FCFS for maximum 100 nodes



GA-Max-min algorithm.

1. For all tasks i in the task set
2. Divide the tasks into classes on basis of burst time or previous history
3. Send the tasks to the appropriate queue
4. Apply different selection algorithms as applicable to the different queues
5. Makespan = Calculate makespan (Task set)
6. Resource utilization = Calculate resource utilization (Task set)
7. End.

The task set is divided into classes based on burst time or previous history. Then for each queue Resource utilization and makespan is calculated by the calculate resource utilization () and calculate makespan () functions. Both these functions take task set as the input.

6 Experimental Evaluation

See (Figs. 2, 3, 4 and 5).

Fig. 3 Resource utilization Vs No. of processor (Max 100)

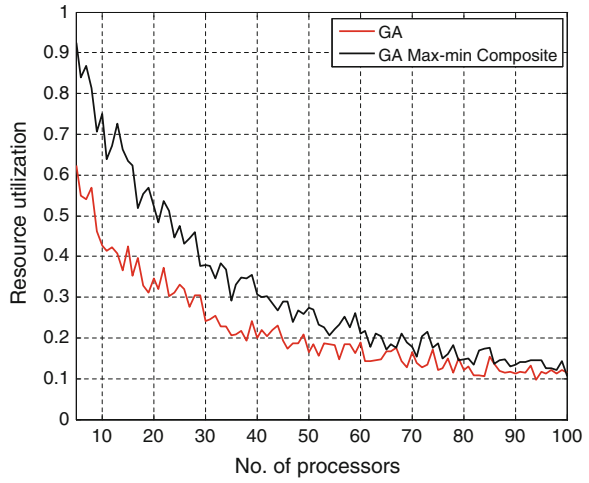


Fig. 4 Resource utilization Vs No. tasks (Max processor 100)

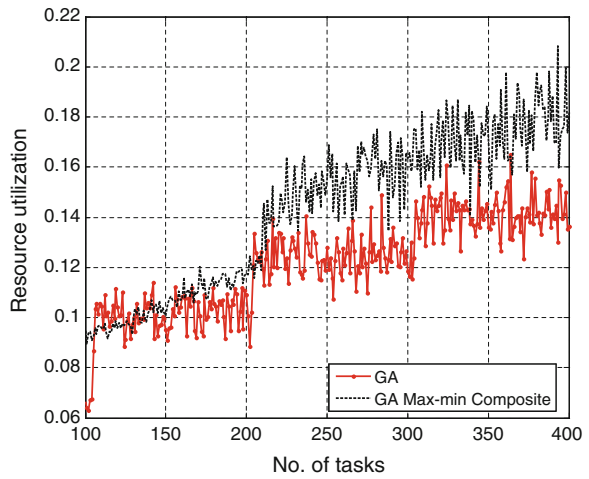
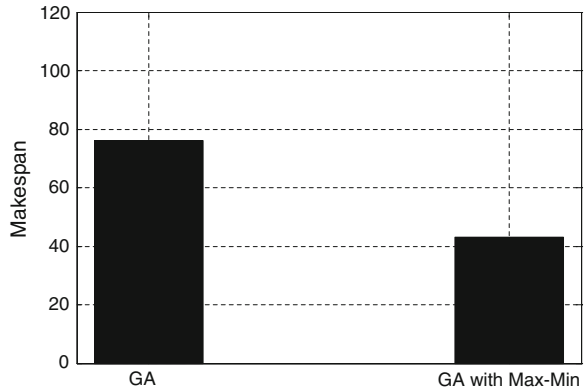


Fig. 5 Makespan comparison between GA and composite GA (max processor = 100)



7 Conclusion

In this paper we compared various resource allocation strategies such as FCFS, Random, Min-min for Video On Demand Services on the basis of makespan and average resource utilization. We also combined two heuristics Genetic algorithm and max min to get a new heuristic GA-max-min. We chose Genetic algorithm as one component of the combined heuristic as it was feasible to apply genetic algorithms for large data sets and the max min algorithm as another component as it provides the best resource utilization. The new heuristic proved to be better in terms of resource utilization and makespan. For unpredictable nature of the tasks genetic algorithms works best as the system learns about the nature through GA and thus utilization is sometimes low. The combined heuristic can, thus be used to enhance the Average resource utilization of the Genetic algorithm and it also decreases the makespan that the genetic algorithm produces.

References

1. Gupta, V., Balter, M.H., Sigman, K., Whitt, W.: Analysis of join-the-shortest-queue routing for web server farms. *Perform. Eval.* **64**(9–12), 1062–1081 (2007)
2. Narasimhan, A.: Distributed multimedia applications-opportunities, issues, risk and challenges: a closer look. In: *IASTED International Conference on Intelligent Information Systems*, pp. 455–460 (1997)
3. Panigrahi, N., Sahoo, B.: Qos based retrieval strategy for video on demand. Available Online at <http://dspace.nitrkl.ac.in:8080/dspace/bitstream/2080/789/1/bdsahoo2009.pdf>. Accessed 08 May 2011
4. Ligang, D., Bharadwaj, V., Ko, C.C.: Efficient movie retrieval strategies for movie-on-demand multimedia services on distributed networks. *Multimedia Tools Appl.* **20**(2), 99133 (2003)
5. Niyato, D., Srinilta, C.: Load balancing algorithms for internet video and audio server. In: *Proceedings of 9th IEEE International Conference on Networks*, p. 76 (2001)

6. Ciardo, G., Riska, A., Smirmi, E.: Equiloat: a load balancing policy for clustered web servers. *Perform. Eval.* **46**(2–3), 101–124 (2001)
7. Zhang, Z., Fan, W.: Web server load balancing: a queuing analysis. *Eur. J. Oper. Res.* **186**(2), 681–693 (2008)
8. Ko, M., Koo, I.: An overview of interactive video on demand system. Technical Report, The University of British Columbia, 13 Dec 1996
9. N. Jian et al.: Hierarchical content routing in large-scale multimedia content delivery network. In: *Proceedings of IEEE International Conference on Communications (ICC)*, Anchorage, May 2003
10. Wang, B., et al.: Optimal proxy cache allocation for efficient streaming media distribution. In: *Proceedings of IEEE Infocom*, New York, June 2002
11. Thouin, F., Coates, M.: VOD networks: design approaches and future challenges. In: *Proceedings of Network IEEE*, Montreal, pp. 42–48 (2007)
12. Shari_an, S., Motamedi, S.A., Akbari, M.K.: A predictive and probabilistic load balancing algorithm for cluster based web servers. In: *Proceedings of Applied Soft Computing*, p. 970, Jan 2011
13. Carlsson, N., Eager, D.L.: Server selection in large scale video on demand. In: *Proceedings of ACM Transactions on Multimedia, Computing and Communications* (2010)
14. Thouin, F.: VOD equipment allocation. Technical Report, Mcgill University, Montreal
15. Chauhan, S.S., Joshi, R.C.: A weighted time min-min max-min selective scheduling strategy for independent tasks on grid. In: *Proceedings of Advance Computing Conference (IACC)*, Patiala, Feb 2010
16. Zomaya, A.Y., Teh Y.H.: On using genetic algorithms for dynamic load balancing. *IEEE Trans. Parallel Distrib. Syst.* **12**(9), 899–911 (2001)

A Novel Co-swarm Gravitational Search Algorithm for Constrained Optimization

Anupam Yadav and Kusum Deep

Abstract In this article a new co-swarm Gravitational Search Algorithm is proposed to solve the non-linear constrained optimization problems. The idea of Gravitational search algorithm (GSA) and Differential Evolution (DE) is inherited to propose a new robust search algorithm. The individual influences of GSA and DE over the particles is incorporated collectively to provide a more effective influence in comparison to the individual influences of the GSA and DE. A new velocity update equation is propose to update the positions of the particles. To evaluate the availability of the proposed algorithm a state-of-the-art problems proposed in IEEE CEC 2006 is solved and the results are compared with GSA and DE. The supremacy of the proposed algorithm is benchmarked over the exhaustive simulation results, feasibility rate and success rate.

Keywords Gravitational search algorithm · Differential evolution · Mutation · Crossover

1 Introduction

Constrained optimization problems (COPs) play very important role in the field of optimization theory because many real life, including engineering problems can be modeled as constrained optimization problems. Mathematically the COPs can be formulated as:

A. Yadav (✉)

Department of Applied Sciences, ITM University, Gurgaon, India
e-mail: anupamyadav@itmindia.edu

K. Deep

Department of Mathematics, Indian Institute of Technology, Roorkee, India
e-mail: kusumfma@iitr.ernet.in

$$\text{Min. or Max. } f(x), \quad x = [x_1, x_2, x_3, \dots, x_D], \quad (1)$$

subject to a set of inequality constraints

$$g_j(x) \leq 0, \quad j = 1, 2, 3, \dots, q, \quad (2)$$

as well as equality constraints

$$h_j(x) = 0, \quad j = q + 1, q + 2, \dots, m, \quad (3)$$

where $f : R^D \rightarrow R$, g_j are q inequality constraints and h_j are the $m - q$. The feasible solution to these problems is a great challenge to the researchers working in this area. Since some of the problems has high level of complexity because of the very small ratio of the feasible region and total search region [1]. Due to the obvious limitations of the deterministic methods available in operations research, the differential free stochastic search techniques are very useful while solving COPs. Many nature inspired algorithms are also established in the literature which are being used to solve COPs, such as GA, PSO, DE and many other optimization techniques are successfully utilized to solve these problems. Since every swarm intelligence or evolutionary heuristics are having their own limitations depending upon the complexity of the problems. To develop a global heuristic which can be applied to a variety of a problems, a hybrid of the existing techniques is reported in the literature [2]. Liao [3] successfully solved engineering design problems using a hybrid of DE. A biogeography based hybrid DE algorithm is also proposed by Gong et al. [4]. A self adaptive DE is also proposed by Brest [5], co-evolutionary DE is also coined by He [6] and Sedki [7]. Xin [8] suggested the supremacy of the hybridized algorithms over a variety of problems. In this article a very recent search algorithm Gravitational search is hybridized with the Differential Evolution. Since these two algorithms are inspired from two very different fundamental natural process which coined the basic idea of hybridization of the GSA and DE. A co-swam approach involving GSA and DE is contrived to develop a novel technique. The paper is organized as follows. In the next section s brief introduction of GSA and DE is discussed. In Sect. 3, a new hybrid co-swarm Gravitational search algorithm is proposed. In Sect. 4, benchmark functions and experimental results are presented. Finally the article is concluded along with the proposed future scope.

2 Gravitational Search Algorithm

Gravitational Search Algorithm (GSA) [9] is a recent heuristic optimization algorithm. It is inspired by Newton's basic physical theory that a force of attraction works between every particle in the universe and this force is directly proportional to the product of their masses and inversely proportional to the square of distance between their positions. All these particles are named as agents or particles. In GSA each agent is equipped with four kinds of properties: position, mass, active

Table 1 Pseudo code of gravitational search algorithm

Gravitational Search Algorithm
<p>Step (1) Initialization Randomly initialize all the particles $(X_1^t, X_2^t, \dots, X_{ps}^t)$ size ps in $[X_{min}, X_{max}]^D$ Set iteration $t=0$ Evaluate the fitness values $(fit_1^t, fit_2^t, \dots, fit_{ps}^t)$ of $X(\text{Agent})$ Calculate G_i^t, $best_i^t$, $worst_i^t$ and M_i^t for $i = 1, 2, \dots, ps$. Calculate the total force in each direction F_i^t Calculate the ac_i^t and velocity. Sort the Swarm with the help of following criterion: Step(2) Reproduction and Updating While (Stopping Criterion is not satisfied) do for $i=1: ps$ do $V_i^{t+1} = rand() \times V_i^t + ac_i^t$ $X_i^{t+1} = X_i^t + V_i^{t+1}$ Evaluate the fitness values (fit_i^t) of $X(\text{Agent})$ Update G_i^t, $best_i^t$, $worst_i^t$ and M_i^t. Using feasibility based rule. Calculate the total force in each direction F_i^t Calculate the ac_i^t and velocity. end of for end while</p>

gravitational mass and passive gravitational mass. The position of the mass provides the solution of the problem. Gravitational masses and inertial masses can be evaluated using fitness function. Each kind of mass follows the following to basic laws of physics:

1. *Law of gravity*
2. *Law of motion*

The exhaustive procedure of GSA is explained in Table 1.

2.1 Differential Evolution

Differential Evolution is again a nature inspired optimization technique, It was proposed by Storn and Price [10] in 1995. This technique is also a population based stochastic optimization algorithm. This technique comes under the umbrella of Evolutionary Algorithms. It employs the simple arithmetic operation including the mutation, crossover and selection to develop a better population from the randomly generated initial population. The implementation of DE is quite simple and easy to synchronize it with different platforms. For the obvious reason it has been used for various optimization problems; constrained as well as unconstrained continuous optimization problems [11]. DE is equipped with two key processes:

Table 2 The pseudo code of differential evolution algorithm

Differential Evolution
<p>Step (1) Initialization Randomly initialize all the particles $(X_1^t, X_2^t, \dots, X_{ps}^t)$ in $[X_{min}, X_{max}]^D$. Set iteration $t=0$.</p> <p>Step (2) Reproduction and updation. While (Terminating Criterion is not met) do. Evaluate the fitness values $(fit_1^t, fit_2^t, \dots, fit_{ps}^t)$ of X. Mutation Create the mutant vector v_i^t. Crossover Create the trial vector u_i^t by crossover operation.) Evaluate the fitness values of v_i^t and u_i^t. Selection for $i=1: ps$ do update the position of the particle end for end while</p>

the fluctuation process which enables the exploration ability throughout the search space and selection process, which enables the exploitation of the search algorithm. DE begins with the random generation of a population which can be expressed as multidimensional vectors of the form, $X_i^t(x_{i1}^t, x_{i2}^t, \dots, x_{iD}^t)$ where $i = 1 : ps$ is the number of particles at any instant t and D is the dimension of space. Initially, these vectors are randomly generated in the fixed size of interval. These generated particles undergo the processes of mutation, crossover and selection. Before proposing a new co-evolutionary algorithm, a brief review of mutation, crossover and selection is presented in the following subsection. An exhaustive procedure of DE is explained in Table 2.

3 A Hybrid Co-swarm Gravitational Search Algorithm

3.1 Motivation

The motivation behind the hybridization of the GSA and DE is to take the advantage of the very basic principle of force of attraction between two particles and the basis of the differential evolution simultaneously. As GSA is a technique based on the laws of motions of particles and DE is the technique inspired from the basic idea of human evolution. The Idea of hybridization is design a new stochastic search technique which is equipped with the power of GSA as well as DE. The guiding ability of the GSA and DE in mixed simultaneously so that the particles can be pushed towards a more better position than the position suggested by GSA

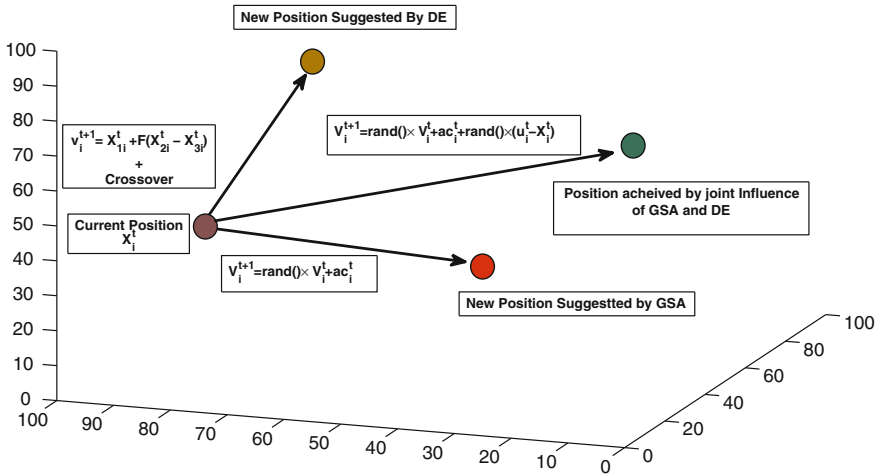


Fig. 1 Three dimensional environment of the position update strategy

and DE individually the proposed algorithm follows the following steps, let $(X_1^t, X_2^t, \dots, X_{ps}^t)$ be the randomly initialized particles in the search domain. These initially generated particles are processed through an independent process of DE and GSA. After applying DE and GSA as explained in the previous sections, we have accelerations ac_i^t evaluated through GSA and a set of trail vector u_i^t obtained by the process mutation and crossover in DE. Instead of updating particles position by the position update equation of GSA or DE, a new velocity update equation is proposed which incorporates the influence of both DE and GSA in a single one. Equation (4) is the proposed velocity update equation for the swarm.

$$V_i^{t+1} = \omega rand() \times V_i^t + ac_i^t + c * rand() \times (u_i^t - X_i^t) \tag{4}$$

$$X_i^t = V_i^{t+1} + X_i^t \tag{5}$$

Figure 1 depicts the three dimensional environment of the position update of the particles. The exhaustive algorithm of the proposed GSADE is explained in Table 3.

4 Experimental Results and Benchmark Functions

In this section the proposed GSADE algorithm is tested on 24 real parameter benchmark problems proposed in IEEE CEC 2006 [1]. The results of the GSADE is compared with the original GSA [9] and DE. The choice of parameters and constraint handling method is explained in the following sections.

Table 3 The pseudo code of the proposed GSADE algorithm

<p>A hybrid of GSA and DE</p> <p>Step (1) Initialization Randomly initialize all the particles $(X_1^t, X_2^t, \dots, X_{ps}^t)$ in $[X_{min}, X_{max}]^D$. Initialize velocity $(V_1^t, V_2^t, \dots, V_{ps}^t)$ set iteration $t=0$ While($t < itermax$)</p> <p>Step (2) Reproduction and Updation Evaluate the fitness values $(fit_1^t, fit_2^t, \dots, fit_{ps}^t)$ of X. for $i = 1 : ps$ Mutation $v_i^t = X_{1i}^t + F(X_{2i}^t - X_{3i}^t)$ Crossover Evaluate u_i^t using crossover Apply Gravitational Search Algorithm $G^t = G^{t0} \times \exp((- \alpha \frac{iter}{itermax}))$ for $j = 1 : ps$ $F_{ij}^t = G^t \times \frac{M_{pi}^t \times M_{aj}^t}{R_{ij}^t} \times (X_i^t - x_j^t)$ $R_{ij}^t = \ X_i^t, X_j^t\ _2$ end for Calculate acceleration $ac_i^t = \frac{F_i^t}{M_{ii}^t}$ Step (3) Velocity and position update equation $V_i^{t+1} = \omega rand() \times V_i^t + ac_i^t + rand() \times (u_i^t - X_i^t)$ $X_i^{t+1} = V_i^{t+1} + X_i^t$ end of for $t=t+1$ end of while</p>

Table 4 Fine tuned parameter values for GSADE, GSA and DE

ω	c	ps	F	CR	itermax
0.9	1.49618	60	0.7	1.1	4000

4.1 Constraint Handling

The parameter-free constraint handling approach based on sorting of the swarm is used to ensure the feasibility of the particles. The degree of constrained violation for a particle x is evaluated by using the equation $G(x) = \frac{1}{m} \sum_{j=1}^m G_j(x)$. In each iteration the swarm is sorted as suggested in Liang et al. [1].

Table 5 Function optimization results for the functions g01 to g12

	Best	Mean	Worse	Stdev	Mean inf.
g01					
GSADE	-15.0000	-15.0000	-15.0000	1.61E - 11	0.0000
GSA	-	-	-	-	541.8225
DE	-15.0000	-15.0000	-15.0000	3.11E - 10	0.0000
g02					
GSADE	-0.7967	-0.7967	-0.7967	3.36E - 16	0.0000
GSA	-0.2423	-0.0983	-0.0465	2.80E - 02	0.0000
DE	-0.7810	-0.7810	-0.7810	4.01E - 09	0.0000
g03					
GSADE	-1.0005	-1.0005	-1.0005	7.63E - 16	0.0000
GSA	-	-	-	-	2.2765
DE	-0.0118	-0.0118	-0.0118	5.18E - 18	0.0000
g04					
GSADE	-30665.5390	-30665.5390	-30665.5390	2.57E - 11	0.0000
GSA	-29510.0520	-27327.3890	-23560.6830	2.11E + 03	1.0715
DE	-30665.5335	-30665.5353	-30665.5347	1.78E - 11	0.0000
g05					
GSADE	5126.4967	5126.4967	5126.4967	5.50E - 12	0.0000
GSA	-	-	-	-	1975.0210
DE	5126.5001	5126.4987	5126.4989	5.43E - 12	0.0000
g06					
GSADE	-6961.8139	-6961.8139	-6961.8139	2.13E - 12	0.0000
GSA	-3744.2747	279310.4500	1020773.7000	2.42E + 05	5809.5648
DE	-6961.8139	-6961.8139	-6961.8139	4.59E - 12	0.0000
g07					
GSADE	24.3062	24.3062	24.3062	2.15E - 14	0.0000
GSA	850.4374	2103.3302	4824.1543	1.08E + 03	1992.8454
DE	24.3062	24.3062	24.3062	4.83E - 11	0.0000
g08					
GSADE	-0.0958	-0.0958	-0.0958	8.40E - 17	0.0000
GSA	-0.0958	0.5679	53.5663	6.47E + 00	33.3236
DE	-0.0958	-0.0958	-0.0958	5.44E - 17	0.0000
g09					
GSADE	680.6301	680.6301	680.6301	5.73E - 13	0.0000
GSA	836.1642	1.4309E + 06	9.5128E + 06	2.27E + 06	6848.2815
DE	680.6301	680.6301	680.6301	3.84E - 11	0.0000
g10					
GSADE	7049.2480	7049.2480	7049.2480	5.50E - 12	0.0000
GSA	-	-	-	-	1750742.8000
DE	7049.2480	7049.2480	7049.2480	7.31E - 10	0.0000

(continued)

Table 5 (continued)

	Best	Mean	Worse	Stdev	Mean inf.
g11					
GSADE	0.7532	0.7534	0.7683	1.23E – 02	0.0000
GSA	0.8452	1.6221	4.5674	1.17E + 00	0.5211
DE	0.7499	0.7499	0.7499	8.96E – 16	0.0000
g12					
GSADE	–1.0000	–1.0000	–1.0000	0.00E + 00	0.0000
GSA	–0.9997	–0.7204	–0.3703	1.34E – 01	0.4205
DE	–1.0000	–1.0000	–1.0000	0.00E + 00	0.0000

4.2 Parameter Setting

The fine tuned parameters involved in GSADE is listed in Table 4. For the experiments a 100 run result is simulated.

5 Results and Discussion

To test the proposed algorithm a state-of-the-art real parameter constrained optimization problems are solved. The results of the GSADE is compared with the results of GSA and DE. Table 5 shows the results of the GSADE, GSA and DE. The results are compiled for the best, mean, worse, standard deviation (STDEV) and mean infeasibility (Mean Inf.) of the particles in the last iteration of each run. A 4000 iteration is taken to simulate the results. From Table 5, it can be observed that for the problems g01, g02, g03, g04, g05, g07, g12, g13 and g17 the proposed GSADE is able to give the best fitness value in comparison to the other algorithms. Even the difference between the best, mean and worse is recorded zero up to the 8–10 decimal places, however only four decimal places results are presented. Except the problems g11, g20, g22 and g23 the standard deviation in the fitness value is less than $O(10^{-10})$. In the last column of the Table 5 the mean infeasibility of the particles in the last iteration is presented, in which it is observed that GSADE is able to give 100 % feasibility to the 22 problems out of 24 problems. To test the feasibility rate and success of the GSADE, feasibility rate and success rate is compared with the feasibility and success of the GSA and DE (Table 6).

1. Feasible Run: A run during which at least one feasible solution is recorded.
Feasibility Rate = No. of Feasible Runs/Total Runs
2. Successful Run(Sruns): A run during which at least one feasible solution is recorded meeting with $|\text{fit}(x) - \text{fit}(x^*)| \leq 0.0001$, where $f(x)$ is the known

Table 6 Function optimization results for the functions g13 to g24

g13					
GSADE	0.4388	0.4388	0.4388	$3.92E - 16$	0
GSA	-	-	-	-	24.9075
DE	0.4933	0.5001	0.5075	$3.02E - 03$	0
g14					
GSADE	-47.7649	-47.7649	-47.7649	$4.30E - 14$	0
GSA	-	-	-	-	85.4441
DE	-47.7649	-47.7649	-47.7649	$2.97E - 13$	0
g15					
GSADE	961.715	961.715	961.715	$8.03E - 13$	0
GSA	963.9578	811.6076	983.4647	$9.78E + 01$	171.1705
DE	961.715	961.715	961.715	$8.05E - 13$	0
g16					
GSADE	-1.9052	-1.9052	-1.9052	$1.34E - 15$	0
GSA	-	-	-	-	28864.923
DE	-1.9052	-1.9052	-1.9052	$3.75E - 16$	0
g17					
GSADE	8853.5339	8853.5339	8853.5339	$8.47E - 12$	0
GSA	-	-	-	-	1203.7903
DE	8854.9729	8854.9971	8855.0434	$1.67E - 02$	0
g18					
GSADE	-0.866	-0.866	-0.866	$6.07E - 16$	0
GSA	-0.2928	0.5234	193.3305	$5.84E + 01$	1296.7228
DE	-0.866	-0.866	-0.866	$7.75E - 10$	0
g19					
GSADE	32.6556	32.6556	32.6556	$5.94E - 12$	0
GSA	954.2394	18959.779	41292.367	$8.89E + 03$	219.0697
DE	32.6556	32.6556	32.6556	$1.17E - 06$	0
g20					
GSADE	-	-	-	-	0.246
GSA	-	-	-	-	235.4983
DE	-	-	-	-	0.2699
g21					
GSADE	324.7028	324.7028	324.7028	$0.00E + 00$	0
GSA	-	-	-	-	2640.1702
DE	324.7028	324.7028	324.7028	$1.86E - 10$	0
g22					
GSADE	-	-	-	-	308.1947
GSA	-	-	-	-	3200071
DE	-	-	-	-	3000.1

(continued)

Table 6 (continued)

g23					
GSADE	-400.0551	-400.0551	-400.0551	2.31E - 06	0
GSA	-	-	-	-	363.0938
DE	-400.0551	-400.0551	-400.0551	7.61E - 08	0
g24					
GSADE	-5.508	-5.508	-5.508	3.58E - 15	0
GSA	-5.4272	-3.7059	-1.2099	1.23E + 00	0.8783
DE	-5.508	-5.508	-5.508	3.46E - 16	0

Table 7 Feasibility rate of GSADE, GSA and DE

	g01	g02	g03	g04	g05	g06	g07	g08
GSADE	100	100	100	100	100	100	100	100
GSA	0	100	0	60	0	20	40	35
DE	100	100	100	100	100	100	100	100
	g09	g10	g11	g12	g13	g14	g15	g16
GSADE	100	100	100	100	100	100	100	100
GSA	24	0	90	85	0	5	2	0
DE	100	100	100	100	95	100	100	90
	g17	g18	g19	g20	g21	g22	g23	g24
GSADE	100	100	100	0	100	0	100	100
GSA	0	20	10	0	40	0	0	90
DE	0	0	0	0	100	0	92	100

Table 8 Success rate of GSADE, GSA and DE

	g01	g02	g03	g04	g05	g06	g07	g08
GSADE	1.00	0.00	0.90	1.00	0.95	1.00	1.00	1.00
GSA	0.00	0.00	0.00	0.00	0.00	0.00	0.00	0.90
DE	1.00	0.00	0.00	1.00	0.90	0.96	1.00	1.00
	g09	g10	g11	g12	g13	g14	g15	g16
GSADE	1.00	1.00	97.00	1.00	1.00	1.00	1.00	1.00
GSA	0.00	0.00	0.00	1.00	0.00	0.00	0.00	0.00
DE	1.00	0.98	0.96	0.65	0.00	1.00	0.96	0.98
	g17	g18	g19	g20	g21	g22	g23	g24
GSADE	1.00	1.00	1.00	0.00	0.00	0.00	1.00	1.00
GSA	0.00	0.00	0.00	0.00	0.00	0.00	0.00	0.00
DE	0.00	1.00	0.68	0.00	0.00	0.00	1.00	0.97

Fig. 2 One dimensional trajectory of acceleration of a typical particle

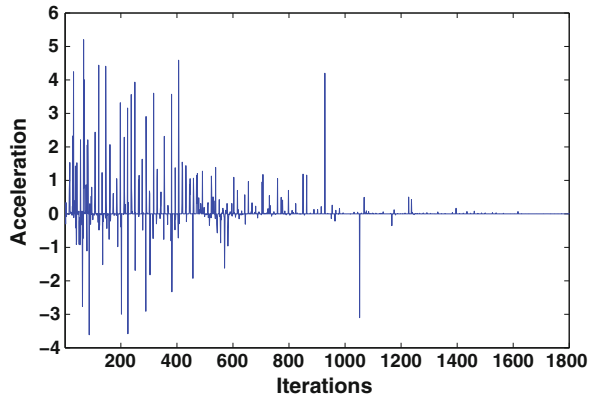
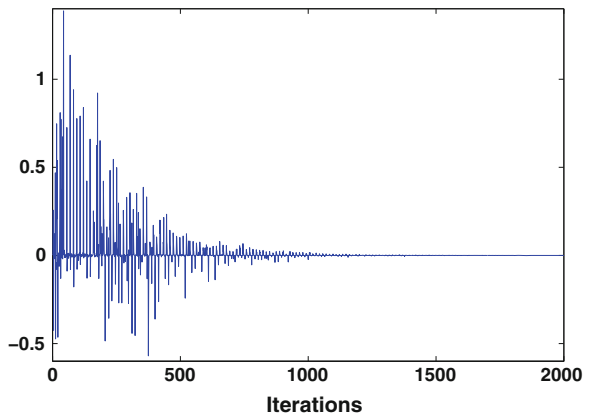


Fig. 3 One dimensional trajectory of acceleration of a typical particle



global minima and $f(x^*)$ is the obtained minima.

Success Rate = No. of Successful Runs/Total Runs

The results of the feasibility rate and success rate are listed in Tables 7 and 8. The success rate of the GSADE is recorded 100 % for 17 problems and more than 90 % for the 3 problems out of total 24 problems. To discover the behavior of the acceleration of the particles a one dimensional trajectory of the acceleration is depicted in Figs. 2 and 3. Over all it can be observed that the performance of the GSADE is very good over the chosen problems, for few problems the performance is excellent and for some problems the results of the GSADE is comparable to DE.

6 Conclusion

This article proposes a new co-swarm gravitational search algorithm which is designed by hybridizing the essential properties of GSA and DE. A new velocity update equation is proposed to implement this hybridization the proposed algorithm is tested over 24 real parameter constrained optimization problems, having a varied level of complexity. The results of the GSADE is compared with the original GSA and DE. The fitness value analysis is performed with feasibility rate and success rate. It is observed that for most of the problems the performance of GSADE is very good in comparison to the other algorithms. In future the utility of the proposed algorithm could be tested over some more benchmark problems and real life problems.

References

1. Liang, J.J., Runarsson, T.P., Mezura-Montes, E., Clerc, M., Suganthan, P.N., Coello, C.A.C., Deb, K.: Problem definitions and evaluation criteria for the cec 2006 special session on constrained real-parameter optimization. *J. Appl. Mech.* **41**
2. Zhang, W.-J., Xie, X.-F.: Depso: hybrid particle swarm with differential evolution operator. In: *IEEE International Conference on Systems, Man and Cybernetics*, vol. 4, pp. 3816–3821. IEEE (2003)
3. Liao, T.W.: Two hybrid differential evolution algorithms for engineering design optimization. *Appl. Soft Comput.* **10**(4), 1188–1199 (2010)
4. Gong, W., Cai, Z., Ling, C.X.: DE/BBO: a hybrid differential evolution with biogeography-based optimization for global numerical optimization. *Soft Comput. Fusion Found. Method. Appl.* **15**(4), 645–665 (2010)
5. Brest, J., Zumer, V., Maucec, M.S.: Self-adaptive differential evolution algorithm in constrained real-parameter optimization. In: *IEEE Congress on Evolutionary Computation, CEC 2006*, pp. 215–222. IEEE
6. He, Q., Wang, L.: An effective co-evolutionary particle swarm optimization for constrained engineering design problems. *Eng. Appl. Artif. Intell.* **20**(1), 89–99 (2007)
7. Sedki, A., Ouazar, D.: Hybrid particle swarm optimization and differential evolution for optimal design of water distribution systems. *Adv. Eng. Inf.* **26**(3), 582–591
8. Xin, B., Chen, J., Zhang, J., Fang, H., Peng, Z.: Hybridizing differential evolution and particle swarm optimization to design powerful optimizers: a review and taxonomy. In: *IEEE Transactions on Systems, Man, and Cybernetics, Part C: Applications and Reviews*, vol. 42 no. 5, pp. 744–767 (2012)
9. Rashedi, E., Nezamabadi-pour, H., Saryazdi, S.: Gsa: a gravitational search algorithm. *Inf. Sci.* **179**(13), 2232–2248 (2009)
10. Storn, R., Price, K.: Differential evolution—a simple and efficient heuristic for global optimization over continuous spaces. *J. Global Optim.* **1**(4), 341–359 (1997)
11. Storn, R.: On the usage of differential evolution for function optimization. In: *Biennial Conference of the North American Fuzzy Information Processing Society, NAFIPS, 1996*, pp. 519–523. IEEE (1996)

An Analytical Investigation on Thermally Induced Vibrations of Non-homogeneous Tapered Rectangular Plate

Anupam Khanna and Narinder Kaur

Abstract The goal of the present investigation is to study the temperature-thickness coupling problem of non-homogeneous rectangular plate with varying thickness. Authors assumed that temperature and thickness of the plate vary exponentially in x-direction only. Four sided clamped boundary condition with two term deflection function is considered. Due to non-homogeneity present in the plate's material, variation in poisson's ratio is assumed exponential in x-direction. An authentic and quite convenient Rayleigh–Ritz technique has been applied to obtain the fundamental frequencies for the first two modes of vibration. The effect of structural parameters such as taper constant, thermal gradient, non-homogeneity constant and aspect ratio on time period and deflection has been illustrated for first two modes of vibration. Results are calculated with great accuracy and presented in tabular form.

Keywords Vibration · Thermal gradient · Taper constant · Aspect ratio · Non-homogeneity constant · Deflection

1 Introduction

Recent development in space technology has stimulated interest in the study and analysis of vibration of plates. With the development of technology, especially in space technology, composite materials i.e. visco-elastic materials became the necessity to reduce or control the effect of vibrations. Plates of variable thickness are frequently used in order to economize the plate material or to lighten the plates,

A. Khanna (✉) · N. Kaur

Department of Mathematics, Maharishi Markandeshwar University, Mullana, Ambala, India
e-mail: rajjeanupam@gmail.com

N. Kaur

e-mail: narinder89.kaur@gmail.com

especially when it is used in the wings of high-speed and high performance aircrafts.

In an up-date survey of literature, authors have come across various models to account for non-homogeneity of plate materials proposed by researchers dealing with vibration but none of them consider non-homogeneity with thermal effect on tapered visco-elastic plates. An appreciable work [1–19] is available in the field of vibrations of plates with different surroundings and conditions but very few of them had worked on non homogeneous visco-elastic plates of variable thickness subject to thermal gradient.

In this paper, our main endeavour is to provide a mathematical model for analyzing the vibrational behaviour of visco-elastic non-homogeneous rectangular plate with exponential varying thickness and temperature variation in x-direction. The non-homogeneity is assumed to arise in exponential order in x-direction due to the variation in the poisson's ratio of the plate material. Rayleigh–Ritz approach had been adopted to calculate time period and defection for the first two modes of vibrations for various values of taper constant, thermal gradient, aspect ratio and non-homogeneity constant. It is also assumed that rectangular visco-elastic plate is isotropic and clamped on all the four edges. All the material constants used in numerical calculation have been taken for 'DURALIUM', an alloy of aluminium. Findings of the present paper are given in tabular form.

2 Mathematical Formulation

2.1 Analysis of Differential Equation of Motion

The differential equation of an isotropic visco-elastic tapered plate is given by Leissa [11]

$$M_{x,xx} + 2M_{xy,xy} + M_{y,yy} = \rho h w_{,tt} \quad (1)$$

where,

$$\begin{aligned} M_x &= -\tilde{D}D_1[w_{,xx} + \nu w_{,yy}], \\ M_y &= -\tilde{D}D_1[w_{,yy} + \nu w_{,xx}], \text{ and} \\ M_{xy} &= -\tilde{D}D_1(1 - \nu)w_{,xy}. \end{aligned} \quad (2)$$

where, M_x , M_y are bending moments, M_{xy} is twisting moment. Here w , h , ρ and ν are deflection, thickness of plate, density and poisson ratio of plate material respectively. A comma in the suffix denotes partial differentiation with respect to suffix variable. After substituting the values of M_x , M_y and M_{xy} from Eq. (2) in Eq. (1), one gets

$$\begin{aligned} \tilde{D} [D_1(w_{,xxxx} + 2w_{,xxyy} + w_{,yyyy}) + 2D_{1,x}(w_{,xxx} + w_{,xyy}) \\ + 2D_{1,y}(w_{,yyy} + w_{,yxx}) + D_{1,xx}(w_{,xx} + vw_{,yy}) \\ + D_{1,yy}(w_{,yy} + vw_{,xx}) + 2(1 - \nu)D_{1,xy}w_{,xy}] + \rho h w_{,tt} = 0. \end{aligned} \tag{3}$$

By using variable separation technique, the solution of Eq. (3) can be taken in the form of product of two functions as,

$$w(x, y, t) = \phi(x, y)\psi(t). \tag{4}$$

where ϕ and ψ are deflection function and time function respectively.

After using Eq. (4) in Eq. (3), one obtains

$$\begin{aligned} [D_1(\phi_{,xxxx} + 2\phi_{,xxyy} + \phi_{,yyyy}) \\ + 2D_{1,x}(\phi_{,xxx} + \phi_{,xyy}) + 2D_{1,y}(\phi_{,yyy} + \phi_{,yxx}) \\ + D_{1,xx}(\phi_{,xx} + \nu\phi_{,yy}) + D_{1,yy}(\phi_{,yy} + \nu\phi_{,xx}) \\ + 2(1 - \nu)D_{1,xy}\phi_{,xy}] / \rho h \phi = - \frac{\ddot{\psi}}{D\psi}. \end{aligned} \tag{5}$$

Here, dot denotes differentiation with respect to t .

The previous equation is satisfied if both of its sides are equal to a constant. Denoting this constant by ξ^2 , one gets

$$\begin{aligned} [D_1(\phi_{,xxxx} + 2\phi_{,xxyy} + \phi_{,yyyy}) \\ + 2D_{1,x}(\phi_{,xxx} + \phi_{,xyy}) + 2D_{1,y}(\phi_{,yyy} + \phi_{,yxx}) \\ + D_{1,xx}(\phi_{,xx} + \nu\phi_{,yy}) + D_{1,yy}(\phi_{,yy} + \nu\phi_{,xx}) \\ + 2(1 - \nu)D_{1,xy}\phi_{,xy}] - \rho \xi^2 h \phi = 0. \end{aligned} \tag{6}$$

and

$$\ddot{\psi} + \xi^2 \tilde{D}\psi = 0. \tag{7}$$

Equations (6) and (7) represent the differential equations of motion and time function for non-homogeneous rectangular plate respectively. Here, D_1 is flexural rigidity of rectangular plate i.e.,

$$D_1 = \frac{Eh^3}{12(1 - \nu^2)}. \tag{8}$$

2.2 Frequency Equation and Assumptions

Rayleigh Ritz technique has been adopted to solve the frequency equation. This method is completely depends upon conservation of energy according to which

maximum strain energy (S_m) must be equal to the maximum kinetic energy (K_m). So, it is necessary for the problem under consideration that [7]

$$(S_m - \lambda^2 K_m) = 0. \quad (9)$$

where,

$$K_m = \frac{1}{2} \rho \dot{\xi}^2 \int_0^a \int_0^b h \phi^2 dy dx. \quad (10)$$

and

$$S_m = \frac{1}{2} \int_0^a \int_0^b D_1 \left\{ (\phi_{,xx})^2 + (\phi_{,yy})^2 + 2\nu \phi_{,xx} \phi_{,yy} + 2(1-\nu)(\phi_{,xy})^2 \right\} dy dx. \quad (11)$$

The authors assumed the exponential temperature variation as:

$$\tau = \tau_0 (1 - e^{\frac{x}{a}}). \quad (12)$$

where τ denotes the temperature excess above the reference temperature at any point on the plate and τ_0 denotes the temperature excess above the reference temperature at $x = y = 0$ and a and b denote the length and breadth of rectangular plate respectively.

For most of engineering materials, the temperature dependence of the modulus of elasticity can be expressed as [8]:

$$E = E_0 (1 - \gamma \tau). \quad (13)$$

where E_0 is the value of the Young's modulus at reference temperature i.e. $\tau = 0$ and γ is the slope of the variation of E. After using Eq. (12) in Eq. (13), one gets

$$E = E_0 (1 - \alpha (1 - e^{\frac{x}{a}})). \quad (14)$$

where, $\alpha = \gamma \tau_0 (0 \leq \alpha < 1)$ is thermal gradient.

It is considered that thickness varies exponentially in x-direction as

$$h = h_0 (e^{\frac{\beta x}{a}}). \quad (15)$$

where, h_0 is thickness of the plate at $x = y = 0$ and β is taper constant in x-direction.

Also, the authors assumed that poisson ratio of material varies exponentially in x-direction as shown below:

$$\nu = \nu_0 e^{\alpha_1 x/a}. \quad (16)$$

where ν_0 denotes poisson ratio at reference temperature i.e. $\tau = 0$ and α_1 is called non homogeneity constant.

After using Eqs. (14), (15) and (16) in Eq. (8), one obtains

$$D_1 = \frac{(E_0(1 - \alpha(1 - e^{\frac{x}{a}}))h_0^3(e^{\frac{\beta x}{a}})^3}{12(1 - \nu_0^2 e^{\frac{2x}{a}})} \tag{17}$$

Since plate is assumed clamped at the boundary, so the boundary conditions are taken as:

$$\left. \begin{aligned} \phi = \phi_{,x} = 0, x = 0, a \\ \phi = \phi_{,y} = 0, y = 0, b \end{aligned} \right\} \tag{18}$$

For arbitrary variations of ϕ satisfying the relevant boundary conditions.

$$\phi(x,y) = \left[\left(\frac{x}{a}\right)\left(\frac{y}{b}\right)\left(1 - \frac{x}{a}\right)\left(1 - \frac{y}{b}\right) \right]^2 \left[U_1 + U_2 \left(\frac{x}{a}\right)\left(\frac{y}{b}\right)\left(1 - \frac{x}{a}\right)\left(1 - \frac{y}{b}\right) \right] \tag{19}$$

where U_1 and U_2 are two arbitrary constants.

2.3 Solution of Equation of Motion

Now assuming the non-dimensional variables as

$$X = \frac{x}{a}, \quad Y = \frac{y}{a} \tag{20}$$

After using Eq. (20) in Eqs. (10) and (11), one gets

$$K_m^* = \frac{1}{2} \rho \xi^2 a^2 h_0 \int_0^1 \int_0^{b/a} (e^{\beta X}) \phi^2 dYdX \tag{21}$$

and

$$\begin{aligned} S_m^* = R \int_0^1 \int_0^{b/a} & \left\{ \frac{(1 - \alpha(1 - e^X))(e^{\beta X})^3}{(1 - \nu_0^2 e^{2X})} \right\} \\ & \left\{ (\phi_{,XX})^2 + (\phi_{,YY})^2 + 2\nu_0 e^{2X} \phi_{,XX} \phi_{,YY} \right. \\ & \left. + 2(1 - \nu_0 e^{2X})(\phi_{,XY})^2 \right\} dYdX \end{aligned} \tag{22}$$

where, $R = \frac{E_0 h_0^3}{24a^2}$. After substituting K_m^* and S_m^* from Eqs. (21) and (22) in Eq. (9), one obtains

$$(S_m^* - \lambda^2 K_m^*) = 0 \tag{23}$$

Here $\lambda^2 = \frac{12\rho\xi^2 a^4}{E_0 h_0^2}$ is a frequency parameter. Equation (23) consists two unknown constants i.e. U_1 and U_2 arising due to the substitution of ϕ . These two constants are to be determined as follows

$$\frac{\delta(S_m^* - \lambda^2 K_m^*)}{\delta U_n} = 0, \quad n = 1, 2. \quad (24)$$

On simplifying Eq. (24), one obtains

$$S_{n1}U_1 + S_{n2}U_2 = 0, \quad n = 1, 2. \quad (25)$$

Choosing $U_1 = 1$, one can easily get U_2 from Eq. (25), which is $\left(\frac{-S_{n1}}{S_{n2}}\right)$.

For a non-trivial solution, the determinant of the coefficient of Eq. (25) must be zero. Therefore one obtains the frequency equation as follows:

$$\begin{vmatrix} S_{11} & S_{12} \\ S_{21} & S_{22} \end{vmatrix} = 0. \quad (26)$$

As Eq. (26) gives a bi-quadratic equation in λ which provides desired values of λ^2 .

After substituting the values of U_1 and U_2 in Eq. (19), one can obtain deflection function ϕ as

$$\phi = \left[XY \left(\frac{a}{b}\right) (1 - X) \left(1 - \left(\frac{aY}{b}\right)\right) \right]^2 \left[1 + \left(\frac{-S_{11}}{S_{12}}\right) XY \left(\frac{a}{b}\right) (1 - X) \left(1 - \left(\frac{aY}{b}\right)\right) \right]. \quad (27)$$

Time period of the vibration of visco-elastic plate is given by

$$K = \frac{2 \times \pi}{\xi}. \quad (28)$$

2.4 Solution of Time Function and Deflection

Time function of vibrations of non-homogeneous rectangular plate are defined by the general ordinary differential Eq. (7) [12].

$$\psi(t) = e^{a_1 t} \left[\cos b_1 t + \left(-\frac{a_1}{b_1}\right) \sin b_1 t \right]. \quad (29)$$

Table 1 Time period ($\times 10^{-5}$) vs non homogeneity constant for fixed aspect ratio ($a/b = 1.5$)

α_1	$\beta = \alpha = 0.0$		$\beta = \alpha = 0.2$		$\beta = \alpha = 0.6$	
	Mode 1	Mode 2	Mode 1	Mode 2	Mode 1	Mode 2
0.0	668.23	169.09	562.92	142.59	393.40	100.17
0.05	665.99	168.52	560.97	142.09	392.01	99.78
0.1	663.62	167.92	558.90	141.55	390.53	99.36
0.15	661.11	167.28	556.70	140.98	388.93	98.91

After using Eqs. (27) and (29) in Eq. (4), deflection function w can be expressed as

$$\begin{aligned}
 w = & \left[XY \left(\frac{a}{b} \right) (1 - X) \left(1 - \left(\frac{aY}{b} \right) \right) \right]^2 \\
 & \left[1 + \left(\frac{-S_{11}}{S_{12}} \right) XY \left(\frac{a}{b} \right) (1 - X) \left(1 - \left(\frac{aY}{b} \right) \right) \right] \\
 & \times \left[e^{a_1 t} \left\{ \cos b_1 t + \left(\frac{-a_1}{b_1} \right) \sin b_1 t \right\} \right].
 \end{aligned} \tag{30}$$

3 Results and Discussion

In calculations, the following parameters are used for duralium i.e.

$$\begin{aligned}
 E &= 7.08 \times 10^{10} \frac{\text{N}}{\text{M}^2}, \\
 G &= 2.632 \times 10^{10} \frac{\text{N}}{\text{M}^2}, \\
 \eta &= 14.612 \times 10^5 \frac{\text{Ns}}{\text{M}^2}, \\
 \rho &= 2.80 \times 10^3 \frac{\text{Kg}}{\text{M}^3}, \\
 v_0 &= 0.345, h_0 = 0.01 \text{ m.}
 \end{aligned}$$

Authors had calculated as well as tabulated the results for time period and deflection for different combinations of taper constant, aspect ratio, thermal gradient and non-homogeneity constant for first two modes of vibration.

Table 1 shows time period ($K \times 10^{-5}$) for increasing values of non homogeneity constant (α_1) for fixed aspect ratio ($a/b = 1.5$) for different combinations of taper constant (β) and thermal gradient (α) i.e.

$$\beta = \alpha = 0.0, \beta = \alpha = 0.2, \beta = \alpha = 0.6.$$

From Table 1, it can be clearly observed that time period for both the modes of vibration continuously decreases (top to bottom) with increasing non-homogeneity constant from 0.0 to 0.15 for fixed value of aspect ratio i.e. $\frac{a}{b} = 1.5$ at different

Table 2 Time period ($\times 10^{-5}$) vs aspect ratio for fixed taper constant ($\beta = 0.2$) and thermal gradient ($\alpha = 0.2$)

$\frac{a}{b}$	$\alpha_1 = 0.0$		$\alpha_1 = 0.1$	
	Mode 1	Mode 2	Mode 1	Mode 2
0.25	1472.26	360.24	1459.84	357.10
0.5	1367.36	341.03	1356.16	338.12
0.75	1177.13	298.85	1167.93	296.41
1.0	944.51	241.33	937.46	239.50
1.25	730.75	186.25	725.46	184.86
1.5	562.92	142.59	558.90	141.55

combination of α and β . Also interesting to note that time period decreases (left to right) as combined values of β and α increase for both the modes of vibration.

Table 2 shows time period ($K \times 10^{-5}$) for increasing value of aspect ratio ($\frac{a}{b}$) for fixed taper constant ($\beta = 0.2$) and thermal gradient ($\alpha = 0.2$) for different values of non homogeneity constant (α_1) i.e.

$$\alpha_1 = 0.0, \alpha_1 = 0.1,$$

From Table 2, it is found that as aspect ratio increases from 0.25 to 1.5, time period decreases (top to bottom) continuously for different values of non-homogeneity constant i.e. $\alpha_1 = 0.0, 0.1$ at fixed value of thermal gradient ($\alpha = 0.2$) and taper constant ($\beta = 0.2$).

In Tables 3, 4 and 5, deflection (for both the modes of vibrations) is calculated for $T = 0$ K and $T = 5$ K at different values of X and Y i.e.

- 3: $\alpha = \beta = 0.0$; $\frac{a}{b} = 1.5$; $\alpha_1 = 0.0, 0.1$
- 4: $\alpha = \beta = 0.6$; $\frac{a}{b} = 1.5$; $\alpha_1 = 0.0, 0.1$
- 5: $\alpha = \beta = 0.2$; $\alpha_1 = 0.1$; $\frac{a}{b} = 0.25, 0.5, 0.75, 1.0, 1.25, 1.5$.

From Tables 3 and 4, it can be seen that at $T = 0$ K, deflection (for both the modes of vibration) increases from 0.0 to its maxima then decreases to 0 (left to right) as X increases from 0.0 to 1.0 for $Y = 0.2$ and $Y = 0.6$. Interesting to see that deflection for $X = 0.2$ and $X = 0.8$ and $X = 0.4$ and $X = 0.6$ are same for both the modes of vibration. Authors noticed that deflection decreases rapidly as Y increases from 0.2 to 0.6 for both the modes of vibrations.

At $T = 5$ K in Table 3, deflection for both the modes of vibration decreases continuously as α_1 varies from 0.0 to 0.1 (top to bottom). In Table 4, at $T = 5$ K, deflection for both the modes of vibration increases at different values of X, Y and α_1 . From Table 5, it can be clearly seen that at $T = 0$ K and $T = 5$ K, deflection at $Y = 0.2$ for first mode of vibration increases as aspect ratio increases from 0.25 to 1.5. At $T = 5$ K deflection for first mode of vibration continuously increases while deflection for the second mode, it firstly increases then it decreases as aspect ratio increases from 0.25 to 1.5 for fixed value of taper constant, thermal gradient and non-homogeneity constant i.e. $\alpha = \beta = 0.2$ and $\alpha_1 = 0.1$.

Table 3 Deflection ($\times 10^{-5}$) vs non-homogeneity constant for $\alpha = \beta = 0.0$; $\frac{\alpha}{\beta} = 1.5$ at $\psi = 0\text{ K}$ and $\psi^a = 5\text{ K}$

$X \rightarrow$	$\alpha_1 \downarrow$	0.0		0.2		0.4		0.6		0.8		1.0	
		Mode 1	Mode 2	Mode 1	Mode 2	Mode 1	Mode 2	Mode 1	Mode 2	Mode 1	Mode 2	Mode 1	Mode 2
0.2	0	0	0	114.6210	39.5098	259.8370	6.3376	259.8370	6.3376	114.6210	39.5098	0	0
		{0}	{0}	{50.4459}	{1.8094}	{114.3570}	{0.2902}	{114.3570}	{0.2902}	{50.4459}	{1.8094}	{0}	{0}
0.1	0	0	0	82.5345	39.5100	151.5460	6.3383	151.5460	6.3383	82.5345	39.5100	0	0
		{0}	{0}	{50.1875}	{1.7987}	{113.7790}	{0.2885}	{113.7790}	{0.2885}	{50.1875}	{1.7987}	{0}	{0}
0.6	0	0	0	20.8718	14.9592	47.1142	27.1595	47.1142	27.1595	20.8718	14.9592	0	0
		{0}	{0}	{9.1859}	{0.6847}	{20.7443}	{1.2435}	{20.7443}	{1.2435}	{9.1859}	{0.6847}	{0}	{0}
0.1	0	0	0	20.8730	14.9593	47.1184	27.1595	47.1184	27.1595	20.8730	14.9593	0	0
		{0}	{0}	{9.1381}	{0.6810}	{20.6283}	{1.2364}	{20.6283}	{1.2364}	{8.9381}	{0.6810}	{0}	{0}

^a All the values written in bold and {} brackets shows deflection for both the modes of vibrations for $\psi = 5\text{ K}$

Table 4 Deflection ($\times 10^{-5}$) vs non-homogeneity constant for $\alpha = \beta = 0.6$; $\frac{\alpha}{\beta} = 1.5$ at $\psi = 0$ K and $\psi^a = 5$ K

$X \rightarrow$	$\alpha_1 \downarrow$	0.2		0.4		0.6		0.8		1.0	
		Mode 1	Mode 2	Mode 1	Mode 2	Mode 1	Mode 2	Mode 1	Mode 2	Mode 1	Mode 2
0.2	0	0	120.9650	39.6305	280.3390	6.7448	280.3390	6.7448	120.9650	39.6305	0
	{0}	{0}	{29.9232}	{71.6024}	{69.5026}	{12.1862}	{69.5026}	{12.1862}	{29.9232}	{71.6024}	{0}
0.1	0	0	120.8890	39.6355	280.9930	6.4042	280.9930	6.4042	120.8890	39.6355	0
	{0}	{0}	{46.2200}	{77.4880}	{105.0800}	{13.2193}	{105.0800}	{13.2193}	{46.2200}	{77.4880}	{0}
0.6	0	0	21.3500	14.9687	48.7281	27.1915	48.7281	27.1915	21.3500	14.9687	0
	{0}	{0}	{5.2931}	{27.0227}	{12.0808}	{49.0538}	{12.0808}	{49.0538}	{5.2931}	{27.0227}	{0}
0.1	0	0	21.3652	14.9691	48.7796	27.1928	48.7796	27.1928	21.3652	14.9691	0
	{0}	{0}	{5.2427}	{29.2649}	{11.9698}	{53.1624}	{11.9698}	{53.1624}	{5.2427}	{29.2649}	{0}

^a All the values written in bold and {} brackets shows deflection for both the modes of vibrations for $\psi = 5$ K

Table 5 Deflection ($\times 10^{-5}$) vs aspect ratio for $\alpha = \beta = 0.2$; $\alpha_1 = 0.1$ at $\psi = 0$ K and $\psi^a = 5$ K

$X \rightarrow$	$a/b \downarrow$	0.0		0.2		0.4		0.6		0.8		1.0	
		Mode 1	Mode 2	Mode 1	Mode 2	Mode 1	Mode 2	Mode 1	Mode 2	Mode 1	Mode 2	Mode 1	Mode 2
0.2	0.25	0	0	5.92258	4.9310	13.4907	10.1443	13.4907	10.1443	13.4907	10.1443	5.92258	4.9310
		{0}	{0}	{4.0690}	{1.0601}	{9.2686}	{2.1806}	{9.2686}	{2.1806}	{9.2686}	{2.1806}	{4.0690}	{1.0601}
	0.5	0	0	21.3832	14.9802	48.8403	27.2303	48.8403	27.2303	48.8403	27.2303	21.3832	14.9802
0.75	0.25	{0}	{0}	{14.2754}	{2.9527}	{32.6058}	{5.3650}	{32.6058}	{5.3650}	{32.6058}	{5.3650}	{14.2754}	{2.9527}
		0	0	42.4659	25.2039	96.5044	38.2452	96.5044	38.2452	96.5044	38.2452	42.4659	25.2039
	0.5	{0}	{0}	{26.5624}	{3.9507}	{60.3635}	{5.9949}	{60.3635}	{5.9949}	{60.3635}	{5.9949}	{26.5624}	{3.9507}
1.0	0.25	0	0	66.2840	33.0759	149.9810	37.9032	149.9810	37.9032	149.9810	37.9032	66.2840	33.0759
		{0}	{0}	{36.9421}	{3.3310}	{83.5888}	{3.8172}	{83.5888}	{3.8172}	{83.5888}	{3.8172}	{36.9421}	{3.3310}
	0.5	0	0	91.2432	37.7618	206.6960	26.1961	206.6960	26.1961	206.6960	26.1961	91.2432	37.7618
1.25	0.25	{0}	{0}	{42.8622}	{2.0186}	{97.0968}	{1.4003}	{97.0968}	{1.4003}	{97.0968}	{1.4003}	{42.8622}	{2.0186}
		0	0	115.591	39.5332	263.113	6.4164	263.113	6.4164	263.113	6.4164	115.591	39.5332
	0.5	{0}	{0}	{43.3414}	{2.8282}	{98.6551}	{0.4590}	{98.6551}	{0.4590}	{98.6551}	{0.4590}	{43.3414}	{2.8282}

^a All the values written in bold and {} brackets shows deflection for both the modes of vibrations for $\psi = 5$ K

4 Conclusion

The main aim of the present study is to provide such kind of a mathematical models which help the scientists and practicing engineers to increase strength, durability and efficiency of designs of machines and structures. They can obtain the desired values of deflection by the appropriate tapering and variation in corresponding parameters. Therefore, authors advised them to go through the findings of the present paper before finalizing any design of machine and structure.

References

1. Abu, A.I., Turhan, D., Mengi, D.: Two dimensional transient wave propagation in visco-elastic layered media. *J. Sound Vib.* **244**, 837–858 (2001)
2. Algazin, S.D.: Vibrations of free edge variable thickness plate of arbitrary shape in plane. *J. Appl. Mech. Tech. Phys.* **5**, 126–131 (2011)
3. Alijani, F., Amabili, M.: Theory and experiments for nonlinear vibrations of imperfect rectangular plates with free edges. *J. Sound Vib.* **332**, 3564–3588 (2013)
4. Avalos, D.R., Laura, P.A.: Transverse vibrations of a simply supported plate of generalized anisotropy with an oblique cut-out. *J. Sound Vib.* **258**, 773–776 (2002)
5. Bhardwaj, N., Gupta, A.P., Choong, K.K., Ohmori, H.: Transverse vibrations of clamped and simply-supported circular plates with two dimensional thickness variation. *Shock Vib.* **19**(2012), 273–285 (2012)
6. Chakraverty, S.: *Vibrations of Plate*, vol. 10. Taylor and Francis, Boca Raton (2009)
7. Gupta, A.K., Khanna, A.: Vibration of visco-elastic rectangular plate with linearly thickness variations in both directions. *J. Sound Vib.* **301**, 450–457 (2007)
8. Gupta, A.K., Kumar, L.: Effect of thermal gradient on vibration of non-homogeneous visco-elastic elliptic plate of variable thickness. *Meccanica* **44**, 507–518 (2009)
9. Khodzhaev, D.A., Eshmatov, BKh: Non linear vibrations of a visco-elastic plate with concentrated masses. *J. Appl. Mech. Tech. Phys.* **48**, 905–914 (2007)
10. Lal, R., Kumar, Y.: Characteristic orthogonal of nonhomogeneous rectangular polynomials in the study of transverse vibrations orthotropic plates of bilinearly varying thickness. *Meccanica* **47**, 175–193 (2012)
11. Leissa, A.W.: *Vibrations of plate*. In: NASA SP-160 in U. S. Govt, Printing Office (1969)
12. Leissa, A.W.: Recent studies in plate vibration 1981–1985. Part II, complicating effects. *Shock Vib. Dig.* **19**, 10–24 (1987)
13. Li, W.L.: Vibration analysis of rectangular plate with general elastic boundary supports. *J. Sound Vib.* **273**, 619–635 (2004)
14. Patel, D.S., Pathan, S.S., Bhoraniya, I.H.: Influence of stiffeners on the natural frequencies of rectangular plate with simply supported edges. *Int. J. Eng. Res. Technol.* **1**, 1–6 (2012)
15. Rezaee, M., Fekrmandi, H.: A theoretical and experimental investigation on free vibration behavior of a cantilever beam with a breathing crack. *Shock Vib.* **19**, 175–186 (2012)
16. Sharma, S., Gupta, U.S., Lal, R.: Effect of pasternak foundation on axisymmetric vibration of polar orthotropic annular plates of varying thickness. *J. Vib. Acoust* **132**, 1–13 (2012)
17. Singh, B., Chakraverty, S.: Transverse vibration of completely-free elliptic and circular plates using orthogonal polynomials in the Rayleigh-Ritz method. *J. Sound Vib.* **33**, 741–751 (1991)
18. Singh, B., Saxena, V.: Transverse vibration of rectangular plate with bidirectional thickness variation. *J. Sound Vib.* **198**, 51–65 (1996)
19. Wang, H.J., Chen, W.L.: Axisymmetric vibration and damping analysis of rotating annular plates with constrained damping layer treatments. *J. Sound Vib.* **271**, 25–45 (2004)

Building of a Competent Mobility Model for Ad Hoc Wireless Networks

Arvind Kumar Shukla, C. K. Jha and Vimal Kumar Mishra

Abstract Mobility is a natural character of Ad Hoc networks. A realistic simulation of user movement in Ad Hoc Network is very important to the network performance. Therefore, by using a realistic mobility model, which is an important aspect in enhancing the self-confidence in the simulation result of the network. Although, each node's movement is random, there are still some underlying disciplines in their mobility. By predicting the mobility of user that truly depicts nodes mobility in an Ad Hoc Network, is the first step of mobility management. In this manuscript an attempt has been made by proposing a new mobility model called restriction models for generating unusual mobility scenarios for Ad Hoc networks such as campus scenario. The propose algorithm performance has been evaluated using network simulator (ns2.35) for dynamic source routing (DSR). The results are compared with other mobility model such as Random way point. The results shows that our proposed algorithm has outperform the available mobility model for campus scenario.

Keywords Ad Hoc network · Mobility models · Mobility patterns · ns 2.35 · Performance parameters · Boonmotion 2.0

A. K. Shukla (✉) · C. K. Jha
Department of AIM and ACT, Banasthali Vidyapith, Rajasthan, India
e-mail: toarvindshukla@gmail.com

C. K. Jha
e-mail: ckjhal@gmail.com

V. K. Mishra
Department of Computer Engineering, Government Girls Polytechnic, Allahabad, India
e-mail: vimal.mishra.upte@gmail.com

1 Introduction

This instruction Individual mobility has been widely studied in many areas like urban planning, traffic forecasting and avoiding the spread of biological and mobile viruses [1, 2]. It's also an essential topic used to improve the Performance of wireless ad-hoc network. For example, protocols can be designed based on the regularity of nodes movement pattern. As the mobile devices are often carried by human, it's important to study the human mobility in order to simulate the Ad Hoc networks in a more perfect and practical way. Modern research has proved that person movement is not random but natural [1, 3–5]. Additionally, it has been indicated that even with the regularity of persons, the individual mobility has some basic presentation. However, it is logical to imagine a high degree of correlation between future and past movement speeds and direction. This motion is totally stateless, that is, the future movement here is completely independent of the past movement and hence there are no boundaries forced on the maximum variation which the nodes can take up for their next movement. This randomness in choosing the next direction vector renders this type of movement entirely changeable. One of the most usually used mobility models is the Random Waypoint model. In this model, every node selects a random point in the simulation area as its destination, and a speed V from an input range $[V_{min}, V_{max}]$. The node then moves to its destination at its selected speed. When the node reaches its destination, it rests for some pause time. At the end of this pause time, it selects a new destination and speed and resumes movement. The properties of the random waypoint model have been extensively studied [3, 6–8]. One of the interesting results of these studies addresses the node spatial distribution of the random waypoint model. It is shown that, due to the characteristics of the model, the concentration of nodes follows a cyclic pattern during the lifetime of the network. The nodes tend to congregate in the center of the simulation area, resulting in non-uniform network density.

In a realistic mobility model the nodes movement is the first step to perform mobility management. Different mobility models have different focuses and different application scenarios [3, 6, 9]. Moreover random mobility models, to get enhanced performance, some emerging mobility research papers have modified a method to organize the movement of a small part of elected nodes and develop this movement to improve the network's overall performance. In this paper we proposed a new variant of mobility model which reflects the realism and diversified walk. In this technique we impose some constraints to find the current and future location of the mobile node. Mobility models are required to describe movement behavior on different scales. The most of the researchers resort to adding their own ad hoc mobility models to the traditional wired models. These ad hoc mobility models seldom reflect actual movement patterns. There are a few models for delineating the mobility of Mobile Users. The common approaches for modeling

human movements are described below. Among these are fluid flow model, diffusion model, gravity model, and markovian chain mobility model. In campus the movement of person is affected by its behavior and each person's mobility differs which can be problematic for mobility modeling. There are still some common facts that could be used to represent person movement pattern for campus. In this paper, we discuss various characteristics of individual mobility: i.e. Pause time; and Return time; Velocity and increase of velocity; Direction angle change; Displacement; The combination of these characteristics can be helpful in predicting the person movement pattern.

In this paper, the next section describes the Classification of the existing mobility models, followed by proposed new mobility model for campus scenario. [Section 4](#) discusses simulation results and finally paper is concluded in [Sect. 5](#).

2 Existing Mobility Models

The Mobility Models can be categorized on the following criteria: measurement, scale of mobility, randomness, geological constraints, destination oriented and by varying parameters [10]. Usually, there are two types of mobility models (I) Trace based mobility models and (II) Synthetic mobility models. Trace models provide mobility patterns based on deterministic approach while synthetic models present movements of mobile nodes in a practical manner. Many mobility models have been proposed in the literature [10–16]. In this section we will review several common mobility models used in the literature. In paper different stochastic mobility models are discussed. In [Fig. 1](#) the Categorization of mobility model has been shown.

In Random walk mobility model each node moves from its existing location to a new location by randomly choosing an arbitrary direction and speed from a specified range. Such a move is performed for either a constant time or a constant distance traveled. Then a new speed and direction are selected. At the limitations, nodes jump off like billiard balls on a pool table. The random walk mobility model is described as a memory less mobility pattern, because it retains no information about its past locations and speed values. In Random waypoint mobility model, this model is equal to the random walk model except that the modification in speed and direction is done after predefined pause time. This model is extensively used for evaluating ad hoc network routing protocols [7, 10, 17, 18]. Random direction mobility model deals with mobility of node where speed and direction are constant and new direction and velocity is chosen after pause time. In this the nodes touches the edge of area after that the velocity on direction is rest. Then, the nodes pause and a fresh direction and velocity are chosen randomly. Then the procedure repeats [7, 17, 19, 20]. A boundless simulation area mobility model contacts the planar rectangular simulation field with a boundless torus.

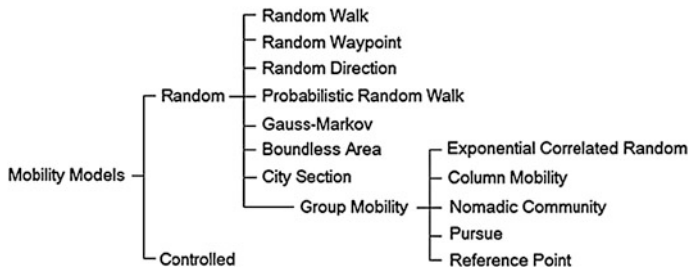


Fig. 1 Categorization of the existing mobility models

In Gauss-Markov mobility model the uses one modification restriction to contrast the degree of randomness in the mobility pattern. The random Gauss-Markov mobility model is introduced as an enhancement above the soft random mobility model. A node's next location is generated by its past location and velocity. Depending upon parameters set, this allows modeling beside a field from random walk to fluid-flow [7, 10, 16–18].

In probabilistic version of the random walk mobility model the last step made by the random walk influences the next one. Under the form that a node has motivated to the right, the probability that it continues to travel in this path is higher than the probability that movement will cease. This leads to a walk that leaves the starting point much faster than the unusual random walk model [17, 19].

In City Section Mobility Model the random waypoint movement is combined with a street map of an implicit city and paths of the mobile nodes are partial to these streets in the field. In a related model, the streets are replaced by Voronoi graphs. Also, obstacles are used, which obstruct radio signals [19, 20].

In group-mobility models [2, 21] are usually an expansion of the above models, where either a function describes the group behavior or the nodes are in some way connected with a group leader or a target.

In Exponential Correlated Random Mobility Model the motion function creates a group activity [16, 18].

In Column Mobility Model, set of mobile nodes form a line and move forward in a particular direction [3, 22, 23].

In Nomadic Community Mobility Model define a set of mobile nodes move mutually from one position to another.

In Pursue Mobility Model, for each group the group members follow a target node moving over the simulation area.

In Reference Point Group Mobility Model the movement of group is based upon the path traveled by a consistent center. Again the logical center moves according to a person mobility model [7, 10, 17, 18, 21].

2.1 Unusual Levels of Mobility

In static networks, the mobility of nodes, users, and the monitored event itself is minimal or ignored. This static model may be extended by introducing mobility in one or more of the below-mentioned three levels of the ad hoc networks:

Node level mobility: the ad hoc nodes themselves may be moving. Examples include nodes mounted on moving cars or flying unmanned airborne vehicles, collecting information as their carriers constantly change their location and/or orientation [16, 24].

Information level mobility: the event (source) monitored by or going on in the network is mobile [1, 4, 14, 25]. Mobility Management in MANETs [2] maintained truck is moving along with the truck.

User level mobility: users (destination) accessing the information composed by the network may themselves be moving, and thus the information that is related to them may change over time [16, 17, 22, 23].

3 Proposed Mobility Model

Here we are proposing restricted mobility model for person movement in the campus model that can be helpful in modeling realistic scenario such as factory, university, etc. It could be interesting to model mobility inside the above campus. In this work we have assume that the nodes mobility pattern is homogenous in nature that means, the entire set of nodes follow any one particular type of mobility pattern. Further, it has been assumed that the speed of the nodes remains constant where as nodes may change their direction. In the next section we have discuss the constriction of Partially Deterministic Mobility Model.

3.1 Partially Deterministic Mobility Model

For constructing the partially deterministic mobility model for person movement in campus, we considered two types of column movement, depending on the maximum acceptable variation from the unusual direction. Thus, if the maximum deviation of the person was less than 15° , then the mobility pattern will follow strict column model. If, however, the maximum deviation was greater than 15° and less the 45° , then it will be termed as less strict column model. The algorithm is given below:

```

Step 1: begin
Step 2: pos old_position = get_current_position (node);
Step 3: speed old_speed = get_current_speed (node);
Step 4: direction old_direction = get_current_direction (node);
Step 5: direction new_direction = get_new_direction ();
Step 6: if the deviation is positive from the location point of ending destination
{
pos new_position_x = old_x + v * t * cos(F) ;
pos new_position_y = old_y + v * t * sin(F) ;
}
Step 7: if the deviation is negative from the location point of ending destination
{
pos new_position_x = old_x - v * t * cos(F) ;
pos new_position_y = old_y - v * t * sin(F) ;
}
Step 8: return (new location);
Step 9: stop

```

Here the mathematical component shows a node (person) at location (old_x, old_y), moving horizontally and now undergoes a deviation of F (i.e. $+15^\circ$). Consider the node (person) continues to travel at the same speed (i.e. v) with which it was moving, the new x and y co-ordinates (i.e. new_x, new_y) are given by $\text{new_x} = \text{old_x} + v * t * \cos(F)$ and $\text{new_y} = \text{old_y} + v * t * \sin(F)$. A probable column model is shown in Fig. 2.

3.2 Constructing Random Mobility Model

For constructing random mobility pattern, there is no predetermined path of the nodes [16, 22]. Here the nodes after each pause choose a random direction, in an accurately random scenario the speed of the nodes would be a random variable, but for our simulations the speed is constant through the duration of simulation. The pseudo code for constructing this type of mobility pattern is similar to the pseudo code for semi-deterministic model shown in Fig. 3, excepting that the, `get_new_direction()` purpose here returns a random value ranging from 0° to 360° .

3.2.1 Constructing Deterministic Mobility Model

For constructing deterministic mobility patterns, the nodes are imparted a exacting velocity through which they travel but they move only in vertical or horizontal tips. When a node hits the border of the outline, it retraces its lane with the same speed. To execute this mobility model, we fed the scenario producer component of NS2.35 with location coordinates as well as the turns which the node would take; resembling an urban traffic model, where the paths and speeds are predefined i.e. the speed of the person is 0–3 km/h.

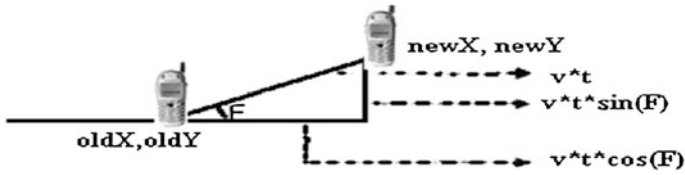


Fig. 2 Coordinates computation model

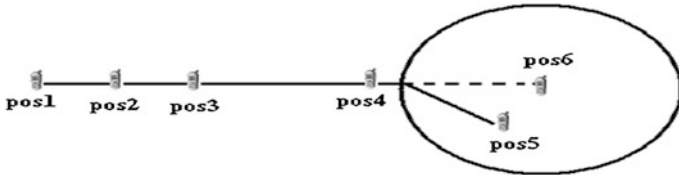


Fig. 3 Location prediction

3.3 *Constructing and Identifying the Position Aware Algorithm for Underlying Mobility Pattern Aware*

To produce the mobility patterns, which the nodes in the mobile Ad Hoc network will follow, the position aware algorithm will be adapted according to node movement. Now assume, the nodes in an Ad Hoc network are imparted a particular type of mobility pattern. The algorithm would have no information of the basic mobility pattern being followed by the nodes. Thus, in order to make the algorithm for mobility pattern aware, it should first be prepared to be able to recognize the mobility models (urban traffic, column or random) of the nodes. Secondly, it will adapt according to the mobility pattern recognized in order to effectively predict the position of the mobile nodes.

In order to categorize mobility, we used F , which is the variation of the new direction of movement of the person from the old direction, as the major constraint to classify mobility. Now when the algorithm has to recognize the mobility pattern being followed by the nodes, it also uses the variation F , as its basis for categorization. To establish this variation F , the record of past position co-ordinates of nodes stored in the past tables is used. The algorithm is given as follows:

Step 1: begin

Step 2: initialization var old_direction, new_direction, deviation,
average_deviation average_deviation = 0;

Step 3: for (each entry in the history table for the node)

```
{
old_direction = diff (node.history_table[i], node.history_table[i+1]);
new_direction = diff (node.history_table[i+1],
node.history_table[i+2]);
deviation = diff (old_direction, new_direction);
average_deviation = average_deviation + deviation;
}
```

Step 4: average_deviation=average_deviation/total_number_of_iterations_in_for_loop;

Step 5: pattern=get_type_of_pattern_based_on_max_deviation (max_deviation);

Step 6: return (pattern);

Step 7: Stop

The logic used for computing the deviation angle is the difference in slopes of two consecutive entries in the history table for any node. For example consider the sample history table entries for node2 stored at node1, (x2,1, y2,1), (x2,2, y2,2), (x2,3, y2,3) and (x2,4, y2,4). Then the slope of the line from (x2,1, y2,1) and (x2,2, y2,2) is given by $(x2,1 - x2,2)/(y2,1 - y2,2)$ and similarly for the line between points (x2,2, y2,2) and (x2,3, y2,3) is given by $(x2,2 - x2,3)/(y2,2 - y2,3)$. And the difference in their slopes will give us the deviation between the two lines. Thus, as can be seen from the algorithm, it is the average deviation, which helps in deciding the mobility pattern and in recognizing the mobility patterns proposed in our study.

3.3.1 Number of Rows in History Table

Till now we have understood that the history table has at least four entries for each node. Clearly, keeping more history will be beneficial and will lead to a more correct classification of the basic mobility pattern. But in our study, however, as the maximum number of possible mobility patterns under concern is only three, it suffices to have four history table entries. Because by keeping four position coordinates, we can calculate two variation angles and from those two deviations we can find the common deviation acceptable, which is enough to classify the mobility being followed into deterministic, semi-deterministic or random.

3.3.2 Adapting to Mobility Patterns

To find a route to the destination node our algorithm will try to get intermediary nodes which will be in the direction of the destination node. The location coordinates from the last location renew from the destination node was used to set up the general direction of the destination. But as the nodes in an Ad Hoc network are

commonly in motion, the last location update received about the destination node, might not be destination node's current location. We accept that this method of location prediction is not error free, but if we are able to predict the future location of the nodes with an error which is less than half of the nodes' transmission range, it suffices our requirements.

The algorithm of location forecast is as follows:

The algorithm of location forecast is as follows:

Step 1: begin

Step 2: This procedure predicts a possible future location for a node if only the pattern type is not random, in which case there is no rational reason to predict future location.

```
if (pattern_type == random)
    return (NULL);
```

Step 3: if (pattern_type == column) predict (old_pos, new_pos, speed, old_deviation);

Step 4: if (pattern_type == pursue)

```
...
```

```
...
```

```
return (predicted_pos);
```

Step 5: Stop

4 Simulation and Performance Metrics

The network simulations have been carried out using Network Simulator ns2.35 and its related tools for animation and study of results. We chose a Linux platform i.e. UBUNTU 12.04 LTS, as Linux offers a number of programming development tools that can be used with the simulation method. We have generated mobility scenarios for Proposed Mobility Model and random way point model using the ns2.35, so that they can be incorporated into TCL scripts. Random traffic associates of CBR can be setup between mobile nodes using a traffic-scenario generator script [21].

For this study, we have used the Proposed mobility Models and random way-point mobility model for the node having pause time of 30 s and speed varying between 0 and 100 m/s with minimum speed of 5 m/s and maximum speed of 20 m/s for simulation time of 300 s.

4.1 Simulation Constraint

The parameters used for carrying out simulation are summarized in Table 1.

Table 1 Simulation parameters

Parameter	Value
Channel type	Channel/Wireless channel
Simulator protocols	NS 2 (Version 2.35) DSR
Simulation duration	300 s
Number of nodes	25, 50, 75, 100
Transmission range	250 m
Movement model	Proposed mobility models and random way point mobility model
MAC layer protocol	802.11
Pause time (s)	0.20, 40, 60
Maximum speed	20
Minimum speed	0.5
Packet rate	4 packet/s
Traffic type	CBR
Data payload	512 bytes/packet
Max of CBR connections	8, 25, 40
Environment size	500 m * 500 m

4.2 Performance Parameters

The performance of routing protocol DSR is using the following important Quality of Services (QoS) metrics:

4.2.1 Packet Delivery Ratio (PDR)

It describes the loss rate that will be seen by the transport protocols, which run on top of the network layer. It is the ratio of data packets delivered to the destination to those generated from the sources. It is calculated by dividing the number of packets received by destination through the number packet originated from the source.

PDF = $(Pr/Ps) * 100$, where Pr is total Packet received and Ps is the total Packet sent.

4.2.2 Throughput

It is the average number of messages successfully delivered per unit time number of bits delivered per second [19, 20].

$$\text{Throughput} = \frac{\text{Total Received Packets}}{\text{Total Simulation Time}} \quad (\text{kbits/sec})$$

where N is the number of data sources.

4.2.3 Average End-to-End Delay

It is defined as the time taken for a data packet to be transmitted across an MANET from source to destination.

$D = (T_r - T_s)$, where T_r is receive Time and T_s is sent Time.

4.3 Results

The simulations are focused on analyzing the performance of routing overhead, throughput and packet delivery ratio. The results also compared with proposed and random way point mobility. The result will show the performance for every mobility model that had been selected.

4.3.1 Throughput

Random Waypoint Model and Proposed model both have more or less same throughput. The high throughput is contributed the lower delay because of the lower number of hop (Fig. 4).

4.3.2 Packet Delivery Ratio (PDR)

Proposed mobility models (Restricted) performed better in delivering packet data to destination by considering the pause time every time changing their directions. The proposed mobility models are improved significant with the increasing of the number of nodes because the number of load is small and the traffic is not heavy (Fig. 5).

4.3.3 Average End to End Delays

It shows that the proposed mobility model is generated the highest routing overhead compared with the Random way point mobility model due to the movement of the each Mobile Node are being enforced to the border of the simulation area before changing track. Proposed Model performs lowest routing overhead and it's good for the routing communication (Fig. 6).

Fig. 4 Throughput versus number of nodes

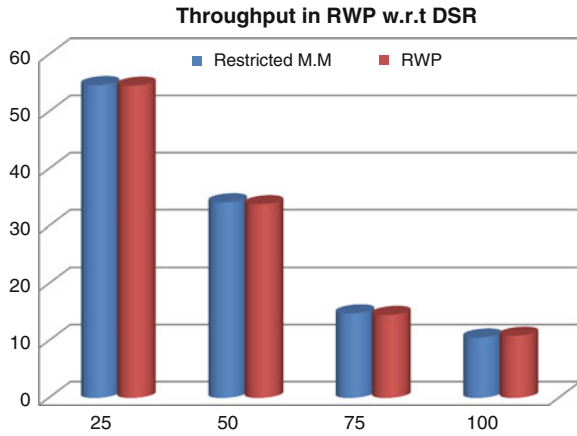


Fig. 5 PDF versus number of nodes

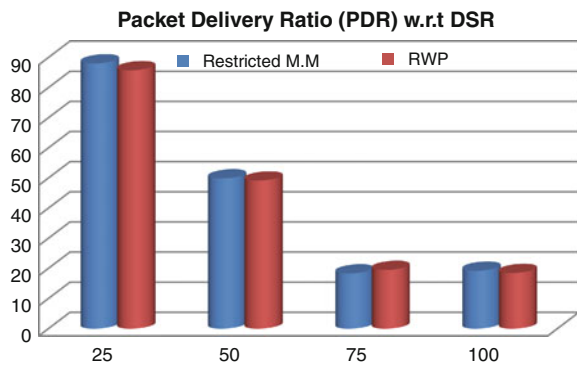
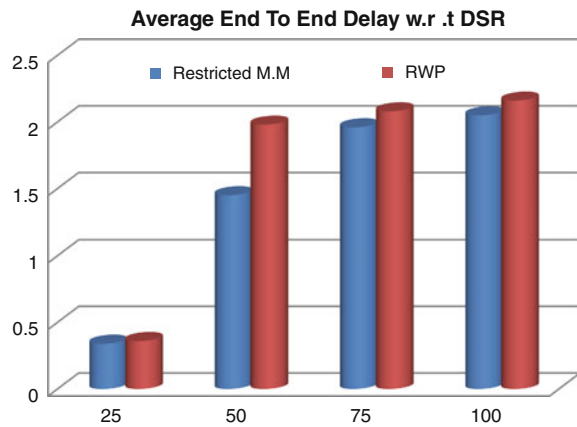


Fig. 6 Routing overhead versus number of nodes



5 Conclusion

In this paper we have proposed a statistical Mobility Model for Ad-hoc Network. For most scenarios, including campus, office buildings etc, and a random movement of nodes on straight lines is much over simplified. Here, we allow nodes to assume more than one role and provide an intuitive way to reconcile their potentially conflicting schedules and path state. This naturally lends itself to a greater diversity of mobility patterns while also being more in line with the way we think, which again facilitates the design of the anticipated scenario in the first place. In the proposed model we have calculated the various Performance Parameters with respect to propose and Random Way point Mobility models using DSR routing protocol. In this paper we have given new mobility models which closely capture the movement of common campus person. The propose model has shown better results in terms of Throughput, PDR and end to end delay where DSR has been taken as a routing protocol. The improvement in performance is achieved by better prediction of nodes movement. Thus we can say that our proposed model can be used for the campus scenario.

References

1. Rhee, I., Shin, M., Hong, S., Lee, K., Chong, S.: On the levy-walk nature of human mobility. In: Proceedings of the IEEE INFOCOM (2008)
2. Zhao, M., Mason, L., Wang, W.: Empirical study on human mobility for mobile wireless networks. In: Proceedings of the IEEE Military Communications Conference (MILCOM 2008), pp. 1–7 (2008)
3. Li, F., Wu, J.: Mobility reduces uncertainty in manets. In: Proceedings of the IEEE INFOCOM (2007)
4. Jardosh, A., Belding-Royer, E.M., Almeroth, K., Suri, S.: Towards realistic mobility models for mobile ad hoc networks. In: Proceedings of the 9th Annual ACM/IEEE International Conference on Mobile Computing and Networking (MobiCom'03), San Diego, September 2003
5. Rhee, I., Shin, M., Hong, S., Lee, K., Chong, S.: On the levy-walk nature of human mobility: do humans walk like monkeys? Technical report, CSC, NCSU (2007)
6. Grossglauser, M., Vetterli, M.: Locating nodes with EASE: mobility diffusion of last encounters in Ad Hoc networks. In: Proceedings of the IEEE Infocom (2003)
7. Hsu, W., Helmy, A.: Impact: Investigation of Mobile-User Patterns Across University Campuses Using WLAN Trace Analysis. Tech. rep., USC, Los Angeles (2005)
8. Balazinska, M., Castro, P.: Characterizing mobility and network usage in a corporate wireless local-area network. Paper presented at the 1st international conference on mobile systems, applications, and services (MobiSys), San Francisco, May 2003
9. Garmin website. In <http://www.garmin.com/>
10. Bai, F., Helmy, A.: A survey of mobility modeling and analysis in wireless adhoc networks. In: Wireless Ad Hoc and Sensor Networks. Springer (2006), ISBN: 978-0-387-25483-8
11. Bettstetter, C., Resta, G., Santi, P.: The node distribution of the random waypoint mobility model for wireless ad hoc networks. IEEE Trans. Mob. Comput. 2(3), 257–269 (2003)

12. Karagiannis, T., Faloutsos, M., Molle, M.: Long-range dependence: ten years of internet traffic modeling. *IEEE Internet Comput.* **8**(5), 57–64 (2004) (special issue in “measuring the internet”)
13. Pawlikowski, K., Jeong, H.-D.J., Lee, J.-S.R.: On credibility of simulation studies of telecommunication networks. *IEEE Commun. Mag.* **40**(1), 132–139 (2002)
14. Camp, T., Boleng, J., Davies, V.: A survey of mobility models for ad hoc, network research. *Wirel. Commun. Mob. Comput.* **2**(5), 483–502 (2002). special issue on mobile ad hoc networking: research, trends, and applications
15. La, R.: Distributional convergence of inter-meeting times under generalized hybrid random walk mobility model. *IEEE Trans. Mob. Comput.* **9**(9), 1201–1211 (2010)
16. Rhee, I., Shin, M., Hong, S., Lee, K.R., Kim, S.J., Chong, S.: On the levy-walk nature of human mobility. *IEEE/ACM Trans. Network.* **19**(3), 630–643 (2011)
17. Aschenbruck, N., Gerhards-Padilla, E., Peter, M.: A survey on mobility models for performance analysis in tactical mobile networks. *J. Telecommun. Inf. Technol.* **2**, 54–61 (2008)
18. Iyer, A., Rosenberg, C., Karnik, A.: What is the right model for wireless channel interference. *IEEE Trans. Wireless Commun.* **8**(5), 2662–2671 (2009)
19. Jayakumar, G., Ganapathy, G.: Performance comparison of mobile ad-hoc network routing protocol. *Int. J. Comput. Sci. Netw. Secur.* **7**(11), 77–84 (2007)
20. Asma, T., Rajneesh, G.M., Sunil, T.: Comparative performance analysis of DSDV, AODV and DSR routing protocols in MANET using NS2. In: *International Conference on Advances in Computer Engineering* (2010)
21. Kumar, S., Sharma, S.C., Suman, B.: Mobility metrics based classification & analysis of mobility model for tactical network. *Int. J. Next Gener. Netw.* **2**(3), 39–51 (2010)
22. Liu, J., Jiang, X., Nishiyama, H., Kato, N.: On the delivery probability of two-hop relay MANETs with erasure coding. *IEEE Trans. Commun.* **61**(4), 1314–1326 (2013)
23. Andrews, J.G., Haenggi, M., Jindal, N.: A primer on spatial modeling and analysis in wireless networks. *IEEE Commun. Mag.* **48**(11), 156–163 (2010)
24. Kotz, D., Essien, K.: Analysis of a campus-wide wireless network. *Wireless Netw.* **11**, 115–133 (2005)
25. Hong, D., Rappaport, S.-S.: Traffic model and performance analysis for cellular mobile radio telephone systems with prioritized and non prioritized handoff procedures. *IEEE Trans. Veh. Technol.* **35**, 77–92 (2003)
26. Su, J., Goel, A., de Lara, E.: An empirical evaluation of the student-net delay tolerant network. In: *International Conference on Mobile and Ubiquitous Systems: Networking & Services (MobiQuitous)*, pp. 1–10 (2006)
27. Karagiannis, T., LeBoudec, J.-Y., Vojnovic, M.: Power law and exponential decay of inter contact times between mobile devices. In: *Proceedings of ACM MOBICOM*, pp. 183–194 (2007)
28. Medina, A., Gursun, G., Basu, P., Matta, I.: On the universal generation of mobility models. In: *Proceedings of the IEEE/ACM MASCOTS 2010, Miami Beach, FL* (2010)

Single Axis Position Control of a Precision Gimbal

Kamna Ashu, Sanoj Kumar and Kanika Chawla

Abstract This paper describes the single axis (azimuth) motion control of a Dual axis Gimbal scanner using a digital signal processor TMS320F28335. Here the Gimbal is being used as an electro-mechanical platform for mounting of electro-optical payloads. Its motion is being controlled by DSP and commanded and monitored by the Graphical User Interface (GUI) designed on LabVIEW. The control system implements a two loop architecture i.e. inner rate loop closed by the Gyro and Outer loop closed by the position encoder. The external disturbing noise or force to the Gimbal is being removed by stabilizing the gyro. The Gimbal Scanner consists of DC motors for driving its two axes i.e., azimuth and elevation. The incremental encoders are used as position sensors.

Keywords Gimbal · Control system · Gyro · LabVIEW · Position control · PID

1 Introduction

A Gimbal is an electro-mechanical arm to isolate the electro-optical payloads from ground disturbances. It provides a platform to mount cameras, sensors, laser source and laser receivers. The laser source and receiver optics will be used for pointing and scanning of moving targets like ships, tanks, military tanks, aerial photography

K. Ashu (✉)

Chandigarh Engineering College, Mohali, India

e-mail: kamnaashu@gmail.com

S. Kumar

LASTEC, Defence Research Development Organization, New Delhi, India

e-mail: kumar.sanoj@yahoo.co.in

K. Chawla

PDM engineering college for women, Bahadurgarh, Haryana, India

e-mail: Kanika.c.26@gmail.com

[1, 2] or Unmanned Aerial Vehicles (UAVs). The platform at which these payloads will be mounted must be a motorized and stabilized platform. Hence, the Gimbal provides this requirement. Apart from this it is widely used in imaging and tracking. The effect of gimbal point displacement on optical axis pointing precision in an image seeker was analyzed [3]. The precision Gimbal has a set of two orthogonal pivot axes.

The project uses Pulse Width Modulation, Analog to Digital Converter, Serial Communication Interface, Serial Peripheral Interface and Quadrature Encoder Pulse modules of TMS320F28335, to control the motion of Gimbal scanner in Azimuth or Horizontal plane. The serial communication is being used between the GUI and the processor for command and feedbacks. The direction of the rotation is a function of the angle made by the averaged axis direction of the rotor and the normal to the plane [4]. The Gimbal responds to the processor by rotating to the specified angle as commanded by the GUI.

1.1 System Requirements

- System should support two way communications between the processor and the GUI.
- System should store data and provide access to Gimbal control parameters.
- System must be field-configurable.
- System should be properly grounded.

1.2 Power Requirements

- The system requires 24 V power supply for motors, ± 15 V for operational amplifiers, +5 V for ADC, Buffers, +3.3 V for DSP buffers and 1.9 V for the DSP core.
- The system takes only +24 V for its operation. The rest of other power supplies are provided by DC–DC converters and regulators.

1.3 Specifications of Gimbal

- Payload: 20 kg
- Slewing rates: 1 deg/sec (min)
60 deg/sec (max)
- Slewing acceleration: 10 deg/sec²
- Azimuth: -80 to $+80$ degree
- Elevation: 0–60 degree.

2 Operation

The Gimbal signals are limit switches and encoder outputs. They both operate at power from 0 to 5 V. However the processor can respond only to 0–3.3 V. This is overcome by the use of level shifter. The level shifter is placed at the interface of the processor and the Gimbal. It brings down the voltage level of Gimbal to the processor level. Hence now in the presence of level shifter, the gimbal operates in the range of 0–3.3 V.

The motion of the Gimbal is programmed in DSP and it is being controlled by using Proportional Integral Differential control. The position encoder provides the angular travel and the gyro provides the rate of move. It is operated in several modes i.e. scan, home, pause, stop and command depending on the command being given on the GUI. In scan mode, a fixed the duty cycle of PWM is fed into the Gimbal through power amplifier, the Gimbal moves in one counter clockwise direction. On reaching the maximum position of encoder it changes the direction by change of duty cycle by DSP and moves clockwise. The mechanical motion of the Gimbal is limited by mechanical stopper and limit switches. The maximum position of encoder counts is set few counts ahead of the limit switch to avoid a mechanical hit. The limit switch in azimuth and elevation are provided for initializing the encoder and to cut off the motor power if the Gimbal arm over travels. The limit switch operates in normally open mode. In open mode it gives 5 V output and in close contact it gives 0 V output. The degree of rotation of Gimbal in azimuth varies by +80 degree to –80 degree. The motion of Gimbal is being controlled by the commands on the GUI designed on Lab VIEW (Fig. 1).

2.1 Position Control

The position of the Gimbal is monitored by the encoder. The angular travel of the Gimbal is controlled by the position encoder. It closes the outer loop of the control system. The encoder also gets the direction and speed information of the Gimbal.

An incremental encoder is used to sense the position of the Gimbal. The counter in the DSP is set up in the up count mode for counting encoder counts. The encoder is initialized at the centre position. The counter starts counting from zero and keeps incrementing. When it reaches the period value of the timer period register, it resets to zero and the counting operation starts again from zero.

The range of the azimuth is set linear to the range of the pulse width modulator. The current-mode linearization was successfully handled via compensation filters and internal model controllers [5]. The range of the pulse width modulator is from 0 to 7500 and the range of the azimuth is from –80 to +80 degree. This is done so that the pace of the Gimbal is linear for both below its centre position and above its centre position.

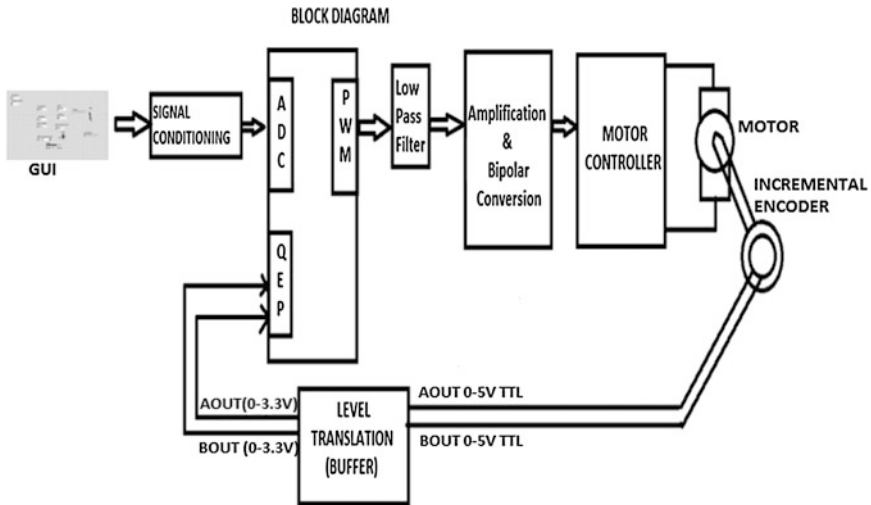


Fig. 1 Block Diagram. Commands are given by GUI. It is then conditioned, amplified and converted to bipolar form to be fed to the motor. The encoder's value is level translated and is given as feedback to the Quadrature Encoder Pulse (QEP)

2.2 Integration of GUI

The GUI is created on LabVIEW. The GUI communicates with the processor via serial communication in full duplex mode. The GUI acts as a mode to change the position of Gimbal by changing the degrees of the Gimbal on GUI in the range of -80 degrees to $+80$ degrees in command mode. The Gimbal is being commanded and monitored via GUI. It works on the principle of VISA communication.

When the write switch is on, the GUI sends the commanded value to the processor by means of serial communication. The processor then feeds the received value to the motor of the Gimbal. The Gimbal in turns responds by moving to the degree value commanded from the GUI.

In addition, when the read switch is turned on, the Gimbal sends its feedback value to the GUI. The received value is indicated by the position of the slider on the GUI. The Gimbal hence works in a closed loop.

$$SCI \text{ Asynchronous Baud} = \frac{LSPCLK}{(BRR + 1)8} \quad (1)$$

$$\begin{aligned} BRR &= \frac{LSPCLK}{SCI \text{ Asynchronous Baud} * 8} - 1 \\ &= \frac{37500000}{9600 * 8} - 1 \\ &= 0x01E7 \end{aligned} \quad (2)$$

The upper two bits of the BRR are set at the high baud value i.e., 0x0001, and the lower two bits of the BRR are set at the lower baud value i.e., 0x00E7. The serial communication is done in first in first out mode (FIFO mode). An interrupt level is fixed to a certain set value. When the status level of the SCI matches to the interrupt level, an interrupt is generated and the data is transferred. Hence serial communication is done.

$$\begin{aligned} \text{SPI Baud Rate} &= \frac{LSPCLK}{(SPIBRR + 1)} \\ &= 0x0063 \end{aligned} \quad (3)$$

The SPI Baud Rate determines the rate at which bit is being transferred to the peripherals. In the master mode there are 125 data transfer rates. In one SPICLK cycle one data bit is shifted. SPI communicates between the processor and the ADC. It is set in the master mode.

2.3 Modes

The modes of the Gimbal can be controlled by scan, command and pause options on the GUI. The scan, command and pause options can be set high and low accordingly to switch to different modes of the Gimbal as per need. The GUI is designed on the LabVIEW to operate the Gimbal in five modes.

HOME MODE: (SCAN = 0, COMMAND = 0 PAUSE = 0)

This is the initial mode of the Gimbal. When the switch to Gimbal is turned on, the Gimbal starts its motion. It takes one complete rotation and sets itself to centre position and rests at this position until other mode is set. At the centre, the duty cycle of the Gimbal is fifty percent.

SCAN MODE: (SCAN = 1, COMMAND = 0, PAUSE = 0)

In this mode the Gimbal is set into free mode. It continuously scans. At the minimum position its duty cycle is hundred percent. As soon as it strikes the maximum position, the direction is reversed. At minimum position the duty cycle is zero percent. When it reaches the minimum position, it again reverses the direction. This operation continues until it is paused or stopped by the operator by setting the pause high.

PAUSE MODE: (SCAN = 1, COMMAND = 0, PAUSE = 1)

The Gimbal in scan mode can be paused by initializing PAUSE. When it is set high, the Gimbal stops at the position its pause command was given. In this mode SCAN command and PAUSE command are set high.

COMMAND MODE: (SCAN = 0, COMMAND = 1, PAUSE = 0)

In command mode, the Gimbal is manually operated. The motion of the Gimbal here is controlled by the operator. The operator varies the angle of the Gimbal on the GUI and the Gimbal turns by the same. The Gimbal can be steered to any direction in the range of -80 degree to 80 degree by varying the slider to different positions.

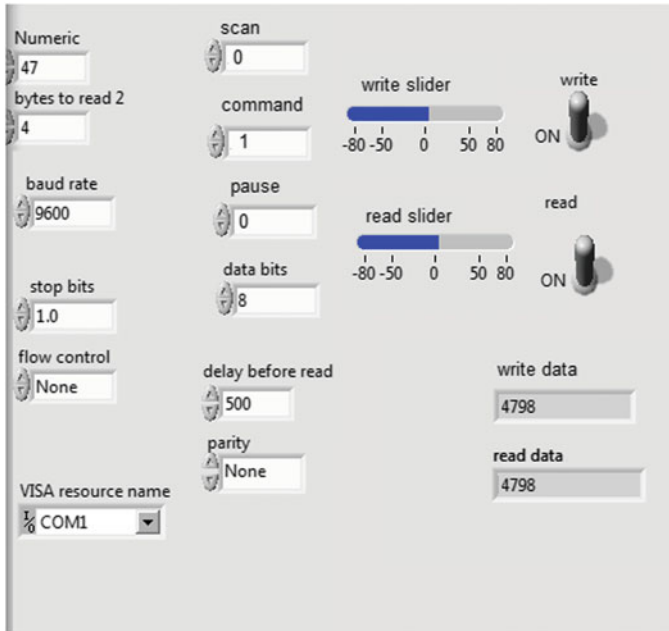


Fig. 2 Graphical user Interface at centre position in command mode. At the centre position the slider is at 0 degree. The centre position of the gimbal is set as 4798 which is retrieved in write data of GUI after feedback response from the gimbal

- At zero degree, the Gimbal is at its centre position.
- At -80 degree, the Gimbal is at its minimum position.
- At $+80$ degree, the Gimbal is at its maximum position.

STOP MODE: (SCAN = 1/0, COMMAND = 0, PAUSE = 0)

In the STOP mode the Gimbal is initially in SCAN mode. When the SCAN is raised low from high along with COMMAND and PAUSE both being low, STOP mode is initialized. Hence the position where this mode is initialized, the Gimbal moves in that direction which is closest to the extreme value and stops there. If it is set in stop mode before the centre position, it will move back to zero position and stop there. If the stop mode is set after the centre position, the Gimbal will move to the maximum position and stop at the maximum position (Fig. 2).

2.4 Noise Reduction

The Gimbal is stabilized by the gyro rate outputs. The gyro senses the external disturbances and the closed control loop are inserted to make the output stable. The Gimbal can also be stabilized by LQG/LTR controller [6]. Noise reduction is

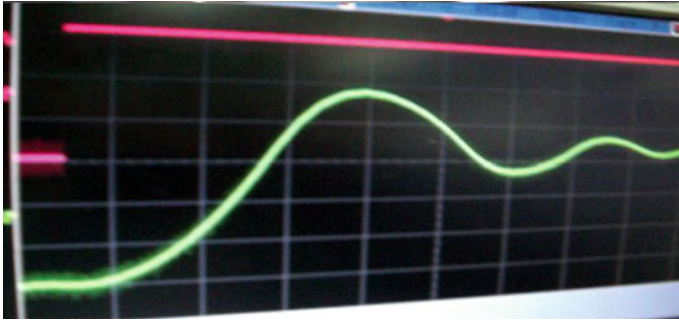


Fig. 3 Gimbals’ response without compensation. This response of gimbal is unstable and has many oscillations. The system thus is not very responsive and is not stable

done by adding the filter and increasing the gain of the control system. At low gains the system becomes slow and sluggish. Whereas when the system is proportionally integrally and derivative controlled, the system becomes more responsive and errors are detected easily. A Finite Impulse response filter having a cut off frequency, f , 100 Hz is inserted to eliminate the gyro noise.

$$\begin{aligned} \frac{Y}{X} &= \frac{2\pi f}{s + 2\pi f} \\ &= \frac{2 * 3.142 * 100}{s + 2 * 3.142 * 100} \\ &= \frac{628.4}{s + 628.4} \end{aligned} \tag{4}$$

Where,

$Y = output,$

$X = input.$

The Laplace transfer function, [7], of the plant and compensator are implemented into DSP by replacing s in terms of z and expressing in terms of past and present input and output (Fig. 3).

$$S = \frac{2(1 - z^{-1})}{T(1 + z^{-1})} \tag{5}$$

$$Y0 = (0.01545 * X0) + (0.01545 * X1) + (0.96908 * Y1) \tag{6}$$

Where,

$Y0 = current output,$

$Y1 = past output,$

$X0 = present input,$

$X1 = past input.$

The sampling frequency of the control loop is at 100 Hz. The system is compensated by implementing Proportional, Integral and Differential (PID) control.

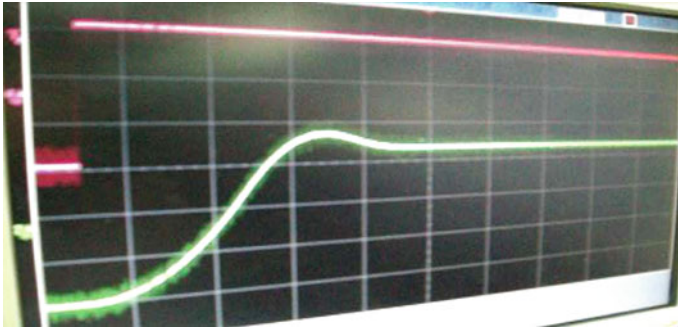


Fig. 4 Gimbals' Response with PID control. When the system is PID controlled, it shows a stable response. The oscillations are removed and errors are reduced. Proportionally, integrally and derivative control increases the system performance making it robust

The proportional action enables easy detection of error. The proportional factor depends on the present error. The derivative factor depends on the past error. Integral factor depends on the analysis of future errors of the closed control loop. The derivative action controls the rate of error with time. It also allows reaching the point in a well tuned manner. Integral action moves the proportional band relative to the set point increasingly until the error is reduced to zero and the set point is achieved. Hence PID is used to improve the performance of the control system by removing oscillations and sluggishness (Fig. 4).

3 Conclusion

The Gimbal is operated in different modes according to the requirement. It is stabilized by using compensators and PID control thereby reducing the external noises and disturbances present in the control loop. The error in the Gimbal is reduced by making it more responsive, removing the oscillations present and increasing the stability of the system. The stabilized Gimbal can now be effectively used for the purpose of scanning and tracking in various modes.

References

1. Kawada K., Shiino T., Yamamoto T., Komichi M.: Data-driven PD gimbal control. In: International Conference on Computational Intelligence for Modelling Control and Automation, December 2008, pp 993–998. (2008)
2. Osborne J., Hicks G., Fuentes R.: Global analysis of the double-gimbal mechanism. IEEE Control Syst. **28**(4) 44–64 (2008)

3. Zhang, X., Jiang, Z., Wei, Q., Jia, H.: Effect of gimbal point displacement on optical axis pointing precision in an image seeker. In: International Conference on Electric Information and Control Engineering (ICEICE), Wuhan April 2011, pp. 3233–3236. (2011)
4. Ishlinsky, AYu.: On Mechanics of Gyroscopes in Gimbal Suspension: International Union of Theoretical and Applied Mechanics, pp. 87–96. Springer, Berlin (1978)
5. Fang, J., Ren, Y.: High-precision control for a single-gimbal magnetically suspended control moment gyro based on inverse system method. *IEEE Trans. Industr. Electron.* **58**(9) 4331–4342 (2010)
6. Seong, K.-J., Kang, H.-G., Yeo, B.-Y., Lee, H.-P.: The stabilization loop design for a two-axis gimbal system using LQG/LTR controller. In: International Joint Conference SICE-ICASE, 2006, pp. 755–759. (2006)
7. Nise, N.: *Control Systems Engineering*, Addison-Wesley, Boston (1994)

An Investigation of Fuzzy PSO and Fuzzy SVD Based RBF Neural Network for Multi-label Classification

Jitendra Agrawal, Shikha Agrawal, Shilpy Kaur and Sanjeev Sharma

Abstract Multi-label classification deals with problems where each instance is associated with multiple labels at the same time. Various techniques exist to solve the multi-label classification problem. One such technique is ML-RBF (Multi-Label Radial Basis Function), which has proved to be quite efficient. However, to further enhance the performance of the ML-RBF for multi-label classification problem, we have proposed two new algorithms. The first proposed algorithm is named as fuzzy PSO based ML-RBF, which is the hybridization of fuzzy PSO and ML-RBF. The second proposed algorithm is named as FSVD-MLRBF that hybridizes fuzzy c-means clustering along with SVD (Singular Value Decomposition). Both the proposed algorithms are applied to real world datasets i.e. yeast and scene dataset. The experimental results show that both the proposed algorithms meets or beats ML-RBF when applied on the test datasets.

Keywords Fuzzy particle swarm optimization · Singular value decomposition · Multi-label classification · Multi-label radial basis function

J. Agrawal (✉) · S. Kaur · S. Sharma
School of Information Technology, RGPV, Bhopal, Madhya Pradesh, India
e-mail: jitendra@rgtu.net

S. Kaur
e-mail: shilpykaur191@gmail.com

S. Sharma
e-mail: sanjeev@rgtu.net

S. Agrawal
University Institute of Technology, RGPV, Bhopal, Madhya Pradesh, India
e-mail: shikha@rgtu.net

1 Introduction

Multi-label classification problems are present everywhere in the real world. An example can be a text document consisting information about the attacks of 26/11 can be categorized as news, movie and terrorist attack. Similarly in medical diagnosis, a patient may be suffering from cancer, diabetes and kidney failure at the same time. In semantic scene classification, a snap can simultaneously belong to more than one class, such as beach, forest, city and people. Similarly a protein can perform many functions simultaneously. For example, enzymatic proteins increase metabolism for digestion in the stomach, functioning of pancreas, blood-clotting and convert glycogen into glucose. In all these examples set of labels are associated with each instance, so the task of multi-label classifier is to output the label set for unseen instances. Thus in multi-label classification each example is associated with a subset of labels Y_i in the given label set L i.e. $Y_i \subseteq L$. The following paragraph contains the literature survey of the work done in so far in multi-label classification using neural networks and particle swarm optimization.

Multi-label k-nearest neighbor (ML-kNN) is introduced by Zhang and Zhou [1] which uses the basic concept of k-nearest neighbor. For each test tuple it first identifies its k-nearest neighbors and according to the classes assigned to these neighbors, test tuple is classified using maximum a posteriori (MAP). Spyromitros et al. [2] proposed kNN in conjunction with Binary Relevance (BR) problem transformation method known as BR-kNN. When BR is paired with kNN same process of calculating kNN is performed L (total number of labels) times. In order to overcome in the proposed BR-kNN independent predictions are made for each label followed by single k-nearest neighbor search. The author identifies two extensions of BR-kNN to improve the performance. The first extension known as BR-kNN-a, handles the empty set that may be produced as an output of BR. In such case, BR-kNN-a outputs the label with highest confidence. The second extension BR-kNN-b works in two steps: in the first step it calculates the average size of label set of k-nearest neighbor and in second step the label with highest confidence is produced. Coelho et al. [3] proposed Multi-Label k-Nearest Michigan Particle Swarm Optimization (ML-KMPSO) which hybridizes MPSO (Michigan Particle Swarm Optimization) and ML-kNN (Multi-Label k-Nearest Neighbor). At first MPSO breaks the MLC into sub classification problems without considering the label correlation. And then ML-kNN is used to establish the correlation among classes.

Zhang and Zhou [4] proposed first neural network based algorithm for multi-label classification and named it as back propagation for multi-label learning (BP-MLL). In this work a single hidden layer feed-forward BP-MLL neural network is used with sigmoidal neurons and bias parameters in the hidden and input layers. The number of output layer neuron is equal to the number of labels. Training is based on the traditional BP (Back Propagation) algorithm. But to deal with the correlation between labels a global error function is proposed in this paper. Grodzicki et al. [5] proposed some modifications in the error function of BP-MLL

proposed in [4], by incorporating a threshold value into the error function used in BP-MLL. Radial Basis Neural Network for Multi-Label (ML-RBF) learning is proposed by Zhang [6]. The training procedure of ML-RBF is a two stage process. In first step k-means clustering is performed on set of instances of each possible class. The parameters of the basis functions are then determined using these centroids. In the second stage, weights are adjusted to minimize the sum-of-square error function. Apart from RBF, ART (Adaptive Resonance Theory) is also applied for multi-label classification. Sapozhnikova [7] presents the extension of fuzzy ARTMAP for multi-label classification called multi-label-FAM. In the proposed methodology a best category set with high activation values are produced based on the fact that if the relative difference of activations of a category lies below a predefined threshold then it is included in the set. After normalizing these activation values the resultant prediction is obtained by calculating weighted sum of individual predictions. Post processing filter is used to produce the labels, having scored more than predefined fraction of the highest score. De Souza et al. [8] Proposed an effective machine learning technique which provides fast training and testing along with simple implementation for automatic multi-label text categorization systems known as VG-RAM WNN (virtual generalizing random access memory weightless neural networks). RAM based neural networks use RAM to store knowledge instead of connections. The networks input values are used as the RAM address the value stored at this address is the neuron's output. Implementation simplicity and high computational speed during the training phase of Probabilistic Neural Network (PNN) motivates Ciarelli et al. [9] to propose a modified version of PNN to solve the multi-label classification problem. The proposed version of PNN is composed of three layers but like original PNN requires only one training step. Chen et al. [10] Proposed an algorithm that consists of two stages of a multilayer perceptron (MLP), named Multi-Instance Multi-Label Neural Network (MIMLNN). The first-stage of MLP is used to establish the relationship between scene regions and labels whereas the second stage of MLP captures the label correlation needed for multi-label classification. The training of MIMLNN is done by Rprop, which is a refined form of back-propagation algorithm.

Although many approaches have been proposed by different researchers to solve multi-label classification problem but population based meta heuristics approaches are yet to be explored. So, this paper introduces two new algorithms for multi-label classification: the first algorithm fuzzy PSO based ML-RBF hybridizes RBF neural network and fuzzy PSO algorithm which is used to optimize the RBF networks connection weights. Briefly, we perform fuzzy c-means on the instances of each possible class. The centroids so obtained are used to determine the first layer basis functions. At the next step, second layer weights of RBF neural network are optimized by minimizing sum-of square error function using fuzzy PSO. Whereas in the second algorithm, RBF is trained using traditional training method SVD (Singular Value Decomposition) and so it is named as FSVD-MLRBF.

The structure of this paper is organized as: [Sect. 2](#) describes the proposed methodology of the two proposed algorithms. [Section 3](#) reports experiments and compares obtained results with the result of the known classifier reported earlier in literature. Finally, [Sect. 4](#) concludes the paper.

2 Proposed Methodology

The proposed algorithms (Fig. 1) are based on ML-RBF (Multi-Label Radial Basis Function) neural network. The training of ML-RBF [6] can be done in two stages: At the first stage we determine the centers and RBF (Radial Basis Function) by applying fuzzy c-means clustering and Gaussian activation function respectively. This leads to the formation of nodes in the hidden layer. In the second stage we determine the weights between hidden layer and output layer. In our proposed methods we have trained the neural network using two different approaches: In the fuzzy PSO based ML-RBF we use fuzzy PSO (fuzzy Particle Swarm Optimization) to obtain optimized weights whereas in FSVD-MLRBF the weights are determined using traditional SVD (Singular Value Decomposition).

2.1 Phase 1: Determination of Hidden Layer

Let D be a multi-label dataset and $L = 1, 2, \dots, L$ be the label set, such that $D = \{(x_i, Y_i) | 1 \leq i \leq m\}$, where x_i is a single instance and $Y_i \in L$ is the set of labels to which x_i belongs.

In this paper, we perform fuzzy c-means clustering on the set of instances with label $l \in L$. We thus have k_l clustered groups and j centroids for each $l \in L$. The number of clusters in each case is determined using following formula used in [6] i.e.

$$k_l = \alpha \times |U_l| \quad (1)$$

where, α is a fraction of the number of instances U_l . k_l and c_j are together form the basis function. We are using Gaussian activation function as the basis function which is given by:

$$\Phi_j(x_i) = \exp\left(-\frac{\text{dist}(x_i, c_j)^2}{2\sigma^2}\right). \quad (2)$$

Here $\text{dist}(x_i, c_j)$ is the Euclidean distance between x_i and the j th centroid c_j . σ is the smoothing parameter and for all the centroids its value remains same and is calculated using:

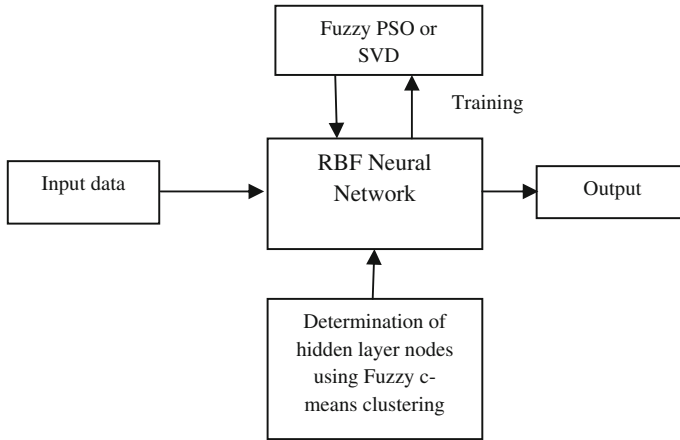


Fig. 1 Proposed Architecture of Fuzzy PSO based ML-RBF and FSVD-MLRBF for multi-label classification

$$\sigma = \mu \times \left(\frac{\sum_{p=1}^{K-1} \sum_{q=p+1}^K dist(c_p, c_q)}{K(K-1)/2} \right) \tag{3}$$

where, μ is the scaling factor. Thus for each label k_l basis functions are obtained hence the total number of basis function retained in the hidden layer will be given as $K = \sum_{l=1}^L k_l$. All the basis functions so obtained are then put together and re-indexed.

2.2 Phase 2: Determination of Weights Between Hidden Layer and Output Layer

Different methods can be applied to train a neural network. The two methods that are used in our proposed work are described in the next paragraph.

A. Weight Adjustment using fuzzy PSO algorithm

In fuzzy PSO [11] instead of only one best particle in the neighborhood, multiple particles in the neighborhood are allowed to influence other particles. Each group member is assigned with the multiplier known as charisma which is a fuzzy variable. The influence of each best particle to others is calculated using this charisma variable and summation is then applied to the original formulation. Thus each particle will update its position and velocity using following two formulas:

$$x_{id} = x_{id} + V_{id} \tag{4}$$

$$V_{id} = wV_{id} + c_1 * rand() * (p_{id} - x_{id}) + \sum_{h=1}^k c_2 * rand() * \Psi(p_{hd})(p_{hd} - x_{id}) \quad (5)$$

where, w is the inertia weight, c_1 and c_2 are the acceleration coefficients and $rand()$ is independent random number, $\Psi(p_{hd})$ is charisma function and is defined as follows:

$$\Psi(p_h) = \frac{1}{1 + \left(l \frac{f(p_h) - f(p_g)}{f(p_g)} \right)^2} \quad (6)$$

$f(.)$ is the fitness function, l is a user specified parameter. The key of the fuzzy PSO algorithm is to choose the fitness function. This paper uses sum-of-square error as the fitness function.

$$E = \frac{1}{2} \sum_{i=1}^m \sum_{l=1}^L (y_l(x_i) - t_l^i)^2 \quad (7)$$

In this formula t_l^i is the desired output of x_i on the l th class. $y_l(x_i)$ is the actual output of x_i on the l th class and is given by $y_l(x_i) = \sum_{j=1}^{L+1} w_{jl} \Phi_j(x_i)$.

The objective is to find such a particle that minimizes the output of the fitness function. At first step, initialize the position and velocity of each particle. Set the values of k and l . At second step, calculate the fitness of each particle using fitness function according to formula (7). In each iteration of neural network training, the particle with smallest fitness function value is considered as g_{best} , which is best position of all the particles till now. Each particle will update its position and velocity using Eqs. (4) and (5) respectively. This process terminates when the minimum fitness function value is achieved or maximum number of iterations is met.

B. Weight Adjustment using SVD

Due to the quadratic nature of the error function, it can be solved using set of linear equations. In order to find the solution, differentiating Eq. (7) with respect to w_{jl} and setting the derivative to zero gives the normal equations for the least sum-of-square problem:

$$(\Phi^T \Phi) W = \Phi^T T. \quad (8)$$

Here, Φ has dimensions $m \times (K + 1)$ with elements $\Phi_j(x_i)$, W has dimensions $(K + 1) \times L$ with elements w_{jl} and T has dimensions $m \times L$ with elements t_l^i . The weights are calculated using Eq. (8) using linear matrix inversion techniques of SVD [12].

Correlation between the classes in RBF is achieved as all the nodes in the hidden layer are connected to all the nodes in the output layer. Thus information present in the hidden layer nodes is completely used to determine the optimized weights as well as for predicting instances for class 1.

3 Experiments

3.1 Dataset

The performance of the two proposed approaches is evaluated on the yeast dataset and scene dataset. Yeast dataset describes the genes of Yeast *Saccharomyces cerevisiae*. 103 features are derived for each gene from the micro-array expression data and phylogenetic profile. For simplicity 14 classes in the top hierarchy are used with average value of 4.24 labels per gene. The dataset contains 2, 417 instances. The scene dataset is composed of 2,407 instances each of which is represented by 294 feature vector. This dataset contains the scenes data. There are 6 classes used in this dataset.

3.2 Evaluation Measures

The performance of multi-label classifier is measured using four evaluation measures [6, 13] which are: Hamming Loss, One Error, Coverage and Ranking Loss. Hamming loss is defined as the number of times an instance is classified incorrectly and is defined as

$$HL = \frac{1}{n} \sum_{i=1}^n \frac{|Z_i \Delta Y_i|}{L}. \quad (9)$$

Δ is the symmetric difference between two sets. Z_i is the set of labels predicted by the classifier and Y_i is the desired set of labels for a given test instance x_i .

One error measures the number of times top-ranked label is not in the set of labels of an instance. It is given by

$$OE = \frac{1}{n} \sum_{i=1}^n \delta([\arg \max f(x_i, l)] \notin Y_i). \quad (10)$$

Here δ is a function that produces 1 if the argument is true and 0 otherwise.

Coverage is used to determine the number of steps needed to cover all the proper labels of the instance and is given by

$$Coverage = \frac{1}{n} \sum_{i=1}^n \max rank(x_i, l) - 1. \quad (11)$$

And last is Ranking Loss that determines the number of label pairs that are reversely ordered for an instance. It is given by

$$RL = \frac{1}{n} \sum_{i=1}^n \frac{|D_i|}{|Y_i| |\bar{Y}_i|} \quad (12)$$

where \bar{Y}_i is complementary of Y_i while $D = \{(l_1, l_2) | f(x_i, l_1) \leq f(x_i, l_2), (l_1, l_2) \in Y_i \times \bar{Y}_i\}$.

All the performance measures described above have best performance when value is zero which implies that smaller the value better the performance of the classifier.

3.3 Classification Results

The experimental results are obtained by performing ten-fold cross validation on the yeast and scene data set. The other parameters that govern the performance of RBF neural network are α and μ , whose value is set to $\alpha = 0.01$ and $\mu = 1$ as in [6]. Fuzzy PSO search dimension (RBF networks weights number) is the product of number of nodes in the hidden layer and number of nodes in the output layer of the neural network. Here the number of hidden nodes is obtained as a result of clustering and the number of output nodes is equals to the number of classes in the dataset. So for yeast dataset, number of nodes in output layer are 14 and in case of scene dataset they are 6. Results are obtained in 50 runs of fuzzy PSO. The termination criterion of fuzzy PSO is either 1,000 iterations or till the value of fitness function reaches 0.001. The values of other parameters are given in the Table 1 below:

Table 1 Values of various parameters used in experiments

Parameter	Range
w	0.4
c_1	2
c_2	2
k	3
l	1.6
E	0.001
m	1.25
V_{\max}	0.5, 1, 2
Number of particles	20

Table 2 Performance of each compared algorithm (mean \pm std. deviation) on Yeast dataset

	Fuzzy PSO based ML-RBF (A_1)	FSVD-MLRBF (A_2)	ML-RBF (A_3)
Hamming loss	0.260 \pm 0.110	0.291 \pm 0.151	0.195 \pm 0.011
One error	0.181 \pm 0.076	0.306 \pm 0.382	0.233 \pm 0.037
Coverage	5.277 \pm 0.570	3.743 \pm 2.145	6.352 \pm 0.244
Ranking loss	0.298 \pm 0.170	0.224 \pm 0.157	0.169 \pm 0.017

Table 3 Performance of each compared algorithm (mean \pm std. deviation) on Scene dataset

	Fuzzy PSO based ML-RBF (A_1)	FSVD-MLRBF (A_2)	ML-RBF (A_3)
Hamming loss	0.211 \pm 0.097	0.236 \pm 0.119	0.163 \pm 0.015
One error	0.150 \pm 0.183	0.196 \pm 0.214	0.294 \pm 0.033
Coverage	0.901 \pm 0.595	0.892 \pm 0.711	0.904 \pm 0.087
Ranking loss	0.503 \pm 0.162	0.552 \pm 0.113	0.158 \pm 0.020

Table 4 Statistical analysis of each algorithm on Yeast dataset

	Hamming loss	One error	Coverage	Ranking loss
Fuzzy PSO based ML-RBF—FSVD-MLRBF	$A_1 \approx A_2$	$A_1 > A_2$	$A_1 < A_2$	$A_1 \approx A_2$
Fuzzy PSO based ML-RBF—ML-RBF	$A_1 \approx A_3$	$A_1 > A_3$	$A_1 \approx A_3$	$A_1 \approx A_3$
FSVD-MLRBF—ML-RBF	$A_2 \approx A_3$	$A_2 \approx A_3$	$A_2 > A_3$	$A_2 \approx A_3$

Table 5 Statistical analysis of each algorithm on Scene dataset

	Hamming loss	One error	Coverage	Ranking loss
Fuzzy PSO based ML-RBF—FSVD-MLRBF	$A_1 \approx A_2$	$A_1 \approx A_2$	$A_1 \approx A_2$	$A_1 \approx A_2$
Fuzzy PSO based ML-RBF—ML-RBF	$A_1 \approx A_3$	$A_1 > A_3$	$A_1 \approx A_3$	$A_1 < A_3$
FSVD-MLRBF—ML-RBF	$A_2 \approx A_3$	$A_2 > A_3$	$A_2 \approx A_3$	$A_2 < A_3$

Tables 2 and 3 shows the experimental results of proposed algorithms and ML-RBF. The values of ML-RBF used in Tables 2 and 3 have been taken from [6]. The results have been reported as mean \pm std. deviation.

Tables 4 and 5 shows statistical results of all the three algorithms. As shown in the tables, for each evaluation metric, $A < B$ indicates that performance of B is statistically significantly better than that of A for one specific metric based on unpaired t test at 95 % confidence interval.

From the experimental results of the Tables 2 and 3, the two proposed algorithms i.e. fuzzy PSO based MLRBF and FSVD-MLRBF outperforms ML-RBF in terms of one error and coverage but hamming loss and ranking loss of ML-RBF is less than both the proposed algorithms. However, statistical analysis of the results on the yeast dataset shows that ML-RBF is equivalent to both the proposed

algorithms in terms of hamming loss and ranking loss. While t-test result on scene dataset shows that ML-RBF outperforms both the proposed algorithms in terms of ranking loss. This may be because we have more number of instances of scene dataset compared to in [6]. In terms of one error fuzzy PSO based MLRBF is outperforming FSVD-MLRBF and ML-RBF while in case of coverage FSVD-MLRBF is outperforming fuzzy PSO based MLRBF and ML-RBF.

4 Conclusion

In this paper, we have proposed two approaches fuzzy PSO based MLRBF and FSVD-MLRBF. The experiments were conducted on two real world datasets i.e. yeast and scene dataset. Results of experiments show that both these algorithms can be successfully used for solving multi-label classification task. The analysis of results show that FSVD-MLRBF and fuzzy PSO based MLRBF outperforms ML-RBF in terms of one error and coverage in both the datasets. Statistical results of PSO based MLRBF and FSVD-MLRBF shows that both the proposed algorithms meets or beats existing ML-RBF. However, ML-RBF performs better in terms of ranking loss. So, in future we can further improve the performance of the proposed algorithms in terms of ranking loss. We can also use other multi-label datasets of varying complexity to fully evaluate the performance of both the proposed algorithms.

References

1. Zhang, M.L., Zhou, Z.H.: ML-KNN: A lazy learning approach to multi-label learning. *Pattern Recogn.* **40**, 2038–3048 (2007)
2. Spyromitros, E., Tsoumakas, G., Vlahavas, I.: An empirical study of lazy multilabel classification algorithms. *artificial intelligence: theories, models and applications. Lect. Notes Artif. Intell.* **5138**, 401–406 (2008)
3. Coelho, T.A., Esmín, A.A.A., Junior, W.M.: Particle swarm optimization for multi-label classification. In *Proceedings of the 13th annual conference companion on Genetic and evolutionary computation*, pp. 17, 18. (2011)
4. Zhang, M.L., Zhou, Z.H.: Multi-label neural networks with applications to functional genomics and text categorization. *IEEE Trans. Knowl. Data Eng.* **18**, 1338–1351 (2006)
5. Grodzicki, R., Mandziuk, J., Wang, L.: Improved multi-label classification with neural networks. *advances in knowledge discovery and data mining. Lect. Notes Comput. Sci.* **5199**, 409–416 (2008)
6. Zhang, M.L.: ML-RBF: RBF neural networks for multi-label learning. *Neural Process Lett.* **29**, 61–74 (2009)
7. Sapozhnikova, E.P.: Art-based neural networks for multi-label classification. In: Adams, N.M., Robardet, C., Siebes, A., Boulicaut, J.F. (eds.): *Advances in Intelligent Data Analysis VIII. Lecture Notes in Computer Science*, Vol. 5772, pp. 167–177 (2009)

8. De Souza, A.F., Pedroni, F., Oliveira, E., Ciarelli, P.M., Henrique, W.F., Veronese, L., Badue, C.: Automated multi-label text categorization with VG-RAM weightless neural networks. *Neurocomputing* **72**, 2209–2217 (2009)
9. Ciarelli, P.M., Oliveria, E., Badue, C., De Souza, A.F.: Multi-label text categorization using a probabilistic neural network. *Int. J. Comput. Inf. Syst. Ind. Manage. Appl. (IJCISIM)* **1**, 133–144 (2009)
10. Chen, Z., Chi, Z., Fu, H., Feng, D.: Multi-instance multi-label scene classification: A neural approach. *Neurocomputing* **99**, 298–306 (2013)
11. Abdelbar, A.M., Abdelshahid, S., Wunsch II, D.C.: Fuzzy PSO: A generalization of particle swarm optimization. In: *Proceedings of International Joint Conference on Neural Networks*, Vol. 2, Montreal, Canada. (2005)
12. Press, W.H., Teukolsky, S.A., Vetterling, W.T., Flannery, B.P.: *Numerical recipes in C: the art of scientific computing*. Cambridge University Press, New York (1992)
13. Tsoumakas, G., Katakis, I.: Multi-Label Classification: An Overview. *Int. J. Data Warehouse. Min.* **3**, 1–13 (2007)

A Peer-to-Peer Single Objective Particle Swarm Optimizer

Hrishikesh Dewan, Raksha B. Nayak and V. Susheela Devi

Abstract Particle Swarm Optimization is a parallel algorithm that spawns particles across a search space searching for an optimized solution. Though inherently parallel, they have distinct synchronizations points which hinders attempts to create completely distributed versions of it. In this paper, we attempt to create a completely distributed peer-to-peer (P2P) particle swarm optimization in a cluster of heterogeneous nodes. Since, the original algorithm requires explicit synchronization points we modified the algorithm in multiple ways to support a P2P system of nodes. We also modify certain aspect of the basic PSO algorithm and show how certain numerical problems can take advantage of the same thereby yielding fast convergence. This paper is based on one of our earlier work where we demonstrated the use of peer-to-peer systems for single objective optimizations functions. In this paper, we present the modifications that have been made to the previous system and test several benchmark functions.

1 Introduction

Particle swarm optimization (PSO) is based on the simulated modeling of birds, schools of fish and is being pursued actively in solving a wide range of computational optimization problems. The algorithm is inherently parallel and requires

H. Dewan (✉) · V. S. Devi
Department of Computer Science and Automation, Indian Institute of Science, Bangalore,
India

e-mail: hrishikesh.dewan@csa.iisc.ernet.in

V. S. Devi
e-mail: susheela@csa.iisc.ernet.in

R. B. Nayak
Knowledge and Innovation, Siemens Corporate Technology and Development Center,
Bangalore, India
e-mail: raksha.nayak@siemens.com

creation of an adequate number of particles that encompass the solution space to find the global minimum or maximum and a range of local optima solutions for a given problem. The initial PSO algorithm is sequential in that a single process when executed with an objective function, also called as a fitness function, is executed sequentially one after another to derive the required result. While, there are attempts to create a distributed based particle swarm optimizer, such attempts are more oriented towards a client–server master slave model with both synchronous and asynchronous model of communication [1–4] etc. are some of the implementations. As evident, such systems due to implicit or explicit dependence on single computing nodes pose problems in the areas of fault-tolerance and availability. Also, client–server distributed system requires significant resource planning and allocation before we execute any optimization problem. In this work, we propose a completely distributed P2P particle swarm optimizer. Our P2P model is resilient towards node failure, churns and has adequate algorithms for maintaining load across a set of heterogeneous systems. Further, the implementation is generic and hence any optimization problem can be plugged in the system without significant change in the underlying source code and the execution. We believe that the present system is a convincing alternative for those where owning a expansive expensive system is not a reality and requires guaranteed result without any dependence of any kind of centralized system. This paper is a revision of our earlier work [5] where we have demonstrated the usefulness of a peer-to-peer system for optimizing functions. In this paper, we introduce the various modifications that has been made to enhance the system and also present new results based on the experiments that has been conducted on top of this new system.

This paper is organized as follows. [Section 2](#) describe related work and shows how our algorithm is different from other peer works. [Section 3](#) describes the main components of our algorithm. [Section 4](#) describes the algorithms. Experiments and Results are described in [Sect. 5](#) and finally we conclude the paper in [Sect. 6](#).

2 Related Work

Distribution of PSO is being tried in several different ways. For example, [1–4, 6–9] lists the several attempts. Almost all of them except for [1] have definite synchronization barriers. As such each swarm agent though distributed in a set of nodes requires a synchronization point. In some implementations, definite synchronization points are defined and they are categorically termed as a synchronized particle swarm optimization whereas in case of others, asynchronous method is being developed by sending individual updates to a centralized server. In such implementations, the remote swarm agent need not wait for other agents for identifying the global best but the design demands a single server to which all nodes are required to send information. In other words, the parallel methods still have a dependency on a single server for information dissipation. We overcome this

anomaly by distributing information to a fixed set of neighbor nodes and a collection of random nodes.

Of all these attempts our work is comparable to [2]. In [2], they have proposed a parallel algorithm for solving a PSO problem and use gossip or epidemic algorithms to disseminate the best particle across a set of nodes. They however have not mentioned any fault-tolerance and load balancing techniques for the distributed PSO. Compared to [2] we have defined explicit load balance and fault tolerant algorithms. Another work in this area is [1]. In [1], authors have defined a multi-objective P2P particle swarm optimization method. In [1], Free Pastry [7] is being used to create the ring of node space. In our work, we have instead used a ring of nodes where the neighbor selection is based on the proximity of the swarm space than the numeric proximity as noted in [1]. Further, in [1], there is no specific scheme that is being defined for fault-tolerance and load balancing of nodes. In a peer-to-peer system, load balancing and fault tolerant are important features as computing systems participating are largely heterogenous in hardware configurations and they may fail without any notice to the other systems. Also, we have introduced swarm skip, a technique to skip ahead already computed swarm space. Ability to skip swarm space nullifies re-work and thereby decreasing the time required to converge to global minima.

3 Components of the Peer-to-Peer PSO

Our model includes the following three basic components. These components work together to create a complete distributed P2P swarm optimization set of nodes.

3.1 *Peer-to-Peer Model*

We follow a distributed system of nodes where every node is a master and a slave at the same time. In essence, each node is a peer and is responsible for all activities of the swarm. In some cases, such a single node acts as a complete PSO node and is capable of executing single or multiple objective functions. The communication model among the peers is asynchronous, meaning that generation and transfer of message is independent of any other node. We don't have distinct master nodes but at a particular time instant, a few of the nodes may be regarded as the leader of the optimization problem. Such leaders are however not static and they are purely formed in an ad-hoc manner and thus can change based on the overall system state. In our base model, we also handle load balance of the nodes. Our system has no strict requirement on homogeneity of nodes and hence handling load balance among the nodes is a necessity. However, unlike [1-4], we do not have a centralized model for calculating load imbalance in the system and subsequent

distribution of work. In our model, load balance is handled in a local manner and gradually load imbalance is solved using a distributed messaging system. In the similar way, fault tolerance is handled by continuous implicit monitoring of nodes and re-starting new swarm optimizers whenever a node fails. The organization of nodes in our model is based on circular ring where each node is connected to its immediate neighbor. Neighbors are however dependent on the dimensionality of the objective function. Thus for each swarm optimization problem, each node maintains a distinct routing table. Entries in the routing tables are used for communication among nodes. Further, each node randomly chooses $\log N$ number of nodes and includes them in the routing table. Each node has a unique identifier of 2^{128} bits and hence the number of systems that can be supported in our existing implementation is of the order of 2^{128} . Node identifier is generated using SHA-1 algorithm, which is known to provide 128 bit pseudo random number with significant probability of randomness. It can be shown that in our system, a message need not require more than $\log K$ number of hops to reach from one position to the other. Hence instead of a purely unstructured P2P network, the system has a deterministic cost for traversing a message. Distributing a PSO algorithm that was being designed to run sequentially and share results at the end of each iteration requires a few modifications. The first modification that we did is the non synchronous global update propagation wherein each iteration need not wait for a synchronization barrier for proceeding to the next interval. The second modification we did is on the swarm agent to subscribe to events precipitated by the particles whenever they try to cross their chunk size. In our method, we don't allow the particles to cross their swarm size. The algorithm detects such anomalies and either blocks the particle or reposition the particle in its own swarm space for more exploration of the candidate solutions. The third modification we introduced is the skipping of swarm exploration space. In our model, before a new swarm is explored, the intelligent agent at each node checks if the swarm space is already being explored. If the swarm space is explored, the swarm is re-positioned in a new candidate solution space or the swarm agent declares itself in its community of neighbor of job completion. We don't however include the following in our existing model. We assume that the system of nodes is trusted and hence byzantine fault tolerant techniques and security policies are not applied. The reason for not implementing the same is due to the fact that optimizers may not require such extra sophisticated algorithms to ensure security and trustworthiness. However, with some minor enhancements and some increasing cost in messaging, such systems can be easily introduced in our system. We envision this implementation in our test bed as a future work. Finally, the present system is capable of handling single objective functions with both convex and non convex types. We do not support multi-modal or multi-objective functions and such single objective functions which changes dynamically.

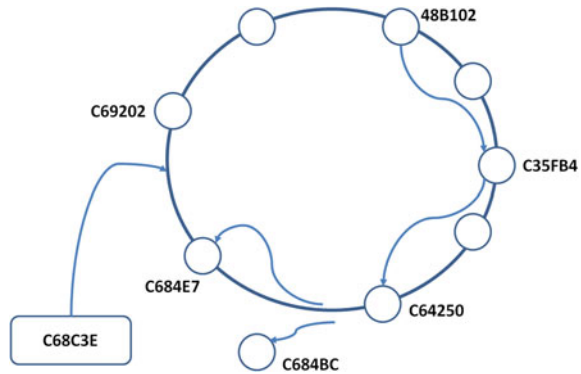
3.2 Network

Each node in our system maintains a routing table. The routing table entries are used for communication, to multicast results, transfer information related to load in the system and for fault tolerance. Like Chord [10, 11], our system arranges the nodes in a circular ring where each node is connected to its immediate successors and predecessors. However, unlike the single dimensional arrangement of [10, 11], we build the neighbor nodes in a multidimensional way. Therefore, the routing protocol in our system of nodes is a multi-dimensional one unlike the single dimensional routing strategies as adopted in most P2P systems. The number of dimensions in the multi-dimensional network is however dependent on the number of variables in the objective function. If the objective function involves a vector of single element, it is the same as in [10, 11] whereas if the system has a vector of D dimensions, routing and selection of nodes happens in D dimensions. Nodes join and leave the system without any prior notice and we do not envision a complete stable system. In a P2P system, the churns rates can be very high and thus measures for ensuring connectivity and completion of work is of utmost concern. Since, our connection of nodes is at random with no reliance on the underlying physical topology, we avoid the churning effect of nodes that might happen due to network partition or failure of a complete failure of a system of nodes. On the other hand due to non-availability of underlying physical network topology, the communication among peer nodes might require a large number of physical hops in the internet.

3.3 Swarm Agent

Each agent runs a sequential PSO and therefore the same agent can be used to find optimal solutions for a given objective function. When a agent starts, it calculates the swarm based on its mode. We support at present two modes of operation; master mode and slave mode. The notion of master is used for only two reasons-one to compute the swarm space and divide into chunks. Each chunk is a workable item and can be shared across a set of nodes requesting for work. The swarm agents receive chunks of data from a remote peer node and via the network component sends it across to the neighbors and the nodes in the routing table. Also swarm agents have distinct roles defined as Cooperative and Island where in each mode the swarm agent declares to its set of neighbors its choice of accepting work share from other nodes.

Fig. 1 An overlay network of nodes



4 Algorithms

The system can be divided into four different sections: Swarm Optimization and Execution, Node Join and Leave, load balancing and fault tolerance. We present below the core set of algorithms that encompasses all these four sections.

4.1 Network Model

We use an overlay network of nodes for communication of system as well as application level messages. The overlay network is a circular ring and is formed by applying consistent hashing functions. When a node joins the network, it is provided with a unique 160 bit identifier. The identifier is derived by concatenating time and MAC address of the node as an input to SHA-1 hash function. Based on the output, the ring is organized lexicographically. Figure 1 is an illustration of the same. For routing messages from one node to the other, each node maintains a routing table. The routing table entries are of three different types. Lexicographic neighbors (bi-directional) in both the clockwise and anti clock wise directions (a configurable number each in either direction), second unidirectional random links (based on the number of 1 s in the identifier) and third objective space neighbors. Objective space neighbors are the areas in decision variable space which are adjacent to the node that is currently being computed. For example, as illustrated in Fig. 3, the decision variable space is divided into equal size squares. Each node at any single point of time computes only one quadrant. For 2D space as illustrated, the number of neighbors is 4 and in general for n-dimensional space there are $2n$ neighbors. The reason for maintaining the objective space neighbors is to refer to it during the strategic re-work negotiation algorithm defined in the subsequent

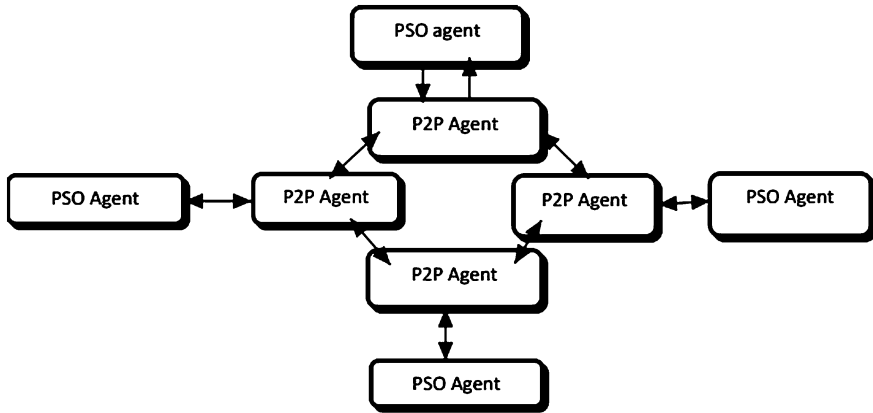


Fig. 2 P2P PSO Architecture

sections. When a node needs to send a message to yet another node, the routing table for the node is consulted to find the nearest node. Nearest node distance is the lexicographic distance. The algorithm then forwards the node to the nearest node and the same procedure is repeated till either the destination node is reached or there is no node of that identifier. In case of the former, the message is consumed by the destination node where as in case of the latter, the message is either consumed by the most preceding node or an error is returned to the user. Due to non-uniformity of node links, the reverse path can be different from the source node. It can be proved that on an average the maximum number of hops required to transfer a message is not more than $\log K$, where K is the number of nodes in the network. Also, due to non-uniformity of processing capability, each node may compute widely disparate function spaces. Therefore the neighbor space routing table changes from time to time and is not bound to be static during the entire life cycle of a node. Our network differs from other DHT-based network such as Chord, Pastry etc. by including extra neighbor node information related to our objective function. This modification is sought to decrease the message overload and also for fast convergence. When a node completes its job of finding the global best, it does not seek to enter into some other nodes dimensional space. Instead, the completed or the lightly loaded node simply skips the region of space and moves to the space which is slowly progressing or not yet processed. Thus, unlike the traditional PSO algorithms where there is a large amount of duplication of work, this design ensures very little duplication of work. Hence, compared to other algorithms, the relative time to convergence is faster (Figs. 5 and 6).

Due to large number of dimensions, the effective neighbors are roughly around $2 N$. This is a large number even for moderately size dimensions. To reduce the effect of introducing a large number of such neighbor nodes, we include a tree base directory structure (Fig. 3). Every node maintains a single indirection to its parent and each parent includes the list of siblings. The number of siblings is not more than

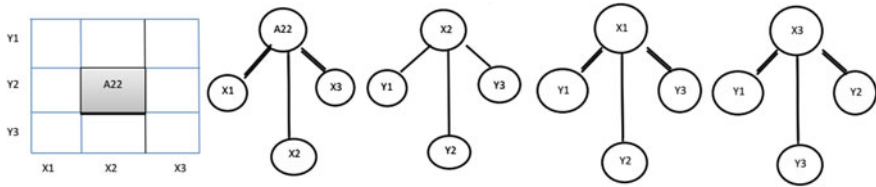


Fig. 3 a Division of search space into equal size partitions

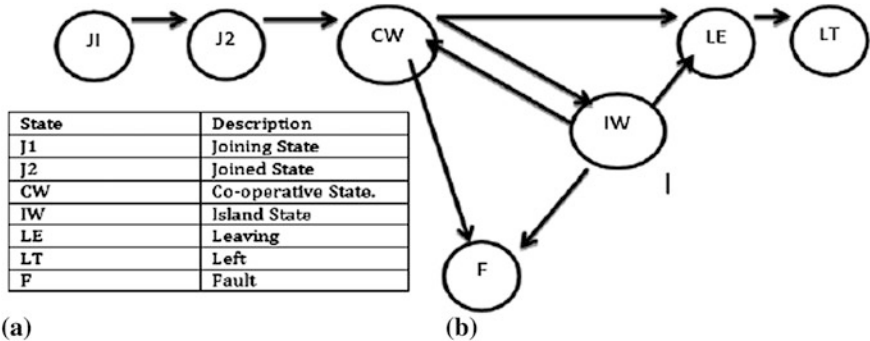


Fig. 4 a States of a Node: b Legends

the number of dimensions that is being used to divide the hyper-plane. Thus, the maximum number of neighbors that a node has to store is dependent upon the problem statement and also on the factors of division. For example, for three dimensional vectors, we first divide the function space in one of its axis. The second level includes the divisions of the second and so on. This increases the time to propagation but it prohibits the overcrowding of the routing table entries of the node.

4.2 Node Management

In a P2P network all nodes are symmetric and equal. Whenever a node has to participate in the function optimization computation, the first operation is the join operation. Upon completion of join, a node acquires a membership to the network and participates in all its activities, which includes function optimization, message passing, load balancing and fault-tolerance. Since each peer-node is responsible for at-least a certain chunk of work, there must be well-defined node leaving protocol. In this section, we define the node joining and leave protocols. It is important to note that in an ad-hoc network with no central administrative unit, nodes can join and leave at any moment. Such abrupt change in the network topology could be due to malfunctioning of hardware, software or the network.

Hence, the join and the leave protocol must handle these extreme but major use cases as well (Fig. 4).

As noted in section A, whenever a node joins, it first creates a new pseudo-random ID of 160 bits. After the ID is created, it then searches for an existing node in the network to communicate with. The list of existing nodes must be supplied to the new node before it starts its operation and is, by and large a manual process. Once, the node is connected to any of the existing nodes, the first message it composes is to find duplication of its own calculated node ID. Such a message is routed to the network using the newly connected existing node. If there are no such nodes, then the node can safely join the network. On the other hand, if such a node exists, the new node creates a new ID and recursively follows the same process. Joining the network involves creating the routing table entries. After the routing table entries are successfully created, the node connects to any node in the network for work units. Since a node already existent in the network is completely participating in the optimization process, the new node requests work from the already existent nodes. In our present protocol, we allow a new node to acquire work from a number of existing nodes and selects the work that seems appropriate. Upon selection of the work unit, the neighbors nodes are identified and the objective neighbor node work is filled. At this stage the routing table entries are complete and also the necessary code and work unit is with the new node. The new node starts executing its own sequential PSO from this point. Note that this type of work selection is completely deterministic and may take some time if the already existing nodes do not have work to allocate to a new node. The other joining protocol that we have investigated is to randomly select a work. Once the new node acquires the necessary code for the functions, its solution space and work division technique, it randomly selects a work unit from the entire available work unit. Since the routing table entries maintains neighbor node information based on the decision space neighbors, a message is sent from the new node to the node which is responsible for the work chunk. If the work chunk is available, then it is allocated to the new node or the node recursively continues the random work unit selection process again until it gets the desired work load. It is important to note that if the number of nodes are larger than the available work units, then neighbor nodes can further partition its work space and allocate a few to the newly joined node.

The node leaving protocol is opposite of what is defined in the node joining protocol. The leaving node broadcast leave messages to all its neighbors and waits for a few seconds before it leaves the network. Upon leaving the network, a hole is created in the overlay network and routing table entries of the neighbor nodes are modified. Dynamic node churns are described in more detail in section E.

4.3 Information Propagation

Information Propagation is done using the routing table entries of each node. Thus each node in the network works as a router and is responsible for forwarding message to the closest (lexicographically) destination node for transmission. In our system,

there are two types of information. The first type is the information related to swarm optimization and second type is the information for maintaining the network. As noted earlier, our objective space is divided into distinct hyper-planes and we maintain a hierarchy of neighbors. The non-dominated solution is only passed to the neighbors. The receiving node takes the responsibility of finding dominated solutions, if any, from this set. Figure 3 shows such neighbor sets for a particular peer that is responsible for a certain hyper-plane of the search space. The other information that is passed in the network is related to the maintenance of the network. Node join and leave, heartbeat messages and that of load balancing information are some of them. More details of these messages are mentioned in their respective subsections.

4.4 Load Balancing and Fault Tolerance

A P2P ad-hoc network is always a mix of diversified components: diversified in terms of hardware resources and software components available for computation. Therefore, there is no uniformity in the completion time of a solution space. Some nodes may take a long time to compute a work unit whereas some nodes may complete the same in 1/10th of the time taken by the other node. As a result, load balancing of nodes is an important requirement in such a diversified P2P network. We balance loads not instantaneously, but after repeated step intervals. A step interval is a finite number of iterations. After completion of each step, the node propagates its load to the neighbors using a broadcast. Nodes that are lagging behind comparatively are further propagated.

For broadcasting, there are two specific rules. For each node we maintain a least and utmost load, which are respectively 20 and 80 %. If the CPU utilization falls below or above this limit, the node broadcasts this information to the neighbors. Every node therefore maintains the load of its neighbors. If, however, the load is not below or above this threshold limit, there is no message sent. Hence, load information table is not as populated as the routing table entries. Once a node receives such information, it compares the load with all the entries and tries to achieve equilibrium by matching low capacity nodes with the high capacity ones. If, on the other hand, there are nodes that are still not yet matched, then the information is passed on to the nodes neighbors. The process is repeated until either there is a match or there are no nodes to match. When a node completes its allocated work unit and there are no more pending works, the computational utilization decreases by 10 %. Under this circumstance, the broadcast is sent from the node to all its neighbors till it receives new chunk of data. It is not difficult to prove that lowest utilized node is always eventually matched with a highly loaded node and the maximum number of steps required to match such a node is no more than $\log N$. Thus the network tries to balance load at the neighborhood first and if unsuccessful, propagates the information to the next level. With this, there are no central co-coordinators required and also the number of messages required for balancing the load is less. As in the case of load balancing, fault tolerance is also

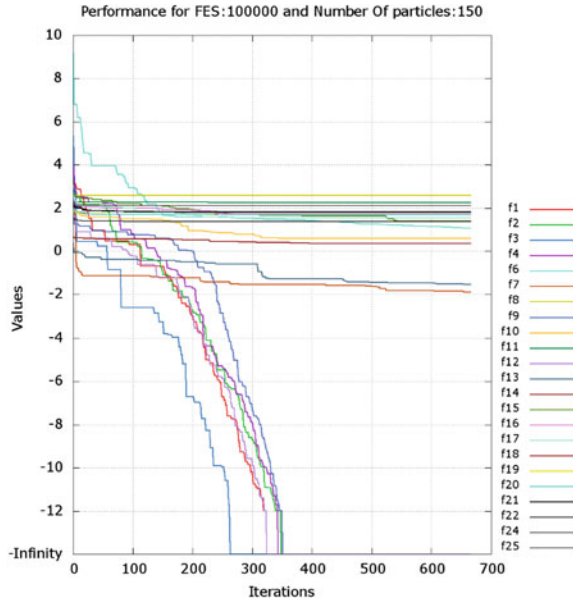
Table 1 FES: 100,000, Number of Particles: 50

	F1	F2	F3	F4	F6	F7	F8	F9
Min	0.0E+00	0.0E+00	0.0E+00	0.0E+00	0.0E+0	5.79E-003	3.77287E+002	0.0E+00
7th	0.0E+00	0.0E+00	0.0E+00	0.0E+00	0.0E0	1.00E-002	3.77297E+002	0.0E+00
13th	0.0E+00	0.0E+00	0.0E+00	0.0E+00	2.35	1.16E-002	3.77381E+002	0.0E+00
19th	0.0E+00	0.0E+00	0.0E+00	0.0E+00	3.43	1.42E-002	3.77460E+002	0.0E+00
Max	0.0E+00	0.0E+00	0.0E+00	0.0E+00	5.16	2.01E-002	3.78283E+002	9.9596E-001
Avg	0.0E+00	0.0E+00	0.0E+00	0.0E+00	2.16	1.21E-002	3.77460E+002	3.9838E-002
Std Dev	0.0E+00	0.0E+00	0.0E+00	0.0E+00	1.84	3.38E-003	2.50976E-001	1.9919E-001

Table 2 FES: 100,000, Number of Particles: 50

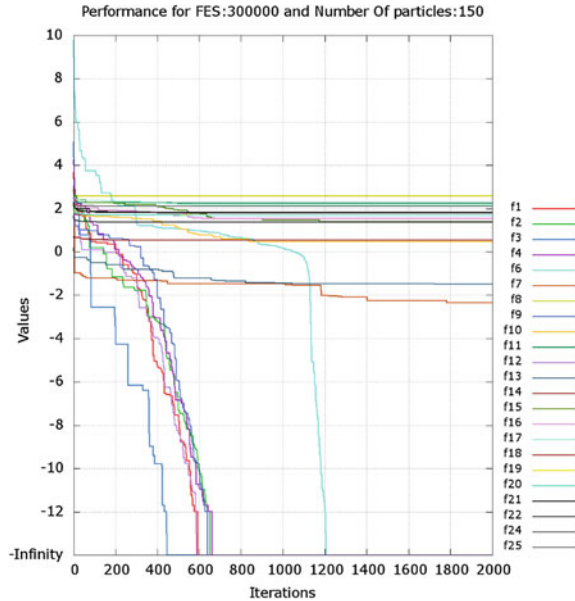
	F10	F11	F12	F13	F14	F15	F16	F17
Min	0.0E+000	1.80E+002	0.0E+00	3.82E-003	2.574E+000	0.0000E+000	2.6317E+001	1.5569E+001
7th	0.000E+000	1.80E+002	0.0E+00	2.33E-002	2.882E+000	2.0184E+001	3.4220E+001	3.1295E+001
13th	9.949E-001	1.80E+002	0.0E+0	3.93E-002	3.036E+000	2.6925E+001	3.9324E+001	3.8313E+001
19th	9.949E-001	1.80E+002	0.0E+00	5.89E-002	3.13E+000	5.0321E+001	4.4351E+001	5.1644E+001
Max	3.979E+000	1.80E+002	0.0E+0	1.48E-001	3.533E+000	2.1612E+002	5.9601E+001	1.9869E+002
Avg	9.551E-001	1.80E+002	0.0E+00	4.84E-002	3.056E+000	6.1540E+001	4.0004E+001	5.3385E+001
Std Dev	1.054E+000	0.00E+000	0.0E+00	3.96E-002	3.20E-001	7.4534E+001	8.7276E+000	4.260E+001

Fig. 5 Convergence plots for F1-F4, F6-F25 for FES 1,00,000, 150 particles



handled co-operatively. Each node upon joining the network maintains three fault tolerant connections to three other nodes. These nodes need not be entries in the routing table and are independent of them. After every successful time interval, which is configurable, the node sends the best positions, work unit in allocation information to each of these nodes. Failure to receive updates by the majority, either due to its software/hardware or network partition, signals the node as dead and a new node is selected for execution of the work. In the traditional algorithm for PSO, particles seem to do repetitive work. In our model, we prune such repetitions. Every particle sub swarm is allocated a chunk of work describing the lower and upper bound for the objective function and whenever a swarm moves beyond its chunk space, it first collaborates with the neighboring nodes for the exploration of the search space. If the swarm space is already explored or exploited, the swarm is allocated a new chunk work and the swarm jumps towards that point. As evident, the swarm computation part has a large number of peer threads or parallel tasks in execution. The execution of such is however asynchronous and event based mechanism is used to inform each tasks or the other. In our system, every peer can compute the whole swarm space, unless it is joined by

Fig. 6 Convergence plots for F1-F4, F6-F25 for FES 3,00,000, 150 particles



other swarm. The actual distribution of swarm happens only when multiple nodes of nodes join together to create a family of swarm agents, collating to solve or find solutions to a single objective function.

5 Experiment and Results

We checked our system and the algorithms by creating a complete PSO implementation from scratch using .NET 4.0 and C# as the implementation language. To support multiple different objective functions, we wrote a generic set of classes and interfaces. The same implementation code is re-usable across multiple objective functions of varied types. Each agent in a node runs as a process and has three main modules: network and routing, sequential PSO implementation, load and fault-tolerance. We have tested our algorithms using the benchmark functions as mentioned in [12]. The test bed is varied from 10 to 100 logical nodes. Each node runs as a process in a computer system and altogether we used 8 computing nodes for running the system. Each system runs either Windows 7 or Linux Operating System and .NET framework is included to execute the programs. Each system includes at-least 1 GB of RAM and dual core processors. The network connecting among the nodes is 100 Mbps Ethernet LAN. Each experiment is run for 25 number of times and we have produced the statistical results in Tables 1 and

Table 3 FES: 100,000, Number of Particles: 50

	F18	F19	F20	F21	F22	F23	F24	F25
Min	4.892E+001	4.926E+001	4.923E+001	6.421E+001	4.221E+001	6.431E+001	2.355E+001	1.277E+002
7th	4.909E+001	4.935E+001	4.940E+001	6.42E+001	4.223E+001	6.434E+001	2.358E+001	1.280E+002
13th	4.927E+001	4.944E+001	4.950E+001	6.444E+001	6.815E+001	6.436E+001	2.359E+001	1.281E+002
19th	4.930E+001	4.955E+001	4.95E+001	6.455E+001	6.830E+001	6.462E+001	2.361E+001	1.283E+002
Max	4.956E+001	4.969E+001	4.978E+001	6.457E+001	6.847E+001	6.505E+001	2.37E+001	1.285E+002
Avg	4.920E+001	4.945E+001	4.951E+001	6.440E+001	5.578E+001	6.448E+001	2.360E+001	1.282E+002
Std Dev	1.579E-001	1.135E-001	1.442E-001	1.161E-001	1.328E+001	2.214E-001	3.649E-002	2.843E-001

Table 4 FES: 150,000, Number of Particles: 150

	F1	F2	F3	F4	F6	F7	F8	F9
Min	0.0E+00	0.0E+00	0.0E+00	0.0E+00	0.0E+00	4.492E-003	3.772E+002	0.0E+00
7th	0.0E+00	0.0E+00	0.0E+00	0.0E+00	0.0E+00	7.056E-003	3.773E+002	0.0E+00
13th	0.0E+00	0.0E+00	0.0E+00	0.0E+00	0.0E+00	8.293E-003	3.77E+002	0.0E+0
19th	0.0E+00	0.0E+00	0.0E+00	0.0E+00	0.0E+00	9.483E-003	3.776E+002	0.0E+00
Max	0.0E+00	0.0E+00	0.0E+00	0.0E+00	8.584E-001	1.111E-002	3.781E+002	0.0E+0
Avg	0.0E+00	0.0E+00	0.0E+00	0.0E+00	7.101E-002	7.932E-003	3.775E+002	0.0E+00
Std Dev	0.0E+00	0.0E+00	0.0E+00	0.0E+00	2.030E-001	1.940E-003	2.332E-001	0.0E+00

Table 5 FES: 150,000, Number of Particles: 150

	F10	F11	F12	F13	F14	F15	F16	F17
Min	0.0E+000	1.80E+002	0.0E+00	3.82E-003	2.574E+000	0.0000E+000	2.6317E+001	1.5569E+001
7th	0.000E+000	1.80E+002	0.0E+00	2.33E-002	2.882E+000	2.0184E+001	3.4220E+001	3.1295E+001
13th	9.949E-001	1.80E+002	0.0E+0	3.93E-002	3.036E+000	2.6925E+001	3.9324E+001	3.8313E+001
19th	9.949E-001	1.80E+002	0.0E+00	5.89E-002	3.13E+000	5.0321E+001	4.4351E+001	5.1644E+001
Max	3.979E+000	1.80E+002	0.0E+0	1.48E-001	3.533E+000	2.1612E+002	5.9601E+001	1.9869E+002
Avg	9.551E-001	1.80E+002	0.0E+00	4.84E-002	3.056E+000	6.1540E+001	4.0004E+001	5.5385E+001
Std Dev	1.054E+000	0.00E+000	0.0E+00	3.96E-002	3.20E-001	7.4534E+001	8.7276E+000	4.7100E+001

Table 6 FES: 150,000, Number of Particles: 150

	F18	F19	F20	F21	F22	F23	F24	F25
Min	4.892E+001	4.926E+001	4.923E+001	6.421E+001	4.221E+001	6.431E+001	2.355E+001	1.277E+002
7th	4.909E+001	4.935E+001	4.940E+001	6.42E+001	4.223E+001	6.434E+001	2.358E+001	1.280E+002
13th	4.927E+001	4.944E+001	4.950E+001	6.444E+001	6.815E+001	6.436E+001	2.359E+001	1.281E+002
19th	4.930E+001	4.955E+001	4.95E+001	6.455E+001	6.830E+001	6.462E+001	2.361E+001	1.283E+002
Max	4.956E+001	4.969E+001	4.978E+001	6.457E+001	6.847E+001	6.505E+001	2.37E+001	1.285E+002
Avg	4.920E+001	4.945E+001	4.951E+001	6.440E+001	5.578E+001	6.448E+001	2.360E+001	1.282E+002
Std Dev	1.579E-001	1.135E-001	1.442E-001	1.161E-001	1.328E+001	2.214E-001	3.649E-002	2.139E-001

2. Initial chunk division of nodes is made to 1/10 of the variable size. The convergence plots for one of the runs for each of these benchmark functions are plotted in Figs. 5 and 6. We clearly observe that if the decision variable size is of large size increase in the number of nodes that participates in the system is essential. PSO algorithm, without any modification, doesn't work well when the number of dimensions of an objective function increases. To mitigate the effect, a large number of nodes are essential to break up the search space into chunks and allocate work to the swarm agents. Increasing the number of particles or the FES is a problem with a single system based particle swarm optimizer. But in a peer-to-peer system, there is no problem of these sort and problems of such kind is solved effectively. We also observed that unlike our semi-structured network as presented in [5], a structured network as implemented in this paper produces better result. But such kind of structured networks are only helpful when the entire peer-to-peer nodes are in close vicinity. If the nodes are far apart and the overlay network is oblivious to the underlying physical network, it may take a long time to transfer messages to desired recipients. We intend to mitigate this problem in the future.

6 Future Work and Conclusion

In the present work, we concentrated on single objective functions and showed how a P2P distributed system can be effectively used to find global minima/maxima of optimization functions. A peer-to-peer system is vulnerable from a security point of view; malicious node may distribute incorrect gbest and make the swarm move in a totally endless solution space where optimal solutions can never be reached. Byzantine fault tolerance, encryption of essential data and identification of nodes may be necessary when internet scale P2P systems are used for solving such problems. We intend to investigate these feature as our future work and also test a new set of scalable test functions for single objective unconstrained optimizations.

References

1. Scriven, I., Lewis, A., Mostaghim, S.: Dynamic search initialisation strategies for multi-objective optimisation in peer-to-peer networks. In: Evolutionary Computation, 2009, pp. 1515–1522. CEC'09. IEEE Congress on, IEEE (2009)
2. Biazini, M., Montresor, A.: p2poem: Function optimization in p2p networks. Peer-to-Peer Networking. Appl. 6(2), 213–232 (2013)
3. Hereford, J.M.: A distributed particle swarm optimization algorithm for swarm robotic applications. In: IEEE Congress on Evolutionary Computation, 2006, pp. 1678–1685. CEC 2006, IEEE (2006)

4. Venter, G., Sobieszczanski-Sobieski, J.: Parallel particle swarm optimization algorithm accelerated by asynchronous evaluations. *J. Aerosp. Comput. Inf. Commun.* **3**(3), 123–137 (2006)
5. Dewan, H., Devi, V.S.: A peer-peer particle swarm optimizer. In: 2012 Sixth International Conference on Genetic and Evolutionary Computing (ICGEC), pp. 140–144. IEEE (2012)
6. Kennedy, J.: Particle swarm optimization. In: *Encyclopedia of Machine Learning*, pp. 760–766. Springer (2010)
7. Rowstron, A., Druschel, P.: Pastry: Scalable, decentralized object location, and routing for large-scale peer-to-peer systems. In: *Middleware 2001*, pp. 329–350. Springer (2001)
8. Schutte, J.F., Reinbolt, J.A., Fregly, B.J., Haftka, R.T., George, A.D.: Parallel global optimization with the particle swarm algorithm. *Int. J. Numer. Meth. Eng.* **61**(13), 2296–2315 (2004)
9. Koh, B.I., George, A.D., Haftka, R.T., Fregly, B.J.: Parallel asynchronous particle swarm optimization. *Int. J. Numer. Meth. Eng.* **67**(4), 578–595 (2006)
10. Nilsson, S., Tikkanen, M.: An experimental study of compression methods for dynamic tries. *Algorithmica* **33**(1), 19–33 (2002)
11. Stoica, I., Morris, R., Karger, D., Kaashoek, M.F., Balakrishnan, H.: Chord: A scalable peer-to-peer lookup service for internet applications. In: *ACM SIGCOMM Computer Communication Review*, vol. 31, pp. 149–160. ACM (2001)
12. Suganthan, P.N., Hansen, N., Liang, J.J., Deb, K., Chen, Y., Auger, A., Tiwari, S.: Problem definitions and evaluation criteria for the cec 2005 special session on real-parameter optimization. *KanGAL Report 2005005* (2005)

F-FDRPSO: A Novel Approach Based on Hybridization of Fuzzy C-means and FDRPSO for Gene Clustering

Arpit Jain, Shikha Agrawal, Jitendra Agrawal and Sanjeev Sharma

Abstract Gene Clustering is one among the most popular issues involve in the field of Bioinformatics and is defined as the process of grouping related genes in the same cluster. Among the various algorithm proposed for clustering, the fuzzy c-means and there hybridization with some other methods has been used by most of the researchers to deal with the problem of premature convergence in fuzzy c-means clustering algorithm, but the results obtained were not satisfactory because the gene expression has huge amounts of ambiguous and uncertain biological data which requires advanced computing tools for processing such data. Particle Swarm Optimization (PSO) one of the variant of Swarm Intelligence (SI) has recently emerged as a nature inspired algorithms, especially known for their ability to produce low cost, fast and reasonably accurate solutions to complex search problems. PSO based Fuzzy C-Means algorithm were proposed but they all uses the traditional PSO algorithm. In traditional PSO algorithm each particle is attracted toward the best ever position discovered by any particle in the swarm, that limits the exploration capability. Instead if particle learn from the experience of the neighbouring that has better fitness than itself, the swarm can be more effectively and efficiently explored. So a method based on hybridization of fuzzy c-means and Fitness Distance Ratio based PSO is proposed. Initially this approach distributes the membership on the basis of the distance between sample and cluster centre making membership meet the constraints of FCM then the ratio of relative fitness and the distance of other particle is used to determine the direction in which

A. Jain (✉) · S. Agrawal · J. Agrawal · S. Sharma
Rajiv Gandhi Proudyogiki Vishwavidyalaya, Bhopal, India
e-mail: arpitcs09@gmail.com

S. Agrawal
e-mail: shikha@rgtu.net

J. Agrawal
e-mail: jitendra@rgtu.net

S. Sharma
e-mail: sanjeev@rgtu.net

each component of the particle position needs to be changed. The experiments were conducted on four real data sets and results shows that F-FDRPSO performs significantly better than FPSO and FCM algorithm.

Keywords Fitness distance ratio based particle swarm optimization · Fuzzy c-means · Gene clustering · Particle swarm optimization

1 Introduction

Bioinformatics field is an application of computational methods which makes biological discoveries. During the past few years a tremendous growth have been made for gathering biological information in the form of protein sequences, gene expression data and genomes. These information were analysed, interpreted and apply on the various Bioinformatics problems such as Gene Clustering Problem, Molecular Docking Problem, Multiple Sequence Alignment Problems, Phylogenetic tree construction, RNA Secondary Structure Prediction, Protein Secondary Structure Prediction, and Fragment Assembly Problem. Gene Clustering is one among the most popular issues involve in the field of Bioinformatics and is defined as the process of assigning related genes in the same cluster. A gene is the basic physical and functional unit of heredity and is made up of DNA which carries the required information that helps in the formation of protein which leads to construction of structural components. Clustering is a process of combining objects into a set of disjoint groups on the basis of some sort of similarity such that the objects in each cluster are more similar to each other than object from different clusters. So, a Gene clustering can be defined as the process of grouping Genes into cluster based on similar Gene expression level. The process through which the coded information of a gene is converted into structures operating in the cell is termed as gene expression. The gene expression helps in knowing the status of gene i.e. a gene has been “turned on” or activated. Gene Clustering is becoming popular nowadays because of increasing power of computing and matured microarray technology. Microarray technology allows monitoring huge amount of gene expression level simultaneously for whole genome through a single chip only.

Number of researchers have put their efforts for clustering the Gene Expression Data in which firstly Hartigan et al. [1] apply the concept of clustering on Gene expression data using classic K-Means algorithm. But it has the drawback of easily getting trapped in local optima. To overcome this problem Zhihua et al. [2] proposed a modified form of K-Means algorithm known as PK-Means in which Particle Pair Optimizer is combined with K-Means clustering algorithm. Due to the addition of exploration factor the PK-Means algorithms outperform K-Means. Lam et al. [3], has proposed a modified version of PK-means in which the concept of cluster matching is introduced where on the basis of closest distance each cluster centroid in a particle is matched with its corresponding centroid in the best

particle. Lam et al. [4] proposes a novel algorithm XK-means which hybridize PSO and K-means so as to integrate the concept of exploration with exploitation. This is done by using K-means and an exploratory vector. Before K-Means iteration the exploratory vector is added to each centroid. The algorithm includes two parameters namely a_i and b_i which are problem dependent and the value of parameter b_i is set in such a way that it decrease monotonically. As a result the search space gets explored and the exploitation level gets increased. In comparison to K-means and PK-means the complexity of the proposed algorithm is low.

A neural network based Gene clustering approach was introduced by Xiao et al. [5] which hybridizes Self Organizing Maps (SOM) and PSO for clustering genetic data. The proposed SOM/PSO algorithm works in two stages. In the first stage of the proposed algorithm, SOM is used to cluster the dataset. In this stage either regular SOM or SOM with a conscience can be used. The SOM normally runs for 100 iterations and generates a group of weights. In the second stage, PSO is initialized with the weights produced by SOM in the first stage. Then PSO is used to refine the clustering process. The experimental result shows that the proposed algorithm outperforms the average quantization error and the typographic error as compared to SOM.

Zhen et al. [6] proposes a Particle Swarm Optimizer (PSO) based memetic algorithm (MA) [7] named as memetic K-means algorithm (MKMA). The aim of the proposed algorithm is to minimize the sum of squared distance. The MA combines both global and local search where the global search in MKMA is achieved with the help of one of the variants of PSO i.e. Comprehensive learning particle swarm optimizer (CLPSO) [8]. CLPSO maintains the diversity of the swarm which help in improving the exploration efficiency of the global search. The experiment were conducted on two gene expression datasets and it was found that, in comparison to K-means, Fuzzy K-means and PK-means the MKMA has consistently attained better performance. Although the PSO algorithm converges fast, but lacks in global convergence and may get trapped in local optima. To overcome this drawback of PSO the Sun et al. [9] proposed the Quantum-behaved Particle Swarm Optimization (QPSO) algorithm. The QPSO possesses better global convergence behavior than PSO, but it also suffers from premature convergence. To overcome the problem of QPSO, Jun Sun introduced the revised version of QPSO by adding a Multi-Elastic strategy for Quantum-behaved Particle Swarm Optimization (QPSO) known as Multi-Elitist QPSO model to update the gbest position of the QPSO algorithm. In the MEQPSO algorithm, the particle's search is not based on the global position i.e. gbest but on the basis of the promising search region so that the particle has more chance to search in this region and obtain the global optimal solution. As a result, the MEQPSO have a stronger global search ability and better overall performance than the original QPSO [10].

This paper presents a novel approach based on hybridization of Fuzzy c-means and Fitness Distance Ratio based Particle Swarm Optimization (FDRPSO) for Gene Clustering named as F-FDRPSO. Particle Swarm Optimization is a newly emerged evolutionary technique based on swarm intelligence theory and FDR-PSO is one of

the variant of PSO. In FDR-PSO each particle not only learns from itself, group best particle but also learns from the experience of the neighbouring particle that has better fitness than itself. So the search space can be more effectively and efficiently explored.

The rest of the paper is organized as follows. In Sect. 2, the detail of Fuzzy c-means and FDR-PSO is presented and a novel approach F-FDRPSO is proposed. In Sect. 3, we evaluated the proposed algorithm with four test datasets and compare it with FPSO and Fuzzy c-means, finally Sect. 4 concludes this study with a short discussion.

2 F-FDRPSO: A Hybrid FDRPSO Based Fuzzy C-means Algorithm

Although Fuzzy C-Means is one of the most popular methods for gene clustering due to its simplicity but facing with the problem of premature convergence. To deal with this problem PSO based Fuzzy C-Means algorithm is proposed (FPSO) by Mehdizadeh et al. [11] but it uses the traditional PSO algorithm, where each particle is attracted toward the best ever position discovered by any particle in the swarm. This limits the exploration. So to enhance the performance, a novel method based on hybridization of FCM with FDRPSO is proposed called F-FDRPSO which maintains the merits of both FCM and PSO algorithms.

2.1 Fuzzy C-means Algorithm

Fuzzy C-Mean (FCM) algorithm was developed by Dunn [12] and improved by Bezdek et al. [13]. It is basically an unsupervised clustering algorithm which has been applied to wide range of problems involving clustering, classifier design and feature analysis. FCM clustering method allows a data to belong to two or more clusters. The clusters are formed using distance between data points and cluster centers.

Fuzzy c-means partition n data points $d = (p_1, p_2, p_3, \dots, p_n)$ into c ($1 < c < n$) clusters with $Z = (z_1, z_2, z_3, \dots, z_n)$ centroids. The classification result is expressed in terms of matrix $U = [\mu_{ik}]_{c \times n}$, where μ_{ik} is the membership degree of data point k with cluster i and satisfies the following conditions:

$$0 \leq \mu_{ik} \leq 1 \quad i = 1, 2, \dots, c, \quad k = 1, 2, \dots, n \tag{1}$$

$$\sum_{i=1}^c \mu_{ik} = 1 \quad k = 1, 2, \dots, n \tag{2}$$

$$0 < \sum_{k=1}^n \mu_{ik} \leq n \quad i = 1, 2, \dots, c \tag{3}$$

The objective function of FCM algorithm is to minimize the Eq. (4):

$$J(p) = \sum_{k=1}^n \sum_{i=1}^c [\mu_{ik}]^m \|x_k - V_i\|^2 \tag{4}$$

where $m > 1$ which controls the influence of membership grade, V_i denotes the cluster center of cluster i , x_k denotes the vector of data point and $\|x_k - V_i\|^2$ imitate the Euclidean distance between x_k and V_i .

where

$$V_i = \frac{\sum_{k=1}^n [\mu_{ij}]^m x_k}{\sum_{k=1}^n [\mu_{ij}]^m} \quad i = 1, 2, \dots, c \tag{5}$$

$$\mu_{ik}^{t+1} = \left[\sum_{j=1}^c \left(\frac{\|x_k - V_i^{(t)}\|^2}{\|x_k - V_j^{(t)}\|^2} \right)^{\frac{1}{m-1}} \right]^{-1} \tag{6}$$

where μ_{ik}^{t+1} is the membership degree of data point k in cluster i .

The Fuzzy c -means clustering is defined as follows:

Step 1: Let $t = 0$, Select an initial fuzzy pseudo-partition.

Step 2: Calculate the c cluster centers V_1^t, \dots, V_c^t by Eq. (5) for $P^{(t)}$ and the value of m which has been taken.

Step 3: Compute $\mu_{ik}^{(t+1)}$ by Eq. (6) and update P^{t+1}

Step 4: Compare P^t and $p^{(t+1)}$ If $|P^{(t+1)} - P^t| \leq \epsilon$, then stop; otherwise increase the value of t by one and go to step 2.

In the above algorithm, the parameter $m > 1$ is selected to suit the problem under consideration, as the value of m increases the partition becomes fuzzier and currently there is no measure to determine the optimal value for it [14].

2.2 Particle Swarm Optimization

Particle swarm optimization (PSO) is a population based stochastic optimization technique proposed by Kennedy and Eberhart [15] in 1995. The concept is stated as; each particle updates its position and velocity on the basis of its own best value and best value in the whole swarm. For a swarm of n particles the i th particle is represented by a position denoted as $x_i = (x_{i1}, x_{i2}, \dots, x_{id})$ and velocity as $v_i = (v_{i1}, v_{i2}, \dots, v_{id})$. The particles were explore in the search space with a velocity

that is updated through its own and that of neighbor's particle performance. In the PSO method the velocity and position of each particle were updated using equation's given below:

$$V_{id}^{t+1} = \omega V_{id}^t + c_1 r_1 (p_{best} - X_{id}) + c_2 r_2 (G_{best} - X_{id}) \quad (7)$$

$$X_{id}^{t+1} = X_{id}^t + V_{id}^{t+1} \quad (8)$$

Here w is an inertia weight, c_1 and c_2 are two positive acceleration constants, P_{best} is the best positions of the i th particle find so far and G_{best} is the group best position of a particle in the swarm and t is the iteration count.

2.3 Fitness Distance Ratio Based Particle Swarm Optimization

Peram et al. [16] proposed a modified particle swarm optimization called Fitness Distance Ratio based Particle Swarm Optimization (FDRPSO) in which each particle is moved towards other nearby particles that have better fitness, instead of just the best position discovered so far.

The learning process defined in the standard PSO is based on a particle's own experience and the best particle in the swarm. The FDRPSO algorithm adds a new dimension to this approach where each particle also learns from the neighbour particles based on the better fitness value than itself. This approach results in changes in the velocity update equations, although the position update equations remain unchanged. The FDR-PSO algorithms consider only one particle at a time and that particle must satisfy two criteria:

1. It must be near the particle being updated.
2. It should have visited a position of higher fitness.

The velocity component is update by selecting a particle which maximizes the ratio i.e. the d th dimension of the i th particle's velocity is updated using a particle called the N_{best} , with prior best position P_j , which maximize the

$$\text{Fitness Distance Ratio} = \frac{\text{Fitness}(P_j) - \text{Fitness}(X_i)}{|P_{jd} - X_{id}|} \quad (9)$$

where $|\dots|$ denotes the absolute value.

$$V_{id}^{t+1} = \omega V_{id}^t + c_1 r_1 (P_{best} - X_{id}) + c_2 r_2 (G_{best} - X_{id}) + c_3 r_3 (N_{best} - X_{id}) \quad (10)$$

$$X_{id}^{t+1} = X_{id}^t + V_{id}^{t+1} \quad (11)$$

The proposed F-FDRPSO algorithm for gene clustering problem can be stated as-

Algorithm F-FDRPSO

Input: dataset, number of cluster.

Output: Minimized value of Objective Function.

Begin

1. Initialize the position and velocity of each particle including G_{best} , P_{best} , ω , c_1 , c_2 , c_3 along with the fuzzy parameters as fuzzy index, number of clusters, where c_1 , c_2 , c_3 , ω are the constants, P_{best} is the best position of the particle discovered so far, G_{best} is the group best position in the swarm. N_{best} is the neighbour particle which is having better fitness value.
2. Find cluster centre for each particle using Eq. (5).
3. Using the value of cluster centre compute the value of objective function according to Eq. (4).
4. Store each particle position as best position P_{best} and each particle Fitness, then choose the particle that has best fitness as G_{best} .
5. Calculate the Fitness Distance Ratio using Eq. (9) and compute the N_{best} value accordingly.
6. Update the position and velocity of each particle according to Eqs. (10) and (11).
7. Based on the updated value, recomputed the fitness value of each particle compare the fitness of each particle with its previous best fitness P_{best} , if better than it, and then set the current position as P_{best} .
8. Compare the fitness of each particle with the group best previous fitness, if better than it, then set the current position as; G_{best} .
9. The algorithm terminates when either the objective function improvement between two consecutive iterations is less than the minimum amount of improvement specified or the maximum number of iterations is reached, if preconditions not met, then return to Step 2; else stop the iteration and output the solution.

3 Experimental Results

3.1 Parameter Settings

This paper presented a novel F-FDRPSO method for clustering Gene Expression Data. The main objective of this study is to access the relative performance of the proposed F-FDRPSO with respect to FPSO and FCM. The performance is measured with respect to the minimization of objective function value as in Eq. (4). For the comparative study, the methods were coded using the fuzzy tools available in MATLAB. For our experimental tests, we used a Dual Core processor with (CPU 2.60 GHz 4 GB RAM) and the values of different parameters used are as follows: $w = 0.72$, $c_1 = c_2 = c_3 = 1.49$, $m = 2$, $\varepsilon = 0.00001$ and number of iterations = 100.

3.2 Performance Metrix

Mean Squared Error

The Mean Squared Error (*MSE*) is used to measure the compactness inside the clusters, and is defined as:

$$MSE = \frac{1}{N} \sum_{j=0}^{K-1} \sum_{x_i \in C_j} \|y_i - z_j\|^2 \quad (12)$$

where y_i is a data point i , z_j is its cluster's centroid and C_j is its cluster.

3.3 Test Dataset

For evaluating the FCM, FPSO, F-FDRPSO methods, four real world dataset were considered:

1. The Iris plants data set is from the UCI Machine Learning Repository. This is perhaps the best known database to be found in pattern recognition literature. The data set has 150 points containing 50 instances of each of three types of Iris plants.
2. The Wine data set has 178 data points and 13 attributes where each data point is classified into three classes. This dataset is taken from UCI Machine Learning Repository.
3. The training Image Segmentation data set has 210 data points and 19 attributes, where each data point is classified into seven classes (i.e., brick face, sky, foliage, cement, window, path, grass). This dataset is from UCI Machine Learning Repository.
4. The Reduced Yeast Cell Cycle (RYCC) data set used in this research is from [17]. It is a data matrix with 384 rows and 17 columns. Each row represents a gene with 17 dimensions where each dimension corresponds to a point in the time series. It contains 384 genes that are grouped based on the five phases of the cell cycle: G1/M, G1, S, G2, and M. The microarray samples, collected at 17 time points taken in 10-min intervals, cover nearly two full cell cycles (170 min).

4 Result

Although the main objective of this research is to cluster the Genes of Yeast cell cycle dataset but we have firstly tested the method on three standard dataset namely iris, wine and image and compared the result with FCM, FPSO and F-FDRPSO as shown in Table 1. In Table 2 the Yeast Cell Cycle dataset is tested with varying the fuzziness parameter value as $m = 2$ and $m = 1.25$ for the FCM, FPSO and F-FDRPSO respectively. The Yeast Cell Cycle data set has been tested

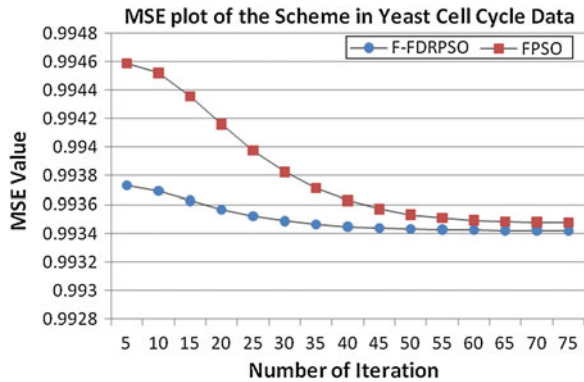
Table 1 Results of FCM, FPSO and F-FDRPSO methods on three standard datasets

Problem	Method	Average OFV	Best OFV	Worst OFV
IRIS	FCM	60.575959	60.575956	60.575963
	FPSO	60.575959	60.575956	60.575963
	F-FDRPSO	60.575959	60.575956	60.575963
WINE	FCM	1796082.759585	1796082.759582	1796082.759588
	FPSO	1796082.759585	1796082.759582	1796082.759588
	F-FDRPSO	1796082.759585	1796082.759582	1796082.759588
IMAGE	FCM	678645.888423	677260.451155	688310.182251
	FPSO	678286.821116	677260.451155	688310.166998
	F-FDRPSO	678125.120520	677260.451154	688310.123091

Table 2 Results of FCM, FPSO and F-FDRPSO methods on yeast cell cycle datasets

Problem	Method	Average OFV	Best OFV	Worst OFV
Yeast cell cycle with $m = 2.0$	FCM	288.786616	288.776441	288.992267
	FPSO	288.788632	288.776277	289.069299
	F-FDRPSO	288.779445	288.776324	288.823331
Yeast cell cycle with $m = 1.25$	FCM	726.376694	725.581488	731.011064
	FPSO	726.386523	725.581451	731.008277
	F-FDRPSO	726.039010	725.581488	731.005278

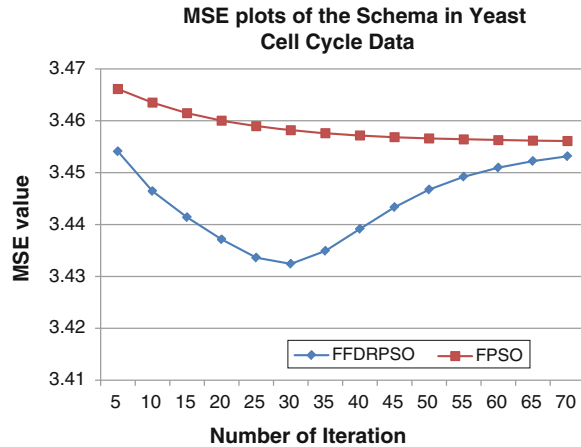
Fig. 1 MSE plots with iterations of the schemes in yeast cell-cycle data with $m = 2.0$



for the first time using Fuzzy c-means and that of PSO and its variant i.e. FDR-PSO. In all cases the result obtained by proposed method outperforms the FCM and FPSO methods.

The average variation of the MSE performance over the iteration of the schemes with the datasets, obtained in a 10 typical runs and with $m = 2$ and $m = 1.25$, is shown in Figs. 1 and 2 respectively. From the result depicted in Fig. 1, it can be seen that the MSE of the FPSO in compare to F-FDRPSO, converges faster. Also with $m = 125$ the graph of F-FDRPSO show that the value of MSE decreasing initially but with the increase in the number of iteration the F-FDRPSO converges to lower value of MSE than FPSO.

Fig. 2 MSE plots with iterations of the schemes in yeast cell-cycle data with $m = 1.25$



5 Conclusion

Gene cluster analysis is the first step in discovering the function of gene in bioinformatics. Although K-means clustering is one of the most popular clustering algorithm in which the data objects are partitioned into k clusters (where the number of clusters is known in advance), such that each data object belongs to exactly one cluster still it is not applicable for real data sets having no definite boundaries between the clusters. In such condition Fuzzy C-Means, due to its fuzziness feature has become the most well-known and powerful method in cluster analysis, but the random selection in centre points makes iterative process falling into the local optimal solution easily. To overcome this problem, recently many evolutionary algorithms such as genetic algorithm (GA), simulated annealing (SA), ant colony optimization (ACO), and particle swarm optimization (PSO) have been applied. Evolutionary algorithm, such as Particle Swarm Optimization (PSO) is incorporated with the fuzzy c-means clustering to achieve both exploration and exploitation. This kind of integrated algorithm can give better clustering results in term of compactness within the clusters, but the problem with the PSO based Fuzzy C-Means is that each particle is attracted toward the best ever position discovered by any particle in the swarm which limit the exploration. Instead if particle learn from the experience of the neighbouring particle that has better fitness than itself then the swarm can be more effectively and efficiently explored. This concept is used in the proposed F-FDRPSO method. The experimental results over four well known data set namely Iris, Wine, Image and Yeast Cell Cycle data set shows that the proposed method is efficient and produce much better results in comparison to PSO based fuzzy c-means and Fuzzy c-means.

References

1. Hartigan, J.A., Wong, M.A.: A k-means clustering algorithm. *Appl. Stat.* **28**, 126–130 (1979)
2. Du, Z., Wang, Y., Ji, Z.: PK-means: a new algorithm for gene clustering. *Comput. Biol. Chem.* **32**, 243–247 (2008)
3. Lam, Y.-K., Tsang, P.W.M., Leung, C.-S.: Improved Gene Clustering Based on Particle Swarm Optimization, K-Means, and Cluster Matching, pp. 654–661. Springer, Berlin (2011)
4. Lam, Y.-K., Tsang, P.W.M., Leung, C.-S.: eXploratory K-means: a new simple and efficient algorithm for gene clustering. *Appl. Soft Comput.* **12**(3), 1149–1157 (2012)
5. Xiao, X., Dow, E.R., Eberhart, R., Miled, Z.B., Oppelt, R.J.: Gene clustering using self-organizing maps and particle swarm optimization (2003)
6. Ji, Z., Liu, W., Zh, Z.: Gene Cluster in using Particle Swarm Optimizer based Memetic Algorithm. Springer, Berlin (2011)
7. Moscato, P.: Memetic Algorithm: A Short Introduction. McGraw-Hill, London (1999)
8. Liang, J.J., Qin, A.K., et al.: Comprehensive learning particle swarm optimizer for global optimization of multimodal functions. *Proc. IEEE Trans. Evol. Comput.* **10**(3), 81–295 (2006)
9. Sun, J., Fang, W.C., Wun, X.J., Xu, W.: Gene expression data analysis with the clustering method based on an improved quantum-behaved particle swarm optimization. *Eng. Appl. Artif. Intell.* **25**, 376–391 (2012)
10. Jain, Arpit, Agrawal, Shikha, Agrawal, Jitendra, Sharma, Sanjeev: Analysis of population based metaheuristic used for gene clustering. *Int. J. Comput. Commun. Eng.* **2**(2), 174–178 (2013)
11. Mehdizadeh, E., Sadi-Nezhad, S., Tavakkoli-Moghaddam, R.: Optimization of fuzzy clustering criteria by a hybrid PSO and fuzzy c-means clustering algorithm. *Iran. J. Fuzzy Syst.* **5**(3), 1–14 (2008)
12. Dunn, J.C.: A fuzzy relative of the isodata process and its use in detecting compact well-separated clusters. *J. Cybern.* **3**, 32–57 (1973)
13. Bezdek, J.C., Ehrlich, R., Full, W.: FCM: the fuzzy c-means clustering algorithm. *Comput. Geosci.* **10**(2–3), 191–203 (1984)
14. Klir, J.G., Yuan, B.: Fuzzy Sets and Fuzzy Logic, Theory and Applications. Prentice-Hall, New Jersey (2003)
15. Kennedy, J., Eberhardt, R.C.: Particle swarm optimization. In: IEEE International Joint Conference on Neural Networks, pp. 1942–1947. IEEE, Piscataway (1995)
16. Peram, T., Veeramachaneni, K., Mohan, C.K.: Fitness-distance-ratio based particle swarm optimization. In: Proceedings of the IEEE/SIS, pp. 174–181 (2003)
17. Yeung, K.Y.: Cluster analysis of gene expression data. Dissertation, Department of Computer Science and Engineering, Washington (2001)

Metaheuristic Approaches for Multiprocessor Scheduling

Lakshmi Kanth Munganda and Alok Singh

Abstract In the multiprocessor scheduling problem, a given list of tasks has to be scheduled on identical parallel processors. Each task in the list is defined by a release date, a due date and a processing time. The objective is to minimize the number of processors used while respecting the constraints imposed by release dates and due dates. This objective is clearly linked with minimizing the cost of hardware needed for implementing a specific application. In this paper, we have proposed two metaheuristic approaches for this problem. The first approach is based on artificial bee colony algorithm, whereas the latter approach is based on invasive weed optimization algorithm. On the standard benchmark instances for the problem, performances of our approaches are comparable to other state-of-the-art approaches.

1 Introduction

A list of n tasks is given and these tasks have to be scheduled on identical parallel processors (each processor has the same computing ability). Each task i has a release date r_i , a due date d_i , and a processing time p_i . Let s_i be the start time of task i . A task i can start only after its release date, i.e., $r_i \leq s_i$ and has to be finished before its due date $s_i + p_i \leq d_i$. The objective of multiprocessor scheduling problem considered in this paper is to schedule the tasks so as to minimize the number of processors used in such a way that the constraints imposed by

L. K. Munganda · A. Singh (✉)

School of Computer and Information Sciences, University of Hyderabad,
Hyderabad 500 046, India
e-mail: alokes@uohyd.ernet.in

L. K. Munganda

e-mail: lakshmikanth.munganda@gmail.com

release dates and due dates should not be violated. This objective is directly linked with minimizing the cost of the hardware needed for implementing a specific application [5, 8], where tasks must be executed on the cheapest possible architecture.

The multiprocessor scheduling problem as defined above is \mathcal{NP} -Hard as it reduces to one-dimensional bin packing problem when all release dates are set to zero and all due dates are set to a unique date greater than or equal to the processing time of the longest task. One-dimensional bin packing problem is a well known \mathcal{NP} -Hard problem.

A tabu search based method is proposed by Sevaux and Sörensen [22] for this problem. This method first computes a lower bound m on the number of processors and then the classical $Pm|r_i|\sum U_i$ scheduling problem is solved using tabu search. The $Pm|r_i|\sum U_i$ problem seeks an allocation of tasks on m processors so as to minimize the number of late tasks, i.e., those tasks that can not be finished before its due date. The binary variable $U_i = 1$, if task i is late, 0 otherwise. If a task is not late then it is called an early task. In case $\sum U_i = 0$ then a solution to the original scheduling problem is found and the method stops, otherwise the tabu search procedure is applied again after incrementing the value of m by 1. This process continues until a solution with $\sum U_i = 0$ is found. Tabu search procedure either inserts a late task in between two early tasks or replaces a late task with some consecutive early tasks. Sum of processing times of late tasks is used as tabu criterion in this method. Inbuilt cycle detection mechanism and dynamic tabu tenure adjustment are two other important features of this method. This method will be referred to as TS-I subsequently.

Sevaux et al. [21] also presented a tabu search based method which follows a reverse approach in comparison to [22]. This method begins with an initial feasible solution to the problem with m processors and then it removes one or two processors randomly from the solution thereby making some tasks unallocated. Tabu search tries to allocate these unallocated tasks one-by-one in some random order. If a solution with m or less than m processors is found after allocating all the tasks then it becomes the new initial solution and the whole process is repeated again, otherwise the new solution is discarded and the original solution is perturbed again. This process is repeated for a fixed number of iterations. Like [22], this tabu search procedure also consists of either inserting an unallocated task between two allocated tasks or exchanging an unallocated task with some consecutively allocated tasks. However, in this approach an exchange operation is performed only when the processing time of the unallocated task is more than the processing time of each consecutively allocated task to be exchanged. Moreover, once an unallocated task becomes allocated, it can not be removed for the duration determined by the tabu tenure. No cycle detection mechanism is needed in this approach as an unallocated task is exchanged with smaller tasks only. In comparison to TS-I, this approach performed better. This approach will be referred to as TS-II subsequently.

A hybrid approach combining a steady-state grouping genetic algorithm with a heuristic is proposed in [24]. This approach employs specially designed crossover and mutation operators which are used in a mutually exclusive manner. After the

application of genetic operators some tasks remain unallocated which are allocated by the heuristic. This hybrid approach outperformed both TS-I and TS-II. Hereafter, this approach will be referred to as HGGA-SSR. HGGA-SSR along with TS-I and TS-II constitute the state-of-the-art for multiprocessor scheduling problem.

In this paper, we have proposed two metaheuristic approaches viz. Artificial Bee Colony (ABC) Algorithm and Invasive Weed Optimization (IWO) Algorithm for multiprocessor scheduling problem. Both ABC and IWO algorithms fall under the category of metaheuristics based on swarm intelligence [4]. ABC algorithm proposed by Karaboga [9] is inspired by intelligent foraging behaviour of honey bee swarm. Mehariban and Lucas [16] proposed IWO algorithm on getting inspiration from colonizing behaviour of weeds. We have evaluated the performance of our proposed approaches on benchmark instances available in the literature. Performance of our approaches is comparable with other state-of-the-art approaches.

The rest of this paper is organized as follows: [Section 2](#) provides a brief introduction to Artificial Bee Colony (ABC) Algorithm. [Section 3](#) describes our ABC approach to multiprocessor scheduling problem. [Sections 4](#) and [5](#) respectively provides a brief introduction to Invasive Weed Optimization (IWO) Algorithm and describes our IWO approach to multiprocessor scheduling problem. Computational results are presented in [Sect. 6](#), whereas [Sect. 7](#) outlines some concluding remarks and directions for future research.

2 Introduction to ABC Algorithm

ABC is a population based meta-heuristic optimization algorithm, which is inspired by the intelligent foraging behavior of natural honey bee swarm. The natural bees are divided into three categories employed, onlooker and scout bees based on their work. The employed bees collect the nectar from the food sources and bring it to the hive. After coming to the hive, the employed bees share the information about food sources with the onlooker bees which are waiting in the hive. To share the information the employed bees perform dances in a common area in the hive, which is called dancing area. Onlooker bees observe the dances performed by employed bees before choosing a food source. The probability of a food source to be chosen by the onlooker bees is proportional to the nectar amount of that food source. Therefore, the food sources which are having high nectar amount attract more bees than the other food sources which are having less nectar amount. When a food source is completely exhausted, all the employed bees associated with it leave it, and become scouts or onlookers. Scouts look for new food sources in the vicinity of the hive. Whenever a bee, whether it is scout or onlooker finds a food source then it becomes employed. So in a way exploration is done by the scouts and exploitation is done by the employed and onlookers.

Inspired by this intelligent foraging behavior of honey bee swarm, Karaboga [9] designed the ABC algorithm which was extended further by [1, 3, 6, 7, 10–13, 17, 23, 25–27] etc. Like real bees, in the ABC algorithm, artificial bees are also classified into scout, employed and onlooker bees with similar functions. In the ABC algorithm a food source and its nectar content respectively represent a candidate solution and its fitness. The ABC algorithm assumes that there is only one employed bee for every food source, i.e., the number of employed bees is same as the number of food sources. Usually, the number of onlooker bees are also taken to be equal to the number of employed bees. The employed bee of an exhausted food source becomes a scout and as soon as it finds a new food source it again becomes employed. The action of a scout bee is simulated by generating a new food source (solution) randomly and associating the scout bee in consideration with this newly generated food source to make it again employed. We will use food source and solution interchangeably throughout this paper.

The ABC algorithm begins with generating certain number of food sources randomly and associating each of these food sources with an employed bee. After that, a search process is carried out repeatedly until termination criteria is met. Each iteration of the ABC algorithm consists of two phases viz. the employed bee phase and the onlooker bee phase. In the employed bee phase, every employed bee determines a new food source in the neighborhood of its associated food source. If the nectar content of this new food source is higher than that of its currently associated food source, then this employed bee associates itself with this new food source abandoning the old one, otherwise it continues with the old one. The actual process of determining a new food source in the neighborhood of a particular food source depends on the problem under consideration.

Once the employed bee phase ends, the onlooker bee phase starts. In this phase, first of all, each onlooker bee selects a food source using some probability based selection criterion. Usually, the selection criterion prefers good food sources over bad ones so that more onlooker bees will be assigned to good food sources which in turn result in more exploitation in the vicinity of these food sources. After all onlookers have selected their food sources, each of them determines a food source in the neighborhood of its chosen food source in a manner similar to employed bee phase and computes its fitness. Among all new food sources determined by onlookers associated with a particular food source i and food source i itself, best food source will be the new position of the food source i . If a food source is not improved over a predetermined number of iterations *limit*, then this food source is assumed to be exhausted and its associated employed bee abandons it and becomes a scout. This scout is again made employed by associating it with a new randomly generated food source. When the new positions of all food sources are determined the onlooker bee phase ends and the next iteration of the ABC algorithm begins.

An excellent literature survey on the ABC algorithm and its applications can be found in [14].

3 ABC Algorithm for Multiprocessor Scheduling

This section describes our ABC algorithm based approach to multiprocessor scheduling. This approach will be referred to as MPS-ABC subsequently.

A solution in ABC algorithm is represented as a set of single processor schedules, i.e., no ordering exists among the single-processor schedules. As the processors are identical, any schedule can be executed on any processor. Therefore, there is no redundancy in our solution representation.

For determining the fitness of a solution we adopted the approach used in [24] which uses two fitness functions. The first fitness function F is the objective function, i.e., the number of processors used in the solution. The second fitness function is needed to determine the relative fitness of two solutions having the same number of processors. The second fitness function f is computed by summing up the square of the relative idle time (idle time in a schedule divided by the duration of the schedule) over all the single-processor schedules. A solution C is said to be more fit than another solution C' , if $(F(C) < F(C'))$ or $(F(C) = F(C'))$ and $(f(C) > f(C'))$.

The algorithm is initialized by assigning a randomly generated solution to each employed bee. The process of generation of an initial solution is described below. This initial solution generation process tries to schedule the tasks as early as possible on one of the available processors. Only when it is not possible to schedule the tasks anywhere, a new processor is added to the solution and task is scheduled on it at the earliest possible time.

- A task is selected uniformly at random for allocation. The selected task is tried for insertion at the beginning of a processor.
- If it is not possible to insert at the beginning of a processor, then it is tried for insertion at the middle of a processor.
- If it is also not possible to insert the task in the middle of some processor, then it is tried for insertion at the end of a processor.
- When it is not possible to insert the task anywhere, then a new processor is added to the solution and the task is allocated to it. This process is repeated until all tasks are allocated.

In the employed bee phase, we generate a neighbouring solution to each and every solution. After generating the neighbouring solution, we check whether the neighbouring solution is better than existing solution or not. If it is, we replace the existing solution with the neighbouring solution. Otherwise, ignore the neighbouring solution.

The process of generating a neighbouring solution (E') for an employed bee solution E with m processors is as follows:

- Randomly remove one or two processors from the solution, thereby creating a set of unallocated tasks.

- The unallocated tasks are tried for allocation on processors in some random order. A task is tried for insertion in the same way, as in the case of generation of an initial solution.
- If a solution with m or fewer than m processors is obtained then it becomes the new solution.
- In case if the neighbouring solution is not generated, then replace E with a random solution.

In the onlooker bee phase, two different methods are used for generating a neighboring solution which are used in a mutually exclusive manner. These methods are derived from the genetic operators used in [24]. The first method is applied with probability p_f , otherwise the second method is used. k -ary tournament selection method ($k = 2$ for first method but $k = 3$ for second method) is used for selecting solutions for onlooker bees. Both methods leave certain tasks unassigned which are processed in the same manner as in initial solution generation.

In the first method, one more solution is selected using binary tournament selection and an iterative process begins. During each iteration, the best of the two participating solutions are selected with probability p_b and the schedule with smallest relative idle time is copied from the selected parent solution to the child solution. After that, all the tasks belonging to this schedule are deleted from the both participating solutions and the relative idle times of the schedules are updated. This method iterates for $\min(m_1, m_2) - 2$ iterations, where m_1 and m_2 are the number of processors in the two participating solutions.

In the second method, from the selected solution, we randomly remove some schedules thereby creating a number of unallocated tasks. The schedules are selected uniformly at random for removal except for the schedule with largest relative idle time which is always removed.

If a solution is not improved over the specified number of iterations (it_{noimp}), then that solution has to be replaced by a random solution which is generated in the same manner as initial solution.

4 Introduction to Invasive Weed Optimization (IWO) Algorithm

Invasive Weed Optimization (IWO) is a meta-heuristic optimization algorithm that is motivated by the colonizing behavior of weeds which is a common phenomenon in agriculture. A weed is considered as an undesirable plant in agriculture because of its robust and adaptive nature. IWO is developed by Mehariban and Lucas [16]. In the IWO algorithm, each weed represents a possible solution to the problem under consideration and the fitness of a weed means the fitness of the solution being represented by that weed. IWO algorithm consists of initialization, reproduction, spatial distribution, and competitive exclusion phases. These phases are summarized below. In the initialization phase, a finite number of weed solutions

are randomly initialized in the search space. In the reproduction phase, each weed of the population is allowed to produce seeds based on their relative fitness (fitness of the individuals and the best and worst fitness of the colony). The weed with the best fitness produce more number of seeds than the weed with the worst fitness. In the spatial distribution phase, these produced seeds are spread randomly in the search space with a particular standard deviation. In competitive exclusion phase, to limit the maximum number of weeds in a colony some kind of competition between weeds is needed. The weeds with better fitness up to colony size are kept and others are removed from the search space. Some recent applications of IWO algorithm can be found in [2, 15, 19, 20].

5 IWO Approach to Multiprocessor Scheduling Problem

In this section, we describe the main features of our Invasive Weed Optimization (IWO) algorithm. Our IWO approach will be referred to as MPS-IWO subsequently. Most of the concepts used in MPS-IWO are borrowed from those of MPS-ABC.

MPS-IWO uses the same solution representation as used in MPS-ABC. Fitness of a solution is also evaluated in the same manner as in MPS-ABC. IWO consists of initialization, reproduction, spatial distribution, and competitive exclusion phases. These phases are described below.

A population of initial weed solutions are generated randomly in the search space. The process of generation of an initial weed solution is same as in MPS-ABC.

In the reproduction phase, we generate seed solutions for each and every weed solution. The solution which has better fitness value will produce more number of seed solutions than the solution which has worst fitness value. The number of seed solutions (range from s_{max} to s_{min}) generated for a weed solution will depend on its fitness value. The process of generation of a seed solution to a weed solution is analogous to neighboring solution generation in MPS-ABC. In our IWO approach, seed solutions are always generated in the same manner, i.e., we have not tried to induce any decrease in the expected standard deviation of seed solutions from their parent weed solution with iterations.

In the competitive exclusion phase, only the solutions which have better fitness value will be retained for future consideration. Actually, due to the generation of seed solutions, number of solutions in the colony will reach its maximum permissible value pop_{max} after some iterations. Under this situation, the competitive exclusion phase removes the solutions with poor fitness from the colony in the following manner: Once the maximum number of solutions in the colony is reached, whenever an iteration completes, i.e., each solution in the colony has produced seed solutions, all the solutions including newly generated seed solutions are sorted according to their fitness. Next, some solutions with lowest fitness are

eliminated so as to retain best pop_{max} solutions in the colony. In this way, only the solutions with better fitness survive and are allowed to reproduce.

6 Computational Results

The MPS-ABC and MPS-IWO have been coded in C and were executed on a linux based 3.0 GHz core2duo system with 2 GB of RAM. In all our computational experiment with MPS-ABC, we have used a population of 200 bees out of which 100 are employed bees and 100 are onlooker bees. We have taken $p_f = 0.8$, $p_b = 0.9$ and $it_{noimp} = 100$. We have allowed MPS-ABC to execute for $10n$ iterations on a problem instance with n tasks. In case of MPS-IWO, we have used an initial population size of 50, $pop_{max} = 20$, $s_{max} = 5$, and $s_{min} = 1$. We have also allowed MPS-IWO to execute for $10n$ generations on a problem instance with n tasks. It is to be noted that for MPS-IWO, competitive exclusion phase will start eliminating solutions since beginning as generated initial solutions are more than pop_{max} .

We have used the same 100 test instances as used in [21, 22] and [24] to evaluate the performance of our approaches. These instances were introduced by Sevaux and Sörensen [22]. There are 20 instances for each value of $n \in \{20, 40, 60, 80, 100\}$, where n is the number of tasks. Therefore, altogether 100 instances were used. Optimal solution for all these instances are also known [18].

Table 1 compares the performance of MPS-ABC and MPS-IWO with HGGA-SSR, TS-I and TS-II in terms of solution quality, where each row shows the number of instances out of 20 solved to optimality by different methods. The optimum solutions for all these instances are obtained through a mixed integer linear programming (MILP) based solver [18]. Table 2 reports the average execution time of each approach on instances of each size in seconds. Data for HGGA-SSR, TS-I and TS-II are taken from [21, 22, 24] respectively.

Tables 1 and 2 clearly show the superiority of MPS-ABC over TS-I and TS-II. In comparison to these two methods, MPS-ABC returned better quality solutions in shorter time. Out of 100 instances it solves 90 instances optimally, whereas TS-I and TS-II respectively solve 45 and 88 instances optimally. For the remaining instances MPS-ABC requires only one processor more than the optimal number of processors. The results are slightly inferior when compared to the HGGA-SSR method. HGGA-SSR solves 97 instances optimally. TS-I, TS-II and HGGA-SSR were executed on a 3.0 GHz Pentium 4 system, whereas MPS-ABC and MPS-IWO have been executed on a 3.0 GHz core2duo system. As the different approaches have been executed on different systems, only a rough comparison regarding the execution times can be made as it is not possible to compare the execution times precisely. Even after compensating for difference in processing powers of machines, we can safely say that MPS-ABC is much faster than TS-I and TS-II. It is also faster than HGGA-SSR. As far as MPS-IWO is concerned,

Table 1 Comparison of MPS-ABC and MPS-IWO with TS-I, TS-II and HGGA-SSR in terms of solution quality

Instance size (n)	Number of instances solved to optimality				
	TS-I	TS-II	HGGA-SSR	MPS-ABC	MPS-IWO
20	20	20	20	20	20
40	16	20	20	20	16
60	7	19	20	19	15
80	0	17	19	18	12
100	2	12	18	13	9

Table 2 Average execution times of MPS-ABC, MPS-IWO, HGGA-SSR, TS-I and TS-II in seconds

Instance size (n)	Average execution time				
	TS-I	TS-II	HGGA-SSR	MPS-ABC	MPS-IWO
20	2.2	0.45	0.05	0.01	0.12
40	8.8	1.73	0.17	0.03	0.25
60	15.5	2.86	0.40	0.07	0.49
80	37.6	3.94	0.88	0.13	0.84
100	49.9	5.24	1.32	0.25	1.34

MPS-IWO returned better quality solutions in shorter time in comparison to TS-I. Out of 100 instances it solves 72 instances optimally, whereas TS-I solves 45 instances optimally. The results of MPS-IWO are inferior when compared to TS-II and HGGA-SSR methods. TS-II and HGGA-SSR respectively solve 88 and 97 instances optimally.

7 Conclusions

In this paper, we have presented two metaheuristic approaches viz. Artificial Bee Colony Algorithm and Invasive Weed Optimization Algorithm, for a multiprocessor scheduling problem where the objective is to minimize the total number of processors used. This objective is directly linked with minimizing the cost of the hardware needed for implementing a specific application. We have compared our ABC and IWO approaches with two tabu search based approaches and a hybrid steady-state grouping genetic algorithm. Our ABC approach outperformed both the tabu search based approaches in terms of solution quality as well as running time. But the ABC approach results are slightly inferior when compared to the HGGA-SSR approach. On the other hand, our IWO approach outperformed the TS-I approach in terms of solution quality as well as running time. But the IWO approach results are inferior when compared to TS-II, HGGA-SSR approaches and our own ABC approach.

We intend to improve our approaches so that they can outperform HGGA-SSR. In this regard, we plan to experiment with some new neighboring solution generation methods. We have assumed throughout this paper that tasks are independent, i.e., there are no precedence constraints among tasks. A possible future work is to extend the ABC and IWO approaches presented here to the version of the problem where there are precedence constraints among tasks.

References

1. Akay, B., Karaboga, D.: A modified artificial bee colony algorithm for real-parameter optimization. *Inf. Sci.* **192**, 120–142 (2012)
2. Basak, A., Maity, D., Das, S.: A differential invasive weed optimization algorithm for improved global numerical optimization. *Appl. Math. Comput.* **219**(12), 6645–6668 (2013)
3. Basturk, B., Karaboga, D.: An artificial bee colony (ABC) algorithm for numeric function optimization. In: *Proceeding of the IEEE Swarm Intelligence Symposium*, pp. 12–14. IEEE, Indianapolis (2006)
4. Bonabeau, E., Dorigo, M., Theraulaz, G.: *Swarm intelligence: from natural to artificial systems*. Oxford University Press, New York (1999)
5. Gajski, D.D., Dutt, N.D., Wu, A.C.-H., Lin, S.Y.-L.: *High level synthesis: Introduction to chip and system design*. Academic Publishers, Boston (1992)
6. Gao, W., Liu, S.: Improved artificial bee colony algorithm for global optimization. *Inform. Process. Lett.* **111**(17), 871–882 (2011)
7. Gao, W., Liu, S., Huang, L.: A global best artificial bee colony algorithm for global optimization. *J. Comput. Appl. Math.* **236**(11), 2741–2753 (2012)
8. Lee, J.-H., Hsu, Y.-C., Lin, Y.-L.: A new integer linear programming formulation for the scheduling problem in data path synthesis. In: *Proceedings of the 1989 IEEE International Conference on Computer-Aided Design*, pp. 20–23. IEEE Computer Society Press, New York (1989)
9. Karaboga, D.: An idea based on honey bee swarm for numerical optimization. Erciyes University, Turkey (2005)
10. Karaboga, D., Akay, B.: A modified artificial bee colony (ABC) algorithm for constrained optimization problems. *Appl. Soft Comput.* **11**, 3021–3031 (2011)
11. Karaboga, D., Basturk, B.: Artificial bee colony (ABC) optimization algorithm for solving constrained optimization problems. In: *Lecture notes in Artificial Intelligence*, vol. 4529, pp. 789–798. Springer, Berlin (2007)
12. Karaboga, D., Basturk, B.: A powerful and efficient algorithm for numeric function optimization: artificial bee colony (ABC) algorithm. *J. Global Optim.* **39**, 459–471 (2007)
13. Karaboga, D., Basturk, B.: On the performance of artificial bee colony (ABC) algorithm. *Appl. Soft Comput.* **8**, 687–697 (2008)
14. Karaboga, D., Gorkemli, B., Ozturk, C., Karaboga, N.: A comprehensive survey: artificial bee colony (ABC) algorithm and applications. *Artif. Intell. Rev.* (2012). (In Press) doi: [10.1007/s10462-012-9328-0](https://doi.org/10.1007/s10462-012-9328-0)
15. Kundu, D., Suresh, K., Ghosh, S., Das, S., Panigrahi, B.K., Das, S.: Multi-objective optimization with artificial weed colonies. *Inf. Sci.* **181**(12), 2441–2454 (2011)
16. Mehrabian, A., Lucas, C.: A novel numerical optimization algorithm inspired from weed colonization. *Ecol. Inform.* **1**(4), 355–366 (2006)
17. Pan, Q.K., Tasgetiren, M., Suganthan, P., Chua, T.: A discrete artificial bee colony algorithm for the lot-streaming flow shop scheduling problem. *Inf. Sci.* **181**, 2455–2468 (2011)
18. Rossi, A., Sevaux, M.: Mixed-integer linear programming formulation for high level synthesis. In: *Proceedings of the Eleventh International Workshop on Project Management and Scheduling*, pp. 222–226. Istanbul, Turkey (2008)

19. Roy, G.G., Chakraborty, P., Zhao, S.Z., Das, S., Suganthan, P.N.: Artificial foraging weeds for global numerical optimization over continuous spaces. In: IEEE Congress on Evolutionary Computation, pp. 1–8 (2010)
20. Roy, S., Islam, S.M., Das, S., Ghosh, S.: Multimodal optimization by artificial weed colonies enhanced with localized group search optimizers. *Appl. Soft Comput.* **13**(1), 27–46 (2013)
21. Sevaux, M., Singh, A., Rossi, A.: Tabu search for multiprocessor scheduling: application to high level synthesis. *Asia-Pac. J. Oper. Res.* **28**, 201–212 (2011)
22. Sevaux, M., Sorensen, K.: A tabu search method for high level synthesis. In: Proceedings of the Franco V/Roadef, pp. 395–396. France (2007)
23. Singh, A.: An artificial bee colony algorithm for the leaf-constrained minimum spanning tree problem. *Appl. Soft Comput.* **9**, 625–631 (2009)
24. Singh, A., Sevaux, M., Rossi, A.: A hybrid grouping genetic algorithm for multiprocessor scheduling. In: Proceedings of the Second International Conference on Contemporary Computing, vol. 40, pp. 1–7. Springer, India (2009)
25. Sundar, S., Singh, A.: A swarm intelligence approach to the quadratic minimum spanning tree problem. *Inf. Sci.* **180**, 3182–3191 (2010)
26. Sundar, S., Singh, A.: A swarm intelligence approach to the quadratic multiple knapsack problem. In: Lecture notes in Computer Science, vol. 6443, pp. 626–633. Springer, Berlin (2010)
27. Sundar, S., Singh, A.: A swarm intelligence approach to the early/tardy scheduling problem. *Swarm Evol. Comput.* **4**, 25–32 (2012)

Fuzzy Slack Based Measure of Data Envelopment Analysis: A Possibility Approach

Shivi Agarwal

Abstract Slack based measure (SBM) model of Data Envelopment Analysis (DEA) is very effective to evaluate the relative efficiency of decision making units (DMUs). It deals with the directly input excess and output shortfall to assess the effect of slacks on efficiency with common crisp inputs and outputs. In some cases, input and output data of DMUs can't be precisely measured, so, the uncertain theory has played an important role in DEA. In these cases, the data can be represented as linguistic variable characterized by fuzzy numbers. This paper attempts to extend the traditional DEA model to a fuzzy framework, thus proposing a fuzzy SBM DEA model based on possibility approach to deal with the efficiency measuring problem with the given fuzzy input and output data. Finally, numerical examples are presented to illustrate the proposed fuzzy SBM model. By extending to fuzzy environment, the DEA approach is made more powerful for application.

Keywords Data envelopment analysis · SBM · Efficiency · Fuzzy LPP · Possibility theory

1 Introduction

Data Envelopment Analysis (DEA) is a non-parametric method for evaluating the relative efficiency of decision making units (DMUs) such as bank branches, schools, transport sectors, hospitals, post offices etc. on the basis of multiple inputs and outputs. There exist many DEA models such as NSM [2], BCC [4], CCR [6] and SBM [17] models. The existing DEA models are usually limited to common

S. Agarwal (✉)

Department of Mathematics, BITS, Pilani 333031, Rajasthan, India
e-mail: shividma@gmail.com

crisp inputs and outputs. In some cases, input and output data of DMUs can't be precisely measured, so, the uncertain theory has played an important role in DEA. In these cases, the data can be represented as linguistic variable characterized by fuzzy sets.

Some researchers have proposed several fuzzy models to evaluate DMUs with fuzzy data [1, 3, 8–12, 14–16, 18]. This study selected a SBM model introduced by Tone [17], because this measure deals directly with the input excesses and the output shortfalls to assess the effect of slacks on efficiency of DMU concerned. This study extended the possibility approach to SBM DEA Model. Saati and Memariani [15] have also proposed SBM model with fuzzy input–output level. In their study only the most favorable or the upper bound of the efficiency was calculated.

In this paper, SBM model is extended with fuzzy environment for evaluating efficiency of DMUs with fuzzy data. The proposed model is based on the possibility approach of fuzzy SBM model. In possibility approach every constraint is considered as fuzzy event. The approach transforms fuzzy DEA models into possibility DEA models. The approach is similar to chance constrained programming method for probabilistic uncertainty problems.

The rest of the paper is organized as follows. In Sect. 2, review of SBM model for crisp data is given. The proposed SBM model with fuzzy data is described in Sect. 3. In Sect. 4, numerical illustration of fuzzy SBM model is exhibited followed by conclusions in the last.

2 SBM DEA Model with Crisp Data

Tone [17] proposed a new measure of efficiency which deals directly with the slacks. This model is known as SBM model. In order to estimate the efficiency of k th DMU, SBM model is given as

$$\begin{aligned}
 \text{Min } \tau_k &= t - \frac{1}{m} \sum_{i=1}^m \frac{S_{ik}^-}{x_{ik}} \\
 &\text{subject to} \\
 t + \frac{1}{s} \sum_{r=1}^s \frac{S_{rk}^+}{y_{rk}} &= 1 \\
 \sum_{j=1}^n \lambda_{jk} y_{rj} - S_{rk}^+ &= t y_{rk} \quad \forall r = 1, \dots, s \\
 \sum_{j=1}^n \lambda_{jk} x_{ij} + S_{ik}^- &= t x_{ik} \quad \forall i = 1, \dots, m \\
 t > 0, \lambda_{jk} &\geq 0 \quad \forall j = 1, \dots, n
 \end{aligned} \tag{1}$$

$$S_{rk}^+, S_{ik}^- \geq 0 ; r = 1, \dots, s, \quad i = 1, \dots, m$$

where y_{rk} = the amount of the r^{th} output produced by the k^{th} DMU, x_{ik} = the amount of the i^{th} input used by the k^{th} DMU, n = number of DMUs; s = number of outputs; m = number of inputs. S_{rk}^+ = slack in the r^{th} output of the k^{th} DMU, S_{ik}^- = slack in the i^{th} input of the k^{th} DMU, λ_{jk} 's = intensity variables.

Let an optimal solution of (1) be $(\tau_k^*, t_k^*, A^*, S^{-*}, S^{+*})$.

The interpretation of the results of the model (1) can be summarized as follows:

- The DMU under reference is said to be Pareto efficient if all slacks are zero i.e. S_{rk}^{+*} and $S_{ik}^{-*} = 0$ for every r and i which is equivalent to $\tau_k^* = 1$.
- The non-zero slacks and (or) $\tau_k^* \leq 1$ identify the sources and amount of any inefficiency that may exist in the DMU $_k$.

3 SBM DEA Model with Fuzzy Data

In a set of DMUs, suppose that the inputs \tilde{X}_{ij} and outputs \tilde{Y}_{rj} are approximately known and can be represented by convex, normal fuzzy sets. Thus, fuzzy SBM model is as follows

$$\begin{aligned}
 \text{Min } \tilde{\tau}_k &= t - \frac{1}{m} \sum_{i=1}^m \frac{S_{ik}^-}{\tilde{X}_{ik}} \\
 &\text{subject to} \\
 t + \frac{1}{s} \sum_{r=1}^s \frac{S_{rk}^+}{\tilde{Y}_{rk}} &= 1 \tag{2} \\
 \sum_{j=1}^n \lambda_{jk} \tilde{Y}_{rj} - S_{rk}^+ &= t \tilde{Y}_{rk} \quad \forall r = 1, \dots, s \\
 \sum_{j=1}^n \lambda_{jk} \tilde{X}_{ij} + S_{ik}^- &= t \tilde{X}_{ik} \quad \forall i = 1, \dots, m \\
 t > 0, \lambda_{jk} &\geq 0 \quad \forall j = 1, \dots, n \\
 S_{rk}^+, S_{ik}^- &\geq 0 ; r = 1, \dots, s, \quad i = 1, \dots, m
 \end{aligned}$$

This study used the concept of possibility of fuzzy events and chance-constrained programming (CCP) to solve the fuzzy linear programming model i.e., fuzzy SBM DEA model. Possibility theory was proposed by Zadeh [19] followed by Dubois and Prade [7]. He defined the concept of “fuzzy variable”, associated with a possibility distribution. In the fuzzy linear programming model, each fuzzy coefficient can be considered as a fuzzy variable and each constraint can be considered to be a fuzzy event. Charnes and Cooper [5], introduced the concept of CCP, which deals with uncertainty by specifying the desired levels of confidence

with which the constraints hold. This concept was extended by Liu [13]. The fuzzy SBM DEA model becomes the following possibility SBM DEA model with the concept of possibility and CCP.

$$\begin{aligned} & \text{Min } \tilde{v}_k = f_k \\ & \text{subject to} \end{aligned} \tag{3}$$

$$\pi \left(t - \frac{1}{m} \sum_{i=1}^m \frac{S_{ik}^-}{\tilde{X}_{ik}} \leq f_k \right) \geq \beta$$

$$\pi \left(t + \frac{1}{s} \sum_{r=1}^s \frac{S_{rk}^+}{\tilde{Y}_{rk}} = 1 \right) \geq \alpha_0 \tag{4}$$

$$\pi \left(\sum_{j=1}^n \lambda_{jk} \tilde{Y}_{rj} - S_{rk}^+ = t \tilde{Y}_{rk} \right) \geq \alpha_{1r} \quad \forall r = 1, \dots, s \tag{5}$$

$$\pi \left(\sum_{j=1}^n \lambda_{jk} \tilde{X}_{ij} + S_{ik}^- = t \tilde{X}_{ik} \right) \geq \alpha_{2i} \quad \forall i = 1, \dots, m \tag{6}$$

$$t > 0, \lambda_{jk} \geq 0 \quad = 1, \dots, n$$

$$S_{rk}^+, S_{ik}^- \geq 0; r = 1, \dots, s, i = 1, \dots, m$$

where $\beta, \alpha_0, \alpha_{1r} (r = 1, \dots, s)$ and $\alpha_{2i} (i = 1, \dots, m) \in [0, 1]$ are pre-specified acceptable levels of possibility for constraints (3), (4), (5) and (6), respectively. The interpretation of the model is that the objective value f_k should be the maximum value that the return function $\left(t - \frac{1}{m} \sum_{i=1}^m \frac{S_{ik}^-}{\tilde{X}_{ik}} \right)$ can achieve with ‘‘possibility’’ level β or higher, subject to the possibility levels of constraints (4), (5) and (6) being at least $\alpha_0, \alpha_{1r} (r = 1, \dots, s)$ and $\alpha_{2i} (i = 1, \dots, m)$ respectively. The model can be solved by applying the lemma given by Lertworasirikul et al. [11]. According to lemma, let $\tilde{a}_1, \tilde{a}_2, \dots, \tilde{a}_n$ be fuzzy numbers and let $(\cdot)_{\alpha_1}^L$ and $(\cdot)_{\alpha_1}^U$ denote the lower and upper bounds of the α level set of $\tilde{a}_i, i = 1, \dots, n$, respectively. Then for any given possibility levels α_1, α_2 and $\alpha_3 \in [0, 1]$.

- (i) $\pi(\tilde{a}_1 + \tilde{a}_2 + \dots + \tilde{a}_n \leq b) \geq \alpha_1$ if and only if $(\tilde{a}_1)_{\alpha_1}^L + \dots + (\tilde{a}_n)_{\alpha_1}^L \leq b$
- (ii) $\pi(\tilde{a}_1 + \tilde{a}_2 + \dots + \tilde{a}_n \geq b) \geq \alpha_2$ if and only if $(\tilde{a}_1)_{\alpha_2}^U + \dots + (\tilde{a}_n)_{\alpha_2}^U \geq b$
- (iii) $\pi(\tilde{a}_1 + \tilde{a}_2 + \dots + \tilde{a}_n = b) \geq \alpha_3$ if and only if $(\tilde{a}_1)_{\alpha_3}^L + \dots + (\tilde{a}_n)_{\alpha_3}^L \leq b$
and $(\tilde{a}_1)_{\alpha_3}^U + \dots + (\tilde{a}_n)_{\alpha_3}^U \geq b$

When fuzzy inputs and fuzzy outputs are trapezoidal fuzzy numbers, then the possibility fuzzy SBM DEA model become the following linear programming model by using the concept given by Liu [13] and the above lemma given by Lertworasirikul et al. [11].

$$\begin{aligned}
 & \text{Min } \tilde{\tau}_k = f_k \\
 & \text{subject to} \\
 & \left(t - \frac{1}{m} \sum_{i=1}^m \frac{S_{ik}^-}{\tilde{X}_{ik}} \right)_{\beta}^L \leq f_k \tag{7}
 \end{aligned}$$

$$\left(t + \frac{1}{s} \sum_{r=1}^s \frac{S_{rk}^+}{\tilde{Y}_{rk}} \right)_{\alpha_0}^L \leq 1 \tag{8}$$

$$\left(t + \frac{1}{s} \sum_{r=1}^s \frac{S_{rk}^+}{\tilde{Y}_{rk}} \right)_{\alpha_0}^U \geq 1 \tag{9}$$

$$\left(\sum_{j=1}^n \lambda_{jk} \tilde{Y}_{rj} - S_{rk}^+ - t \tilde{Y}_{rk} \right)_{\alpha_{1r}}^L \leq 0 \quad \forall r = 1, \dots, s \tag{10}$$

$$\left(\sum_{j=1}^n \lambda_{jk} \tilde{Y}_{rj} - S_{rk}^+ - t \tilde{Y}_{rk} \right)_{\alpha_{1r}}^U \geq 0 \quad \forall r = 1, \dots, s \tag{11}$$

$$\left(\sum_{j=1}^n \lambda_{jk} \tilde{X}_{ij} + S_{ik}^- - t \tilde{X}_{ik} \right)_{\alpha_{2i}}^L \leq 0 \quad \forall i = 1, \dots, m \tag{12}$$

$$\left(\sum_{j=1}^n \lambda_{jk} \tilde{X}_{ij} + S_{ik}^- - t \tilde{X}_{ik} \right)_{\alpha_{2i}}^L \leq 0 \quad \forall i = 1, \dots, m \tag{13}$$

$$\begin{aligned}
 & t > 0, \lambda_{jk} > 0 \quad \forall j = 1, \dots, n \\
 & S_{rk}^+, S_{ik}^- \geq 0; r = 1, \dots, s, i = 1, \dots, m
 \end{aligned}$$

The fuzzy SBM DEA model is become crisp linear programming problem which can be solved by any software related to LPP. According to Lertworasirikul et al. [11]. DMU k is α -possibilistic efficient if f_k value at the α possibility level is greater than or equal to one; otherwise, it is α -possibilistic inefficient. Where α be the set of $\beta, \alpha_0, \alpha_{1r} (r = 1, \dots, s)$ and $\alpha_{2i} (i = 1, \dots, m)$. However, to make a reasonable efficiency comparison of DMUs, the possibility levels of constraints (α) for these DMUs should be set at the same possibility level.

Table 1 Input and output data of five DMUs

DMU	A	B	C	D	E
Input 1	(3.5,4,4.5)	(2.9,2.9,2.9)	(4.4,4.9,5.4)	(3.4,4.1,4.8)	(5.9,6.5,7.1)
Input 2	(1.9,2.1,2.3)	(1.4,1.5,1.6)	(2.2,2.6,3.0)	(2.2,2.3,2.4)	(3.6,4.1,4.6)
Output 1	(2.4,2.6,2.8)	(2.2,2.2,2.2)	(2.7,3.2,3.7)	(2.5,2.9,3.3)	(4.4,5.1,5.8)
Output 2	(3.8,4.1,4.4)	(3.3,3.5,3.7)	(4.3,5.1,5.9)	(5.5,5.7,5.9)	(6.5,7.4,8.3)

Source Guo and Tanaka [8]

Table 2 Efficiency scores of five DMUs

Possibility level	DMU A	DMU B	DMU C	DMU D	DMU E
0	1.00	1.00	1.00	1.00	1.00
0.25	1.00	1.00	1.00	1.00	1.00
0.50	1.00	1.00	1.00	1.00	1.00
0.75	1.00	1.00	1.00	1.00	1.00
1.0	0.697	1.00	0.705	1.00	1.00

4 Numerical Illustration

To illustrate the proposed fuzzy SBM DEA model, consider the data taken by Guo and Tanaka [8]. Data consists of five DMUs with two inputs and two outputs which is shown in Table 1. The inputs and outputs have symmetrical triangular membership functions.

The efficiencies of all DMU are calculated by the proposed fuzzy SBM DEA model at five different possibility levels using MATLAB. Table 2 depicts the results of efficiency for five possibility levels $\alpha = \beta = \alpha_0 = \alpha_{1r} (r = 1, \dots, s) = \alpha_{2i} (i = 1, \dots, m)$ as 0, 0.25, 0.50, 0.75, 1.0.

In Table 2, the efficiency scores at the possibility level 1 indicates the efficiency that is most likely to be and at possibility level 0 indicates the maximum value of the efficiency. For example, the efficiency scores of DMU A and DMU C at possibility level 1 is 0.697 and 0.705 respectively, which indicates the DMU A and DMU C are possibilistically inefficient with possibility level 1 whereas they are possibilistically efficient with all other possibility levels. The remaining DMUs are possibilistically efficient at all possibility levels. These results are comparable with the results obtained by Lertworasirikul et al. [11], with fuzzy CCR model for the same example.

5 Conclusions

DEA has wide application to evaluate the relative efficiency of a set of DMUs using multiple inputs to produce multiple outputs. The existing DEA models are usually limited to common crisp inputs and outputs. In some cases, input and

output data of DMUs can't be precisely measured, for example, quality of service, quality of input resource, degree of satisfaction etc. So, the uncertain theory has played an important role in DEA. In these cases, the data with crisp number will not satisfy the real needs and this restriction will diminish the practical flexibility of DEA in application. Thus, the data can be represented as linguistic variable characterized by fuzzy sets. This paper attempts to extend the traditional DEA model to a fuzzy framework, thus proposing a fuzzy SBM DEA model based on possibility theory and chance-constrained programming (CCP) to deal with the efficiency measuring problem with the given fuzzy input and output data. The proposed method provides the ability to offer more objective measurement of efficiency of DMUs in vague environment. This method is efficient and effective for a large quantity of fuzzy numbers. Finally, numerical examples are presented to illustrate the proposed fuzzy SBM DEA model. The study reveals that the efficiency scores are crisp at any possibility level so the manager can rank the DMUs based on the efficiency scores at any required possibility level. Thus, the calculated efficiency measure provides the more information for management. By extending to fuzzy environment, the DEA approach is made more powerful for application.

References

1. Agarwal, S.: Efficiency measure by fuzzy data envelopment analysis model. In: *IXX International Conference: (IMST 2010–FIM XIX) on Interdisciplinary Mathematical and Statistical Techniques held at Patna University, Patna, 18–20 Dec 2010*
2. Agarwal, S., Yadav, S.P., Singh, S.P.: A new slack DEA model to estimate the impact of slacks on the efficiencies. *Int. J. Oper. Res.* **12**(3), 241–256 (2011)
3. Ammar, S., Wright, R.: Applying fuzzy set theory to performance evaluation. *Socio-Econ. Plann. Sci.* **34**, 285–302 (2000)
4. Banker, R.D., Charnes, A., Cooper, W.W.: Some models for the estimation of technical and scale inefficiencies in data envelopment analysis. *Manage. Sci.* **30**, 1078–1092 (1984)
5. Charnes, A., Cooper, W.W.: Chance-constrained programming. *Manage. Sci.* **6**, 73–79 (1959)
6. Charnes, A., Cooper, W.W., Rhodes, E.: Measuring the efficiency of decision making units. *Eur. J. Oper. Res.* **2**, 429–441 (1978)
7. Dubois, D., Prade, H.: *Possibility theory: an approach to computerized processing of uncertainty*. Plenum Press, New York (1988)
8. Guo, P., Tanaka, H.: Fuzzy DEA: a perceptual evaluation method. *Fuzzy Sets Syst.* **119**, 149–160 (2001)
9. Hougaard, J.L.: Fuzzy scores of technical efficiency. *Eur. J. Oper. Res.* **115**, 529–541 (1999)
10. Kao, C., Liu, S.T.: Fuzzy efficiency measure in data envelopment analysis. *Fuzzy Sets Syst.* **113**, 427–437 (2000)
11. Lertworasirikul, S., Fang, S., Joines, J.A., Nuttle, H.L.W.: Fuzzy data envelopment analysis (DEA): a possibility approach. *Fuzzy Sets Syst.* **139**, 379–394 (2003)
12. Lertworasirikul, S., Fang, S., Nuttle, H.L.W., Joines, J.A.: Fuzzy BCC model for data envelopment analysis. *Fuzzy Optim. Decis. Making* **2**, 337–358 (2003)
13. Liu, B.: *Uncertain programming*. Wiley-Interscience Publication, New York (1999)
14. Liu, S.T., Chuang, M.: Fuzzy efficiency measure in fuzzy DEA/AR with application to university libraries. *Fuzzy Sets Syst.* **36**(2), 1105–1113 (2009)

15. Saati, S., Memariani, A.: SBM model with fuzzy input-output levels in DEA. *Aust. J. Basic Appl. Sci.* **3**(2), 352–357 (2009)
16. Sengupta, J.K.: A fuzzy system approach in data envelopment analysis. *Comput. Math. Appl.* **24**, 259–266 (1992)
17. Tone, K.: A slack based measure of efficiency in data envelopment analysis. *Eur. J. Oper. Res.* **130**, 498–509 (2001)
18. Wen, M., Li, H.: Fuzzy data envelopment analysis (DEA): model and ranking method. *J. Comput. Appl. Math.* **223**(2), 872–878 (2009)
19. Zadeh, L.A.: Fuzzy sets as a basis for a theory of possibility. *Fuzzy Sets Syst.* **1**, 3–28 (1978)

Application of Ant Algorithm Variants to Single Track Railway Scheduling Problem

G. S. Raghavendra and N. Prasanna Kumar

Abstract This paper proposes the methodology to solve the railway time tabling problem using the ant algorithm variants. The aim of the paper is to arrive at the conflict free schedules for the set of trains, considering all the operational constraints. A well defined model is used to solve the scheduling problem on single line track with few parallel lines occurring at frequent periods for crossing purpose. The model makes a realistic assumptions that set of trains will be scheduled in a zone that covers set of cities and scheduling is optimized with respect to number of conflicts. The paper investigates the performance by simulation considering realistic parameter values for both Ant Colony Optimization (ACO) and train scheduling problem. Finally, conclusion is drawn by comparing with other ants algorithm variants.

Keywords Ant · Conflict · Railway · Schedules · Train

1 Introduction

The train timetable generation is a challenging task. Traditionally, timetable is generated manually by trial and error method based on experience and information. The advent of computer aided tools have helped the planner to come up with the effective timetable [1, 2] and effectiveness can be accessed in terms of robustness in routing [3], revenue profitability etc. The aim of the train scheduling problem is to come with the ideal timetable that satisfies several objectives and imposed constraints. The objectives can be maximizing the number of passengers,

G. S. Raghavendra · N. Prasanna Kumar (✉)
BITS Pilani K. K. Birla Goa Campus, Zuarinagar, Goa, India
e-mail: prasannak@goa.bits-pilani.ac.in

G. S. Raghavendra
e-mail: gsr@goa.bits-pilani.ac.in

minimizing the number of conflicts, waiting time of the passengers, revenue maximization and so on. Hence, scheduling is a multi-objective optimization problem. In addition, timetable needs to satisfy the set of constraints that can be grouped into three categories [4] namely *User Requirements*, *Traffic Constraints* and *Infrastructure Constraints*. It is possible to deduce many more constraints to reflect the realistic railway schedules. The scope of this work is to apply the punished ACO [5] and Dynamic Ants Systems [6] variant to train scheduling problem and compare the results with the basic ant variants.

2 Literature Review

2.1 Railway Scheduling

The Rail transportation planning provides rich number of problems that can be modeled and solved using optimization techniques. The problems can be classified into two groups [7] namely Train Routing Problem and Train Scheduling Problem. These problems itself contains a lot of sub-problems and mathematical models can be developed to tackle each of these problems. Several optimization techniques like mathematical programming, mixed integer linear programming, branch and bound have been used to solve the train problems. Although they were able to provide consistently good solutions, but need large memory space and time to compute the solution. Heuristics techniques were employed to obtain results in reasonable amount of time. These techniques use the domain knowledge of the problem to arrive at the solution. Cai and Goh [8] used the greedy heuristic approach to resolve the conflicts. The set of rules were devised to resolve the conflicts in a best way. The results obtained using heuristics often deviates more from the optimal solution. Kraay et al. [9] proposed a heuristics based on Local Heuristics Search (LSH), that tries to resolve the conflicts by looking into previous schedules. The LSH technique replace the existing solution with the better solution by searching in the neighborhood region. The train conflicts that happen at sidings will be shifted by one position and solution is accepted, if it results in minimum conflict delay. Higgins et al. [10] proposed a methodology that combines LSH and tabu search to shift more than one conflicts at a time to have a reduced total conflict delay. Kwan and Mistry [11] used the co-evolutionary approach to generate the automatic timetable. Tormos et al. [12] used genetic algorithms to solve the train timetable problem. The chromosomes were encoded using the activity list representation and genes are represented with sequence of (train, section) pairs. The genes were organized to satisfy the operational constraints. The problem involves generating a population of chromosomes that satisfy the operational constraints and selecting the best chromosome that results in minimum conflict delay.

2.2 Ant Colony Optimization

In recent years there has been splurge in the algorithms that belongs to a meta-heuristic class. One such algorithm is ACO, a nature inspired population based algorithm fascinated by the foraging behavior of the ants. The tiny creature ants, which are almost blind can establish the shortest path from nest to the food source. The food hunting activity provides the formal framework to solve the combinatorial optimization. Ants are guided by the chemical substance called pheromone trail, which is laid by them during their journey. The pheromone trail has a crucial role to play in ACO framework by acting as an indirect medium of communication between the ants to share their journey experience. This indirect mechanism helps the ants to establish the shortest path between food source and the nest. The pheromone trail is a volatile substance, it evaporates over the period of time and this mechanism helps to forget the bad experiences of the journey. The first algorithmic framework that captures the essence of ant activity was given by Dorigo [13]. Ant algorithms combine the greedy mechanism and heuristic information to arrive at the optimal solution. In literature, several variants of algorithm [14–16] have been proposed and each of them tries to balance the exploration of new solutions and the exploitation of good solutions in the search space. ACO algorithms have been successfully applied to other problems like Telecommunication Networks [17], Graph Coloring [18] to name a few.

3 A Model for Train Scheduling Problem

The paper [4] provides the general definition, notations and the input requirements of the model. A model is described by objective functions and the constraints that are supposed to be satisfied. The objective function is to minimize the total conflict delay that arises due to unavoidable sidings.

$$Min_{cd} = \sum_{i \in T} \sum_{k \in DL} A_k^{t_i} - D_k^{t_i} \quad (1)$$

subject to **Constraint** satisfaction like **Line time constraints, Headway constraints, Train Dispatch constraint and Stop time Constraints.**

4 Punished Ants and Performance Linked Ant System

Raghavendra et al. [5, 6] proposed the incorporation of punishment mechanism and Dynamic ants selection mechanism to two versions of ant systems namely Elitist ant and Rank ant. This paper extends the application of these algorithms to the ACO framework to train scheduling problem proposed by [4]. The intention

behind the punishment mechanism is to favor exploitation process in the search space by removing pheromone trial on non elite paths. The quantity of pheromone to be removed will be specified by the algorithmic specification. The algorithmic specification for EA specifies to decrease the quantity of pheromone trial proportional to the solution quality found on non elite paths and in case of RA, all the non elite paths are weighted according to their performances and accordingly decreased. The punishment feature for EA and RA is given by the equation:

$$\tau_{t_i t_j} = \tau_{t_i t_j} - \Delta\tau_{t_i t_j}^* \tag{2}$$

where $\Delta\tau_{t_i t_j}^*$ is

$$\Delta\tau_{t_i t_j}^* = \sum_{k=1}^l \Delta\tau_{t_i t_j}^k$$

where $\Delta\tau_{t_i t_j}^k$ in case of EA is given by the equation:

$$\Delta\tau_{t_i t_j}^k = \begin{cases} Q^*/L_k & \text{if } (t_i, t_j) \in \text{k-th ant's non performing tour list} \\ 0 & \text{otherwise.} \end{cases}$$

The $\Delta\tau_{t_i t_j}^k$ in case of RA is given by the equation:

$$\Delta\tau_{t_i t_j}^k = \begin{cases} Q^* \cdot (l - k)/L_k & \text{if } (t_i, t_j)\text{-th ant's non performing tour list} \\ 0 & \text{otherwise} \end{cases}$$

where Q^* is the algorithmic constant. If m and e represent the number of ants and elite ants respectively, then l represents the non-elite ants given by the expression $l = m - e$.

The algorithms here on-wards will be termed as Punished Elitist Ant System (PEAS) and Punished Rank Ant System (PRAS) due to punishment mechanism incorporation.

Similarly, dynamic ant selection mechanism will place all the performing ants into one class and non-performing ants into another class based on statistical function. The following statistical functions were used; Mid-range, mean and median. Mid-range function computes the value by considering the best and worst TCT values. Similarly mean and median values are computed using all the TCT in a given iteration. Suppose, if mean function is used for classification then tour performances lesser than mean will be in performing class and rest of the ants in non-performing class. The performing ants get chance for additional reinforcement according to the following equation:

$$\tau_{t_i t_j} = \tau_{t_i t_j} + \Delta\tau_{t_i t_j}^* \tag{3}$$

where $\Delta\tau_{t_i t_j}^*$ is

$$\Delta\tau_{t_i t_j}^* = \sum_{k=1}^l \Delta\tau_{t_i t_j}^k$$

where $\Delta\tau_{t_i t_j}^k$ in case of EA is given by the equation:

$$\Delta\tau_{t_i t_j}^k = \begin{cases} Q^*/L_k & \text{if } (t_i, t_j) \in \text{k-th ant's performing tour list} \\ 0 & \text{otherwise.} \end{cases}$$

The $\Delta\tau_{t_i t_j}^k$ in case of RA is given by the equation:

$$\Delta\tau_{t_i t_j}^k = \begin{cases} Q^* \cdot (e - k)/L_k & \text{if } (t_i, t_j) \in \text{k-th ant's performing tour list} \\ 0 & \text{otherwise.} \end{cases}$$

Since the number of selected ants varies across the iteration, we will name them as *Dynamic Ants*(DA). The proposed algorithms here on-wards are named as *Dynamic Elitist Ants* (DEA) and *Dynamic Rank Ants* (DRA) due to incorporation of DA in EA and RA. The integration of proposed algorithms and statistical tool results in several variant of ant algorithms Dynamic Elitist Ant—Mid-Range (DEAMR), Dynamic Elitist Ant—Mean (DEAM), Dynamic Elitist Ant—Median (DEAMed), Dynamic Rank Ant—Mid-Range (DRAMR), Dynamic Rank Ant—Mean(DRAM) and Dynamic Rank Ant—Median (DRAMed).

The dynamic elitism was extended by incorporating punishment feature. The algorithmic specification for pheromone removal is same as Eq. 2. The incorporation of punishment mechanism results in Punished Dynamic Elitist Ant—Mid-Range (DEAMR), Punished Dynamic Elitist Ant—Mean (DEAM), Punished Dynamic Elitist Ant—Median (DEAMed), Punished Dynamic Rank Ant—Mid-Range (DRAMR), Punished Dynamic Rank Ant—Mean (DRAM) and Punished Dynamic Rank Ant—Median (DRAMed). It should be noted that the composition of elite and non-elite ants varies in this system.

5 Experimental Study

5.1 Parameter Settings and Input to the Algorithm

The proposed model was extensively simulated to identify the schedule that has minimal conflict delay. The parameters relevant to ACO and train scheduling problem were varied for simulation as mentioned in paper [4].

Table 1 Comparative analysis of train scheduling problem for Punished Ants, Dynamic Ants System and Punished Dynamic Ants System

Algorithms	Fixed commercial waiting time		Variable commercial waiting time	
	pml = 2		pml = 2	
	TCT	Parameter details	TCT	Parameter details
PEAS	788	$\alpha = 4 \beta = 3 \rho = 0.85$	1372	$\alpha = 4 \beta = 4 \rho = 0.9$
PRAS	792	$\alpha = 1 \beta = 3 \rho = 0.95$	1366	$\alpha = 5 \beta = 1 \rho = 0.8$
DEASMR	793	$\alpha = 3 \beta = 1 \rho = 0.75$	1376	$\alpha = 5 \beta = 1 \rho = 0.75$
DEASM	794	$\alpha = 4 \beta = 1 \rho = 0.75$	1371	$\alpha = 5 \beta = 1 \rho = 0.95$
DEASMed	783	$\alpha = 5 \beta = 1 \rho = 0.70$	1393	$\alpha = 4 \beta = 1 \rho = 0.95$
DRASMR	776	$\alpha = 5 \beta = 1 \rho = 0.8$	1376	$\alpha = 4 \beta = 3 \rho = 0.7$
DRASM	770	$\alpha = 3 \beta = 1 \rho = 0.7$	1372	$\alpha = 5 \beta = 4 \rho = 0.7$
DRASMed	776	$\alpha = 5 \beta = 1 \rho = 0.8$	1376	$\alpha = 4 \beta = 3 \rho = 0.7$
PDEASMR	800	$\alpha = 5 \beta = 3 \rho = 0.75$	1361	$\alpha = 4 \beta = 2 \rho = 0.7$
PDEASM	792	$\alpha = 4 \beta = 1 \rho = 0.95$	1366	$\alpha = 4 \beta = 3 \rho = 0.85$
PDEASMed	800	$\alpha = 5 \beta = 3 \rho = 0.75$	1361	$\alpha = 4 \beta = 2 \rho = 0.7$
PDRASMR	805	$\alpha = 5 \beta = 5 \rho = 0.85$	1363	$\alpha = 2 \beta = 1 \rho = 0.75$
PDRASM	777	$\alpha = 5 \beta = 1 \rho = 0.85$	1360	$\alpha = 3 \beta = 4 \rho = 0.90$
PDRASMed	793	$\alpha = 5 \beta = 1 \rho = 0.75$	1368	$\alpha = 5 \beta = 1 \rho = 0.85$

5.2 Comparative Analysis

The Table 1 shows the comparative analysis for Punished Ants, Dynamic Ants and Punished Dynamic Ants. The assessment was done with respect to TCT and better schedule order will have a smaller TCT. The Table 1 reports the TCT and the corresponding parameters values, when extra line is available for sidings (pml = 2). A detailed analysis is carried for Fixed Commercial Waiting Time and Variable Commercial Waiting Time. The best results along with parameter value are highlighted. In Punished ant system, PEAS provides the best TCT value and its performance is at par with basic ant variants (see [4] for pml = 2). Similarly, in DEAS and PDEAS class, DRASM and PDRASM provide the best TCT value with decrease in waiting time of 1.66 and 0.70 % respectively, when compared with the basic ant variants. Another interesting observation is that punishment mechanism hasn't improved the performance of DA selection mechanism and shows an overall increase in waiting time of 0.90 %. In general, it can be observed that punished and dynamic ant variants provide improved TCT values than the basic ant variants. Similar observation can be made on Variable Commercial Waiting Time. The performance of PRAS in punished ant system class is slightly better than that of basic variants (see [4] pml = 2) with decrease in waiting time of 0.43 %. Similarly, DEASM and PDRASM in DEAS and PDEAS class show an improvement with decreased waiting for time of 0.07 and 0.87 % respectively. However, among the proposed approaches PDRASM shows an improvement of 0.43 % over PRAS and 0.80 % over DEASM in terms of best results.

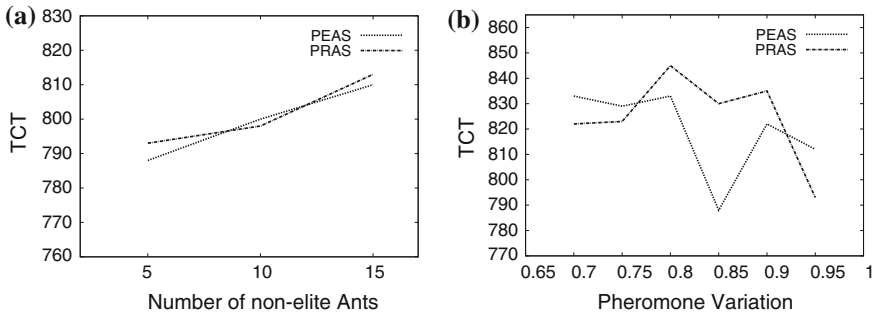


Fig. 1 Performance comparison of Punished Ant Systems for fixed commercial waiting time. **a** Variation in number of Ants. **b** Variation in Pheromone trials quantity

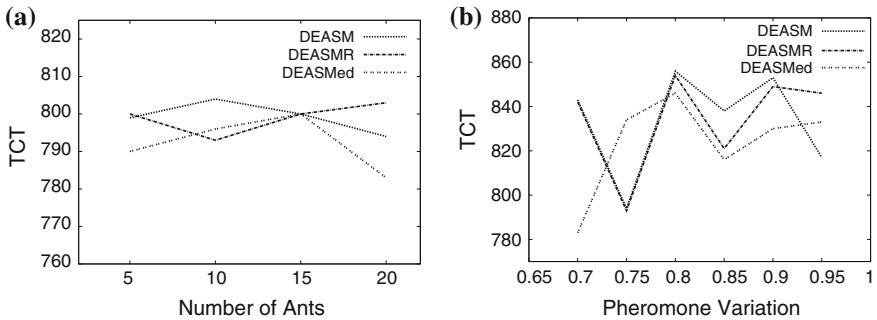


Fig. 2 Performance comparison of Dynamic Elitist Ant Systems for fixed commercial waiting time. **a** Variation in number of Ants. **b** Variation in Pheromone trials quantity

5.3 Performance Analysis

Figure 1 reveals the performance of the ants for Punished Ant Systems. Figure 1a reveals that both the PEAS and PRAS variants provide the best waiting time for smaller number of non-elite ants population *nea* size of 5. It can be observed that, waiting time increased with the increase in the number of punished ants indicating the negative effect of larger punished ants. Figure 1b shows the comparative analysis of algorithms for different trial strength. The figure reveals that PEAS variant provides better waiting time for higher trail strength than the lower trial strength and least waiting time is observed for $\rho = 0.85$. Similarly, for PRAS variant, trains experience more conflicts leading to longer waiting time for ρ setting in the range of $0.8 < \rho < 0.9$ and provides better TCT values for $\rho = 0.95$.

Figure 2 shows the comparative performance of DEAS for train scheduling problem. One of the interesting observations that can be made from Fig. 2a is that, DEASM, DEASMR and DEASMed have similar waiting times for $n = 15$. The DEASM, DEASMR and DEASMed provide least waiting time, when the number

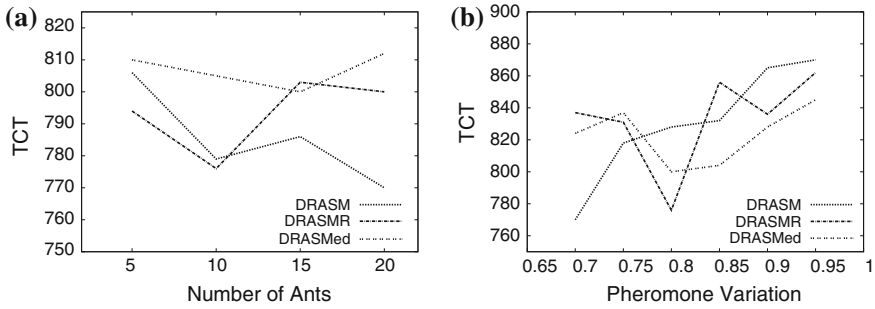


Fig. 3 Performance comparison of Dynamic Rank Ant Systems for fixed commercial waiting time. **a** Variation in number of Ants. **b** Variation in Pheromone trials quantity

of ants settings n is 20, 10, 20 respectively. Figure 2b shows the performance of DEAS algorithms for varying pheromone trial. The variants exhibit larger deviation in the observed waiting time for lower pheromone trial compared to the higher pheromone trial and provide least waiting time for ρ in the range of 0.7–0.75 for all the variants.

Figure 3 reveals the comparative analysis of DRAS variants. It can be observed from Fig. 3a that waiting time of DRASMed is comparatively longer than the DRASMR and DRASM for varying number of ants. It is interesting to see that DRASMR has a better waiting time for smaller ant population and DRASM for larger ant population. The DRASM, DRASMR and DRASMed provide least waiting time for ants population size of 20, 10 and 15 respectively. Figure 3b shows that conflict among the trains increases rapidly for DRASM variant compared to other variants with the increase in trial strength. In general, it can be concluded that higher pheromone persistence factor increases the waiting time of trains for all the variants.

Figure 4 shows the performance of PDEAS variants, when applied to train scheduling problem. Figure 4a shows that PDEASM has least sensitiveness in waiting time variation compared to the other variants for varying ants population. The PDEASMR variant has comparatively longer waiting time than the other variants. The PDEASM, PDEASMR and PDEASMed provide minimal waiting time, when number of ants n was set to 20, 10, 15 respectively. Figure 4b shows that PDEASMR is sensitive to the varying pheromone trial. The waiting time increased rapidly with the increase in the pheromone strength. The PDEASM variant is comparatively insensitive to the varying trial strength compared to its other peer variants. The PDEASM, PDEASMR and PDEASMed provide optimal waiting time, when trail strength ρ was 0.95, 0.75 and 0.85 respectively.

Figure 5 shows the comparative analysis of PDRAS variant. Figure 5a reveals that PDRASM provides the smallest waiting time for most of the varying size of ants population. The PDRASM and PDRASMR variants deliver best waiting time

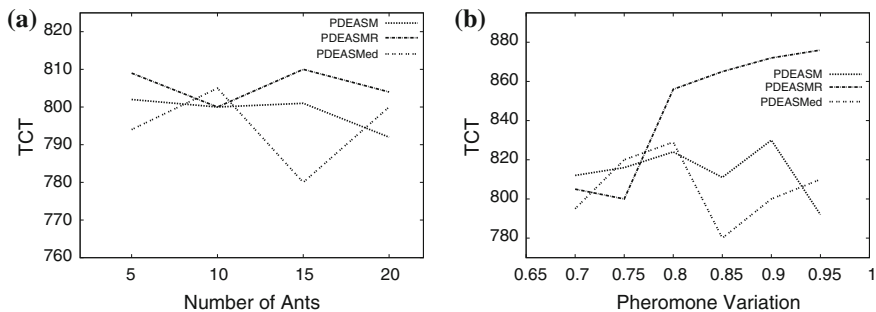


Fig. 4 Performance comparison of Punished Dynamic Elitist Ant Systems for fixed commercial waiting time. **a** Variation in number of Ants. **b** Variation in Pheromone trials quantity

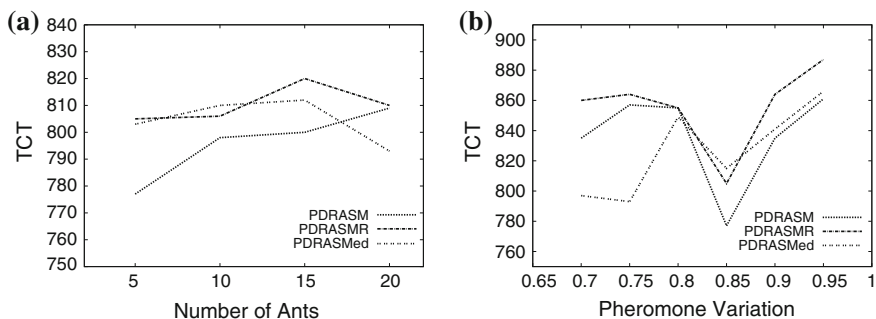


Fig. 5 Performance comparison of Punished Dynamic Rank Ant Systems for fixed commercial waiting time. **a** Variation in number of Ants. **b** Variation in Pheromone trials quantity

for smaller ant population size n of 5 and 10 respectively. Similarly, PDRASMed provides least waiting time for larger population of size 20. Similarly, Fig. 5b reveals that, algorithms exhibit most of the time a similar trend in the variation of waiting time for the varying pheromone trial strength. The PDRASM, PDRASMR and PDRASMed provide least waiting time for trail strength ρ of 0.85, 0.85 and 0.75 respectively.

Figure 6 displays the performance of punished ant systems for the variable commercial waiting time. Figure 6a reveals that observed TCT values of PRAS is slightly better than PEAS variant. The PRAS variant has the best TCT value for non-elite ant’s population nea of size 5. However, same waiting time is observed for the higher number of non-elite ants population. Similarly, Fig. 6 reveals that PRAS has comparatively shorter waiting time than PEAS for varying trial strength. The PEAS variant has the least waiting time for trial strength $\rho = 0.9$ and PRAS for $\rho = 0.8$.

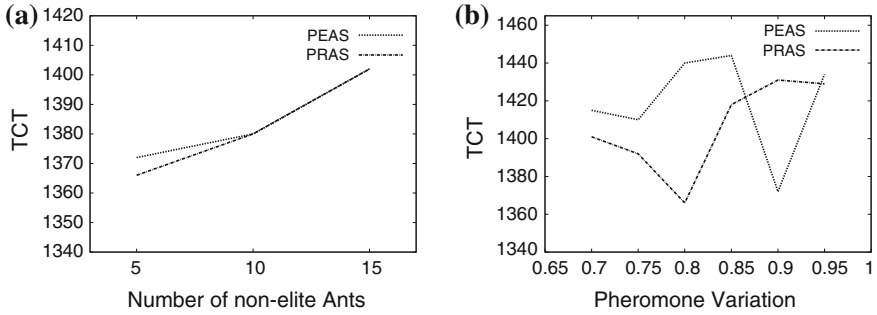


Fig. 6 Performance comparison of Punished Ant Systems for variable commercial waiting time. **a** Variation in number of Ants. **b** Variation in Pheromone trials quantity

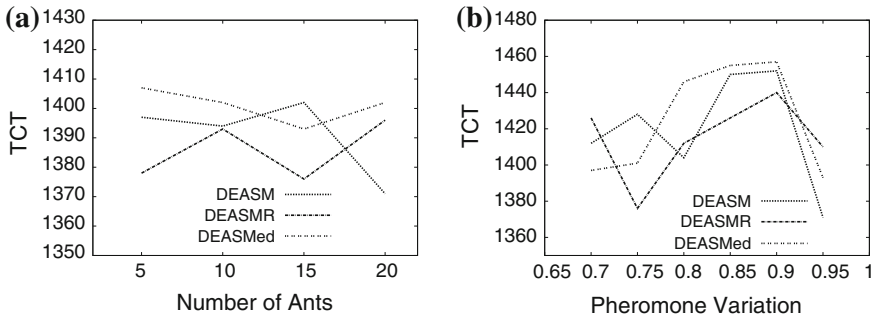


Fig. 7 Performance comparison of Dynamic Elitist Ant Systems for variable commercial waiting time. **a** Variation in number of Ants. **b** Variation in Pheromone trials quantity

Figure 7 displays the performance of DEAS for the variable commercial waiting time. Figure 7a shows that DEASMed variant provides sub-optimal TCT values compared to other variants for varying ant’s diversity. Figure 7b reveals some interesting patterns for the varying trial strength. In general, all the variants show increase in waiting time for the higher pheromone persistence factor and shows sharp decrease in waiting time for $\rho = 0.95$.

Figure 8 depicts the behavior of DRAS class for train scheduling problem. Figure 8a reveals an interesting behavior of DRASMR variant, which reacts sharply to the varying ants population. However, DRASM and DRASMed variants report lesser volatility in waiting time for varying ants population. The trend analysis of Fig. 8b reveals an increase in waiting time with the increase in pheromone persistence factor for DRASM and DRASMed variants and all the variants provide shorter waiting time for trial settings ρ in the range of 0.7–0.75.

Figure 9 shows the behavior of PDEAS for the varying parameters. Figure 9a reveals that all the variants have nearby waiting times for smaller and higher number of ant’s population n of size 5 and 20 respectively. However, shorter

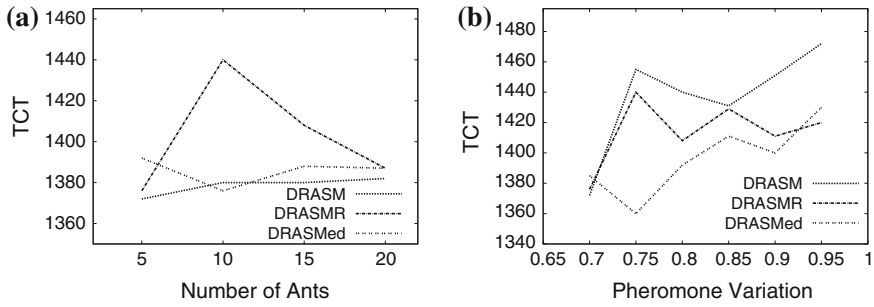


Fig. 8 Performance comparison of Dynamic Rank Ant Systems for variable commercial waiting time. **a** Variation in number of Ants. **b** Variation in Pheromone trials quantity

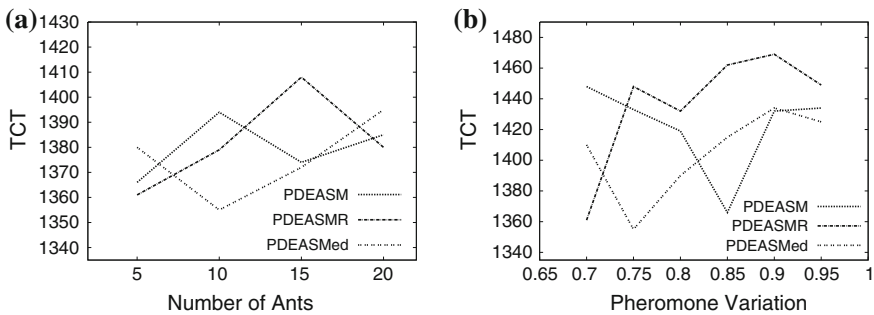


Fig. 9 Performance comparison of Punished Dynamic Elitist Ant Systems for variable commercial waiting time. **a** Variation in number of Ants. **b** Variation in Pheromone trials quantity

waiting times were observed for ants population size in the range of 5–10. Similarly, PDEASMR reacts sharply with an increase in waiting time, as the number of ants in the system increases. The higher concentration of pheromone trial has a bad effect on PDEASMR variant and waiting time increases with the increase in the pheromone persistence factor as seen from Fig. 9b. The shorter waiting time observed for varying ρ and for all the variants it is in the range of $0.7 \leq \rho \leq 0.85$.

Figure 10 shows the performance of PDRAS class for parameter settings pertaining to ACO algorithm. Figure 10a reveals that PDRASM variant has consistently delivered larger TCT values compared to other variants for varying ants population. Similarly, Fig. 10b shows larger fluctuation in waiting times for all the variants indicating their sensitiveness to the pheromone trial strength.

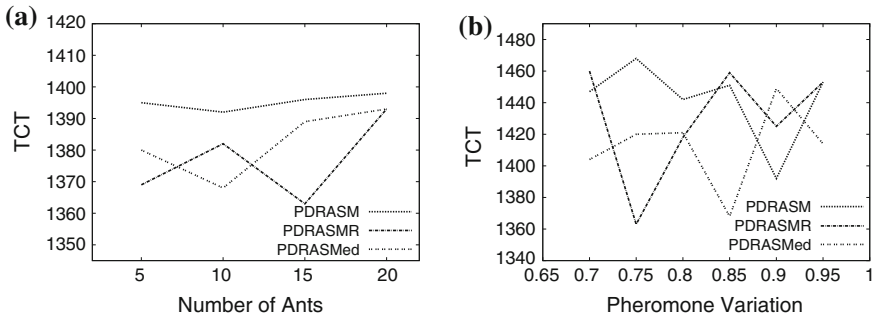


Fig. 10 Performance comparison of Punished Dynamic Rank Ant Systems for variable commercial waiting time. **a** Variation in number of Ants. **b** Variation in Pheromone trials quantity

6 Conclusion and Future Direction

In this paper, we have applied ACO variants to a well defined ACO model for solving the train scheduling problem. The model can be made more realistic by adding few more constraints like specifying the time bound for the departure of a train to a particular destination, scheduling different type of trains that travels with different speed etc. to name few. The future direction includes extending the model for multi track scheduling, incorporation of local search to improve the solution and compare the performance with other variants of ant algorithm.

References

1. Caprara, A.M., Kroon, L.G., Monaci, M., Peeters, M., Toth, P.: Passenger railway optimization. *Transp. Sci. (Elsevier)* **14**, 129–187 (2007)
2. Kroon, L., Huisman, D., Abbink, E., Fioole, P., Fischetti, M., Maroti, G., Schrijver, A., Steenbeek, A., Ybema, R.: The new Dutch timetable: the OR revolution. *Interfaces* **39**(1), 6–17 (2009)
3. Zwaneveld, P.J., Kroon, L.G., van Hoesel, S.P.M.: Routing trains through a railway station based on a node packing model. *Eur. J. Oper. Res.* **128**, 14–33 (2001)
4. Raghavendra, G.S., Prasanna Kumar, N.: An ACO framework for Single Track Railway Scheduling Problem. In: *Proceedings of Seventh International Conference on Bio-Inspired Computation: Theories and Applications. Advances in Intelligent System and Computing (AISC)*, vol. 201, pp 39–51. Springer, Gwalior (2013)
5. Raghavendra, G.S., Prasanna Kumar, N.: On the incorporation of punishment mechanism to Ant System (Unpublished work)
6. Raghavendra, G.S., Prasanna Kumar, N.: Statistical approach for selecting Elite Ants. *Ann. Comput. Sci. Ser.* **9**(2), 69–90 (2011)
7. Cordeau, J., Toth, P., Vigo, D.: A survey of optimization models for train routing and scheduling. *Transp. Sci. (Elsevier)* **32**(4), 380–404 (1998)

8. Cai, X., Goh, C.J.: A fast heuristic for the train scheduling problem. *Comput. Oper. Res.* **21**(5), 499–510 (1994)
9. Kraay, D., Harker, P., Chen, B.: Optimal pacing of trains in freight railroads. *Oper. Res.* **39**(1), 82–99 (1991)
10. Higgins, A., Kozan, E., Ferreira, L.: Heuristic techniques for single line train scheduling. *J. Heuristics* **3**, 43–62 (1997)
11. Kwan, R.S.K., Mistry, P.: A co-evolutionary algorithm for train timetabling. Research Report Series 13, School of Computing, University of Leeds, Leeds (2003)
12. Tormos, P., Lova, A., Barber, F., Ingolotti, L., Abril, M., Salido, M.A.: A genetic algorithm for railway scheduling problems. *Stud. Comput. Intell.* **128**, 255–276 (2008)
13. Dorigo, M., Maniezzo, V., Colorni, A.: Ant System: optimization by a colony of cooperating agents. *IEEE Trans. Syst. Man Cybern.* **26**(1), 29–41 (1996)
14. Bullnheimer, B., Hartl, R.F., Strauss, C.: A new rank based version of the Ant System: a computational study. *Central Eur J Oper Res Econ* **7**(1), 25–38 (1999)
15. Blum, C., Roli, A., Dorigo, M.: HC-ACO: The Hypercube framework for Ant Colony Optimization. *IEEE Trans. Syst. Man Cybern.* **34**(2), 1161–1172 (2004)
16. Stutzle, T., Hoos, H.H.: MAX—MIN Ant System. *Futur. Gener. Comput. Syst.* **8**(16), 889–914 (2000)
17. Di Caro, G., Dorigo, M.: Ant Colonies for adaptive routing in packet-switched communication networks. In: *Proceedings of the 5th International Conference on Parallel Problem Solving from Nature (PPSN V)*, pp. 673–682 (1998)
18. Costa, D., Hertz, A.: Ants can colour graphs. *J. Oper. Res. Soc.* **48**, 295–305 (1997)
19. Vansteenwegen, P., Souffriau, W., Van Oudheusden, D.: The orienteering problem: a survey. *Eur. J. Oper. Res.* **209**, 110 (2011)

An ICA Mixture Model Based Approach for Sub-pixel Classification of Hyperspectral Data

N. Prabhu, Manoj K. Arora, R. Balasubramanian and Kapil Gupta

Abstract Hyperspectral sensors are capable of collecting information in hundreds of contiguous spectral bands to expand the capability of multispectral sensors that use tens of discrete spectral bands. The contiguous bands play a vital role in study of types of vegetation, minerals, forest and soil types. In this paper, an iteratively learning parameter algorithm has been implemented to classify the hyperspectral image in an unsupervised way. The methodology followed in learning the parameters of ICA mixture model (ICAMM) has been discussed and the proportionality constant has been fixed as 0.7 to obtain the linear transformation for estimating the class membership probability of each pixel of a hyperspectral data. The ICAMM algorithm models class distributions as non-Gaussian densities, has been employed for unsupervised classification. Here the data have been transformed into new space in which, the data are as independent as possible by exploiting higher order statistics. This algorithm produces an average overall accuracy of around 65 % and outperforms the conventional K-means clustering and ISODATA.

Keywords Hyperspectral data · ICAMM algorithm · Kurtosis · Parametric classifier · Unsupervised classification

N. Prabhu (✉) · M. K. Arora
Department of Civil Engineering, IIT Roorkee, Roorkee 247667, India
e-mail: lord.n.prabhu@gmail.com

M. K. Arora
e-mail: manojfce@iitr.ernet.in

R. Balasubramanian · K. Gupta
Department of Mathematics, IIT Roorkee, Roorkee 247667, India
e-mail: balarfma@iitr.ernet.in

K. Gupta
e-mail: kapilgupta1020@gmail.com

1 Introduction

Hyperspectral sensors are capable of acquiring information of land use land cover in hundreds of narrow width, contiguous spectral bands, which give more information to study types of vegetation, minerals, soil classification, etc. The land use land cover classes may be extracted from remote sensing data in both supervised and unsupervised ways using a number of classification algorithms. For supervised classification, training data is required for further processing, which is, in general a set of pure pixels. But in most of the cases it is hard to get the required number of pure pixels from the image. Also, the supervised classification of hyperspectral data requires an optimum number of pure pixels which depends upon the number of bands used in classification process, in order to avoid Hughes phenomenon [1]. So, in such case, typically, unsupervised classification may be performed that clusters the data into various natural groups.

The sensors providing data at coarse spatial resolutions such as AVIRIS, Hyperion and MODIS increase the possibility occurrence of mixed pixels. Hence, the conventional per pixel classification algorithms that allocate one class to each pixel may not be appropriate for the classification of mixed pixels. Alternative approaches for classifying mixed pixels are, therefore, sought. Some sub-pixel classification techniques include, maximum likelihood classification (MLC) [2] in soft form, linear mixture model (LMM) [3, 4], fuzzy set based methods [5], artificial neural networks (ANN) [3], support vector machines (SVMs) [6] in soft form, decision-tree regression [7] and logistic regression [8]. These algorithms have their own mathematical background and modeled accordingly. So, an algorithm which is capable of estimating the class member probability for each pixel is required. An approach for unsupervised classification of hyperspectral images is based on a mixture model, where the distribution of the entire data is modeled as a weighted sum of the class-conditional densities. If the classes are modeled as multivariate Gaussian distribution the mixture model is known as Gaussian Mixture Model (GMM) [9] while, if the classes are modeled as multivariate non-Gaussian distribution then the mixture model is Independent Component Analysis Mixture Model (ICAMM).

GMM works by considering the lower order statistics of the data. Classification is done on the basis of second order statistical parameters derived from spectral characteristics of each class, which may not be sufficient in discriminating the within-class variation. For example, in Fig. 1a and b, both the spectral data sets are having same mean and same variance values; however, there are four clusters in Fig. 1a and only one cluster in Fig. 1b [10]. Thus, second order statistics are not capable of revealing the information available in the data. Also, to extract the non-Gaussian hidden features from different phases [11], ICAMM, which is capable of handling multiphase process with non-Gaussianity present within individual phases have been used.

Hence when the lower order statistics are not helpful in retrieving information from hyperspectral data, higher order statistics may be helpful to do so. In ICAMM, kurtosis, a higher order statistics, plays an important role in making the

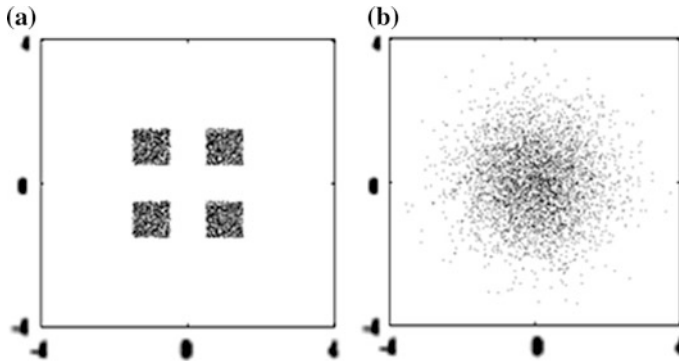


Fig. 1 Two data sets having identical second order statistics. **a** 4 clusters **b** Single cluster [10]

clusters as independent as possible. The ICAMM algorithm finds the linear transformation from the data to independent components for each cluster.

The aim of this paper is to provide a brief description of ICA mixture model, to produce fraction cover through ICAMM unsupervised classification of remotely sensed hyperspectral data to extract information from complicated land cover region covered by shadows and snow.

2 The ICAMM Algorithm

Imagine that in a room two persons are talking simultaneously. It was recorded by two microphones placed at two different locations in the room, but the positions of microphones are fixed throughout the recording process. These two microphones record the speech by both the persons but with different intensities. Let $x_1(t)$ and $x_2(t)$ be the intensities of the recorded signals at the two microphones at time t . Now this situation may be modeled as a linear combination of source signals weighed by parameters which depends upon the distance between microphones and the speakers. This situation has been expressed as [11],

$$\begin{aligned} x_1(t) &= a_{11}s_1 + a_{12}s_2 \\ x_2(t) &= a_{21}s_1 + a_{22}s_2 \end{aligned} \tag{1}$$

where $a_{11}, a_{12}, a_{21}, a_{22}$ are the mixing parameters in which a_{ij} corresponds to distance between microphone i and person j and s_1 and s_2 are intensities of the original speech signals. In its simple form, the system of equations are written as $\mathbf{x} = \mathbf{A}\mathbf{s}$. Recovering the original signal from the obtained sensor signal without having the knowledge about the mixing process is called as blind source separation (BSS) [12, 13]. Also, ICA is used to identify the hidden signals from the brain (such as activations) [14]. In that paper, a review on independent component analysis has been given. The hyperspectral data may also be modeled as,

$$\mathbf{x}_t = A_j \mathbf{s}_{j,t} + b_j, \quad (2)$$

where \mathbf{x}_t is the intensity values of the pixels of hyperspectral data in various bands, A_j is the mixing matrix for class j which is unknown, $\mathbf{s}_{j,t}$ is the source signal and b_j is the bias. Thus, in the present context, the solution of BSS problem leads to finding fractional cover given the observed hyperspectral data.

The solution for ICA exists when the following restrictions are implicitly executed by the algorithm:

- (i) The number of bands should be greater than or equal to the number of independent components (the required clusters are projected into new space whose axes are called as components).
- (ii) Among the K components, at most one distribution can be Gaussian. Remaining components are to be non-Gaussian.
- (iii) For each class/cluster, either no sensor noise or only low additive noise signals are permitted.

Based on the same concept, the hyperspectral data can be represented as a set of pixel vectors of dimension equal to the number of bands. The matrix A is the linear combination that transforms the data \mathbf{x} into independent components \mathbf{s} . Every class is modeled as a linear combination of sensor values weighed by the class-component densities.

Let the number of spectral bands of a hyperspectral data be N . Then each pixel vector \mathbf{x}_t , denoted as $\mathbf{x}_t = (x_1, x_2, \dots, x_N)^T$, is an N dimensional vector. Assuming that there are T pixels to be unmixed and are given by $X = \{\mathbf{x}_1, \mathbf{x}_2, \dots, \mathbf{x}_T\}$. The likelihood of the data [15] is given by the joint density,

$$p(X|\Theta) = \prod_{t=1}^T p(\mathbf{x}_t|\Theta), \quad (3)$$

where $\Theta = (\theta_1, \theta_2, \dots, \theta_K)$ are the K class parameters. The maximum likelihood estimate of Θ is the value that maximizes the value $p(X|\Theta)$ [16].

Let the pixel vectors from the hyperspectral data be obtained probabilistically from the set of spectral classes $\{C_1, C_2, \dots, C_K\}$. The probability of selecting the spectral class C_j is $P(C_j)$ and hence the probability of a pixel \mathbf{x}_t having the parameter Θ is given by the probability density function (pdf) of \mathbf{x}_t , which may be expressed by the mixture density model [15] given in Eq. (4),

$$p(\mathbf{x}_t|\Theta) = \sum_{j=1}^K p(\mathbf{x}_t|C_j, \theta_j) \cdot P(C_j), \quad (4)$$

The conditional density for class C_j is given by [15],

$$p(\mathbf{x}_t|C_j, \theta_j) = \frac{p(\mathbf{s}_{j,t})}{|\det(A_j)|} \quad (5)$$

where,

$$\log [p(\mathbf{s}_{j,t})] \propto - \sum_{i=1}^n \left\{ \phi_{i,j} \log [\cosh(s_{j,i,t})] - \frac{s_{j,i,t}^2}{2} \right\}. \quad (6)$$

Here $p(s_{j,t})$ is the prior source probability and normalize $p(s_{j,t})$, such that the fraction abundance in (6) becomes non-negative and less than one [17]. The classes are assumed to follow multivariate non-Gaussian distribution and the ICAMM algorithm is capable of finding the non-orthogonal directions of the data distributed. Since the distribution of the entire data is modeled as a weighted sum of the class-component densities of all the classes, it is represented as follows:

$$\mathbf{x}_t = A_j \mathbf{s}_{j,t} + b_j \quad (7)$$

where A_j is a full-rank matrix assumed as the basis matrix or mixing matrix which specifies the linear combination of independent sources [18]. By knowing only the observed mixed signals \mathbf{x}_t , the aim of ICAMM is to find the mixing matrix A_j for each class and the bias b_j and hence the fraction cover for each pixel.

Each A_j consists of M rows such that each data is represented by these M hyperplanes. In general, $N \geq M$. For simplicity, let the number of bands be the same as number of components ($N = M$). Such assumption can be met by transforming the hyperspectral data to reduced feature space. The bias b_j are the translation parameters which give the position of the center of cluster C_j . From (3) we get,

$$\mathbf{s}_{j,t} = A_j^{-1}(\mathbf{x}_t - b_j) \quad (8)$$

For each pixel vector \mathbf{x}_t , calculate the class-component density, given by Eq. (5).

Adapt A_j 's and b_j 's by using gradient ascent for learning the parameters [19–21]. Learning the parameters is a process in which the parameters A_j and b_j are updated iteratively until they fit into the data as perfect as possible. They are adapted as follows:

$$\Delta A_j \propto P(\mathbf{x}_t | C_j, \Theta) A_j [I - \Phi_j \tanh(\mathbf{s}_{j,t}) \mathbf{s}_{j,t}^T - \mathbf{s}_{j,t} \mathbf{s}_{j,t}^T] \quad (9)$$

where I is an identity matrix and a proportionality constant is introduced. In general the proportionality constant is kept between 0 and 1. In this paper, it has been taken as 0.7. The proportionality constant has been fixed to 0.7 by trial and error method. The experiment has been done for all values between 0 and 1 by taking interval 0.05. Here, Φ_j is an N -dimensional diagonal matrix corresponding to class j and is composed of $\phi_{i,j}$ [20] defined by:

$$\phi_{i,j} = \frac{m_4(s_{j,i,t})}{m_2^2(s_{j,i,t})} - 3, \quad (10)$$

where, m_p corresponds to the p th moment of the independent source. The value of kurtosis $\phi_{i,j}$ is positive for super-Gaussian, negative for sub-Gaussian and zero for Gaussian $s_{j,i}$.

For each class j , the bias b_j is updated by,

$$b_j = \frac{\sum_{t=1}^T x_t P(C_j|x_t, \Theta)}{\sum_{t=1}^T P(C_j|x_t, \Theta)}, \quad (11)$$

The kurtosis for i th independent component over class j is used to find the class-component density and is given by (7). The independency of the component is checked from the joint probability density given as in (1). Once the A_j 's and b_j 's are adapted, the class member probability for each pixel is calculated from Bayes theorem, given as:

$$p(C_j|\mathbf{x}_t, \Theta) = \frac{p(\mathbf{x}_t|C_j, \theta_j)P(C_j)}{\sum_{j=1}^K p(\mathbf{x}_t|C_j, \theta_j)P(C_j)}, \quad (12)$$

where all $P(C_j)$'s are assumed to be equal.

The convergence occurs once the transformed clusters are as independent as possible. At this iteration A_j and b_j values are taken and then from (9) the fraction cover is obtained. If required, the fractional cover of various classes may be converted to a land cover map, by replacing the fractional cover by its class attribute having maximum fractional value. A pseudo code for the algorithm is given as follows:

Pseudo code of ICAMM [21]

Initialize the mixing matrices and bias

For each pixel vector \mathbf{x}_t ,

Repeat

For each class

Calculate $s_{j,t}$

Calculate $p(\mathbf{x}_t|\Theta)$

Calculate $p(C_j|\mathbf{x}_t, \Theta)$

Check for independence

Adapt A_j

Adapt b_j

Repeat the entire process for all $t = 1, 2, \dots, T$.

Convert into hard classification output, if required.

3 Experimental Dataset

The experiment has been carried out on Terra MODIS image consisting of 36 bands. The first two bands are of spatial resolution 250 m and bands 3–7 have spatial resolution of 500 m. The remaining bands from band 8 to band 36 are of 1000 m spatial resolution. The area belongs to a Himalayan region with many

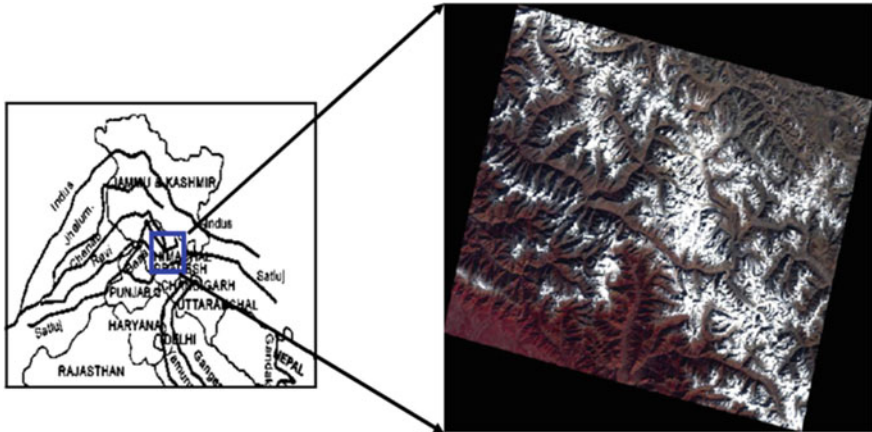


Fig. 2 The MODIS FCC (Red B6, Green B5, Blue B4)

glaciers (Fig. 1). In the region there are four major classes, namely, valley rock, vegetation, snow and shadow, are present. The area has many big glaciers such as Samudra Tapu glacier. The study area contains Samudra Tapu watershed with an areal extent of about 110 Km² (latitude 31° 12' 22''N to 32° 05' 19''N and longitude 77° 31' 59''E to 77° 57' 34''E) and is covered in 161 × 157 pixels of the MODIS sub-scene under investigation (Fig. 2).

Even though two bands B1 and B2 are of fine resolution (250 m) it requires at least 4 bands of same resolution to do classification. On the other hand, bands from B8 to B36 are plenty in number of bands, but the spatial resolution is coarse (1000 m). Hence the 500 m spatial resolution bands B3 to B7 are used for classification purpose. Moreover these bands are suitable for studies of land/cloud/aerosols/boundaries [22]. Hence only these bands are used for classification purpose.

4 Methodology

Using the ICAMM algorithm we run the dataset MODIS by taking only 4 bands (as the available classes are only 4, to make the number of classes same as that of the number of bands, a separability analysis has been done and found that the best minimum separability obtained by taking bands B4, B5, B6 and B7). Since, the mixing matrices and bias vectors are random, to check the performance of the algorithm, it was run for 6 times. Since the clustering is based upon the random initialization of mixing matrices and bias vectors, there are 4 factorial (number of clusters K = 4) ways of representing the clusters. First, the fraction images are converted into thematic map by considering the maximum class member probability of that pixel [21]. Then the classification accuracy was assessed by using an

Table 1 The overall accuracy, user’s and producer’s accuracies and kappa coefficient at each run

	Overall accuracy	Average user’s accuracy	Average producer’s accuracy	Kappa coefficient
Run 1	87.34	77.33	89.55	0.77
Run 2	80.46	73.89	71.99	0.59
Run 3	42.06	46.86	48.73	0.21
Run 4	71.28	57.03	50.25	0.47
Run 5	72.39	51.40	54.42	0.45
Run 6	61.04	67.71	71.78	0.43
Run 7	59.31	65.00	70.36	0.40
Run 8	70.04	46.97	48.28	0.45
Run 9	67.99	50.30	52.20	0.45
Run 10	65.14	56.14	68.32	0.45
Average	67.71	59.26	62.59	0.47

Table 2 Comparison of user’s and producer’s accuracies for each class at each run

	User’s accuracy				Producer’s accuracy			
	Valley rock	Vegetation	Snow	Shadow	Valley rock	Vegetation	Snow	Shadow
Run 1	97.86	65.09	70.22	76.15	88.46	100	100	69.73
Run 2	84.14	73.91	67.81	69.70	93.08	77.27	100	17.63
Run 3	80.96	7.43	52.27	46.77	35.73	42.73	58.23	58.24
Run 4	95.72	1.03	41.36	90	88.84	1.82	100	10.35
Run 5	86.64	11.63	87.71	19.61	88.64	18.18	99.37	11.49
Run 6	95.39	17.27	62.21	95.98	55.40	100	67.72	63.99
Run 7	94.77	17.16	58.10	90	53.56	100	65.82	62.10
Run 8	95.30	1.02	40.55	51.02	88.10	1.82	93.67	9.58
Run 9	98.07	11.81	52.02	39.29	79.69	30	56.96	42.15
Run 10	98	20.84	50.33	55.39	67.96	80.91	96.84	27.59
Average	92.69	22.719	58.26	63.39	73.95	55.27	83.86	37.29

error matrix based assessment [23, 24]. Apart from analyzing using the overall accuracies, the user’s and producer’s accuracies have also been analyzed, to check quality of the output for each class. Table 1 shows the overall, user’s and producer’s accuracies and kappa coefficients for each run.

It can be seen from Table 1 that the minimum overall classification accuracy is 42.06 %, while the maximum is 87.34 %. Also it can be seen that, due to the class shadow mixed with vegetation there is a dip in both user’s accuracy and producer’s accuracy for class vegetation. From Table 2, it is evident that the user’s accuracy for class valley rock is consistent while the vegetation was wrongly classified as valley rock (at one run) and shadow (at another run). Figure 3a is the classified image while fraction images of valley rock, vegetation, snow and shadow are given in Fig. 3b–e. The class shadow appears only at the location where valley rock is present, so shadow mixed up by valley rock. Finally a thematic map is generated from the fraction images by taking the maximum class member

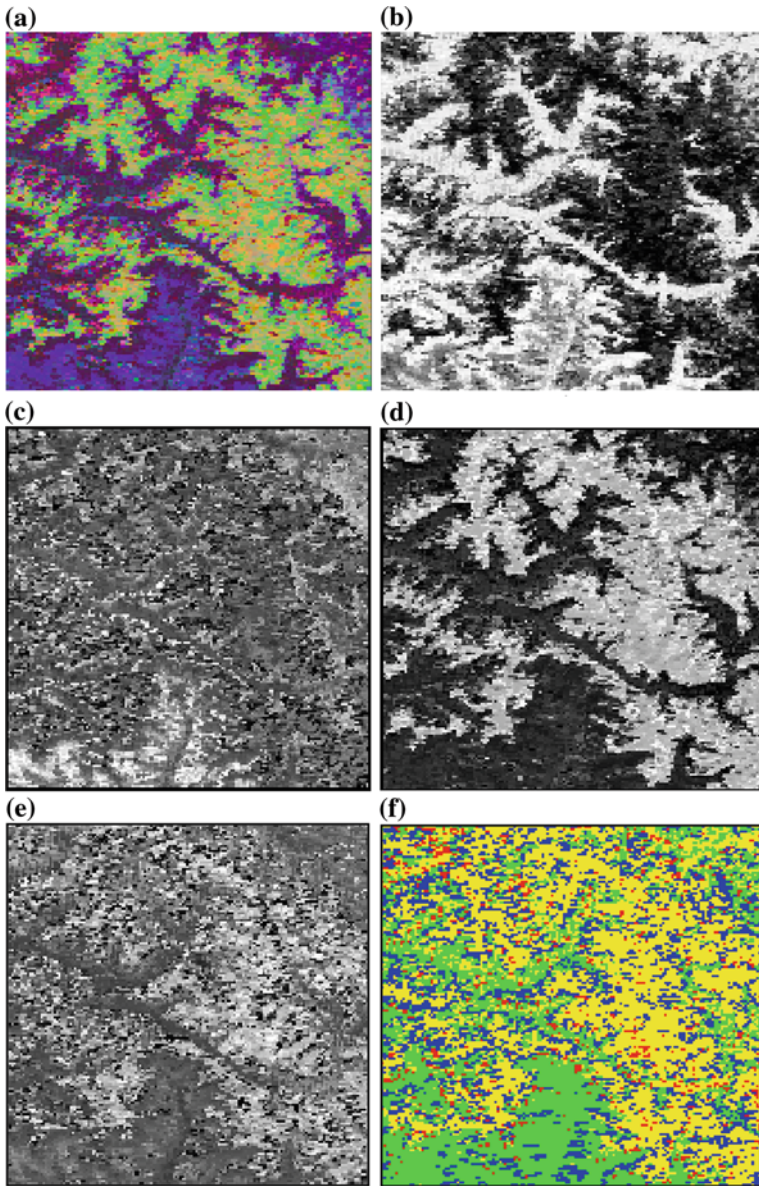


Fig. 3 a–f The classified image along with the fraction images and thematic map, **a** the classified image, **b** fraction image for class valley rock, **c** fraction image for class vegetation, **d** fraction image for class snow, **e** fraction image for class shadow, **f** thematic map got from the fraction images by taking the maximum class member probability of each pixel. Here *green color* for valley rock, *blue* for vegetation, *yellow* represents snow and *red* for shadow

Table 3 Average user's accuracy and average producer's accuracy of the 4 classes got by classifying the dataset by ISODATA algorithm for 10 times

Sl. No.	Classes	User's accuracy	Producer's accuracy
1	Valley Rock	88.67	44.04
2	Vegetation	10.59	60.91
3	Snow	56.16	51.91
4	Shadow	61.70	69.73
	Average	54.28	56.65

probability of each pixel. Here green color represents valley rock, blue for vegetation, yellow represents snow and red color for shadow. For the proportionality constant 0.7 we get some better results while comparing with other values.

For comparison, the dataset has been classified by using another unsupervised classifier, ISODATA, which is available in ERDAS IMAGINE 2010. Here also the classification has been performed for 10 times. The average overall accuracy comes to be 50.12 % while the average user's and producer's accuracies for various classes are given in the Table 3. From Tables 2 and 3, we get that the average overall accuracy of ICAMM is better than the ISODATA algorithm. Moreover the user's accuracy of snow is slightly better by classification using ICAMM than ISODATA, while the producer's accuracy for snow is significantly better for ICAMM.

5 Conclusion and Future Scope

The classification accuracy and rate of convergence depends upon the parameters, random matrices and the bias vectors, which are initialized at the beginning. The ability of unmixing the classes using ICAMM is more when compared over other conventional unsupervised classifiers (K-means clustering, ISODATA). The overall accuracy for K-means clustering is around 50 % [18] in general. Particularly for this dataset, by using ISODATA classification, the overall accuracy is 51 % while that of ICAMM is 65 %. The proportionality constant has been fixed at 0.7 which is able to extract more information from hyperspectral data through this algorithm.

References

1. Hughes, G.F.: On the mean accuracy of statistical pattern recognizers. *IEEE Trans. Inf. Theory* **14**(1), 55–63 (1968)
2. Jia, X., Richards, J.A.: Efficient maximum likelihood classification for imaging spectrometer data sets. *IEEE Trans. Geosci. Remote Sens.* **32**(2), 274–281 (1994)

3. Foody, G.M., Arora, M.K.: Incorporating mixed pixels in the training, allocation and testing stages of supervised classifications. *Pattern Recogn. Lett.* **17**, 1389–1398 (1996)
4. Kasetkasem, T., Arora, M.K., Varshney, P.K., Areekul, V.: Improving subpixel classification by incorporating prior information in linear mixture models. *IEEE Trans. Geosci. Remote Sens.* **49**(3), 1001–1013 (2011)
5. Chanussot, J., Benediktsson, J.A., Fauvel, M.: Classification of remote sensing images from urban areas using a fuzzy probabilistic model. *IEEE Geosci. Remote Sens. Lett.* **3**(1), 40–44 (2006)
6. Platt, J.C.: Probabilistic outputs for support vector machines and comparisons to regularized likelihood methods. In: Smola, A. et al. (ed.), *Advances in Large Margin Classifiers*. MIT Press, Cambridge (2000)
7. Xu, M., Watanachaturaporn, P., Varshney, P.K., Arora, M.K.: Decision tree regression for soft classification of remote sensing data. *Remote Sens. Environ.* **97**(3), 322–336 (2005)
8. Cheng, Q., Varshney, P.K., Arora, M.K.: Logistic regression for feature selection and soft classification of remote sensing data. *IEEE Geosci. Remote Sens. Lett.* **3**(4), 491–494 (2006)
9. Duda, R.O., Hart, P.E., Stork, D.G.: *Pattern Classification*, 2nd edn. Wiley, New York (2001)
10. Shah, C.A., Varshney, P.K.: A higher order statistical approach to spectral unmixing of remote sensing imagery. In: *Proceedings of Geoscience Remote Sensing Symposium, IGARSS'*, vol. 2, pp. 1065–1068 (2004)
11. Yu, J., Chen, J., Rashid, M.M.: Multiway independent component analysis mixture model and mutual information based fault detection and diagnosis approach of multiphase batch processes. *Process Syst. Eng.* **59**(8), 2761–2779 (2013). (Wiley Online Library AICHe Journal)
12. Hyvärinen, A., Oja, E.: Independent component analysis: algorithms and applications. *Neural Netw. Official J. Int. Neural Netw. Soc.* **13**(4–5), 411–430 (2000)
13. Common, P.: Independent component analysis, a new concept? *Signal Process* **36**, 287–314 (1994)
14. Beckmann, C.F.: Modelling with independent components. *NeuroImage* **62**, 891–901 (2012)
15. Lee, T.W., Lewicki, M.S., Sejnowski, T.J.: ICA mixture models for unsupervised classification of non-gaussian classes and automatic context switching in blind signal separation. *IEEE Trans. Pattern Anal. Mach. Learn.* **22**(10), 1078–1089 (2000)
16. Shah, C.A., Arora, M.K., Robila, S.A., Varshney, P.K.: ICA mixture model based unsupervised classification of hyperspectral imagery. In: *IEEE Computer Society Applications on Image Pattern Recognition Workshop, Proceedings*, pp. 29–35 (2002)
17. Plumbley, M.D.: Algorithms for nonnegative independent component analysis. *IEEE Trans. Neural Netw.* **14**(3), 534–543 (2003). (A publication of the IEEE Neural Networks Council)
18. Shah, C., Arora, M., Varshney, P.: Unsupervised classification of hyperspectral data: an ICA mixture model based approach. *Int. J. Remote Sens.* **25**(2), 481–487 (2004)
19. Lee, T.W., Girolami, M., Sejnowski, T.J.: Independent component analysis using an extended informax algorithm for mixed sub-Gaussian and super-Gaussian sources. *Neural Comput.* **11**(2), 417–441 (1999)
20. Shah, C.A., Varshney, P.K.: A higher order statistical approach to spectral unmixing of remote sensing imagery. In: *Geoscience and Remote Sensing Symposium*, pp. 1065–1068 (2004)
21. Lee, T.W., Lewicki, M.S.: Unsupervised image classification, segmentation and enhancement using ICA mixture models. *IEEE Trans. Image Process.* **11**(3), 270–279 (2002). (A publication of the IEEE Signal Processing Society)
22. National Aeronautics and Space Administration: <http://modis.gsfc.nasa.gov/about/specifications.php>. MODIS Homepage
23. Story, M., Congalton, R.: Accuracy assessment: a user's perspective. *Photogramm. Eng. Remote Sens.* **52**(3), 397–399 (1986)
24. Congalton, R.G.: A review of assessing the accuracy of classifications of remotely sensed data. *Remote Sens. Environ.* **46**, 35–46 (1991)

Network Connectivity in VANETs

**Ranjeet Singh Tomar, Brijesh Kumar Chaurasia, Shekhar Verma
and Rajendra Singh Kushwah**

Abstract VANETs are targeted to improve the traffic safety and driving experience on the road. Vehicular connectivity based communication in VANETs to be used for safety critical, safety related and non safety related messages dissemination in the networks. A key challenge in developing such network connectivity mechanism is that quickly adaptation the changes in the network topology due to the vehicular mobility. In this work we investigate the feasibility of developing the location based network connectivity for communication in VANETs in the spatial localized time domain for safety applications. The vehicular mobility and maximization of network connectivity duration between the vehicles have been identified as two important design goals in this work. However, these two goals are in conflict in nature, which makes it challenging to achieve both of these two goals in VANETs. To balance the trade-off between vehicular mobility and network connectivity, the average number of vehicle links, average link duration and connection time of each vehicle is ensured and subject to this constraint, aggregate network connectivity is maximized for efficient communication in VANETs.

Keywords Medium access control (MAC) · Vehicular ad hoc networks (VANETs) · Vehicular connectivity

R. S. Tomar (✉) · B. K. Chaurasia
ITM University, Gwalior, India
e-mail: er.ranjeetsingh@gmail.com

B. K. Chaurasia
e-mail: bkchaurasia.itm@gmail.com

S. Verma
Indian Institute of Information Technology, Allahabad, India
e-mail: sverma@iiita.ac.in

R. S. Kushwah
Institute of Technology & Management, Gwalior, India
e-mail: rajendrasingh.ind@rediffmail.com

1 Introduction

Driving behavior, traffic congestion, and treacherous driving conditions have caused numerous accidents every year all over the world. Under such circumstances the challenge of improving safety has become critical and has been subject of extensive research efforts. Vehicle manufacturers have made great efforts to improve the safety of their vehicles by developing passive vehicle safety systems, which aim to minimize post-crash human injury [1]. The active vehicle safety systems, explore collision prevention and avoidance techniques. The limitations of the current techniques stem from the lack of information to the vehicle beyond immediate line of sight. Intelligent transportation system significant by enhance the quality of transportation systems by reducing traffic congestion, increasing road safety and traveler convenience [2]. ITS constitute a basket of technologies and is combination of vehicle information and communication system. VANET is a component of ITS. In VANET, vehicles are equipped with communication devices, processors, and micro controller along with sensors, display, global positioning system (GPS), RADAR and other electronics equipment [3]. Integration of these devices enables vehicles to communicate with each others as well as RSUs providing communication infrastructure for VANET. These RSUs places at a fixed optimal places like road intersections. Communication between vehicles is known as inter-vehicle communication (IVC or V2V) and communication between vehicles and roadside infrastructure is known as vehicle-to-roadside communication (V2R) [4]. A typical VANET is characterized by high mobility, dynamic topology, QoS requirements which are different from a MANET and availability of sufficient storage and power [5].

The rest of the paper is organized as follows. [Section 2](#) describes the problem definition. In [Sect. 3](#), network connectivity of vehicular traffic are given. [Section 4](#) is presented analytical evaluation. The simulation and results are presented in [Sect. 5](#) followed by conclusion in [Sect. 6](#).

2 Problem Definition

Vehicles move in bidirectional single or multi lanes on the road with different speeds and accelerations. They also turn in different directions at junctions. There are different classes of lane on the road as per the speed limits to be followed vehicles i.e. low, medium and high speed lane on the road. Each vehicle starts moving from definite segment, travels on the road and can change its lane or overtake another vehicle. After reaching destination or at traffic lights, vehicle stops for a pause of some time and then repeat the same process i.e. randomly and predefined the next destination on the road. The density of the vehicular traffic also varies from one place to another and with respect to time. This requires benchmarking of the temporal state of neighborhood as vehicles move under different traffic conditions and transmission powers.

3 Network Connectivity

With the advent of wireless technologies, connectivity in VANETs has become common place. An ad hoc network is formed by groups of vehicular nodes that communicate amongst themselves and set up connectivity in the VANETs. Connectivity in vehicular ad hoc networks may degrade dramatically in sparse traffic and also high speed highways [6]. Queuing model $M/G/\infty$ theory is investigating the connectivity in the vehicular network. This model based media access control mechanism provides a way to improve the connectivity by adding some extra nodes with higher transmission range called as mobile base stations. This model takes into account the case when some of the vehicles do not participate in the network either because they are not equipped with wireless transceivers or some other security reasons. Moreover, connectivity in presence of fixed roadside units (RSUs) is also considered [7]. This analytical model can be used to find out the optimum values of the number of base stations as well as their transmission range in order to achieve a desired degree of connectivity in the network [8]. The exact probability based vehicle connectivity model in one dimensional stationary vehicular ad hoc wireless network is composed of at most C clusters is proposed in the literature. The probability of vehicular network connectivity, i.e. the case of $C = 1$, can be derived as a special case in the network connectivity. A very simple approximation is presented for the exact probability of network connectivity. This model provides approximation heuristically, which validate the analytical exact probability calculation in vehicular network by computing the probability of network connectivity and maintain the accuracy of analysis with the Monte Carlo simulation analysis. The networks theoretically used the percolation theory for the network connectivity. Percolation theory provided the quantitative relationship among network connectivity, vehicle density and transmission range [9]. Based on this percolation theory, there is a jump for the network connectivity when vehicle density or transmission range is large enough. This theory also calculates the threshold values of vehicle density and transmission range in the vehicle network. A large transmission range can have better network connectivity, but it can also cause serious collisions in wireless links in the network. For a fixed vehicle density, this theorem gave the minimum transmission range to achieve better network connectivity. Below the minimum transmission range, collisions might be few due to the network connectivity. The analytical framework of network connectivity helps to approximately estimate the minimum number of RSUs required covering a road segment, for a low density VANET. This framework provided probabilistic vehicle-to-RSU delay guarantee with intermittent multi hop connectivity between vehicles and RSUs. This framework proposed the two analytical models to study spatial propagation of information for one and two lane straight roads, without consideration of bandwidth constraints and data traffic characteristics based on probability based connectivity. It also calculates the average length of a connected path from any given vehicle to an RSU. IEEE 802.11p and 1609 standards are currently under development to support vehicle to vehicle and

vehicle to infrastructure communications in vehicular networks. In infrastructure based vehicular relay model, access probability and connectivity probability are important measures. This model derives close form equations for calculating these two probabilities using parameters such as inter base station distance, vehicle density, transmission ranges of base station. The statistical connectivity based model derives the probability distribution of the node population size on the highway and the node's location distribution also determines the mean cluster size and the probability that the nodes will form a single cluster. The analysis of this model applies to any path in a network of highways. This model also shows the significance effect of mobility on the connectivity of VANETs.

4 Analytical Evaluation

4.1 Road Model and Input Traffic

A road with multiple unidirectional lanes is considered. The vehicles move in a single direction with different speeds and multiplicity of the lanes allows vehicles to overtake each other without any restriction in the number of lanes. The road has S segments of D m each. The road length is $S \cdot D$ m. Vehicles can enter and exit at the end points of a segment and there is no waiting period or queue required to enter the road. There are two end points of the road and there is no exit point at the start of the initial segment or entry at the end of the last segment. Vehicles arrive at the beginning of a segment follow a Poisson distribution $p_y(y)$ and travel towards the end point independently of other existing vehicles on the road. The arrival rate at the (ij) th segment at (i) th point is λ_i with the departure rate at the (j) th point being δ_j ($\lambda_i = 0$ for $i = 0$ and δ_j for $j = S$). Once a vehicle enters the road at an entry point, it cannot exit from the same point i.e., every vehicle must traverse at least one segment as soon as it enters the road. An arriving vehicle is admitted in the road and starts traversing on the road without any waiting period i.e., no vehicle has to wait at the side of the road to enter the road. Once on the road, a vehicle cannot exit from the same junction and must traverse at least one segment before it can depart at one of the junctions. The time which a vehicle spends on the road is assumed to be independent general random variable.

When the traffic density is small, the vehicles cruise freely. This is free flow traffic condition. In the steady state, vehicles follow and move at fixed safe distance their preceding vehicle. The velocities of the vehicles are almost constant in the free flow traffic condition. As the traffic density increases, random perturbations set in and phantom jams appear. Reaction to these phantom jams renders the velocities of vehicles variable. With further increase in vehicular density, the traffic becomes more turbulent. The speeds of the vehicles decrease, the variation in mobility increases as congestion on the road. In addition to the effect of traffic instability on mobility, other road conditions and maneuvers also affect the motion of vehicles.

Lane change is a frequent action undertaken by vehicles on the road and usually results in a definite gain to the vehicle in terms of driving comfort or reduced time to travel. However, it destabilizes the traffic in both the original and target lanes. Lane merging maneuvers increase the density of the traffic in the merging lane suddenly. This induces large change in vehicular mobility as vehicles adjust to the traffic conditions in the new lane. Traffic lights are used at every intersection of roads as a traffic control mechanism. When a vehicle reaches at intersection then it decelerates and stops there for a predefined time called pause time. When the traffic light is red then a vehicle stops and waits for light to turn green. This maneuver supports overtaking of vehicles on multilane roads. When many vehicles reach at the intersection then a queue is formed at the crossing of each lane. This may leads to congestion on junction. To model the mobility of a vehicle in different conditions we assume that vehicles travel with variable velocity. The velocity of a vehicle v_i of a vehicles moving in one direction follows a normal distribution with mean speed μ and variance $\sigma^2:N(\mu, \sigma^2)$. Vehicles in different lanes moving in the same direction have different mean and variance. The vehicles moving in opposite directions in corresponding lanes have similar parameters.

4.2 Size of Neighborhood

The number of vehicles in the communication range R_c of V_c is governed by a Poisson distribution. The probability that V_c has exactly n vehicles in its communication range R_c is given by

$$\frac{\exp(-\lambda R_c)(\lambda R_c)^n}{n!}$$

As vehicles move, the state of the neighborhood changes with time. New vehicles enter and current vehicles exit the neighborhood. The distribution, however, remains the same.

4.3 Neighborhood Stability and Link Duration

In the multilane highway, vehicles move in different directions with normally distributed velocities $N(\mu_i, \sigma_i^2)$, where i is the number of lanes in one direction. All the k vehicles in the neighborhood of the chosen vehicle, V_c , also move along their lanes. Due to variation in speeds, their distances from V_c change with time. The relative speeds of vehicles moving in direction opposite to V_c is large while the relative speeds of vehicles in the same direction lanes are quite small. Thus, vehicles moving in the opposite direction leave the neighborhood faster as compared to same direction vehicles. If the distance covered by a vehicle in time T is

such that it is not within the radius R_c of V_c , then, it leaves the neighborhood. A vehicle may lag behind or surge ahead to leave the neighborhood. Following cases may arise.

Case I: A neighbor V_k of V_c be at an initial distance d_0^k at time t_0 ahead of V_k in the same lane. The distance x traveled in time T can be given as

$$x = vT$$

where, v is the relative velocity of the vehicle V_k with respect to V_c . Since, the velocities of V_k and V_c are normally distributed with means μ_k, μ_c and variances σ_k^2, σ_c^2 , the relative velocity v will also be normally distributed with mean $\mu_v = \mu_k + \mu_c$ ($\mu_k - \mu_c$) if they are moving in opposite (same) direction and variance $\sigma_v^2 = \sigma_k^2 + \sigma_c^2$. Thus, x is also normally distributed with mean $\mu_v T$ and variance $\sigma_v^2 T$. The probability that the distance traveled x is larger than d_T^k can be given as

$$\int_0^x \frac{1}{\sqrt{2\pi\sigma_v^2}} \exp\left(-\frac{(x - \mu_v)^2}{2\sigma_v^2}\right) dx$$

This can be represented by an error function as

$$erf(y) = \int_0^y \frac{2}{\sqrt{\pi}} \exp(-y^2) dy$$

Vehicle V_k will leave the neighborhood of V_c if $d_0^k + d_T^k > R$.

Case II: A neighbor V_k of V_c be at an initial distance d_0^k at time t_0 behind of V_k in the same lane. V_k cannot overtake V_c in the same lane. Hence, it can only lag behind to leave the neighborhood by travelling at a speed lower than V_c . V_k will leave the neighborhood of V_c if $d_0^k + |d_T^k| > R$.

Case III: A neighbor V_k of V_c be at an initial distance d_0^k at time t_0 ahead of V_k in a opposite lane. A vehicle in the opposite lane has to travel at high relative speed to cross V_c and then travel a distance more than R to leave the neighborhood of V_c . Thus, V_k will leave the neighborhood of V_c if $d_T^k - d_0^k > R$.

Case IV: A neighbor V_k of V_c be at an initial distance d_0^k at time t_0 behind of V_k in a opposite lane. A vehicle in the opposite lane has to just increase its distance from V_c to more than R to leave the neighborhood. Thus, V_k will leave the neighborhood of V_c if $d_T^k + d_0^k > R$.

Case V: A neighbor V_k of V_c be at an initial distance d_0^k at time t_0 ahead of V_k in a different lane in the same direction. This case is identical to case I. V_k will leave the neighborhood of V_c if $d_0^k + |d_T^k| > R$.

Case VI: A neighbor V_k of V_c be at an initial distance d_0^k at time t_0 behind of V_k in a different lane in the same direction. V_k can overtake V_c as they are in different lanes. Hence, it can lag behind to leave the neighborhood by travelling at a speed lower than V_c . This is same as Case II. V_k will leave the neighborhood of V_c if $d_0^k + |d_T^k| > R$. V_k can only leave the neighborhood of V_c by surging ahead. For this, the condition is, $d_T^k + d_0^k > R$ as in Case III.

The duration of a link between two vehicles V_k and V_c is T . It can be observed that volatility of a link depends directly on variation in mobility which is determined by σ_v^2 . Higher μ_v and σ_v^2 induces faster rate of change of the neighborhood of a vehicle. Thus, high vehicular densities and traffic turbulence make the link volatile. High relative speeds in the same lane that characterize traffic turbulence also make the link transient. In free flow conditions, same lane neighbors have long duration links though, as expected, the links between vehicles moving in different directions have small term relationships.

The neighborhood may also change due traffic perturbations like phantom jams, lane change, lane merge etc. The neighborhood changes abruptly at an intersection or junction. New vehicles join and some current neighbors leave in very small time duration. Let $X(t)$ be the number of vehicles on the road at time t with total number of vehicles arriving on the road in the semi closed time interval $(0, t]$ be $N(t)$. The number of departures from the road at different junctions would be $N(t) - X(t)$. Since, n vehicles have entered the road and each has a probability p of continuing on the road by time t , this becomes a sequence of n Bernoulli trials.

$$P[X(t) = j|N(t) = n] = \begin{cases} \binom{n}{j} p^j (1-p)^{n-j}, j = 0, 1, \dots, n \\ 0 \text{ otherwise} \end{cases}$$

As above, the probability distribution function of the number of vehicles on the road at time t will have a Poisson distribution with parameter equal to

$$P[X(t) = j] = \exp(-\lambda tp) \frac{\lambda tp}{j!}$$

5 Simulation and Results

In this section, we present the network connectivity based simulation using NCTUns5.0 real time traffic simulator [10] in different density of vehicles and with respect to the transmission range and interference range of the vehicle in the VANET environment. Furthermore, we consider the impact of traffic light junctions and high density traffic on network connectivity with respect to the transmission range and interference range. Vehicles are permitted to travel in the straight jacket road at the speed limit between 30 and 120 km/hr. Initially, 40 vehicles per lane are considered in a 1000 m distance on the road. We considered the six lane policy system on the road, so 240 vehicles are travelling on the road. Out of 240 vehicles, 120 vehicles travelling in the one direction and other 120 vehicles travelling in the opposite direction. The transmission range of the vehicles is fixed to be 150 m.

Figures 1 and 2 show the simulation results of the vehicular network connectivity. They include the influences of the no traffic light junction, traffic light junction, lane changing traffic and high density traffic respectively. Traffic lights

Fig. 1 Average link duration at traffic light junction for network connectivity

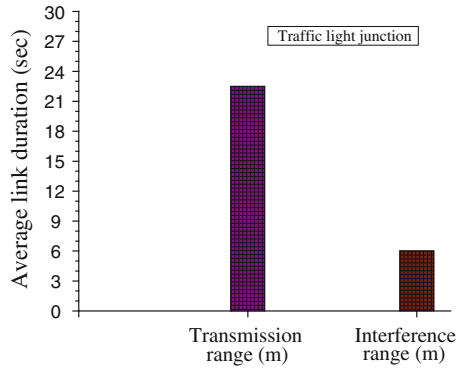
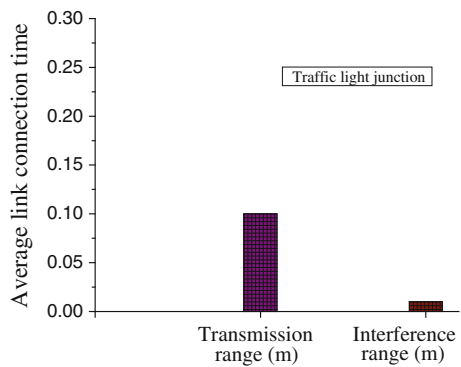


Fig. 2 Average link connection time at traffic light junction for network connectivity



are located at the junction of the road and the mechanism of the traffic light signal consists of 30 s for green signal followed by 30 s for red signal and 15 s for the yellow signal. With traffic lights the number of vehicle communication pairs increases significantly, this is due to the bunching of the vehicles caused by the traffic signal at the junction in Fig. 1.

From Fig. 2, the average link connection time decreases than the average link duration in the transmission range of the vehicles in the network. For interference range vehicles, the average link connection time decreases even when if the average link duration time increases. This shows that the amount of delay of vehicle during travelling by traffic signals is longer than the amount of link connection time of vehicles at traffic light signals.

6 Conclusion

In this paper, we have presented the location based network connectivity in VANETs for message dissemination in the vehicular network. Vehicular mobility and network connectivity are the two important balancing parameters to enhance

the vehicle safety in the VANETs. Average number of vehicle links, average link duration and connection time of the vehicles are ensured that the network connectivity in VANETs is maximized the efficient communication between the vehicles.

References

1. Malta, L., Miyajima, C., Takeda, K.: A study of driver behavior under potential threats in vehicle traffic. *IEEE Trans. Intell. Trans. Syst.* **10**(2), 201–210 (2009)
2. Biswas, S., Tatchikou, R., Dion, F.: Vehicle-to-vehicle wireless communication protocols for enhancing highway traffic safety. *IEEE Commun. Mag.* **44**(1), 74–82 (2006)
3. Kerner, B.S.: *Introduction to Modern Traffic Flow Theory and Control: The Long Road to Three-Phase Traffic Theory*, pp. 1–255. Springer, Berlin (2009)
4. Shiller, Z., Sundar, S.: Emergency lane-change maneuvers of autonomous vehicles. *J. Dyn. Syst. Meas. Contr. ASME* **120**(1), 37–44 (1998)
5. Hossein, J., Kosmatopoulos, E.B., Ioannou, P.A.: Collision avoidance analysis for lane changing and merging. *IEEE Trans. Veh. Tech* **49**(6), 2295–2308 (2000)
6. Ngai, D.C.K., Yung, N.H.C.: A multiple-goal reinforcement learning method for complex vehicle overtaking maneuvers. *IEEE Trans. Intell. Trans. Syst.* **12**(2), 509–522 (2011)
7. Abbas, M.K., Karsiti, M.N., Napiah, M., Samir, B.B.: Traffic light control via VANET system Architecture. In: *Proceedings of the IEEE International Symposium on Wireless Technology and Applications*, pp.174–179, Sept 2011
8. Durrani, S., Zhou, X., Chandra, A.: Effect of vehicle mobility on connectivity of vehicular ad hoc networks. *Proceedings of the 72nd IEEE International Vehicular Technology Conference (VTC-Fall)*, pp. 1–5, Sept 2010
9. Jin, X., Su, W., Wei Y.: A study of the VANET connectivity by percolation theory. *Proceedings of the 3rd IEEE International Workshop on Intelligent Vehicular Communications System*, pp. 85–89, Jan 2011
10. NCTUns. <http://nsl.csie.nctu.edu.tw/nctuns.html>

Proposal and Survey of Various Data Mining Aspects in Mobile Computing Environment

Harcharan Singh Pabla, Sukhdeep Singh, Niyati Gupta,
Palak Makhija, Prabhjot Kaur and Gurpal Singh

Abstract Data mining has its own statutory position in the communication industry. The other term coined for data mining is knowledge discovery of databases it might be mobile databases also. The analysis and discussion of different aspects of mining on mobile environment has been carried out in this paper. Firstly we have proposed two mining approaches for mobile environment i.e. CSU (Create, Select, Update) algorithm and CSA (Create, Select, Alter) algorithm. These two algorithms are achieved by CLDC component of J2ME which has also been discussed in the same paper. Secondly, we have proposed a new term i.e. Ambulatory Data Mining (ADM) which is used to perform collaborative mining of data streams in mobile environments. Wireless communication technologies like Wi-Fi and Bluetooth, which interconnect the mobile devices, have opened doors for collaborative mining amongst the mobile devices targeting the same applications which are used for running data mining techniques on mobile devices. This collaborative mining has been achieved with the help of various mobile software

H. S. Pabla (✉) · P. Kaur

Department of Engineering and Computer Science, Concordia University, Montreal,
QC, Canada

e-mail: h_pabla@encs.concordia.ca

P. Kaur

e-mail: p_sekhon@encs.concordia.ca

S. Singh · N. Gupta · P. Makhija

Department of Computer Science and Engineering, Gyan Vihar University, Jaipur,
Rajasthan, India

e-mail: sukhdeepsingh90@gmail.com

N. Gupta

e-mail: niyati1707@gmail.com

P. Makhija

e-mail: pals.makhija@gmail.com

G. Singh

Department of Information and Technology, Gyan Vihar University, Jaipur, Rajasthan, India

e-mail: gurpal.singh@india.com

agents. So, in the last section we have conducted a survey of various mobile software agents like INTELLIMINER, PADMA, PAPYRUS, HYBRID, KENSINGTON and DKN and discussed their salient features.

Keywords Mining · CSU · CSA · CLDC · Mobile software agents

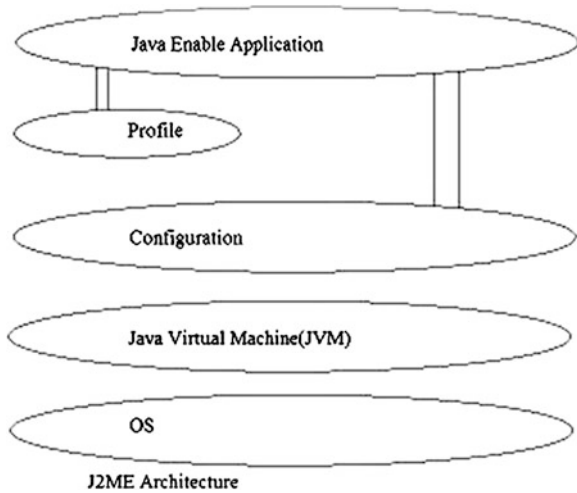
1 Introduction

The embrasive and extensive adoption of computers and the advancement in Database have bestowed the abundant amount of datasets. The deviation in the computer science have made it feasible to procure to accumulate and massive quantity of data electronically in databases, presently in gigabytes or terabytes in a single database only. The exuberant augmentation of data in database has evolved a crucial need for affirmative data mining methods to device relevant information and knowledge. Viewing the other side of coin, the evolution in the network based computing like private intranet, internet, etc. has constituted appeal for the development of such kinds of techniques of data mining that can emerge as a boon in different computing environments. Few years ago, mobile enlargement to Grid System have been progressively considered in order to support universal admittance and preference to the Grid and to involve mobile devices as an appended mobile resources [1, 2]. In the late 1980s the inculcation of data mining and knowledge discovery appeared to scrutinize the information material of data. Mobile devices also use it with the help of MIDLET and CLDC constituent of J2ME [3, 4]. The major hurdle in the path of development of mobile data mining is finding the customary mobile user behavior and pattern in ample amount of data. Initially, the algorithms in finding the frequent user behavior pattern have been analyzed thoroughly in the recent years. The prominent characteristics in all the algorithms is that they make use of a particular data set and frequent item set dwelled by the mobile user. But the area of concern that occurred in this case is that the algorithms do not acknowledged that the behavior of mobile user changes periodically as the time moves on.

2 CLDC & J2ME

CLDC stands for Connected Limited Device Configuration (CLDC) came out as a J2ME standard for the development of mobile applications which re utilized with DMS services. The main of CLDC is to implement applications of data mining in mobile devices. Before the development of J2ME technology, its architecture was introduced. It was also discussed that for what purpose of J2ME is developed and how its services will be provided to the users. The highly optimized environment

Fig. 1 J2ME architecture

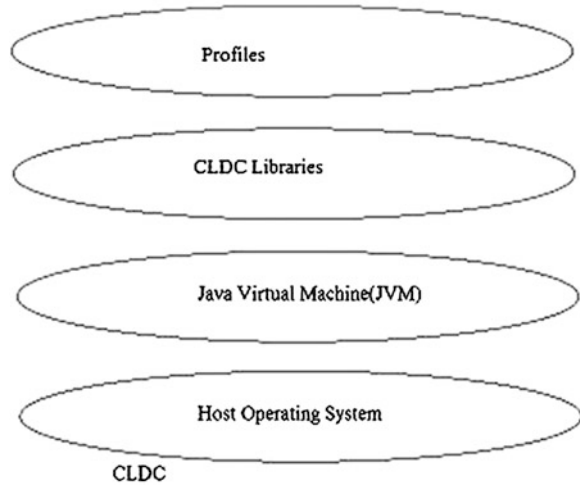


of java runtime is J2EE. The main aim of J2EE was the customer and embedded device markets which consists of the equipment's like Personal Digital Assistant, cellular telephones etc. The architecture of J2ME is shown in the Fig. 1.

Configurations are the most important branch of J2ME. A configuration can be defined as a stipulation that delineate a Java Virtual Machine and a group of APIs that intended towards a particular class of device. This kind of stipulation is Connected, Limited Device Configuration. The CLDC stipulates the devices which contain less than 512 kb of RAM attainable for the java system and a restricted network connection. It also stipulates, a stripped down virtual machine, which is called as KVM, as well as a group of APIs for important application services. The three types of packages used in J2ME are java.io, java.lang and java.util package. Another package which is used for implementation of Generic Connection Framework is javax.microedition.io; it is specifically used for establishment of network connections.

There are already thousands of games present which totally rely on the concept of J2ME and especially with the youth generation. In order to develop new mobile applications, there was an urgent need of object oriented programming languages which is fulfilled by Java. Configurations implements the basic functionality and a path to provide efficient flexibility, but there is one drawback as no services are provided for the management of life cycle of application, user interface, modifying and managing data on the device and the absolute approach to information stored on the network [5]. The CLDC position in J2ME Architecture is shown in the Fig. 2.

Fig. 2 CLDC in J2ME architecture



3 Proposed CSU and CSA Algorithms

In this paper we are also proposing two techniques i.e. CSU [6] and CSA [6] viz. Create Select Update and Create Select Alter based data mining techniques for mobile computing environments.

CSU (Create Select Update) Algorithm:

Step1: Select the data source on which mining has to be performed.

Step2: Create table tablename Column 1 Data Type 1, Column 2 Data Type 2 ,....., Column n Data Type n with condition from data source selected in Step1.

Step3: Insert into tablename Value 1, Value 2,....,Value n.

Step4: Select Column 1, Column 2,..., Column n from data source created in Step2. (to select all the columns). Select Column 1, Column 2,....., Column n WHERE condition from data source created in Step2. (to select the specified columns).

Step5: Update tablename set Column 1 = Value a1, Column 2 = Value a2,....., Column n = Value an (to update all the rows). Update tablename set Column 1 = Value a1, Column 2 = Value a2,....., Column n = Value an WHERE condition (to update the specified rows).

Step6: Apply CLDC profile.

Step7: Establish the connection.

Step8: According to the requirement apply J2ME packages.

Step9: Using Wireless tool kit see the results on simulator.

Step10: Apply the best Data mining techniques available.

Step11: Finish.

CSA (Create Select Alter) Algorithm:

Step1: Select the data source on which mining has to be performed.

Step2: Create table tablename Column 1 Data Type 1, Column 2 Data Type 2,....., Column n Data Type n with condition from data source selected in Step1.

Step3: Insert into tablename Value 1, Value 2,....., Value n.

Step4: Select Column 1, Column 2,....., Column n from data source created in Step2. (to select all the columns). Select Column 1, Column 2,....., Column n WHERE condition from data source created in Step2. (to select the specified columns).

Step5: Alter table tablename add Column A1 data type A1, Column A2 data type A2,....., Column An data type An. Alter table tablename modify Column A1 data type A1, Column A2 data type A2,....., Column An data type An. **Step6:** Apply CLDC profile.

Step7: Establish the connection.

Step8: According to the requirement apply J2ME packages.

Step9: Using Wireless tool kit, see the results on simulator.

Step10: Apply the best Data mining techniques available.

Step11: Finish.

4 Proposed Ambulatory Data Mining (ADM)

Wide range of opportunities has been created to perform data analysis task with continuous advancement in the field of Mobile devices including smart phones. This data analysis task is performed in an ad hoc computing environment which includes number of computational devices such as smart phones or sensors and the applications which run on such devices used for mining and analysis. Then all devices should use a common platform like we have Java Agent Development Framework that is JADE [7] which will be running on all the devices. Then one of these device will initiate the computational task. This same device is responsible for firing mobile software agents. These mobile software agents roam in an ad hoc network formed and perform the following three tasks:

1. It will search for the available applications on the devices in the network.
2. It will discover the computational capabilities of all the devices in a network.
3. It will also search for the available data sources in a network.

Agents after performing the above three tasks will divide the tasks into sub tasks to perform the initiated task. This division will be a collective decision based on certain criteria like proximity to the source of data, the available applications to perform the process, etc. When we collaboratively perform the mining task with the help of different devices connected in an ad hoc network then we use following types of software agents [8]:

1. There are certain agents which are already there on the mobile device or are distributed over the network when mining task is initiated.

2. Then we have second type of agents which are used to process available techniques and data sources and also used to find out the available computational resources in a network.
3. Third type of agents are the agents which roam in the network and collaboratively reach the final decision by consulting the different mobile agent miners available in the network.

Based on the above agents following are the steps that will be carried out in Ambulatory Data Mining (ADM) [8]:

1. Mining task is given an initiation call.
2. All the available mobiles are collected and an ad hoc network is formed.
3. Then data sources and the respective computational sources will be searched for.
4. Then the available techniques will be analyzed and out of all best technique will be selected to perform the mining task.
5. Then we will decide which mobile agent is to be kept stationary and which is to be kept in a mobile state.
6. Mining will be performed on the streaming data with the help of mining models.
7. If the model fails to supplement the desired result then next model is chosen and if it produces the desirous results then the results are forwarded back to decision maker agents.

5 Survey of Mobile Software Agents for Distributed Data Mining in Mobile Environment

Here we are trying to examine the use of mobile software agents for distributed data mining in mobile environment. We have shown a survey of a variety of present mobile software agents based Distributed Data Mining systems like INTELLIMINER, PADMA, PAPYRUS, HYBRID KENSINGTON and DKN and also have mentioned their significant characteristics. Flexibility and self-sufficiency of mobile software agents make them an appropriate tool form software deployment in mobile environment. In centralized data mining method, every bit of data should be actually placed at the same position. The raise in data production needs that large amount of data be communicated to a central location where the data would be mined.

For mobile networks, communication takes more power and therefore communicating big quantity of data over extensive distances is not a viable option. This method also takes an elongated response time. Using a centralized method for mining data which came into existence by distributed applications does not fulfill with the distributed computing concept thereby can't make use of distributed resources fully [9].

Distributed Data Mining (DDM) is a technique that permits data to be mined in a distributed style. The data analysis is done locally and a global data model is made by joining the local results [10]. Distributed Data Mining removes the need to combine data that is distributed, which help avoiding several issues like privacy of data and communication [11].

There has been a quantity of job on the performance examination of the agent-based systems when equated to the conventional DDM systems. The conventional systems were based on the method of sending all data to a centralized repository where it was mined. The agent based system had agents which used to go to the distant data site, computed local models which were then sent to a centralized position for producing the final result.

A bunch of work has been done and is still being done in the field of agent-based DDM systems. Software agent technology is rising as the most capable technology to supply to the requirements of DDM. All the agent-based systems discussed here have a roughly alike architecture having local data agents conducting data mining job at an information source, an organization and management mechanism to see agent’s access to the data source and an approach to unite and present details.

Generally all the systems were planned for DDM activities carried out over the Internet with the exemption of the Papyrus system which was created for clusters, meta- clusters and super-clusters of work stations. Most of the systems are made using Java, thereby they are platform independent.

Comparison between different types of DDM systems:

DDM system name	Platform	Characteristics
INTELLIMINER	JAVA	<ul style="list-style-type: none"> • Support distributed do all loop primitive over clusters of SMP workstation
PADMA	C++	<ul style="list-style-type: none"> • Its network type is internet • Backs up for SQL based requests • Parallel data access process
PAPYRUS	JAVA AGLETS	<ul style="list-style-type: none"> • Its network type is internet • Approach selection support • Provides a layered architecture • Its network type is clusters
HYBRID	DAME	<ul style="list-style-type: none"> • Cost matrix • Allocation time is better • Its network type is internet
KENSINGTON	JAVA	<ul style="list-style-type: none"> • Identifies analysis algorithms as class objects
DKN	Voyager	<ul style="list-style-type: none"> • Knowledge discovery • Retrieval of customized information • Mobile Agent Infrastructure • Its network type is internet

6 Conclusion

In our research paper, we have tried to examine distinct features and elements of data mining on mobile environments. We have considered in our writing, two algorithms CSU and CSA, which are attained by CLDC component of J2ME. And for the purpose of collaborative data mining in mobile environment, we have also explained a new terminology ADM, which is short for Ambulatory Data Mining. To conclude our work we have compared all the data mining systems for mobile networks, on the basis of surveys done to give a detailed view about their important characteristics.

References

1. Migliardi, M., Maheswaran, M., Maniyaran, B., Card, P.: Mobile interfaces to computational, data, and service grid systems. *ACM SIGMOBILE Mob. Comput. Commun. Rev.* **6**(4), 8–15 (2004)
2. Wesner, S., Dimitrakos, T., Jeffrey, K.: Akogrimo—the grid goes mobile. In: *ERCIM*, vol. 59 (2004)
3. Arcelus, A., Jones, M.H., Goubran, R., Knoefel, F.: Advanced information networking and applications workshops, 2007, AINAW. In: *21st International Conference*, May 2007
4. Bahati, R.M., Bauer, M.A.: In: *ICAS'08: Proceedings of the Fourth International Conference on Autonomic and Autonomous Systems (ICAS'08)*, pp. 88–93, IEEE Computer Society, Washington, DC, USA (2008)
5. Ortiz, 2004a, A Survey of J2ME Today, Sun Developer Network (SDN), viewed 13 August 2007
6. Dubey, A.K., Kushwaha, G.R., Prakash, J.: A novel CSUA based data mining approach for mobile computing environments. *Int. J. Comput. Appl.* (0975–8887) **7**(4), 23–26 (2010)
7. Bellifemine, F., Poggi, A., Rimassa, G.: Developing multi-agent systems with JADE. In: Castelfranchi, C., Lesperance, Y. (eds.) *Intelligent Agents VII. Agent Theories Architectures and Languages*, 7th International Workshop, ATAL 2000, Boston, MA, USA, July 7–9, 2000, Proceedings. *Lecture Notes in Computer Science*, vol. 1986, pp. 89–103. Springer Verlag (2000)
8. Stahl, F., Gaber, M.M., Bramer, M., Yu, P.S.: Pocket data mining: towards collaborative data mining in mobile computing environments. In: *Tools with Artificial Intelligence (ICTAI)*, 2010 22nd IEEE International Conference on, vol. 2, pp. 323, 330, 27–29 Oct 2010 doi: [10.1109/ICTAI.2010.118](https://doi.org/10.1109/ICTAI.2010.118)
9. Park, B.-H., Kargupta, H.: Distributed data mining: algorithms, systems, and applications. In: Ye, N. (ed.) *Handbook of Data Mining*, p. 341361. Lawrence Erlbaum, Hillsdale (2003)
10. Provost, F.: Distributed data mining: scaling up and beyond. In: *Advances in Distributed and Parallel Knowledge Discovery*, pp. 3–27. MIT Press (2000)
11. Kargupta, H., Park, B.-H., Hershberger, D., Johnson, E.: Collective data mining: a new perspective toward distributed data analysis. In: *Advances in Distributed and Parallel Knowledge Discovery*, pp. 133–184. AAAI/MIT Press (1999)

Ant Colony Optimization Model for Discrete Tomography Problems

Divyesh Patel and Tanuja Srivastava

Abstract Ant Colony Optimization (ACO) algorithms have been applied to get the solution of many hard discrete optimization problems. But ACO algorithms have not been applied to Discrete Tomography (DT) problems yet. In this paper, we propose a framework of ACO meta-heuristic for DT problems. Some variations in the framework have also been discussed.

Keywords Ant colony optimization · Discrete tomography · Convex binary matrices

1 Introduction

Discrete Tomography (DT) [1] is the reconstruction of discrete sets from its projections. The number of projections is usually 2 to 4. The primary problem of DT is the reconstruction of binary matrices from its row and column sums. As the solution space is very large, some additional geometrical constraints are imposed on the binary matrices. Mostly, convexity, connectivity and periodicity constraints are used.

In 2001, Woeginger [2] proved that the reconstruction of an hv-convex binary matrix from its row and column projections is NP-complete. This NP-complete problem of reconstructing hv-convex binary matrices from two projections was reformulated as an integer programming problem and approximated by Simulated Annealing method by Jarray and Tlig [3] in 2010.

D. Patel (✉) · T. Srivastava
Department of Mathematics, IIT Roorkee, Roorkee, India
e-mail: divyshpatel@gmail.com

T. Srivastava
e-mail: tanujfma@iitr.ernet.in

Ant Colony Optimization (ACO) is a meta-heuristic used to solve hard combinatorial optimization problems. It is based on the foraging behavior of real ants. History of ant algorithms starts from the early nineties. An algorithm called Ant System (AS) [4, 5] was developed by Dorigo et al. in 1991, 96. Later improved versions of AS were proposed. ACS [6] was proposed in 1997, AS_{rank} [7] in 1999, MAX-MIN Ant System [8] in 2000. These algorithms have been applied to various optimization problems. Examples are Traveling Salesman Problem (TSP), Quadratic Assignment, vehicle routing, graph coloring, shortest common super-sequence, etc. We have applied the foraging paradigm of ant colonies in DT problems and we present an Ant Colony Optimization framework for reconstruction of hv-convex matrices from two orthogonal projections.

The present paper is divided into following sections. Section 2 describes the basic notions of DT required in this paper. Section 3 introduces the structure of the ACO meta-heuristic for DT problems. In Sect. 4 we give a formal description of the ACO algorithm to obtain the solution of the problem of reconstruction of hv-convex binary matrices from its row and column sums. Section 5 mentions some variants that can be applied to the above proposed model. Lastly we conclude in Sect. 6.

2 Preliminaries of Discrete Tomography

Let $R = (r_1, r_2, \dots, r_m)$ and $C = (c_1, c_2, \dots, c_n)$ be non-negative integer vectors. Denote by $\mathfrak{U}(R, C)$ the class of all binary matrices $A = (a_{ij})$ satisfying

$$\sum_{j=1}^n a_{ij} = r_i \quad i = 1, 2, \dots, m$$

$$\sum_{i=1}^m a_{ij} = c_j \quad j = 1, 2, \dots, n$$

The vectors R and C are called row and column sum vectors respectively. Figure 1 shows a binary matrix and its row and column sums.

Let $A \in \mathfrak{U}(R, C)$. A switching component of A is a 2×2 sub-matrix of A of the form $\begin{pmatrix} 1 & 0 \\ 0 & 1 \end{pmatrix}$ or $\begin{pmatrix} 0 & 1 \\ 1 & 0 \end{pmatrix}$.

By a switching operation we mean a transformation of the sub-matrix $\begin{pmatrix} 1 & 0 \\ 0 & 1 \end{pmatrix}$ into the sub-matrix $\begin{pmatrix} 0 & 1 \\ 1 & 0 \end{pmatrix}$ or vice versa. It is evident that by performing a switching operation the row and column sums of a binary matrix does not change.

Theorem 2.1 [9] Let $A, B \in \mathfrak{U}(R, C)$. Then A is transformable into B (or vice versa) by a finite sequence of switching operations.

Fig. 1 A 5×5 binary matrix and its row (R) and column (C) sums

						R
						↓
						3
						2
						2
						4
						4
C →	3	2	3	4	3	

A binary matrix is said to be horizontally-convex or h-convex if in each row, all the ones are consecutive. Similarly a binary matrix is said to be vertically-convex or v-convex if in each column, all the ones are consecutive. A binary matrix is said to be hv-convex (or simply convex) if it is both h-convex as well as v-convex. Examples are illustrated in Fig. 2.

To measure the convexity of a binary matrix $A = (a_{ij})$ of size $m \times n$, we introduce the following function

$$f(A) = \sum_{i=1}^m \sum_{j=1}^{n-1} a_{ij}a_{i,j+1} + \sum_{i=1}^{m-1} \sum_{j=1}^n a_{ij}a_{i+1,j}$$

Proposition 2.2 [3] Let $A = (a_{ij})$ be an $m \times n$ binary matrix with (R, C) as row and column sum vectors respectively. Then A is hv-convex iff $f(A) = 2 \sum_{i=1}^m r_i - m - n$ or $f(A) = 2 \sum_{j=1}^n c_j - m - n$.

Reconstruction Problem (R1) Instance: Two non-negative vectors $R = (r_1, \dots, r_m), C = (c_1, \dots, c_n)$ Task: Construct an hv-convex binary matrix $A = (a_{ij})$ having R and C as row and column sums respectively.

3 ACO Model Building for Problem R1

ACO is a meta-heuristic in which a population of artificial ants cooperates in determining good solutions to difficult discrete optimization problems. These artificial ants are stochastic solution building subroutines which probabilistically construct a solution for the optimization problem. These ants iteratively add solution components to partial solutions by using (i) the heuristic values of the problem instance, and (ii) the pheromone trails which change dynamically at runtime reflecting the ants acquired search experience.

Reconstruction problem R1 can be formulated as a maximization problem given by

$$\text{Maximize } f(A) = \sum_{i=1}^m \sum_{j=1}^{n-1} a_{ij}a_{i,j+1} + \sum_{i=1}^{m-1} \sum_{j=1}^n a_{ij}a_{i+1,j} \tag{1}$$

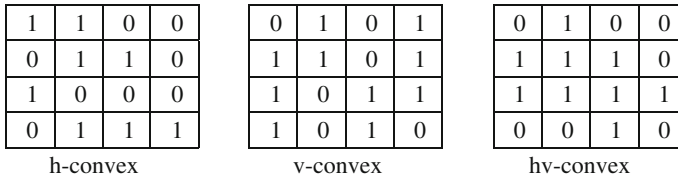


Fig. 2 Examples of h-convex, v-convex and hv-convex binary matrices

$$\text{subject to } \sum_{j=1}^n a_{ij} = r_i \quad i = 1, 2, \dots, m \tag{2}$$

$$\sum_{i=1}^m a_{ij} = c_j \quad j = 1, 2, \dots, n \tag{3}$$

$$a_{ij} \in \{0, 1\} \tag{4}$$

The above reconstruction problem of DT can be written as a maximization problem (S, f, Π) , where S (set of candidate solutions) is the set of all binary matrices of order $m \times n$, f is the objective function given by Eq. (1) and Π is the set of constraints given by Eqs. (2), (3), (4).

The objective is to find a binary matrix $A \in S$ satisfying the constraints given by Π having maximum objective function value.

In order to apply ACO, the optimization problem (S, f, Π) is characterized by the following parameters:

Parameters	Description
$\mathcal{C} = \{C_1, C_2, \dots, C_N\}$	\mathcal{C} is the set of feasible matrices
$L = \{l_{C_i, C_j} : C_i, C_j \in \mathcal{C}\}$	L is the set of possible transformations (by switching operations) between the matrices in $\mathcal{C} \subseteq \mathcal{C}$
$\Pi \equiv \Pi(\mathcal{C}, L)$	Π is the set of problem constraints imposed on the elements of the sets \mathcal{C} and L
$s = (C_i, \dots, C_j)$	s is a state of the problem defined by a finite sequence of the elements in set \mathcal{C}
P	P is the set of all possible sequences over the elements of \mathcal{C}
\bar{P}	\bar{P} is the set of all feasible sequences with respect to the constraints Π . Thus $\bar{P} \subseteq P$
Neighbor states	Two states s_1 and s_2 are neighbors if s_1 can be reached from s_2 or vice versa using only one switching operation (i.e. if C_j is the last matrix in the sequence defining state s_1 then there must exist a matrix $C_j \in \mathcal{C}$ such that $l_{C_i, C_j} \in L$ and state $s_2 = (s_1, C_j)$)
N_s	N_s is the set of all neighbors of state s . It is called neighborhood of s
φ	φ is a solution state if $\varphi \in \bar{P}$ and satisfies all the problem's requirements

The graph $G(\mathcal{C}, L)$ gives a representation of the above defined discrete optimization problem where \mathcal{C} is the set of vertices and L is the set of edges.

Feasible paths on the graph G lead to the solution of our maximization problem. ACO algorithms can be used to find the feasible paths leading to the solution. ACO algorithm uses artificial ants to solve the optimization problem with the aid of above defined graph representation. Artificial ants have the following properties:

- An ant searches for optimal feasible matrix by moving through the graph G .
- An ant i has a memory M^i which can be used to store information of the path it followed so far.
- An ant i has a start state s^i and termination conditions e^i .
- An ant in a particular state can move to only its neighboring feasible states using probabilistic decision rules.
- While moving from one state to another, ants build the solution in an incremental way. Ants stop when any of the termination conditions is satisfied.
- The ant's probabilistic decision rule is defined as a function of (i) the pheromone trails of the available nodes and the heuristic values, (ii) the ant's memory, and (iii) the problem's constraints.
- Ants update pheromone trail τ_{ij} on the edge (i,j) after moving from node i to node j .
- After reaching a solution, an ant can travel backwards (in order to help in finding the shortest path) on the same path with the help of its memory and update the pheromone trails on the edges it traverses.

There is also an additional procedure other than the ants activities called as pheromone trail evaporation. This evaporation procedure is the process of reducing the pheromone trail intensity over time on the edges of the problem graph. Pheromone evaporation is required so that the algorithm do not converge too rapidly to a sub-optimal region.

Thus the ant's behavior is summarized as follows. Ants concurrently move through the neighbor states of the problem by moving along the adjacent nodes of the graph. Ants travel by making a stochastic decision based on the pheromone trails and the heuristic values. In this whole process, ants incrementally construct the solutions to our optimization problem.

The ACO meta-heuristic algorithm is described below:

function ACO()

 initialization()

 while(termination condition is not satisfied)

 for each ant repeat

 antcycle()

 end for

 pheromone evaporation()

 end while

end function

function antcycle()

 initialize ant()

 move to next state based on stochastic decision policy()

 evaluate solution()

 update pheromone trails()

 update ant memory()

end function()

Discrete tomography problems are readily transformed into graph theory problems and ACO method is well suited for graph theory problems because of their multi-agent feature. So ACO is an ideal algorithm for DT problems. Also due to the multi-agent feature of ACO paradigm, more area of feasible region can be explored yielding better optimal solution value qualitatively. Further in ACO the search for the optimal solution proceeds in multi-dimension in the sense that multiple ants choose multiple nodes of the graph during their journey. Also ants communicate indirectly among themselves in order to move to the next node in the graph. These are the significance and advantages of using ACO to search for the solution of an optimization problem represented by a graph.

4 Solution of R1 Based on ACO Model

According to the parameters introduced in Sect. 3, the reconstruction problem R1 can be described as:

Let \mathcal{C} be the set of binary matrices of order $m \times n$ having $H \in \mathbb{N}^m, V \in \mathbb{N}^n$ as the row and column projections respectively. Let L be the set of transformations or connections among the matrices in \mathcal{C} such that matrices C_i and C_j are connected if and only if C_i can be obtained from C_j or vice versa by a single switching operation. Associated with each matrix $C_i \in \mathcal{C}$, there is a heuristic value given by the objective function value $f(C_i)$ which is used in the stochastic decision policy by the ants. So the reconstruction problem is to find a matrix $C_0 \in \mathcal{C}$ in the graph $G(\mathcal{C}, L)$ such that $f(C_0)$ is maximum. According to theorem 2.1, any matrix $M \in \mathcal{U}(H, V)$ can be transformed to the matrix we seek, i.e. an hv-convex matrix $M_0 \in \mathcal{U}(H, V)$. Thus ACO can be adapted easily to solve this reconstruction problem. Hence it is an appropriate algorithm for Discrete Tomography problems.

In the following we explain the working of ACO paradigm for the problem R1. Starting state of all the ants is a state of unit length, i.e. ants start from a state consisting of a single feasible matrix. This matrix is called initial solution of the problem. Initial solution matrix C_1 is obtained by the classical Ryser's algorithm. All the ants start from this matrix C_1 . Matrix C_1 is added to the ants memory and objective function value is calculated for matrix C_1 . Then ants enter a cycle which lasts until termination condition is not satisfied, i.e. until an ant reaches an hv-convex feasible matrix.

During each step of the ant cycle, an ant situated on node i considers the feasible neighbor states, computes their transition probabilities, and applies its decision policy for choosing the next node to move to. It then moves to the new node j and updates its memory as well as the pheromone trail value τ_{ij} . In the process, the solution is evaluated for the optimal value and also the pheromone evaporation function is invoked. As in this reconstruction problem we only seek an hv-convex feasible matrix, we stop the algorithm once an ant reaches a node representing an hv-convex matrix.

The values of pheromone trail τ_{ij} on the connection l_{ij} represents the desirability of moving to node j from node i . The pheromone trail information is changed by the ants to reflect their experience during their journey through the graph G . Pheromone trail information is more useful in finding the minimum number of transformations (in terms of switching operations) from the initial matrix solution to the optimal hv-convex matrix.

The memory of each ant contains the already visited nodes and some other useful information depending upon the problem. By exploiting its memory, an ant can avoid nodes that are already visited. This prevents an ant to fall into a loop. The memory of an ant can also be used to find the length of its tour from initial solution state to optimal solution state and to travel the same path backwards in case of finding the shortest path from the initial node to the optimal node.

The probability P_{ij}^k with which an ant k at node i selects node $j \in N_i^k$ to move to is given by the following probabilistic decision rule:

$$P_{ij}^k = \frac{(\tau_{ij})^\alpha [f(C_j)]^\beta}{\sum_{t \in N_i^k} (\tau_{it})^\alpha [f(C_t)]^\beta}$$

where $N_i^k \subseteq N_i$ is the feasible neighborhood of node i for ant k , α and β are parameters to vary the relative weight of pheromone trail τ_{ij} on edge (i, j) and heuristic value $f(C_t)$ associated with node t respectively.

After moving from node i to node j , an ant k deposits a quantity of pheromone given by $\Delta\tau^k = f(C_j) - f(C_i)$ on the connection l_{ij} that it has used. Thus pheromone trail value for the edge (i, j) is updated as

$$\tau_{ij} \leftarrow \tau_{ij} + \Delta\tau^k$$

Pheromone evaporation is applied to all edges l_{ij} of graph G by the following rule:

$$\tau_{ij} \leftarrow (1 - \rho)\tau_{ij}$$

where $\rho \in (0, 1]$ is the decay coefficient for pheromone trail.

5 Some Variations to the ACO Model

- i. All the ants are starting from a single matrix obtained by Ryser’s algorithm. So the first variation we can have is that to start the algorithm from different starting matrices. This can be achieved by a variation in the Ryser’s algorithm. Ryser’s algorithm constructs a feasible matrix by constructing the columns in the order $1, 2, \dots, n$. We can have $n!$ different permutations of the indices of columns to construct the initial matrix. So ants can start from different starting matrices obtained by using permutation of columns. By having different starting matrices we can get the solution much faster than all the ants starting from a single matrix.

- ii. In order to get the required solution (i.e. an hv-convex matrix) in minimum number of switching operations from the initial matrix, ants on reaching the solution node have to travel back to its starting node using its private memory. Thus in the process depositing more amount of pheromone on the shortest path between the initial and the final nodes. This makes the shortest path more favorable for the future ants to pass through.
- iii. If we are not strict about obtaining an absolute hv-convex matrix or we only require a nearly hv-convex matrix then we can actually get the solution much faster. We can halt the algorithm and get the solution as soon as within the desired value of convexity measure is achieved. This can be done by appending a termination condition on the value of the objective function.
- iv. This algorithm can be applied to reconstruct binary matrices of other classes as well. By changing the objective function used in the algorithm, we can get matrices of a desired class of binary matrices.

6 Conclusion

In this paper, we have given a brief description of a framework of Ant Colony Optimization method applicable to Discrete Tomography problems. We have then given a formal description of the ACO algorithm to the DT problem of reconstruction of an hv-convex binary matrix from its row and column sums. Some variants to the ACO model have also been discussed. Further work can be done in the analysis of parameter settings in a problem specific as well as general framework. Moreover comparison of ACO algorithm with other heuristic algorithms is also a direction for further research.

References

1. Herman, G.T., Kuba, A.: *Discrete tomography: foundations algorithms and applications*. Birkhäuser, Boston (1999)
2. Woeginger, G.J.: The reconstruction of polyominoes from their orthogonal projections. *Inf. Process. Lett.* **77**, 225–229 (2001)
3. Jarray, F., Tlig, G.: A simulated annealing for reconstructing hv-convex binary matrices. *Electro. Notes Discrete Math.* **36**, 447–454 (2010)
4. Dorigo, M., Maniezzo, V., Colomi, A.: Positive feedback as a search strategy. Technical Report 91-016, Dipartimento di Elettronica, Politecnico di Milano, Italy (1991)
5. Dorigo, M., Maniezzo, V., Colomi, A.: The Ant System: optimization by a colony of cooperating agents. *IEEE Trans. Syst. Man Cybern. Part B* **26**(1), 29–41 (1996)
6. Dorigo, M., Gambardella, L.M.: Ant colony system: a cooperative learning approach to the traveling salesman problem. *IEEE Trans. Evol. Comput.* **1**(1), 53–66 (1997)
7. Bullnheimer, B., Hartl, R.F., Strauss, C.: A new rank based version of the ant system: a computational study. *Central Eur. J. Oper. Res. Econ.* **7**(1), 25–38 (1999)
8. Stützle, T., Hoos, H.: MAX-MIN ant system. *Future Gener. Comput. Syst.* **16**, 889–914 (2000)
9. Ryser, H.J.: Matrices of zeros and ones. *Bull. Amer. Math. Soc.* **66**, 442–464 (1960)

Object Recognition Using Gabor Wavelet Features with Various Classification Techniques

Divya Sahgal and Manoranjan Parida

Abstract Object recognition is a process of detection and recognition of certain classes of objects like chairs, guitars, buildings etc., from an image or video sequence. Various researches have been done till now for extraction of object's features from real-world images using various approaches varying from appearance based approaches like PCA, LDA, ICA, moment invariant, shape context, SIFT etc. or model based approaches. We used a well known model based approach "Gabor wavelet transform" to extract the features. Gabor wavelets exhibit desirable characteristics of spatial locality and orientation selectivity. It has several advantages against robustness, illumination, multi-resolution, and multi-orientation. Classifications of objects are important areas in a variety of fields, such as pattern recognition, artificial intelligence and vision analysis. So using the Gabor wavelet features classification is done by various well known classifiers like KNN, Neural Network (NN), SVM, and Naive Bayes classifiers. So results are compared using these classifiers as well we have given various pros and cons for these methods.

Keywords Gabor wavelet · KNN · SVM · NN · Naive bayes

1 Introduction

Introduction goes here Object detection and recognition has attracted significant attention over the past few years in the field of computer vision, pattern recognition and image processing [1–3]. *Object detection* approach first came into existence in

D. Sahgal (✉) · M. Parida
Centre for Transportation Systems, IIT Roorkee, Roorkee, India
e-mail: divyasahgal1@gmail.com

M. Parida
e-mail: ctrans.iitr@gmail.com

1974 by Yoram Yakimovsky, who provided automatic location of objects in digital images [2]. It is a process of detection and recognition of certain classes like guitars, buildings etc. in image or video sequence. Humans are capable of recognizing the world around them based on the visual clues which they perceive from the environment with little effort, despite the fact that the image can contain objects of many different sizes/scales or they can be translated or rotated and can vary in different viewpoints [4, 5]. Various researches have been done till now for detection of objects from real-world images [2, 6], objects from noisy images [3, 7], objects from videos [8, 9], objects moving in space [1] and also tracking multiple objects [10]. Various approaches like feature classification [6], combination of appearance, structural and shape features [10], viewpoint independent object detection [9], wavelet transform methods [7] were adopted for efficient object detection.

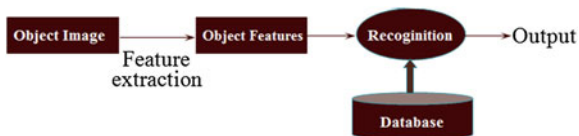
The computer vision literature is rich with approaches in solving the object recognition problem and based on the applied features these methods can be subdivided along many different lines on the basis of architecture point of view such as: *Appearance-based approaches*, which are directly based on images and extracts features corresponding to a particular appearance of the object, which is usually captured by different two-dimensional views of the object-of-interest. Appearance-based methods span a wide spectrum of algorithms, such as Edge matching [11], Gradient matching, Corners [11], Moment Invariants [12], Shape Context [12], Linear Analysis which includes Principal Component Analysis (PCA) [13], Independent Component Analysis (ICA) [14] and Linear Discriminant Analysis (LDA) [15] and Non-Linear Analysis which are kernel based methods and have been successfully applied to solve pattern recognition problems because of their capacity in handling nonlinear data includes methods such as Kernel Principal Component Analysis (KPCA) and Generalized Discriminant Analysis (GDA). Several other methods have been proposed for feature detection, among which the most popular is the Harris corner detector [2], Shi-Tomasi features, SIFT features, and Maximally Stable Extremal Regions [12] and *Model-(or shape-, or geometry-) based approaches*, the information about the objects is represented explicitly.

In this paper we select commonly used method Gabor wavelet (GW) method for feature extraction. Gabor wavelet had been used in the past for object detection in Infrared images [16], 3D object recognition in [17], and object tracking in [18]. The main aim to use Gabor wavelets is due to their multi-resolution, multiorientation properties. For recognition many different classifiers have been employed over the years like KNN, Neural Network (NN), GMM, HMM, SVM, LDA.

In our work, we focus on image-based object recognition, in which the goal is to determine what category or class an image belongs to, by using complete image means extracting the Gabor Wavelet features from whole image. In our work we used NN classifier which uses GW features obtained from whole image and its performance analysis is carried out with respect to KNN, Naive Bayes, and SVM classifiers. The model presented in this paper is effectively used to achieve computationally efficient object recognition as shown in Fig. 1.

The organization of this paper is as follows. Section 2 describes review of Gabor Wavelet feature extraction method. This section gives a brief discussion on

Fig. 1 Proposed model for object recognition



Gabor Wavelet method, which is used in our work in feature extraction for object recognition. Section 3 discusses various classifiers and their pros and cons which have been used for comparison. Section 4 will present the experimental results; here we have shown the results of various recognition systems. Lastly in Sect. 5 the concluding remarks and future work are stated.

2 Feature Extraction

In our work we select commonly used method Gabor Wavelets (GWs) with good characteristics of space-frequency localization are commonly used for extracting local features for various applications like object detection, recognition and tracking. Motivated by biological findings on the similarity of two-dimensional (2D) Gabor filters there has been increased interest in deploying Gabor filters in various computer vision applications and to texture analysis and image retrieval. The general functionality of the 2D Gabor filter family can be represented as a Gaussian function modulated by a complex sinusoidal signal. In our work we use a bank of filters built from these Gabor functions for texture feature extraction. The Gabor wavelet representation of an image is the convolution of the image with a family of Gabor Wavelets [19]. Gabor wavelets detect the edge detector, face region and facial features regions. GWs use Gabor functions which was first proposed in 1946 by Dennis Gabor [8]. Gabor transform is the short-time Fourier transform, used to determine the sinusoidal frequency and phase content of a signal which changes with time [20]. A complex Gabor filter is defined as the product of a Gaussian kernel times a complex sinusoid which is then transformed with a Fourier transform to derive the time–frequency analysis and is defined as [21].

$$\Psi_{u,v}(Z) = \sigma^2 \frac{\|K_{u,v}\|^2 \|Z\|^2}{e} 2\sigma^2 \frac{-\|K_{u,v}\|^2 \|Z\|^2}{[e^{-iK_{u,v}Z} - e^{-\sigma^2/2}]} \tag{1}$$

where $e^{-iKZ_{u,v}}$ is a complex plane wave and $e^{-\sigma^2/2}$ is a term compensates for the DC value which makes the kernel DC-free [22]. The parameter $z = (x, y)$ indicates a point with horizontal and vertical coordinate of image obtained after Otsu thresholding. The operator $\| \|$ denotes the norm operator. Parameters u and v defines the angular orientation and the spatial frequency of the Gabor kernel where v determines scale of kernel. The standard deviation of Gaussian window $\sigma = 2\pi$. The wave vector $k_{u,v}$ is

$$K_{u,v} = K_v e^{i\phi_u} \quad (2)$$

where $k_v = k_{\max}/f_v$ and $\phi_u = u\pi/4$ with $u \in \{0, \dots, 3\}$ if four different orientations are chosen. The maximum frequency $k_{\max} = \pi/2$ and the spatial factor $f = \sqrt{2}$ with $v = \{0, \dots, 3\}$ if four different scales are chosen.

To extract the features from images using GW following steps are carried out (shown in Fig. 2):

- Step 1: Create Gabor Wavelet filter and set the parameters for Gabor wavelet such as Gabor kernel size is 24×24 , orientations $0, \pi/4, \pi/2, 3\pi/4$ and scales $0, 1, 2, 3$.
- Step 2: Gabor kernel is composed of real and imaginary parts with 4 orientations and 4 scales (shown in Figs. 2, 3).
- Step 3: Now convert an input image to Gray scale and reduce its size to 40×40 .
- Step 4: Convolve the image with real and imaginary part of Gabor filter separately.
- Step 5: Calculate magnitude using Real and Imaginary values obtained from Step 3.
- Step 6: Repeat the above steps for all the images. So feature vector of size 25600×1 ($4 \times 4 \times 40 \times 40$) containing magnitude response corresponding to each image is obtained.

3 Recognition

In machine learning and statistics, classification is the problem of identifying which of a set of categories (sub-populations) a new observation belongs, on the basis of a training set of data containing observations (or instances) whose category membership is known. For recognition many different classifiers have been employed over the years like KNN, Neural Network (NN), GMM, HMM, SVM, LDA. We have used Naive Bayes, SVM, KNN and multi-Perceptron Neural Network classifiers which are explained as under with their pros and cons.

The Naïve Bayes Classifiers are based on Bayesian theorem with strong (naive) independence assumptions and is particularly suited when the dimensionality of the inputs is high. Despite its simplicity, it can often outperform more sophisticated classification methods. A more descriptive term for the underlying probability model would be “independent feature model”. In simple terms, a naive Bayes classifier assumes that the presence (or absence) of a particular feature of a class is unrelated to the presence (or absence) of any other feature, given the class variable [23, 24].

Pros: Easy to implement.

- Good results obtained in most of the cases.
- Fast.

Fig. 2 The real part of 4×4 Gabor wavelets

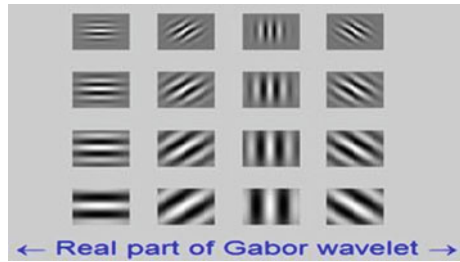
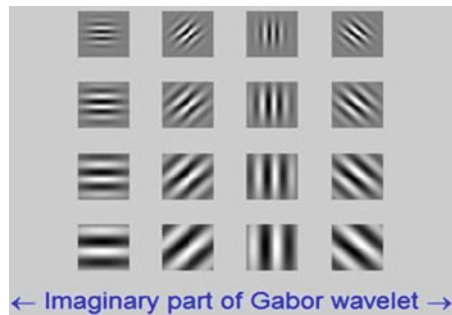


Fig. 3 The imaginary part of 4×4 Gabor wavelets



- Induced classifiers are easy to interpret.
- Robust to irrelevant attributes.
- Uses evidence from many attributes.

Cons:

- Assumption: class conditional independence, therefore loss of accuracy.
- Practically, dependencies exist among variables. E.g., hospitals: patients: Profile: age, family history etc. Symptoms: fever, cough etc., Disease: lung cancer, diabetes etc.
- Dependencies among these cannot be modeled by Naïve Bayesian Classifier.
- Low performance ceiling on large databases.

k-Nearest neighbour classifiers (KNN): In pattern recognition, *the K-nearest neighbour algorithm (k-NN)* is a method for classifying objects based on closest training examples in the feature space. k-NN classification is one of the most fundamental and simple classification methods and should be one of the first choices for a classification study when there is little or no prior knowledge about the distribution of the data. It is a type of instance-based learning, or lazy learning where the function is only approximated locally and all computation is deferred until classification. KNN classification was developed from the need to perform discriminant analysis when reliable parametric estimates of probability densities are unknown or difficult to determine [25, 26].

Pros:

- Simple to implement and easy to compute.
- Flexible to feature/distance choices.
- Straightforward logic.
- Naturally handles multi-class cases.
- Fast training.
- Excellent performance on a wide range of tasks.

Cons:

- Large search problem to find nearest neighbours.
- Basic method.
- It is not sensitive to complex patterns unless extended to include more than just nearest neighbours.

SVM classifiers were relatively new concept having nice generalization properties. They are hard to learn—learned in batch mode using quadratic programming techniques. Using kernels can learn very complex functions. Originating from the hyperplane classifier proposed in [27], *the support vector machine (SVM)* has been greatly developed and widely applied in machine learning, classification and pattern recognition ever since. The original SVM algorithm was invented by Vladimir N. Vapnik and the current standard incarnation (soft margin) was proposed by Vapnik and Corinna Cortes in 1995. Support vector machine (SVM) [28] is the youngest part in statistical learning theory. It is a concept in statistics and computer science for a set of related supervised learning methods that analyze data and recognize patterns, used for classification and regression analysis. The standard SVM takes a set of input data and predicts, for each given input, which of two possible classes forms the input, making the SVM a non-probabilistic binary linear classifier. Given a set of training examples, each marked as belonging to one of two categories, an SVM training algorithm builds a model that assigns new examples into one category or the other. As a classifier, Support Vector Machines (SVM) are used to cluster data into two classes by finding the maximum marginal hyperplane that separates one class from the other by Boser et al. [27]. The margin of the hyperplane, which is maximized, is defined by the distance between the hyperplane and the closest data points. The data points that lie on the boundary of the margin of the hyperplane are called the support vectors. SVMs have been used for multi-class classification problems [29]. Many publicly available SVM packages at <http://www.kernel-machines.org/software>.

Pros:

- Kernel-based framework is very powerful, flexible.
- SVMs work very well in practice, even with very small training sample sizes.
- Often a sparse set of support vectors—compact at test time.

Cons:

- No “direct” multi-class SVM, must combine two-class SVMs.
- Computation, memory.
- During training time, must compute matrix of kernel values for every example pair.
- Learning can take a very long time for large-scale problems.
- Can be tricky to select best kernel function for a problem.

Neural Network Classifier is a quiet old technique. It can easily be learned in incremental fashion. To learn complex functions—use multilayer perceptron (not that trivial). An artificial neural network (ANN), also called a simulated neural network (SNN) or commonly just *neural network (NN)* is an interconnected group of artificial neurons that uses a mathematical or computational model for information processing based on a connectionist approach to computation. In most cases a NN is an adaptive system that changes its structure based on external or internal information that flows through the network [30]. The earliest work in neural computing goes back to the 1940s when McCulloch and Pitts introduced the first neural network computing model. In the 1950s, Rosenblatt’s work resulted in a two-layer network, the perceptron, which was capable of learning certain classifications by adjusting connection weights. Although the perceptron was successful in classifying certain patterns, it had a number of limitations. The perceptron was not able to solve the classic XOR (exclusive or) problem. Such limitations led to the decline of the field of neural networks. However, the perceptron had laid foundations for later work in neural computing. In the early 1980s, researchers showed renewed interest in neural networks. Recent work includes Boltzmann machines, Hopfield nets, competitive learning models, multilayer networks, and adaptive resonance theory models [31]. In more practical terms neural networks are non-linear statistical data modelling tools. They can be used to model complex relationships between inputs and outputs or to find patterns in data. There are various types of neural networks. Explanation of all these types will not be possible due to constraint in space. We are using specific type of neural network “The Multi-layer Perceptron (MLP)” for our object recognition system [30].

Pros:

- Can learn more complicated class boundaries.
- Fast application.
- Can handle large number of features.

Cons:

- Require Rigorous training.
- Hard to interpret.

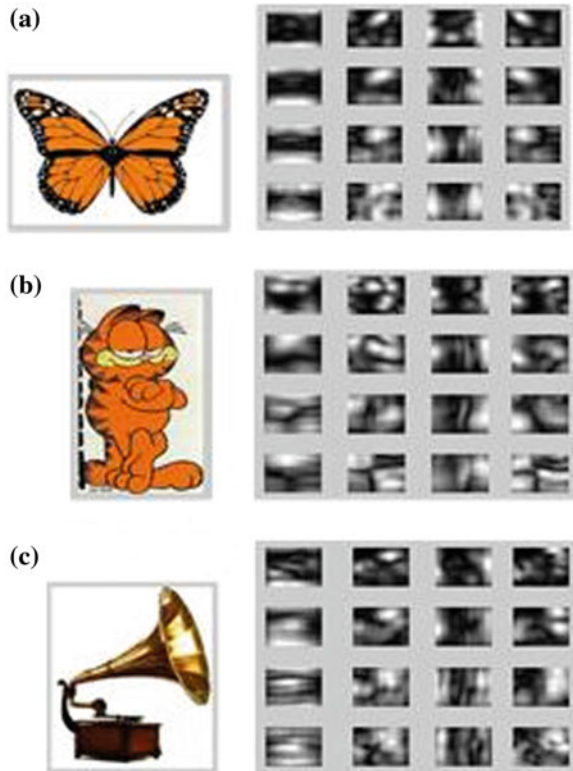


Fig. 4 Images of objects used in training our system for object recognition

4 Experimental Results

We experiment our work using 32-bit OS, MATLAB 7.9.0 and processor used is Intel (R) Core (TM) 2 Duo CPU T6570 with a speed of 2.10 GHz. Here we are presenting the extensive performance evaluation of various recognition methods. The experimental work is performed on samples of the dataset consists of images of various objects. It contains a total of 9146 images of objects belonging to 101 categories (including faces, watches, ants, pianos, chairs, guitars, etc.). Most categories have about 50 images with the size of 300 * 200 pixels. It is intended to facilitate Computer Vision research and techniques. It is most applicable to techniques interested in recognition, classification, and categorization. In our research work we have included 10 different objects classes from dataset selecting all the images present in the selected classes. We have included objects classes such as Butterfly, Ketch, Garfield, Gramophone, Electric Guitar, Hedgehog, Mandolin, Menorah, Panda, and Pyramid. Fifteen exemplars were chosen

Fig. 5 Images of some objects and their corresponding magnitude response image of size 25600*1. **a** butterfly object, **b** garfield object, **c** gramophone object



randomly from each of the 10 object classes for training and remaining images are chosen for testing, yielding a total 644 exemplars. The no of images originally contained in dataset in each class are 81 images in Butterfly class, 34 in Ketch, 51 in Garfield, 75 in Gramophone, 54 in Electric Guitar, 114 in Hedgehog, 43 in Mandolin, 87 in Menorah, 38 in Panda, and 57 in Pyramid. Therefore it consists of a total of 644 images. Out of these 150 images are used for training and rest 494 images are used for testing. Figure 4 shows some of the images used for training. In Fig. 5 we have shown some objects and their corresponding magnitude response which is set as feature vector for training as well as recognition.

After calculating feature vectors we train our system with 150 feature vectors (object images) and then test 494 object images and results are shown in Table 1. The results have been compared for various systems such as Neural Network, KNearest Neighbour, Support Vector Machine, and Naive Bayes. With Neural Network approach we are able to obtain 65.79 % Recognition Rate or we can say 65.79 % of test objects were correctly classified as shown in Table 1. It can be seen that Neural Network system gives highest performance in comparison to SVM, Naive bayes and KNN systems having performance such as 51.62, 45.34 and 44.33 % correspondingly.

Table 1 Comparison of results with various systems

System	Total images corresponding each object class	K-Nearest neighbour classifier (no. of correctly classified object images)	Naïve Bayes classifier (no. of correctly classified object images)	Support vector machine classifier (no. of correctly classified object images)	Neural network classifier (no. of correctly classified object images)
Butterfly	76	21	19	27	39
Garfield	19	6	8	6	11
Gramophone	36	11	14	5	12
Electric guitar	60	11	18	21	32
Hedgehog	39	21	29	22	21
Ketch	99	54	53	71	86
Mandolin	28	9	18	13	20
Menorach	72	51	31	52	62
Panda	23	11	11	12	12
Pyramid	42	24	23	26	30
Average (% age of correctly classified object images)	494	44.33	45.34	51.62	65.79

5 Conclusion

The object recognition has been used in several application fields, in high definition video [32], for high-resolution satellite images [33], in driver assistance systems [34], Automatic Target Detection and Recognition, Autonomous Robots, Vehicle navigation and obstacle avoidance, Industrial Visual Inspection, Face Recognition, Medical Image Analysis [35], Optical character recognition, Web search, Searching image databases, Online dating, Security, Airport baggage screening and Car safety systems [36]. Object recognition has proven to be a significantly difficult challenge especially with the complexity of real world data, in which there is great variation in both the appearance of objects within a single object class (e.g., mugs may come in many shapes and colors), and in the appearance of the same object under various circumstances (e.g., the same object can appear different with changes in pose, size and lighting). The varying appearances and circumstances can extremely change the pixel values in an image for the same object. So variations in geometry, photometry and viewing angle, noise, occlusions and incomplete data are some of the problems with which object recognition systems faced.

Gabor wavelets exhibit desirable characteristics of spatial locality and orientation selectivity. As described earlier this approach has several advantages against robustness, illumination, multi-resolution, and multi-orientation. These extracted

features are used for classification. The results were shown for each object which shows that the Performance of Neural Network system outperforms in maximum of the classes compared to other systems. Object recognition can be used for various applications such as Robotics, driver assistance systems, Airport baggage screening and Car safety systems and so on which means that this technique can be used for security purposes which require the Recognition Rate must be as high as possible rate and minimum misclassification rate. So as future work we will try to extend this work in order to reduce the misclassification rate. So, one of the biggest challenges for the future remains to improve the performance of the system as to achieve exceptionally good results in order to make our system much reliable.

References

1. Roach, J.W., Aggarwal, J.K.: Computer tracking of objects moving in space. *IEEE Trans. Pattern Anal. Mach. Intell.* **PAMI-1**(2), 127–135 (1979)
2. Yakimovsky, Y.: Boundary and object detection in real world images. In: *IEEE Conference on Decision and Control Including the 13th Symposium on Adaptive Processes*, vol. 13, Part 1 (1974)
3. Nahi, N.E., Lopez-Mora, S.: Estimation of object boundaries in noisy images. In: *IEEE Conference on Decision and Control including the 15th Symposium on Adaptive Processes*, vol. 15, Part 1 (1976)
4. Würtz, R.P.: Object recognition robust under translations, deformations, and changes in background. *IEEE Trans. Pattern Anal. Mach. Intell.* **19**, 769–799 (1997)
5. Ozer, H.U., Sundaram, R.: object recognition with generic self organizing feature extractors and fast gabor wavelet transform. In: *Proceedings of International Joint Conference on Neural Networks, Florida*, 12–17 August 2007
6. Dornaika, F., Chakik, F.: Efficient object detection and matching using feature classification. In: *IEEE Conference Pattern Recognition (ICPR), 2010 20th International Conference*, pp. 3073–3076 (2010)
7. Strickland R.N., Hahn H.I.: Wavelet transform methods for object detect ion and recovery. *IEEE Trans. Image Process.* **6**(5), 724–735 1997
8. Xiaoyan, Z., Lingxia L., Xuchun Z.: An automatic video object segment action scheme. In: *IEEE Conference Intelligent Signal Processing and Communication Systems (ISPACS), 2007, International Symposium*, pp. 272–275 (2007)
9. Lee, P.-H., Lin, Y.-L., Chen, S.-C., Wu, C.-H., Tsai, C.-C., Hung, Y.-P.: Viewpoint-independent object detection based on two-dimensional contours and three-dimensional sizes. *IEEE Trans. Intell. Transp. Syst.* **12**(4), 1599–1608 (2011)
10. He L., Wang H., Zhang H.: Object detection by parts using appearance, structural and shape features. In: *IEEE Conference Mechatronics and Automation (ICMA), 2011 International Conference*, pp. 489–494 (2011)
11. Lei, B.J., Hendriks, E.A., Reinders, M.J.T.: On feature extraction from images. In: *MCCWS Project Information and Communication Theory Group* (1999)
12. Peter, M.R., Winter, M.: Survey of Appearance-Based Methods for Object Recognition. Survey available at www.icg.tu-graz.ac.at (2008)
13. Turk, M., Pentland, A.: Eigenfaces for recognition. *J. Cognitive Neurosci.* **3**, 71–86 (1991)
14. Bartlett, M.S., Lades, H.M., Sejnowski, T.J.: Independent component representations for face recognition. In: *Proceedings of SPIE*, pp. 528–539 (1998)
15. D.L. Swet and J. Weng, “Using discriminant eigenfeatures for image retrieval”, *IEEE Transactions on Pattern Analysis and Machine Intelligence*, pp. 831–836, 1996

16. Braithwaite, R.N., Bhanu, B.: Hierarchical Gabor filters for object detection in infrared images. In: Proceedings of CVPR '94, 1994 IEEE Computer Society Conference on Computer Vision and Pattern Recognition (1994)
17. Wu, X., Bhanu, B.: Gabor wavelets for 3-D object recognition. In: Proceedings Fifth International Conference on Computer Vision (1995)
18. Zhang, L., Qin, D.: The object tracking study based on the Gabor wavelet character. In: IEEE International Conference on Mechatronics and Automation (2006)
19. Fergus, R., Perona, P.: Caltech object category datasets. http://www.vision.caltech.edu/Image_Datasets/Caltech101/Caltech101.html (2003)
20. Gabor Transform: http://en.wikipedia.org/wiki/Gabor_transform
21. Zhou, M.: Gabor-boosting face recognition. Thesis at det.tjfsu.edu.cn/faculty/Thesis.pdf. Sept 2008
22. Kepenekci, B.: Face recognition using Gabor wavelets transform. Thesis at citeseerx.ist.psu.edu/viewdoc/download?doi=10.1.1.100.pdf. Sept 2001
23. Naive-Bayes-Classifer: http://en.wikipedia.org/wiki/Naive_Bayes_classifier
24. Naive-Bayes-Classifer: <http://www.statsoft.com/textbook/naive-bayes-classifier/>
25. K-Nearest-Neighbor: http://www.scholarpedia.org/article/K-nearest_neighbor
26. K-Nearest-Neighbor Algo: http://en.wikipedia.org/wiki/K-nearest_neighbor_algorithm
27. Boser, B.E., Guyon, I.M., Vapnik, V.: A training algorithm for optimal margin classifiers. In: Proceedings of the 5th Annual Workshop on Computational Learning Theory, Pittsburgh, pp. 144–152 (1992)
28. Burges, C.: A tutorial on support vector machines for pattern recognition. *Data Min. Knowl. Discov.* **2**, 121–127 (1998)
29. Akay, M.F.: Support vector machines combined with feature selection for breast cancer diagnosis. *Expert Syst. Appl.* **36**, 3240–3247 (2009)
30. Vinay Kumar B, “A Thesis on Face Recognition Using Gabor Wavelets”, *Visvesvaray echnological University, Belgaum*, 2006
31. Neural Network, <http://uhaweb.hartford.edu/compsci/neural-networks-history.html>
32. T. Warsop, S. Singh, “A survey of object recognition methods for automatic asset detection in high-definition video”, *IEEE 9th International Conference on Cybernetic Intelligent Systems (CIS) 2010*, pp. 1 – 6, 2010
33. T. Modegi, “Small object recognition techniques based on structured template matching for high-resolution satellite images”, *IEEE conference on SICE*, pp. 2168 – 2173, 2008
34. Laika, A., Stechele, W.: A review of different object recognition methods for the application in driver assistance systems. *IEEE conference on Image Analysis for Multimedia Interactive Services 2007*, 10 (2007)
35. Martin Garcia Keller, “Matching Algorithms and Feature Match Quality Measures for Model-Based Object Recognition with Applications to Automatic Target Recognition”, Thesis at www.dtic.mil/cgi-bin/GetTRDoc?AD=ADA440328, 1999
36. Fergus R.: Visual object category recognition. In: Proceedings of the IEEE Conference on Computer Vision and Pattern Recognition (2005)

Cryptanalytic Attacks and Countermeasures on RSA

Manish Kant Dubey, Ram Ratan, Neelam Verma
and Pramod Kumar Saxena

Abstract RSA cryptosystem is based on the difficulty of factoring large integers. It is used in encryption as well as in digital signature for providing security and authenticity of information. RSA is employed in various security applications. RSA has been extensively analyzed for flaws and cryptanalytic attacks but it is still considered secure due to adequate countermeasures and improvements reported. In this paper, we present a brief overview on RSA, discuss various flaws and cryptanalytic attacks including applicability of genetic algorithm and some countermeasures to overcome from certain flaws and cryptanalytic attacks. The review study shows that RSA is a most popular secure asymmetric cryptosystem and its strength would remain intact until availability of quantum computers.

Keywords Public key cryptography · Information security · Digital signature · Cryptanalytic attack · Countermeasure · Soft computing · Genetic algorithm

1 Introduction

Cryptography is being used in securing messages and is recognized as a core technology for achieving ‘Confidentiality’—one of the three major goals of Information Security, other two being ‘Integrity’ and ‘Authenticity’. Though

M. K. Dubey (✉) · R. Ratan · N. Verma · P. K. Saxena
Scientific Analysis Group, Defence Research and Development Organization, Delhi, India
e-mail: kantmanish@yahoo.com

R. Ratan
e-mail: ramratan_sag@hotmail.com

N. Verma
e-mail: neelamverma123@gmail.com

P. K. Saxena
e-mail: saxenapk@hotmail.com

cryptography started as an 'Art' and was used in the past in a primitive manner, major developments in cryptography, however, happened with classical paper of Claude E Shannon [1] when he introduced the concepts of measuring information through 'Entropy' and that of 'Perfect Secrecy'. Presently, cryptography is a well developed Science, which is multidisciplinary and has got wide applications, not only in securing military communications but also in variety of areas including security in Control Systems, Application Software, Data Security etc. The term cryptology was first coined by James Howell in 1645, reported in a book by Mollin [2]. It includes 'Cryptography'—the science of securing information as well as 'Cryptanalysis'—the science of extracting plain information from encrypted/secured information without knowing the 'Key' and/or 'encryption algorithm'.

Though different cryptographic schemes/methods can be classified in different manner based on the context, but broadly these can be put in two categories as per present encryption principles. The one is called 'Symmetric Key Cryptography'—where single secret key is required for encryption as well as decryption operations. In the second category lie those cryptographic schemes/methods which require a 'pair of keys'—one for encryption operation and the other corresponding one for decryption operation. This is known as 'Asymmetric Key Cryptography'. In case of symmetric key cryptography one needs secure key management procedure for sharing the 'key' between communications parties through some other means. Whereas, in case of asymmetric key cryptography, such a thing is not required. In fact one 'key' out of the 'key pair' is available publically and other one is totally private, linked to the concerned party communicating. That is why, this category of cryptography is also known as 'Public Key Cryptography' (PKC). The concept of PKC was first introduced in 1976 by Diffie and Hellman [3]. The same was also invented by Merkle [4] at the same time but appeared in 1978. Almost all PKC concepts are based on one-way trapdoor functions. This is done to ensure that 'one key' (private key) out of the 'pair of keys' corresponding to specific person can not be drawn from the 'other key' (public key), unless one knows the trap-door function.

In 1977, three mathematicians—Ronald Rivest, Adi Shamir and Leonard Adleman [5] of MIT invented an encryption scheme, known as RSA scheme, using the difficulty of factorization of large integers as its base. Though the complexity of factorization and the ideas used in RSA scheme were initially known in 1970 to James Ellis and proved in 1973 by Clifford Cocks, while they were working in Communications Electronics Security Group (CESG)—a branch of the British Government Communications Headquarters (GCHQ) [6]. Also, in 1974, Williamson of GCHQ/CESG [6] described the concept of PKC in a manner almost similar to what Diffie-Hellman proposed. These concepts/ideas have been converted to practical system—RSA, which is being used extensively for many applications in Govt. as well as commercial domain. RSA is also being used in many security protocols such as SSL/TLS, SET, SSH, S/MIME, PGP etc. It is being extensively used in E-Banking, Secure Telephony, Smart Cards and communications in different types of Networks. In present day applications, RSA normally uses 1024 bit integer N chosen as the product of two integers (primes)

p and q of the size nearly equal to each other (≈ 512 bits). It is known that the encryption/decryption time in RSA system increases fast as we increase sizes of integers N , p , q . Though, the security provided by the system to information increases with increase in size of key parameters such as N , p , q , one has to accept some trade-offs due to permissible encryption/decryption timing in specific applications.

Due to such trade-offs and also because of the manner in which RSA has actually been implemented, there are several attacks possible on this system. According to Lenstra et al. [7], the results of poorly implemented random number generators for Rivest's 'multiple secrets' tends to include more often identical prime number factors. Also, Diffie's 'single secret' would never encounter such defect. They conclude that '1024-bit RSA provides 99.8 % security at best' and cryptosystems based on the Diffie-Hellman techniques are 'less risky'. The attacks on RSA may be applicable due to mathematical weaknesses in its design and inappropriate software/hardware implementation. The cryptanalysts have exploited such bugs/flaws and reported several attacks on RSA. The genetic algorithm (GA) has also been attempted on RSA for finding keys [8]. Some of the countermeasures have also been reported to defeat developed attacks. In this survey paper, we present some cryptanalytic attacks and countermeasures on RSA.

The paper is organized as follows: In Sect. 2 we present brief of RSA algorithm. In Sect. 3, we discuss certain cryptanalytic attacks along with flaws and their countermeasures on RSA cryptosystems. Finally, the paper is concluded in Sect. 4 followed by the references.

2 RSA Algorithm

We begin with basic construction of RSA Algorithm. Let n -bit integer $N = pq$ be the product of two large primes p and q of almost same size. Select an integer $1 < e < \phi(N)$ such that $\gcd(e, \phi(N)) = 1$, where $\phi(N) = (p - 1)(q - 1)$ is the Euler totient function of N which gives number of integers $1 \leq i < N$ that are relatively prime to N . Find unique integer d satisfying $ed \equiv 1 \pmod{\phi(N)}$. Such a d must exist since $\gcd(e, \phi(N)) = 1$ and there exists k such that $ed = 1 + k\phi(N)$. These integers e and d are called encryption exponent and decryption exponent respectively. The pair (e, N) denotes 'public key' and is made publicly known and (d, N) denote 'private key' of the user. Sender encrypts message $m \in \mathbb{Z}_N$ with (e, N) and sends ciphertext ($c \equiv m^e \pmod{N}$) to receiver who decrypts the cipher text with (d, N) and recovers message ($m \equiv c^d \pmod{N}$).

RSA is computationally highly expensive and time consuming because of multiplications/exponentiations of larger integers. Chinese Remainder Theorem (CRT) can be used to speed up RSA encryption/decryption known as CRT-RSA. Instead of computing $m \equiv c^d \pmod{N}$, we compute $m_p \equiv c^{d_p} \pmod{p}$ and $m_q \equiv c^{d_q} \pmod{q}$, where private exponents $d_p \equiv d \pmod{p - 1}$ and $d_q \equiv d \pmod{q - 1}$. Use CRT to compute $m \equiv c^d \pmod{N} \equiv (m_p \cdot q \cdot q^{-1} \pmod{p} + m_q \cdot p \cdot p^{-1} \pmod{q}) \pmod{N}$.

$N \in \mathbb{Z}_N$ or $m \equiv (m_p + ((m_p - m_q)q^{-1} \bmod p)q) \bmod N$. Qiao and Lam [9] proposed the use of CRT-RSA with $d_p - d_q = 2$ for reducing storage space for CRT-RSA parameters. This variant of CRT-RSA is very useful in low storage capacities of hardware like smart card. However, Jochemsz and May [10] studied lattice-based attacks on this variant of CRT-RSA. In addition to message confidentiality, RSA algorithm is also used for signing messages to provide authentication, data integrity and non-repudiation. Sender takes message m and calculates hash values $h(m)$ and signs hash value $S \equiv (h(m))^d \bmod N$ with its private key d . Receiver computes hash value $S^e \bmod N \equiv (h(m)^d \bmod N)^e \bmod N \equiv h(m)$ with its public key e .

RSA is a trapdoor function which is defined as $f(x) \equiv x^e \bmod N$. A function is said to be one-way if it is easy to compute but hard to invert. Here, trapdoor is d because if function $f(x)$ is given then we can find x by $(x^e \bmod N)^d \equiv x^{ed} \bmod N \equiv x$. Security of RSA depends on private exponent d which relies on factorization of large integer N . If factors of N are known then one can easily calculate private exponent d by solving above congruence. The problems of calculating private exponent d and factorization of N are equivalent as mentioned by Boneh [11]. RSA Problem (RSAP) can be defined as: given (e, N, c) such that $c \equiv m^e \bmod N$ then how can we find m ? In complexity-theoretical point of view RSAP polynomial time reduces to integer factorization problem (IFP), i.e., $(\text{RSAP} \leq_p \text{IFP})$. This means that RSA function can be solved if one can solve IFP but converse is not known to be true. It can also be considered as NP-hard problem. Thus the main aim of cryptanalyst is to construct a polynomial time algorithm to solve either RSA problem or factorization problem. We study the difficulty of finding trapdoor of RSA function on random input that implies given (e, N, c) , how difficult for an adversary is to deduce any information about m ?

3 Cryptanalytic Attacks and Countermeasures

Security of RSA cryptosystem depends on the difficulty of inverting encryption function on an average, i.e. extracting e th roots in the ring \mathbb{Z}_N as well as factorization of the modulus N . Factoring modulus N is an obvious attack of RSA. Factorization problem may be found in Jevons's book [12].

3.1 Factoring Attack

There are several factoring methods such as Trial Division, Pollard's $p - 1$ Method, Elliptic Curve Method etc. available in literature. Among these methods, Quadratic Sieve (QS) and Number Field Sieve (NFS) [13] are most widely used factoring methods. The General NFS (GNFS) algorithm is the fastest known

method for factoring large integers. It factors N in sub-exponential time and the complexity of the algorithm is $e^{c(\log N)^{1/3}(\log \log N)^{2/3}}$ for $c \approx 1.9$. Both the algorithms are based on Fermat's 'difference of squares' method which depends upon the observation that if integers x and y are such that $x \pm y \pmod N$ and $x^2 \equiv y^2 \pmod N$ then the $\gcd(x - y, N)$ and $\gcd(x + y, N)$ are non-trivial factors of N with probability of 50 %. A specialized version of GNFS called Special NFS (SNFS) is also used for factoring special number of the form $r^e + s$. For example, 1039-bit number $2^{1039} - 1$ has been factored in 2007 [14]. As an open challenge to factorize large integers, several RSA challenge numbers have been targeted and prize money associated to encourage researchers. RSA-768, a 232-digit number was factored in 2010 [15]. RSA-704, a 212 digit number was factored using NFS method in 2012 [16]. Shamir proposed theoretical hardware devices TWINKLE and TWIRL in 1999 and 2003 [17, 18] to achieve seed up but most of the success reported is credited to distributed computing in a planned and coordinated manner. The challenges of factorizations of RSA-896, RSA-1024, RSA-1536, RSA-2048 still exist.

3.2 *eth Root Attack*

Suppose $c \equiv m^e \pmod N$ is given then m is obtained directly as $m = \sqrt[e]{c} \pmod N$. It is proved that breaking RSA encryption by computing e th root, assuming $\phi(N)$ is known, is as hard problems as factoring N .

3.3 *Common Modulus Attack*

This attack can be mounted by generating different public key pairs of i th user (e_i, N) and different private key of i th user (d_i, N) with same modulus. For example, suppose (N, e_1) and (N, e_2) be the public keys of first user and second user respectively. The message m is then encrypted as $c_1 \equiv m^{e_1} \pmod N$ and $c_2 \equiv m^{e_2} \pmod N$. If an adversary intercepts ciphers and calculates $t_1 \equiv e_1^{-1} \pmod e_2$, $t_2 \equiv (t_1 e_1 - 1)/e_2$ then one can find $c_1^{t_1} c_2^{-t_2} = m$. Therefore, a modulus N should never be used by more than one entity. In other words, prime numbers used to generate moduli must be unique.

3.4 *Homomorphic Attack*

This exploits multiplicative structure of RSA function. An adversary who knows two ciphertext $c_1 \equiv m_1^{e_1} \pmod N$ and $c_2 \equiv m_2^{e_2} \pmod N$, obtained with same public key, can easily construct ciphertext $c = c_1 c_2 \equiv (m_1 m_2)^e \pmod N$ for message

$m = m_1 m_2$ without knowing it. Under chosen ciphertext attack, an adversary can easily deduce m . Suppose an adversary wants to decrypt $c \equiv m^e \pmod N$ under such attack. He computes $c' \equiv cr^e \pmod N$ and deduces m from $rm \pmod N$. Situation is more worrisome when digital signature is used in RSA function. To avoid this attack, m is padded with OAEP (Optimum Asymmetric Encryption Padding) introduced by Bellare and Rogway [19].

3.5 Cyclic Attack

This attack was invented in 1978. Let $c \equiv m^e \pmod N$ and let there exists positive integer k such that $c^{e^k} \equiv c \pmod N$ as $m \in Z_N$ (called fixed point), then $c^{e^{k-1}} \equiv m \pmod N$. An adversary computes $c^e \pmod N, c^{e^2} \pmod N, c^{e^3} \pmod N, \dots$ until c is obtained for the first time. It is also used for factorization of N by considering prime $(p \text{ or } q)/\gcd(c^{e^k} - c, N)$. Strong primes or randomly chosen pair of large primes for an RSA modulus can be used to avoid such attacks. Number p is a strong prime if $p - 1$ has a large prime factor q , $q - 1$ has a large prime factor s and $p + 1$ has a large prime factor r .

3.6 Private Exponents Attacks

3.6.1 Low Private Exponent

To speed up computation in RSA decryption and signature generation, it often uses small value of d rather than a random d . If RSA private exponent d is chosen too small i.e. $d < \sqrt[4]{N}/3$ and $q < p < 2q$ then by Wiener's Diophantine attack [20], d can be efficiently computed in polynomial time from public exponent e . Boneh and Durfee [21] improved Wiener's method by showing that RSA is insecure for any $d < N^{0.292}$ from powerful LLL-based techniques due to Coppersmith. Roughly we can say that if N is 1024 bits, it follows that d must be at least 300 bits long in order to avoid this attack. In 2005, Steinfeld et al. [22] showed that a sub-exponential-time attack on RSA with private key $d > N^{0.25}$ cannot be obtained just by using Wiener's approach.

3.6.2 Low Private CRT Exponent

Wiener used private CRT-exponents d_p and d_q chosen significantly smaller than p and q for speed up of RSA in decryption phase. Jochemsz and May [23] improved the results. Let $N = pq$ be a n -bit RSA modulus with p and q primes of $n/2$ bits. Then under some condition, N can be factorized in polynomial-time if

$d_p, d_q < N^{0.073}$. Bleichenbacher and May [24] presented an attack on CRT-RSA when CRT-exponents d_p and d_q are suitably small. Nitaj [25] show that RSA is insecure if public exponent e satisfies an equation $ex + y \equiv 0 \pmod p$ with $|x||y| < N^{\sqrt{2}-1/2}$ and $ex + y \equiv 0 \pmod p$. He improved the cryptanalysis of CRT-RSA if one of private exponents d_p satisfies $d_p < N^{\sqrt{2}/4}/\sqrt{e}$.

3.7 Partial Key Exposure Attack

The problem to find fraction of private exponent d that has to be made available to an attacker in order to break the system is defined to be partial key exposure attack. Boneh et al. [26] described several attacks against RSA enabling an attacker given a fraction of bits of d to recover its all bits. They proved that as long as $e < \sqrt{N}$, it is possible to reconstruct all bits of d from just a fraction of its bits using copersmith theorem. Suppose N is n bits long. Then given $\lceil n/4 \rceil$ least significant bits (lsb) of d , one can reconstruct d in time linear in $e \log_2 e$. This relies on theorem due to Coppersmith: let $N = pq$ be an n -bit RSA modulus then given $n = 4$ lsb of p or $n = 4$ most significant bits (msb) of p , one can efficiently factor N . Blomer and May [27] described number of attacks that allow larger public exponents $e < N^{0.725}$. Ernst et al. [28] proposed new partial key exposure attacks for full size public exponent that work up to full size private/public exponent. They use Coppersmith's ideas of finding small roots of polynomials which is reformulated by Coron [29]. This result was improved by using lattice of smaller dimension [30]. Joye and Lepoint [31] imposed this attack by considering private exponents d that are larger than N to improve the performance or to increase the security. They use the concept of Jochemsz and May [23, 32] for solving multivariate polynomials with small integer or modular roots. To defend RSA against partial private key exposure attack, it is suggested to keep d secure, and not try to use small e , since if small e is used, RSA system leaks half of msb of corresponding d .

3.8 Public Exponent Attack

There are several attacks on public exponents e but most important and powerful cryptanalytic attacks on short e are due to a theorem given by Coppersmith [11] for finding small roots of polynomials modulo a composite N . Howgrave-Graham studied [33] for special case $d = 1$, i.e., for degree-1 polynomials. The claim of Coppersmith theorem [11] was generalized by May [34] who established a deterministic polynomial time equivalence of two problems, i.e., computing d from (N, e) and factorization of N .

3.8.1 Broadcast Attack

The attack on small e for same messages is known as Hastad's broadcasting attack [35] which is based on application of Coppersmith theorem. This can be easily explained by simple example illustrated below in which smallest possible exponent $e = 3$ in RSA encryption is vulnerable. Suppose that same message m was sent to three different recipients using $(e, N_1), (e, N_2), (e, N_3)$, where $\gcd(N_i, N_j) = 1$ for $i, j = 1, 2, 3$ with $i \neq j$, and $m < N_i$. Cryptanalyst can compute the ciphertexts $c_1 \equiv m^3 \pmod{N_1}, c_2 \equiv m^3 \pmod{N_2}$ and $c_3 \equiv m^3 \pmod{N_3}$ and then m can easily be computed by CRT using $m^3 \equiv c \pmod{N}$ and $m \equiv \sqrt[3]{c} \pmod{N}$. A stronger version of Hastad's attack was proved by Boneh [36] and states that let N_1, N_2, \dots, N_k be pairwise relatively prime with $N_1 \leq N_i$ for all $i = 1, 2, \dots, k$ and $p_i \in \mathbb{Z}_{N_i}[x]$ for $i = 1, 2, \dots, k$ be the polynomials with maximum degree d . Suppose there exists a unique $M < N_i$ such that $p_i \equiv 0 \pmod{N_i}$ for all $i = 1, 2, \dots, k$ and $k \leq d$, then M can be computed in polynomial time. May and Ritzenhofen [37] improved this attack. This attack is prevented by random padding.

3.8.2 Related Message Attack

Franklin and Reiter [38] proved that when two plaintexts are related polynomially and encrypted with small public exponent e using same RSA modulus N , then RSA may be broken in polynomial time. This result was later improved by Coppersmith et al. [39]. Suppose $m_1, m_2 \in \mathbb{Z}_N$ are two distinct polynomially related messages $m_2 \equiv \alpha m_1 + \beta \pmod{N}$ for some known $\alpha, \beta \in \mathbb{Z}_N$ and $e = 3$ then $c_1 \equiv m_1^3 \pmod{N}, c_2 \equiv m_2^3 \pmod{N}$. Therefore, m_1 and m_2 can be computed as $\beta(c_2 + 2\alpha^3 c_1 - \beta^3) / \alpha(c_2 - \alpha^3 c_1 + 2\beta^3) \equiv m_1 \pmod{N}$ and $m_2 \equiv \alpha m_1 + \beta \pmod{N}$. This attack can be prevented by removing relation between messages by random padding.

3.8.3 Short Pad Attack

Coppersmith shown that adding random padding to messages is not enough. He imposed an attack on random padded and related messages to RSA. Let N be n -bit RSA modulus with encryption key e , and set $\lfloor n/e^2 \rfloor$. Suppose $m \in \mathbb{Z}_N^*$ is a plaintext message unit of bit length at most $n - k$, and set $m_1 = 2^k m + r_1$ and $m_2 = 2^k m + r_2$ with $r_1, r_2 \in \mathbb{Z}, r_1 \neq r_2, 0 \leq r_1, r_2 < 2^k$. Then with knowledge of N, e, m_1, m_2 (but not r_1, r_2), m can be efficiently recovered. From this attack, it easy to verify that short pad attack can be mounted as soon as the pad length is less than $1/9$ of message length when $e = 3$.

3.9 Fault and Bug Attacks

As RSA decryption and signature verification with CRT is four time faster than standard RSA, it is very useful in smart cards and systems-on-chip technologies but due to errors in software/hardware implementations and an attack due to Boneh [40], one can easily factor N and hence break the system. This attack is successful under assumption that cryptanalyst has the knowledge of implementation details. This attack is based on obtaining the difference between correct and incorrect signature of same message. Suppose sender computes $h(m)$ of m to produce $H = h(m)$ for signature then receiver computes $S_p \equiv H^{d_p} \equiv H^{d(\text{mod}(p-1))} \pmod{p}$ and $S_q \equiv H^{d_q} \equiv H^{d(\text{mod}(q-1))} \pmod{q}$. Using CRT, receiver computes signature S . Assuming an error occurs in computation of either S_p or S_q denoted by \overline{S}_p or \overline{S}_q . Suppose cryptanalyst receives wrong S denoted as \overline{S} because $\overline{S}^e \equiv H \pmod{N}$. If S_p is wrong, then $\overline{S}^e \equiv H \pmod{p}$ and $\overline{S}^e \equiv H \pmod{q}$ and therefore compute $q = \text{gcd}(S^e - H, N)$. Similarly, other factor can be obtained by assuming that S_q is wrong. Random padding procedure or verification of correctness of signer's signature S before sending the signature can defeat the attack. Shamir's countermeasure presented [41] relies on selecting a random integer t and computations of $S_{pt} \equiv H^d \pmod{pt}$ and $S_{qt} \equiv H^d \pmod{qt}$. In case of $S_{pt} \equiv S_{qt} \pmod{t}$, the computation is defined to be error free. Their countermeasure is later improved [42].

Biham et al. [43] presented a new attack called bug attack on some public key cryptosystems which have bugs in hardware implementation of computer instructions. Example of such a bug is Intel division bug, which resulted in slightly inaccurate results for extremely rare inputs. Since microprocessors of Personal Computers (PC's) perform multiplications involving tens of words, verification of the correctness of multiplications between all pairs of values is difficult. They have shown that if some intelligence organization discovers even one pair of single-word integers a and b whose product is computed incorrectly by a microprocessor, then the key in RSA-based security program running on any one of the millions of PC's that contain faulty microprocessor can be easily broken unless appropriate countermeasures are taken. In some cases, full key can be retrieved with a single chosen ciphertext while in other cases such as padded with OAEP RSA a larger number of ciphertexts are required. They demonstrate that there are lot of similarity between bug attacks and fault attacks but their countermeasures can be very different. For example, just stopping an erroneous computation or re-computing the result with a different exponentiation algorithm may protect the scheme against fault attacks, but will leak full key via a bug attack.

Pellegrini et al. [44], proposed a fault based attack in 2010 on RSA authentication to recover private key by varying the power voltage of central processing unit (CPU) outside limits caused multiple power faults on server or hardware. They attack original Open SSL authentication library running on a SPARC Linux system implemented on FPGA, and extract system's 1024-bit RSA private key in approximately 100 h. Actually, due to hardware designs and occurrence of

transient hardware failures, errors can be introduced to the system by forcing operative conditions. Modular exponentiation $m^d \bmod N$ is also responsible for this attack.

3.10 Implementation Attacks

There are attacks which are not related to weakness of mathematical construction or algorithm of RSA. Instead, these attacks exploit specific implementations on a particular computing device that allow leak secret information, i.e., private exponent d to leak. These attacks are called implementation attacks and referred as side-channel attacks. They include but not limited to timing attacks, power attacks and so on.

3.10.1 Timing Attack

Kocher [45] invented a new attack on RSA cryptosystem to get d without factoring N . Kocher finds that if attacker has sufficient knowledge of hardware then by measuring time taken to perform the RSA decryption or signature scheme that uses modular exponentiation algorithm, he can recover private exponent d by using some knowledge of probability and statistics. Actually, RSA fast-exponential algorithm uses only squaring if corresponding bit in d is 0, this requires shorter time to decrypt and both squaring and multiplication if corresponding bit is 1. This timing difference allows attacker to find bits in d , one by one. Schindler [46] introduced an efficient new attack on RSA implementations that use CRT with Montgomery's multiplication algorithm. Under optimal conditions, it takes about 300 timing measurements to factorize 1024-bit RSA moduli. Open SSL implementation of RSA is highly optimized using CRT, Sliding windows, Montgomery multiplication, and Karatsuba's algorithm. These optimizations cause both known timing attacks on RSA to fail in practice. Boneh and Brumley [47] devise a new timing attack that is able to extract private key from Open SSL. This is most widely used open source attacks crypto library based server which takes advantage of information leaked by CRT optimization used by many RSA implementations. They improve the efficiency of their attack by a factor of more than 10. Bortz, Boneh and Nangy [36] presented two types of timing attacks that exploit weaknesses in server side application software, specifically when execution time depends on sensitive information. There are two basic methods to avoid this attack. First method is to add random delays to the exponentiations to make each exponentiation that takes same amount of computing time and second method known as blinding suggested by Rivest is to multiply ciphertext by a random number before decryption.

3.10.2 Power Attack

Kocher [48] has given another concept based on measurement of the computer's power consumption during decryption, known as power cryptanalysis to recover d . Since computer's power consumption is necessarily higher during multi-precision multiplications than it would normally be therefore an attacker can measure the length of these high consumption episodes and can easily decide when the computer is performing one or two multiplications, and computes d . Simple power analysis attacks work directly by observing a system's power consumption. Differential power analysis attacks are more powerful which use statistical analysis and error correction techniques to extract information correlated to private keys. There are a couple of possibilities to countermeasures against power analysis, such as keeping power consumption stable or blinding data before cryptographic operations.

3.10.3 RSA Prime Key Generation

Finke et al. [49] introduced a side-channel attack on a straightforward implementation of RSA key generation step. This attack exploits power information to determine number of trial divisions for each prime candidate. They discussed its implementation and countermeasures.

3.11 Bleichenbacher's Attack

3.11.1 First Attack on PKCS#1

PKCS#1 is a cryptographic standard maintained by RSA laboratory. Bleichenbacher's [50] first attack exists due to chosen ciphertext attack. As plain RSA is not secure so before encrypting any message through RSA, it is natural to pad with random bits. In old version, encryption of a message M was in fact an encryption of n bits: $02 \parallel \text{Random Padding} \parallel 00 \parallel M$. He shows that when a protocol decrypting a ciphertext c by checking initial block consist of bytes 0 and 2. This causes problems when an error is found. Actually, an attacker can intercept c , and send $c' \equiv rc \pmod N$ to receiver to decrypt the message, for some random r . Now an attacker will learn whether or not 16 msb are equal to 02. Hence, an attacker told to the receiver to decrypt c' against chosen ciphertext attack. Now attacker can easily find correct initial block by eliminating r . Bleichenbacher shows that this is enough to decrypt c .

3.11.2 Second Attack on PKCS#1

Bleichenbacher [51] presented a new forgery attack against signature scheme defined in PKCS#1. Some implementations extract number of bits for hash value by their position relative to padding without checking for unexpected data after hash value. In case of PKCS#1, hash value is selected by finding the end of padding. A PKCS#1 digital signature is computed on a hash value $H(M)$ that is padded as: $0001FFFF\dots FF00\| \text{data bytes (message } M \text{ in ASN.1 Format)}\| H(M)$, where $0001FFFF\dots FF00$ is a padding value. Padded message shown above is obtained using $e = 3$. When PKCS#1 padding is used, for any message M' with hash value $H(M')$, it is rather easy to find a cubic root of a string like $0001FFFF\dots FF0000\| \text{data bytes in ASN.1 Format}\| H(M')\| \text{Garbage}$, where number of occurrences of FF in padding is reduced and garbage is cleverly chosen to make the modified string into a cube of some value. If one can submit a signature equal to the cube root of M then signature is valid. In this case an attacker can easily apply by choosing extra bits freely in order to create a perfect cube. Izu et al. [52] extended Bleichenbacher's attack and show that when 1024 bit composite and public exponent $e = 3$ are used, the extended attack succeeds forgery with probability $2^{-16.6}$. Jager et al. [53] found several attacks against PKCS#1 key transport mechanism of XML encryption. Public exponent $e = 3$ should be avoided and it should be higher for RSA signatures to avoid such attacks. Moreover, if padding is used then verify that there is no garbage after hash value.

3.12 GA Attack

A timing attack using genetic algorithm for RSA was reported in [8]. The method searches large key space by utilizing the features of GA to produce improved set of keys. A single key having correct key bits survives at the end of search. The search utilizes the idea of timing attack as computation time information that may leak due to different modular operations. This approach suggests a speed up process, aiming at reducing the required number of plaintext-ciphertext samples needed for a successful timing attack. The proposed attack outlined in this work with its preliminary implementation, have given encouraging results.

3.13 Quantum Computing Attack

Shor [54] presented an algorithm for solving factorization problem in time and space polynomial in bit-length of N , provided that the model of Turing machine is replaced by the model of quantum Turing machines. He showed that whenever quantum computers with sufficiently large registers would be constructed then it

would be able to factor a large integer in polynomial time, i.e., RSA would be cracked. Quantum factoring is still in its very early stages and will not threaten the security of RSA at least at present, as current quantum computer can factor $15(5 \times 3)$ only which is of 2 digits number.

4 Conclusion

An introduction to RSA and the role of its parameters has been described along with the survey on proposed different attacks and countermeasures on the system. Whereas some of these attacks are based on bad choices of parameters, others depend on the way RSA is actually implemented. None of the available attacks poses any serious threats to RSA as on date if proper care is taken against the vulnerabilities. The main direction of breaking RSA still remains dependent on 'speed of factorization' of large integers. Accordingly the admissible sizes of parameters p , q and N are increasing with efficient implementations. The factorization methods based on QS, NFS and GNFS have some limitations and these work up to certain sizes of N but for N of size 1024/2048 bits, as on date no efficient sieving and other algorithm exist which can pose any problem to use of RSA. Unless some revolutionary technology such as quantum computing or an altogether different method to factorize large integers come, RSA is going to stay and is expected to be used for quite some time in future.

References

1. Shannon, C.E.: A mathematical theory of communication. *Bell Syst. Tech. J.* **27**(3/4), 379–423/623–656 (1948)
2. Mollin, R.A.: *An Introduction to Cryptography*. Chapman & Hall, CRC Press (2010)
3. Diffie, W., Hellman, M.: New directions in cryptography. *Trans. Inf. Theory* **22**(6), 644–654 (1976)
4. Merkle, R.C., Hellman, M.E.: Hiding information and receipts in trapdoor Knapsacks. In: *International Symposium on Information Theory*, Cornell University, Ithaca, New York (1977)
5. Rivest, R., Shamir, A., Adleman, L.: A method for obtaining digital signatures and public-key cryptosystems. *Commun. ACM* **21**(2), 120–126 (1978)
6. Ellis, J.H.: *The History of Non-secret Encryption*. GCHQ-CESG Publication, London (1987)
7. Lenstra, A.K., James, P.H., Augier, M., Bos, J.W., Kleinjung, T., Wachter, C.: Ron was wrong, Whit is right. <http://eprint.iacr.org/2012/064> (2012)
8. Ali, H., Al-Salami, M.: Timing attack prospect for RSA cryptanalysis using genetic algorithm technique. *Int. Arab J. Inf. Tech.* **1**(1), 80–84 (2004)
9. Qiao, G., Lam, K.-Y.: RSA signature algorithm for microcontroller implementation. In: *Proceedings of CARDIS'98, LNCS*, vol. 1820, pp. 353–356 (1998)
10. Jochemsz, E., May, A.: A strategy for finding roots of multivariate polynomials with new applications in attacking RSA variants. In: *Proceedings of ASIACRYPT'06, LNCS*, vol. 4284, pp. 267–282 (2006)

11. Boneh, D.: Twenty years of attacks on the RSA cryptosystem. *Notices Amer. Math. Soc.* **46**(2), 203–213 (1999)
12. Jevons, W.S.: *The Principles of Science: A Treatise on Logic and Scientific Method.* Macmillan & Co., London (1874)
13. Crandall, R., Pomerance, C.: *Prime Numbers: A Computational Perspective.* 2nd edn. Springer-Verlag, New York (2005)
14. Aoki, K., Franke, J., Kleinjung, T., Lenstra, A.K., Osvis, D.A.: A kilobit special number field sieve factorization. In: *Proceedings of ASIACRYPT'07*, LNCS, vol. 4833, pp. 1–12 (2007)
15. Kleinjung, T., Aoki, K., Franke, J., Lenstra, A.K., Thome, E., Bos, J.W., Gaudry, P., Kruppa, A., Montgomery, P.L., Osvis, D.A., Riele, H., Timofeev, A., Zimmermann, P.: Factorization of a 768-bit RSA modulus. *Advances in Cryptology*, LNCS, vol. 6223, pp. 333–350 (2010)
16. Bai, S., Thome, E., Zimmermann, P.: Factorisation of RSA-704 with CADO-NFS. *cryptoeprint archive*, 369 (2012)
17. Shamir, A.: Factoring large numbers with the TWINKLE device. *CHES'99*, LNCS, vol. 1717, pp. 2–12 (1999)
18. Shamir, A., Tromer, E.: Factoring large numbers with the TWIRL device. *CRYPTO'03*, LNCS, vol. 2729, pp. 1–26 (2003)
19. Bellare, M., Rogaway, P.: Optimal asymmetric encryption. *EUROCRYPT'94*, LNCS, vol. 950, pp. 92–111 (1995)
20. Wiener, H.: Cryptanalysis of short RSA secret exponents. *Trans. Inf. Theory* **36**(3), 553–558 (1990)
21. Boneh, D., Durfee, G.: Cryptanalysis of RSA with private key d less than $N^{0.292}$. *Trans. Inf. Theory* **46**(4), 1339–1349 (2000)
22. Steinfeld, R., Contini, S., Wang, H., Pieprzyk, J.: Converse results to the Wiener attack on RSA. *PKC'05*, LNCS, vol. 3386, pp. 184–198 (2005)
23. Jochemsz, E., May, A.: A polynomial time attack on RSA with private CRT-exponents smaller than $N^{0.73}$. *Advances in Cryptology*, LNCS, vol. 4622, pp. 395–411 (2007)
24. Bleichenbacher, D., May, A.: New attacks on RSA with small secret CRT-exponents. *PKC'06*, LNCS, vol. 3958, pp. 1–13 (2006)
25. Nitaj, A.: A new attack on RSA and CRT-RSA. *AFRICACRYPT'12*, LNCS, vol. 7374, pp. 221–233 (2012)
26. Boneh, D., Durfee, G., Frankel, Y.: An attack on RSA given a small fraction of the private key bits. *ASIACRYPT'98*, LNCS, vol. 1514, pp. 25–34 (1998)
27. Blomer, J., May, A.: New partial key exposure attacks on RSA. *CRYPTO'03*, LNCS, vol. 2729, pp. 27–43 (2003)
28. Ernst, M., Jochemsz, E., May, A., de Weger, B.: Partial key exposure attacks on RSA up to full size exponents. *EUROCRYPT'05*, LNCS, vol. 3494, pp. 371–386 (2005)
29. Coron, J.-S.: Finding small roots of bivariate integer equations revisited. *EUROCRYPT'04*, LNCS, vol. 3027, pp. 492–505 (2004)
30. Sarkar, S., Gupta, S., Maitra, S.: Partial key exposure attack on RSAC improvements for limited lattice dimensions. *INDOCRYPT'10*, LNCS, vol. 6498, pp. 2–16 (2010)
31. Joye, M., Lepoint, T.: Partial key exposure on RSA with private exponents larger than N . *ISPEC'12*, LNCS, vol. 7232, pp. 369–380 (2012)
32. Jochemsz, E., May, A.: A strategy for finding roots of multivariate polynomials with new applications in attacking RSA variants. *ASIACRYPT'06*. LNCS, vol. 4284, pp. 267–282 (2006)
33. Howgrave, N., Graham: Finding small roots of univariate modular equations revisited. *A cryptography and coding*, LNCS, vol. 1355, pp. 131–142 (1997)
34. May, A.: *New RSA vulnerabilities using lattice reduction methods.* PhD thesis, University of Paderborn (2003)
35. Hastad, J.: Solving simultaneous modular equations of low degree. *SIAM J. Comput.* **17**, 336–341 (1988)

36. Bortz, A., Boneh, D., Nangy, P.: Exposing private information by timing web applications. In: Proceedings of the 16th International World Wide Web. Conference, Banff, Alberta, pp. 8–12 (2007)
37. May, A., Ritzenhofen, M.: Solving systems of modular equations in one variable: how many RSA-encrypted messages does Eve need to know? PKC'08, LNCS, vol. 2146, pp. 37–46 (2008)
38. Franklin, M.K., Reiter, M.K.: A linear protocol failure for RSA with exponent three. Crypto'95 Rump Session (1995)
39. Coppersmith, D., Franklin, M., Patarin, J., Reiter, M.: Low-exponent RSA with related messages. EUROCRYPT'96, LNCS, vol. 1070, pp. 1–9 (1996)
40. Boneh, D., DeMillo, R.A., Lipton, R. J.: On the importance of checking cryptographic protocols for faults. EUROCRYPT'97, LNCS, vol. 1233, pp. 37–51 (1997)
41. Shamir, A.: Method and apparatus for protecting public key schemes from timing and fault attacks. U.S. Patent Number 5, 991,415 (1999)
42. Joye, M., Pailler, P., Yen, S.-M.: Secure evaluation of modular functions. In: International Workshop on Cryptology and Network Security, pp.227–229 (2001)
43. Biham, E., Carmeli, Y., Shamir, A.: Bug attacks. CRYPTO'08, LNCS, vol. 5157, pp. 221–240 (2008)
44. Pellegrini, A., Bertacco, V., Austin, T.: Fault based attack of RSA authentication. In: Proceedings of the Conference on Design, Automation and Test, pp. 855–860 (2010)
45. Kocher, P.: Timing attacks on implementations of Diffie-Hellman, RSA, DSS and other systems. CRYPTO'96, LNCS, vol. 1109, pp. 104–113 (1996)
46. Schindler, W.: A timing attack against RSA with the Chinese remainder theorem. CHES'2000, LNCS, vol. 1965, pp. 110–125 (2000)
47. Brumley, D., Boneh, D.: Remote timing attacks are practical. In: Proceedings of the 12th Usenix Security Symposium, pp. 1-14 (2003)
48. Kocher, P., Jae, J., Jun, B.: Differential power analysis. CYRPTO'99, LNCS, vol. 1666, pp. 388–397 (1999)
49. Finke, T., Gebhardt, M., Schindler, W.: New side-channel attack on RSA prime generation. CHES'09, LNCS, vol. 5747, pp. 141–155 (2009)
50. Bleichenbacher, D.: Chosen ciphertext attacks against protocols based on the RSA encryption standard PKCS#1. CRYPTO'98, LNCS, vol. 1462, pp.1–12 (1998)
51. Bleichenbacher, D.: Forging some RSA signature on pencil and paper. Rump Session, CRYPTO'06 (2006)
52. Izu, T., Shimoyama, T., Takenaka, M.: Extending Bleichenbacher's forgery attack. J. Inf. Process. **16**, 122–129 (2008)
53. Jager, T., Schinzel, S., Somorovsky, J.: Bleichenbacher's attack strikes again: breaking PKCS# 1 v1.5 in XML encryption? ESORICS'12, LNCS, vol. 7459, pp.752–769 (2012)
54. Shor, P.W.: Algorithms for quantum computation: discrete logarithms and factoring. FOCS'94, pp. 124–134 (1994)

Applications of Genetic Algorithms in Cryptology

Ram Ratan

Abstract Cryptology deals with the design and analysis of secure communication and information management systems. Cryptography protects vital information from adversaries by the process of encryption and cryptanalysis provides adversaries information being communicated by exploiting cryptographic weaknesses. Cryptography is the key technology which is used in various information security applications to achieve security solutions such as confidentiality, authenticity, integrity, availability and non repudiation. Nature inspired computing applied successfully in various artificial intelligence and pattern recognition problems of various fields gives an inspiration to apply in cryptology. Evolutionary computing is being applied nowadays to achieve solutions of cryptographic and cryptanalytic problems. In this paper, we present brief on cryptosystem and overview on applications of genetic algorithms in cryptology. Findings show that the work on nature inspired computing in cryptology is minimal but the applications of genetic algorithms are increasing. The genetic algorithms are not only applied on less complex and classical ciphers but some block ciphers are also attempted for their solutions. Further insight research is needed to tackle various problems of modern cryptography using genetic or other evolutionary computing techniques.

Keywords Evolutionary computing · Genetic algorithm · Information security · Cryptography · Cryptanalysis · Cryptosystem

R. Ratan (✉)

Scientific Analysis Group, Defence Research and Development Organization, Delhi, India
e-mail: ramratan_sag@hotmail.com

1 Introduction

Cryptology is the Art and the Science of securing information and it has two branches Cryptography and Cryptanalysis. Cryptography concerns to the design of cryptographic schemes, algorithms and systems. Crypto algorithm performs encryption using encryption key at sender site and decryption using decryption key at receiver site through mathematical operations. Encryption key and decryption key remain same in symmetric key cryptography but these keys remain different in asymmetric key cryptography. In symmetric key cryptography, the key is kept secret and appropriate key management is required to maintain its secrecy. In asymmetric key cryptography, encryption key is kept public whereas decryption key is kept private. Cryptanalysis concerns to extraction of secret information or secret key without knowing the decryption key. Cryptography is being applied in information security applications since long time back. Until World War II, it was used in securing messages in some specific areas of military and Govt. communications. A measure of information 'entropy' and the term perfect secrecy was defined by Shannon [1]. A system is known perfectly secure if one could not get any information about the system or the messages from given enciphered messages. Cryptography has been grown tremendously and is being used, nowadays, in several security applications. Cryptographic schemes are designed to ensure the security of vital information from adversaries while its exchange and storage on media. Information security deals with the services of confidentiality, authenticity, integrity, non-repudiation and availability.

Another branch of cryptology is cryptanalysis that concerned to analysis of ciphers to decrypt encrypted messages or to find secret keys. Transmission of vital information is becoming more vulnerable to adversary attacks because the computer and communication environment has become more distributed, diverse, open and global. Advancement in computer technology provides more computational power for cryptanalyst to crack ciphers. Moreover, any weakness left in the design of cryptosystem could be exploited by cryptanalysts to break such cryptosystems. Cracking or breaking of a cipher means to find any weakness that could be exploited with a complexity less than brute-force to solve cipher for obtaining plain secret information or to find secret key even in partial or in distorted form. So, strong design of cryptographic schemes is necessary to counter cryptanalytic attacks. One may refer [2–7] for more detail on cryptology.

Nature inspired system known as sophisticated information processing system in which the computing of natural biological system is modeled and simulated. There has been a growing interest in the use of nature and biology as a source of inspiration for solving computational problems which are ambiguous and difficult to compute. The motivation of evolutionary computing is to extract useful metaphors from natural biological systems and to create effective computational solutions to complex problems. However, the models of computation developed do not exactly correspond to actually happen in biological systems except at a fairly superficial level. Artificial Neural Network, Fuzzy Set, Rough set, Cellular

Automata, Particle Swarm Optimization, Genetic Algorithm etc. are some of the techniques inspired by nature and have been applied successfully in various Artificial Intelligence and Pattern Recognition problems which are complex and ambiguous. The successful uses of such approaches give an inspiration to apply these in solving the problems of cryptology. Evolutionary computing techniques have been applied in cryptography and cryptanalysis to design crypto algorithms and break ciphers [8–17]. The focus of this paper is on Genetic Algorithm (GA) which has been successfully applied in the field of search and optimization. GA techniques have also been tried and found useful in the area of cryptology. The research on GA in cryptology is increasing and gaining popularity among crypto community.

In this paper, we present an overview on applications of GA in cryptology. We present brief detail on cryptosystem, its components and some good cryptographic characteristics of secure cryptosystem in Sect. 2. We present GA briefly in Sect. 3. The applications of GA in cryptography and cryptanalysis are presented in Sect. 4. The paper is concluded in Sect. 5 followed by the references.

2 Cryptosystem

Block diagram of a ‘Cryptosystem’ and its major components are shown in Fig. 1. A Cryptosystem consists of ‘Crypto-algorithm’ which includes ‘Encryption’ and ‘Decryption’ algorithms. The Encryption and Decryption algorithms are initialized with the bits of ‘Initial Vector’ (IV) to fill initials of crypto-algorithm and select desired input parameters from ‘Family Key’ (FK) Data. The IV is obtained from ‘Key Scheduler’ which consists of ‘Key Scheduling Algorithm’ which takes input from ‘User Key’ (UK) Data and ‘Message Key’ (MK). The MK is generated randomly by ‘MK Generator’. The FK and UK data which meet desired cryptographic characteristics are generated separately by ‘Key Generator’ and loaded faithfully into the Cryptosystem through ‘Key Loader’. Key Generator and Key Loader are external components which use to generate and load FK and UK Data into the Cryptosystem.

The ‘plain data’ is encrypted by encryption algorithm which produces ‘crypt data’ to the sender for secure communication. Decryption algorithm decrypts crypt data received from sender and produces plain data to the receiver. Plain data is the input and crypt data is the output of the Cryptosystem during encryption. Similarly, crypt data is the input and decrypt data is the output of the Cryptosystem during decryption.

For a secure Cryptosystem, each component should possess good cryptographic characteristics. Some of these are:

- (i) Size of MK should be adequate to meet security cover.
- (ii) MK Generator should generate random and non repeating MKs.
- (iii) For each MK, Key Scheduler should generate unique IV.
- (iv) Each UK data should be random and different.

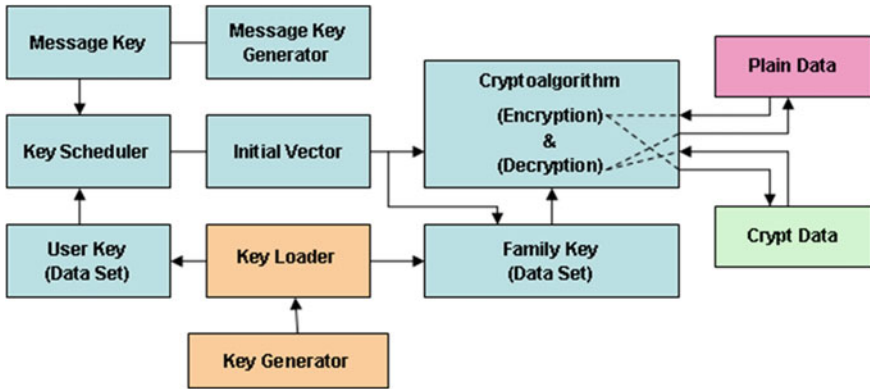


Fig. 1 Block diagram of a cryptosystem

- (v) FK data should meet certain desired characteristics.
- (vi) Key Loader should load UK data and FK data correctly into crypto system regularly at appropriate time interval.
- (vii) Crypto-primitives used in a crypto algorithm should be strong enough.
- (viii) Crypto-algorithm should be resilient against existing attacks.
- (ix) Key sequences generated by crypto algorithm should be unpredictable and follow randomness properties.
- (x) Crypts should be random and unintelligible.

If a Cryptosystem does not follow any of above cryptographic properties then it becomes insecure and vulnerable to attack. The weaknesses persist could be exploited by adversaries/opponents in breaking inappropriately designed Cryptosystems. For a Cryptosystem to be developed with limited hardware resources, the crypto-algorithm should be fast enough and easy to implement without any compromise with required security. The knowledge of cryptanalysis helps the designers to design secure Cryptosystems resilient against existing cryptanalytic attacks.

3 Genetic Algorithm

GA mimics the evolutionary principles rooted in biological evolution. GAs are adaptive search procedures which are footed on Charles Darwin theory [6] of the survival of the fittest. GAs follows nature to a great extent and produce a population in such a way that the attribute which is trendy, i.e., has higher fitness value is replicated more, as is done by the nature. This is also the fundamental concept behind evolution. So, these algorithms are also referred as the evolutionary algorithms. The computer finds better and better solutions to a problem just as species evolve to better adapt to their environment [7]. GA was developed by Prof. J. Holland and his colleagues at the University of Michigan [8]. It is an iterative

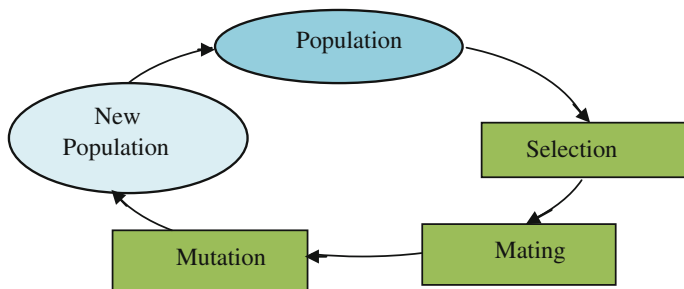


Fig. 2 Basic cycle of genetic algorithm

procedure that consists of a constant-size population of individuals known as chromosomes whereby the initial population is generated at random or heuristically. The binary alphabet $\{0, 1\}$ is often used to represent chromosome cells but integers can be used depending on the application. The fitness value is a function or rationale against which chromosome is tested for its suitability to the problem in hand.

The population evolves by applying three basic operations, selection of solutions, mating of genes and occasional mutation [9]. In selection operation, the individuals are selected for survival and reproduction according to their fitness. In mating operation, new individuals are created by recombining and/or introducing genetic variation into the selected individuals. In mutation, a candidate solution is randomly perturbed for a better individual. The basic cycle of GA is shown in Fig. 2. The cycle continues until a certain number of generations whereby the surviving individuals represent a solution to the problem [10].

Reproduction operator selects chromosomes from the initial population and enters them into the mating procedure. The crossover operator mimics biological recombination between two single chromosomes organisms. For example, the strings 10000100 to 11111111 could be crossed over after the third locus in each to produce the two offspring 10011111 to 11100100. Crossover rate determines the probability of producing a new chromosome form the parents. Mutation operator randomly changes its genetic makeup by flips some of the chromosome cells. For example, the string 00000100 might be mutated in its second position to yield 01000100. Mutation can occur at some chosen cells or at each cell in a string of cells depending on the problems with very small probability.

4 GA in Cryptology

Major works reported that involve GA is focussed on cryptanalysis of crypto-algorithms and design of crypto-primitives. The design of cryptographic schemes using GA has also initiated and some cryptographic schemes have been reported. Mostly, cryptanalytic research using GA has been done on classical ciphers but some work on new ciphers has also attempted.

4.1 *Cryptanalysis of Classical Ciphers*

An initial attempt was reported by Spillman et al. [18] where GA is exploited in cryptanalysis of simple substitution cipher. Since known cryptanalytic attack for simple substitution cipher employs frequency distribution of characters in the message, Spillman derived a fitness function based on single character and bigram frequency distributions. He was successful as GA was proven to be highly useful in cryptanalysis. He suggested the use of trigram frequency distribution and variations on crossover and mutation procedures as future research. Cryptanalysis of simple substitution was carried out further by many researchers using GAs [19–23].

Another initial attempt conducted by Matthews [24] who investigated the use of GA in cryptanalysis of transposition ciphers. In this work the fitness function is based on the message length, frequency distribution of bigrams and trigrams tested for the number of bigrams and trigrams checked and the likelihood of occurrence in successful deciphered messages. Further, the cryptanalysis of transposition cipher was also carried out by other researchers [25–29]. An extensive research on classical cipher cryptanalysis was investigated by Bagnall [26] and Clark [30]. Clark's cryptanalytic attack work covers a variety of classical ciphers that include simple substitution, transposition as well as poly-alphabetic ciphers. He proposed new attacks on these ciphers, which utilize simulated annealing and the tabu search and compared these attacks with GA attack. A comparison of search techniques of GA, simulated annealing and tabu search for cryptanalysis of simple substitutions was performed by Clark and Dawson [10] where it is shown that the tabu search outperformed the other techniques. The comparison of these techniques was also carried out by Garg [28] for cryptanalysis of transposition cipher. An Evolutionary Approach for the Playfair cipher cryptanalysis was applied by Negara [31] to construct key-square. GA for searching key-space of poly-alphabetic substitution ciphers was reported by Ragheb and Subbanagounder [32]. The parallel GA's were proposed by Clark and Dimovski [33, 34] for attacking the poly-alphabetic substitution cipher. Through experimental evidence, he showed that parallel GA is highly efficient in solving poly alphabetic ciphers even with a large period. On the other hand, Bagnall et al. [35] concentrated his work on cryptanalysis of Rotor machine. He used a fitness function based on phi test for non-randomness of text and showed that an unknown three rotor machines can be crypt-analyzed with about 4000 letters of ciphertext. Study of heuristic search algorithms for breaking short cryptograms was reported by Morelli [36, 37]. GA was investigated for decryption of poly-alphabetic Alberti Cipher [38]. It is considered in many ways to be the backbone of modern encryption. This differs from simple substitution cipher where a given letter always receives the same substitute because each consecutive letter in the Alberti cipher is encrypted using a different alphabet than the one preceding it.

Further work on cryptanalytic attack on classical cipher is still continuing while the work on modern ciphers is emerging.

4.2 Cryptanalysis of Public Key Ciphers

Spillman continued his analysis work and illustrated that GA can also be used in the cryptanalysts of public key cryptosystems. He applied GA in cryptanalysis of knapsack ciphers [39]. Compact genetic algorithm was applied by Dawoud Hassan [40] for cryptanalysis of trapdoor 0–1 knapsack cipher. A timing attack prospect for RSA cryptanalysis using GA was reported by Ali and Salami [41].

4.3 Cryptanalysis of Block Ciphers

Genetic algorithm cryptanalysis of the basic substitution permutation network was reported by Albaassal and Joseph [42, 43] for finding of weak keys. An attack was reported by Garg [44] using genetic algorithm with ring crossover and other operators for the cryptanalysis on S-DES where GA perform far better than Brute Force search algorithm. Cryptanalysis of Simplified Data Encryption Standard Algorithm using GA was reported by Sharma and Song [45, 46]. Normadic genetic algorithm for cryptanalysis of DES 16 was reported by Sathya et al. [47]. Genetic algorithm based cryptanalysis of a Feistel type block cipher was reported by Albaasal and Wahdan [48]. Hu [49] reported the Cryptanalysis of TEA Using Quantum-Inspired Genetic Algorithms.

4.4 Design of Cryptographic Primitives and Schemes

The Boolean function is an important cryptographic primitive for block and stream ciphers. The choice of Boolean functions is to be considered carefully in designing of cryptosystems to avoid vulnerabilities and cryptanalytic attacks. Cryptographically, the Boolean functions must be highly non-linear and balanced apart from other characteristics such as algebraic degree, correlation immunity etc. The conventional methods of Boolean function design are random generation and direct construction. By using random generation, it is difficult to find functions with truly excellent properties due to the vast size of the search space while direct constructions may only meet certain design criteria. Millan [50, 51] enhanced his earlier work in designing balanced Boolean function using GA by combining it with the two-step hill climbing algorithm. The hill climbing technique has improved the performance of GA in generating highly non-linear and balanced Boolean functions. Dimovski and Gligoroski [52] employed similar techniques but only tested for non-linearity criteria and compared it with random search which proved to be more powerful technique.

Other application of GA in cryptology is the design of cryptographic schemes and protocols. Clark [53] showed how simulated annealing and GA can be used to

evolve efficient and provably correct protocols. An ICIGA: Improved Cryptography Inspired by Genetic Algorithms for block encryption is proposed by Tragha et al. [54]. A new algorithm was proposed by Agarwal [55] for secret key cryptography based on GA in which the powerful features of the Crossover and Mutation operations of GA were exploited for image encryption. A Novel Approach to Genetic Algorithm Based Cryptography was proposed by Khan and Bhatia [56] which uses standard genetic operators like mutation and crossover to generate secret keys satisfying random tests. A public key cryptography scheme using genetic algorithm was reported by Mishra and Bali [57] where encryption and decryption keys were found.

5 Discussions and Conclusions

Applications of genetic algorithms in cryptology presented in the paper indicate that the evolutionary computing using genetic algorithms is gaining momentum and found useful for solving problems of cryptology whether cryptography or cryptanalysis. Genetic algorithms have been successfully applied in the design of crypto-primitives, new encryption schemes and in the cryptanalysis of ciphers. So far, mostly classical ciphers such as simple substitution, transposition and poly-graphic and poly-alphabetic substitution ciphers have been attempted for their solutions using linguistic characteristics. Attempts have been initiated to analyze some block ciphers such as DES, Fiestal cipher and TEA etc. for distinguishing or identifying weak keys. Apart from symmetric ciphers, the analysis of asymmetric public key systems RSA has also been attempted for obtaining keys using genetic algorithm. Attempts have also been initiated to generate secret keys and crypto primitives to be used in the design of crypto-algorithms.

Although simple and little complex problems of cryptology have been attempted mainly for solving crypts of English text, same problems still to be tackled for solving crypts of other languages and other form of information such as speech and image. Many more issues of cryptology that arrive in cryptography and cryptanalysis are to be tackled for attempting modern ciphers using genetic algorithm. The GAs have been used for solving the problems of cryptology but other evolutionary algorithms being emerged that may give better solutions are also to be tried and evaluated for their performances.

References

1. Shannon, C.E.: Communication theory of secrecy systems. *Bell Syst. Tech. J.* **28**(4), 656–715 (1949)
2. Menezes, A.J., Van Oorschot, P.C., Vanstone, S.A.: *Handbook of Applied Cryptography*. CRC Press, Boca Raton (1996)

3. Beker, H., Piper, F.: Cipher Systems: The Protection of Communications. Northwood Books, London (1982)
4. Stallings, W.: Cryptography and Network Security Principles and Practice. Prentice Hall, Boston (2011)
5. Gaines, H.F.: Cryptanalysis: a Study of Ciphers and Their Solution. Dover Publications, London (1956)
6. Bonissone, P.P., Chen, Y., Goebel, K., Khedkar, P.S.: Hybrid soft computing systems: industrial and commercial applications. Proc. IEEE **87**(9), 1641–1667 (1999)
7. Munakata, T.: Fundamentals of the New Artificial Intelligence: Beyond Traditional Paradigms. Springer, New York (1998)
8. Deb, K.: Genetic algorithms in search and optimization: the technique and applications. In: Proceedings of International Workshop on Soft Computing and Intelligent Systems, Calcutta, India: Indian Statistical Institute, pp. 58–87 (1998)
9. Tomassini, M.: Evolutionary algorithms. In: Proceedings of International Workshop: Towards Evolvable Hardware, Springer LNCS 1062, (1996)
10. Clark, A., Dawson, E.: Optimization heuristics for the automated cryptanalysis of classical ciphers. JCOMMCC **28**, 63–86 (1998)
11. Yang, X.-S., Deb, S.: Cuckoo search via levy flights. In: Nature Biologically Inspired Computing. NaBIC 2009. World Congress, pp. 210–214 (2009)
12. Ibrahim, S., Maarof, M.A.: A review on biological inspired computation in cryptology. http://eprints.utm.my/3248/1/JIT_15Jun2005.pdf (2005)
13. Rod, H.: Automated cryptanalysis of monoalphabetic substitution ciphers using stochastic optimization algorithms. <http://cse.ucdenver.edu/%7Eerhilton/docs/Cryptanalysis-Against-Monosub-Ciphers.pdf>
14. Uddin, M.F., Youssef, A.M.: Cryptanalysis of simple substitution ciphers using particle swarm optimization, evolutionary computation. In: CEC 2006, IEEE Congress on Evolutionary Computing, pp. 677–680 (2006)
15. Kirkpatrick, S., Gelatt, C.D., Vecchi, M.P.: Optimization by simulated annealing. Science **220**(4598), 671–680 (1983)
16. Abdul Halim, M.F., Attea, B.A., Hammed, S.M.: A binary particle swarm optimization for attacking knapsacks cipher algorithm. In: ICCCE08 Conference, Malaysia, May (2008)
17. Goldberg, D.E.: Genetic Algorithms in Search, Optimization and Machine Learning. Addison- Wesley Pub.Co., Boston (1989)
18. Spillman, R., Janssen, M., Nelson, B., Kepner, N.: Use of genetic algorithm in cryptanalysis of simple substitution cipher. Cryptologia **17**(4), 367–377 (1993)
19. Forsyth, W.S., Safavi-Naini, R.: Automated cryptanalysis of substitution ciphers. Cryptologia **17**(4), 407–418 (1993)
20. Thomas, J.: A fast method for cryptanalysis of substitution ciphers. Cryptologia **19**(3), 265–274 (1995)
21. Faldt, E., Nilsson, S.: Solving simple substitution ciphers using genetic programming. <http://target0.be/madchat/crypto/codebreakers/SubstGen.pdf> (2001)
22. Verma, A.K., Mayank, D., Joshi, R.C.: Genetic algorithm and tabu search attack on the mono-alphabetic substitution cipher in adhoc networks. J. Comput. Sci. **3**, 134–137 (2007)
23. Omran, S.S., Al-Khalid, A.S., Al-Saady, D.M.: Using genetic algorithm to break a monoalphabetic substitution cipher. In: Proceedings of IEEE Conference on Open Systems (ICOS 2010), pp. 63–67 (2010)
24. Matthews, R.A.J.: The use of genetic algorithms in cryptanalysis. J. Cryptologia **17**(2), 187–201 (1993)
25. Al-Khalid, A.S., Omran, S.S., Hammod, D.A.: Using genetic algorithms to break a simple transposition cipher. In: 6th International Conference on Information Technology ICIT 2013 (2013)
26. Bagnall, A. J.: The applications of genetic algorithms in cryptanalysis. School of Information Systems, University Of East Anglia (1996)

27. Dimovski, A., Gligoroski, D.: Attacks on the transposition ciphers using optimization heuristics. In Proceedings of ICEST 2003, Oct 2003
28. Garg, P.: Genetic algorithms, tabu search and simulated annealing: a comparison between three approaches for cryptanalysis of transposition cipher. *J. Theor Appl. Inf. Technol.* 5(4):387–392 (2009)
29. Heydari, M., Shabgahi, G.L., Heydari, M.M.: Cryptanalysis of transposition ciphers with long key lengths using an improved genetic algorithm. *World Appl. Sci. J.* 21(8), 1194–1199 (2013)
30. Clark, A.: Optimization heuristics for cryptology. Ph.D. Dissertation, Faculty of Information Technology, Queensland University of Technology, Australia (1998)
31. Negara, G.: An evolutionary approach for the playfair cipher cryptanalysis. <http://elrond.informatik.tu-freiberg.de/papers/WorldComp2012/SAM9762.pdf> (2012)
32. Ragheb, T., Subbanagounder, A.: Applying genetic algorithms for searching key-space of polyalphabetic substitution ciphers. *Int. Arab J. Inf. Technol.* 5(1), 87–91 (2008)
33. Clark, A., Dawson, E.: A parallel genetic algorithm for cryptanalysis of the polyalphabetic substitution cipher. *Cryptologia* 21(2), 129–138 (1997)
34. Dimovski, A., Gligoroski, D.: Attack on the Polyalphabetic substitution cipher using a parallel genetic algorithm. Technical Report, Swiss-Macedonian Scientific Cooperation through SCOPES Project, Ohrid (2003)
35. Bagnall, A.J., Mckeown, G.P., Rayward-smith, V.J.: The cryptanalysis of a three rotor machine using a genetic algorithm. In Proceedings of the Seventh International Conference on Genetic Algorithms (ICGA97), Morgan Kaufmann (1997)
36. Morelli, R.A., Walde, R.E.: A word-based genetic algorithm for cryptanalysis of short cryptograms. In Proceedings of the 2003 Florida Artificial Intelligence Research Symposium (FLAIRS—2003), pp. 229–233 (2003)
37. Morelli, R.A., Walde, R.E., Servos, W.: A study of heuristic search algorithms for breaking short cryptograms. *Int. J. Artif. Intell. Tools (IJAIT)* 13(1), 45–64 (2004) (World Scientific Publishing Company)
38. Servos, W.: Using genetic algorithm to break Alberti cipher. *J. Comput. Sci. Coll.* 19(5), 294–295 (2004)
39. Spillman, R.: Cryptanalysis of knapsack ciphers using genetic algorithms. *Cryptologia* 17(4), 367–377 (1993)
40. Al-Dabbagh, R.D.H.: Compact genetic algorithm for cryptanalysis of trapdoor 0–1 knapsack cipher. *J. Al-Nahrain Univ.* 12(2), 137–145 (2009)
41. Ali, H., Al-Salami, M.: Timing attack prospect for RSA cryptanalysis using genetic algorithm technique. *Int. Arab J. Inf. Technol.* 1(1), 17–27 (2004)
42. Albaassal, A.M.B., Wahdan, A.-M.A.: Genetic algorithm cryptanalysis of the basic substitution permutation network. In: Proceedings of the IEEE Midwest Symposium on Circuits and Systems, pp. 471–415 (2003)
43. Joseph, A.B., Sheridan, H.: Genetic algorithm cryptanalysis of a substitution permutation network. In: IEEE Symposium on Computational Intelligence in Cyber Security, CICS '09, pp. 115–121 (2009)
44. Garg, P.: Genetic algorithm attack on simplified data encryption standard algorithm. *Int. J. Res. Comput. Sci.* ISSN1870-4069 (2006)
45. Sharma, L., Pathak, B.K., Sharma, R.: Breaking of simplified data encryption standard. *Glob. J. Comput. Sci. Technol.* 12(5) (2012) (Version 1.0)
46. Song, J., Zhang, H., Meng, Q. and Wang, Z.: Cryptanalysis of four-round DES based on genetic algorithms. In: Proceedings of the International Conference on Wireless Communications, Networking and Mobile Computing, vol. 4683, pp. 583–590, Springer-Verlag, LNCS (2007)
47. Sathya, S., Chitralakha, S.T., Ananda Kumar, P.: Normadic genetic algorithm for cryptanalysis of DES 16. *Int. J. Comput. Theor. Eng.* 2(3), 411–415 (2010)

48. Albaasal, A.M.B., Wahdan, A.-M.A.: Genetic algorithm cryptanalysis of a feistel type block cipher. In: Proceedings of Electrical, Electronic and Computer Engineering Conference, 217–221 (2004)
49. Hu, W.: Cryptanalysis of TEA using quantum-inspired genetic algorithms. *J. Softw. Eng. Appl.* **3**, 50–57 (2010)
50. Millan, W., Clark, A., Dawson, E.: Smart hill climbing finds better boolean functions. In: Proceedings of 4th Annual Workshop on Selected Areas in Cryptography, SAC 1997, 11–12 Aug 1997
51. Millan, W., Clark, A., Dawson, E.: Heuristic design of cryptographically strong balanced boolean functions. In: *Advances in Cryptology—EUROCRYPT’98*, LNCS 1403, pp. 489–499 (1998)
52. Dimovski, A., Gligoroski, D.: Generating highly nonlinear boolean functions using a genetic algorithm. In: Proceedings of 1st Balcan Conference on Informatics, Thessaloniki, Greece, Nov (2003)
53. Clark, J.A.: Metaheuristic search as cryptological tool. PhD Dissertation, Dept. Comput. Sci, University of York, UK (2000)
54. Tragha A., Omary F., Mouloudi A.: ICIGA: improved cryptography inspired by genetic algorithms. In Proceedings of the International Conference on Hybrid Information Technology (ICHIT’06), pp. 335–341 (2006)
55. Agarwal, A.: Secret key encryption algorithm using genetic algorithm. *Int. J. Adv. Res. Comput. Sci. Softw. Eng.* **2**(4), 216–218 (2012)
56. Khan, F.U., Bhatia, S.: A novel approach to genetic algorithm based cryptography. *Int. J. Res. Comput. Sci.* **2**(3), 7–10 (2012)
57. Mishra, S., Bali, S.: Public key cryptography using genetic algorithm. *International J Recent Technol. Eng. (IJRTE)* **2**(2), 150–154 (2013)

An Ontology and Pattern Clustering Approach for Activity Recognition in Smart Environments

K. S. Gayathri, Susan Elias and S. Shivashankar

Abstract Activity recognition aims at modeling the occupants' behavior by analyzing the sensor data collected from the smart environment. Though most of the activity recognition systems use supervised learning techniques for building such models there is a shift towards the unsupervised learning paradigm as the process of annotating and labeling the data is prone to errors. This paper proposes an *Event Pattern Activity Modeling Framework (EPAM)* to identify the occupant activity pattern from the sensor data by using an unsupervised machine learning approach and further analysis is done with a knowledge driven approach. In the context of smart environments, an activity is considered as a sequence of events that are generated continuously from the sensor data. The segmentation algorithm proposed in *EPAM* is used to identify appropriate event patterns for an activity that are then grouped together using a pattern clustering algorithm that presents a hierarchy of activities. The set of activities of the occupant, observed in a smart environment is not always sequential but is highly interleaved and discontinuous. The proposed algorithm accommodates this valid factor by an innovative use of the *Jaro Winkler* similarity measure. The hierarchy of activity generated by the pattern clustering approach is used for activity modeling. Ontology based activity modeling is preferred over other modeling techniques because of its unified modeling, representation and semantically clear reasoning. The experimental

K. S. Gayathri (✉) · S. Elias
Department of Computer Science and Engineering,
Sri Venkateswara College of Engineering,
Sriperumbudur 602117, India
e-mail: gayasuku@svce.ac.in

S. Elias
e-mail: susanelias70@gmail.com

S. Shivashankar
Ericsson Research India, Chennai, India
e-mail: s.shivashankar@ericsson.com

results show that the proposed *EPAM* framework of segmentation, pattern clustering and ontological modeling is efficient and more effective than the existing approach of activity modeling.

1 Introduction and Related Work

The concept of smart environment has evolved over the years into applications that are very challenging to design, develop and deploy [1–3]. The availability of low cost sensors, paradigms such as the Internet of Things (IoT), and research contributions from the fields of machine learning, ambient intelligence and ubiquitous computing together help in the conceptualization of smart environments [4]. The key to smart environments lies in capturing the data in real time from the environment and in applying reasoning dynamically to achieve a specified goal. Smart environment applications can be integrated in socially relevant scenarios that would have a profound impact on the future of society. Some of the popular smart home applications range from elder and child care [5–7] energy efficiency, surveillance, offices, hospitals, agriculture, disaster assessment, to name a few. The focus of our research work is in the building of a reasoning system for smart environments. The application use case in this research work is the design of a smart home [8] that assists the occupant with *Activities of Daily Living (ADL)*. Activity recognition is the key part in a reasoning system and it is built by training the system on occupants' behavior. The trained system or the activity model can then be used for detection, prediction and decision making [1].

Learning the behavioral pattern of the occupant is essential for effectively reasoning and training the activity recognition system. Information on the normal activities can be obtained from various sources such as data from previous observations or from domain experts, text corpus and web services in specific cases [9–11]. Besides video and audio capturing devices, sensors are largely used to capture the behavior of the occupants in smart environments. Wearable and object based sensors can be efficiently utilized to continuously report about the environment in a pre-specified manner. Extensive research work is being carried out in video based activity recognition, but it has the limitation of violating the privacy of the occupants' especially in smart home applications [9]. Hence the current research focus is towards sensor based activity recognition which includes the generation of models from the data collected from these sensors. Sensor based activity recognition system modeling can be carried out using two approaches namely Data driven and Knowledge driven approaches and this classification is based on the source of the information and the strategies used for training [1, 9]. Data driven approaches analyze the data that describes the occupants' behavior collected from the various sensors deployed in the environment [3, 10]. Machine learning approaches are then used to build an activity model that further learns from the occupants' behavioral data. Sensor data used for training the activity model will either be annotated or unlabelled. Supervised learning techniques [3, 9]

are applied if the data is labeled and unsupervised or semi supervised techniques [12, 13] are applied to unlabelled data. Semantically clear activity modeling can be achieved using knowledge driven approaches that use rich domain knowledge for activity modeling and pattern recognition [9, 14, 15]. Representation of activities in the form of knowledge helps in reusability and scalability as most Activity Daily Living (ADL) activities are similar functions for all occupants. A hybrid Data driven and Knowledge driven approach is used to build an Activity recognition model. The proposed framework employs a data driven approach for extracting the activity patterns from sensor data through behavioral clustering and variability analysis and then models the extracted activity pattern through an ontology based Knowledge driven approach.

2 Proposed Work

The information on *ADL* plays a vital role in building an activity recognition system for assisted living. This demands the mining of sensor data for various activities of an occupant using data mining and machine learning techniques. The proposed Event Pattern Activity Modeling (EPAM) framework is shown in Fig. 1 and it works on an unsupervised machine learning technique to extract meaningful activity patterns from large volumes of unlabelled sensor data and performs activity modeling using an ontology based technique.

2.1 Segmenting Sensor Data

Sensors deployed in smart environments record information about both the occupant and the environment. The received sensor data is in the form of events that are represented as a set containing information such as date, time, sensor identification and status. Event pattern represents an activity and are mined from sensor data through appropriate segmentation approach. Segmentation of sensor data can be done using various approaches: Fixed time interval based, Variable time interval based, Dominant sensor based and Location based. Fixed interval based approach used in [8], segments the sensor data at fixed time interval for generating event patterns. This approach has the drawback of omitting some useful information for an activity if the activity prolongs for more than the fixed time period or it may combine two activity patterns together if the fixed time interval is large than the activity duration. Hence a fixed time interval based approach is not appropriate for segmenting sensor information in smart home applications. Variable interval based approach [14] can be used to vary the time period based on the activity. Since the sensor data is unlabelled and the domain knowledge related to the duration of activity is not available, the time period cannot be varied for different situations. Dominant sensors [16] are sensors that is very important for

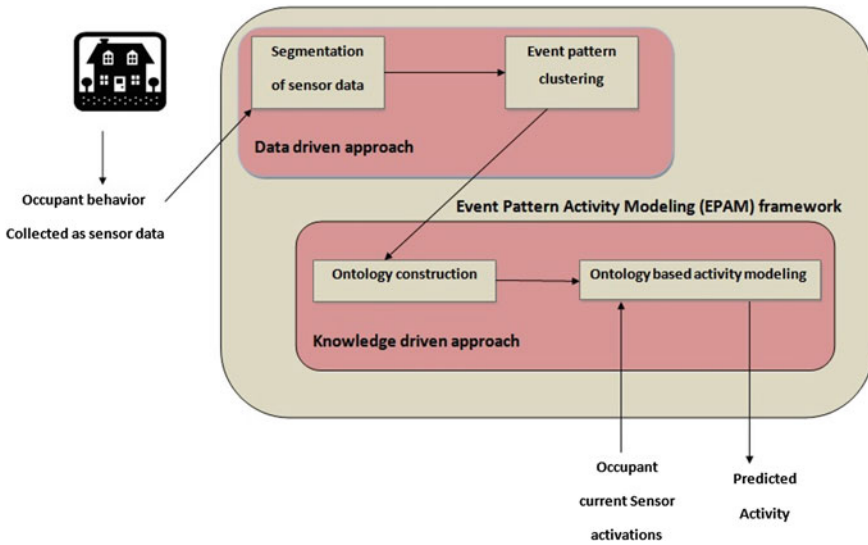


Fig. 1 Event pattern activity modelling (EPAM) framework

each activity. E.g. In “sleep activity”, bed sensors should be ‘ON’ though there are other co existing sensor activations and therefore bed sensors are dominant for sleeping activity. Event patterns are generated in such a way that they contain sequence of events collected with at least one dominant sensor. It is not always possible to define dominant sensors for all activities since an unsupervised approach is used. Another approach is location based where a majority of occupant activity is location specific such as sleeping is associated with bedroom, cooking is done in kitchen and so on. The sensor sequences are segmented based on their spatial location and it will result in event patterns that will be more appropriate for a smart home scenario. The proposed Algorithm 1—Segmentation algorithm takes the continuous sensor data stream as the input and outputs the various event patterns generated based on the spatial location. The line 6 in Algorithm 1 first makes a comparison as to whether any two subsequent events occur in the same location. In such a case, using line 9 in the algorithm they are appended to the sequence of events pertaining to that location else they get represented as event sequences belonging to other relevant spatial locations. This segmentation helps in identifying all activities within a specific location. The segmented sequences are maintained on different data structures for different location.

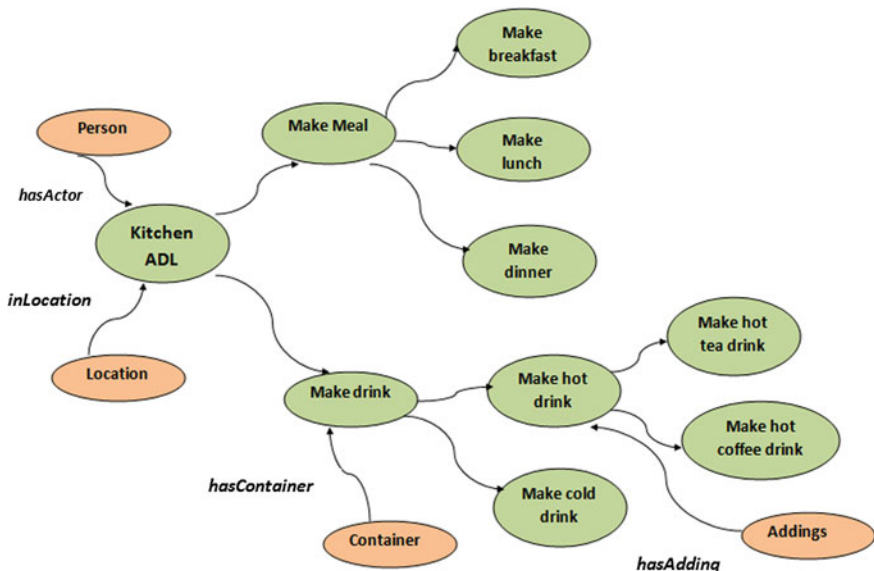


Fig. 2 Hierarchy of kitchen ADL activities

Algorithm 1: Segmenting sensor data

```

1 Procedure Segmenting Sensor data(Sensordata)
2 Sensordata is a sequence of event spatiotemporaldata
3 Initialise the spatial tables to empty
4 Initialise sp.spatio as empty for all spatial location
5 foreach event  $e_i$  in Sensor data do
6   if  $e_i.spatio == e_{i+1}.spatio$  then
7     | sp.spatio  $\leftarrow$  sp +  $e_i$ 
8   end
9   add sp.spatio to spatio table
10  set sp.spatio to empty
11 end
    
```

2.2 Event Pattern Clustering

Event pattern clustering algorithm handles unlabelled sensor data and groups the various sequences together to identify the relevant activity of the occupant in a particular spatial region. The proposed approach identifies all the sub activities pertaining to a particular activity of the occupant and in a way follows hierarchical clustering. The reason behind preferring hierarchical clustering compared to the other clustering approach is that, the activity of the occupant in smart home can be viewed as hierarchy of activities as shown in Fig. 2. What makes it different from

conventional hierarchical technique is that it clusters similar sequences of events rather than grouping discrete events.

The following are the steps involved in event pattern clustering algorithm:

Step 1—Initializing the clusters

The event patterns generated by the location based segmentation algorithm are taken as the input to the event pattern clustering algorithm. Each event pattern available in the spatial table is initialized as a separate cluster with event pattern as the center for the cluster.

Step 2—Extracting temporal information from event pattern

The temporal information from event pattern is extracted by storing the start time of every event pattern with the duration of the activity. This is very essential in order to build the personal occupant profile containing the information regarding the time range around which the occupant does the activity and the duration taken for that activity.

Step 3—Calculate the similarity measure

Similarity between event patterns can be measured by a number of similarity measures like Euclidean distance, Manhattan distance and Levenshtein edit distance [12] but all these do not address issues related to event sequences in a smart environment. In such scenarios the event patterns need not be of the same length, the events may not occur in the same order every time or there may be interleaving of event sequences between different activities. In order to handle the above mentioned issues effectively, our approach uses *Jaro Winkler* similarity measure as given in Eq. 2. The approach allows a range within which the event sequences may be discontinuous as given in Eq. 3 and no two event sequences can represent an activity if they are completely discontinuous.

$$d_j = \begin{cases} 0, & \text{if } m \text{ is } 0 \\ \frac{1}{3} \left(\frac{m}{|S_1|} + \frac{m}{|S_2|} + \frac{m-t}{m} \right) & \text{otherwise} \end{cases} \quad (1)$$

$$d_w = d_j + (l * p(1 - d_j)) \quad (2)$$

$$w_l = \frac{\max(|S_1|, |S_2|)}{2} - 1. \quad (3)$$

The distance measure is given in Eq. 1 and it takes any value between [0, 1]. It takes a maximum value of 1 if the events are completely equal, values closer to 1 represent more similar sequences and it is zero if they are unequal. Equation 2 gives the Jaro distance for strings S_1 and S_2 , l is the length of common prefix at the start of a string and can take a maximum of 4 characters, p is a scaling factor that indicates how much the score is adjusted upwards for strings with common prefixes, m is the number of matching characters, t is half the number of transpositions w_l is the window limit within which the discontinuity is allowed. To understand how the *Jaro distance* measure works, consider an example as shown in Fig. 3



Fig. 3 Illustration for event sequence

where the each event is represented as a character. Two patterns are observed in the sequence of events for which m takes a value of 3, w_l is 1, t is 0, length of S_1 and S_2 is 5. Jaro distance is calculated as 0.6 and Jaro Winkler distance is 0.64. The result gives a similarity measure of 64 %. Using the above mentioned similarity measure a similarity matrix is constructed with the similarity value between every cluster.

Step 4—Merging of clusters

Clusters are to be merged to form hierarchy of activity patterns and clusters which have minimum similarity distance are merged together. After the clusters are merged the similarity measures are to be recalculated between newly formed cluster patterns and every other cluster. Lines 9–13 in the Algorithm 2—Event pattern clustering does the process of merging and recalculating similarity measure. This calculation is based on single linkage clustering approach where the link between two patterns is made by a single event pattern that is formed from two event patterns (one in each cluster) that are closest to each other. The steps 2–4 needs to be repeated until all clusters are merged into a single cluster. Since, the event patterns with respect to the spatial location is taken, the event pattern clustering algorithm is able to identify the various activities done by the occupant in that particular spatial location.

Algorithm 2: Event pattern clustering

```

1 Procedure Event pattern clustering(Event patterns)
2 Event patterns set of event patterns spatioeventtable
3 begin
4   foreach spatial location  $s_i$  do
5     foreach event pattern  $e_i$  in the Spatial location table  $s_i$  do
6       | calculate similarity measure with other event patterns
7     end
8     set each event patterns as cluster pattern center set clusnum = no of event patterns
9     repeat
10    | merge two closest event patterns
11    | update the similarity measure for every event pattern
12    | reduce clusnum by one
13    until clusnum == 1
14   end
15 end

```

2.3 Activity Modeling: Ontology Construction

Activity modeling is required to increase the comfort of the occupant through automation which assists the occupant in performing ADL activities. There are several ways by which modeling can be done, the most commonly used approaches are Artificial Neural Network (ANN), Hidden Markov Model (HMM) and Dynamic Bayesian Network (DBN). The activity models built by the above methods cannot be reused for activity modeling for different occupants. Information about the occupant activity is usually obtained from the domain expert, which makes the system highly dependent on the domain expert. The information given by the expert may not provide the complete knowledge about the occupant activities posing a limitation to the knowledge driven approach. So, we put forth a method of extracting information about the occupant activities through a data driven approach. The extracted information is then represented using knowledge representation techniques such as logics, ontologies. The Fig. 2 shows that the activity of the occupant is hierarchical in nature, so the best approach to represent and reflect this information is through ontology representation. Ontology is preferred because of its systematic representation and its advantage of interoperability, reusability and scalability. Two levels of ontology are constructed 1. ADL ontology is constructed by representing the activities of the occupant and 2. User profile ontology is constructed to represent personal information of the occupant. The information extracted in step 2 of the event pattern clustering algorithm is used for constructing user profile ontology and clustered patterns for constructing ADL ontology. Subsumption, equivalence reasoning techniques can be applied on ontology to perform semantic reasoning for assisting the occupant in his activities.

3 Experimental Analysis

Sensor data used for the experimental analysis were collected from WSU CASAS smart home project [12]. Java API is used to implement the Location based segmentation and event pattern clustering algorithm. The Fig. 4 shows the event patterns that are generated by applying the location based segmentation algorithm on the smart home sensor data. The ontology is constructed using Protege, an ontology editor and FACT ++ is used for ontology reasoning. Figure 5 shows the class constructed using ontology. The efficiency of the proposed system is measured through *misclassification rate* which is the ratio between total number of incorrect classification of activity to total number of activity classification during activity recognition. The experiment was conducted with smart home data set [12]

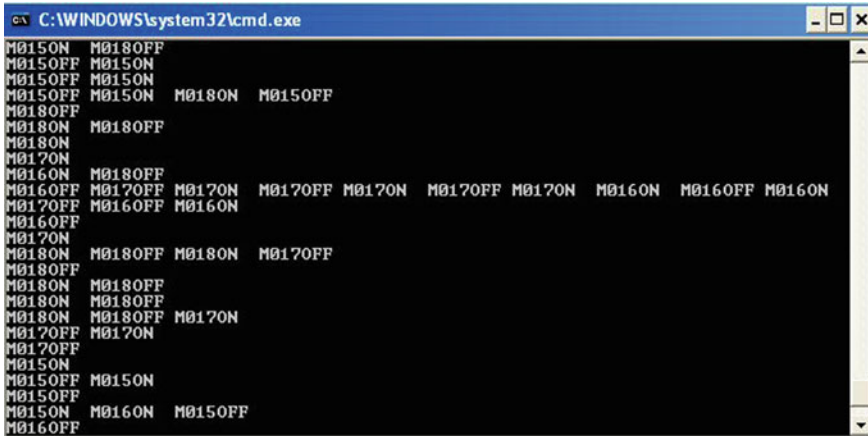


Fig. 4 Event patterns from location based segmentation of sensor data

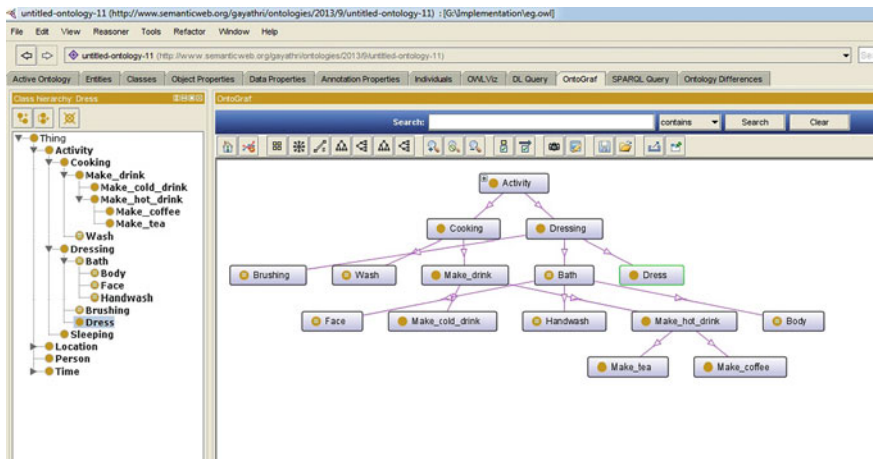
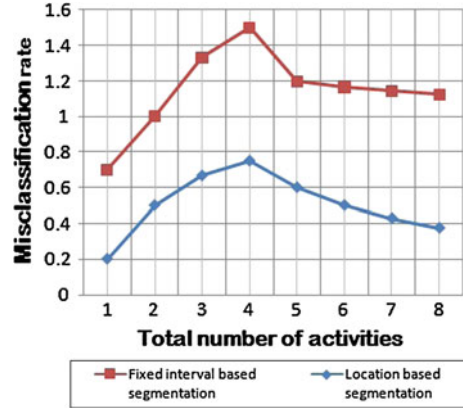


Fig. 5 Ontology construction using protege tool

and the results showed that the misclassification rate is much less in location based rather than fixed interval based segmentation as shown in Fig. 6 thus confirming location based segmentation most suitable for efficient activity modeling.

Fig. 6 Comparison between fixed interval based and location based segmentation



4 Conclusion

Today sensors technology has augmented the field of ubiquitous computing with massive reduction in cost and size thereby enabling the deployment of very challenging applications. A smart environment is an application that effectively utilizes sensors to create Ambient Intelligence for automation in a wide range of domains from entertainment to health care. The most important task in such environments is the identification of occupant activity. Our proposed Event Pattern Activity Modeling (EPAM) follows unsupervised machine learning approach to identify the patterns in the unlabeled collection of sensor data through pattern clustering. We have identified that Jaro Winkler similarity measure compares patterns efficiently in smart environments. The proposed pattern clustering also organizes the clusters into a hierarchy thus identifying the various sub activities of the occupant. Ontology is constructed using the event patterns for each activity which is used for semantic reasoning of new sensor data (test input). The experimental study shows that the proposed approach of combining data driven approach and knowledge driven approach gives better prediction than using a data driven approach. The future enhancement of this work will focus on context based pattern clustering that would augment the Ambient Intelligence (AmI) in smart environments.

References

1. Cook, D.J., Augusto, J.C., Jakkula, V.R.: Ambient intelligence: technologies, applications, and opportunities. *Pervasive Mob. Comput.* **5**(4), 277–298 (2009)
2. Cook, D.J., Das, S.K.: How smart are our environments? An updated look at the state of the art. *Pervasive Mob. Comput.* **3**(2), 53–73 (2007)

3. Augusto, J.C., Nakashima, H., Aghajan, H.: Ambient intelligence and smart environments: a state of the art. In: *Handbook of Ambient Intelligence and Smart Environments*, pp. 3–31 (2010)
4. Alam, M.R., Reaz, M.B.I., Ali, M.A.M.: A review of smart homes - past, present, and future. *IEEE Trans. Syst. Man Cybern. Part C* **42**(6), 1190–1203 (2012)
5. Lotfi, A., Langensiepen, C.S., Mahmoud, S.M., Akhlaghinia, M.J.: Smart homes for the elderly dementia sufferers: identification and prediction of abnormal behaviour. *J. Ambient Intell. Humanized Comput.* **3**(3), 205–218 (2012)
6. Corts, U., Urdiales, C., Annicchiaric, R.: *Intelligent Healthcare Managing: An Assistive Technology Approach*, pp. 1045–1051. Springer-Verlag Berlin Heidelberg (2007)
7. Augusto, J.C., Huch, M., Kameas, A., Maitland, J.: *Handbook of ambient assisted living-technology for healthcare, rehabilitation and well-being. Handbook of Ambient Assisted Living*, vol. 11. IOS Press, US (2012)
8. Sukanya, P., Gayathri, K.S.: An unsupervised pattern clustering approach for identifying abnormal user behaviors in smart homes. *Int. J. Comput. Sci. Netw.* **2**(2), 115–122 (2013)
9. Chen, L., Hoey, J., Nugent, C.D., Cook, D.J., Zhiwen, Y.: Sensor-based activity recognition. *IEEE Trans. Syst. Man Cybern. Part C* **42**(6), 790–808 (2012)
10. Aztiria, A., Izaguirre, A., Augusto, J.C.: Learning patterns in ambient intelligence environments: a survey. *Artif. Intell. Rev.* **34**(1), 35–51. Springer, Netherlands (2010)
11. Atallah, L., Yang, G.-Z.: The use of pervasive sensing for behaviour profiling—a survey. *Pervasive Mob. Comput.* **5**(5), 447–464 (2009)
12. Rashidi, P., Cook, D.J., Holder, L.B., Schmitter-Edgecombe, M.: Discovering activities to recognize and track in a smart environment. *IEEE Trans. Knowl. Data Eng.* **23**(4), 527–539 (2011)
13. Rashidi, P., Cook, D.J.: Keeping the resident in the loop: Adapting the smart home to the user. *IEEE Trans. Syst. Man Cybern. Part A* **39**(5), 949–959 (2009)
14. Chen, L., Nugent, C.D., Wang, H.: A knowledge-driven approach to activity recognition in smart homes. *IEEE Trans. Knowl. Data Eng.* **24**(6), 961–974 (2012)
15. Riboni, D., Bettini, C.: Cosar: hybrid reasoning for context-aware activity recognition. *Pers. Ubiquit. Comput.* **15**(3), 271–289 (2011)
16. Aztiria, A., Augusto, J.C., Basagoiti, R., Izaguirre, A., Cook, D.J.: Discovering frequent user–environment interactions in intelligent environments. *Personal Ubiquitous Comput.* **16**(1), 91–103 (2012)

A Note on Constructing Fuzzy Homomorphism Map for a Given Fuzzy Formal Context

Prem Kumar Singh and Aswani Kumar Ch.

Abstract Formal Concept Analysis is a well established mathematical model for data analysis and processing tasks. Computing all the fuzzy formal concepts and their visualization is an important concern for its practical applications. In this process a major problem is how to control the size of concept lattice. For this purpose current study focus on constructing a fuzzy homomorphism map $h: \mathbf{F} = (O_i, P_j, \tilde{R}) \rightarrow \mathbf{D} = (X_m, Y_n, \tilde{\varphi})$ for the given fuzzy formal context \mathbf{F} where, $m \leq i$ and $n \leq j$. We show that reduced fuzzy concept lattice preserves the generalization and specialization with an illustrative example.

Keywords Formal concept analysis · Fuzzy concept lattice · Fuzzy relation · Fuzzy homomorphism · Fuzzy graph

1 Introduction

Formal Concept Analysis (FCA) is a mathematical model for data analysis and processing task, introduced by Wille [1]. FCA starts analysis from the notion formal context describing a set of objects, a set of attributes and a binary relation between them. The main output of FCA is formal concept, concept lattice and implications. The concept lattice represents generalization and specialization between the concepts, which plays vital role in data analysis. Formal concept is a pair consisting a subset of object (called as extension) and a subset of attributes (intension) closed with Galois connection. Implications shows dependency

P. K. Singh (✉) · A. K. Ch.
School of Information Technology and Engineering, VIT University,
Vellore, Tamilnadu 632014, India
e-mail: premsingh.csjm@gmail.com

A. K. Ch.
e-mail: cherukuri@acm.org

Table 1 The possible conditions in a given fuzzy formal context

Conditions	Objects	Attributes	Fuzzy relation
a	Complete	Complete	Incomplete
b	Incomplete	Complete	Complete
c	Complete	Incomplete	Complete
d	Incomplete	Incomplete	Complete
e	Crisp	Crisp	Fuzzy
f	Crisp	Fuzzy	Fuzzy
g	Fuzzy	Crisp	Fuzzy
h	Fuzzy	Fuzzy	Fuzzy

between attributes. FCA is successfully applied in various domains for knowledge processing tasks as discussed by Poelmans et al. [2]. To represent uncertainty and vagueness in data FCA was incorporated with fuzzy setting by Burusco and Gonzales [3]. Thereafter, several approaches investigated for generating fuzzy concept lattice as given in Belohlavek and Vychodil [4]. In this process a major issue is how to reduce the size of concept lattice.

Generally, reduction can be applied on concept lattice or formal context. Several methods are available related to concept lattice [4–11] or formal context [12–16] as well. Recently, Prem Kumar and Aswani Kumar [11] introduced interval-valued fuzzy graph representation of concept lattice. Belohlavek [12, 13] discussed ordinary equivalent data of given context. Very recently, a method is proposed on homomorphism of attributes in crisp formal context [13–15]. A fuzzy homomorphism is a mapping between two defined informational systems [16–18]. Recently, it is applied in lattice theory [19] and in fuzzy informational system for data compression [20, 21]. In this paper we aim at constructing fuzzy homomorphism map of given context for reducing the concepts with an illustrative example. Table 1 discusses some possible conditions in a given fuzzy formal contexts. The notions complete and incomplete discusses about availability or non-availability of data in the given fuzzy formal context. Recently, incomplete data in FCA is studied extensively [22, 23]. However, in this paper we focus on the conditions in which data is complete for illustration of proposed method.

Remaining part of the paper is organized as follows: Sect. 2 provides a brief background about FCA in the fuzzy setting. Section 3 contains the proposed method. In Sect. 4 we provide illustrative example for the proposed method followed by conclusions, acknowledgements and References.

2 Formal Concept Analysis in the Fuzzy Setting

A fuzzy formal context is a triplet $\mathbf{F} = (O, P, \tilde{R})$, where O is a set of objects, P is a set of attributes and \tilde{R} is an L -relation between O and P , $\tilde{R}: O \times P \rightarrow L$ [3–5]. Each $\tilde{R}(o, p) \in L$ represents the membership value at which the object $o \in O$ has

the attribute $p \in P$ with a certain degree in $[0, 1]$ (L is a support set of some complete residuated lattice \mathbf{L}).

A residuated lattice $\mathbf{L} = (L, \wedge, \vee, \otimes, \rightarrow, 0, 1)$ is the basic structure of truth degrees, where 0 and 1 represent least and greatest elements respectively. \mathbf{L} is a complete residuated lattice iff [4, 9, 24, 25]:

- (1) $(L, \wedge, \vee, 0, 1)$ is a complete lattice.
- (2) $(L, \otimes, 1)$ is commutative monoid.
- (3) \otimes and \rightarrow are adjoint operators (called as multiplication and residuum, respectively), that is $a \otimes b \leq c$ iff $a \leq b \rightarrow c, \forall a, b, c \in L$.

The operators \otimes and \rightarrow are defined distinctly by Lukasiewicz, Godel, and Goguen t-norms and their residua [4, 9, 10].

For any \mathbf{L} -set $A \in L^O$ of objects, and $B \in L^P$ of attributes, we can define an \mathbf{L} -set $A^\uparrow \in L^P$ of attributes and an \mathbf{L} -set $B^\downarrow \in L^O$ of objects as follows [4, 10]:

- (1) $A^\uparrow(p) = \bigwedge_{o \in O} (A(o) \rightarrow \tilde{R}(o, p))$;
- (2) $B^\downarrow(o) = \bigwedge_{p \in P} (B(p) \rightarrow \tilde{R}(o, p))$.

$A^\uparrow(p)$ is interpreted as the \mathbf{L} -set of all attribute $p \in P$ shared by objects from A . Similarly, $B^\downarrow(o)$ is interpreted as the \mathbf{L} -set of all objects $o \in O$ having the attributes from B in common. The fuzzy formal concept is a pair of $(A, B) \in L^O \times L^P$ satisfying $A^\uparrow = B$ and $B^\downarrow = A$, where fuzzy set of objects A called as extent and fuzzy set of attributes B called as intent. The pair (\uparrow, \downarrow) are known as a Galois connection [4, 9, 10, 24, 25].

The set of fuzzy formal concepts FC_F , generated from a given fuzzy formal context \mathbf{F} , defines the partial ordering principle i.e. $(A_1, B_1) \leq (A_2, B_2) \Leftrightarrow A_1 \subseteq A_2 (\Leftrightarrow B_2 \subseteq B_1)$ for every fuzzy formal concept. Together with this ordering, in the complete lattice there exist an infimum and a supremum for some formal concepts [1–4, 9, 10]:

- $\bigwedge_{j \in J} (A_j, B_j) = (\bigcap_{j \in J} A_j, (\bigcup_{j \in J} B_j)^\downarrow^\uparrow)$,
- $\bigvee_{j \in J} (A_j, B_j) = ((\bigcup_{j \in J} A_j)^\uparrow^\downarrow, \bigcap_{j \in J} B_j)$.

3 Proposed Method

Proposed method focus on the conditions in which data is complete for a given fuzzy context shown in Table 1. Then a fuzzy homomorphism map can be defined as given below:

Step 1 Let us suppose a fuzzy formal context $\mathbf{D} = (X_m, Y_n, \tilde{\varphi})$. Now we want to define a fuzzy homomorphism map for the given fuzzy formal context $\mathbf{F} = (O_i, P_j, \tilde{R})$ onto the fuzzy context \mathbf{D} , where $m \leq i$ and $n \leq j$.

Step 2 Then suppose a fuzzy homomorphism map $h: \mathbf{F} = (O_i, P_j, \tilde{R}) \rightarrow \mathbf{D} = (X_m, Y_n, \tilde{\varphi})$ defined as: $\mu_{\tilde{R}}((o_i, p_j)) \leq \mu_{\tilde{\varphi}}(h(o_i), h(p_j)), \forall (o_i, p_j) \in \tilde{R}$ and

their images $(h(o_i), h(p_j)) \in \tilde{\varphi}$. Hence, a fuzzy homomorphism map defines the map for objects and attributes of the given fuzzy formal context \mathbf{F} to \mathbf{D} .

Step 3 The strength of obtained fuzzy relation $\tilde{\varphi}$ of homomorphic fuzzy formal context \mathbf{D} is equaled or exceeded by the strength of fuzzy relation \tilde{R} of given fuzzy formal context \mathbf{F} through the defined map: $\mu_{\tilde{R}}(o_i, p_j) \leq \mu_{\tilde{\varphi}}(h(o_i), h(p_j))$. Thus it is possible to define a fuzzy homomorphism map h as $\max_{\mu_{\tilde{R}}}(o_i, p_j) = \mu_{\tilde{\varphi}}(h(o_i), h(p_j))$ which provide a homomorphic relation $\tilde{\varphi}$ between two objects or attributes that are unrelated under the fuzzy relation \tilde{R} . If it is not the case then h is called as a strong homomorphism. However, given relations \tilde{R} and $\tilde{\varphi}$ are fuzzy then h satisfies properties of strong homomorphism given in Step 4.

Step 4 The homomorphism map h satisfies following two implications:

- (1) $\mu(o_i, p_j) \in \tilde{R} \rightarrow (h(o_i), h(p_j)) \in \tilde{\varphi}$ for all $(o_i, p_j, \tilde{R}) \in \mathbf{F}$.
- (2) $\mu(x_m, y_n) \in \tilde{\varphi} \rightarrow (o_i, p_j) \in \tilde{R}$ for all $(x_m, y_n, \tilde{\varphi}) \in \mathbf{D}$, where $o_i \in h^{-1}(x_m)$ and $p_j \in h^{-1}(y_n)$. We can observe that fuzzy homomorphism map h is many-to-one. However the inverse of h for each relation of $\mu(x_m, y_n) \in \tilde{\varphi}$ is a set of relations from $(o_i, p_j) \in \tilde{R}$.

Step 5 The map h provides compact representation of given fuzzy context $\mathbf{F} = (O_i, P_j, \tilde{R})$ through a defined fuzzy homomorphism. The objects (attributes) in obtained homomorphic context $\mathbf{D} = (X_m, Y_n, \tilde{\varphi})$ belongs to the same block of the partition created by the function h on the set $X_m (Y_n)$. However, a homomorphism map $f: L \rightarrow L'$ in residuated lattice called as complete if it preserves the arbitrary supremum and infimum:

- $\bigvee_{j \in J} h(a_j) = h(\bigvee_{j \in J} (a_j))$,
- $\bigwedge_{j \in J} h(a_j) = h(\bigwedge_{j \in J} (a_j))$.

Proposed method define a many-to-one fuzzy homomorphism for a given fuzzy context \mathbf{F} . The relation between two objects or attributes of obtained homomorphic context (\mathbf{D}) can be computed as per the Step 2 and 3 formally, $\max_{\mu_{\tilde{R}}}(o_i, p_j) = \mu_{\tilde{\varphi}}(h(o_i), h(p_j))$. Since, both relations \tilde{R} and $(\tilde{\varphi})$ are fuzzy then map h satisfies two another implications given in Step 4, which helps to get the elements of \mathbf{F} from \mathbf{D} . In this process we have not reduced any objects and attributes of given fuzzy formal context. hence it is useful for the data analysis and processing tasks. To understand the proposed method in the next section we provide an illustrative example.

4 Illustration

For illustrations of proposed method firstly we provide an example on fuzzy homomorphism map thereafter we describe it for a given fuzzy formal context. For this purpose we have consider a fuzzy matrix shown in Table 2, which represent

Table 2 Fuzzy matrix for the relation $M(X, X)$

	a	b	c	d
a	0.0	0.5	0.0	0.0
b	0.0	0.0	0.9	0.0
c	1.0	0.0	0.0	0.5
d	0.0	0.6	0.0	0.0

relation $M(X, X)$ defined on the set $X = \{a, b, c, d\}$. The fuzzy graph representation for elements of Table 2 is shown in Fig. 1 [17].

Now we want to define a fuzzy homomorphism on the set $X = \{a, b, c, d\}$ as: (1) a and $b \rightarrow \alpha$, (2) $c \rightarrow \beta$ and (3) $d \rightarrow \gamma$. The obtained fuzzy relation suppose $N(Y, Y)$ can be defined on a set $Y = \{\alpha, \beta, \gamma\}$ as depicted in Table 3. The corresponding fuzzy graph for Table 3 is shown in Fig. 2 [17]. Similarly we can define the homomorphism for the objects and attributes of given fuzzy formal context. For this purpose we have considered a fuzzy formal context shown in Table 4 [9].

The generated fuzzy formal concepts from the fuzzy formal context shown in Table 4 are [9]:

1. $\{\emptyset, 1.0/p_1 + 1.0/p_2 + 1.0/p_3 + 1.0/p_4 + 1.0/p_5 + 1.0/p_6\}$
2. $\{0.5/o_1, 1.0/p_2 + 1.0/p_3 + 1.0/p_4 + 1.0/p_5\}$
3. $\{1.0/o_2, 1.0/p_1 + 1.0/p_2 + 1.0/p_3\}$
4. $\{0.5/o_3, 1.0/p_1 + 1.0/p_2 + 1.0/p_6\}$
5. $\{0.5/o_1 + 0.5/o_5, 1.0/p_3 + 1.0/p_4\}$
6. $\{0.5/o_1 + 0.5/o_4, 1.0/p_4 + 1.0/p_5\}$
7. $\{1.0/o_1, 1.0/p_2 + 0.5/p_3 + 0.5/p_4 + 1.0/p_5\}$
8. $\{0.5/o_1 + 1.0/o_2, 1.0/p_2 + 1.0/p_3\}$
9. $\{1.0/o_2 + 0.5/o_3, 1.0/p_1 + 1.0/p_2\}$
10. $\{1.0/o_3, 0.5/p_1 + 0.5/p_2 + 1.0/p_6\}$
11. $\{0.5/o_1 + 1.0/o_5, 1.0/p_3 + 0.5/p_4\}$
12. $\{0.5/o_1 + 1.0/o_4, 1.0/p_4 + 0.5/p_5\}$
13. $\{1.0/o_1 + 0.5/o_4, 0.5/p_4 + 1.0/p_5\}$
14. $\{1.0/o_1 + 1.0/o_5, 0.5/p_3 + 0.5/p_4\}$
15. $\{0.5/o_1 + 1.0/o_2 + 1.0/o_5, 1.0/p_3\}$
16. $\{1.0/o_1 + 1.0/o_2, 1.0/p_2 + 0.5/p_3\}$
17. $\{1.0/o_2 + 0.5/o_3 + 0.5/o_6, 1.0/p_1\}$
18. $\{1.0/o_2 + 1.0/o_3, 0.5/p_1 + 0.5/p_2\}$
19. $\{0.5/o_1 + 1.0/o_4 + 0.5/o_5, 1.0/p_4\}$
20. $\{1.0/o_1 + 1.0/o_4, 0.5/p_4 + 0.5/p_5\}$
21. $\{1.0/o_1 + 1.0/o_2 + 1.0/o_5, 0.5/p_3\}$
22. $\{1.0/o_1 + 1.0/o_2 + 0.5/o_3, 1.0/p_2\}$
23. $\{1.0/o_1 + 1.0/o_4 + 1.0/o_5, 0.5/p_4\}$
24. $\{1.0/o_1 + 1.0/o_2 + 1.0/o_3, 0.5/p_2\}$
25. $\{1.0/o_2 + 1.0/o_3 + 1.0/o_6, 0.5/p_1\}$
26. $\{1.0/o_1 + 1.0/o_2 + 1.0/o_3 + 1.0/o_4 + 1.0/o_5 + 1.0/o_6, \emptyset\}$

Fig. 1 Fuzzy graph for context of Table 2

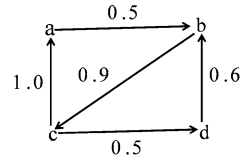


Table 3 Homomorphic image for Table 2

	α	β	γ
α	0.5	0.9	0.0
β	1.0	0.0	0.9
γ	1.0	0.9	0.0

Fig. 2 Fuzzy graph for context of Table 3

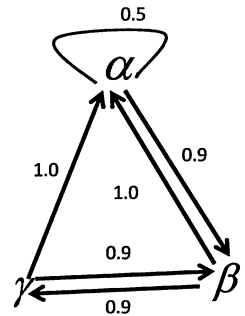


Table 4 Fuzzy formal context

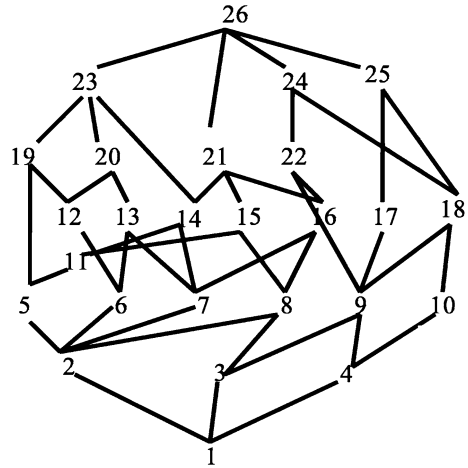
	p_1	p_2	p_3	p_4	p_5	p_6
o_1	0.0	1.0	0.5	0.5	1.0	0.0
o_2	1.0	1.0	1.0	0.0	0.0	0.0
o_3	0.5	0.5	0.0	0.0	0.0	1.0
o_4	0.0	0.0	0.0	1.0	0.5	0.0
o_5	0.0	0.0	1.0	0.5	0.0	0.0
o_6	0.5	0.0	0.0	0.0	0.0	0.0

where \emptyset represents null set. The fuzzy graph representation of concept lattice generated from above concepts is shown in Fig. 3 [9], which represents following information:

- The concepts 25 (attribute- p_1), 24(attribute- p_2), 21 (attribute- p_3) and 23 (attribute- p_4) shows generalization in the concept lattice.
- The concepts 2(object- o_1), 3(object- o_2) and 4 (object- o_3) shows specialization in the concept lattice.

Now we can define a fuzzy homomorphic map $h: \mathbf{F} = (O_i, P_j, \tilde{R}) \rightarrow \mathbf{D} = (X_m, Y_n, \tilde{\varphi})$ on attributes as: (1) p_1 and $p_2 \rightarrow y_1$, (2) p_3 and $p_4 \rightarrow y_2$, (3) $p_5 \rightarrow y_3$ and (4) $p_6 \rightarrow y_4$. The corresponding membership values can be computed through

Fig. 3 Fuzzy concept lattice for context shown in Table 4



Step 3 of proposed method as given below: $(o_1, y_1) = 1.0, (o_1, y_2) = 0.5, (o_1, y_3) = 1.0, (o_1, y_4) = 0.0, (o_2, y_1) = 1.0, (o_2, y_2) = 1.0, (o_2, y_3) = 0.0, (o_2, y_4) = 0.0, (o_3, y_1) = 0.5, (o_3, y_2) = 0.0, (o_3, y_3) = 0.0, (o_3, y_4) = 1.0, (o_4, y_1) = 0.0, (o_4, y_2) = 1.0, (o_4, y_3) = 0.5, (o_4, y_4) = 0.0, (o_5, y_1) = 0.0, (o_5, y_2) = 1.0, (o_5, y_3) = 0.0, (o_5, y_4) = 0.0, (o_6, y_1) = 0.5, (o_6, y_2) = 0.0, (o_6, y_3) = 0.0, (o_6, y_4) = 0.0$. These membership values are shown in Table 5.

Similarly, a fuzzy homomorphism map $h: \mathbf{F} = (O_i, P_j, \tilde{R}) \rightarrow \mathbf{D} = (X_m, Y_n, \tilde{\varphi})$ can be defined on objects as given below: 1. $o_1 \rightarrow x_1$, 2. o_2 and $o_3 \rightarrow x_2$, 3. o_4 and $o_5 \rightarrow x_3$, and 4. $o_6 \rightarrow x_4$. The membership values can be computed as per Step 3 of proposed method described as below: $(x_1, y_1) = 1.0, (x_1, y_2) = 0.5, (x_1, y_3) = 1.0, (x_1, y_4) = 0.0, (x_2, y_1) = 1.0, (x_2, y_2) = 1.0, (x_2, y_3) = 0.0, (x_2, y_4) = 1.0, (x_3, y_1) = 0.0, (x_3, y_2) = 1.0, (x_3, y_3) = 0.5, (x_4, y_4) = 0.0, (x_4, y_1) = 0.5, (x_4, y_2) = 0.0, (x_4, y_3) = 0.0, (x_4, y_4) = 0.0$. These membership values are shown in Table 6. Hence, the final homomorphic context for Table 4 is shown in Tables 7 followed by Table 6.

The fuzzy formal concepts generated from Table 7 are:

1. $\{\emptyset, 1.0/y_1 + 1.0/y_2 + 1.0/y_3 + 1.0/y_4\}$
2. $\{1.0/x_1, 1.0/y_1 + 0.5/y_2 + 1.0/y_3\}$
3. $\{1.0/x_2, 1.0/y_1 + 1.0/y_2 + 1.0/y_4\}$
4. $\{0.5/x_1 + 1.0/x_3, 1.0/y_2 + 0.5/y_3\}$
5. $\{1.0/x_1 + 1.0/x_2 + 1.0/x_4, 0.5/y_1\}$
6. $\{0.5/x_1 + 1.0/x_2 + 1.0/x_3, 1.0/y_2\}$
7. $\{1.0/x_1 + 1.0/x_2, 1.0/y_1 + 0.5/y_2\}$
8. $\{0.5/x_1 + 0.5/x_3, 1.0/y_2 + 1.0/y_3\}$
9. $\{1.0/x_1 + 1.0/x_2 + 0.5/x_4, 0.5/y_1\}$
10. $\{1.0/x_1 + 1.0/x_2 + 1.0/x_3 + 1.0/x_4, \emptyset\}$

Table 5 Homomorphism on attributes of Table 4

	y_1	y_2	y_3	y_4
o_1	1.0	0.5	1.0	0.0
o_2	1.0	1.0	0.0	0.0
o_3	0.5	0.0	0.0	1.0
o_4	0.0	1.0	0.5	0.0
o_5	0.0	1.0	0.0	0.0
o_6	0.5	0.0	0.0	0.0

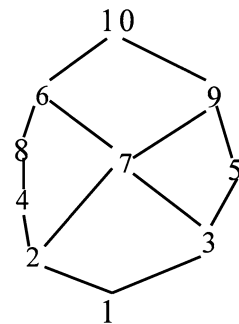
Table 6 Homomorphism on objects of Table 5 followed by Table 6

	y_1	y_2	y_3	y_4
x_1	1.0	0.5	1.0	0.0
x_2	1.0	1.0	0.0	1.0
x_3	0.0	1.0	0.5	0.0
x_4	0.5	0.0	0.0	0.0

Table 7 A homomorphic context for fuzzy context shown in Table 4

	y_1	y_2	y_3	y_4
x_1	1.0	0.5	1.0	0.0
x_2	1.0	1.0	0.0	1.0
x_3	0.0	1.0	0.5	0.0
x_4	0.5	0.0	0.0	0.0

Fig. 4 Fuzzy concept lattice for context shown in Table 7



The fuzzy concept lattice obtained from above generated concepts is shown in Fig. 4, which represents following informations:

- The concepts 9 (attribute- y_1) and 6(attribute- y_2) shows generalization. It means they represents attributes p_1, p_2, p_3, p_4 of original context.
- The concepts 2(object- x_1) and 3 (object- x_2) shows specialization. It means they represents objects o_1, o_2, o_3 of original context.

Now we can observe that the proposed method preserves the information represented in form of specialization and generalization in its original concept lattice. Similarly, we can analyze for other concepts also.

Table 8 Formal concept reduction through homomorphism

	Fuzzy context	Homomorphic context
Example	Table 4	Table 7
Context size	36	16
Number of concepts	26	10
Concept lattice	Fig. 3	Fig. 4
Generalized attributes	p_1, p_2, p_3, p_4	p_1, p_2, p_3, p_4
Specialized objects	o_1, o_2, o_3	o_1, o_2, o_3

From above analysis and with the help of Table 8, we can conclude that:

- A fuzzy homomorphism map can be defined for a given fuzzy formal context for concept lattice reduction.
- The reduced fuzzy concept lattice generated from homomorphism map preserves specialization and generalization, which plays vital role in data analysis and processing tasks.

We believe that proposed method in this study can be helpful for the various applications of FCA in knowledge discovery and processing tasks [1–4, 7–10, 25–29].

5 Conclusions

The current study focused on FCA in the fuzzy setting and defines a fuzzy homomorphism map for the given fuzzy formal context. The motivation of constructing fuzzy homomorphism map is to control the size of concept lattice. The summary of study is as follows:

- A fuzzy homomorphism map can be defined for a given fuzzy formal context for reducing the number of fuzzy formal concepts.
- The reduced fuzzy concept lattice generated from homomorphism map preserves specialization and generalization as shown in Table 8.

Acknowledgments Authors sincerely acknowledge the financial support from NBHM, DAE, Govt. of India under the grant number 2/48(11)/2010-R&D II/10806.

References

1. Wille, R.: Restructuring lattice theory: an approach based on hierarchies of concepts. In: Rival, I. (eds.) *Ordered Sets*, pp. 445–470. Springer, Reidel Dordrecht-Boston (1982)
2. Poelmans, J., Ignatov, D.I., Kuznetsov, S.O., Dedene, G.: Formal concept analysis in knowledge processing: a survey on application. *Exp. Syst. Appl.* **40**(16), 6538–6560 (2013)

3. Burusco, A., Fuentes-Gonzalez, R.: The study of L -fuzzy concept lattice. *Math. Soft Comput.* **1**(3), 209–218 (1994)
4. Belohlavek, R., Vychodil V.: What is fuzzy concept lattice. In: Proceedings 3rd International Conference on Concept Lattices and Their Applications, Czech Republic, pp. 34–45 (2005)
5. Belohalavek, R., Vychodil, V.: Reducing the size of fuzzy concept lattice through hedges. In: Proceedings of 14th IEEE International Conference on Fuzzy Systems, pp. 663–668 (2005)
6. Li, L., Jhang, J.: Attribute reduction in fuzzy concept lattices based on the T-implication. *Knowl. Based Syst.* **23**, 497–503 (2010)
7. Aswani Kumar, Ch., Srinivas, S.: Concept lattice reduction using fuzzy K-means clustering. *Exp. Syst. Appl.* **37**(3), 2696–2704 (2010)
8. Gely, A.: Links between modular decomposition of concept lattices and bimodular decomposition of a context. In: 8th International Conference on Concept Lattices and Their Applications, pp. 393–403 (2011)
9. Ghosh, P., Kundu, K., Sarkar, D.: Fuzzy graph representation of a fuzzy concept lattice. *Fuzzy Sets Syst.* **161**, 1669–1675 (2010)
10. Pocs, J.: Note on generating fuzzy concept lattices via Galois connections. *Inf. Sci.* **185**, 128–136 (2012)
11. Prem Kumar Singh, Ch. Aswani Kumar.: Interval-valued fuzzy graph representation of concept lattice. In: Proceedings of Twelfth International Conference on Intelligent Systems Design and Applications (ISDA), IEEE 27–29 Nov 2012, pp. 604–609 (2012)
12. Singh, P.K., Aswani Kumar, Ch.: A method for reduction of fuzzy relation in fuzzy formal context. In: Proceedings of International Conference on Mathematical Modelling and Scientific Computation 2012, CCIS, vol. 283, pp. 343–350, Springer, Berlin (2012)
13. Belohlavek, R.: Ordinally equivalent data: a measurement-theoretic look at formal concept analysis of fuzzy attributes. *Int. J. Approx. Reason.* (2013)
14. Belohlavek, R., Konecny, J.: Closure spaces of isotone galois connections and their morphisms. In: Proceedings of 24th International Conference on Advances in Artificial Intelligence 2011, pp. 182–191. Springer, Berlin (2011)
15. Shao, M.W., Leung, Y., Wu, W.Z.: Rule acquisition and complexity reduction in formal decision contexts. *Int. J. Approx. Reason.* (2013)
16. Yang, H.Z., Shao, M.W.: attribute characters of formal contexts under homomorphisms. In: Proceedings of IEEE International Conference on Granular Computing 2008, pp. 724–729 (2008)
17. Klir, G.J., Folger, T.A.: *Fuzzy Sets, Uncertainty, and Information*. New Jersey (USA) PHI, (2008)
18. Perchant, A., Bloch, I.: Fuzzy morphisms between graphs. *Fuzzy Sets Syst.* **128**, 149–168 (2002)
19. Kwuida, L., Lehtonen, E.: On the homomorphism order of labeled posets. *Order* **28**, 251–268 (2011)
20. Wang, C., Chen, D., Zhu, L.: Homomorphism between fuzzy information systems. *Appl. Math. Lett.* **22**, 1045–1050 (2009)
21. Wang, C., Chen, D., Hu, Q.: Data compression with homomorphism in covering information systems. *Int. J. Approx. Reason.* **52**, 519–525 (2011)
22. Krupka, M., Lastovicka, J.: Concept lattices of incomplete data. In: Domenach, F., Ignatov, D.I., Poelmans, J.(eds.) ICFCA 2012, LNAI, vol. 7278, pp. 180–194. Springer, Berlin (2012)
23. Li, J., Mei, C., Lv, Y.: Incomplete decision contexts: approximate concept construction, rule acquisition and knowledge reduction. *Int. J. Approx. Reason.* **54**(1), 149–165 (2012)
24. Pollandt, S.: *Fuzzy Begriffe*. Springer, Berlin-Heidelberg (1997)
25. Medina, J., Ojeda-Aciego, M.: On multi-adjoint concept lattice based on heterogeneous conjunctors. *Fuzzy Sets Syst.* **208**, 95–110 (2012)
26. Aswani Kumar, Ch.: Knowledge discovery in data using formal concept analysis and random projections. *Int. J. Appl. Math. Comput. Sci.* **21**(4), 745–756 (2011)
27. Aswani Kumar, Ch.: Fuzzy clustering based formal concept analysis for association rules mining. *Appl. Artif. Intell.* **26**(3), 274–301 (2012)

28. Aswani Kumar, Ch.: designing role-based access control using formal concept analysis. Secur. Commun. Netw. **6**(3), 373–383 (2013)
29. Singh, P.K., Ch. Aswani Kumar: A note on computing crisp order context of a given fuzzy formal context for knowledge reduction. J. Inf. Process. Syst. (2014) (Accepted for Publication)

Application of Ratio Property in Searching of M-Ambiguous Words and Its Generalization

Amrita Bhattacharjee and Bipul Syam Purkayastha

Abstract In this paper ratio property of words are investigated. Concept of ratio property and weak ratio property are extended for n th order alphabet. A relationship of ratio property with M-ambiguity is established. Various lemmas already proved about ratio property over ternary alphabet are investigated for tertiary alphabets. M-ambiguous words are formed by concatenating words satisfying ratio property.

Keywords Parikh matrix · Sub-word or scattered sub-word · M-ambiguity · Ratio property · Weak ratio property

1 Introduction

The notion of Parikh matrix is a well-developed as well as a developing area of research interest. It was introduced in [2] and is an extension of Parikh Mapping [1]. It has become an area of research interest due to its vast scope. In this paper we investigate on some problems on Parikh Matrices of words. A word is a finite or infinite sequence of symbols taken from a finite set called alphabet. With every word over an ordered alphabet, a Parikh Matrix can be associated and it is a triangular matrix. All the entries of the main diagonal of this matrix is 1 and every entry below the main diagonal has the value 0 but the entries above the main diagonal provide information on the number of certain sub-words in w . Although Parikh Matrix of a word is achieving better results, it still faces on some

A. Bhattacharjee (✉) · B. S. Purkayastha
Department of Computer Science, Assam University Silchar, Silchar 788011, India
e-mail: amritabhattacharjee10@gmail.com

B. S. Purkayastha
e-mail: bipulsyam@gmail.com

challenging problems, such as Parikh Matrix is not injective. To overcome the shortcomings, in recent decade scientists have developed many techniques to solve complex problems of words using Parikh Matrix.

Two words of the same alphabet may have the same Parikh matrix. This property is known as M-ambiguity. To find M-ambiguous words is a research problem. Various methods are used to find M-ambiguous words and to solve the problems of M-ambiguity. Ratio property and weak-ratio property introduced in [3] also throws light in this direction. The weak-ratio property is used in [4] to prove some interesting lemma regarding the commutativity of the Parikh matrix of two words over binary and ternary alphabets. In the paper [5] the weak-ratio property is extended to binary arrays and new extensions of this property namely row-ratio property and column-ratio property are introduced. Various results are also investigated in that field. Weak-ratio property is also used in [6] with association with Istrail morphism to explore a new area of investigation of morphic images of words.

In this paper effort has been given to study ratio property and weak ratio property in a generalized approach. Words over tertiary alphabet are discussed in the light of ratio property. We see that two words satisfying ratio property makes M-ambiguous words when they are allied in certain ways.

The paper is organized as follows. The following Sect. 2 reviews the basic preliminaries of Parikh Matrix. Section 3 goes toward developing the generalized definition of ratio property. Section 4 gives generalization of weak-ratio property. In Sect. 5 relationship of ratio property with M-ambiguity is discussed and various lemmas already proved for ternary sequences in [3] are investigated for tertiary sequences. We conclude the paper in Sect. 6 by summarizing the observations.

2 Preliminaries

Ordered alphabet: An ordered alphabet is a set of symbols $\Sigma = \{a_1, a_2, a_3, \dots, a_n\}$ where the symbols are arranged maintaining a relation of order (" $<$ ") on it. For example if $a_1 < a_2 < a_3 < \dots < a_n$, then we use notation: $\Sigma = \{a_1, a_2, a_3, \dots, a_n\}$

Word: A word is a finite or infinite sequence of symbols taken from a finite set called an alphabet. Let $\Sigma = \{a_1, a_2, a_3, \dots, a_n\}$ be the alphabet. The set of all words over Σ is Σ^* . The empty word is denoted by λ .

$|w|_{a_i}$: Let $a_i \in \Sigma = \{a_1, a_2, a_3, \dots, a_n\}$ be a letter. The number of occurrences of a_i in a word $w \in \Sigma^*$ is denoted by $|w|_{a_i}$.

Sub-word: A word u is a sub-word of a word w , if there exists words $x_1 \dots x_n$ and $y_0 \dots y_n$, (some of them possibly empty), such that $u = x_1 \dots x_n$ and $w = y_0 x_1 y_1 \dots x_n y_n$. For example if $w = abcaddbcd$ is a word over the alphabet $\Sigma = \{a, b, c, d\}$ then $abcd$ is a sub-word of w . Two occurrences of a sub-word are considered different if they differed by at least one position of some letter. In the

word $w = abcaddbcd$, the number of occurrences of the word $abcd$ as a sub-word of w is $|w|_{abcd} = 10$.

Concatenation of words: Operation of joining of two words end-to-end is called concatenation.

Triangle matrix: A triangle matrix is a square matrix $m = (m_{ij})_{1 \leq i, j \leq n}$ such that:

1. $m_{ij} \in N$ ($1 \leq i, j \leq n$), N is set of Natural number including zero.
2. $m_{ij} = 0$ for all $1 \leq j < i \leq n$,
3. $m_{ij} = 0$ for all $1 \leq j < i \leq n$.

Parikh matrix: Let $\Sigma = \{a_1 < a_2 < a_3 < \dots < a_n\}$ be an ordered alphabet, where $n \geq 1$. The Parikh matrix mapping, denoted Ψ_{M_n} , is the homomorphism $\Psi_{M_n} : \Sigma^* \rightarrow M_{n+1}$ defined as follows:

if $\Psi_{M_n}(a_q) = (m_{ij})_{1 \leq i, j \leq n+1}$ then $m_{i,i} = 1$, $m_{q,q+1} = 1$ and all other elements are zero.

Parikh matrix of a word: Let $\Sigma = \{a_1 < a_2 < a_3 \dots < a_n\}$ be an n th ordered alphabet. The Parikh matrix of $a_1, a_2, a_3, \dots, a_n$ are as follows:

$$\Psi_{M_n}(a_1) = \begin{pmatrix} 1 & 1 & \dots & 0 & 0 \\ 0 & 1 & \dots & 0 & 0 \\ \vdots & \vdots & \dots & \vdots & \vdots \\ 0 & 0 & \dots & 1 & 0 \\ 0 & 0 & \dots & 0 & 1 \end{pmatrix}_{(n+1) \times (n+1)},$$

$$\Psi_{M_n}(a_2) = \begin{pmatrix} 1 & 0 & \dots & 0 & 0 \\ 0 & 1 & 1 & \vdots & 0 \\ \vdots & \vdots & \dots & \vdots & \vdots \\ 0 & 0 & \dots & 1 & 0 \\ 0 & 0 & \dots & 0 & 1 \end{pmatrix}_{(n+1) \times (n+1)}, \dots,$$

$$\Psi_{M_n}(a_n) = \begin{pmatrix} 1 & 0 & \dots & 0 & 0 \\ 0 & 1 & \dots & 0 & 0 \\ \vdots & \vdots & \dots & \vdots & \vdots \\ 0 & 0 & \dots & 1 & 1 \\ 0 & 0 & \dots & 0 & 1 \end{pmatrix}_{(n+1) \times (n+1)}$$

Any word w over the n th order alphabet has a unique Parikh Matrix. This matrix is given by

$$\Psi_{M_n}(w) = \begin{pmatrix} 1 & |w|_{a_1} & |w|_{a_1 a_2} & \cdots & |w|_{a_1 a_2 \cdots a_{n-2}} & |w|_{a_1 a_2 \cdots a_{n-1}} & |w|_{a_1 a_2 \cdots a_n} \\ 0 & 1 & |w|_{a_2} & \cdots & |w|_{a_2 \cdots a_{n-2}} & |w|_{a_2 \cdots a_{n-1}} & |w|_{a_2 \cdots a_n} \\ \vdots & \vdots & \vdots & \cdots & \vdots & \vdots & \vdots \\ \vdots & \vdots & \vdots & \cdots & \vdots & \vdots & \vdots \\ 0 & 0 & 0 & \cdots & 1 & |w|_{a_{n-1}} & |w|_{a_{n-1} a_n} \\ 0 & 0 & 0 & \cdots & 0 & 1 & |w|_{a_n} \\ 0 & 0 & 0 & \cdots & 0 & 0 & 1 \end{pmatrix}_{(n+1) \times (n+1)}$$

where $|w|_{a_1 \cdots a_i}$ is the number of occurrences of $a_1 \cdots a_i$ in the word $w \in \Sigma^*$, here $i \in [1, n]$.

M-ambiguity: Two words w_1, w_2 over the same alphabet Σ may have the same Parikh matrix. Then the words w_1, w_2 are called M-ambiguous.

Ratio property of words over ternary sequence:

Let $\Sigma = \{a < b < c\}$ be a ternary alphabet. Two words w_1, w_2 over $\Sigma = \{a < b < c\}$ are said to satisfy the ratio property, written $w_1 \sim_r w_2$,

$$\text{If } \Psi_{M_3}(w_1) = \begin{pmatrix} 1 & p_1 & p_{1,2} & p_{1,3} \\ 0 & 1 & p_2 & p_{2,3} \\ 0 & 0 & 1 & p_3 \\ 0 & 0 & 0 & 1 \end{pmatrix} \text{ and } \Psi_{M_3}(w_2) = \begin{pmatrix} 1 & q_1 & q_{1,2} & q_{1,3} \\ 0 & 1 & q_2 & q_{2,3} \\ 0 & 0 & 1 & q_3 \\ 0 & 0 & 0 & 1 \end{pmatrix}$$

satisfy the conditions $p_i = s \cdot q_i$ ($i = 1, 2, 3$), $p_{i,i+1} = s \cdot q_{i,i+1}$ ($i = 1, 2$), where s is a constant.

Weak-ratio property of words over ternary sequence:

Let $\Sigma = \{a < b < c\}$ be a ternary alphabet. Two words w_1, w_2 over $\Sigma = \{a < b < c\}$ are said to satisfy the weak-ratio property, written $w_1 \sim_{wr} w_2$, if

$$\Phi(w_1) = \begin{pmatrix} p_1 & p_{1,2} & p_{1,3} \\ p_{2,1} & p_2 & p_{2,3} \\ p_{3,1} & p_{3,2} & p_3 \end{pmatrix} \text{ and } \Phi(w_2) = \begin{pmatrix} q_1 & q_{1,2} & q_{1,3} \\ q_{2,1} & q_2 & q_{2,3} \\ q_{3,1} & q_{3,2} & q_3 \end{pmatrix} \text{ satisfy the condition } p_i = s \cdot q_i, \{i = 1, 2, 3\} \text{ where } s, (s > 0) \text{ is a constant.}$$

3 Generalization of Ratio Property

Let $\Sigma = \{a_1 < a_2 < a_3 \cdots < a_n\}$ be an n th ordered alphabet. Two words w_1, w_2 over $\Sigma = \{a_1 < a_2 < a_3 \cdots < a_n\}$ are said to satisfy the ratio property, written $w_1 \sim_r w_2$,

$$\text{If } \Psi_{M_n}(w_1) = \begin{pmatrix} 1 & p_1 & p_{1,2} & \cdots & p_{1,n-2} & p_{1,n-1} & p_{1,n} \\ 0 & 1 & p_2 & \cdots & p_{2,n-2} & p_{2,n-1} & p_{2,n} \\ \vdots & \vdots & \vdots & \cdots & \vdots & \vdots & \vdots \\ \vdots & \vdots & \vdots & \cdots & \vdots & \vdots & \vdots \\ 0 & 0 & 0 & \cdots & 1 & p_{n-1} & p_{n-1,n} \\ 0 & 0 & 0 & \cdots & 0 & 1 & p_n \\ 0 & 0 & 0 & \cdots & 0 & 0 & 1 \end{pmatrix} \quad \text{and}$$

$$\Psi_{M_n}(w_2) = \begin{pmatrix} 1 & q_1 & q_{1,2} & \cdots & q_{1,n-2} & q_{1,n-1} & q_{1,n} \\ 0 & 1 & q_2 & \cdots & q_{2,n-2} & q_{2,n-1} & q_{2,n} \\ \vdots & \vdots & \vdots & \cdots & \vdots & \vdots & \vdots \\ \vdots & \vdots & \vdots & \cdots & \vdots & \vdots & \vdots \\ 0 & 0 & 0 & \cdots & 1 & q_{n-1} & q_{n-1,n} \\ 0 & 0 & 0 & \cdots & 0 & 1 & q_n \\ 0 & 0 & 0 & \cdots & 0 & 0 & 1 \end{pmatrix} \quad (n+1) \times (n+1)$$

satisfy the conditions

$$\begin{aligned} p_i &= s \cdot q_i, (i = 1, 2, 3, \dots, n), \\ p_{i,i+1} &= s \cdot q_{i,i+1}, (i = 1, 2, 3, \dots, n - 1), \dots, \\ p_{i,i+(n-2)} &= s \cdot q_{i,i+(n-2)}, (i = 1, 2) \end{aligned}$$

where s is a constant.

4 Generalization of Weak-Ratio Property

Let $\Sigma = \{a_1 < a_2 < a_3 \cdots < a_n\}$ be an n th ordered alphabet. Two words w_1, w_2 over $\Sigma = \{a_1 < a_2 < a_3 \cdots < a_n\}$ are said to satisfy the weak ratio property, written $w_1 \sim_{wr} w_2$,

$$\text{If } \Phi(w_1) = \begin{pmatrix} p_1 & p_{1,2} & \cdots & p_{1,n} \\ p_{2,1} & p_2 & \cdots & p_{2,n} \\ \vdots & \vdots & \vdots & \vdots \\ p_{n,1} & p_{n,2} & \cdots & p_n \end{pmatrix} \text{ and } \Phi(w_2) = \begin{pmatrix} q_1 & q_{1,2} & \cdots & q_{1,n} \\ q_{2,1} & p_2 & \cdots & p_{2,n} \\ \vdots & \vdots & \vdots & \vdots \\ p_{n,1} & p_{n,2} & \cdots & p_n \end{pmatrix}$$

satisfy the conditions $p_i = s \cdot q_i, (i = 1, 2, 3, \dots, n)$, where $s, (s > 0)$ is a constant.

5 Searching M-Ambiguous Words Using Ratio Property

In this section the relationship of ratio property and M-ambiguity is investigated. For simplicity tertiary sequences and definition of ratio property on tertiary alphabet are used. By connecting words satisfying ratio property we form some suitable new words. Using some lemmas about ratio property we show that the newly formed concatenated words are M-ambiguous words.

Ratio property of words over tertiary alphabet: Two words w_1, w_2 over $\Sigma = \{a < b < c < d\}$ are said to satisfy the ratio property, written $w_1 \sim_r w_2$, if

$$\Psi_4(w_1) = \begin{pmatrix} 1 & p_1 & p_{1,2} & p_{1,3} & p_{1,4} \\ 0 & 1 & p_2 & p_{2,3} & p_{2,4} \\ 0 & 0 & 1 & p_3 & p_{3,4} \\ 0 & 0 & 0 & 1 & p_4 \\ 0 & 0 & 0 & 0 & 1 \end{pmatrix} \text{ and}$$

$$\Psi_4(w_2) = \begin{pmatrix} 1 & q_1 & q_{1,2} & q_{1,3} & q_{1,4} \\ 0 & 1 & q_2 & q_{2,3} & q_{2,4} \\ 0 & 0 & 1 & q_3 & q_{3,4} \\ 0 & 0 & 0 & 1 & q_4 \\ 0 & 0 & 0 & 0 & 1 \end{pmatrix}$$

satisfy the conditions

$$p_i = s \cdot q_i, (i = 1, 2, 3, 4), p_{i,i+1} = s \cdot q_{i,i+1}, (i = 1, 2, 3), p_{i,i+2} = s \cdot q_{i,i+2}, (i = 1, 2)$$

where s is a constant.

The ratio property gives a sufficient condition for equality of the Parikh matrices. Let w_1, w_2, w_3 be two tertiary words such that the words satisfy the ratio property. We can form some words from w_1, w_2, w_3 as follows:

$$w^i = w_1 w_2, w^{ii} = w_2 w_1, w^{iii} = w_1^n w_2^n, w^{iv} = (w_1 w_2)^n;$$

$$w^v = w_1^n w_2^n w_3^n, w^{vi} = (w_1 w_2 w_3)^n, w^{vii} = w_1^n w_3^n, w^{viii} = (w_1 w_3)^n$$

It can be proved that the words formed by w_1, w_2, w_3 connecting them by the above way taking them as sub-words give M-ambiguous words. Concatenation of two words satisfying the ratio property by making them sub-word of a word w makes w an M-ambiguous word. Thus the ratio property helps in finding certain M-ambiguous words out of certain sets of words satisfying ratio property.

For $\Sigma = \{a < b < c < d\}$, the following lemmas inspired from [3] give some assistance in this direction.

Lemma 5.1 For any three words w_1, w_2, w_3 over $\Sigma = \{a < b < c < d\}$ having the ratio property so that $w_1 \sim_r w_2, w_2 \sim_r w_3$ we have for $n \geq 0$,

- (a) $\Psi_4(w_1w_2) = \Psi_4(w_2w_1)$ i.e. w^i and w^{ii} are M-ambiguous.
 - (b) $\Psi_4(w_1^n w_2^n) = \Psi_4((w_1w_2)^n)$ i.e. w^{iii} and w^{iv} are M-ambiguous.
 - (c) $\Psi_4(w_1^n w_2^n w_3^n) = \Psi_4((w_1w_2w_3)^n)$ i.e. w^v and w^{vi} are M-ambiguous.
- (a) Proof: if $\Psi_4(w_1)$ and $\Psi_4(w_2)$ are as in definition, then

$$\Psi_4(w_1w_2) = \begin{pmatrix} 1 & p_1 + q_1 & p_{1,2} + p_1q_2 + q_{1,2} & p_{1,3} + p_{1,2}q_3 + p_1q_{2,3} + q_{1,3} & p_{1,4} + p_{1,3}q_4 + p_{1,2}q_{3,4} + p_1q_{2,4} + q_{1,4} \\ 0 & 1 & p_2 + q_2 & p_{2,3} + p_2q_3 + q_{2,3} & p_{2,4} + p_{2,3}q_4 + p_2q_{3,4} + q_{2,4} \\ 0 & 0 & 1 & p_3 + q_3 & p_{3,4} + p_3q_4 + q_{3,4} \\ 0 & 0 & 0 & 1 & p_4 + q_4 \\ 0 & 0 & 0 & 0 & 1 \end{pmatrix}$$

and

$$\Psi_4(w_2w_1) = \begin{pmatrix} 1 & p_1 + q_1 & p_{1,2} + p_2q_1 + q_{1,2} & p_{1,3} + p_{2,3}q_1 + p_3q_{1,2} + q_{1,3} & p_{1,4} + p_{2,4}q_1 + p_{3,4}q_{1,2} + p_4q_{1,3} + q_{1,4} \\ 0 & 1 & p_2 + q_2 & p_{2,3} + p_3q_2 + q_{2,3} & p_{2,4} + p_{3,4}q_2 + p_4q_{2,3} + q_{2,4} \\ 0 & 0 & 1 & p_3 + q_3 & p_{3,4} + p_4q_3 + q_{3,4} \\ 0 & 0 & 0 & 1 & p_4 + q_4 \\ 0 & 0 & 0 & 0 & 1 \end{pmatrix}$$

If the ratio property is satisfied for w_1, w_2 then we have

$$\frac{p_1}{q_1} = \frac{p_2}{q_2} = \frac{p_3}{q_3} = \frac{p_4}{q_4} = \frac{p_{1,2}}{q_{1,2}} = \frac{p_{1,3}}{q_{1,3}} = \frac{p_{2,3}}{q_{2,3}} = \frac{p_{2,4}}{q_{2,4}} = \frac{p_{3,4}}{q_{3,4}} = s$$

These give $p_1q_2 = p_2q_1, p_1q_{2,3} = p_{2,3}q_1, p_1q_{2,4} = p_{2,4}q_1,$

$$p_2q_3 = p_3q_2, p_2q_{3,4} = p_{3,4}q_2,$$

$$p_3q_4 = p_4q_3, p_3q_{1,2} = p_{1,2}q_3,$$

$$p_4q_{2,3} = p_{2,3}q_4,$$

$$p_{1,2}q_{3,4} = p_{3,4}q_{1,2},$$

And thus $\Psi_4(w_1w_2) = \Psi_4(w_2w_1)$. That proves that w^i and w^{ii} are M-ambiguous.

- (b) Proof: $\Psi_4(w_1^n w_2^n) = \Psi_4(w_1^{n-1} w_1 w_2 w_2^{n-1})$
 $= \Psi_4(w_1^{n-1}) \Psi_4(w_1 w_2) \Psi_4(w_2^{n-1})$
 $= \Psi_4(w_1^{n-1}) \Psi_4(w_2 w_1) \Psi_4(w_2^{n-1})$ Using property (a)
 $= \Psi_4(w_1^{n-1} w_2 w_1 w_2^{n-1})$

Repeatedly using property (a) we obtain $\Psi_4(w_1^n w_2^n) = \Psi_4((w_1w_2)^n)$. That proves that w^{iii} and w^{iv} are M-ambiguous.

- (c) The proof is similar to the proof of (b). Noting that $w_1 \sim_r w_3$. Which gives w^v and w^{vi} are M-ambiguous.

Lemma 5.2 Let w_1, w_2, w_3 be three nonempty words with $w_1 \sim_r w_2, w_2 \sim_r w_3$ and $x = w_1 w_2$ then

- (a) $\Psi_4(x^n w_3^n) = \Psi_4((xw_3)^n)$ i.e. w^{vii} and w^{viii} are M-ambiguous.
- (b) x is not related to w_3 under \sim .

The proof of lemma 5.2 (a) is obvious from the lemma 5.1. i.e. $\Psi_4(x^n w_3^n) = \Psi_4(xw_3)^n$, from which we get w^{vii} and w^{viii} are M-ambiguous.

The following example satisfies the lemma 5.2 (b).

$$\text{Let } w_1 = \begin{pmatrix} 1 & 2 & 2 & 1 & 1 \\ 0 & 1 & 1 & 1 & 1 \\ 0 & 0 & 1 & 1 & 1 \\ 0 & 0 & 0 & 1 & 1 \\ 0 & 0 & 0 & 0 & 1 \end{pmatrix}, w_2 = \begin{pmatrix} 1 & 6 & 6 & 3 & 2 \\ 0 & 1 & 3 & 3 & 3 \\ 0 & 0 & 1 & 3 & 3 \\ 0 & 0 & 0 & 1 & 3 \\ 0 & 0 & 0 & 0 & 1 \end{pmatrix},$$

$$w_3 = \begin{pmatrix} 1 & 12 & 12 & 6 & 5 \\ 0 & 1 & 6 & 6 & 6 \\ 0 & 0 & 1 & 6 & 6 \\ 0 & 0 & 0 & 1 & 6 \\ 0 & 0 & 0 & 0 & 1 \end{pmatrix}$$

be three nonempty words. Here $w_1 \sim_r w_2, w_2 \sim_r w_3$.

Now $x = w_1 w_2$

$$= \begin{pmatrix} 1 & 2 & 2 & 1 & 1 \\ 0 & 1 & 1 & 1 & 1 \\ 0 & 0 & 1 & 1 & 1 \\ 0 & 0 & 0 & 1 & 1 \\ 0 & 0 & 0 & 0 & 1 \end{pmatrix} \cdot \begin{pmatrix} 1 & 6 & 6 & 3 & 2 \\ 0 & 1 & 3 & 3 & 3 \\ 0 & 0 & 1 & 3 & 3 \\ 0 & 0 & 0 & 1 & 3 \\ 0 & 0 & 0 & 0 & 1 \end{pmatrix} = \begin{pmatrix} 1 & 8 & 14 & 16 & 18 \\ 0 & 1 & 4 & 7 & 10 \\ 0 & 0 & 1 & 4 & 7 \\ 0 & 0 & 0 & 1 & 4 \\ 0 & 0 & 0 & 0 & 1 \end{pmatrix}$$

The above matrix is not related to w_3 . It is an example that x is not related to w_3 under \sim_r .

6 Conclusion

Ratio property is a property of words introduced in [3] helps in connecting words in an interesting way. The words satisfying ratio property can make certain M-ambiguous words. M-ambiguity of words is the problem for which Parikh matrices cannot be used in the injective way. That is for a single Parikh matrix

satisfying M-ambiguity there may be more than one word corresponding to the matrix. This paper presents generalization of ratio property and weak ratio property. Some lemmas proved for ternary sequences are investigated for tertiary words. Using those lemmas certain M-ambiguous words are formed from words satisfying ratio property by concatenating them in certain ways. We have discussed some ways of concatenation. To find all the possible ways of concatenating words satisfying ratio property to make M-ambiguous words is an open problem.

References

1. Parikh, R.J.: On the context-free languages. *J. Assoc. Comput. Mach.* **13**, 570–581 (1966)
2. Mateescu, A., Salomaa, A., Salomaa, K., Yu, S.: A sharpening of the Parikh mapping. *Theoret. Informatics Appl.* **35**, 551–564 (2001)
3. Subramanian, K.G., Huey, A.M., Nagar, A.K.: On Parikh matrices. *Int. J. Found. Comput. Sci.* **20**(2), 211–219 (2009)
4. Mahalingam, Kalpana, Subramanian, K.G.: Product of Parikh matrices and commutativity. *Int. J. Found. Comput. Sci.* **23**(1), 207–223 (2012)
5. Subramanian, K.G., Mahalingam, K., Abdullah, R., Nagar, A.K.: Binary images, M -vectors, and ambiguity, IWCIA 2011, LNCS 6636, pp. 248–260, 2011. Springer-Verlag, Berlin, Heidelberg (2011)
6. Subramanian, K.G., Isawasan, Pradeep, Venkat, Ibrahim: Parikh matrices and Istrail morphism. *Malays. J. Fundam. Appl. Sci.* **9**(1), 5–9 (2013)

Two Storage Inventory Model for Deteriorating Items Under Fuzzy Environment

S. R. Singh and Anuradha

Abstract In the present study, we investigate a two-warehouse economic order quantity model for deteriorating items in which demand increases with respect to time. Shortages are allowed and partially backlogged. This study has been done with two types of model, first one is crisp model and the second is fuzzy model. In crisp model the capacity of the own-warehouse, holding cost, unit cost, shortage cost and opportunity cost are taken as the form of real numbers and in fuzzy model, these are taken as a triangular fuzzy numbers. Graded Mean Representation method is used to defuzzify the total cost function in case of fuzzy model. To illustrate the model numerical examples are given and sensitivity analysis has been done.

Keywords Inventory · Deterioration · Shortage · Two warehouses · Fuzzy

1 Introduction

In most of the inventory models that had been projected within the early literature, the associated prices are described as real numbers, though the \$64000 world inventory prices sometimes exist with imprecise elements. Once uncertainty becomes a matter of discussion, standard approaches to treating uncertainty in internal control specialize in applied math. During this case, client demand united of the key parameters and supply of uncertainty is most frequently treated by a

S. R. Singh (✉) · Anuradha
Department of Mathematics, D.N. College, Meerut, India
e-mail: shivrajpundir@gmail.com

Anuradha
e-mail: anuradha.tanwar@gmail.com

S. R. Singh · Anuradha
Department of Mathematics, Banasthali University, Banasthali, Rajasthan, India

chance distribution. However, the probability-based approaches might not be sufficient enough to replicate all uncertainties which will arise during a globe inventory system. Modelers might face some difficulties whereas attempting to create a sound model of a list system, during which the connected prices cannot be determined exactly. For instance, prices are also obsessed with some foreign unit. In such a case, as a result of the amendment within the exchange rates, the prices are usually not known exactly. Another supply of uncertainty might arise owing to the issue of crucial actual price elements. In some cases attempting to see the precise values of such price elements is also terribly troublesome and expensive, if not possible. For instance, inventory-carrying price is usually obsessed with some parameters like current charge per unit and stock keeping the market value of the unit, which cannot be known exactly. To prevail over this obscurity, many practitioners and academician made use of fuzzy set theory. Initially, Zadeh [1] introduced the concept of fuzzy set. Park [2] applied the fuzzy set concepts to EOQ formula by representing the inventory carrying cost with a fuzzy number and solved the economic order quantity model using fuzzy number operations based on the extension principle. Vujosevic et al. [3] used trapezoidal fuzzy number to fuzzify the order cost in the total cost of the inventory model without backorder, and got fuzzy total cost. Lee and Yao [4] proposed the inventory without backorder models in the fuzzy sense and the order quantity is fuzzified as the triangular fuzzy number. Dutta et al. [5] developed a model in presence of fuzzy variable demand in which the optimum is achieved using a graded mean integration representation. Roy and Samanta [6] discussed a fuzzy continuous review inventory model without backorder for deteriorating items in which the cycle time is taken as a symmetric fuzzy number. Some recent work in this direction has been done by Singh et al. [7, 8].

Two storage facility is an important topic in that it enables firms to store the items. Generally, we have limited storage space in own warehouses and rented warehouse with unlimited storage space. This helps in reducing inventory costs as well as in obtaining the best prices due to large volume of the purchases. Hartely [9] was the first to address the problem of two warehouses. Murdeshwar and Sathe [10] formulated some aspects of lot size models with two level of storage. A two warehouses inventory model with linearly time dependent demand is developed by Goswami and Chaudhuri [11]. Bhunia and Maity [12] developed a deterministic inventory model with two warehouses for deteriorating items taking linearly increasing demand with time, shortages were allowed and excess demand was backlogged as well. Yang [13] proposed a two-warehouse inventory model for deteriorating items with shortages. Yang [14] extended Yang [13] to incorporate partial backlogging and then compared the two models based on the minimum cost approach. Singh et al. [8] discussed the two-warehouse model with permissible delay in payment in fuzzy environment. Sett et al. [15] formulated a two-warehouse inventory model with increasing demand and time varying deterioration.

Deterioration is responsible for decreasing the original economic value of the items after a certain period. Several researchers have been worked in this direction. The analysis of deteriorating inventory problems began with Ghare and Schrader [16], who developed a simple inventory model with a constant rate of

deterioration. Aggarwal [17] presented a inventory model for constant deteriorating items. Dutta and Pal [18] extended Mandal and Phaujdar [19] work for deteriorating items with the assumption that the demand rate is a linear function of the on-hand inventory by allowing shortages, which are completely backlogged. Balkhi [20] presented a production lot-size inventory model for deteriorating items over a finite planning horizon. Panda et al. [21] formulated an economic order quantity model. In which deterioration is weibull distribution in two parameters. Sana [22] analyzed an optimal policy for the deteriorating items. Sarkar and Sarkar [23] presented an inventory model for deteriorating items with inventory dependent demand function.

The above-mentioned literature reveals that inventory models for deteriorating items under the facility of two storage space in imprecise environment. In which demand increases with time and shortages are allowed and partially backlogged. The capacity of the own-warehouse, holding cost, unit cost, shortage cost and opportunity cost are taken as a triangular fuzzy numbers. Graded Mean Representation method is used to defuzzify the total cost function. To illustrate the study, numerical examples are provided and sensitivity analyses are also discussed.

2 Assumptions and Notations

The mathematical models of the two-warehouse inventory problems are based on the following assumptions:

2.1 Assumptions

1. The demand rate is an increasing and linear function of time.
2. Shortages are allowed and partially backlogged which is an exponentially decreasing function of time t , where t is the waiting time up to the next replenishment.
3. Deterioration rate is constant for both the warehouses.
4. The goods of the RW are consumed only after consuming the goods kept in the OW.
5. The inventory costs (including holding cost and deterioration cost) in the RW are higher than those in the OW.
6. With the viewpoint of cost-minimization, the opportunity cost due to lost sale is the sum of the revenue loss and the cost of goodwill. Hence, the opportunity cost due to lost sale here is greater than the unit purchase cost.
7. Replenishment rate is infinite.
8. Lead time is zero.

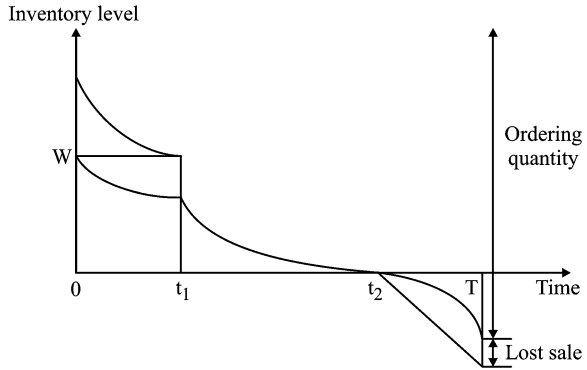
2.2 Notations

- $D(t)$: Demand rate of the items and given by $D(t) = a + bt$, where a and b are positive constants.
- α : Deterioration rate in the OW, where $0 < \alpha < 1$.
- β : Deterioration rate in the RW, where $0 < \beta < 1$.
- $e^{-\sigma t}$: Backlogging rate, σ , backlogging parameter, $0 < \sigma < 1$.
- W : Capacity of the owned warehouse (OW).
- Z : The initial inventory for the period.
- A : Replenishment cost per order.
- C : Deterioration cost per unit.
- C_S : Shortage cost per unit time.
- L : Opportunity cost due to lost sale, if the shortage is lost.
- H : Holding cost per unit per unit time in the OW.
- F : Holding cost per unit per unit time in the RW, $F > H$.
- $I_1(t)$: The inventory level in the RW during the time $[0, t_1]$.
- $I_2(t)$: The inventory level in the OW during the time $[0, t_1]$.
- $I_3(t)$: The inventory level in the OW during the time $[t_1, t_2]$.
- $I_4(t)$: The inventory level during the time $[t_2, T]$.
- t_1 : The time at which the inventory level reaches zero in the RW.
- t_2 : The time at which the inventory level reaches zero in the OW and shortages occur.
- T : The time at which the shortage level reaches the lowest point in the replenishment cycle.
- TC : The total inventory cost per unit time.
- \tilde{TC} : The fuzzy total inventory cost per unit time.

3 Mathematical Formulation of the Model

At time $t = 0$, the initial inventory for the period T is Z and out of these Z units W units are kept in the OW and rest $(Z-W)$ units are stored in the RW provided $Z > W$, otherwise zero units are stored in the RW. The goods of the OW are consumed only after consuming the goods kept in the RW. At time t_1 , inventory level in the RW reaches to zero due to the combined effect of demand and deterioration, and the inventory level W in the OW also reduces due to the effect of deterioration only. During (t_1, t_2) , inventory level in the OW reaches to zero due to the combined effect of demand and deterioration. At the time t_2 , both warehouses are empty and there after shortages occur. The partially backlogged quantity is supplied to the customers at the beginning of the next cycle. The inventory situation described as above can be represented as shown in Fig. 1.

Fig. 1 Two-warehouse inventory system



3.1 Crisp Model

During the interval (0, T), the inventory level at time t in the RW and the OW are governed by the following differential equations:

$$I'_1(t) + \beta I_1(t) = -(a + bt), \quad 0 \leq t \leq t_1 \quad \text{with } I_1(t_1) = 0 \tag{1}$$

$$I'_2(t) + \alpha I_2(t) = 0, \quad 0 \leq t \leq t_1 \quad \text{with } I_2(0) = W \tag{2}$$

$$I'_3(t) + \alpha I_3(t) = -(a + bt), \quad t_1 \leq t \leq t_2 \quad \text{with } I_3(t_2) = 0 \tag{3}$$

$$I'_4(t) = e^{-\sigma(T-t)}(a + bt), \quad t_2 \leq t \leq T \quad \text{with } I_4(t_2) = 0 \tag{4}$$

Using the boundary conditions, the solution of above differential equations are given by as follows:

$$I_1(t) = \frac{1}{\beta^2} \left\{ (\beta(a + bt_1) - b)e^{\beta(t_1-t)} - (\beta(a + bt) - b) \right\}, \quad 0 \leq t \leq t_1 \tag{5}$$

$$I_2(t) = We^{-\alpha t}, \quad 0 \leq t \leq t_1 \tag{6}$$

$$I_3(t) = \frac{1}{\alpha^2} \left\{ (\alpha(a + bt_2) - b)e^{\alpha(t_2-t)} - (\alpha(a + bt) - b) \right\}, \quad t_1 \leq t \leq t_2 \tag{7}$$

$$I_4(t) = \frac{a}{\sigma} \left(e^{-\sigma(T-t)} - e^{-\sigma(T-t_2)} \right) + \frac{b}{\sigma} \left(te^{-\sigma(T-t)} - t_2 e^{-\sigma(T-t_2)} \right) - \frac{b}{\sigma^2} \left(e^{-\sigma(T-t)} - e^{-\sigma(T-t_2)} \right), \quad t_2 \leq t \leq T \tag{8}$$

Due to the continuity at $t = t_1$, from the Eqs. (5) and (7), we have

$$\begin{aligned}
 I_2(t_1) &= I_3(t_1) \\
 \Rightarrow W e^{-\alpha t_1} &= \frac{1}{\alpha^2} \left\{ (\alpha(a + bt_2) - b)e^{\alpha(t_2-t_1)} - (\alpha(a + bt_1) - b) \right\} \\
 \Rightarrow W &= \frac{1}{\alpha^2} e^{\alpha t_1} \left\{ (\alpha(a + bt_2) - b)e^{\alpha(t_2-t_1)} - (\alpha(a + bt_1) - b) \right\}
 \end{aligned} \tag{9}$$

Now, using Taylor series expansion for the exponential function and ignoring higher order terms, Eq. (9) reduces to

$$t_2 = \frac{1}{(b + \alpha x - 2b\alpha t_1)} \left[\frac{-(a - \alpha x t_1 + b\alpha t_1^2)}{\sqrt{\left\{ (a - \alpha x t_1 + b\alpha t_1^2)^2 + (b + \alpha x - 2b\alpha t_1) \left(\begin{matrix} (2\alpha t_1 + b t_1^2 - \alpha x t_1^2) \\ + 2W(1 - \alpha t_1 + \alpha^2 t_1^2/2) \end{matrix} \right) \right\}}} \right] \tag{10}$$

Equation (10) shows that t_2 is a function of t_1 , so, t_2 is not a decision variable. Since, $I_1(t) = Z - W$ at $t = 0$, therefore, we have

$$Z = W + \frac{\{(\beta(a + bt_1) - b)e^{\beta t_1} - (a\beta - b)\}}{\beta^2} \tag{11}$$

Now the total cost consists of following components:

1. Ordering cost = A (12)

2. Holding cost per cycle in RW

$$\begin{aligned}
 HC_{RW} &= F \int_0^{t_1} I_1(t) dt \\
 HC_{RW} &= \frac{F}{\beta^2} \left\{ \frac{1}{\beta} (\beta(a + bt_1) - b)(e^{\beta t_1} - 1) - t_1 \left(\beta \left(a + b \frac{t_1}{2} \right) - b \right) \right\}
 \end{aligned} \tag{13}$$

3. Holding cost per cycle in OW

$$\begin{aligned}
 HC_{OW} &= H \left\{ \int_0^{t_1} I_2(t) dt + \int_{t_1}^{t_2} I_3(t) dt \right\} \\
 HC_{OW} &= H \left\{ \frac{W}{\alpha} (1 - e^{-\alpha t_1}) + \frac{1}{\alpha^2} \left\{ \frac{1}{\alpha} (\alpha(a + bt_2) - b) (e^{\alpha(t_2-t_1)} - 1) \right. \right. \\
 &\quad \left. \left. - (t_2 - t_1) \left(\alpha \left(a + \frac{b}{2} (t_2 - t_1) \right) - b \right) \right\} \right\}
 \end{aligned} \tag{14}$$

4. Shortage cost per cycle

$$\begin{aligned}
 SC &= -C_s \int_{t_2}^T I_4(t) dt \\
 SC &= -C_s \left\{ \frac{a}{\sigma} \left(\frac{1}{\sigma} (1 - e^{-\sigma(T-t_2)}) - (T - t_2)e^{-\sigma(T-t_2)} \right) + \frac{b}{\sigma} \left(\frac{T}{\sigma} - \frac{t_2}{\sigma} e^{-\sigma(T-t_2)} - \frac{1}{\sigma^2} \right. \right. \\
 &\quad \left. \left. + \frac{e^{-\sigma(T-t_2)}}{\sigma^2} - t_2(T - t_2)e^{-\sigma(T-t_2)} \right) - \frac{b}{\sigma^2} \left(\frac{1}{\sigma} (1 - e^{-\sigma(T-t_2)}) - (T - t_2)e^{-\sigma(T-t_2)} \right) \right\} \tag{15}
 \end{aligned}$$

5. Opportunity cost due to lost sales per cycle

$$\begin{aligned}
 OP &= L \int_{t_2}^T (1 - B(T - t))(a + bt) dt = L \int_{t_2}^T (1 - e^{-\sigma(T-t)})(a + bt) dt \\
 OP &= L \left\{ a(T - t_2) + \frac{b}{2}(T^2 - t_2^2) - \frac{a}{\sigma} (1 - e^{-\sigma(T-t_2)}) - b \left(\frac{T - e^{-\sigma(T-t_2)}}{\sigma} - \frac{1 - e^{-\sigma(T-t_2)}}{\sigma^2} \right) \right\} \tag{16}
 \end{aligned}$$

6. Deterioration cost per cycle

$$\begin{aligned}
 DC &= C \left(\beta \int_0^{t_1} I_1(t) dt + \alpha \int_0^{t_1} I_2(t) dt + \alpha \int_{t_1}^{t_2} I_3(t) dt \right) \\
 DC &= C \left(\frac{1}{\beta} \left\{ \frac{1}{\beta} (\beta(a + bt_1) - b) (e^{\beta t_1} - 1) - t_1 \left(\beta \left(a + b \frac{t_1}{2} \right) - b \right) \right\} + W(1 - e^{-\alpha t_1}) \right. \\
 &\quad \left. + \frac{1}{\alpha^2} \left\{ \frac{1}{\alpha} (\alpha(a + bt_2) - b) (e^{\alpha(t_2-t_1)} - 1) \right\} \right. \\
 &\quad \left. - (t_2 - t_1) \left(\alpha \left(a + \frac{b}{2}(t_2 - t_1) \right) - b \right) \right\} \tag{17}
 \end{aligned}$$

Therefore total average cost per unit time is

$$\begin{aligned}
 TC(t_1, T) &= \frac{1}{T} [OC + HO_{RW} + HO_{OW} + SC + OP + DC] \\
 TC(t_1, T) &= \frac{1}{T} \left\{ A + \frac{(F + C\beta)}{\beta^2} \left\{ \frac{1}{\beta} (\beta(a + bt_1) - b) (e^{\beta t_1} - 1) - t_1 \left(\beta \left(a + b \frac{t_1}{2} \right) - b \right) \right\} \right. \\
 &\quad + (H + C\alpha) \left[\frac{W}{\alpha} (1 - e^{-\alpha t_1}) + \frac{1}{\alpha^2} \left\{ \frac{1}{\alpha} (\alpha(a + bt_2) - b) (e^{\alpha(t_2-t_1)} - 1) \right. \right. \\
 &\quad \left. \left. - (t_2 - t_1) \left(\alpha \left(a + \frac{b}{2} (t_2 - t_1) \right) - b \right) \right\} \right] - C_s \left(\left(\frac{a}{\sigma} \left(\frac{1}{\sigma} \right) \right. \right. \right. \\
 &\quad \left. \left. \times \left(1 - e^{-\sigma(T-t_2)} \right) - (T - t_2) e^{-\sigma(T-t_2)} \right) \right. \\
 &\quad \left. + \frac{b}{\sigma} \left(\frac{T}{\sigma} - \frac{t_2}{\sigma} e^{-\sigma(T-t_2)} - \frac{1}{\sigma^2} + \frac{e^{-\sigma(T-t_2)}}{\sigma^2} - t_2(T - t_2) e^{-\sigma(T-t_2)} \right) \right. \\
 &\quad \left. - \frac{b}{\sigma^2} \left(\frac{1}{\sigma} \left(1 - e^{-\sigma(T-t_2)} \right) - (T - t_2) e^{-\sigma(T-t_2)} \right) \right) \right) + L \left(a(T - t_2) + \frac{b}{2} (T^2 - t_2^2) \right. \\
 &\quad \left. - \frac{a}{\sigma} \left(1 - e^{-\sigma(T-t_2)} \right) - b \left(\frac{T - e^{-\sigma(T-t_2)}}{\sigma} - \frac{1 - e^{-\sigma(T-t_2)}}{\sigma^2} \right) \right) \left. \right\}
 \end{aligned}
 \tag{18}$$

Now, for minimizing the total average cost per unit time, the optimal values of t_1 and T (say t_1^* and T^*) can be obtained by solving the following equations simultaneously:

$$\frac{\partial TC(t_1, T)}{\partial t_1} = 0 \quad \text{and} \quad \frac{\partial TC(t_1, T)}{\partial T} = 0
 \tag{19}$$

which satisfies the conditions

$$\begin{aligned}
 \frac{\partial^2 TC(t_1, T)}{\partial t_1^2} > 0, \quad \frac{\partial^2 TC(t_1, T)}{\partial T^2} > 0 \quad \text{and} \quad \left(\frac{\partial^2 TC(t_1, T)}{\partial t_1^2} \right) \left(\frac{\partial^2 TC(t_1, T)}{\partial T^2} \right) \\
 - \left(\frac{\partial^2 TC(t_1, T)}{\partial t_1 \partial T} \right)^2 > 0
 \end{aligned}
 \tag{20}$$

3.2 Fuzzy Model

Due to uncertainty in the environment it is not easy to define all the parameters precisely, accordingly we assume some of these parameters namely \tilde{A} , \tilde{W} , \tilde{C} , \tilde{C}_s , \tilde{H} , \tilde{F} and \tilde{L} are taken as in fuzzy sense, which may change within some limits.

Let $\tilde{A} = (a_1, a_2, a_3)$, $\tilde{W} = (w_1, w_2, w_3)$, $\tilde{C} = (c_1, c_2, c_3)$, $\tilde{C}_s = (C_{S1}, C_{S2}, C_{S3})$, $\tilde{H} = (h_1, h_2, h_3)$, $\tilde{F} = (f_1, f_2, f_3)$ and $\tilde{L} = (l_1, l_2, l_3)$ are as triangular fuzzy numbers.

Total cost of the system per unit time in fuzzy sense is given by

$$\begin{aligned}
 \tilde{TC}(t_1, T) = & \frac{1}{T} \left\{ \tilde{A} + \frac{(\tilde{F} + \tilde{C}\beta)}{\beta^2} \left\{ \frac{1}{\beta} (\beta(a + bt_1) - b) (e^{\beta t_1} - 1) - t_1 \left(\beta \left(a + b \frac{t_1}{2} \right) - b \right) \right\} \right. \\
 & + (\tilde{H} + \tilde{C}\alpha) \left[\frac{\tilde{W}}{\alpha} (1 - e^{-\alpha t_1}) + \frac{1}{\alpha^2} \left\{ \frac{1}{\alpha} (\alpha(a + bt_2) - b) (e^{\alpha(t_2 - t_1)} - 1) \right. \right. \\
 & \left. \left. - (t_2 - t_1) \left(\alpha \left(a + \frac{b}{2} (t_2 - t_1) \right) - b \right) \right\} \right] \\
 & - \tilde{C}_s \left(\left(\frac{a}{\sigma} \cdot \left(\frac{1}{\sigma} \times (1 - e^{-\sigma(T-t_2)}) \right) - (T - t_2) e^{-\sigma(T-t_2)} \right) \right. \\
 & + \frac{b}{\sigma} \left(\frac{T}{\sigma} - \frac{t_2}{\sigma} e^{-\sigma(T-t_2)} - \frac{1}{\sigma^2} + \frac{e^{-\sigma(T-t_2)}}{\sigma^2} - t_2(T - t_2) e^{-\sigma(T-t_2)} \right) \\
 & \left. \left. - \frac{b}{\sigma^2} \left(\frac{1}{\sigma} (1 - e^{-\sigma(T-t_2)}) - (T - t_2) e^{-\sigma(T-t_2)} \right) \right) \right) \\
 & + \tilde{L} \left(a(T - t_2) + \frac{b}{2} (T^2 - t_2^2) - \frac{a}{\sigma} (1 - e^{-\sigma(T-t_2)}) \right. \\
 & \left. \left. - b \left(\frac{T - e^{-\sigma(T-t_2)}}{\sigma} - \frac{1 - e^{-\sigma(T-t_2)}}{\sigma^2} \right) \right) \right\} \tag{21}
 \end{aligned}$$

We defuzzify the fuzzy total cost $\tilde{TC}(t_1, T)$ by graded mean representation, which is given by

$$TC_{DGMRM}(t_1, T) = \frac{1}{6} [\tilde{TC}_1(t_1, T)(t_1, T) + 4\tilde{TC}_2(t_1, T) + \tilde{TC}_3(t_1, T)] \tag{22}$$

where,

$$\begin{aligned}
 \tilde{TC}_i(t_1, T) = & \frac{1}{T} \left\{ a_i + \frac{(f_i + c_i\beta)}{\beta^2} \left\{ \frac{1}{\beta} (\beta(a + bt_1) - b) (e^{\beta t_1} - 1) \right. \right. \\
 & \left. \left. - t_1 \left(\beta \left(a + b \frac{t_1}{2} \right) - b \right) \right\} \right. \\
 & + (h_i + c_i\alpha) \left[\frac{w_i}{\alpha} (1 - e^{-\alpha t_1}) + \frac{1}{\alpha^2} \left\{ \frac{1}{\alpha} (\alpha(a + bt_2) - b) (e^{\alpha(t_2 - t_1)} - 1) \right. \right. \\
 & \left. \left. - (t_2 - t_1) \left(\alpha \left(a + \frac{b}{2} (t_2 - t_1) \right) - b \right) \right\} \right] \\
 & - c_{s_i} \left(\left(\frac{a}{\sigma} \cdot \left(\frac{1}{\sigma} \times (1 - e^{-\sigma(T-t_2)}) \right) - (T - t_2) e^{-\sigma(T-t_2)} \right) \right. \\
 & + \frac{b}{\sigma} \left(\frac{T}{\sigma} - \frac{t_2}{\sigma} e^{-\sigma(T-t_2)} - \frac{1}{\sigma^2} + \frac{e^{-\sigma(T-t_2)}}{\sigma^2} - t_2(T - t_2) e^{-\sigma(T-t_2)} \right) \\
 & \left. \left. - \frac{b}{\sigma^2} \left(\frac{1}{\sigma} (1 - e^{-\sigma(T-t_2)}) - (T - t_2) e^{-\sigma(T-t_2)} \right) \right) \right) \\
 & + l_i \left(a(T - t_2) + \frac{b}{2} (T^2 - t_2^2) - \frac{a}{\sigma} (1 - e^{-\sigma(T-t_2)}) \right. \\
 & \left. \left. - b \left(\frac{T - e^{-\sigma(T-t_2)}}{\sigma} - \frac{1 - e^{-\sigma(T-t_2)}}{\sigma^2} \right) \right) \right\} \tag{23}
 \end{aligned}$$

where $i = 1, 2, 3$.

Now, for minimizing the fuzzy total average cost per unit time, the optimal values of t_1 and T (say t_1^* and T^*) can be obtained by solving the following equations simultaneously:

$$\frac{\partial TC_{DGMRM}(t_1, T)}{\partial t_1} = 0 \text{ and } \frac{\partial TC_{DGMRM}(t_1, T)}{\partial T} = 0 \tag{24}$$

which also satisfies the conditions

$$\begin{aligned} \frac{\partial^2 TC_{DGMRM}(t_1, T)}{\partial t_1^2} > 0, \frac{\partial^2 TC_{DGMRM}(t_1, T)}{\partial T^2} > 0 \text{ and } \frac{\partial^2 TC_{DGMRM}(t_1, T)}{\partial t_1^2} \frac{\partial^2 TC_{DGMRM}(t_1, T)}{\partial T^2} \\ - \left(\frac{\partial^2 TC_{DGMRM}(t_1, T)}{\partial t_1 \partial T} \right)^2 > 0 \end{aligned} \tag{25}$$

4 Numerical Example and Sensitivity Analysis

4.1 Example 1: For Crisp Model

To illustrate the model, we consider the following numerical values of the parameters from the previous studies in the appropriate units:

$W = 200$, $A = \text{Rs. } 150$ per order, $a = 50$ units per year, $b = 0.2$ units per year, $H = \text{Rs. } 10$ per unit per year, $F = \text{Rs. } 12$ per unit per year, $C = \text{Rs. } 20$ per unit, $C_s = \text{Rs. } 15$ per unit, $L = \text{Rs. } 18$ per unit, $\alpha = 0.05$, $\beta = 0.06$, $\sigma = 0.08$.

Applying the above solution procedure, by using the mathematical software **MATHEMATICA-8.0**, we get the following optimal values of $t_1 = 0.5729$ year, $T = 0.7241$ year and $TC = \text{Rs } 4670.6982$.

4.2 Example 2: For Fuzzy Model

To illustrate the model, we consider the following data in appropriate units:

$a = 50$ units per year, $b = 0.2$ units per year, $\alpha = 0.05$, $\beta = 0.06$, $\sigma = 0.08$,

$$\begin{aligned} \tilde{A} &= (142.5, 150, 157.5), \tilde{W} = (190, 200, 210), \tilde{C} = (19, 20, 21), \tilde{C}_s \\ &= (14.25, 15, 15.75), \\ \tilde{H} &= (9.5, 10, 10.5), \tilde{F} = (11.4, 12, 12.6) \text{ and } \tilde{L} = (17.1, 18, 18.9). \end{aligned}$$

Applying the above solution procedure, by using the mathematical software **MATHEMATICA-8.0**, we get the optimal values of $t_1 = 0.6129$ year, $T = 0.8124$ year and $TC_{DGMRM} = \text{Rs } 4714.7809$.

Table 1 Sensitivity analysis of various parameters

Parameters	% changes	t_1	T	TC	% change in TC
A	-20	0.3721	0.5031	3970.2260	-14.99
	-10	0.3727	0.5425	4170.6362	-10.70
	10	0.4724	0.5978	5670.4687	+21.41
	20	0.5720	0.6268	5870.7498	+25.69
W	-20	0.4729	0.4587	4670.0672	0
	-10	0.4829	0.5253	4700.5967	+0.64
	10	0.7929	0.8065	5270.8646	+12.09
	20	0.8929	0.9879	6170.5621	+32.02
H	-20	0.4525	0.5146	3170.6424	-32.03
	-10	0.5646	0.6758	3670.3478	-21.3
	10	0.7768	0.8931	6670.4634	+42
	20	0.8742	0.9246	7670.3426	+64
F	-20	0.2154	0.3223	2670.3282	-42.28
	-10	0.3965	0.4202	3070.6522	-34.25
	10	0.5532	0.5756	4670.1653	0
	20	0.5776	0.7235	6670.6451	+42
a	-20	0.4729	0.6854	3670.1782	-21.42
	-10	0.5710	0.7200	4178.1047	-10.54
	10	0.6729	0.8200	5600.5432	+19.04
	20	0.6780	0.8250	5700.7753	+22.05
b	-20	0.3629	0.6943	3670.7628	-21.04
	-10	0.4001	0.7002	4000.6782	-14.30
	10	0.6772	0.8345	6360.1653	+36.17
	20	0.7020	0.8504	6908.7821	+47.91
α	-20	0.4651	0.6286	4031.4879	-13.64
	-10	0.5125	0.6932	4376.6587	-6.23
	10	0.6308	0.7587	4856.7808	+3.9
	20	0.6823	0.7903	5189.6880	+11.11
β	-20	0.5134	0.6803	4100.8754	-12.11
	-10	0.5379	0.7068	4356.5879	-6.75
	10	0.5969	0.7486	4746.9701	+1.64
	20	0.6297	0.7843	4945.6709	+5.81

4.3 Sensitivity Analysis

In order to study how the parameters affect the optimal solution, the sensitivity analysis is carried out with respect to the various parameters. The result of the sensitivity analysis are given in the Table 1.

From sensitivity Table 1 the following inferences are drawn:

1. From Table 1, it is observed that as ordering cost 'A' increases then t_1 , T and total cost 'TC' increase.
2. t_1 , T and total cost 'TC' increase with an increases in capacity of own warehouse.

3. On seeing the above table, t_1 , T and total cost 'TC' increase with an increases in holding cost of own warehouse as well as rented warehouse. But, percentage change in total cost in own warehouse is more than rented warehouse.
4. As demand parameters 'a' and 'b' increases then t_1 , T and total cost 'TC' increases but percentage change in total cost 'TC' with respect to negative change is equal for both the parameters whereas with respect to positive change in b is more than a.
5. On increases the deterioration rate ' α ' and ' β ' for both the warehouses then t_1 , T and total cost 'TC' increases.

5 Conclusions

This paper presents a two-warehouse fuzzy inventory model for deteriorating items in which demand is an increasing function of time. This paper is including two types of model one is crisp model and the second is fuzzy model. In crisp model, the capacity of own warehouse, deterioration rate, inventory holding cost, unit cost and shortage cost are represented by a real numbers where as in fuzzy model these are represented by triangular fuzzy numbers. The graded mean method is employed to evaluate the optimal time period of positive stock t_1 and total cycle length T which minimizes the total cost. By numerical examples the model is illustrated in a well manner. A sensitivity analysis is also conducted on the different parameters. A future study would be to extend the proposed model for finite replenishment rate, stock outs, which are partially backlogged, price dependent demand, stock dependent demand and many more.

References

1. Zadeh, L.A.: Fuzzy sets. *Inf. Control* **8**(3), 338–353 (1965)
2. Park, K.: Fuzzy-set theoretic interpretation of economic order quantity. In: *IEEE Transactions on Systems, Man, and Cybernetics SMC-17*, pp. 1082–1084 (1987)
3. Vujosevic, M., Petrovic, D., Petrovic, R.: EOQ formula when inventory cost is fuzzy. *Int. J. Prod. Econ.* **45**, 499–504 (1996)
4. Lee, H.M., Yao, J.S.: Economic order quantity in fuzzy sense for inventory without backorder model. *Fuzzy Sets Syst.* **105**, 13–31 (1999)
5. Dutta, P., Chakraborty, D., Roy, A.R.: A single-period inventory model with fuzzy random variable demand. *Math. Comput. Model.* **41**(8–9), 915–922 (2005)
6. Roy, A., Samanta, G.P.: Fuzzy continuous review inventory model without backorder for deteriorating items. *Electron. J. Appl. Stat. Anal.* **2**(1), 58–66 (2009)
7. Singh, S.R., Jain, S., Pareek, S.: A warehouse imperfect fuzzified production model with shortages under inflationary conditions. *Adv. Decis. Sci.* **12**, 1–16 (2013)
8. Singh, S.R., Kumar, N., Kumari, R.: Two-warehouse fuzzy inventory model under the conditions of permissible delay in payments. *Int. J. Oper. Res.* **11**(1), 78–99 (2011)

9. Hartely, V.R.: *Operations Research—A Managerial Emphasis*, pp. 315–317. Good Year, Santa Monica (1976)
10. Murdeshwar, T.M., Sathe, Y.S.: Some aspects of lot size models with two levels of storage. *Opsearch* **22**, 255–262 (1985)
11. Goswami, A., Chaudhuri, K.S.: An economic order quantity model for items with two levels of storage for a linear trend in demand. *J. Oper. Res. Soc.* **43**, 157–167 (1992)
12. Bhunia, A.K., Maity, M.: A two-warehouse inventory model for deteriorating items with linear trend in demand and shortages. *J. Oper. Res. Soc.* **49**, 287–292 (1998)
13. Yang, H.L.: A two-warehouse inventory models for deteriorating items with shortages under inflation. *Eur. J. Oper. Res.* **157**, 344–356 (2004)
14. Yang, H.L.: Two-warehouse partial backlogging inventory models for deteriorating items under inflation. *Int. J. Prod. Econ.* **103**(1), 362–370 (2006)
15. Sett, B.K., Sarkar, B., Goswami, A.: A two-warehouse inventory model with increasing demand and time varying deterioration. *Scientia Iranica* **19**, 1969–1977 (2012)
16. Ghare, P.M., Schrader, G.P.: A model for exponentially decaying inventory. *J. Ind. Eng.* **14**, 228–243 (1963)
17. Aggarwal, S.P.: A note on an order level inventory model for a system with constant rate of deterioration. *Opsearch* **15**, 184–187 (1978)
18. Dutta, T.K., Pal, A.K.: A note on an inventory model with inventory—level—dependent demand rate. *J. Oper. Res. Soc.* **41**, 971–975 (1990)
19. Mandal, B.N., Phaujdar, S.: An inventory model for deteriorating items and stock dependent consumption rate. *J. Oper. Res. Soc.* **40**, 483–488 (1989)
20. Balkhi, Z.T.: On a finite horizon production lot size inventory model for deteriorating items: an optimal solution. *Eur. J. Oper. Res.* **132**, 210–223 (2001)
21. Panda, S., Saha, S., Basu, M.: An EOQ model with generalized ramp-type demand and Weibull distribution deterioration. *Asia Pac. J. Oper. Res.* **24**, 1–17 (2007)
22. Sana, S.S.: Demand influenced by enterprises' initiatives—a multi-item EOQ model of deteriorating and ameliorating items. *Math. Comput. Model.* **52**, 284–302 (2010)
23. Sarkar, B., Sarkar, S.: An improved inventory model with partial backlogging, time varying deterioration and stock-dependent demand. *Econ. Model.* **30**, 924–932 (2013)

Fuzzy Optimal Solution of Interval-Valued Fuzzy Transportation Problems

Deepika Rani and T. R. Gulati

Abstract There are several methods to solve the unbalanced fully fuzzy transportation problems in which the total availability is less than the total demand. In these methods a dummy source, is added to balance the problem. As this added dummy source does not exist actually, it is not genuine to apply existing methods to get real life solutions. So, in this paper a method is proposed to solve such unbalanced transportation problems and the obtained fuzzy optimal solution is in terms of original sources only. By applying the proposed method, we can get the information that the availability of which original source should actually be increased so that the total fuzzy demand is met and the total fuzzy transportation cost is minimum.

Keywords Interval-valued fuzzy numbers · Fully fuzzy transportation problem · Fuzzy optimal solution

1 Introduction

In global economics, the supply chain management is becoming increasingly important day by day. So, the knowledge of the transportation system is fundamental to the efficient and economical operation of a company. Transportation model plays an important role in supply chain management for reducing cost and improving services. Appa [1] discussed several variations of the transportation problem.

D. Rani (✉) · T. R. Gulati
Department of Mathematics, Indian Institute of Technology Roorkee, Roorkee,
247667, India
e-mail: deepikaitroorkee@gmail.com

T. R. Gulati
e-mail: trgulati@gmail.com

There exist effective algorithms [2] for the basic transportation problem [3] which assumes that the parameters of the problem are exactly known. However, there may be some situations when the parameters are not known in a precise manner. A frequently used way to express the imprecision are fuzzy numbers proposed by Zadeh [4]. Use of fuzzy numbers to represent the imprecision in parameters enriches and enhances the suggested solution methodologies. It enlarges the range of applications of linear programming. Several techniques [5–9] have been proposed to solve the transportation problem in fuzzy environment.

In this paper, a method is proposed to obtain the fuzzy optimal solution in terms of the original sources and destinations only keeping the total transportation cost minimum. Here, we use (λ, ρ) interval-valued fuzzy numbers to represent the fuzziness in parameters. The signed distance ranking is used to defuzzify the problem.

This paper is organised as follows. Basic definitions, arithmetic operations and comparison of interval-valued fuzzy numbers are contained in Sect. 2. In Sect. 3, fully fuzzy transportation problem is formulated using (λ, ρ) interval-valued fuzzy numbers. Algorithm for obtaining fuzzy optimal solution is proposed in Sect. 4. A numerical example is solved in Sect. 5.

2 Preliminaries [10, 11]

2.1 Basic Definitions

Definition 1. If the membership function of the fuzzy set \tilde{b}_α on $\mathbb{R} = (-\infty, \infty)$ is

$$\mu_{\tilde{b}_\alpha}(x) = \begin{cases} \alpha, & \text{if } x = b \\ 0, & \text{if } x \neq b \end{cases}$$

then \tilde{b}_α is called a level α fuzzy point.

Definition 2. If the membership function of the fuzzy set \tilde{A} on \mathbb{R} is given by

$$\mu_{\tilde{A}}(x) = \begin{cases} \frac{\lambda(x-l)}{(m-l)}, & \text{if } l \leq x \leq m \\ \frac{\lambda(n-x)}{(n-m)}, & \text{if } m \leq x \leq n, \quad l \leq m \leq n \\ 0 & \text{otherwise} \end{cases}$$

then \tilde{A} is called a level λ fuzzy number, $0 < \lambda \leq 1$ and is denoted by $\tilde{A} = (l, m, n; \lambda)$.

Definition 3. If the membership function of the fuzzy set $[b_\alpha, c_\alpha]$ on \mathbb{R} is

$$\mu_{[b_\alpha, c_\alpha]}(x) = \begin{cases} \alpha, & \text{if } b \leq x \leq c, \quad b \leq c \\ 0, & \text{otherwise} \end{cases}$$

then $[b_x, c_x]$ is called a level α fuzzy interval, $0 < \alpha \leq 1$.

Definition 4. An interval-valued fuzzy set (*i-v* fuzzy set) \tilde{A} on \mathbb{R} is given by $\tilde{A} = \{x, [\mu_{\tilde{A}^L}, \mu_{\tilde{A}^U}]\}, x \in \mathbb{R}, \mu_{\tilde{A}^L}(x), \mu_{\tilde{A}^U}(x) \in [0, 1], \mu_{\tilde{A}^L}(x) \leq \mu_{\tilde{A}^U}(x), \forall x \in \mathbb{R}$ and is denoted by $\tilde{A} = [\tilde{A}^L, \tilde{A}^U]$.

If $\mu_{\tilde{A}^L}(x)$ and $\mu_{\tilde{A}^U}(x)$ are according to Definition 2 as follows:

$$\mu_{\tilde{A}^L}(x) = \begin{cases} \frac{\lambda(x-l)}{(m-l)}, & \text{if } l \leq x \leq m \\ \frac{\lambda(n-x)}{(n-m)}, & \text{if } m \leq x \leq n, l < m < n \\ 0 & \text{otherwise} \end{cases}$$

and

$$\mu_{\tilde{A}^U}(x) = \begin{cases} \frac{\lambda(x-p)}{(m-p)}, & \text{if } p \leq x \leq m \\ \frac{\lambda(r-x)}{(r-m)}, & \text{if } m \leq x \leq r, p < m < r \\ 0 & \text{otherwise} \end{cases}$$

then $\tilde{A} = [\tilde{A}^L, \tilde{A}^U] = [(l, m, n; \lambda), (p, m, r; \rho)]$, where $0 < \lambda \leq \rho \leq 1, p < l < m < n < r$ and is called level (λ, ρ) interval-valued fuzzy number.

Let $F_{IV}(\lambda, \rho) = [(l, m, n; \lambda), (p, m, r; \rho)] \quad \forall p < l < m < n < r, 0 < \lambda \leq \rho \leq 1$.

Let $\tilde{A} = [(l_1, m_1, n_1; \lambda), (p_1, m_1, r_1; \rho)], \tilde{B} = [(l_2, m_2, n_2; \lambda), (p_2, m_2, r_2; \rho)] \in F_{IV}(\lambda, \rho)$.

2.2 Arithmetic Operations

- (i) $\tilde{A} \oplus \tilde{B} = [(l_1 + l_2, m_1 + m_2, n_1 + n_2; \lambda), (p_1 + p_2, m_1 + m_2, r_1 + r_2; \rho)]$
- (ii) $\tilde{A} \ominus \tilde{B} = [(l_1 - n_2, m_1 - m_2, n_1 - l_2; \lambda), (p_1 - r_2, m_1 - m_2, r_1 - p_2; \rho)]$
- (iii) $k\tilde{A} = \begin{cases} [(kl_1, km_1, kn_1; \lambda), (kp_1, km_1, kr_1; \rho)] & \text{if } k > 0 \\ [(kn_1, km_1, kl_1; \lambda), (kr_1, km_1, kp_1; \rho)] & \text{if } k < 0 \\ [(0, 0, 0; \lambda), (0, 0, 0; \rho)] & \text{if } k = 0 \end{cases}$

2.3 Comparison of Interval Valued Fuzzy Numbers

- (i) $\tilde{A} \succ \tilde{B}$ if $d(\tilde{A}, \tilde{0}) > d(\tilde{B}, \tilde{0})$
- (ii) $\tilde{A} \succcurlyeq \tilde{B}$ if $d(\tilde{A}, \tilde{0}) \geq d(\tilde{B}, \tilde{0})$
- (iii) $\tilde{A} \approx \tilde{B}$ if $d(\tilde{A}, \tilde{0}) = d(\tilde{B}, \tilde{0})$

where $d(\tilde{A}, \tilde{0}) = \frac{1}{8}[6m_1 + l_1 + n_1 + 4p_1 + 4r_1 + 3(2m_1 - p_1 - r_1)\frac{\delta}{\rho}]$ is called the signed distance of \tilde{A} from $\tilde{0}$. The signed distance has same order properties as those of real numbers, so this has been preferred for defuzzification of the fuzzy numbers in this paper.

If the interval-valued fuzzy number \tilde{A} is such that $d(\tilde{A}, \tilde{0}) = 0$, then it is called zero interval-valued fuzzy number and is denoted as $\tilde{A} \approx \tilde{0}$.

3 Problem Formulation

An unbalanced interval-valued fully fuzzy transportation problem having m sources and n destinations can be formulated as follows:

$$\begin{aligned} &\text{Minimize } \sum_{i=1}^m \sum_{j=1}^n (\tilde{c}_{ij} \otimes \tilde{x}_{ij}), \\ &\text{Subject to} \\ &\sum_{j=1}^n \tilde{x}_{ij} \succcurlyeq \tilde{a}_i \quad (1 \leq i \leq m), \\ &\sum_{i=1}^m \tilde{x}_{ij} \preccurlyeq \tilde{b}_j \quad (1 \leq j \leq n), \\ &\tilde{x}_{ij} \succcurlyeq \tilde{0}, \\ &\sum_{i=1}^m \tilde{a}_i \prec \sum_{j=1}^n \tilde{b}_j \end{aligned} \tag{P1}$$

where \tilde{a}_i : the fuzzy availability of the product at i th source S_i ,
 \tilde{b}_j : the fuzzy demand of the product at j th destination D_j ,
 \tilde{c}_{ij} : the fuzzy cost for transporting one unit of the product from S_i to D_j ,
 \tilde{x}_{ij} : the fuzzy quantity of the product to be transported from S_i to D_j ,
 and $\tilde{a}_i, \tilde{b}_j, \tilde{c}_{ij}, \tilde{x}_{ij}$ are all interval-valued fuzzy numbers.

4 Proposed Algorithm

A method to solve the problem (P_1) is proposed in this section. To do so, we first prove the following result.

Theorem 1 *Let (P_2) be the fuzzy linear formulation of balanced interval-valued FFTP obtained by adding a dummy source S_{m+1} to (P_1) with unit fuzzy transportation costs $\tilde{c}_{(m+1)j} = \min_{1 \leq i \leq m} (\tilde{c}_{ij}), 1 \leq j \leq n$. Also, let (\tilde{u}, \tilde{v}) and (\tilde{u}', \tilde{v}') be the optimal solutions of the duals of (P_1) and (P_2) , respectively, where*

$(\tilde{u}, \tilde{v}) = (\tilde{u}_1, \tilde{u}_2, \dots, \tilde{u}_m, \tilde{v}_1, \tilde{v}_2, \dots, \tilde{v}_n)$. Then $\tilde{u}_i = \tilde{u}'_i, 1 \leq i \leq m$ and $\tilde{v}_j = \tilde{v}'_j, 1 \leq j \leq n$ provided $\tilde{u}'_{m+1} = \tilde{0}$.

Proof The problem (P_2) is:

$$\begin{aligned} \text{Minimize } & \sum_{i=1}^{m+1} \sum_{j=1}^n (\tilde{c}_{ij} \otimes \tilde{x}_{ij}), \text{ subject to} \\ & \sum_{j=1}^n \tilde{x}_{ij} \approx \tilde{a}_i (1 \leq i \leq m+1), \quad \sum_{i=1}^m \tilde{x}_{ij} \approx \tilde{b}_j (1 \leq j \leq n), \tilde{x}_{ij} \succcurlyeq \tilde{0}, \\ & \text{where } \tilde{a}_{m+1} = \sum_{j=1}^n \tilde{b}_j \ominus \sum_{i=1}^m \tilde{a}_i. \end{aligned}$$

Since (\tilde{u}, \tilde{v}) is the optimal solution of the dual of (P_1) , so

$$\tilde{u}_i \oplus \tilde{v}_j \preccurlyeq \tilde{c}_{ij}, \forall 1 \leq i \leq m, 1 \leq j \leq n \text{ and } \tilde{u}_i \succcurlyeq \tilde{0}, \forall 1 \leq i \leq m.$$

To show that (\tilde{u}', \tilde{v}') is also an optimal solution of the dual of (P_1) , it is sufficient to show that

- (i) $\tilde{u}'_i \oplus \tilde{v}'_j \preccurlyeq \tilde{c}_{ij}, \forall 1 \leq i \leq m, 1 \leq j \leq n$ and
- (ii) $\tilde{u}'_i \succcurlyeq \tilde{0}, \forall 1 \leq i \leq m.$

(i) Since (\tilde{u}', \tilde{v}') is the optimal solution of the dual to problem (P_2) , so

$$\tilde{u}'_i \oplus \tilde{v}'_j \preccurlyeq \tilde{c}_{ij}, \forall 1 \leq i \leq m+1, 1 \leq j \leq n$$

Therefore $\tilde{u}'_i \oplus \tilde{v}'_j \preccurlyeq \tilde{c}_{ij}, \forall 1 \leq i \leq m, 1 \leq j \leq n.$

(ii) In particular for $i = m + 1$, for all j , $\tilde{u}'_{m+1} \oplus \tilde{v}'_j \preccurlyeq \tilde{c}_{(m+1)j}$, which implies

$$\tilde{v}'_j \preccurlyeq \tilde{c}_{(m+1)j} \text{ (since } \tilde{u}'_{m+1} = \tilde{0}) \Rightarrow \tilde{v}'_j \preccurlyeq \tilde{c}_{ij} \text{ for all } i \text{ (since } \tilde{c}_{(m+1)j} = \min_{1 \leq i \leq m} (\tilde{c}_{ij}))$$

$$\Rightarrow \tilde{c}_{ij} \ominus \tilde{v}'_j \succcurlyeq \tilde{0}$$

$\Rightarrow \tilde{u}'_i \succcurlyeq \tilde{0}$ (since corresponding to each \tilde{v}'_j , there exist \tilde{u}'_i such that $\tilde{u}'_i \oplus \tilde{v}'_j = \tilde{c}_{ij}$).

The steps of the proposed method are as follows:

Step 1: Find the fuzzy optimal solution of the unbalanced interval-valued FFTP (P_1) by fuzzy vogel approximation method using the fuzzy transportation costs $\tilde{c}_{(m+1)j} = \min_{1 \leq i \leq m} (\tilde{c}_{ij})$ from the dummy source to all the destinations. Because the

excess demand has to be transported, the relative costs associated with transporting more than \tilde{a}_i from different sources will tell which source should supply excess demand.

Let $\tilde{x}_{ij}, \forall 1 \leq i \leq m + 1, 1 \leq j \leq n$ be the obtained fuzzy optimal solution.

Step 2: Assuming $\tilde{u}'_{(m+1)} = [(0, 0, 0; \lambda), (0, 0, 0; \rho)]$ (the signed distance of the fuzzy dual variable corresponding to dummy source in the balanced interval-valued FFTP (P_2) equal to 0), find the dual variables for the fuzzy optimal solution obtained in Step 1.

Step 3: Now by Theorem 4, the dual solution of FFTP (P_1) is same as that of FFTP (P_2). To find the fuzzy optimal solution in terms of original sources only with the help of fuzzy optimal solution obtained in Step 1, find the dual variables $\tilde{u}_i, 1 \leq i \leq m$ such that $\tilde{u}_i \approx \tilde{0}$ (because availability of only these sources can be increased [12]).

Step 4: Let $\tilde{x}_{(m+1)p}$ be the fuzzy basic variable. Following two cases arise:

Case 1: If i , such that the dual variable $\tilde{u}_i \approx \tilde{0}$ is unique (say r), then increase the value of the cell (r,p) in the fuzzy optimal solution obtained in Step 1 by $\tilde{x}_{(m+1)p}$.

Case 2: If i , such that the dual variable $\tilde{u}_i \approx \tilde{0}$ is not unique, then increase the value of the cell having least fuzzy transportation cost in column p by $\tilde{x}_{(m+1)p}$. This cell may or may not be a basic cell in the optimal solution obtained in Step 1.

If there is a tie in the least cost cells, then any one of these cells may be selected to increase the value of the corresponding variable.

5 Numerical Example

By using the methods proposed in the literature for obtaining fuzzy optimal solution for fuzzy transportation problems with total availability less than total demand, it is not possible to find that the availability of which source should be increased to accomplish the total demand. This information can be obtained by using the proposed method and we show the same by solving the following example:

Consider the fully fuzzy transportation problem with 3 sources and 3 destinations. Transportation costs, supply and demand coefficients are interval-valued fuzzy numbers as shown in Table 1.

We find that the problem is not balanced since the total fuzzy availability is $[(30, 38, 42; 0.9), (25, 38, 50; 1)]$ and the total fuzzy demand is $[(41, 45, 50; 0.9), (35, 45, 53; 1)]$.

According to Step 1 of the proposed method balance the interval-valued FFTP by introducing a dummy source S_4 with fuzzy availability equal to $[(41, 45, 50; 0.9)(35, 45, 53; 1)] \ominus [(30, 38, 42; 0.9), (25, 38, 50; 1)] = [(-1, 7, 20; 0.9)(-15, 7, 28; 1)]$ and unit fuzzy transportation costs as shown in Table 2.

Table 1 Intial data (Transportation cost, supply, demand)

Destinations → Sources ↓	D_1	D_2	D_3	Fuzzy availability
S_1	[(3, 6, 9; 0.9), (1, 6, 10; 1)]	[(3, 4, 7; 0.9), (1, 4, 9; 1)]	[(3, 6, 9; 0.9), (1, 6, 10; 1)]	[(17, 20, 21; 0.9), (16, 20, 24; 1)]
S_2	[(4, 8, 10; 0.9), (2, 8, 14; 1)]	[(2, 3, 7; 0.9), (1, 3, 8; 1)]	[(3, 5, 7; 0.9), (1, 5, 8; 1)]	[(9, 10, 11; 0.9), (7, 10, 12; 1)]
S_3	[(8, 9, 10; 0.9), (7, 9, 11; 1)]	[(3, 5, 7; 0.9), (1, 5, 8; 1)]	[(2, 3, 7; 0.9), (1, 3, 8; 1)]	[(4, 8, 10; 0.9), (2, 8, 14; 1)]
Fuzzy demand	[(10, 12, 15; 0.9), (8, 12, 16; 1)]	[(22, 23, 24; 0.9), (20, 23, 25; 1)]	[(9, 10, 11; 0.9), (7, 10, 12; 1)]	

Table 2 Balanced interval-valued FFTP

Destinations → Sources ↓	D_1	D_2	D_3	Fuzzy availability
S_1	[(3, 6, 9; 0.9), (1, 6, 10; 1)]	[(3, 4, 7; 0.9), (1, 4, 9; 1)]	[(3, 6, 9; 0.9), (1, 6, 10; 1)]	[(17, 20, 21; 0.9), (16, 20, 24; 1)]
S_2	[(4, 8, 10; 0.9), (2, 8, 14; 1)]	[(2, 3, 7; 0.9), (1, 3, 8; 1)]	[(3, 5, 7; 0.9), (1, 5, 8; 1)]	[(9, 10, 11; 0.9), (7, 10, 12; 1)]
S_3	[(8, 9, 10; 0.9), (7, 9, 11; 1)]	[(3, 5, 7; 0.9), (1, 5, 8; 1)]	[(2, 3, 7; 0.9), (1, 3, 8; 1)]	[(4, 8, 10; 0.9), (2, 8, 14; 1)]
S_4	[(3, 6, 9; 0.9), (1, 6, 10; 1)]	[(2, 3, 7; 0.9), (1, 3, 8; 1)]	[(2, 3, 7; 0.9), (1, 3, 8; 1)]	[(−1, 7, 20; 0.9), (−15, 7, 28; 1)]
Fuzzy demand	[(10, 12, 15; 0.9), (8, 12, 16; 1)]	[(22, 23, 24; 0.9), (20, 23, 25; 1)]	[(9, 10, 11; 0.9), (7, 10, 12; 1)]	

Now, using the fuzzy Vogel’s approximation method to the balanced interval-valued FFTP represented by Table 2, the following fuzzy optimal solution is found:

$$\tilde{x}_{11} = [(10, 12, 15; 0.9), (8, 12, 16; 1)], \tilde{x}_{12} = [(-10, 8, 23; 0.9), (-27, 8, 43; 1)], \tilde{x}_{22} = [(9, 10, 11; 0.9), (7, 10, 12; 1)], \tilde{x}_{33} = [(4, 8, 10; 0.9), (2, 8, 14; 1)], \tilde{x}_{42} = [(-8, 5, 21; 0.9), (-25, 5, 35; 1)], \tilde{x}_{43} = [(-1, 2, 7; 0.9), (-7, 2, 10; 1)].$$

Assuming $\tilde{u}'_4 = [(0, 0, 0; 0.9), (0, 0, 0; 1)]$, find the values of all the dual variables corresponding to the obtained fuzzy optimal solution and by Step 3 of the proposed method the values for the dual variables $\tilde{u}_i, 1 \leq i \leq 3$ and $\tilde{v}_j, 1 \leq j \leq 3$ are:

$$\tilde{u}_1 = [(-17, 5, 21; 0.9), (-35, 5, 42; 1)], \tilde{u}_2 = [(-5, 0, 5; 0.9), (-7, 0, 7; 1)], \tilde{u}_3 = [(-5, 0, 5; 0.9), (-7, 0, 7; 1)], \tilde{v}_1 = [(-11, 7, 32; 0.9), (-34, 7, 51; 1)], \tilde{v}_2 = [(2, 3, 7; 0.9), (1, 3, 8; 1)], and \tilde{v}_3 = [(2, 3, 7; 0.9), (1, 3, 8; 1)].$$

From these values we find that $d(\tilde{u}_2, \tilde{0}) = d(\tilde{u}_3, \tilde{0}) = 0$. So, the availability of S_2 and S_3 should be increased.

By using Step 4 of the proposed method, the fuzzy optimal solution is found to be:

$$\begin{aligned} \tilde{x}_{11} &= [(10, 12, 15; 0.9), (8, 12, 16; 1)], \tilde{x}_{12} = [(-10, 8, 23; 0.9), (-27, 8, 43; 1)], \\ \tilde{x}_{22} &= [(9, 10, 11; 0.9), (7, 10, 12; 1)] \oplus [(-8, 5, 21; 0.9), (-25, 5, 35; 1)] = [(1, 15, 32; 0.9), (-18, 15, 47; 1)] \\ \text{and } \tilde{x}_{33} &= [(4, 8, 10; 0.9), (2, 8, 14; 1)] \oplus [(-1, 2, 7; 0.9), (-7, 2, 10; 1)] = [(3, 10, 17; 0.9), (-5, 10, 24; 1)]. \end{aligned}$$

Acknowledgments The first author thanks CSIR, Government of India for providing financial support.

References

1. Appa, G.M.: The transportation problem and its variants. *Oper. Res. Q.* **24**, 79–99 (1973)
2. Taha, H.A.: *Operations Research: An Introduction*, 8th edn. Prentice-Hall, New Jersey (2007)
3. Hitchcock, F.L.: The distribution of a product from several sources to numerous localities. *J. Math. Phys.* **20**, 224–230 (1941)
4. Zadeh, L.A.: Fuzzy Sets. *Inf. Control* **8**, 338–353 (1965)
5. Basirzadeh, H.: An approach for solving fuzzy transportation problem. *Appl. Math. Sci.* **5**, 1549–1566 (2011)
6. Chiang, J.: The optimal solution of the transportation problem with fuzzy demand and fuzzy product. *J. Inf. Sci. Eng.* **21**, 439–451 (2005)
7. Dinagar, D.S., Palanivel, K.: The transportation problem in fuzzy environment. *Int. J. Algorithms Comput. Math.* **2**, 65–71 (2009)
8. Gupta, P., Mehlawat, M.K.: An algorithm for a fuzzy transportation problem to select a new type of coal for a steel manufacturing unit. *TOP* **15**, 114–137 (2007)
9. Pandian, P., Natrajan, G.: A new algorithm for finding a fuzzy optimal solution for fuzzy transportation problems. *Appl. Math. Sci.* **4**, 79–90 (2010)
10. Chiang, J.: Fuzzy linear programming based on statistical confidence interval and interval-valued fuzzy set. *Eur. J. Oper. Res.* **129**, 65–86 (2001)
11. Yao, J.S., Wu, K.: Ranking fuzzy numbers based on decomposition principle and signed distance. *Fuzzy Sets Syst.* **116**, 275–288 (2000)
12. Ebrahimnejad, A., Nasserri, S.H.: Using complementary slackness property to solve linear programming with fuzzy parameters. *Fuzzy Inf. Eng.* **3**, 233–245 (2009)

Comparative Study for Brain Tumor Classification on MR/CT Images

Ankit Vidyarthi and Namita Mittal

Abstract The objective of this study is to find out the algorithms and approaches that have been used for the classification of multiclass brain tumors as specified by the World Health Organization (WHO) in Computed Tomography (CT) or Magnetic Resonance (MR) images. From the past several years lot of researchers focused in current domain and came up with new ideas and facts for proper diagnosis of the tumor cells. The accuracy results of their study give the implication of how well their ideas was found to give more accurate results of classifying tumors type into their correct classes. In this whole study, focus was made on supervised classification approaches on 2D MRI or CT images of multi class brain tumors. This paper gives the comparative study of various approaches that was used to identify the tumor cells with correct class labels.

Keywords Brain tumor classification · Magnetic resonance imaging · Computed tomography

1 Introduction

An uncontrolled growth of cells inside a human body is termed as tumor. Tumor forms a group of solid mass of lesions'. There is not a specific position of the initiation and growth of a tumor thus it can affect any part of the human body. Human brain is the most sensitive part of the body. The brain is the center of thoughts, emotions, memory and speech. It control muscle movements and

A. Vidyarthi (✉) · N. Mittal
Malaviya National Institute of Technology, Jaipur, India
e-mail: ankit.09303022@gmail.com

N. Mittal
e-mail: mittalnamita@gmail.com

Table 1 Performance evaluation

Metric	Equation
Precision	$\frac{TP}{TP+FP}$
Recall	$\frac{TP}{TP+FN}$
Accuracy	$\frac{TP+TN}{TP+TN+FP+FN}$

interpretation of sensory information like sight, sound, touch, taste, pain etc. when such form of abnormality is formed inside brain is known as brain tumor. Brain tumor can be categorized into benign and malignant. Benign brain tumors are the primary tumors that have no cancer cells while the malignant tumors have cancer cells that grow rapidly inside the body [1].

On the basis of malignancy of tumor World Health Organization (WHO) categorized it into four groups or grades [2, 3]. Stage 1 of brain cancer is the least serious and the easiest to treat. Some cells still resemble normal cells, and the growth is slow. The cells have not yet invaded the surrounding tissue in stage 1. The whole tumor is usually able to be removed. In Stage 2, the tumor is larger. It has usually spread to the surrounding tissue. It is still treatable with surgery. During stage 3, the tumor is more aggressive, and the growth of the tumor is apparent. Cancer cells now look different from normal cells. Surrounding tissue is infected, and chemotherapy is the treatment used. Stage 4 is difficult to treat, but luckily not impossible [4].

In the past, many researchers [5, 6] from various domains like medical science, neuroscience, and computer science came in front to classify this life threaten disease in its early stage only. The classification or discrimination between benign and malignant tumor is necessary to identify that which type of tumor really suffered by patients. Whenever there is an abnormal growth of tissues that starts from the brain and doesn't spread to another parts of the body, is termed as a primary brain tumor. This tumor can be further categorized into benign and malignant (Table 1).

A benign brain tumor grows slowly, has distinct boundaries and spreads rarely. While a malignant brain tumor grows quickly and spreads to nearby brain areas. These have irregular boundaries but don't spread to organs outside the brain that's why they are also known as brain cancers [7].

Secondary brain tumors, also called Metastatic, begin as a cancer in any part of the body and spread to the brain when cancer cells are carried in blood stream to the brain. Since the brain is enclosed completely within the skull, the cells haven't got the area to expand. Thus whenever a tumor forms inside the brain it compresses and displaces normal brain tissues [8].

The predictable methods which are present in diagnosis includes Computed Tomography (CT) scan, Magnetic Resonance Imaging (MRI) scan, Positron Emission Tomography (PET) scan, Biopsy, Spinal Tap etc. [9]. Imaging tests are

used to help pinpoint where exactly the brain tumor is located. CT scan is a safe, non-disturbing test that uses an X-ray beam and a computer to make 2D image of the brain. On the other hand, MRI scan is a non-disturbing test that uses a magnetic field and radio frequency waves to give a detailed view of the soft tissues of the brain [10, 11]. A biopsy is used to identify the type of brain tumor. It is a procedure to remove a small amount of tumor to be examined by a pathologist under a microscope. A spinal tap is used so that spinal fluid can be taken and examined for cancer cells [11].

The rest of this paper is organized as follows: Section 2 discusses about the previous literature survey. Section 3, describes the overall contribution of the researchers with their methodology and classification accuracy. Section 4, gives the conclusion of the paper.

2 Related Work

From the past several Years, significant efforts on differentiating brain neoplasm have been made by incorporating MR/CT imaging features into pattern classification frameworks using machine learning approaches.

In [12], authors proposed mix technique consists of a combination of ANN and KNN as a classifier. The proposed work follows three steps, feature extraction using Discrete Wavelet Transformation (DWT), feature selection using PCA and proposed classifier ANN + KNN. The dataset contains total of 275 MR images of 256×256 pixels size. Dataset are categorized into normal (94) and abnormal (181) brain MR images. There are nearly 278 textures, shape features are extracted using GLCM. These features are being fed into neural network classifier and KNN classifier separately. The final class label has provided by the majority voting of the two classifiers. The proposed hybrid classifier approach gives good overall results.

Authors [13], proposed a new indexing based approach called Feature Database Tree (KD-Tree) for faster retrieval of the result in CBIR system. Total 82 images were used, out of those, 42 were of normal images and 40 were malignant ones. This dataset was processed by 10 folds randomly. In each fold, wavelet transformation [14] and modified fuzzy c-means algorithms [15] are used for image segmentation. The segmented tumor portion was processed for feature extraction using Gray Level Co-occurrence Matrix (GLCM) [15], Shape features followed by feature reduction using Principal Component Analysis (PCA) [15]. The reduced feature set was classified using ensemble classifier using Support Vector Machine (SVM), Artificial Neural Network (ANN), and K-Nearest Neighbor (KNN) [15]. The class labels along with feature set are stored in feature database for faster retrieval using KD-Tree indexing. This approach gives the classification accuracy of 97 % approximately.

An ANN and its variants based classification has described in [16–19]. Here the authors have used the GLCM based texture features along with some intensity based features [16]. The dimensionality of feature vector is further reduced by PCA. Using ANN and its variants for classification, various authors used a variable dataset lies between 60–428 MR images of 256×256 dimension. It has been seen that for small dataset of 60 or 80 images classifier gives accuracy rate of nearly 91 % [16] but as the size of dataset increases up to 273, the classification accuracy decreases up to 64 % [19] and varies in a range of (64–94 %) using Bayesian ANN. While using a huge dataset of 428 MR images, the author of [16] claims an accuracy of 85 %.

In [8, 20, 21–23], a SVM based classification approach was used. A dual intensity based features are been extracted using DCT and DWT [20] while GA followed by PCA is used for feature selection. Thus on a dataset of 120 images categorized into normal or abnormal MR images a classification accuracy achieved is 96 %. While using texture, shape based features with ranking mechanism for feature selection the classifier accuracy decreases to 88 % [22]. When the dataset of images increases or decreases the accuracy fluctuates between [80–90 %] as described in [8, 23]. It has been noted that SVM gives good results at Intensity based features rather than texture features.

A new probabilistic approach using neural network used in [21, 24, 25] named PNN. Using the same intensity based features and texture based features, when PNN is applied to a small dataset of 20 images the accuracy achieved is 100 % [24] but as the classifier is tested on a dataset of 120 MR images the accuracy decreases to 96 % [25]. It has been noted during the experiments that PNN works well for frequency based features set extracted using either Discrete Wavelet Transformation (DWT) or Discrete Cosine Transformation (DCT) but degrades the performance with texture based features extracted using Gray Level Co-occurrence Matrix (GLCM).

In [26], a new neuron classifier Simplified Bi-directional Associative Memory (sBAM) is been proposed for brain tumor classification which hasn't been used in such domain ever before. Here the author gives the comparative study of three neuron classifiers operated for tumor classification on MR images. For the comparative purpose the author used the two supervised learning neuron-classifier algorithms like Error Correcting Learning Algorithm and Hebbian Learning Algorithm with one unsupervised learning algorithm named sBAM. sBAM is given by Rajasekaran and Pai for classification of data but such algorithm hasn't been tested for tumor classification. The methodology adopted here is to first segment the tumor image. On the segmented tumor Region texture based features are computed using GLCM. These computed features are been fed into neuron classifiers and corresponding accuracy is been noted. For the experimental purpose an MRI dataset of 200 images is been considered having tumors of class I, II, III, IV respectively. It has been noted that for a sample of size 50 and 200 images,

supervised neuron classifiers accuracy reduced drastically while for sBAM classifier, for variable dataset the accuracy obtained is 95 %. The author also claimed that the computational time for sBAM is also less than for supervised algorithms.

3 Dataset used and Experimental Setup

For the evaluation of the classification methods, this paper basically focused on a dataset of CT/MR images which is used by the researchers. Here the detailed results are presented including the classes of tumors being analyzed with the proper dataset strength. Feature Extraction, Feature selection, Classification Algorithms used by various authors with corresponding accuracy value is shown below in Table 2.

3.1 Evaluation Metrics

Precision, Recall, Accuracy and F-measure are used for evaluating performance of brain tumor classification. Precision for a class is the fraction of total number of images that are correctly classified to the total number of images that classified to the class (sum of True Positives (TP) and False Positives (FP)). Recall is the fraction of total number of correctly classified images to the total number of images that belongs to class (sum of True Positives and False Negative (FN)). F-measure is the combination of both precision and recall. F-measure is used to report the performance of classifiers for the tumor classification.

The statistical evaluation of performance is shown below in table, through confusion matrix.

3.2 Comparative Results and Discussions

See Table 2.

Table 2 Comparison of previous studies on classification of brain tumors

Author- year	Brain tumor classes/Images per class	Image dataset	Feature extraction	Feature selection	Classifier	Accuracy obtained (%)
Megha.P. Arakeri, Springer, 2013	1. Primary (42) 2. Malignant (40)	82	Shape + Texture (GLCM)	PCA + KD-Tree indexing	SVM, ANN, K-NN	97
Jainysachdeva, Vinodkr, Springer, 2013	Astocytoma, Glioblastoma, Medulloblastoma, Meningioma, Metastatic Abnormal (60)	428	GLCM + LoG + IBF + RULBP	PCA	ANN + PCA-ANN	85.23
N. HemaRajni, R. Bhavani, Springer, 2013	Normal (20) Abnormal (60)	80	DWT	PCA	ANN,K-NN, SVM	91, 93, 95
D. Sridhar, Murali Krishna- IEEE, 2013	Primary, Secondary	20	DCT	DCT	PNN	100
Padma Nanthagopal, Springer, 2012	Normal (40) Benign (37) Malignant (43)	120	DWT + WCT	GA	PNN	96
Padma Nanthagopal, Springer, 2012	Normal (40) Benign (37) Malignant (43)	120	DWT + WCT	GA + PCA	SVM	96
Prof. Vikas Gupta, IEEE, 2012	Class I, II, III, IV	60	GLCM	-	ANN	89
P. Rejendran, M. Madheswaran- IEEE, 2012 [27]	Normal (151), Benign (22), Malignant (27)	200	Shape features	ASM	Decision Tree	90
DrMohdFauzi Bin Othman, IEEE, 2012	Normal, Abnormal	15	DWT	-	Kernel-SVM	N (98) AB (67)
Amer Al. Badameh, IEEE/ACM 2012	1. Normal (10) 2. Abnormal (60)	70	DWT	PCA	ANN + KNN	N (96.77) AB (97.56)
Evangelia I. Zacharaki, Springer, 2011	Meningioma,Glioma Grade II, III, IV, Metastatis	100	Age, shape, intensity	PCA	J48,KNN,VFI,SVM, Naive Bayes	85, 93.5, 95, 93
MohdFauzi Othman, IEEE, 2011	Normal, malignant	15	PCA	PCA	PNN	73-80

(continued)

Table 2 (continued)

Author- year	Brain tumor classes/Images per class	Image dataset	Feature extraction	Feature selection	Classifier	Accuracy obtained(%)
Carlos-Arizmendi, Alfredo Vellido, IEEE, 2011	Normal, Primary Grades, Secondary Grades	273	PCA	MWVA	Bayesian ANN	64-95
S. N. Deepa, B. Aruna Devi, IEEE, 2011 [28]	Normal, Abnormal	42	GLCM	-	RBFN	85.71
Jainysachdeva, Vinodkr, IEEE 2011	1. Astrocytoma (118) 2. Glioblastoma (59) 3. Meningioma (97) 4. Medulloblastoma (88) 5. Metastasis (66)	428	GLCM + LoG + IBF + RILBP	PCA	GA-SVM	89.8, 83.3, 96, 91.8, 97.1
Dipali M. Joshi, Dr. N. K. Rana, IEEE, 2010	Normal, Abnormal	80	GLCM	-	Neuro-fuzzy	Based on segmentation (75)
Evangelia I. Zacharaki, IEEE, 2009	Grade I, II, III, IV	98	Age, shape, Texture	Ranking based method	SVM	88.2
Evangelia I. Zacharaki, IEEE, 2009	1. Metastatic (24) 2. Grade Gliomas (22) 3. Glioblastomas (34) 4. Gliomas Grade III (18)	98	Age, shape, Texture	PCA	SVM-RFE	91.7, 90.9, 41.2, 33.4

4 Conclusion

In this paper main focus has given to the contribution of various research works published in digital repository like IEEE, Springer for Brain Tumor classification from 2009 to 2013 onwards. The comparative study clearly shows the achievements being done in tumor classification with proper accuracy rate from the past several years. For the classification of tumors, the researchers used a techniques of feature extraction which includes texture and frequency based features extracted using GLCM and DWT which is followed by feature selection techniques like PCA or Genetic algorithm. Main emphasis was given on classification accuracies. For such various researcher's have proposed a variants of classifiers like PNN and KD-tree indexing mechanism for faster retrieval in CBIR system. The results shows that the classifiers like ANN, PNN, BPNN works well for frequency based features while classifiers like KNN is good for texture based features. It has also been seen that as the size of dataset varies the corresponding accuracy rate shuffles. With the increase in the dataset of images the corresponding accuracy starts decreasing. Most of the researchers used a dataset of MR images between 80 to 120 images. There is still a requirement of some new algorithms and techniques which can give better efficiency rate on a larger datasets.

References

1. http://www.hopkinsmedicine.org/healthlibrary/conditions/nervous_system_disorders/brain_tumors_85,P00775/
2. Ratan, R., Sharma, S., Sharma, S.K.: Multiparameter segmentation and quantization of brain tumor from MR images. *Indian J. Sci. Technol.* **2**(2), 11–15 (2009)
3. Joshi, D., Rana, N.K., Misra, V.: Classification of brain cancer using artificial neural network. In: *International Conference on Electronic Computer Technology*, pp. 112–116. (2010)
4. Astrocytomas grading and their malignancy. <http://en.wikipedia.org/wiki/Astrocytoma>
5. Tatter, S.B.: The new WHO classification of tumors affecting the central nervous system. <http://neurosurgery.mgh.harvard.edu/newwhobt.htm>
6. Kleihues, P., Burger, P.C., Scheithauer, B.W.: The new WHO classification of brain tumours. *Brain Pathol. (US National Library of Medicine National Institutes of Health)* **3**(3):255–268 (1993)
7. <http://www.nhs.uk/Conditions/Brain-tumour/Pages/Introduction.aspx>
8. Zacharaki, E.I., Wang, S., Chawla, S., Yoo, D.S.: MRI-based classification of brain tumor type and grade using SVM_RFE. In: *IEEE International Symposium on Biomedical Imaging: from Nano to Macro* (2009)
9. Borden, N., Forseen, S.E.: *Pattern Recognition Neuroradiology*. Cambridge University Press, New York (2011)
10. <http://www.brainumor.org/patients-family-friends/about-brain-tumors/symptoms-and-diagnosis.html>
11. <http://www.cancer.gov/cancertopics/wyntk/brain/page1/AllPages>
12. Badarneh, A., Najadat, H., Alaraziqi, A.M.: A classifier to detect tumor disease in MR brain images. In: *IEEE International Conference on Advances in Social Networks Analysis and Mining* (2012)

13. Arakeri, M.P., Reddy, G.R.M.: An intelligent content-based image retrieval system for clinical decision support in brain tumor diagnosis. *Int. J. Multimedia Inf. Retrieval* (2013) (Springer)
14. Lin, C., Liu.: A Tutorial of the Wavelet Transform, Google scholar article, 23 Feb (2010)
15. <http://en.wikipedia.org>
16. Sachdeva, J., Kumar, V., Gupta, I.: Segmentation, feature extraction and multiclass brain tumor classification. *Int. J. Digit. Imaging* **26**, 1141–1150 (2013) (Springer)
17. Rajni, N.H., Bhavani, R.: Automatic classification of CT brain images using ANN, KNN and SVM. *Int. J. Artif Intell.Soc.* (2013) (Springer)
18. Gupta, V., Sagale, K.S.: Implementation of classification system for brain cancer using back propagation network and MRI. In: *IEEE International Conference on Engineering (Nuicone)*, (2012)
19. Arizmendi, C., Vellido, A., Romero E.: Binary classification of brain tumors using a discrete wavelet transform and energy criteria. In: *IEEE Second Latin American Symposium on Circuits and Systems (LASCAS)*, (2011)
20. Nanthagopal, A.P., Rajamony, R.S.: Classification of benign and malignant brain tumor CT images using wavelet texture parameters and neural network classifier. *Int. J. Comput. Vision*, (2012) (Springer)
21. Othman, M.F., Ariffanan, M., Basri M.: Probabilistic neural network for brain tumor classification. In: *Second International Conference on Intelligent Systems, Modeling and Simulation*, (2011)
22. Zacharak,i E.I., Kanas, V.G.: Investigating machine learning techniques for MRI based classification of brain neoplasm. *Int. J. Comput. Assist. Radiol. Surg.* **6**(6):821–828 (2011) (Springer)
23. Fauzi, M., Othman, B., Abdullah, N.B.: MRI brain classification using support vector machine. In: *IEEE 4th International Conference on Modeling, Simulation and Applied Optimization (ICMSAO)*, (2011)
24. Sridhar, D., Krishna M.: Brain tumor classification using discrete cosine transform and probabilistic neural network. In: *IEEE International Conference on Signal Processing, Image Processing and Pattern Recognition*, (2013)
25. Nanthagopal, A.P., Rajamony, R.S.: Automatic classification of brain computed tomography images using wavelet-based statistical texture features. *Int. J. Comput. Vision*, (2012) (Springer)
26. Rehman, Y., Azim, F.: Comparison of different artificial neural networks for brain tumor classification via magnetic resonance images. In: *IEEE 14th International Conference on Modeling and Simulation*, (2012)
27. Rajendran, P., Madheswaran, M., Naganandhini K.: An improved pre-processing technique with image mining approach for the medical image classification. In: *Second International Conference on Computing, Communication and Networking Technologies*, (2012)
28. Deepa, S.N., Devi, B.A.: Artificial neural networks design for classification of brain tumor. In: *IEEE International Conference on Computer Communication and Informatics*, (2011)

Anonymous Remote User Authentication and Key Agreement for Cloud Computing

Raghavendra Mishra

Abstract Cloud computing is a remote provision computing technology, which enables user for convenient on-demand access to networks, servers, storage, applications, and services with minimal management effort. Some of the popular cloud services are data storage as services (DSAS) and software as a service (SAAS). In these services, cloud provides the infrastructure for the remote user to store its data or to access software anytime and anywhere without the knowledge or expertise or control over the cloud. Since, a user accesses the remote server through a public channel where an attacker may have full control over the public network. If user and server do not establish a secure session, an attacker gets an opportunity to perform various attacks. Moreover, an attacker can acquire user's sensitive personal information if message includes user's original identity. Therefore, an anonymous mutual authentication mechanism is the paramount requirement to restrict illegal access of cloud server and to ensure user's privacy. In this article, we present a cloud user-server anonymous mutual authentication framework in which user and server authenticate each other and establish a session key without disclosing users' original identity over the public channels. Moreover, user can change its private key periodically to avoid key compromise impersonation attack, which also enhances anonymity during communication. Further, we analyze our scheme to illustrate that the proposed scheme is efficient to establish a secure session between the user and server without losing user anonymity.

Keywords Cloud computing · Anonymity · Certificateless cryptography · Mutual authentication

R. Mishra (✉)

School of Studies in Tourism and Travel Management, Jiwaji University, Gwalior, India
e-mail: mraghavendra86@gmail.com

1 Introduction

Advancement in computing and network technology has presented various computing services for users. Cloud computing is a computing technology, which provides unlimited infrastructure where a remote user can access computing resources. It is an on-demand technology that employs computing resources to present convenient on-demand access to networks, servers, services, storage and applications. It provides the capability to servers to address a wide range of requirement of clients over the network [1].

Cloud computing has emerged as the cutting-edge of scalable technology, which is at the meeting of three major requirements such as service orientation, visualization and standardization of computing. The cloud offers the services which can be provisioned and accessed with minimal management effort from user side. And, user enables to utilize the services without the expertise, knowledge and control over the infrastructure. Some of the major cloud service providers are Google, Amazon, VMware, Sun Microsystems, IBM, Yahoo, Microsoft [2–6]. They are accelerating their paces in developing cloud computing system and enhancing its services to the large numbers of users. Service providers are offering various range of services in the cloud such as Software as a Service (SAAS), Platform as a Service (PAAS), Data Storage as a Service (DSAAS) and Infrastructure as a Service (IAAS) [6].

Cloud offers a client–server architecture in which user accesses the remote servers through the internet in order to get data storage and software services where user utilizes the computing resources on a short-term basis and make the payment for the services. The SAAS and DSAAS have many advantages, some of them are (i) The server can be accessed at anytime and from anywhere, (ii) A physical storage space and computing device are no longer needed to user, (iii) Charged in terms of computing resources usage on a short-term basis, (iv) User need not to invest over the infrastructure and maintenance, (v) User can achieve infinite storage space and computing power immediately, (vi) Enables user to access the services without any proper understanding, knowledge and expertise over the infrastructure. These advantages encourage the user to utilize cloud services.

In spite of development in cloud infrastructure, there are many research challenges occurring in cloud environment [7]. Some of them are, how to control breaching of privacy and security during the access of services while client–server are communicating over the public channel [8–10]. Specifically, user stores its data or access software from a remote server via public channel. An attacker can get full control over the public channel such that he can track the message and source, can intercept the message, and can perform various attacks. An attacker can perform attacks during data transmission and can make services vulnerable. Vulnerability in secure and trusted communication, raise the question mark over the use of cloud service. This makes user uncomfortable in the system. As a result, users try to find some alternate as they don't feel comfortable in cloud system [11].

This may cause revenue loss. However, the session key agreement protocol can prevent the attacks over transmitted data. Moreover, in general architecture, user does not authenticate the server and only server authenticate the user. This scenario creates the full possibility of wrong server selection or server impersonation. However, the mutual authentication mechanism has the potential to make sure that the user and the server can correctly identify each other. Mutual authentication and session key agreement enables the user to transfer their data or to access the server correctly and securely over the public network [12].

In addition, the leakage of the user's specific information, enables the adversary to track the user current location and login history [13]. Although user's anonymity ensures user's privacy by preventing an attacker from acquiring user's sensitive personal information. Moreover, anonymity makes remote user authentication mechanism more robust, as an attacker could not track which user-server are interacting'. The straightforward way to preserve anonymity is to conceal entities real identity during communication [14]. Therefore, to achieve secure and anonymous communication, a cloud infrastructure should support efficient mutual authentication protocols in which user and server can anonymously authenticate each other so that a secure session can be established.

In the past few years, many identity-based mutual authentication protocols have been proposed for cloud infrastructure [12, 15–18]. During mutual authentication, user and server interact with each other and verifies the legitimacy of each other, then establish a shared session key using a shared secret. In this regard, Yang and Chang [17] proposed an identity-based remote user authentication protocol for mobile users based on elliptic curve cryptography (ECC). Their scheme inherits the merits of both identity based cryptosystem and elliptic curve. In 2009, Chen et al. [15] identified two security flaws, namely, insider attack and impersonation attack in Yang-Chang's scheme. To remove these security flaws, they presented an advanced password based authentication scheme using ECC. The authors claimed that their protocol is secured to provide mutual authentication and is appropriated for cloud computing environment. However, Wang et al. [19] showed that Chen et al. [15] protocol is not secure and is vulnerable to offline password guessing attack, and key compromise impersonation attack and also suffers from the clock synchronization problem. In 2010, Wang et al. [16] proposed a public auditing protocol where auditing protocols are used to ensure authenticity and integrity of the out-source data. However, in 2012, Xu et al. [20] analyzed serious security flaws and showed that Wang et al. [16] protocol is vulnerable to existential forgeries using known message attacks from a malicious Cloud server and an outside attacker. Kang and Zhang [21] also presented short key size identity based authentication scheme, although it suffers forward secrecy attack and does not maintain users' anonymity.

Presently, most of the mutual authentication protocol does not prevent key compromise impersonation attack. Moreover, if the users' long-term private key is compromised, then it cannot change its private key by itself (without server or private key generator (PKG) support). To achieve, the user has to communicate with PKG [15, 17, 21]. As a result, the attacker gets success to perform

impersonation attacks. If a user will be able to change its private and public keys periodically, then the leaked key (key compromise) situation can be handled in a better way. In addition, periodical change of private–public keys will enhance user anonymity scenario, as the attacker cannot identify the user with the public key of the user, which is used to establish session. Anonymity protects consumer privacy and makes remote user authentication more robust during communication. Moreover, user anonymity restrains an attacker from acquiring sensitive personal information about an individual’s preferences, lifestyles, shopping patterns, expenses, etc., by analyzing the content consumption and accessing communications [22].

In this paper, we will apply the pairing based certificateless authenticated key agreement protocol for cloud infrastructure which is introduced by Al-Riyami and Paterson [23]. This proposed approach removes key escrow problem as PKG generates only partial key of the user and the entity secret key depends on the entity’s generated share. In this scheme, server and user achieve their partial private keys from PKG and can generate secret value to achieve their public–private keys. Moreover, user and server can change their private–public keys whenever they required without the involvement of PKG. Further, both parties can mutually authenticate each other and establish a session key to communicate securely. Moreover, user and server’s real identity and public key are not revealed during communication, which makes the communication completely anonymous.

The rest of the paper is organized as follows: In Sect. 2, first we define some notations that we will use throughout the paper, then recall the concept of elliptic curve cryptography, identity based public key cryptography and certificateless public key cryptography. We present proposed protocol in Sect. 3. The scheme is analyzed in Sect. 4. Finally, in Sect. 5, we draw a conclusion.

2 Preliminaries

2.1 Background of Elliptic Curve group

The concept of elliptic curve cryptography (ECC) is introduced by Miller [24] and Koblitz [25]. In ECC, E/F_q denotes an elliptic curve E over a prime finite field F_q , defined by an equation

$$y^2 = x^3 + ax + b, \quad \text{for } a, b \in F_q, q \text{ is a large prime number}$$

and with the discriminate

$$\Delta = 4a^3 + 27b^2 \neq 0$$

The points on E/F_q together jointly an extra point Θ form a group

$$G = \{(x, y) : x, y \in F_q; (x, y) \in E\} \cup \{\Theta\},$$

where the point Θ is known as “point at infinity” which acts as the identity element in G . The elliptic curve group G satisfies the properties of the additive Abelian group.

For a given point $P = (x_P, y_P)$, x_P is called the X - coordinate of P , and y_P is called the Y - coordinate of P where P is the generator of group G . The group addition operation in G is defined as:

- (i) $P + \Theta = \Theta + P = P$ for all $P \in G$.
- (ii) If $P = (x_P, y_P) \in G$, then $-P = (x_P, -y_P)$ and $(x_P, y_P) + (x_P, -y_P) = \Theta$.
- (iii) If $P = (x_P, y_P) \in G$, and $Q = (x_Q, y_Q) \in G$, where $P \neq \pm Q$, then $P + Q = (x_3, y_3)$, where $x_3 = (\lambda^2 - x_P, x_Q) \bmod q$, $y_3 = (\lambda(x_P, x_Q) - y_P)$ and $\lambda = \frac{y_Q - y_P}{x_Q - x_P}$.

The scalar multiplication on the group G is defined like $k \cdot P = P + P + \dots + P$ (k times). For smallest integer $n > 1$, if $n \cdot P = \Theta$ then n is said to be the order of P or P has order n . The details of the elliptic curve group are given in [26].

2.2 Bilinear pairings

Let $(G_1, +)$ and (G_2, \cdot) be the additive and multiplicative cyclic groups of order q respectively where q is a k -bit large prime. The bilinear pairing $e : G_1 \times G_1 \rightarrow G_2$ defined by $e(\cdot, \cdot)$ has the following properties as discussed in [27, 28]:

- **Bilinear:** $e(aP, bQ) = e(P, Q)^{ab}$, for all $P, Q \in G_1$ and $a, b \in \mathbb{Z}_q^*$;
- **Non-degenerate:** There exist $P, Q \in G_1$ such that $e(P, Q) \neq 1$;
- **Computable:** There exists an efficient algorithm to compute $e(P, Q)$, for all $P, Q \in G_1$.

The security of CL-PKC in $e(\cdot, \cdot)$ based on the hardness of follow computational problems [23]:

Discrete Logarithm Problem: For a given generator P of G_1 and $Q \in G_1$, find an element $a \in \mathbb{Z}_q^*$ such that $aP = Q$.

Computational Diffie-Hellman (CDH) Problem: Let P be a generator of G_1 . Given $\langle P, aP, bP \rangle \in G_1$ compute $e(P, P)^{ab}$ for $a, b \in \mathbb{Z}_q^*$.

Bilinear Diffie-Hellman (BDH) Problem: Let P be a generator of G_1 . Given $\langle P, aP, bP, cP \rangle \in G_1$ compute $e(P, P)^{abc}$, for $a, b, c \in \mathbb{Z}_q^*$.

2.3 Certificateless Public Key Cryptography (CL-PKI)

Certificateless cryptography is introduced in 2003 by Al-Riyami and Paterson [23]. It eliminates the use of certificate in the system and removes key escrow problem. It comprises of the seven algorithms which are as follows:

Setup: It is a probabilistic algorithm run by The Private Key Generator (PKG) which takes a security parameter, randomly chosen master key and a list of public parameters such as description of message space and ciphertext space.

Partial Private Key-Extract: It is a probabilistic algorithm which is run by the PKG. It takes input as user identity $ID \in \{0, 1\}^*$ and the master key. It returns partial private key.

Set Secret Value: It is a probabilistic algorithm which is performed by the entity. It takes list of public parameters and produces a random secret value for the entity.

Set Private Key: It is a deterministic private key generation algorithm which is run by the entity. It takes input as an entity partial private key and secret value, then returns a private key.

Set Public Key: It is a deterministic public key generation algorithm which runs by entity. It takes parameter and entity secret value, then computes entity public key.

Encrypt: It is a probabilistic algorithm which takes input as message, receiver identity and public key. It outputs ciphertext.

Decrypt: It is a deterministic algorithm which takes a ciphertext and receiver private key. It returns message.

3 Proposed scheme

In this section, we present an anonymous mutual authentication scheme. This scheme has three phases. First phase is the setup phase where the user and server submit their identities separately to the private key generator (PKG) and in return get their partial private keys. Once the user gets the private key, he can submit his registration request to the cloud server. Upon receiving the registration request, the cloud server verifies the authenticity of the user and registers the authorized users. Further, user and server mutually authenticate each other and establish a secure session. During authentication, the user does not reveal his identity over the public channel to achieve anonymity. The protocol is composed of the following four algorithms:

- Setup.
- Extract.
- Registration and secure session establishment.
- Key update.

3.1 Setup

Private key generator (PKG) chooses an arbitrary generator $P \in G_1$, selects a master key $m \in Z_q^*$ and sets $PK = mP$. Let $h : \{0, 1\}^* \times G_1 \rightarrow G_1$ be a map-to-point hash function. $h_0 : G_2 \rightarrow \{0, 1\}^k$, $h_1 : G_1 \times G_1 \times G_1 \times G_2 \rightarrow \{0, 1\}^k$, $h_2 : G_1 \times G_1 \times \{0, 1\}^k \rightarrow \{0, 1\}^k$. PKG publishes system parameters $\langle G_1, G_2, e(\cdot, \cdot), k, P, PK, h(\cdot), h_0(\cdot), h_1(\cdot), h_2(\cdot) \rangle$ and keeps the master key m secret.

3.2 Extract

Server's partial private key extraction: Server (S) submits its public identities ID_S to the PKG. Then, PKG verifies the proof of the identity. If the verification succeeds, then generates the partial private key as follows:

- Compute $Q_S = h(ID_S || mP) \in G_1$.
- By using its master key m , generates the partial private keys $W_S = mQ_S$ and delivers (Q_S, W_S) to S through a secure channel.

On receiving the partial private keys, S verifies its partial keys as:

$$e(W_S, P) = e(mQ_S, P) = e(Q_S, mP) = e(Q_S, PK)$$

Server's private and public key extraction: Cloud server S selects a secret value $x_S \in Z_q^*$ at random and keeps x_S secret. Then, it generates its private key SK_S by computing $SK_S = x_S W_S = x_S m Q_S$. It constructs its public key $PK_S = \langle X_S, Y_S \rangle$ where $X_S = x_S P$ and $Y_S = x_S PK = x_S m P$. Then, it keeps $\langle ID_S, Q_S, PK_S \rangle$ in its public directory.

User's partial private key extraction: User U submits his public identity ID_U to the PKG. Then, PKG verifies the proof of identity. If the verification succeeds, then generates the partial private key in the following way:

- Compute $Q_U = h(ID_U || mP) \in G_1$.
- By using its master key m , generates the partial private key $W_U = mQ_U$ and delivers (Q_U, W_U) to U through a secure channel.

On receiving the key U can verify as:

$$e(W_U, P) = e(mQ_U, P) = e(Q_U, mP) = e(Q_U, PK).$$

User's private and public key extraction: Cloud user U selects a random value $x_U \in Z_q^*$ and keeps it secret. Then, U generates its private key SK_U by computing $SK_U = x_U W_U = x_U m Q_U$ and constructs its public key $PK_U = \langle X_U, Y_U \rangle$ where $X_U = x_U P$ and $Y_U = x_U PK = x_U m P$. U stores its keys in secure place and does not make public the likability between its identity and public key.

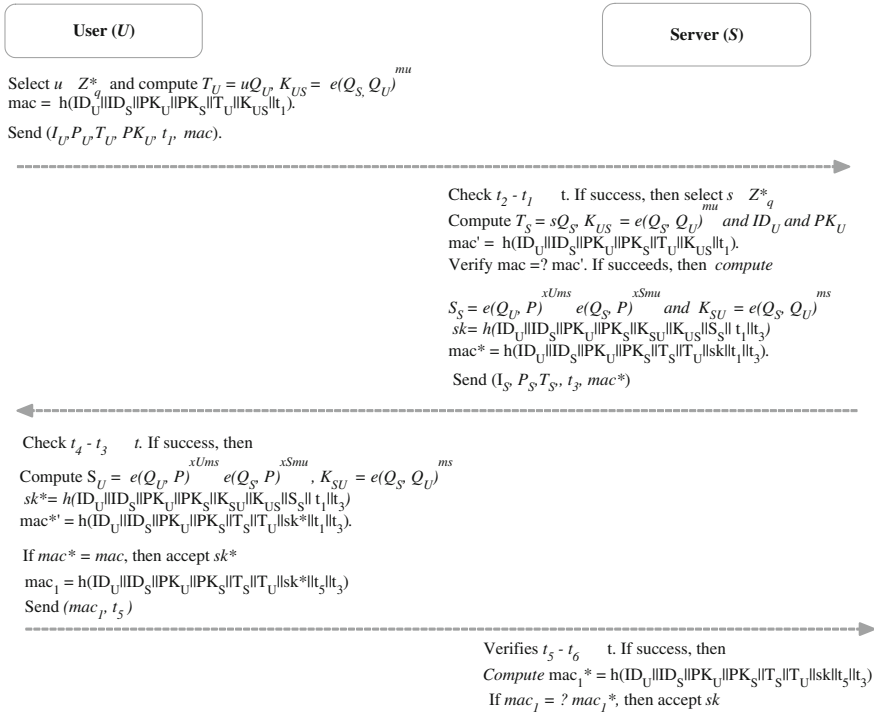


Fig. 1 Proposed mutual authentication mechanism between cloud user and server

3.3 Registration and Secure Session Establishment

User U submits his registration request with identity ID_U to the server S . S verifies the authenticity of U . If U is authorized user, then S registers U 's identity ID_U . Otherwise, denies the registration request (Fig. 1).

When a user wishes to access the cloud services, the user first establishes a secure session with S . To establish a session, U sends "HELLO" message to S . S replies to U with a "HELLO" message. On receiving S response, U initiates the session with S as follows:

- **Step 1.** U achieves $\langle ID_S, Q_S, PK_S \rangle$ from S 's public directory, then chooses a random value $u \in Z_q^*$ and computes $T_U = uQ_U$ and $h_0(k_{US})$ and mac at time t_1 where

$$K_{US} = e(Q_S, W_U)^u = e(Q_S, mQ_U)^u = e(Q_S, Q_U)^{um},$$

$$mac = h_2(ID_U || ID_S || PK_U || PK_S || T_U || k_{US} || t_1).$$

Then, U computes $P_U = PK_U \oplus h_0(k_{US})$ and $I_U = ID_U \oplus h_0(k_{US})$, and sends $\langle I_U, P_U, T_U, t_1, mac \rangle$ to S .

- **Step 2.** On receiving the user message, S computes $t_2 - t_1 \leq \Delta t$, where t_2 is the message receiving time and Δt is the valid time delay in message transmission. If the time delay in message transmission is valid, then S computes $h_0(K_{SU}^*)$ where

$$k_{US}^* = e(W_S, T_U) = e(mQ_S, uQ_U) = e(Q_S, Q_U)^{mu}.$$

Then, it achieves U 's public key and identity as:

$$ID_U = ID_U \oplus h_0(k_{US}) \oplus h_0(K_{US}^*) \text{ and } PK_U = PK_U \oplus h_0(k_{US}) \oplus h(K_{US}^*),$$

since $mu = um$ as $m, u \in Z_q^*$. S verifies the authenticity and the registration of U . If U is unauthorized or revoked user, then S denies the request. Otherwise, computes message authentication code as:

$$\text{mac}' = h_2(ID_U || ID_S || PK_U || PK_S || T_U || k_{US}^* || t_1),$$

and verifies $\text{mac} = ? \text{mac}'$.

- **Step 3.** If verification succeeds, S selects a random value $s \in Z_q^*$ and computes $T_S = sQ_S$, $Q_U = h(ID_U || PK)$, then computes k_{SU} and S_S as:

$$\begin{aligned} S_S &= e(Q_U, Y_U)^s \cdot e(SK_S, T_U) \\ &= e(Q_U, P)^{x_{Ums}} \cdot e(Q_S, P)^{x_{Sms}} \end{aligned}$$

$$k_{SU} = e(W_S, Q_U)^s = e(mQ_S, Q_U)^s = e(Q_S, Q_U)^{ms}$$

Then, S computes session key sk and mac^* as:

$$\begin{aligned} sk &= h_1(ID_U || ID_S || PK_U || PK_S || k_{SU} || K_{US} || S_S || t_1 || t_3), \\ \text{mac}^* &= h_2(ID_U || ID_S || PK_U || PK_S || T_S || T_U || sk || t_1 || t_3). \end{aligned}$$

S computes $h_0(k_{SU})$, $I_S = ID_S \oplus h_0(k_{SU})$ and $P_S = PK_S \oplus h_0(k_{SU})$. Then, U sends $\langle I_S, P_S, T_S, t_3, \text{mac}^* \rangle$ to U , where t_3 is the current timestamp.

- **Step 4.** On receiving the message, U computes $t_4 - t_3 \leq \Delta t$, where t_4 is the message receiving time. If t_3 is not fresh, U aborts the current session. Otherwise, U computes S_U as:

$$k_{SU}^* = e(T_S, W_U) = e(sQ_S, mQ_U) = e(Q_S, Q_U)^{sm}.$$

Then, it achieves S 's public key and identity as:

$$ID_S = ID_S \oplus h_0(k_{SU}) \oplus h_0(K_{SU}^*) \text{ and } PK_S = PK_S \oplus h_0(k_{SU}) \oplus h_0(K_{SU}^*).$$

$$S_U = e(Q_S, Y_S)^u \cdot e(SK_U, T_S) = e(Q_S, P)^{x_S^{mu}} \cdot e(Q_U, P)^{x_U^{ms}}$$

then computes the session key sk' and mac^{*} as:

$$sk^* = h_1(ID_U || ID_S || PK_U || PK_S || K_{S_U}^* || K_{U_S} || S_U || t_1 || t_3),$$

$$mac^{*'} = h_2(ID_U || ID_S || PK_U || PK_S || T_S || T_U || sk^* || t_1 || t_3).$$

U verifies the server authenticity by the condition $mac^{*' } = ? mac^*$. If the verification succeeds, then U considers sk^* as the session key.

- **Step 5.** U computes mac_1 at time t_5 and sends $\langle mac_1, t_5 \rangle$ to S where

$$mac_1 = h_2(ID_U || ID_S || PK_U || PK_S || T_S || T_U || sk^* || t_5 || t_3).$$

- **Step 6.** On receiving the message S computes

$$mac_1^* = h_2(ID_U || ID_S || PK_U || PK_S || T_S || T_U || sk^* || t_5 || t_3),$$

then verifies $mac_1 = ? mac_1^*$. If the verification succeeds, then S considers sk as the session key.

- **Step 7.** Once the secure session is established, user and server can communicate securely using the established session key sk over the insecure network.

3.4 Updating the Leaked Private Key

Once a user private key is compromised or leaked, user can reconstruct his/her public and private keys as follows:

- Generate a random number x_U^* and computes x_U^*P .
- Achieve his/her private and public keys using secret value x_U^* as follows:

$$SK_U^* = x_U^*W_U = x_U^*mQ_U \text{ and } PK_U = x_U^*PK = x_U^*mP.$$

4 Security Analysis

In this section, we will analyze the security of the proposed scheme.

4.1 User anonymity

In the proposed scheme, the anonymity of U is hidden by XORing identical with a hash value of $K_{US} = e(Q_U, Q_S)^{mu}$. Although to compute $e(Q_S, Q_U)^{mu}$ for given $\langle uQ_U, Q_S, PK = mP \rangle$, an attacker has to achieve m for given $\langle mP, P \rangle$, which is equivalent to discrete logarithm problem. Moreover, the user uses different K_{US} for each session. So, a previous compromised values of K_{US} does not help the attacker to know which user is establishing current session. This dynamic identity mechanism helps to protect user anonymity. Moreover, the attacker can not identify with which server a user is communicating, as server identity and public key is also hidden in communication. Anonymity of both user-server identity and public key makes the communication completely anonymous.

4.2 Man in the Middle Attack

User and server authenticate each other without knowing each other. An adversary or malicious PKG can try man in the middle attack by sending the forge message. However, to authenticate each other the server and the user exchange message authentication code mac with each other. To compute mac, an adversary needs to compute sk . To compute sk the secret values S_S or S_U and $e(Q_S, Q_U)^{mu}$ is needed. Although to compute $e(Q_S, Q_U)^{mu}$ for given $\langle uQ_U, Q_S, PK = mP \rangle$, the attacker has to achieve m for given $\langle mP, P \rangle$, which is equivalent to discrete logarithm problem. Moreover, to compute S_S or S_U require secret share x_U or x_S and session secret values u or s respectively. which are with U and S only. And, to compute $e(Q_S, P)^{x_S mu}$ for given $\langle Q_S, uP, x_S mP \rangle$ and to compute $e(Q_U, P)^{x_U ms}$ for given $\langle Q_U, lP, x_U mP \rangle$ is equivalent to BDH problem in ECC.

4.3 Known Key Secrecy

If an attacker achieves some past session keys. Then, compromise of previously established session keys does not help to generate other session keys or new session key. As, each session key hashed with a one way hash function, which cannot be reverted. Therefore, no information can be extracted from session key. In addition, each session key involves different secret session values s and u and time-stems for each session, which ensure different session keys for different sessions. These facts show that compromise of any session key does not result the compromise of current session keys.

4.4 Forward Secrecy

A compromise of private key (x_U, SK_U) of user does not reveal previously established session keys because to achieve a session key, short time secret key information and partial private key W_S or W_U is needed. However, for given $\langle P, mP, Q_U, Q_S \rangle$, to compute $Q_U, Q_S m$ is equivalent to CDH problem.

4.5 Perfect Forward Security

Compromise of the PKG master key reveals the information about partial private key $W_S = Q_S m$ and $W_U = Q_U m$, but does not reveal any information about session key because to achieve session key, the value (x_U, x_S) and (u, s) are needed. However, x_U and x_S cannot be computed from master key. Moreover, to compute $e(Q_U, P)^{x_U m s}$ from given $\langle Q_U, P, x_U P, sP, mP \rangle$, $e(Q_S, P)^{x_S m u}$, and $\langle Q_S, P, x_S P, uP, mP \rangle$ are equivalent to BDH problem.

4.6 Known Session-Specific Temporary Information Attack

If short term secret keys u and s compromise, then the attacker can compute $A_1 = e(Q_U, Y_U)^s = e(Q_U, P)^{x_U m s}$ and $A_2 = e(Q_S, Y_S)^u = e(Q_S, P)^{x_S m u}$. An adversary can compute S_S or S_U using A_1 and A_2 as:

$$\begin{aligned} S_U &= A_1 \cdot A_2 \\ &= e(Q_S, P)^{x_S m u} \cdot e(Q_U, P)^{x_U m s} \end{aligned}$$

Although an attacker cannot construct the session keys, as each session key includes $Q_U Q_S m$, and to compute $Q_U Q_S m$ knowledge of the master key is needed, where to compute the master key m for given $\langle P, mP \rangle$ is equivalent to DLP in ECC.

4.7 Replay Attack

Replay attack is the most common attack in authentication process. However, the common countermeasures are timestamp scheme and random number scheme. In our scheme, we adopt both the mechanism the timestamp and in each communication message authentication code (mac) includes a timestamp. In addition, mac is unchangeable, as it is protected with one way collision free hash function $(h(\cdot))$. Therefore, the proposed scheme is secure against replay attack.

4.8 Impersonation Attack

Let us assume that the attacker (A) achieves private key SK_U of the user U . Then, E tries to impersonate the user by forging the message. However, knowledge of private key does not enable the adversary to perform the impersonation attack. A detailed decryption of impersonation attack failure is as:

- U initiates the session with S .
- U chooses a random number $u \in Z_q^*$ and computes $T_U = uP$, $k_{US} =$ and mac . Then, U sends the message $\langle ID_U \oplus h(k_{US}, PK_U \oplus h(k_{US}, T_U, t_1, mac)) \rangle$ to S .
- To verify that the message is sent by U , A needs to extract the ID_U from $ID_U \oplus h(k_{US})$. Which requires the computation of K_{US} . Although, to compute $K_{US} = e(Q_S, Q_U)^{mu}$ from $\langle uQ_U, mQ_U, Q_S \rangle$, A needs to compute u for given $\langle Q_U, uQ_U \rangle$, which is equivalent to DLP.
- If A assume that the message is from U , then A does not intercept the U 's message.
- On receiving the message, S chooses a random number $s \in Z_q^*$ and computes $T_S = sP$, k_{US} , mac^* and verifies $mac = ? mac^*$. Then, S computes S_S , sk and mac' , and responds with the message $\langle ID_S \oplus h(k_{SU}, PK_S \oplus h(k_{SU}, T_S, t_3, mac^*)) \rangle$.
- A intercepts the S 's message and tries to replace it. A generates $a \in Z_q^*$ and can replace T_S by $T_A = aQ_S$. However, A can not computes mac with T_A , as mac includes sk , and sk includes K_{US} . Although to compute $K_{US} = e(Q_S, Q_U)^{mu}$ from $\langle uQ_U, mQ_U, Q_S \rangle$, A needs to compute u for given $\langle Q_U, uQ_U \rangle$, which is equivalent to DLP. Moreover, A has to compute $e(Q_S, P)^{x_S mu}$ to compute S_S . However, to compute $e(Q_S, P)^{x_S mu}$ for given $\langle Q_S, uQ_U, x_S mP \rangle$ is equivalent to the BDH problem in the ECC. Therefore, impersonation attacks are not possible in proposed protocol.

4.9 Mutual Authentication

In mutual authentication mechanism user must prove its identity to the server and the server must prove its identity to the user. In the proposed scheme user and server both authenticate each other. To achieve it, user and server exchange message authentication codes, which includes entities' identities and secret keys. In authentication phase server's verifies user authenticity in step 2 and vice versa is done in step 4. No unauthorized party can forge either of the entities, as message authentication codes involve secret shares of entities. In addition, to construct message authentication code form publicly available information is hard as mentioned in proposition 2 and 7.

Table 1 Comparison of the schemes with related schemes for different security scenarios

Security attributes	[17]	[15]	[21]	Proposed
Key freshness	Yes	Yes	No	Yes
Known session keys	Yes	Yes	No	Yes
Impersonation attack	No	No	Yes	Yes
Replay attack	No	No	Yes	Yes
Known session-specific temporary information attack	No	No	Yes	Yes
Perfect forward secrecy	No	No	No	Yes
Mutual authentication	Yes	Yes	Yes	Yes
Session key establishment	Yes	Yes	Yes	Yes
Anonymity	No	No	No	Yes

No: does not prevent the attack; Yes: prevents the attack

4.10 Session Key Computation

In the proposed scheme, the session key (sK) is constructed by the shared secret of both the user and server. Moreover, both the user and the server verify the shared secret key (session key) in *steps 4* and *6* respectively to ensure the correctness of the key (Table 1).

5 Conclusion

In cloud computing, mutual authentication between cloud users and server is essential to ensure authorized communication which restricts the adversary from intercepting the communication. In this paper, we have proposed certificateless identity based mutual authentication mechanism which removes key escrow problem and ensure authorized and secure communication between remote user and server. Moreover, cloud user and server establish a session key which they use for secure communication.

References

1. Armbrust, M., Fox, A., Griffith, R., Joseph, A.D., Katz, R., Konwinski, A., et al.: A view of cloud computing. *Commun. ACM.* **53**(4), 50–58 (2010)
2. Amazon Web Service, <http://aws.amazon.com>
3. “Google App Engine”. <http://appengine.google.com>
4. Microsoft Azure, <http://www.microsoft.com/azure/>
5. <http://www.softwarehouse.com.cn/news/show/101593.html>
6. Zhou, M., Zhang, R., Zeng, D., Qian, W.: Services in the cloud computing era: A survey. In: *Proceeding of the 4th International Universal Communication Symposium (IUCS)*. IEEE, pp. 40–46 (2010)
7. Zhang, Q., Cheng, L., Boutaba, R.: Cloud computing: state-of-the-art and research challenges. *J. Internet. Serv. Appl.* **1**(1), 7–18 (2010)

8. Takabi, H., Joshi, J.B.D., Ahn, G.J.: Security and privacy challenges in cloud computing environments. *Security and Privacy, IEEE*. **8**(6), 24–31 (1991)
9. Zhou, M., Zhang, R., Xie, W., Qian, W., Zhou, A.: Security and privacy in cloud computing: A survey. In: *Proceeding of the Sixth International Conference on Semantics Knowledge and Grid (SKG)*, pp. 105–12 (2010)
10. Zissis, D., Lekkas, D.: Addressing cloud computing security issues. *Future. Gener. Comput. Syst.* **28**(3), 583–592 (2012)
11. Siani, P., Azzedine, B.: Privacy, security and trust issues arising from cloud computing. In: *Proceeding of the IEEE Second International Conference on Cloud Computing Technology and Science (CloudCom)*, pp. 693–02 (2010)
12. Chang, H., Choi, E.: *User authentication in cloud computing. Ubiquitous Computing and Multimedia Applications*. Springer, Heidelberg (2011)
13. Caimu, T., Dapeng, O.W.: Mobile privacy in wireless networks-revisited. *IEEE Trans. Wireless Commun.* **7**(3), 1035–1042 (2008)
14. Ronald, P., Christoph, S.: Privacy-preserving DRM for cloud computing. In: *Proceeding of the 26th International Conference on Advanced Information Networking and Applications Workshops (WAINA)*, pp. 1286–91 (2012)
15. Chen, T.H., Yeh, H., Shih, W.K.: An advanced ecc dynamic id-based remote mutual authentication scheme for cloud computing. In: *Proceeding of the 5th FTRA International Conference on Multimedia and Ubiquitous Engineering (MUE)*, pp. 155–59 (2011)
16. Wang, C., Wang, Q., Ren, K., Lou, W.: Privacy-Preserving public auditing for data storage security in cloud computing. In: *Proceeding of the IEEE INFOCOM*, pp. 1–9 (2010)
17. Yang, J.H., Chang, C.C.: An ID-based remote mutual authentication with key agreement scheme for mobile devices on elliptic curve cryptosystem. *Comput. Secur.* **28**(3), 138–143 (2009)
18. Zhi-hua, Z., Jian-jun, L., Wei, J., Yong, Z., Bei, G.: An new anonymous authentication scheme for cloud computing. In: *Proceeding of the 7th International Conference on Computer Science and Education (ICCSE)*. IEEE, pp. 896–98 (2012)
19. Wang, D., Mei, Y., Ma, C., Cui, Z.: Comments on an advanced dynamic id-based authentication scheme for cloud computing. *Web Information Systems and Mining*, pp. 246–53 (2012)
20. Xu, C., He, X., Abraha-Weldemariam, D.: Cryptanalysis of Wang’s auditing protocol for data storage security in cloud computing. *Information Computing and Applications*, pp. 422–28 (2012)
21. Kang, L., Zhang, X.: Identity-based authentication in cloud storage sharing. *International Conference on Multimedia Information Network and Security(MINES)*. IEEE Computer Society, pp. 851–55 (2010)
22. Feng, B., Robert, D.: Privacy protection for transactions of digital goods. *International Conference on Information and Communication Security (ICICS)*, pp. 202–13 (2001)
23. Al-Riyami, S., Paterson, k.: Certificateless public key cryptography. In: *Proceeding of the Advances in Cryptology-ASIACRYPT*, pp. 452–73 (2003)
24. Miller, V.: Use of elliptic curves in cryptography. In: *Proceeding of the Advances in Cryptology—CRYPTO’85*, pp. 417–26 (1986)
25. Elliptic, K.N.: Cryptosystems curve. *Math. Comput.* **48**(177), 203–209 (1987)
26. Hankerson, D., Menezes, A.J., Vanstone, S.: *Guide to Elliptic Curve Cryptography*. Springer, New York (2004)
27. Boneh, D., Franklin, M.: Identity-Based encryption from weil pairing. In: Kilian J. (ed) *Proceeding of the Crypto. Lecture Notes in Computer Science*, vol. 2139, pp. 213–29. Springer Heidelberg (2001)
28. Dutta, R., Barua, R., Sarkar, P.: Pairing based cryptographic protocols : A survey. <http://eprint.iacr.org/2004/064> (2004)

Automatic Identification of an Epileptic Spike Pattern in an EEG Signals Using ANN

Mohd. Zuhair, Sonia Thomas, Anup Kumar Keshri,
Rakesh Kumar Sinha, Kirat Pal and Dhrubes Biswas

Abstract This work emphasizes to automatically detect the pattern called 'epileptic spike' from electroencephalogram (EEG) signal using multilayer perceptron (MLP). The analysis work is carried out through using the receiver operating characteristics (ROC). Electroencephalograph is used to record the electrical activity of the brain. Classification of the (EEG) signal plays a vital role in the diagnosis of epilepsy. The verification of epileptic seizure requires long-term EEG monitoring of 24 h or more. The signal is a huge collection of data and unfortunately, medicos uses the traditional method of visually interpreting EEG signal through personal experience to identify the transient event of epilepsy. This method of visual interpretation is tedious and time-consuming and, may result in an erroneous judgment. Hence, efficient EEG signal analysis is required for the diagnosis of epilepsy. This model is evaluated on the basis of sensitivity and selectivity and experimental result highlights the good precision of the model. The overall accuracy of the model is computed as 99.11 %.

Keywords EEG · ROC · MLP

M. Zuhair (✉) · D. Biswas
Rajendra Mishra School of Engineering Entrepreneurship, Indian Institute of Technology,
Kharagpur, India
e-mail: md.zuhair.cs@gmail.com

S. Thomas · K. Pal
Earthquake Engineering, Indian Institute of Technology, Roorkee, India

A. K. Keshri
Department of Information Technology, Birla Institute of Technology, Ranchi, India

R. K. Sinha
Department of Biomedical Instrumentation, Birla Institute of Technology, Ranchi, India

1 Introduction

Epilepsy is a chronic brain disorder that affects people of every age around the globe. Around 50 million people worldwide are suffering from epilepsy which accounts for 0.5 % of the global diseases. Studies reveal that close to 80 % of epilepsy cases worldwide are diagnosed in developing countries. Recent studies indicate that in both developed and developing countries up to 70 % of diagnosed cases can be successfully treated with anti-epileptic drugs (AEDs) [1]. The Electroencephalogram (EEG) is conventional source of information used to monitor, manage and diagnose neurological disorder associated with epilepsy. Epilepsy is a neurological condition having the tendency to have recurrent seizures. Seizures are manifested as sharp abrupt changes in the amplitude of EEG signal in a short span of time, as shown in the Fig. 1a. The data recorded by EEG monitoring devices are enormous and hence, analysis by visual inspection of extensive recordings of EEG, in order to locate traces of epilepsy is not routinely possible. Therefore, automatic detection of epilepsy has been the intent of many researchers.

Various techniques have been established for ‘automatic epileptic detection system’ from EEG signal for medicos. Some of the methods applicable are using artificial neural networks [2–9], fuzzy logic [10], DFA [11, 12], genetic programming [13], Hidden Markov model [14] and various other time and frequency domain analysis [15–22]. ANNs play a vital role in ‘decision making’ issues. Thus, ANN have remarkably gained attention and so-cause interest in many fields like modern information technology, production technique, decision making, pattern recognition, diagnostics, data analysis etc. This paper attributes to the automation of an epileptic spike detection model using a feed-forward neural network, with four features as input. The model comprises of a two-layered back propagation neural network with a feedback connection from the output of hidden layer to its input. The four features are extracted from a one second window of EEG signal using basic signal processing functions.

2 Data Recording and Processing

The EEG data is recorded from male Charles Foster rats weighing between 200–250 g. The recording electrodes were implanted on the rat’s head under urethane (Sigma, USA) anesthesia (1.5 gm/kg i.p). Two electrodes for EEG recording were placed on the frontal and occipital parts of the skull and one reference electrode was placed on the anterior most part of the skull. Three stainless steel screw electrodes of 1 mm diameter soldered with flexible radio wires were implanted extradural. To actuate epileptic seizure, a 10 ml benzyl penicillin solution having 50 units of benzyl penicillin was injected below the cortical surface of the parietal region of the brain [11]. The intra cerebral injection

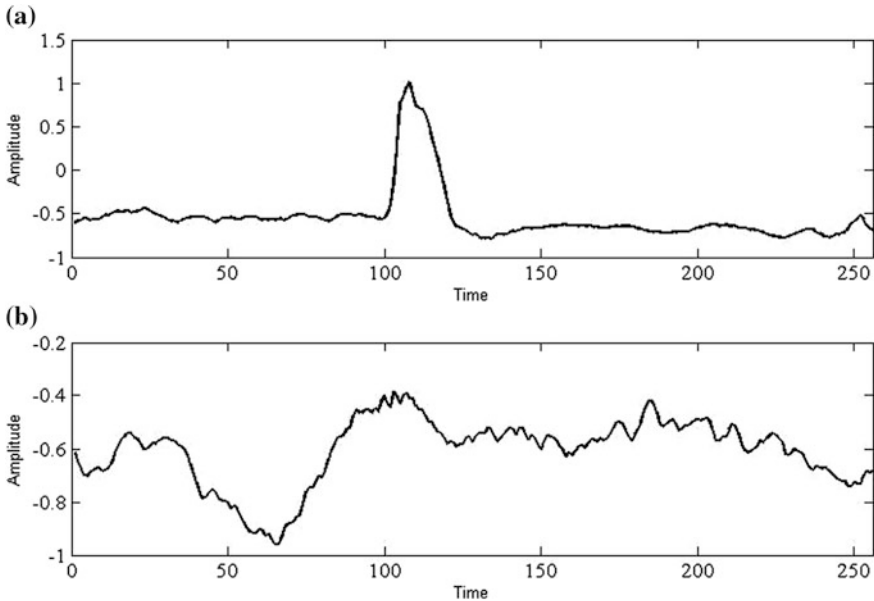


Fig. 1 1 s window of **a** Spike data. **b** Non spike data

dose of benzyl penicillin produces spontaneous seizure. The seizure was initiated within 3–5 min of injection.

The single channel bipolar EEG signal was recorded with standard amplifier setting as suggested by [23], continuously for 45 min through an electroencephalograph (EEG-8, Medicare, India) from the time of injection of penicillin to the end of seizure patterns. The EEG signal was recorded in separate data files for duration of two minutes. The files are then, stored to the computer hard disk after digitization of the traces at 256 Hz. Visual Lab-M software (AD Link Technology Inc., Taiwan) has been used for the data collection. After the recording, whole data was pre-processed for the removal of baseline shift and band pass filter using an infinite impulse response (IIR) 4th order Butterworth filter with a lower cut-off of 0.25 Hz and a higher cut-off of 35 Hz [24, 25]. Whole experiment procedure in this case has been designed and conducted in compliance with the committee for purpose of control and supervision of experiments on animals (CPCSEA), India as well as in accordance with internal institutional policies and guidelines.

3 Feature Extraction for ANN

Various signal processing techniques as well as computational methodologies have been used by different authors for recognizing an epileptic spike. In this paper, a feed-forward neural network is used to detect the epileptic spike pattern. The

processing of EEG data for feature extraction can be done in the time domain as well as frequency domain [2], and, also, using wavelet transforms [10]. The feature extraction from EEG signal is done by considering a fixed window frame size of one second. The sampling rate of the signal is 256 Hz and each window has 'n' samples. The one second EEG signal of a healthy person (non-epileptic patient) is shown in the Fig. 1b and, that of an epileptic patient containing epileptic spike in the Fig. 1a. Considering x as the sampled signal, then, (i) x_k will be the k th sampled signal, (ii) x_{k+1} will be next sampled signal, (iii) x_{k-1} will be the previous signal. Some representations are expressed below which gives a basic idea of the mathematical equations involved in the feature extraction of EEG signal. The basic building block of a signal is a window. Each window is characterized by a set of four tuples, where each tuple is resolved by a mathematical expression as defined below.

3.1 Zero Crossing (ZC)

ZC is the number of zero crossings of the wave. ZC is incremented when either condition p_1 (crossing zero downwards) or p_2 (crossing zero upwards) is arrived, and, this is not a noise-condition p_3 . The threshold is used to make the counter less sensible to noise.

$$ZC = \begin{cases} ZC + 1, & \text{if } (p_1 \vee p_2) \wedge p_3 \\ ZC, & \text{otherwise} \end{cases} \quad (1)$$

$$p_1 = (x_k \geq 0) \wedge (x_{k+1} < 0)$$

$$p_2 = (x_k \leq 0) \wedge (x_{k+1} > 0)$$

$$p_3 = |x_k - x_{k+1}| \geq \text{threshold}$$

3.2 Frequency of Slope Changes (FSC)

FSC is incremented when the current data point is either a positive peak (condition p_4) or a negative peak (condition p_5) and, these are not attributed to the noise conditions p_3 (previously defined) and p_6 .

$$FSC = \begin{cases} FSC + 1, & \text{if } (p_4 \vee p_5) \wedge (p_3 \vee p_6) \\ FSC, & \text{otherwise} \end{cases} \quad (2)$$

$$p_4 = (x_k > x_{k-1}) \wedge (x_k > x_{k+1})$$

$$p_5 = (x_k < x_{k-1}) \wedge (x_k < x_{k+1})$$

$$p_6 = |x_k - x_{k-1}| \geq \text{threshold}$$

3.3 Upslope Distance (UD)

UD is the distance travelled by the wave while the slope is positive. The condition is checked by p_7 and, if the condition is true for p_8 , then, the distance UD is determined as;

$$UD = \sum_{k=2}^N p_7, \text{ if } p_8 \quad (3)$$

where,

$$p_8 = \begin{cases} 1 & \text{if } (p_7 > 0) \\ 0, & \text{otherwise} \end{cases}$$

$$p_7 = (x_k - x_{k-1})$$

3.4 Downslope Distance (DD)

DD is the distance travelled by the signal while the slope is negative. The condition is checked by p_7 , if the condition is true for p_8 , then, the distance is calculated as;

$$DD = \sum_{k=2}^N p_7, \text{ if } p_8 \quad (4)$$

where,

$$p_8 = \begin{cases} 1 & \text{if } (p_7 < 0) \\ 0, & \text{otherwise} \end{cases}$$

4 Artificial Neural Network (ANN) Implementation

ANN are inspired by biological neural networks, consisting of neuron like units connected through input and output paths having adjustable weights [26]. Each neuron produces an output which is function of sum of its input. A three-layered feed-forward back-propagation ANN is applied to classify the spike and non-spike windows from EEG signals. From the EEG data, four features are extracted from a

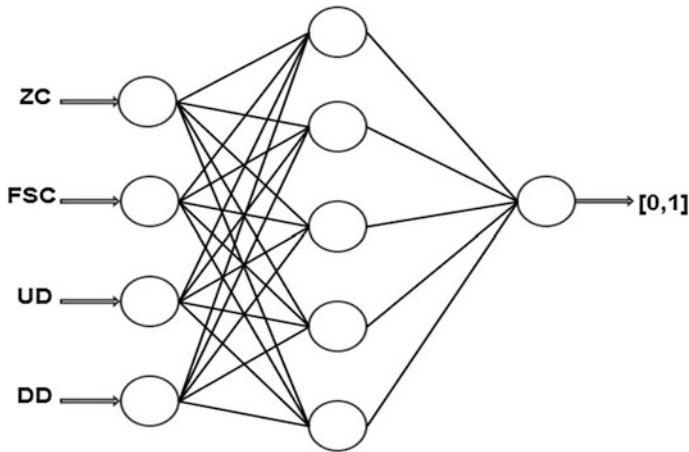


Fig. 2 Architecture of neural network

window of one second. These four features are input to the neural network, as illustrated in the Fig. 2. ANN has three-layer architecture with the structure 4-5-1. Training algorithm is feed-forward back propagation algorithm with sigmoidal function as an activation function. The output of the ANN is $[0, 1]$ where, 0 represents non spike EEG data of one second epoch and, 1 represents spike data of one second epoch. 120 data points of one second is used in training the ANN. Training data contains 60 spike data and 60 non spike data points of 1 s.

5 Performance Evaluation Parameters

Receiver operating characteristics (ROC) [4] is widely applied in the field of radar communications for detecting missile. It signifies the trade-off between missing and incoming missile and raising the false alarm. The analogy is used to specify a missing seizure and raising a false alarm. Various cases are illustrated as,

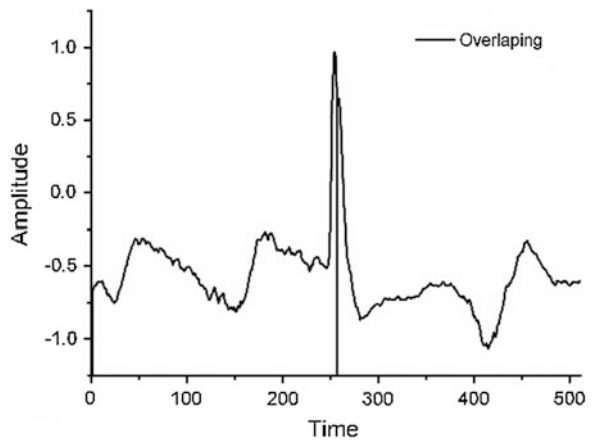
1. True Positive (TP)—The ANN identifies a spike pattern that was labelled as a spike by the expert.
2. True Negative (TN)—The ANN and the expert both agree that the EEG pattern is normal.
3. False Positive (FP)—The ANN detects a spike in an EEG segment that was labelled normal by the expert.
4. False Negative (FN)—The ANN has missed a spike that the expert has identified in the segment.

Table 1 ROC analysis

Data set	TP	TN	FP	FN
Data 1	38	102	0	0
Data 2	30	96	0	1
Data 3	23	96	2	0
Data 4	19	101	1	0
Data 5	19	116	0	0
Data 6	20	126	0	1

Table 2 Result comparison of ANN and manual detection

Data set	Data length	Manual spike detected	ANN spike detected	ANN non spike detected	Accuracy percentage
Data 1	140	38	38	102	100
Data 2	127	31	30	97	98.34
Data 3	121	23	25	96	98.98
Data 4	121	19	20	101	99.51
Data 5	135	19	19	116	100
Data 6	150	21	20	130	97.62
				Accuracy	99.11

Fig. 3 EEG data containing spike in overlapping window

The equations used for the computation are expressed as;

$$1. \text{ Sensitivity} = TP / (TP + FN) * 100. \quad (5)$$

$$2. \text{ Specificity} = TN / (TN + FP) * 100. \quad (6)$$

$$3. \text{ Selectivity} = TP / (TP + FP) * 100. \quad (7)$$

$$4. \text{ Accuracy} = (\text{Sensitivity} + \text{Specificity}) / 2 * 100. \quad (8)$$

6 Results and Discussion

Table 1 gives the illustration of ROC analysis of the result interpreted from the proposed ANN model. It is indicated that the number of spikes detected by ANN was almost equal to the number of spike recognized by the expert. Table 2 estimates the accuracy of the proposed ANN model as 99.11 % which is better than [8, 11, 14], the previous work done in this research domain. The ROC analysis results into the proposed ANN missed to detect a spike in the data set 2 and dataset 6, as shown in the Table 1 (the false negative is 1 for both the dataset). This is because the spike exists at the border of two consecutive windows (i.e. overlapping windows). In such cases of overlapping windows, the spike gets itself split into two windows and hence, goes undetected. In the data set 2, the spike is present at the overlapping of window at 40 and 41 s. In the data set 6, the spike is present at the overlapping of window at 121 and 122 s. The overlapping is illustrated in the Fig. 3.

7 Conclusion

The results as computed in the Tables 1 and 2 clearly highlights that the proposed ANN architecture has very high precision and accuracy in detecting the epileptic spikes from EEG signals. There are of course minute losses in the interfacing between the devices. As interpreted from the Fig. 3, it can be accessed that the accuracy could be further improved if the overlapping of spike can be treated efficiently. Besides the overlapping spikes, the proposed ANN architecture has not missed out any other spikes present in the dataset.

References

1. World Health Organization Media centre factsheet. <http://who.int/mediacentre/factsheets/fs999/en/index.html> (2012)
2. Srinivasan, V., Eswaran, C., Sriram, N.: Artificial neural network based epileptic detection using time-domain and frequency-domain features. *J. Med. Syst.* **29**, 647–660 (2005). doi:10.1007/s10916-005-6133-1
3. Kutlu, K., Kuntalp, M., Kuntalp, D.: Optimizing the performance of an MLP classifier for the automatic detection of epileptic spikes. *Expert Syst. Appl.* **36**, 7567–7575 (2009). doi:10.1016/j.eswa.2008.09.052
4. Sezer, E., Isik, H., Saracoglu, E.: Employment and comparison of different artificial neural networks for epilepsy diagnosis from EEG signals. *J. Med. Syst.* **36**, 347–362 (2010). doi:10.1007/s10916-010-9480-5
5. Subasi, A., Ercelebi, E.: Classification of eeg signal using neural network and logistic regression. *Comput. Methods Programs Biomed.* **78**, 87–99 (2005). doi:10.1016/j.cmpb.2004.10.009
6. Sahin, C., Ogulata, N.S., Aslan, K., Bozdemir, H.: The application of neural networks in classification of epilepsy using EEG signals. In: Mele, F., et al. (eds.) BVAI 2007. LNCS, vol. 4729, pp. 499–508. Springer, Heidelberg (2007)

7. Pradhan, N., Sadasivan, P.K., Arunodaya, G.R.: Detection of seizure activity in EEG by an artificial neural network: a preliminary study. *Comput. Biomed. Res.* **29**, 303–313 (1996)
8. Jahankani, P., Kodogiannis, V., Lygouras, J.: Adaptive fuzzy inference neural network system for EEG signal classification. In: Jain, L.C., Lim, C. P. (eds.) *Handbook on Decision Making*. ISRL vol. 4, pp. 453–471. Springer, Heidelberg (2010)
9. Kumar, Y., Dewal, M.L., Anand, R.S.: Epileptic seizures detection in EEG using dwt-based ApEn and artificial neural network. *SIViP* (2012). doi:[10.1007/s11760-012-0362-9](https://doi.org/10.1007/s11760-012-0362-9)
10. Geva, A. B.: Forecasting generalized epileptic seizure from the eeg signal by wavelet analysis and dynamic unsupervised fuzzy clustering. *IEEE Trans. Biomed. Eng.* **45**, 1205–1216 (1998)
11. Keshri, A.K., Sinha, R.K., Hatwal, R., Das, B.N.: Epileptic spike recognition in electroencephalogram using deterministic automata. *J. Med. Syst.* **33**, 173–179 (2009). doi:[10.1007/s10916-008-9177-1](https://doi.org/10.1007/s10916-008-9177-1)
12. Keshri, A.K., Sinha, R.K., Mallik, D.K., Das, B.N.: Parallel algorithm to analyze the brain signals: application on epileptic spike. *J. Med. Syst.* **35**, 93–104 (2011). doi:[10.1007/s10916-009-9345-y](https://doi.org/10.1007/s10916-009-9345-y)
13. Lopes, H.S.: Genetic programming for epileptic pattern recognition in electroencephalographic signals. *Appl. Soft Comput.* **7**, 343–352 (2007). doi:[10.1016/j.asoc.2005.07.004](https://doi.org/10.1016/j.asoc.2005.07.004)
14. Abdullah, M. A., Abdullah, J. M., Abdullah, M. Z.: Seizure detection by means of Hidden Markov model and stationary wavelet transform of electroencephalogram signal. In: *Proceedings of the IEEE-EMBS International Conference on Biomedical and health (BHI (2012))*, Hong Kong and Shenzhen (2012)
15. Gotman, J., Flanagan, D., Zhang, J., Rosenblatt, B.: Automatic seizure detection in the newborn: methods and initial evaluation. *Electroencephalogr. Clin. Neurophysiol.* **103**, 356–362 (1997)
16. Zoubir, M., Boashash, B.: Seizure detection of newborn EEG using a model-based approach. *IEEE Trans. Biomed. Eng.* **45**, 673–685 (1998)
17. Shaker, M.M.: EEG wave classifier using wavelet transform and fourier transform. *Int. J. Biol. med. Sci.* **12**, 85–90 (2006)
18. Qu, H., Gotman, J.: A patient specific algorithm for the detection of seizure onset in long-term EEG monitoring: possible use of warning system. *IEEE Trans. Biomed. Eng.* **44**(2), 115–122 (1997)
19. Litt, B., Echauz, J.: Prediction of epileptic seizures. *Lancet Neurol.* **1**, 22–30 (2002)
20. Othman, M.Z., Shaker, M.M., Abdullah, M.F.: EEG spike detection, sorting and localization. In: *Proceedings of World Academy Science, Engineering and Technology*, vol. 9, ISSN 1307-6884 (2005)
21. Indiradevi, K.P., Elias, E., Shathidevi, P.S., Nayak, D.S., Radhakrishnan, K.: A multi-level wavelet approach for automatic detection of epileptic spike in electroencephalogram. *Comput. Biol. Med.* **38**, 805–816 (2008)
22. Tzallas, A.T., Oikonomou, V.P., Fotiadis, D.I.: Epileptic spike detection using a Kalman filter based approach. In: *Proceedings of the 28th Conference of the IEEE Engineering in Medicine and Biological Society*, New York City, Aug 30–Sept 3 2006
23. Sarbadhikari, S.N.: A neural network confirms that physical exercise reverses EEG changes in depressed rats. *Med. Eng. Phys.* **17**, 579–582 (1995)
24. Sinha, R.K.: Electro-encephalogram disturbances in different sleep-awake states following exposure of high environmental heat. *Med. Biol. Eng. Comput.* **42**, 282–287 (2004)
25. Sinha, R.K.: Artificial neural network detects changes in electro-encephalogram power spectrum of different sleep-awake states in an animal model of heat stress. *Med. Biol. Eng. Comput.* **41**, 595–600 (2003)
26. Haykin, S.: *Neural Networks*. McMaster University, Ontario (1999)

About the Editors

Dr. Millie Pant is Associate Professor with the Department of Paper Technology, Indian Institute of Technology Roorkee, Roorkee, India. She has to her credit several research papers in journals of national and international repute and is a well known figure in the field of Swarm Intelligence and Evolutionary Algorithms.

Prof. Kusum Deep is with the Department of Mathematics, Indian Institute of Technology Roorkee, Roorkee, India. Over the last 25 years, her research is increasingly well-cited making her a central International figure in the area of Nature Inspired Optimization Techniques, Genetic Algorithms and Particle Swarm Optimization.

Dr. Jagdish Chand Bansal is Assistant Professor with the South Asian University, New Delhi, India. He is holding an excellent academic record and an excellent researcher in the field of Swarm Intelligence at the National and International Level. He has several research papers in journals of national and international repute.

Prof. Atulya Nagar holds the Foundation Chair of Computer and Mathematical Sciences and Heads the Department of Computer Science at Liverpool Hope University, Liverpool, UK. Prof. Nagar is an internationally recognised scholar working at the cutting edge of theoretical computer science, applied mathematical analysis, operations research, and systems engineering and his work is underpinned by strong complexity-theoretic foundations.

Author Index

A

Abdi, Lida, 589
Agarwal, Rashi, 203
Agarwal, Saumya, 121
Agarwal, Shivi, 733
Aggarwal, Remica, 427
Agrawal, Jitendra, 677, 709
Agrawal, S. P., 1
Agrawal, Seema, 225
Agrawal, Shikha, 677, 709
Ahn, Chang Wook, 413
Alberti, Riccardo, 503
Ali, Musrrat, 413
Anand, Darpan, 211
Anand, Sanjay Kumar, 561
Anju Alias, M., 85
Anuradha, 867
Arora, Manoj K., 755
Arumugam, S., 25, 35
Asady, B., 183
Ashu, Kamna, 667

B

Balasubramanian, R., 755
Bathla, Ravitashaw, 321
Berciano, Ainhoa, 45
Bhardwaj, Tushar, 355
Bhargava, Deepshikha, 133
Bhattacharjee, Amrita, 857
Bhattacharyya, Dhruva Kr., 601
Biswas, Dhruves, 915
Buckley, Neil, 25, 35

C

Ch., Aswani Kumar, 845
Chandrakant, N., 247, 259
Chaturvedi, D. K., 193, 267

Chauhan, P. K. S., 441
Chaurasia, Brijesh Kumar, 767
Chawla, Kanika, 667
Christinal, Hepzibah A., 45

D

Dare, V. R., 481
Das, Kedar Nath, 143
Deep, Aakash, 343
Deep, Kusum, 395, 495, 629
Deepa, S. N., 547
Devi, Gayatri, 441
Devi, V. Susheela, 689
Dewan, Hrishikesh, 689
Dhall, Sakshi, 365
Díaz-Pernil, Daniel, 45
Diwakar, Manoj, 403
Dubey, Manish Kant, 805
Dubey, Om Prakash, 495
Dwivedi, Bharti, 333

E

Elias, Susan, 833

G

Gayathri, K. S., 833
Geethanjali, M., 85
Gogoi, Minakshi, 601
Gulati, T. R., 881
Gupta, N., 183
Gupta, Gourav, 535
Gupta, Kapil, 755
Gupta, Manish, 211
Gupta, Niyati, 777
Gupta, Praneesh, 539
Gutiérrez-Naranjo, Miguel A., 45

H

Hashemi, Sattar, 589
Himakshi, 109

J

Jain, Arpit, 709
Jain, Shilpi, 121
Jain, Shubham, 321
Jauhar, Sunil, 343
Jha, C. K., 653
Joshil Raj, K., 95

K

Kalyani, T., 481
Kapoor, Monit, 513
Karpaga Senthil Pandey, T., 85
Kaul, Uarvarshi, 121
Kaur, Narinder, 641
Kaur, Prabhjeet, 561
Kaur, Prabhjot, 777
Kaur, Shilpy, 677
Keshri, Anup Kumar, 915
Khalid, Saifullah, 333
Khanna, Anupam, 641
Khanna, Kavita, 451, 459
Kumar, Amit, 281, 535
Kumar, Anil, 1
Kumar, Bhawya, 579
Kumar, Pardeep, 403
Kumar, Sanoj, 667
Kumar, Vineet, 281, 379
Kushwah, Rajendra Singh, 767

L

Lal, Roshan, 169
Lather, J. S., 55
Lellouch, Gabriel, 525

M

Maheshwari, Sanjeev, 161
Makhija, Palak, 777
Manju, A., 69
Mansouri, P., 183
Mishra, Amit Kumar, 525
Mishra, Prasanna Raghaw, 539
Mishra, Puneet, 281
Mishra, Raghavendra, 899
Mishra, Vimal Kumar, 653
Mittal, Abha, 441
Mittal, Namita, 889

Mogha, Sandeep Kumar, 467
Munganda, Lakshmi Kanth, 721

N

Nagar, Atulya K., 25, 35, 503
Nair, Sreejith S., 281
Nayak, Raksha B., 689
Nigam, M. J., 69

P

Pabla, Harcharan Singh, 777
Pal, Kirat, 915
Pal, Saibal K., 365
Pandit, Manu Ram, 355
Pant, Millie, 343, 413
Parida, Manoranjan, 793
Parouha, Raghav Prasad, 143
Patel, Divyesh, 785
Prabhu, N., 755
Prasad, Ajay, 495
Prasanna Kumar, N., 741
Prateek, Manish, 513
Prusty, Alok Kumar, 615
Purkayastha, Bipul Syam, 857

R

Raghavendra, G. S., 741
Rajan, C. Christober Asir, 11
Rajaselvi, V. Devi, 481
Rajpal, Navin, 451, 459
Rana, K. P. S., 281, 379
Rani, Deepika, 881
Rani, Rashmi, 169
Rastogi, Rohit, 121
Ratan, Ram, 805, 821
Roy, B. K., 297

S

Sahgal, Divya, 793
Sahoo, Bibhudatta, 615
Samuel, G. Giftson, 11
Santhosh, K. V., 297
Saxena, Pramod Kumar, 805
Saxena, Sameer, 133
Sharma, Amit Kumar, 561
Sharma, Kapil, 365
Sharma, M. K., 535
Sharma, Palak, 121
Sharma, Piyush, 55
Sharma, Pratibha, 403

Sharma, Richa, 281, 379
Sharma, Sanjeev, 677, 709
Sharma, Tarun Kumar, 355
Shivashankar, S., 833
Shukla, Anupam, 307
Shukla, Arvind Kumar, 653
Shukla, Pankaj, 579
Singh, Alok, 721
Singh, Arunesh Kumar, 193
Singh, Chandan, 235
Singh, Charan Kamaljit, 109
Singh, Dipti, 225
Singh, Garima, 395
Singh, Gurpal, 777
Singh, Jitendra, 193
Singh, Manu Pratap, 211
Singh, Mayank Pratap, 267
Singh, Nidhi, 225
Singh, Prem Kumar, 845
Singh, Rajeev, 321
Singh, Ravindra Kumar, 109
Singh, S. P., 467
Singh, S. R., 867
Singh, Satya Narayan, 495
Singh, Sukhdeep, 777
Sinha, Rakesh Kumar, 915
Sinha, S. K., 55
SivaSathya, S., 95
Srivastava, Tanuja, 785
Sudha, G., 547

Sur, Chiranjib, 307
Swarnakar, Sandip, 403

T

Tayal, V. K., 55
Thomas, D. G., 481
Thomas, Sonia, 915
Tomar, Ranjeet Singh, 767

V

Verma, Harsh Kumar, 109
Verma, Neelam, 805
Verma, Shekhar, 767
Vidyarthi, Ankit, 889
Vijay, Rahul, 579
Vimal, Vrinice, 161

Y

Yadav, Anupam, 629
Yadav, Dhananjay, 235
Yadav, Shiv Prasad, 467

Z

Zuhair, Mohd., 915